VOL.
8
1959

Vol.8, 1959

# THE PHYSICS AND CHEMISTRY OF SOLIDS

AN INTERNATIONAL JOURNAL

*Editor-in-Chief*
**HARVEY BROOKS**
*Cambridge, Mass.*

*Associate Editors*

**H. B. G. CASIMIR**
*Eindhoven*

**G. J. DIENES**
*Brookhaven*

**JACQUES FRIEDEL**
*Paris*

**E. M. LIFSHITZ**
*Moscow*

**Proceedings of 1958 International Conference on Semiconductors**

**PERGAMON PRESS**

**NEW YORK · LONDON · PARIS · LOS ANGELES**

# THE JOURNAL OF THE PHYSICS AND CHEMISTRY OF SOLIDS


*Editors*

PROF. HARVEY BROOKS (*Editor-in-Chief*), 224 *Lyman Laboratory, Harvard University, Cambridge* 38 *Mass., U.S.A.*

PROF. Dr. H. B. G. CASIMIR, *N.V. Philips' Gloeilampenfabrieken, Eindhoven, The Netherlands*

DR. G. J. DIENES, *Brookhaven National Laboratory, Upton, Long Island, New York, U.S.A.*

PROF. JACQUES FRIEDEL, *École Nationale Supérieure des Mines, 60 Blvd. St. Michel, Paris, France*

PROF. E. M. LIFSHITZ, *The Academy of Sciences of the U.S.S.R., Moscow, U.S.S.R.*

*Editorial Advisory Board*

*U.S.A.:* E. N. ADAMS, Pittsburgh · D. L. ALPERT, Illinois · L. APKER, Schenectady · J. BARDEEN, Illinois · D. S. BILLINGTON, Oak Ridge · R. G. BRECKENRIDGE, Cleveland · LEO BREWER, Berkeley, Calif. · E. BURSTEIN, Penn. · J. A. BURTON, New Jersey · N. CABRERA, Virginia · G. C. DANIELSON, Iowa · I. ESTERMANN, Washington, D.C. · J. C. FISHER, Schenectady · F. HERMAN, Princeton · CONYERS HERRING, New Jersey · A. R. VON HIPPEL, Cambridge, Mass. · J. H. HOLLOMON, Schenectady · W. V. HOUSTON, Houston · H. B. HUNTINGTON, Troy · H. M. JAMES, Purdue · JOHN G. KIRKWOOD, Yale · C. KITTEL, Berkeley, Calif. · W. KOHN, Pittsburgh · J. A. KRUMHANSL, Cleveland · A. W. LAWSON, Chicago · H. W. LEVERENZ, Princeton · O. T. MARZKE, Pittsburgh · B. T. MATTHIAS, New Jersey · L. R. MAXWELL, Silver Spring · JOSEPH E. MAYER, Chicago · E. W. MONTROLL, Maryland · DAVID PINES, Princeton · H. REISS, New Jersey · J. R. REITZ, Cleveland · A. ROSE, Princeton · O. C. SIMPSON, Argonne R. SMOLUCHOWSKI, Pittsburgh · F. H. SPEDDING, Iowa · D. TURNBULL, Schenectady · J. H. VAN VLECK, Harvard · B. E. WARREN, Cambridge, Mass. · EUGENE P. WIGNER, Princeton · B. H. ZIMM, Schenectady.

*Canada:* R. E. BURGESS, Vancouver · D. K. C. MACDONALD, Ottawa.

*United Kingdom:* A. CHARLESBY, Shrivenham, Berks · W. J. DUNNING and F. C. FRANK, Bristol · H. K. HENISCH, Reading · H. JONES, London · J. W. MITCHELL, Bristol · A. B. PIPPARD, Cambridge · M. H. L. PRYCE, Bristol R. A. SMITH, Malvern · K. W. H. STEVENS, Nottingham · F. C. TOMPKINS, London.

*France:* E. F. BERTAUT, Grenoble · A. GUINIER, Paris · LOUIS NÉEL and LOUIS WEIL, Grenoble.

*Germany:* M. BORN, Bad Pyrmont · ULRICH DEHLINGER, Stuttgart · R. HILSCH, Göttingen · G. LEIBFRIED, Aachen E. MOLLWO, Erlangen · H. PICK, Stuttgart · M. VON LAUE, Berlin · H. WELKER, Erlangen.

*Italy:* F. G. FUMI, Pavia.

*Czechoslovakia:* J. TAUC, Praha.

*Japan:* TOSHINOSUKE MUTO, Tokyo.

*The Netherlands:* A. MICHELS and G. W. RATHENAU, Amsterdam. *Sweden:* J. O. LINDE, Stockholm · PER-OLOV LÖWDIN, Uppsala.

*Switzerland:* G. BUSCH and P. SCHERRER, Zurich. *U.S.S.R.:* G. S. ZHDANOV, Moscow.



*Publishing Offices*

*American Continent: Pergamon Press, Inc., 122 East 55th Street, New York 22, N.Y.*

*Rest of the World: Pergamon Press Ltd., 4 & 5 Fitzroy Square, London W.1*

*Issued in parts. Subscription rates: (A)* £6 (*U.S.A.* $17.00) per volume; *(B) for subscribers who write directly to the publishers certifying that the subscription is for their own personal use,* £8 5*s.* (*U.S.A.* $22.50) per annum, *including postage.*



*Pergamon Press are also the publishers of the following journals:*

JOURNAL OF NUCLEAR ENERGY (*including* •THE SOVIET JOURNAL OF ATOMIC ENERGY. Part A: REACTOR SCIENCE. Part B: REACTOR TECHNOLOGY
HEALTH PHYSICS (*The Official Journal of the Health Physics Society*)
JOURNAL OF INORGANIC AND NUCLEAR CHEMISTRY
TETRAHEDRON (*The International Journal of Organic Chemistry*)
TALANTA (*An International Journal of Analytical Chemistry*)
INTERNATIONAL JOURNAL OF APPLIED RADIATION AND ISOTOPES
BIOCHEMICAL PHARMACOLOGY
•BIOPHYSICS
•JOURNAL OF MICROBIOLOGY, EPIDEMIOLOGY AND IMMUNOBIOLOGY
•PROBLEMS OF HEMATOLOGY AND BLOOD TRANSFUSION
•PROBLEMS OF ONCOLOGY
•PROBLEMS OF VIROLOGY
•SECHENOV PHYSIOLOGICAL JOURNAL OF THE U.S.S.R.
•PAVLOV JOURNAL OF HIGHER NERVOUS ACTIVITY
•ELECTRIC TECHNOLOGY U.S.S.R.
•RADIO ENGINEERING
•RADIO ENGINEERING AND ELECTRONICS
•TELECOMMUNICATIONS
•THE PHYSICS OF METALS AND METALLOGRAPHY
•THE ABSTRACTS JOURNAL OF METALLURGY
APPLIED MATHEMATICS AND MECHANICS
CHEMICAL ENGINEERING SCIENCE
JOURNAL OF ATMOSPHERIC AND TERRESTRIAL PHYSICS
ANNALS OF THE INTERNATIONAL GEOPHYSICAL YEAR
GEOCHIMICA ET COSMOCHIMICA ACTA
SPECTROCHIMICA ACTA
BULLETIN GEODESIQUE
JOURNAL OF THE MECHANICS AND PHYSICS OF SOLIDS
ACTA METALLURGICA (*for the Board of Governors of Acta Metallurgica*)
DEEP-SEA RESEARCH
JOURNAL OF NEUROCHEMISTRY
JOURNAL OF PSYCHOSOMATIC RESEARCH
JOURNAL OF INSECT PHYSIOLOGY
JOURNAL OF AIR POLLUTION
INTERNATIONAL ABSTRACTS OF BIOLOGICAL SCIENCES (*for Biological and Medical Abstracts Ltd.*)
RHEOLOGY ABSTRACTS
VACUUM
OPERATIONAL RESEARCH QUARTERLY
ANNALS OF OCCUPATIONAL HYGIENE

•Translations of Russian Journals published on behalf of Pergamon Institute, a non-profit-making foundation.

*Leaflets giving further details and subscription rates for each of these journals are available on request*

Copyright © 1959 Pergamon Press, Ltd.



PERGAMON PRESS, INC.

122 EAST 55TH STREET, NEW YORK 22, N.Y. 4 & 5 FITZROY SQUARE, LONDON W.1



VOL
8
195

VOL.
8
1959

VOL
8
195

VOL.
8
1959

# TABLE OF CONTENTS

M. H. HEBB: Introduction. . . . . 1

## A. OPENING SESSION

A.2 J. BARDEEN: Trends in semiconductor research . . . . . 2
A.3 A. JOFFÉ: Properties of various semiconductors . . . . . 6
*Discussion:* Compiled by W. SHOCKLEY . . . . . 13
A.4 O. G. FOLBERTH and H. WELKER: Binding and semiconductor properties of $A^{III}B^{V}$-compounds . . . . . 14
*Discussion:* Compiled by F. HERMAN . . . . . 20

## B. BAND THEORY

B.1 J. C. SLATER: Band theory . . . . . 21
B.2 C. ZENER: *D*-band and mixed-valency semiconductors . . . . . 26
B.3 D. E. SOULE and J. W. MCCLURE: Band structure and transport properties of single-crystal graphite . . . . . 29
B.4 J. L. BIRMAN: Calculation of electronic energy bands in ZnS . . . . . 35
B.5 E. O. KANE: The semi-empirical approach to band structure . . . . . 38
B.6 W. KOHN: Motion of electrons and holes in semiconductors from a many-electron point of view. 45
B.7 L. M. ROTH and G. W. PRATT, JR.: A many-body treatment of dielectric screening for impurity states and excitons in semiconductors . . . . . 47
*Discussion:* Compiled by H. EHRENREICH . . . . . 50

## C. RECOMBINATION AND IMPURITY CENTERS

C.1 S. G. KALASHNIKOV: Studies on the recombination of electrons and holes in germanium . 52
C.2 W. W. TYLER: Deep level impurities in germanium . . . . . 59
C.3 M. LAX: Giant traps . . . . . 66
C.4 P. T. LANDSBERG and A. R. BEATTIE: Auger effect in semiconductors . . . . . 73
C.5 P. H. BRILL and R. F. SCHWARZ: Radiative recombination and lifetime in germanium . 75
C.6 S. GOLDSTEIN: H. METTE and W. W. GÄRTNER: Carrier recombination in germanium as a function of temperature between 100°K and 550°K . . . . . 78
C.7 R. O. CARLSON, R. N. HALL and E. M. PELL: Sulfur in silicon . . . . . 81
C.8 V. E. LASHKAREV, E. G. MISELYUK and K. D. GLINCHUK: Effect of annealing on the state of certain impurities in Ge . . . . . 84
*Discussion:* Compiled by A. ROSE . . . . . 85

## D. SURFACES

D.1 A. MANY: The electrical structure of semiconductor surfaces . . . . . 87
D.2 E. HARNIK and Y. MARGONINSKI: The effect of some surface treatments on the characteristics of fast states on germanium surfaces . . . . . 96
D.3 R. BRAY and R. W. CUNNINGHAM: Optical and magnetic surface studies on germanium . 99
D.4 J. N. ZEMEL and R. L. PETRITZ: Magneto-surface properties of near intrinsic germanium . 102
D.5 N. J. HARRICK: Effect of the metal-to-semiconductor potential on the semiconductor surface barrier height . . . . . 106
D.6 R. MISSMAN and P. HANDLER: Hall mobility of a cleaned germanium surface . . . 109
D.7 G. A. BARNES and P. C. BANBURY: Electrical properties of clean germanium surfaces . . 111
D.8 S. P. WOLSKY: Germanium and silicon surfaces . . . . . 114
D.9 H. E. FARNSWORTH, R. E. SCHLIER and J. A. DILLON, JR.: Surface-structure and work-function determinations for silicon crystals . . . . . 116
D.10 F. G. ALLEN: Work function and emission studies on clean silicon surfaces . . . . 119
*Discussion:* Compiled by H. STATZ . . . . . 121

## E. THEORY II

E.1 J. M. LUTTINGER: Transport theory . . . 123
E.2 L. STILBANS: The scattering mechanism of carriers on phonon and lattice defects . . 123
E.3 A. R. REGEL: On the role of the short and long-range order in the electrical properties of substances . . . 124
E.4 P. N. ARGYRES: Galvanomagnetic effects in the quantum limit . . . 124
E.5 H. EHRENREICH: Screening effects in polar semiconductors . . . 130
E.6 P. J. PRICE: On the theory of strong-field conduction . . . 136
E.7 G. E. TAUBER and L. SOFFER: Transport phenomena in semiconductors for warped energy surfaces . . . 138

## F. DISLOCATIONS

F.1 L. SOSNOWSKI: Electronic processes at grain boundaries . . . 142
F.2 A. F. GIBSON: The mobility, diffusion constant, and lifetime of minority carriers in heavily dislocated germanium . . . 147
F.3 C. BENOIT À LA GUILLAUME: Recombinaison radiative par l'intermédiaire des dislocations dans le germanium . . . 150
F.4 P. BARUCH: Centres de recombinaison introduits dans le germanium par des electrons de 2 MeV . . . 153
F.5 R. K. MUELLER: Capture diameter of dislocations in low angle grain boundaries in germanium 157
F.6 H. KAWAMURA and H. OKURA: Trapping of photoelectrons around dislocation lines in alkali-halides . . . 161
*Discussion:* Compiled by G. L. PEARSON . . . 164

## G. EXCITONS

G.1 H. HAKEN: On the theory of excitons in solids . . . 166
G.2 E. F. GROSS: Optical spectrum and magneto-optical properties of excitons . . . 172
G.3 I. BROSER and R. BROSER-WARMINSKY: Concerning the problem of exciton diffusion in photoconductors . . . 177
G.4 M. BALKANSKI: Energy transfer in semiconductors . . . 179
G.5 G. DIEMER, G. J. VAN GURP and W. HOOGENSTRAATEN: An analysis ofmix ed ambipolar and exciton diffusion in CdS crystals . . . 182
G.6 E. GRILLOT and M. BANCIE-GRILLOT: Fluorescent emission ascribable to exciton annihilation in pure CdS crystals . . . 187
G.7 S. NIKITINE: Spectroscopie du corps solide et spectres d'excitons . . . 190
*Discussion:* Compiled by B. LAX . . . 193

## H. GENERAL

H.1 W. PAUL: The effect of pressure on the properties of germanium and silicon . . . 196
H.2 M. CARDONA, W. PAUL and H. BROOKS: Dielectric constant of germanium and silicon as a function of volume . . . 204
H.3 R. BOWERS: The magnetic susceptibility of semiconductors . . . 206
H.4 H. D. HAGSTRUM: State density in the valence band of silicon . . . 211
H.5 G. WEINREICH: Chemical shift of donor states germanium . . . 216
*Discussion:* Compiled by J. H. CRAWFORD . . . 218

## I. TRANSPORT

I.1 J. TAUC: Electron impact ionization in semiconductors . . . 219
I.1a V. S. VAVILOV: On photo-ionization and ionization by fast electrons in germanium and silicon 223
I.2 S. H. KOENIG: Hot and warm electrons—A review . . . 227
I.3 E. CONWELL: Lattice mobility of hot carriers . . . 234
I.4 J. B. GUNN: Effect of electron and impurity density on the field-dependence of mobility in germanium . . . 239
I.5 M. C. STEELE and M. GLICKSMAN: High electric field effects in *u*-indium antimonide . . . 242
I.6 T. N. MORGAN: The mobility of electrons heated by microwave fields in *n*-type germanium . 245
I.7 W. SASAKI, M. SHIBUYA, K. MIZUGUCHI and G. M. HATOYAMA: Anisotropy of hot electrons in germanium . . . 250
I.8 H. FRITZSCHE: The effect of uniaxial tensile stress on impurity conduction in germanium . 257
I.9 T. A. LONGO, R. K. RAY and K. LARK-HOROVITZ: Low temperature impurity conduction in silicon . . . 259
*Discussion:* Compiled by R. W. KEYES . . . 262

VOL. 8 1959

## J. OPTICAL PROPERTIES

J.1 H. J. G. Meyer: Theory of infrared absorption by conduction electrons in germanium . 264
J.2 H. Y. Fan and P. Fisher: Absorption spectra of group V donors in germanium . . . 270
J.2a H. Y. Fan and A. K. Ramdas: Infrared absorption in neutron irradiated silicon . . . 272
J.3 F. R. Kessler: Infrared absorption of free carriers produced in semiconductors by photoeffect 275
J.4 F. Stern: Effects associated with a linear energy term in the valence band of intermetallic semi-conductors . . . . . 277
J.5 R. Braunstein: Intervalence band transitions in gallium arsenide . . . . . 280
J.6 G. Picus, E. Burstein, B. W. Henvis and M. Hass: Infrared lattice vibration studies of polar character in compound semiconductors . . . . . 282
*Discussion:* Compiled by E. Burstein . . . . . 285

## K. IONIC CRYSTALS

K.1 T. Muto, S. Oyama and H. Okuno: Electronic structure of an exciton in alkali halides . 286
K.2 Y. Toyozawa: Exciton-lattice interaction and a theory of the line shape of exciton absorption bands . . . . . 289
K.3 B. Goodman and O. S. Oen: Interaction of excitons with lattice vibrations . . . . 291
K.4 W. Martienssen: The optical absorption edge in ionic crystals . . . . . 294
K.5 E. A. Braun and J. W. Mitchell: Photoconductivity in crystals of silver bromide . . 297
K.6 F. C. Brown and K. Kobayashi: Electronic processes in the silver halides at low temperature 300
*Discussion:* Compiled by D. Dutton . . . . . 302

## L. MAGNETO-OPTICAL EFFECTS

L.1 E. Burstein, G. S. Picus, R. F. Wallis and F. Blatt: Zeeman type magneto-optic studies of energy band structure . . . . . 305
L.2 B. Lax, L. M. Roth and S. Zwerdling: Quantum magneto-absorption phenomena in semiconductors . . . . . 311
L.3 R. F. Wallis and H. J. Bowlden: Theory of the Zeeman effect in the photo-ionization of impurities . . . . . 318
L.4 W. S. Boyle: Far infrared magneto-optic effects from impurities in germanium . . . . 321
L.5 T. S. Moss, S. D. Smith and K. W. Taylor: The infrared Faraday effect due to free carriers in indium antimonide . . . . . 323
L.6 A. M. Portis: Microwave Faraday rotation: measurement of the conductivity tensor . . 326
L.7 G. E. Hambleton and W. W. Gärtner: Microwave Hall effect in germanium and silicon at 20 kmc/s . . . . . 329
L.8 M. Bernard: Effet electromagnetophotonique dans le germanium . . . . . 332
*Discussion:* Compiled by H. Y. Fan . . . . . 336

## M. THERMAL CONDUCTION AND THERMOMAGNETIC EFFECTS

M.1 Y. Kanai and R. Nii: Experimental studies on the thermal conductivity in semiconductors . 338
M.2 B. Abeles: Thermal conductivity of germanium in the temperature range 300°–1080°K . 340
M.3 J. A. Krumhansl: Thermal conductivity in semiconductors . . . . . 343
M.4 P. G. Klemens: Thermal resistance due to isotopes and other point defects . . . . 345
M.5 T. H. Geballe, C. Herring and J. E. Kunzler: Phonon-drag thermomagnetic effects in *n*-germanium . . . . . 347
M.6 J. Appel: Theory of thermoelectric and thermomagnetic effects in nonpolar isotropic semiconductors . . . . . 353
M.7 M. Rodot: Sur les effets de transport dans l'antimoniure d'indium . . . . . 358
*Discussion:* Compiled by H. P. R. Frederikse . . . . . 361

## N. THEORY III

N.1 A. Morita: Cohesive energies and band structures of covalence and ionic crystals . . 363
N.2 Ph. Choquard, A. Janner and E. Ascher: On the connection between bonds and bands in metals and semiconductors . . . . . 366
N.3 J. C. Phillips: Energy bands of silicon and germanium . . . . . 369
N.4 B. Segall: Band structure calculations of semiconductors by the Kohn–Rostoker–Korringa method: application to germanium . . . . . 371
N.5 F. Bassani: Energy band structure of sodium atoms in the diamond lattice . . . . 375
N.6 F. W. G. Rose: The mass-action laws for free carriers and amphoteric impurities in semiconductors . . . . . 377
*Discussion:* Compiled by F. Herman . . . . . 379

## O. EXCITONS AND PHOTONS


O.1 R. J. Elliott and R. Loudon: Theory of fine structure on the absorption edge in semiconductors . . . 382
O.2 G. G. Macfarlane, T. P. McLean, J. E. Quarrington and V. Roberts: Exciton and phonon effects in the absorption spectra of germanium and silicon . . . 388
O.3 J. R. Haynes, M. Lax and W. F. Flood: Analysis of intrinsic recombination radiation . 394
O.4 S. Zwerdling, L. Roth and B. Lax: The direct and indirect transition excitons in germanium 397
O.5 B. N. Brockhouse: Lattice vibrations of semiconductors by neutron spectrometry . . 400
O.6 Frank Herman: Lattice vibrational spectrum of germanium . . . 405
O.7 C. Domb, A. A. Maradudin, E. W. Montroll and G. H. Weiss: The vibration spectra of disordered lattices . . . 419
*Discussion:* Compiled by M. Lax . . . 421


## P. SEMICONDUCTING COMPOUNDS


P.1 W. W. Scanlon: Recent advances in the optical and electronic properties of PbS, PbSe, PbTe and their alloys . . . 423
P.2 T. Okada: The electrical properties and crystal structure of $IV_b$–$VI_b$ intermetallic-compounds 428
P.3 J. R. Drabble: Galvanomagnetic effects in bismuth telluride . . . 428
P.4 N. Fuschillo, J. N. Bierly and F. J. Donahoe: Transport properties of the pseudo-binary alloy system $Bi_2Te_{3-y}Se_y$ . . . 430
P.5 P. Fielding, G. Fischer and E. Mooser: Semiconductors of the type $A^{III}B^{VI}$ . . . 434
P.6 W. E. Spicer and A. H. Sommer: Intermetallic semiconductors containing alkali metals . 437
P.7 D. Fox: Conducting states in organic molecular crystals . . . 439
*Discussion:* Compiled by P. Keck . . . 442


## Q. LARGE BAND GAP SEMICONDUCTORS


Q.1 E. W. J. Mitchell: A review of recent work on diamond . . . 444
Q.2 G. F. J. Garlick: Infrared phosphor-semiconductors . . . 449
Q.3 W. W. Piper, P. D. Johnson and D. T. F. Marple: Temperature dependence of the optical band gap in ZnS . . . 457
Q.4 J. S. Prener and F. E. Williams: Some characteristics of large band gap compound semiconductors . . . 461
Q.5 M. A. Lampert, A. Rose and R. W. Smith: Space-charge-limited currents as a technique for the study of imperfections in pure crystals . . . 464
Q.6 A. R. Hutson: Electronic properties of ZnO . . . 467
Q.7 D. L. Dexter: Optical investigation of semiconductors at the University of Rochester . . 473
Q.8 C. D. Clark: The absorption edge spectrum of diamond . . . 481
*Discussion:* Compiled by W. C. Dunlap, Jr. . . . 484


## R. RESONANCE


R.1 G. Feher: Donor wavefunctions in silicon by the ENDOR techniques . . . 486
R.2 G. W. Ludwig, H. H. Woodbury and R. O. Carlson: Spin resonance of deep level impurities in germanium and silicon . . . 490
R.3 J. Lambe and C. Kikuchi: Spin resonance of donors in CdS . . . 492
R.4 R. N. Dexter: Cyclotron resonance in cadmium sulfide . . . 494
R.5 H. J. Zeiger, C. J. Rauch and M. E. Behrndt: Cross modulation of DC resistance by microwave cyclotron resonance . . . 496
R.6 E. H. Rhoderick: Nuclear magnetic resonance studies of doped III–V compounds . . 498
R.7 O. Kraus: Nuclear magnetic resonance in semiconductors . . . 504
*Discussion:* Compiled by A. F. Kip . . . 506


## S. GALVOMAGNETIC EFFECTS


S.1 A. C. Beer: Fine structure in the Hall coefficient . . . 507
S.2 M. Glicksman: The magnetoresistance of electrons in InP and GaAs . . . 511
S.3 R. J. Sladek: Impurity band conduction in strong magnetic fields . . . 515
S.4 J. C. Haslett and W. F. Love: Galvanomagnetic effects in *n*-InSb at low temperatures in strong magnetic fields . . . 518
S.5 A. W. Ewald and O. N. Tufte: Electronic properties of gray tin single crystals . . 523
S.6 H. Roth: Measurement of the galvanomagnetic effects in pure tellurium . . . 525
*Discussion:* Compiled by P. J. Price . . . 530


VOL 8 195

## T. SUMMARY SESSION

T.1 H. Brooks: Stationary states of semiconductors . . . . . 531
T.2 D. Polder: Fundamental transition processes . . . . . 535
T.3 L. Apker: Recombination, trapping and optical phenomena . . . . . 537
T.4 W. H. Brattain: Surfaces . . . . . 540
T.5 C. Herring: Transport . . . . . 542

AUTHOR INDEX . . . . . 551

VOL. 8 1959

VOL
8
195

# INDEX OF AUTHORS


B. Abeles, M2
F. G. Allen, D10
L. Apker, T3
J. Appel, M6
P. N. Argyres, E4
E. Ascher, N2
M. Balkanski, G4
P. C. Banbury, D7
M. Bancie-Grillot, G6
J. Bardeen, A2
G. A. Barnes, D7
F. Bassani, N5
P. Baruch, F4
A. R. Beattie, C4
A. C. Beer, S1
M. E. Behrndt, R5
C. Benoit à la Guillaume, F3
M. Bernard, L8
J. S. Bierly, P4
J. L. Birman, B4
F. Blatt, L1
R. Bowers, H3
H. J. Bowlden, L3
W. S. Boyle, L4
W. H. Brattain, T4
E. A. Braun, K5
R. Braunstein, J5
R. Bray, D3
P. H. Brill, C5
B. N. Brockhouse, O5
H. Brooks, H2, T1
I. Broser, G3
R. Broser-Warminsky, G3
F. C. Brown, K6
E. Burstein, J6, L1
M. Cardona, H2
R. O. Carlson, C7, R2
Ph. Choquard, N2
C. D. Clark, Q8
E. M. Conwell, 13
J. H. Crawford, Jr.
R. W. Cunningham, D3
D. L. Dexter, Q7
R. N. Dexter, R4
G. Diemer, G5
J. A. Dillon, Jr., D9
C. Domb, O7
F. J. Donahoe, P4
J. R. Drabble, P3
H. Ehrenreich, E5
R. J. Elliott, O1
A. W. Ewald, S5
H. Y. Fan, J2, J2a
H. E. Farnsworth, D9
G. Feher, R1
P. Fielding, P5
G. Fischer, P5
P. Fisher, J2
W. F. Flood, O3
O. G. Folberth, A4
D. Fox, P7
H. Fritzsche, I8
N. Fuschillo, P4
G. F. J. Garlick, Q2
W. W. Gärtner, C6, L7
T. H. Geballe, M5
A. F. Gibson, F2
M. Glicksman, I5, S2
K. D. Glinchuk, C8
S. Goldstein, C6
B. Goodman, K3
E. Grillot, G6
E. F. Gross, G2
J. B. Gunn, I4
M. Haas, J6
H. D. Hagstrum, H4
H. Haken, G1
R. N. Hall, C7
G. E. Hambleton, L7
P. Handler, D6
E. Harnik, D2
N. J. Harrick, D5
J. Haslett, S4
G. M. Hatoyama, I7
J. R. Haynes, O3
M. H. Hebb, A1
B. Henvis, J6
F. Herman, O6
C. Herring, T5
W. Hoogenstraaten, G5
A. R. Hutson, Q6
A. Janner, N2
A. Joffé, A3
P. D. Johnson, Q3
S. G. Kalashnikov, C1
Y. Kanai, M1
E. O. Kane, B5
H. Kawamura, F6
F. R. Kessler, J3
C. Kikuchi, R3
P. G. Klemens, M4
S. H. Koenig, I2
W. Kohn, B6
K. Kobayashi, K6
O. Kraus, R7
J. A. Krumhansl, M3
J. Lambe, R3
M. A. Lampert, Q5
P. T. Landsberg, C4
K. Lark-Horovitz, I9
V. E. Lashkarev, C8
B. Lax, G, L2, O4
M. Lax, C3, O3
T. A. Longo, I9
R. Loudon, O1
W. F. Love, S4
G. W. Ludwig, R2
J. M. Luttinger, E1
G. G. Macfarlane, O2
A. Many, D1
A. A. Maradudin, O7
Y. Margoninski, D2
D. T. F. Marple, Q3
W. Martienssen, K4
J. W. McClure, B3
T. P. McLean, O2
H. Mette, C6
H. J. G. Meyer, J1
E. G. Miselyuk, C8
R. Missman, D6
E. W. J. Mitchell, Q1
J. W. Mitchell, K5
K. Mizuguchi, I7
E. W. Montroll, O7
E. Mooser, P5
T. N. Morgan, I6
A. Morita, N1
T. S. Moss, L5
R. K. Mueller, F5
T. Muto, K1
R. Nii, M1
S. Nikitine, G7
O. S. Oen, K3
T. Okada, P2
H. Okuno, K1
H. Okura, F6
S. Oyama, K1
W. Paul, H1, H2
E. M. Pell, C7
R. L. Petritz, D4
J. C. Phillips, N3
G. Picus, J6, L1
W. W. Piper, Q3
D. Polder, T2
A. M. Portis, L6
G. W. Pratt, Jr., B7
J. S. Prener, Q4
P. J. Price, E6
J. E. Quarrington, O2
A. K. Ramdas, J2a
C. J. Rauch, R5
R. K. Ray, I9

A. R. Regel, E3
E. H. Rhoderick, R6
V. Roberts, O2
M. Rodot, M7
A. Rose, C, Q5
F. W. G. Rose, N6
H. Roth, S6
L. M. Roth, B7, L2, O4
W. Sasaki, I7
W. W. Scanlon, P1
R. E. Schlier, D9
R. F. Schwarz, C5
B. Segall, N4
M. Shibuya, I7
R. J. Sladek, S3
J. C. Slater, B1
S. D. Smith, L5
R. W. Smith, Q5
L. Soffer, E7
A. H. Sommer, P6
L. Sosnowski, F1
D. E. Soule, B3
W. E. Spicer, P6
M. C. Steele, I5
F. Stern, J4
L. Stilbans, E2
G. E. Tauber, E7
J. Tauc, I1
K. W. Taylor, L5
Y. Toyozawa, K2
O. N. Tufte, S5
W. W. Tyler, C2
G. J. van Gurp, G5
V. S. Vavilov, I1a
R. F. Wallis, L1, L3
G. Weinreich, H5
G. H. Weiss, O7
H. Welker, A4
F. E. Williams, Q4
S. P. Wolsky, D8
H. H. Woodbury, R2
H. J. Zeiger, R5
J. N. Zemel, D4
C. Zener, B2
S. Zwerdling, L2, O4

VOL
8
195

VOL.
8
1959

VOL
8
195

*J. Phys. Chem. Solids* Pergamon Press 1959. Vol. 8. p. 1. Printed in Great Britain

# INTRODUCTION

**M. H. HEBB**

General Electric Research Laboratory, Schenectady, N.Y.

VOL.
8
1959

THE 1958 International Conference on Semiconductors was held during the week 18–22 August, at the University of Rochester, Rochester, New York. Doubtless, it will become known as the Rochester Conference, just as its predecessors are known by the names Reading, Amsterdam, and Garmisch-Partenkirchen.

The Proceedings of the Conference are published as a single issue of the *Journal of the Physics and Chemistry of Solids*. Great efforts have been made to meet the early deadline for publication. Credit goes to the authors of papers for their promptness in submission of manuscripts, to the editorial committee for their work in preparing the manuscripts for publication and to the staff of Pergamon Press for its accomplishment of a difficult task.

The selection of the papers presented at the Conference from those submitted, as well as their logical arrangement in sessions, was the responsibility of the Program Committee. Its members should be congratulated for their efforts. In addition to the formal program, a valuable part of any conference is the discussion that follows the formal papers. The organizing and editing of these questions and comments to make them available to others is a challenging assignment. The Conference is indebted to the co-chairmen for the discussion reported in these Proceedings.

Special recognition is due to the speakers in the summary session, whose incisive comments set the subject presented at the Conference in perspective. The remarks made at this session were invaluable to the participants of the Conference. They have been recorded in the Proceedings so that even those unable to attend the Conference can benefit from them. Some of the flavor of the talks is inevitably lost in a literary transcription. This loss is particularly regrettable in the case of the introductory remarks made by CONYERS HERRING, who organized the summary session.

For those interested in statistics, the total attendance was officially 500, of whom 412 were from the United States, 18 were from Canada, and the remaining 70 from 14 countries overseas.

There remains the pleasant task of acknowledgment to several organizations for their parts in the success of the Conference..

Foremost is the University of Rochester. The facilities provided by our host were ideal and the arrangements—even including the weather—were excellent.

Without financial support the Conference would not have been possible. Our principal support came from the Atomic Energy Commission, the National Science Foundation, the Office of Naval Research, and the Office of Scientific Research of the Air Research and Development Command. Substantial contributions were made by a number of industrial organizations. Local industry groups in Rochester assumed the burden of many of our extra-Conference activities.

Many of the delegates from overseas were able to attend the Conference only because of the support provided by the Military Air Transport Service, whose help was generously made available to the Conference through the courtesy of the Office of Scientific Research.

Finally, sponsorship of the Conference by the International Union of Pure and Applied Physics formalized its international character and expedited participation by delegates from abroad.

*J. Phys. Chem. Solids* Pergamon Press 1959. Vol. 8. pp. 2–6. Printed in Great Britain

SESSION A:
OPENING SESSION*

A.2

# TRENDS IN SEMICONDUCTOR RESEARCH

J. BARDEEN

University of Illinois, Urbana, Ill.

VOL
8
195

THE rapid expansion of scientific research in recent years has created a real problem in communications. It is a problem which involves mass, time, and distance, but you can't find the answers in a physics text. If for no other reason than the sheer mass of published work, it is impossible to keep up with what's going on by reading journals, as one could do not so long ago. Another important difficulty concerns the speed of research. Work being done now in one laboratory may depend on what's been done in another laboratory in a distant part of the world only months before. Preprints and journal articles help one keep up to date in one's own narrow field, but they have their limitations. Books on special subjects and review articles in periodical or book form help one keep up with related fields.

Conferences on special subjects, such as this one, are becoming of increasing importance in scientific communication. They allow one to meet and talk with co-workers and to have an up-to-date summary of current work presented. The main limitation is that of the human mind to absorb all with which it is confronted. This meeting should provide everyone with a good opportunity to review research programs in the light of what is going on elsewhere, to put current semiconductor research into better perspective, and perhaps, most likely in private conversations, to get hints as to how one might surmount one difficulty or another in his own research.

It may be of interest to spend a few minutes this morning with a brief survey of trends in semiconductor research. What have we accomplished and where are we heading? It was not until the advent of quantum theory, some thirty-odd years ago, that there was an adequate basis for understanding the many properties of solids. Many facts now can be correlated on the basis of the Bloch theory and the corresponding energy-band model, in spite of its limitations. Left out of the Bloch model are interactions between electrons and lattice vibrations, except for scattering processes, and correlations between electrons resulting from Coulomb interactions, which are by no means small. Because of its simplicity, and the mathematical difficulties involved in going beyond it, the Bloch theory has been applied to many problems in metals and semiconductors, and with what must be regarded as remarkable success in view of its basic limitations. It is, in fact, only in recent years that we are beginning to understand why the Bloch model works as well as it does. It is, of course, much more satisfactory for *s–p* valence electrons than for the more tightly bound *d*-electrons.

In this afternoon's session on band theory, SLATER will give a general review and ZENER will discuss applications to *d*-band semiconductors.

There is now considerable interest in many-particle theories which go beyond the Bloch one-particle model to take into account dynamical correlations between the particles. A method which has proved useful in metal theory and is now being applied to semiconductors is to introduce screening of electrons by means of a complex frequency-dependent dielectric constant. This is a rather general method which involves taking pair correlations properly into account. Electrons and holes may be regarded as elementary excitations described by many-particle wave functions. It

* *Chairmen:* J. BARDEEN and D. L. DEXTER.

turns out, as will be discussed by KOHN and others, that some results of the Bloch model, such as introduction of quasi-particle excitations with an effective mass and use of a static dielectric constant in the force between a conduction electron or hole and a charged impurity center, follow from the many-particle treatment.

Most of the basic ideas and concepts used in semiconductors go back to the 'thirties. A. H. WILSON in 1931, was the first to introduce the concept of a hole from the modern point of view and to show how impurities can influence the carrier concentrations. It was recognized that photoconductivity could arise from excitation of electrons from the valence to the conduction band, and that the excess carriers introduced in this way would have a finite lifetime before recombination occurs. Not long after, in 1935, FRENKEL applied the concepts of generation of electron–hole pairs by light, diffusion in a concentration gradient, and flow of carriers in electric and magnetic fields, to account for experimental results of KIKOIN and NOSKOV on the photomagnetoelectric effect in $Cu_2O$ and of DEMBER on the change of contact potential with light.

FRENKEL also suggested the exciton as a localized atomic excitation which could be transferred from atom to atom in the crystal. Another concept of an exciton as a bound state of an electron and a hole was suggested by SLATER and SHOCKLEY, and the theory developed further with the use of effective masses and dielectric constants by WANNIER. It was in the paper of WANNIER that the localized electron functions which now bear his name were introduced. These two different approaches to the exciton have since been developed by many people. Some recent theoretical developments will be discussed at this meeting by HAKEN and by MUTO, the latter work applying particularly to the alkali halides. TOYOZAWA and also GOODMAN and OEN will discuss interactions between excitons and lattice vibrations.

For a long time excitons were regarded as a theoretical possibility, but there was no real experimental demonstration of their existence. The first experimental proof of energy transfer by excitons was obtained several years ago by APKER and TAFT from their studies of photoelectric emission of electrons from alkali halide crystals. Excitons are now coming into their own, as shown by the fact that they are the principal subject of two sessions at this meeting.

Among the most interesting papers at the Garmisch meeting two years ago were those of GROSS on the discrete line absorption spectrum observed near the band edge of $Cu_2O$, with term values which could be fitted so remarkably well with a hydrogen-like formula, and of BROSER and BALKANSKI, who presented evidence for diffusion of excitons in CdS crystals. There is still controversy about this latter work and related experiments done since. BROSER now takes the view that his experiments can be accounted for by scattering and reabsorption of fluorescent radiation, while BALKANSKI and also DIEMER and his co-workers believe that true exciton diffusion has been observed in certain specimens. You will be able to hear both sides of the story tomorrow afternoon and form your own conclusions.

GROSS has extended his work on line spectra in $Cu_2O$ and CdS to observe the Zeeman splitting, and has found evidence for both the electron–hole-type exciton and the localized-type exciton of FRENKEL. In a long series of experiments, NIKITINE has observed in a large number of different substances line spectra in emission and absorption which can be interpreted in terms of excitons.

Excitons are stable in germanium and silicon only at low temperatures. Evidence for excitons in these materials has come from analysis of the fine structure of the absorption spectrum obtained under high resolution near the band edge by MACFARLANE and his co-workers and from the corresponding emission spectrum of the recombination radiation by HAYNES and his co-workers. These experiments also give detailed information about the phonons involved in the indirect transitions. ZWERDLING and his co-workers have observed the Zeeman effect of the exciton absorption spectrum in germanium. All of this work on germanium and silicon will be discussed on Thursday afternoon. The first paper of this session is an important one by ELLIOT on the theory of the fine structure of the absorption edge.

A distinct trend of semiconductor research in the past few years is that it has become a quantitative science with a close coordination between theory and experiment. This is, of course, due in large part to the availability of very perfect single crystals of germanium, silicon, and now an

increasing number of other substances. These materials are ideal for the theorists because they are at once simple enough to understand and sufficiently complex to yield a rich variety of phenomena. Theory is not only able to account for the gross features, but also in many cases the fine details of complex phenomena. The main basis for the theory is the band model, with modifications in some cases for many-particle aspects or for intereactions between electrons and lattice vibrations. The theory forms a framework for analysis and interpretation of experiments. Parameters of the theory, such as effective masses, dielectric constants, energy gaps, and mobilities, which would be extremely difficult to evaluate theoretically from first principles, usually are obtained from experiment as empirical parameters.

The first experiments to give precise information on effective masses were the cyclotron-resonance experiments of KIP, KITTEL and their co-workers at California, and of LAX and his co-workers at the Lincoln Laboratory. This work was presented at the Amsterdam meeting four years ago. These experiments showed the complex nature of both the conduction and valence bands of germanium and silicon, as had been indicated earlier from magneto-resistance studies. The cyclotron-resonance method is limited to materials with a long relaxation time for collisions of the carriers, so that they can make a number of orbits in a magnetic field between collisions. Shorter relaxation times can be tolerated if the magnetic field is increased, but then direct observation of resonance is not easy because the cyclotron frequencies usually come in the most difficult region of the spectrum in which to work, the far infrared.

Ways out of this difficulty have been shown independently by BURSTEIN and by LAX, who detected the quantitized LANDAU-type levels of the carriers in a magnetic field in the optical absorption spectra near the band edge, either in interband transitions or in transitions from an impurity level to one of the bands. These powerful methods for getting information on band structure will be discussed in a series of papers on Thursday morning.

At one time traps were traps, and that was the end of it. Now we try to understand the energy levels of particular impurity atoms or other imperfections, and the trapping cross-sections of these for electrons and holes. Through careful research by a number of investigators, a large amount of information has been accumulated. Of particular interest and technological importance are the recombination centers. Several interesting papers dealing with these subjects are to be given in one of the sessions this afternoon. The theory of recombination via traps as worked out by SHOCKLEY and READ and by HALL is well confirmed by experiments, although generalizations are required in some cases. An important problem for the future is to get a more detailed and quantitative picture of luminescent centers.

A very ingenious and powerful method for investigating wave functions of electrons at impurity levels is the Electron Nuclear Double Resonance (ENDOR) method of FEHER. This method, which involves saturating the electron resonance and then observing the nuclear resonance lines, will be discussed by him on Friday morning, in a session which includes a number of other interesting papers on spin-resonance phenomena in semiconductors. We can expect an expansion of activity in this very interesting field in the years to come.

There has always been a close connection between semiconductor science and semiconductor technology, and I think this is a good thing for both. In the 'thirties, semiconductors were used mainly as rectifiers, and the important materials were copper oxide and selenium. Theories of rectification were worked out independently by MOTT, SCHOTTKY and DAVYDOV. From SCHOTTKY come most of our ideas concerning space-charge layers in which the space charge comes from uncompensated donor or acceptor ions. He had the concept of an inversion layer in which the conductance changes from *n*- to *p*-type as a result of the change in potential in the barrier region, and this came close to the ideas required for transistors. What he failed to recognize is the importance of minority carriers in the current flow. DAVYDOV, as early as 1938, came close to an adequate theory of *p*–*n* junctions, but the assumptions he made to get a mathematical solution were such as to mask minority carrier injection, which is of course one of the most important features of modern junctions and is a consequence of SHOCKLEY's theory. No doubt SCHOTTKY and others were thinking of their work in semiconductors such as copper

oxide in which minority carrier flow is unimportant.

Much of the semiconductor research in America and elsewhere during the past ten or fifteen years has been on germanium and silicon. As you know, this work has been greatly stimulated by applications first to radar detectors and then to diodes and transistors. Of great importance to the study is ability to make exceptionally perfect single crystals and to control the impurities present to a very high degree. As we have mentioned, these materials have served and are continuing to serve as a splendid testing ground for theoretical developments.

VOL. 8 1959

A large part of this research has been associated with transistor development, a great deal of it pioneered by SHOCKLEY. I will discuss just two of these briefly, the so-called "hot" electron problem, or change in mobility with electric field, as first observed by SHOCKLEY and RYDER, and the semiconductor surface-barrier problem, in which BRATTAIN has played a leading role.

There are several papers devoted to each of these subjects at this meeting. TAUC will discuss the increased quantum yield which occurs when the absorbed photon has so much energy that the excited electron or hole has sufficient energy to create further pairs by impact ionization.

A general review of the hot electron problem will be given by KOENIG. He himself has been investigating the change in ionization of impurities at low temperatures which occurs when the electrons are heated by a pulsed electric field to a higher temperature than the lattice. Such experiments give information about ionization and recombination processes. Several other interesting papers on the same general subject will be given on Wednesday morning.

During the past few years methods have been developed for determining the energy distribution of *surface* traps and capture cross-sections of electrons and holes. A general review will be given by MANY. Of particular theoretical interest is whether or not states exist on a surface free of any oxide layer or other contamination. The possibility of such states was first pointed out by TAMM, and SHOCKLEY later developed a more elaborate theory for valence crystals, in which he showed that surface states in the forbidden gap may be associated with uncompensated or dangling chemical bonds. For example, in germanium an interior atom forms four bonds with its near neighbors, but a surface atom can form only three. The unfilled orbital corresponding to the fourth bond is free to be occupied by electrons.

FARNSWORTH has shown that an apparently clean surface can be formed on germanium or silicon by an ion-bombardment technique. Several investigators have studied the electrical properties of surfaces cleaned in this way. HANDLER found that a germanium surface cleaned by bombardment is strongly *p*-type with a very high density of surface states. BARNES and BANBURY report different results for a freshly cleaved surface maintained in high vacuum. There should be some interesting discussions at the session on surfaces tomorrow morning.

This meeting reflects the increasing interest in compound semiconductors. Some of this stems from WELKER's pioneer work on the III–V compounds, whose properties are roughly similar to those of germanium and silicon. There is also great interest in compounds useful for thermoelectric elements. Much of the early work in this field was purely empirical. The first real scientific study of electron mobility, thermal conductivity, and other factors important for thermal elements, and the way they depend on composition was made by JOFFÉ and his co-workers. Results they have obtained clearly demonstrate the virtue of the scientific over the purely empirical approach. We are honored to have both JOFFÉ and WELKER on this morning's program.

Research on thermoelectric effects and on thermal conduction in semiconductors has yielded a number of interesting phenomena, involving phonon scattering, phonon drag, and heat transfer by ambipolar diffusion. Much remains to be done in this field. No doubt Professor JOFFÉ will discuss some of the accomplishments and outstanding problems in his talk. More details on thermal conduction will be given by KANAI and others in the session on Thursday morning.

In this brief review I have had time to indicate only a small fraction of the interesting papers to be presented, and many of those I have discussed were picked more or less at random or from personal interest rather than intrinsic importance.

Questions are often asked as to whether any new revolutionary discoveries can be expected in

the semiconductor field. In one sense, I believe the answer is no. Practically all of our basic ideas —energy bands, electrons and holes, phonons, excitons, polarons, dislocations, thermal generation and recombination of carriers, and so forth —date from the 'thirties or earlier. But the application of these ideas to particular situations, making them more precise and quantitative, and the working out of the wide variety of interactions possible among the elementary excitations have provided and will continue to provide many interesting and important problems with unexpected results and new applications. This meeting shows that the semiconductor field is a very live one, and there is no reason to expect interest to decline in the years to come.

*J. Phys. Chem. Solids* Pergamon Press 1959. Vol. 8. pp. 6–14. Printed in Great Britain

# PROPERTIES OF VARIOUS SEMICONDUCTORS

A. JOFFÉ

A.3

Institute of Semiconductors, Leningrad, U.S.S.R.

**Abstract**—The discovery of a $p$–$n$ transition inside a monocrystal of Ge and of analogous materials (instead of a boundary between two semiconductors with a hole and electron conductivity which we investigated in 1938), the simple crystal structure, and the highest purity of Ge justify the extensive interest in these materials.

A neglect of the immense diversity of semiconductors is however a disadvantage. Contrary to Ge, for a large number of low mobility or of liquid semiconductors even the notion of velocity and effective mass cannot be defined; the scattering time is no longer short compared to the relaxation time. Melting of such semiconductors does not influence their properties, while a radical change appears if the number or the position of the next neighbours becomes involved.

Thus the interest must be directed toward the chemical bond and toward the structure of the electronic cloud inside a unit cell. Professor SAMOILOVICH has succeeded in explaining in this way the appearance of two effective masses for holes in Ge, the right dependence of mobility on temperature $\mu \sim T^{-2.3}$, the influence of a magnetic field, etc. The use of semiconductors for thermoelectric devices raises problems concerning their thermal, electric and mechanical behavior.

A systematic study of a variety of semiconductors, of solid solutions, of phenomena determining the ratio of thermal conductivity to the electron mobility, a favorable choice of the degree of degeneration, a consideration of the anisotropy, and of the anharmonicity of the chemical bond—all those fundamental problems must be taken into account. Some of the results achieved in this direction will illustrate the importance of the problems involved. While many of such problems are still rather obscure, some success has already been achieved. The figure of merit $z=\alpha^2/\varkappa\rho$ ($\alpha$—thermoelectric power per °C) has increased up to and over $z=3\times10^{-3}$/deg. (some papers use $\sqrt{z}$ instead of $z$) which means a cooling by one thermocouple from 112°C to 0°C or from +27°C to −45°C.

The problems of thermoelectric cooling, heating and energy production have become a promising field of research.

THIRTY years ago the discovery of rectification in an oxidized copper plate, and shortly afterwards the discovery of copper oxide and selenium photocells, directed the interest of physicists to the field of semiconductors and especially to copper oxide and selenium. A new era arose after the war due to the discovery of phenomena at a $p$–$n$ boundary inside a monocrystal of germanium or silicon. The modern semiconductors are the germanium-like materials. Thus the

VOL. 8 1959

immense diversity of semiconductors became neglected in spite of the fact that they include resistivities from $10^{10}$ to $10^{-4}$ Ω-cm, mobilities from 0·1 to $10^5$ cm²/V sec, impurities between $10^{-8}$ and 50 per cent, and all possible types of chemical bond.

We came to the problem of semiconductors from another point of view and therefore investigated somewhat different materials. Allow me to describe some of the results of our work.

The diversity of properties of semiconductors as depending on their structure may be illustrated by the various mechanisms of thermal conductivity we met during our researches in the domain of thermoelectricity.

(1) In semiconductors with impurity conduction, the conductivity may be divided into two parts: the phonon term $\kappa_{ph}$ and the Wiedemann–Franz term $\kappa_{el}$ due to free charges:

$$\kappa = \kappa_{ph} + \kappa_{el} \tag{1}$$

$$\kappa_{el} = A\frac{k^2}{e^2}T\sigma = L\sigma, \tag{2}$$

where $A = \pi^2/3$ for a degenerate state of charges and $A = (r+2)$ for nondegenerate charges; $r$ denotes the exponent in the expression for the free path $l$ as a function of the kinetic energy

$$l \sim \epsilon^r \tag{3}$$

Increasing the impurity conduction $\sigma$ of some $Bi_2Te_3$ materials from 1000 to 4500 $\Omega^{-1}cm^{-1}$, we checked the Wiedemann–Franz ratio $L$ for the nondegenerate state ($\sigma < 2500$ $\Omega^{-1}cm^{-1}$) and found an increase of $L$ for the degenerate state ($\sigma > 3500$ $\Omega^{-1}cm^{-1}$). For $r$, we found $r = 0$, in good agreement with the value following from other considerations (Fig. 1).

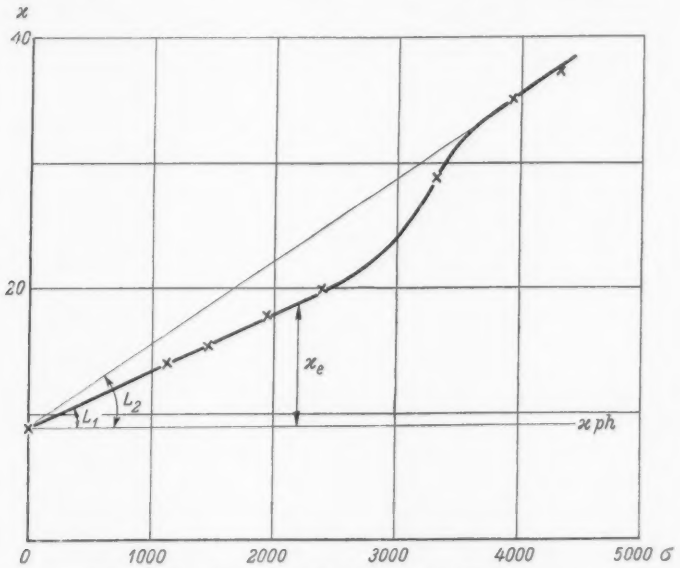


FIG. 1. The thermal conductivity $\kappa$ in mW/cm°C as a function of the electrical conductivity $\sigma$ in $\Omega^{-1}cm^{-1}$ $Bi_2Te_3$.

(2) As soon as intrinsic conductivity appears, and charges of both signs begin to take part in the electric conduction, an additional energy transport becomes noticeable. In 1940, DAVYDOV and SHMUSHKEVICH and later Dr. P. J. PRICE and others derived a formula for the additional thermal conductivity $\Delta\kappa_{el}$ due to the ambipolar diffusion of charges in the direction of the temperature gradient:

$$\Delta\kappa = L\frac{\sigma_1\sigma_2}{\sigma_1+\sigma_2}\left(\frac{\Delta E_0}{2kT}+r+2\right)^2, \tag{4}$$

where $L$ denotes the Wiedemann–Franz ratio, $\Delta E_0$ the width of the forbidden zone, and $\sigma_1$ and $\sigma_2$ are the conductivities due to holes and electrons respectively. Fig. 2, representing the best measurement on $Bi_2Te_3$ by C. B. SATTERTHWAITE and R. W. URE, shows that the deviation from a straight line for $\kappa_{ph}^{-1} \sim T$ starts at the temperature where the intrinsic electric conduction and a drop in the Hall constant $R$ become noticeable.

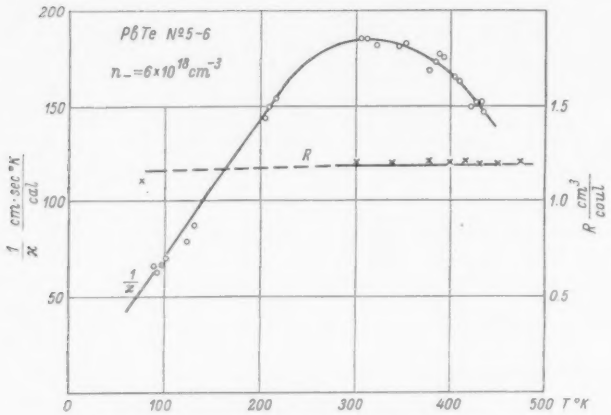


FIG. 3. The thermal resistivity $\kappa^{-1}$ and the Hall constant $R$ versus temperature for $n$-type PbTe.

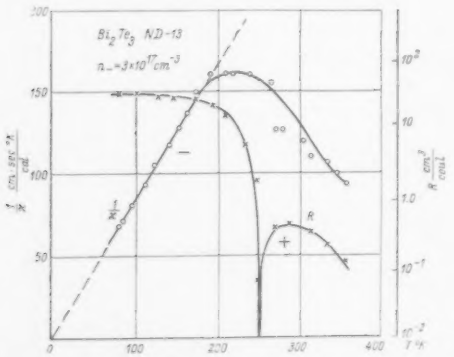


FIG. 2. The thermal resistivity $\kappa^{-1}$ and the Hall constant $R$ versus temperature for $Bi_2Te_3$.

(3) We met, however, semiconductors (PbTe and PbSe) in which the additional thermal conductivity appears at temperatures much lower than the intrinsic conductivity. In our samples of PbTe the measurements of the Hall effect and of the thermoelectric power proved that the intrinsic conductivity did not exist below 600°K, while $\Delta\kappa$ already appeared at 200°K and rose as $\exp(-0{\cdot}1/kT)$, see Fig. 3. The only explanation we were able to find led to a hypothesis of states with a low excitation energy of 0·1 eV, which are able to diffuse along the gradient of temperature.

The notion of excitons was first developed by FRENKEL in 1931. G. E. PIKUS and Dr. PRICE gave a formula for the additional thermal conductivity due to excitons:

$$\Delta\kappa_{ex} = kND\left[\left(\frac{\Delta E}{kT}+2\right)^2+2\right]. \qquad (5)$$

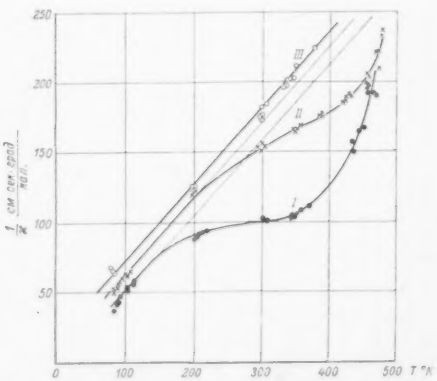


FIG. 4. The thermal resistivity $\kappa^{-1}$ versus temperature for tellurium samples with various impurity contents.

But the excitons we have in mind are different from the Frenkel–Mott excitons of the positronium type with an excitation energy $\Delta E$ close to $\Delta E_0$. The excited states able to produce an additional thermal conductivity must have a value of $\Delta E < \frac{1}{2}\Delta E_0$. In the case of PbTe $\Delta E = 0{\cdot}1$ eV, while $\Delta E_0 > 0{\cdot}35$ eV. It would therefore be confusing to call them "excitons". Such diffusing energy states may exist in some semiconductors and be absent in others. It is possible, however, that they are not detectable by optical means.

(4) Mrs. DEVYATKOVA investigated recently the thermal conductivity of several samples of tellurium. Her results are shown in Fig. 4. Curve

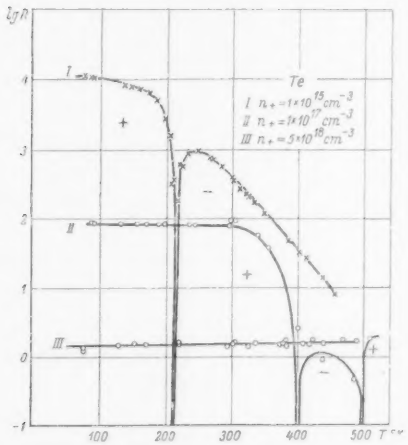


FIG. 4a. The Hall constant $R$ versus temperature for tellurium samples with various impurity contents.

1 represents the properties of the purest sample with $n = 10^{15}$cm$^{-3}$; curve 2 is for a sample with $n = 10^{17}$, and curve 3 gives the results for a sample with $n = 10^{18}$. Fig. 4a shows the electrical properties of the three samples.

The explanation of this strange behaviour of tellurium can be found in its optical properties. Below a frequency $\nu < \Delta E_0/h$, the pure semiconductor is transparent except for impurities, defects, and free charges present. The dependence of the infrared absorption of tellurium on the concentration of free charges can be taken from a publication by FAN. The heat transmitted by infrared radiation and the additional conductivity was computed long ago by GENZEL:

$$\Delta\kappa_{\text{rad}} = \frac{16}{3}\cdot\frac{\alpha n^2}{K}T^3 \qquad (6)$$

where $n$ denotes the refraction, $K$ the absorption, and $\alpha$ the coefficient in the Stephan formula for the energy of a black body $u = \alpha T^4$. B. J. MOYGES calculated on the basis of the optical data the thermal conductivity of tellurium and obtained exactly the curves shown in Fig. 4.

(5) The drag of phonons provides one more way of influencing the thermal conductivity of semiconductors.

(6) At concentrations of free charges exceeding $10^{20}$cm$^{-3}$, the scattering of phonons at electrons becomes essential.

We see that the same physical phenomenon may depend on a number of different mechanisms in different semiconductors. More than this, there is a danger that some conclusions drawn on the basis of germanium may have a limited value and cannot be generalized.

We are used to a picture of the movement of free charges in a semiconductor which reminds one of the kinetic theory of gases. This is satisfactory as long as we consider metals or semiconductors such as germanium with a high mobility. The mean free path $l$ may be estimated from the formula:

$$l \cong 10^{-8}\sqrt{\frac{\overline{m}}{m_0}}\mu \text{ cm}.$$

However, $l$ becomes less than the wavelength of nondegenerate electrons for semiconductors with $\mu < 100$ cm$^2$/V sec. For semiconductors with $\mu < 5$ cm$^2$/V sec, the mean free path $l$ becomes smaller than the lattice constant. Most of the known semiconductors belong to this group of materials. The scattering time is then no longer small as compared with the duration of the movement between two collisions. The notion of a mean velocity of a distribution of velocities does not exist.

Dr. JUSE has investigated samples of $In_2Se_3$, $In_2Te_3$, $Ga_2Se_3$, and $Ga_2Te_3$ with empty metal sites and accordingly with a very low mobility. It turns out that the mobility of electrons (Fig. 5) increases with temperature as $\exp(-E/kT)$, thus suggesting statistical jumps from one cell to the next one with an excitation energy $E$ instead of

the usually assumed free paths each traversing several periods of the crystal lattice. A different law must be applied to the mobility of holes (Fig. 6), as we shall see later. Semiconductors of the Juse type with small mobilities are quite numerous. For instance, Dr. REGEL investigated liquid semiconductors and was able to show that during melting the properties of semiconductors remain unchanged if the distribution of the nearest neighbors does not change. The mobility is, however, small in the liquid state. Mrs. GORJUNOVA and Dr. KOLOMIEZ prepared several series of semiconducting glasses with an amorphous structure and a very small mobility.

Thus it seems that our contemporary theory, using a distribution of velocities of free charges, is applicable only to semiconductors possessing high mobility. For materials with a low mobility, other ideas and other methods must be used.

Until recently, the thermal conductivity of semiconductors at room temperature and above did not attract the attention of physicists. It is, however, of primary importance in the use of thermoelements. The efficiency of a thermoelectric generator of electric energy for any cooling and heating device depends on the figure of merit, $z$, of the materials used:

$$z = \alpha^2 \frac{\sigma}{\kappa_{ph} + \kappa_{el}}, \tag{7}$$

where $\alpha$ denotes the thermoelectric power per °C. Still better would be the use of the product of $z$ and the mean temperature $\bar{T}$ of the thermo-

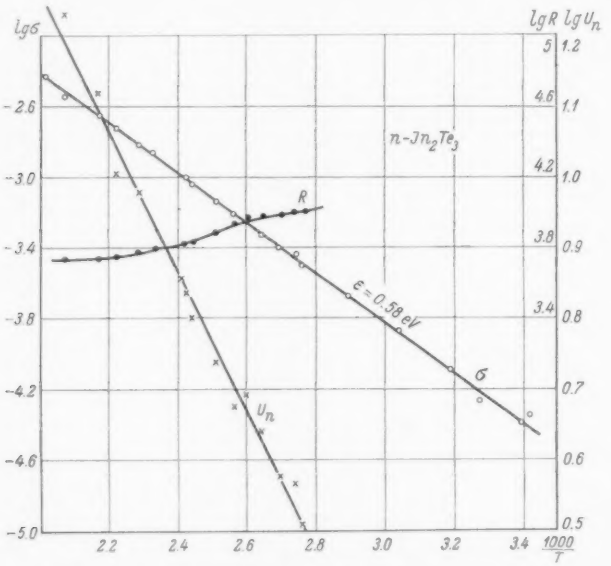


FIG. 5. The electrical conductivity $\sigma$, Hall constant $R$, and mobility $u$ of $n$-type $In_2Te_3$ as a function of inverse temperature ($1/T$).

couple. $z\bar{T}$ is a dimensionless number of magnitude 0·1—1. The efficiency of a thermocouple between $T_1$ and $T_2$ may be represented as:

$$\eta = f(T_2/T_1, z\bar{T}).$$

We had to investigate the phonon conductivity of semiconductors of every kind in order to choose the right materials for thermocouples. We found that at a given temperature the phonon conductivity becomes smaller the higher the atomic weight and the anharmonicity (depending on the chemical bond) and the lower the Debye temperature of the substance.

VOL. 8 1959

The value of $\kappa_{ph}$ may be reduced still further by impurities. By introducing $N$ foreign atoms into a lattice with $N_0$ atoms, we decrease the conductivity $\kappa_0$ to a value $\kappa$, given by:

$$\frac{\kappa_0}{\kappa} = 1 + \frac{N}{N_0} \cdot \frac{\lambda_0}{a} S, \qquad (8)$$

where $\lambda_0$ is the mean free path of the pure substance, $a$ is the lattice parameter, and $S$ is the scattering cross-section expressed in $a^2$ units.

In view of the fact that the wavelength of nondegenerate free charges is an order of magnitude larger than the wavelength of the most active phonons, we expected that isolated impurity atoms would have a smaller cross-section for electrons than for phonons. Moreover, the scattering of charges will depend on the sign of impurity ions, while the scattering of phonons must be independent of the sign. The experiments conducted by Dr. STILBANS convincingly proved that this difference is more important than one would

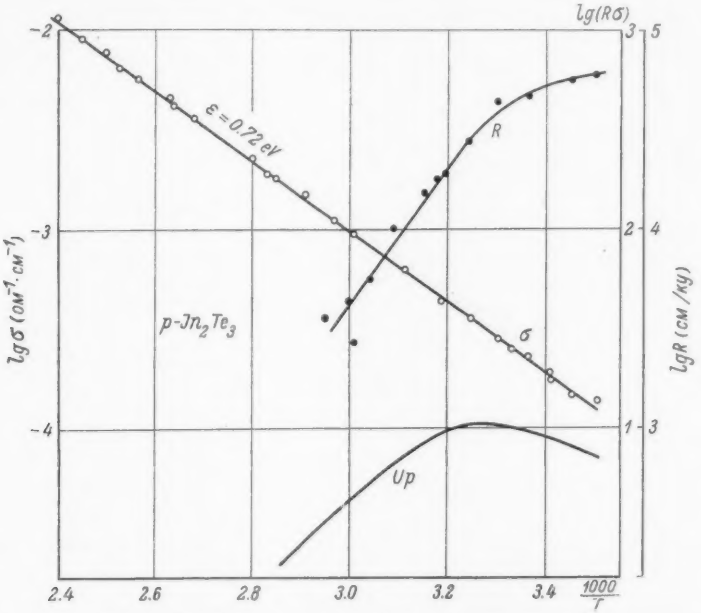


FIG. 6. The electrical conductivity $\sigma$, Hall constant $R$, and mobility $u$ of $p$-type $In_2Te_3$ as a function of inverse temperature $(1/T)$.

Large amounts of impurities may be introduced in the case of the solid solutions used and investigated by Mrs. JOFFÉ. At concentrations near 50 per cent the mean free path drops many times and approaches a value of one or two atomic distances. Accordingly $\kappa_{ph}$ becomes small. At the same time, however, the mobility $\mu$ of free charges and the electrical conductivity may decrease. What we want to achieve is an increase of $\mu/\kappa_{ph}$. This presents the problem of the influence of impurities on the scattering of phonons as compared to electrons.

expect. The modulation of electron waves leads to a decisive predominance of scattering at the defects charged by the opposite sign. A disturbance of the sublattice of positive ions (metals) decreases the mobility of negative electrons. A disturbance of metalloids (negative ions) influences the mobility of holes.

Fig. 7 represents the mobility of electrons and holes as a function of the concentration of $Bi_2S_3$ in $Bi_2Te_3$. One may see that the statistically mixed negative ions Te and S decrease the mobility of holes many times, while the mobility of electrons

is only slightly changed. In a solid solution of PbSe and PbTe, the mobility of holes decreases 2·5 times, while the electrons are retarded by 25 per cent. In Fig. 8, the case of a solid solution $Bi_2Te_3$–$Sb_2Te_3$ is shown. The irregularity of positive ions (Bi–Sb) leads to a decrease in the mobility of the electrons, while the mobility of the holes even increases as a result of an ordering process. The solid solution PbTe–SnTe behaves similarly. The difference between electrons and holes in $In_2Te_3$ (Figs. 5 and 6) may be explained in the same way.

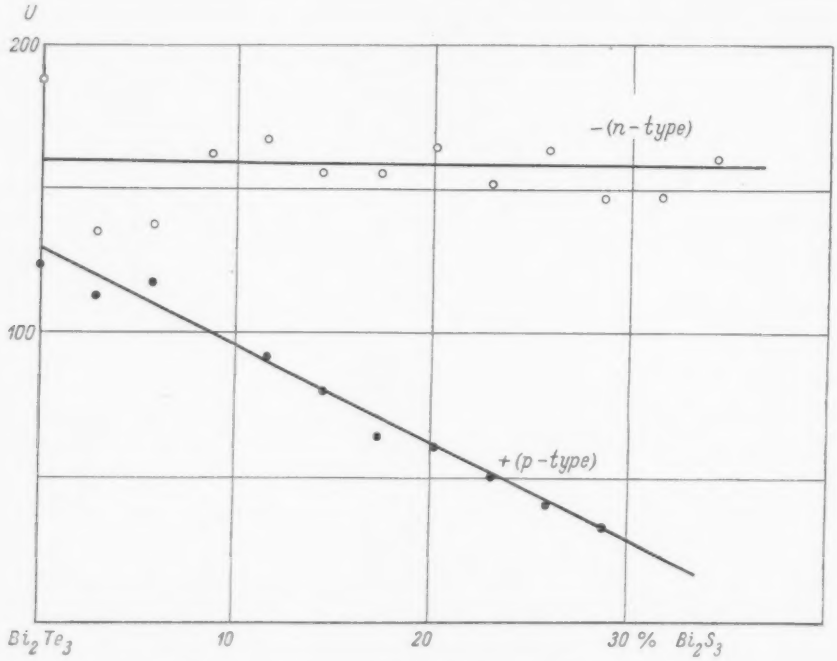


FIG. 7. The carrier mobility in $Bi_2Te_3$–$Bi_2S_3$ mixtures as a function of the $Bi_2S_3$ concentration.

By investigating the process of scattering at a large concentration of ions, we could see that they do not act as the sum of independent ions. If the mean distance between neighboring impurity ions becomes much smaller than the wavelength of moving charges, the ions must be considered as a continuous medium with fluctuations of its density leading to scattering.

The application of thermocouples over a wide range of temperatures and in concentrations of free charges at various degrees of degeneration allowed us to investigate separately the influence on the mobility of the velocity of free charges and of the heat movement of the crystal lattice. By gradually increasing the concentration of impurities, the Fermi level and the velocity of free charges could be varied at constant temperature. On the other hand, at a high degree of degeneration, a constant velocity has been maintained at varying temperatures.

We found that the probability of scattering at a given velocity is proportional to $T$ at low temperatures and to $T^2$ at higher temperatures. Apparently at a large concentration of phonons besides the usual process with one phonon of a large wavelength, a two-phonon process becomes essential.

The nature of the chemical bond or the density distribution of the electron cloud inside the crystal cell becomes of primary importance.

Guided by the requirements of thermoelectric devices, we were developing both the physics and

the applications of semiconductors. We could not solve all of the problems; some of them were discussed rather qualitatively. The figure of merit, $z$, we were able to reach does not exceed 2·5—3·5 × $10^{-3}$ $deg^{-1}$, and $z\bar{T}$ was not greater than 1. Nevertheless, our thermocouples found some applications. A home refrigerator, a cooling apparatus suitable for temperatures down to −50°C, high-precision thermostats with an accuracy of 0·001°C, and some biological, meteorological, and agricultural apparatus provided useful applications. The efficiency of our generators of electric energy does not exceed 8–10 per cent. Nevertheless, they found practical applications. Thus, the thermoelectricity of semiconductors represents a promising field of research and offers a variety of useful applications.

I am glad that the interest in this field is growing in the United States, in England and France, in Czechoslovakia and China.

I am convinced that every approach to semiconductors from a new direction will lead to a better understanding of their properties and to the introduction of new materials. They are needed because our existing theory is inadequate and the number of known semiconductors is meager.

I hope that the cooperation of physicists, chemists, and engineers such as we meet at our Conference will further still more the success of the physics of semiconductors and the importance of their technical applications.

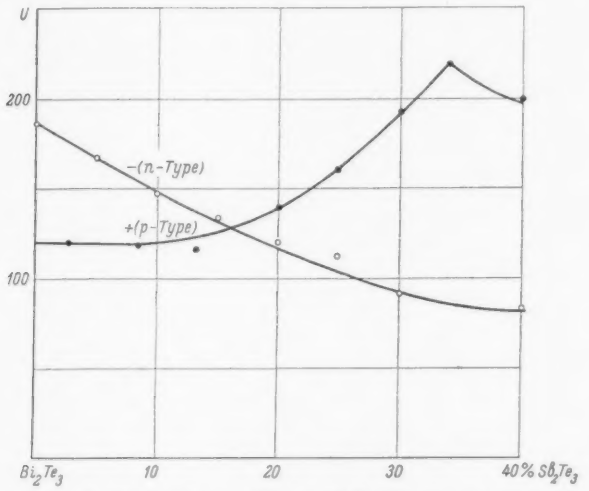


FIG. 8. The carrier mobility in $Bi_2Te_3$–$Sb_2Te_3$ mixtures as a function of the $Sb_2Te_3$ concentration.

## DISCUSSION

W. SHOCKLEY: Professor JOFFÉ reports some very interesting results in connection with the mobility of electrons and holes in bismuth telluride to which has been added some bismuth sulphide. He reports a negligible change in electron mobilities up to quite substantial additions of sulphur, so that as much as one-third of the tellurium atoms were replaced. On the other hand, there are appreciable reductions of hole mobility, as is to be generally expected when atomic disorder is present.

In this comment I wish to propose a possible explanation for the very small change in electron mobility in these mixed crystals, based upon a picture of the behavior of the electrons in the $Te^{--}$ and the $S^{--}$ ions. In keeping with some observations on $O^{--}$ quoted later in this comment, it is proposed that the electrons of these doubly negative ions tend to spread out in these crystals. Thus, unlike the highly ionic structure of an alkali halide, one electron from each $Te^{--}$ ion forms a sort of electron gas. If this picture represents at all correctly the situation surrounding the bismuth ion, then it is evident that there will be little change on replacing tellurium by sulphur so far as the surrounding of the bismuth ions is concerned.

An excess electron in this crystal will use a wave function for the lowest unoccupied level, which must be, of course, orthogonal to wave functions for the electrons in the valence band. The valence-band electrons are those at the highest level and are those wave functions occupied by the most loosely bound electrons of the tellurium and sulphur ions. Accordingly, we would assume that an excess electron uses a wave function which tends to become concentrated around the bismuth ions and to have very small values near the suphur or tellurium ions, since its wave function there must be orthogonal to the electrons of the valence band.

On the basis of this picture, it follows that an excess electron has a very slight interaction with the cores of the sulphur and tellurium ions. Accordingly, its scattering by disorder among these ions will be very small. Apparently it is so small as to be imperceptible in the experiments carried out at Professor JOFFE's laboratory.

On the other hand, the wave functions used by holes are large around the tellurium and sulphur ions and consequently are affected by the potential-energy distribution in the interior of these ions. These will evidently be different for these two ions, and thus the scattering of the holes will be strongly influenced by disorder among these positive ions.

Some evidence to support this interpretation is found in the crystal structure of $Bi_2Te_3$ (tellurobismuthite) and $Bi_2Te_2S$ (tetradymite).[1] These two structures differ by having 33 atomic per cent of the tellurium atoms replaced by sulphur atoms. This replacement apparently changes the interatomic distances by no more than about 2 per cent. This is in keeping with the idea that the core of the $Te^{--}$ and $S^{--}$ ions is not very important, so that it is largely the distribution of a loosely bound outer electron which is most important.

The assumption that the electrons of the $Te^{--}$ and $S^{--}$ ions spread out is in keeping with the observations made on the polarizability of the oxygen $O^{--}$ ion in various compounds.[2] It has been found that in the sequence of alkaline–earth ions the electronic polarizability which must be assigned to $O^{--}$ in order to account for the refractive index varies approximately linearly with the volume available for the $O^{--}$ ion. Assigned polarizabilities for $Al_2O_3$ and $Li_2O$ appear to fit well on this same scheme.

## REFERENCES

1. WYCKOFF R. W., *Crystal Structures* Interscience Publishers, Inc., New York (1948).
   WYCKOFF quotes the following references:
   GARRIDO J. and FEO R., *Bull. Soc. Franc. Minér.* **61**, 196 (1938); FRONDEL C., *Amer. Min.* **24**, No. 12, Part II, 7 (1939); LANGE P. W., *Naturwissenschaften* **27**, 133 (1939).
2. SHOCKLEY W., *Phys. Rev.* **73**, 1273 (1948), TESSMAN J. R., KAHN A. H. and SHOCKLEY W., *Phys. Rev.* **92**, 890 (1953).

VOL
8
195

*J. Phys. Chem. Solids* Pergamon Press 1959. Vol. 8. pp. 14–20. Printed in Great Britain

A.4

# BINDING AND SEMICONDUCTOR PROPERTIES OF $A^{III}B^{V}$ COMPOUNDS

**O. G. FOLBERTH and H. WELKER**

Siemens-Schuckert Forschungslaboratorium, Erlangen, Germany

**Abstract**—A model for the interpretation of the characteristic properties of the $A^{III}B^{V}$ compounds is proposed which takes into account the polarization of the valence electrons towards the $B^{V}$ ions. It is supposed that the polarization increases with increasing ionic part of the chemical bond and with increasing mean atomic weight. The influence of polarization on the lattice potential is investigated. It is shown that for $A^{III}B^{V}$ compounds, especially InSb, a neutral binding is to be expected, as proposed by J. C. SLATER and G. F. KOSTER (*Phys. Rev.* **94**, 1948 (1954)). The results are used to provide an explanation of the characteristic differences between the values of the energy gap $\Delta E$ and the mobility ratio $\mu_n/\mu_p$ in the various $A^{III}B^{V}$ compounds. Some pecularities concerning the mutual solubilities of $A^{III}B^{V}$ compounds and the solubilities of elements of the Group IV of the Periodic System in the $A^{III}B^{V}$ compounds are discussed. It is shown that for a continuous solid solution to be formed the polarizations must not differ too greatly. This rule allows the preferential formation of continuous solid solutions in the systems InAs–InP and GaAs–GaP to be explained.

VOL. 8 1959

If we consider the various groups of semiconducting materials, we find some general rules governing the variation of the energy gap. Thus it is well known that the energy gap decreases with increasing atomic number; for instance, the energy gap of the elements of Group IV of the Periodic System decreases from diamond to gray tin. A similar rule exists also for the semiconducting $A^{III}B^{V}$ compounds.

Furthermore the $A^{III}B^{V}$ compounds all have higher energy gaps than the corresponding isoelectronic elements of Group IV. These rules were set forth by Welker[1] in 1952, on the basis of binding theory. The essential basis of the argument was that for the $A^{III}B^{V}$ compounds there exists a small additional ionic bond which arises from the inequality between the two kinds of atoms, namely the $A^{III}$ and the $B^{V}$ atoms. The covalent bond and the ionic bond come to resonance according to Pauling[2] and the result is a larger total binding strength and from this a larger energy gap.

However, it is not possible to explain by this concept alone the differences between the energy gaps of $A^{III}B^{V}$ compounds with the same mean atomic weight, the so-called isoelectronic compounds. The binding strength increases in the isoelectronic sequences AlSb–GaAs–InP and GaSb–InAs, whereas the energy gap decreases. This behaviour cannot be accounted for by the preceding considerations, because an increasing binding strength should cause an increase in the energy gap.

Therefore a further factor must exist, whose effect is greater than that of the binding strength. Such an effect has been known for a long time, but, in our opinion, it has not as yet been applied correctly to $A^{III}B^{V}$ compounds. Seraphin,[3] Adavi[4] and Gubanow[5] have shown—partly in a different manner—that the energy gap increases with increasing difference between the potential valleys at the $A$ and $B$ atoms, with otherwise constant binding strength. In this way it is possible to understand why the energy gap increases markedly from an element of Group IV to the isoelectronic $A^{III}B^{V}$, $A^{II}B^{VI}$, and $A^{I}B^{VII}$ compounds. The very large energy gaps of nearly pure ionic crystals, like the alkali halides, can be explained only in this manner. To a first approximation all $A^{III}B^{V}$ compounds have the same difference between the potential valleys at the sites of the $A^{III}$ and $B^{V}$ atoms. In this approximation it is assumed that every $B^{V}$ atom gives one valence electron to an $A^{III}$ atom, so that all atoms now share equally four valence electrons. These charged atoms could now build up a crystal having a tetrahedral structure like the elements of Group IV. The resulting structure has the ZnS lattice. In this approximation the difference in charge between the $B^{V}$ and the $A^{III}$ sites amounts to two electronic charges uniformly for all $A^{III}B^{V}$ compounds.

For a better approximation it is still necessary to consider the deformation of the electronic structure caused by the above-mentioned charge difference, namely the polarization of the valence and the inner-shell electrons in the direction towards the $B^{V}$ atoms. This polarization differs for the various $A^{III}B^{V}$ compounds; it increases with increasing difference in electronegativity between the $B^{V}$ and $A^{III}$ atoms, and therefore it increases with increasing ionic bond. It increases also with the atomic weight.[6]

How does this polarization influence the lattice potential? If the polarization is very small, the valence electrons are almost equally distributed over the valence bridges in the same manner as in the elements of Group IV. So the potential is essentially determined by the difference of charge between $B^{V}$ and $A^{III}$ sites. The conduction electrons then find deeper potential valleys at the $B^{V}$ sites. Increasing polarization causes a variation of the potential valley in such a way that the deep $B^{V}$ valleys become narrower and the shallow $A^{III}$ valleys become broader. If we approximate the potential by Dirac functions, we may say that the polarization causes a reduction of the potential difference between $B^{V}$ and $A^{III}$ sites. This difference will be called $\epsilon$ in the following figures; $\epsilon$ vanishes completely if the polarization is so large that on the average three valence electrons correspond to the $A^{III}$ sites and five electrons correspond to the $B^{V}$ sites. On further increase in the polarization, the relations are reversed, so that for the conduction electrons the potential at an $A^{III}$ site is stronger than at a $B^{V}$ site.

By making certain assumptions it is possible to estimate the polarization in arbitrary units by the following formula:[6]

$$J = \frac{E_{ion}}{E_{cov}}(Z^{III}+Z^{V})^{3/2}$$

where $E_{ion}$ is the ionic extra energy according to PAULING, $E_{cov}$ is the convalent binding energy, and $Z^{III}$ and $Z^{V}$ are the atomic numbers of the elements $A^{III}$ and $B^{V}$, respectively.

It is easy to see now that the experimental values of the energy gaps can be explained. To show this, the potential differences $|\epsilon|$ and the energy gaps of the two isoelectronic groups AlSb–GaAs–InP and GaSb–InAs are given in Fig. 2. One sees that these differences vary in the same sense as the energy gaps. This effect should then overcompensate the effect of binding strength discussed

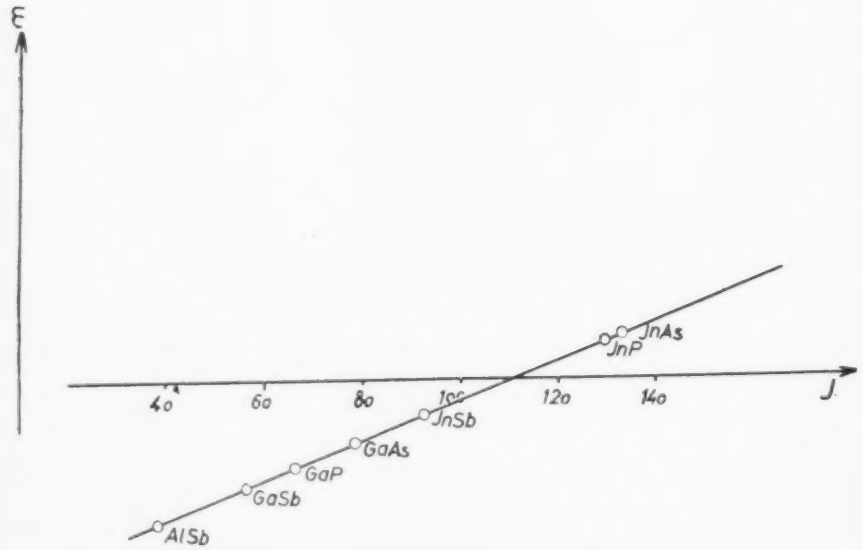


FIG. 1. Hypothetical relationship between the difference in the potential strength $\epsilon$ at $A^{III}$ and $B^{V}$ sites and the polarization $J$.

The principal hypothesis is taken from SLATER and KOSTER,[7] who suggest a nearly "neutral binding" for the $A^{III}B^{V}$ compounds. This means that the polarization is such that parameter $\epsilon$ is in the neighbourhood of zero for $A^{III}B^{V}$ compounds. Further we assume a linear relation between $\epsilon$ and $J$, with the neutral point at a $J$ value between InSb and InAs (Fig. 1). We can see that the polarization increases from 38 units for AlSb to 118 units for InAs, whereas the potential difference $\epsilon$ increases from a negative value for AlSb to zero and then to a positive value for InAs.

earlier. It is worth noting that, if the proposed model is true, the increase of the energy gaps of $A^{III}B^{V}$ compounds with regard to the energy gap of the corresponding isoelectronic element of Group IV is caused to a great extent by the potential difference at AlSb and GaSb, whereas the effect of binding strength is predominant in InP and InAs. GaAs occupies an intérmediate position.

It seems that the model developed may also explain other features of the semiconducting properties of the $A^{III}B^{V}$ compounds. At first we shall apply the proposed ideas to the following

question: what is the reason for the peculiar, abnormally high values of the mobility ratio $b(=\mu_n/\mu_p)$ in the various $A^{III}B^{V}$ compounds? For the elements of Group IV it is known that the ratio $b$ is of the order of 2. This ratio $b$ is larger (up to $b \approx 100$) for many $A^{III}B^{V}$ compounds. The high values of $b$ are not only based on an increased electron mobility $\mu_n$, but also on a decreased hole mobility $\mu_p$.

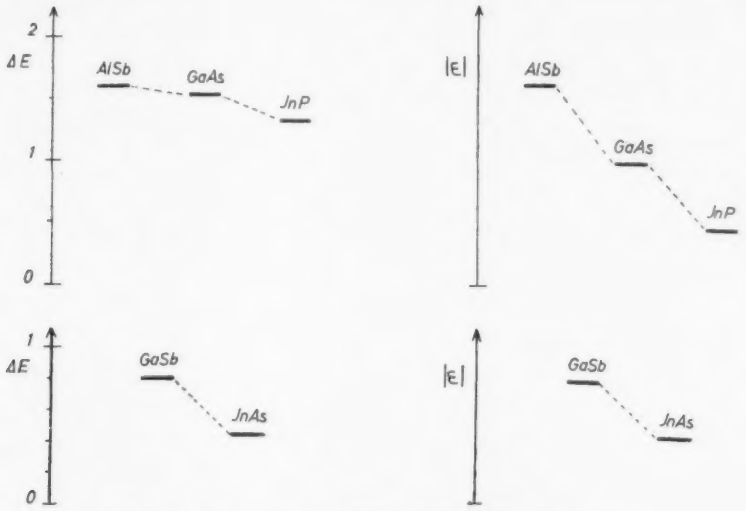


FIG. 2. The energy gap $\Delta E$ and the difference in the potential strength between $A^{III}$ and $B^{V}$ sites $|\epsilon|$ for $A^{III}B^{V}$ compounds.

Such a decrease of the hole mobility $\mu_p$ in a ZnS lattice may be explained by the polarization of the valence electrons in the following way.[6] In a diamond lattice the valence electrons are distributed symmetrically over the valence bridges. If anywhere an electron is missing, a hole is created. Such a hole moves if a valence electron from one of the six neighbouring valence bridges jumps into the hole. Each of these six possibilities has the same probability. In a ZnS lattice with polarization, the mechanism of hole motion is slightly different. The valence electrons are not distributed symmetrically in the valence bridges, being closer to the $B^{V}$ than to the $A^{III}$ atoms. Thus from the six neighbouring positions of valence electrons which surround a hole, three have come nearer, whilst the other three are more distant. This means that for the first group the jump probabilities are increased, whilst for the second group these probabilities are decreased. Movement of a hole through the lattice is possible only with the participation of this second group of jumps. In this way the smaller jump probability determines the hole mobility. This is equivalent to an increase of the effective masses of the holes. If we remove other influences, especially the influence on the electron mass, we may expect $b$ to increase with increasing polarization. That such a relation between the mobility ratio and the polarization really exists may be seen from Fig. 3, where the experimental values of $b$ are plotted against the estimated values of polarization $J$.

It is more difficult to explain the very high electron mobilities, e.g. those in InSb and InAs. These two compounds are located near the "neutral point" (see Fig. 1). Therefore the lattice scattering should be of the same order as that in the elements of Group IV. The higher binding strength is also favourable to a small lattice scattering. The second reason for the high mobility in $A^{III}B^{V}$ compounds—the small effective mass—is not yet fully understood.

The polarization effect may also explain some

pecularities which are connected with the formation of solid solutions.[6] From metallic alloy systems it is known that a continuous solid solution exists if the two components crystallize in the same crystal system and if the lattice constants do not differ by more than approximately 10 per cent. These conditions also apply in semiconducting systems, but they are not always sufficient. A study of the quasi-binary systems between $A^{III}B^{V}$ compounds shows that in some of these systems continuous solid solutions do not form or form only to a limited extent. This is the case even though the lattice constants satisfy the above-mentioned conditions well.

These facts may be explained in the following way. If the polarization values of the two compounds differ too greatly, a considerable distortion of the electronic structure results. Consequently the internal energy is raised and decomposition is favoured, since the system then passes into a state with lower energy. In Table 1 the relative disparity between the lattice constants and the difference in the polarization values are listed for various quasi-binary systems. Evidently a continuous solid solution exists only in those systems for which the polarization values and the lattice constants do not differ very markedly. For the same reason, continuous solid solutions do not exist between $A^{III}B^{V}$ compounds and elements of Group IV. For example, GaAs and germanium do not mix together over a wide range in spite of having almost equal lattice

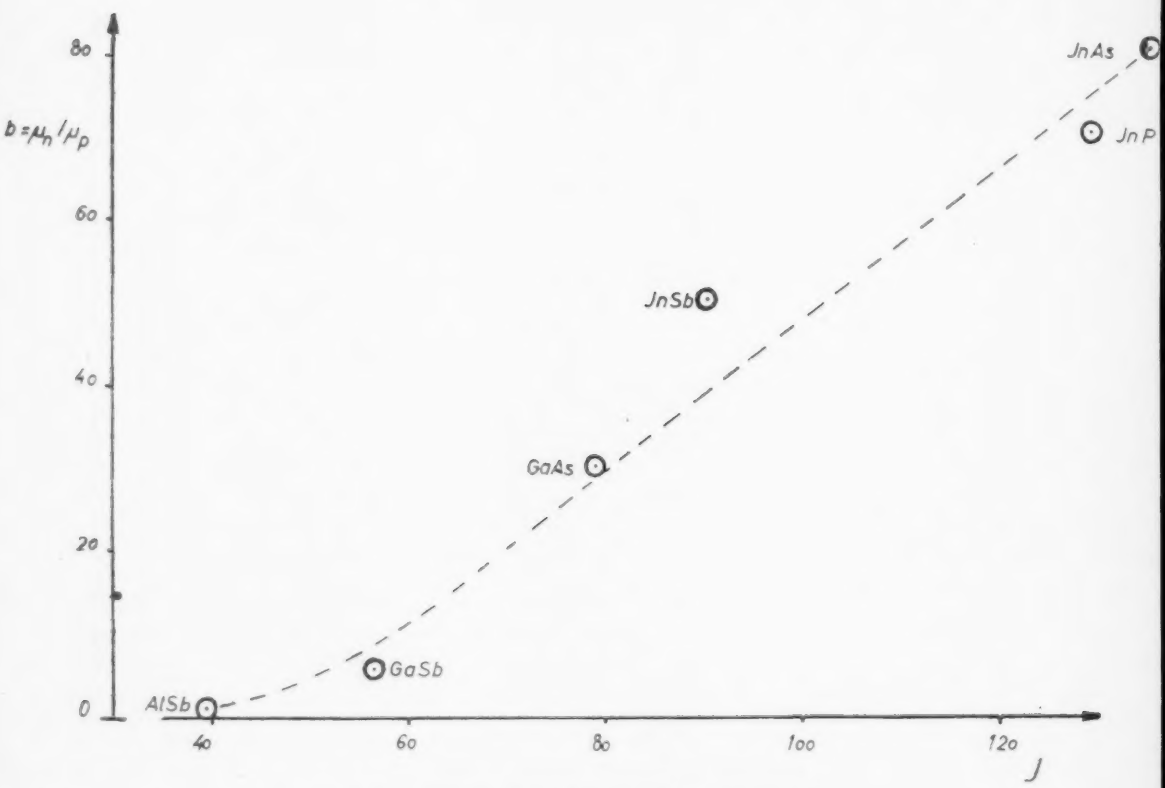


FIG. 3. Polarization $J$ as a function of the mobility ratio $b = \mu_n\mu_p$ for $A^{III}B^{V}$ compounds.

constants. By the same reasoning it follows that continuous solution between a $A^{III}B^{V}$ compound and a $A^{III}B^{V}$ compound is not possible.

Near the ends of the quasi-binary systems, the formation of solid solutions is favoured by the increased influence of the entropy in these regions. up to 2 per cent, but germanium dissolves only much smaller amounts of GaAs.

It is known that in the $A^{III}B^{V}$ compounds with components of almost equal atomic radii, elements of Group IV are more likely to replace $B^{V}$ than $A^{III}$ atoms.[9] This behaviour appears

*Table 1. Solid solutions in systems with various $A^{III}B^{V}$ compounds*

| Continous solid solution | | | | | | No continuous solid solution | | |
|---|---|---|---|---|---|---|---|---|
| Without tendency to decomposition | | | With tendency to decomposition | | | | | |
| System | $\Delta a$ | $\Delta J$ | System | $\Delta a$ | $\Delta J$ | System | $\Delta a$ | $\Delta J$ |
| InAs in InP | 3·2% | 3·5 | InSb in GaSb | 6·1% | 35·9 | InSb in InAs | 6·7% | 41 |
| GaAs in GaP | 3·7% | 11·9 | InSb in AlSb | 5·5% | 54·5 | InSb in InP | 9·9% | 37·5 |
| | | | GaSb in AlSb | 0·7% | 18·6 | GaSb in GaAs | 7·5% | 22 |
| | | | InAs in GaAs | 6·9% | 54·9 | InP in GaP | 7·4% | 63·3 |
| | | | | | | GaSb in GaP | 11·2% | 10·1 |

In these cases solid solutions may exist even if the above-mentioned rules are not satisfied. The region of solid solution, however, is larger the smaller the increase in internal energy resulting from the solution process. Such an increase is small if an $A^{III}B^{V}$ compound with a small polarization is dissolved in an $A^{III}B^{V}$ compound with a high polarization. The opposite case—an $A^{III}B^{V}$ compound with high polarization dissolved in an $A^{III}B^{V}$ compound with small polarization—would give a relatively high increase of internal energy. To understand this, it is necessary to remember that in a ZnS lattice the polarization of the valence electrons exerts a stress on the lattice. On dissolving a compound with a lower polarization, this stress is reduced and a state with lower energy is reached.*

From these considerations it can be understood why InAs dissolves InSb up to 2 per cent, whereas InSb dissolves only a negligible amount of InAs.[8] For the same reason GaAs dissolves germanium to arise from the fact that the polarization is reduced more by substitution of a $B^{V}$ site than of an $A^{III}$ site, because the valence electrons are nearer to the $B^{V}$ sites. For energy gaps larger than $\approx 1$ eV, it appears that the above-mentioned effect is negligible and it becomes energetically favourable, if the atoms of Group IV are distributed equally over $A^{III}$ and $B^{V}$ sites.[10]

Finally, it is worth pointing out that it may be possible to treat $A^{II}B^{VI}$ compounds in a similar manner.

* The ZnS lattice is held together by means of the covalent bond. If an ionic bond is added, this structure remains stable, up to values of the ionic bond of the order of the covalent bond. Consider, for example, the compound CuBr, which crystallizes in the ZnS lattice. If the ionic bond predominates, the ZnS lattice becomes unstable, because the NaCl or CsCl lattice is now more favourable.

## REFERENCES


1. Welker H., *Z. Naturf.* **7a,** 744 (1952).
2. Pauling L., *The Nature of the Chemical Bond* Oxford University Press (1950).
3. Seraphin B., *Z. Naturf.* **9a,** 450 (1954).
4. Adavi J., *Phys. Rev.* **105,** 789 (1957).
5. Gubanow A. J., *Zh. tekh. fiz., Moscow* **26,** 2170 (1956).
6. Folberth O. G., *Z. Naturf.* (to be published). In this paper a detailed description of the problem presented here can be found.
7. Slater J. C. and Koster G. F., *Phys. Rev.* **94,** 1948 (1954).
8. Shih C. and Peretti E. A., *J. Amer. Chem. Soc.* **75,** 608 (1953).
9. Folberth O. G. and Schillimann E., *Z. Naturf.* **12a,** 943 (1957).
10. Kolm C., Kulin S. A. and Averbach B. S., *Phys. Rev.* **108,** 965 (1957).

## DISCUSSION

F. HERMAN: It is difficult to believe that the observed differences in energy gaps, effective masses, and carrier mobilities in the various III–V compounds can be interpreted solely and directly in terms of differences in the chemical binding. A minimum requirement for such an interpretation would be the knowledge that all the III–V compounds have the same type of energy-band structure. Then differences from crystal to crystal might bear some relationship to differences in the covalent and ionic components of the binding, and to differences in the polarization of the constituent atoms. However, this knowledge is lacking, and in fact there is good reason to believe that the symmetry classification and location in the reduced zone of the valence and conduction-band edges of different III–V compounds are not identical. In such circumstances, there would be differences between crystals arising from differences in the detailed nature of the energy-band structure, which, at the present time, can hardly be predicted from rough estimates of differences in the chemical binding.

To support this point of view, let us consider the four crystals germanium, GaAs, InP and AlSb. It is well known that in germanium there are [111]-, [000]-, and [100]-type minima in the lowest conduction band.[1] Since these three sets of minima are no more than 0·1—0·2 eV apart, and since GaAs, InP, and AlSb may be regarded as perturbed germanium crystals,[2,3] it is reasonable to expect the conduction-band edge in these three compounds to be defined by the [111] minima (as in germanium), by the [000] minimum, or by the [100] minima. (The occurrence of minima in other locations in the reduced zone is possible, but less likely.)

In point of fact, there is experimental evidence for a [000] conduction-band edge in both InP[4] and GaAs.[4,5] In the case of InP, there is also evidence[4,6] for another set of minima, possibly of the [100] type, just above the [000] minimum. In the case of GaAs, there is again evidence[7,8] for a second set of minima. The conduction-band structure of AlSb is presently unknown.

In view of the large difference in electron mobilities in AlSb ($\mu_n \approx 200$) on the one hand, and in GaAs ($\mu_n > 3400$) and InP ($\mu_n > 3400$) on the other, it is tempting to assume that the conduction-band edge in AlSb does not lie at [000], but elsewhere in the zone, for example along the [100] axes. This would provide a natural explanation for the large difference in $\mu_n$, since it would be reasonable to expect different effective masses and different relaxation times to be associated with different types of band edges.

The latter point is strikingly demonstrated in the case of germanium and GaAs. According to the theory of WELKER and FOLBERTH, the change in the electronic properties in going from germanium to GaAs should be due to a change of the ionic to covalent binding ratio, and to a change in the atomic polarizations. While such a picture may be true enough, it completely misses the important switch of the conduction-band edge from the [111] face points to the zone center, and the associated changes in $m^*$ and $\tau$.

Finally, it should be noted that the occurrence of two distinct sets of nearly degenerate minima (as is apparently not quite the case in InP or GaAs) would lead to effective mass and mobility values that would be incomprehensible on the basis of WELKER and FOLBERTH's model alone.

### REFERENCES


1. HERMAN F., *Proc. Inst. Radio Engrs.* **43,** 1703 (1955); *Rev. Mod. Phys.* **30,** 102 (1958).
2. HERMAN F., *J. Electronics* **1,** 103 (1955).
3. CALLAWAY J., *J. Electronics* **2,** 330 (1957).
4. GLICKSMAN M., *J. Phys. Chem. Solids* **8,** 52 (1959).
5. SPITZER W. G. and FAN H. Y., *Phys. Rev.* **106,** 882 (1957); BARCUS L. C., PERLMUTTER A. and CALLAWAY J., *Phys. Rev.* **111,** 167 (1958).
6. NEWMAN R., Private communication.
7. EHRENREICH H., Private communication.
8. SPITZER W. G., Private communication.

*J. Phys. Chem. Solids* Pergamon Press 1959. Vol. 8. pp. 21–25. Printed in Great Britain

SESSION B:
THEORY I*

B.1

# BAND THEORY†

J. C. SLATER

Massachusetts Institute of Technology, Cambridge, Mass.

VOL. 8 1959

**Abstract**—The band theory of solids represents a one-electron theory, in which an electron moves in a periodic potential representing the nucleus and the averaged potential of other electrons, in the sense of HARTREE's self-consistent field. It is really broader than a one-electron theory, however, in that group theory shows that a perfect crystal of a semiconductor, having only one electron in the conduction band, or one vacancy in the valence band, will have energy levels of the same general type, so that so long as the interaction of electrons and holes with each other, and the distortion of the lattice by the charges (polaron formation) can be neglected, it forms an adequate approximation. Important advances have been made in the last few years in the approximate solution of SCHRÖDINGER's equation for a periodic potential, in the detailed understanding of the band structure of particular semiconductors, and in the use of experiments to clarify many important points of these band structures. Some of these advances will be described.

THIS paper is intended as a general survey, to open our discussion on the theory of semiconductors. Every worker in semiconductors must be aware of the debt which the theory owes to BLOCH, BRILLOUIN, WILSON, and others[1] who, in the early 1930's developed the idea of energy bands in solids, and the relation between the existence or lack of energy gaps and the distinction between insulators, semiconductors, and metals. We are aware also of the fact that our Soviet colleagues believe that in the last few years the concept of band theory has been overplayed, and that they feel that the American workers, in particular, have taken this theory too literally.[2] I do not agree with their point of view, but I believe that these are questions to be considered on their scientific merits, and I should like to use this paper to discuss in an elementary manner the way in which a theorist now regards the band theory, and fits it in with his broader understanding of the theory of solids in general.

We realize in the first place that the theory of energy bands is a one-electron theory. An electron moving according to the principles of wave mechanics in a periodic potential, repeating in each unit cell of a perfect crystal, will have wave functions of the form of a plane wave, symbolized mathematically by the exponential $e^{i\mathbf{k}\cdot\mathbf{r}}$, where $\mathbf{k}$ is a propagation vector, $\mathbf{r}$ the position vector, multiplied by a periodic function $u_{kn}(\mathbf{r})$. This periodic function is characterized by $\mathbf{k}$, which acts as a quantum number, and by another quantum number which we may denote as $n$. The corresponding energy of the electron in the periodic potential is $E(\mathbf{k}n)$, again determined by the same quantum numbers. The quantity $\mathbf{k}$ takes on independent values only within a polyhedron surrounding the origin in $\mathbf{k}$ space, called the central unit cell of the reciprocal lattice, or the central Brillouin zone; a value of $\mathbf{k}$ outside this polyhedron leads to wave functions repeating those already found from $\mathbf{k}$'s inside the central Brillouin zone. We may describe the quantum number $n$ in a simple way. For a given value of $\mathbf{k}$, the periodic potential problem will have an infinite number of energy values. We may label the lowest energy value $n = 1$, the next $n = 2$, and so on. The energies in general will not be degenerate; degeneracy comes only for certain values of $\mathbf{k}$ having particular symmetry properties, as has been very throughly studied in the last few years. Thus there

* *Chairman*: W. SHOCKLEY; *Co-Chairman*: H. EHRENREICH.

† Supported in part by the Office of Naval Research under contract with the Massachusetts Institute of Technology.

is no ambiguity in general regarding this labelling. For a given value of $n$, the energy and wave functions vary as smooth functions of $\mathbf{k}$. We then define the energy levels associated with the same value of $n$, and with all values of $\mathbf{k}$ within the central Brillouin zone, as constituting an energy band.

Pauli's principle, coupled with band theory, shows that there are just enough independent stationary states in an energy band to accommodate one electron of each spin per unit cell in the crystal. The theory of electrical conductivity shows that if the electrons fill the lowest possible states, and if these fill certain energy bands, leaving an empty gap above between the topmost filled band and the lowest empty band, we shall have an insulator or semiconductor, depending on the width of the gap, while if the electrons partly fill certain bands, leaving unoccupied states immediately above, we have a metal.

These are the elementary and familiar principles of the energy-band theory. No one questions them as forming a correct deduction from wave mechanics, provided we accept the one-electron picture on which they are based. The real question is, to what extent does this oversimplified model correspond to reality? We could attempt to answer this question in either of two ways. First, there is the empirical or pragmatic answer: to what extent do the consequences of such a picture agree with experiment? Secondly, there is the more theoretical answer: to what extent do they agree with the more elaborate theory which we should find by rigorously applying the principles of wave mechanics to the problem of a solid? To me, as a theoretical physicist, the second type of answer is more satisfying than the first. If the results of the simple theory disagree with experiment, then it is wrong; but if they agree with experiment, it is not necessarily right: other theories as well might give the right answer. Nevertheless we must realize that the plausibility of the theory is greatly strengthened by the many types of agreement with experiment that have been discovered in the last few years, many of which will be reported on at this conference.

In the first place, calculations of energy bands,[1,3] using reasonable postulates regarding the one-electron potential, have agreed with experiment in the sense that they indicate filled bands with gaps above in cases where it is known that we have insulators or semiconductors, and they indicate partly filled bands in cases known to be metals. This is about as far as the agreement went until the last few years. Even ten years ago, the complicated structure of the bands indicated by such theory as was then available was a purely hypothetical thing, with no experiments available to check it. Now, however, the situation has completely changed, particularly as concerns the behavior of germanium and the 3–5 compounds. The beautiful experiments on cyclotron resonance, carried out by Kip and his associates in Berkeley, and by Lax and his associates at M.I.T.,[4] have given us a very powerful tool for determining the details of the energy bands for those materials for which the experiments have been possible. The even more recent experiments on the oscillatory magneto-optic effect verify and extend these results, and give very elaborate and convincing confirmations of the energy-band type of theory. Experiments which are now being planned seem likely to extend these powerful methods to many types of materials which cannot be examined by present techniques. It seems very likely that these experimental methods, depending on the interactions of strong magnetic fields and very high-frequency electromagnetic oscillations in solids, will eventually be capable of giving very complete information about the energy levels in solids, information comparable with that given about individual atoms by atomic spectroscopy and the Zeeman effect. And the further we go in this direction, the more it seems that an energy-band picture is capable of explaining what we are finding. In other words, the empirical answer to our question about the legitimacy of energy-band theory seems to be definite: the more we find out about it, the better it works, at least for materials similar to germanium.

Let us then go to the other type of answer, that depending on the analysis of more rigorous approaches to the theory of solids. There are three major types of approximations made in using the energy-band model of a solid. First is the assumption of the self-consistent field: the assumption that the action of other electrons on the electron in question can be replaced by a periodic potential, arising from the averaged behavior of the other electrons. Secondly, there is the closely related

VOL. 8 1959

approximation that we can disregard anything of the nature of multiplet structure, treating the problem like that of one electron outside closed shells. Thirdly, there is the quite separate postulate that we can treat the electronic motion separately from the nuclear motion, as in the approximation of BORN and OPPENHEIMER for a molecule, solving for the energy bands in an approximation in which the nuclei are held fixed at the positions which they would occupy in an ideal crystal at the absolute zero of temperature, and bringing in the interaction with the lattice only as a perturbation at a later stage of the calculation. Let us take up these three approximations, all of which are very significant, in order. For the first two approximations it pays to recall the similar and familiar example of the theory of isolated atoms, where the same two approximations must be made in the first stages of our calculation.

A semiconductor is an inherently simpler problem in quantum mechanics than a metal, just as an alkali atom is simpler than one with more outer electrons. The reason is that the semiconductor ordinarily has so few electrons in the conduction band, or so few holes in the valence band, that they can be treated independently of each other, so that we are essentially dealing with a single electron outside closed shells. We know that the alkali atoms can be handled with great success by a central field model, of a single electron moving in a properly chosen potential field, determined ordinarily by the HARTREE–FOCK method. This is no accident. By group theory we can show that the behavior of the orbital and spin angular momenta of an isolated atom show properties like those of a single electron. The reason is that the angular momentum operator and the rotation operator are closely related to each other, so that the fact that the potential energy of the atom as a whole is independent of rotation leads directly to the angular momentum properties, like those of single electrons moving in central fields.

Similarly the operation of translation through one lattice spacing is related to the quantity **k**, similar to a linear momentum, and often called a pseudo-momentum, and the fact that the behavior of a semiconducting crystal is unchanged when we make a translation through a lattice spacing directly leads to a classification of its stationary states by means of a pseudo-momentum **k** like that of a single electron. In other words, it is necessary that the lower stationary states of a semiconductor with a single electron in the conduction band (or a single hole in the valence band) show the same type of behavior as those of a single electron in a periodic potential. This similarity holds not only as far as the translation is concerned, but also for the rotational operations which result in the interesting degeneracy and symmetry properties of the energy bands. This point of view has been emphasized by a number of physicists recently,[5] and probably will be brought out more clearly in some of the later papers in this series, by KOHN and others, dealing with semiconductor problems by means of a many-electron approach.

The second approximation met in the energy-band theory, namely that we can disregard any analogy to multiplet structure, or any interaction of the electrons outside the closed shells, holds only to a limited extent, though we are familiar with phenomena where it does not hold, but where this has long been recognized. The most familiar of these examples is that of the exciton, resulting from the interaction between an electron and a hole. This has close analogy to the atomic problem of an inert-gas atom, in which one electron is removed from the filled shell and placed in an outer shell. For instance, in neon, where we have the configuration $1s^2 2s^2 2p^6$ in the ground state, we could go to the state $1s^2 2s^2 2p^5 3s$, leaving a hole in the $2p$ shell and an extra electron in the $3s$ state. In such a case, we know from the vector model of the atom that we have a vector coupling problem between the $2p$ shell, which acts like a single $2p$ hole, and the $3s$ electron, resulting in $^1P$ and $^3P$ states. This is a simple example of multiplet structure, replacing the doublet spectra arising in the case of alkali atoms. But this situation as applied to excitons is now well understood. The work of OVERHAUSER[6] and others has shown that the multiplet structure of excitons, as complicated by the fact that we are in a crystalline field rather than a central field, really exists. Here is a simple case where we must consider a two-electron problem, and there are other such cases. They do not invalidate the picture of energy bands, but merely show that we must expect to extend it in appropriate cases.

We may remark at this point that it is here that the theory of metals, and of magnetic media, becomes so much more complicated than that of semiconductors. We know from atomic theory that a partially filled shell has much more complicated multiplet structure than a shell with only two electrons. Thus, for instance, there are five multiplets for the configuration $d^2$, eight for $d^3$, and sixteen each for $d^4$ and $d^5$. In the $f$ shell, even $f^4$ has 47 multiplets, and $f^7$, the half-filled shell, has no fewer than 119. A partially filled energy band in a metal acts, as far as its multiplet structure is concerned, somewhat like an atom with a shell capable of holding two electrons for each unit cell of the crystal, partially filled with electrons. This is something that cannot possibly be handled completely and rigorously, and we are pushed into approximations for treating the multiplet structure, which often are far from satisfactory. In the case of paramagnetism, this situation is not so serious. Here we can treat each paramagnetic atom separately, so long as their wave functions do not overlap or interact by superexchange mechanisms through intermediate electrons. Thus the problem is no more difficult than that of a single paramagnetic atom in a crystalline field, and there has been widespread success in treating such cases. But once the orbitals of the various atoms overlap or show superexchange phenomena, we must consider all the unit cells of the crystal as forming a single problem and consequently in ferromagnetism and antiferromagnetism we meet theoretical problems of an altogether higher order of difficulty. Fortunately, in an ordinary non-magnetic semiconductor, these situations do not arise, and it is here that we may expect the energy-band theory in its simpler forms to hold with relative accuracy.

Now let us consider the third and final approximation made in the energy-band theory. We conventionally start by fixing the nuclei at the positions which they would have in a perfect crystal at the absolute zero of temperature, setting up a self-consistent potential, and solving the energy bands in that potential. Then, as a later stage in the approximation, we try to bring in the interaction with lattice vibrations as a perturbation. It is this approximation which the Soviet workers have mainly questioned: they feel that the interaction is so strong that it cannot be handled by perturbation methods. This would be expected to be the case more particularly in ionic crystals, where an isolated electron can produce large distortion of the lattice of ions, rather than in a covalent crystal such as germanium. Here we are meeting problems which are the hardest ones in semiconductor theory, and where I believe that we still do not have enough information to decide the question completely. There seem to be at least two methods of approach to its solution.

First, there is the experimental approach. The electron–lattice interaction in such a covalent crystal as germanium is not likely to be large, as I have just mentioned. It can well be that this is a partial explanation of the fact that it is in germanium that the energy-band approach has worked best. But fortunately now there is more and more work on the III–V compounds like InSb, and on the II–VI compounds like ZnS and ZnSe. Surely these compounds will be increasingly ionic, and in the I–VII compounds like CuBr we shall have an almost completely ionic case, though with the same type of crystal structure. Intensive study of these groups of compounds, such as is going on at present, is bound to show if, or where, the energy-band picture begins to break down as the crystal becomes more ionic. The evidence is pretty clear that the situation in the III–V compounds is not very different from that in germanium; but those compounds might well be nearly covalent, and the ionic behavior may begin to come in only with the II–VI and I–VII compounds.

The second approach, which still must be developed much further, though very good steps toward it have been taken, is the theoretical study of electron–lattice interactions, in the limit where they are large. Some theoretical studies of polarons in alkali halides, which have been carried out so far,[7] suggest that the lattice polarization by the conduction electrons, though appreciable, is not enough to affect the properties of the crystal in a very profound fashion. But these studies have hardly gone far enough to be conclusive. The whole question of interaction of electron waves with lattice waves, and of lattice waves with each other, is to my mind the leading theoretical problem in the study of solids at present. Very good starts toward its solution have been made, for example by VAN HOVE,[8] using methods which

were originally developed for the study of field theory. But these studies must be carried much further than they have already, before they can give really conclusive answers to the behavior of polar crystals. It is almost certain that in such a study, the simple energy-band theory will appear as a first approximation for the electronic motion, as the simple harmonic theory of elastic vibrations will appear as the first approximation for the nuclear motion. But it is the higher approximations that will count, and the encouraging thing about the recent studies in the field is that rigorous methods are being found to apply perturbation theory to such problems.

Let me close by describing a few of the many problems that await solution along this line, but whose treatment is in sight, and probably will be worked out in the next few years. First we have the problems of ordinary elastic vibrations of crystals. Here we are beginning, through the work of LAVAL, WARREN,[9] and their colleagues with X-ray thermal diffuse scattering, and through the work of BROCKHOUSE[10] and others with neutron scattering, to have good experimental knowledge of the elastic spectra of a few simple crystals. We must tie these results in with fundamental calculations of microscopic elastic constants, from energy-band theory or improvements on it. Then we must consider the scattering of one thermal wave by another, leading to thermal conductivity on the one hand and thermal expansion on the other. Here VAN HOVE[8] has carried out a thorough theoretical analysis, which awaits comparison with detailed calculations on individual crystals. Next we must consider the interaction of electron waves with these elastic waves, resulting on the one hand in a theory of electron mobility and electrical resistivity, and on the other in an understanding of the damping of ultrasonic waves by electron waves which has been the subject of interesting experimental investigations recently.[11]

These are but a few of the aspects of these interactions between waves, as far as semiconductors are concerned; I have already indicated that the problems of metals, and particularly of ferromagnetic metals, are far more complicated. Fortunately, as I have mentioned, the theoretical means of handling these problems are becoming more powerful; and I have a great deal of confidence that through such advances in theory, we shall eventually find to what extent a simple energy-band approach is adequate for ionic semiconductors, as it seems to be from empirical evidence for the covalent semiconductors. At least, we seem to have here a fruitful direction of attack, and I believe we shall find that it is work along these lines which will make the most useful advance in semiconductor theory in the coming years. As far as I know, this point of view is in agreement with that of the Soviet workers, who are actively pursuing theoretical work along the lines I have described, and have been making good progress toward an understanding of these difficult problems.

## REFERENCES


1. SLATER J. C., *The Electronic Structure of Solids* from *Encyclopedia of Physics* Vol. 19. Springer, Berlin (1956), for bibliography on the band theory.
2. DUNLAP Jr. W. C., *Phys. Today* **11,** 14 (1958).
3. HERMAN F., *Rev. Mod. Phys.* **30,** 102 (1958), for references not given in (1).
4. LAX B., *Rev. Mod. Phys.*, **30,** 122 (1958), for references on experimental methods of studying energy bands.
5. KOHN W., *Phys. Rev.* **105,** 509 (1957).
6. OVERHAUSER A. W., *Phys. Rev.* **101,** 1702 (1956).
7. SCHULTZ T. D., *Solid-State and Molecular Theory Group M.I.T. Tech. Rep.* No. 9 (1956) (unpublished), including references.
8. VAN HOVE L., Unpublished. To be available as *Solid-State and Molecular Theory Group M.I.T. Tech. Rep.*
9. LAVAL J., *Rev. Mod. Phys.* **30,** 222 (1958); CRIBIER D., *ibid.* p. 228; JACOBSEN E. H., *ibid.* p. 234. including references.
10. BROCKHOUSE B. N. and STEWART A. T., *Rev. Mod. Phys.* **30,** 236 (1958); STEWART A. T. and BROCKHOUSE B. N., *ibid* p. 250.
11. MORSE R. W., *Phys. Rev.* **97,** 1716 (L) (1955).

*J. Phys. Chem. Solids* Pergamon Press 1959. Vol. 8. pp. 26–28. Printed in Great Britain

# *D*-BAND AND MIXED-VALENCY SEMICONDUCTORS

C. ZENER

B.2

Westinghouse Research Laboratories, Pittsburgh, Pa.

**Abstract**—In many cases the shell and band models predict identical or similar results. In such cases it is only a matter of personal preference as to which model is used. However, there are other cases where the two models make different predictions. Here it becomes necessary to ascertain the proper model by checking the agreement with experiment. The purpose of the present paper is to discuss the relevant theoretical and experimental information which is of aid in deciding on the most appropriate model.

VOL
8
195

THOSE of us from industrial research laboratories dream of the day when we can sit down at a drawing board and design solid-state materials to specifications. While this day has not yet arrived, some of us nonetheless make brave attempts. In such attempts one question we ask is: "what is the most appropriate model for the electronic structure?" In many cases we conclude that the band model is the best representation, together with its conceptual paraphernalia of band width, band gap, effective mass, &c. In those cases where our curiosity extends beyond germanium and silicon, beyond the III–V compounds, beyond the II–VI compounds, doubts begin to haunt us as to whether the band concept is any longer applicable, as to whether, in fact, we should not adopt a localized concept for the charge carriers.

My own doubts stem from two considerations. Consider first that if we insist upon using the band concept, the conduction band is only sparsely occupied. Now let us go through the mental exercise of forming localized wave packets (see Fig. 1). The increase in kinetic energy will then correspond to essentially half the band width. If the lattice is of a polar nature, we may now gain back a considerable amount of energy by allowing a relaxation of the lattice around the localized charge carriers. If the final energy lies above the bottom of the conduction band, we are justified in our preference for the band concept. If the final energy lies below the bottom of the conduction band, our preference for the band concept is questionable.

Next consider the case where the conduction band can have at least four electrons per atom, and where the conduction band is about half filled. When we now form localized wave packets, we again have an increase in kinetic energy. Let us now be clever in allowing only wave packets with parallel spins on the same lattice site. We then experience a decrease in energy due to spin correlation. The band concept will be unjustified if the final energy is below the original energy.

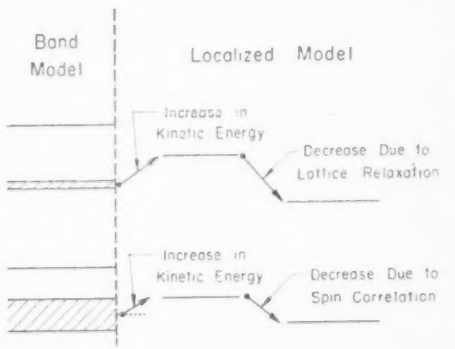


FIG. 1

Let us now look at the experimental facts. No example has come to my attention for which we would appear justified to attribute a localization of charge carriers to solely the lattice relaxation surrounding the charge carriers. Many examples have come to my attention, primarily through the work of my colleague, Dr. R. R. HEIKES, where the desire of electrons to associate only with other electrons with parallel spins forces us to abandon the band model in favor of a localized model. These examples I shall now review.

First, let me review the case of the *d*-electrons in iron. As long as we are well below the Cur

temperature, i.e. as long as all the spins are parallel, no advantage would be gained through a localization of the *d*-electrons. In fact, there is no way of experimentally distinguishing between the behavior of two specimens, one of which conforms to the band model, the other to the localized model. Only when we begin to uncouple the spins through a rise in temperature can we obtain an advantage by localization, or can we distinguish experimentally between specimens conforming to the two models. I shall now review the experimental evidence which forces us to adopt the localized model for the *d*-electrons in iron at elevated temperatures.

On the band model, demagnetization associated with a rise in temperature implies a complete uncoupling of all spins with one another. Such complete spin uncoupling would give an entropy increase of $R \ln 4$ cal/mole°C. On the localized model, demagnetization associated with a rise in temperature implies a complete uncoupling only of the spins of one atom with the spins of neighboring atoms. The spins within the same atom remain firmly coupled to one another. The increase in entropy associated with demagnetization is thus, according to the localized model, only $R \ln 3$ cal/mole°C. A careful examination of the specific-heat anomaly of iron up to its melting temperature has led Dr. LARRY DARKEN to an experimental value of 2·1 for the entropy of demagnetization. The following figures provide strong evidence in favor of the localized model:

| Theory | Exp. |
|---|---|
| $R \ln 4 = 2{\cdot}75$ | ... |
| $R \ln 3 = 2{\cdot}18$ | 2·1 |

Iron manifests a well known anomaly in resistivity as we uncouple the spins by a rise in temperature as illustrated in Fig. 2. Band enthusiasts like to interpret this anomaly by ascribing it to a scattering of electrons from the conduction band into the *d*-band. According to this viewpoint, demagnetization opens up more levels in the *d*-band into which the conduction electrons may be scattered. KASUGA has recently pointed out, however, that such an interpretation would lead to a different $\rho$ versus $T$ curve than is observed. Since, according to this model, scattering is still by phonon–electron interaction, above the Curie temperature, the $\rho$ versus $T$ curve would have a slope which would extrapolate back through the origin. Since this is not the case, rather since demagnetization appears to add a constant value to the $\rho$ versus $T$ dependence, KASUGA concluded that the *d*-electrons in iron could be represented only by a localized model. Above the Curie temperature the randomness in orientation of the spins of the individual atoms gives rise to a random fluctuation in the effective potential seen by the conduction electrons as they wander through the lattice. This random fluctuation in effective potential gives rise to an added temperature–independent resistivity.

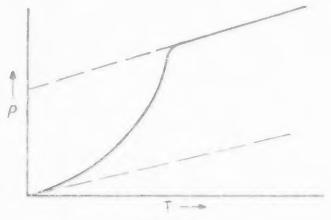


FIG. 2

Next, let us look at the transition metal oxides of the type MnO . . . NiO. These oxides have been thoroughly studied in our laboratory by a group guided by Dr. HEIKES. These oxides are well known to be semiconductors in their pure state, i.e. resistivity decreases rapidly with a rise in temperature. Now the term "semiconductor" has in recent years acquired a connotation which is associated with the conceptual paraphernalia of band width, band gap, effective mass, &c. The Westinghouse group has conclusively demonstrated that these conceptual paraphernalia are inappropriate when applied to these transition-metal oxides. I shall review the experimental observations which have led to this conclusion.

Positive carriers are introduced into the transition-metal oxides by substituting lithium atoms for some of the transition-metal atoms. Such doped oxides still have a resistivity which decreases rapidly with increasing temperature. According to the band model, a certain energy is necessary to free the positive charges from the doping atoms. According to such a model this energy would, however, approach zero as the concentration of doping atoms increased. Experimentally one finds that the heat of activation for electrical conduction remains essentially constant if the doping concentration is increased from 1 atomic per cent up

to the maximum solubility limit of some 20 atomic per cent. We therefore conclude that the observed heat of activation for conduction is associated with the mobility of the charge carriers rather than with their number. We are thus led to the viewpoint that electrical conduction takes place by the activated exchange of electrons from doubly ionized transition-metal ions to triply ionized transition-metal ions. Such an exchange requires a heat of activation presumably because of the lattice distortion which surrounds a triply ionized transition-metal ion in a lattice where the ions are predominantly doubly ionized.

This concept of electrical conduction by the activated jumping of localized charge carriers leads to certain predictions.

The first prediction relates to the internal friction of doped transition-metal oxides. Metal physicists are familiar with an internal-friction peak associated with pairs of solute atoms. Thus consider brass, which is a solid solution of zinc in copper. Two zinc atoms which happen to be nearest neighbors of one another will cause a lattice distortion having a tetragonal symmetry. Under zero applied stress, these axes of tetragonal symmetry will be randomly oriented. Under an applied tensile stress, the equilibrium distribution of these tetragonal axes will be one in which more tend to be parallel to the tensile axis than perpendicular. Such an equilibrium distribution will, however, require time to be established. As a consequence, the internal friction measured under conditions of gradually rising temperature will show a peak at that temperature where the time of relaxation is comparable to the period of vibration used in the measurement. Measurements on the internal friction of mixed-valence oxides were made expressly to see if such a peak did exist. These measurements did indeed verify the presence of such a peak associated with pairs of triply ionized transition-metal ions, and thus furnished strong corroborative evidence of the correctness of the model of electrical conduction by localized charge carriers.

The second prediction relates to the thermoelectric power of doped transition-metal oxides. From simple arguments based on entropy of mixing, one concludes that the thermoelectric power will be given by:

$$\frac{dE}{dT} = (k/e) \ln (1-2c)/c.$$

Thus an atomic concentration of 8 per cent should give a thermoelectric power of 204 $\mu$V/°C. Extensive thermoelectric measurements on doped transition-metal oxides have verified the essential correctness of the viewpoint that the charge carriers are randomly localized on the positive ion sites.

I now return to the physical basis for the localization of the charge carriers in the transition-metal oxides. Two possible cases have previously been discussed, namely the relaxation of a polar lattice surrounding an excess charge, and the desire of electrons to associate only with other electrons having common spin directions. The relative importance of these two effects cannot be decided by observations on the transition-metal oxides, since here both effects are present. Thus, in these oxides the transition-metal ions themselves have *d*-electrons whose spins are highly correlated, and also the presence of a heat of activation for charge movement implies a lattice distortion surrounding the charge carriers. A distinction may, however, be made in going from MnO to MnTe. In the latter material the electrical characteristics are profoundly influenced by the spin structure. Below the magnetic transformation temperature, doped MnTe behaves in every way as if the charge carriers moved in a conduction band. The electrical resistivity is low and increases linearly with temperature. The thermoelectric power likewise is metallic, being of the order of 20 $\mu$V/°C. Above the magnetic-transformation temperature, the electrical resistance is higher by at least an order of magnitude. An order-of-magnitude rise in the thermoelectric power in going past the magnetic-transformation temperature is strong indication that the random spin orientation at the higher temperature favors localization of the charge carriers, in contrast to the band model which appears appropriate in the temperature range where the spins are ordered.

In closing I wish to join Professor JOFFÉ in reiterating the danger of blindly applying the band concept to semiconductors once we leave the area of germanium and silicon, of the III–V compounds, of the II–VI compounds, and of the I–VII compounds.

VOL
8
195

*J. Phys. Chem. Solids* Pergamon Press 1959. Vol. 8. pp. 29–35. Printed in Great Britain

# BAND STRUCTURE AND TRANSPORT PROPERTIES OF SINGLE-CRYSTAL GRAPHITE

B.3

D. E. SOULE and J. W. McCLURE

National Carbon Research Laboratories,* Cleveland, Ohio

**Abstract**—Understanding of the band structure of graphite has developed to the point where satisfactory correlation can be made with single-crystal measurements. These include cyclotron resonance, de Haas–van Alphen effect, electrical conductivity, Hall effect, and magneto-resistance. The band model, a result of the efforts of many workers, is consistent with group theory and fundamental calculations. The most important features of the model are: the valence and conduction bands overlap by about 0·03 eV; there are about $10^{-5}$ per atom of both electrons and holes at absolute zero contained in highly anisotropic (12 to 1) Fermi surfaces; the effective masses in the basal plane are 0·03 $m_0$ for electrons and 0·06 $m_0$ for holes; and there is fine structure warping near the ends of the Fermi surfaces. Thus, the foundation has been laid for systematic studies of doping and electron scattering. In the lattice-scattering region (for present samples $\gtrsim 25°K$), the mobilities obey a $T^{-1·2}$ law. This temperature-dependence can be understood on a simple deformation-potential theory. The "knee" in the resistivity temperature curve at $\sim 110°K$ can be accounted for by a transition with increasing temperature from degenerate to classical behavior. While the above results are encouraging, the explanation of the exact origin of the large diamagnetic susceptibility is believed to be as yet unsatisfactory.

VOL. 8 1959

## 1. INTRODUCTION

MANY of the electronic properties of graphite can be correlated with our present knowledge of the energy-band structure. However, some of the main features can be deduced directly from the crystal structure itself. For this reason, it is appropriate first to inspect the crystal lattice, which is shown in Fig. 1. The lattice is made up of hexagonal layers in an *abab* stacking scheme. Each carbon atom has four valence electrons, three of which form tight covalent bonds with the three nearest neighbors in the plane. These electrons are known as $\sigma$ electrons. The fourth electron, or $\pi$ electron, is more loosely bound. The density of $\pi$ electrons is greatest just above and just below a given plane. Thus the first main feature of the lattice is the close proximity (1·42 Å) and tight bonding of atoms in the layers compared to the wide spacing (3·35 Å) and loose bonding between layers. This important feature causes strong anisotropy in the mechanical and electrical properties of graphite. The second characteristic feature of the lattice is the hexagonal symmetry of the layer planes. Consequently, one would expect to see hexagonal symmetry in the properties of graphite; for example, the Brillouin zone is a flat hexagonal cylinder. The third main feature is the stacking scheme in which alternate layers are laterally displaced, producing two types of lattice sites with distinctly different environments. Those atoms designated by *A* in Fig. 1 have neighbors directly above and below in the adjacent planes. On the other hand, those designated by *B* are located above and below the centers of open

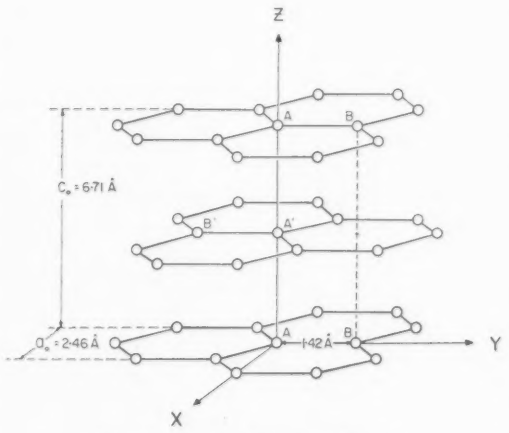


FIG. 1. The graphite crystal lattice.

* National Carbon Company, Division of Union Carbide Corporation.

hexagons in adjacent planes. It will be seen that this type of stacking affects the degree of band overlap.

## 2. DESCRIPTION OF BAND MODEL

Many workers have contributed to the band calculations for graphite, and only a brief résumé can be given here. First of all, the simplest approximation which suggests itself is to neglect the weak interlayer interaction and study the two-dimensional case of a single layer. As it turns out, such an approximation is valid because the interaction between in-plane neighbors is almost one hundred times that between layers. WALLACE* was the first to make such calculations, using the tight-binding method for nearest neighbors. More refined calculations were subsequently made by other workers. The most rigorous were those of CORBATO, which included the effects of neighbors up to ninth order. The composite picture of the band structure is as follows: there is a large energy gap in the $\sigma$-band system, and the two $\pi$-bands touch at the six Brillouin-zone corners, with the touching energy lying within the $\sigma$-band gap. The counting of states is such that the lower $\pi$-band is nearly filled, and the upper $\pi$-band is nearly empty. For an understanding of transport properties, then, attention need only be given to the $\pi$-bands near the zone corners.

The second phase of the band calculation included the interlayer interaction. Though the gross features of the two-dimensional model were unchanged, important changes were produced in the critical regions near the six vertical Brillouin-zone edges. WALLACE also made the first three-dimensional calculation. CARTER and KRUMHANSL discovered a band shift due to the $A$ and $B$ site difference, while JOHNSTON investigated higher-order effects and found extra degeneracies, band overlap, and trigonal warping of the energy surfaces.

In the third phase in the development of the band model, SLONCZEWSKI and WEISS[1] made a group-theoretical, perturbation treatment which laid the foundation for a minimum-parameter general model. The parameters have been determined from such experiments as the de Haas–van Alphen effect,[2] cyclotron resonance,[3] and infrared emissivity.[4]

Fig. 2 shows what is believed to be the best representation of the band structure to date. The variation of energy along a vertical zone edge is shown using a double-zone convention. The curves pass smoothly through the zone boundaries due to the required degeneracy on the horizontal zone faces in hexagonal close-packed lattices. At any value of $k_z$, the lower curve represents the top of the valence band, and the upper curve represents the bottom of the conduction band. The resulting occupation of states is indicated by the cross-hatched region in the figure, where the Fermi level is for perfect graphite.

Though the band model is more general than any special approximation, the essential features of the $E$ versus $k_z$ diagram can be qualitatively related to the interaction between neighboring atoms, as shown in the lattice schematic in the figure. The strongest interaction, between $A$ and $B$ atoms in the plane, dominates the energy variation perpendicular to the zone edge and is represented by $\gamma_0$ (not shown in the figure). The largest interlayer interaction, between $A$ and $A'$ atoms, is represented in the figure by the parameter $\gamma_1$. Next in order would be the interaction between $B$ and $B'$ atoms, but it is cancelled exactly on the zone edge, due to phase relations. The $B$–$B'$ interaction does, however, cause warping of the energy surfaces near the zone edge. Finally, the small next-nearest-layer interaction between $B$ atoms, represented by $\gamma_2$, causes the actual band overlap. The value of $\gamma_1$ (0·14 eV) was derived from the infrared measurements, and the other two parameter values were derived from the de Haas–van Alphen effect.

The anisotropy of the energy surfaces for electrons and holes at a series of energies is shown in Fig. 3. The diagram can be regarded as showing a progression of Fermi surfaces for various doping levels. Each surface is a figure of rotation about a zone edge, as is shown in the diagram for the particular energies $A$ and $B$. In actuality, the axial symmetry is not perfect, but the trigonal warping is appreciable only near the ends of the closed surfaces.

## 3. CORRELATION OF EXPERIMENT WITH THE BAND MODEL

The effects of the three principal features of the band structure (anisotropy, band overlap, and trigonal warping) can be seen in the experimental results. Cyclotron-resonance experiments by GALT

* References to work cited here by author's name only may be found in reference 2.

VOL 8 195

*et al.* indicate that roughly equal numbers of electrons and holes are simultaneously present in graphite at low temperatures. Fine structure in the cyclotron resonance has been interpreted as being due to the trigonal warping.[3] Additional evidence for the band overlap comes from the all the oscillations arise from the same cause, which is the oscillations in the density of states due to the quantization of the carrier energies in the magnetic field. The theory of the susceptibility oscillations was worked out by PEIERLS and LANDAU for free electrons, and generalized to

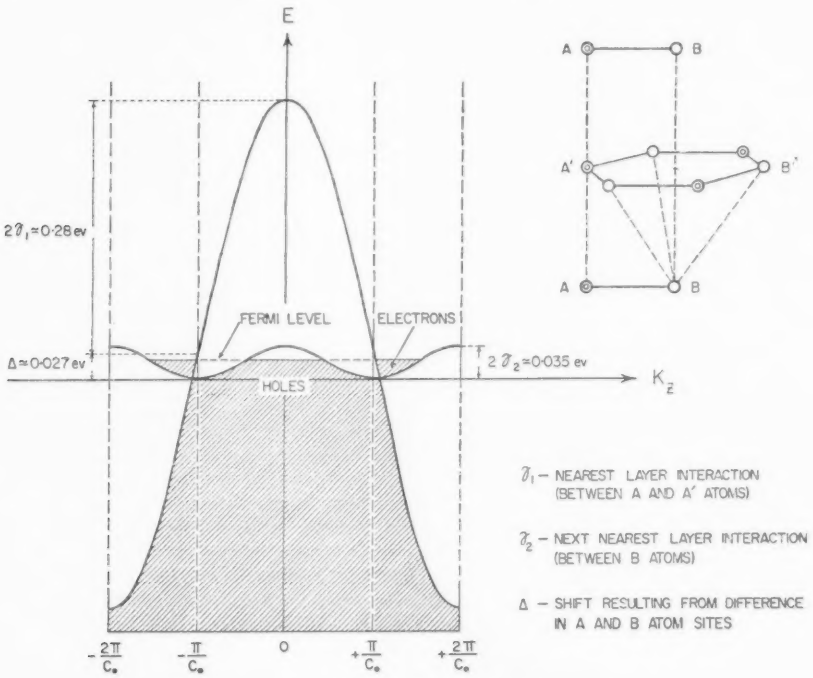


FIG. 2. Energy variation of the $\pi$-bands along a vertical Brillouin-zone edge. A "double-zone" convention is used.

Hall-coefficient change of sign with magnetic field.[5,6] Such a change in sign can only be due to the simultaneous presence of electrons and holes. Also, sharp variations in the Hall coefficient at very low fields indicate the presence of high-mobility minority carriers,[6] which may be identified with the trigonal warping.

De Haas–van Alphen oscillations as a function of magnetic field have been observed in the susceptibility, Hall effect, and magnetoresistance at low temperatures. In the work of BERLINCOURT and STEELE all three properties were measured on the same crystal, and all three exhibited the same period of oscillation. This result establishes that arbitrary band structures by ONSAGER and by LIFSHITZ and KOSEVICH. The susceptibility theory agrees well with experiment and provides a way to obtain information about the Fermi surfaces and effective masses. Attention has been given to the theory of the galvanomagnetic oscillations only more recently by several authors.[7] While these authors do not agree on some details, the interpretation of the period of oscillation is the same as in the susceptibility theory, where it is inversely proportional to the extremum of the Fermi surface cross-section perpendicular to the applied magnetic field.

The de Haas–van Alphen results can be used

to calculate carrier densities. Thus it is possible to make two independent calculations of the carrier densities using the same set of galvanomagnetic data on the same crystal.[6] Table 1 shows such a comparison. From the good agreement of the two methods it can be concluded that the majority carriers are responsible for the de Haas–van Alphen oscillations; a situation which may be unique with graphite. Table 1 also shows a comparison of effective mass values in the layer plane for electrons and holes. Actually, there is a distribution of mass values in graphite; the de Haas–van Alphen effect measures the mass at maximum (or minimum) cross-section of the Fermi surface. The cyclotron-resonance effect, on the other hand, depends upon the entire mass distribution. The values in the table for cyclotron resonance were calculated by NOZIÈRES for comparison with the de Haas–van Alphen values.

Recently,[8] the anisotropy of the Fermi surface has been measured directly by measuring the period of magnetoresistance oscillations as a function of the angle between the magnetic field and the $c_0$-axis. The results are shown in Fig. 4, where they have been fitted by the curve corresponding to an ellipsoid with an anisotropy of 11·6 to 1. The results shown represent an average of the electron and hole periods, giving a mean value for the anisotropy. For comparison, the band model with parameters determined from other experimental data had predicted[2] anisotropies in the range 11 or 13 to 1.

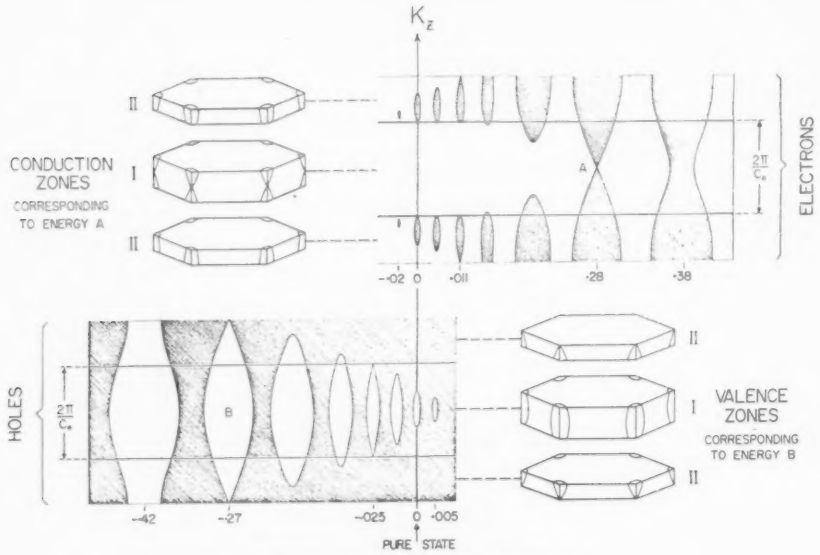


FIG. 3. Surfaces of constant energy in graphite. Cross-sections of the energy surfaces (which are figures of rotation about zone edges) are shown for a number of different energies. The vertical scale has been compressed by a factor of about 2·5. The placement in the zone of the surfaces labeled *A* and *B* is shown (the surfaces have been magnified by about a factor 10 in horizontal dimensions). The same "double-zone" convention is used as in Fig. 2.

## 4. EFFECTS OF SCATTERING

The mobilities of the carriers in graphite are high, as is evidenced by the very large magnetoresistance. (The in-plane resistance increases by a factor of 8000 at 25 kG at 4·2°K.) Furthermore,

*Table* 1. *Correlation of majority carrier densities and effective masses in graphite*

| Method | Carrier density × $10^{18}$ ($cm^{-3}$) | | Sample |
|---|---|---|---|
| | Electrons | Holes | |
| Non-oscillatory galvanomagnetic effects | 3·1 | 2·7 | EP–14 |
| De Haas–van Alphen galvanomagnetic effects | 2·8 | 2·2 | EP–14 |

| Measurement | Effective mass ratio | | Reference |
|---|---|---|---|
| | Electrons | Holes | |
| Susceptibility, de Haas–van Alphen vs. temperature | 0·036 | ~0·07 | SHOENBERG |
| | 0·038 | 0·057 | BERLINCOURT and STEELE; McCLURE |
| Cyclotron resonance | 0·031 | 0·066 | GALT *et al.*; NOZIÈRES |
| Galvanomagnetic effects, de Haas–van Alphen vs. field | 0·030 | 0·060 | SOULE |

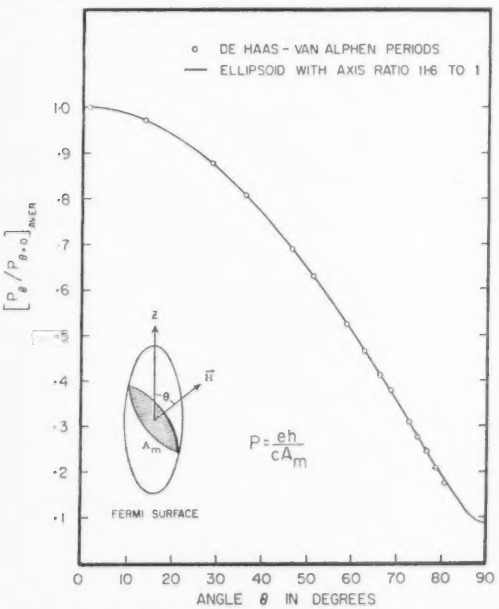


FIG. 4. Dependence of de Haas–van Alphen period (from magnetoresistance measurements) on the angle between the magnetic field and the $c_0$-axis. The ordinate is the ratio of the period at a given angle to the period with the magnetic field parallel to the $c_0$-axis.

large anisotropies are exhibited by the resistivity (100 or 1000 to 1) and magnetoresistivity (130 to 1). Such anisotropies depend both upon the mass anisotropy and the relaxation-time anisotropy. The average mobilities have been determined experimentally from magnetoresistance measurements and are shown in Fig. 5. The temperature-dependence of the mobility follows a $T^{-1.2}$ law in the lattice scattering region above about 25°K for these samples. In contrast to the mobility temperature-dependence, which is smooth, the resistivity curve has a "knee" in the temperature region between 80 and 150°K (see Fig. 5). The degeneracy temperatures of the carriers (as determined by the de Haas–van Alphen effect) are in roughly the same region, being 140°K for electrons and 210°K for holes. Below this temperature region, the carrier concentrations are relatively independent of temperature, but above the region the concentrations increase markedly with temperature, thereby slowing down the rate of increase of resistivity and producing the "knee".

The simplest theory of lattice scattering gives the result that the scattering power (inverse of relaxation time) should be proportional to the

phonon density times the density of states of the carriers. The first factor is proportional to the temperature (above $\sim 50°K$), while the second depends upon the carrier energy. However, the average density of states in the "Fermi surface region" has a weak temperature-dependence which can be roughly represented by $T^{\frac{1}{4}}$ (the same factor would be constant for a good metal and would be proportional to $T^{\frac{1}{4}}$ for an ideal semiconductor). Thus, the simple theory gives about the same temperature-dependence for the relaxation time as is observed in the experimentally determined mobilities. The theoretical fit of the resistivity is shown in Fig. 5. Besides the band parameters, the curve depends upon three adjustable parameters, the Fermi energy and the deformation-potential constant for electrons and that for holes. The degree of agreement shown in the figure serves as further substantiation of the band model.

The major unexplained phenomena which depends only upon the band structure is the large steady diamagnetic susceptibility.[9] The Landau–Peierls formula fails for touching bands, and as yet no rigorous calculation for the present band model has been reported. It is worth noting that the "degeneracy temperature" deduced from the susceptibility is about 400–500°K, much higher than the degeneracy temperature deduced from the conductivity. Thus, the susceptibility "degeneracy temperature" must correspond to some other feature of the band structure than the Fermi energy. In any case, the extent of the overall correlation with experiment cited above gives us confidence that the band model is essentially correct.

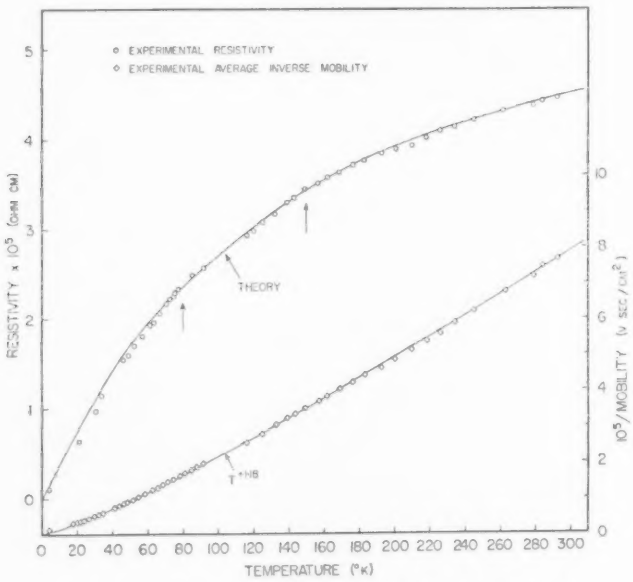
EXPERIMENTAL RESISTIVITY
EXPERIMENTAL AVERAGE INVERSE MOBILITY
THEORY
$T^{+N\beta}$
RESISTIVITY x $10^5$ (ohm cm)
$10^5$/MOBILITY (v sec/cm$^2$)
TEMPERATURE (°K)
0 20 40 60 80 100 120 140 160 180 200 220 240 260 280 300
0 1 2 3 4 5
0 2 4 6 8 10

FIG. 5. Temperature-dependence of electrical resistivity and average mobility (derived from magnetoresistance measurements) for graphite. Note that the inverse of the mobility is plotted, and that the zeros of the two scales do not coincide. The arrows mark the breaks in the resistivity curve.

**REFERENCES**

1. SLONCZEWSKI J. C. and WEISS P. R., *Phys. Rev.* **109,** 272 (1958).
2. MCCLURE I. W., *Phys. Rev.* **108,** 612 (1957).
3. NOZIÈRES P., *Phys. Rev.* **109,** 1510 (1958).
4. BOYLE W. S. and NOZIÈRES P., *Phys. Rev.* (to be published).
5. KINCHIN G. H., *Proc. Roy. Soc.* **A217,** 9 (1953).
6. SOULE D. E., submitted to *Phys. Rev.*
7. ZILBERMAN G. E., *Zh. eksp. teor. fiz.* **29,** 762 (1955). LIFSHITZ I. M. and KOSEVICH A. M., *J. Phys. Chem. Solids* **4,** 1 (1958). ARGYRES P. N., *Phys. Rev.* **109,** 1115 (1958).
8. SOULE D. E., *Bull. Amer. Phys. Soc.* **3,** 105 (1958).
9. See HAERING R. R. and WALLACE P. R., *J. Phys. Chem. Solids* **3,** 253 (1957); MASE S., *J. Phys. Soc. Japan* **13,** 563 (1958).


*J. Phys. Chem. Solids* Pergamon Press 1959. Vol. 8. pp. 35–37. Printed in Great Britain

VOL. 8 1959

B.4

# CALCULATION OF ELECTRONIC ENERGY BANDS IN ZnS


JOSEPH L. BIRMAN

Research Laboratories, Sylvania Electric Products Inc., Bayside, New York


INTEREST in the nature of the band structure of ZnS arises from several sources. There is a considerable amount of empirical information on the behavior of luminescent (phosphor) ZnS which has been correlated, with varying degrees of success, by means of the SCHON-KLASENS[1] band model; this simple model requires quantitative elaboration. There is also the electroluminescent activity of the ZnS systems,[2] which leads one to inquire whether any peculiarity of band structure may underlie the susceptibility of ZnS as a favorable base material for this process. In addition, ZnS may be a prototype of materials with mixed covalent–ionic binding (e.g. ZnSe, CdS, &c.), so that an understanding of its band structure may give insight into that of the related materials. Finally there is the challenging problem of the effect upon the band structure of structural defects which commonly occur in synthetic ZnS crystals.[3] Here, too, ZnS is a prototype exhibiting faulting (random and periodic) and mixed crystals (regions of zinc blende (ZB) twinned on regions of wurtzite (W)), also shown by other materials (SiC, $CdI_2$, &c.).[4]

Consequently an attempt has been made to provide some answers to the questions: (1) Is the magnitude of the effective charge a satisfactory measure of the nature of the bond in ZnS? (2) Can the polar properties of ZnS (and other materials with related structures) lead to an understanding of how to parameterize the bond? (3) Making reasonable assumptions about the bond, what are the calculated band structures for the two ideal modifications ZB and W? (4) What relation is there between the ZB and W band structures, and also between the band structures of these ideal modifications and that of the *actual* faulted and twinned crystals?

It is not possible to characterize the ZnS bond unambiguously by means of a single number —"effective charge."[5] On the other hand, on the basis of simple theories, the polar properties may yield meaningful bond parameters (bond moment, bond polarizability, &c.).[6] An accurate energy-band calculation[7] has been carried out by the cellular method at points of high symmetry in the Jones Zone of ZB (points $\Gamma$, $A$, X) and W (points $\Gamma$, $\Gamma'$, $K$, $K'$). The calculation* indicates normal order of states in valence and conduction bands (*s*-like states lowest, *p*-like states higher) and

* As of Aug. 1958.

minimum energy-band separations (optical gap) at the center of the zone in both modifications, and the optical gap of ZB some tenths of a volt smaller than that of W. Using the tight-binding method[8] as a qualitative guide (it could *not* be used as a quantitative interpolation method), it is found that for **k** vectors along the "polar" zone directions ($\Gamma$–$A$ in ZB; $\Gamma$–$A$–$\Gamma'$ in W) states in wurtzite may be considered as derived from corresponding (same $|\mathbf{k}|$) zinc blende states by means of a perturbation which takes into account the lower site

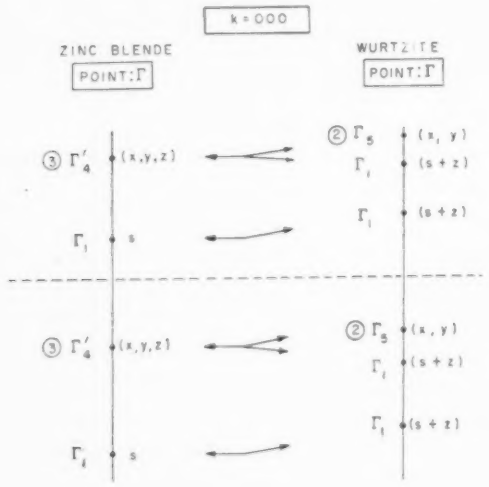


FIG. 1. Correspondence between ZB and W states at $\mathbf{k} = 000$. The atomic (tight-binding) correspondence of each state is shown in parentheses, the degeneracy in the circle. This diagram illustrates the splitting and shifting of ZB states due to the lower W potential symmetry.

(potential) symmetry: $C_{3v}$ in wurtzite, $T_d$ in zinc blende. This "crystallographic splitting" of corresponding states depends upon **k**, and diminishes as **k** approaches the zone edges, that is there are *smaller* energy differences between corresponding states at the zone edges. Correspondence between states in the zones, in two directions perpendicular to the polar directions ($\Gamma$–$M$ and $\Gamma$–$K$, in both ZB and W) has also been examined by the tight-binding method.

Now consider a model mixed crystal consisting of ZB regions twinned on, and alternating with, W regions. For electron (or hole) propagation *along* the polar direction, an energy barrier exists at each twin plane interface region as a result of two effects. There is the barrier due to the **k**-dependent

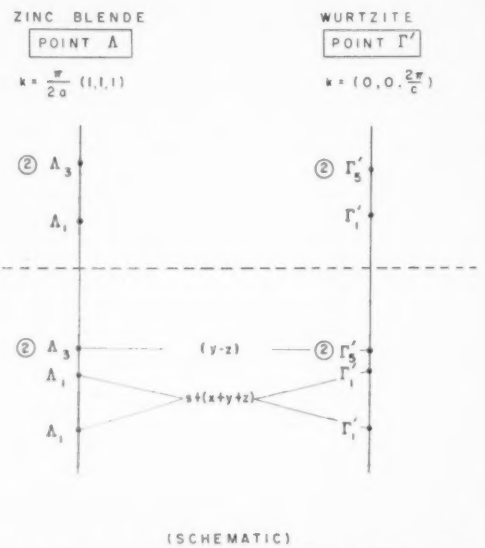


FIG. 2. Correspondence between ZB and W states for **k** at the zone edge in the polar direction. The shift of corresponding states is smaller than at $\mathbf{k} = 000$. In both Figs. 1 and 2 the order of states is that given by the current results of the cellular calculation (Aug. 1958).

"crystallographic splitting" or corresponding states. Otherwise stated, we may preserve a given **k** as a "good" crystal quantum number on both ZB and W sides of the twin plane, but at the expense of an energy discontinuity. In addition an energy barrier (discontinuity) exists due to the locked-in strain, to which is coupled a locked-in polarization, in the twin plane region. Consider the case of the rotation twin in ZB: the environment of atoms in this region is W-like, i.e. corresponds to a three-layer inclusion of W in ZB. Since W is pyroelectric, this dipole layer of W is equivalent to a plane double layer of charge perpendicular to the polar direction and hence gives rise to a discontinuity of electrostatic potential[9] or barrier in this direction. Electron propagation perpendicular to the polar direction may occur (i) within the barrier regions, (ii) within ZB regions, and (iii) within W regions; presumably all occur simultaneously in an experiment on an actual crystal. The reported anisotropy of conductivity and electroluminescence in ZnS

crystals[10] is probably related to the existence of these barriers, while transverse conductivity may be related to carrier transport in regions (i), (ii), (iii). It is not possible at this time to make a quantitative analysis of the cited data due to still uncertain

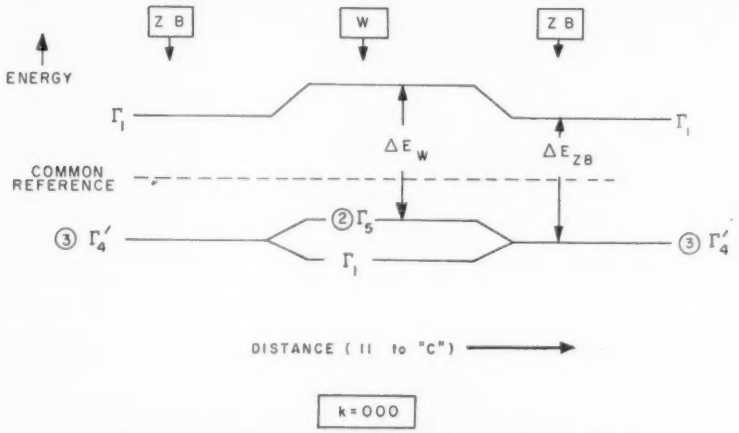


FIG. 3. Illustration of the barrier in a mixed crystal due to change in crystal symmetry. The barrier heights, as well as $\Delta E_W$ and $\Delta E_{2B}$ depend on **k**.

contact effects. In addition, the mixed crystal may be expected to show some evidence of the simultaneous existence of both ZB and W gaps (for example in edge absorption or emission); perhaps the wavelength-dependence of the recently reported photovoltage in unactivated ZnS may relate to this.[11] For a model crystal with random faulting, the average crystal band gap will depend upon the probability of faulting (the latter affects the magnitude of the hexagonal part of the potential at a site).

This work is continuing and will later be reported in detail.

## REFERENCES

1. See SCHON M. *Physica* **20,** 930 (1954) and literature cited therein; also KLICK C. C. and SCHULMAN J. H. *Solid State Physics* (Ed. F. SEITZ and D. TURNBULL), Vol. 5. p. 157. Academic Press, New York (1957).
2. A review is given and further literature cited by PIPER W. W. and WILLIAMS F. E. *Solid State Physics* (Ed. F. SEITZ and D. TURNBULL) Vol. 6. Academic Press, New York (1958).
3. AMINOFF G. and BROOME A. *Z. Krist.* **80,** 355 (1931). MUELLER H. *Neues Jb. Miner. Abh.* **84,** 1, 43 (1952). STROCK L. W. and BROPHY V. A. *Amer. Min.* **40** 94 (1955).
4. MITCHELL R. S. *Z. Krist.* **109,** 1 (1957).
5. BIRMAN J. L. *Phys. Rev.* **109,** 810 (1957).
6. A simple theory of the piezoelectric effect has been discussed by BIRMAN J. L. *Phys. Rev.* **111,** 1510 (1958) from which bond moments might be obtained.
7. Preliminary ZB results are given by SHAKIN C. and BIRMAN J. L. *Phys. Rev.* **109,** 818 (1957). More accurate results are to be published.
8. SLATER I. C. and KOSTER G. *Phys. Rev.* **94,** 1498 (1954); BIRMAN J. L. to be published.
9. STRATTON J. A. *Electromagnetic Theory* p. 189. McGraw-Hill, New York (1941).
10. ZALM P. *Phillips Res. Rep.* **11,** 398 (1956). LEMPICKI A., FRANKL D. and BROPHY V. *Phys. Rev.* **107,** 1238 (1957) and other references cited therein.
11. CHEROFF G. and KELLER S. *Phys. Rev.* **111,** 98 (1958). LEMPICKI A. Private communication.

*J. Phys. Chem. Solids* Pergamon Press 1959. Vol. 8. pp. 38–44. Printed in Great Britain

# THE SEMI-EMPIRICAL APPROACH TO BAND STRUCTURE

B.5

EVAN O. KANE

General Electric Research Laboratory, Schenectady, New York

**Abstract**—A review of the **k·p** approach to band structure will be given. An effective Hamiltonian for the cell-periodic part of the Bloch function consists of diagonal elements corresponding to the band energies at $\mathbf{k}=0$ and off diagonal elements of $(h/m)$ **k·p** connecting the bands and causing mutual repulsion unless symmetry forbids interaction. When $(h/m)$ **k·p** is small compared to the energy separation between bands, second order perturbation theory can be used to obtain effective masses. $E$ vs. $k^2$ expressions involve a small number of parameters which are determined by experiments such as cyclotron resonance. Perturbation theory can be improved upon by treating strongly interacting bands exactly and subsequently handling weak interactions by perturbation theory. Such a procedure inevitably increases the number of parameters to be determined. Optical band gap measurements are needed for this extension. In addition, absolute optical absorption determines momentum matrix elements between bands. The feasibility of using such an approach to determine band structure empirically throughout the zone will be examined. In addition to **k·p**, there are less important **k** dependent terms which must be considered in some cases. The linear **k** terms at $\mathbf{k}=0$ in the III–V compounds are an example. The inclusion of exchange terms in the one particle Schröedinger equation introduces modifications in the above treatment. The interband matrix elements determining the effective mass contain contributions from both momentum and exchange terms, whereas optical absorption involves only the momentum matrix element. Exchange terms contribute *first* order perturbation corrections to the effective mass. Estimates of exchange effects indicate that they are small. The symmetry approach of LUTTINGER may serve to indicate inadequacies of the one particle viewpoint.

VOL
8
195

## INTRODUCTION

BEFORE the advent of cyclotron resonance most information about band structure was based on calculations from first principles. The obvious advantages of such calculations are partly offset by two drawbacks, one theoretical and one practical.

The theoretical drawback is that one does not yet know how to formulate the "best" one-particle Hamiltonian, $H_0$, whose eigenvalues and eigenfunctions describe the solid.*

The practical drawback to direct energy-band calculations is the large amount of labor required to achieve self-consistency, assuming that a model for the Hamiltonian has been chosen.

The above difficulties make it desirable to deduce as much information about band structure as possible directly from experiment. A useful tool in this process is the **k·p** representation of the Hamiltonian. We will first describe the **k·p** representation in its simplest form and then discuss the effects contributed by spin-orbit interaction and exchange.

The **k·p** matrix has been largely treated by perturbation theory. The problems of extending this approach will be presented. Finally, the problem of the validity of the one-electron approximation will be touched on briefly.

We limit ourselves throughout to the task of describing the energy versus **k** curves for a solid. We will not attempt to discuss the important problems of effective-mass theory[1] which deal with how to use this information to calculate impurity levels, energy states in magnetic fields, and other interesting properties.

## k·p REPRESENTATION

A one-particle Schrödinger equation is assumed:

$$H_0\psi_{n\mathbf{k}} = E_{n\mathbf{k}}\psi_{n\mathbf{k}} \tag{1}$$

$$H_0 = (\mathbf{p}^2/2m)+V(\mathbf{r}) \tag{2}$$

* The "best" one-particle Hamiltonian presumably depends on what is to be calculated. The Hartree–Fock equation gives the lowest total energy to be obtained from a single Slater determinant, but need not give the best one-particle Hamiltonian for calculating $E$ versus **k** for an electron or hole.

where $V(\mathbf{r})$ has lattice periodicity. The band index $n$ is needed, since we restrict $\mathbf{k}$ to the first Brillouin zone. BLOCH showed in 1928 that $\psi_{\mathbf{k}}$ can be written in the form

$$\psi_{n\mathbf{k}} = e^{i\mathbf{k}\cdot\mathbf{r}} u_{n\mathbf{k}}(\mathbf{r}). \tag{3}$$

Substituting equation (3) in equation (1) gives the following equation for $u_{\mathbf{k}}$:

$$\{H_0+(\hbar/m)\mathbf{k}\cdot\mathbf{p}+\hbar^2\mathbf{k}^2/2m\}u_{n\mathbf{k}} = E_{n\mathbf{k}}u_{n\mathbf{k}} \tag{4}$$

The two terms involving $\mathbf{k}$ which have been added to the Hamiltonian, $H_0$, clearly result from operating on $e^{i\mathbf{k}\cdot\mathbf{r}}$ with $\mathbf{p}^2/2m$. For any given $\mathbf{k}$ the eigenfunctions of equation (4) form a complete set of cell-periodic functions. This set may be used as the basis for a representation of the Hamiltonian.

Various points $\mathbf{k}$ have proved useful in providing representations, but for the sake of simplicity we shall consider the case $\mathbf{k} = 0$, which has received the most attention.

Using the $\mathbf{k} = 0$ representation, the operator $H_0$ of equation (4) is diagonal with eigenvalues equal to the energy of the bands at $\mathbf{k} = 0$. The operator $(\hbar/m)\ \mathbf{k}\cdot\mathbf{p}$ provides only off-diagonal elements, since $\mathbf{P}_{nn} = 0$ due to the reality of $H_0$.[2]* The number of matrix elements can be reduced to an essential minimum by the use of group theory.[3,4] Group theory also gives the degeneracies of the bands at symmetry points such as $\mathbf{k} = 0$.

The band structure in the vicinity of $\mathbf{k} = 0$ may be investigated with the aid of perturbation theory. This method was used by SEITZ[5] in 1935 in calculating the band structure of lithium. To lowest order the bands are parabolas centred at $\mathbf{k} = 0$,† as given by the formula:

$$E_n(\mathbf{k}) = E_n(0)+\frac{\hbar^2\mathbf{k}^2}{2m}+\sum_{n'\neq n}\frac{(\mathbf{k}\cdot\mathbf{p}_{nn'}\mathbf{k}\cdot\mathbf{p}_{n'n})}{E_n-E_{n'}}. \tag{5}$$

When the bands are degenerate, the expressions for energy versus $\mathbf{k}$ become more complicated. The energies are then given by the eigenvalues of the matrix

$$H_{ni,nj} = \left\{E_n(0)+\frac{\hbar^2\mathbf{k}^2}{2m}\right\}\delta_{ij}+\sum_{n'\neq n}\frac{\mathbf{k}\cdot\mathbf{p}_{ni,n'}\mathbf{k}\cdot\mathbf{p}_{n',nj}}{E_n-E_{n'}}, \tag{6}$$

where $i$ and $j$ represent degenerate eigenfunctions of band $n$. These energy surfaces were discussed by SHOCKLEY[6] in 1950. SHOCKLEY also indicated how symmetry could be used to minimize the number of parameters in the energy expressions.

For many purposes one is not interested in the explicit form of equations (5) and (6). Equation (5) may be written more simply as:

$$E_n(\mathbf{k}) = E_n(0)+\hbar^2\left(\frac{\mathbf{k}_x^2}{2m_x^*}+\frac{\mathbf{k}_y^2}{2m_y^*}+\frac{\mathbf{k}_z^2}{2m_z^*}\right) \tag{7}$$

The quantities $m_x^*$, $m_y^*$, $m_z^*$ are then to be determined by experiment. Symmetry requires $m_x^* = m_y^* = m_z^*$ in a solid having cubic symmetry. Equation (6) may also be simplified in a similar manner as SHOCKLEY has shown.

## SPIN-ORBIT INTERACTION

The application of the above results to germanium and silicon had to await the cyclotron-resonance measurements which were begun at Berkeley[3] and Lincoln Labs[7] in 1953. The effects of spin-orbit interaction are important in the interpretation of the experimental data.

The spin-orbit energy, $H_{s.o.}$ is given by:

$$H_{s.o.} = (\tfrac{1}{2}m^2c^2)[\nabla V\times\mathbf{p}]\cdot\mathbf{s}. \tag{8}$$

This term must be added to the Hamiltonian $H_0$ of equation (2). A further term $\mathcal{H}_{s.o.}$ should be added to equation (4) for $u_{\mathbf{k}}$, namely

$$\mathcal{H}_{s.o.} = (\hbar/2m^2c^2)[\nabla V\times\mathbf{k}]\cdot\mathbf{s}. \tag{9}$$

Since the main contribution to the spin-orbit interaction occurs deep in the atomic core where $\mathbf{p} \gg \hbar\mathbf{k}$, it seems adequate for most applications to neglect the term $\mathcal{H}_{s.o.}$ in comparsion with $H_{s.o.}$

The preponderant importance of the core also permits us to write equation (8) in the more familiar atomic form:

$$H_{s.o.} = \frac{1}{2m^2c^2}\cdot\frac{1}{r}\cdot\frac{dV}{dr}\mathbf{l}\cdot\mathbf{s} \tag{10}$$

Spin-orbit effects in solids are of the same order of magnitude as in free atoms. $H_{s.o.}$ tends to be increased

* For a non-degenerate band this may be seen very simply. Since $H_0$ is real, the functions $u_n(\mathbf{k} = 0)$ may be taken to be real. Hence $\mathbf{p}_{nn} = \langle u_n|-i\hbar\nabla|u_n\rangle = 0$, since $\mathbf{p}_{nn}$ must be real.

† This statement is no longer true in crystals lacking inversion symmetry when spin-orbit effects are included.

by the higher electron density in the solid and decreased by the admixture of higher angular momentum terms which keep the electron away from the nucleus. In germanium the net effect is an increase from 0·2 eV in the atom to 0·3 eV[8] in the solid for the holes at $\mathbf{k} = 0$. The difference is small enough that spin-orbit energy determinations may be useful in investigating the ionicity of III–V[9] and other appropriate compounds.

In principle, one could consider a set of basic functions, $u_n(\mathbf{k} = 0)$ defined as eigenfunctions of the operator $H_0 + H_{s.o.}$ In cases where the spin-orbit energy is less than the appropriate $\mathbf{k} = 0$ energy gaps, it is sufficient to consider a basis defined by $H_0$ and treat $H_{s.o.}$ as a perturbation. This latter approach is simpler and provides more information. This was the method adopted by ADAMS,[3] DRESSELHAUS *et al.*[3] and OVERHAUSER.[10]

To illustrate the validity of this approach for germanium, we refer to Fig. 1, which shows the energy bands at $\mathbf{k} = 0$ as computed by HERMAN. Of the bands shown, the upper $\Gamma_{25}^+$ band is the only one which interacts via $H_{s.o.}$ with the $\Gamma_{25}^+$ valence band and thereby mixes the non-degenerate eigenfunctions of $H_0$. Since the appropriate energy gap is thus ~17 eV, whereas the spin-orbit energy is only 0·3 eV, the approximation is quite good. The approximation is even better than indicated, since the upper $\Gamma_{25}^+$ band presumably has a large amount of *d*-function and higher-angular-momentum components which have small spin-orbit energies.

In crystals lacking inversion symmetry, spin-orbit effects give rise to linear $\mathbf{k}$-terms [2,11] which have the effect of shifting the band minima and maxima slightly away from $\mathbf{k} = 0$. Linear terms arise either from the operator $\mathcal{H}_{s.o.}$ of equation (9) or by a "mixed" second-order perturbation term involving the operators $H_{s.o.}$ of equation (8) and $(\hbar/m)\,\mathbf{k}\cdot\mathbf{p}$.[12] Terms of this sort may be important in the III–V compounds. Rough theoretical estimates[2,11] indicate that the linear terms in InSb displace the valence-band maximum about $10^{-4}$ eV above the energy at $\mathbf{k} = 0$. A good experimental determination of this number has not yet been made. In general, spin-orbit effects become increasingly important going down or to the right in the Periodic Table.

## EXCHANGE

The contribution of exchange to the $\mathbf{k}\cdot\mathbf{p}$ formalism was noted by HERRING[13] in 1937. More recently, the problem has been discussed by the present author [14] and by PHILLIPS.[15] The Hamiltonian with exchange is given by:

$$H_{ox} = (\mathbf{p}^2/2m) + V + Z, \tag{10}$$

where $Z$ is the self-consistent exchange operator

$$Z(\mathbf{r}_1, \mathbf{r}_2) = -e^2 \sum_i \frac{\psi_i(\mathbf{r}_1)\psi_i^*(\mathbf{r}_2)}{\mathbf{r}_{12}} \tag{11}$$

and

$$Z\psi = \int Z(\mathbf{r}_1, \mathbf{r}_2)\psi(\mathbf{r}_2)\mathrm{d}\mathbf{r}_2. \tag{12}$$

The Schrödinger equation for $u_\mathbf{k}$ becomes

$$\{e^{-i\mathbf{k}\cdot\mathbf{r}} H_{ox} e^{i\mathbf{k}\cdot\mathbf{r}}\} u_\mathbf{k} = E_\mathbf{k} u_\mathbf{k}. \tag{13}$$

If the exponential factors in equation (13) are expanded, the following expression may be derived:

$$\left\{H_{ox} + \sum_\mu i\mathbf{k}^\mu [H_{ox}, \mathbf{r}^\mu] + \sum_{\mu,\nu} \frac{i^2}{2!}\mathbf{k}^\mu\mathbf{k}^\nu [[H_{ox}, \mathbf{r}^\mu], \mathbf{r}^\nu] + \right.$$

$$\left. + \sum_{\mu,\nu,\lambda} \frac{i^3}{3!}\mathbf{k}^\mu\mathbf{k}^\nu\mathbf{k}^\lambda [[[H_{ox}, \mathbf{r}^\mu], \mathbf{r}^\nu], \mathbf{r}^\nu] + \ldots\right\} u_\mathbf{k} = E_\mathbf{k} u_\mathbf{k}, \tag{14}$$

where

$$i[H_{ox}, \mathbf{r}^\mu] = (\hbar/m)\mathbf{p}^\mu + i\int (\mathbf{r}_2{}^\mu - \mathbf{r}_1{}^\mu) Z(\mathbf{r}_1, \mathbf{r}_2) d\mathbf{r}_2 \tag{15}$$

$$i^2[[H_{ox}, \mathbf{r}^\mu], \mathbf{r}^\nu] = (\hbar^2/m)\delta^{\mu\nu} + i^2\int (\mathbf{r}_2{}^\mu - \mathbf{r}_1{}^\nu)(\mathbf{r}_2{}^\nu - \mathbf{r}_1{}^\nu) Z(\mathbf{r}_1, \mathbf{r}_2) d\mathbf{r}_2 \tag{16}$$

$$i^3[[[H_{ox}, \mathbf{r}^\mu], \mathbf{r}^\nu], \mathbf{r}^\lambda] = i^3[[[Z, \mathbf{r}^\mu], \mathbf{r}^\nu], \mathbf{r}^\lambda] \tag{17}$$

All commutators higher than the second result from $Z$ alone. It may be noted that equation (14) remains valid for the most general one-electron operator $H_0$. Only the evaluation of the commutators depends on the terms considered in the Hamiltonian. For this reason the following

discussion of the effects of exchange on the $\mathbf{k}\cdot\mathbf{p}$ representation is actually valid for the most general possible one-electron operator. We can estimate the effects of exchange from first principles, but we have no way at present of estimating the contribution of more general one-electron operators which might conceivably be needed to take account of correlation effects as accurately as is possible for a one-particle theory. The fact that the experimental information available so far indicates that the effects we shall discuss are small is thus of more intrinsic interest than it would be if it merely confirmed the estimates made of the exchange effects. Since $i[H_{ox}, \mathbf{r}]$ has the same symmetry as $\mathbf{p}$ under the operations which leave $H_{ox}$ unchanged, any work in which $i[H_{ox}, \mathbf{r}]$ is treated as an unknown constant subject only to symmetry restrictions is obviously not affected by the introduction of exchange into this term. The contribution of exchange may be estimated if $i[H_{ox}, \mathbf{r}]$ is evaluated theoretically.[15]

The term $i^2[[H_{ox}, \mathbf{r}^\mu], \mathbf{r}^\nu]_{nn}$ may exhibit effects due to exchange. In the absence of exchange this term is a universal constant, $(\hbar^2/m)$, but with exchange it is a function of the crystal and the band in question. When general expressions with arbitrary constants such as equation (7) are employed, all $\mathbf{k}^2$ terms are automatically included. However, when comparison is made between the mass constants of different bands, effects due to the second-order commutator might be observed, as can be seen from the following argument. The mutual "repulsion" of two bands $n$ and $n'$ connected by a matrix element $i[H_{ox}, \mathbf{r}^\mu]_{nn'}$ gives rise to an equal and opposite contribution to the curvature of the bands. If the two bands are very close together, so that interactions with other bands can be neglected, the mass of band $n$ could be inferred from a measurement of the mass in band $n'$. A large exchange effect due to the term $i^2[[H_{ox}, \mathbf{r}^\mu], \mathbf{r}^\nu]_{nn}$ would spoil this relationship. A recent determination of the conduction-band mass at $\mathbf{k} = 0$ in germanium has provided a test of this relationship.[17] No measurable effect from the second-order commutator was found within the accuracy of measurement ($\sim 2$ per cent). A large second-order commutator would also contribute a large parabolic term to energy versus $\mathbf{k}$ and invalidate the author's calculations [12] of non-parabolic effects in $n$-type InSb.

Rough estimates of the effect of exchange have been made, using a Slater exchange hole and taking the expansion of $\psi(\mathbf{r}_2)$ about $\mathbf{r}_1$

$$\psi(\mathbf{r}_2) = \psi(\mathbf{r}_1) + (\mathbf{r}_2 - \mathbf{r}_1) \cdot \nabla\psi(\mathbf{r}_1) \qquad (18)$$

to lowest non-vanishing order.[14] These estimates indicated a 60 per cent increase in the interband matrix elements due to exchange and a contribution of $+0{\cdot}6$ reciprocal mass units to the reciprocal effective mass from the second-order commutator $i^2[[Z, \mathbf{r}^\mu], \mathbf{r}^\nu]$ for the case of germanium. In this crude approximation the results did not depend on the band considered.

PHILLIPS[15] has estimated a 30 per cent contribution from exchange to the commutator $i[H_{ox}, \mathbf{r}]$ on the basis of theoretical estimates of the momentum matrix elements for germanium.

The $n^{\text{th}}$ term of equation (14) is of the order $(\mathbf{k}\mathbf{r}_0)^n H_{ox}/n!$ where $\mathbf{r}_0$ is the radius of the exchange hole, 1·4Å for germanium. At the zone edge $\mathbf{k}\mathbf{r}_0 \sim 1$; hence the terms considered above may not be adequate for an accurate description of the bands, though they should still give a reasonable approximation even out to the zone boundary.

## EXTENSION OF PERTURBATION THEORY

The straightforward perturbation-theory treatment of the $(\hbar/m)\ \mathbf{k}\cdot\mathbf{p}$ matrix is limited to a small region of $\mathbf{k}$-space. When the off-diagonal elements become of the order of the diagonal separations (band gaps at $\mathbf{k} = 0$), the perturbation series no longer converges. In cases where the band gap is unusually small, as in InSb, the limitations of perturbation theory can be partially circumvented by treating the interactions between closely adjacent bands exactly and treating more distant bands by perturbation theory.[12]

The importance of non-parabolic effects in InSb was first inferred from experiment by HROSTOWSKI *et al.*[18] and later by other workers.[19] EHRENREICH *et al.*[20, 21] have found satisfactory agreement with experiment for a number of phenomena, using the non-parabolic bands given by the $\mathbf{k}\cdot\mathbf{p}$ method.

In principle, of course, the greater the number of bands which are treated exactly, the greater the region of $\mathbf{k}$-space which can be described correctly. The practical difficulty is that the number of unknown parameters increases very

rapidly with the number of bands, and many accurate experimental results and much labor are needed to fit the parameters.

An attempt has been made to extend the approach used in InSb to cover the entire Brillouin zone for the case of germanium. In this calculation the seven lowest bands of Fig. 1 are treated exactly and the effect of the eighth band is estimated by perturbation theory. More distant bands, not shown in Fig. 1, are also neglected.

The seven bands considered give a total of fourteen parameters; 6 band energies at $\mathbf{k} = 0$ and 8 momentum matrix elements. The most reliable experimental information consists of 3 mass constants for holes at $\mathbf{k} = 0$;[3] 2 mass constants for electrons at $\mathbf{k} = (\frac{1}{2}, \frac{1}{2}, \frac{1}{2})$[3] the energies of the conduction band minima at $\mathbf{k} = 0$,[16] $\mathbf{k} = (\frac{1}{2}, \frac{1}{2}, \frac{1}{2})$,[16] and $\mathbf{k} = (x, 0, 0)$.[22] ($x$ represents the unknown position of the minimum in the (100) direction.) This gives 8 experimental numbers, and hence 6 additional conditions are needed to determine the 14 parameters of the theory. The additional conditions may be obtained by requiring the energy to be periodic and continuous in $\mathbf{k}$-space, a condition which is not automatically satisfied by the $\mathbf{k}\cdot\mathbf{p}$ representation. It is not clear how many periodicity conditions may meaningfully be installed. The number should be kept as low as possible, since these conditions are entirely independent of the potential. The most appropriate conditions are those for the lower bands, since they are furthest from the bands which have been ignored. Periodicity conditions for bands 1, 2, and 3 in both the (100) and (111) directions were chosen to determine the remaining 6 parameters.

The matrix element of $(\hbar/m)\,\mathbf{k}\cdot\mathbf{p}$ between bands 2 and 3 evaluated at the zone edge in the (100) direction is 11 eV. If the matrix element between bands 8 and 2 is assumed to be half as large as the matrix element between bands 2 and 3, the perturbation correction to the energy of band 2 due to band 8 would be $\sim 1$ eV. Since the actual corrections may be even larger than this, it would be very desirable to supplement the $\mathbf{k}\cdot\mathbf{p}$ method with reliable estimates of energies and matrix elements for higher and lower bands. A less satisfactory alternative would be to estimate contributions from neglected bands by requiring more periodicity conditions to be satisfied.

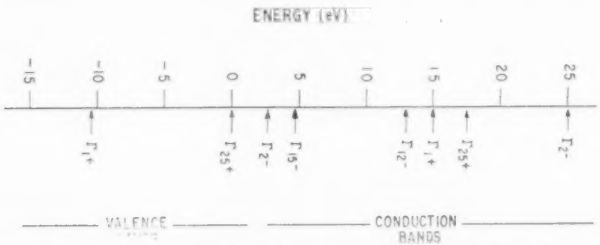


FIG. 1. Energy levels at $\mathbf{k} = 0$ based on calculations by F. HERMAN. Reproduced from DRESSELHAUS *et al.*[3]

The effects of exchange due to the term $i[Z, \mathbf{r}]_{nn'}$ are automatically included in the above treatment. The second-order term $i^2[[Z, \mathbf{r}^\mu], \mathbf{r}^\mu]_{nn'}$ as well as higher terms have not been included. To do so would require the introduction of additional undetermined parameters. If the second-order term contributes 0·25 reciprocal mass units, it will give a correction $\sim$1 eV at the zone edge. A method of undetermined parameters will generally partly compensate for the corrections discussed above.

The problem of fitting 14 parameters appears to be tractable. Four parameters may be evaluated immediately from the experimental data at $\mathbf{k} = 0$. The remaining 10 parameters are to be determined by solving the secular equations for the (111) and (100) direction and using periodicity conditions as well as experimental data.

The largest secular equation is fourth order for the (100) direction and sixth order for the (111) direction. In a general direction the secular equation would be fourteenth order; fortunately, only the (111) and (100) directions enter into the parameter-fitting problem. The numerical technique

adopted requires a reasonable starting point and iterative improvement by linear extrapolation.

There are other methods by which the extensive experimental information on germanium may be used to deduce the band structure. ALLEN[23] has discussed a method of determining parameters in an OPW treatment. More recently PHILLIPS[24] has fitted the experimental data for germanium and silicon, using a "pseudopotential" with remarkably few parameters. The limitations of this method remain to be investigated.

## MANY-PARTICLE VIEWPOINT

The discussion in this paper has been based entirely on the one-particle approximation. KOHN[25] has demonstrated that in some cases a rigorous many-particle treatment leads to the same results as were previously obtained by using the one-particle approximation. KOHN's treatment depends on the following facts.

(1) The excited states of a perfect insulator are at a finite energy (equal to the band gap of the one-electron theory) above the ground state.

(2) Because of translational symmetry, the many-electron states may be characterized by a $\mathbf{k}$ vector, so that one can still speak of energy versus $\mathbf{k}$ curves.

The excited states of interest to semiconductors are the extrema ($\partial E/\partial \mathbf{k} = 0$). If the energy is expanded to second order in $\mathbf{k}$, symmetry arguments may be used to reduce the number of constants. General expressions for energy versus $\mathbf{k}$ such as that given in equation (7) can be obtained without recourse to the one-particle theory.

The interpretation of the constants in terms of perturbation contributions from higher bands, as shown in equation (5), is, of course, specific to the one-particle approach.

KOHN's treatment derives the effective-mass equation for an impurity center and shows that the dielectric constant results from the theory in a natural way. KOHN's work does not include magnetic fields, an obvious requirement for the understanding of cyclotron resonance, but it appears quite likely that those aspects of semiconductor theory which depend only on an expansion of the energy to order $\mathbf{k}^2$ and the use of symmetry arguments may be entirely rigorous.*

Some of the successes of the one-electron approach such as the computation of the germanium conduction band mass at $\mathbf{k} = 0$ from the valence-band masses at $\mathbf{k} = 0$,[17] and the calculation of non-parabolic effects[12,17] clearly do not follow from the many-particle approach, since we have already noted that these derivations would be invalidated by the most general one-electron approach.

Even though the above facts tend to validate the one-particle approach for certain semiconductors, there remains the important problem of how to determine the optimum one-particle Hamiltonian from first principles. The solution of this problem may result from further progress in many-particle theory.†

## ERRATUM

The author erroneously stated at the Rochester conference and also in reference (14) that optical absorption measurements could be used to determine the momentum matrix element $p_{nn'}$ between bands. This deduction was based on an interaction Hamiltonian which did not satisfy gauge-invariance requirements.

Gauge invariance demands [28] that the Hamiltonian satisfy the relation

$$H\left(A^\mu+\frac{\partial g}{\partial x^\mu}\right) = \exp\left(\frac{ie}{\hbar c}g\right)H(A^\mu)\exp\left(-\frac{ie}{\hbar c}g\right) \quad (19)$$

where $g(r)$ is an arbitrary gauge function. Let us expand $H(A^\mu)$ in powers of $A^\mu$

$$H(A^\mu) = H(\mathrm{o}) + \sum_\mu \left\{A^\mu, H^\mu_{1a}\right\}^+ + \sum_\mu \left[A^\mu, iH^\mu_{1b}\right]^- + \ldots \quad (20)$$

Braces denote the anticommutator and brackets

* For an illuminating illustration of the use of symmetry in effective-mass theory including magnetic fields (but not considering many-particle effects), see LUTTINGER.[26] The present discussion in terms of the properties ofenergy vs. $\mathbf{k}^2$ is somewhat of an oversimplification. KOHN's work is also considerably oversimplified in the above discussion.

† See, for example, BRUECKNER and LEVINSON.[27]

denote the commutator. If we set $A = 0$ in equation (19), expand in powers of $g$ and equate terms linear in $g$ we obtain the relation:

$$\sum_{\mu}\left\{\frac{\partial g}{\partial x^{\mu}}, H_{1a}{}^{\mu}\right\}^{+}+\sum_{\mu}\left[\frac{\partial g}{\partial x^{\mu}}, iH_{1b}{}^{\mu}\right]^{-} = \left(\frac{ie}{\hbar c}\right)[g, H(\mathrm{o})]^{-}, \tag{21}$$

where $H_{1a}{}^{\mu}$ and $H_{1b}{}^{\mu}$ are Hermitian operators. Relations between higher powers of $g$ may also be obtained if desired. Taking $g = x^{\mu}$ in equation (21) gives:

$$H_{1a}{}^{\mu} = \tfrac{1}{2}\left(\frac{ie}{\hbar c}\right)[x^{\mu}, H(\mathrm{o})]^{-} \tag{22}$$

which shows that the optical absorption depends on the commutator of $x$ with $H$ in the same way as the matrix elements in the effective-mass formalism given in equations (14) and (15).

Information about the operator $H_{1b}{}^{\mu}$ can be obtained by substituting the gauge function $g = x^{\mu}x^{\nu}$ in equation (21):

$$[x^{\mu}, iH_{1b}{}^{\nu}]^{-}+[x^{\nu}, iH_{1b}{}^{\mu}]^{-} = -\{x^{\nu}, H_{1a}{}^{\mu}\}^{+} -\{x^{\mu}, H_{1a}{}^{\nu}\}^{+}+\left(\frac{ie}{\hbar c}\right)[x^{\mu}x^{\nu}, H(\mathrm{o})]^{-}. \tag{23}$$

Further relations can be obtained by using higher powers of $x$ in the gauge function. The information in this form is useful if $A^{\mu}$ is expanded in powers of $x$. However, not all the information about $H_{1b}^{\mu}$ which one might desire can be obtained in this way. It may be seen directly from equation (19) that a term of the form $\mathscr{H}$ (curl $A$) automatically satisfies gauge-invariance requirements if $\mathscr{H}$ (curl $A$) commutes with $\boldsymbol{r}$. Thus the requirements of gauge invariance do not fully specify the form of operators which depend explicitly on the magnetic field.

## REFERENCES


1. Wannier G. H. *Phys. Rev.* **52,** 191 (1937).
   Adams E. N. *J. Chem. Phys.* **21,** 2013 (1953).
   Luttinger J. M. and Kohn W. *Phys. Rev.* **97,** 869 (1955).
2. Dresselhaus G. *Phys. Rev.* **100,** 580 (1955).
3. Dresselhaus G., Kip A. F. and Kittel C. *Phys. Rev.* **98,** 368 (1955).
4. Koster G. F. *Solid State Physics* (Ed. F. Seitz and D. Turnbull) Vol. 5, p. 173, Academic Press, New York (1957).
5. Seitz F. *Phys. Rev.* **47,** 400 (1935).
6. Shockley W. *Phys. Rev.* **78,** 173 (1950).
7. Dexter R. N., Zeiger H. J., and Lax B. *Phys. Rev.* **104,** 637 (1956).
8. Kahn A. H. *Phys. Rev.* **97,** 1647 (1955).
9. Braunstein R. *J. Phys. Chem. Solids,* **8,** 280 (1959).
10. Overhauser A. W. Private communication.
11. Parmenter R. H. *Phys. Rev.* **100,** 573 (1955).
12. Kane E. O. *J. Phys. Chem. Solids* **1,** 249 (1957).
13. Herring C. *Phys. Rev.* **52,** 365 (1937).
14. Kane E. O. *J. Phys. Chem. Solids.* **6,** 236 (1958).
15. Phillips, J. C. *J. Phys. Chem. Solids.* **7,** 52 (1958).
16. Dash W. C. and Newman R. *Phys. Rev.* **99,** 1151 (1955).
17. Roth, L. M., Lax B. and Zwerdling S. *Phys. Rev.* To be published.
18. Hrostowski H. J., Wheatley G. H. and Flood W. F. *Phys. Rev.* **95,** 1683 (1954).
19. Barrie R. and Edmond J. T. *J. Electronics* **1,** 161 (1955).
    Chasmar R. P. and Stratton R. *Phys. Rev.* **102,** 1686 (1956).
    Keyes R. J., Zwerdling S., Foner S., Kolm H. H. and Lax B. *Phys. Rev.* **104,** 1804 (1956).
20. Ehrenreich H. *J. Phys. Chem Solids* **2,** 131 (1957); *ibid.* To be published.
21. Wallis R. F. *J. Phys. Chem. Solids* **4,** 101, (1958).
    Bowers R. *Bull. Amer. Phys. Soc.* **3,** 120 (1958); *J. Phys. Chem. Solids,* **8,** 206 (1959).
22. Johnson E. R. and Christian S. M. *Phys. Rev.* **95,** 560 (1954).
23. Allen L. C. *Phys. Rev.* **98,** 993 (1955).
24. Phillips J. C. To be published.
25. Kohn W. *Phys. Rev.* **105,** 509 (1957); **110,** 857 (1958).
26 Luttinger J. M. *Phys. Rev.* **102,** 1030 (1956).
27. Brueckner K. A. and Levinson C. A. *Phys. Rev.* **97,** 1344 (1955).
28. Sachs R. G. and Austern N. *Phys. Rev.* **81,** 705 (1951).
    The author is indebted to Dr. J. J. Tiemann for acquainting him with this reference.


VOL
8
195

*J. Phys. Chem. Solids* Pergamon Press 1959. Vol. 8. pp. 45–47. Printed in Great Britain

# MOTION OF ELECTRONS AND HOLES IN SEMICONDUCTORS FROM A MANY-ELECTRON POINT OF VIEW

3.6

W. KOHN

Carnegie Institute of Technology, Pittsburgh, Pennsylvania

**Abstract**—The physical properties of a conduction electron or hole in a semiconductor are customarily interpreted in terms of a model in which they are regarded much like free electrons or positrons. The only modifications are the following: the free electron mass $m$ is replaced by an effective mass $m^*$ (or some appropriate generalization); and the interaction with an embedded charge $q$ (impurity) is taken as $eq/\kappa r$, where $\kappa$ is the static dielectric constant of the semiconductor.

It will be shown (KOHN *Phys. Rev.* **105**, 509 (1957); **110**, 857 (1958)) that this model can be strictly derived from the many-electron Schrödinger equation, provided only that the interaction of the carrier with the field produced by the embedded charge is weak enough. The effects of the electron–electron interaction are summed to all orders of perturbation theory, using the techniques of FEYNMAN and GOLDSTONE. This result constitutes one of the simplest cases of a (finite) mass and charge renormalization.

VOL. 8 1959

THIS audience, which is attending a conference on semiconductors, need hardly be reminded that physicists have come to think of electrons and holes in semiconductors as very analogous to free electrons and free positrons. The necessary modifications are conceptually quite simple, though quantitatively often very large. One must replace the free electron mass $m$ by an effective mass

$$m \to m^* \tag{1}$$

(or some suitable generalization), and one must modify the Coulomb interaction between two charges by the static dielectric constant $\kappa$

$$\frac{q_1 q_2}{r} \to \frac{q_1 q_2}{\kappa r} \tag{2}$$

For example, it is customary to describe an electron bound by an extra charge $q$ in the semiconductor by an effective-mass equation

$$\left(\frac{-\hbar^2}{2m^*}\nabla^2 - \frac{eq}{\kappa r}\right)F = EF. \tag{3}$$

Naturally one cannot expect such an equation to be valid unless the orbits of the electron are large compared to atomic dimensions. For in the case of small orbits, neither the dielectric constant nor the effective mass is a meaningful concept. However, for highly excited orbits, the eigenvalues of equation (3)—calculated with independently determined values of $m^*$ and $\kappa$—have in many cases been found to be in excellent quantitative agreement with experiment.[1]

Now from a certain point of view, this success of the effective-mass equation (3) may appear surprising. For so-called exchange and correlation effects do not seem to have been explicitly included. However, one may wonder whether they are not implicitly contained in the parameters $m^*$ and $\kappa$. This has in fact been shown to be the case.[2] It has been proved that under the single assumption that the electron orbit is large, equation (3) is *exact* and that all effects of the exclusion principle and the electron–electron interaction are completely included in the values of $m^*$ and $\kappa$.†

I would like now to outline the considerations which lead to this conclusion.

## EFFECTIVE MASS

Let us denote by $N$ the number of electrons in a perfect semiconductor without free carriers.

† In this demonstration the nuclei have been regarded as fixed.

Then, as has been noted by many authors, the eigenfunctions for the $N\pm1$ electron system can be labelled by a set of quantum numbers, one of which—denoted by $\mathbf{K}$—plays the role of a propagation vector. This is a direct consequence of the periodicity of the total Hamiltonian. We write these wave functions and the corresponding energies as:

$$\Psi_{n,\mathbf{K}};\ E_{n,\mathbf{K}} \tag{4}$$

where $\psi_{n,\mathbf{K}}$ has the following property. If $\mathbf{r}_i$ are the position vectors of the electrons and $\boldsymbol{\tau}$ is a lattice vector,

$$\Psi_{n,\mathbf{K}}(\mathbf{r}_1+\boldsymbol{\tau},\ \mathbf{r}_2+\boldsymbol{\tau},\ \ldots) = e^{i\mathbf{K}\cdot\boldsymbol{\tau}}\Psi_{n,\mathbf{K}}(\mathbf{r}_1,\ \mathbf{r}_2,\ldots) \tag{5}$$

Let the lowest-energy eigenvalue be $E_{0,0}$. Then, if for simplicity we take a cubic crystal, we can write $E_{0,\mathbf{K}}$ for small values of $\mathbf{K}$ in the form

$$E_{0,\mathbf{K}} = E_{0,0}+\frac{\hbar^2}{2m^*}\mathbf{K}^2. \tag{6}$$

The constant $m^*$ is by definition the effective mass of our "electron" or "hole". It will be seen that it is really a property of the entire $N\pm1$ electron system.

## DIELECTRIC CONSTANT

It is now not difficult to show that if an external charge is introduced into this $N\pm1$ electron system the full many-body Schrödinger equation can be reduced to an effective mass equation of the form

$$\left(\frac{-\hbar^2}{2m^*}\nabla^2\mp\frac{eq}{\kappa^* r}\right)F = EF \tag{7}$$

provided only that the orbit of the bound carrier is large enough. Here $\kappa^*$ is a constant defined as:

$$\frac{1}{\kappa^*} = \lim_{\substack{\mathbf{K},\mathbf{K}'\to 0\\ \mathbf{K}\neq\mathbf{K}'}} \left(\Psi_{0,\mathbf{K}},\ \sum e^{i(\mathbf{K}-\mathbf{K}')\cdot\mathbf{r}_i}\Psi_{0,\mathbf{K}'}\right).$$

It determines the strength of the Coulomb interaction between the external charge $q$ and the carrier.

It remained to show that this constant $\kappa^*$ is equal to the dielectric constant $\kappa$ which enters into the expression for the force between two external charges, $q_1$ and $q_2$, immersed in the medium at a distance $R$

$$F = \frac{q_1 q_2}{\kappa R^2} \tag{8}$$

The equality of $\kappa$ and $\kappa^*$ was established by treating the electron–electron interaction by perturbation theory and showing that $\kappa = \kappa^*$ to all orders in the perturbation expansion. The proof of this identity was greatly facilitated by the use of FEYMAN diagrams and the linked cluster expansions of GOLDSTONE.[3] It expresses the fact that two distant external charges exert the same force on each other as an external charge and a carrier.

## CONCLUSION

One will note the great similarity of this situation with renormalization in quantum electrodynamics. The replacement of $m$ by $m^*$ can be viewed as a mass renormalization, while our results concerning the dielectric constant can be expressed by saying that in a semiconductor charges interact with each other like charges in a vacuum, but as though they had an effective charge

$$Q_{\text{eff}} = \frac{Q}{\kappa^{\frac{1}{2}}}. \tag{9}$$

This is the analog of charge renormalization.

In quantum electrodynamics one has learned that a "real" electron (in contrast to a so-called "bare" one) is really a very complicated excitation of the electron and photon fields and yet it can for many purposes be completely described by its effective mass and charge. Similarly in a semiconductor a so-called electron or hole constitutes a very complicated disturbance of the perfect crystal, yet it can in many situations be completely characterized by an effective mass and charge. Thus the "naive" one-particle picture is seen to have a rather deep validity.

A number of things remain to be done. The idea of renormalization should be extended to a wider class of situations, such as excitons, motion of carriers in static magnetic fields or under the

influence of light waves, &c. Then it will be of interest to study the corrections which become necessary when the de Broglie wavelengths of the carriers are no longer large compared to a lattice spacing, and their description by an effective mass and charge ceases to be adequate.

REFERENCES

1. See, for example, KOHN W. *Solid State Physics* (Ed. F. FEITZ and D. TURNBULL) Vol. V, p. 257. Academic Press, New York (1957).
2. KOHN W. *Phys. Rev.* **105,** 509 (1957); **110,** 857 (1958).
3. GOLDSTONE J. *Proc. Roy. Soc.* **A293,** 267 (1957).

*J. Phys. Chem. Solids* Pergamon Press 1959. Vol. 8. pp. 47–51. Printed in Great Britain

VOL. 8 959

# A MANY-BODY TREATMENT OF DIELECTRIC SCREENING FOR IMPURITY STATES AND EXCITONS IN SEMICONDUCTORS*

**LAURA M. ROTH and G. W. PRATT, Jr.**

Lincoln Laboratory, Massachusetts Institute of Technology, Lexington, Massachusetts

IN the preceding paper Professor KOHN[1] has demonstrated that the long-range interaction between an electron and an impurity is screened by an effective dielectric constant $\kappa^*$ and that $\kappa^*$ is in fact equal to the static dielectric constant $\kappa$. In the present paper the effective dielectric constant is derived from an effective one-electron Hamiltonian. We shall apply this approach to the problem of a single-donor impurity, although it is equally applicable to other cases such as the acceptor or exciton problems. An approximate evaluation of the formal expression obtained for $\kappa^*$ is given.

The most naive description of the problem of a single-donor impurity and an excess electron is to express the perturbed wave function as a linear combination of determinants each corresponding to a full valence band with one electron in the conduction band. Here the electron–electron interaction is approximated by an averaged, periodic, one-electron potential. In this way one is led to the usual one-particle effective mass equation but with a dielectric constant of unity. Phenomenologically one retains the one-particle equation but substitutes the static dielectric constant of the material in the impurity potential.

The phenomenological result can be rigorously derived as follows. Let the set of states corresponding to a full valence band and one electron in the conduction band be denoted by set $A$. All other possible states make up set $B$. The Hamiltonian is taken as the complete many-electron energy operator including the perturbation $U = eQ/r$ of the impurity whose charge is $Q$. The exact solutions of this perturbed many-electron problem come from the corresponding infinite secular equation. However, this secular equation bears no resemblance to a one-particle effective mass equation due to the inclusion of excited states with holes–electron pairs. Physically such states are necessary in order that dielectric polarization take place.

The one-particle description can be recovered by projecting the exact Hamiltonian onto the space of the states in set $A$. States in set $B$ instead of appearing in the perturbed wave function now appear indirectly in an effective Hamiltonian whose perturbation expansion[2] is:

* The research reported in this document was supported jointly by the Army, Navy and Air Force under contract with the Massachusetts Institute of Technology.

$$(H_{\text{eff}})_{ij} = H_{ij}{}^{0} + H_{ij}{}' - \\ - \sum_{\alpha}^{B} \frac{H_{i\alpha}{}' H_{\alpha j}{}'}{H_{\alpha\alpha}{}^{0} - \epsilon} + \sum_{\alpha,\beta}^{B} \frac{H_{i\alpha}{}' H_{\alpha\beta}{}' H_{\beta j}{}'}{(H_{\alpha\alpha}{}^{0} - \epsilon)(H_{\beta\beta}{}^{0} - \epsilon)} \quad (1)$$

Here $H^0$ is the unperturbed Hamiltonian, $H'$ includes the difference between the exact Coulomb electron–electron interaction and the averaged periodic potential, and also includes the impurity potential $U$. Roman subscripts refer to states in set $A$ and Greek subscripts to states in $B$. $\epsilon$ is the final energy for any given final state.

A difficulty arises, however, in that all the corrections to the energy of the filled valence band are included in $H_{\text{eff}}$ and cannot be simply subtracted off due to the inclusion of $\epsilon$ in the denominators. The difficulty can be overcome by using the methods of HUGENHOLTZ[3] and VAN HOVE.[4] The various terms in equation (1) can be represented by FEYNMAN diagrams similar to those used by GOLDSTONE.[5] The result is that equation (1) is valid if (*a*) the sum is extended over diagrams without disconnected ground state (valence band) components,[3] and (*b*) $\epsilon$ is regarded as relative to the perturbed ground state energy. There are then no quantities in the sum depending on the volume of the crystal.

In the generalized one-particle equation $(H_{\text{eff}})_{ij}$ is the effective interaction between electrons in Bloch states $i$ and $j$ of the conduction band. The dielectric constant is found by considering only those terms of equation (1) linear in the impurity charge and going as $(\mathbf{k}_i - \mathbf{k}_j)^{-2}$. This $\mathbf{k}$ behavior becomes a $1/r$ dependence when one takes the Fourier transform of the secular equation.

The first-order contribution to the effective interaction is given in Fig. 1a, in which the excess electron, represented by the line with the arrow pointed up, is scattered by the impurity potential $U$ from the state $n$, $\mathbf{k}$ to the state $n'$, $\mathbf{k}+\mathbf{q}$. Here $n$ is the band index and $\mathbf{k}$ the reduced wave vector. In the limit of small $\mathbf{q}$ the matrix element for $n = n'$ is:

$$U_1| = <n\mathbf{k}+\mathbf{q}|\frac{eQ}{r}|n\mathbf{k}> \sim \frac{4\pi eQ}{\Omega q^2} \quad (2)$$

The second-order contribution is shown in Fig. 1b. This represents the process in which the electron in $n\mathbf{k}$ is scattered to $n\mathbf{k}+\mathbf{q}$ due to its interaction with the valence electron in state $m\mathbf{k}'$ which becomes raised to state $m'\mathbf{k}'-\mathbf{q}$. Here momentum is conserved. The interaction at the upper vertex represents the annihilation of the hole–electron

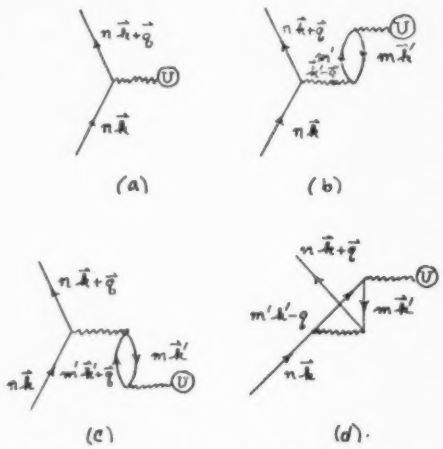


FIG. 1. First- and second-order diagrams.

pair by $U$. The hole in $m\mathbf{k}'$ is shown by a line with an arrow pointing down. The total contribution of these processes is:

$$-\sum_{\substack{m',m \\ \mathbf{k}}} \frac{(m\mathbf{k}'|U|m'\mathbf{k}'-\mathbf{q})(m'\mathbf{k}-\mathbf{q}, n\mathbf{k}+\mathbf{q}|V|m\mathbf{k}', n\mathbf{k})}{\epsilon_{m'}(\mathbf{k}'-\mathbf{q}) - \epsilon_m(\mathbf{k}')}$$

$$\sim -\left[\frac{4\pi e^2}{\Omega q^2} \sum_{\substack{m,\ m \\ \mathbf{k}}} \frac{|\int u_{m\mathbf{k}}{}^{*}(\partial/\partial k_1) u_{m\mathbf{k}}{}'|}{\epsilon_{m'}(\mathbf{k}') - \epsilon_m(\mathbf{k}')}\right]^2 \frac{4\pi eQ}{\Omega q^2} \quad (3)$$

in the limit of small $q$ for cubic crystals.[1] This result is of the form of a constant times the first-order contribution in equation (1). The $1/q^2$ singularity comes partly from $U$ and partly from the Coulomb interaction $V$. (A pair annihilation or creation contributes a factor of $q$ and the Fourier component of $U$ or $V$ a factor of $1/q^2$.) The energy denominator should be the sum of the energies of all the particles (holes counting negative) in the intermediate state, less the final energy $\epsilon$. We have omitted the term $\epsilon_n(\mathbf{k}+\mathbf{q}) - \epsilon$ in the denominator

of equation (3). This would vanish for elastic scattering except that $\epsilon$ includes the energy shift for the electron due to the many-particle interactions. This point is discussed below. The other second-order diagram contributing to the long-range interaction is Fig. 1c, which can be shown to be the same as equation (3). Diagrams such as Fig. 1d do not give a long-range interaction, since the Coulomb matrix element goes as $1/(\mathbf{k}'-\mathbf{k}+\mathbf{q})^2$, which is not singular in $q$. The long-range contribution from second order is, therefore, $-4\pi\alpha U_1$, if the quantity in brackets of equation (3) is denoted by $2\pi\alpha$.

Let us consider those third-order diagrams which are derived from the second-order graphs by adding another hole–electron pair loop as in going from 1b to 2a. Fig. 2a can be shown to give

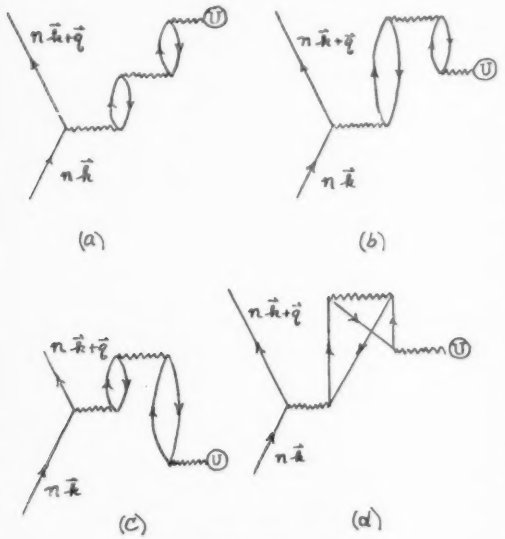


FIG. 2. Third-order diagrams.

$(2\pi\alpha)^2U_1$, each loop contributing a factor $2\pi\alpha$, if (*a*) the energy shift is again omitted and (*b*) momentum transfers $\mathbf{q}+\mathbf{K}$, $\mathbf{K}\neq 0$, where $\mathbf{K}$ is a vector of the reciprocal lattice, are neglected (i.e. the *Umklapp* processes). There are five more permutations of the vertices of Fig. 2a. The two shown in Figs. 2b and 2c combine from identities involving the energy denominators to yield also $(2\pi\alpha)^2U_1$. The total contribution of all six third-order diagrams of this type is $4(2\pi\alpha)^2U_1$. The argument can be extended to all orders, the contribution from $n$'th order being $(-4\pi\alpha)^{n-1}U_1$. The effective interaction is then

$$U'=\sum_{n=1}^{\infty}(-4\pi\alpha)^{n-1}U_1=\frac{1}{1+4\pi\alpha}U_1. \quad (4)$$

Thus we obtain an expression for the dielectric constant in terms of the quantity $\alpha$, which is readily identified as a static electronic polarizability. This result without a local-field correction is identical with that obtained by NOZIÈRES and PINES[6] who neglected exchange effects and the short-range part, $H_{sr}$, of the Coulomb interaction. It can be shown that the *Umklapp* processes described above which essentially correspond to $H_{sr}$ will lead to a local-field correction. Exchange effects first appear in third-order, for example, the graph shown in Fig. 2d. It is difficult to estimate the importance of these terms. The neglect of exchange in the long-range Coulomb interaction is equivalent to the random phase approximation of the Bohm–Pines theory. It should be pointed out that the expansion of $1/\kappa$ in powers of $\alpha$ does not converge for $\kappa>2$. One must, therefore, envision the use of analytic continuation in order that the result apply to most actual dielectrics.

The problem of eliminating the energy shift in $H_{\text{eff}}$ can be solved by including a more general class of diagrams than those shown here, in which case our result becomes identical with KOHN'S, where "clothed" rather than "bare" particles interact with the impurity potential. This is equivalent to including the exact electron–electron interaction in $H^0$ reducing $H'$ simply to $U$ for the impurity problem. The present method, based on VAN HOVE'S and HUGENHOLTZ'S formalism, can be extended to the case of the interaction of several particles, for example the exciton problem. One finds that the interaction is again screened by the static dielectric constant. This will be more fully described in a future publication.

## REFERENCES

1. KOHN W. *J. Phys. Chem. of Solids* **8**, 45 (1959); *Phys. Rev.* **110**, 857 (1958).
2. LOWDIN P. *J. Chem. Phys.* **19**, 1396 (1951).
3. HUGENHOLTZ N. M. *Physica* **23**, 481 (1957).
4. VAN HOVE L. *Physica* **21**, 901 (1955); **22**, 343 (1956).
5. GOLDSTONE J. *Proc. Roy. Soc.* **A293**, 267 (1957).
6. NOZIÈRES P. and PINES D. *Phys. Rev.* **109**, 762 (1958).

## DISCUSSION

*Compiled by* H. EHRENREICH

### B.1. J. C. SLATER

P. MARCUS (Carnegie Institute of Technology): In reference to J. C. SLATER's comments on band theory in disordered alloys, is it necessary to distinguish the problem of disordered lattices from that involving lattices with temperature oscillations?

J. C. SLATER replied that these are in fact distinct problems with the second the more difficult. The reason for this is that it is necessary to take account of the lattice vibrations and the resultant energy loss, a situation that does not arise in the case of static disordered alloys.

### B.2. C. ZENER

A most interesting discussion concerning the existence of a Hall effect in *d*-band semiconductors followed ZENER's paper.

F. H. HORN (General Electric Research Laboratory) asked how, with the localized band model, one accounts for the high Hall mobility (~1000 cm²/V-sec) reported for NiO.

After several comments concerning the experimental observations that bear on the existence of a Hall effect in such systems, the Chairman (W. SHOCKLEY) called on F. J. MORIN (Bell Telephone Laboratories) to present his views concerning the Hall effect in oxides of the 3*d* transition metals.

F. J. MORIN pointed out that in the oxides at the beginning of the 3*d* series, i.e. those involving Sc, Ti, and V, the *d* wave functions extend out far enough to overlap and form a 3*d* conduction band. As one moves across the series, however, these wave functions contract until, for Cr and the remaining members of the series, the *d*-band has essentially zero width. Thus oxides such as TiO and $V_2O_2$ are metals, whereas oxides from $Cr_2O_3$ to the end of the series are insulators. The room-temperature mobility is ~1 cm²/V-sec in $TiO_2$ and decreases to ~0·01 in $V_2O_3$. In the oxides having a zero-width *d* band, the mobility is ~0·001. Whereas a Hall effect has been obtained in TiO, none due to *d*-band transport has been observed in materials where the width of the *d*-band is zero. There is, however, an extraordinary Hall effect due to magnetization in such oxides as $Fe_2O_3$ and $Fe_3O_4$, which disappears at the Curie temperature. These oxides also contain a wide, filled 2*p*-band due to the oxygen lattice. The Hall mobility of carriers in this band, generated by thermal excitation, is normal and about 100 cm²/V-sec. In a pure and stoichiometric sample of NiO, for example, when transport in the 3*d*-levels is minimized, a Hall effect due to conduction in the 2*p*-band can be seen.*

H. BROOKS (Harvard University) commented that there was some theoretical justification for expecting a Hall effect, even though small, in a material where electronic transport is characterized by an activation energy. The magnitude of the Hall field should be obtainable simply from the Lorentz force—$(e/c)(\mathbf{v}\times\mathbf{H})$ with the velocity $\mathbf{v}$ taken to be the drift velocity associated with the jumping processes in the presence of an electric field.

R. LANDAUER (IBM Research Laboratory) agreed with this viewpoint. In an extended comment (not presented orally at the session), he gave the following arguments. The intuitive notion that every jump is completely uncorrelated with the previous jump is not correct, for if there is a non-vanishing jump rate, then the thermal relaxation in a trap is not complete, and there exists some correlation with previous events. The classical equation of motion is:

$$d\mathbf{p}/dt = -e\mathbf{E}_0-(e/mc)\mathbf{p}\times\mathbf{H}-(\mathbf{p}/\tau)+\mathbf{F}_T+\mathbf{F}_L$$

where $\tau$ is the relaxation time (here assumed constant), $\mathbf{F}_T$ is the fluctuating force due to the thermal environment and $\mathbf{F}_L$ is the force producing trapping. Averaging over long time (many jumps) and noting that $\langle\mathbf{F}_T\rangle = 0$, one finds:

$$\langle\mathbf{p}\rangle = \tau[\langle\mathbf{F}_L\rangle-e\mathbf{E}_0-(e/mc)\langle\mathbf{p}\rangle\times\mathbf{H}].$$

The situation described by the preceding equation is qualitatively equivalent to one where the same field $E_0$ is supplemented by an electric field $\mathbf{E}_L$ such that $-e\mathbf{E}_L$ is equal to the *average* Lorentz force. This is true because $\langle\mathbf{F}_L\rangle$ is of the same magnitude in the two situations.

H. P. R. FREDERIKSE (National Bureau of Standards) then inquired whether the Hall coefficient occurring in a crystal where the conduction mechanism is a jump process is still proportional to $1/n$.

H. BROOKS replied that he believed it was, but its usefulness might be limited by the difficulties encountered in measuring these very small Hall voltages.

### B.4. JOSEPH L. BIRMAN

H. BROOKS asked how many match points were used in computing eigenvalues of the different states in the cellular calculation.

J. L. BIRMAN replied that the eigenfunction for each state in each structure was expanded in a series of spherical harmonics up to and including $l = 6$, and hence the number of match points used depended upon the particular state. For some states as many as 16 match points were used in the calculation.

P. MARCUS inquired concerning the accuracy of the calculated eigenvalues.

J. L. BIRMAN stated that each eigenvalue was determined by averaging the results obtained from several sets of match points. Not all sets of match points gave a match. In general 10–15 good sets were used for each state, and the deviation from the mean was about 10 per cent.

* A full account of the material contained in the preceding comment by MORIN may be found in a recent paper in the *Bell Syst. Tech. J.* **37,** 1047 (1958).

VOL 8 195

E. H. RHODERICK (S.E.R.L., Baldock, England) asked about the distinction made between choice of effective charge and choice of ion size. It was felt that these are connected, i.e. once the ion size is specified the effective charge is also completely determined.

J. L. BIRMAN agreed that this is true. In his calculation, however, the effective charge was determined from various theories of the lattice properties (*reststrahlen* &c.) in which the assumption is made that the ions are point charges, or have non-overlapping charge distributions. These point charges were "blown up" into ion-charge densities within some (assumed) ion sphere. In this sense BIRMAN argued that ion charge and size are independent.

F. E. WILLIAMS (General Electric Research Laboratory) commented on the fact that the magnitude of the calculated band gaps agrees with experiment better than do the calculated difference in band gaps for the two structures. He inquired whether the calculated difference being too large indicates that the charges on the Zn and S should be less than $\pm\frac{1}{2}$, since the difference in the potential for the two structures arises from the Ewald potential at third and greater nearest neighbors.

J. L. BIRMAN indicated that because of the mechanics of carrying out the cell calculation, it is not possible to estimate the influence of change of effective charge upon the location of various eigenstates. He expressed the hope that other and more extensive band calculations now in progress, by OPW and variational methods, for the ZB–W structures would shed light on this important problem. He added that it may also be that the effective charges are not the same for a given material in the different structures, although this seems a good approximation for ZnS.

R. W. KEYES (Westinghouse Electric Corp.) inquired concerning the choice of the common reference energy for comparison of the zinc blende and Wurtzite levels.

J. L. BIRMAN answered that relative energies could be computed because the same atomic potentials were used for both structures.

### B.6. W. KOHN

G. WEINREICH (Bell Telephone Laboratories) asked whether the state of one electron in the conduction band can be *defined* as a state such that near it $\mathbf{K}$ is the only continuously varying quantum number.

W. KOHN replied that near $\mathbf{K} = 0$ this is possible.

H. HAKEN (University of Erlangen, Germany) made two comments concerning KOHN's paper:

(1) As has been stressed by Professor KOHN, the one-particle approximation of an impurity centre using an effective mass and a dielectric constant within the Coulomb law is asymptotically exact for large orbits, a result which for the case of *excitons* has also been obtained along different lines (HAKEN, H. *Int. Conf. Semiconductors, Garmisch* (1956)). On the other hand one may ask how well the description by means of a dielectric constant works for smaller orbital radii. With the aid of a simple model, it was shown by SCHOTTKY and HAKEN that the description mentioned above holds rather well up to distances of the order of $l \sim \sqrt{\hbar^2/2m\Delta E}$, where $m$ is the effective electron mass and $\Delta E$ is the energy gap.

(2) The occurrence of a dielectric constant within the Coulomb law is not only due to the electron–electron interaction (core-electron polarization), but also due to the electron-lattice interaction. Here once again it may be shown, that at large distances the usual Coulomb law is asymptotically correct, whereas at smaller distances deviations occur, which arise from the fact that the ions can no longer follow the motion of the electron.

### B.7. LAURA M. ROTH and G. W. PRATT

H. HAKEN commented that when the effective interaction between the electron and the impurity centre has the form of the Coulomb law, then one can show that this law is valid even in the strong-coupling case when perturbation theory breaks down. One treats first the motion of an excess electron in a strictly periodic lattice and then takes into account the interaction with the impurity center. Whereas in the neighbourhood of the excess electron the cloud of virtual electron–hole states might differ considerably from the cloud determined by perturbation theory, the long-range part of the cloud leads to the usual Coulomb law.

*J. Phys. Chem. Solids* Pergamon Press 1959. Vol. 8. pp. 52–59. Printed in Great Britain

SESSION C:

RECOMBINATION AND IMPURITY CENTERS*

# STUDIES ON THE RECOMBINATION OF ELECTRONS AND HOLES IN GERMANIUM

C.1

**S. G. KALASHNIKOV**

Institute of Radio and Electronics, Academy of Sciences, Moscow, U.S.S.R.

**Abstract**—The life time of nonequilibrium charge carriers in *n*- and *p*-type germanium was measured as a function of the equilibrium carrier concentrations. The concentration range from the intrinsic region up to $\sim 10^{18}$ cm$^{-3}$ was covered. Both electron and hole capture coefficients were found to be independent of concentration up to the concentrations of at least $\sim 10^{17}$ cm$^{-3}$. The temperature dependence of the hole life times in copper-doped *n*-type germanium was investigated. The experimental data were compared with the statistics of recombination on many-level centres and a good agreement was shown to be obtainable. From the data obtained some conclusions on the nature of elementary capture processes in germanium were drawn.

VOL
8
195

## 1. INTRODUCTION

ACCORDING to the data available,[1]† direct electron–hole recombination does not play any significant role in germanium under the usual conditions. The principal recombination processes are related to nonradiative electron transitions to trapping states, the latter being due to impurity atoms and structural imperfections. The energy released at the capture process may be transferred to elementary excitations of some kind—phonons, excitons, free charge carriers (impact recombination) or to the plasma oscillations of the electron–hole gas (plasma recombination).

The specific form of the concentration—and temperature dependence of the capture coefficients (or capture cross sections) must be different for different capture mechanisms. In the phonon recombination case capture coefficients do not depend upon concentration and for the shallow traps are but weakly temperature dependent.[2,3] In the case of exciton recombination, capture cross-sections may or may not be strongly temperature dependent according to whether the minimum exciton energy is greater or smaller than the ionization energy of the centre;[4] in both cases no serious concentration dependence is expected. If the recombination process is of the impact type, the capture coefficients must be concentration dependent, being approximately proportional to the concentration.[5] Finally, the plasma mechanism[6] is characterized by a sharp increase of the capture coefficients at a certain critical concentration. (It should be noted, however, that in germanium this mechanism may be effective only under very special conditions.) The temperature dependence of the cross sections may also be due to the Coulomb repulsion.

One may hope to obtain some information on the relative importance of the different elementary capture mechanisms by measuring the dependence of the charge carrier life time upon the carrier concentration and the temperature. In the following some results are described of the relevant recent investigations by the author and his co-workers.

## 2. THE CONCENTRATION DEPENDENCE OF THE LIFE TIME

The dependence of the capture coefficients on concentration was studied by investigating the influence of different 3 and 5 group elements upon the life time. It had been shown earlier[7] that at high concentrations of these elements they affect the life time in different ways. Bi and Tl, being characterized by rather big atomic radii, small segregation coefficients and relatively small solubilities strongly increase the recombination rate, while the other elements, such as Sb and Ga, having smaller atomic radii and readily soluble in

*Chairman: J. Tauc, *Co-Chairman:* A. Rose.

†The list of references does not pretend to be complete, the papers being mentioned only in connection with the concentration—or temperature dependence of the capture coefficients.

germanium, influence the recombination to a lesser extent. The reason for this difference is now being investigated in more detail.

In view of these results the doping elements possessing high segregation coefficients and high solubilities (Al, B, P) were used. The recombination centres in Al- and P-doped samples were of unknown origin; in B-doped samples they were mainly copper atoms.

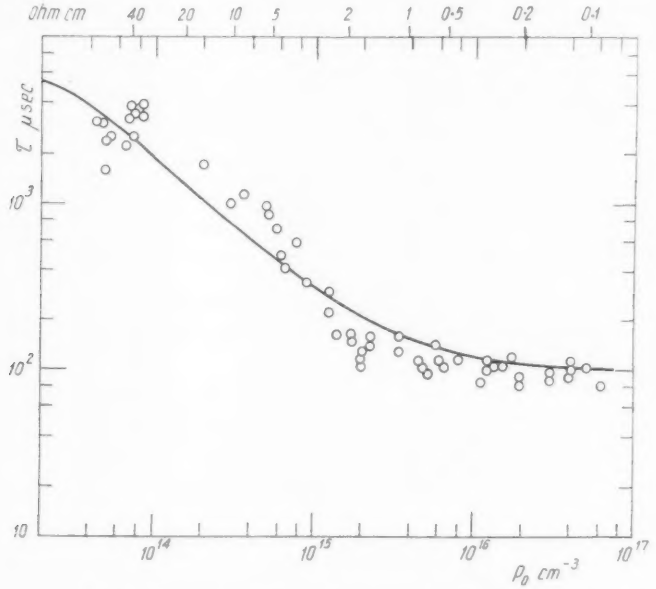


FIG. 1. Dependence of the electrons life time on the equilibrium hole concentration. Al = doped samples; traps of unknown origin. The curve is drawn according to the expression $\tau = \tau_{n0}(1+(a/\rho_0))$, with $\tau_{n0} = 100$ $\mu$ sec, $a = 2{\cdot}1 \times 10^{15}$ cm$^{-3}$.

The dependence of the electron life time in Al-doped samples upon the equilibrium hole concentration is shown in Fig. 1.[8] The life time was measured by the light spot method[9] with the constant collector response.[10] The mobility values were taken from reference (11).

Fig. 2 gives the dependence of the hole life time in P-doped samples upon the equilibrium electron concentration.[12] In some of the samples the diffusion length was determined by a simultaneous measurement of the photomagnetoelectric effect and photoconductivity.[13] The experimental technique used is described in detail in reference (14). Both methods gave results coinciding within experimental error $\sim 20$ per cent. Mobility values at the concentrations over $1 \times 10^{17}$ cm$^{-3}$ were obtained by extrapolating the data of (11) according to the theoretical expression (both lattice and ionised impurity scattering being taken account of).

The concentration dependence of the life time in boron-doped samples is shown in Fig. 3.[12] In this case a sharp decrease of the life time was observed at equilibrium hole concentrations $\lesssim 2 \times 10^{17}$ cm$^{-3}$. This effect is to be discussed below in more detail.

The most important feature of the curves obtained is the existence of the well-defined plateau in the high concentration region. An analogous (but not so well-defined) plateau had been observed in reference (15) as well as in references (16–18).

According to the recombination statistics[19,20] for the life time to be concentration independent it is necessary that (1) recombination be due to only one trapping level and (2) capture cross sections be constant. Therefore it follows from our

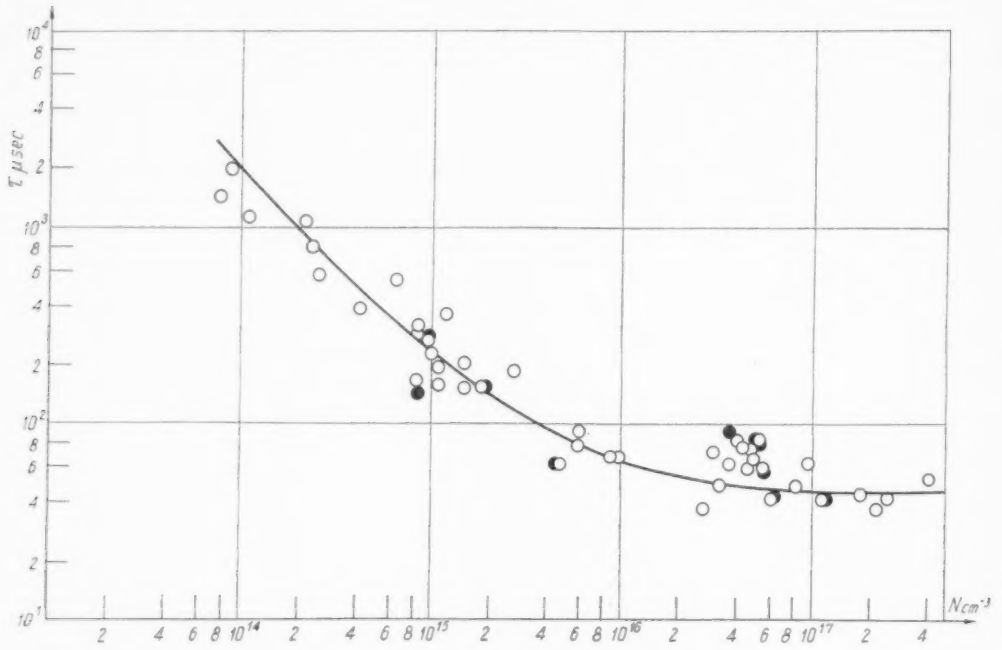


FIG. 2. Dependence of the hole life time on the equilibrium electron concentration. P = doped samples; traps of unknown origin. ○—light spot method, ● = PME method. The theoretical curve corresponds to $\tau_{p0} = 50\ \mu$ sec, $a = 4{\cdot}4 \times 10^{15}$ cm$^{-3}$.

data that in all cases studied, capture cross sections in Ge do not depend upon concentration up to the values of the latter of at last $\sim 10^{17}$ cm$^{-3}$.

In what follows the experimental data are interpreted on the basis of the statistics of recombination on many-level traps, recently discussed by SAH and SHOCKLEY.[20]* Assume a small concentration of excess carriers as well as of traps and let the sample be nondegenerate. (These conditions were met in our experiments). Then the life time, $\tau$, under stationary conditions may be written in the form:

$$\frac{1}{\tau} = (n_0+p_0)\sum_{j=1}^{M}\frac{f_j{}^0+f_{j-1}{}^0}{C_{pj}{}^{-1}(n_0+n_j)+C_{nj}{}^{-1}(p_0+p_j)} \quad (1)$$

Here $C_{pj}$ is the product of the trap concentration and the coefficient of hole capture to the $j$th level of the trap (the trap possessing $j$ electrons before the hole is captured); $C_{nj}$ is an analogous electron quantity (the electron being captured becomes the $j$th one in the trap); $M$ is the maximum number of electrons that a trap can capture. The quantities $n_j$ and $p_j$ are defined by the equations:

$$n_j = N_c \exp\left(\frac{E_j{}^*-E_c}{kT}\right),\ p_j = N_v \exp\left(-\frac{E_j{}^*}{kT}\right),\ (j = 1, 2, \ldots . M) \quad (2)$$

$N_c$ and $N_v$ being effective densities of states in the conduction, and valence bands respectively, $E_c$—the bottom of the conduction band, $E_j{}^*$—some effective energy levels describing the traps (all the

*Some of the following relations are written in a form somewhat different from that of reference (20) but are identical to the equations of this paper. In this connection see Appendix to reference (23).

energies are calculated with respect to the top of the valence band). $E_j^*$ is the increment of the trap free energy when one of the electrons is transferred from the crystal to the trap. Finally $f_j^0$ is the equilibrium probability of finding $j$ electrons in a trap:

$$f_j^0 = \frac{\prod_{K=0}^{j} \frac{n_0}{n_K}}{\sum_{j=0}^{M} \prod_{K=0}^{j} \frac{n_0}{n_K}} = \frac{\prod_{K=0}^{j} \frac{p_K}{p_0}}{\sum_{j=0}^{M} \prod_{K=0}^{j} \frac{p_K}{p_0}} \qquad (3)$$

*The problem of equilibrium electron distribution in traps had been considered in reference (21).

These relations were employed to discuss the experimental results in somewhat more detail.

If there is some concentration range where only one recombination level is of importance, then only one of the terms in (1) is dominant, and equation (1) reduces to the well-known Hall–Shockley–Read expression[19] for the simple traps. We compared this expression (for extrinsic range and small trap concentration) with our experimental data. The theoretical curves are shown in Figs. 1–3 as full lines. We see that (the boron-doped samples excluded) the general fit is satisfactory.

The sharp decrease of the life time at the boron concentration of about $2\times10^{17}$ cm$^{-3}$ may be due either to the onset of some new recombination process or to the effect of another recombination level lying close to the valence band. As pointed out above, the main recombination centres in these

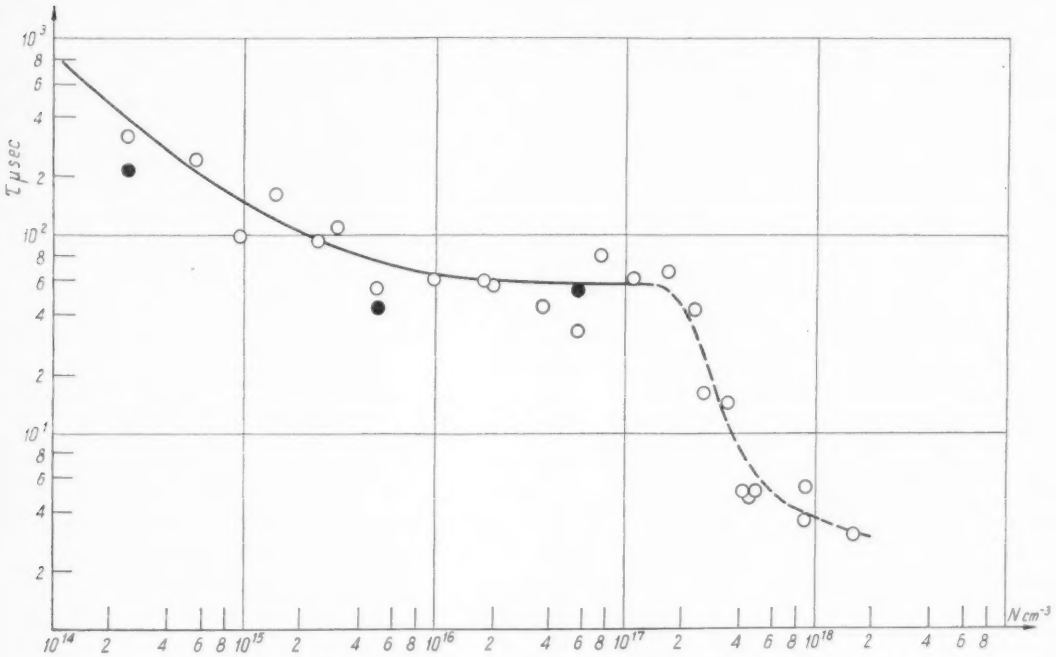


FIG. 3. The concentration dependence of the life time in boron-doped samples. The main recombination centres are Cu-atoms. ○=PME method, ●=the light spot method. The full curve corresponds to the theoretical expression with $\tau_{n0} = 60$ μsec, $a = 1{\cdot}6\times10^{15}$ cm$^{-3}$.

samples were copper atoms. It is known[22] that copper introduced three acceptor levels in germanium, lying respectively at 0·04 eV, 0·32 eV from the valence band and at 0·26 eV from the conduction band. Therefore we tried to estimate the capture cross section that should be ascribed to the 0·04 level to explain the observed decrease in $\tau$. Let us assume for an approximate estimate that $E_j^* \cong E_j$ and that the capture cross sections for different levels do not differ by many orders of magnitude. Then for the case of high hole concentration and copper controlled recombination equations (1)–(3) reduce to

$$\tau \cong \frac{p_0+p_1}{C_{n1}p_0+C_{n2}p_1}$$

Now, the experiment gives $C_{n2}^{-1} \equiv \tau_{n0} = 60\mu$sec, and $\tau \cong 4\mu$sec for $p_0 = 1\times10^{18}$ cm$^{-3}$. Hence, assuming $p \sim 1\times10^{18}$ cm$^{-3}$, one finds that $C_{n1}$ must be of the order of ten times larger than $C_{n2}$—a result that seems to be quite possible. Therefore it seems probable that a sharp decrease in life time at high boron concentrations may be due to the effect of the lowest copper level.

attempt was made to take into account more exactly that traps possess several energy levels.

The dependence of the capture coefficient on temperature is obtained most directly for heavily doped samples corresponding to the plateau on the life time vs. concentration curves. In this case only one level is effective, and the recombination rate is controlled by the capture of minority carriers. The experimental data for such samples are shown in Fig. 4. It is seen that the diffusion length and, hence, the capture coefficient $C_{p3}$ is but weakly temperature dependent. This is in agreement with results of reference (25).

At the lower doping level the diffusion length was found to be somewhat more temperature dependent. Making use of the mobility temperature dependence as given in reference (11), one can obtain the temperature dependence of the life time. For one of the samples this is shown in Fig. 5.

The data thus obtained were compared with the theory. It is easily seen from equation (3) that the 0·04 level cannot play any role under our conditions of concentration and temperature, since there are practically no single-charged copper ions. Besides that $n_2/n_0 \ll 1$, $p_0/n_0 \ll 1$. Therefore one obtains, using equations (1) and (3):

$$\frac{1}{\tau} = \left(1+\frac{n^3}{n_0}\right)^{-1}\left[\left(C_{p3}^{-1}+C_{n3}^{-1}\frac{p_3}{n_0}\right)^{-1}+\frac{n_3}{n_0}\left(C_{p2}^{-1}+C_{n2}^{-1}\frac{p_2}{n_0}\right)^{-1}\right] \quad (4)$$

### 3. THE TEMPERATURE DEPENDENCE OF THE LIFE TIME

In the experiments to be described the temperature dependence of the life time was investigated on $n$-type germanium samples doped with phosphorus and antimony. The temperature range covered extended from 120° to 300°K. Equilibrium electron concentration ranged from $3{\cdot}5\times10^{14}$ cm$^{-3}$ to $6\times10^{16}$ cm$^{-3}$. The recombination centres were diffusion introduced copper atoms in concentration of about $1\times10^{14}$ cm$^{-3}$. The life time was measured by the light spot technique. The sample with a holder was placed in a hermetically sealed and dried chamber with a transparent window.

It should be noted that the temperature dependence of the Cu capture cross sections in germanium had been investigated earlier.[24,25] In our experiments another type of doping was used and an

This expression can be further simplified since the term $C_{n3}^{-1}(p_3/n_0)$ may be safely neglected relative to $C_{p3}^{-1}$; furthermore, $n_0 \cong$ const in the temperature range considered.

The quantity $C_{p3}^{-1} \equiv \tau_{p0}$, entering equation (4), is known from experiment, as well as its temperature dependence. This is shown by the dotted lines in Figs. 5 and 6.† Now the experimental data by Burton *et al.*[15] however they are interpreted, lead to the conclusion that $C_{p3}/C_{n2} \cong 10$. Therefore there are three unknown quantities in the equation (4): $C_{p3}/C_{p2}$, $E_3^*$ and $E_2^*$. They were

†Experiment shows that at $n_0 \sim 10^{15}$ cm$^{-3}$ and $T \gtrsim 170$°K the diffusion length was temperature independent. Hence, $\tau_{p0}$ as a function of temperature is inversely proportional to the diffusion constant in this range. Taking account of the hole diffusion constant varying as $\sim T^{-1.3}$[11] one obtains $\tau_{p0} \sim T^{1.3}$. The dotted curves in Figs. 5 and 6 correspond to this relation.

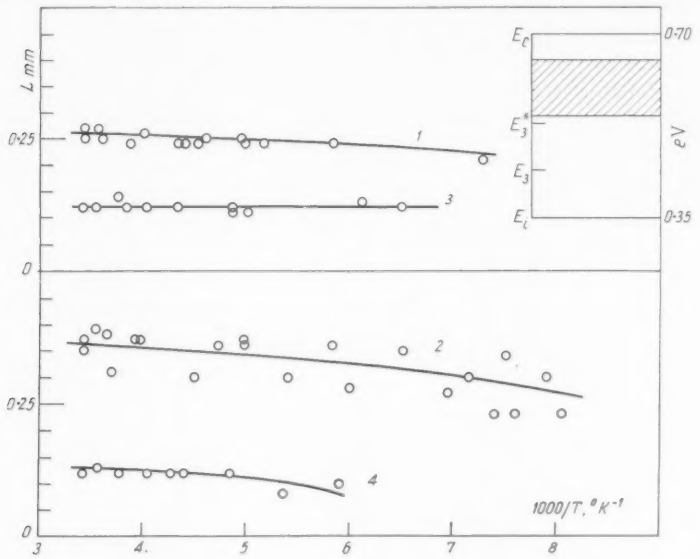


FIG. 4. The temperature dependence of the diffusion length in phosphorus-doped germanium samples (heavy doping).
1—$n_0 = 2{\cdot}9 \times 10^{16}$ cm$^{-3}$, Cu not introduced.
2—$n_0 = 5{\cdot}7 \times 10^{16}$ cm$^{-3}$, Cu not introduced.
3, 4—$n_0 = 5{\cdot}7 \times 10^{16}$ cm$^{-3}$, Cu introduced.

considered as temperature independent and chosen as to obtain the best fit to experimental data at all the values of concentration used. The result is shown in Figs. 5 and 6. It is seen that equation (4) fits well to the experimental points, as soon as one assumes that in all four cases $C_{p3}/C_{p2} \cong 20$; $E_c - E_3^* = 0{\cdot}16 - 0{\cdot}18$ eV and $E_2^* - E_v = 0{\cdot}24$ eV (the last figure being of importance only for $n_0 = 3{\cdot}5 \times 10^{14}$ cm$^{-3}$). The copper concentration and the value of $\tau_{p0}$ being known one can obtain the absolute value of the hole cross-section for the highest copper level. It turns out to be of the order of $10^{-16}$ cm$^{-2}$.

A still more convincing agreement of equations (1)–(3) with experiment was obtained recently with $p$-type Ni-doped germanium (to be published). In this case as well no experimental evidence of the strong temperature dependence of the capture coefficients was obtained.

## 4. CONCLUSIONS

According to the data obtained the capture coefficients for both electrons and holes in germanium are independent of the concentration of the free carriers. This is valid at least up to the concentrations of about $10^{17}$ cm$^{-3}$. Hence it follows that the impact recombination processes do not play any significant role in germanium in this concentration range. It should be noted that the same conclusion was obtained recently in reference (26) in connection with the other experiments. There is as well no experimental evidence pointing to a significant role of the plasma excitation processes.* Therefore it may be concluded that the charge

*It should be noted however that the plasma type recombination could not be observed in our experiments, since for this process to occur, the plasmon energy must not be less than the level depth. This means that at the concentrations we worked with, the plasma mechanism could be effective only for shallow traps (supplied, for instance, by accidental 5-group donors in boron–doped samples). Yet in this case, because of the sharp increase of the electron capture cross-sections, the net recombination rate would have been controlled by the hole capture. Therefore the increase of the electron capture cross-sections could have been overlooked.

carrier recombination in germanium proceeds mainly via phonon and exciton process.

The coefficient of the hole capture to the highest copper level in germanium is but weakly temperature dependent. The same seems to be true for the middle copper level, as well as for the traps of unknown origin. In all these cases capture coefficients increase relatively slowly as the temperature is decreased.

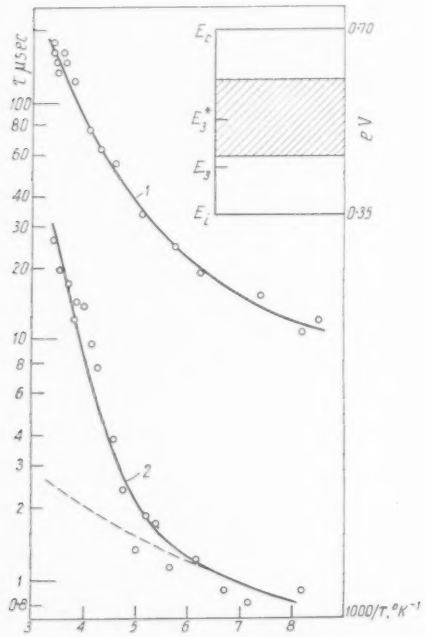


FIG. 5. The temperature dependence of life time $n_0 = 1{\cdot}8 \times 10^{15}$ cm$^{-3}$ (Sb = doped samples). 1—before Cu was introduced; 2—after Cu was introduced. The full curve 2 corresponds to the theoretical expression, with $E_c - E_3^* = 0{\cdot}17$ eV. The dotted curve shows the temperature dependence of $\tau_{p0}$. In the right upper corner the range of Fermi level values is indicated.

An observed temperature dependence of minority carrier life time in copper-doped germanium may be well fitted into the theoretical frame; yet this is possible only if due account is taken of the statistics of recombination on many-level traps. The influence of temperature on the recombination process is not in general confined just to a change of the relative role of electron and hole capture by each particular level, as is the case for the simple traps. For many-level traps still another effect must be taken into account—the change of relative concentrations of different levels (i.e. of ions in different charge conditions) with changing temperature.

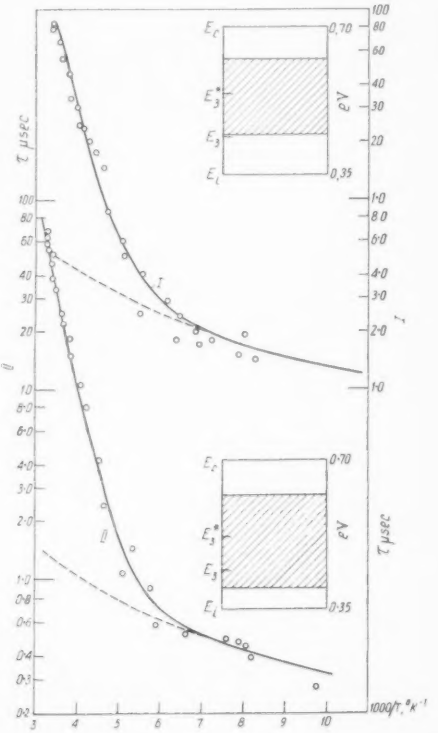


FIG. 6. The temperature dependence of life time. P = doped samples containing Cu. The full curves correspond to the theoretical expressions.
1—$n_0 = 3{\cdot}5 \times 10^{14}$ cm$^{-3}$, $E_c - E_3^* = 0{\cdot}18$ eV.
2—$n_0 = 1{\cdot}0 \times 10^{15}$ cm$^{-3}$, $E_c - E_3^* = 0{\cdot}16$ eV.

*Acknowledgments*—The author wishes to express his gratitude to V. G. ALEXEEVA, I. V. KARPOVA, A. I. MOROZOV and K. P. TISSEN for their consent to use the results of our common work in this paper and to V. L. BONCH-BRUEVICH for valuable discussion of the theoretical problems.

The Institute of Radio and Electronics A.S. U.S.S.R., Moscow State University.

**REFERENCES**

1. v. Roosbroeck W. and Shockley W., *Phys. Rev.* **94,** 1558 (1954).
2. Cubo R. and Toyozawa Y., *Progr. Theor. Phys* .**13,** 160 (1955).
3. Gummel H. and Lax M., *Phys. Rev.* **97,** 1469 (1955).
4. Bonch-Bruevich V. L., *Zh. exp. teor. fiz. SSSR.* **32,** 1470 (1957).
5. Sclar N. and Burstein E., *Phys. Rev.* **98,** 1757 (1955); Bess L., *Phys. Rev.* **105,** 1469 (1957); Nagae M., *Progr. Theor. Phys.* **19,** 339 (1958).
6. Bonch-Bruevich V. L., *Dokl. Akad. Nauk. SSSR,* **21,** 87 (1957); *Zh. tekh. fiz., Moscow* **28,** (in press). (1958).
7. Alexeeva V. G. *et al., Zh. tekh. fiz., Moscow* **27,** 1931 (1957).
8. Kalashnikov S. G. and Tissen R. P., *Zh. tekh. fiz., Moscow* **28,** (1958) (in press).
9. Valdes L. B., *Proc. Inst. Radio Engrs. N.Y.* **40,** 1420 (1952).
10. Rashba E. I. and Tolpygo R. B., *Dokl. Akad. Nauk. Ukr. SSR, fiz. ser. Sci.* Ukraina **1,** 29, 1956.
11. Prince M., *Phys. Rev.* **92,** 681 (1953).
12. Alexeeva V. G., Karpova I. V. and Kalashnikov S. G., *Zh. tekh. fiz., Moscow* **28,** (1958).
13. Aigrain P., *Ann. Radio elect.* CGTSE **9,** 219 (1954); v. Roosbroeck W., *Phys. Rev.* **101,** 1713 (1956).
14. Landsberg E. G. and Kalashnikov S. G., *Zh. tekh. fiz. Moscow* **28,** (in press) (1958).
15. Burton J. A. *et al., J. Phys. Chem.* **57,** 853 (1953).
16. Kalashnikov S. G., Lvova E. U. and Ostroborodova V. V., *Zh. tekh. fiz., Moscow* **27,** 1925 (1957).
17. Lashkarev V. E. *et al., Zh. tekh. fiz., Moscow* **27,** 2437 (1957).
18. Glinchuk K. D., Miseluk E. G. and Fortunatova N. N., *Zh. tekh. fiz., Moscow* **27,** 2451 (1957).
19. Shockley W. and Read W. T., *Phys. Rev.* **87,** 835 (1952); Hall R. N., *Phys. Rev.*
20. Chin-Tang Sah and Shockley W., *Phys. Rev.* **109,** 1103 (1958).
21. Landsberg P. T., *Proc. Phys. Soc.* A**65,** 604 (1952); *Ibid.* B**69,** 1056 (1956); Samoilovitch A. G. *Thermodyn. a. Stat. Phys.*, 2nd Edn., 1955; Pekar S. J., *Zh. exp. teor. fiz. SSSR* **31,** 351 (1954); Champness C. H., *Proc. Phys. Soc.* B**69,** 1335 (1956); Shockley W. and Last J. T., *Phys. Rev.* **107,** 392 (1957).
22. Woodbury H. H. and Tyler W. W., *Phys. Rev.* **105,** 84 (1957).
23. Zdanova N. G., Kalashnikov S. G. and Morosov A. I., *Zh. tekh. fiz., Moscow* (in press).
24. Baum R. M. and Battey J. F., *Phys. Rev.*, **98,** 923 (1955).
25. Shulman R. G. and Wyluda B. J., *Phys. Rev.* **102,** 1455 (1956).
26. Brown D. A. H., *J. Electron. Control* **4,** 341 (1958).


*J. Phys. Chem. Solids* Pergamon Press 1959. Vol. 8. pp. 59–65. Printed in Great Britain

# DEEP LEVEL IMPURITIES IN GERMANIUM

C.2

**W. W. TYLER**

General Electric Research Laboratory, Schenectady, New York

**Abstract**—This paper will review the properties of deep level impurities in germanium. With the exception of the well known hydrogen-like impurities, all of the electrically active impurities which have been studied in detail act as multiple acceptors or donors introducing deep impurity levels ($\geq$ ·03 eV). The number and type of levels are consistent with the tetrahedral bonding model. As examples, Zn (with a $4s^2$ outer orbit configuration) acts as a double acceptor in Ge ($4s^24p^2$); Cu ($4s^1$) acts as a triple acceptor and Te ($5s^25p^4$) acts as a double donor. However, no theoretical treatment has proven adequate for calculation of the positions of energy levels for the deep level impurities. Hall coefficient studies have determined the positions of deep acceptor levels introduced into Ge by the elements Zn, Cd, Mn, Fe, Co, Ni, Cu, Ag and Au. Deep donor levels are introduced by S, Se and Te. For most of these impurities the positions of the energy levels have been confirmed by studies of extrinsic photoconductivity or optical absorption. Values of diffusivity and the temperature dependence of solubility are also known for many of these impurities. The interpretation of both steady state and

transient photoconductivity studies has demonstrated the importance of the charge state at deep level impurities in determining recombination processes. At low temperatures, multiply charged negative centers are effective hole traps; multiply charged positive centers act as electron traps. Some quantitative values of capture cross sections have been obtained for different charge states of multiple acceptor impurities. Reference will be made to other electrical, optical and magnetic experiments made possible because of the present knowledge of deep level impurities in Ge and the control now possible over crystal preparation.

## 1. INTRODUCTION

ELECTRICALLY active impurity elements in germanium are classified as hydrogen-like and deep level impurities. Hydrogen-like impurities, which consist of Li and elements of Columns V and III of the periodic table, act as single donors or acceptors, introducing levels about 0·01 eV from the band edges. Deep level impurities include all other electrically active elements whose properties have been studied. Properties of hydrogen-like impurities and earlier work on deep level impurities in both Ge and Si have been summarized in previous reviews.[1–6] This paper will summarize available information concerning ionization energies, the number and type of levels introduced by deep level impurities in Ge. Other properties of these impurities will be discussed briefly.

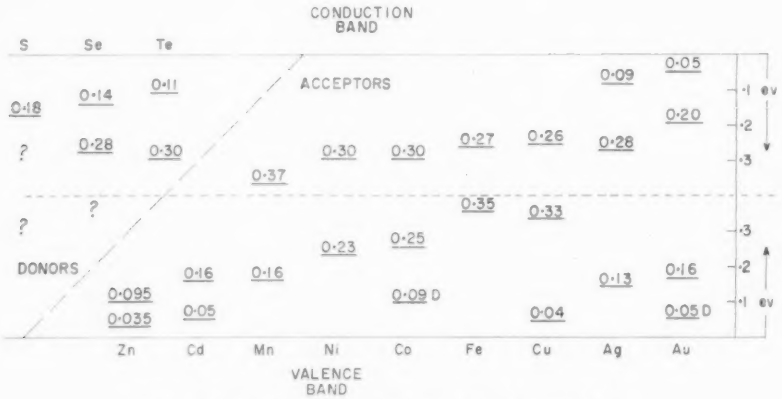


FIG. 1 Ionization energies for deep level impurities in Ge obtained from Hall coefficient studies. Energy values (in eV) are measured from the nearest band edge and represent values at absolute zero. For Se and S only the upper donor levels have been accurately measured.

## 2. SUMMARY OF IMPURITY LEVELS

An empirical correlation exists between the electron configurations and the type and number of energy levels introduced by many impurities in Ge. It has been recognized that the hydrogen-like impurities, such as As ($4s^24p^3$) and Ga ($4s^24p^1$), act as single donors and acceptors respectively because of an excess or deficit of one electron from the four needed to form valence bonds with nearest neighbor Ge atoms ($4s^24p^2$). Similar considerations are applicable for many of the deep level impurities. For example, Zn($4s^2$) acts as a double acceptor,[7] Cu($4s^1$) acts as a triple acceptor[8] and Te($4s^24p^6$) acts as a double donor.[9] The applicability of this tetrahedral bonding model constitutes evidence that these impurities are substitutional in the Ge lattice. At present no adequate theory has been proposed for the calculation of energy values for the deep level impurities.[10]

Figure 1 summarizes the positions of energy levels for the deep level impurities in Ge. Acceptor impurities will be discussed first. Zn,[7,11] Cd[12] and the transition metal impurities Mn,[13] Fe,[14] Co[15] and Ni[16,17,18] act as double acceptor

impurities. Cu,[8,11b,19,20] Ag[21] and Au[8,22] act as triple acceptor impurities. The method of introduction of these impurities into Ge and the determination of the positions of energy levels by Hall coefficient studies have been described in the original publications. In most cases the positions of the levels have been confirmed by studies of the spectral dependence of the extrinsic photoconductivity.[5]

As indicated in Fig. 1, Au[23] and Co[24] also introduce donor levels below the acceptor levels. No donor level is found for Ni[24] which in many respects is similar to Co. The donor levels found for Au and Co may be characteristic of interstitial sites. However, the approximate equality in concentration of donor and acceptor states for both Au[23,8] and Co makes it probable that they are associated with the same substitutional site.

Experimental evidence for all of the multiple level models represented in Fig. 1 is primarily this approximate equality in concentrations of the different levels for a given impurity. This equality in level concentration has been confirmed over a range of impurity concentrations for Zn, Cu, Ni and Au. In addition, studies of mobility have confirmed the presence of doubly charged sites in Zn[7] and Ni[24] doped crystals.* Mobility studies also indicate that both Cu and Au are probably triply charged under proper conditions of temperature and compensation.[8]

In addition to the levels of Fig. 1 which are thought to be characteristic of substitutional impurities, the introduction of a given impurity may also give rise indirectly to shallow acceptor levels, usually at lower concentrations. Such auxiliary levels have been observed in Ni, Mn[13] and Ag[21] doped Ge, and have been studied in most detail for the case of Ni doped Ge.[25,26] Ni-doped samples may be prepared (by diffusion at high temperature and rapid quenching) so that the shallow acceptor levels (0·05 eV and 0·01 eV) are in very low concentration relative to the deeper acceptor levels. On heat treatment at temperatures as low as 400°C the deep levels may be largely converted into shallow levels. Subsequent level treatment at high temperatures followed by quenching converts the shallow levels back to deep levels.[24] It seems likely that supersaturated Ni in substitutional solution may precipitate at low temperatures leaving vacancies, vacancy aggregates or Ni complexes which give rise to the shallow acceptor levels. The possibility[27] that the 0·05 eV acceptor states are attributable to Cu does not seem to be consistent with radiotracer studies of the diffusion of Cu in Ni-doped Ge at 400°C.[28]

Less complete information is available for several other acceptor impurities in Ge. Cr[29] seems to introduce several shallow acceptor levels between 0·12 eV and the valence band. Its solubility is low and accurate measurements of the concentrations of these several levels have not been made. Pt introduces an acceptor level at 0·04 eV and also deeper acceptor levels in appreciably lower concentrations.[11b,29] Thus it is not clear that Pt acts simply as a multiple acceptor impurity. Attempts to see electrical activity associated with Ti and V in Ge have not been successful.[29,13]

Figure 1 also summarizes information presently available for deep level donor impurities. It is fairly well established that Te acts as a double donor impurity, consistent with the tetrahedral bonding model. The two donor levels indicated are observed in approximately equal concentrations for crystals doped from the melt[9a] or by diffusion.[9b] Other levels seen in Te-doped samples grown from the melt are present at lower concentrations in diffused samples. For Se[24] and S[24] the positions of the upper donor levels have been well established. However, it is not clear that Se and S act simply as double donors. There is some evidence for two other deep donor levels associated with both of these elements. The approximate positions of these levels are indicated in Fig. 2. For Se the 0·28 eV level is present in concentrations which are several times greater than that of the 0·14 eV level for both diffused and melt doped crystals. It does not seem probable that either of these elements should act as a triple donor impurity. However they may be present in both substitutional and interstitial sites, giving donor levels at each site.

*These studies of Hall coefficient and mobility in Ge samples containing $8 \times 10^{15}$ Ni atoms/cm$^3$ do not show the anomalous phenomena reported in reference (18b) and interpreted as impurity banding.

These donor elements are difficult to introduce into Ge because of their high vapor pressure, resulting in a high rate of loss from the Ge melt, and because of their relatively low diffusion coefficients in solid Ge. However, for both Te and Se the positions of the levels have

been observed in both melt doped and diffused samples. For S the results have been obtained only for diffused samples. Diffusion studies have been made in a sealed quartz capsule at 920°C. The problem of Cu contamination was less serious than anticipated, probably because of gettering by the Te, Se or S. For all of these elements effective diffusion rates in Ge can be enhanced by prior deformation of the Ge, presumably because of dislocation piping.

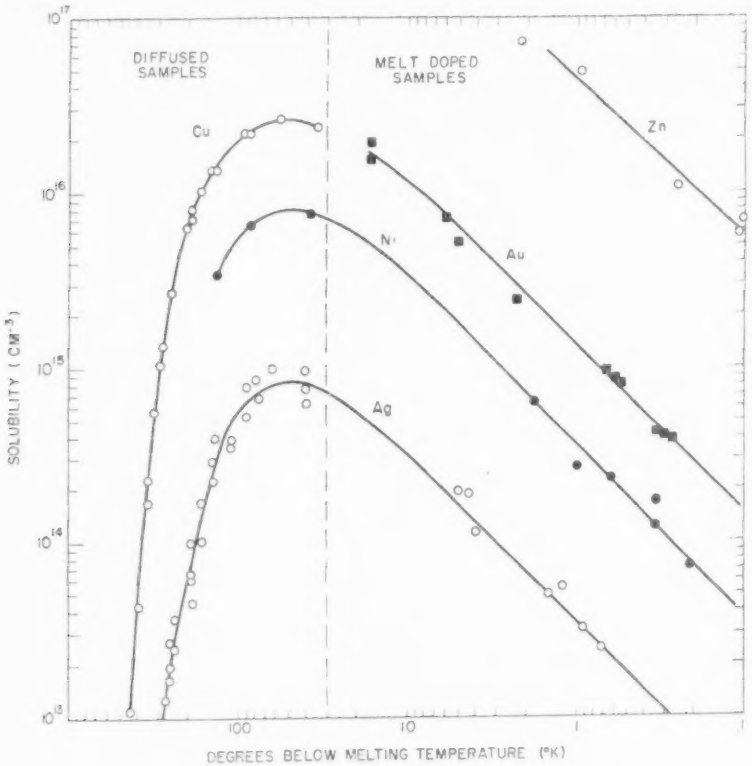


FIG. 2. Solubility of several deep level impurities in Ge plotted as a function of temperature in degrees (°K) below the melting temperature. The dotted line separates data obtained on diffused samples from that obtained on melt-doped samples.

In addition to impurities discussed above, Si,[30] Sn[31] and Pb[31] are soluble in Ge but are electrically neutral. Assuming that it requires less energy to break a Sn–Ge bond than a Ge–Ge bond, it might be expected that Sn (or Pb) would introduce a donor level near the valence band which would show up in Ge doped with comparable concentrations of both Ga and Sn. Such a level is not found for Sn.[24] The presence of electrically inactive hydrogen and oxygen has been reported[32] at concentrations as high as $10^{18}$ cm$^{-3}$ in Ge.*

*G. ELLIOT, *Nature* **180**, 1350 (1957), has recently indicated that oxygen acts as a donor impurity in Ge. His results have been confirmed and extended.[24] There is evidence for a deep donor level attributable to oxygen.

VOL. 8 1959

### 3. SOLUBILITY AND DIFFUSIVITY OF DEEP LEVEL IMPURITIES

The solubilities of the deep level impurities are appreciably lower than for the hydrogen like impurities. Fig. 3 shows solubility values derived from Hall coefficient studies plotted as a function of temperature (degrees below the melting temperature of Ge). The vertical dotted line separates data points obtained with diffused samples from data points obtained with samples grown from doped melts. The temperature of the melt was calculated from the known concentration of impurity in the melt.[33] All of the deep level impurities show a retrograde solubility.[34]

Data for Zn[7] are in agreement with published values for lower temperatures.[35] Both Zn and Au have low diffusion constants and solubility studies are not conveniently made using diffusion. The data given here for Au[24] indicate that the maximum solubility is at least as great as that of Cu. Data for Cu[8] shown in Fig. 3 are in good agreement with radiotracer studies.[36] Solubility values for Ni, which were obtained[26] by measuring the As concentration needed to completely compensate the 0·23 eV Ni level, are somewhat higher than published values[37] obtained from resistivity measurements in uncompensated samples. Ag has the lowest distribution coefficient and solubility of the impurities which have been studied in any detail. Values shown here[21] are in reasonable agreement with radiotracer studies.[38] Table 1 gives a compilation of distribution coefficients and maximum solubility values for deep level impurities. These values have not been confirmed using radiotracer methods for any of the deep donor impurities.

*Table* 1.

| Element | Maximum solubility ($cm^{-3}$) | Distribution coefficient | References |
|---|---|---|---|
| Zn | $5{\cdot}5\times10^{18}$ | $4\times10^{-4}$ | 35, 7 |
| Cd | | $>1\times10^{-5}$ | 12 |
| Mn | | $\sim10^{-6}$ | 13 |
| Ni | $8\times10^{15}$ | $3\times10^{-6}$ | 26, |
| Co | $\sim2\times10^{15}$ | $\sim10^{-6}$ | 24, 15 |
| Fe | $\sim1{\cdot}5\times10^{15}$ | | 39 |
| Cu | $2{\cdot}6\times10^{16}$ | $\sim10^{-5}$ | 8, 36, 24 |
| Ag | $8\times10^{14}$ | $4\times10^{-7}$ | 21, 38 |
| Au | $>2\times10^{16}$ | $1{\cdot}3\times10^{-5}$ | 24, 22 |
| Te | $>2\times10^{15}$ | $\sim10^{-6}$ | 9, 24 |
| Se | $>5\times10^{15}$ | | 24 |
| S | $>5\times10^{15}$ | | 24 |

Diffusion in Ge is of particular interest because of the wide range of values observed and the several possible mechanisms. It is generally believed that impurities of low diffusion coefficients remain substitutional and diffuse by the vacancy mechanism.[4,40] Impurities with large diffusion coefficients, such as Cu,[36] are thought to diffuse as interstitial positive ions. The time required for such impurities to attain equilibrium substitutional solubility will depend not only on the interstitial diffusivity but also on the rate of association with vacancies. For these impurities, the effective diffusivity may be structure sensitive.[41–43]

Table 2 lists approximate values of diffusion constants for some of the deep level impurities. No attempt is made to review the details of the temperature or structure dependence. Except for Zn, it is observed that diffusion constants for the deep level impurities are large compared to the self diffusion of Ge[44,45] and diffusion coefficients of the III–V column elements.[46]

Table 2.

| Element | Temp. (°C) | Diffusivity ($cm^2$/sec) | References |
|---|---|---|---|
| Zn | 900 | $1\times10^{-11}$ | 46 |
| Ni | 875 | $5\times10^{-5}$ | 37 |
| Fe | 930 | $4\times10^{-6}$ | 39 |
| Cu | 900 | $3\times10^{-5}$ | 36, 43 |
| Ag | 900 | $2\times10^{-6}$ | 38 |
| Au | 900 | $4\times10^{-9}$ | 22 |
| Se | 920 | $\sim10^{-10}$ | 24 |
| S | 920 | $\sim10^{-9}$ | 24 |
| Te | 920 | $\sim10^{-11}$ | 24 |

### 4. OTHER STUDIES OF DEEP LEVEL IMPURITIES

Knowledge of the energy level structure, the solubility and diffusivity of many impurities in Ge has stimulated a variety of additional research studies. Particular emphasis has been placed on optical studies.[5] The extrinsic photoconductance spectrum has been measured for the different charge states for most of the deep level impurities. In general, the threshold for photoconductive response is consistent with the position of the level measured by Hall coefficient studies. Because of the

variety of deep levels now known, Ge samples may be prepared with extrinsic thresholds from 3 $\mu$ out to 40 $\mu$. Control of the charge at the impurity site permits control of the response time of the photoconductivity because of the effect of coulomb fields on capture cross-sections.[5] Response times for extrinsic photoconductivity vary from $10^{-10}$ sec to $> 10$ sec depending on the dominant impurity, its charge state and the temperature. This ability to control spectral response and response time of the extrinsic photoconductivity makes Ge of considerable interest from the point of view of infrared detection.

Direct measurement of the optical absorption cross-sections for deep level impurities is difficult because of their low solubilities. However, measurements have been made for Zn,[47] Cu[48] and Ni[5] in Ge. For both Cu and Ni the photoconduction and absorption spectra are similar. Recent far infrared studies of the absorption spectrum of neutral Zn in Ge[49] has shown structure possibly attributable to excited states. With this exception there is no experimental evidence for excited states of deep level impurities.

The recognized importance of deep level impurities as recombination centers in Ge stimulated many of the initial studies.[16,36] However, in spite of the extensive knowledge now available about equilibrium properties of impurities in Ge, values of capture cross-sections for possible recombination processes are incomplete and approximate. Several authors have treated the statistics of recombination processes.[50] A recent review[51] discusses methods of measuring lifetime in Ge and Si and summarizes published values of capture cross-sections deduced from these measurements. One aspect of recombination which has been demonstrated in Ge studies is the importance of the charge at the impurity site in determining relative capture cross-sections for electrons and holes.[5]

Detailed studies of spin resonance of Mn[52] and Ni[53] in Ge have been reported. The resonances observed are attributed to $Mn^{-}$ and $Ni^{-}$; spin resonance for the other possible charge states of these impurities has not been observed. As for recombination studies, the control over the charge at the impurity site is important in permitting the observation and interpretation of resonance studies.

The spin resonance studies of Mn and Ni tend to confirm the double acceptor model and indicate that these impurities are isolated and not associated with vacancies, dislocations or other impurities. For the case of Ni in particular spin resonance studies have yielded information about the hyperfine interaction with $Ge^{73}$ in the nearest neighbor positions. Such information permits estimates of the spatial extent of wave functions associated with deep level impurities and may eventually stimulate the development of a theory of deep levels.

Preliminary studies[54] indicate that under certain conditions spin resonance absorption is observable in Ge crystals containing Fe or Co. At present the experimental control over impurity concentrations and the charge at impurity sites is less effective for Fe and Co than for Ni and the interpretation of resonance studies is more difficult. Initial attempts[54] to detect spin resonance associated with any of the charge states of Au, Zn and Te in Ge have not been successful. The reasons for this are not understood in detail. However, the information presently available indicates that the application of spin resonance studies to Ge may perhaps be limited to those impurities with unfilled *d*-shells.

*Acknowledgments*—The author is indebted to R. NEWMAN and H. H. WOODBURY whose co-operation was essential to many aspects of this review, and to E. O. KANE for many valuable discussions.

## REFERENCES

1. BURTON J. A., *Physica* **20,** 845 (1954).
2. BURSTEIN E. and EGLI P. H., *Advances in Electronics and Electron Physics,* Vol. VII, p. 1. Academic Press, New York (1955).
3. BROOKS H., *Advances in Electronics and Electron Physics,* Vol. VII, p. 85, Academic Press, New York (1955).
4. DUNLAP W. C. Jr., *Progress in Semiconductors,* Vol. 2, p. 167. John Wiley & Sons, New York (1957).
5. NEWMAN R. and TYLER W. W., "Photoconductivity in Germanium", to be published in *Solid State Physics.* Academic Press, New York.
6a. COLLINS C. B. and CARLSON R. O., *Phys. Rev.* **108,** 1409 (1957).
6b. HANNAY N. B., *Progress in Semiconductors,* Vol. 1. Heywood and Company Ltd., London (1956).
7a. TYLER W. W. and WOODBURY H. H., *Phys. Rev.* **102,** 647 (1956).
7b. KALASHNIKOV S. G., LVOVA E. IU. and OSTROBORODOVA V. V., *Zh. tekh. fiz., Moscow* **27,** 1925 (1957).

8. WOODBURY H. H. and TYLER W. W., *Phys. Rev.* **105,** 84 (1957).
9a. ARMSTRONG J. A., TYLER W. W. and WOODBURY H. H., *Bull. Amer. Phys. Soc.* **2,** 265 (1957).
9b. TYLER W. W., unpublished work.
10. See KOHN, W. *Solid State Physics,* Vol. 5, p. 257. for a review of the effective mass theory applied to hydrogen-like impurities in Ge and Si. Academic Press, New York (1957).
11a. DUNLAP Jr. W. C., *Phys. Rev.* **85,** 945 (1952).
11b. DUNLAP Jr. W. C., *Phys. Rev.* **96,** 40 (1954).
12. WOODBURY H. H. and TYLER W. W., *Bull. Amer. Phys. Soc.* **1,** 127 (1956).
13. WOODBURY H. H. and TYLER W. W., *Phys. Rev.* **100,** 659 (1955).
14a. TYLER W. W. and WOODBURY H. H., *Phys. Rev.* **96,** 874 (1954).
14b. GLINCHUK K. D., MISELUK E. G. and FORTUNATOVA N. N., *Zh. tekh. fiz., Moscow* **27,** 2451 (1957).
15. TYLER W. W., NEWMAN R. and WOODBURY H. H., *Phys. Rev.* **97,** 669 (1955).
16. BURTON J. A., HULL G. W., MORIN F. J. and SEVERIENS J. C., *J. Phys. Chem.* **57,** 853 (1953).
17. TYLER W. W., NEWMAN R. and WOODBURY H. H., *Phys. Rev.* **98,** 461 (1955).
18a. BATTEY J. F. and BAUM R. M., *Phys. Rev.* **100,** 1634 (1955).
18b. KANAI Y. and NII R., *J. Phys. Soc. Japan* **12,** 125 (1957).
19. MORIN F. J. and MAITA J. P., *Phys. Rev.* **90,** 337 (A) (1953).
20. BATTEY J. F. and BAUM R. M., *Phys. Rev.* **94,** 1393 (1954).
21. TYLER W. W., *Bull. Amer. Phys. Soc.* **3,** 128 (1958) (details to be published).
22. DUNLAP Jr. W. C., *Phys. Rev.* **97,** 614 (1955).
23a. DUNLAP Jr. W. C., *Phys. Rev.* **100,** 1629 (1955).
23b. SCHULTZ M. L. and MORTON G. A., *Proc. Inst. Radio Engrs., N.Y.,* **43,** 1819 (1955).
24. TYLER W. W., unpublished work.
25. PENNING P., *Phys. Rev.* **102,** 1414 (1956).
26. TYLER W. W. and WOODBURY H. H., *Bull. Amer. Phys. Soc.* **2,** 135 (1957). See also TWEET A. G., *Phys. Rev.* **111,** 67 (1958) for similar studies in Cu-doped Ge.
27. PENNING P., Philips Res. Rep. **13,** 17 (1958).
28. TWEET A. G. and TYLER W. W., *J. Appl. Phys.* **29,** 1578 (1958).
29. WOODBURY H. H. and TYLER W. W., unpublished work.
30. See JOHNSON E. R. and CHRISTIAN S. M., *Phys. Rev.* **95,** 560 (1954) and cited references.
31. TRUMBORE F. A., RICHARDS W. H. and ISENBERG C. R., Bell Telephone Laboratories Technical Memorandum; TRUMBORE F. A., *J. Electrochem. Soc.* **103,** 597 (1956).
32. THURMOND C. D., GULDNER W. G. and BEACH A. L., *J. Electrochem. Soc.* **103,** 603 (1956).
33. HALL, R. N., *J. Phys. Chem. Solids* **3,** 63 (1957).
34. THURMOND C. D. and STRUTHERS J. D., *J. Phys. Chem.* **57,** 831 (1953).
35. THURMOND C. O., TRUMBORE F. A. and KOWALCHIK M., *J. Chem. Phys.* **25,** 799 (1956).
36. FULLER C. S., STRUTHERS J. D., DITZENBERGER J. A., and WOLFSTIRN K. B., *Phys. Rev.* **93,** 1182 (1954).
37. VAN DER MAESEN F. and BRENKMAN J. A., *Philips Res. Rep.* **9,** 225 (1954).
38. BUGAY A. A., KOSENKO V.E. and MISELUK E.G., *Zh. tekh. fiz., Moscow* **27,** 1671 (1957).
39. BUGAY A. A., KOSENKO V. E. and MISELUK E. G., *Zh. tekh. fiz., Moscow* **27,** 210 (1957).
40. VALENTA M. W., *Bull. Amer. Phys. Soc.* **3,** 102 (1958).
41. TWEET A. G. and GALLAGHER C. J., *Phys. Rev.* **103,** 828 (1956).
42. FRANK F. C. and TURNBULL D., *Phys. Rev.* **104,** 617 (1956).
43. FULLER C. S. and DITZENBERGER J. A., *J. Appl. Phys.* **28,** 40 (1957).
44. LETAW H., PORTNOY W. N. and SLIFKIN L., *Phys. Rev.* **102,** 636 (1956).
45. VALENTA M. W. and RAMASASTRY C., *Phys. Rev.* **106,** 73 (1957).
46. DUNLAP Jr. W. C., *Phys. Rev.* **94,** 1531 (1954).
47. BURSTEIN E., PICUS G. and SCLAR N., *Photoconductivity Conference,* p. 353, John Wiley & Sons, New York (1956).
48. KAISER W. and FAN H. Y., *Phys. Rev.* **93,** 977 (1954).
49. PICUS G. and BURSTEIN E., private communication.
50a. HALL R. N., *Phys. Rev.* **87,** 387 (1952).
50b. SHOCKLEY W. and READ W. T., *Phys. Rev.* **87,** 835 (1952).
50c. See also KALASHNIKOV S. G. *J. Phys. Chem. Solids,* **8,** 52 (1959).
51. BEMSKI G., *Proc. Inst. Radio Engrs., N.Y.* **46,** 990 (1958).
52. WATKINS G. D., *Bull. Amer. Phys. Soc.* **2,** 345 (1957).
53. LUDWIG G. W. and WOODBURY H. H., *Bull. Amer. Phys. Soc.* **3,** 135 (1958).
54. WOODBURY H. H. and LUDWIG G. W., private communication.


VOL. 8 1959

*J. Phys. Chem. Solids* Pergamon Press 1959. Vol. 8. pp. 66–73. Printed in Great Britain

# GIANT TRAPS

MELVIN LAX

C.3

Bell Telephone Laboratories, Incorported, Murray Hill, New Jersey

**Abstract**—Enormous cross-sections in the range $10^{-15}$ cm$^2$ to $10^{-13}$ cm$^2$ have been observed for a wide variety of traps in Si and Ge some involving binding energies many times the Debye energy. Direct transitions to the ground states of these traps require simultaneous emission of many phonons. Such multiphonon emission is a highly unlikely event in these materials where the electron lattice interaction is weak and yields cross-sections too small by five to ten orders of magnitude. Cross-sections comparable to, or within an order of magnitude of those observed can be calculated on the basis of capture into the highly excited states of coulomb attractive centers followed by a cascade process involving successive emissions and absorptions of single phonons until the electron enters the ground state or escapes. The initial capturing event is likely to involve an optical phonon or an intervalley collision in the room temperature range, but the acoustic phonon contribution will predominate at low temperatures.

The large cross-sections $10^{-17}$ cm$^2$ to $10^{-15}$ cm$^2$ found for neutral centers can be explained on the same basis, the attractive potential in this case being provided by the large polarizability of the neutral center.

VOL.
8
195

## 1. INTRODUCTION

THE phenomenological description of an impurity as a trap or a recombination center makes use of the cross-section presented by the impurity for the capture of an electron or a hole. The cross-sections reported in the literature (see Table 1) cover an enormous range $10^{-12}$ cm$^2$ to $10^{-22}$ cm$^2$. The giant trapping cross-sections $10^{-15}$ cm$^2$ to $10^{-12}$ cm$^2$ seem to be associated with attractive centers. The large cross-sections $10^{-17}$ cm$^2$ to $10^{-15}$ cm$^2$ seem to be associated with neutral cross-sections and the minuscule cross-sections $10^{-22}$ cm$^2$ are certainly associated with repulsive centers.

While a cross-section of $10^{-15}$ cm$^2$ might seem reasonable in view of the geometrical size of an impurity state, one must remember that the electron not only must come to the vicinity of the center, it must on arrival perform the unlikely task of disposing of perhaps 0·5 eV (and it may take ten phonons to carry away this energy). Thus the geometrical cross-section would have to be multiplied by the (small) probability of such an unlikely energy losing collision.*

Our present task is to explain (1) how giant cross-sections are possible for attractive centers, (2) how large cross-sections are possible for neutral centers, (3) why the cross-section is so sensitive to the charge on the center. We have previously suggested[2] that large cross-sections are made possible by capture into excited states possessing large orbits. The large energy loss is accomplished by a cascade process involving the successive emission of single phonons as the electron plummets down the excited states. Such excited states of large orbit are clearly available to a coulomb attractive center, and as we shall see permit (classically calculated) enormous cross-sections that depend on the charge of the center but not on details of its potential. For neutral centers a moderately long range inverse fourth power potential is available because of the interaction between the charge carrier and the polarizability of the center. Since the polarizability of an atom varies inversely as the square of the ionization energy, and ionization energies of centers in solids are an order of magnitude lower than free atom ionization energies, large polarizabilities result. These polarizabilities will sometimes, but not always, be large enough to permit a ladder of excited states sufficient to allow a cascade process. Thus cross-sections of neutral centers will be more sensitive to the detailed

*Estimates of cross-sections for multi phonon processes are given by H. GUMMEL and M. LAX,[1] and are shown to be quite small $< 10^{-20}$ cm$^2$ in materials like Si and Ge.

*Table* 1. *Capture cross-sections and their temperature dependence*
(the exponent $n$ in $T^{-n}$ is shown in the last column).

| Host | Center | Charge | $T$ | $\sigma_n$ | $\sigma_p$ | $n$ | Author |
|---|---|---|---|---|---|---|---|
| Si | $Au^+$ | Attract. | 300° | $3{\cdot}5\times10^{-15}$ | | 2·5 | Bemski[a] |
| | | | 77° | $1\times10^{-13}$ | | | Davis[b] |
| | $Au^-$ | Attract. | 300° | | $1{\cdot}0\times10^{-15}$ | 4 | Bemski[a] |
| | | | 77° | | $3\times10^{-13}$ | | Davis[b] |
| | $Au^\circ$ | Neutral | 300° | $5\times10^{-16}$ | $>3\times10^{-16}$ | 0 for $\sigma_n$ | Bemski[a] |
| | | | 77° | $4\times10^{-15}$ | $4\times10^{-15}$ | | Davis[b] |
| | $In^-$ | Attract. | 100° | | $1{\cdot}5\times10^{-13}$ | 2 | Wertheim[c] |
| | $In^\circ$ | Neutral | 100° | $1{\cdot}1\times10^{-16}$ | | 1 | Wertheim[c] |
| Ge | $Sb^+$ | Attract. | 4° | $10^{-12}$ | | 2·7 | Koenig[d] |
| | $Ni^-$? | Attract. | 300° | | $>4\times10^{-15}$ | | Burton *et al.*[e] |
| | | | | | $3{\cdot}5\times10^{-14}$ | | Battey and Baum[f] |
| | | | | | $1{\cdot}2\times10^{-16}$ | | Okada[g] |
| | | | 70° | | $10^{-13}$ | | Newman and Tyler[h] |
| | $Cu^-$? | Attract. | 300° | | $10^{-16}$ | | Burton *et al.*[e] |
| | $Cu^-$? | Attract. | 130–200° | | $10^{-16}$ | 0 | Shulman and Wyluda[i] |
| | $Fe^-$ | Attract. | 300° | | $3\times10^{-15}$ | | Glinchunk *et al.*[j] |
| | $Fe^{--}$ | Attract. | 300° | | $1\times10^{-14}$ | | Glinchunk *et al.*[j] |
| | $Ni^\circ$? | Neutral? | 300° | $8\times10^{-17}$ | | | Burton *et al.*[e] |
| | | | | $8\times10^{-16}$ | | | Battey and Baum[f] |
| | | | | $9\times10^{-17}$ | | | Okada[g] |
| | $Cu^\circ$? | Neutral? | 300° | $10^{-17}$ | | | Burton *et al.*[e] |
| | $Fe^\circ$, $Co^\circ$, $Ni^\circ$, $Mn^\circ$ | | 300° | $10^{-16}-10^{-15}$ | | | Tyler and Woodbury[k] |
| | $Mn^-$ | Repulsive | 300° | $<10^{-22}$ | | | Tyler and Woodbury[k] |


a Bemski G., *Phys. Rev.* (to be published).
b Davis W. D. (Private communication).
c Wertheim G. K., *Bull. Amer. Phys. Soc.* Ser. II, **2**, 314 (1957).
d Koenig S., *Phys. Rev.* **110**, 986, 988 (1958).
e Burton J., Hull R., Morin F. and Severiens J., *J. Phys. Chem.* **57**, 853 (1953).
f Battey J. F. and Baum R. M. *Phys. Rev.* **100**, 1634 (1955).
g Okada J., *J. Phys. Soc. Japan* **12**, 741, 1338 (1957).
h Newman R. and Tyler W. W., *Bull. Amer. Phys. Soc.* Ser II, **3**, 15 (1958).
i Shulman R. G. and Wyluda B. J., *Phys. Rev.* **102**, 1455 (1956).
j Glinchunk K. D., Miseluk E. G. and Fortunatova N. N., *Zh. tekh. fiz., Moscow* **27**, 2451 (1957).
k Tyler W. W. and Woodbury H. H., *Bull. Amer. Phys. Soc.* Ser. II **1**, 127 (1956) paper L7.

potential of the centers and will exhibit more variability from one center to another than cross-sections for attractive centers.

Repulsive centers will surely not have excited states of large orbit, indeed they may not possess excited states at all. Thus repulsive centers do not permit a cascade process and might actually proceed by multi-phonon emission with very small cross-section.

Thus a cascade process would explain the sensitivity of the cross-sections to the state of charge, and an appreciable variability of cross-sections in the neutral and repulsive cases. The primary tasks that remain are (1) to show that for attractive centers cross-sections as large as those observed are possible, (2) to make a crude estimate for neutral centers supposing that such excited states exist.

## 2. ASSUMPTIONS

Our calculation will be based on the following assumptions,

(1) Between collisions the motion of the electron may be described by its classical orbit in the presence of an attractive center.*

(2) The probability per unit time of a collision with a given energy loss, at any point of the orbit, may be computed (quantum-mechanically) as if the electron were moving uniformly (in a plane wave) with the momentum appropriate to that point on the orbit. (This implies that the change in momentum on the orbit over a time interval of the order of the duration of a collision may be neglected.)

(3) The ionization energy of the ground state of the center is large compared to $kT$ (otherwise the center would not act as a trap).

(4) For binding energies in the vicinity of $kT$ there are enough excited states to permit the use of classical mechanics for calculating transitions into such states or between them.

(5) Motion up and down among the excited states is so rapid that electrons which escape in effect come out instantaneously (as compared with the rate at which electrons disappear from the conduction band during the capture process) so that one need not be concerned with time delays but only with the fraction $P(U)$ of electrons that are captured with binding energy $U$ that stick (i.e. enter the ground state before emerging). The overall cross-section for capture of electrons with kinetic energy $E_0$ can therefore be written in the form

$$\sigma(E_0) = \int \sigma(E_0, U)\, dU\, P(U) \qquad (2.1)$$

where $\sigma(E_0, U)dU$ is the differential cross-section for a collision with energy loss $E_0+U$ into a state of binding energy $U$.

(6) Equation (2.1) already neglects the possible dependence of the sticking probability $P(U)$ on the angular momentum of the state as well as its binding energy.

(7) The sticking probability $P(U)$ does not depend on the history of arrival into state $U$. Thus if $K(U, \hbar\omega)d(\hbar\omega)$ is the probability (not per unit time) that an electron in state $U$ will emit a phonon $\hbar\omega$ in $d(\hbar\omega)$ then

$$P(U) = \int_{U+\hbar\omega>0} K(U, \hbar\omega)d(\hbar\omega)P(U+\hbar\omega) \qquad (2.2)$$

represents the probability of entering the ground state as the probability of any first step times the probability that the first step leads to eventual capture.

(8) The total probability of all possible steps including emission: $\hbar\omega > 0$ and absorption: $\hbar\omega < 0$ is by definition unity.

$$\int K(U, \hbar\omega)d(\hbar\omega) = 1. \qquad (2.3)$$

(9) If an electron in making transitions among the states $U$ reaches a state of positive energy ($U < 0$) it has definitely escaped. Hence $P(U) = 0$ for $U < 0$, and this explains the lower limit $U+\hbar\omega > 0$ in equation (2.2).

(10) For a coulomb attractive center the virial theorem implies that the average kinetic energy in a closed orbit is equal to the binding energy $U$. If $[1/l(E, \hbar\omega)]d(\hbar\omega)$ is the differential reciprocal mean free path for a collision with energy loss between $\hbar\omega$ and $\hbar\omega+d(\hbar\omega)$ we may take

$$K(U, \hbar\omega) = \frac{1/l(U, \hbar\omega)}{\int(1/l(U, \hbar\omega)]d(\hbar\omega)} \qquad (2.4)$$

*For a coulomb attractive center this assumption is valid at distances greater than the solid state Bohr radius.

by neglecting fluctuations in the kinetic energy along the orbit and normalizing in accord with equation (2.3).

(11) For acoustic phonon collisions we may use the deformation potential theory[3] without neglecting the phonon energy to show that the differential reciprocal mean free path $1/l(E, \hbar\omega)$ is given by*

$$\frac{1}{l(E,\hbar\omega)} = \frac{1}{l_c}\frac{1}{8Emc^2}|\hbar\omega|\frac{\lambda}{1-\exp(-\lambda)} \quad (2.5)$$

where

$$\lambda = \hbar\omega/kT \quad (2.6)$$

and the "classical" mean free path $l_c$ is given by

$$1/l_c = E_1^2 kTm^{5/2}/(\pi\hbar\rho c^2) \quad (2.7)$$

where $c$ is the velocity of sound, $m$ is the effective mass of the electron $\rho$ is the crystal density and $E_1$ is the deformation potential constant. (In practice we shall determine $l_c$ from the experimental mobility rather than equation (2.7).) Conservation of energy and momentum limit the possible phonons in equation (2.5) that may be emitted or absorbed respectively to

$$(\hbar\omega/\tfrac{1}{2}mc^2) \leqslant 4[(E/\tfrac{1}{2}mc^2)^{\frac{1}{2}}-1] \quad (2.8)$$

$$(\hbar\omega/\tfrac{1}{2}mc^2) \geqslant -4[(E/\tfrac{1}{2}mc^2)^{\frac{1}{2}}+1]. \quad (2.9)$$

(12) In computing the sticking probability $P(U)$ from equations (2.2) and (2.4) we actually used only acoustic phonon collisions in our initial calculation, although optical phonons may also have some influence.

(13) A starting approximation to $P(U)$ may be obtained by noticing that when $U \sim kT \gg \frac{1}{2}mc^2$ the maximum energy changes by equations (2.8) and (2.9) are of the order $4(U\frac{1}{2}mc^2)^{\frac{1}{2}} \ll U$. Thus in equation (2.2) $P(U+\hbar\omega)$ may be expanded, regarding $\hbar\omega$ is small, to second order in $\hbar\omega$. This "Fokker–Planck" type approximation leads to a second order differential equation whose solution if we neglect terms of order $mc^2/kT$, $mc^2/E$ and $4(U\frac{1}{2}mc^2)^{\frac{1}{2}}/kT$ can be written:

$$P(U) = 1-(1+\alpha+\tfrac{1}{2}\alpha^2)\exp(-\alpha) \quad (2.10)$$

with

$$\alpha = (U-\tfrac{1}{2}mc^2)/kT$$

The solution has been written in this form to emphasize that $P(U) = 0$ for $U \leqslant \frac{1}{2}mc^2$ since electrons with a velocity less than that of sound cannot emit phonons and hence must escape. A plot of equation (2.10) is shown in Fig. 1. In Fig. 2 we show the correct solutions at four temperatures obtained by iterating equation (2.2) using (2.10) as a

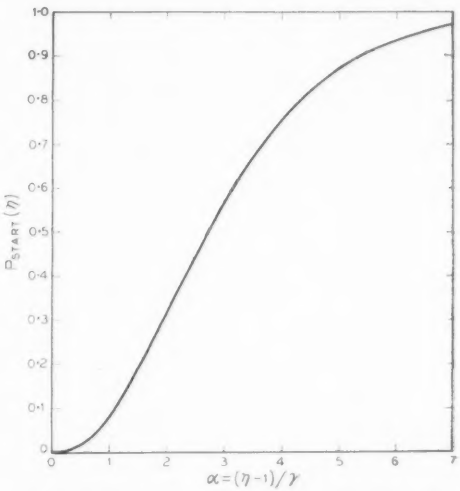


FIG. 1. A starting approximation $P_{start}$ for the sticking probability is plotted against $\alpha = (U-\frac{1}{2}mc^2)/kT$ where $U$ is the binding energy, $m$ the effective mass of the carrier $c$ the velocity of sound, $T$ the absolute temperature and $k$ is Boltzmann's constant.

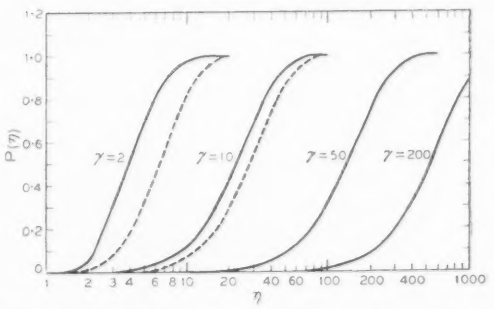


FIG. 2. Numerical solutions $P(\eta)$ of the sticking probability integral equation are plotted against $\eta = U/\frac{1}{2}mc^2$ for $\gamma \equiv kT/\frac{1}{2}mc^2 = 200$, 50, 10 and 2. These solutions were obtained by iteration using the starting approximation shown in Fig. 1. For $\gamma = 50$ and 200 (and hence also larger $\gamma$) the correct solution is indistinguishable from the (dotted) starting approximation on the scale shown.

*A more detailed presentation of the subject matter sketched in this paper will be presented to the Physical Review.

starting approximation. In all cases, the sticking probability becomes close to unity for binding energies large compared to $kT$.

(14) The fate of the electron is decided in the vicinity $U \sim kT$. Hence all previous assumptions, concerning the validity of classical mechanics and the rapidity of diffusion up and down the energy scale need only relate to this region. The last step (or two) from the first excited state to the ground state may be a slow one requiring multi-phonon emission or the emission of radiation and a fully quantum mechanical treatment. However, if these states are deep compared to $kT$ the fate of the electron will have already been decided. Although such a last step may limit the rate at which the electron enters the ground state, it will not affect the rate at which electrons leave the conduction band or the observed trapping cross-section.*

### 3. IMPACT PARAMETER CROSS-SECTION CALCULATION

The motion of an electron (between collisions with phonons) is assumed to follow a classical orbit in the vicinity of a trapping center. The probability per unit time of a collision at some point on the orbit is computed quantum mechanically for an electron whose momentum is equal to the classical momentum at that point on the orbit. The cross-section for energy loss $E_0+U$ (see equation (2.1)), is computed from the area struck, $2\pi bdb$ times the probability that a collision with energy loss $E_0+U$ will occur somewhere along an orbit that starts with an energy $E_0$ and an impact parameter $b$:

$$\sigma(E_0, U) = \int 2\pi bdb \int dtW(E(t), E_0+U) \quad (3.1)$$

where $W(E, \hbar\omega)d(\hbar\omega)$ is the transition probability per unit time for a collision with energy loss between $\hbar\omega$ and $\hbar\omega+d(\hbar\omega)$.

The kinetic energy $E(t)$ at the time $t$ is given by

$$E(t) = E_0 - V(r(t)) \quad (3.2)$$

where $V(r)$ is the potential energy associated with the center ($-Ze^2/\kappa r$ for a coulomb attractive center with charge $Ze$ in a dielectric constant $\kappa$) and $r(t)$ is the instantaneous position on the orbit. The variable of integration may be changed from $t$ to $r$ by means of the Jacobian:

$$\frac{dr}{dt} = \left[\frac{2}{m}\left(E(r) - E_0\frac{b^2}{r^2}\right)\right]^{\frac{1}{2}} \quad (3.3)$$

The integration over $b$ can then be performed explicitly giving

$$\sigma(E_0, U) = \int_0^{r_0} 4\pi r^2 dr(E(r)/E_0)[1/l(E(r), E_0+U)] \quad (3.4)$$

where $1/l(E, \hbar\omega)$, the differential mean free path, is related to $W(E, \hbar\omega)$ by a factor $(2E/m)^{-\frac{1}{2}}$, and is given for acoustic phonons by equation (2.5).

The upper limit $r_0$ is the largest radius at which a collision with energy loss $E_0+U$ is possible i.e. for which $1/l(E(r), E_0+U)$ does not vanish. The ability of an electron to lose more than its initial energy is made possible by the speed up to the new kinetic energy $E(r)$.

For acoustic phonons, the differential reciprocal mean free path is given by equation (2.5). For optical phonons we shall take

$$\frac{1}{l(E, E_0+U)} = \frac{w}{2l_c}\frac{\lambda}{1-\exp(-\lambda)}\frac{(E-\hbar\omega)^{\frac{1}{2}}}{E^{\frac{1}{2}}}\delta(\hbar\omega - E_0 - U) \quad (3.5)$$

where $\hbar\omega$ is the optical phonon energy, $\lambda = \hbar\omega/kT$ and $w$ is HERRING's[4] factor describing the squared ratio of optical to acoustic matrix elements.

A thermal average cross-section can be computed from

$$\sigma = \int E_0 \exp(-E_0/kT)\sigma(E_0)dE_0 / \int E_0 \exp(-E_0/kT)dE_0 \quad (3.6)$$

where one factor of $E_0^{\frac{1}{2}}$ arises from the density of states and another because transition rates are proportional to the velocity times the cross-section.

*The author is indebted to ALBERT ROSE and GREGORY WANNIER for illuminating discussions of this point.

VOL. 8 1959

## 4. SUMMARY OF RESULTS

The total thermal average cross-section for capture of an electron on a coulomb attractive center may be computed by combining equations (2.5), (3.4) and (3.6) with the numerically computed sticking probability shown in Fig. 2. In the region $\gamma \equiv kT/\frac{1}{2}mc^2 \gg 1$ the total cross-section may be represented approximately by

$$\sigma \simeq \frac{4^5}{6}\frac{\sigma_1}{\gamma^4}\int_{\delta/\gamma}^{\infty}\frac{\exp(-x)}{x}dx$$

$$\simeq \frac{4^5}{6}\frac{\sigma_1}{\gamma^4}\left[\ln\left(\frac{\gamma}{1{\cdot}78\delta}\right)+\frac{\delta}{\gamma}\right] \qquad (4.1)$$

where

$$\sigma_1 = \frac{\pi}{12}\left(\frac{Ze^2}{\kappa\frac{1}{2}mc^2}\right)^3\frac{1}{l_c\gamma}. \qquad (4.2)$$

$\delta$ is represented as a function of $\gamma$ by Fig. 3, and

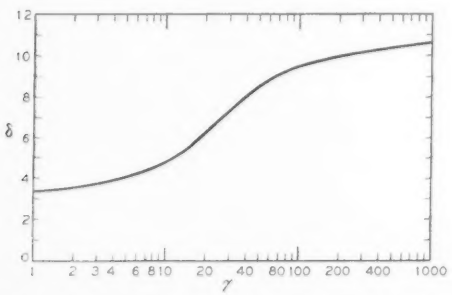


FIG. 3. The parameter $\delta$ is chosen as a function of $\gamma$ so that the simplified formula equation (4.1) agrees with numerically computed results at $\gamma = 200$, 50, 10 and 2. Equation (4.1) can now be used to interpolate for cross-sections at other temperatures.

$\kappa$ is the dielectric constant. Within a factor of three uncertainty, $\sigma_1$ for germanium is $7\times10^{-9}Z^3\,\mathrm{cm}^2$ and $\frac{1}{2}mc^2$ is $1{\cdot}13\times10^{-5}\,\mathrm{eV} = 0{\cdot}131°\mathrm{K}$. A plot of $\sigma$ vs. temperature is compared in Fig. 4 and S. KOENIG's[5] data for ordinary donors in germanium. Theoretical and experimental cross-sections increase from about $10^{-13}\,\mathrm{cm}^2$ at 10°K to $10^{-12}\,\mathrm{cm}^2$ at 4°K. The experimental results show a definite levelling off at 4°K. This levelling off may be attributed to the fact that at 4°K we have that $e^2/\kappa kT \simeq d$ where $d$ is the mean separation between traps, and $r_0 \simeq d$ where $r_0$ is the cut-off radius of equation (3.4) for the case of a thermal electron captured into a state with binding energy of order $kT$. Thus the cross-sections level off because one cannot count capture into orbits whose radius is larger than the separation between centers.

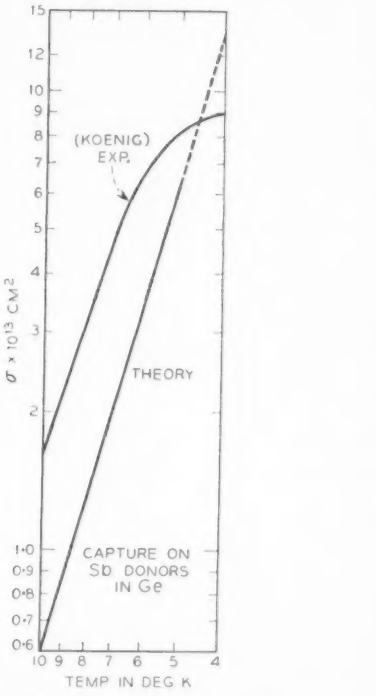


FIG. 4. The Cascade theory with acoustic phonons as the mechanism, i.e. equation (4.1) is compared with experimental results of S. Koenig for capture of electrons by Sb donors in germanium.

In the absence of such cut-offs, the characteristic temperature dependence of $1/T^4$ comes from (see equation 3.4))

$$\frac{r_0^3}{l_c}\frac{E(r_0)}{E_0} \simeq \frac{(1/T^2)^3}{1/T}\cdot\frac{T^2}{T} \sim \frac{1}{T^4} \qquad (4.3)$$

where the dependence of $E(r_0)$ (and hence $r_0 \sim \sim 1/E(r_0)$) on temperature can be seen by setting $\hbar\omega \simeq kT$ in equation (2.8) and solving for $E$.

For electrons in silicon, we have roughly $\sigma_1 \simeq 5{\cdot}5\times10^{-10}\,\mathrm{cm}^2$ and $\sigma \simeq 0{\cdot}5\times10^{-16}\,\mathrm{cm}^2$ at room temperature which is about one order of magnitude smaller than BEMSKI's reported cross-section for electrons on $Au^+$ of $3{\cdot}5\times10^{-15}\mathrm{cm}^2$. However, BEMSKI's cross-sections in the range

200° to 500° show a $T^{-2.5}$ behavior rather than a $T^{-4}$ behavior. We believe this implies that the observed cross-section is partly or predominantly due to intervalley and optical phonon processes.

Our results for optical phonons based on equation (3.5) can be summarized in the form

$$\sigma = \sigma_0 \lambda[1-\exp(-\lambda)]^{-1} D(\lambda) \tag{4.4}$$

where

$$\sigma_0 = \frac{8\pi}{15} \frac{w Z^3}{l_c} \frac{e^2}{\kappa k T} \left(\frac{e^2}{\kappa \hbar \omega}\right)^2 \tag{4.5}$$

is a temperature independent unit of cross-section, $\lambda = \hbar\omega/kT$ and $D(\lambda)$ is defined by

$$D(\lambda) = \lambda^{5/2} e^{-\lambda} \int_0^\lambda y^{-5/2} P(y) e^y dy \tag{4.6}$$

where

$$P(y) \simeq 1-e^{-y}(1+y+\tfrac{1}{2}y^2) \tag{4.7}$$

is the sticking probability in units $y = U/kT$. A plot of $D(\lambda)$ and the complete temperature dependence of $\sigma$ is shown in Fig. 5.

For electrons in silicon

$$\sigma_0 \sim 3{\cdot}5 \times 10^{-13} w Z^3 (\cdot 01 \text{ eV}/\hbar\omega)^2. \tag{4.8}$$

At room temperature $\lambda = \hbar\omega/kT \simeq 4$, so that $\lambda[1-\exp(-\lambda)]^{-1} D(\lambda)$ is about 5 and the total cross-section $\sigma$ is about $10^{-14}$ cm$^2$ if $w$ is of order unity. However, optical phonon transitions may be unimportant because of a selection rule. Intervalley transitions may be important because the ellipses for each valley are roughly 83 per cent of the way to the zone boundary in the 100 direction. Thus a small longitudinal acoustic phonon of perhaps 0·017 eV could cause an umklapp transition into the neighboring valley just across the zone boundary. This would yield $\sigma_0 \simeq 10^{-13}\, wZ^3$ and $\sigma \simeq 1{\cdot}7 \times 10^{-15}\, wZ^3$ cm$^2$ in rough agreement with Bemski's value of $3{\cdot}5 \times 10^{-15}$ cm$^2$ for electron on $Au^+$ in silicon.

For neutral centers, we shall assume a potential of the form

$$\begin{aligned} V(r) &= -A/r^4 \qquad r > R \\ &= -A/R^4 \qquad r < R \end{aligned} \tag{4.9}$$

where $A$ is determined by the polarizability $\alpha$ of the neutral center and the dielectric constant $\kappa$ of the lattice:

$$A = \tfrac{1}{2}\alpha e^2/\kappa^2 \tag{4.10}$$

and $\alpha$ can be estimated by comparison with the polarizability of a hydrogen atom

$$\alpha_H = \frac{9}{2}(a_H)^3 \simeq 0{\cdot}666 \times 10^{-24} \text{ cm}^3 \tag{4.11}$$

by means of the relationship

$$\alpha/\alpha_H \simeq (m_0/m)(I_H/I)^2 \tag{4.12}$$

where $m/m_0$ is the effective mass in units of the free electron mass, $I_H = 13{\cdot}6$ eV and $I$ is the ionization energy of the neutral center.

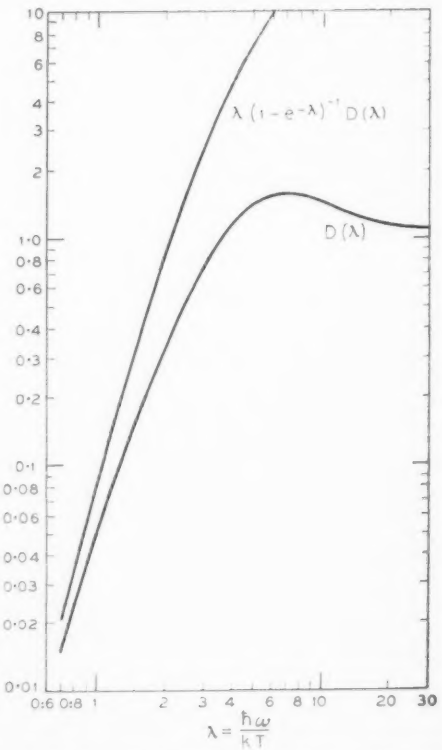


FIG. 5. The cross-section for capture via optical phonons is given by

$$\sigma = \sigma_0\, \lambda[1-\exp(-\lambda)]^{-1}\, D(\lambda)$$

where $\sigma_0$ (equation (4.5)) is independent of temperature and $\lambda = \hbar\omega/kT$.

The cross-section for capture via acoustic phonons is then given roughly by

$$\sigma \simeq \frac{4\pi}{9}\left(\frac{A}{\tfrac{1}{2}mc^2}\right)^{3/4}\frac{1}{l_c}\frac{[\tfrac{1}{2}mc^2(\hbar\omega_m)^3]^{\frac{1}{2}}}{(kT)^2} \qquad (4.13)$$

where $\hbar\omega_m$ is the maximum acoustic phonon that it is possible to emit:

$$\hbar\omega_m = 4[(A/R^4)(\tfrac{1}{2}mc^2)]^{\frac{1}{2}}$$
or
$$\hbar\omega_m = k\theta_{\text{Debye}} \qquad (4.14)$$

whichever is smaller.

The corresponding cross-section for neutral capture via optical phonon emission is roughly

$$\sigma \sim \frac{8\pi}{3}\frac{w}{l_c}\frac{A}{kTR}\frac{\lambda}{1-\exp(-\lambda)}. \qquad (4.15)$$

If one assumes $I \simeq 0{\cdot}5$ eV and adjusts $R$ so that the potential energy of equation (4.9) yields this binding energy (in W. K. B. approximation) one obtains $R \simeq 1{\cdot}16$ Ä. Both the optical and acoustic cross-sections then turn out to have the surprisingly high value of roughly $10^{-15}$ cm$^2$ at room temperature. It must be remembered, of course, that the potential we are using barely admits of excited states so that our cross-sections may be mild or gross overestimates depending critically on the actual polarizability and the details of the potential near the center which varies markedly from one impurity to another.

*Acknowledgments*—It is a pleasure to acknowledge the assistance of MRS. GWEN HANSEN and MRS. LILLIAN LEE with the analogue and digital machine computations.

## REFERENCES

1. GUMMEL H. and LAX M., *Annals of Physics* **2**, 28 (1957).
2. LAX M., *Bull. Amer. Phys. Soc.* Ser. II **1**, 128 (1956); *Ibid.* **2**, 147 (1957).
3. BARDEEN J. and SHOCKLEY W., *Phys. Rev.* **80**, 72 (1950).
4. HERRING C., *Bell. Syst. Tech. J.* **34**, 237 (1955).
5. KOENIG S. H., *Phys. Rev.* **110**, 986, 988 (1958); *J. Phys. Chem. Solids* **8**, 227 (1959).

*J. Phys. Chem. Solids* Pergamon Press 1959. Vol. 8. pp. 73–75. Printed in Great Britain

# AUGER EFFECT IN SEMICONDUCTORS

C.4

P. T. LANDSBERG and A. R. BEATTIE

Marischal College, University of Aberdeen, Scotland

THE recombination rate of excess electrons and holes by electron–electron collisions (band–band Auger effect) has been investigated on the basis of the following assumptions: (1) Perturbation theory, using determinants of Bloch functions to describe initial and final states of the two-band electron system; (2) the effective Coulomb potential of a carrier at a distance $r$ is $(e/\epsilon r)\exp(-\lambda r)$, where $\epsilon$ is an effective dielectric constant, and $\lambda^{-1}$ a screening radius; (3) parabolic bands with effective masses $m_c$, $m_v$ ($m_c \neq m_v$) for the conduction and valence bands respectively; (4) the electrons in each band are in equilibrium among themselves, but the electrons in different bands are not in equilibrium with each other (i.e. use of Fermi–Dirac statistics with two quasi-Fermi levels); (5) small departures from equilibrium.

The details of the calculation will be published in the *Proceedings of the Royal Society*, and a summary of results will be given here, together with comments, most of which are not contained in the Royal Society paper. References to equations in this latter paper will be prefixed by the symbol I.

One may commence this study by calculating the rate $R$ at which electron–hole pairs combine under conditions of thermal equilibrium, assuming the band–band Auger effect to be the only recombination mechanism. This rate $R$ is equal to the

electron–hole pair generation rate. If $n_0$ is the equilibrium electron concentration in the semiconductor of volume $V$, an electron Auger effect lifetime for thermal equilibrium may be defined by

$$\tau_{e0} \equiv n_0 V/R. \tag{1}$$

This lifetime may be written as

$$\tau_{e0} \equiv 2An_0/I. \tag{2}$$

Here $I$ involves dimensionless integrals, and is of order unity for near intrinsic specimens. Also

$$A = \frac{\pi^3\epsilon^2\hbar^6}{\kappa\sqrt{2}e^4m_c^{5/2}}\left(\frac{\eta_G}{kT}\right)^{3/2}|F|^{-2}\exp\left[\frac{1+2\mu}{1+\mu}\eta_G+\eta_c-F_0\right].$$

Here $F$ is believed to be order 0·1 for InSb, and involves overlap integrals of pairs of periodic parts of Bloch functions; $\mu \equiv m_c/m_v$; $\eta_G \equiv E_G(T)/kT$, where $E_G$ is the energy gap; $F_0$ is the Fermi energy for thermal equilibrium divided by $kT$. The notation $\eta_c$, $\eta_v$ for the energies, divided by $kT$, at conduction and valence band edges will also be used.

The result (2) may be obtained by comparing (1) and (I 5·4), using (I 3·5) and (I 5·7). The analogous lifetime for holes is $\tau_{h0} = 2Ap_0/I$.

Suppose next that there are excess carriers, so that the carrier concentrations are $n = n_0+\delta n$, $p = p_0+\delta p$, then the lifetime of excess electrons is found to be simply

$$\tau_e = (\alpha_c/2)[1+(\alpha_c n_0/\alpha_v p_0)(\delta p/\delta n)]^{-1}\tau_{e0}. \tag{3}$$

Here

$$\alpha_c \equiv \frac{F_{-\frac{1}{2}}(F_0-\eta_c)}{F_{\frac{1}{2}}(F_0-\eta_c)},\ \alpha_v \equiv \frac{F_{-\frac{1}{2}}(\eta_v-F_0)}{F_{\frac{1}{2}}(\eta_v-F_0)},$$

where

$$F_r(a) \equiv \int_0^\infty \frac{x^r dx}{1+\exp(x-a)}$$

is a Fermi integral. The $\alpha$'s have the value two for non-degenerate samples. (3) may be obtained by comparing (2) and (I 5·7). The lifetime (3) is obtained from the difference between the recombination and the generation rate, which are not equal away from thermal equilibrium. This rate may be called the net recombination rate. The lifetime of excess holes can be obtained from (3) by evaluating $\tau_h = (\delta p/\delta n)\tau_e$.

It is easiest to investigate the lifetimes under the neglect of exchange effects. Adding primes to lifetimes calculated in this way, one can show that $(2/3)\tau_i' < \tau_i < \tau_i'(i = e \text{ or } h)$.

In the case of InSb the effect of screening on the lifetime has been estimated as less than 5 per cent. If screening is neglected, and nondegeneracy is assumed, one finds

$$\tau_e' = 7{\cdot}58\times10^{-18}\frac{\epsilon^2}{|F|^2}(1+2\mu)\sqrt{(1+\mu)}\left\{1+\frac{\sqrt{\mu}(1+2\mu)}{2+\mu}\frac{p_0}{n_0}\exp\left(-\frac{1-\mu}{1+\mu}\eta_G\right)\right\}^{-1}\times$$
$$\times\left[1+\frac{n_0}{p_0}\frac{\delta p}{\delta n}\right]^{-1}\eta_G^{\frac{1}{2}}\exp\left(\frac{1+2\mu}{1+\mu}\eta_G\right)\text{sec}. \tag{4}$$

The first term in the curly brackets arises from electron collisions in the conduction band, and the second term from hole collisions in the valence band. It is seen that for an intrinsic specimen for which $\delta p = \delta n$ the temperature dependence of the lifetime is governed by the factor

$$\left[\frac{E_G(T)}{kT}\right]^{\frac{1}{2}}\times\begin{cases}\exp\left(\dfrac{1+2\mu}{1+\mu}\eta_G\right) & (\mu<1),\\ \exp\left(\dfrac{1+2\mu^{-1}}{1+\mu^{-1}}\eta_G\right) & (\mu>1).\end{cases}$$

This shows that for such specimens ln $\tau_e'$ increases with $1/T$ approximately linearly with an activation energy of *approximately* $[(1+2\mu)/(1+\mu)]E_G(0)$. If the temperature is kept fixed and the concentration is changed, (4) shows that for a non-degenerate

sample the concentration dependence of $\tau_e'$ is given by

$$(C/D)p_0^{-2}(n_0 \ll p_0), \qquad Cn_0^{-2}(n_0 \gg p_0),$$

where the ratio of the factors of proportionality is

$$D = \frac{\sqrt{\mu}(1+2\mu)}{2+\mu} \exp\left[-\frac{1-\mu}{1+\mu}\eta_G\right].$$

Between these two extreme ranges there is a relatively constant plateau. The $(p_0^{-1}, n_0^{-1})$-law on either side of the lifetime maximum, familiar from the recombination via traps, is seen to be replaced by a $(p_0^{-2}, n_0^{-2})$-law. But, because of the broad plateau, it is *not correct* to suppose that the Auger effect can be a dominant mechanism only if an inverse square concentration dependence of the lifetime has been established experimentally.

The above analysis has applications to three different experimental situations: (1) the lifetimes $\tau_{e0}$, $\tau_{h0}$ of carriers due to the recombination rate $R$ in thermal equilibrium can be discussed; (2) if an external influence, such as radiation, keeps the non-equilibrium number of pairs at a constant value, the above lifetimes $\tau_e$, $\tau_h$ give the average time before a newly created carrier recombines, assuming the Auger effect to be the only recombination mechanism; (3) suppose the trapped electrons (concentration $n_t$) are near enough to a band to be in equilibrium with it. The equation $\delta n - -\delta p + \delta n_t = 0$ for charge conservation leads then to a relation for $\delta F_c/\delta F_v$ in terms of time-independent (thermal equilibrium) quantities. In the equation $d(\delta n)/dt = -\delta n/\tau_e$ for the change in $\delta n$ with time after the disturbance has been switched off, $\tau_e$, though it depends on $\delta p/\delta n$, i.e. on $\delta F_c/\delta F_v$, is therefore independent of time. Hence, under these conditions, an exponential decay of $\delta n$ must be expected, with the same time constant as calculated for case (2).

The effect under investigation is likely to be most important when $E_G/kT$ is small, and seems to yield the correct order of magnitude for the measured lifetimes in InSb above room temperatures.

*J. Phys. Chem. Solids* Pergamon Press 1959. Vol. 8. pp. 75–77. Printed in Great Britain

# RADIATIVE RECOMBINATION AND LIFETIME IN GERMANIUM*

C.5

**PATRICIA H. BRILL and RUTH F. SCHWARZ**

Philco Corporation, Philadelphia 34, Pennsylvania

ACCORDING to the theory of VAN ROOSBROECK and SHOCKLEY,[1] band to band recombination in germanium is proportional to the product of the hole and electron densities. Thus if excess carriers are generated, the net rate of radiation per unit volume, $U$, resulting from the recombination should be given by

$$U = \mathscr{R}[(n_0+p_0)\delta p + \delta p^2]/n_i^2 \qquad (1)$$

where $n_0$ and $p_0$ are the equilibrium concentrations of electrons and holes respectively, $\delta p$ is the excess concentration of holes or electrons, $n_i$ is the intrinsic concentration of carriers, and $\mathscr{R}$ is the radiation constant of reference (1). The present work consists of a direct verification of this law by simultaneous measurements of the output radiation and optically induced excess carrier concentrations, the latter being determined from photoconductivity measurements.

Light from a microscope lamp was chopped at 750 c/s, passed through a water filter, and focused

*The work described here was supported in part by the BuShips under Contract No. NObsr—72695 (1718).

on one face of an etched Ge sample. Kodak neutral density filters provided a range of approximately 100 to 1 in. incident light intensity. The recombination radiation, which peaked at 0·70 eV, was detected by a PbS cell whose absolute sensitivity was known. Simultaneous measurements of the change in resistance of the samples with light level were made. Both $n$- and $p$-type Ge ranging in resistivity from 0·2 to 12 Ω cm, were used. The thickness of the illuminated regions varied from 0·2 to 0·4 mm.

The excess carrier density was calculated from the photoconductivity data by assuming a uniform distribution of these carriers over an effective length, $l$, of the crystal. This excess carrier density gives a change in conductivity, $\Delta\sigma$, which is related to the measured change in resistance, $\Delta R$, by the equation

$$\frac{(\mu_n+\mu_p)\delta p}{\mu_n n_0+\mu_p p_0}=\frac{\Delta\sigma}{\sigma_0}=\frac{\Delta R/R_{\text{dark}}}{1-\Delta R/R_{\text{dark}}} \qquad (2)$$

Here $\sigma_0$ is the dark conductivity of the sample, $\mu_n$ and $\mu_p$ are the mobilities of electrons and holes respectively, and $R_{\text{dark}}$ is the resistance in the dark corresponding to the length, $l$.

$R_{\text{dark}}$ was first calculated from the resistivity and dimensions of the sample with $l$ taken to be the length of the illuminated region. For the cases where $\delta p$ was small compared with $(n_0+p_0)$, a log–log plot of output radiation vs. $\delta p$ gave a slope of 1·0 as expected. For the cases where $\delta p$ was comparable to $(n_0+p_0)$ it was found that the exact curvature of the log–log plots depended critically on the value chosen for $R_{\text{dark}}$. This value is not known accurately because of possible errors in the measured resistivity of the samples, and errors in the effective length, $l$, arising from possible variations in the excess carrier concentrations near the electrical contacts. $R_{\text{dark}}$ was therefore determined empirically to give the best fit between theory and experiment, and this value was compared with the value of $R_{\text{dark}}$ calculated from the measurements. Percentage changes in $\delta p$ determined from the two values of $R_{\text{dark}}$ were of the same order as the percentage changes in $R_{\text{dark}}$. An equivalent error in $R_{\text{dark}}$ in the linear cases would not affect the curvature.

A comparison of experimental and theoretical results is shown in Fig. 1 for three samples of widely different resistivity. The other seven samples tested gave similar results. In all cases the agreement between theory and experiment seemed within experimental error.

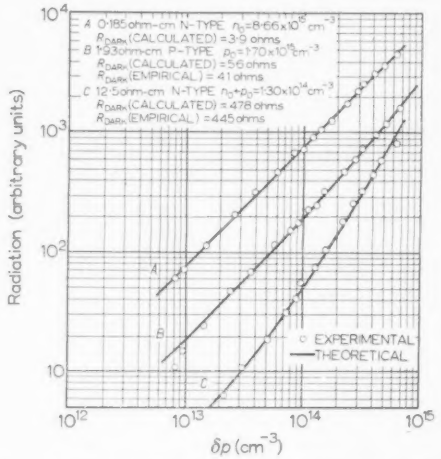


FIG. 1. Recombination radiation as a function of excess carrier density, $\delta p$, for three samples of germanium.

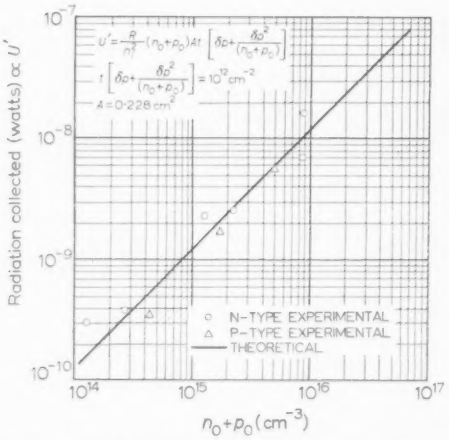


FIG. 2. Recombination radiation from various samples of germanium as a function of equilibrium carrier density.

Fig. 2 is a log–log plot of output radiation vs. the equilibrium carrier density, $(n_0+p_0)$, for the various samples for a constant value of $tA[\delta p+\delta p^2/(n_0+p_0)]$ where $t$ is the thickness and

$A$ is the radiating area. As may be seen from equation (1), this plot should be a straight line with a slope of 1. Although there is considerable spread in the data, a variation from the curve of a factor of two or more is not unreasonable from the differences in the surface optical properties alone.

A numerical estimate of the radiation constant $\mathscr{R}$ was made using the line drawn in Fig. 2, which effectively averages all the samples measured. The following factors were taken into account. Of the total radiation emitted approximately 1·5 per cent falls within the critical angle of 14° from the normal to the surface. Of this, approximately $\frac{1}{3}$ gets further internally reflected. From the geometry of the system, an estimated 10 per cent of the radiation leaving the germanium is collected. An experimental value of $\mathscr{R}$ was thus determined as $2{\cdot}5 \times 10^{13}$ $cm^{-3}sec^{-1}$ which may be compared with the theoretical value of $1{\cdot}57 \times 10^{13}$ $cm^{-3}sec^{-1}$ given by VAN ROOSBROECK and SHOCKLEY.[1] This agreement is better than might have been anticipated.

The effective sample lifetime, $\tau_{eff}$, is related to $\delta p$ by the equation

$$\tau_{eff} = t\delta p/I_0$$

where $t$ is the thickness of the sample and $I_0$ is the number of hole–electron pairs generated per sec per $cm^2$ of illuminated surface. $I_0$ is proportional to the incident light intensity.

In most cases, the slope of a log–log plot of $\delta p$ vs. incident light was somewhat greater than 1·0 indicating a slow increase in $\tau_{eff}$ with increasing injection. In many of the samples tested, both the resistance and the output radiation drifted slowly with time after the incident light level had been altered. Most of the data were taken in a quasi-steady state before the drifting was appreciable, but a few tests were also made after the drift was completed. All of the samples tested showed a greater dependence of lifetime on injection level after drift than before. For example, over the range of $\delta p$ tested for sample B of Fig. 1, $\tau_{eff}$ increased by 60 per cent before drift, while after drift, it increased by a factor of 5.

The time constant involved in the drifting phenomena suggest a change in charge in the outer surface states and a consequent change in surface potential. Therefore, the large variation in lifetime with $\delta p$ after drift probably reflects changes in surface recombination velocity rather than changes in bulk lifetime. This is reasonable from the geometry of the samples. It is important to note that the curves of radiation vs. injected carrier density were completely independent of whether the data were taken before or after drift.

Curves of output radiation versus current were taken on many diodes made by alloying indium into $n$-type germanium of various resistivities. These curves indicated that the output radiation almost always increased with the current as a power between about 1·3 and 1·7 over approximately two decades of output radiation where heating was not appreciable. The simple power law dependence over so much of the range tested is surprising considering the following facts. (1) In this current range the radiation should begin to increase faster than linearly with injected carrier density according to equation (1). (2) In the same current range the injection efficiency should start to decrease. (3) Effective sample lifetime is changing with current and is known to be increasing in the lower range.

*Acknowledgments*—The authors wish to thank Dr. P. J. DANIEL for calibration of the PbS detector, as well as for many helpful discussions and suggestions on the major portion of this work. They also wish to thank Dr. M. E. LASSER, Mr. J. WALSH, Dr. S. ZAROMB, and Mr. L. W. HERSHINGER for their useful comments and advice, and Mr. J. COSGROVE for his preparation of the diodes used in the electrical experiments.

## REFERENCES

1. VAN ROOSBROEK W. and SHOCKLEY W., *Phys. Rev.* **94**, 1558 (1954).

*J. Phys. Chem. Solids* Pergamon Press 1959. Vol. 8. pp. 78–80. Printed in Great Britain

# CARRIER RECOMBINATION IN GERMANIUM AS A FUNCTION OF TEMPERATURE BETWEEN 100°K AND 550°K

C.6

**S. GOLDSTEIN, H. METTE and W. W. GÄRTNER**

U.S. Army Signal Research and Development Laboratory, Fort Monmouth, New Jersey

LIFETIMES in germanium have been measured by the photomagnetoelectric method using a previously described technique.[1] The sample is mounted in an evacuated quartz tube which is then inserted in a transparent dewar. The whole apparatus is placed in a magnetic field of 1000 G. Illumination of the sample is obtained by a beam light source from the outside which is used in conjunction with a filter. This insures pure surface generation necessary for the interpretation by the simplest form of the theory of the PME effect.[2] Temperatures below 250°K are attained by partially filling the dewar with liquid nitrogen, thus lowering the ambient around the quartz tube. The high temperature region is reached by partially filling the dewar with silicone oil which is then heated by an auxiliary coil in the dewar. The temperature of the sample itself is measured by a thermocouple cemented to the back surface. A simple a.c. Wheatstone bridge is employed for the determination of conductivity as well as photoconductance of the sample, whereas open-circuit voltage is measured in a d.c. potentiometer compensating circuit. The exposure to light is always kept very short to avoid an influence on the temperature of the sample. Since thermomagnetoelectric effects may introduce serious errors, they have been measured separately and an estimate has shown that they are unimportant for the light intensities used. Careful etching of the front surface for minimum surface recombination velocity is important and greatly increases the accuracy of the measurements. An estimate has shown that in order to determine the energy of a recombination level by the PME method to within $\pm 0{\cdot}01$ eV, the initial readings of the open-circuit voltage and of photoconductance must be accurate to within $\pm 1{\cdot}2$ per cent. The accuracy of our measurement is approximately 0·03 eV.

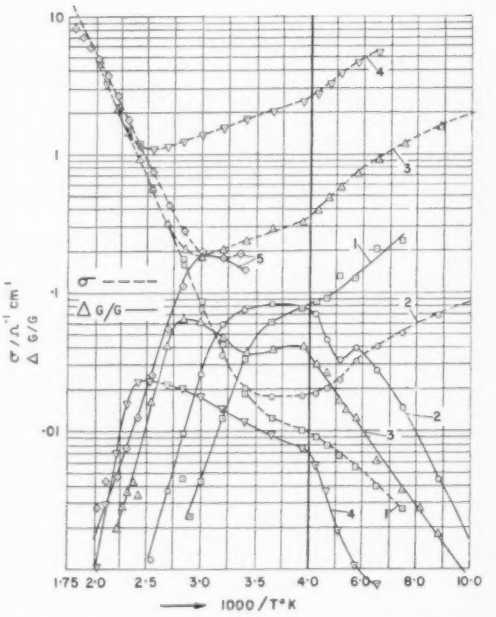


FIG. 1: Conductivity, $\sigma$, and photoconductance, $\Delta G/G$, in various germanium crystals as a function of temperature, $T$.

| Sample No. | Type | 20°C/Ω cm |
|---|---|---|
| 1 | *p* | 51·84 |
| 2 | *p* | 49·75 |
| 3 | *p* | 4·31 |
| 4 | *p* | 0·556 |
| 5 | *n* | 5·13 |

The evaluation of lifetime from PME data involves the mobilities and diffusion constants of both types of carriers. Therefore, if measurements are taken over a wide temperature range it is imperative to measure the mobility of the charge carriers at the same time. This has been done in these experiments by measuring conductivity and Hall effect.

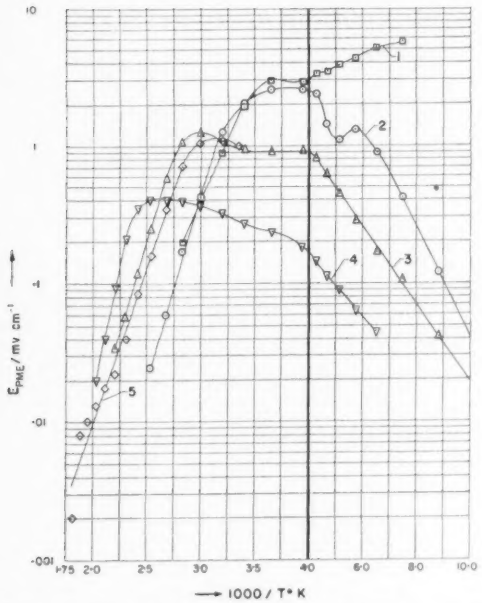


FIG. 2: Open-circuit PME field, $E_{PME}$, in various germanium crystals as a function of temperature, $T$.

| Sample No. | Type | 20°C/Ω cm |
|---|---|---|
| 1 | $p$ | 51·84 |
| 2 | $p$ | 49·75 |
| 3 | $p$ | 4·31 |
| 4 | $p$ | 0·556 |
| 5 | $n$ | 5·13 |

Figs. 1 and 2 show the conductivity, photoconductance and open circuit PME field measured on various germanium crystals, mostly $p$-type for reasons pointed out below. In Fig. 3 the lifetimes evaluated from the data in Figs. 1 and 2 are given as a function of temperature. Among the five samples shown, two samples (2 and 3) can apparently be fitted by an equation of the form

$$\tau_0 = \tau_{p0}\frac{n_0+n_1}{n_0+p_0}+\tau_{n0}\frac{p_0+p_1}{n_0+p_0}$$

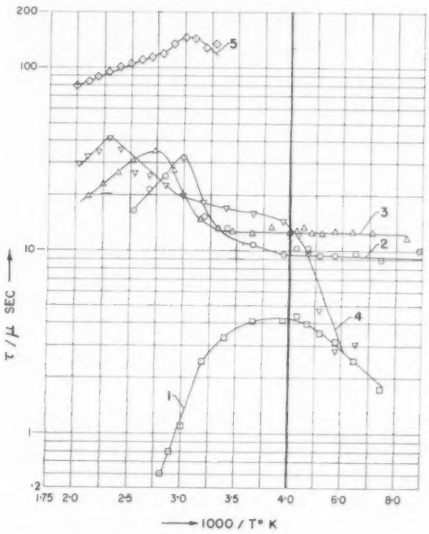


FIG. 3: Lifetime, $\tau$, in various germanium crystals as a function of temperature, T.

| Sample No. | Type | 20°C/Ω cm |
|---|---|---|
| 1 | $p$ | 51·84 |
| 2 | $p$ | 49·75 |
| 3 | $p$ | 4·31 |
| 4 | $p$ | 0·556 |
| 5 | $n$ | 5·13 |

and thus seem to follow the Hall–Schockley–Read recombination mechanism[3] with constant recombination level and constant recombination cross section. The notation in this equation follows that of SHOCKLEY–READ.[3] The dependence of lifetime on injection level has been checked and the absence of any strong dependence up to the levels employed in the measurements indicates that in the $p$-type material $\tau_{p0}$ must be smaller than, or of the order of, $\tau_{n0}$, which is in agreement with the observations of Burton *et al.*[4] This is of importance in these measurements because otherwise the theory of the PME effects[2] would not be applicable in its present form since it assumes

constant lifetimes throughout the sample. The curves shown are for constant light intensity. Since the light intensity does not enter the evaluation explicitly one may use lower light intensities for long-lifetime samples and higher light intensities for short-lifetime samples. In particular, one could also monitor the light intensity in such a way that $\delta n/p_0$ remains constant in a thin sample. This would, for example, be imperative in cases where the lifetime is a strongly varying function of injection level even for small excess densities.[5]

Curve 2 can apparently be fitted by the following parameters: $\tau_{n0} = 9{\cdot}5\ \mu$sec, $E_c - E_t = 0{\cdot}31$ eV, $\tau_{p0} \simeq 9{\cdot}5\ \mu$sec or $\tau_{n0} = 9{\cdot}5\ \mu$sec, $E_t - E_v = 0{\cdot}31$ eV, $\tau_{p0} \ll 9{\cdot}5\ \mu$sec; similarly curve 3 can be fitted by $\tau_{n0} = 13{\cdot}5\ \mu$sec, $E_c - E_t = 0{\cdot}31$ eV, $\tau_{p0} \simeq 13{\cdot}5\ \mu$sec or $\tau_{n0} = 13{\cdot}5\ \mu$sec, $E_t - E_v = 0{\cdot}31$ eV, $\tau_{p0} \ll 13{\cdot}5\ \mu$sec. Since the recombination level is so close to the middle of the gap it is difficult to determine whether it lies in the upper or lower half of the gap. The origin of our levels is unknown but Tyler has reported several levels in this range earlier in this Session. The slope of the curves in the intrinsic range is steeper than would be expected from a formal extrapolation of the Shockley–Read theory to high temperatures, and it appears that a more efficient recombination mechanism begins to predominate or that recombination level and recombination cross section themselves become temperature dependent.

Difficulty in reproducibility of lifetime values measured by the PME method in $n$-type material particularly at low temperatures made it inadvisable to report these measurements. Curve 5 in the figures corresponds to a typical $n$-type sample at higher temperatures. If the Shockley–Read mechanism is applicable to this case the high temperature slope could be associated with a recombination level 0·043 eV removed from the intrinsic Fermi level. The remaining two curves (1 and 4) apparently do not fit the Hall–Shockley–Read single level mechanism. In particular, the double break in the low-temperature portion of curve 4 is unaccounted for. Other more complicated mechanisms have been proposed for such cases[6] but the larger number of parameters to be fitted requires more extensive measurements, in particular as a function of injection level.

We have seen that lifetime measurements taken over a wide range of temperatures are a very good check for the recombination mechanism involved, and in certain cases recombination in germanium follows the simple Hall–Shockley–Read mechanism. In other cases the mechanisms are more involved, and the most promising approach to clarify the situation is to take a large number of lifetime measurements as a function of temperature at least over the range reported here and over a wide range of injection levels.

VOL 8 195

## REFERENCES

1. Goldstein S., Mette H. and Gärtner W. W., *Bull. Amer. Phys. Soc.* Ser. II, **3,** 101 (1958).
2. van Roosbroeck W., *Phys. Rev.* **101,** 1713 (1956).
3. Hall R. N., *Phys. Rev.* **87,** 387 (1952); Shockley W. and Read W. T., *Phys. Rev.* **87,** 835 (1952).
4. Burton J. A., Hull G. W., Morin F. J. and Severiens J. C., *J. Phys. Chem.* **57,** 853 (1953).
5. see e.g. Bemski G., *Phys. Rev.* **100,** 523 (1955); Blakemore J. S., *Phys. Rev.* **110,** 1301 (1958).
6. for such mechanisms see Sah C. T. and Shockley W., *Phys. Rev.* **109,** 1103 (1958); Blakemore J. S., *Phys. Rev.* **110,** 1301 (1958); Shockley W., *Proc. Inst. Radio Engrs., N.Y.* **46,** 973 (1958); Bemski G., *Proc. Inst. Radio Engrs. N.Y.* **36,** 990 (1958); and the references in these articles.

*J. Phys. Chem. Solids* Pergamon Press 1959. Vol. 8. pp. 81–83. Printed in Great Britain

# SULFUR IN SILICON

R. O. CARLSON, R. N. HALL and E. M. PELL

C.7

General Electric Research Laboratory, Schenectady, New York

## 1. INTRODUCTION

THE systematic study of the effects of impurities in silicon[1] has added greatly to our scientific and technological knowledge. Well understood is the action of the Group III elements as acceptor impurities and the Group V elements as donor impurities. As substitutional impurities in the silicon lattice, the Group VI elements are expected to be donor impurities since only four of their six outer valence electrons are needed to form tetrahedral bonds with neighboring silicon atoms. This donor action is revealed in our experiments with sulfur. Oxygen in silicon shows donor behavior,[2] but it appears to be active only in combination with other impurities present.[3] In germanium, the elements sulfur, selenium, and tellurium are donors and levels have been determined for each of them.[4] Donor activity has also been claimed for oxygen in germanium.[5]

## 2. PROCEDURE

The first evidence for the donor nature of sulfur in silicon was obtained by admitting some hydrogen sulphide gas into the argon protective gas during part of the growth period of a single crystal by the Czochralski technique. The crystal was grown from a *p*-type melt but it was *n*-type in the middle section in which the hydrogen sulphide gas had been present in growth. No further doping of growing crystals was attempted since diffusion proved to be a more controllable process of introducing sulfur.

In the diffusion process, less than 1 mg of 99·85 per cent pure sulfur was sealed off in an evacuated quartz tube with silicon samples of dimensions $\sim 1{\cdot}5 \times 3 \times 10\ \text{mm}^3$. Times of the order of one day were sufficient to saturate these samples at high temperatures. Sulfur reacted with the silicon samples and excess sulfur in some cases caused a mass transport of the silicon and eroded the samples. There is evidence in the literature[6] for silicon sulfides (both SiS and $SiS_2$) and these probably form in an intermediate stage. Contacts to the samples were made by spring wires against gold-plated regions. The magnetic field used in the cryostat arrangement was 6000 G.

## 3. ELECTRICAL ACTIVITY

From measurements of resistivity and Hall coefficient over the range 80°–700°K, as shown in Fig. 1 for a typical sample, CD-490, a level of 0·18 eV from the conduction band was attributed

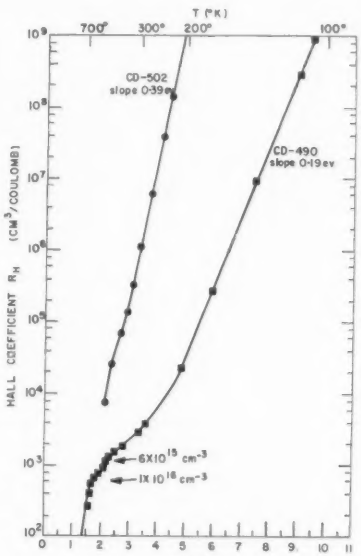


FIG. 1. Hall coefficient vs. reciprocal temperature for typical samples of sulfur-doped silicon, showing the two observed levels. Samples were *p*-type before diffusion of sulfur. The slopes of the Hall coefficient curves must be corrected for the $T^{3/2}$ dependence of the density of states near the bottom of the conduction band. This correction gives the levels as 0·18 and 0·37 eV from the conduction band edge.

to sulfur. This level was observed in samples of both floating zone and crucible grown silicon into which sulfur was diffused and also in samples cut from the one grown crystal doped with hydrogen sulfide. In addition, one $p$-type crystal was grown dominated by gallium rather than the usual acceptor, boron, and the same level was observed on diffusing in sulfur. The observed donor activity of sulfur was not dependent on the concentration or nature of the acceptor present so that an ion-pairing mechanism for the level can be ruled out.

At higher temperatures a second level is evident in CD-490 and in other samples with the 0·18 eV level, leading one to suspect that sulfur has two levels above the middle of the gap. In samples in which the 0·18 eV level is completely empty and the deeper level partially empty by compensation ($2N_S > N_A > N_S$, where $N_S$ is the sulfur concentration and $N_A$ the shallow acceptor concentration), then a level at 0·37 eV from the conduction band is observed, as in CD-502 of Fig. 1.

Spectroscopic analysis of the sulfur revealed that the five previously studied elements[1] which give rise to deep levels in silicon, namely iron, manganese, copper, gold, and zinc were present to less than 1 part in $10^5$. Thus these elements could not be responsible for either of the levels observed. No evidence for any acceptor activity of sulfur was observed on diffusing into $n$-type samples.

## 4. SOLUBILITY AND DIFFUSION COEFFICIENT

Initial electrical studies at 1200°C revealed a solubility of $\sim 10^{15}$ cm$^{-3}$ for sulfur. However, it was found that insufficient sulfur was present in these samples to saturate them, the amount of sulfur having been kept low because of its reactivity with silicon. Further samples showed that up to $3 \times 10^{16}$ cm$^{-3}$ could be introduced into silicon as plotted in Fig. 2. Retrograde solubility is evident close to the silicon melting point. Comparison of this solubility curve with HALL's curves[7] indicates that the segregation coefficient of sulfur in silicon is $\sim 10^{-5}$, of the same order of magnitude as the other deep level impurities studied. The concentration in the 0·18 eV level was approximately equal to that in the 0·37 eV level in various samples, allowing for partial compensation of the shallower level by acceptors present and for the fact that the 0·37 eV level is not completely emptied before intrinsic generation of carriers competes.

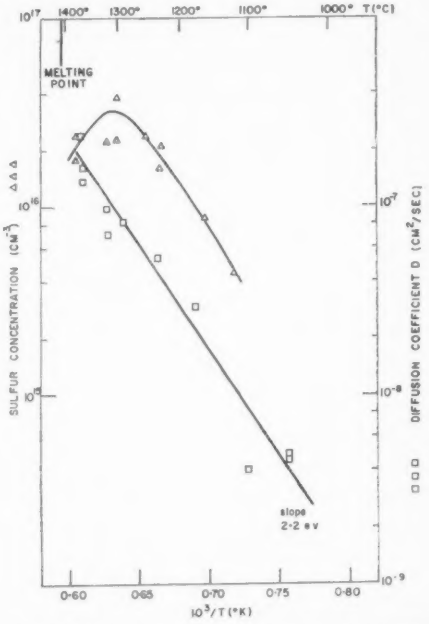


FIG. 2. Solubility and diffusion coefficient of sulfur in silicon as determined from electrical measurements.

Radiotracer studies using $S^{35}$ did not give accurate results. The beta particles for $S^{35}$ are so weak (0·17 MeV) that only a very thin layer of silicon is effectively counted and sample activity was close to background. The radiotracer studies do suggest, however, that the total sulfur content cannot be much more than that measured as electrically active.

The diffusion coefficient, also plotted in Fig. 2, was determined by measuring the depth of the $p$-$n$ junction formed on diffusion of sulfur into $p$-type silicon. The surface donor concentration was determined from the solubility curve, multiplying by two to account for the two observed levels. The values of diffusion coefficient are intermediate between very fast diffusers such as copper or nickel ($D \sim 5 \times 10^{-5}$ cm$^2$/sec) and the Group III-V elements ($D \sim 10^{-11}$ to $10^{-13}$ cm$^2$/sec at 1200°C). The activation energy for

sulfur diffusion ($D = D_0 \exp -E/kT$) is given by the slope as 2·2 eV or 51,000 cal. This compares with ~ 1 eV for iron and gold[8] and 3·5 to 4·7 eV for the III-V elements.[9] The diffusion coefficient for oxygen is $\sim 10^{-8}$ cm$^2$/sec at the melting point of silicon, with an activation energy of 3·5 eV.[10]

## 5. PHOTOCONDUCTIVITY SPECTRA

Samples in which the 0·18 eV and the 0·37 eV levels were dominant were studied using Newman's technique.[11] Results, plotted in Fig. 3,

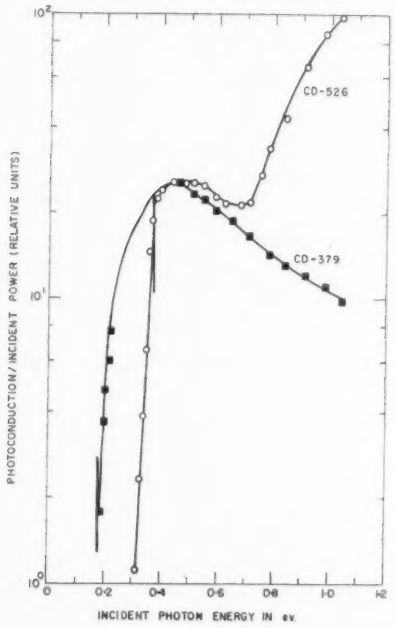


FIG. 3. Photoconductive spectra of *n*-type sulfur-doped silicon. Thermal ionization energies are indicated for comparison with the optical curves. The spectra were shifted vertically to coincide at 0·45 eV.

show that these spectra support the level positions determined from electrical measurements. In addition, in the sample with the 0·37 eV level, CD-526, there appears to be a very deep level, whose origin is not understood.

## 6. CONCLUSIONS

Sulfur introduces two donor levels into the forbidden band of silicon, at 0·18 eV and 0·37 eV from the conduction band. Its maximum solubility of $3 \times 10^{16}$ cm$^{-3}$ at 1320°C is comparable to that of iron, manganese and zinc, but diffusivity is somewhat lower. $D = 0{\cdot}92 \exp(-2{\cdot}2/kT)$, roughly $D(1300°\text{C}) = 10^{-7}$ cm$^2$/sec and $D(1100°\text{C}) = 10^{-8}$ cm$^2$/sec. The double donor activity of sulfur suggests that it is a substitutional impurity in the silicon lattice, but it presumably diffuses as an interstitial impurity. Its solubility is only ~1/50 that of oxygen in silicon, but apparently oxygen is electrically active only in combination with other impurities or defects.

*Acknowledgments*—Much of the sample preparation and electrical measurement was carried out by G. D. BROWER, the photoconductivity spectra by R. NEWMAN and R. CHRENKO, while D. LOCKE and Miss S. SCHWARZ aided in parts of the experiment.

## REFERENCES

1. CONWELL E. M., *Proc. Inst. Radio Engrs., N.Y.* **46,** 1281 (1958); COLLINS C. B. and CARLSON R. O., *Phys. Rev.* **108,** 1409 (1957); HANNAY N. B. in *Progress in Semiconductors,* Vol. 1, pp. 1–35. Heywood & Company Ltd., London (1956).
2. KAISER W. and KECK P. H., *J. Appl. Phys.* **28,** 882 (1957); KAISER W., *Phys. Rev.* **105,** 1751 (1957).
3. FULLER C. S. and LOGAN R. A., *J. Appl. Phys.* **28,** 1427 (1957); FULLER C. S. and DOLEIDEN F. H., *J. Appl. Phys.* **29,** 1264 (1958).
4. ARMSTRONG J., TYLER W. W. and WOODBURY H. H., *Bull. Amer. Phys. Soc.* Ser. II, **2,** 265 (1957); TYLER W. W., *J. Phys. Chem. Solids* **8,** 59 (1959).
5. ELLIOTT G., *Nature, Lond.* **180,** 1350 (1957).
6. ZINTL E. and LOOSEN K., *Z. Phys. Chem.* **174,** 301 (1935).
7. HALL R. N., *J. Phys. Chem. Solids* **3,** 63 (1957).
8. STRUTHERS J. D., *J. Appl. Phys.* **27,** 1560 (1956).
9. FULLER C. S. and DITZENBERGER J. A., *J. Appl. Phys.* **27,** 544 (1956).
10. LOGAN R. A. and PETERS A. J., paper presented before 5th Annual Semiconductor Symposium of the Electrochemical Society, May 1957. Referred to in the text and in footnote 20 of Reference (3) (FULLER and LOGAN).
11. NEWMAN R., *Phys. Rev.* **99,** 465 (1955).

*J. Phys. Chem. Solids* Pergamon Press 1959. Vol. 8. pp. 84–86. Printed in Great Britain

# EFFECT OF ANNEALING ON THE STATE OF CERTAIN IMPURITIES IN GE*

C.8

V. E. LASHKAREV, E. G. MISELYUK and K. D. GLINCHUK

Institute of Physics, Academy of Sciences, Kiev, U.S.S.R.

THE effect of annealing Ge alloyed with Fe, Ni, Co, at average temperatures ($t° < 500°C$) on the concentration of equilibrium carriers ($n$) and volume life-time ($\tau$) of non-equilibrium current carriers is studied. Studies of the temperature dependence $n$ (using the Hall effect) and of $\tau$ made it possible to determine energy levels and change of acceptor level states, which resulted from these impurities. Shallow level impurities (Sb, Ga) were also included in the Ge specimens.

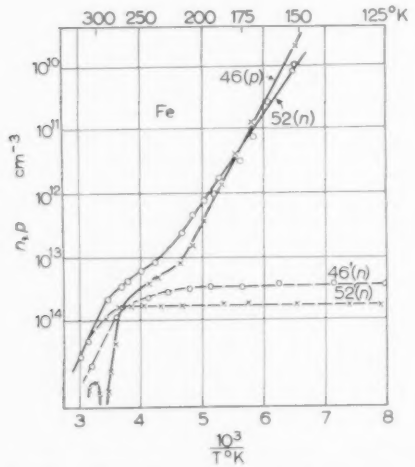


FIG. 1. The effect of annealing on the concentration of carriers in germanium doped with iron: 46-$p$-type, 52-$n$-type. After annealing (24 hr at 500°C)—46′ and 52′. The sample 46 converted to $n$-type.

We obtained the following results:

(1) Before annealing—the decrease of the concentration of equilibrium current carriers is monotonic with decreasing temperature and the value of $\tau$ is low (fractions of microseconds).

(2) After annealing—the concentration of current carriers remains steady in a wide temperature range (~100°K–350°K) and $\tau$ exhibits a steep increase (tens and hundreds of times).

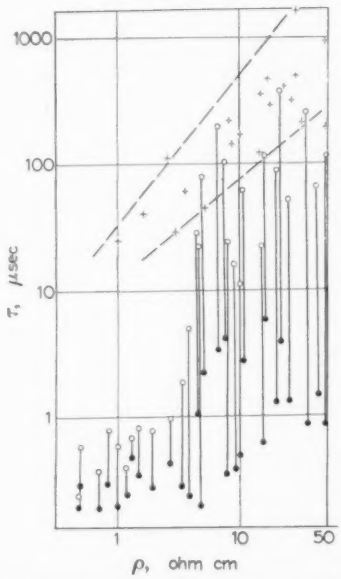


FIG. 2. Effect of annealing on $\tau$ at 20°C for germanium doped with Fe, Ni, Co as a function of specific resistivity: ●—before annealing, ○—after annealing (48 hr at 500°C), ×—data for samples doped with Sb or Ga with no Fe, Ni, Co impurities (annealing has no effect on $\tau$).

This kind of an annealing effect is explained by the de-activation of acceptor levels due to the release of the impurity atoms from the solid solution.

*Not presented at Conference.

The values obtained for the activation energy of recombination centers in annealed specimens (~0·10–0·18 eV) are approximately the same as the ones obtained for Ge which does not contain any of the impurities under consideration.

The given experimental data are compared with the other properties of these impurities in Ge—rate of diffusion and solubility.

It is assumed that the observed de-activation effect of Fe-, Ni-, Co- impurities is valid also for other impurities having substantial diffusion coefficients at annealing temperatures.

## DISCUSSION

*Compiled by* A. ROSE

### C.2 W. W. TYLER

O. SIMPSON (S.E.R.L. Baldock, England): Ni, Fe or Mn doped germanium show shallow levels after annealing. If these levels are due to vacancies resulting from super saturation they should all have the same ionization energy. Has this been observed?

W. W. TYLER: The shallow levels introduced during the annealing of Ni, Mn and Ag—doped Ge all appear at about 0·05 eV and 0·01 eV. It is suggested but not proven that these levels are associated with vacancies. P. Penning who first observed these levels in Ni-doped Ge has suggested that the ·05 eV level may be due to Cu introduced during the annealing process. This will be discussed in the written report.

S. H. KOENIG (IBM Watson Labs.): What is the mentioned evidence for electrical activity of $O_2$ dissolved in Ge?

W. W. TYLER: Thurmond *et al.* have indicated that oxygen may be present in Ge at high concentrations but be electrically inactive. However G. Elliot has indicated that under certain conditions oxygen may act as a donor impurity in Ge. We have repeated Elliot's experiment and agree with his results.

### C.3 M. LAX

H. J. MEYER (Philips): Do you not think that one should make a rather sharp distinction between capture into traps and capture into recombination centers, this last process not being covered by your theory. In fact it may well be that the cross-section for this process is determined by the last stage of the capture process: transition from the first excited state to the ground state, which then would require consideration of a many-phonon process.

M. LAX: If the time delay in the last few steps is significant, recombination cross-sections could be affected (although capture cross-sections should not) because it may delay the subsequent capture of a carrier of opposite sign. Under these circumstances, *recombination* centers with the same charge could have effective cross-sections which varied from one another and depended on the details of the center (particularly, location of the first few excited states).

S. H. KOENIG (IBM Watson Labs.): Apropos of the answer to Meyer's question, the work of Weinreich at BTL shows that the capture cross-section into the excited states is larger than that for the ground state.

M. BERNARD (C NET France): Experiments which I have reported at the Brussels Conference seem to be in satisfactory agreement with your theory: they concern capture of a hole by $Ni^{--}$, $Co^{--}$ or $Fe^{--}$ ion (pretty large orbits); first the capture cross-sections are very large ($10^{-15}$ to $10^{-12}$ cm$^2$); it seems they increase strongly with decreasing temperature.

### C.4 P. T. LANDSBERG and R. A. BEATTIE

L. SOSNOWSKI (Warsaw University, Poland): (1) Have you considered the collision recombination of a free electron with a trapped hole and vice versa? Is the probability for such a process not greater due to lack of limitation caused by momentum conservation law?

(2) The attention of the author is drawn to the experimental results on thalium sulphide published partly in 1954 showing $\tau \sim 1/p^2$ dependence (SOSNOWSKI, L. and OSTROWSKI, T. W. *Bull. Acad. Pol. Sci.* C1 III, **8**, 356 (1954)), over a long range of concentration. The work has been continued and further results containing an

estimation of absolute values of coefficients involved will be published soon in *Acta Physica Polonia*.

P. T. LANDSBERG: I quite agree with Dr. Sosnowski that the auger effect with the participation of traps ought also to be considered, and I am grateful for the reference to his paper. We have worked on this effect, but we are not yet able to present any results. As to its importance compared with band–band Auger effect, one can probably not make any completely general statement.

JAN TAUC (Inst. of Technical Physics, Prague): In the paper read by Dr. Landsberg an entirely spherically symmetrical energy band structure was assumed. This may lead to incorrect results when applied for Ge, Si or InSb. An essential difference is caused by the fact that in an asymmetrical band structure the conservation laws may be in some cases fulfilled only in some directions of **k** vectors which in a symmetrical structure are independent of directions.

P. T. LANDSBERG: I also agree with Dr. Tauc's remark that the use of simple bands is somewhat unrealistic. The calculation is, however, extremely involved even with this assumption; the simplest reasonable model had to be adopted in order to discover the basic trends of the lifetime.

### C.5 P. BRILL and R. F. SCHWARTZ

G. C. DOUSMANIS (RCA Labs.): The increase of lifetime with injection, as a result of surface effects, is not to be expected in the general case. Injection, on the contrary, tends to flatten the bands at the surface, hence move the surface recombination ($s$) towards its maximum value in the curve of $s$ *vs.* surface potential $\phi_s$. The maximum of $s$ occurs usually at $|\phi_s|$ small, which, for fairly pure material, corresponds to flat bands at the surface.

### C.6 S. GOLDSTEIN, H. METTE and W. W. GARTNER

R. N. HALL (G.E.): Lifetimes seemed quite short. Were the samples deliberately doped with deep level impurities? Is there any explanation for the great difference between lifetimes of samples 1 and 5, which were both about 50 Ω cm at room temperature?

S. GOLDSTEIN: The samples were obtained through the courtesy of various industrial organizations and were used as supplied. The origin of the recombination levels found is unknown.

S. D. ROSENBAUM (Northern Electric Co. Ltd. Montreal): Were precautions taken to look for shallow trapping, and if necessary make allowances for errors due to this effect?

S. GOLDSTEIN: In agreement with Shulman and Wylunda[1] no evidence of trapping has been found in $p$-type germanium. Trapping, if present to any significant degree, usually reduces the PME response to extremely low levels and the whole method of measurement becomes inapplicable.

#### REFERENCE

1. SHULMAN R. G. and WYLUNDA B. J., *Phys. Rev.* **102**, 1455–1457 (1956).

VOL 8 195

*J. Phys. Chem. Solids* Pergamon Press 1959. Vol. 8. pp. 87–96. Printed in Great Britain

SESSION D:
SURFACES*

D.1

# THE ELECTRICAL STRUCTURE OF SEMICONDUCTOR SURFACES

A. MANY†

Research Laboratories, Sylvania Electric Products Inc., Bayside, New York

VOL. 8 1959

**Abstract**—The present status of semiconductor surface research is briefly reviewed. The properties of the space-charge region, the oxide layer normally present on a real surface, and the slow and fast states are considered. Various measurements, such as those of field effect over a wide frequency range and surface recombination velocity are discussed. The energy distribution and hole and electron capture cross-sections of the fast states in germanium and silicon, as deduced from such measurements by various workers, are then summarized. The good experimental agreement among workers in this field as to the general characteristics of the fast states is particularly significant in view of the widely different treatments given to the surface in the different laboratories. Although the information available on the surface states is appreciable, particularly on germanium, the important question of their origin is still largely open. Some implications of the meagre available data bearing on this problem will be discussed.

## 1. INTRODUCTION

MAJOR advances in our understanding of semiconductor surfaces have taken place in the past few years. The various surface phenomena fall into a definite pattern and can be described in general, if not always in detail in terms of well established models.

The bulk of the information available on the surface electrical structure is derived from work on germanium and silicon, the most extensively studied semiconductors. It is fairly safe to assume, however, that most of the concepts and models relevant to the surfaces of these materials can be extended with only minor modifications to surfaces of other semiconductors. This is indicated, for example, by the results obtained on lead salts[1] and zinc oxide[2] surfaces. The discussions that follow will accordingly be given most in terms of germanium.

Two types of surfaces can be considered, "clean" and "real". Ideally clean and perfect surfaces can be thought of as the outer crystallographic planes of a perfect crystal, with no foreign impurities or localized imperfections. Such planes will not necessarily be the same as parallel internal planes, due to the different environments of an atom in the plane in the two cases. The break in lattice periodicity at the surface could give rise to localized levels in the band gap, or TAMM states.[3] SHOCKLEY, by considering a simplified model, concluded that such states would be present on surfaces of germanium and other crystals of the diamond lattice.[4] These states can be considered as the unfilled orbitals or dangling bonds of the surface atoms. They are therefore expected to be acceptor states and present with a maximum density corresponding to that of the surface atoms, i.e. of the order of $10^{15}$ cm$^{-2}$.

Surfaces that have undergone a change from the clean state, either intentionally or by insufficient isolation from external effects, are referred to as real surfaces. The real surfaces most commonly studied are prepared by mechanical polishing followed by chemical etching. The characteristics of a real surface will depend, of course, both on the crystal in question and on the particular treatment given to the surface. In the case of germanium or silicon, an oxide layer and absorbed impurities are normally present on the

*Chairman: W. H. BRATTAIN; Co-Chairman: H. STATZ.

†On leave of absence from the Hebrew University, Jerusalem, Israel.

surface. The foreign atoms may bond with the surface atoms thereby partially or totally saturating the dangling bonds. Operationally, two types of states are found on such surfaces: the fast states, which are presumably situated on the interface of the crystal and the oxide, and are possibly related to the original Tamm levels; and the slow states, which are predominantly situated on the outer surface of the oxide layer and arise entirely from adsorbed gas molecules.

Clean surfaces have been approximated in practice by cleavage in ultra-high vacuum,[5.5a] and, more commonly, by the FARNSWORTH technique of ion bombardment and subsequent annealing in ultra high vacuum.[6] Although an appreciable amount of effort has gone into the preparation and study of such surfaces, the results reported on the electrical structure are as yet mostly of a qualitative nature. It has been found, for example, that clean surfaces are strongly $p$-type,[5.7] as is to be expected from acceptor levels of the Tamm type. Only rough estimates of the density of states are available.[7,8] Work on real surfaces, on the other hand, has yielded much richer information on the detailed electrical structure. Particularly noteworthy is the comprehensive quantitative information now available on the characteristics of the fast states on real germanium surfaces. In this paper we shall attempt a brief review of the present state of surface research, and particular attention will be given to the electrical structure of the fast states.

## 2. THE FREE "REAL" SURFACE

Fig. 1 shows the accepted energy level diagram at the free surface of an $n$-type semiconductor for the case of an inversion layer (a), and an accumulation layer (b). The bulk crystal is on the right with $E_c$, $E_v$, $E_F$ and $E_i$ denoting respectively the conduction band edge, the valence band edge, the Fermi level and the so-called intrinsic Fermi level, the latter being very close to the midgap. The oxide layer with its conduction and valence bands is shown next to the semiconductor, with the midgaps of the two materials arbitrarily assumed at the same energy level. The fast and slow states are each schematically represented by a discrete set of levels. The surface states give rise to a potential barrier of such a height, $qV_s$, that the total charge on the states is balanced by that in the space-charge region. A more convenient measure of the potential barrier than $V_s$ is the surface potential, $\phi_s$, defined as the difference between the Fermi level and the intrinsic Fermi level at the surface. The surface potential is taken as negative when the Fermi level is below $E_i$ (Fig. 1a), positive when above (Fig. 1b). Actually, the density of the slow states ($> 10^{13}\,\mathrm{cm}^{-2}$) is so much larger than that of the fast states ($\sim 10^{11}\,\mathrm{cm}^{-2}$) that they completely dominate in controlling $\phi_s$. Gas ambients like oxygen and ozone, having a strong electron afinity, induce acceptor-type slow states and thus give rise to a negatively-charged surface (Fig. 1a). Other gases, like water vapor and ammonia, give rise to donor-type slow

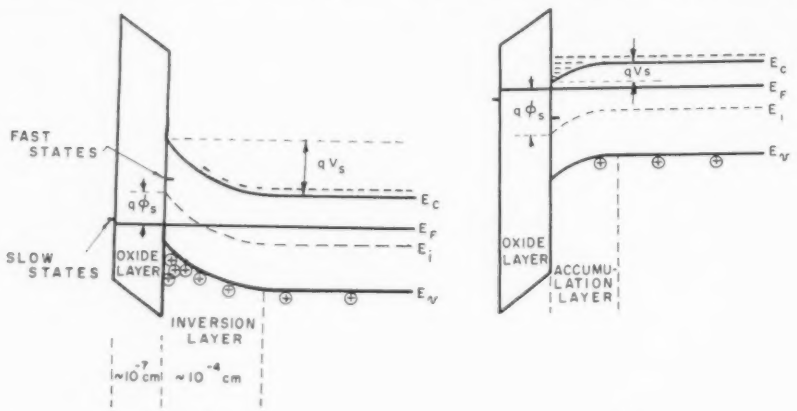


FIG. 1. Energy level diagram for the free real surface of an $n$-type semiconductor.

states and thus to a positively-charged surface (Fig. 1b). The fast states, on the other hand, are affected only slightly by gas ambients, as is to be expected from their location inside the oxide layer.

In order to determine the characteristics of the surface states it is necessary to vary the surface potential and follow the resulting changes in surface properties. This is usually achieved by exposing the surface to a cycle of gas ambients or by applying electric fields normal to the surface. For any work of quantitative nature it is essential to determine throughout this procedure the magnitude of $\phi_s$. A powerful technique for this purpose is the measurement of surface conductance, $\Delta\sigma$, which for a given type, resistivity and temperature is a unique function of $\phi_s$. The carrier densities in the space-charge region which enter into the expression of $\Delta\sigma$ are directly obtainable from a solution of Poisson's equation for any given $\phi_s$. There is, however, some question as to the effective mobilities of the carriers when constrained to move along a potential well of width comparable to or less than a mean free path. Assuming the surface to be a completely diffuse scatterer, SCHRIEFFER[10] has calculated the surface mobilities as a function of $\phi_s$. Measurements of surface magneto effects seem to confirm these calculations,[11] but more direct evidence is desirable. In any case, there is a substantial region of interest, corresponding to low barrier heights where the departures of the surface mobilities from the bulk values are sufficiently small to permit the use of the latter in calculating $\Delta\sigma$.

### 3. FIELD EFFECT MEASUREMENTS

Field effect measurements over a wide frequency range have proved to be an invaluable tool for studying the various surface states. For discussion of the frequency dependence of the field effect, suppose that a steady electric field is suddenly applied normal to the surface of an extrinsic semiconductor. The field, which momentarily penetrates the semiconductor, will cause a flow of predominantly majority carriers through the contacts into or out of the sample. This condition is established in a very short time, comparable to the dielectric relaxation time. We shall first consider the simpler case of an accumulation layer in which minority carriers can be neglected. The induced charge then appears as a change in the majority carrier density at the surface, giving rise to a sharp change in surface conductance. Non-equilibrium now exists between the majority carrier band and the various surface states. The fast states, being in good electrical contact with the bulk, are the first to interact with the space charge. As majority carriers are being trapped by or released from these states, $\Delta\sigma$ relaxes rapidly to a quasi-stationary value as equilibrium is reached. The time constant of this relaxation for germanium at room temperature is of the order of $10^{-8}$ sec.[12] In the case of an inversion layer, the relaxation process is quite different as it involves both types of carriers. At the onset of the field the initial current through the body will be carried by majority carriers as before, whereas at quasi-equilibrium the induced charge must appear as a change in the surface excess of minority carriers. The relaxation process would thus involve also hole–electron recombination or generation, whether via the fast states or by some other process in the sample, giving rise to a longer time constant, comparable to the sample effective lifetime.

Following the fast relaxation process, the slow states begin to interact with the induced charge, giving rise to a further relaxation in $\Delta\sigma$, but with a time constant many orders of magnitude larger than that associated with the fast states. This time constant may amount to seconds, minutes or even hours, depending on the surface condition. Due to the extremely large density of states normally present at the surfce, $\Delta\sigma$ relaxes to almost its original value corresponding to zero applied field. This final condition corresponds to practically all the induced charge residing in the slow states, thus effectively screening the space-charge region from the external field.

To summarize, there are three frequency ranges that can be studied: (1) d.c. fields for investigating the charge transfer mechanism between the slow states and the bulk, (2) low frequencies such that the effect of the slow states is eliminated, while, at the same time, the fast states are in equilibrium with the space charge, and (3) high frequencies where the interaction of the fast states with the bands can be studied. We shall now discuss measurements in these ranges in the order listed.

### 3.1. *Slow states*

Measurements pertaining to the slow states were mostly concerned with the study of the relaxation in $\Delta\sigma$ accompanying the d.c. field effect. The relaxation time has been found to increase very rapidly with a decrease in temperature[14] and with an increase in the oxide-layer thickness.[15] While the former results suggest a mechanism of charge transfer over a potential barrier, the latter point out to a tunneling process through the oxide layer. None of these models seems to account separately for the two sets of results but a combination of the two probably will. It should be noted that the dependence of the relaxation time on the oxide thickness strongly indicates that the slow states are predominantly situated on the outer surface of the oxide.[15]

The relaxation time has also been found to depend very strongly on the surrounding gas ambient, which is to be expected since the latter determines the density of slow states induced. Water vapor, for example, seems to induce a particularly large density of states, as judged from its drastic effect in reducing the relaxation time. In fact, such a large density of states may give rise, by mutual interaction between neighboring molecules, to electronic conductance through the layer of adsorbed molecules. Evidence for such conductance was found by STATZ and co-workers[16] on surfaces with thick adsorbed water layers.

### 3.2. *Fast states–low-frequency range*

The surface properties most commonly studied are the trapped charge in the fast states, surface recombination velocity and surface photovoltage, all measured as a function of surface potential. The trapped-charge density is derived from field effect measurements. The total charge $Q_T$ induced by the field at the surface is made up partly of a change in carrier density in the space-charge region, $\Delta Q_{sc}$ and partly of a change in charge on the fast states, $\Delta Q_{ss}$. (The charge in the slow states is assumed to be unaltered in this frequency range.) The change in $\Delta\sigma$ results entirely from $\Delta Q_{sc}$ and can be used to determine both $\Delta Q_{sc}$ and $\phi_s$. Thus, by varying the amplitude of the applied field, $\Delta Q_{ss} = Q_T - \Delta Q_{sc}$ can be evaluated as a function of $\phi_s$. This can be compared with the Fermi–Dirac distribution function given by

$$Q_{ss}/q = -\sum \frac{N_t}{1+\frac{1}{2}\exp[(E_t - E_i - q\phi_s)/kT]} \quad (1)$$

where each term in the summation corresponds to one set of discrete levels of energy $E_t$ and density $N_t$. This comparison can yield, in principle, the density and energy distribution of the various fast states. In practice, however, unless the swing in $\phi_s$ is sufficiently large, in fact larger than can be achieved experimentally, it is practically impossible to determine uniquely these parameters. BROWN,[17] who initiated these measurements, found, in fact, that different distribution functions, ranging from a discrete scheme to a continuous one, could equally account for the experimental data.

Obviously, additional and independent data are required for an unambiguous determination of the fast-state structure. This is supplied most effectively by the measurement of surface recombination velocity $s$ as a function of $\phi_s$. As in the bulk, surface recombination in germanium and silicon proceeds predominantly through intermediate energy levels, in this case the fast surface states. By applying the Shockley–Read theory of bulk recombination to a semiconductor surface, one obtains in the case of one discrete set of states[18]

$$s = \frac{N_t c_p (p_0 + n_0)}{2n_i \exp(q\phi_0/kT)\{\cosh[(E_t - E_i - q\phi_0)/kT] + \cosh[q(\phi_s - \phi_0)/kT]\}}, \quad (2)$$

where

$$q\phi_0 \equiv (kT/2)\ln(c_p/c_n)$$

and $c_p$ and $c_n$ are the hole and electron capture probabilities, given by the products of the thermal-velocity $v$ and the respective capture cross-sections $A_p$ and $A_n$. Equation (2) predicts that $s$ is symmetrical around $\phi_s = \phi_0$, this value being a measure of the ratio of hole to electron capture

cross-sections. In the region around $\phi_0$, $s$ is constant, but falls off rapidly for large $\phi_s$ values.

Typical experimental results for $\Delta Q_{ss}$ and $s$ vs. $\phi_s$ on germanium are shown in Fig. 2.[19] The recombination data (Fig. 2a) can be fitted very satisfactorily with the theoretical curve (equation (2)) corresponding to *one* discrete set of recombination levels, giving a striking confirmation of the theoretical model of surface recombinations. The fact that only one set of levels is dominant in the recombination, repeatedly found for most surfaces studied by us, is perhaps the strongest argument for the essentially discrete nature of the fast-state distribution on germanium. The energy level can be determined from this fit with a high precision. With the use of this information, the analysis of the field effect data in Fig. 2(b) becomes much more reliable. First the dashed curve corresponding to a Fermi–Dirac function of trapped charge in the recombination level is plotted. This obviously cannot account completely for the observed results, indicating that other sets of levels with negligible effect on recombination are also present at the surface. One of these sets is found to be situated at about one $kT$ below $E_i$. The solid curve is the combined effect of the two sets and accounts for the experimental results over a considerable range. The departures at extreme $\phi_s$ values indicates that two other sets of levels, one near the conduction band and one near the valence band, are also present, but the swing in $\phi_s$ was insufficient to permit their study in any detail beyond a rough estimate of their positions. More detailed information on the two outer sets was obtained by BARDEEN *et al.*[20] and by STATZ *et al.*[16,21] by studying strong inversion layers on both $p$- and $n$-type samples, corresponding to extreme $\phi_s$ values.

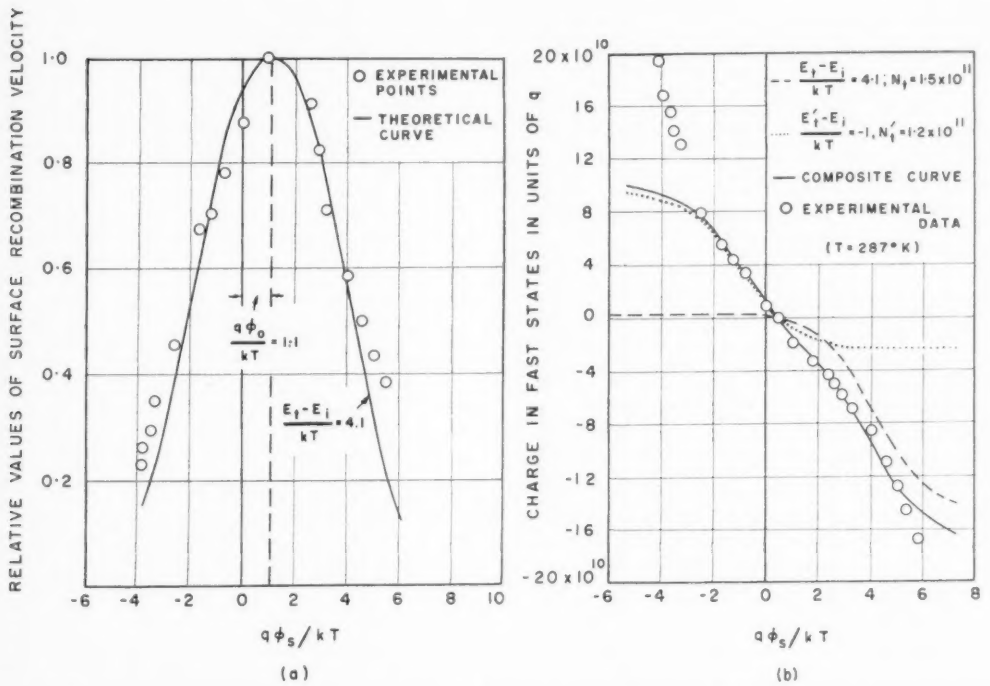


FIG. 2. Surface recombination velocity (a) and trapped charge density (b) vs. $q\phi_s/kT$ for an $n$-type germanium samp e

Finally, the measurement of surface photovoltage, i.e. the change of contact potential with illumination, affords yet another independent technique for studying the fast states. When the surface is illuminated, the carrier densities in the bulk are changed. The surface has then to

readjust itself to the changed availability of holes and electrons. This is done by rearrangement of charge in the space-charge region and in the occupation of the fast states. By analysing these effects, BRATTAIN *et al.* could arrive at conclusions regarding the fast state structure.[22]

Table 1 summarizes the characteristics of the fast states on real (etched) germanium surfaces, as determined by different workers using the techniques just described. Listed in the Table are the energy levels of the various sets with respect to the gap center in units of $kT$, their density per $cm^2$ and their capture cross-sections in $cm^2$. Except for the continuous distribution found by BRATTAIN and co-workers[22], most of the results indicate an essentially discrete distribution. There are four sets of levels grouped in four columns, in order of diminishing energy in the gap. The results reported by different workers are in good agreement considering that the fast states are affected by both the initial treatment of the surface and the subsequent history. For example, measurements on one sample at different gas ambients and over an extended period of time show a variation in the energy level of the recombination states from 3 to 6 $kT$.[19] There is also surprisingly good agreement regarding the densities of the states, which in all cases are of the order of $10^{11}$ per $cm^2$. Of the two intermediate sets, only the one above the gap center contributes to the recombination velocity, indicating that the capture cross-sections for the other set are negligible. The recombination is associated with a larger cross-section for holes than for electrons. These levels are therefore acceptor-like and may arise, for example, from states that are neutral when empty and negatively charged when occupied by an electron. Due to Coulomb attraction, a negatively charged state will have a larger cross-section for holes than a neutral state for electrons.

Silicon surfaces have received less attention than germanium surfaces, mainly because of the greater difficulties of measurement and the lack of as good bulk material. Work by STATZ *et al.*[16,21] and BUCK and MCKIM[23] indicates that the structure is not very different from that in germanium, with the density of fast states about one order of magnitude larger than that in germanium.

As for clean surfaces, very few results of the kind discussed above were reported. The difficulties of preparing and maintaining clean surfaces make the application of the rather elaborate techniques used in the study of real surfaces prohibitive. It has been found[7,8] that clean surfaces obtained by the FARNSWORTH technique[6] are strongly $p$-type. These results indicate that the density of states is very large, approaching the value for Tamm levels. For cleaved surfaces, PALMER and DAUENBAUGH[5] report much the same behavior whereas BARNES and BANBURY[5a] find these surfaces to be near intrinsic. On the whole it seems that most of the experimental evidence points at the presence of Tamm-like states on a clean surface. Such surfaces also exhibit low values of surface recombination velocity. For state densities as high as those of the Tamm levels, such low values of recombination velocity can only be obtained at very extreme values of surface potential. This indeed is the case in the strongly $p$-type surfaces observed on clean surfaces.

### 3.3. *Fast states–high frequency range*

Field effect measurements in this range were carried out by LOW *et al.*[13] using pulsed fields and by MONTGOMERY *et al.*[12,24] using sinusoidal fields. LOW's measurements, carried out on accumulation layers show that the time constant associated with the relaxation between the fast states and the majority-carrier band is of the order of microseconds at room temperature. MONTGOMERY's measurements, on the other hand, show no dispersion in the a.c. field effect due to this type of relaxation up to a frequency of several megacycles, indicating that the time constant is of the order of $10^{-8}$ sec. Most probably, the accumulation layers studied by LOW were not sufficiently developed so that the much longer time constants could arise from minority carrier effects. GARRETT[25] carried out a detailed theoretical analysis of the high-frequency field effect and obtained good agreement with MONTGOMERY's data[12] provided the fast states involved were assumed to be situated at a distance of about $7\,kT$ from $E_i$, corresponding either to the recombination levels or to the outer sets of levels listed in Table 1. This analysis indicates further that the presence of any significant number of states near the midgap is unlikely. The fact that

*Table* 1. *Summary of results obtained by different workers on the energy levels, densities and capture cross-sections of the fast states on real germanium surfaces*

| $\frac{E_t-E_i}{kT}$ | $N_t$ | $\frac{E_t-E_i}{kT}$ | $N_t$ | $A_p = c_p/v$ | $A_p/A_n$ | $\frac{E_t-E_i}{kT}$ | $N_t$ | $\frac{E_t-E_i}{kT}$ | $N_t$ | Source |
|---|---|---|---|---|---|---|---|---|---|---|
| 8 | $25N$ | 3 | $N$ | | | $-1$ | $N$ | $-6$ | $25N$ | MONTGOMERY and BROWN [24] |
| $>4$ | | ..... | $1\text{–}10\times10^{11}$ | $6\times10^{-15}$ | 150 | Continuous near $E$ | | $<-4$ | | BROWN *et al.*[22] |
| $>7$ | | 3–6 | $1\text{–}4\times10^{11}$ | $6\text{–}15\times10^{-15}$ | 2–30 | $-1$ | $1\text{–}10\times10^{10}$ | $<-5$ | | MANY *et al.*[18,19] |
| $>5{\cdot}5$ | | | ..... | Small continuous distribution | | ..... | | $(-5)$–$(-6)$ | $1\text{–}3\times10^{11}$ | BARDEEN *et al.*[20] |
| 7 | | 3·5–4·5 | $1\text{–}10\times10^{10}$ | $3\text{–}10\times10^{-15}$ | 10–50 | $-1$ | $2\text{–}20\times10^{10}$ | | | WANG and WALLIS[26] |
| 5–7 | $1\text{–}10\times10^{11}$ | | | | | | | $-5{\cdot}5$ | $1{\cdot}4\times10^{11}$ | STATZ *et al.*[16,21] |

this latter conclusion is incompatible with the low frequency data, as summarized in Table 1, was attributed by GARRETT to inhomogeneities in $\phi_s$ from point to point at the surface. This seems difficult to accept in view of the excellent agreement of the surface recombination data with the heoretical expression (equation (2)).[18,19] Such an agreement could only be obtained if the surface is homogeneous. Unfortunately, neither LOW nor MONTGOMERY specified the values of $\phi_s$ existing at the surfaces studied. It is conceivable that the accumulation layers studied by MONTGOMERY were highly developed so that only the states close to the band edges were involved in the charge transfer, the states near the gap center being practically empty in the *p*-type samples and completely filled in the *n*-type samples.

## 4. CONCLUSION

In conclusion we shall make a few general remarks concerning the surface structure as presently known. The properties of the space-charge region are fairly well understood. Further work is required to elucidate the scattering processes limiting carrier mobilities at the surface. The measurement of surface capacitance[22] and field effect at very high frequencies,[26] over a wide range of surface potential values, may be promising approaches.

As to the fast states, a rather complete description of their characteristics on real germanium surfaces is available. Little, however, can yet be said about their origin. Although the surrounding gas ambient is found to affect the structure of the fast states,[19] the changes are small enough to

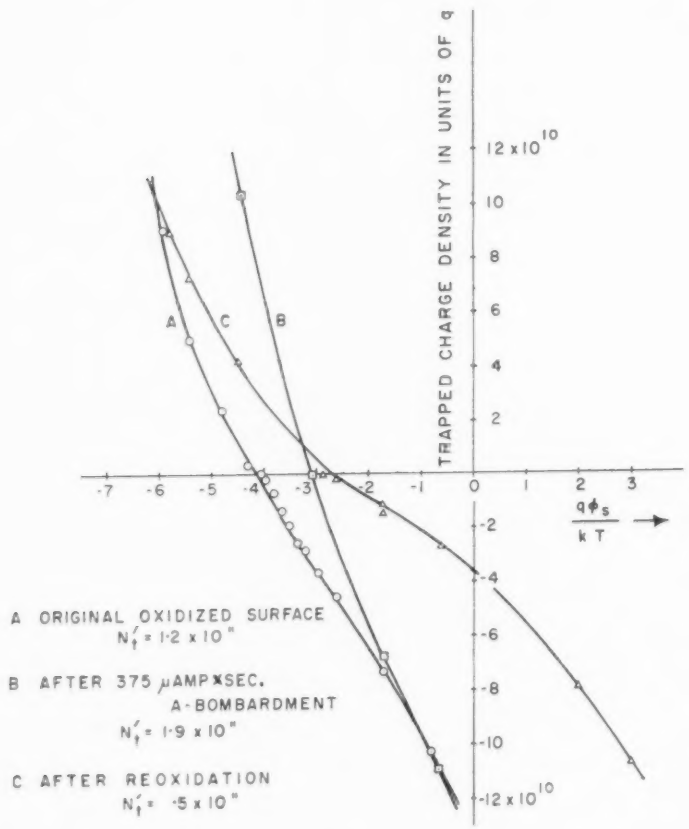


FIG. 3.

preclude the possibility of the states being associated with easily desorbed atoms. If there is a density of some $10^{15}$ Tamm levels per cm$^2$ on a clean surface, as indicated by theoretical reasoning[4] and supported to some extent by experiment,[7,8] how can one explain the much lower density of $10^{11}$ states found on a real surface? One possibility is that the oxide bonds to the surface atoms, saturating most of the dangling bonds that would give rise to the Tamm levels. The remaining $10^{11}$ states may then arise from the relatively small number of misfits between the germanium and oxide lattices, possibly due to dislocations or other imperfections. If it were possible to correlate the density of states with the condition of the oxide layer on a real surface, this would provide some evidence for this model. Preliminary results obtained by A. Feuersanger in this Laboratory indeed seem to point in this direction. Fig. 3 shows the measurement of trapped charge density vs. surface potential for three different conditions of the surface. The slopes of the curves in the neighborhood of $q\phi_s = 1kT$ are proportional to the densities of the set of states at this energy level. As discussed previously this is one of the inner levels found on germanium surfaces. Curve A was obtained on an etched surface and corresponds to a state density of about $1{\cdot}2\times10^{11}$ per cm$^2$. Curve B was obtained after argon bombardment which is known to knock off oxygen atoms from the oxide, and corresponds to a larger density of $1{\cdot}9\times10^{11}$. Finally, after reoxidizing (curve C), the density of states reduces to $0{\cdot}5\times10^{11}$. This cycle is reproducible for not too heavy bombardment doses and seems to indicate that removal of oxygen is associated with a larger state density, while reoxidation results in a reduction in density, as is to be expected from the role of oxygen in the model discussed.

Even though work of this nature on real surfaces may shed some light on the nature and origin of the fast states, the most promising approach, despite the formidable experimental difficulties, to this question would be the study of clean surfaces. A fundamental difficulty might arise here from the large density of states presumably present on a clean surface, as the swing in surface potential that might be achieved would be too small to allow for any detailed study of the surface structure. The study of the transition stages between the clean and real states under carefully controlled conditions might therefore prove more successful.

## REFERENCES


1. Petritz R. L., Lummis F. L., Sorrows H. E. and Scanlon W. W., *Semiconductor Surface Physics.* University of Pennsylvania Press, Philadelphia (1957).
2. Heiland G., *Z. Phys.* **142,** 415 (1955); *Ibid.* **148,** 15 (1957).
3. Tamm I., *Phys. Z. Sowjet.* **1,** 733 (1932).
4. Shockley W., *Phys. Rev.* **56,** 317 (1939).
5. Palmer D. R. and Dauenbaugh C. E., *Bull. Amer. Phys. Soc.* Ser. II, **3** (1958).

5a. Barnes G. A. and Banbury P. C., *Proc. Phys. Soc.* **71,** 1020 (1958).

6. Schlier R. E. and Farnsworth H., *Semiconductor Surface Physics.* University of Pennsylvania Press, Philadelphia (1957).
7. Madden H. H. and Farnsworth H. E., *Bull. Amer. Phys. Soc.* **1,** 53 (1956); Autler S. H., McWhorter A. L., Gebbie H. A., *Bull. Amer. Phys. Soc.* **1,** 145 (1956); Law J. T. and Garrett C. G. B., *J. Appl. Phys.* **27,** 656 (1956).
8. Handler P., *Semiconductor Surface Physics.* University of Pennsylvania Press, Philadelphia (1957).
9. Kingston R. H. and Neustadter S. F., *J. Appl. Phys.* **26,** 718 (1955); Garrett C. G. B. and Brattain W. H., *Phys. Rev.* **99,** 376 (1955).
10. Schrieffer J. R., *Phys. Rev.* **97,** 641 (1955).
11. Petritz R. L. *Phys. Rev.* **110,** 1254 (1955); Zemel J. N. and Petritz R. L., *Phys. Rev.* **110,** 1263 (1958).
12. Montgomery H. C., *Phys. Rev.* **106,** 441 (1957).
13. Banbury P. C., Low G. G. E. and Nixon J. D., *Semiconductor Surface Physics.* University of Pennsylvania Press, Philadelphia (1957); Low G. G. E., *Proc. Phys. Soc.* **68,** 1154 (1956), and *Report on Conference on Semiconductors.* Physical Society, London (April 1956).
14. Morrison S. R., *Semiconductor Surface Physics.* University of Pennsylvania Press, Philadelphia (1957).
15. Lasser M., Wysocki C. and Bernstein B., *Semiconductor Surface Physics.* University of Pennsylvania Press, Philadelphia (1957).
16. Statz H., DeMars G. A., Davis Jr. L., and Adams Jr. A. A., *Semiconductor Surface Physics.* University of Pennsylvania Press, Philadelphia (1957).
17. Brown W. L., *Phys. Rev.* **100,** 590 (1955).
18. Many A., Harnik E. and Margoninski Y., *Semiconductor Surface Physics.* University of Pennsylvania Press, Philadelphia (1957).
19. Many A. and Gerlich D., *Phys. Rev.* **107,** 404 (1957).
20. Bardeen J., Coovert R. E., Morrison S. R., Schrieffer J. R. and Sun R., *Phys. Rev.* **104,** 47 (1956).

21. STATZ H., DEMARS G., DAVIS L. Jr. and ADAMS Jr. A., *Phys. Rev.* **106,** 455 (1957).
22. BROWN W. L., BRATTAIN W. H., GARRETT C. G. B. and MONTGOMERY H. C., *Semiconductor Surface Physics*, Parts 1 and 2. University of Pennsylvania Press, Philadelphia (1957).
23. BUCK T. M. and MCKIM F. S., *J. Electrochem. Soc.* **105,** 709 (1958).
24. MONTGOMERY H. C. and BROWN W. L., *Phys. Rev.* **103,** 865 (1956).
25. GARRETT C. G. B., *Phys. Rev.* **107,** 478 (1957).
26. WANG S. and WALLIS G., *Phys. Rev.* **105,** 1459 (1957); Private communication, to be published.

*J. Phys. Chem. Solids* Pergamon Press 1959. Vol. 8. pp. 96–99. Printed in Great Britain

D.2

# THE EFFECT OF SOME SURFACE TREATMENTS ON THE CHARACTERISTICS OF FAST STATES ON GERMANIUM SURFACES

E. HARNIK and Y. MARGONINSKI

Department of Physics, The Hebrew University, Jerusalem, Israel

## 1. INTRODUCTION

LITTLE is known at present on the physical origin of fast states on germanium surfaces. With recent improvements in techniques[1,2] it appears that a systematic investigation of changes induced in the structure of fast states by various surface treatments and their correlation with the appropriate factors may supply useful information relevant to this problem. The results of some experiments carried out along these lines are reported and discussed in the present communication.

The surface treatments undertaken were chosen with a view to investigate the relation between the germanium oxide and some fast state characteristics. Accordingly, remanent changes induced by ozone and by $HNO_3$ on freshly etched, unstabilized surfaces were compared on the same filament.

## 2. EXPERIMENTAL METHOD AND RESULTS

The following surface treatments were independently employed: (1) etching in CP4-A* for 30 sec at 30°C, (2) passing dry ozonized oxygen (ozone), produced by ultraviolet irradiation, through the cryostat for 15 min at 25°C, (3) dipping into concentrated $HNO_3$ for 2 min at 30°C. The samples studied were $n$-type filaments of 25 Ω cm resistivity and (110) crystallographic orientation. Following a chemical treatment they were placed between two metal electrodes with mica insulation and introduced into a cryostat—all this within 10 min. All measurements were taken in vacuum of less than $10^{-4}$ mm Hg, within 1 hr after the application of a treatment. The experiments were carried out in cycles of two or more consecutive treatments. Care was taken to reduce to a minimum exposure to air between two consecutive treatments.

Simultaneous measurements, at constant temperatures, of filament lifetime and resistivity were carried out as a function of the voltage applied between the electrodes and the filament. Details on the method of measurement and on the interpretation of data are described elsewhere.[2] From the experimental data the fractional surface recombination velocity, $s/s_M$, where $s_M$ is the maximum value of $s$, and trapped charge density, $Q_{ss}$, were calculated and plotted vs. the surface potential, $\phi_s$. The difference between the energy of the recombination center, $E_t$, and the intrinsic Fermi level, $E_i$, was calculated from the larger of the two values of $\phi_s$ at which $s/s_M = 0{\cdot}5$. The ratio of capture probabilities for holes and electrons respectively, $c_p/c_n$, was determined from the relation $\phi_0 = (kT/2q) \cdot \ln(c_p/c_n)$, where $\phi_0$ is the value of $\phi_s$ about which the $s(\phi_s)$ curve is symmetrical and $q$ is the electronic charge. The density of the recombination centers, $N_t$, was derived from the slope of the $Q_{ss}(\phi_s)$ curve at $q\phi_s = (E_t - E_i)$ according to the relation $N_t = (4kT/q)(dQ_{ss}/d\phi_s)$. Finally the $(\phi_s)$ curve was analysed and the values for the energy, $E'_t$, and the density, $N'_t$, of a second set of fast states determined.

*The same as CP4 but without $Br_2$.

The results are summarized in Table 1. The data in (a) and (b) show the reproducibility of results with consecutive CP4–A treatments performed on the same filament. In (a) the results on partly etched surfaces are given. Here the treatments were started on a rough surface, ground with No. 800 carborundum. It can be seen that subsequent treatments gradually reduce the parameters of the recombination centers to values found on well-etched surfaces. The reproducibility on the latter is shown in (b). It appears that both $(E_t-E_1)$ and $c_p$ are fairly reproducible but large variations are observed in $c_p/c_n$.

The effect of ozone is shown in Fig. 1 and Table 1, (c) and (e). It is seen that while $(E_t-E_1)$ is hardly affected, the value of $c_p/c_n$ is considerably reduced. The $Q_{ss}$ curves show additional changes in fast state structure. The levels below $E_1$ appear to be shifted towards the valence band and the center level—towards the conduction band. Changes in the density of the center states induced by ozone on freshly etched surfaces have been

*Table.* 1 *The characteristics of two sets of levels,* $E_tE'_t$, *on n-type samples of* 25 Ω cm *resistivity and crystallographic orientation* (110) *as affected by various surface treatments.*

| Treatment | $(E_t-E_1)/kT$ | $c_p/c_n$ | $N_t\times10^{-11}$ ($cm^{-2}$) | $s_M$ | $(c_p/v_t)\times10^{14}$ ($cm^2$) | $(E'_t-E_1)/kT$ | $N'_t\times10^{-11}$ ($cm^{-2}$) |
|---|---|---|---|---|---|---|---|
| (a) 1. CP4-A | > 10·0 | $> 2\times10^4$ | > 10·0 | 900 | | | |
| 2. | 8·5 | $8\times10^3$ | 8·0 | 795 | 17·4 | | |
| 3. | 6·6 | 100 | 1·0 | 446 | 11·0 | −1·2 | 1·4 |
| (b) 1. CP4-A | 5·8 | 36 | 0·9 | 264 | 3·7 | 0·6 | 0·4 |
| 2. | 6·2 | 2400 | 2·4 | 260 | 2·9 | 1·2 | 0·4 |
| 3. | 6·2 | 150 | 1·2 | 198 | 3·2 | −0·6 | 1·0 |
| 4. | 5·8 | 55 | 1·1 | 269 | 3·1 | −1·8 | 1·4 |
| (c) 1. CP4-A | 6·2 | 2000 | 1·0 | 160 | 4·0 | 1·3 | 0·3 |
| Ozone | 6·2 | 270 | 2·2 | 328 | 3·2 | 3·0 (−1·0)* | 0·9(0·5)* |
| 2. CP4-A | 6·2 | 150 | 1·2 | 198 | 3·2 | −0·6 | 1·0 |
| Ozone | 5·8 | 55 | 1·8 | 153 | 1·1 | 0·2 | 0·5 |
| (d) 1. CP4-A | 6·2 | 2400 | 2·4 | 260 | 2·9 | 1·2 | 0·4 |
| $HNO_3$ | 7·0 | 9900 | 3·2 | 146 | 2·9 | 1·2 | 0·4 |
| 2. CP4-A | 5·8 | 55 | 1·1 | 269 | 3·1 | −1·8(2·0)* | 0·6(0·4)* |
| $HNO_3$ | 7·0 | 150 | 2·0 | 246 | 5·1 | −1·8 | 1·4 |
| (e) 1. CP4-A | 6·2 | 150 | 1·2 | 198 | 3·2 | −0·6 | 1·0 |
| Ozone | 5·8 | 55 | 1·8 | 153 | 1·1 | 0·2 | 0·5 |
| $HNO_3$ | 7·3 | 800 | 4·1 | 232 | 3·3 | 0·2 | 0·6 |
| 2. CP4-A | 5·8 | 55 | 1·1 | 269 | 3·1 | −1·8(2·0)* | 0·6(0·4)* |
| $HNO_3$ | 7·0 | 150 | 2·0 | 246 | 5·1 | −1·8 | 1·4 |
| Ozone | 6·2 | 37 | 3·2 | 211 | 1·2 | 0·8 | 0·6 |

(a) Consecutive treatments of CP4-A on partly etched surfaces.
(b) Consecutive treatments of CP4-A on well etched surfaces.
(c) The effect of ozone treatment on CP4-A treated surfaces.
(d) The effect of $HNO_3$ treatment on CP4-A treated surfaces.
(e) Results of cycles of three consecutive treatments.
All measurements were carried out in vacuum of less than $10^{-4}$ mm Hg, at 298°K. The thermal velocity, $v_t$, was taken as $10^7$ cm/sec.

*A third set of levels identified on the $Q_{ss}$ curve.

reported by WALLIS.[3] RZHANOV *et al.*[4] have identified two sets of fast states on ozone treated stabilized surfaces which lie close to the values of $E_t$ and $E'_t$ found here.

The effect of $HNO_3$ is shown in Fig. 2 and Table 1, (d) and (e). Here both $E_t - E_i$ and $c_p/c_n$ are appreciably increased, in contrast to the effect of ozone treatment. The changes in the $Q_{ss}$ curves can be interpreted either as a shift of the levels below $E_i$ towards the conduction band or as an increase in their density. The center levels are little affected. The same trend was observed in the changes induced by $HNO_3$ on stabilized surfaces.

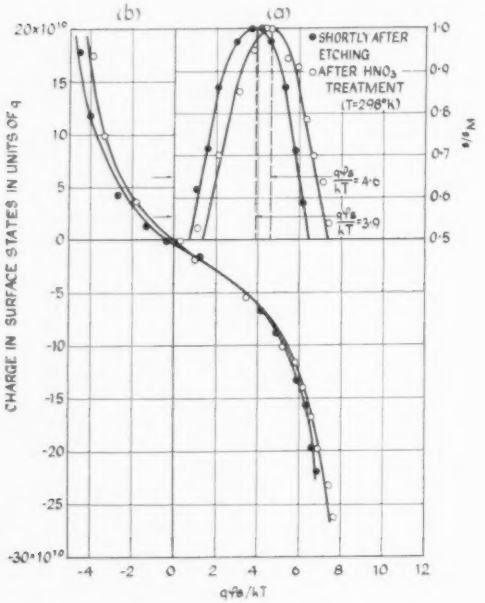


FIG. 1. Surface recombination velocity (a) and trapped charge density (b) versus $q\phi_s/kT$ for an $n$-type sample of 25 Ω cm resistivity, showing the effect of ozone treatment on a CP4-A treated surface.

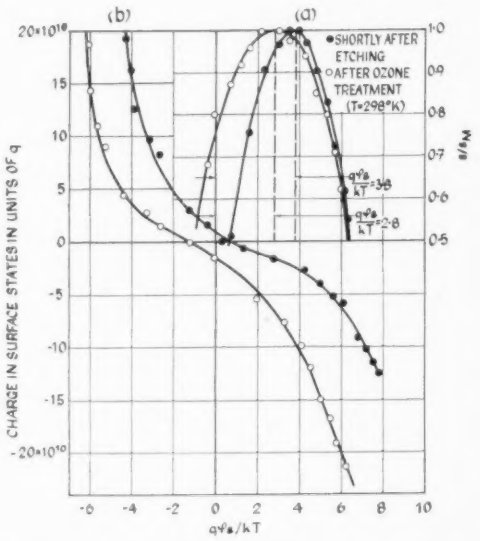


FIG. 2. Surface recombination velocity (a) and trapped charge density (b) versus $q\phi_s/kT$ for an $n$-type sample of 25 Ω cm resistivity, showing the effect of $HNO_3$ treatment on a CP4-A treated surface.

### 3. DISCUSSION

The data presented in Table 1 show clearly that the changes induced by ozone and $HNO_3$ in the characteristics of the recombination centers follow systematically a definite trend, and may, therefore, be associated with the action of these reagents. It may seem surprising that ozone and $HNO_3$, both oxidizing agents, should show so different, almost opposing, effects. This may, however, be connected with the difference in their reactivity. It has been pointed out by WALLIS[3] that ozone being a strong, rapidly acting oxidizing agent will produce a rather imperfect, amorphous oxide layer. On the other hand, $HNO_3$ is a milder oxidizer and will form more perfect, crystalline oxide layers. It is, therefore, tentatively suggested that the recombination centers, and probably some unidentified levels below $E_i$, are associated with misfits between the oxide and the underlying germanium structure, as these would be sensitive to the perfection and crystalline structure of the oxide layer.

In conclusion it should be pointed out that mechanical damages give rise to a rather complicated fast state structure, with a very high density of acceptor type levels near the conduction band which, in spite of their very large $c_p/c_n$ ratio, dominate the recombination process by

sheer superiority in density. This is evident from Table 1 (a). As more damaged parts are in general etched away more rapidly than others the recombination process gradually shifts, with consecutive etchings, to levels having lower $c_p/c_n$ ratio, until mechanical damage ceases to dominate the process.

**REFERENCES**

1. WANG S. and WALLIS G., *Phys. Rev.* **105,** 1459 (1957).
2. MANY A. and GERLICH D., *Phys. Rev.* **107,** 404 (1957).
3. WALLIS G., *Syl. Tech.* **11,** 6 (1958).
4. RZHANOV A. V., NOVOTOTSKY-VLASOV YU. F. and NEIZVESTNY I. G., *Zh. tekh. fiz., Moscow* **27,** 2440 (1957).

*J. Phys. Chem. Solids* Pergamon Press 1959. Vol. 8. pp. 99–102. Printed in Great Britain

# D.3 OPTICAL AND MAGNETIC SURFACE STUDIES ON GERMANIUM*

**RALPH BRAY and R. W. CUNNINGHAM†**

Purdue University, Lafayette, Indiana

GOLD-DOPED germanium at liquid nitrogen temperature has been very useful for studying surface behavior.[1] The high bulk resistivity of the material $\sim 10^6\ \Omega$ cm at 85°K, permits sensitive detection of surface conductive and galvanomagnetic properties. At the low temperature, communication between the "bulk" and "slow" surface states becomes so ineffective that changes in surface potential, induced by external field-effect, or illumination are very stable. This makes possible detailed measurements of surface properties at various values of the surface potential.

Illumination[2] of the surface of the samples at 80°K with intense white light produces, in addition to the usual fast bulk photoconductivity, a very slowly decaying component which may be called a retentive conductance, $G_r$. An appreciable fraction of this conductance remains even several days after the light is shut off. $G_r$ may be built up to values several orders of magnitude higher than the initial dark conductance, $G_0$. $G_r$ depends on the integrated flux which has fallen on the sample, and may be built up for hours without reaching saturation. Recovery to the initial $G_0$ value is facilitated by heating the sample. Complete recovery is achieved rapidly at $T \geqslant 250$°K.

That the retentive conductance is a surface effect, requiring the presence of an oxide layer, is shown by its dependence on surface treatment. Thus the slow decay effects are observed with aged surfaces, or surfaces etched in various oxidizing agents (e.g. $HNO_3$, $HF$–$HNO_3$, $H_2O_2$), but not with surfaces freshly reduced in HF etch. Field effect measurements show that, prior to any illumination, the surfaces are near the conduction minimum. However, corresponding to higher $G_r$, the surfaces become increasingly more $p$-type. It is therefore concluded that, the effect of the illumination is to increase the electron charge in the slow states inside or on the oxide layer; free holes form a thin, compensating space charge layer (accumulation layer, since all samples were $p$-type) to provide the excess conductance. The retentiveness of the effect may then be attributed to the ineffective communication between the slow states and the bulk. A slow state density of at least $10^{12}/\text{cm}^2$ is necessary to give thousand-fold changes in conductance.

*Work supported by Signal Corps contract.
†Present address: Texas Instruments, Dallas, Texas.

The stable control of the surface permits measurement of the Hall coefficient, $R$, and the magnetoresistive ratio, $\Delta\rho/\rho_0$ at different levels of dark surface conductance. Fig. 1 shows $R\sigma$ and $\Delta\rho/\rho_0$ (taken on different samples) plotted against $(G-G_0)/G_0$, the relative change in sample conductance from the minimum value. The data are for the whole sample, and do not show the separate bulk and surface contributions. Nevertheless, the large decrease in $R\sigma$ and $\Delta\rho/\rho_0$ attest to the relatively low mobility of holes in the thin, space charge layer, due to random scattering of the holes at the surface as predicted by SCHRIEFFER.[3]

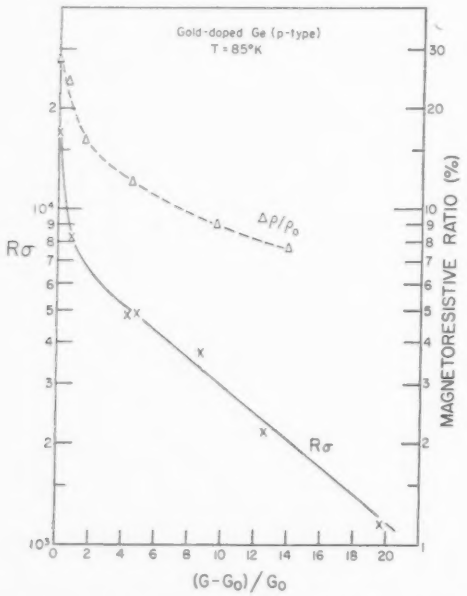


FIG. 1. The Hall mobility ($R\sigma$) and magnetoresistive ratio ($\Delta\rho/\rho_0$) vs. the relative change in sample conductance due to surface conduction. The two results are measured on different samples. Both the surface and bulk contribute to the plotted values.

The spectral dependence of the slow component of the photoconductivity was studied in the range 0·25—1·4 $\mu$ with a grating monochromator. It is usually necessary to build up $G_r$ by prolonged irradiation at short wavelength ($\sim$0·37$\mu$) to obtain the full details of the spectral response, as illustrated in Fig. 2. The initial low sensitivity may be attributed to operation near the conductance minimum of the surface. Because of the practical impossibility of obtaining steady state changes in the slow photoconductivity with illumination, it was necessary to resort to the following expedient. The sample was illuminated for an arbitrary interval (5 min.) and the conductance was then allowed to decay in the dark an equal time interval. The response was then taken as the difference between the values of dark conductance just before illumination and at the end of the light–dark cycle. This response, normalized for the incident light intensity, is plotted as the ordinate in Fig. 2. Note that the fast bulk photoconductive contribution is automatically eliminated.

The main features of the spectral response can be summarized as follows: (1) Most characteristic is the very strong response with a threshold near 0·45 $\mu$ and peaking near 0·37 $\mu$. It is this short wavelength response which contributes the very

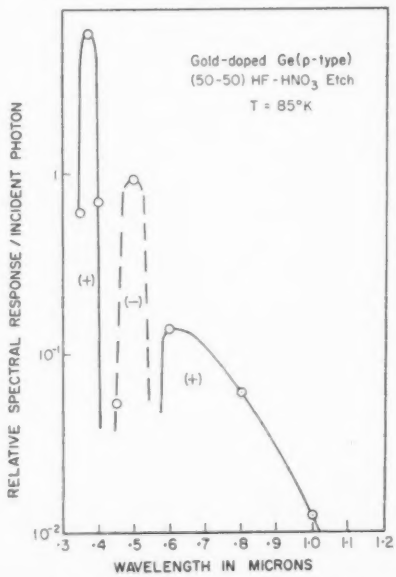


FIG. 2. Relative spectral response of the slow photoconductive effect per incident photon; (+) and (−) represent positive and negative slow photoconductive effects. The bulk photoconductive effect is eliminated from the plot.

prolonged retentive effects, measurable in hours. A more rapidly decaying component, in order of minutes, may also be distinguished. (2) A much weaker response occurs at longer wavelengths, peaking at $\sim$0·6 $\mu$ and decreasing monotonically in the infra-red. The decay here corresponds to that of the faster component above. (3) The dashed curve centering $\sim$0·5 $\mu$ represents a negative photoconductive effect, which accelerates

the decay of the retentive conductance previously built up at other wavelengths. It quenches particularly the faster component, irrespective of its origin. (4) Not shown in the figure is another negative effect, at $\lambda \leqslant 0{\cdot}31\ \mu$ which gradually quenches the very slow component of the retentive conductance built up in the $0{\cdot}37\ \mu$ range.

A two trap model is suggested by the various spectral and decay rate observations. The usual surface model[4] is illustrated in Fig. 3. Consider first the very slow, short wavelength effects (1), associated with internal oxide states, close enough to the bulk Ge to communicate by tunnel effect. The drop in response of this component of the photoconductivity with increasing wavelength can be attributed to the decrease in number of generated electrons that can reach the surface as the absorption coefficient of the incident radiation decreases. The $0{\cdot}5\ \mu$ quench (corresponding to a threshold of $\sim 2{\cdot}2$ eV) may be associated either with direct excitation of electrons out of oxide traps, or excitation of free holes in the Ge to the

Two Trap Model

| | Slow Adsorption States | Internal Oxide States |
|---|---|---|
| Natural Recovery Time | Days | Minutes |
| Electron Capture Threshold | ~ 3 ev | << 1 ev |
| Quench Threshold | ~ 4 ev | ~ 2·2 ev |

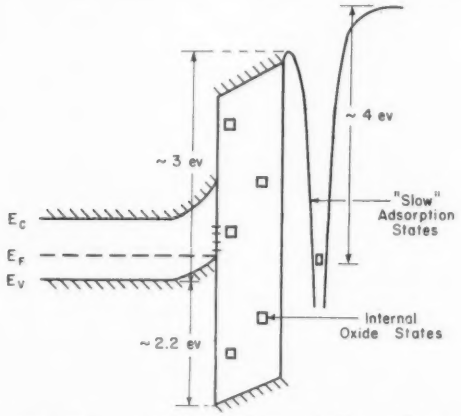


FIG. 3. Usual model of the semiconductor surface with an oxide layer, for $p$-type Ge with an accumulation space charge layer.

which may be associated with the slow states on the outside of the oxide layer. We suppose the short wavelength light ($\lesssim 0{\cdot}45\mu$) excites hole–electron pairs in the Ge with enough energy for the electrons to pass over the oxide barrier to the outer traps. The requirement that such electrons must be generated within a mean free path of the surface is compatible with absorption data[5] for these wavelengths. This sets a height of about 3 eV for the oxide barrier (Fig. 3). The quench (4) of the slow effect suggests that $\geqslant$ 4 eV is required to free the trapped electrons. The faster decaying components of (1) and (2) are tentatively oxide valence band where they can recombine with trapped electrons. The relatively long decay time and the high quench energy seem to rule out the interface states as the trap for these effects. It should be noted that an oxide gap[6] of about 5·5 eV is compatible with the picture presented here.

In conclusion, it is apparent that a modulation of the surface potential is possible by proper selection of the wavelength of the exciting radiation. The control of the surface by light is especially valuable at low temperature where the use of gaseous ambients for this purpose is impractical. The study of spectral effects appears to be useful for specifying details of the surface

model. The results reported here were obtained primarily on surfaces etched in $HNO_3$ or $HF$–$HNO_3$. Correlation of the spectral response with other surface treatment should be rewarding.

### REFERENCES

1. CUNNINGHAM R. W. and BRAY R., *Bull. Amer. Phys. Soc.* Ser. II. **2**, 348 (1957); *Ibid.* **3**, 115 (1958).
2. MORRISON S. R., *Phys. Rev.* **102**, 1297 (1956).
3. SCHRIEFFER J. R., *Phys. Rev.* **97**, 641 (1955). See also PETRITZ R. L., *Phys. Rev.* **110**, 1254 (1958); ZEMEL J. N. and PETRITZ R. L., *Ibid.* **110**, 1263 (1958).
4. KINGSTON R. H., *J. Appl. Phys.* **27**, 101 (1956).
5. ARCHER R. J., *Phys. Rev.* **110**, 354 (1958).
6. PAPAZIN H. A., *J. Appl. Phys.* **27**, 1253 (1956).

*J. Phys. Chem. Solids* Pergamon Press 1959. Vol. 8. pp. 102–105. Printed in Great Britain

VOL 8 195

D.4

# MAGNETO-SURFACE PROPERTIES OF NEAR INTRINSIC GERMANIUM

**J. N. ZEMEL and R. L. PETRITZ***

U.S. Naval Ordnance Laboratory, White Oak, Maryland

## 1. INTRODUCTION

RECENTLY, ZEMEL and PETRITZ[1] reported on the use of the galvanomagnetic coefficients for determining the electrical transport properties of excess carriers at the surface of germanium. Using the analysis of PETRITZ,[2] the authors deduced the following: the conventional model of the surface[3] is substantially correct; light holes play an important role in surface charge transport for $p$-type layers; the existence of a mobility correction for the surface carriers[4] was confirmed. In order to study these last two properties in greater detail, a series of experiments has been carried out on a slightly $p$-type, near intrinsic germanium sample, using the same techniques reported in (I). The analysis is quite similar to the one presented in (I) with certain modifications.

## 2. EXPERIMENTAL PROCEDURE AND RESULTS

The sample used in this experiment had a resistivity of 48 Ω cm at 25°C and a thickness of 27 $\mu$. Leads were soldered to eccentrically placed side arms and the resulting mixed signal was measured with a Brown Type 15 electrometer. The surface conditions were modulated by a modified Bardeen–Brattain cycle consisting of wet, dry and sparked oxygen. Several values of the magnetic field were used to explore the dependence of the Hall coefficient and magnetoresistance on the field but only the low field data will be reported here. In Fig. 1, a composite of experimental and theoretical curves for the Hall coefficient are presented as functions of the fractional change in sample conductance with respect to the conductance minimum, $\Delta\sigma_{min}/\sigma_{min}$. In Fig. 2 corresponding curves for magnetoresistance are similarly plotted. All the data were taken at 25°C. This temperature was regulated to better than 0·1°C.

## 3. DISCUSSION OF THE DATA

The data in Figs. 1 and 2 are composites of runs carried out at two different values of the magnetic field (1600 and 1910 G). The data substantially overlap throughout the entire range of $\Delta\sigma_{min}/\sigma_{min}$. The swings in the conductance are quite substantial as indicated by the fact that

*Currently on leave at Texas Instruments, Inc., Dallas, Texas.

the maximum value of $\Delta\sigma_{min}/\sigma_{min}$ on the $p$ side of the minimum was $\sim$2·5. The Hall data show very little scatter but the magnetoresistance at large values of $\Delta\sigma_{min}/\sigma_{min}$ does. The resistivity in this region is small and the changes due to the magnetic field are also small. As a result the measurement errors increase substantially. The relative precision of the Hall data is within $\pm$5 per cent and of the magnetoresistance data is within $\pm$10 per cent for conductance changes less than 250 per cent. Above that point the Hall data precision is approximately $\pm$20 per cent, while the magnetoresistance precision is no better than $\pm$40 per cent. The absolute value of the conductance and Hall data are good to 20 per cent, the error here being the uncertainty in the thickness measurement.

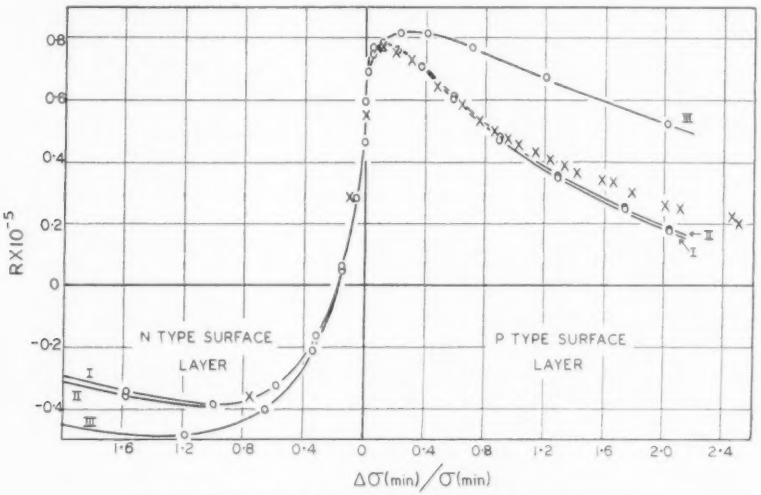


FIG. 1. Hall coefficient as a function of the fractional change in conductance with respect to the conductance minimum. (×) refers to experimental data and (○) refers to theoretical data. Curve I uses the Hall effective mobility expression of ZEMEL.[5] Curve II uses the square of the conductivity effective mobility for $\langle\mu_s^2\rangle/\langle\mu_b^2\rangle$. Curve III has all the mobilities set equal to the bulk mobilities.

## 4. ANALYSIS

The methods used in I for analyzing the data were employed here with only minor modifications. Since the curves were calculated on an IBM 650 computer, it was desirable to use a closed form expression for the effective mobilities. The constant field space-charge potential[4,5] yields closed forms for the effective mobilities and these were used in the analysis. Three cases are treated here: (1) the Hall effective mobility ($\langle\mu_s^2\rangle/\langle\mu_b^2\rangle$, equation (20) of I) was set equal to the square of the conductivity effective mobility, and the magnetoresistance effective mobility ($\langle\mu_s^3\rangle/\langle\mu_b^3\rangle$, equation (21) of I) was set equal to the cube of the conductivity effective mobility; (2) the Hall effective mobility derived by ZEMEL[5] was used, and the magnetoresistance effective mobility was set equal to the three-halves power of the Hall effective mobility; and (3) all mobilities were set equal to the bulk mobilities.

In Table 1 the constants used for calculating the curves are given. In order to obtain a good fit the carrier mobilities and the density of light holes can be varied. A cut and try method was used to fit the curves. The bulk potential was estimated from the general fit of the curves and is probably within 10 per cent of the correct value. As can be seen in Table 1, the ratio of electron to hole mobilities is somewhat low. Additional adjustment of the light to heavy hole mobility ratio

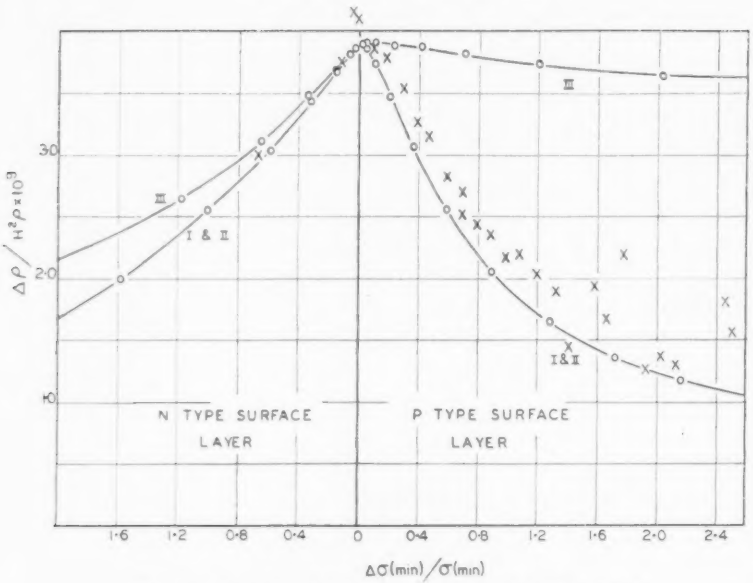


FIG. 2. Magnetoresistance as a function of the fractional change in conductance with respect to the conductance minimum. (×) refers to experimental data and (○) refers to theoretical data. In curve I, $\langle\mu_n^3\rangle/\langle\mu_b^3\rangle = (\langle\mu_n^2\rangle/\langle\mu_b^2\rangle)^{3/2}$, in II, $\langle\mu_n^3\rangle/\langle\mu_b^3\rangle = (\langle\mu_n\rangle/\langle\mu_b\rangle)^3$ and in curve III all the mobilities are set equal to the bulk mobilities.

and density would probably eliminate this discrepancy. However, since the space-charge region model is not quite correct, the adjustment would not yield better information.

### 5. COMPARISON OF THEORY AND EXPERIMENT

The most striking result of a comparison of the calculated curves with the data is confirmation of the importance of diffuse surface scattering of the excess carriers on surface transport measurements. It is obvious that elimination of surface scattering destroys the good qualitative agreement between theory and experiment. This is shown by curve III in Figs. 1 and 2. The Hall data were normalized to agree with the maximum of the theoretical curves by multiplying the data by 0·944. Even without this normalization, the data would have

*Table* 1. *Parameters used in the calculation*

| | |
|---|---|
| $\mu_n = 3650$ cm²/V sec | electron mobility |
| $\mu_p = 2010$ cm²/V sec | average hole mobility |
| $b_{32} = 7{\cdot}5$ | ratio of light to heavy hole mobility |
| $r = 2{\cdot}25\times10^{-2}$ | density of light holes relative to heavy holes |
| $L_D = 7{\cdot}24\times10^{-5}$ cm | Debye length |
| $d = 2{\cdot}7\times10^{-3}$ cm | sample thickness |
| $n_i = 2{\cdot}1\times10^{13}$ carriers/cm³ | bulk intrinsic carrier density |
| $m_1/m_e = 0{\cdot}1$ | electron effective mass to free electron mass |
| $m_2/m_e = 0{\cdot}3$ | heavy hole effective mass to free electron mass |
| $m_3/m_e = 0{\cdot}1333$ | light hole effective mass to free electron mass |

still agreed to within 6 per cent. The magnetoresistance data were not normalized. While the agreement is only good to about 15 per cent over the range of $\Delta\sigma_{min}/\sigma_{min}$, there are several significant points to be noticed. The theoretical curves tend to deviate the most when $\Delta\sigma_{min}/\sigma_{min}$ is large. This corresponds to values of the surface potential less than $-5kT$. In this region, the effective mobility based on the linear potential model falls below the Poisson potential mobility. Thus the deviation of the theory is in the right direction.

The mobility theory used here is based on a bounded solution to the Boltzmann equation. Making use of a diffuse surface scattering boundary condition, one obtains expressions for the galvanomagnetic coefficients in excellent agreement with experiment as shown above. However, the theory does not deal with the source of the diffuse scattering mechanism. Diffraction effects such as those disucssed by MÜSER[6] in metals would not apply here because of the long de Broglie wavelengths of the carriers. Thus another mechanism is needed to account for the phenomena. One possibility is the trapping and subsequent emission of carriers from surface states. However, the full explanation for this behavior must await additional theoretical and experimental developments.

Examination of the values of $r$ and $b_{32}$ (the density and mobility ratios of light to heavy holes) indicates good agreement with the work of WILLARDSON, HARMAN and BEER.[7] However, further work is needed since the values are at best order of magnitude quantities.

## 6. CONCLUSIONS

The comparison of theory and experiment strongly confirms the existence of a diffuse surface scattering mechanism. The density and mobility ratio for light holes agrees with an earlier estimate but uncertainties in the fit require further work before reliable values can be obtained.

*Acknowledgments*—The authors would like to acknowledge the assistance given by the Applied Mathematics Department in obtaining the numerical values for the theoretical curves and in particular, the help of Mr. ARTHUR HILT. The material used was kindly supplied by Dr. WILLIS ADCOCK of Texas Instruments, Inc. Mr. JAMES R. BURKE assisted in the data reduction.

## REFERENCES

1. ZEMEL J. N. and PETRITZ R. L., *Phys. Rev.* **110,** 1263 (1958). Referred to hereafter as I.
2. PETRITZ R. L., *Phys. Rev.* **110,** 1254 (1958).
3. *Semiconductor Surface Physics* (Edited by R. H., KINGSTON). University of Pennsylvania Press Philadelphia (1957).
4. SCHRIEFFER J. R., *Phys. Rev.* **97,** 641 (1955).
5. ZEMEL J. N., *Phys. Rev.*, to be published.
6. MÜSER H., private communication.
7. WILLARDSON R. K., HARMAN T. C. and BEER A. C., *Phys. Rev.* **96,** 1512 (1954).

*J. Phys. Chem. Solids* Pergamon Press 1959. Vol. 8. pp. 106–108. Printed in Great Britain

D.5

# EFFECT OF THE METAL-TO-SEMICONDUCTOR POTENTIAL ON THE SEMICONDUCTOR SURFACE BARRIER HEIGHT

**N. J. HARRICK**

Philips Laboratories, Irvington-on-Hudson, New York

## 1. INTRODUCTION

THEORIES of metal-to-semiconductor contacts generally contain the assumption that the contact potential is a factor in controlling the surface barrier height. This assumption, however, has remained unverified. From numerous experiments, conclusions have been drawn that sometimes the contact potential did affect the barrier height and other times the contact potential did not affect the barrier height. To explain these latter results, BARDEEN[1] proposed the presence of surface states and described the effective shielding of the semiconductor by means of them. Since BARDEEN's proposal, additional positive and negative results have appeared in the literature. Thus some uncertainty in regard to this assumption still persists.

In the past experiments, attempts were made to check this assumption by measuring the voltage–current characteristics of metal-to-semiconductor contacts, using different metals for the contacts. This is not necessarily a good test, as the voltage–current characteristics are not always sensitive functions of the barrier height, especially with the existing uncertainties in the theories of metal-to-semiconductor contacts. In the ideal experiment one would measure the barrier height before and after the metal is brought into contact with the semiconductor. This cannot be done by the standard field-effect technique because the surface conductivity cannot be measured when a metal is in contact with the surface. The surface conductivity can, however, be monitored by passing infrared radiation near the surface inside the semiconductor. The object of the present experiment is to monitor the surface conductivity with infrared radiation as the metal is brought into contact and to attempt to relate any observed changes to changes in surface barrier height.

## 2. EXPERIMENTAL

The use of infrared radiation to measure an excess or deficit of carriers in semiconductors is discussed elsewhere.[2] Schematic diagrams of the techniques employed in the present experiments are shown in Fig. 1. The observations consist of measurements of infrared intensity transmitted by the germanium sample before and after a metal is brought into contact. Liquid metals are used in the present experiment as they can easily be removed from contact with the semiconductor and also observations can be taken while the contact is being made. As we are interested in surface effects, it is necessary to bring the beam near the surface. This can be done by passing the beam parallel to and near the surface or by internally reflecting the beam at the germanium surface (Fig. 1b). In the former case only qualitative results can be obtained because the distance of the beam from the surface cannot be known precisely. Most of the results described here were obtained using this technique, but the latter technique (Fig. 1a) will be described because it leads to a better understanding of the experimental approach and can in principle be used to obtain quantitative results. In the latter case, the ratio of the change in transmitted intensity due to bringing a metal into contact, to the transmitted intensity for total internal reflection at the Ge–air interface (angle of incidence greater than 14·5°) is given by the following relationship:*

$$\pm\frac{\Delta I}{I_T} = 1-R^n \exp\left[\mp(k_h\Delta P+k_e\Delta N)\frac{2n}{\cos\theta}\right].$$

$R$ is the reflectivity from the metal-semiconductor interface, $\Delta P$ and $\Delta N$ the total number of excess holes and electrons per cm$^2$, respectively, introduced into the surface barrier by the presence of the metal, $\theta$ the angle of incidence, $n$ the number of reflections and the $k$'s are the extinction coefficients for holes and electrons. The change in surface barrier height can be determined[3] from $\Delta P$, $\Delta N$ and knowledge of the original surface barrier height. Unfortunately, for an Hg–Ge interface, $R$ turns out to be only 45 per cent at three

* This relationship can be derived following a procedure similar to that given in Reference (2), but now considering only changes in the carrier concentration in the surface barrier and changes in the reflectivity of the surfaces which come into contact with the metal.

microns, except for grazing incidence, while the exponential term is in general small. Hence, unless $R$ can be increased, it would be difficult to obtain quantitative or even qualitative evaluation of the surface barrier height. However, an upper limit of the change in surface barrier height can be established using this technique. For a beam nominally parallel to the surface, the effect

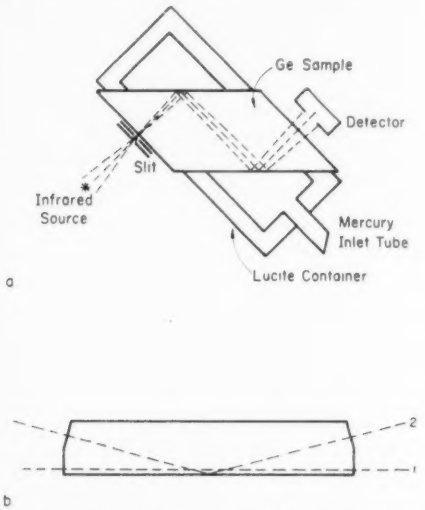


FIG. 1. Experimental set-up used to observe changes in the semiconductor surface conductivity due to bringing a metal into contact with a semiconductor.

of the reflectivity is not completely eliminated but greatly reduced for two reasons: Firstly, due to the usual uncollimated nature of a light beam, only part of the beam is reflected from the interface. Secondly, any rays striking the interface, do so at near grazing incidence when the reflectivity approaches 100 per cent.[4] The qualitative results described in this next section were obtained by passing the beam parallel to the surface.

### 3. RESULTS AND DISCUSSION

Changes in transmitted infrared intensity were observed when mercury or gallium was brought into contact with an etched (CP–4) germanium surface. The magnitude and sign of these changes could be controlled by the gaseous ambient. Typical signals observed are those shown in Fig. 2 for Hg and Ga. These curves are similar to those observed in the standard field-effect experiments. The interpretation for the signal represented by the curve of Fig. 2(a) is that the surfacewas initially $p$-type and driven further $p$-type by the presence of the mercury. The subsequent decay of the signal represents the return of the surface to its original condition. Similarly, when the contact was removed, the surface was driven less $p$-type and was subsequently restored with a somewhat longer time constant. The decay curve of Fig. 2(b) was obtained with mercury after the germanium surface was driven strongly $n$-type with water vapor and ammonia. A similar curve was obtained by the use of gallium in place of mercury when the surface was originally $p$-type. The signal here shows that the surface was driven strongly to the opposite type and subsequently returned to its original state. These interpretations are demonstrated schematically in the accompanying surface conductance vs. surface barrier potential diagrams. The above interpretations are consistent with the signs of the contact potentials measured by us for Hg and Ga with respect to Ge in air ($-0{\cdot}5$ V for Hg and $+0{\cdot}2$ V for Ga). The final sign of the surface barrier potential was checked by passing a current through the metal–semiconductor interface and noting whether injection or extraction occurred. The results of these observations are generally found to be consistent with the previous interpretations.

Our interpretations are strengthened by the fact that the general behavior of the change in transmission of infrared by the sample could be accounted for by a change in the surface barrier height in the following instances:

(1) Without a metal in contact, the transmission of the sample changed in the expected manner with gaseous ambient (wet air, $O_2$, $O_3$, $NH_3$).

(2) An increase of transmission by the sample when a metal comes into contact cannot be explained by the effect of the reflectivity. With mercury, this increase of transmission by the sample was obtained only after the surface was known to be $n$-type from the injection–extraction experiment of the previous paragraph.

(3) The field-effect experiment was set up and the sample conductivity monitored by means of infrared radiation. The expected changes in transmitted infrared radiation with applied field were, indeed, observed. These changes could also be controlled by the gaseous ambient and the magnitude and decays of the observed signals were quite like those shown in Fig. 2.

(4) In the set-up shown in Fig. 1(b), the signals for beams (1) and (2) due to bringing a metal into contact with an etched Ge surface changed quite differently when the state of the surface was changed by varying the ambient. In one particular case, for instance, signal (1) changed by a factor of 3 (from 0·5 per cent to 1·5 per cent) and exhibited a time constant as well as a reversal in sign in the manner of Fig.2(b), while signal (2) exhibited no time constant and remained unchanged at about 50 per cent. Our interpretation is that the

signal for beam (1) arose principally from a change in surface barrier height while signal (2) was due largely to the loss by reflection from the Ge–Hg interface.[4]

## 4. CONCLUSION

In conclusion we can say that changes in surface conductivity with relaxation times (of the order of tens of seconds) have been observed as a metal (Hg or Ga) was brought into contact with etched germanium surfaces. These changes and relaxation times are interpreted to be due to changes in the semiconductor surface barrier height and presence of surface states. The direction of the observed changes are consistent with the sign of the contact potential involved and the initial type of the semiconductor surfaces. Because of the large contribution to the signal from the reflectivity loss when a metal is brought into contact with germanium,[4] nothing definite can be said about permanent changes in the surface barrier height while the metal is in contact. Quantitative measurement can be obtained only in the cases, such as when transients are observed, when the signals involved can definitely be established to have resulted from changes in surface barrier height. For mercury, whose work function is about one-half of a volt higher than that of germanium, and for an etched or diamond polished surface on the germanium, there is not a permanent change in the surface barrier height of more than 0·25 V for the cases studied. This was deduced from careful correlation between experiment and theory of the reflectivity of a germanium–mercury interface and using the technique shown in Fig. 1(a).[4]

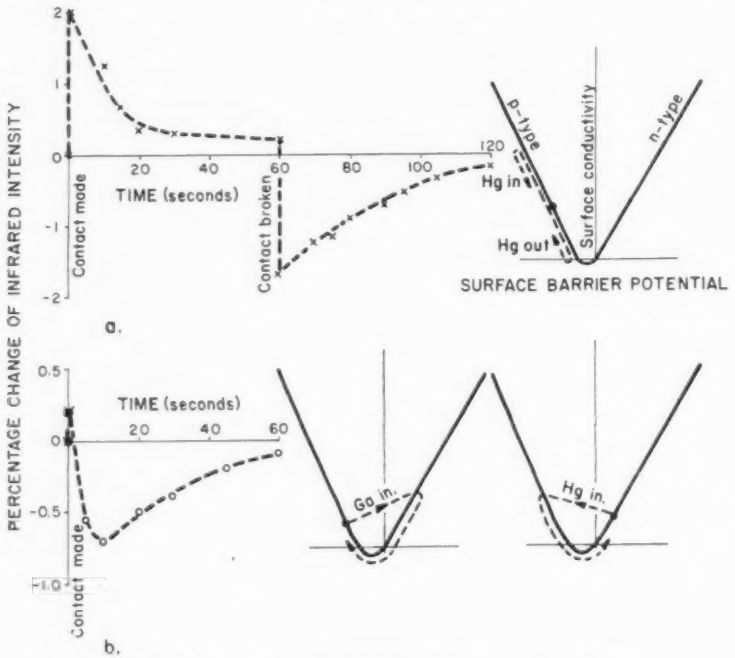


FIG. 2. Observations and interpretations of some decay curves resulting from bringing a metal into contact with germanium.

*Acknowledgment*—The author has profited from several helpful discussions with Dr. P. H. DOWLING during the course of this work.

## REFERENCES

1. BARDEEN J., *Phys. Rev.* **71,** 717 (1947).
2. HARRICK N. J., *Phys. Rev.* **103,** 1173 (1956).
3. KINGSTON R. H. and NEUSTADTER S. F., *J. Appl. Phys.* **26,** 718 (1955).
4. HARRICK N. J., to be published.

*J. Phys. Chem. Solids* Pergamon Press 1959. Vol. 8. pp. 109–111. Printed in Great Britain

D.6

# HALL MOBILITY OF A CLEANED GERMANIUM SURFACE*

ROLLAND MISSMAN and PAUL HANDLER

University of Illinois

VOL. 8 959

ONE of the important properties necessary for the study of semiconductor surfaces is the mobility of the carriers in the space-charge potential well. As is often the case the width of the potential well is small compared to the mean free path of the carriers and the effect of surface scattering will become important. If the scattering at the surface is diffuse, the mobility of the carriers will be reduced below their bulk value. The dependence of the conductivity mobility of these carriers on the depth of the well has been calculated by SCHRIEFFER.[1] The dependence of the Hall mobility has been calculated for the case of a constant electric field by ZEMEL[2] and agrees within 10–20 per cent of the reduced conductivity mobility found by SCHRIEFFER. PETRITZ[3] has derived expressions for surface densities and mobilities which are functions of the experimental galvanomagnetic data and are independent of the shape of the space charge region. These expressions with certain simplifying assumptions will be used to evaluate the experimental data in this paper. The first experimental study of the surface Hall coefficient and magnetoresistance has been carried out by ZEMEL and PETRITZ.[4] They showed that for shallow space-charge potential wells there is a reduction of the bulk mobility which is in qualitative agreement with the predictions of SCHRIEFFER. Since the reduction in mobility is small for shallow potential wells, additional data for deep potential wells are needed to test the theory of diffuse scattering at semiconductor surfaces. The space-charge potential well of a cleaned germanium surface in ultra-high vacuum may be varied over a range almost three times as large[5] as that investigated by ZEMEL[4] and this system has been used in the present investigation to determine the dependence of the mobility on the depth of the space-charge potential well. Data were obtained only in the range of deep potential wells and were found to be in good agreement with Schrieffer's theory.

A thin (0·2 mm) *n*-type, 20 Ω cm sample of germanium was mounted in an ultra-high vacuum system by means of molybdenum clip leads in a manner similar to that described by HANDLER.[5] The experimental tube was designed to fit between the pole pieces if a small electromagnet capable of reaching fields of 0·3 Wb/m². The sample was cleaned by argon ion bombardment, annealed at 650°C overnight, and then cooled to room temperature over a period of 2 hr.

Simultaneous measurements of the conductivity and Hall voltage were made with a Type B Rubicon Precision Potentiometer as oxygen was admitted to the system.

Fig. 1 shows the total conductivity, $\sigma$, of the germanium sample after cleaning as a function of time. The oxygen pressures are approximate and

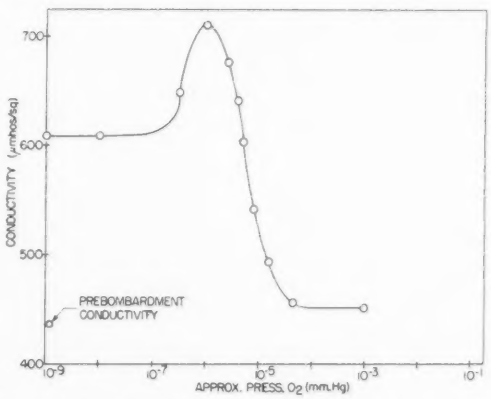


FIG. 1. Conductivity of a germanium slab with an argon bombarded and annealed surface as a function of oxygen coverage.

*This research was supported by the Office of Naval Research.

are used only to indicate the sequential relationship of the conductivity with admission of oxygen. The results are similar to those reported earlier.[5] The final point is taken to be the value of the bulk conductivity. Although the minimum of the conductivity was not observed, it is estimated that the final point is within 10 $\mu$mhos of it. All conductivity above the final point is associated with the surface. Since the clean germanium surface is $p$-type and degenerate,[5] the increase

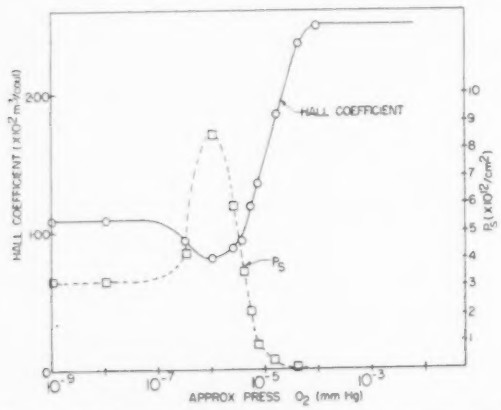


FIG. 2. Hall coefficient and surface carrier density/cm$^2$ on an argon bombarded and annealed germanium slab as a function of oxygen coverage.

in conductivity with the adsorption of oxygen indicates a further increase in degeneracy. With the addition of oxygen beyond the maximum in the conductivity, the surface region returns to a condition where the energy bands are flat right up to the surface. This picture is strongly supported by the results of the Hall measurements. Fig. 2 shows the Hall coefficient, $R$, for the sample and $P$, the number of carriers in the space charge region as a function of oxygen adsorption. The Hall coefficient first decreases, indicating the addition of holes to the $n$-type sample and then increases indicating the removal of holes. The dashed line and the right-hand ordinate indicate the number of holes in the space-charge potential well. Since the holes are the predominant source of charge in the space-charge region the electric field at the surface may be calculated from Gauss's Law. The dependence of the electric field on $q\psi_s/kT$, the difference in electrostatic potential between the bulk and the surface, has been discussed by SIEWATZ and GREEN[6] for partially degenerate space charge regions, and may be used to relate the number of holes in the space charge region to $q\psi_s/kT$. Fig. 3 shows an energy band representation of the space charge region: (a) at the clean surface, (b) at the conductivity maximum, (c) at the flat band condition. The Fermi energy is approximately $0{\cdot}5kT$ below the edge of the valence band at the clean surface and $4kT$ below at the maximum of the conductivity.

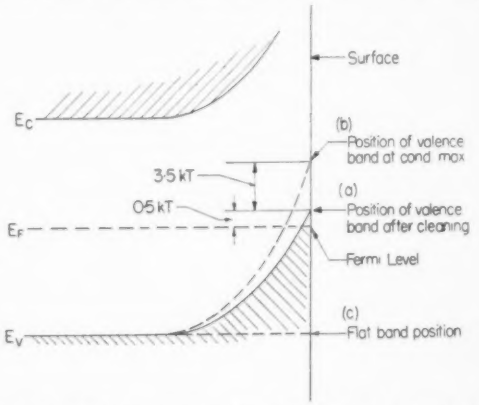


FIG. 3. Band representation showing position of the energy bands at the surface when, (a) the surface has been cleaned, (b) the conductivity is a maximum during $O_2$ exposure, (c) after $O_2$ exposure.

The value of the Hall mobility of the holes in the space-charge region was calculated from the following formula:

$$\mu_{ps} = \frac{R\sigma^2 - R_B\sigma_B^2}{\sigma - \sigma_B}$$

and the hole density/cm$^2$ was calculated from

$$P = \frac{(\sigma - \sigma_B)t}{2q\mu_{ps}}$$

The subscript $B$ refers to the value of $R$ and $\sigma$ at or near the flat band condition and $t$ is the slab thickness. This formula involves several simplifying assumptions: (1) $\mu_{ps}$ (conductivity) $= \mu_{ps}$ (Hall); (2) neglect of fast holes and electrons in the space charge region; (3) neglect of correlation effects and bulk terms as discussed by ZEMEL and PETRITZ.[4] The measurements were made at 298°K and the Hall voltage was observed to be linear with magnetic field. Fig. 4 shows the values

of $\mu_{pS}/\mu_{pB}$ as a function of $q\psi_S/kT$, for three different oxygen admissions. The mobility is definitely below its bulk value. The solid line represents the value of the reduced mobility based on Schrieffer's theory. The fit is good considering the approximations used in interpreting the data and strongly supports the model of diffuse scattering at the surface. However, since some joints lie above the curve, some specular scattering may occur. Further interpretation would include the effect of fast holes and quantum effects. For the extreme degenerate situation shown in Fig. 3 the width of the well at the Fermi energy is approximately 10 Å. This represents a few atom layers and one wonders whether the band representation or Poisson's equation can be applied to such narrow space charge regions. Moreover, the Heisenberg uncertainty principle indicates that states should not exist at the bottom of the well.

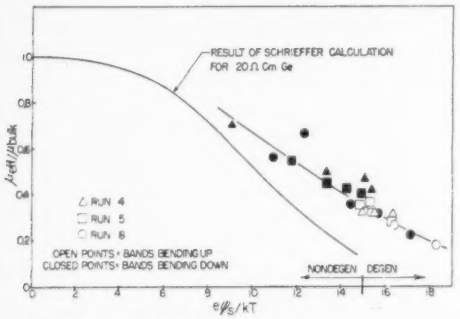


FIG. 4. The ratio of the effective mobility of the $p$-type surface carriers to the bulk mobility as a function of the depth of the space charge potential well.

## REFERENCES

1. SCHRIEFFER J. R., *Phys. Rev.* **97,** 641 (1955).
2. ZEMEL J. N., *Bull. Amer. Phys. Soc.* **3,** 105 (1958).
3. PETRITZ R. L., *Phys. Rev.* **110,** 1254 (1958).
4. ZEMEL J. N. and PETRITZ R. L., *Phys. Rev.* **110,** 1263 (1958).
5. HANDLER P., *Semiconductor Surface Physics* p. 39. University of Pennsylvania Press, Philadelphia (1957).
6. SELWATZ R. and GREEN M., *J. Appl. Phys.* **29,** 1034 (1958).

*J. Phys. Chem. Solids* Pergamon Press 1959. Vol. 8. pp. 111–113. Printed in Great Britain

# ELECTRICAL PROPERTIES OF CLEAN GERMANIUM SURFACES

G. A. BARNES and P. C. BANBURY

Department of Physics, University of Reading

## 1. INTRODUCTION

THE technique developed by FARNSWORTH for the cleaning of surfaces by ion bombardment, has recently been applied in investigations of the electrical properties of semiconductor surfaces,[1] in an attempt to improve understanding of the nature and origin of surface states. The procedure involves bombarding the surface with positive ions from an inert gas discharge, evacuating to a high vacuum, and annealing at a moderate temperature to restore crystalline order at the surface. The bombardment process itself may be regarded as a means of removing a part of the crystal by sputtering; an alternative approach to the problem of obtaining a clean surface is to expose a new face by fracture.

Contamination of a fresh surface may, in principle, arise from the presence of foreign atoms previously located in the region now exposed, and by their arrival by surface diffusion, bulk

diffusion, or adsorption from the gaseous ambient. The removal of the vacuum limitation imposed by the discharge, and of the annealing process, will tend to reduce the effect of the last two sources. At a pressure of $10^{-10}$ mm Hg the time taken to establish a tenth of a monolayer of contaminant by adsorption, even assuming a sticking coefficient of unity, is $\sim$30 min. It has been assumed that the other sources of progressive contamination are not more rapid than this at room temperature.

We have measured the field effect on conductance, and the photoconductance, in specimens of germanium with freshly cleaved surfaces under these conditions.

## 2. EXPERIMENTAL PROCEDURE

The nature of the field effect measurement (the effective transverse mobility of induced surface charge) requires that the surface shall be plane. The measurements reported here have been taken on surfaces exposed by cleavage on a (111) plane.

For convenience the final specimen should be in the form of a rectangular filament, say of length, $l$, breadth $b$, and thickness $t$, where the thickness $t$ of the specimen beneath the freshly exposed surface should be small. In practice, to obtain cleavage it has been found necessary to make it greater than $b$; values of $t = 0{\cdot}2$ cm and $b = 0{\cdot}1$ cm have been attained.

The system for supporting and cleaving the specimen has been described elsewhere.[2] An oriented crystal of size about $2{\cdot}5 \times 1{\cdot}0 \times 0{\cdot}1$ cm, with welded low-resistance molybdenum and contacts near one side is mounted by this side in close-fitting jaws of glass. A magnetically operated lever carrying a diamond at the tip, is arranged to provide a short scratch at one end of the specimen. The cleaving stress is applied by a glass lever hung on to the main body of the specimen near the end where the scratch is applied; this lever is again magnetically operated. The cleavage thus commences at the scratched end of the specimen, and is allowed to run freely along the length of the crystal, leaving a filament of approximate dimensions $2{\cdot}5 \times 0{\cdot}2 \times 0{\cdot}1$ cm, with a freshly exposed surface of $2{\cdot}5 \times 0{\cdot}1$ cm. After cleavage a field electrode of metal with bead spacers of glass or mica with a metal film on the reverse side may be allowed to fall into position near the fresh surface for the application of electric fields; alternatively, the surface may be illuminated through a nearby slit.

The best surfaces obtained by this means have shown little irregularity to the naked eye except in the region beneath the diamond scratch, which is not used in the field effect measurement for this reason. Microscopic examination down to $\sim 1\ \mu$ generally fails to reveal any sudden steps, but irregular deviations from the (111) plane over the 2 cm length are sufficient to make examination by interference techniques difficult. Typically these deviations are estimated as of height a few microns. Spacings between this surface and the field electrode of $\sim 0{\cdot}3$ mm have been employed.

It may be remarked that all attempts to perform cleavage on specimens to which the diamond scratch had been applied before assembly and evacuation were unsuccessful. The failure was associated with the prolonged baking.

The whole system occupies a volume of less than one litre, and contains little metal apart from the specimen itself. By continuous pumping with a mercury diffusion pump with two cold traps, and the use of an Alpert ion pump, pressures in the region of $10^{-10}$ mm Hg, are obtained after many hours baking at 420°C. The gauge is not normally operated during the cleavage process, nor while the electrical measurements are being taken. An initial set of measurements of either kind can be completed within a few minutes of cleavage.

## 3. RESULTS

Measurements have been taken of the d.c. field effect on the clean surface, and of the 50 c/s a.c. field effect and the low-level photoconductance, both on the fresh surface and, in preliminary measurements, during contamination by air. An approximate calibration for the lifetime was obtained by a comparison, after contamination, of the photoconductance and photoconductive decay.

In the measurements of d.c. field effect induced conductance changes were observed over periods up to 1 min and found to remain constant (to better than 30 per cent), indicating that slow surface states with relaxation times of less than 100 sec, if present, must have much lower densities than occur on oxidized surfaces.

The photoconductance measurements have been carried out on 20 Ω cm *n*-type material. Values of surface recombination velocity obtained were in the region of 100 to 300 cm/sec. During progressive contamination by air to atmospheric pressure the *s*-value was found to rise monotonically by a factor of ~6.

Attempts to observe the large signal surface conductance curve in the a.c. field effect measurement involved the application of high voltages (~$10^4$ V) to the field electrode, and spurious conductances invalidated the measurements. It was not practicable to reduce the Ge to electrode spacing by a large factor, and observations were therefore limited to small-signal field effect mobility, with a consequent inability to evaluate a barrier height in the general case.

The results of such measurements are shown in Fig. 1. In the case of the near intrinsic material,

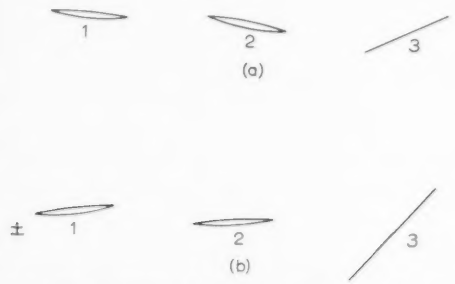


FIG. 1. Small-signal a.c. field effect curves before and during contamination of surfaces, (a) near-intrinsic material, (b) ~20 Ω cm *n*-type material.

the field effect mobility on the fresh surface was very low. In one case a minimum appeared detectable, indicating a zero field barrier height of approximately $2kT$. During contamination an initial swing towards a *p*-type mobility was followed by a much larger change to an *n*-type condition. On *n*-type material an initial *n*-type mobility was seen, which underwent first a small reduction, and then a large increase, during contamination.

The results on intrinsic material might be interpreted as indicating a near-intrinsic surface with little or no barrier in the clean condition, with the surface becoming first *p*-type and then more *n*-type on contamination. In the results on the *n*-type material, since the slope does not change sign it is not possible to distinguish between changes of barrier height and of surface state density, but the similarity in behaviour between the two sets of results suggests that the surface again moves during contamination first towards a *p*-type and then a more strongly *n*-type condition. The initial barrier height appears to be less than $4kT$, since the conductivity is *n*-type. It might be supposed, for example, that in all cases the fresh surface is near the intrinsic condition.

Alternatively, as pointed out by HANDLER (private communication), the results might be reconcilable with the model established from measurements on bombarded surfaces in which the fresh surface is supposed to be highly *p*-type with a high surface state density, if the observed effects are attributed to a balance between a low *p*-type effective mobility on the fresh surface and a high *n*-type mobility associated with the stray capacity to the uncleaved side surfaces. It is hoped that further measurements will give more decisive information as to barrier heights.

*Acknowledgments*—Thanks are due to Professor R. W. DITCHBURN for his support of the work, and to the Admiralty for permission to publish this paper.

## REFERENCES

1. SCHLIER R. E. and FARNSWORTH H. E., *Semiconductor Surface Physics*, Proceedings of Conference on Physics of Semiconductor Surfaces, June 1956. University of Pennsylvania Press, Philadelphia.
2. HANDLER P., *Semiconductor Surface Physics*, Proceedings of Conference in Physics of Semiconductor Surface, June 1956. University of Pennsylvania Press, Philadelphia.
3. BARNES G. A. and BANBURY P. C., *Proceedings of First International Congress on Vacuum Techniques*, June, 1958. Pergamon Press, London.

VOL. 8 1959

*J. Phys. Chem. Solids* Pergamon Press 1959. Vol. 8. pp. 114–118. Printed in Great Britain

D.8

# GERMANIUM AND SILICON SURFACES

SUMNER P. WOLSKY

Raytheon Manufacturing Company, Research Division, Waltham 54, Massachusetts

## 1. INTRODUCTION

THE oxidation of germanium surfaces has been widely studied. The data available, however, have been obtained, for the most part, with powdered surfaces prepared by chemical reduction or by crushing in vacuum. This paper reports information concerning the room temperature oxidation kinetics of positive ion bombarded and vacuum-baked single crystal slices of germanium. A comparison is made with the oxidation data reported by others. Preliminary measurements with silicon surfaces are discussed.

## 2. EXPERIMENTAL

The apparatus consisted chiefly of a quartz microbalance housed in an ultra-high vacuum system. The sensitivity was 0·15 $\mu$g. A detailed description of the apparatus and experimental method, including the argon bombardment procedure, has been presented elsewhere.[1]

Only single crystal slices were used in this work. The germanium and silicon samples were (100) oriented. The samples were prepared by a polishing procedure followed by a CP-4 etch to a final thickness of 2–4 mils. All samples were thoroughly baked in vacuum prior to any experiments.

Geometric sample areas were 10 to 15 cm$^2$. The actual surface areas were determined by the BET technique[2] using nitrogen or krypton. The roughness factor for a CP-4 etched (100) surface was found to be in agreement with the value of 1·3 reported by others.[3] This factor, therefore, was used to determine the surface area in some instances where microscopic examination revealed no change in the nature of the sample surface due to the experimental process.

The argon–ion bombardment procedure was sufficient to remove at least ten monolayers of germanium from the sample surface.[1] The samples were baked at 450° to 625°C for up to 1 hr following the bombardment. The time interval between the end of the post-bombardment heating and the admission of oxygen varied from 1 to 2 hr. It was not possible in most experiments to obtain reliable readings with the balance for 3 to 10 min following the admission of oxygen to the system.

## 3. RESULTS AND DISCUSSION

The oxidation data are summarized in Fig. 1.* Plots A, B, and C were obtained from germanium samples, while D is the result of an experiment with silicon. Samples in runs A and B were prepared by the argon-bombardment procedure prior to exposure to pressures of 3 mm and 0·1 mm, respectively. C was prepared by vacuum bakeout at 775° to 850°C for an approximate total of seven hours in a vacuum of $10^{-7}$ mm. At least 4 hr of the baking occurred after the sample had been accidentally oxidized due to a power failure. The silicon sample, D, was ion-bombarded, exposed to air for several hours, and subsequently baked for 1 hr at 950°–1000°C. The vacuum at the bakeout temperature had deteriorated to $10^{-7}$ mm. Both experiments C and D were at 3 mm oxygen pressure.

In experiment B, considerable etching of the surface occurred during the experiment. Unfortunately, the sample was destroyed before the surface area determination could be performed. Since the roughness factor of 1·3 could not apply in this instance, the area was calculated on the assumption that the immediate oxygen uptake, i.e., that occurring in the first minutes, was equivalent to the adsorption of one oxygen per surface germanium atom. Since such an uptake is consistent with our experience and with the results of others,[4,5] this assumption probably does not introduce any significant error.

The following conclusions may be drawn from a consideration of experiments A, B and D shown in Fig. 1. (1) The room temperature oxidation of germanium and silicon surfaces proceeds according to a logarithmic rate law of the type determined in experiment A, i.e.,

$$N = 8{\cdot}9\times10^{14}+0{\cdot}95\times10^{14}\log_{10}t$$

where $N$ is the number of oxygen atoms adsorbed in $t$ minutes of exposure to oxygen. Earlier measurements which indicated little, if any,

* The experimental points have been omitted in order to simplify the plot. The averaged observed weight changes, however, were reproducible to at least $\pm0{\cdot}06$ $\mu$g or less than $1\times10^{14}$ atoms/cm$^2$. A more detailed presentation of this and additional data will be published elsewhere.

further adsorption after the initial uptake have been found to be limited to occasional unusual instances. (2) The behavior of germanium and silicon surfaces is similar to that of many other solids whose oxidation have been shown to follow a logarithmic rate law.[6] (3) The results of the germanium experiments are in agreement with those obtained by others[4,5,7] using powdered or crushed surface prepared by a variety of techniques. (4) The result of the single experiment with silicon performed at 3 mm oxygen pressure there is no dependence of the rate upon pressure. This conclusion is contrary to the observations with evaporated films. (8) From the comparatively low initial uptake, it may be assumed that the silicon surface was not clean to less than half a monolayer of oxygen. It is not possible to decide from this experiment whether this was due exclusively to the bakeout or was really the partial regeneration of an ion-bombarded surface.

Prolonged bakeout at high temperatures has been used by some in hopes of obtaining a clean

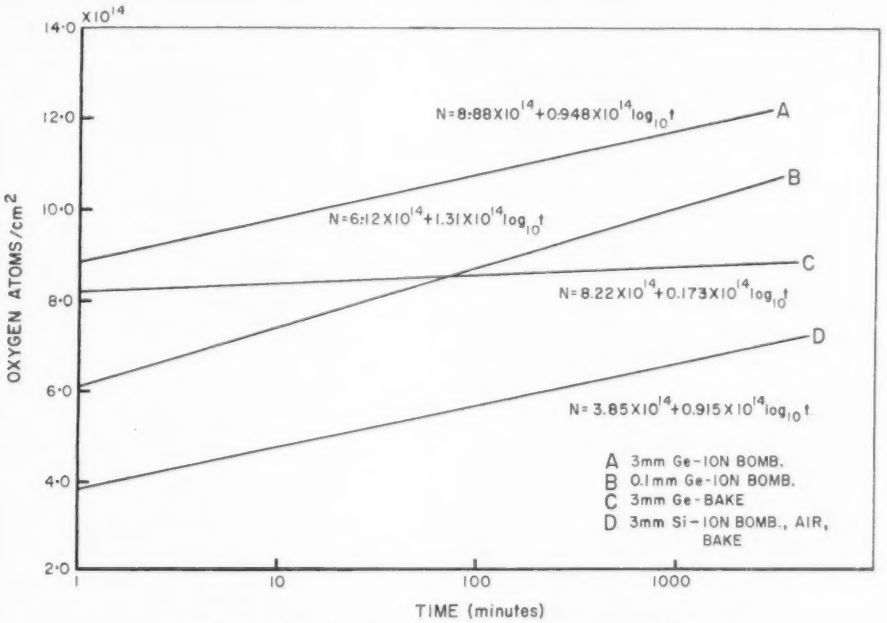


FIG. 1. The oxidation of germanium and silicon at 22°C.

is in agreement with the data of GREEN at 0·1 mm[8] but disagrees with the recent work of LAW on evaporated films.[9] (5) The rate of oxidation appears to be the same for germanium and silicon surfaces. (6) The rate of the oxidation of germanium has been reported[4] to be proportional to the square root of the oxygen pressure, i.e. $dN/dT\alpha(P_{O_2})^{\frac{1}{2}}$. Since the rates of oxygen uptake in experiments A and B were essentially the same even though the oxygen pressure differed by a factor of 30, no evidence of such a pressure dependence has been noted. (7) A comparison of our silicon results with those of GREEN at a lower oxygen pressure indicates that for silicon, also, germanium surface.[10,11] In general, only partial success was achieved with subsequent ion-bombardment necessary for adequate preparation of the surface. The results of our vacuum-baking experiment are presented in plot C. The initial uptake of approximately one monolayer of oxygen is consistent with the behavior of bombarded surfaces. The rate of further oxygen uptake, however, was only one-fourth of that observed in A and B. Due probably to the condition of the sample surface and the vigorous bakeout, the surface area, as determined from BET measurement, increased by a factor of 16. This can be compared to a sandblasted germanium surface

with a roughness factor of only 3 to 4.[12] That the nature of the surface and the rate of oxidation were both anomalous indicates a possible relationship between the structure of the surface and the kinetics of the oxidation process. Further work, however, is necessary to justify such a conclusion. Probably the most significant contribution of experiment C is that it indicates the feasibility of preparing a clean germanium surface by high temperature bakeout.

A sticking coefficient, $S$, of approximately $10^{-3}$ for oxygen on germanium has been determined from electron diffraction[11] and contact potential measurements.[13] This value, however, represents an average $S$ for the region of coverage up to a monolayer of oxygen, i.e. $\theta = 1$. From an experiment in which a sample was ion-bombarded and the weight gain subsequently followed in a dynamic vacuum, it has been possible to determine sticking coefficients as a function of coverage. Inherent in our experiment are the assumptions that (1) the observed weight gain is due to the interaction of the surface with oxygen, and (2) the oxygen pressure is constant and equivalent to the pre-experimental pressure of the system, in this instance $5\times10^{-10}$ mm. On the basis, $S$ was found to vary from $2\times10^{-3}$ for $\theta = 0{\cdot}1$ to $6\times10^{-5}$ at $\theta = 1{\cdot}0$. Other oxidation experiments have indicated an average value of $S = 5\times10^{-4}$ for the range of oxygen coverage up to $\theta = 0{\cdot}8$. Although no detailed measurements have been made for oxygen on silicon, observations of the behavior of ion-bombarded silicon samples in the residual vacuum indicate a sticking coefficient of the same order of magnitude as that for germanium.

Thermal or ion-bombardment etching of our silicon samples has not been observed when the usual rigorous conditions of cleanliness have prevailed. In those occasional instances in which etching during the experiment has occurred, it has been possible to correlate the effect with the presence of an oxide film on the sample or with a leak in the system. It may be speculated, therefore, that the etching due to high temperature bakeout or to sputtering with positive ions is related to the nature of the sample surface and to the concentration of reactive species such as oxygen in the sample environment.

VOL
8
195

**REFERENCES**

1. Wolsky S. P., *Phys. Rev.* **108,** 1131 (1957).
2. Brunauer S., Emmett P. H. and Teller E., *J. Amer. Chem. Soc.* **60,** 309 (1938).
3. Law J. T., *J. Phys. Chem.* **59,** 543 (1955).
4. Green M., Kafalas J. A. and Robinson P. H., *Semiconductor Surface Physics* p. 349. University of Pennsylvania Press, Philadelphia (1957).
5. Ligenza J. R., *Bull. Amer. Phys. Soc.* **2,** 371 (1957).
6. Landsberg P. T., *J. Chem. Phys.* **23,** 1079 (1955).
7. Dell R., *J. Phys. Chem.* **61,** 1584 (1958).
8. Green M. and Kafalas J. A., *Phys. Rev.* **98,** 1566 (1955).
9. Law J. T., *J. Phys. Chem. Solids* **4,** 91 (1958).
10. Allen F. G. and Fowler A. B., *J. Phys. Chem. Solids* **3,** 107 (1957).
11. Schlier R. E. and Farnsworth H. E., *Semiconductor Surface Physics* p. 3. University of Pennsylvania Press, Philadelphia (1957).
12. Law J. T. and Francois E. E., *Ann. N.Y. Acad. Sci.* **58,** 925 (1954).
13. Dillon J. and Farnsworth H. E., *J. Appl. Phys.* **28,** 174 (1957).

*J. Phys. Chem. Solids* Pergamon Press 1959. Vol. 8. pp. 116–118. Printed in Great Britain

D.9

# SURFACE-STRUCTURE AND WORK-FUNCTION DETERMINATIONS FOR SILICON CRYSTALS*

**H. E. FARNSWORTH, R. E. SCHLIER and J. A. DILLON, Jr.**
Barus Research Laboratory, Brown University, Providence, R.I.

The low-energy electron diffraction method[1] has been used to determine the structure of clean surfaces and of adsorbed gas layers. Work-function determinations have been made in a separate experimental tube by determining the photoelectric work function of a reference metal and then measuring the contact potential difference

*This work was supported by a contract with the U.S. Air Force, Air Force Cambridge Research Center, Air Research and Development Command.

between this metal and the silicon crystal.[2] The high vacuum techniques and the method of cleaning the crystal surfaces have been described elsewhere.[1]

In addition to the normal surface lattice spacings, the structures of clean (111) and (100) surfaces were found to contain larger spacings, most of which depended on the conditions of ion bombardment and subsequent heat treatment. Two very large-spaced structures were found on the (111) surface. They depended on the energy at which the crystal was ion bombarded, and the heat treatment that followed the ion bombardment. Two different large-spaced structures, not affected by the energy of ion bombardment, were found on the (100) surface. Reference is made to Table 1.

appropriate treatment. The above structures which resulted from quenching and annealing treatments were not obtained until the crystals had received about 5 cycles of alternate ion bombardment and heating resulting in a total bombardment of 2 hr at 100 $\mu$A/cm$^2$ and a total heating of 100 hr at about 800°C.

The rates of oxygen adsorption depended on the condition of the surface, as well as the crystal plane forming the surface. Fig. 1 shows the estimated fractional coverage of the surface as a function of the exposure to oxygen. The fractional coverages were estimated from the changes in diffracted beam intensities with oxygen exposure, assuming that the beam was scattered coherently by covered and uncovered regions of the surface. The difference between the rates of adsorption

*Table 1. Structures of large surface lattices*

| | Treatments | Structures |
|---|---|---|
| (A) (111) surface | Annealed at 650° for a few hours after heating at 1000°C for a few minutes following ion bombardment at 150 to 500 eV. | A spacing 7 times that of silicon and an orientation of silicon. |
| (B) (111) surface | Radiation quenched from 1000°C after bombardment at 500 eV. | A spacing $\sqrt{19}$ times that of silicon but rotated $\pm 23{\cdot}5°$ from silicon lattice. |
| (C) (111) surface | Radiation quenched from 1000°C after bombardment at 150 eV. | Too weak to determine structure (probably similar to one of above structures).* |
| (D) (100) surface | Annealed at 650°C for a few hours subsequent to heating at 1000°C for a few minutes or subsequent to argon-ion bombardment. | Double-spaced surface lattice in azimuths having even sums of indices. Results are similar to those for (100) Ge, and have the same interpretation.[3] |
| (E) (100) surface | Radiation quenched from 1000°C. | A spacing about 8 per cent greater than that of normal silicon plus the structures† in (D). |

* Diffraction beams from the normal lattice were stronger [50% greater than (A) and 200% to 300% greater than (B)].

† Diffraction patterns from these structures were about 30% weaker than those in (D).

The quenched patterns on the (111) surface were affected only by the ion-bombarding energy; i.e. after oxygen adsorption or annealing, the original structure characteristic of the bombarding energy was restored by heating to 1000°C and quenching. Changes from one structure to another could be effected repeatedly for both crystals by

on quenched and annealed surfaces of the same crystal orientation is quite apparent, and has also been found by the work-function method.[4]

Since the results on work function have been described in detail,[4] only a brief summary will be given here. For "floating-zone" purified crystals, the work functions were independent of

the type of heat treatment and hence were insensitive to the differences in surface structure observed by electron diffraction. While there were no apparent differences between the electron-diffraction results for "floating-zone" purified and oxygen-doped samples, the values of work function for oxygen-doped crystals were higher after radiation quenching than they were after annealing. Increases in work function due to oxygen adsorption were dependent on the type of heat treatment and could be correlated with differences in adsorption rates observed by electron diffraction.

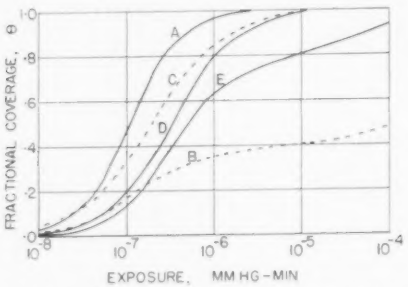


FIG. 1. Adsorption of oxygen. The letters on the curves correspond to the letters in Table 1.

A comparison of the work function and photoelectric threshold energy values for the cleaned silicon surfaces indicated that the Fermi level was near or even below the top of the valence band. This same result has been reported previously for the case of ion-bombardment cleaned germanium,[2,5,6] and has been interpreted in terms of the cut bonds at the surface acting as traps which result in an upward bending of the valence band. The degenerate condition was relieved by oxygen adsorption; i.e. the increase in work function was always smaller than the increase in the threshold energy value. This suggests that, while the total energy barrier was increased (due to the adsorbed dipole layer), the adsorbed oxygen also saturated a number of the surface traps and allowed the valence band to move downward somewhat.

When silicon was heated in vacuum at a temperature of about 1000°C for a few hours, the surface became thermally etched. At this temperature, evaporation of the silicon also became appreciable. The etch patterns, which seemed to be due to the formation of pits rather than hillocks, were triangular on the (111), rectangular on the (100) and hexagonal on the (110) face. Electron microscope photographs* of the pits on the (110) and (111) faces are shown in Figs. 2 and 3. The pits appear to be due to the preferential development of (111), (113), (131) and (311) planes. This is in agreement with the observation that the (111) face was much more stable under thermal etching than were the (100) and (110) faces. At temperatures higher than 1000°C the thermal etching proceeded very rapidly so that after about 24 hr heating at 1100°C the (110) and (100) faces had a sandblasted appearance. Under the same conditions, the (111) face still exhibited the same triangular patterns. Since the pitting seemed to develop more rapidly in the vicinity of scratches on the surface, the pits may have originated in the vicinity of surface defects. The etch patterns which appeared on the (111) faces may have been due to the fact that a chemically etched surface always exhibited some degree of waviness. NEWMAN and WAKEFIELD[7] have reported similar results for surfaces which had been heated in an inert atmosphere. We have noted in the electron–diffraction system that it was possible to produce clean surfaces with a minimum of thermal etching by using ion-bombardment cleaning followed by heating at temperatures in the vicinity of 900°C. By thus keeping the high temperature heating to a minimum, thermal etching has been avoided almost completely.

VOL
8
195

## REFERENCES

1. FARNSWORTH H. E., SCHLIER R. E., GEORGE and BURGER, *J. Appl. Phys.* **29,** (1958).
2. DILLON Jr. J. A. and FARNSWORTH H. E., *J. Appl. Phys.* **28,** 174 (1957).
3. SCHLIER R. E. and FARNSWORTH H. E., *Semiconductor Surface Physics* p. 3. University of Pennsylvania Press, Philadelphia (1957).
4. DILLON Jr. J. A. and FARNSWORTH H. E., *J. Appl. Phys.* **29,** (1958).
5. HANDLER P., *Semiconductor Surface Physics* p. 23. University of Pennsylvania Press, Philadelphia (1957); GREEN M., *Ibid.*, p. 362.
6. FORMAN R., *Bull. Amer. Phys. Soc.* Ser. II **3,** 260 (1958).
7. NEWMAN R. C. and WAKEFIELD J., Resumes des Communications, Congres International sur la Physique de l'Etat Solide etc., Brussels, June 1958, p. 54.

*These photographs were obtained through the courtesy of Drs. G. A. WOLFF and F. LEONHARD of the Signal Corps Engineering Laboratories at Fort Monmouth, N.J.

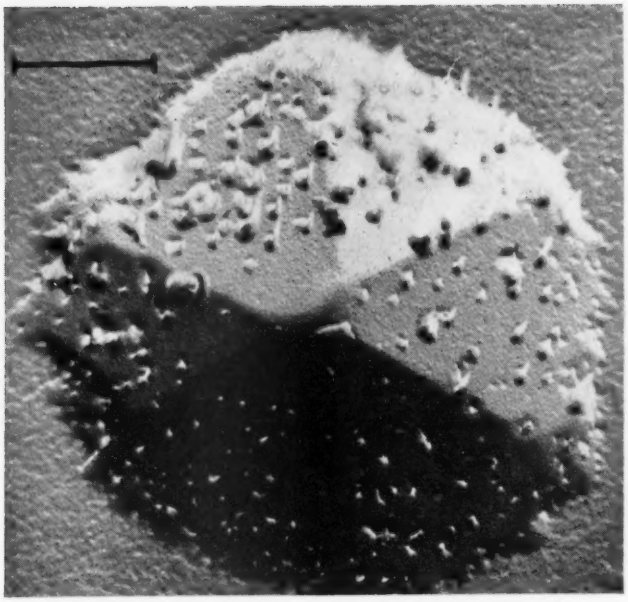

FIG. 2. Electron microscope photograph of a thermal etch pit on a (110) silicon face after heating in high vacuum for 45 min at 1100°C. Scale length is 0·5 $\mu$.

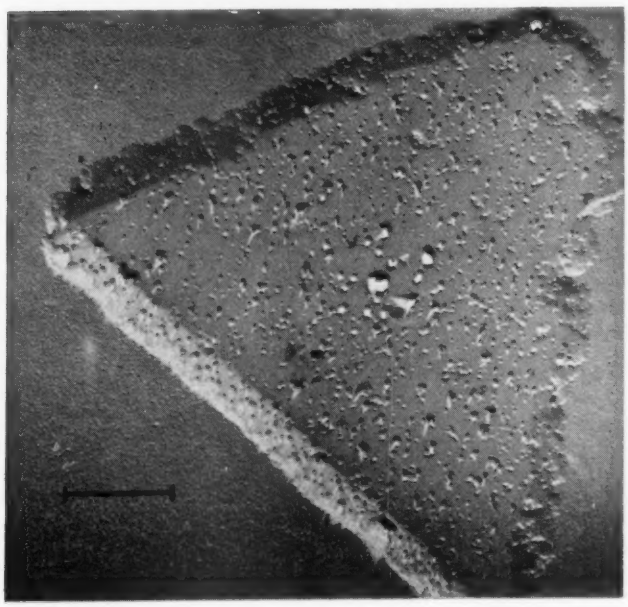

FIG. 3. Electron microscope photograph of a thermal etch pit on a (111) silicon face after heating in high vacuum for 45 min at 1100°C. Scale length is 1 $\mu$.

[facing page 118

VOL
8
195

*J. Phys. Chem. Solids* Pergamon Press 1959. Vol. 8. pp. 119–122. Printed in Great Britain

# WORK FUNCTION AND EMISSION STUDIES ON CLEAN SILICON SURFACES

**FREDERICK G. ALLEN**

Bell Telephone Laboratories Inc., Murray Hill, New Jersey

## 1. EXPERIMENTS

THE three experiments to be described here were all carried out on the surfaces of single crystal silicon of high purity, cleaned by high temperature heating in a mercury pumped high vacuum system ($10^{-9}$ to $10^{-10}$ mm Hg), and all yield data on the cleanliness or on the parameters of the energy level diagram of a clean semiconductor surface.

The first makes use of the MÜLLER field emission microscope,[1] using a silicon tip as the emitter. Experience has shown that the field emission pattern from a metal tip is a sensitive gauge of the cleanliness of the surface. Small fractions of a single atomic layer of contaminant on the surface from the gas phase, or very small percentages of foreign atoms in the bulk of the crystal are readily detected from changes in the pattern.

Using techniques similar to those described by D'ASARO[2] we are able to obtain a completely reproducible field emission pattern, having correct symmetry and orientation, after heating freshly etched and rinsed silicon tips to 1550°K for as little as three minutes in high vacuum. (See Fig. 1.) This pattern has been reproduced with 13 different samples from 6 different crystals including a zone-refined crystal of high purity. The clean pattern does not change with long annealing at intermediate temperatures (1100–1200°K) nor after flashing up to the melting point—treatments that change emission patterns when impurities are present in the tip. The clean pattern contaminates rapidly upon exposure to gases with an initial sticking coefficient for oxygen of about 1/60. These results are considered strong evidence that one is dealing with the atomically clean silicon surface.

Three properties of the field emission current from silicon thus far established are (1) the plot of log $I$ vs. $1/V$, where $I$ is total emission current and $V$ the anode potential, is linear over at least 3 decades in $I$ to within a 20 per cent scatter in $I$ values. Maximum current densities are estimated as $\geqslant$ 500 A/cm$^2$; (2) the emission current at given field strength is independent of temperature to within 20 per cent from room temperature up to at least 1200°K; (3) the emission is independent of strong illumination of the tip with visible light at room temperature.

In the second experiment, the work function of silicon crystal faces is measured with the Kelvin technique by finding the contact potential difference between the sample face and a tungsten single crystal ribbon reference face of known work function immediately after flashing both surfaces to high temperatures. The silicon surface was flashed many minutes above 1550°K till reproducible values resulted—a treatment shown by the field emission study to produce a surface that is believed atomically clean. The results thus far have shown that for silicon surfaces cut parallel to the (100) and (111) planes and etched smooth in HF-$HNO_3$ mixtures, the work functions are $4{\cdot}91 \pm 0{\cdot}05$ eV for the (100) and $4{\cdot}74 \pm 0{\cdot}05$ for the (111) faces. The samples were 15 Ω cm boron-doped pulled silicon crystals grown at these Laboratories. These results are in close agreement with similar values reported by DILLON,[3] and show the same face sequence as values reported for germanium.[4]

On identical samples cut from the same crystal as the above, and under the same vacuum and cleaning conditions, EISINGER[5] has measured a photo-threshold of $4{\cdot}74 \pm 0{\cdot}03$ eV for the (111) face, and a less certain value of $5{\cdot}05 \pm 0{\cdot}05$ eV for the (100) face.

The combined data indicate that for these samples at least, filled electron energy levels of high density lie within 0·05 eV of the Fermi level at the cleaned surface. If, as seems most likely here from the nature of the photo-yield plot of EISINGER's data, the photo-threshold corresponds to emission from the top of the valence band,[6] the cleaned silicon surfaces reported here must be degenerately $p$-type at room temperature with no field applied. Such a $p$-type surface could be due to surface states lying close to the top of the valence band in the gap in excess of $10^{13}$/cm$^2$.

It is known that the high temperature heating treatments in vacuum used to clean the surface may alter the resistivity of both surface and

bulk. In particular, it has been found that a strong $p$-type layer of as yet unknown origin remains at the surface after removal from the vacuum system. Many thousands of angstroms of material must be removed from the surface before it disappears. Until this effect can be controlled or eliminated, the $p$-characteristic of our cleaned surfaces cannot be definitely ascribed to the surface states mentioned.

In the last experiment, the thermionic emission was measured from silicon samples as used in the field emission and the contact potential experiments to determine the work function at high temperatures. Since the field emission samples had already produced clean field emission patterns and since most of the thermionically emitting surface had been heated even to higher temperatures than the tip, there was especially strong evidence for a clean surface condition during the thermionic runs. Though the samples in the field emission and contact potential experiments were of completely different geometry, the thermionic emission results agreed very well.

Richardson plots of the data from four samples give good fit to straight lines of slope $\Phi^* = 4{\cdot}30$ eV with intercepts, $A^*$, ranging from 0·8 to 1·6 A/cm$^2$ deg$^2$. If the reflection coefficient $r$ may be neglected in the Richardson equation $J = (1-r)AT^2\exp(-\Phi/kT)$ and if $A$ is taken as the theoretical value of 120 A/cm$^2$ deg$^2$ one finds the true work function $\Phi(T)$ vs. $T$ to be shown as in Fig. 2 for two typical samples. [(100) and 110) faces on surfaces.] An almost linear temperature dependence of $\Phi$ is seen to result and the values are well fitted over this temperature range by $\Phi = 4{\cdot}30 + 3{\cdot}75\times10^{-4}T$ eV, for $T$ in degrees Kelvin.

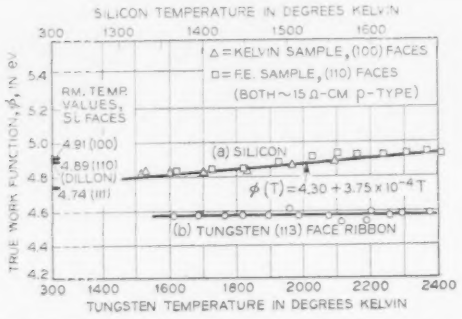


FIG. 2. Thermionically determined work function of silicon vs. temperature. $\Phi$ is found at each $T$ from the Richardson equation assuming $A = 120$ A/cm$^2$deg$^2$ and $r \cong 0$. (a) The data for two silicon samples; (b) the data for the tungsten (113) face single crystal ribbon. Room temperature values for individual silicon faces were determined by the Kelvin method.

This strong positive temperature dependence is illustrated by comparing with the temperature-insensitive values of $\Phi$ measured and shown in the same figure for the tungsten reference surface used in the same Kelvin tube. The work function values for silicon faces at room temperature measured here [or by Dillon for the (100) face] are also shown.

These thermionic emission results are in fair agreement with those of ESAKI[7] when the correct values of emissivity for silicon[8] are used with his data.

## 2. DISCUSSION

The source of the field emission electrons from silicon and the space charge condition at the surface in the presence of the high fields ($2\times10^7$ V/cm) are not yet known. The temperature independence does rule out the possibility of emission of electrons from thermally filled states lying above the Fermi level at the surface. The linearity of the emission plot suggests that either the bottom of the conduction band lies below the Fermi level at the surface (degenerate $n$-type) due to the large induced negative charge for all fields studied, or else that the energy levels at the surface are held clamped with respect to the Fermi level by surface state densities in excess of $10^{13}$/cm$^2$ eV lying close to the Fermi level.[9,10]

The positive temperature dependence of the work function at high temperatures found here (and by ESAKI) cannot be simply explained from data on temperature dependence of the energy gap.[11] In order to match the room temperature values of work function, this temperature dependence must decrease or even change sign between 300 and 1300°K (note the break in the temperature scale, Fig. 2) where the silicon goes from extrinsic to intrinsic. Drastic changes in work function over this range were not, however, observed with the field emission samples, and while the high field present in that case may change matters, other work has also failed to find large changes in this range.[9,12]

VOL.
8
1959

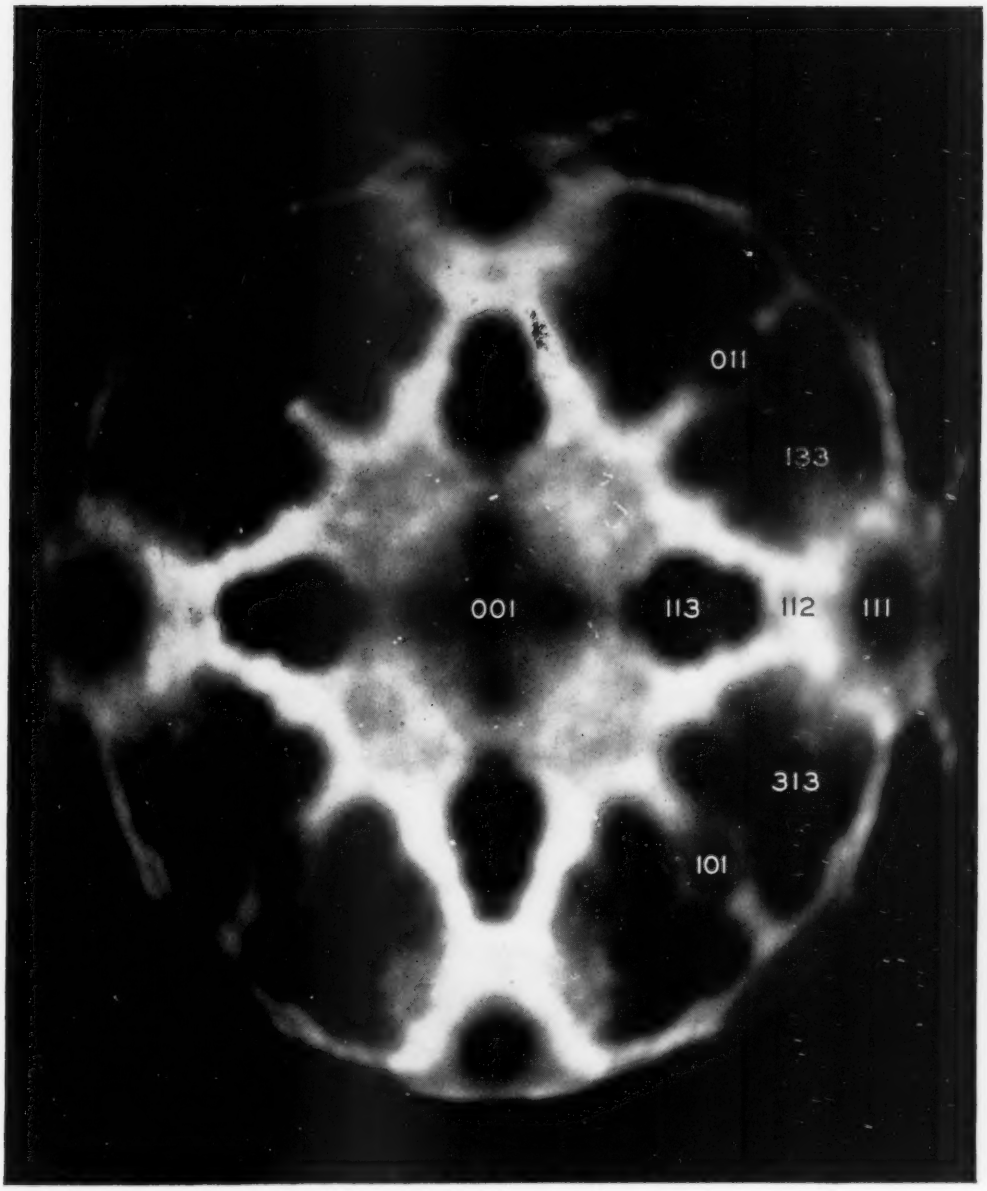


FIG. 1. Field emission pattern from an (001) oriented silicon tip just after flashing at 1550°K, with some of the principal planes indicated.

[facing page 120

VOL.
8
195

**REFERENCES**

1. Good R. and Müller E., *Handbuch der Physik* XXI, pp. 206–214.
2. D'Asaro L. A., *J. Appl. Phys.* **29,** 33 (1958). In the present work, doping the legs of the sample and applying a high field during cleaning has been found unnecessary.
3. Dillon J. A., *Bull. Amer. Phys. Soc.* **3,** (1958).
4. Allen F. G. and Fowler A. B., *J. Phys. Chem. Solids* **3,** 107 (1957).
5. Eisinger J., unpublished.
6. See also Apker L., Taft E. and Dickey J., *Phys. Rev.* **74,** 1462 (1948).
7. Esaki L., *J. Phys. Soc. Japan* **8,** 347 (1953).
8. Allen F. G., *J. Appl. Phys.* **28,** 1510 (1957).
9. Allen F. G., Ph. D. Thesis, Harvard University (1955).
10. Stratton R., *Proc. Phys. Soc.* B**68,** 746 (1955).
11. Morin F. and Maita J., *Phys. Rev.* **96,** 28 (1954).
12. Smith A. H., *Phys. Rev.* **75,** 953 (1949).

## DISCUSSION

*Compiled by* H. Statz

After paper D1, W. H. Brattain (B.T.L.) commented that his early experiments, which were carried out together with C. G. B. Garrett, were not accurate enough to distinguish between discrete and continuous fast surface states near the middle of the gap. However, at the present time they believe, in agreement with other workers, that the states are discrete.

G. F. J. Garlick (University of Hull, U.K.) asked after D3 whether the quenching of photocurrent at short wavelength could be due to a photo-desorption effect at the outer layer. R. Bray answered that the short wavelength quench excites trapped electrons out of the slow states. This restores the original charge on the adsorbed atoms. Subsequent desorption appears possible but not necessary. Garlick's other question was whether, because of the long-time growth and decay effects, it might not be profitable to use controlled warming rate measurements of collapse of conductance and effects of different spectral illuminations. Different state levels should be resolved as in experiments on thermoluminescence and on annealing of radiation damage in metals. The answer was that thermal annealing runs have been made and it was found that the very slow effects disappear even below room temperature. This implies that the mechanism of recovery cannot involve thermal activation of trapped electrons over the oxide barrier, since the latter is some 3 eV high. Recovery by tunnel effect is ruled out by the strong temperature dependence. Possibly ionic conduction in the oxide layer is responsible for the recovery, in which case activation energies from warming experiments would have no relation to observed optical quenching energies.

Also, after D3, W. E. Spicer (R.C.A.) asked whether the authors compared their results with those of Seeger on external electron emission from surface states. The answer was that external electron emission for the recovery of the conductance does not seem compatible with the observation of the 4 eV quenching energy.

R. L. Williams (Carde, Quebec, Canada) asked after D3 whether the time constants for establishing the excess conductivity and its decay were effected by the light intensity. In the answer, it was pointed out that the time decays are complicated and it is difficult to characterize them by any time constants. However, there is evidence that the relative magnitudes of the slow and fast components, built-up by short wavelengths, are dependent on the light intensity.

On a question from M. M. Atalla (B.T.L.), R. Bray stated that in the calculations it was taken into account that the gold atoms in the space charge are not all ionized.

Concerning paper D4, R. Bray (Purdue University) asked whether the dependence of the apparent Hall coefficient and Hall mobility on surface recombination for near intrinsic samples had any influence on the measurements. In his answer, J. N. Zemel stated that the geometry used minimized such effects and that probably the influence was negligible. R. Bray then asked how the ratio of light to heavy hole mobility changes from bulk to surface space charge layer. The answer was that the two mobilities change differently because of the differences in both

bulk mobilities and effective masses. These differences were taken into account in the calculations.

G. HEILAND (Universität Erlangen, Germany) commented in regard to paper D6 that he observed similar increases in *p*-type surface conductivity by admitting atomic hydrogen to a bombardment-cleaned surface. Apparently a germanium–hydrogen bond is formed which gives a negative surface charge and a large increase in the density of holes at the surface.

To a question from J. T. LAW (B.T.L.), P. HANDLER stated that the maximum conductivity was only estimated to correspond to the adsorption of one monolayer of oxygen. Regarding another question by J. T. LAW, P. HANDLER said that the surface was uncontaminated after the annealing process before the admission of oxygen since the ion gauge was in continuous operation during the annealing process.

J. N. ZEMEL's (N.O.L.) comment on D6 was that in spite of the substantially different surface treatments in the region of overlap, there is agreement in the Hall effect measurements carried out by himself and PETRITZ and those reported in D6.

In regard to D7, K. C. NOMURA (Honeywell) made the remark that similar measurements had been reported by PALMER and DAUENBAUGH at the March 1958 Meeting of the A.P.S. at Chicago. In the answer, however, it was pointed out that the cited measurements showed a strong *p*-type surface in contradiction with the findings of BARNES and BANBURY.

After paper D8, F. G. ALLEN (B.T.L.) made the comment that he could produce thermal etch pits on silicon crystals in oxygen pressures between $10^{-3}$ and $10^{-6}$ mm Hg; however, no thermal etch pits were produced in vacua of about $10^{-9}$ mm Hg, even after heavy and prolonged evaporation. These findings are in agreement with those of WOLSKY.

On a question of J. BARDEEN (University of Illinois) after D8, WOLSKY said that measurements, as yet, have only been made on (100) crystal faces.

To a question by C. G. B. GARRETT (B.T.L.) in regard to paper D9, H. E. FARNSWORTH stated that oxygen covered silicon surfaces could be completely regenerated by heating at 900°C for a few minutes. For floating zone refined samples, regeneration was complete after heating at 650°C for 1 hr. However, after several cycles of adsorption and heating, a temperature of 750°C was required for regeneration. These results suggest that regeneration occurred as a result of diffusion of oxygen into the interior.

After paper D10, J. BARDEEN (University of Illinois) raised the question whether the double periodicity on (100) faces observed by FARNSWORTH *et al.* could be detected from the field emission patterns. The answer was that an ion field microscope might have enough resolution but not the electron field microscope.

W. H. BRATTAIN (B.T.L.) made another comment after paper D10. F. G. ALLEN observed a strong *p*-type skin on his samples after the cleaning operation which was not due to surface states but rather to bulk acceptors in a layer under the surface. The question arises whether, in other work dealing with clean surfaces, the observed *p*-type surface layers were due to surface charges or whether they were due to a conversion of the bulk material in the vicinity of the surface.

*J. Phys. Chem. Solids* Pergamon Press 1959. Vol. 8. p. 123. Printed in Great Britain

SESSION E:*
THEORY II

E.1

# TRANSPORT THEORY

J. M. LUTTINGER†
École Normale Supérieure, Paris, and University of Michigan, Ann Arbor, Michigan

**Abstract**—The usual theories of electrical conductivity suffer from a number of weaknesses. A more general theory will be described which gives the entire density matrix of a system of charge carriers in the steady state. It will be shown that the usual theory is valid under certain limiting conditions, but that in general there are rather complicated corrections to it.

VOL. 8 1959

* *Chairman:* R. KUBO; *Co-Chairman:* E. N. ADAMS.
† This paper was read by W. Kohn.

*J. Phys. Chem. Solids* Pergamon Press 1959. Vol. 8. pp. 123–124. Printed in Great Britain

E.2

# THE SCATTERING MECHANISM OF CARRIERS ON PHONON AND LATTICE DEFECTS

L. STILBANS

Institute for Semiconductors, Academy of Sciences, Leningrad, U.S.S.R.

**Abstract**—We have studied the scattering mechanism of carriers by phonons, and by neutral and charged defects.

The free path, and the mobility of electrons scattered by lattice vibrations both depend upon the kinetic energy of the electrons and on the thermal motion of the crystal lattice. In order to separate the influence of the two variables, we investigated:

(1) The dependence of the mobility on the degree at degeneration (i.e. on the concentration of carriers) at constant temperature. In this way, we found that in bismuth and lead telluride, the free path of carriers is independent of their kinetic energy. As for the temperature dependence of the mobility of strongly degenerated carriers with a kinetic energy independent of temperature, we found that at low temperature the free path is inversely proportional to temperature, and at high temperature to the square of the temperature. The last result could be explained only by the inclusion of two-phonon processes at a high concentration of phonons.

(2) The scattering on neutral and ionized impurities. We have found in both cases that the mobility of electrons is strongly influenced by defects localized in the positive ion sublattice, while defects localized in the anion sublattice have little importance. An opposite regularity has been found for holes. In the case of neutral impurities in accordance with the theory of ERGINSOY, the scattering

cross section is practically independent of energy, but does depend strongly upon the number of phonons. The last result is completely unexpected from the point of the usual theory. We may assume, however, that the impurity atoms increase the probability of scattering of electrons on phonons of short wave length by taking up the surplus momentum during the collision.

In the case of scattering by ions, it turned out that at high concentration of impurity ions the decrease of the mobility is unexpectedly weak. It seems that the carriers are not scattered by each ion, but are only influenced by statistical fluctuations of their arrangement. The dependences of the free path upon the energy does not agree with the Conwell–Weiskopf theory.

*J. Phys. Chem. Solids* Pergamon Press 1959. Vol. 8. p. 124. Printed in Great Britain

E.3

# ON THE ROLE OF THE SHORT AND LONG-RANGE ORDER IN THE ELECTRICAL PROPERTIES OF SUBSTANCES*

**A. R. REGEL**

Institute for Semiconductors, Academy of Sciences, Leningrad, U.S.S.R.

**Abstract**—The study of the change of electrical properties during the melting process of a variety of materials permits one to establish the relative importance of short and long-range order.

The investigation of a wide range of substances shows that there are three principal types which do not change in the presence of impurities. The three types can be characterized briefly in the following way:

(1) The substance is a semiconductor both in the solid and in the liquid state. Practically all the oxides and sulfides and most of the selenides and tellurides of metals, especially of light metals, may be included in this type.

(2) The substance is a semiconductor or semimetal in the solid state but becomes a metal upon being melted. Nearly all the elemental semiconductors and a number of intermetallic compounds belong to this type. Some tellurides and selenides of heavy metals can be included in this type too.

(3) The substance is a metal in the solid state and retains the metallic properties upon being melted. All the metals and alloys and a number of intermetallic compounds can be included in this type.

A comparison of the properties of each of these types with the structure of the substance and the character of the chemical bonds leads to the conclusion that the zone structure of the substance depends on the short-range order only, while the periodicity of the crystal lattice becomes responsible for the value of the mobility.

The change of the short-range order either at the melting point or during the heating in the liquid state has been investigated.

* Paper not presented.

*J. Phys. Chem. Solids* Pergamon Press 1959. Vol. 8. pp. 124–130. Printed in Great Britain

E.4

# GALVANOMAGNETIC EFFECTS IN THE QUANTUM LIMIT

**PETROS N. ARGYRES**

Westinghouse Research Laboratories, Pittsburgh, Pennsylvania

**Abstract**—In magnetic fields so large that all conduction electrons are in the lowest oscillator state, the time between collisions is a strong function of the magnetic field and the scattering mechanism. The galvanomagnetic effects, through their magnetic field dependences in this region provide,

therefore, a sensitive tool for the study of the various scattering mechanisms. It can be established that scattering by phonons or randomly distributed ionized impurities can be described in the quantum limit by a relaxation time, for both longitudinal and transverse effects. The Hall coefficient and the transverse and longitudinal resistivities are calculated and compared for the two scattering mechanisms.

THE usual Boltzmann equation for the distribution function of free carriers in electric and magnetic fields is correct for small values of the magnetic field. The effect of the field on the scattering is not taken into account, and in addition the quantum mechanical nature of the motion of the carrier in the magnetic field is neglected.

The results of this equation, if extrapolated to arbitrarily high magnetic fields, are that the resistivity due to free carriers reaches a value independent of the magnetic field and that the Hall coefficient is a constant inversely proportional to the density of the carriers.

In semiconductors with small effective carrier mass it is feasible with presently available magnetic fields to reach cyclotron frequencies

$$\omega = eH/mc \tag{1}$$

such that

$$\omega\tau \gtrsim 1, \tag{2}$$

where $\tau$ is a measure of the time between successive collisions, and also

$$\hbar\omega \gtrsim kT. \tag{3}$$

Under these conditions it is essential that we consider the quantum mechanical character of the motion of the electron in the magnetic field. Its Hamiltonian, for the particular gauge $A = (0, Hx, 0)$ for a magnetic field $H$ in the $z$-direction, is

$$H_0 = (1/2m)[p_x^2+(p_y+m\omega x)^2+p_z^2]. \tag{4}$$

The eigenfunctions and eigenvalues can be taken to be

$$\psi_n\mathbf{k}(\mathbf{r}) = \phi_n\left(x+\frac{\hbar k_y}{m\omega}\right)e^{ik_y y}e^{ik_z z}(L_yL_z)^{-\frac{1}{2}}, \tag{5}$$

$$\epsilon_{n\mathbf{k}} = \hbar\omega_{n\mathbf{k}} = n\hbar\omega+\hbar^2k_z^2/2m. \tag{6}$$

$\phi_n(x+\hbar k_y/m\omega)$ are the orthonormalized eigenfunctions of a one-dimensional simple harmonic oscillator. It is seen that the motion of the electron perpendicular to the magnetic field is quantized, the characteristic magnetic energy quantum being $\hbar\omega$. Energies are measured from the lowest oscillator level.

We now want to make a transport theory of charge on the basis of these states. In other words, we shall treat the action of the electric field and the scattering by the imperfections in the crystal as small perturbations on the exact motion of the electrons in the magnetic field.

We notice immediately that in the representation of the $\psi$'s the longitudinal component of the velocity operator has only diagonal matrix elements, whereas the transverse components have off-diagonal matrix elements in the oscillator quantum number $n$. We thus have

$$(n\mathbf{k}|v_x+iv_y|n'\mathbf{k}') = 2i(\hbar\omega/2m)^{\frac{1}{2}}n^{\frac{1}{2}}\delta_{n',n-1}\delta_{\mathbf{k}'\mathbf{k}} \tag{7}$$

$$(n\mathbf{k}|v_z|n'\mathbf{k}') = (\hbar k_z/2m)\delta_{n'n}\delta_{\mathbf{k}'\mathbf{k}}. \tag{8}$$

The current density $\mathbf{J}$ is given in general by the trace of the velocity operator $\mathbf{v}$ and the steady-state density operator $f$, i.e.

$$\mathbf{J} = (e/\Omega)Tr\{\mathbf{v}f\} \tag{9}$$

with the normalization

$$(1/\Omega)Tr\{f\} = N = \text{electron concentration}, \tag{10}$$

where $\Omega$ = volume of the specimen. From the nature of the matrix elements of $\mathbf{v}$, we observe that for the calculation of the current in general knowledge of the diagonal elements of the density operator, the so-called distribution function, is not sufficient; we need some matrix elements off-diagonal in the oscillator index $n$.

The determination of the steady-state density matrix $f$ is thus the main problem. A number of different approaches to this problem have been made recently. We shall follow here what is perhaps the most elementary approach.[1-3] We shall sketch this briefly here.

In the one electron approximation the assembly of the conduction electrons is described by the

density operator $f$ that satisfies the equation of motion

$$ihdf/dt = [H_T, f], \tag{11}$$

where $$H_T = H_0 + H_e + H_s. \tag{12}$$

$H_0$ is the Hamiltonian of the electron in the magnetic field and we have discussed it previously. The second term

$$H_e = -e\mathbf{E}\cdot\mathbf{r} \tag{13}$$

stands for the interaction of the electron (charge $e$) with the external uniform electric field $\mathbf{E}$. $H_s$ is the scattering potential energy.

We shall consider here two scattering mechanisms: (1) A set of impurities localized at the points $r_i$, each of potential $V(r)$, i.e.

$$\text{(i)}\quad H_s = \sum_i V(\mathbf{r}-\mathbf{r}_i) = (1/\Omega)\sum_{\mathbf{q}} v(\mathbf{q}) e^{i\mathbf{q}\cdot\mathbf{r}} \sum_i e^{-i\mathbf{q}\cdot\mathbf{r}_i}, \tag{14}$$

where $$v(\mathbf{q}) = \int V(\mathbf{r}) e^{-i\mathbf{q}\cdot\mathbf{r}} d\mathbf{r}. \tag{15}$$

(2) Acoustic lattice vibrations

$$\text{(ii)}\quad H_s = C\,div\,u(\mathbf{r}) = (C^2kT/s^2\mu\Omega)^{\frac{1}{2}} \sum_{\mathbf{q}} e^{i\mathbf{q}\cdot\mathbf{r}}, \tag{16}$$

where $u(\mathbf{r})$ denotes the displacement of the lattice due to thermal vibrations. We are considering only elastic scattering; in semiconductors, acoustic phonon scattering is elastic for almost all temperatures.

From the equation of motion of the density matrix $f$, the effect of the scattering potential $H_s$ can be found by second-order perturbation theory to be

$$[\partial(n'\mathbf{k}|f|n\mathbf{k})/\partial t]_{sc} = (n'\mathbf{k}|Sf|n\mathbf{k}), \tag{17}$$

where the scattering operator $S$ is given by

$$(n'\mathbf{k}|Sf|n\mathbf{k}) = \sum_{n''\mathbf{q}} [(n''+n'-n|f(\mathbf{k}+\mathbf{q})|n'')W_{n'n}{}^{n''}(\mathbf{k}+\mathbf{q},\mathbf{k})] - (n'|f(\mathbf{k})|n)\sum_{n''\mathbf{q}} [\tfrac{1}{2}W_{n''n''}{}^{n}(\mathbf{k},\mathbf{k}+\mathbf{q}) + \tfrac{1}{2}W_{n''n''}{}^{n'}(\mathbf{k},\mathbf{k}+\mathbf{q})]. \tag{18}$$

The $W$'s play the role of rates of transition probabilities and are for the two scattering mechanisms considered:

(1) $$W_{n'n}{}^{n''}(\mathbf{k}+\mathbf{q},\mathbf{k}) = (2\pi/\hbar)(N_1/\Omega)V^2(\mathbf{q})J^*{}_{n',n''+n'-n}J_{nn''}\delta(\epsilon_{n'',\mathbf{k}+\mathbf{q}}-\epsilon_{n\mathbf{k}}) \tag{19}$$

for impurity scattering, and

(2) $$W_{n'n}{}^{n''}(\mathbf{k}+\mathbf{q},\mathbf{k}) = (2\pi/\hbar)(C^2kT/s^2\mu\Omega)J^*{}_{n',n''+n'-n}J_{nn''}\delta(\epsilon_{n'',\mathbf{k}+\mathbf{q}}-\epsilon_{n\mathbf{k}}) \tag{20}$$

for acoustic phonon scattering, where:

$$J_{nn'} = \int \phi_n\left(x+\frac{\hbar k_y}{m\omega}\right)e^{iq_x x}\phi_{n'}\left(x+\frac{\hbar[k_y+q_y]}{m\omega}\right)dx. \tag{21}$$

We note that for the diagonal matrix elements ($n' = n$) we can use the usual corpuscular description of the collisions in terms of the transition probabilities from one state to another and the probabilities of occupation of these states.

In deriving the above mentioned results we made use of the fact that the impurities are randomly distributed in space, i.e. we replaced matrix elements of $H_s$ and their products by their ensemble averages, and that the phonons remain always in thermal equilibrium. We have also dropped the terms that describe the shifting of the oscillator levels due to the interaction with the imperfections. These can be shown to be negligible.

With this treatment of the scattering term we get from the equation of motion of the density matrix a Boltzmann equation for the matrix

VOL 8 195

elements of interest of the density operator, namely.

$$d(n'\mathbf{k}|f|n\mathbf{k})/dt = (i/\hbar)(n'\mathbf{k}|[f, H_0+H_e]|n\mathbf{k})+ \\ +(n'\mathbf{k}|Sf|n\mathbf{k}) \quad (22)$$

In the absence of the electric field, it is easy to verify that the thermal equilibrium distribution

$$(n'\mathbf{k}|f_0|n\mathbf{k} = f_0(\epsilon_{n\mathbf{k}})\delta_{n'n} = [1+e^{(\zeta-\epsilon^{n\mathbf{k}})/kT}]^{-1}\delta_{n'n} \quad (23)$$

is a stationary solution of the Boltzmann equation.

To the first order in the electric field we can then write for the steady-state density matrix

$$f = f_0+f_1, \quad (24)$$

where now $f_1$ satisfies the equation

$$i\omega(n'-n)(n'|f_1(\mathbf{k})|n)+(n'\mathbf{k}|Sf_1|n\mathbf{k}) \\ = (i/\hbar)(n'\mathbf{k}|[H_e, f_0]/n\mathbf{k}). \quad (25)$$

The solution of this equation is in general difficult on account of the complicated nature of the scattering operator, equation (18), or, more specifically, its first term. In the cases, however, where the scattering is isotropic in the absence of any magnetic field, one can prove that for a transverse electric field the first term of the scattering matrix vanishes, just as

$$\int W(\mathbf{k}, \mathbf{k}')f(\mathbf{k}')d\mathbf{k}' = 0 \quad (26)$$

for the case of zero magnetic field. Two such well-known cases are the scattering by acoustic phonons and that by infinitely localized impurities. We then see that a single relaxation time for the appropriate off-diagonal matrix elements of the density operator exists and it is equal to the inverse sum of one half the transition probably from states $|n\mathbf{k})$ and $|n'\mathbf{k})$ to all other states. For the longitudinal case the relaxation time is, as in the case of zero magnetic field, equal to the momentum relaxation time, the transition probabilities referring now to the Landau states.

For scattering potentials with varying Fourier components the first term of the scattering matrix does not vanish and this complicates matters. In the case of the quantum limit, however, the situation becomes tractable again. By "quantum limit" we understand the case where all conduction electrons occupy the ground oscillator state, i.e.

$$n = 0, \epsilon_z = \hbar^2k_z^2/2m < \hbar\omega \quad (27)$$

As we shall see below, the scattering in this case can always be described by a scalar relaxation time and thus experimental results can be easily analyzed.

We shall study and compare here the galvanomagnetic effects in the quantum limit in the cases of acoustic phonon and ionized-impurity scattering, the scattering potential of each impurity taken to be of the screened Coulomb type, i.e.

$$V(\mathbf{r}) = (\pm e^2/\kappa)e^{-r/r_s}/r \quad (28)$$

We present this primarily as a model calculation to demonstrate how sensitive the galvanomagnetic effects in the quantum limit are to different scattering mechanisms. It can be proved, however, that equation (28) is the self-consistent potential of an ionized-impurity of charge $\pm e$ in a specimen of dielectric constant $\kappa$ and in the presence of a magnetic field in the Fermi-Thomas approximation. The field affects, in general, only the screening length $r_s$.

Let us consider first the case of the electric field being *transverse* to the magnetic field, i.e. in the $xy$-plane. The driving term of the Boltzmann equation (25) is then

$$ie(2m\hbar\omega)^{-\frac{1}{2}}(E_x-iE_y)[f_0(\epsilon_{n'})-f_0(\epsilon_n)](n+1)^{\frac{1}{2}}\delta_{n'n+1}+ \\ +(\text{herm. conj.}), \quad (29)$$

i.e. it combines states differing in the oscillator quantum number by 1. We note that the first term of the scattering matrix brings in only the intermediate states of the same energy as the initial state $|n\mathbf{k})$ and that it does not depend on $k_y$. This enables us to find very simply a solution of the transport equation in the quantum limit of the form

$$(n'|f_1(\mathbf{k})|n) = \chi_n(\epsilon_z)\delta_{n'n+1}+(\text{herm. conj.}) \quad (30)$$

For then the collision term of the Boltzmann equation for $\chi_0(\epsilon_z)$ becomes simply

$$-\chi_0(\epsilon_z)/\tau(\epsilon_z), \quad (31)$$

where

$$\tau^{-1}(\epsilon_z) = \sum_{n'\mathbf{q}}[\tfrac{1}{2}W_{n'n'}{}^0(\mathbf{k}, \mathbf{k}+\mathbf{q})+\tfrac{1}{2}W_{n'n'}{}^1(\mathbf{k}, \mathbf{k}+\mathbf{q})- \\ -W_{10}{}^{n'}(\mathbf{k}+\mathbf{q}, \mathbf{k})] \quad (32)$$

which, as we shall see below, is a function of $\epsilon_z$. For scattering by ionized impurities we find from equation (19)

$$(1) \qquad \tau^{-1}(\epsilon_z) \cong \frac{\pi e^4 N_I}{\mathbf{k}^2(2m)^{\frac{1}{2}}} \frac{I_I(\epsilon_s/\hbar\omega)}{\hbar\omega} \epsilon_z^{-\frac{1}{2}}, \tag{33}$$

where

$$I_I(x) = 2\int_0^\infty [t^2 e^{-t}/(t+x)^2]dt, \quad \epsilon_s = \hbar^2/2mr_s^2. \tag{34}$$

The $I_I(x)$ is a slowly varying function of $x$ that decreases monotonically from the value 1 to 0. [In the range $x$: 0–10 it can be fairly well approximated by the function $2/(1+4x)$.] For acoustic phonon scattering the relaxation time is found with the use of equation (20) to be

$$(2) \quad \tau^{-1}(\epsilon_z) \cong (C^2kT/\mu s^2)(m^{\frac{3}{2}}/2^{\frac{1}{2}}\pi\hbar^4)\hbar\omega\epsilon_z^{-\frac{1}{2}} \tag{35}$$

We note that the relaxation time has the same energy dependence for both scattering mechanisms, whereas it differs drastically in its dependence on the magnetic field. Large magnetic fields lengthen the relaxation time in the impurity scattering region, whereas they shorten it in the acoustic phonon region. This has the important consequence that for a given temperature and impurity concentration the relative importance of phonon over that of impurity scattering is very much enhanced in the quantum limit.

Thus the assumed functions $\chi_n(\epsilon_z)$ do exist and are

$$\chi_0(\epsilon_z) = ie(E_x - iE_y)(2m\hbar\omega)^{-\frac{1}{2}}[f_0(\epsilon_z)/(\tau^{-1}(\epsilon_z)+i\omega)] \tag{36}$$

$$\chi_n(\epsilon_z) = 0, \text{ for } n \neq 0. \tag{37}$$

All $\chi_n(\epsilon_z)$ for $n = 0$ are simply zero because the driving term vanishes for $\epsilon_{n\mathbf{k}} > \hbar\omega$.

For the *longitudinal* case, the driving term in the Boltzmann equation is

$$eE_z(\hbar k_z/m)f_0'(\epsilon_{n\mathbf{k}})\delta_{n'n}. \tag{38}$$

Again taking advantage of the properties of the scattering operator we can find a solution of the transport equation of the form

$$(n'|f_1(\mathbf{k})|n) = k_z\sigma_n(\epsilon_z)\delta_{n'n} \tag{39}$$

For then the collision term for $n = 0$ becomes

$$-k_z\sigma_0(\epsilon_z)/\tau_l(\epsilon_z), \tag{40}$$

where

$$\tau_l^{-1}(\epsilon_z) = \sum_{n'\mathbf{q}} W_{n'n'}{}^0(\mathbf{k}, \mathbf{k}+\mathbf{q}). \tag{41}$$

For ionized-impurity scattering this gives

$$(1) \quad \tau_l^{-1}(\epsilon_z) = \frac{\pi e^4 N_1}{\kappa^2(2m)^{\frac{1}{2}}} \frac{I_l[(4\epsilon_z+\epsilon_s)/\hbar\omega]}{\epsilon_z+(\epsilon_s/4)} \epsilon_z^{-\frac{1}{2}}, \tag{42}$$

where

$$I_l(x) = \int_0^\infty [te^{-t}/(t+x)]dt \tag{43}$$

is a slowly varying function of $x$ that decreases monotonically from 1 to 0. [In the range $x$ : 0–10 it can be approximated by the function $1/(2+x)$.] For acoustic phonon scattering equation (41) yields

$$(2) \quad \tau_l^{-1}(\epsilon_z) = (C^2kT/\mu s^2)(m^{\frac{3}{2}}/2^{\frac{1}{2}}\pi\hbar^4)\hbar\omega\epsilon_z^{-\frac{1}{2}} \tag{44}$$

Again we note that high magnetic fields lengthen the longitudinal relaxation time in the impurity scattering region, whereas in the phonon region they shorten it. The functions $\sigma_n(\epsilon_z)$ are then

$$\sigma_0(\epsilon_z) = (-e\hbar/m)E_z\tau_l(\epsilon_z)f_0'(\epsilon_z) \tag{45}$$

$$\sigma_n(\epsilon_z) = 0, \text{ for } n \neq 0. \tag{46}$$

Having determined the steady-state density matrix, we can now calculate the current density. For the *transverse* case it is convenient to calculate

$$J_x + iJ_y = (e/\Omega)Tr\{(v_x+iv_y)f\}$$

$$= 2(e/\Omega)\sum_{\mathbf{k}} (1\mathbf{k}|v_x+iv_y|0\mathbf{k})\chi_0^*(\epsilon_z) \tag{47}$$

$$= (e^2/m)(E_x+iE_y)(2\pi)^{-2}(2m/\hbar^2)^{\frac{1}{2}}\hbar\omega \int_0^{\hbar\omega} \frac{f_0(\epsilon_z)\epsilon_z^{-\frac{1}{2}}\, d\epsilon_z}{\tau^{-1}(\epsilon_z)-i\omega}$$

This equation along with the corresponding expressions for the appropriate relaxation times, equations (33) and (35), constitute the fundamental equations for the transverse phenomena. Writing the transverse current density in terms of the conductivity tensor

$$\begin{pmatrix} J_x \\ J_y \end{pmatrix} = \begin{pmatrix} \sigma_1 & -\sigma_2 \\ \sigma_2 & \sigma_1 \end{pmatrix} \begin{pmatrix} E_x \\ E_y \end{pmatrix}, \tag{48}$$

we have for the Hall coefficient and transverse resistivity, respectively,

$$R = (-1/H)\sigma_2/(\sigma_1^2+\sigma_2^2) \tag{49}$$

$$\rho_t = \sigma_1/(\sigma_1^2+\sigma_2^2) \tag{50}$$

For the *longitudinal* case we have simply

$$J_z = (e/\Omega)Tr\{v_z f\}$$
$$= 2(e/\Omega)\sum_{\mathbf{k}} (0\mathbf{k}|v_z|0\mathbf{k})k_z\sigma_0(\epsilon_z)$$
$$= -(2e^2/m)E_z(2\pi)^{-2}(2m/\hbar^2)^{\frac{1}{2}}\hbar\omega \times$$
$$\times \int_0^{\hbar\omega} \epsilon_z^{\frac{1}{2}}\tau_l(\epsilon_z)f'_0(\epsilon_z)\,d\epsilon_z. \tag{51}$$

The appropriate relaxation times are given by equations (42) and (44). The longitudinal resistivity is, of course,

$$\rho_l = E_z/J_z. \tag{52}$$

We shall discuss these quantities in the limiting cases of degenerate and classical statistics.

It is convenient to express some parameters in terms of the relaxation time $\tau_0$ in zero magnetic field, which for impurity scattering is given by

$$\tau_0^{-1}(\epsilon) = (\pi e^4 N_I/\kappa^2 2^{\frac{1}{2}}m^{\frac{1}{2}})I_0(4\epsilon/\epsilon_s^0)\epsilon^{-\frac{1}{2}}, \tag{53}$$

where

$$I_0(x) = \ln(1+x) - x/(1+x), \tag{54}$$

and the corresponding conductivity

$$\sigma_0 = 1/\rho_0 = -(4e^2/3m)(2\pi)^{-2}(2m/\hbar^2)^{\frac{1}{2}}$$
$$\int_0^{\infty} \epsilon^{\frac{1}{2}}\tau_0(\epsilon)f'_0(\epsilon)\,d\epsilon. \tag{55}$$

We find for the Hall coefficient and resistivity for degenerate statistics and for weak scattering $[kT \ll (4/9)(\zeta_0/\hbar\omega)^2\zeta_0 \ll \hbar\omega]$:

| | Impurity scattering | Phonon scattering |
|---|---|---|
| $R$ | $\dfrac{1}{Nec}\left[1+\dfrac{3\pi}{4\tau_0\omega_f}\dfrac{I_t(\epsilon_s/\hbar\omega)}{I_0(4\zeta_0/\epsilon_s^0)}\dfrac{\zeta_0}{\hbar\omega}\right]$ | $\dfrac{1}{Nec}\left[1+\dfrac{3\pi}{8\tau_0\omega_f}\dfrac{\hbar\omega}{\zeta_0}\right]$ |
| $\dfrac{\rho_t}{\rho_0}$ | $\dfrac{3}{2}\dfrac{I_t(\epsilon_s/\hbar\omega)}{I_0(4\zeta_0/\epsilon_{0s})}\ln\left[\dfrac{2\tau_0\omega_f}{3}\dfrac{I_0(4\zeta_0/\epsilon_s^0)}{I_t(\epsilon_s/\hbar\omega)}\dfrac{\hbar\omega}{\zeta_0}\right]$ | $\dfrac{3}{4}\left(\dfrac{\hbar\omega}{\zeta_0}\right)^2\ln\left(\dfrac{4\tau_0\omega_f}{3}\dfrac{\zeta_0}{\hbar\omega}\right)$ |
| $\dfrac{\rho_e}{\rho_0}$ | $\dfrac{\epsilon_s^0}{\hbar\omega}\left[1+\dfrac{3}{4}\dfrac{\hbar\omega}{\zeta_0}\right]^{-1}$ (for $4\zeta_0/\epsilon_s^0 \ll 1$) | $\dfrac{3}{4}\left(\dfrac{\hbar\omega}{\zeta_0}\right)^2$ |

According to the simple theory of screening, under degenerate conditions

$$\epsilon_s/\hbar\omega = (e^2/2\pi^3\kappa)(2m/\hbar^2)^2(\hbar\omega/N).$$

Since, $I_t$ is a monotonically decreasing function of its argument, we see that for the quantum limit under degenerate conditions the Hall coefficient decreases slightly faster than $H^{-1}$ with the magnetic field in the impurity scattering range, whereas it increases as $H$ in the phonon region. The transverse resistivity is a slowly increasing function

of $H$ in the impurity range, while it increases essentially as $H^2$ in the phonon scattering region. On the other hand, the longitudinal resistivity varies essentially as $H^{-2}$ for impurity scattering, whereas for phonon scattering it varies as $H^2$ with the magnetic field.

For classical statistics $[\hbar\omega \gg kT \gg 16\pi^3(\hbar^2/2m)^3 (N/\hbar\omega)^2]$ we have, again in the limit of weak scattering:

| | Impurity scattering | Phonon scattering |
|---|---|---|
| $R$ | $\frac{1}{Nec}\left[1+\frac{I_t(\epsilon_s/\hbar\omega)}{I_0(4kT/\epsilon_s{}^0)}\frac{\pi}{\tau_0\omega}\frac{kT}{\hbar\omega}\right]$ | $\frac{1}{Nec}\left[1+\frac{\sqrt{\pi}}{2}\frac{\hbar/\tau_0}{kT}\right]$ |
| $\frac{\rho_t}{\rho_0}$ | $\frac{16}{\pi}\frac{I_t(\epsilon_s/\hbar\omega)}{I_0(12kT/\epsilon_s{}^0)}\frac{kT}{\hbar\omega}\ln\left[\frac{I_t(4kT/\epsilon^0{}_s)}{I_0(\epsilon_s/\hbar\omega)}\tau_0\omega\frac{\hbar\omega}{kT}\right]$ | $\frac{4}{3\pi}\frac{\hbar\omega}{kT}\ln\frac{kT}{\hbar/\tau_0}$ |
| $\frac{\rho_l}{\rho_0}$ | $I_0{}^{-1}(b)\left(\frac{4b}{3+2b}\right)\left[1+12\left(\frac{3+2b+b^2}{3b+2b^2}\right)\frac{kT}{\hbar\omega}\right]^{-1}$ | $\frac{1}{3}\frac{\hbar\omega}{kT}$ |

Thus for classical statistics the Hall coefficient decreases essentially as $H^{-2}$ with the magnetic field in the impurity scattering region, whereas in the phonon range it does not vary with the magnetic field (although it depends on temperature). The transverse resistivity decreases essentially as $H^{-1}$ for impurity scattering, while it increases as $H$ for phonon scattering. The same is roughly true for the longitudinal resistivity.

We thus conclude that in magnetic fields so large that all conduction electrons are in the lowest oscillator state the time between collisions is a strong function of the magnetic field strength and the scattering mechanism. The galvanomagnetic effects, through their magnetic field dependences in this region, provide, therefore, a sensitive tool for the study of the various scattering mechanisms.

VOL
8
195

REFERENCES

1. ARGYRES P. N. and ADAMS E. N., *Phys. Rev.* **104**, 900 (1956).
2. ARGYRES P. N., *Phys. Rev.* **109**, 1115 (1958).
3. ARGYRES P. N., *Westingho. Res. Rep.* 6–94760-2-R10 (Unpublished).

*J. Phys. Chem. Solids* Pergamon Press 1959. Vol. 8. pp. 130–135. Printed in Great Britain

# E.5 SCREENING EFFECTS IN POLAR SEMICONDUCTORS

H. EHRENREICH

General Electric Research Laboratory, Schenectady, New York

SCREENING effects in a semiconductor containing conduction electrons or holes modify both the electron–phonon interaction and the frequency of longitudinal lattice vibrations. In a material where scattering due to the polar character of optical modes is the principal mechanism determining the transport properties, the modified interaction potential and longitudinal optical frequency are

obtained from the following four equations:

$$\ddot{\mathbf{w}} = b_{11}\mathbf{w} + b_{12}\mathscr{E} + (2/\tau_l)\dot{\mathbf{w}} \tag{1}$$

$$\mathbf{P} = b_{21}\mathbf{w} + b_{22}\mathscr{E} \tag{2}$$

$$\nabla \cdot \mathbf{D} = -4\pi e \langle \rho^{(1)} \rangle \tag{3}$$

$$i\hbar(\partial\rho/\partial t) = [H, \rho]. \tag{4}$$

Equations (1) and (2) are macroscopic equations given by BORN and HUANG[1] describing the optical lattice vibrations of long wavelengths. The first of these is the equation of motion for the relative displacement $\mathbf{u}_+ - \mathbf{u}_- \equiv (v_a/M)^{\frac{1}{2}}\mathbf{w}$ of the two ions having a reduced mass $M$ in a unit cell of volume $v_a$. The forces acting are the Hooke's Law force and the self-consistent electric field $\mathscr{E}$. The third term of equation (1) causes the amplitude of the lattice vibration to *build up* in time. Its behavior is in accord with the boundary condition we shall impose: at $t = -\infty$ the lattice is at rest. Thus $\mathbf{w}(t = -\infty) = \mathscr{E}(t = -\infty) = \mathbf{P}(t = -\infty) = 0$. Equation (2) relates the macroscopic polarization $\mathbf{P}$ in a given region to the relative displacements as well as to the field $\mathscr{E}$ polarizing the ions. The coefficients $b_{ij}$ can be related to the low and high frequency dielectric constants $\epsilon_0$, $\epsilon_\infty$ when no free charges are present and to the transverse optical (reststrahlen) frequency $\omega_t$. BORN and HUANG[1] show that $b_{11} = -\omega_t^2$, $b_{12} = b_{21} = \omega_t[(\epsilon_0 - \epsilon_\infty)/4\pi]^{\frac{1}{2}}$, and $b_{22} = (\epsilon_\infty - 1)/4\pi$. We shall assume that these constants are not appreciably altered by the introduction of conduction electrons and holes in concentrations typical of semiconductors.

Equations (3) and (4) give a quantum mechanical description of the influence of the screening electrons. The former is Poisson's equation, relating the screening charge to the self-consistent field $\mathscr{E} = \mathbf{D} - 4\pi\mathbf{P}$; the latter is the Liouville equation describing the dynamical response of the screening electrons to the self-consistent field. The Hamiltonian $H$ has the form $H = H_0 + Ve^{t/\tau_e}$, where the self-consistent potential energy determined by the vibrating lattice plus screening electrons is $V = -e\phi$ which in turn is related to the electric field by $\mathscr{E} = -\nabla\phi$. $H_0$ is the Hamiltonian for free particles with wave function $|k\rangle \sim e^{ik\cdot r}$ which satisfies the Schrödinger equation $H_0|k\rangle = E_k|k\rangle$. The density matrix $\rho$ will be written in the form $\rho^{(0)} + \rho^{(1)}e^{t/\tau_e}$ and treated using perturbation theory. The unperturbed density matrix $\rho^{(0)}$ is an operator having the property $\rho^{(0)}|k\rangle = f_0(E_k)|k\rangle$ where $f_0(E_k)$ is the distribution function which may correspond either to Boltzmann or Fermi statistics. We note that $\rho(t = -\infty) = \rho^{(0)}$ and $H(t = -\infty) = H_0$, in accord with the assumption that there is no interaction with the lattice at time $t = -\infty$. The term $\langle \rho^{(1)} \rangle = Tr(C\rho^{(1)})/Tr(\rho^{(0)})$ in equation (3) yields the spatial distribution of the charge density. Here $C$ is the charge density operator which has matrix elements $\langle k|C|k'\rangle = e^{i(k'-k)\cdot r}$.

We shall solve equations (1)–(4) for the case of longitudinal optical vibrations since the transverse modes are not coupled to the electrons by the polar interaction. We consider Fourier components corresponding to right and left travelling lattice waves characterized by wave number $q$ and the actual frequency $\omega$ $(q)$ as modified by screening effects. This frequency is a function of $q$ and must be regarded as a quantity to be determined. The Fourier components of the screened and unscreened potentials corresponding to the two directions of propagation will be denoted $\phi_S{}^{\pm}(\omega, q)$ and $\phi_U{}^{\pm}(q)$. Thus we write

$$\phi_S(r) = \sum_q [\phi_S{}^+(\omega, q)e^{i(\mathbf{q}\cdot\mathbf{r}-\omega t)} + \phi_S{}^-(\omega, q)e^{-i(\mathbf{q}\cdot\mathbf{r}-\omega t)}]$$

and similarly for $\mathbf{P}$, $\mathscr{E}$, and $\mathbf{w}$. In order to simplify the notation, we shall suppress the $\pm$ superscripts and consider only positive components associated with right-travelling waves. It is easily shown that the results for the negative components are obtained by taking the complex conjugate of all quantities involved. The solution of equation (4) shows the Fourier components of $\langle \rho^{(1)} \rangle$ to be proportional to $V(\omega, q)$. We shall therefore write these components in the form $\rho(\omega,q)\ V(\omega, q)$. Explicit expressions for $\rho(\omega, q)$ are calculated in the quantum mechanical and classical limits when $\omega\tau_e \gg 1$ for both Fermi and Boltzmann statistics in another paper[2] to be published in collaboration with M. H. COHEN. For the classical case and Boltzmann statistics it is found that

$$\rho(\omega, q) = -(n/KT)[\{1 - 2u\exp(-u^2)\int_0^u \exp(x^2)dx\} + i\pi^{\frac{1}{2}}u\exp(-u^2)] \tag{5}$$

where $n$ is the carrier concentration, $u = (\omega/q)(m^*/2KT)^{\frac{1}{2}}$ is the ratio of the phase velocity to the electron velocity corresponding to an energy $KT$, and $m^*$ is the effective mass. The integral leading to equation (5) involves a complex energy denominator. In evaluating this integral we have assumed $(\omega\tau_e)^{-1} \equiv \epsilon \to 0$ and linearized the denominator by writing it in the form $(x \mp i\epsilon)^{-1} = \mathscr{P}(x^{-1}) \pm i\pi\delta(x)$. The resulting expression (5) therefore does not depend explicitly on $\tau_e$. As shown in Ref. 2, the imaginary term can be associated with the lifetime of plasma oscillations.

Simple and physically meaningful expressions for the screened interaction potential and the actual lattice frequency can be obtained by introducing the complex frequency and wave number dependent dielectric constant discussed in reference (2). This dielectric constant may be obtained from the density matrix by calculating a complex current and using familiar expressions involving the conductivity and electric susceptibility. In the low frequency limit we find

$$\epsilon_0(\omega, q) = \epsilon_0 + \gamma(\omega, q) = \epsilon_0^{(1)}(\omega, q) + i\epsilon^{(2)}(\omega, q), \quad (6)$$

and similarly for $\epsilon_\infty(\omega, q)$ in the high frequency limit. The complex contribution $\gamma(\omega, q) = -(4\pi e^2/q^2)\rho(\omega, q)$ is due to free carriers and is the same in both limits.

The screened longitudinal optical frequency is obtained from the condition requiring equations (1)–(4) to be self-consistent. The necessity for such a condition is recognized by noting that the Fourier transforms of equations (1) and (2) and those of equations (3) and (4) each lead to an equation of the form $P(\omega, q) = \lambda(\omega, q)\mathscr{E}(\omega, q)$ and that $\lambda(\omega, q)$ must be the same for both equations. We must linearize the imaginary term involving $\tau_l$ in order to be consistent with the condition $\omega\tau_e \gg 1$ used earlier. We find the transcendental equation

$$\omega^2/\omega_t^2 = \epsilon_0^{(1)}(\omega, q)/\epsilon_\infty^{(1)}(\omega, q) \quad (7)$$

which determines $\omega$ and also an expression for $\tau_l$ showing it to be related to the damping of the lattice waves resulting from the interaction with the free carriers.

A revealing expression relating the screened and unscreened potentials $\phi_S(\omega, q)$, $\phi_U(q)$ can be obtained upon generalizing the effective ionic charge $e^*$ determining the strength of the electron–phonon coupling[3] which appears in the familiar expression for $\phi_U(q)$. We express the unscreened charge $e^*$ in terms of $\epsilon_0$, $\epsilon_\infty$, and $\omega_t$, noting that the transverse frequency is not modified by the screening electrons. The screened charge $e_S^*(\omega, q)$ is found simply by replacing the dielectric constants with those defined in equation (6). The result, depending on frequency and wave number, is

$$e_S^*(\omega, q) = (v_a M/4\pi)^{\frac{1}{2}} \times \times [\epsilon_0(\omega, q) - \epsilon_\infty(\omega, q)]^{\frac{1}{2}}\omega_t/\epsilon_\infty(\omega, q). \quad (8)$$

With the help of equation (8) it can be shown that

$$\phi_S(\omega, q)/\phi_U(q) = e_S^*(\omega, q)/e^* = \epsilon_\infty/\epsilon_\infty(\omega, q). \quad (9)$$

The screened interaction potential is therefore obtained by substituting in the expression for the unscreened potential the natural generalizations of the effective ionic charge and lattice frequency as obtained from equations (7) and (8).

In the quantum mechanical limit and for Boltzmann statistics, equations (7) and (9) can be shown to correspond precisely to the results of BARDEEN and PINES[4] when damping is neglected and their unscreened electron–phonon interaction is specialized to the present $\phi_U(q)$. The expression (9) in terms of the ratio of dielectric constants is similar to that given in reference (2) for an arbitrary electron–phonon interaction. If the unrenormalized frequency $\omega_U$ is used in equation (9), one finds that $\epsilon_\infty^{(1)}(\omega_U, q) = 0$ whenever $\omega_U(q)$ equals the frequency $\omega_P(q)$ of a plasmon having wave number $q$. As shown below, this resonance behavior is absent when the actual frequency is used.

Fig. 1 exhibits the behavior of $\omega^2/\omega_t^2$, and of $|\phi_S(\omega, q)/\phi_U(q)|$, as a function of $\sigma = q/2k_T$, where $k_T = (2m^*KT)^{\frac{1}{2}}/\hbar$ is the wave number of an electron having energy $KT$. We visualize a weakly polar semiconductor characterized by $\epsilon_0/\epsilon_\infty = 1{\cdot}2$ in the classical limit for which equation (5) applies, and assume the validity of Boltzmann statistics, as well as a temperature such that $\hbar\omega_t/KT = 1$. Further we consider a typical carrier concentration corresponding to $(\omega_t/\omega_P)^2 = 1$ where $\omega_P^2 = 4\pi ne^2/\epsilon_\infty m^*$ is the plasma frequency. The curve for $\omega^2/\omega_t^2$ vs. $\sigma$ results from solving equation (7). The actual frequency $\omega$ is then used in arriving at the results for $|\phi_S(\omega, q)/\phi_U(q)|$ obtained from equation (9). The general appearance of the curves shown in Fig. 1 is seen to be quite similar. For small $\sigma$ we note that both the screened potential and lattice frequency are actually greater than in the unscreened case. This results from the fact that in this range of $\sigma$ the phase velocity of the lattice wave $v_\phi = \omega/q$ is much larger than the thermal velocity of the electrons. In the frame of reference for which the lattice wave is at rest, the electrons are rushing over the potential hills and valleys associated with the wave with a velocity $v_\phi$ so large that there is no opportunity for the achievement of thermal equilibrium in the valleys. Because of acceleration effects the electrons spend more time on the hills than in the valleys and

*anti-screening* effects occur which produce the behavior at small $q$ shown. Indeed, this effect increases as $q$ increases and $v_\phi$ decreases since the potential hills and valleys become more noticeable to the electrons. This behavior continues until $v_\phi$ begins to become comparable with the thermal velocity. For larger $q$ thermal equilibrium in the valleys can be achieved and the behavior of the frequency and potential exhibits the expected become more appreciable. The dashed portion of the curve indicates the region where damping effects are sufficiently important that the linearization used to arrive at equation (5) is no longer a valid approximation.

In applications to many transport calculations it is a fair approximation to neglect time-dependent and quantum mechanical effects, that is, to consider equation (5) in the limit $u = 0$. The

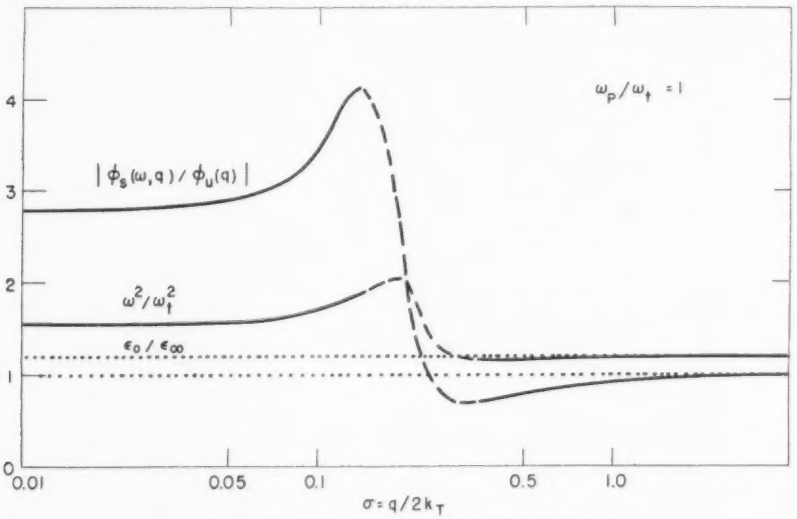


FIG. 1. $\phi_s(\omega, q)/\phi_U(q)$ and $\omega^2/\omega_t^2$ vs. $\sigma = q/2k_T$ for a weakly polar semiconductor characterized by $\epsilon_0/\epsilon_\infty = 1{\cdot}2$, $\hbar\omega_t/KT = 1$, and carrier concentration such that $\omega_t/\omega_P = 1$. The validity of Boltzmann statistics is assumed.

reduction due to screening. In the limit that

$$q\lambda_D \gg 1, \text{ where } \lambda_D = [\epsilon_\infty KT/4\pi ne^2]^{\frac{1}{2}}$$

is the Debye length, screening effects vanish and $\phi_S(\omega, q)/\phi_U(q) \to 1$. In this limit we find the familiar relation $\omega^2/\omega^2_t = \epsilon_0/\epsilon_\infty$ between the longitudinal and transverse frequencies. It should be noted that equation (7) obviously is a generalization of this last relationship. Quantum mechanical effects which are not shown in Fig. 1, become important only for $q > k_T$ where they reduce the screening. The uncertainty principle then does not permit the electrons to be as localized as is required by classical considerations. As the carrier concentration increases, the results shown in Fig. 1 are altered in that the maximum at small $\sigma$ and the reduction at larger $\sigma$ due to screening effects both

validity of this approach depends on the fact that the phonons that contribute appreciably to electron scattering in many transport processes are characterized by $\sigma \sim 1$. In this range of $\sigma$ the anti-screening effects have disappeared. This approximation somewhat overestimates the influence of screening; however, the transport calculations, which are already complicated because of the failure of the relaxation time approximation,[5-3] remain tractable. In this limit $\phi_S(\omega, q)/\phi_U(q) = (1+q^{-2}\lambda_D^{-2})^{-1}$ and $\omega^2/\omega_t^2 = (\epsilon_0/\epsilon_\infty + q^{-2}\lambda_D^{-2})/(1+q^{-2}\lambda_D^{-2})$. The mobility for various carrier concentrations resulting from this form of the electron–phonon interaction is easily obtained from the curves shown in Fig. 2. These results represent the generalization of Fig. 1 (Curve 2) given in the paper of HOWARTH and SONDHEIMER[5] where

the transport properties of weakly polar semiconductors are calculated in the absence of screening effects using Kohler's variational principle. To obtain Fig. 2 we have multiplied the transition probabilities given by equation (6) of reference (5) by $(1+q^{-2}\lambda_D^{-2})^{-2}$ to take account of the screening effects and carried through the analogous variational calculation for Boltzmann statistics and a simple parabolic band.* The dependence of $\omega$ on wave number which is weak in this approximation has been neglected. The functions $G^{(1)}e^{-\xi}$ plotted in Fig. 2 as a function of $z = \hbar\omega/KT$ are the generalizations of those defined in equation (44) and (47) of reference (5). The accuracy of these functions, which is limited by the choice of the trial function used in the variational calculation, is believed to be better than 20 per cent, as in reference (5). The carrier concentrations are expressed in terms of the plasma frequency. For $\omega_P = 0$ the results reduce to those given by HOWARTH and SONDHEIMER. Using Fig. 2, the mobility may be computed by simple substitution in the following equation:

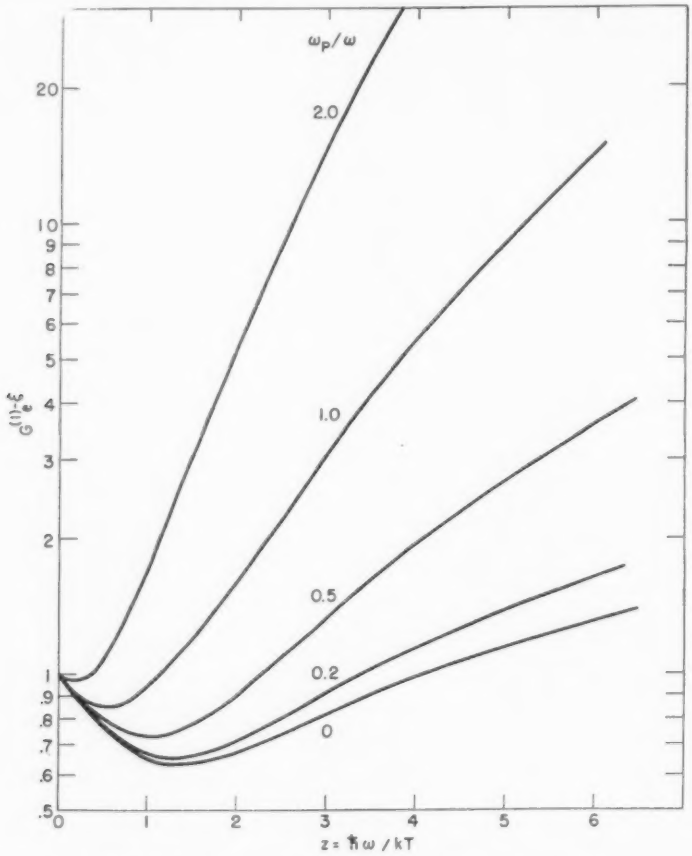


FIG. 2. $G^{(1)}e^{-\xi}$ vs. $z = \hbar\omega/KT$ (notation of reference (5)) for various carrier concentrations characterized by $\omega_P^2 = 4\pi ne^2/\epsilon_\infty m^*$. These results may be used in conjunction with equation (10) to determine the mobility due to screened polar scattering.

$$\mu(\mathrm{cm^2/V\ sec}) = 0{\cdot}199(T/300)^{\frac{1}{2}}(e/e^*)^2(m/m^*)^{\frac{1}{2}} \times \times (10^{22}M)(10^{23}v_a)(10^{-13}\omega)(e^z-1)(e^{-\xi}G^{(1)}) \quad (10)$$

* The resulting matrix element for scattering is also discussed in references (3) and (6).

which is obtained from equation (43) of reference 5.

We note that the screening effects can be very important at low temperatures for reasonable carrier concentrations. For example, the lattice mobility of a polar semiconductor characterized by $\epsilon_\infty = 16$, $m^* = 0{\cdot}1$, $n = 10^{18}\text{cm}^{-3}$, and $\hbar\omega = KT$ at room temperature is proportional to the curve labelled $\omega_P = \omega$. At high temperatures the screening effects gradually disappear since $\lambda_D$ becomes large. It should be recognized, however, that a semiconductor containing a carrier concentration $n$ will also contain at least $n$ charged impurities which will dominate the scattering at low temperatures where the effect of screening on the electron–phonon interaction is most pronounced. The combination of the two scattering mechanisms in a calculation of the mobility therefore tends partially to mask the effect produced by the screening of the lattice waves.†

The following interesting situation can occur. In two samples A and B of a given polar semiconductor characterized by impurity concentrations $n_I(A) > n_I(B)$ and carrier concentrations $n(A) > n(B)$, the mobilities $\mu(A)$ and $\mu(B)$ may have the property that at low temperatures when impurity scattering predominates, $\mu(A) < \mu(B)$, whereas at higher temperatures where lattice scattering is most important and the screening effects under discussion come into play, $\mu(A) > > \mu(B)$. The mobilities therefore intersect at some intermediate temperature. This effect should be observable in materials for which e* is sufficiently large that polar scattering can compete effectively with ionized impurity scattering for the impurity concentrations involved at temperatures $T \lesssim \hbar\omega/K$ where screening effects are important. For example in two samples of a material characterized by $e^* = 0{\cdot}5$, $\hbar\omega/K = 560°\text{K}$, $m^* = 0{\cdot}08$, $M = 0{\cdot}4\times10^{-22}\text{g}$, $v_a = 5\times10^{-23}\text{cm}^3$, $n_I(A) = n(A) = 10^{18}\text{cm}^{-3}$, $n_I(B) = n(B) = 4\times10^{15}$, one calculates that an intersection of the mobilities should occur at about 300°K.‡

Screening effects are also important in InSb in the range of temperatures where polar scattering predominates because of the large intrinsic carrier concentrations that occur. In another paper[6] it is shown that the mobility can be understood quantitatively if they are taken into account.

A further consequence of screening effects that has considerable theoretical importance is that the constant $\alpha$ which determines the strength of the electron–phonon coupling[8] can be appreciably reduced for phonons that predominantly scatter electrons in semiconductors. When free carriers are present $\alpha$ becomes a function of $\omega$ and $q$ and may be written in the form

$$\alpha(\omega, q) = 2^{\frac{1}{2}}\pi m^{*\frac{1}{2}}e^2e^{*2}(\omega, q)/\hbar^{\frac{1}{2}}\omega^{\frac{1}{2}}Mv_a.$$

Using equation (9), we find that in PbS containing $10^{18}$ carriers $\alpha(\omega, q)$ is a factor two smaller than the coupling constant in the absence of screening for a phonon having wave number $q = k_T$ at 100°K. The constants needed to compute $\alpha(\omega, q)$ are those given by PETRITZ and SCANLON.[9] Such a reduction of the coupling constant may validate the use of weak-coupling theory in some materials containing an appreciable carrier concentration where it would be inapplicable in the absence of screening charges.

## REFERENCES


1. BORN M. and HUANG K., *Dynamical Theory of Crystal Lattices*, pp. 82–84. Oxford Press (1954).
2. EHRENREICH H. and COHEN M. H., to be published. See also *Bull. Amer. Phys. Soc.* Ser. II, **3**, 271 (1958).
3. EHRENREICH H., *J. Phys. Chem. Solids* **2**, 131 (1957).
4. BARDEEN J. and PINES D., *Phys. Rev.* **99**, 1140 (1955).
5. HOWARTH D. J. and SONDHEIMER E. H., *Proc. Roy. Soc.* **A219**, 53 (1953).
6. EHRENREICH H., *J. Phys. Chem. Solids*, **9**, 129 (1959).
7. REID F. J. and WILLARDSON R. K., *J. Electron. and Control* **5**, 54 (1958).
8. FRÖHLICH H., *Advanc. Phys.* **3**, 325 (1954).
9. PETRITZ R. L. and SCANLON W. W., *Phys. Rev.* **97**, 1620 (1955).


† This may not be true, however, in the hot electron problem where the lattice interaction is needed to dissipate energy. The reduction of the magnitude of the lattice interaction in this case may cause the electrons to heat up more rapidly than they would in the absence of screening effects.

‡ An effect of this type has been recently observed in *n*-type InP.[7] Indeed, with the exception of $e^*$ which is somewhat too large, the parameters used in the preceding example are characteristic of this material. Although the polar interaction appears to give rise to the dominant lattice scattering mechanism, there is still too much uncertainty at the present time concerning the value of $m^*$ and the conduction band structure in InP to attribute this effect to screening.

*J. Phys. Chem. Solids* Pergamon Press 1959. Vol. 8. pp. 136–137. Printed in Great Britain

# E.6 ON THE THEORY OF STRONG-FIELD CONDUCTION

P. J. PRICE
International Business Machines Corporation, Watson Laboratory, New York City

In the theory of electronic transport in solids, the following transformation is useful:[1] Let the Boltzmann equation[2] be written

$$(\partial f/\partial t)_{\text{coll}} = g \tag{1}$$

Then the expectation of some function $\psi$ of electron state, if this expectation is zero for thermal equilibrium, is[3]

$$I\psi f = -Ig\int_0^\infty dt\langle\psi; t\rangle, \tag{2}$$

where the integrand $\langle\ ;\ \rangle$ stands for the expectation of $\psi$, after an interval $t$, for an electron starting from a definite state (which is the independent variable for the sum-integral $I$) and undergoing Brownian motion. When $\psi$ is the electron velocity $\mathbf{v}$, we obtain an expression for the current in terms of the mean free path[4] [5]

$$\mathbf{l} \equiv \int_0^\infty dt\langle\mathbf{v}; t\rangle \tag{3}$$

from which a formula corresponding to the usual ones for the Ohmic mobility and conductivity follows.[4] For electric conduction in general, since

$$g = \mathbf{F}\cdot(\partial/\partial\mathbf{p})f$$

where $\mathbf{F}$ is the Lorentz force, the drift velocity is[6]

$$\mathbf{u} \equiv I\mathbf{v}f = I\{f\mathbf{F}\cdot(\partial/\partial\mathbf{p})\mathbf{l}\}. \tag{4}$$

If there is a magnetic (as well as an electric) field, $\mathbf{H}$, its effect on $\mathbf{u}$ may be represented either by the term proportional to $\mathbf{H}$ in $\mathbf{F}$ on the right of (4) or by transferring the corresponding term in (1) from the right to the left and[5] generalizing the integrand $\langle\ ;\ \rangle$ in (2) to include the effect of $\mathbf{H}$ in the Brownian motion. Neither is satisfactory for non-Ohmic conduction because one still gets $\mathbf{u}$ in terms of an integral over $f(\mathbf{E}, \mathbf{H})$, whereas one wants a formula for the change in $\mathbf{u}$ due to $\mathbf{H}$ in terms of the situation for $H = 0$. The following generalization[7] provides such a result, and also a theory of diffusion, of differential mobility, and of the change in the expectation of magnitudes (such as energy) whose thermal average is not zero, for hot electrons.

When the Lorentz force is $\mathbf{F}_a$, let $f_a$ be the solution of the Boltzmann equation. Then when the Lorentz force is $\mathbf{F}_a+\mathbf{F}_b$ we have

$$I\{(f-f_a)\psi\} = If_a\mathbf{F}_b\cdot(\partial/\partial\mathbf{p})\int_0^\infty dt(\langle\psi; t, \mathbf{F}_a\rangle-\psi_a)+O(\mathbf{F}_b^2), \tag{5}$$

where the $\mathbf{F}_a$ in $\langle\ ;\ \rangle$ signifies that the Brownian motion is with this force acting (accelerating the electron between scatterings) and

$$\psi_a \equiv \langle\psi; \infty, \mathbf{F}_a\rangle = If_a\psi.$$

Thus the required formulas contain the *differential mean free path*[7]

$$\mathbf{l}' \equiv \int_0^\infty dt(\langle\mathbf{v}; t, \mathbf{F}\rangle-\mathbf{u}). \tag{6}$$

It can be shown[5] that this satisfies the integro-differential equation

$$\{1-\mathscr{L}-\tau\mathbf{F}\cdot(\partial/\partial\mathbf{p})\}\mathbf{l}' = \tau(\mathbf{v}-\mathbf{u}), \tag{7}$$

where $1/\tau$ is the collision frequency and $\mathscr{L}\psi$ is the expectation of $\psi$ after one scattering from the given (initial) state. If the wrong value were substituted for $\psi_a$ in (5) or $\mathbf{u}$ in (6), the integral would diverge. Correspondingly, if the wrong value of $\mathbf{u}$ is used in (7) there will not be a bounded solution. Thus $\mathbf{u}$ *is the eigenvalue of* $\mathbf{v}$ *in* (7). The corresponding situation also obtains, of course, for any function $\psi$, of electron state, other than $\mathbf{v}$.

The eigenvalue feature of (7) may be verified for the "standard" case, already studied, in which the electron energy $\epsilon$ is $p^2/2m^*$ and scattering is by weak non-polar interaction with longitudinal Debye modes of velocity $s \ll \sqrt{(kT/m^*)}$. This case has the characteristic that $f$ becomes altogether different from the thermal equilibrium function for modest field strengths at which the surfaces of constant $f$ remain almost spherical. For $H = 0$ one may expand $\mathbf{l}' \cdot \mathbf{E}$ in ascending powers of $\mathbf{E} \cdot \mathbf{v}$ (the coefficients being functions of $\epsilon$) and obtain a simple differential equation in $\epsilon$ for the lowest term. One finds that the solution for $\mathbf{l}'$ is bounded for one value of $\mathbf{u}$ only, and that this value is indeed just the drift velocity given by the well known solution for $f$ in this case.[8] For the eigenfunction one finds

$$\mathbf{l}' \simeq -\tau_0(\epsilon)\mathbf{u} + \tau\mathbf{v} \tag{8}$$

where $\tau_0(\epsilon)$ is a positive monotonic-increasing function, of complicated form. The linear Hall effect is represented by (5) with $\mathbf{l}'$ substituted from (8) and $\mathbf{F}_b = -(e/c)\mathbf{v}\times\mathbf{H}$. The first term of (8) contributes nothing, and in consequence the Hall component of $\mathbf{u}$ is just $(e/m^*c)\mathbf{H}\times I\tau\mathbf{v}f$. One may reduce this expression to the usual form of an expectation of an *even* function of $\mathbf{p}$ either by applying the foregoing method to get the eigenvalue of $\tau\mathbf{v}$ or by using the formula connecting odd and even parts of $f$ together with PISARENKO's result.[8] The resulting expression is that used by SODHA and EASTMAN,[9] and could have been obtained from (4) by assuming the change in $f$ due to the magnetic field to be negligible on the right hand side.[10] For the "many valley" case, by assuming the tensor generalization, according to the HERRING–VOGT approximation, of (8) to hold, one obtains for the Hall component of $\mathbf{u}$ *in one valley*:

$$-(e^2/3c)\mathbf{H}\cdot\langle\boldsymbol{\lambda}(\epsilon)\rangle\times\mathbf{E}.$$

Here $\langle\ \rangle$ denotes the expectation for a single valley distribution and $\boldsymbol{\lambda}$ is the tensor with components $\lambda_{11} = \tau_2\tau_3/m_2^*m_3^*$, etc., in the usual notation.[11] To deal with diffusion, one replaces the *operator* $f_a\mathbf{F}_b \cdot (\partial/\partial\mathbf{p})$ in (5) by a *function* which is the rate of change of $f$ due to the space gradient. Then according to (8) the flux of electrons is

$$\mathbf{N} = -(2/3m^*)\{\mathbf{u}\ \mathrm{div}(ne\mathbf{E}If\tau d(\epsilon\tau_0)/d\epsilon) + \\ +\mathrm{grad}(nIf\tau\epsilon)\}, \tag{9}$$

where $n$ is the electron concentration. Evidently diffusion perpendicular to $\mathbf{u}$ is given by a simple generalization of the usual formula (but the EINSTEIN relation no longer holds). Diffusion parallel to $\mathbf{u}$ is more complicated. (However, for a steady state with div $n\mathbf{u} = 0$ the first term of (9) comes from the space gradient of $f$ only and does not depend on grad $n$.)

## REFERENCES


1. See references (4) and (5). An earlier paper, PRICE, P. J., *IBM J.* **1,** 147 (1957), gives some aspects of the mathematics in more detail.
2. This means the linear equation. The results following apply to linear transport (e.g. Ohmic conduction) with (1) the linearized equation, and to non-linear transport also when Boltzmann (rather than Fermi) statistics applies.
3. Here $I$ stands for integration over the Brillouin zone and summation over spin states and bands. To simplify the exposition, the normalization throughout is such that $If = 1$ : This should be remembered when one is comparing equations here with those in references (1), (4) and (5).
4. PRICE P. J., *IBM J.* **1,** 239 (1957).
5. PRICE P. J., *IBM J.* **2,** 200 (1958).
6. See also CONWELL E. M., *Phys. Rev.* **88,** 1379 (1952).
7. See the footnote on page 201 of reference (5).
8. For example PISARENKO N. L., *Izv. Akad. Nauk. SSSR, Mathematical and Natural Sciences*, p. 631 (1938).
9. SODHA M. S. and EASTMAN P. C., *Phys. Rev.* **110,** 1314 (1958).
10. Using this formula for the Hall mobility, the value 1·06 given by SODHA and EASTMAN for the ratio of Hall mobility to drift mobility, at field strengths $E$ for which $u$ is proportional to $\sqrt{E}$, was obtained by Mr. P. B. Linhart at Watson Laboratory in 1956.
11. Here the subscripts denote components in the valley axis directions. The off-diagonal elements are zero. This result for the Hall effect corresponds to those for Ohmic conduction given by HERRING C., *Bell Syst. Tech. J.* **34,** 237, Section 6 (1955). See also HERRING C., and VOGT E., *Phys. Rev.* **101,** 944, equation (19) (1956).

*J. Phys. Chem. Solids* Pergamon Press 1959. Vol. 8. pp. 138–141. Printed in Great Britain

E.7

# TRANSPORT PHENOMENA IN SEMICONDUCTORS FOR WARPED ENERGY SURFACES

G. E. TAUBER* and L. SOFFER†

*Dept. of Physics, Western Reserve University, Cleveland and
The Franklin Institute Laboratories, Philadelphia
†Dept. of Physics, Western Reserve University, Cleveland.

VOL
8
195

PREVIOUS calculations of the transport coefficients in semiconductors[1] assumed that the energy–momentum dependence can be described by spherical energy surfaces. Recent work on cyclotron resonance,[2] however, shows that the actual surfaces depart from the spherical form, and, in the case of germanium and silicon in particular, the energy momentum dependence is given by an expression of the form[3]

$$E_{1,2} = -(1/2m)(Ap^2 + \pm[B^2p^4 + C^2(p_x^2p_y^2 + p_y^2p_z^2 + p_z^2p_x^2)]^{\frac{1}{2}}) \quad (1)$$
$$E_0 = -D - (1/2m)Ap^2$$

where $A$, $B$ and $C$ are constants determined from the cyclotron resonance experiments,[2] $D$ is the spin–orbit splitting energy and the plus and minus sign refers to the surface of the light and heavy holes respectively.

In addition to the complication introduced by the non-spherical nature of the energy surface (1), it becomes also necessary to consider the effect of the transitions between bands. It is known[4] that the Boltzmann transport equation for the problem can be written as integral operator equations, which in our case become

$$\sum_n L_{mn}(f_{1i}^n) = v_i \partial f_0/\partial \epsilon_m = x_{1i}^m,$$
$$\sum_n L_{mn}(f_{2i}^n) = v_i \epsilon_m \partial f_0/\partial \epsilon_m = x_{2i}^m \quad (2)$$

where $L_{mn}$ is the integral operator defined by

$$L_{mn}(\Phi_n) = (1/kT)\int V(\mathbf{k}_m, \mathbf{k}_n)[\Phi_m(\mathbf{k}_m) - \Phi_n(\mathbf{k}_n)]d\mathbf{k}_n \quad (3)$$

and $m$, $n$ ($m$, $n = 0$, 1, 2) denote the possible energy $\Phi_n$ bands. Here is a function, which measures the deviation of the carrier distribution function $f$ from its equilibrium value $f_0$*

$$f^n = f_0^n - (\partial f_0^n/\partial \epsilon_n)\Phi_n \quad (4)$$

$f_{1i}^n$ and $f_{2i}^n$ are the components of $\Phi_n$ obtained by separating it in the usual fashion according[4] to

$$\Phi_n(\mathbf{k}) = [eE_i + T\partial/\partial x^i(\zeta/T)]f_{1i}^n + 1/T\ \partial T/\partial x^i f_{2i}^n \quad (5)$$

It has been shown by KOHLER[5] that the Boltzmann equation can be derived from a variational principle, for which the extremal function is given by the inner product[6]

$$(\Phi;\ \Phi) = \int \Phi(\mathbf{k})L(\Phi)d\mathbf{k} \quad (6)$$

subject to the subsidiary condition

$$(\Phi,\ X) = \int \Phi(\mathbf{k})Xd\mathbf{k} = (\Phi;\ \Phi) \quad (7)$$

In applying this to the system of equations (2) we simply have to replace (6) and (7) by a sum of terms. The new extremal function is thus given by†

$$(f_{pi};\ f_{pj}) = \sum_{mn}(f_{pi}^m;\ f_{pj}^n) \qquad (p = 1, 2) \quad (8)$$

subject to the subsidiary conditions

$$(f_{pi},\ x_{pj}) = \sum_m (f_{pi}^m,\ x_{pj}^m)$$

* For the Maxwell–Boltzmann distribution $\Phi$ should be replaced by $\Phi/(1-f_0)$.

† It can easily be seen that (8) is positive definite by using $f = f_1 + f_2$ and substituting in (8) making use of the symmetry properties of $L$.

$$= \sum_{m,n} (f_{pi}{}^m; f_{pj}{}^n) = (f_{pi}; f_{pj}) \qquad (p = 1, 2) \quad (9)$$

where we have introduced the notation

$$(f^m; f^n) = \int f^m L_{mn}(f^n) d\mathbf{k}_m;$$
$$(f^m, x^m) = \int f^m x^m d\mathbf{k}_m. \qquad (10)$$

This variational principle can be solved by an application of the Ritz method. For this purpose we expand the functions $f_{1i}{}^m$ and $f_{2i}{}^m$ as an infinite power series in the energy $\epsilon$

$$f_{1i}{}^m = k_i \sum_r a_{mr}(\epsilon_m)^r \text{ and } f_{2i}{}^m = k_i \sum_r b_{mr}(\epsilon_m)^r \qquad (11)$$

where $k_i$ are the components of $\mathbf{k}$ and $a_{mr}$ the unknown coefficients to be determined by the variational principle. Substituting (11) into (8) and (9) we obtain finally a set of linear equations for the unknowns $a_{mr}$, $b_{mr}$ which satisfy the stationary condition (8) and the subsidiary conditions (9)

$$\alpha_{pq}{}^{ij} = \sum_{m,s} a_{ms} d_{pq,ms}{}^{ij}, \quad \beta_{pq}{}^{ij} = \sum_{m,s} b_{ms} d_{pq,ms}{}^{ij} \qquad (12)$$

where we have introduced the notation

$$d_{mr,ns}{}^{ij} = (k_i \epsilon_m{}^r; k_j \epsilon_n{}^s) = d_{ns,mr}{}^{ij}$$
$$\alpha_{mr}{}^{ij} = (k_i \epsilon_m{}^r, x_{1j}{}^m), \quad \beta_{mr}{}^{ij} = (k_i \epsilon_m{}^r, x_{2j}{}^m) \qquad (13)$$

The advantage of the use of the variational principle and its solution (12) lies in the fact that the transport coefficients can be expressed in terms of infinite determinants[7] which can be evaluated to any required degree of accuracy without requiring an explicit solution of the transport equations. The electric and energy current densities may be considered to be given as the sum of the appropriate expressions for each band. The result can be written in the same form as in the standard theory:

$$J_i = K_{ij}{}^1[e^2 E_j + eT\partial/\partial x_j(\zeta/T)] + K_{ij}{}^2/e/T/\partial T/\partial x_j \qquad (14)$$

$$W_i = -K_{ij}{}^3[e^2 E_j + eT\partial/\partial x_j(\zeta/T)] - K_{ij}{}^4/e/T/\partial T/\partial x_j \qquad (15)$$

where now the $K_{ij}$'s are sums of energy integrals over the bands, i.e.

$$8\pi^3 K_{ij}{}^1 = \sum_m (f_{ij}{}^m x_{ii}{}^m), \text{ etc.} \qquad (16)$$

The energy integrals, and hence the transport coefficients can be obtained explicitly by a generalization of an elegant method due to ENSKOG.[8] Let $D^{ij}$ denote the determinant obtained from the matrix $d_{mr,no}{}^{ij}$ where the elements are grouped according to increasing $m$ (and $n$) for a given $r$ (and $s$). Furthermore, let $D_{\alpha\beta}{}^{ij}$ be the determinant obtained from $D^{ij}$ by bordering it with a row of $\alpha_{mr}$ and a column of $\beta_{mr}$, the last diagonal element being zero. Then it is possible to show that the $K_{ij}$ are given by

$$K_{ij}{}^1 = D_{\alpha\alpha}{}^{ij}/D^{ij}, \; K_{ij}{}^2 = D_{\alpha\beta}{}^{ij}/D^{ij},$$
$$K_{ij}{}^3 = D_{\beta\alpha}{}^{ij}/D^{ij}, \; K_{ij}{}^4 = D_{\beta\beta}{}^{ij}/D^{ij} \qquad (17)$$

which is in accordance with the standard results, the only difference being that now we have more rows and columns corresponding to the different values of $(mr, ns)$. The various transport coefficients are then obtained from (17) and the appropriate formulae.

In order to calculate the matrix elements (13), it is necessary to make definite assumptions about the nature of the energy–momentum dependence, such as (1). It is convenient to express (1) in terms of polar co-ordinates with $\mathbf{k}$ as the polar vector, in which case we can write

$$(2m/\hbar^2)\epsilon_n = k^2 g_n(\theta, \phi) \qquad (18)$$

where

$$g_0 = A$$
$$g_{1,2}(\theta, \phi) \qquad (19)$$
$$= A \pm [B^2 + C^2(\sin^4\theta \cos^2\phi \sin^2\phi + \cos^2\theta \sin^2\theta)]^{\frac{1}{2}}.$$

It has not been feasible to carry out the angular integrations for the functions $g(\theta, \phi)$ given by (19) in closed form, but from a study of the constants $A$, $B$ and $C$ it follows that $g_n(\theta, \phi)$ can be expanded in terms of cubic harmonics[9]

$$g_n(\theta, \phi) = F_n{}^2[1 - G_n Y_4{}^c - H_n(Y_4{}^c)^2 \ldots] \qquad (20)$$

where

$$Y_4^c = P_4(\cos\theta) + /1/168/P_4^4(\cos\theta)\cos 4\phi \quad (21)$$

$P_m^n$ being the Legendre polynomials of the first kind and $F_m$, $G_m$ appropriate combinations of the constants $A$, $B$ and $C$.*

If we restrict ourselves to directions of the electric field and temperature gradient parallel to the $z$-direction, which can be done without loss of generality in the absence of magnetic fields, we obtain for the integrals $\alpha_{mr}$ and $\beta_{mr}$ up to first order in the expansion (20)

$$\alpha_{mr} = \frac{\pi^3(2r+3)!!}{3h2r} n(kT)^r F_m^{-5} \quad (22)$$

with similar expressions for $\beta_{mr}$ obtained by replacing $r$ by $r+1$ in (22).

For the evaluation of the matrix elements $d_{mr,no}{}^{ij}$ (13) we require the explicit form of the operator $L_{mn}$ obtained by generalizing the standard expression to several surfaces.[10] It is given by

$$L_{mn}(\Phi) = 1/kT \int U(\mathbf{k}_m, \mathbf{k}'_n) f_{0m}(1-f'_{0n}) \times$$
$$\times [N_0\delta(\epsilon_m - \epsilon'_n + \hbar\omega_q) + (N_0+1)\times \quad (23)$$
$$\times \delta(\epsilon_m - \epsilon'_n - \hbar\omega_q)](\Phi'_n - \Phi_m)\, d\mathbf{k}'_n.$$

Let $\theta$ be the angle between $\mathbf{k}$ and $\mathbf{k}'$, $\alpha$ and $\beta$ the angles between $\mathbf{k}$ and $\mathbf{k}'$ and the $k_z$-axis respectively, and let $\phi$ be the angle between the plane containing $\mathbf{k}$ and the $\mathbf{k}_z$-axis, and the plane containing $\mathbf{k}$ and $\mathbf{k}'$. For this spherical triangle we have

$$\cos\beta = \cos\alpha\cos\theta + \sin\alpha\sin\theta\cos\phi. \quad (24)$$

Furthermore, if $\omega$ and $\gamma$ are the azimuthal angles of $\mathbf{k}$ and $\mathbf{k}'$ (with the $k_z$-axis) we also have

$$\sin\beta\sin(\omega-\gamma) = \sin\theta\sin\phi. \quad (25)$$

It is thus possible to express any functions of the angles $\beta$, $\gamma$ in terms of the relative angles $\alpha$ and $\omega$ by (24) ,(25) and the addition formula for Legendre functions.[11] In order to make use of the $\delta$-functions, it is necessary to change $k$ and $k'$ into $\epsilon$ and $\epsilon'$ through (18), which gives rise to the presence of the functions $g_m(\alpha, \omega)$ and $g_n(\beta, \gamma)$ in the integrand of (23). Using the expansion (20) and the properties of the Legendre functions the angular integration over $\phi$, $\omega$ and $\alpha$ can be readily carried out and results in expressions of the form

$$I_{mn}{}^1(\cos\theta) = \int \cos\alpha\, d\alpha \int g_m{}^{-2}(\alpha, \omega)\, d\omega \int \cos\beta g_n{}^{-2}(\beta, \gamma)\, d\phi = \sum_{t=0}^{2} a_{mn}{}^{2t+1}(\cos\theta)^{2t+1}$$

$$I_{mn}{}^2(\cos\theta) = \int \cos^2\alpha\, d\alpha \int g_m{}^{-5/2}(\alpha, \omega)\, d\omega \int g_n{}^{-3/2}(\beta, \gamma)\, d\phi = \quad (26)$$

$$\sum_{t=0}^{2} a_{mn}{}^{2t}(\cos\theta)^{2t}$$

where the coefficients $a_{mn}{}^t$ for the various bands have been obtained, but are not given here for lack of space. The integration over $\theta$ is replaced by integration over $x$ through*

$$x^2 u = \eta + \eta' - 2(\eta\eta')^{\frac{1}{2}}\cos\theta \quad (27)$$

where we have defined

$$x = \hbar\omega/kT,\ \omega = c_s q,\ \eta = \epsilon/kT \text{ and } \eta' = \epsilon'/kT$$

The integration over $\eta'$ can now be carried out with the use of the delta functions giving two contributions corresponding to $\eta' = \eta \pm x$ which can be combined into one integral between the limits $\Theta/T$ and $-\Theta/T$, where $\Theta$ is the effective Debye temperature, yielding for $d_{rm,ns}$

$$d_{mr,ns} = \int_0^\infty \eta^{r+\frac{1}{2}} e^{-\eta}\, d\eta \int_{-\Theta/T}^{\Theta/T} W(m, n)(1 - Ce^{-\eta}) \frac{x^2\, dx}{|1-e^{-x}|} [(\eta+x)^{s+\frac{1}{2}} I_{mn}{}^1 - \eta^{s+\frac{1}{2}} I_{mn}{}^2] \quad (28)$$

* Lack of space does not permit us to give any numerical results at this time.

* As our approximation is only valid up to first orders in $Y_4{}^c$ it is sufficient to use the zeroth order approximation in replacing $k$ by $\epsilon$.

Here $W(m, n)$ denotes the probability for transitions from band $m$ to $n$.[12]* The integration over $\eta$ involves integrals of the form

$$I_{m,n,p} = \int_0^\infty d\eta e^{-m\eta}\eta^p/(x+\eta)^n \qquad (29)$$

which can be reduced to elementary functions and $Ei(-x)$ integrals, leaving only the integration over $x$. Except for very low temperatures which are of no interest, since the conductivity is negligible there, we can expand the integrand in powers of $x$, and then integrate term by term. It can be shown that the $x$-integrals involved can be reduced to the $J$-integrals which have been tabulated elsewhere.[13]

We are now in the position to evaluate the matrix elements for the various energy bands ($m, n = 0, 1, 2$) and powers of the expansion in the energy ($r, s = 0, 1, 2$ etc.) and obtain the energy integrals (17) and thus the transport coefficients. Details of the calculations and final numerical results will be given elsewhere.

* We are indebted to Dr. Price for drawing our attention to this paper.

## REFERENCES


1. Blatt F. J., *Solid State Physics* **4,** 200 (1957).
2. Lax B., *Rev. Mod. Phys.* **30,** 122 (1958) and refs. given there.
3. Dresselhaus G., Kip A. F. and Kittel C., *Phys. Rev.* **95,** 568 (1954); *Ibid.* **98,** 368 (1955).
4. Wilson A. H., *The Theory of Metals.* University Press, Cambridge (1954).
5. Kohler M., *Z. Phys.* **124,** 772 (1948); *Ibid.* **125,** 679 (1949).
6. Ziman J. M., *Canad. J. Phys.* **34,** 1256 (1956).
7. Sondheimer E. H., *Proc. Roy. Soc.* A**203,** 75 (1950).
8. Enskog D., Dissertation Upsala (1917).
9. Davis L., *Phys. Rev.* **56,** 93 (1939).
10. Mott N. F., *Proc. Roy. Soc.* A**151,** 699 (1936).
11. Jahnke E. and Emde F., *Tables of Functions.* Dover Publications, New York (1943).
12. Ehrenreich H. and Overhauser A. W., *Phys. Rev.* **104,** 331 (1956).
13. MacDonald D. K. C. and Towle L. T., *Canad. J. Phys.* **34**, 418 (1956).

*J. Phys. Chem. Solids* Pergamon Press 1959. Vol. 8, pp. 142–146. Printed in Great Britain

SESSION F:
DISLOCATIONS*

# F.1 ELECTRONIC PROCESSES AT GRAIN BOUNDARIES

L. SOSNOWSKI
Institute of Physics, Warsaw, Poland

**Abstract**—The electrical properties of grain boundaries of several kinds, such as the low angle boundary and the coherent and incoherent twin boundaries, will be discussed in connection with experimental work on Si and Ge crystals.

The nature of the boundaries was established by optical, X-ray, and electron microscopy methods. Diffusion of minority carriers, recombination rates, photovoltaic effects, and transient phenomena were investigated. The occurrence of *n–p–n* junctions at some types of boundaries is assumed. The experimental data are discussed in terms of the density of electronic states at the boundary.

VOL
8
195

INVESTIGATIONS of electronic phenomena occurring at intercrystalline boundaries have been going on for some time at our laboratory in Warsaw.† Some of the results were reported at the recent Brussels Conference.[1] I shall summarize these briefly before discussing more recent studies.

The work has been carried out on silicon and germanium of both *n*- and *p*-types. Samples were prepared either by growing crystals from a suitable seed or by zone melting a single crystal. In this way one obtains twin crystals containing low-angle and high-angle boundaries. Samples of regular form (usually $10\times2\times0{\cdot}5$ mm) were cut from such crystals with a boundary perpendicular to the longest dimension of the sample. The boundaries were made visible under either an optical or an electron microscope by appropriate etching; the crystallographic orientations of both parts of the bicrystal were established by X-ray diffraction methods.

The occurrence of two kinds of boundaries, of essentially different electronic properties, was found. We shall call them henceforth boundaries of type I and type II. Type I corresponds to low-angle dislocation boundaries; type II to high-angle boundaries and incoherent twins.

Type I boundaries act as regions of enhanced recombination. This behaviour of the grain boundary has been observed by many authors (VOGEL *et al.*[2]). The diffusion curve shows a sudden drop at the boundary, when measured in the direction perpendicular to the boundary. Along the boundary one observes a marked decrease in the diffusion length. A typical case is shown in Fig. 1.

Assuming that surface recombination at the grain boundary equals $S$, and putting $\alpha_1$ and $\alpha_2$ for the angles of inclination of tangents to the diffusion curve at the grain boundary, the boundary condition takes the form:

$$\operatorname{tg}\alpha_1-\operatorname{tg}\alpha_2 = S/D.$$

Owing, however, to the finite size of a generating light spot, these angles could not be accurately measured directly. Solving the diffusion equation:

$$\frac{\partial^2 p}{\partial x^2}-\frac{p}{L^2}=0,$$

with the above boundary conditions, and putting $\log K = \log p_{1e}-\log p_{2e}$, where $p_{1e}$ and $p_{2e}$ are values at the boundary of extrapolated linear parts of the diffusion curve, one obtains:

$$\frac{S}{D}=\frac{2K-1}{L_1}-\frac{1}{L_2}.$$

$K$, $L_1$, and $L_2$ could be read off directly from the graph.

The values of $S$ are of the order of $10^3$ cm/sec;

* *Chairman*: J. W. MITCHELL; *Co-Chairman*: G. L. PEARSON.

† The work on electronic properties of grain boundaries in germanium has been carried out by T. FIGIELSKI, extended to silicon by M. JASTRZEBSKA; X-rays studies of grain boundaries by J. AULEYTNER amd M. LEFELD; technological group W. GIRIAT (Ge) and T. NIEMYSKI (Si).

for instance, for the case shown in Fig. 1, $S = 790$ cm/sec.

The boundaries of type II, whose properties are the main subject of the present paper, show a number of striking and rather unexpected features.

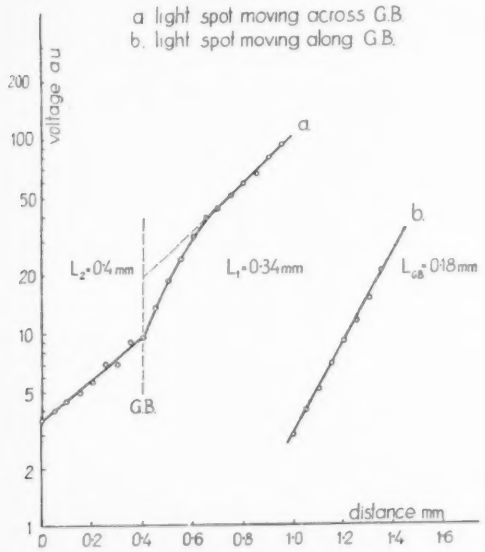


FIG. 1. Diffusion curve for type-I boundary. Collector voltage is plotted versus distance from boundary.
(*a*) Light spot moves in direction perpendicular to boundary.
(*b*) Light spot moves parallel to boundary.

Their main properties are as follows:

(1) Occurrence of a photo-emf when the boundary is asymmetrically illuminated.[3] This photo-emf changes its sign when the light spot crosses the boundary. For *n*-type samples, the illuminated part of the bicrystal becomes negatively charged; for *p*-type, positively (see Fig. 2).

(2) Photoconductivity of a sample shows a pronounced peak when the light spot crosses the boundary. The slope of the logarithm of the photocurrent versus distance from the boundary curve corresponds to the diffusion length of the minority carriers (see Fig. 3).

(3) The transverse diffusion curve shows deviations from regular behaviour;[4, 5] near the boundary one observes usually a maximum of the collector current (see Fig. 4). This deviation from a monotonic fall is connected, however, with the influence of photo voltages on the collector, and can be partly or wholly eliminated by increased

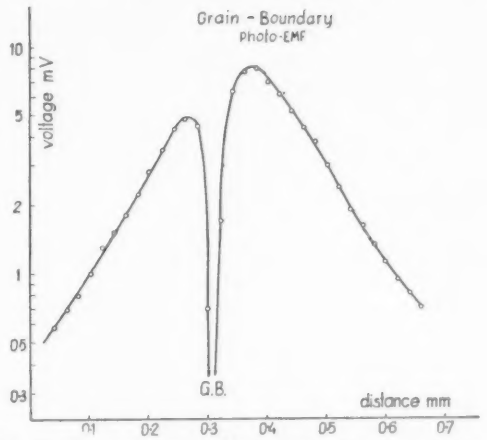


FIG. 2. Photo-emf as a function of light-spot position, type-II boundary. An inversion of sign occurs when light spot crosses the boundary.

collector selectivity for minority carriers or by background illumination of a sample. Corrected diffusion curves do not show any discontinuity at the boundary, thus indicating apparent $S = 0$.

(4) Diffusion length measured along or parallel to the boundary is increased above that of the bulk material. This increase may be so marked that the collector current is almost constant over the whole length of the boundary which amounts to 1–2 mm. Strong background illumination or a polarizing voltage of a few volts applied to the boundary reduces the apparent diffusion length to its normal value (see Fig. 5).

(5) The current/voltage relation for samples

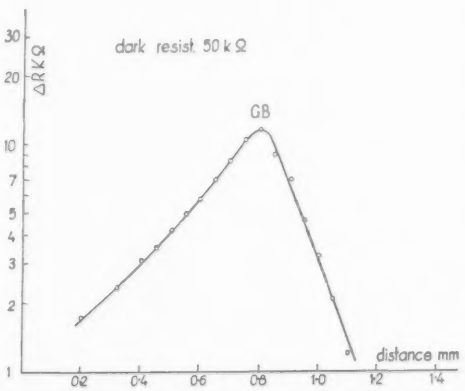


FIG. 3. Change of resistance of a sample under illumination by light spot. Type-II boundary.

containing such boundaries is similar to the diode characteristic in the blocking direction.

The above-mentioned facts lead us to the conclusion that an inversion layer exists at the boundary, i.e. an $n$–$p$–$n$ junction for an $n$-type sample and a $p$–$n$–$p$ junction for a $p$-type. We take for

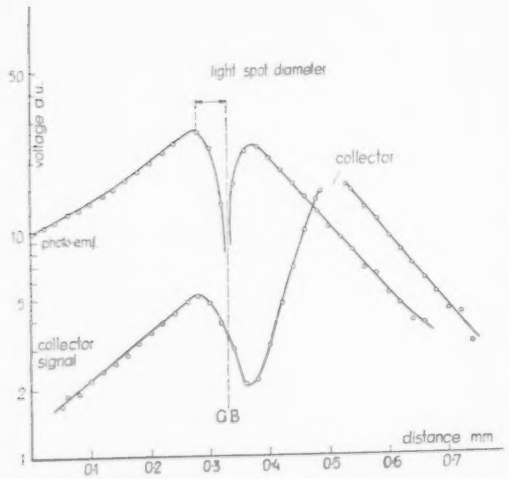


FIG. 4. Transverse diffusion curve for type-II boundary. Note maximum in the vicinity of the grain boundary. A photo-emf curve for the same boundary is shown for comparison.

further discussion the first case, i.e. an $n$–$p$–$n$ junction.

Let us assume an $n$-type semiconductor with a potential barrier at the boundary of height $\phi$. We put $\psi$ for the electrostatic potential and $e\Phi$ for the Fermi level. $w$ is the width of a boundary region, which we assume is small compared with the diffusion length $L$. The photo-emf, $V$, will depend on separation by the barrier of holes and electrons. Assuming that $j_0$ is a current of holes produced by light and crossing the boundary, one might obtain $V$ from the equilibrium condition $j_0+j_+=j_-$, where $j_+$ and $j_-$ are the diffusion currents of holes and electrons respectively. After simple calculations one obtains, for small illumination:

$$V=\frac{kT}{e}\,\frac{j_0 w}{D_+ p}\left\{1+b\exp\frac{e}{kT}[2(\Phi-\psi)-\phi]\right\}^{-1}$$

$$=Aj_0\left(1+b\frac{n}{p_b}\right)^{-1};$$

where $b=\mu_e/\mu_h$, $n$ is the density of electrons in the bulk of the sample and $p_b$ is the density of holes in the boundary region. From the above formula one can see that appreciable values of $V$ occur only when $p_b \geqslant n$, i.e. when the boundary is of the $n$–$p^+$–$n$ type.

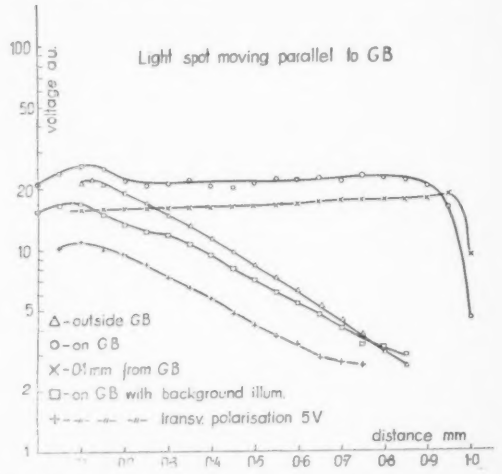


FIG. 5. Longitudinal diffusion curve for type-II boundary. Note practically constant value of collector signal when light spot moves along the boundary.

As the occurrence of the photo-emf is the most important feature of grain boundaries of type II, we are forced to assume the existence of a $p^+$ region at such a boundary. This assumption is sufficient to explain all other features of this type of grain boundary.

The irregular behaviour of the diffusion curve can then be connected with the "feed-in feed-out effect", first noticed by MOORE and WEBSTER for $n$–$p^+$ junctions.[6] Essential to the "feed-in, feed-out effect" (hereafter ffe) is the interaction between the holes and their electrostatic field; the hole entering the $p^+$ region disturbs, by its charge, the barrier-layer potential and thus causes the expulsion from the $p^+$ region of some other hole. Thus the transfer of holes through the boundary region is, in this case, essentially not a diffusion process.

Let us assume that the disturbance of the barrier height caused by one hole is equal $\delta\phi$. In the stationary state $\phi$ must, of course, be constant, and $\delta\phi$ must be compensated either by an incoming electron or by an outgoing hole. Calculating the

diffusion currents of holes and electrons caused by the change of the barrier height, $\delta\phi$, one obtains for the probability of expulsion of a hole:

$$W_p = \left(1+b\frac{n}{p_b}\right)^{-1}.$$

Ffe is effective when $W_p \simeq 1$. As the expression for $W_p$ is identical with the binomial coefficient for the photo-emf, one can see that both these effects should occur simultaneously. At a grain boundary showing photo-emf, the ffe should be effective and vice versa. Of course, the recombination of a hole in the boundary region will have no influence on a hole current crossing the grain boundary; thus the ffe explains immediately the continuity of the transverse diffusion curve.

One can also understand the apparent increase of the longitudinal diffusion length. Let us follow the propagation along the boundary region of a small potential disturbance caused by injection of some holes at one point. The problem is analogous to that of a transmission line, with capacity per unit length $\alpha$, and conductivity $\xi$. One has also to introduce a damping constant $\chi$ accounting for leakage of holes from the boundary region to the bulk material. We look for a stationary solution of the differential equation:

$$\alpha\frac{\partial\Phi}{dt} = \zeta\frac{\partial^2\Phi}{\partial z^2} - \chi\Phi, \text{ where } \Phi = \phi - \phi_0$$

is the measure of the deviation from equilibrium.

For a stationary state $\partial\Phi/\partial\chi = 0$, and one obtains solutions in the form $\Phi = \Phi_0 e^{-2/\lambda}$ with $\lambda = \xi/\chi$. Simple considerations give:

$$\chi = \frac{\sigma_m}{L}\left(1+b\frac{n}{p_b}\right),$$

where $\sigma_m = e\mu_h p$ is the minority-carrier contribution to the conductivity of the bulk material. For boundaries of type II, such as we are now considering, one may put $1+b(n/p_b) \simeq 1$. Then:

$$\lambda/L = \left(\frac{\sigma_b}{\sigma_m}\frac{w}{L}\right)^{\frac{1}{2}},$$

where $\sigma_b$ is the conductivity along the boundary layer, and $w$ is the barrier width.

Putting $\mu_b = \chi\mu$; $p_b/n = \gamma$, one finally obtains

$$\frac{\lambda}{L} = \left(\chi\cdot\gamma\cdot\frac{w}{L}\right)^{\frac{1}{2}}\frac{n}{n_i}.$$

We do not know the exact values of $\chi$, $\gamma$, or $w$.

However, making reasonable estimations ($w \sim 100-1000$ Å, $\gamma \sim 100$, $\chi \sim 1$) one can easily obtain $\lambda \simeq (10-100)L$, which is amply sufficient to account for the observations.

Further information can be gained from investigations of transient phenomena. Experimental data are shown in Fig. 6. The square-wave voltage

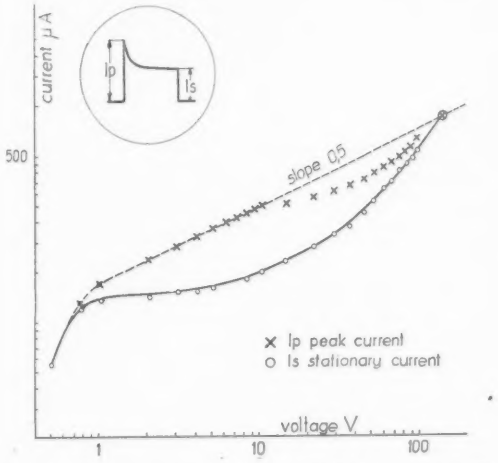


FIG. 6. Square-wave voltage applied to type-II boundary. Note that peak current is proportional to $V^{\frac{1}{2}}$ in the middle of the voltage range.

pulses have been applied through ohmic electrodes to a sample containing a type II boundary and the current through the sample observed on the screen of an oscilloscope. The circuit constants were so adjusted that the initial peak of the current corresponded to charging of a boundary. Crosses on the graph represent the peak values, circles, stationary values of a current.

No initial peak appears for low voltages applied to the barrier.

For voltages in the range 1–20 V the peak follows a $V^{\frac{1}{2}}$ law; for voltages of about 100V it disappears again. The last value of the voltage agrees with the crossing point of an extrapolated $V^{\frac{1}{2}}$ line with the experimental curve.

Let us estimate the influence of an applied voltage on the charge and potential height of the boundary layer. Let the density of electrons in surface states be equal to $S$ cm$^{-2}$, and let the maximum concentration of holes in the boundary

region be $p_0$ cm$^{-3}$. Then from the solution of the Poisson equation one obtains the relation:

$$\left(\phi - \frac{kT}{e}\right) + \frac{kT}{e}\frac{P_0}{n} = \frac{\pi e}{2\epsilon}\frac{s^2}{n},$$

where $\epsilon$ is the dielectric constant.

We may introduce now the concept of effective concentration of holes per unit area, partly compensating the negative surface charge:

$$p_{ef} = \int p d\chi \simeq \left(\frac{\epsilon}{2\pi e n \phi \beta^2}\right)^{\frac{1}{2}} p_0,$$

where $\beta = e/kT$. Putting

$$\phi = \frac{\pi e s^2_{ef}}{2n\epsilon},$$

and assuming $(kT/e)p_0 < n\phi$, one obtains $s_{ef} = sp_{ef}$.

One can consider thus, that the barrier height $\phi$ depends on the total charge $es_{ef}$ in the boundary region, which is equal to the difference between the charge of electrons in surface states and the charge of holes in the inverson layer.

To account for the influence of an applied voltage, $V$, we shall consider a parabolic potential barrier caused by the effective charge $es_{ef}$.

Let $\phi_0$ be the height of the boundary barrier when the external voltage is zero and $\phi$ the height when the external voltage is $V$. Let $es_{ef}{}^0$ and $es_{ef}$ be the corresponding charge densities. Putting $k^2 = (\pi e/2u\,\epsilon)s^2_{ef}$, we have $\phi = (k - eV/hk)^2$ with $\phi_0 = k_0{}^2$. The numbers of electrons in surface states is an increasing function of $\Delta\phi = \phi_0 - \phi$. That is $s = f(\Delta\phi)$. The exact shape of the function $f$ depends on the energy spectrum of the surface states. For a single energy level:

$$S = n_s f = n_s[\exp(E_s - \Phi + \phi)\beta + 1]^{-1};$$

where $n_s$ is the number of surface states of energy $E_s$. For high energy levels one obtains approximately

$$S = S_0 e^{-\beta\Delta\phi}; \text{ thus } \phi = (k_0 e^{\beta\Delta\phi} - V/nk_0 e^{-\beta\Delta\phi})^2.$$

According to this formula the dependence of $\phi$ on $V$ is a very small one; for not too high voltages $\Delta\phi \simeq V/4\beta\phi_0$; for high voltages $\Delta\ \phi = (1/2\beta)\log V/2\phi_0$. In this range $k \sim V^{\frac{1}{2}}$ in agreement with our experimental results for the range of 2–50 V. When, however, the surface states become saturated, i.e. $f \simeq 1$, $s$ becomes constant and nearly equal to $n_s$ and the barrier height quickly drops. In this condition the peak in Fig. 6 should disappear. From the value of voltage at which the peak disappears, we can estimate the density of surface states, which for most samples is of the order of magnitude of $10^{11}$–$10^{12}$ cm$^{-2}$.

The simple assumption of a single energy level of surface states does not seem to account for all of the observed facts. The experimental data for the dependence of longitudinal diffusion length on applied voltage, and the current/voltage characteristic of the photocurrent show that in the range 0·5–2 V the barrier height falls considerably. The photocurrent voltage characteristic is shown in Fig. 7. Note the strong increase of the current at some fairly low voltage, which varies from sample to sample. This behaviour of the photocurrent indicates that the electronic component of a current becomes appreciable at these fairly low voltages, which is possible only when $\phi$ decreases by some $kT/e$ below its initial value. One may hope to obtain from such measurements an energy spectrum for the boundary surface states.

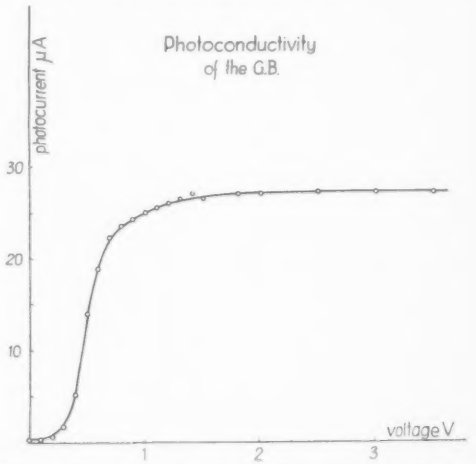


FIG. 7. Photocurrent versus voltage characteristic for type-II grain boundary.

VOL
8
195

## REFERENCES

1. FIGIELSKI T. and SOSNOWSKI L., *International Conference on Solid State Physics in Electronics and Telecommunications. Brussels* (June 1958).
2. VOGEL F. L., READ W. T., and LOVELL, L. C., *Phys. Rev.* **94,** 1791 (1954).
3. PEARSON G., *Phys. Rev.* **76,** 459 (1949).
4. MATARÉ H. F., *Z. Naturf.* **10a,** 640 (1955).
5. MATARÉ H. F., *Z. Natur.* **11a,** 876 (1956).
6. MOORE A. R. and WEBSTER W. M., *Proc. Inst. Radio Engrs.* **43,** 427 (1955).

*J. Phys. Chem. Solids* Pergamon Press 1959. Vol. 8. pp. 147–149. Printed in Great Britain

# F.2 THE MOBILITY, DIFFUSION CONSTANT, AND LIFETIME OF MINORITY CARRIERS IN HEAVILY DISLOCATED GERMANIUM

A. F. GIBSON

Royal Radar Establishment, Malvern, England

## 1. INTRODUCTION

BELL and HOGARTH[1] have shown that the diffusion length, $L$, of minority carriers in germanium and silicon, measured by the travelling-light-spot technique, may be anisotropic if the crystal contains a high density of parallel edge dislocations. The diffusion length measured parallel to the dislocation array was typically a factor of two or three greater than that measured perpendicular to the array.

It is well known that dislocations in germanium or silicon crystals act as efficient recombination centres (WERTHEIM and PEARSON[2]). As BELL and HOGARTH[1] point out, however, a significant anisotropy in carrier lifetime, assuming the diffusion constant to be isotropic, can be obtained only if two additional assumptions are made, namely:

(*a*) The dislocations are largely polygonized into "walls", and

(*b*) the dislocations are surrounded by a potential barrier which tends to exclude minority carriers from the high recombination region.

The object of the work to be described in the present paper was, primarily, to check the validity of the assumption that the diffusion constant, $D$, is isotropic and equal to the normal value in heavily dislocated material. Two approaches to the measurement of $D$ have been made, namely drift-mobility measurements and the simultaneous measurement of phase and amplitude in the travelling-light-spot experiment. We shall show that in $n$-type germanium $D$ is not isotropic. In $p$-type germanium, on the other hand, $D$ is isotropic and all the anisotropy appears to reside in the lifetime, $\tau$. In addition measurements of drift mobility at high electric fields will be described, the results obtained giving valuable quantitative support for the model proposed.

## 2. EXPERIMENTAL RESULTS

The experimental results for germanium are summarized in Table 1.

*Table* 1.

| Experimental Method | Results | |
|---|---|---|
| | Holes in $n$-type Ge | Electrons in $p$-type Ge |
| Travelling light spot | $L_\parallel > L_x$<br>$D_\parallel > D_x = D_0$<br>$\tau_\parallel \approx \tau_x$ | $L_\parallel > L_x$<br>$D_\parallel = D_x = D_0$<br>$\tau_\parallel > \tau_x$ |
| Drift mobility at low fields ($E < 100$ V/cm) | $\mu_\parallel = \mu_x = \mu_0$<br>$D_\parallel > D_x = D_0$ | |
| Drift mobility at high fields (100 V/cm $< E <$ 5000 V/cm) | $\mu_x < \mu_\parallel = \mu_0$ | $\mu_\parallel = \mu_x = \mu_0$ |
| Electrical resistance | Isotropic | |

(a) *Travelling-light-spot experiments*

By the simultaneous measurement of phase and amplitude, using "chopped" light, the diffusion constant and lifetime of injected carriers can be obtained separately in this experiment. As shown in Table 1, the diffusion constant of holes in $n$-type germanium was found to be about two or three times greater parallel to the dislocation array than across it, the latter having the normal diffusion constant. No comparable effect was observed in high-resistivity $p$-type germanium, all the anisotropy in diffusion length being accounted

for by an anisotropy in effective electron lifetime.

(b) *Low-field drift-mobility experiments*

In view of the above results, the drift mobility of holes in *n*-type germanium was measured by the HAYNES–SHOCKLEY[3] technique in filaments cut parallel and perpendicular to the dislocation array. In the same experiment the diffusion constant could be deduced from the broadening of the hole pulse arriving at the collector. As shown in Table 1, the diffusion constant was found to be anisotropic, in agreement with the travelling-light-spot data, but the drift mobility, at least at low fields, was isotropic. It would appear, therefore, that the Einstein relation between $D$ and $\mu$ is not applicable to heavily dislocated *n*-type material.

## 4. DISCUSSION OF RESULTS

SHOCKLEY[5] has suggested that the dangling bonds associated with edge dislocations produce a row of acceptor levels. If a significant fraction of these levels are occupied, the potential energy of electrons is raised locally and the dislocation may be considered as a thread of *p*-type material embedded in the crystal. We shall now show, qualitatively, that this model can account for our results.

(a) *N-type germanium*

As a *p*-type region in an *n*-type bulk crystal represents a potential minimum for holes, injected carriers will be captured by the dislocations where they will become majority carriers. For space-charge compensation, another hole will be

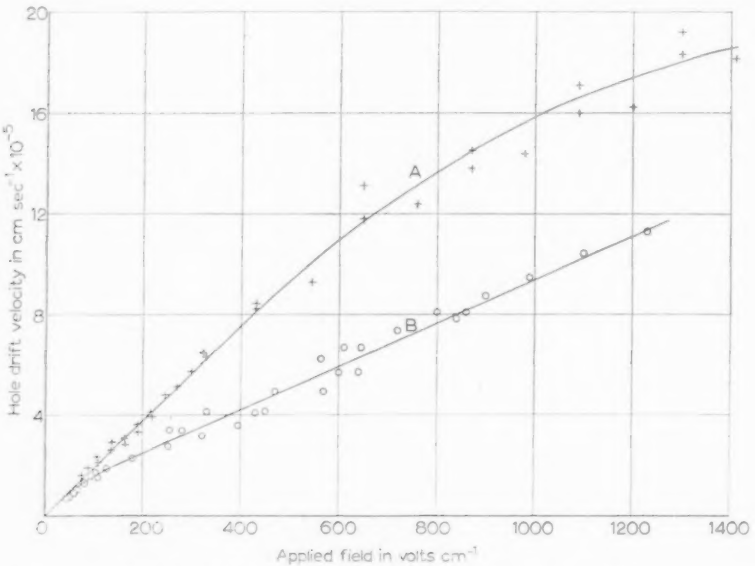


FIG. 1. Drift velocity of electrons parallel (curve A) and perpendicular (curve B) to dislocation arrays in germanium.

At high electric fields ($E > 100$ V cm$^{-1}$), some anisotropy in the drift mobility of holes was observed. The drift mobility was measured by the technique described by GIBSON and GRANVILLE[4] and some typical results are shown in Fig. 1. The mobility parallel to the dislocation array (curve A) is the same as that in undislocated material, whereas that across the dislocation array (curve B) is significantly less.

emitted somewhere along the line.* Release of a hole will occur with equal probability on either side of the point of capture, so that, in the absence of an external field, the mean position of the hole is unaffected. It follows therefore that dislocations provide a mechanism for enhanced diffusion of

* Compare the propagation of a hole through a "floating" *p* region on *n* material (MOORE and WEBSTER[6]).

holes along the dislocations without any increase in hole mobility, so that the Einstein relation is not applicable to this system. Clearly the dislocations cannot assist the diffusion of holes perpendicular to the dislocation array.

In as much as the dislocations act as traps for holes, the drift mobility in *n*-type germanium will be reduced by the dislocations. A trap of finite dimensions is effective, however, only if an untrapped carrier drifts in the applied field a distance greater than the dimensions of the trap in the mean escape time of the trap. This condition will be achieved at relatively low fields for drift across the dislocations, and is the basis of the interpretation of the results shown in Fig. 1. The data given in this figure indicate that the dislocations have an effective diameter of about $0{\cdot}8\times10^{-4}$ cm and that, in a sample containing $10^6$ dislocations per cm$^2$, a hole spends about half its total life trapped at a dislocation.

The above interpretation of enhanced diffusion has been developed quantitatively by GIBSON and PAIGE.[7] The dislocation in *n*-type material will be surrounded by a *p*–*n* junction and may be treated as a coaxial line formed from iterative elements of the form shown in Fig. 2. The capacity

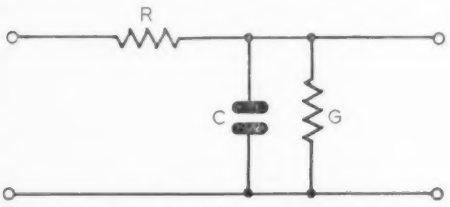


FIG. 2. Equivalent circuit for one element of a transmission line analogue of a dislocation in *n*-type germanium (see text).

*C* and conductance *G* per unit length of the *p*–*n* junction may be calculated from *p*–*n* junction theory in cylindrical co-ordinates, the diameter of the space-charge cylinder being known from the high-field drift-mobility data. The resistance per unit length of the inner conductor is calculated on the assumption that the occupation density of the acceptor levels is about 10 per cent (READ[8]). The results indicate that, with a dislocation density of about $10^6$ cm$^{-2}$, the diffusion constant of holes parallel to the dislocations will be about 100–200 cm$^{-2}$ sec$^{-1}$, in adequate agreement with the experimental data. If polygonization of the dislocations is assumed, two additional adjustable parameters become available and a much larger anisotropy in diffusion constant can be accounted for.

(b) *P-type germanium*

In *p*-type material the dislocations are, of course, still *p*-type. However, the negative charge density along the dislocation may be significantly higher than the acceptor density in the high-resistivity bulk material, so that there is still a space-charge region in which the electron potential energy is increased. The presence of this barrier will impede the capture of minority carriers (electrons) by the dislocations and, following the argument given by BELL and HOGARTH, provides a mechanism by which $\tau$ may be anisotropic. The dislocations will clearly have no significant effect on the diffusion constant of the electrons, however, and no anisotropy of *D* can be expected.

*Acknowledgments*—In preparing this contribution I have drawn on the results of various colleagues at R.R.E., notably Mr. J. B. ARTHUR, Dr. J. W. GRANVILLE, and Dr. E. G. S. PAIGE. We are in turn indebted to Mr. P. J. HOYLAND, who supplied the dislocated crystals. The paper is published by permission of the H.B.M. Stationery Office, London.

## REFERENCES

1. BELL R. L. and HOGARTH C. A., *J. Electronics and Control* **3**, 455 (1957).
2. WERTHEIM G. K. and PEARSON G. L., *Phys. Rev.* **107**, 694 (1957).
3. HAYNES J. R. and SHOCKLEY W., *Phys. Rev.* **81**, 835 (1951).
4. GIBSON A. F. and GRANVILLE J. W., *J. Electronics* **2**, 259 (1956).
5. SHOCKLEY W., *Phys. Rev.*, **91**, 228 (1953).
6. MOORE A. R. and WEBSTER W. M., *Proc. Inst. Radio Engrs.* **43**, 427 (1955).
7. GIBSON A. F. and PAIGE E. G. S., *Phil. Mag.* (to be published).
8. READ W. T., *Phil. Mag.* **45**, 775 (1954).

*J. Phys. Chem. Solids* Pergamon Press 1959. Vol. 8. pp. 150–153. Printed in Great Britain

# F.3 RECOMBINAISON RADIATIVE PAR L'INTERMÉDIAIRE DES DISLOCATIONS DANS LE GERMANIUM

C. BENOIT À LA GUILLAUME

Laboratoire de Physique, Ecole Normale Supérieure, Paris, France

## 1. INTRODUCTION

L'ÉTUDE de la lumière émise par la recombinaison des porteurs en excès dans le germanium est un moyen d'analyse très puissant des processus de recombinaison.

Dans le germanium, on distingue deux types de processus:

(*a*) La recombinaison bande à bande, qui doit s'effectuer avec émission ou absorption d'un phonon pour assurer la conservation de la quantité de mouvement. La vitesse de recombination par ce processus est de la forme:

$$R_1 = A(np - n_i^2),$$

$n$ et $p$ désignant les densités d'électrons et de trous libres. $A$ est un coefficient que l'on peut calculer à partir du coefficient d'absorption $\alpha(E)$.[1] A dépend peu de la température ($A \sim 3 \cdot 10^{-14}$). Ce processus est radiatif, et l'émission correspondante a été observée dès 1952.[2, 3]

(*b*) La recombinaison par l'intermédiaire de centres recombinants, l'énergie de l'électron lié au centre étant située dans la bande interdite. SHOCKLEY *et al.*[4, 5] ont calculé la vitesse de recombinaison par ce processus

$$R_2 = \frac{N_t C_n C_p (np - n_i^2)}{C_n(n+n_1) + C_p(p+p_1)}.$$

$N_t$ désigne la densité de centres recombinants, $C_n$ et $C_p$ les probabilités de capture d'un électron libre par un centre vide et d'un trou libre par un centre occupé, $n_1$ et $p_1$ les densités d'électrons et de trous libres dans du germanium à l'équilibre lorsque le niveau de Fermi est sur les centres.

## 2. COMPÉTITION ENTRE CES DEUX PROCESSUS

On a calculé, dans le cas d'une jonction $p$–$n$ (la région $p$ étant fortement dopée) plane, polarisée dans le sens direct et à fort niveau d'injection, les nombres $N_1$ et $N_2$ de paires électron–trou qui se recombinent par cm$^2$ et par seconde par ces deux processus.

L'excès de porteurs $\delta(x)$ obéit à l'équation:

$$D\frac{d^2\delta(x)}{dx^2} = A\delta^2(x) + B\delta(x).$$

$D$ est le coefficient de diffusion, $A\delta^2(x)$ est le terme de recombinaison bande à bande, $B\delta(x)$ est le terme de recombinaison par centres (pour $\delta \gg n_0$).

On obtient:

$$\left.\begin{aligned} N_1 &= \tfrac{2}{3}C(\beta^3 + 3\beta^2) \\ N_2 &= 3C\beta \\ N_1 + N_2 &= I_0 \end{aligned}\right\} \qquad (1)$$

$I_0$ est la densité de courant, $C = D^{\frac{1}{2}}B^{\frac{1}{2}}A^{-1}$ et $\beta$ un paramètre. Pour $I_0$ assez faible les formules, (1) ($\delta < B/A$) devient:

$$\left.\begin{aligned} N_1 &= \frac{1}{2C}I_0^2 \\ N_2 &= I_0 - \frac{1}{2C}I_0^2 \end{aligned}\right\} \qquad (2)$$

Les intensités correspondantes $J_1$ et $J_2$, exprimées en nombres de photons, seront de la forme: $J_1 = N_1$, $J_2 = \eta N_2$, si on suppose les rendements radiatifs des deux processus égaux respectivement à 1 et $\eta$.

Lorsque $I_0$ est assez faible, la mesure de $J_2$ donne $\eta$ et la mesure de $J_1$ donne $C$, d'où l'on tire $B$ qui est l'inverse de la durée de vie à fort niveau d'injection.

## 3. TECHNIQUE EXPERIMENTALE

Le spècimen de germanium est taillé en forme de sphére de Weierstrass, et on fait une jonction alliée au point de Weierstrass du dioptre. On amèliore ainsi par

un facteur 20 le rendement optique du système.[6] Le spécimen est refroidi, soit dans un cryostat métallique muni d'une fenêtre de quartz ou de KCl, soit dans un Dewar de verre mince partiellement argenté, le spécimen étant plongé dans le réfrigerant ($N_2$ ou $H_2$ liquide). Ce dernier procédé donne une température mieux définie, mais présente quelques inconvénients (raies d'absorption de $H_2$ liquide). Le courant dans le spécimen est modulé en ondes carrées à 13 Hz. La lumière émise est analysée à l'aide d'un spectrographe Perkin–Elmer avec prisme en NaCl et détecteur PbS.

## 4. RÉSULTATS EXPERIMENTAUX

Les résultats suivants ont été obtenus avec un spécimen de germanium monocristallin de type $n$, résistivité 2Ω cm, durée de vie $\tau$ de 70$\mu$sec, densité de dislocations $N_d = 5 \cdot 10^4$ par cm$^2$. Dans ce spécimen, les dislocations jouent un rôle prépondérant dans la recombinaison.[7] La Fig. 1 donne la répartition spectrale de la lumière émise à différentes températures. On observe en plus de la raie bande à bande (vers 0,70 eV), une émission que l'on peut décomposer en plusieurs raies larges qui se situent à 63°K vers 0,50, 0,545, 0,61 et 0,68 eV.

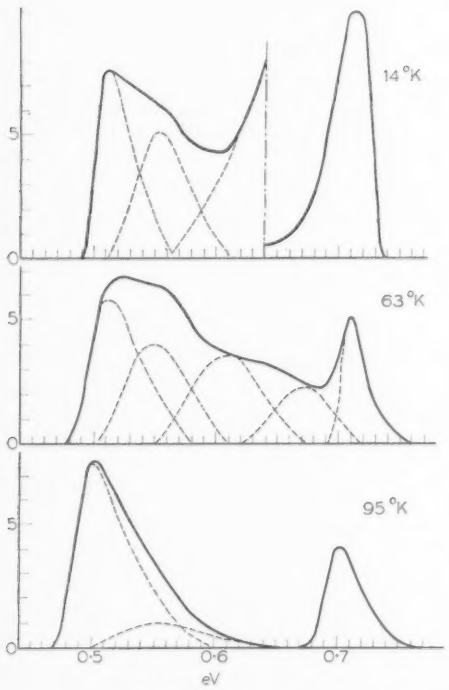


FIG. 1. Répartition spectrale de la lumière de recombinaison dans du germanium contenant $5 \times 10^4$ dislocations par cm$^2$, pour une densité de courant de 0,5 A/cm$^2$, à différentes températures. A 14°K, la raie à 0,71 eV due aux dislocations masque complétement la raie due à la recombinaison bande à bande.

*Procédé de séparation des raies*—On utilise le fait que les intensités de ces différentes raies varient de façon différente en fonction de l'intensité du courant. Soit la répartition spectrale $F(E)$ composée de deux raies $f_a(E)$ et $f_b(E)$:

$$F(E) = af_a(E) + bf_b(E).$$

Formons la combinaison linéaire des répartitions $F_1(E)$ et $F_2(E)$ obtenues pour deux valeurs différentes du courant, $I_1 < I_2$.

$$F_1(E) - yF_2(E) = (a_1 - ya_2)f_a(E) + (b_1 - yb_2)f_b(E).$$

Si les intensités des raies varient de façon différente en fonction de $I$ ($a_1/a_2 \neq b_1/b_2$), en prenant $y = a_1/a_2$, on isole la raie $f_b(E)$ et en prenant $y = b_1/b_2$, on isole la raie $f_a(E)$. Un procédé expérimental permet d'enregistrer directement $F_1(E) - yF_2(E)$: on alimente la source en signaux carrés entre les valeurs $I_1$ et $I_2$ et pendant la demi-période où le courant vaut $I_2$, on obture une fraction $(1-y)$ de la fente d'entrée du spectrographe à l'aide d'une roue dentée.

L'application de ce procédé vers 90°K permet de séparer les deux raies à 0,50 et 0,545 eV qui sont seules présentes à cette température. Puis, vers 63°K, on peut séparer les deux raies à 0,61 et 0,68 eV qui ont alors des lois de variation différente de celle du groupe 0,51 et 0,545 eV.

A 20°K, on note une forte augmentation de la raie à 0,68 eV et un déplacement de son maximum jusque vers 0,71 eV. La Fig. 2 donne la variation de l'intensité de certaines de ces raies en fonction de l'intensité du courant, à 77 et à 20°K. A 77°K, les formules (1) sont assez bien vérifiées, et en faisant coincider les courbes théoriques et expérimentales, en diagramme log–log, on peut en déduire une valeur du rendement radiatif $\eta$ voisine de 0,1.

L'étude de l'intensité de la raie à 0,50 eV entre 100 et 200°K conduit à un rendement radiatif $\eta$ de la forme:

$$\eta = \frac{\eta_0}{1 + a \exp(-W/kT)} \qquad (3)$$

avec $W = 0{,}14$ eV. De plus, l'étude de l'intensité

de la raie bande à bande entre 100 et 300°K permet de conclure que $B$ (inverse de la durée de vie à fort nivau d'injection) croît lorsque $T$ décroît.

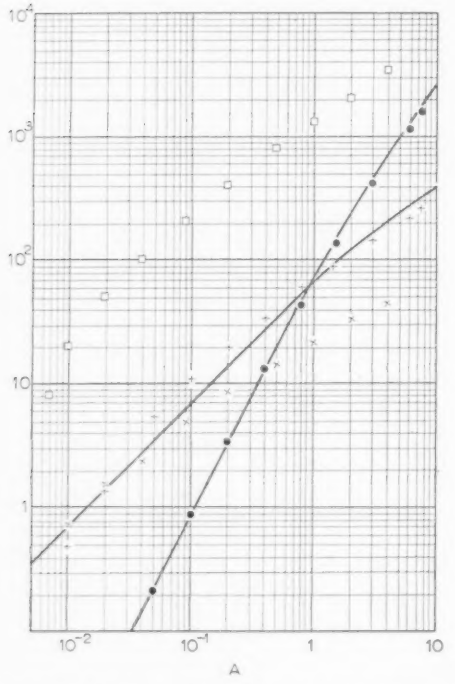


FIG. 2. Variation de l'intensité des raies de recombinaison en fonction de l'intensité du courant. A 77°K = (● raie bande à bande, + raie à 0,50 eV due aux dislocations, et en trait plein les courbes théoriques tirées des formules (1) pour $\eta = 0{,}1$.
A 20°K = X-raie à 0,51 eV, □ raie à 0,71 eV due aux dislocations.

## 5. NATURE DES CENTRES RECOMBINANTS

On a trouvé une bonne corrélation entre l'intensité des raies ci-dessus et la densité de dislocations. Ceci est en bon accord avec les résultats de NEWMAN.[8] D'autre part, l'introduction dans du germanium contenant peu de dislocations, de défauts tels que Cu, Ni, Co, lacunes et intersticielles, ne provoque pas l'apparition de ces raies. Dans le spécimen principalement étudié et contenant $5 \cdot 10^4$ dislocations par cm$^2$, la technique de jonction par alliage introduit une quantité de défauts négligeable. En effet, l'injection optique de porteurs en excès donne les mêmes résultats que l'injection par une jonction alliée.

## 6. MODÈLE PROPOSÉ

On suppose que les dislocations introduisent dans le germanium une série de niveaux d'énergie pour l'électron. A température ordinaire, la recombinaison par les dislocations s'effectue par l'intermédiaire d'un niveau $E_0$ assez profond, proche du milieu de la bande interdite, et ce processus, qui peut être du type de SHOCKLEY–READ, n'est pas radiatif. Lorsque la température des processus de recombinaison par l'intermédiaire de niveaux $E_i^-$ proches de la bande de conduction et $E_j^+$ proches de la bande de valence, interviennent. On suppose que, le long de la ligne de dislocation, se trouvent un certain nombre de sites régulièrement répartis. Un site dans l'état normal (o) peut capter un électron libre au niveau $E_i^-$ pour donner un site $(i)^-$. Le site $(i)^-$ peut alors capter un trou libre au niveau $E_j^+$ pour donner un site $(i.j)^0$. Le site $(i.j)^0$ retombe alors à l'état (O) par émission d'un photon d'énergie $(E_i^- - E_j^+)$. On propose d'identifier les états $E_i^-$ et $E_j^+$ avec les états liés du potentiel de déformation des bandes d'énergie [9] introduit par les compressions et dilatations autour d'une dislocation.[10]

On a pu montrer[11] que l'expression de la vitesse de recombinaison par un couple de niveau $E_i^-$ et $E_j^+$ est de la même forme que celle obtenue dans le modèle de SHOCKLEY–READ et HALL, à condition que la durée de vie de l'état excité $(i.j)^0$ soit assez faible. On a montré aussi que la compétition entre la recombinaison non-radiative par l'intermédiaire de $E_0$ et la recombinaison par l'intermédiaire de $E_i^-$ et $E_j^+$ conduit à un rendement radiatif de la forme (3) avec $W = E_c - E_i^-$ ($E_c$ désigne l'énergie au bas de la bande de conduction) et permet d'expliquer la chute de l'émission pour les faibles valeurs du courant. Ce modèle conduit à une valeur de $B$ croissante lorsque la température décroît. Il conserve aux dislocations un rôle d'accepteur.

Le Tableau 1 donne les valeurs $E_i^-$ et $E_j^+$ proposées (à 20°K).

Le Tableau 2 donne les états excités correspondants aux raies observées. $E_3^-$ et $E_2^+$ désignent en réalité une série de niveaux, ce qui explique le fort déplacement et la forte augmentation de

*Tableau* 1. *Position des niveaux d'énergie introduits par les dislocations*

| $E_c^-$ | $E_i - E_i^-$(eV) | $E_j^+$ | $E_j^+ - E_v$ (eV) |
|---|---|---|---|
| $E_1^-$ | 0,14 | $E_1^+$ | 0,19 |
| $E_2^-$ | 0,095 | $E_2^+$ | 0,05 |
| | 0,05 | | . |
| | . | | . |
| $E_3^-$ | . | | . |
| | . | | 0 |
| | 0 | | |

*Tableau* 2. *Correspondance entre les états excités et l'énergie des raies émises*

| Raies | Etats excités |
|---|---|
| 0,51 | $(1, 1)^0$ |
| 0,555 | $(2, 1)^0$ |
| 0,61 | $(1, 2)^0$, $(2, 1)^0$, $(3, 1)^0$ |
| 0,71 | $(3, 2)^0$ |

l'intensité de la dernière raie lorsque la température décroît de 63 à 20°K.

Je remercie le Professeur P. AIGRAIN qui m'a constammant guidé au cours de ce travail.

**REFERENCES**

1. VAN ROOSBROECK W. et SHOCKLEY W., *Phys. Rev.* **94,** 1558 (1954).
2. HAYNES J. R. et BRIGGS H. B., *Phys. Rev.* **86,** 647 (1952).
3. NEWMAN R., *Phys. Rev.* **91,** 1313 (1953).
4. SHOCKLEY W. et READ W. T., *Phys. Rev.* **87,** 835 (1952).
5. HALL R. N., *Phys. Rev.* **87,** 387 (1952).
6. AIGRAIN P., *Physica* **22,** 1010 (1954).
7. WERTHEIM G. K. et PEARSON G. L., *Phys. Rev.* **107,** 694 (1957).
8. NEWMAN R., *Phys. Rev.* **105,** 1715 (1957).
9. BARDEEN J. et SHOCKLEY W., *Phys. Rev.* **80,** 72 (1950).
10. KULIN S. A. et KURTZ A. D., *Acta Met.* **2,** 354 (1954).
11. BENOIT À LA GUILLAUME C., Thèse (Juin 1958).

*J. Phys. Chem. Solids* Pergamon Press 1959. Vol. 8. pp. 153–157. Printed in Great Britain

# F.4 CENTRES DE RECOMBINAISON INTRODUITS DANS LE GERMANIUM PAR DES ELECTRONS DE 2 MeV

**P. BARUCH**

Ecole Normale Supérieure, Paris, France

NOUS avons cherché à déterminer les propriétés des centres de recombinaison introduits par le germanium à la suite du bombardement par des électrons de 2 MeV. Il s'agit de connaître la position des niveaux dans la bande interdite, les sections efficaces de capture pour les trous et les électrons, et de vérifier s'il y a identité avec les centres, accepteurs et donneurs, dont la présence a été constatée à la suite d'irradiations.[1]

Des expériences analogues, utilisant des neutrons rapides,[2, 3] des rayonnements $\gamma$ du $^{60}Co$,[2] des électrons de 700 à 1000 keV[4] ont été décrites par d'autres auteurs.

Le dispositif expérimental dont nous nous sommes servis comportant un accélérateur Van de Graaff de 2 MeV dont le faisceau traversait une fenêtre mince d'aluminium pour venir frapper les échantillons en germanium de $20 \times 5 \times 1$ mm. La densité de courant moyenne sur l'échantillon était de 0,1 $\mu A/cm^2$. Les échantillons se trouvaient

dans le vide et leur température pouvait être contrôlée entre+100 et −180°C; la plupart des échantillons ont été bombardés à 0°C, quelques-uns à −180°C. On mesurait, entre deux bombardements successifs, la conductivité et la durée de vie. Pour cette dernière mesure, nous avons employé la méthode consistant à découper en impulsions courtes—de 0,5 μsec—le faisceau du Van de Graaff, afin d'introduire un excès de porteurs minoritaires.[5]

L'épaisseur—1 mm—des échantillons a été choisie plus petite que la pénétration—1,8 mm—des électrons de 2 MeV dans le germanium, afin d'éviter de trop grandes inhomogénéités dans la répartition des défauts. En contre-partie, la recombinaison en surface joue un grand rôle dans la mesure de la durée de vie, et, pour minimiser l'importance de cette contribution de surface, nous avons été conduit à prendre des échantillons ayant une faible durée de vie initiale ($\tau < 40$ μsec). Ceci pose d'ailleurs le problème de l'interaction entre les défauts.

Nous avons aussi, occasionnellement, utilisé l'effet "électron-voltaïque"[6, 7] pour évaluer la durée de vie (Fig. 1).

D'après la théorie de SHOCKLEY–READ et HALL,[8] on peut écrire:

$$\frac{1}{\tau} - \frac{1}{\tau_0} = N_t \times f[F, E_t, \sigma_p, \sigma_n] \qquad (1)$$

où $N_t$ est le nombre de centres recombinants, $F$ la position du niveau de Fermi, $E_t$ la position du niveau de recombinaison, $\sigma_p$ et $\sigma_n$ les sections efficaces de capture pour les trous et les électrons. Si la guérison est supposée négligeable, on peut écrire $N_t = \lambda N_b$ où $N_b$ est le nombre total d'électrons par cm² ayant frappé le cristal. On voit qu'en première approximation $1/\tau$ varie linéairement avec $N_b$. Cependant quand $N_t$

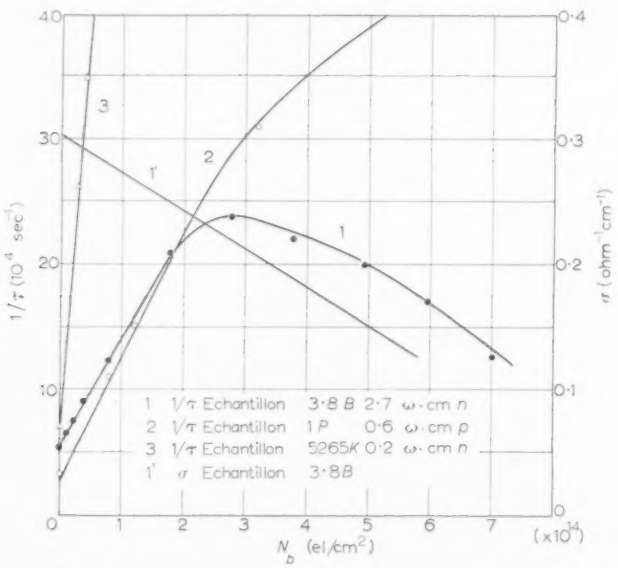


FIG. 1. Courant de court-circuit "électron-voltaïque" d'une diode bombardée à 100°K. La courbe A correspond à un premier bombardement par un faisceau de $4 \cdot 10^{-8}$ A/cm², la courbe B à un deuxième bombardement, avec une intensité de $3{,}3 \cdot 10^{-8}$ A/cm² et aprés un recuit de 15 min à 100°C. Les deux courbes normalisées à la même intensité de faisceau, coïncident initialement, ce qui montre que la guérison est presque totale pour la durée de vie, cependant que le décalage du minimum indique une guérison partielle de conductivité.

atteint une valeur importante devant le nombre de porteurs initial, la conductivité de l'échantillon varie par l'introduction d'accepteurs profonds, en même temps qu'un terme supplementaire en $N_t$ vient modifier légèrement l'expression de SHOCKLEY–READ. On doit donc s'attendre à un écart à la linéarité, qui sera le plus sensible pour un échantillon $n$ de forte résistivité, qui tend, par le bombardement, à devenir intrinsèque. Le degré d'occupation des pièges varie fortement, en diminuant leur efficacité statistique. Cet effet peut s'opposer efficacement à l'introduction de pièges en nombre croissant, conduisant à une inversion de sens de variation et à un minimum de la durée de vie, que WERTHEIM a observé sur un échantillon de silicium,[9] et que nous avons observé sur divers échantillons (Fig. 2), l'exemple le plus frappant étant celui représenté sur la Fig. 1 d'une diode $p$–$n$ (par alliage d'indium) bombardée à température de l'air liquide.

Pour caractériser les centres de recombinaison divers échantillons de concentrations électroniques différentes ont été bombardés, et l'on a tracé la courbe de variation de la durée de vie en fonction de la position initiale du niveau de Fermi. En effet, pour de faibles irradiations ne changeant pas la conductivité, on peut appliquer la théorie de SHOCKLEY–READ et la formule (1) s'écrit, avec les notations de la référence (7):

$$\left[\frac{d(1/\tau)}{dN_b}\right]^{-1}_{N_b=0} = \lambda^{-1}\left[\frac{1}{\alpha_p}\cdot\frac{n_0+n_1}{n_0+p_0}+\frac{1}{\alpha_n}\frac{p_0+p_1}{n_0+p_0}\right].$$

Sur la Fig. 3 on a marqué les points expérimentaux; malgré leur large dispersion, ils se situent bien sur une courbe théorique de SHOCKLEY–READ, tracée ici en traits pleins, avec les valeurs suivantes des paramètres:

$\lambda = 0{,}5\ \text{cm}^{-1}$
(déduit des mesures de conductivité)

$\sigma_p = 16\cdot10^{-16}\ \text{cm}^2$

$\sigma_n = 16\cdot10^{-17}\ \text{cm}^2$

$E_c - E_t = 0{,}18\ \text{eV}$

ou

$E_t - E_V = 0{,}23\ \text{eV}$

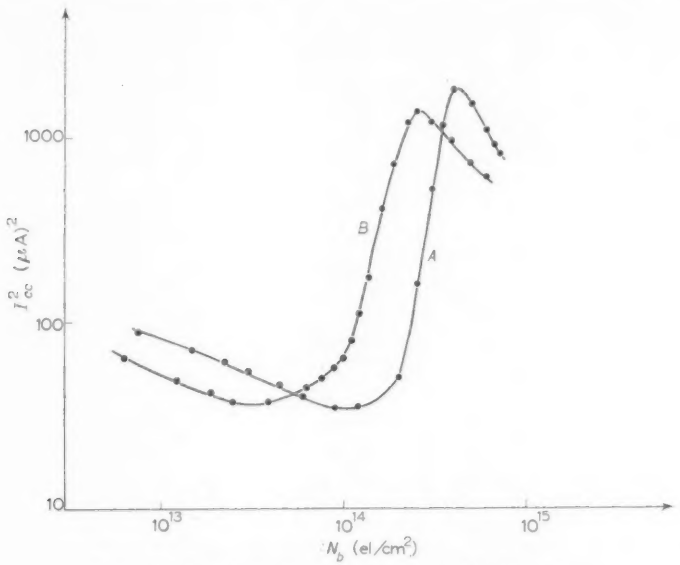


FIG. 2. Variation du taux de recombinaison sous l'action du bombardement pour trois échantillons de compositions différentes. La variation de la conductivitè $\sigma$ de l'échantillon de type $n$ de haute résistivité a aussi été représentée.

La valeur de $\sigma_n$ est douteuse, étant donnée le faible nombre de résultats expérimentaux pour des échantillons de type $p$.

Le choix du niveau de recombinaison à 0,18 eV de la bande de conduction semble le plus probable, étant donnée la valeur de la section efficace $\sigma_p$ qui correspond sensiblement à celle d'un atome neutre; surtout, il existe à cette position un niveau accepteur, attribué à l'interstitiel, comme l'ont montré les travaux de CRAWFORD *et al.*[1] sont instables thermiquement. Un court recuit à 100°C en fait disparaître une grande partie; on a cependant remarqué que l'effet de guérison est plus marqué sur la durée de vie que sur la conductivité, comme le montre la Fig. 1.

De même des bombardements à température de l'azote liquide indiquent pour la conductivité et la durée de vie une efficacité beaucoup grande qu'à 0°C. Nous avons cependant observé une grosse différence de comportement entre les

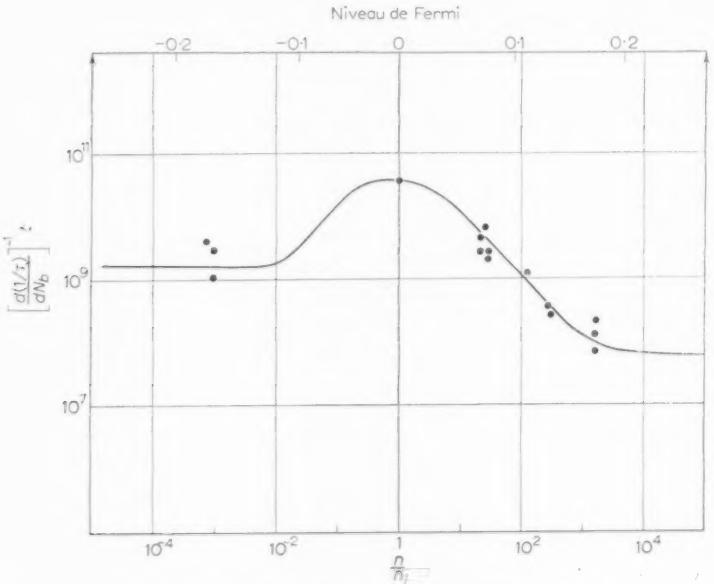


FIG. 3. Influence de la position du niveau de Fermi sur la variation de la durée de vie.

Cette détermination du niveau de recombinaison est en accord avec des déterminations par d'autres auteurs.[2, 4]

L'étude de la durée de vie en fonction de la température aurait pu aider à lever l'indétermination entre les deux niveaux possibles, mais pour les échantillons utilisés, avec les flux élevés auxquels ils ont été soumis, cette variation ne suit pas les lois de SHOCKLEY–READ; le nombre de pièges, grand devant celui des porteurs restants, donne une durée de vie sensiblement constante de 25 à −50°C, comme on peut le voir d'après les relations données par WERTHEIM[10] et SANDIFORD[11].

Les défauts créés par les électrons de 2 MeV échantillons $p$ et $n$: dans le germanium $n$ la guérison de la durée de vie est étalée entre −180 et 0°C, tandis que dans un échantillon $p$, elle se produit brusquement à −90°C. Si l'on suppose le processus de guérison comme monomoléculaire, on trouve une énergie d'activation de l'ordre de 0,5 eV.

Les études de FLETCHER et BROWN[12] et de WAITE[13] ont montré que la guérison pouvait être attribuée, au-dessus de 160°C, à la recombinaison de paires lacunes–interstitiels, les défauts voisins, issus du même noeud du réseau, se recombinant les premiers, et l'énergie d'activation est voisine de 1,4 eV. En extrapolant leurs résultats aux températures inférieures à 100°C, on voit que ce

processus ne peut pas rendre compte de nos expériences. On doit supposer que les défauts qui disparaissent sont plus mobiles que les lacunes, ou qu'ils sont plus instables de nature, comme une paire lacune–interstitiel très rapprochés; cependant BROWN—cité par WAITE[13]—a montré que ce type de défaut était stable même à température ordinaire. CRAWFORD suppose que l'interstitiel est le plus mobile à température ordinaire, et nous penchons vers cette explication. Dans ce cas, il faudrait expliquer pourquoi l'interstitiel perd sa mobilité à haute température.

Pour contrôler si la guérison à 0°C est due à une dissociation de centres complexes ou à une diffusion de défauts mobiles suivie d'annihilation dans des puits fixes, tels que les dislocations, on peut étudier des échantillons ayant des concentrations différentes de dislocation.

Dans ce but, nous avons dans une expérience préliminaire bombardé des échantillons déformés plastiquement à chaud, ce qui a introduit $3 \cdot 10^6$ dislocations par cm$^2$. Les expériences sont assez douteuses, cependant on a noté, pour l'un au moins des échantillons, une diminution de l'efficacité d'introduction des accepteurs par le bombardement: on trouve 0,15 électron enlevé par électron incident dans l'échantillon déformé, contre 0,6 dans le cristal normal de même résistivité (3Ω cm). On aurait donc une diffusion et annihilation très rapide des défauts instables et cette annihilation se ferait sur les dislocations. Ce résultat, s'il est confirmé, appuierait l'hypothèse de défauts ponctuels très mobiles, probablement les interstitiels.

Un compte-rendu plus détaillé de ce travail sera publié ailleurs.[14]

## BIBLIOGRAPHIE


1. Voir, par exemple, CRAWFORD J. H. et CLELAND J. W., *Progress in Semiconductors* Vol. II, p. 67. Heywood, Londres (1957).
2. CURTIS O. L., CLELAND J. W., CRAWFORD J. H., et PIGG J. C., *J. Appl. Phys.* **28,** 1161 (1957).
3. MESSENGER G. C. and SPRATT J. P., *Proc. Inst. Radio Engrs.* **46,** 1038 (1958).
4. VAVILOV V. S., SMIRNOV L. S., PATSKEVITCH V. M., SPITZIN A. V., et GALKIN G. N., *Zh. tekh. fiz.* **26,** 1865 (1956).
5. WERTHEIM G. K. et AUGUSTYNIAK W., *Rev. Sci. Instrum.* **27,** 1062 (1956).
6. RAPPAPORT P. et LOFERSKI J. J., *Phys. Rev.* **98,** 1861 (1955).
7. KOCH L. et VAN DONG N., Conférence de Bruxelles 1958 (à paraître).
   BARUCH P. et VAN DONG N., à paraître aux *C. R. Acad. Sci., Paris.*
8. SHOCKLEY W. et READ W. T., *Phys. Rev.* **87,** 835 (1952); HALL R. N., *Phys. Rev.* **87,** 387 (1952).
9. WERTHEIM G. K., *Phys. Rev.* **105,** 1730 (1957).
10. WERTHEIM G. K., *Phys. Rev.* **109,** 1086 (1958).
11. SANDIFORD D. J., *Phys. Rev.* **105,** 524 (1957).
12. FLETCHER R. C. et BROWN W. L., *Phys. Rev.* **92,** 585 (1953).
13. WAITE T. R., *Phys. Rev.* **107,** 471 (1957).
14. BARUCH P. et ANDRÉ P., Conférence de Bruxelles 1958 (à paraître).


*J. Phys. Chem. Solids* Pergamon Press 1959. Vol. 8. pp. 157–161. Printed in Great Britain

F.5

# CAPTURE DIAMETER OF DISLOCATIONS IN LOW-ANGLE GRAIN BOUNDARIES IN GERMANIUM

ROLF K. MUELLER

Mechanical Division of General Mills, Inc.

EXPERIMENTS with grain boundaries of known crystallographic configuration in *n*-type germanium will be described briefly. An interpretation of these experiments will be given, and it will be shown that the rate of electron capture at the boundary can be determined from observed data. With the assumption of a dislocation array model for the low-angle boundaries, a capture diameter for electrons of the dislocation can be derived.

The grain boundaries investigated are tilt

boundaries with misfit angles of 4°, 6° and 25°. The tilt axis was in all cases in a common ⟨100⟩ direction and the boundary plane a mean {110} plane.

Rods of rectangular cross-section with the grain boundary perpendicular to the main axis were prepared (see insert in Fig. 1). Ohmic contacts

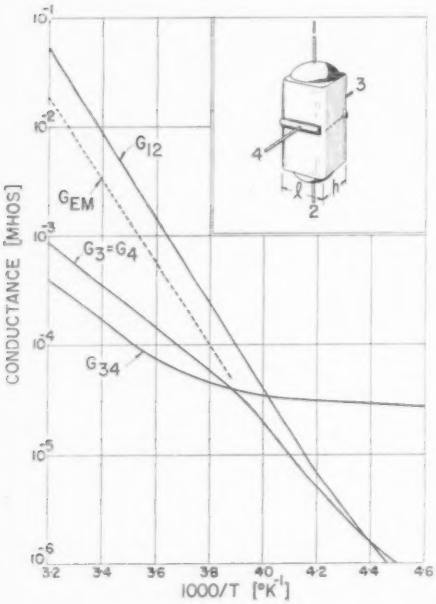


FIG. 1. Experimental values of the conductances $G_{12}$, $G_3$, $G_4$, and $G_{34}$ as a function of inverse temperature for a 4° sample. $G_{em}$ determined according to equation (15) is given as a dashed line. The insert shows the sample geometry and contact arrangement.

(1 and 2) were applied to the ends of the sample and indium contacts (3 and 4) alloyed on opposite sides of the sample covering the grain boundary. The alloyed contacts were applied in all cases to sides perpendicular to the tilt axis. With these samples voltage/current characteristics for different contact combinations have been measured as a function of temperature in the range 350–200°K. For applied voltages small compared to $kT/q$ (<20 mV), the voltage/current relation is linear and a low-voltage conductance can be defined. We shall be concerned in this paper only with these low-voltage conductances. Experimental details of the preparation of the bicrystals and methods of measuring these conductances are described elsewhere.[1]

The following symbols for the different conductances under study are in accordance with the numbering of the four contacts shown in Fig. 1:

- $G_{12}$ conductance across the grain boundary between contacts 1 and 2. Contacts 3 and 4 are floating.
- $G_{34}$ conductance along the grain boundary between contacts 3 and 4. Contacts 1 and 2 are connected and floating.
- $G_3(G_4)$ "diode conductance" between contact 3(4) and the connected contacts 1 and 2. Contact 4(3) is floating.

Typical experimental data for a 4° and a 25° boundary are shown in Figs. 1 and 2.

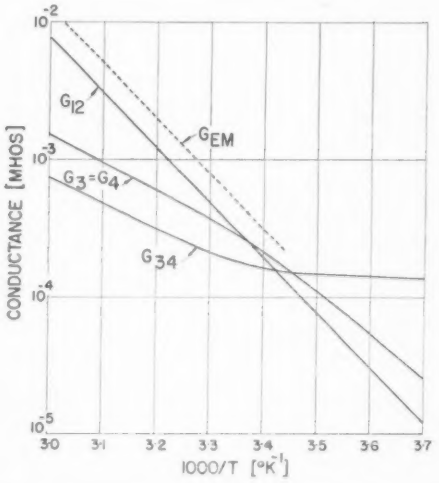


FIG. 2. Experimental values of the conductances $G_{12}$, $G_3$, $G_4$, and $G_{34}$ as a function of inverse temperature for a 25° sample. $G_{em}$ determined according to equation (15) is given as a dashed line.

It has been shown in a previous paper[2] that the conductance $G_{12}$ can be expressed in terms of the electron generation per cm² of boundary per sec, $i_{em}$. The quantity $i_{em}$ which depends exponentially on temperature, has the dimension of a current density and can be visualized as the electron emission current per cm² of boundary:

$$G_{12} = lh\frac{1-\gamma/2}{2\gamma} i_{em} q/kT \qquad (1)$$

where $l$ and $h$ are the cross-sectional dimensions of the sample (Fig. 1) and $\gamma$ is the capture rate of the boundary, i.e. the ratio between electrons striking the boundary to electrons captured at the boundary. It is further shown in reference (2) that the hole contribution to $G_{12}$ is negligible in a temperature range where the enhanced pair generation in the space-charge region can be neglected. Its effect at low temperatures will be discussed below.

The conductances $G_{34}$ and $G_3(G_4)$ show identical temperature-dependence in the high-temperature range, corresponding to an apparent activation energy of half the gap energy (indicated by the slope of the log $G$ versus $1/T$ characteristic). The ratio $G_3/G_{34}$ is equal to two in this temperature range. At lower temperatures $G_{34}$ shows an activation energy of $0{\cdot}04 \pm 0{\cdot}01$ [eV], indicating a conducting sheet at the grain boundary. An activation energy for this interface conductance of the same order has been found by TWEET[3] for grain boundaries in gold-doped germanium. The diode conductances, $G_3(G_4)$, at lower temperatures tend to follow the temperature-dependence of $G_{12}$ modified by the increasing effect of generation in the space-charge region. The apparent activation energy of half the gap energy for $G_3$ and $G_{34}$ in the upper temperature range indicates that no appreciable contribution to the observed conductance is due to hole current to the indium contacts proper, since such a contribution would show an activation energy close to the gap energy. A further indication to this effect is the close agreement of $G_3$ and $G_4$ which could not be expected if the hole current were appreciable because of unavoidable differences in the contact areas.

The identical temperature-dependence of $G_{34}$ and $G_3(G_4)$ in the upper temperature range suggests that in both cases the current flow is governed by the same mechanism. The current carried by the conducting sheet at the grain boundary modifies the potential of the boundary proper against the bulk along the extension of the boundary between the two contacts 3 and 4 and thereby modifies the amount of current flow from the boundary to the bulk.

The potential gradient in the conducting sheet as a function of the distance $x$ from one of the contacts (3) or (4) is given by:

$$\frac{dV}{dx} = -\frac{I(x)}{g \cdot l} \tag{2}$$

where $I(x)$ is the total current in the sheet, $l$ the width of the sample (see Fig. 1) and $g$ the conductance of a square of the sheet.

If we define $V$ as the deviation of the grain-boundary potential from its equilibrium value against the bulk, the net current density $i_B$ flowing from the boundary to the bulk for sufficiently small values of $V$ ($V < kT/q$) is given by:

$$i_B = i_{em}\frac{qV}{kT}. \tag{3}$$

The divergence of the current $I(x)$ in the conducting sheet is therefore:

$$\frac{dI(x)}{dx} = -i_{em}\frac{qV}{kT} \cdot l. \tag{4}$$

If we define a characteristic length, $\lambda$, by:

$$\lambda = \left(\frac{g \cdot kT}{q \cdot i_{em}}\right)^{\frac{1}{2}} \tag{5}$$

we get from equations (2) and (4) an equation for $I(x)$ or $V(x)$:

$$\frac{d^2I(x)}{dx^2} = \lambda^{-2} \cdot I(x) \text{ or } \frac{d^2V(x)}{dx^2} = \lambda^{-2}V(x). \tag{6}$$

This equation, together with appropriate boundary conditions, allows the determination of the conductances $G_3(G_4)$ and $G_{34}$. We shall first determine $G_3(G_4)$. Let the applied voltage between contact 3 and the bulk (contacts 1 and 2) be $U$. The boundary conditions then are: $V(0) = U$ and $I(h) = 0$. The second boundary condition is the condition for the floating contact (4) at $x = h$. Considering that $G_3$ by definition is:

$$G_3 = \frac{I(0)}{U} \tag{7}$$

we find for $G_3$ and likewise for $G_4$:

$$G_3 = G_4 = g \cdot \frac{l}{\lambda} \tanh(h/\lambda). \tag{8}$$

The boundary conditions appropriate for the determination of $G_{34}$ are, because of the symmetry

of the system, $V(x) = -V(h-x)$ and $V(0)-V(h) = U$.

With this boundary condition we find for $G_{34}$:

$$G_{34} = g \cdot \frac{l}{2\lambda} \coth(h/2\lambda). \tag{9}$$

It is easier to compare the expressions for $G_3$ and $G_{34}$ with the experimental data if we consider a high- and low-temperature approximation. For sufficiently high temperatures, $\lambda$ is small compared to $h$ due to the exponentially increasing quantity $i_{em}$. The hyperbolic tangent and cotangent can therefore be replaced by unity, and we get from equations (8) and (9):

$$G_3 = G_4 = 2G_{34} = \frac{l}{\lambda} g = l \cdot \left(\frac{q i_{em} g}{kT}\right)^{\frac{1}{2}} \text{ for } \lambda < h. \tag{10}$$

Equation (10) shows directly the observed factor 2 between $G_3(G_4)$ and $G_{34}$ and describes correctly the observed temperature-dependence. According to equation (1), $G_{12}$ is proportional to $i_{em}$ and according to equation (12) below, $G_{34}$ for low temperatures is proportional to $g$. The slope of log $G_3$ in the high-temperature range is therefore according to equation (10) equal to half the sum of the slopes of log $G_{12}$ and the slope of the low-temperature branch of log $G_{34}$. This is in excellent agreement with the experiment.

For sufficiently low temperatures $\lambda$ becomes large compared to $h$, and we can replace the hyperbolic tangent by its argument. This gives:

$$G_3 = G_4 = l \cdot h \frac{q}{kT} i_{em} = G_{em} \text{ for } \lambda > h \tag{11}$$

and

$$G_{34} = \frac{l}{h} g \text{ for } \lambda > h. \tag{12}$$

In the low-temperature case we cannot, however, neglect the effect of the enhanced generation in the space-charge region on the observed conductances. For small applied voltages this effect can be approximately described by the introduction of two additional conductances, $G_{S_1} = G_{S_2} = G_S$ between the boundary (the sheet conductance $g$ is large compared to $G_S$) and either side of the bulk (represented by the contacts 1 and 2). If we denote the total diode conductance by $\bar{G}_3$, we can represent $\bar{G}_3$ by the parallel combination of the above considered electron part $G_3$ and the two conductances $G_{S_1}$ and $G_{S_2}$:

$$\bar{G}_3 = G_3 + 2G_S. \tag{13}$$

The total grain-boundary conductance $\bar{G}_{12}$, however, is determined by the series combination of $G_{S_1}$ and $G_{S_2}$ in parallel to the above considered electron part $G_{12}$:

$$\bar{G}_{12} = \tfrac{1}{2} G_S + G_{12}. \tag{14}$$

For low enough temperatures, $G_S$ becomes the leading term in equations (13) and (14) due to its smaller activation energy, so that $\bar{G}_3$ ultimately becomes four times as large as $\bar{G}_{12}$. This explains the observed lower slope in the experimentally determined log $G_3$ versus $1/T$ characteristic of Fig. 1 and 2 compared to the slope of the log $G_{12}$ versus $1/T$ characteristic and the crossover of $G_3$ and $G_{12}$ for the 4° boundary.

The foregoing consideration shows that the experimental values of the low-temperature branch of $\bar{G}_3(\bar{G}_4)$ do not represent the electron part $G_3 = G_{em}$ which we would like to compare with $G_{12}$.

The validity of equation (11), however, is not affected by the space-charge generation because of the relatively high value of $g$ and its low activation energy. We can therefore extrapolate $gl/h$ from the low-temperature branch of $G_{34}$ to higher temperatures and determine $G_{em}$ from:

$$G_{em} = \frac{(G_{34})^2}{gl/h} = lhi_{em}\frac{q}{kT} \tag{15}$$

in the high-temperature region where the space-charge generation can be neglected.

Comparison of equation (1) with equation (15) shows that the ratio $G_{12}/G_{em}$ depends only upon the capture rate $\gamma$:

$$G_{12}/G_{em} = \frac{1-\gamma/2}{2\gamma}. \tag{16}$$

The values of $\gamma$ determined according to equation (16) from the experimental data are given in Table 1. As expected, $\gamma$ increases with increasing misfit angle of the boundaries. If one assumes for the low-angle boundaries a dislocation array model with the smallest crystallographically

possible number of dislocations, one finds for the 4° samples a relative separation, $S$, of 56 Å and for the 6° samples a relative separation of 35 Å. Underlying this model one can relate the value

*Table* 1

| Misfit angle | Number of samples | Capture rate of boundary, $\gamma$ | Capture diameter $d$ (Å) |
|---|---|---|---|
| 4° | 3 | 0·16, 0·18, 0·22 | 5·6, 6·4, 7·8 |
| 6° | 2 | 0·33, 0·25 | 7·0, 5·6 |
| 25° | 2 | 0·61, 0·56 | |

of $\gamma$ with the capture diameter, $d$, of the individual dislocations:

$$\gamma = \frac{\pi d}{2S}. \qquad (17)$$

This relation yields for the capture diameter, $d$, the values given in Table 1. For comparison, values for the capture diameter determined with random dislocations[4] and with dislocation arrays of wider separation[5] are given in Table 2.

*Table* 2

| $d$ (Average) | $d$ (Wertheim[4]) | $d$ (McKelvy[5]) |
|---|---|---|
| 6·5 | 6·8 | 5·6 |


**REFERENCES**

1. Mueller R. K. To be published.
2. Mueller R. K., *Report on 18th Annual Conference on Physical Electronics, MIT*, p. 29 (1958).
3. Tweet A. G., *Phys. Rev.*, **99**, 1182 (1955).
4. Wertheim G. K. and Pearson G. L., *Phys. Rev.* **107**, 694 (1957).
5. McKelvy T. P., *Phys. Rev.* **106**, 910 (1957).


*J. Phys. Chem. Solids* Pergamon Press 1959. Vol. 8. pp. 161–165. Printed in Great Britain

F.6

# TRAPPING OF PHOTOELECTRONS AROUND DISLOCATION LINES IN ALKALI HALIDES


**HAZIMU KAWAMURA and HIROSHI OKURA**

Department of Physics, Osaka City University, Osaka, Japan


The effect of mechanical working upon the photocurrents in colored KCl and KBr single crystals was investigated in the temperature range from −200 up to 0°C. The irradiation was performed by chopping the light from a tungsten incandescent lamp at 30 c/s, the photocurrent being lock-in detected. An a.c. field of 1000 c/s was applied to the crystal so that the space charges were eliminated.

Although it is to be expected that the range of a photoelectron is shortened as the result of the trapping by a dislocation line or by its jog, the effect is complicated by the formation of complex centers such as $M$- or $R$-centers, which accompany mechanical working or irradiation with $F$-light. Fig. 1a shows how rapidly the complex centers are formed in the deformed crystal upon irradiation with $F$-light. However, when the crystal was purified by recrystallization from the melt, these complex centers did not appear even with much longer irradiation, as shown in Fig. 1b. Thus, by employing such a pure crystal, we were assured of freedom from parasitic effects due to complex centers.

The recrystallized pure single crystals of KCl and KBr were additively colored by heating at 420 ∼ 560°C in sodium or potassium vapor. The densities of $F$-centers were $10^{16} \sim 10^{17}$ cm$^{-3}$ as shown in Table 1. The crystal was cleaved into several pieces, which were then mechanically

worked to varying degrees. Each specimen was pulse-annealed at 400°C for 1 min. The mechanical working consisted of linear compression by a weight tester, and the degree of deformation was measured by the fractional thickness reduction.

Typical results are shown in Figs. 2a and 2b, in which the solid line relates to the undeformed crystal and the dotted line to the deformed one. Each specimen was obtained from the same piece of colored crystal. These curves may be interpreted in terms of the shortening of the range of the photoelectron due to shallow trapping centers produced by mechanical working, which become ineffective above −120°C. If $T_F$ is the mean lifetime of a photoelectron due to the trapping by $F$-centers and $T_D$ that arising from shallow traps, the net mean lifetime $T$ for the deformed crystal is given by the relation $1/T = 1/T_F + 1/T_D$. Since the photocurrent for the undeformed sample is proportional to $T_F$ and that for the deformed one proportional to $T$, we have

$$1/T_D = 1/T - 1/T_F \sim 1/I - 1/I_0, \qquad (1)$$

and

$$T_F/T_D = I_0/I - 1; \qquad (2)$$

where $I_0$ and $I$ are the photoconductances for

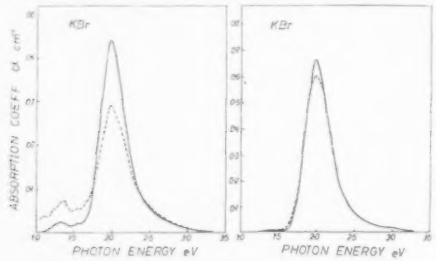


(a) (b)

FIG. 1. Absorption coefficients of colored KBr as functions of photon energies. (a) Usual crystal which underwent 13 per cent deformation; — before irradiation and – – – after 10 min irradiation. (b) Recrystallized specimen which underwent 19 per cent deformation; — before irradiation and – – – 30 min irradiation with $F$-light.

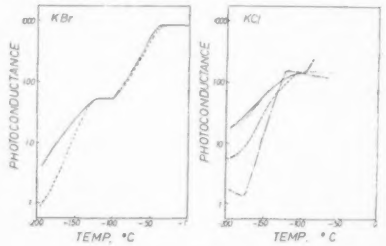


FIG. 2. Photoconductance for KBr and KCl as the functions of temperature. (a) KBr; — undeformed crystal and – – – crystal 9 per cent deformed. (b) KCl; — undeformed, – – – crystal 19 per cent deformed, · · · · · quantum efficiency for $F$–$F'$ transition, and —·— the photoconductance according to POHL.[3]

*Table* 1

| | $N_F$(cm$^{-3}$) | Degree of deformation (per cent) | $T^*$(°C) | $N_D tv/N_F \sigma$ | $N_D tv$(cm$^{-1}$) | $N_D$(cm$^{-2}$) | $w$(cm) |
|---|---|---|---|---|---|---|---|
| | | | | | $\times 10^2$ | $\times 10^9$ | $\times 10^{-8}$ |
| KBr | $1{\cdot}5 \times 10^{16}$ | 16 | −170 | 1·4 | 2·0 | 7·6 | 2·6 |
| | $1{\cdot}5 \times 10^{16}$ | 21 | −167 | 2·3 | 3·3 | 9·6 | 3·4 |
| | $4{\cdot}3 \times 10^{16}$ | 8 | −170 | 0·7 | 3·2 | 4·5 | 7·1 |
| | $4{\cdot}0 \times 10^{16}$ | 9 | −167 | 1·0 | 3·9 | 4·6 | 8·5 |
| | $3{\cdot}8 \times 10^{16}$ | 11 | −167 | 3·3 | 12·5 | 5·8 | 22 |
| | $7{\cdot}7 \times 10^{16}$ | 9 | −167 | 0·9 | 6·6 | 4·6 | 14 |
| | $1{\cdot}3 \times 10^{17}$ | 18 | | 0·6 | 7·8 | 8·4 | 9·3 |
| | Mean | | −168 | | | | 9·3 |
| | | | | | $\times 10^3$ | | |
| KCl | $4{\cdot}0 \times 10^{16}$ | 16 | −165 | 3·8 | 1·5 | | |
| | $4{\cdot}0 \times 10^{16}$ | 25 | −150 | 7·6 | 3·0 | | |
| | $1{\cdot}6 \times 10^{17}$ | 19 | −150 | 2·2 | 3·5 | | |
| | $1{\cdot}6 \times 10^{17}$ | 21 | −153 | 3·4 | 5·5 | | |
| | Mean | | −155 | | | | |

undeformed and deformed crystals, respectively. Making use of the relation (1), we can obtain the temperature-dependence of $1/T_D$ from the experimental curves as shown in Fig. 3. The temperature at which the derivative of this curve becomes a maximum can be used to give an order-of-magnitude estimate of the trap depth. It is about −170°C for KBr and −155°C for KCl. If the trap depth is $E$, the releasing frequency may be expressed as $\nu = \nu_0 \exp(-E/kT)$, where $\nu_0$ is of the order of $10^{10}$ sec$^{-1}$. Since it would be reasonable to assume that $\nu$ becomes of the order 1 sec$^{-1}$ at the above characteristic temperature, we can estimate the trap depth $E$ to be 0·21 and 0·24 eV for KBr and KCl, respectively.

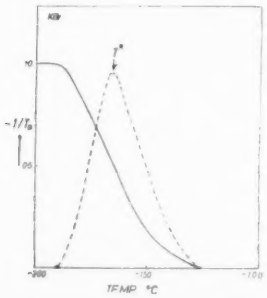


FIG. 3. The reciprocal of the mean lifetime of a photoelectron due to trapping by dislocation line as a function of temperature and its derivative curve.

Since, as shown later, the cross-section becomes much too large if only the jog of a dislocation line is responsible for trapping, we shall assume that the dislocation line itself traps a photoelectron. $T_F/T_D$ can be obtained by analyzing the experimental data with the aid of equation (2). It becomes constant at low temperature where release from the trap is negligible. If $N_D$ is the number of dislocation lines per cm$^2$ and $w$ is the effective width of the dislocation line for trapping, $1/T_D$ is proportional to $N_D w$. On the other hand, $1/T_F$ is proportional to $N_F \sigma$, where $N_F$ is the density of $F$-centers and $\sigma$ is the effective cross-section for electron trapping. Hence we have

$$N_D w / N_F \sigma = T_F/T_D = I_0/I - 1, \qquad (3)$$

from which we get $N_D w$, assuming $\sigma$ to be $10^{-14}$ cm$^2$. The values obtained are shown in the fourth and fifth columns of Table 1. In a separate experiment we estimated the density of dislocations in deformed crystals of KBr by the use of nuclear magnetic resonance. Results are shown in the sixth column. Using these values, we obtain the effective width $w$ as shown in the last column. If this effect is attributed only to the jogs of the dislocation lines, their cross-section must be as large as $10^{-13}$ cm$^2$, even if they were spaced every ten atomic distances along the dislocation line.

The potential field around dislocation line is estimated by making use of the deformation potential. It can trap an electron at either the compressed or dilated side, according to the sign of the deformation potential. Although an electron may be trapped as a moving polaron along a dislocation line or self-trapped by polarizing the medium, the latter state is little more stable than the former according to a rough estimate. The energy of the self-trapped state was estimated by a variational method. Employing the value of 5·4 eV as the deformation potential for KCl, which we have obtained by the use of the cellular method, we found that the energy required to release the electron from the self-trapped state to the bottom of the conduction band is 0·27 eV, which is to be compared with the experimental value of 0·24 eV.

The temperature range where trapping is effective just overlaps the range where the optically excited $F$-electrons can escape thermally into the conduction band. In this range the quantum efficiency $\eta$ for the production of photoelectrons is less than unity and is temperature-dependent. In Fig. 2b, $\eta$ obtained by experiment[2] on the $F$–$F'$ transition is shown together with the photocurrent for KCl due to POHL.[3] It seems likely that POHL's specimen was considerably strained, since the trend of the photoconductivity curve should be similar to that of the $\eta$ curve, if the temperature variation of electron mobility is neglected. The photoconductivity curve may thus fall further when electron trapping becomes effective at low temperature.

## REFERENCES

1. OTSUKA E. and KAWAMURA H., *J. Phys. Soc. Japan* **12**, 1071 (1957).
2. PICK H., *Ann. Phys., Lzg.* **31**, 365 (1938).
3. POHL R. W., *Proc. Phys. Soc.* **49**, 13 (1937).

## DISCUSSION

*Compiled by* G. L. PEARSON

### F.1 L. SOSNOWSKI

R. K. MUELLER (General Mills): We have obtained results very similar to those of Fig. 6 (18th Annual Conference on Physical Electronics (M.I.T., 1958) p. 29). We have also made calculations of the fraction of the current across the grain-boundary layer carried by electrons. The calculations indicate that, even at very low voltages ($< kT/e$), the current is substantially electronic. Experiment and theory are in good agreement.

A. SOSNOWSKI: We plan to investigate this point in more detail to find whether such is the case for the grain boundaries which we have studied.

A. G. TWEET (General Electric Co.): Could you tell us what the orientation was for the grain boundaries of the second kind?

A. SOSNOWSKI: Fig. 8 shows the results of the X-ray determination of the orientation of the two halves of the germanium bicrystal on which we made the measurements for Fig. 5.

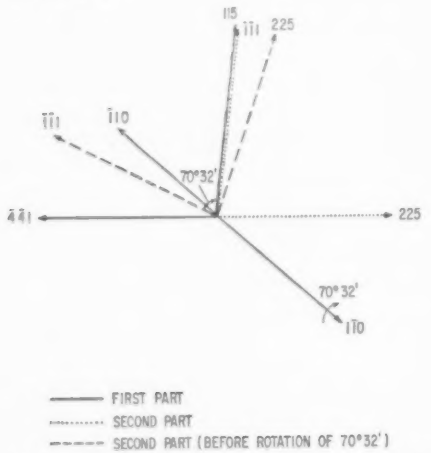


FIG. 8. Crystallographic orientation of a typical germanium bicrystal with a type-II boundary, as determined by X-ray diffraction.

### F.2 A. F. GIBSON

E. E. LOEBNER (R.C.A.): The models used by SOSNOWSKI (paper F.1) for tilt boundaries and that of GIBSON for edge dislocations are similar. This $n$–$p$–$n$ type of structure is essentially symmetrical. We (at R.C.A.) studied plastically deformed II-VI compounds, such as CdS, and in these materials the barriers were asymmetric due to the oppositely charged ions. Very large photovoltages, up to 200 V, could be developed across crystals containing a number of such barriers in series.

W. SHOCKLEY (Beckman Instrument Co.): What can be the explanation of a lifetime which is direction-dependent? It would seem that lifetime is a scalar quantity and cannot have directional dependence.

A. F. GIBSON replied that his model indicated anisotropy of lifetime of electrons in $p$-type material but that he knew of no explanation of the effect in $n$-type.

In subsequent discussion with A. G. TWEET, A. F. GIBSON said that most of the crystals used were bent around a 111 axis or cut from crystals grown on seeds bent around that axis. Bending around a 111 axis gave two arrays of dislocations running at 60° to one another and, in effect, only a resolved component was measured. Some measurements were made on crystals bent around a 112 axis as this type of deformation gave more nearly single slip. Measurements of X-ray broadening in two directions at right angles in these crystals have been described by BELL and HOGARTH (Reference 1 of paper).

### F.3 C. BENOIT À LA GUILLAUME

P. T. LANDSBERG (University of Aberdeen): How sure can one be that the peaks on the right-hand side of your slides arise from band-to-band transitions rather than from localized impurities located near the band edge?

C. BENOIT À LA GUILLAUME replied that these peaks are structure-independent. They are found in all samples and are independent of the impurity content and dislocation density.

### F.4 P. BARUCH

W. SHOCKLEY (Beckman Instrument Co.): It was proposed by the speaker that a given type of defect when increased in number can cause both a decrease in number of electrons and an increase in lifetime. I would like to comment that this could not occur for a single level with transition change ($-1$ to 0) but could occur for transition change ($-2$ to $-1$).

P. BARUCH: I agree with W. SHOCKLEY's objection that in terms of a single acceptor center in the upper half of the forbidden gap which acts as a recombination center, it is impossible to get a turnover of lifetime with increasing center recombination. One can see readily that the number of centers available to recombination is kept almost constant, and the variation of lifetime should be saturable. However, if there is another acceptor level below the recombination center regardless of whether it belongs to the same defect, which is then a multiple acceptor, or to another defect introduced by bombardment (either vacancy or interstitial) a turnover is possible, since the Fermi level can be pulled down below the recombination level. This is the hypothesis which we made and which is supported by the study of variation of conductivity by bombardment.

R. N. HALL (General Electric Co.): Curve 1 of Fig. 2 shows a sample with recombination rate first increasing

rapidly, and then decreasing with continued bombardment. At the same time, the conductivity decreases relatively slowly. The change in lifetime is too great to be explained by the SHOCKLEY–READ recombination model as suggested, since lifetime should increase only linearly with resistivity. I doubt that any combination of levels can give the observed behavior. Have you any other explanation? (How about surface recombination to account for the initial rapid rise in apparent recombination rate?)

P. BARUCH: The steepness of the increase of lifetime depends strongly on the initial position of the Fermi level, as can be seen from the expression:

$$\tau = \frac{1}{\alpha_p N_t}\left[1+\frac{\eta_1}{N_D N_t}\right]$$

(usual symbols of HALL–SHOCKLEY–READ theory, $N_D$ being the number of chemical donors) which applies for an $n$-type sample with a recombination level in the upper half of the gap and an acceptor level near the valence band, both with the same concentration. Such a model is rather crude, and has to be improved, but it shows the essential features of the problem. For a high-resistivity $n$-type sample ($N_D < n_1$) this reduces to:

$$\tau = \frac{1}{\alpha_p N_t}\,\frac{\eta_1}{N_D - N_t}$$

and $\tau$ has a minimum for $N_t = N_D/2$. For $N_t > N_D/2$ one sees that the occupancy factor of the traps is more important than their density, and tends to lower the efficiency for recombination. This situation seems to apply reasonably well to sample 38-B, the conductivity of which varied by a factor of 2 (within experimental error).

P. AIGRAIN (Ecole Normale Supérieure): The possibility that both the interstitial and vacancy can be amphoterous defects (charge states $-1$, 0, 1) seems to have been overlooked and would explain many seemingly strange points.

F.5 L. ROLF K. MUELLER

A. G. TWEET (General Electric Company): I would like to call attention to a phenomenon which shows that different kinds of grain boundaries can exhibit different electrical properties. R. K. MUELLER's measurements indicate that the conductivity of the boundary decreases with an activation energy $\sim$0·5 eV, at least down to liquid-nitrogen temperature. At the Brussels Conference earlier this year, MATARÉ and his co-workers at Sylvania presented evidence that grain boundaries continue to conduct with no freeze-out down to 4°K. The point I wish to make is that these results are not inconsistent. Older work on grain boundaries in gold-doped germanium showed the existence of both these kinds of behavior in a single piece of germanium, depending upon the orientation of the boundary. At that time it was not clear that the gold was not influencing the properties of the boundary. These interesting new results now indicate the possibility that the electrical properties are directly related to the characteristics of the dislocation arrays in the boundary.

*J. Phys. Chem. Solids* Pergamon Press 1959. Vol. 8. pp. 166–171. Printed in Great Britain

SESSION G:
EXCITONS

G.1

# ON THE THEORY OF EXCITONS IN SOLIDS*

HERMANN HAKEN

Institut für Theoretische Physik der Universität, Erlangen

**Abstract**—The different kinds of excitons are considered taking into account the electron–electron interaction as well as the electron–lattice interaction. Some earlier results published by TOYOZAWA, HELLER and MARCUS are obtained as special cases. A refined theory of dielectric screening due to lattice vibrations is given. Optical properties of excitons with large orbital radii are discussed. Certain selection rules as well as a possible explanation of dichroitic effects are given and compared with the corresponding ones of impurity atoms. Finally a quantitative theory of the elementary process of energy transfer by excitons is given and compared with the resonance energy transfer process investigated by Dexter.

## 1. DIFFERENT KINDS OF EXCITONS AND THEIR MUTUAL INTERACTION

THE exciton is generally assumed to consist of an electron and a hole coupled together electrostatically. Two limiting cases of this concept are well known.

(1) The electron and the hole are situated at the same lattice cell and jump simultaneously from one cell to the next one (FRENKEL[1]).

(2) The electron and the hole are separated by a distance which is large compared with the lattice constant. In this case the electron and the hole may be treated approximately as point charges having an effective mass and interacting through a Coulomb potential (hydrogen-like excitons, WANNIER[2]).

While experimental evidence for excitons of type (1) was given by HILSCH and POHL[3] (and later on by others) as long as 30 years ago (alkali-halides) the existence of excitons of type (2) became evident only in recent years especially through the experiments of GROSS,[4] HAYASHI,[5] NIKITINE[6] and their co-workers. However, from these experiments it became clear that even in cases in which the orbital radius of the exciton is rather large the exciton is hydrogen-like only in special cases.

It is the purpose of this paper to present a more refined treatment of the stationary states of excitons as well as their optical transitions, especially for large orbits. Many of our results are also applicable to impurity electrons if this problem is treated as a limiting case in which the mass of the hole tends to infinity.

We begin by reporting some results of a paper of SCHOTTKY and the author[7] in which both kinds of excitons are treated in the framework of the many electron problem, taking into account explicitly the mutual Coulomb interaction between electrons. We used the following simple model: The crystal is assumed to have cubic symmetry and to be an insulator. The atomic orbitals (or Wannier functions) of the valence band are assumed to have $s$-symmetry, whereas those of the conduction bands have $p$-symmetry. We assume further that, within a zeroth approximation, the following two types of elementary excitations are possible:

(1) Local pair states, the excited electron being fixed at the same lattice site as the hole. This kind of excitation will be treated as a new particle.

(2) A free extra electron or a free hole.

If we ignore overlap of the atomic orbitals at different lattice sites in the Coulomb integrals we obtain the following effective Hamiltonian:

$$H_{\text{el}}+H_{\text{hole}}+H_{\text{el-hole}}+H_{p}+H_{\text{el}-p}+$$
$$H_{\text{hole}-p}+H_{p-p}+H_{\text{diss.}}$$

$H_{\text{el}}$ and $H_{\text{hole}}$ describe respectively the motion of

*Chairman: F. SEITZ; *Co-Chairman;* B. LAX.

the surplus electron and of the hole in the field of the nuclei and that of all valence (and core) electrons. $H_{\text{el-hole}}$ describes the Coulomb interaction between the charge cloud of the surplus electron and that of the hole. These three parts are the same as those obtained in WANNIER's paper.[2] Further,

$$H_p = \sum_{n,\mu} \beta_{n,\mu}{}^{+}\beta_{n,\mu}\Delta E$$

represents the energy of the local pair states ($\beta$, pair state operators, $\Delta E$, activation energy) and

$$H_{p-p} = \sum_{m,n;\,\mu,\nu} \beta_{m,\mu}{}^{+}\beta_{n,\nu}\times$$

$$\times \tfrac{1}{2}\langle n,0;\, m,\mu|e^2/r|m,0;\, n,\nu\rangle + \text{conj.}$$

describes the interaction between local states. Here

$$\langle n,i;\, m,j|e^2/r|m,k;\, n,l\rangle = \int a_i{}^{*}(x-n)\times$$

$$\times a_j{}^{*}(x'-m)(e^2/r)a_k(x'-m)a_l(x-n)\,dx\,dx'$$

where $a_l(x-n)$ is a Wannier function and the indices $i$, $j$, $k$, $l$ assume the value 0 for the valence band and 1, 2, 3 for the three $p$-functions describing the conduction band. The terms with $\mu = \nu$ have already been obtained by HELLER and MARCUS[8] but the other terms were not considered. In the total Hamiltonian $H_{\text{el}-p}$ and $H_{\text{hole}-p}$ represent respectively the interaction between the local pair states and the extra electron or hole. For instance

$$H_{\text{el}-p} = \sum \hat{\alpha}_{n,\nu}{}^{+}\hat{\alpha}_{n,\nu}\beta_{m,\mu}\langle n,\nu;\, m,\mu|e^2/r|m,0;\, n,\nu\rangle$$

where $\alpha_{n,\nu}$ are electron operators. Such terms are already known from TOYOZAWA's[9] treatment of the interaction of impurity electrons with excitons. Finally $H_{\text{diss}}$ describes the possibility that the pair states dissociate into a free electron and a free hole.

In consequence of the interaction terms between the different kinds of "particles" neither the pair states nor the free electron or the free hole states are stationary. The interaction $H_{p-p}$ may be partially removed by constructing "running" pair states and completely by building up wave functions in which the orientation of the $p$-function is perpendicular or parallel to the direction of motion. We thus find, in contrast to the paper of HELLER and MARCUS[8] that only these two kinds of running pair states are stationary* (insofar as the other terms $H_{\text{diss}}$ are neglected). On account of $H_{\text{diss}}$, even in the absence of holes or excess electrons, running pair states are not strictly stationary but are surrounded by other electron–hole pairs. This has been recently shown in detail by TAKEUTI[10] along somewhat different lines. In the following however, we shall not discuss the corrections to the local pair states but only to "extended" pairs consisting of a "free" hole and a "free" electron.

## 2. THEORY OF SCREENING EFFECTS FOR EXCITONS (AND IMPURITY CENTRES) IN SEMICONDUCTORS

### 2.1. *Asymptotically exact solution for large distances*

If we evaluate $H_{\text{el-hole}}$ for a large distance between the excess electron and the hole, we get $-e^2/r$, as has already been shown by Wannier. This result is however not completely satisfactory as in a dielectric material we expect the interaction law to be given by something like $-e^2/(\epsilon r)$, where $\epsilon$ is an effective dielectric constant, which comes from the polarization of the crystal. This polarization is due to the core electrons as well as to the displacement of the ions as a whole. In order to treat this polarization let us ignore for the moment the model introduced above and treat it quite generally (for sufficiently large distances) by proceeding in two steps:†

(1) If only one particle, for instance an excess electron, moves through the lattice it is accompanied by a polarization "cloud" built up of displaced ions and core electrons. The corresponding wave function which we assume to be already determined, may be written as:

$$F_{\text{el}}(a,a^{+},b)\Phi_0$$

where $a$, $a^{+}$ are the annihilation and creation

* This result however is of limited interest only, as it was derived for the special model described above. If the crystal has other symmetry properties, more general considerations are necessary.

† The results of this Section 2.1 have already been reported by the author at the International Conference on Semiconductors and Phosphors, Garmisch, 1956.

operators of electrons and holes and $b$ those of polarization quanta of the lattice vibrations, $\Phi_0$ represents the electronic and ionic ground state of the crystal (valence band filled up, conduction band empty). Owing to the translational invariance of the total Hamiltonian the stationary states may be denoted by a wave vector quantum number $k$ (HAKEN[11]): $F_{\mathrm{el}} = F_{\mathrm{el}}{}^{k}$.

(2) If now an excess electron and a hole are present and their orbital distance is not too small, their polarization clouds may be superposed practically undisturbed, which may be accounted for by writing the total wave function in the form

$$F^{kk'} = F_{\mathrm{el}}{}^{k} F_{\mathrm{hole}}{}^{k'} \Phi_0. \tag{2.1}$$

Due to the direct Coulomb interaction between the electron and the hole as well as to the interaction brought about by the two clouds the wave function (2.1) is not yet stationary. Instead we have to build up linear combinations

$$\Sigma c_{kk'} F^{kk'}.$$

In order to determine the coefficients $c_{kk'}$ we put (2.1) into the Schrödinger equation of the whole problem. Using $HF^k = E(k)F^k$ and the approximate orthogonality of the $F^{kk'}$ (for distances not too small) we obtain for $c_{kk'}$ the equation

$$[(E_{\mathrm{el}}(k) + E_{\mathrm{hole}}(k')c_{kk'} + \\ + \sum_{w,w'} G(kk';\, ww')c_{ww'} = Ec_{kk'}.$$

If the orbital radius of the electron–hole pair (exciton!) is large and the extrema of the bands are situated at $k = 0$ we may approximate $E(k)$ by $E_0 + \hbar^2k^2/2m^+$. Under rather general assumptions $G$ may be written as the Fourier transform of $(1/c)$ $(e^2/r)$. If we therefore introduce instead of the $c_{kk'}$ its Fourier transform $\phi$ we get the Schrödinger equation

$$\left(-\frac{\hbar^2}{2m_{\mathrm{e}}}\Delta_{\mathrm{el}} - \frac{\hbar^2}{2m_{\mathrm{h}}}\Delta_{\mathrm{hole}} + \frac{e^2}{cr} + \mathrm{const}\right)\phi = E\phi$$

for $\phi$ which describes the motion of the electron and the hole in a screened Coulomb field.

In order to get the value of $c$ explicitly and to obtain the interaction law at small distances we have used the model described above[7] to treat the core electron polarization. To treat the exciton–lattice interaction we used the well known polaron approach (FRÖHLICH[12]). We obtained for $H_{\mathrm{interaction}}$:

$$-\frac{e^2}{r} + \left(\frac{e^2}{r}\right)\{1 - \tfrac{1}{2}[\exp(-u_1 r) + \\ + \exp(-u_2 r)]\}[1 - (1/\epsilon_\infty)] + \left(\frac{e^2}{r}\right) \times \\ \times \{1 - (\tfrac{1}{2})[\exp(-v_1 r) + \exp(-v_2 r)]\}[1/\epsilon_\infty) - (1/\epsilon)] \\ u_i = (2m_i \Delta E/\hbar^2)^{\frac{1}{2}},\ v_i = (2m_i\omega/\hbar)^{\frac{1}{2}} \tag{2.2}$$

($\Delta E$, excitation energy of pair states (Frenkel excitons); $\hbar\omega$, energy of longitudinal lattice vibrations, optical branch; $\epsilon$, static dielectric constant; $\epsilon_\infty$, high frequency dielectric constant).

For large distances the exponential functions may be neglected and we obtain the usual Coulomb law $-(e^2/(\epsilon r))$. For small distances, however, deviations occur. Thus for $u_i^{-1} < r < v_i^{-1}$ we obtain approximately $-(e^2/\epsilon_\infty r)$, whereas for $r < u_i^{-1}$ we get $-e^2/r$. Thus the interaction law derived above describes in a reasonable manner that as the orbital radius of the exciton becomes smaller and therefore the particles of the exciton move more rapidly the ions and finally the core electrons can no longer follow the motion of the electron and hole and therefore no polarization can be brought about.

### 2.2. *Refined theory of dielectric screening brought about by polarizational lattice vibrations*

While the above treatment describes the exact behaviour of the effective interaction law for large orbital radii of the exciton it provides only a qualitatively correct description for small distances. This failure stems partially from the fact that the microscopic structure of the crystal was neglected in deriving (2.2), partially the fact that exchange terms between neighbouring ions are neglected. These alterations may be accounted for in a reasonable manner by applying perturbation theory or the intermediate coupling theory to the electron–electron interaction, which we shall not discuss here. Finally it is not evident how good or bad the above interaction law (2.2) is at small distances even in a continuum, for the procedure

described above was adapted especially to large orbital radii. While in the case of electron–electron interaction this problem may also be treated in a reasonable manner by perturbation or intermediate coupling theory† in the case of the exciton lattice interaction these two methods may fail due to the rather strong electron–phonon interaction. We therefore confine ourselves to this latter problem, applying a new variational technique developed by FEYNMAN[13] for treating the polaron problem. Rather than approximating a single wave function by a trial function, in this principle the whole Hamiltonian is approximated by a "trial Hamiltonian". We treated this problem in the well known continuum approximation for the electron, the hole, and the polarizational lattice vibrations (FRÖHLICH[12]). In accord with Feynman's idea of representing the "cloud effect" by auxiliary particles, we choose the following trial Hamiltonian

$$H_{\text{trial}} = H_1 + H_2 + f(r)$$

$$H_i = -\frac{\hbar^2}{2m_i}\Delta_{x_i} - \frac{\hbar^2}{2\tilde{m}_i}\Delta_{z_i} + \frac{\tilde{m}_i\tilde{\omega}_i^2}{2}(x_i - z_i)^2 - \frac{3}{2}\hbar\omega.$$

where $x_i$ = coordinate of electron or hole, $z_i$ = coordinate of auxiliary particle, and $\tilde{m}_i$, $\tilde{\omega}_i$, $f(r)$ are variational parameters. In extension of FEYNMAN's considerations for deriving the ground state energy (of the polaron) at $T = 0°\text{K}$ we obtain also expressions for the energy $E_k$ of the excited exciton states at $T > 0°\text{K}$ (the variational principle, however, holds in general only for the lowest state and $T = 0°\text{K}$):

$$\tilde{E}_n \approx E_n - \langle\phi_n\left(f(r) + \frac{e^2}{\epsilon_\infty r}\right)\phi_n\rangle - Z +$$

$$+\sum_w\sum_m\left\{(\bar{n}_w+1)|\langle\phi_n{}^*H_w\phi_m\rangle|^2\frac{P}{E_n - E_m - \hbar\omega_w} + \right.$$

$$\left. +\bar{n}_w|\langle\phi_m{}^*H_w\phi_n\rangle|^2\frac{P}{E_n - E_m + \hbar\omega_w}\right\}$$

with

$$Z = \sum_{i=1,2}\left\{\frac{\tilde{m}_i\tilde{\omega}_i^2}{2}\langle\phi_n{}^*X_i{}^2\phi_n\rangle - \right.$$

$$\left. -\hbar\sum_m\frac{\tilde{m}_i\tilde{\omega}_i^3}{2}\frac{|\langle\phi_n{}^*X_i\phi_m\rangle|^2}{E_n - E_m - \hbar\tilde{\omega}_i}\right\}.$$

Here $E_n$, $\phi_n$ are respectively eigenvalues and eigenfunctions belonging to $H_{\text{trial}}$,

$$\bar{n}_w + 1 = (1 - \exp(-\hbar\omega_w/kT)^{-1}$$

and $w$ is the phonon wave vector. $H_w$ is the exciton–phonon interaction Hamiltonian which applies to both optical and acoustical phonons and $P$ is the principal value.

All results hitherto published by other authors[14–18] treating the same problem are contained as special cases in the present theory. (H. J. G. MEYER,[14] TULUB,[15] IPATOVA,[16] DYKMAN and PEKAR,[17] MOSKALENKO[18]). For large orbital radii the two particles behave like polarons according to FEYNMAN's theory, coupled by $-e^2/\epsilon r$. For small distances, however, the result is still rather involved but qualitatively similar to (2.2).

The procedure enables one also to derive the line breadth† for at least the case, in which the effective ("renormalized") exciton–lattice coupling is weak. One has to replace $P/E$ by $\pi\delta(E)$ in the above formula and to disregard the contribution $Z$.

### 3. OPTICAL PROPERTIES OF EXCITONS WITH LARGE ORBITAL RADII

These properties have been investigated independently by DRESSELHAUS,[19] ELLIOTT[20] and the author[21] (following a suggestion by S. NIKITINE). In these theories the matrix element responsible for the optical transitions

$$M = i\hbar\frac{e}{m}\int\psi_e{}^*\left\{\sum_{j=1}^{n}\exp(ilx_j)\mathbf{e}\cdot\text{grad}_j\right\}\psi_g\,d\tau$$

is evaluated by inserting for the initial state (ground state) a determinant of Bloch functions of the valence band and for the final (exciton) state a

† This remark applies only to semiconductors where an energy gap arises, but not for metals.

† Recently remarkable progress in determining the exciton line shape has been achieved in a very important paper by TOYOZAWA. It seems to us that especially in cases where the "cloud effect" becomes important the treatment described above might be successfully incorporated in the general method of TOYOZAWA. I am very much indebted to Prof. TOYOZAWA for sending me a preprint of his work.

superposition of determinants according to Wannier's theory (but including an effective $\epsilon$). By expanding the resulting matrix element into a series of powers of the $k$-vectors of the Bloch wave functions one obtains in particular for the first two terms:

$$M = i\hbar\frac{e}{m}\left(\int u_{0,L}^{*}\,\mathbf{e}\cdot\operatorname{grad} u_{0,V}\,d\tau\right)\sqrt{V}\phi(0) \quad (3.1)$$

and

$$M = -\hbar\frac{e}{m}\{\operatorname{grad}_k \int u_{k\,L}^{*}\,\mathbf{e}\,\operatorname{grad}_x u_{k,V}\,d\tau\}_{k=0}\operatorname{grad}\phi|_0 \quad (3.2)$$

where $\exp(ikx)u_{k,L}$ and $\exp(ikx)u_{k,V}$ are Bloch functions of the conduction and valence bands, respectively, and $\phi$ is the solution of Wannier's two particle equation. $V$ is the crystal volume.

Since details of the calculations as well as the selection rules which follow from the factors $\phi(0)$ resp. $\operatorname{grad}\phi|_0$ presumably will be found in the paper of ELLIOTT* in this issue the reader is referred for these questions to ELLIOTT's paper. Here, however, we want to discuss further some aspects of (3.1) and (3.2) which have not yet been discussed in the literature. One question of interest is whether the spectra following from (3.1) and (3.2) may be obtained simultaneously. We find that if the crystal possesses a centre of inversion and if the conduction and valence bands are not degenerate, either (3.1) or (3.2) must be necessarily zero. Therefore in this case the transitions belonging to (3.1) and (3.2) cannot occur simultaneously. The proof runs as follows. Under the assumptions made above it follows almost immediately that

$$u_{-k}(-x) = \pm u_k(x).$$

If the positive sign applies (3.2) might be different from zero but (3.1) definitely vanishes. If, however, the negative sign applies (3.2) definitely vanishes.

As pointed out by NIKITINE, this exclusion principle does not hold if the symmetry of the crystal is destroyed, for instance by impurity centres or dislocations. We investigated this proposal quantitatively, confining ourselves to the case in which the Bloch functions of the valence band are strongly disturbed only in the neighbourhood of the perturbation centres, whereas the wave-functions for small $k$ of the conduction electrons are not strongly disturbed. We discuss here only some points of the change of (3.1): If the impurity centres (or other types of perturbations) are distributed and oriented at random, (3.1) remains practically zero. If, however, the impurity wave functions are oriented in a definite manner, for instance by internal fields or by stress, (3.1) is proportional to the density of impurity centres, and the transition probability itself to the square. Such considerations might have application to observations made by Nikitine and Reiss on CuI (compare the contribution of Nikitine to the proceedings).

A second point we wish to discuss concerns a possible explanation of dichroitic effects. Within the framework of the approximation used above, dichroitic effects must be contained in the first factor of (3.1), as was pointed out by Nikitine. Our proposal runs as follows: If two conduction bands are present it may happen that (3.1) $\neq 0$ for wave functions of conduction band 1 and $= 0$ for that of conduction band 2 when the polarization of light is given by $\mathbf{e}_1$ and vice versa when a second direction of polarization is chosen. As the two bands may possess different effective masses and a different energy gap two different (dichroitic) exciton series may occur.

Finally a short comparison with the optical behaviour of impurity centres will be made: H. J. G. MEYER[22] has pointed out, that due to the screening effect discussed in Section 2 and to the variation of the effective mass with the orbital radius impurity centres may also have absorption series similar to those hitherto attributed to excitons. This implies that the orbital radius of the ground state of the impurity atom is very small (atomic size) whereas that of the excited state is rather large (up to several hundred Angstroms). In order to calculate the matrix element of the optical transition we therefore used for the ground state the atomic wave function $a$ of the impurity centre, and for the excited state a linear-combination of Bloch functions or Wannier functions $b$. We obtain in a zeroth approximation for large orbits

* ELLIOTT[20] moreover investigated the influence of lattice vibrations as well as the absorption at the band edge.

$$M = i\hbar\frac{e}{m}\phi(0)\int a^* \mathbf{e}\,\mathrm{grad}\,b\,d\tau. \qquad (3.3)$$

$\phi$ describes the overall behaviour of the excited impurity electron. From (3.3) we see, that on account of the hydrogen-like function $\phi$ the *same* selection rules apply as those for excitons, whereas a difference is brought about by the factor $\int a^* \mathbf{e}\,\mathrm{grad}\,b\,d\tau$ which depends sensitively on the symmetry properties of the atomic orbital and the Wannier function. On account of the smallness of $\phi(0)$ in the case of large orbits the transition probability is considerably decreased, compared with free atomic transitions. Of course, in contrast to the case of excitons, the absorption coefficient is proportional to the concentration of impurity centres. On account of these considerations recent calculations of the absorption coefficient of CuI performed by NIKITINE[23] using ELLIOTT's[20] formula for the exciton absorption coefficient seem to favour an explanation of the absorption lines as exciton lines.

## 4. ENERGY TRANSFER BY EXCITONS, ESPECIALLY IN SENSITIZED PHOSPHORS

We compare the following two mechanisms:
(1) direct energy transfer by resonance between sensitizer and activator
(2) energy transfer by exchange of excitons.

Whereas (1) has already been thoroughly investigated (for the case of solids by DEXTER[24]) a quantitative treatment of (2) seems still to be lacking in the literature. We attempted to treat both mechanisms simultaneously by means of the "effective Hamiltonian" described in Section 1. We report here only results for the case where the electronic states of sensitizer and activator are of atomic size. Since the final result is rather lengthy we mention here only two characteristic limiting cases: (i) If the activation energy is much smaller than the energy for creating an exciton, the exchange of excitons results in a dielectric screening which reduces the transition probability $P$ for the transfer of energy by direct resonance by $(1/\epsilon_\infty)^2$, that is, $P \sim 1/\epsilon_\infty^2 R^6$, where $R$ is the distance between sensitizer and activator.

If on the other hand the activation energy has approximately the same magnitude as the creation energy of the exciton, the decrease of $P$ as a function of $R$ is mainly determined by

$$\frac{1}{R^2}\exp[-2R(m^*/(2\hbar t_0)^{\frac{1}{2}}] \qquad (4.1)$$

where $m^*$ is the effective mass of the exciton, and $t_0$ the mean exciton life time. Therefore the range of the energy transfer is in this case mainly determined by the life time of the exciton.*

Since the mean life time is temperature dependent, (4.1) also becomes temperature dependent. A further temperature dependence is brought about by the lattice vibrations in the neighbourhood of the impurity centre. This can be accounted for in a manner similar to DEXTER's[24] treatment of direct energy transfer by resonance.

## REFERENCES


1. FRENKEL J., *Phys. Rev.* **37,** 17, 1276 (1931).
2. WANNIER G. H., *Phys. Rev.*. **52,** 191 (1937).
3. HILSCH R. and POHL R. W., *Z. Phys.* **48,** 384 (1928).
4. GROSS E. F., *Suppl. 4 Nuovo Cim.* 672 (1956).
5. HAYASHI M. and KATSUKI K., *J. Phys. Soc., Japan* **5,** 381 (1950).
6. NIKITINE S., *J. Phys. Radium* **17,** 817 (1956).
7. HAKEN H. and SCHOTTKY W., *Z. Phys. Chem.*, in press.
8. HELLER W. R. and MARCUS A., *Phys. Rev.* **84,** 809 (1951).
9. TOYOZAWA Y., *Progr. Th. Phys.* **12,** 421 (1954).
10. TAKEUTI Y., *Progr. Th. Phys.* **18,** 421 (1957).
11. HAKEN H., *Z. Naturf.* **10a,** 253 (1955).
12. FRÖHLICH H., *Advanc. Phys.* **3,** 325 (1954).
13. FEYNMAN R. P., *Phys. Rev.* **97,** 660 (1955).
14. MEYER H. J. G., *Physica* **22,** 109 (1956).
15. TULUB A. W., *Isv. Leningr. Univ., Ser. fiz. khim.* **4,** 53 (1957).
16. IPATOVA I. P., *Zh. tekh fiz. SSSR* **26,** 2787 (1956).
17. DYKMAN I. M. and PEKAR S. J., *Dokl. Akad. Nauk. SSSR* **83,** 825 (1952).
18. MOSKALENKO V. A., *Zn. eksp. teor. fiz. SSSR* **30,** 959 (1956).
19. DRESSELHAUS G., *Phys. Rev.* **106,** 76 (1957).
20. ELLIOTT R. J., *Phys. Rev.* **108,** 1384 (1957).
21. HAKEN H., Lectures given at Strasbourg, May, 1957, and April 1958.
22. MEYER H. J. G., *Halbleiterprobleme–IV,* edited by W. SCHOTTKY. Vieweg (1958) in press.
23. NIKITINE S., *Proceedings of the 8th annual meeting of the Société de Chimie Physique. J. Chim. Phys.* in press.
24. DEXTER D. L., *J. Chem. Phys.*, **21,** 836 (1953).


* A somewhat more detailed report also including impurity centres with large radii is given in the Proceedings of the 8 Annual Meeting of the Société de Chimie Physique, Paris, 1958, to be published in *J. Chim. Phys.*

*J. Phys. Chem. Solids* Pergamon Press 1959. Vol. 8. pp. 172–176. Printed in Great Britain

G.2

# OPTICAL SPECTRUM AND MAGNETO-OPTICAL PROPERTIES OF EXCITONS

**E. F. GROSS**

Physico-Technological Institute, Academy of Sciences,
Leningrad, U.S.S.R.

**Abstract**—In a number of crystals at low temperatures a complex structure of distinct strong lines at the edge of fundamental absorption is observed. There is reason to believe that the structure is connected with the creation of excitons predicted by FRENKEL.

In $Cu_2O$ one can observe a hydrogen-like series of narrow lines:

$$\nu_n = \nu_\infty - \frac{B}{n^2}; \; n = 2, 3, 4, 5, 6, 7, 8, 9, 10 \ldots$$

showing the existence of Mott excitons in the crystal. The fact that their diameters are very large is confirmed by ionization (dissociation) of excitons observed even in weak electric fields (1 kV/cm).

The quadratic diamagnetic Zeeman effect is detected in $Cu_2O$ and CdS which is a proof of the large dimensions of excitons and their enormous diamagnetism. The linear paramagnetic Zeeman effect of the members of the $Cu_2O$ series was not observed. That proves the existence of positronium-like excitons with equal effective masses of electron and hole. On the other hand some of the $Cu_2O$ and CdS absorption lines show the linear Zeeman splitting only. This can be explained by excitation of localized excitons whose radii do not exceed the size of the crystal cell. In such a case the spectra of ortho- and para-excitons may be different.

Another phenomenon was observed in a magnetic field near the series limit of the $Cu_2O$ exciton spectrum. A group of almost equidistant absorption maxima beyond the exciton series limit with a fine structure has been detected. These maxima are due to the diamagnetic levels of LANDAU. The spacing between successive maxima is determined by the exciton cyclotron frequency which is equal to the halfsum of the cyclotron frequencies of the electron and hole.

In luminescence in a number of crystals, narrow emission lines are observed at the very edge of the fundamental absorption nearly coinciding with the absorption lines. Some of these may have appeared as a result of annihilation of excitons with the emission of light. Some of the crystals show a fine structure of the spectral dependence of photoconductivity which is closely related to the line structure of the absorption edge. This reveals the role of excitons in photoconductivity.

A COMPLEX structure consisting of narrow strong absorption lines is observed at the edge of the fundamental absorption of a number of crystals at low temperatures. A structure of this kind has already been known well in crystals of alkali halides since the time of HILSCH and POHL.[1] Recent work has established that the structure of the fundamental absorption edge is some common phenomenon, detected in a number of crystals:* $Cu_2O$, CdS, CdSe, ZnS, $HgT_2$, $PbT_2$, CuCl, CuBr, CuT, BaO and others.

The large absorption coefficient in structure lines allows us to refer them to the crystal lattice. This very fact, together with the disposition of the lines at the very edge of the fundamental absorption give us grounds to connect the linear structure with formation of excitons, theoretically forecast by FRENKEL[2].*

I shall mainly dwell on the investigations of my laboratory in Leningrad carried on with the active participation of N.A. KARRYEV, B. P. ZAHARČENJA, A. A. KAPLYANSKY, B. S. RAZBYRIN, B. V. NOVYIKOV, V. B. SOBOLEV, M. A. JAKOBSON and others.

The most interesting and clear results have been obtained on the cuprous oxide crystal where, at the absorption edge, two series of narrow lines,

* However, it must be noted that in some crystals, such as: $V_2O_5$, $MoO_3$, $As_2S_3$, $Bi_2O_3$, $TiO_2$ and some others the structure at the absorption edge has not been found.

* However, one should always bear in mind that some narrow absorption lines may be connected with impurity centres and defects in the crystal lattice.

"yellow" and "green", can be observed (Fig. 1). The frequencies of these lines, converging to the series limits, well satisfy the hydrogen-like relation of the kind:

$$\nu_n = \nu_\infty - \frac{R_{ex}}{n^2} \qquad (1)$$

$n = 2, 3, 4, 5, 6, 7, 8, 9, 10 \ldots$ for "yellow" series

$n = 2, 3, 4, 5 \ldots$ for "green" series

where $\nu_\infty$ is the frequency of the series limit (the photodissociation of exciton), $n$ the quantum number and $R_{ex}$ the Rydberg constant for the exciton, connected with the Rydberg constant $R$ by the relation:

$$R_{ex} = \frac{R\mu^*/m}{n_0^4}$$

where $n_0$ is the index of refraction, $m$ is the electron mass in vacuum and $\mu^*$ is the reduced effective mass of the exciton,

$$\frac{1}{\mu^*} = \frac{1}{\mu_e^*} + \frac{1}{\mu_h^*}$$

where $\mu_e^*$ and $\mu_h^*$ are the effective masses of the electron and the hole.

The hydrogen-like series in cuprous oxide points to existence of Mott excitons in the crystal.

Considering the hydrogen-like model of the WANNIER-MOTT exciton[3] one can calculate the exciton diameter in the cuprous oxide crystal with the formula:

$$d_{ex} = 2(\hbar^2/\mu^* e^2) n_0^2 n^2 \qquad (2)$$

where $n_0$ is the index of refraction ($n_0 = 2{\cdot}5$ for $Cu_2O$), $\mu^*$ is the reduced effective mass of the exciton.

Defining $\mu^*$ from the exciton series ($\mu^* \cong 0{\cdot}25$ m), we obtain from the formula (2) for lowest and highest experimental values of $n$ the sizes of the exciton diameters:

$$n = 2 \qquad d_{2ex} \cong 100\,\text{Å}$$
$$n = 10 \qquad d_{10ex} \cong 2500\,\text{Å}$$

Hence, it is evident that the exciton diameters for high excitation states (great quantum numbers) are extremely large.

Naturally, mistrust and doubt may arise as to whether there can really exist in crystals quasi-atoms-excitons consisting of electron and hole of such large size. Perhaps this idea of exciton is a result of a wrong interpretation of experimental fact—the existence in the $Cu_2O$ crystal spectrum of a ten-member series. However, we must necessarily come to the conclusion that such great excitons do exist in crystals. This is pointed at by two independent phenomena which we were able to observe in the exciton spectrum—the Stark effect and the Zeeman effect.

ZAHARČENJA, REGNOV and I were able to observe[4] the Stark effect on the members of the exciton series even in a weak electric field $E = 5$ kv/cm. That is possible only when the exciton sizes are very large. It is further possible to observe the phenomenon of the ionization (dissociation) of exciton by a weak electric field. Beginning with the field strength $E = 6$ kV/cm the high members of the series gradually disappear being covered by the fundamental absorption edge shifting on the exciton series (Fig. 2). As the field increases the absorption edge covers more and more series members so that when the field $E = 30$ kV/cm, the whole exciton yellow series disappears. The exciton dissociates under the influence of the field which tears off the electron from the hole. The tearing off of the electrons by the electric field is also observed in atoms though the field then is very strong, $E = 1000$ kV/cm. The fact that the same phenomenon is observed in excitons with fields a hundred times less points to the large size of the exciton's orbits.

Further, our research work with ZAHARČENJA has shown[5] that the members of the exciton series in $Cu_2O$ do not display an ordinary paramagnetic Zeeman effect proportional to the magnetic field $H$ but a diamagnetic one proportional to the square of the magnetic field. Under the influence of the magnetic field there takes place a shift of the split exciton lines to the violet part of the spectrum towards the series limit (Fig. 3). The shift is greater the higher the quantum number $n$ of the series member and increases with the increase of the magnetic field. Investigations have shown[5] that the shift is proportional to $H^2$ and $n^4$.

These experimental results are in full agreement with the theory of the diamagnetic quadratic Zeeman effect according to which the diamagnetic

shift is proportional to the square of the electron orbit radius and, therefore, to quantum number to the fourth power.[6]

$$\Delta W = \frac{e^2}{8mc^2}(x^2+y^2)H^2. \qquad (3)$$

Agreement between experiment and theory shows that the observed shift of the series members of exciton in a magnetic field is due to the diamagnetism of the exciton. The diamagnetic shift in the Zeeman effect is very great as can readily be observed with the series member having the quantum number $n = 3$, while in atomic spectra such a shift is observed[7] on very high series members ($n = 30$) only. This shows that the exciton diamagnetism is very great; that, in its turn, is a consequence of very large exciton orbits.*

The diamagnetic shift in the exciton spectrum (equation (3)) allows one to determine the exciton radius. The shift for series member $n = 5$ measured experimentally is 1·8 $cm^{-1}$. This value determines the exciton diameter according to equation (3). When $H = 28000$ oersted, the exciton diameter becomes $d_{5ex} = 400$ Å. The size of the diameter for the same excited state of the exciton calculated (equation (2)) from the Mott exciton model was found to be $d_{5ex} = 500$ Å. The agreement between the calculated value is good enough considering the approximate manner of calculation.

Thus, the study of the Zeeman effect independently of the Stark effect and the series relations (equations (1) and (2)), also point to the extremely great dimensions of the exciton in cuprous oxide crystals.†

A more thorough study of the Zeeman effect in the exciton spectrum leads to the conclusion[8] that an ordinary paramagnetic Zeeman effect observed in free atoms is fully absent or rather small in the series members ($n = 3, 4, 5, 6$) of the exciton in $Cu_2O$ crystals. The splitting of the series members is caused by the diamagnetic effect only. This conclusion follows from a number of observations and from the experimentally established fact that the picture of magnetic splitting is completely or almost completely identical in $\pi$ and $\sigma$ components (Fig. 4). This is not observed in the Zeeman effect in free atomic systems.

The value of magnetic splitting $\Delta\nu$ of a normal Zeeman triplet in the exciton spectrum must be proportional to $(\mu_e^* - \mu_h^*)$—the difference between the effective masses of electron and hole in the crystal.[9] The magnetic splitting $\Delta\nu$ may be equal to 0, i.e. the linear Zeeman effect may be absent only when $\mu_e^* \cong \mu_h^*$. Thus it follows that in a cuprous oxide crystal there exists an exciton of the quasipositronium type with equal or almost equal masses of electron and hole.

This conclusion based on the absence of the ordinary paramagnetic Zeeman effect in the series members in $Cu_2O$ is at the same time a proof that the hydrogen-like series of narrow lines in the $Cu_2O$ crystal is really due to the exciton and not to some kind of impurity centres or defects in the $Cu_2O$ lattice. Were the series connected with such centres and not with excitons, the ordinary linear Zeeman effect would have to be observed in the series lines. However this is not observed.

The study of the magnetic field action upon the cuprous oxide exciton spectrum has brought Zaharčenja and myself to one more rather interesting phenomenon.[10] We have discovered that near the series limit, where the diamagnetic shift is comparable with the distance between the neighbouring series members, there appears a spectrum consisting of almost equidistant lines. The distance between the lines when $H = 30000$ oersted is about 2 $cm^{-1}$. Gradually weakening and becoming

* It would be of great interest to observe the high diamagnetism of the exciton with the aid of direct measurements of magnetic susceptibility. Some time ago, Sel'kin and I made experiments of this kind illuminating the crystal with light which excites excitons. Experimental difficulties, however, caused by the perturbing action of the photomagnetic effect which appears during illumination of the crystal in the magnetic field did not make it possible to obtain as yet clear and definite data.

† While Zaharcenja and I were investigating the exciton spectrum in cuprous oxide there arose of course the question of whether very thin $Cu_2O$ plates could hold such large excitons.

If the $Cu_2O$ plates are thin enough, some of the large excitons especially those which get excited near the surface cannot be formed and cannot exist in plates. This phenomenon must be manifest in the disappearance of those lines at the exciton series limit which are connected with the excitation of very large excitons. Perhaps this is why in the experiments of Zaharčenja and myself in thin plates the highest members of the exciton series seem to be weakened near the very limit of the series.

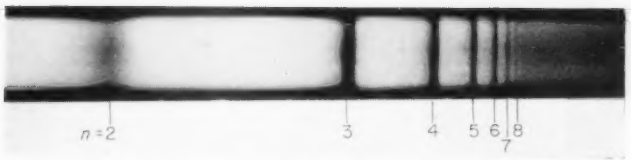


FIG. 1. Yellow series of the exciton in a $Cu_2O$ crystal at $T = 1{\cdot}3°K$

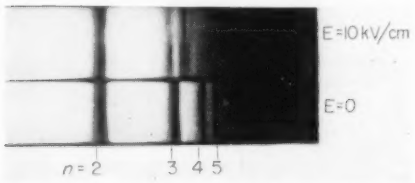


FIG. 2. Stark effect on the lines of the exciton yellow series in a $Cu_2O$ crystal at $T = 77{\cdot}3°K$.

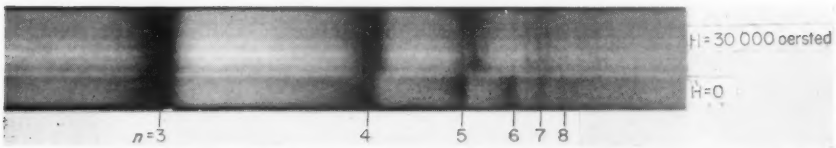


FIG. 3. Diamagnetic Zeeman effect on the lines of the exciton yellow-series in a $Cu_2O$ crystal at $T = 4{\cdot}2°K$.

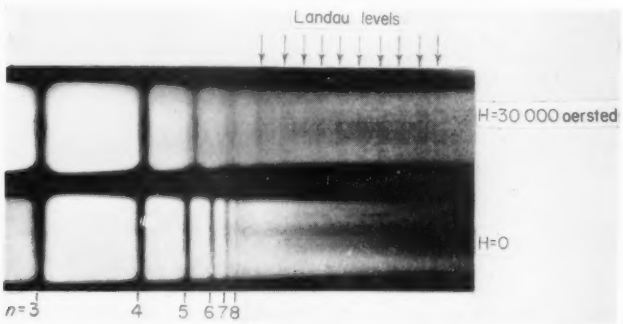


FIG. 4. Diamagnetic Zeeman effect on the lines of the exciton yellow series in a $Cu_2O$ crystal at $4{\cdot}2°K$. $\pi$ and $\sigma$ components

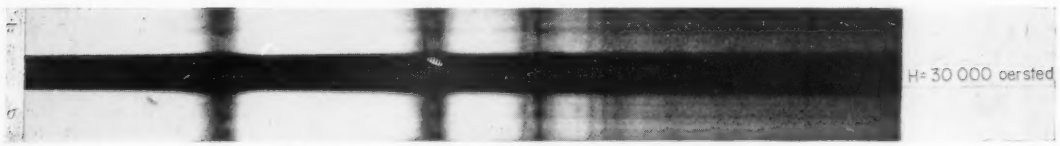


FIG. 5. Absorption maxima due to Landau levels in the continuous background beyond the exciton series limit of a $Cu_2O$ crystal in a magnetic field at $T = 4{\cdot}2°K$.

[facing page 174

VOL. 8 1959

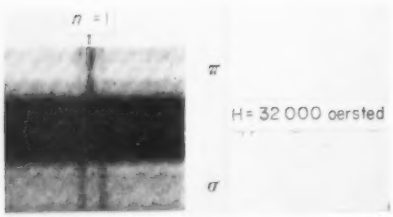


FIG. 6. Zeeman triplet of a sharp absorption line in the $Cu_2O$ crystal spectrum at $T = 4{\cdot}2°K$.

VOL
8
195

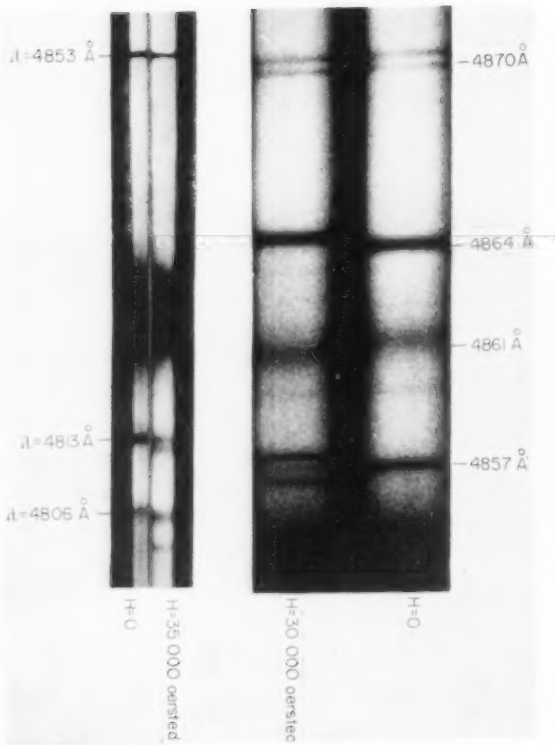


FIG. 7. Zeeman effect on the lines of the CdS crystal spectrum at the edge of the fundamental absorption.

irregular this linear spectrum extends beyond the series limit where in the absence of a magnetic field a continuous spectrum corresponding to the exciton dissociation is observed. In addition, beyond the exciton series limit on the background of the continuous spectrum there appears in the magnetic field case almost equidistant diffuse absorption maxima (Fig. 5). When the field $H = 30000$ oersted, the distance between the absorption maxima is about 7 $cm^{-1}$. On these maxima are superposed barely resolved lines corresponding to some kind of fine structure. Thus in a magnetic field the continuous spectrum beyond the exciton series limit is no longer continuous, but reveals two phenomena: (1) absorption maxima beyond the series limit and (2) a fine structure on them. The further the absorption maxima from the series limit (when $H = 0$) the weaker their intensity and they gradually melt into the continuous absorption background. At a magnetic field equal to $H = 30000$ oersted we could observe up to ten such maxima.

The described picture of an exciton spectrum in a magnetic field is not to be interpreted as a strong diamagnetic shift of highest series members. The approximate equidistance of absorption maxima beyond the series limit does not correspond to the $H^2$ law of diamagnetic shift, but the distance between the maxima is proportional to the magnetic field $H$.

This makes us suppose that here we have to do with a new phenomenon of the appearance of diamagnetic levels of the exciton similar in their characteristics to diamagnetic levels of a charge carrier moving in the magnetic field in accordance with LANDAU theory[11] and observed in cyclotron resonance experiments. However, for excitons this phenomenon must have specific outlines. The electron and hole in the exciton are not free; they are bound by coulomb forces. The coulomb forces are strong for the low states of the exciton and predominant as compared with Lorenz forces arising from a magnetic field $H$. On the contrary the coulomb forces are weak at the highest excited states. The magnetic forces are predominant here determining the regularities near the series limit and call forth the equidistant maxima in the exciton spectrum.

Owing to the magnetic field there can exist some nondissociated states of the exciton beyond the series limit. The magnetic field does not let the electron tear off from the hole, i.e. dissociate the exciton and on the contrary keeps the electron and hole in stable discrete states.

The general picture of continuous absorption with diffuse maxima beyond the exciton series limit (without fine structure) given above is well explained by the Landau[11] level scheme. It needs no coulomb interaction for its interpretation and might be also observed for free electrons and holes not bound into an exciton. On the contrary the appearance of discrete lines in the form of some fine structure on these diffuse absorption maxima is called forth by the presence of the coulomb field between electrons and holes even though a weak one at long distances between electron and hole. The appearance of discrete fine structure is typical namely for the bound state of electron and hole, i.e. typical for an exciton.

The theoretical study of the exciton energy spectrum in a magnetic field made by Prof. P. P. Pavinsky, confirms these considerations.

The Schrödinger equation for the motion of the hole and electron of the exciton in a coulomb force field and a magnetic field $H$ (directed along $Z$ axis) may be written as follows:

$$\left[-\frac{\hbar^2}{2\mu^*}\Delta+\frac{e^2H^2}{8\mu^*c^2}(x^2+y^2)-\frac{e^2}{\epsilon r}\right]\psi = E\psi \quad (4)$$

where $\mu^*$ is the reduced effective exciton mass, $\epsilon = n_0^2$ is the optical dielectric constant. In the equation a member is missing that characterized the paramagnetism of an exciton. As the effective masses of electron and hole in a cuprous oxide crystal are approximately equal $\mu_e^* \cong \mu_h^*$, this member of the equation (4) is small and need not be taken into account. Weak magnetic effects connected with the shift of the centre of gravity of the exciton are also disregarded.

A mathematical analysis of the solutions of the equation (4) shows that the energy distance $\Delta E$ between the absorption maxima beyond the series limit, equals $\Delta E = \hbar\Omega$ where $\Omega = eH/\mu^*c$—cyclotron frequency, corresponding to the magnetic field $H$. When $H = 29000$ oersted and the reduced effective mass $\mu^* = 0{\cdot}25\ m_e$, the calculated value of $\Omega$ becomes $\Omega_{calc} = 11$ $cm^{-1}$, while the experimental value $\Omega_{exp} = 7$ $cm^{-1}$. The difference between these values may be connected

with some inaccuracy of the experiment or, possibly, with the dependence of the effective exciton mass on the magnetic field.

The frequency $\Omega$, found from the exciton spectrum in a magnetic field is equal to the sum† of cyclotron frequencies $\Omega_e$ and $\Omega_h$ of electron and hole forming the exciton.

$$\Omega = (\Omega_e + \Omega_h);\ \Omega_e = \frac{eH}{\mu_e^* c};\ \Omega_h = \frac{eH}{\mu_h^* c}.$$

$\Omega$ may be called "the cyclotron frequency of the exciton" as it might have appeared in the absorption of a low-frequency electromagnetic radiation in cyclotron resonance experiments.

It seems to us that the phenomena we have observed—the equidistant structure beyond the exciton series limit of $Cu_2O$ in a magnetic field is by its very nature similar to the oscillatory magneto absorption effect observed by ZWERDLING and LAX[12] in germanium as well as by BURSTEIN and PICUS[13] in InSb.

Now I should like to return to the problem of exciton sizes in crystals. In addition to excitons of large radii there may also exist excitons of small radii in the crystal lattice. Zaharčenja, Razbyrin and I have observed in the spectra of the crystals of cadmium sulfide, groups of lines at the edge of the fundamental absorption which show an ordinary Zeeman splitting in the magnetic field and do not reveal any diamagnetic shift (Figs. 6 and 7). In other words, their Zeeman effect, as it is, differs little from the phenomena observed in free atoms and ions or, for example, in rare earth crystals. It shows that the electron excitation radii here are not large, and probably do not pass the limit of the elementary crystal cell.

Excitons in crystals can differ not only in size but in mutual spin orientation of electron and hole. That leads to two different kinds of excitons: *para*-excitons and *ortho*-excitons having different physical properties.

Under the influence of light there may arise in the crystal only *para*-excitons. *Ortho*-excitons may appear under the action of light waves only in case of some simultaneous disturbing influence which may cause the turn-over of the spins in the exciton. Such a disturbing action at the formation of an *ortho*-exciton may be caused, for example, by an electron lattice defect or a paramagnetic ion as well.

The "life-time" of an *ortho*-exciton in a crystal must be substantially longer than of *para*-exciton, as its annihilation is less probable. The Zeeman effect of the *ortho*-exciton must differ from the Zeeman effect of *para*-exciton.

The energy difference between the levels of *para*- and *ortho*-excitons for excitons of large radii is very little (as for *para*- and *ortho*-positronium). It can be considerably greater only for excitons of small radii because of the interaction between the electron of the exciton with other electrons of the ion in the lattice, near which the exciton was created. As it is revealed with a helium atom, the levels of an *ortho*-exciton energetically are believed to be lower than the levels of a *para*-exciton. Thus, the absorption (excitation) spectrum of an *ortho*-exciton, which must be very weak, as well as its emission (luminescence) spectrum at its annihilation must be shifted to the long-wave side from the *para*-exciton spectra.

It seems possible that the so-called edge emission observed in the luminescence of a number of crystals, is connected with the formation and annihilation of *ortho*-excitons.

Lately there appeared some theoretical work by TAKEUTI[14] and TRLIFAJ[15] studying some aspects of *para*- and *ortho*-excitons.

† Theoretically it has not been quite cleared up whether the frequency of $\Omega$ should be equal to a sum or a half-sum of the cyclotron frequencies of $\Omega_e$ and $\Omega_h$.

## REFERENCES


1. HILSCH R. and POHL R. W., *Z. Phys.* **59,** 812 (1930).
2. FRENKEL J., *Phys. Rev.* **37,** 17, 1276 (1931).
3. WANNIER G. H., *Phys. Rev.* **52,** 191 (1937); MOTT N. F., *Proc. Roy. Soc.* A **167,** 384 (1938).
4. GROSS E. F., ZAHARČENJA B. P. and REJNOV N. M., *Dokl. Akad. Nauk. SSSR* **97,** 57, 221 (1954).
5. GROSS E. F. and ZAHARČENJA B. P., *J. Phys. Radium* **1,** 68 (1957).
6. VAN VLECK J. H., *Theory of Electric and Magnetic Susceptibilities*, p. 178. Oxford Press (1939).
7. JENKINS F. A. and SEGRE E., *Phys. Rev,* **55,** 52 (1939); HARTING D. and KLINKENBERG P. F. A., *Physica* **24,** 669 (1949).
8. GROSS E. F. and ZAHARČENJA B. P., *Zh. tekh. fiz.* **27,** 1940 (1957).
9. SAMOJLOVIC A. G. and KORENBLIT L. L., *Dokl. Akad. Nauk. SSSR* **101,** 55 (1955).
10. GROSS E. F., ZAHARČENJA B. P. and PAVINSKIJ P., *Zh. tekh. fiz.* **27,** 2177 (1957).
11. LANDAU L. D., *Z. Phys.* **64,** 629 (1930).
12. ZWERDLING S. and LAX B., *Phys. Rev.* **106,** 51 (1957).
13. BURSTEIN E. and PICUS G. S., *Phys. Rev.* **105,** 1123 (1957).
14. TAKEUTI Y., *Prog. Theor. Phys.* **18,** 421 (1957).
15. TRLIFAJ M., *Czech. J. Phys.* **7,** 673 (1957).

*J. Phys. Chem. Solids* Pergamon Press 1959. Vol. 8. pp. 177–179. Printed in Great Britain

# G.3 CONCERNING THE PROBLEM OF EXCITON DIFFUSION IN PHOTOCONDUCTORS

**I. BROSER and R. BROSER-WARMINSKY**

Institut für Elektronenmikroskopie am Fritz-Haber-Institut
der Max-Planck-Gesellschaft, Berlin-Dahlem

IT has been reported by BALKANSKI and one of the authors[1] (I. BROSER) as well as by DIEMER and HOOGENSTRAATEN[2] that the propagation of photoconductivity over long distances in partially illuminated crystals of cadmium and zinc sulfide may be related with an energy transport by thermal diffusion of excitons. However, another effect for explaining the existence of long range photodiffusion appears, i.e. the scattering of the incident or luminescent light and the reabsorption of this radiation in the non-illuminated region of the crystal.[3] In order to clear up this problem, we performed a number of investigations by measuring simultaneously the photoconductivity and the flux of the luminescent light in that part of the crystal which is shielded from direct illumination; another part of the crystal is irradiated either by visible light of different wavelengths or by X-rays and $\alpha$-particles respectively. In all those cases in which the primary radiation could not reach the region of the investigated crystal directly, it could be shown[4] that the scattered and reabsorbed luminescent light was responsible for the photoconductivity when the same photocurrent was produced by scattered luminescent radiation or by monochromatic light of a wavelength in the region of the emission band, no measurable difference between the luminous fluxes could be observed. This fact is to be seen from Fig. 1 (curves I), where the wavelength dependence of photoconductivity and luminous flux of a not directly illuminated part of a CdS crystal is shown. The values of photoconductivity and luminous flux were set equal in the region of strong absorption ($\lambda < 510$ m$\mu$). We note that the curves intersect again at about 720 m$\mu$, this point being the position of the maximum of the emission spectrum of the crystal. The same relation between photoconductivity and luminous flux holds, if the time dependence of a photocurrent pulse produced by a short light pulse is investigated. No marked difference in the shape of the photocurrent can be observed, if the light pulse arises from luminescent or from equivalent monochromatic light.

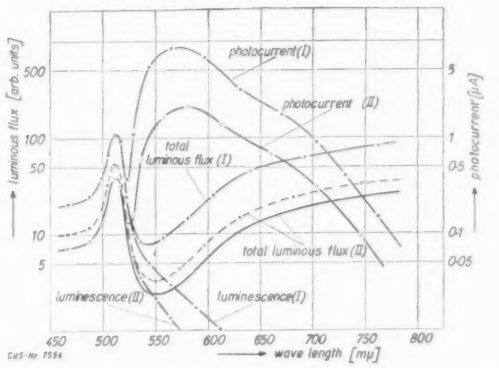


FIG. 1. Photocurrent, flux of luminescent light, and total luminous flux as function of the wavelength of the incident light in a not directly irradiated part of a CdS crystal: (I) before and (II) after cleaving the crystal.

Another proof of the non-validity of the exciton diffusion theory follows from the experiment shown in Fig. 1 (curves II). It indicates in contrast to the measurements of BALKANSKI and WALDRON[5] that energy transfer over long distances is still possible if the crystal has been cleaved into two parts and cemented with a substance of a high refractive index. The only effect of cleaving is that both photoconductivity and light current decrease in consequence of the loss of light near the cemented area, whereas the shape of the curves does not change. A similar experiment, the influence of $\alpha$-particle bombardment on the diffusion of photoconductivity, is shown in Fig. 2. If one assumes that energy transfer is by excitons,

it must be expected that any region of the crystal being damaged by α-particles would diminish the intensity of the flux of excitons, due to the increase of recombination processes at the perturbed lattice. On the other hand, no decrease of photoconductivity should occur if the energy propagation is caused by light scattering, as the α-particles do not produce visible defects. The latter observation was found to be true for the case of strongly-absorbed blue light as well as for weakly-absorbed yellow light. The change of the electrical properties of the bombarded zone is shown by the decrease of the diffused conductivity by indirect excitation with α-particles (decrease of luminescent light[6]) and by the increase of α-conductivity within the bombarded zone.[6]

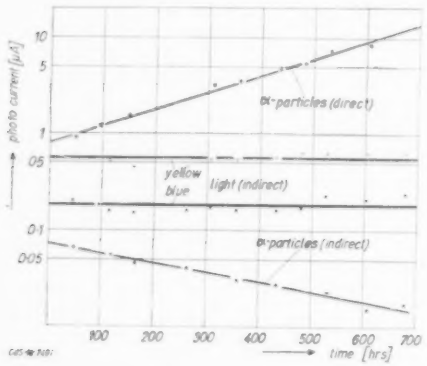


FIG. 2. Effect of α-particle bombardment on the photoconductivity of a CdS crystal:
Upper curve: Bombarded zone is site of irradiation and site of measurement
Middle curves: Bombarded zone lies between site of irradiation and site of measurement
Lower curve: Bombarded zone is site of irradiation, but not site of measurement.

An argument against the explanation of photodiffusion by light scattering was the behavior of this effect at low temperatures.[7] As shown in Fig. 3 the photocurrent in a not directly illuminated part of the crystal increases with decreasing temperature much more if excited in the region of lattice absorption than if irradiated with monochromatic yellow or red light. In terms of the exciton theory this means that the lifetime of excitons would increase with decreasing temperature, thus increasing the diffusion length for the indirectly excited photoconductivity. But in

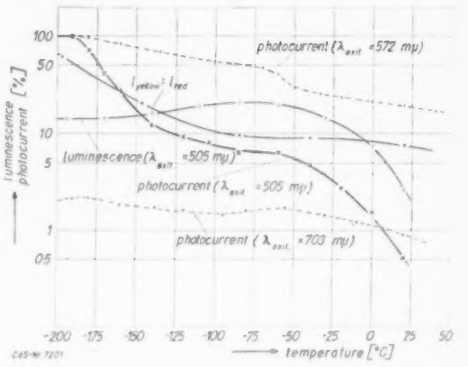


FIG. 3. Temperature dependence of photoconductivity, of the flux of luminescent light, and of the ratio of yellow and red luminescence in a not directly irradiated part of a CdS crystal.

reality, the temperature dependence of the photoconductivity comes from the change of the luminescence colour from red ($\lambda \max \approx 700\ m\mu$) to yellow ($\lambda \max \approx 575\ m\mu$), the ratio of the intensity of these two emission bands being drawn in Fig. 3. Besides, the sharp decline of conductivity from −50 to +25°C may be explained by the decrease of luminescent efficiency in this region of temperature. The fact that at lower temperatures the not directly excited photoconductivity will be caused by luminescent radiation of a short wavelength is to be seen more accurately in Fig. 4. Here, the photoconductivity, the total luminous flux, and the luminous flux of the total luminescence and of the red and the yellow luminescence especially, is reproduced as a function of the wavelength of the exciting illumination. Normalizing

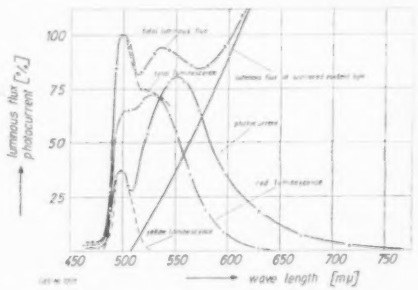


FIG. 4. Photocurrent, flux of luminescent light, and scattered incident light as function of the wavelength of the incident light in a not directly irradiated part of a CdS crystal at 77°K.

the photoconductivity peak at 500 mμ and the peak of the yellow band, we find that a monochromatic radiation of 575 mμ with the same intensity as that of the yellow luminescence will give the same photoconductivity. Indeed, 575 mμ is exactly the wavelength of the band maximum of the yellow luminescence. Measurements in the region of liquid-helium temperature have recently been performed. With the crystals investigated up to now no measurable diffusion of photoconductivity could be observed. This may be also an indirect argument for the light scattering theory, as in this case no excitation of photoconductivity with direct light in the long wavelength tail of the absorption band could be found, and therefore, neither the luminescent nor the scattered light could produce photoconductivity in the not directly illuminated part of the crystal.

Summarizing the results of our measurements, we may state that there is no cogent reason to assume exciton diffusion in order to explain the propagation of photoconductivity in photoconductors. On the other hand, it cannot be concluded from our investigations that exciton diffusion in the crystals does not occur at all, but if there is any energy transport by excitons, it will be masked by the much more effective mechanism of scattering and reabsorption of luminescent light.

VOL. 8 1959

## REFERENCES


1. BALKANSKI M. and BROSER I., paper given at *International Conference on Semiconductors and Phosphors, Garmisch-Partenkirchen, Germany*, August 28–September 1 (1956).
2. DIEMER G. and HOOGENSTRAATEN W., *J. Phys. Chem. Solids* **2**, 119 (1957).
3. BALKANSKI M. and BROSER I., *Z. Elektrochem.* **61**, 715 (1957).
4. BROSER I. and BROSER-WARMINSKY R., *J. Phys. Chem. Solids* **6**, 386 (1958).
5. BALKANSKI M. and WALDRON R. D., *Tech. Rep.* 123, *Laboratory for Insulation Research.* Massachusetts Institute of Technology, Cambridge, Mass., U.S.A. (Nov. 1957).
6. BROSER I. and WARMINSKY R., *Z. Naturf.* **6a**, 85 (1951).
7. DIEMER G., Private communication.


*J. Phys. Chem. Solids* Pergamon Press 1959. Vol. 8. pp. 179–181. Printed in Great Britain

G.4

# ENERGY TRANSFER IN SEMICONDUCTORS

**M. BALKANSKI**

Laboratoire de Physique, Ecole Normale Supérieure, Paris, France

WHEN an exciton produced in a semiconductor annihilates after propagation by returning in its fundamental state emitting a photon, this photon can be reabsorbed creating a new exciton if its frequency corresponds to the resonance energy. The processes can repeat themselves as long as the photon emission takes place in the interior of the crystal at a few λ beneath the surface. The energy propagates by alternative creation and annihilation of excitons coupled by the radiation field until the excited state reaches the surface where the photon is emitted out of the system and detected. This mechanism has as a model the multiple diffusion demonstrated for the first time in the case of gases in the Laboratory of Prof. Kastler by J. E. Blamont. The idea for introducing multiple diffusion in the treatment of exciton diffusion was given by P. Aigrain and is based on two experimental facts observed in cadmium sulfide.

(1) Migration of the excitation in the solid for a large distance from the point where it has been created.

(2) The lifetime of the macroscopically observed excitation is much longer than the lifetime of a single excited state.

The mechanism we are proposing to describe the energy transfer at great distances includes two successive steps repeated alternately.

(a) Absorption of light and creation of an electron–hole pair strongly interacting between them whose zeroth order excited wave function can be constructed as[1]

$$\psi(\boldsymbol{k}-\boldsymbol{K},\boldsymbol{k}) = \frac{1}{\sqrt{(2N)!}} \sum_P (-)^P P\Phi(\boldsymbol{k}-\boldsymbol{K},\boldsymbol{k})P\chi$$

where

$$\Phi(\boldsymbol{k}-\boldsymbol{K},\boldsymbol{k}) = u_{k_1}(\boldsymbol{r}_1)\dots u_k{}^e(\boldsymbol{r}_i)\dots u_{k_N}(\boldsymbol{r}_N)\cdot$$
$$u_{k_1}(\boldsymbol{r}_{N+1})\dots u_{k-K}(\boldsymbol{r}_{N+i})\dots u_{k_N}(\boldsymbol{r}_{2N})$$

$P$ means the permutation of order $(2N)!$, $u_k(\boldsymbol{r})$ is the Bloch function in the valence band and $u_k{}^e(\boldsymbol{r})$ that in the conduction band. For each spin state we have $N^2$ wave functions $\psi(\boldsymbol{k}-\boldsymbol{K},\boldsymbol{k})$ defined by vectors $\boldsymbol{k}-\boldsymbol{K}, \boldsymbol{k}$ representing respectively the Bloch function of the valence band from which an electron is missing and the Bloch function of the conduction band to which an electron has been raised. From these $N^2$ wave functions of the zeroth order we get, by a unitary transformation, $N^2$ new wave functions:

$$\Psi(\boldsymbol{K},\boldsymbol{R}) = \frac{1}{\sqrt{N}} \sum_k \exp[-i\boldsymbol{k}\boldsymbol{R}]\Psi(\boldsymbol{k}-\boldsymbol{K},\boldsymbol{k}).$$

Each of these represents a so-called excitation wave which corresponds to an electron–hole complex separated by $\boldsymbol{R}$ in space and moving with a wave vector $\boldsymbol{K}$. Since we do not wish to consider phonons in this treatment we will take $K = 0$.

(b) The excited electron returning to its ground state emits a photon. This corresponds to a coupling of the excitation wave with the radiation field. The emitted photon can be reabsorbed regenerating the excitation wave.

This second step may seem similar to the mechanism evoked in the theory[2] of sensitized luminescence but actually it differs not only phenomenologically but also in theoretical treatment. The excitation we are considering is a property of the pure lattice and the transitions involve coupling between the excitation waves and the radiation field.

The propagation of the excitation energy can be considered as exciton diffusion if the two following conditions are satisfied:

(i) The excitation wave conserves the wave vector $|\boldsymbol{K}|$ over the whole process

(ii) The multiple diffusion of the photon by the excitation waves is a coherent process. The coherence being defined as in the case of the multiple diffusion involved in optical resonance, which for a gas is as follows:

If the state of an atom I after absorption of a photon is described by the wave function $\psi_{\mathrm{I}}(t)$, this excitation can be re-emitted after a time $\tau$ and reabsorbed by a second atom. The wave function $\psi_{\mathrm{II}}(t)$ which will describe the second excited state after reabsorption can be considered in two different ways:[3]

(1) If $\psi_{\mathrm{II}}(t)$ is a proper atomic state, i.e., if between the coefficients of the expansion of the wave functions of the first atom $C_i$ and the second atom $C'_i$ only an intensity relationship exists (in $|C'_i|^2$ and $|C'_i|^2$) then the diffusion is incoherent. The processes I and II are distinct and independent. We shall ignore such processes.

(2) If $\psi_{\mathrm{II}}(t)$ takes the form

$$\psi_{\mathrm{II}}(t) = \sum_i C_i'(t)\psi_i{}^{\mathrm{II}}$$

where the $C'_i$ are determined in phase and magnitude by the $C_i$ of the first atom then the diffusion is coherent. In the case where $C_i$ and $C'_i$ are equal in phase and magnitude one can say that the two atoms are exchanging their wave functions and in this case the notion of coherent multiple diffusion covers completely that of exciton propagation.

A complete theoretical treatment of the multiple diffusion in the case of gases is carried out by J. P. Barrat which will be published soon in *J. Phys. Radium*.

The method used in the theoretical treatment of multiple diffusion involves time dependent perturbation theory. The system first considered is set up from $N$ atoms and the radiation field. The states taken into account are

(1) the ground states plus a photon
(2) one excited state (exciton) and no photon present.

The system Hamiltonian is built up from a diagonal part $\mathscr{H}_0$ whose matrix elements are the energies $\epsilon_0$ and $\epsilon_n$ of the levels, and an off-diagonal part $\mathscr{H}_{\mathrm{int}}$ which has non-zero matrix elements only between the ground state and the excited state. $\mathscr{H}_{\mathrm{int}}$ is the part of the radiation field responsible for the dipolar electronic transitions between the ground and excited states with absorption and

emission of a photon. Only this part of the radiation field is quantised and all the possible states of the system for which the principal of energy conservation shall not be respected would not be accounted for. The exciton of energy $E_k$ migrates through the crystal with a group velocity $\boldsymbol{v}_k = 1/\hbar \operatorname{grad}_k E_k$ and as the matrix elements of $\mathscr{H}_{\text{int}}$ depend on the position of the excited state, the matrix elements of $\mathscr{H}_{\text{int}}$ are consequently time dependent.

We are considering in this treatment, in addition to the pure radiation field, the contribution of its interaction with particles. As we are considering the interaction as a perturbation, it is suitable to introduce the interaction representation which has the advantage of removing the trivial time dependence of the free fields and of introducing the time variation of the state vector due only to the interaction.

Thus the computed radiative emission by recombination of an exciton is:

$$|b_{\mu,\,\boldsymbol{k}_{ph},\,\lambda(t=\infty)}|^2 = \frac{|a_k|^2\,|\langle\mu|\boldsymbol{e}_\lambda\cdot\boldsymbol{D}|m_0\rangle|^2}{(\epsilon_0-\epsilon_n-\boldsymbol{k}\cdot\boldsymbol{v}_k)^2+\gamma^2/4}\times Q.$$

For a small or negligible exciton-phonon interaction, i.e., when the effective mass of the exciton is not too large, the emitted optical line has the Lorentz form displaced by Doppler effect (connected with the term $\boldsymbol{k}\cdot\boldsymbol{v}_k$ due to the velocity of propagation of the excitation wave). The breadth of the line is $\gamma$. The exciton being propagated in a crystalline medium the right hand member is multiplied by the square of the ratio of the electrical field within the crystal and that of the exciton which is not homogeneous and depends on an effective dielectric constant, $K = 1/f(r)$, function of the radius of the electronic orbit $r$.

For a strong phonon interaction the lattice vibrations which interfere with the radiation field have to be introduced as a probability function $b_p(t)$ of the states $|p\rangle$ which should be normalized on the atomic scale. The exciton effective mass will then be large and the absorbed and emitted line will have a Gaussian shape. The experimental study by optical and magnetic resonance will give information as to the degree of exciton-phonon interaction. This should also give information on exciton propagation or degree of binding of the excited state.

Considering two excitation waves one of which annihilates when the other is created by passage of the photon from one to the other one finds a probability of passage of the photon from exciton 1 to exciton 2 or $1/\epsilon_0^2 R_{12}^2$.

Extending this treatment to $p$ passages of a photon after successive creation and annihilation of $n$ excitons one finds an apparent lifetime

$$T = -\frac{1}{\gamma(1-\alpha x)} = \frac{\tau}{1-\alpha x} > \tau$$

$\tau$ is the proper lifetime of the individual exciton. $T$ is the macroscopic value measurable by magnetic resonance.

On the other hand, the total probability of finding one exciton is

$$\text{Trace } \rho(t) = e^{-\gamma(1-x)t}$$

with $x = 1-e^{-2\boldsymbol{k}\cdot\boldsymbol{\nu}\boldsymbol{R}}$.

The time of trapping the radiation in the crystal is then

$$\tau' = \frac{1}{\gamma(1-x)} = \frac{\tau}{1-x}.$$

This shows that in the solids where a reabsorption of the emitted photon is possible one should find the apparent lifetime of the exciton greater than that given by simple estimation on one excited state. Because this multiple process is possible it is also natural to find great diffusion length. This explains the known experimental results. Further experimentation on optical and magnetic resonance should give data on the velocity of exciton propagation and presumably on their effective mass as well. When it will become possible to resolve the lines from electron spin resonance one will become aware of the fine structure of the exciton.

## REFERENCES

1. Takeuti Y., *Prog. Theor. Phys.* **18,** 421 (1957).
2. Dexter D. L., *J. Chem. Phys.* **21,** 836 (1953).
3. Guiochon M. A., Blamont J. E. and Brossel J., *C.R. Acad. Sci., Paris.* **243,** 1859 (1956) and *J. Phys.* **18,** 99 (1957).

*J. Phys. Chem. Solids* Pergamon Press 1959. Vol. 8. pp. 182–187. Printed in Great Britain

# G.5 AN ANALYSIS OF MIXED AMBIPOLAR AND EXCITON DIFFUSION IN CdS CRYSTALS

G. DIEMER, G. J. VAN GURP AND W. HOOGENSTRAATEN

Philips Research Laboratories
N. V. Philips' Gloeilampenfabrieken, Eindhoven–Netherlands

**Abstract**—The experimental set-up for studying photo-diffusion in CdS crystals is discussed. After careful elimination of possible interfering effects (especially the influence of fluorescence light) it is concluded from photo-diffusion measurements at various temperatures that excitation energy can diffuse in an electrically neutral, non-ambipolar form with a finite velocity of propagation. For this exciton type of migration, in one case a diffusion length of 3 mm and a propagation velocity of $10^4$ cm/sec was found.

## 1. INTRODUCTION

THOUGH the theoretical concept of the exciton has been discussed already since 1931[1] only since 1951 experimental evidence for the existence of excitons was found.[2,3] More recently, photo-diffusion measurements on CdS crystals have been performed,[4,5] from which it was concluded that excitons do migrate in this material over rather large distances (of the order of millimetres). From similar experiments, however, BROSER[6] concluded that the migration of excitation energy over such large distances was due to self-excitation by fluorescence light. Admittedly, excitons and light quanta in a solid have many properties in common and this is perhaps the main cause that such a controversy could arise.

It is the aim of this article to throw some light on this problem by pointing out what the properties of a single crystal should be like in order that the effects of exciton diffusion should not be drowned in the interfering effects. On the basis of experiments, performed on one particular, extensively studied CdS crystal which fulfilled the necessary requirements, it will be shown that excitation energy can migrate in an electrically neutral, non-ambipolar form over the distances mentioned with a velocity of propagation much smaller than that of light. For the sake of brevity, only the most salient points will be mentioned here. A more extensive discussion will be given in a forthcoming paper.[7]

## 2. NECESSARY REQUIREMENTS

It is our experience that the following properties of a crystal favour the experimental detection of exciton migration:

(1) Optical clearness and absence of macroscopic physical defects and inhomogeneities.

(2) Large sample dimensions to prevent annihilation at the surface.

(3) Moderate concentration of activator centres from which excitons can eject electrons, resulting in conductivity (very pure samples showed, in general, no large diffusion lengths).

(4) Overlap between the photoconductivity and fluorescence spectra as small as possible.

(5) Low temperature is favourable as long as the overlap (4) does not become too large.

In view of the diffculties encountered in growing and activating large CdS crystals in a well-defined way, one must not be surprised that there still exist large discrepancies between the results of various experimenters.

## 3. EXPERIMENTAL METHOD AND INTERFERING EFFECTS

With the experimental set-up shown framed in Fig. 1 the photocurrent is measured as a function of the shadow width $x$. In the sample under discussion the Hall mobility proved to be equal to that of $n$-type samples. Hence $I(x)$ is a measure for the electron concentration $n(x)$, in which relationship the electrode geometry and the spatial distribution of the charge carriers enter as parameters.

P.E.M. measurements on this sample revealed an ambipolar diffusion length as small as $0{\cdot}1\mu$. The dark conductivity was very low ($\approx 10^{-11}$ $\Omega^{-1}\text{cm}^{-1}$). Ohmic In-amalgam electrodes were used.

Fig. 1 shows $I(x)$ curves, obtained with various

screening conditions. We will now summarize the perturbing effects to be taken into account before the $I(x)$ curves can be interpreted in terms of diffusion lengths.

3.1. *Local inhomogeneities* in the dark-conductivity and in the photoconductivity are revealed by moving a narrow line of shadow or light, respectively, along the crystal, while the current through the crystal is measured by means of two electrodes applied to opposite ends of the crystal[5]. Our sample proved to be sufficiently homogeneous.

3.2. *Irregularities near the probe electrodes and end effects* make it impossible to derive an ambipolar diffusion length from the steep part of the $I(x)$ curves at small $x$-values. Other experimental arrangements are more adequate in this respect.[5] These effects, which do influence the apparent contribution of the tail of the diffusion curve but not its slope, are the following:

(*a*) Divergence of the incident beam and diffraction of the light.

(*b*) Deviations of the electrode edges from a straight line parallel to the edge of the mask.

(*c*) Inhomogeneity of the probe field both parallel to the crystal surface and perpendicular to it. This will spread out the ambipolar drop of the $I(x)$ curve over a distance of the order of the inter-electrode distance $\Delta$ and change the apparent contribution of the tail. If the width of the slit 3 in Fig. 1 exceeds $\Delta$, the region of small $x$-values is even more difficult to interpret. We may furthermore point out the possibility of sudden changes in the $I$, $V$ characteristic if the illumination of a non-transparent electrode is changed.[5]

(*d*) When the area of illumination is reduced to the order of the smallest crystal dimension (large values of $x$) another drop of the $I(x)$ curve occurs, in accordance with the boundary conditions of the diffusion equation.

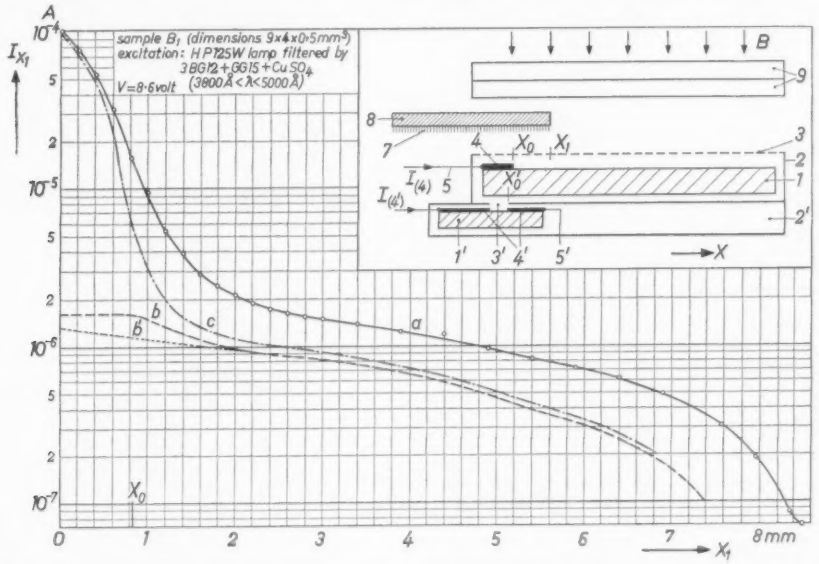


FIG. 1. Framed part: experimental arrangement for studying large photo-diffusion lengths in single crystals (side view). (1) Crystal with probe electrodes (4) and leads (5), mounted inside a black box (2) with a slit (3). The surface of the movable shadow mask (8) is covered with an anti-reflection layer (7) of black velvet paper. The intensity and spectral distribution of the exciting light may be varied by the filters (9). Below box (2) a second light-tight box (2′) contains a sintered CdS–Cu photocell (electrodes (4′), leads (5′)), which measures the intensity of the light falling through a narrow slit (3′) (perpendicular to the $x$-direction) below the probes (4) in the common wall of the two boxes.

Curves: probe current as a function of shadow position $x$. Curve (a): no velvet layer (7) or black paint on probe electrodes; (b) after application of a layer of black paint on and around the probes (4); (c): with velvet paper (7) but without paint; (b′): curve (b) extrapolated to $x = x_0$, showing a tail contribution of about 10 per cent to the photocurrent.

3.3. *Scattering and multiple reflection outside the crystal.* Its influence on the tail contribution is shown by the curves *c* and *a* of Fig. 1. Complete suppression of this scattering is obtained by application of a velvet layer to the shadow mask (curve c). The tail, occurring with curves *b* and *c* can thus not be due to light scattered outside the crystal.

3.4. *Scattering and multiple reflection inside the crystal.* This cannot play a role in our diffusion measurements since we have confined ourselves to excitation by strongly absorbed light. By careful filtering all radiation with a penetration depth larger than about $1\mu$ was eliminated.*

3.5. *Deviations from a monomolecular recombination* of the charge carriers, which is usually assumed for theoretical treatment, reveals itself in a non-linear relation between photocurrent $I$ and excitation intensity $B$. In the intensity region of interest our sample was slightly sublinear ($I \propto B^{0.8}$). With a strongly sublinear dependence or a saturation the diffusion curve will show a tail, even in the case of pure ambipolar diffusion.[5] In our case the correction for non-linearity is not important, changing the diffusion length of the tail from the measured value of about 4 mm to about 3 mm.

3.6. *Influence of fluorescence light.* At room temperature the crystal showed a rather weak fluorescence with a maximum in the near infra-red. At higher excitation densities the spectral distribution $F(\lambda)$ shifted to shorter wavelengths. It was, therefore, difficult to determine $F(\lambda)$ at the moderate excitation densities at which the diffusion measurements were performed. The most reliable results were obtained by using a sintered CdS pellet as a radiation detector, combined with a series of interference filters. This combination proved to be much more sensitive than a monochromator + cooled IP22, even when working with a wide slit. Fig. 2 shows various curves for $F(\lambda)$ obtained in different ways, as well as the spectral response of the crystal and of the CdS monitor. A sharp drop in crystal response in the wavelength region of the fluorescence is observed, which is a favourable factor in preventing an exciton contribution from being drowned in the interfering effect of the fluorescence. In order to determine the contribution of diffused fluorescence light to the probe current, we performed the following measurements (see Fig. 1):

(*a*) The sample (1) was excited by 4358 Å and both the crystal probe current and monitor current were measured (values $I_c$ and $I_m$). The crystal current $I_c$ may contain a contribution $I_{cf}$ due to fluorescence.

(*b*) Excitation by 7230 Å of such an intensity that the monitor current $I'_m$ equals $I_m$ of case (*a*). Now the crystal current was $I'_c = 0{\cdot}010 I_c$ ($\pm$ 20 per cent). With 7490 Å excitation the result was, within the experimental error, the same.

(*c*) Excitation by a simulation spectrum, shown by curve *s* of Fig. 2 (this is somewhat more short-wave than the fluorescence spectrum), and such an intensity that the monitor current $I''_m = I_m$. Now $I''_c = 0{\cdot}10 I_c$.

An analysis[7] shows that from these experiments it can be concluded that the contribution by fluorescence light cannot be larger than about 1 per cent.

## 4. QUENCHING BY INFRA-RED

Infra-red illumination with $\lambda > 8500$ Å (from an incandescent lamp + filter UG 12) reduced the contribution of the tail by a factor of 10, whilst with overall excitation of the sample, such that the probe current was the same as in the diffusion case, the quenching amounted to a factor of 1·3 only. The nature of the influence of I.R. on the diffusion mechanism is not yet understood. With monochromatic I.R. no selective quenching was observed in the region between 0·8 and $10\mu$. On the contrary, two weak stimulation maxima were found (at 1·1 and $1{\cdot}45\mu$).

## 5. TEMPERATURE DEPENDENCE OF THE DIFFUSION

The measurement described in section 3.6 was repeated at a series of temperatures between −196°C and +85°C. The results are shown in Fig. 3. At low temperature the diffused photocurrent increases much more strongly than the photosensitivity at direct illumination (see curve *a*/*b*). Only a small part of this increase is due to the increase of fluorescence and its shift to shorter wavelengths. By means of a simulation spectrum it was found that at −196°C only 20

* When weakly absorbed light is used it is, in principle, possible to investigate its contribution by means of a monitor photocell (cf. ref. (5)).

VOL 8 195

per cent of the observed current was caused by diffused fluorescence radiation.

The temperature dependence of $a/b$, however, may not be interpreted as the temperature dependence of the exciton-diffusion length $l_{De}$ (in the form of $l_{De}^{-1} \propto -\log(a/b)$), because the extrapolated value $I(o)$ of the tail may also depend on temperature. With the help of the data of curve $c$ of Fig. 1, however, we were able to prove that at $-190°C$ the value of $l_{De}$ must be at least four times as large as at room temperature.[7]

### 6. VELOCITY OF PROPAGATION

This was measured with the arrangement of Fig. 1, but using a sinusoidally modulated excitation, the average intensity of which was increased with increasing $x$ in such a way that the average probe current remained constant. The fundamental

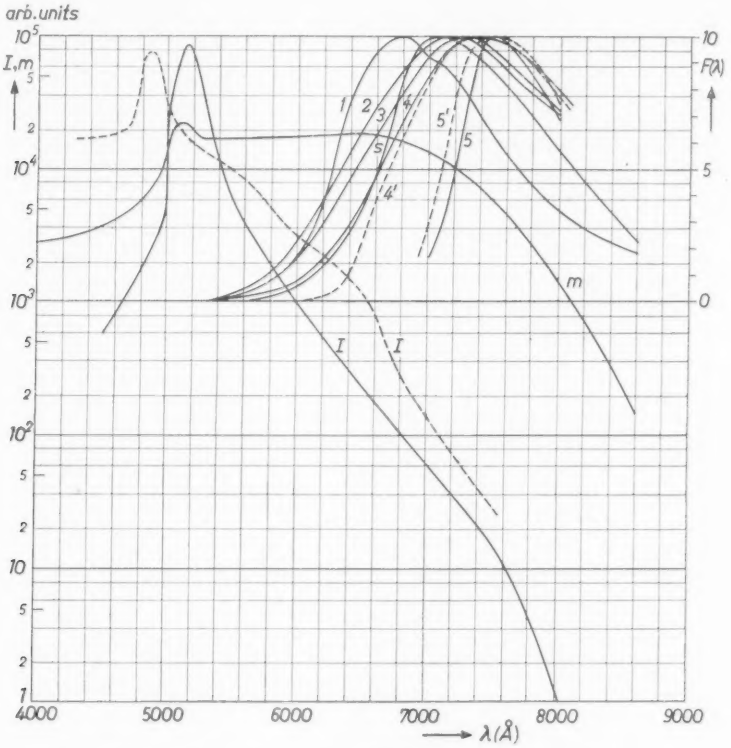


FIG. 2. Spectral response of photoconduction ($I$) at 293°K (solid curve) and 77°K (dashed curve). Curve m: spectral response of monitor cell. Curves 1–5′: spectral distribution of fluorescence at room temperature.

(1) Very strong excitation (H.P. xenon lamp, $\lambda < 5100$ Å resolving power $\Delta\lambda = 100$ Å),

(2), (3) and (4) Decreasing exciting intensity; $\Delta\lambda = 400$–$600$ Å.

(4′) Curve (4) corrected to infinitely small slit width.

(5) Very low excitation and measured with CdS cell and interference filters ($\Delta\lambda = 125$ Å).

(5′) Curve (5) corrected to a resolving power of $\Delta\lambda = 550$ Å.

(s) Simulation spectrum obtained by filters and measured like curves (2)–(4).

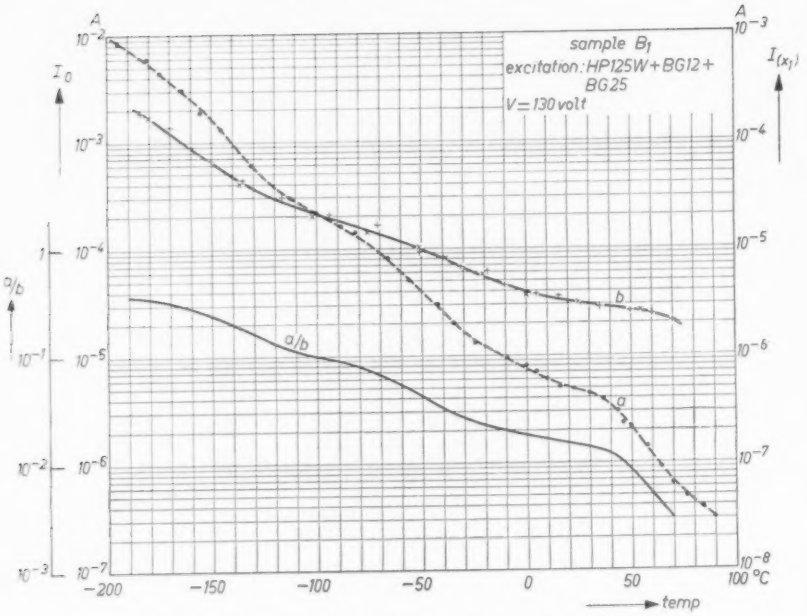


FIG. 3. Temperature dependence of the diffused photoconductivity $I(x)$ obtained with constant shadow width of 3 mm (curve a) compared with the variation of the photocurrent $I(o)$ with overall excitation (b). Curve a/b (framed part) shows the ratio of the two curves.

frequency (5000 c/s) of the modulated probe current was filtered out and its phase lag $\omega\tau_D$ relative to the phase of the modulated excitation was determined as a function of $x$. By measuring in this way the effect on the phase of a possible non-monomolecular annihilation rate of the free electrons could be eliminated.[7] Fig. 4 shows the result as $\tau_D$ vs $x$. Both the gradual decrease of $\tau_D$ in the region $x < x_0$ and the sudden increase as soon as the shadow edge passes beyond the electrode edge ($x < x_0$) are due to rather trivial electrode effects. The linear increase between $x = 1{\cdot}2$ and $x = 2{\cdot}0$ mm shows the time lag due to diffusion. The decrease at larger $x$-values must be ascribed to the relatively increasing influence of diffused and scattered fluorescence and exciting radiation, which causes no or only a slight phase lag in the resulting conductivity.

From the linear part of the curve between $x = 1{\cdot}2$ and $2{\cdot}0$ mm we derived a propagation velocity $v_e = 10^4$ cm/sec at room temperature. From this value and from the diffusion length $l_{De} = 0{\cdot}3$ cm, obtained from stationary measure-

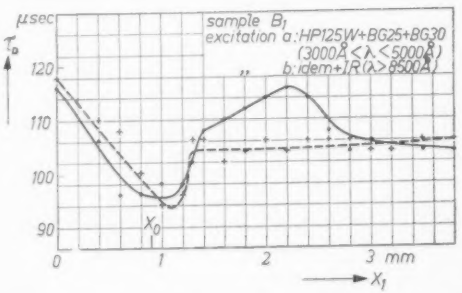


FIG. 4. Time lag $\tau_D$ of modulated photocurrent relative to the modulated excitation, as a function of the shadow width $x_1 - x_0$. Curve (a) without infra-red; curve (b) with additional I.R. illumination of the whole crystal.

ments, we can obtain the exciton lifetime $\tau_e$:

$$v_e = \sqrt{2}\omega l_{De}(\sqrt{1+\omega^2\tau_e^2}-1)^{-\frac{1}{2}},\ l_{De} = \sqrt{D_e\tau_e}.$$

which gives $\tau_e = 80$ μsec, and hence a diffusion coefficient $D_e = 1100$ cm²/sec. Although the latter value is rather large, it does not appear theoretically improbable as a diffusion coefficient of

excitons. In view of the stationary measurements, reported in sections 3 and 5, we think that in the crystal under discussion a contribution of diffused excitons to the shadow conductivity is well established.

We are indebted to Messrs A. J. van der Houven van Oordt and A. T. Vink for their assistance in the measurement of spectral distributions.

## REFERENCES

1. FRENKEL J., *Phys. Rev.* **37**, 17, 1276 (1931); WANNIER, G. H. *Phys. Rev.* **52**, 191 (1937); HELLER W. R. and MARCUS A., *Phys. Rev.* **84**, 809 (1951).
2. GROSS E. F. *et al.*, *Soujet fiz. tekh. fiz.* **1**, 674, 677, 900, 1340 (1957); NIKITINE S., *C.R. Acad. Sci. Paris.*, **244**, 1478 (1957). MARTIENSSEN W., *J. Phys. Chem. Solids* **2**, 257 (1957). (For further references see ref. (7)).
3. APKER L. and TAFT E. A., *Phys. Rev.* **79**, 964 (1950); *Ibid.* **81**, 698 (1951); *Ibid.* **82**, 814 (1951). PHILIPP H. R. and TAFT E. A., *Phys. Rev.* **106**, 671 (1957). (For further references see ref. (7)).
4. BALKANSKI M. and BROSER I., paper given at *International Conference on Semiconductors and Phosphors, Garmisch-Partenkirchen* (1956). BALKANSKI M., *Bull. Amer. Phys. Soc.* **2**, 120 (1957). BALKANSKI M. and WALDRON R. D., *Tech. Rep. Industr. Res. Mass. Inst. Tech.* 123 (1957); *Progr. Rep. Insul. Res. Mass. Inst. Tech.* **21**, 26 (1957).
5. DIMER G. and HOOGENSTRAATEN W., *J. Phys. Chem. Solids* **2**, 119 (1957).
6. BROSER I., Physiker Tagung, Heidelberg (1957); see also BALKANSKI M. and BROSER I., *Z. Elektrochem.* **61**, 715 (1957).
7. DIEMER G., VAN GURP G. J. and HOOGENSTRAATEN W. to be published in Philips Res. Rept. (1958).

*J. Phys. Chem. Solids* Pergamon Press 1959. Vol. 8. pp. 187–190. Printed in Great Britain

# G.6 FLUORESCENT EMISSION ASCRIBABLE TO EXCITON ANNIHILATION IN PURE CdS CRYSTALS*

**EDMOND GRILLOT and MARGUERITE BANCIE-GRILLOT**

Laboratoire de Luminescence—Faculté des Sciences de Paris—France

THE very pure, non-activated cadmium sulfide, which is not luminescent at room temperature, becomes fluorescent at 100°K or lower, the emission band showing an unusual structure consisting of some maxima spaced equidistantly about 300 $cm^{-1}$ apart.[1] This particular structure, owing to the great purity of these substances (no impurity atoms intentionally introduced) led to the assumption that this *green emission* might be due to a non-classical mechanism. It was first proposed that it could result from a direct free electron–free hole recombination (band–band) which would be non-localizable around a lattice defect. More recently,[2] another mechanism has been considered, consisting of exciton annihilation in conjunction with lattice vibrations.

In previous papers,[3] it has been shown that certain characteristics of this green fluorescence of very pure CdS at very low temperatures vary considerably from one sample to another, according to the method of their chemical preparation and, for some of them, according to the ageing time. These characteristics are: (1) the resolution of the band structure, the number of its maxima and their relative intensity, (2) the luminescence efficiency, (3) the spectral position of the structure maxima, which actually consist of two series.

Such a behaviour could not be explained if it were assumed that this green emission would not be localizable around a lattice defect, i.e. if it were a fundamental property of the greenockite lattice. On the other hand, the sorts of lattice defects existing in the crystal, and their concentration, strongly depend on the chemical way it was

* Not presented at Conference.

prepared, and a strong variation of the properties connected with these lattice defects might be expected. As two series of structure maxima are observed, either in different crystals or sometimes also co-existing in the same crystal, one may expect the presence of two kinds of luminogene centres, built up around two kinds of lattice defects, which could be sulfur vacancies and cadmium vacancies.

Growing CdS single crystals by the sublimation method at as low a temperature as possible i.e. from CdS gas as little as possible dissociated into its components, have been obtained samples, which actually did not show any fluorescence when cooled to 100° or 77° K.[4] They become fluorescent only at much more lower temperatures but then their emission appears very different from the usual green "edge-emission". At 20°K, the green band is still very weak but, at the same time a new blue fluorescence appears, whose spectrum is composed of 9 narrow lines. The frequencies of the six shorter wave lengths obey (in good enough approximation) hydrogen-like law:

$$\nu_n = A - B/n^2$$

where $A = 20{,}700$ cm$^{-1}$ (approximately fundamental absorption edge) and $B = 6{,}500$ cm$^{-1}$ (order of magnitude of the ratio: Rydberg constant to dielectric constant square) and $n = 3$, 4, 5, 6, 7 and 8. Owing to all these facts, this new special fluorescence emission has been treated[4] as due to the annihilation of excitons, only observable in a lattice in which the defect concentration is very low.

The same crystals, cooled to 4°K, show a more complex fluorescence spectrum.[5] The former lines persist but new lines are now observed, the whole constituting a kind of fine structure, with 3 triplets and one doublet, the distance between components being everywhere about 60 cm$^{-1}$. The frequencies of the lines composing the longer wave length triplet are exactly the same as those of the three longer wave length lines observed at 20°K, which did not obey the hydrogen-like law: therefore, they seem also to belong to the same system.

New results have been obtained last winter, in collaboration with E. F. Gross and his co-workers. The first results concern the polarization properties of this peculiar fluorescence light. When a Nicol prism is interposed between the fluorescent single crystal and the spectrograph, the spectrum described above is not modified by the analyser orientation: $E \perp c$ axis of the crystal. But, for $E \| c$, the whole spectrum is almost entirely quenched.[6]

In certain CdS powders, as well as in certain CdS single crystals prepared by the gaseous phase method, lines were also previously observed. The difference between them and the hydrogen-like system here described lies not only in the fact that they appeared weak, in addition to an intensive green emission band: it lies also in their frequencies. Concerning their possible polarization, nothing was written. We have also carried out some researches on single crystals showing also at 4°K some weak blue fluorescence lines, in addition to an intensive green fluorescence band (the two series of structure maxima being present). The system constituted by these weak blue lines was very different from our former one. Moreover, except for the lines whose wave lengths are less than 4,868 Å, which can become weakened because of the dichroism of the CdS crystal,[6] all the other lines, as well as the green band, did not show such a polarization. This seems to prove that they originate in quite different conditions (perhaps surface defects or dislocations).

Researches were also undertaken concerning the influence of a magnetic field on the hydrogen-like fluorescence.[7] A single crystal, showing such peculiar fluorescence lines, cooled at 4°K was introduced into the air-gap of a magnet, its $c$-axis being perpendicular to the magnetic field. Then it became possible to observe three doublets replacing the three narrower fluorescence lines. For a magnetic field $H = 28{,}000$ oersteds, the more intensive one $\lambda = 4870{\cdot}0$ Å gave a doublet with $\Delta\lambda = 0{\cdot}58$ Å, disposed approximately symmetrically with reference to the position of the line observed without the field. Similarly, the line $\lambda = 4868{\cdot}2$ Å[6] gave a doublet with $\Delta\lambda = 0{\cdot}8$ Å and, much more weakly, the line $\lambda = 4{\cdot}861{\cdot}4$ Å a doublet with $\Delta\lambda = 1{\cdot}2$ or $1{\cdot}3$ Å. It must be emphasized that these doublets can only be seen when the orientation of the single crystal is $c \perp H$. On the other hand, when $c \| H$, there are no doublets but only single lines, in the same position as the lines observed without a magnetic field. Then, for each level, the magnetic

field gives rise to a Zeeman triplet. But, according to its orientation with reference to the axis of the crystal, only either the central line or the lateral ones can be observed. Due to the polarization of the emitted light, either the doublets (when $c \perp H$), or the single lines (when $c \| H$) can be easily seen through a Nicol prism whose orientation is $E \perp c$, while all are quenched for $E \| c$. It is obvious that the single lines are $\sigma$-components, while the two lines of the doublets are $\pi$-components, which means that the observed Zeeman triplets are not normal ones, but inverse ones.

Another important difference between the behaviour of the CdS single crystals prepared by sublimation with large temperature gradient (those showing the hydrogen-like fluorescence) and that of CdS samples obtained by other ways, lies in their light absorption spectra. For the latter crystals, it has been previously shown[8] that a complex series of absorption lines could be observed at 4°K near the fundamental absorption edge, the relative intensity of certain of these lines varying from one sample to another.[9] By contrast, for the former crystals, it is important to note that the absorption spectra obtained were uniform for all the examined samples. Moreover, the spectrum is especially simple: near the fundamental absorption edge, only three narrow absorption lines were found,[6] whose frequencies are just a little different from those of the three fluorescence lines corresponding to the upper levels. This absorption spectrum is unchanged when observed through an analyser in the position $E \| c$. But, for $E \perp c$, the absorption edge is shifted by about 20 Å, recovering the two absorption lines at higher frequencies. Placing the crystal in a magnetic field $H = 28{,}000$ oersted, perpendicular to the $c$-axis and interposing a Nicol prism in the position $E \perp c$ the last remaining absorption line appears clearly enlarged. This can be also explained as a Zeeman effect. But the doublet lines would then be $\pi$-components and the matter would be, once again, an inverse Zeeman effect.

## DISCUSSION

The similarities in the fine structure observed at 4°K were the first evidence that all the blue fluorescence lines emitted by this kind of CdS samples might belong to the same system.[5] The uniformity of the light polarization of this whole system adds new evidence that they should all originate in the same kind of atom or quasi-atom which furthermore should have a definite orientation with reference to the crystallographic axis. The hydrogen-like relation between frequencies suggests a very simple constitution of this atom or quasi-atom which, from the superposition of the series limit and the fundamental absorption edge, seems strongly related to the fundamental lattice. All these results may be considered as convergent arguments in favour of the assumption of an emission ascribable to exciton annihilation in the lattice of pure CdS.

The correspondence between the frequencies of the three higher fluorescence levels and the three absorption lines observed only in this kind of crystal is probably not accidental. The parallel between the magnetic behaviour of the corresponding absorption line (4869·1 Å) and emission line (4870·0 Å) seems to indicate that the same kind of transitions give rise to both phenomena. Accordingly, these three absorption lines can be regarded due to the generations of excitons.

On the other hand, the inverse Zeeman effect observed for the three fluorescence lines and probably for the one absorption line is a rare enough phenomena. Only a few examples are known. It may be interpreted as resulting from the magnetic dipolar character of the transition involved, which, in this case, would be an almost forbidden one. Such transitions as the formation and annihilation of excitons, which have no equivalence in actual atoms, are likely to have a small probability. It was observed that the output of the hydrogen-like fluorescence is much weaker than that of the usual fluorescence (as, for example, CdS green "edge-emission").

Two kinds of processes may be considered concerning the energy transfers involving excitons.[10] First, a reversible transformation exciton –photon on the upper observed levels. Resulting from the annihilation of an exciton, a photon is seen after it gets out of the crystal: but it could be also reabsorbed in another point of the lattice, giving rise to a new exciton, which then moves slowly. This process can be repeated many times. The following observation agrees with such an assumption. The narrow fluorescence lines are in reality accompanied by a background of light,

situated between 4870 and 4942 Å[4,5] and polarized in the same way as the lines. The relative intensity of this background, referred to the intensity of the lines, is small when the observed fluorescence light emerges from the crystal through the excited side: but, by contrast, it is much stronger when the light emerges through the other face, after crossing a crystal 50$\mu$ thick.[10]

The excitation with Wood ultra-violet rays, which gives rise to the hydrogen-like fluorescence of these crystals, can first generate only free electrons and free holes moving in the lattice. It can be assumed that the accidental meeting of one electron and one positive hole with approximately the same momentum may produce the formation of one exciton. If this is the case, the probability of such an encounter must decrease under the influence of an electric field. Such a decrease has been actually found.[10] Conversely, only little energy is needed to ionize excitons.

The possibility, simultaneously, of these two processes:

$$\text{electron} + \text{hole} \rightleftharpoons \text{exciton} \rightleftharpoons \text{photon}$$

may be one of the reasons for the complexity of the energy transfers in such crystals.

## REFERENCES


1. KROEGER F. A., *Physica* **7**, 1 (1940).
2. KROEGER F. A. and MEYER H. J. G., *Physica* **20**, 1149 (1954).
3. GRILLOT E., *Internationales Kolloquium über Halbleiter und Phosphore Garmish Parten kirchon*, 561 (1956); *J. Chim. Phys.* **54**, 118 (1957).
   GRILLOT E. and BANCIE-GRILLOT M., *Kolloquium für Festkörperphysik* Erfurt, to be published (1957); and *Sovietchania no spectroscopia liouminestsentsia*, To be published, Moscow (1957).
4. GRILLOT E., BANCIE-GRILLOT M., PESTEIL P. and ZMERLI A., *C.R. Acad. Sci., Paris* **232**, 1794 (1956).
5. GRILLOT E., *J. Phys. Radium*, **17**, 822 (1956).
6. BANCIE-GRILLOT M., GROSS E. F., GRILLOT E., and RAZBIRINE B. S., *C. R. Acad. Sci., Paris*, to be published (1958).
7. GROSS E. F., GRILLOT E., BANCIE-GRILLOT M. and ZAKHARTCHENIA B. P., *C.R. Acad. Sci., Paris* to be published (1958).
8. GROSS E. F. and IAKOBSON M. A., *Dokl. Akad. Nauk. SSSR* **102**, 485 (1955).
9. GROSS E. F., RAZBIRINE B. S. and IAKOBSON M. A., *Zh. tekh. fiz. SSSR* **27**, 1149 (1957).
10. GRILLOT E., *Colloque: transferts d'énergie lumineuse et photosensibilisation, Paris*, May 1958; *J. Chim. Phys.* to be published (1958).


VOL 8 195

*J. Phys. Chem. Solids* Pergamon Press 1959. Vol. 8. pp. 190–195. Printed in Great Britain

# G.7 SPECTROSCOPIE DU CORPS SOLIDE ET SPECTRES D'EXCITONS

S. NIKITINE

Laboratoire de Spectroscopie et d'Optique du Corps Solide
Institut de Physique, Université de Strasbourg, France

## 1. INTRODUCTION

DEPUIS quelques années, un nombre considérable de travaux ont été consacrés à la spectroscopie du corps solide. En particulier, les spectres de $Cu_2O$, CuI, CuBr, CuCl, $HgI_2$, $PbI_2$, AgI, TlI, TlBr, TlCl, CdS, BaO ont été étudiés aux trés basses températures.[1] Tous ces corps présentent, aux très basses températures, des spectres d'absorption composés d'une ou de plusieurs raies d'absorption et d'un spectre continu de plus courtes longueurs d'onde. Dans beaucoup de cas, les raies observées forment une série convergeant vers le spectre continu. Il y a lieu de classer ces spectres en plusieurs classes distinctes.

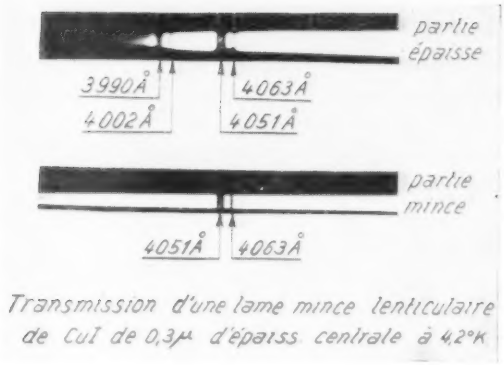


FIG. 1. Les deux premières raies de la série et le bord d'absorption de CuI à 4·2°K. Les raies comportent une structure de doublet.

FIG. 2. Doublet de la raie ultime de CuI à 4·2° K observée avec une lame très mince.

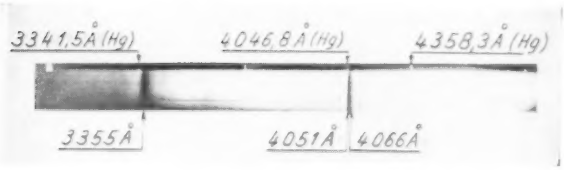


FIG. 3. Première et deuxième raies ultimes de CuI à 77°K observées avec une lame très mince.

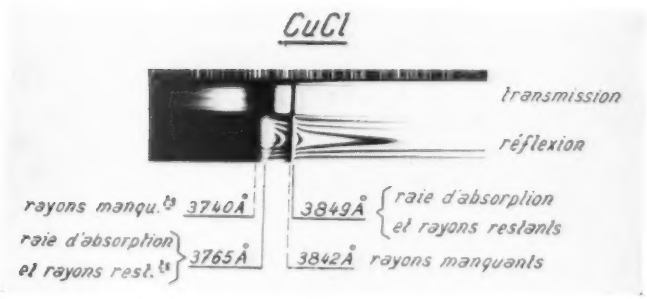


FIG. 4. Bandes de rayons restants et rayons manquants de CuCl et spectre d'une lame mince à 77°K.

[facing page 190

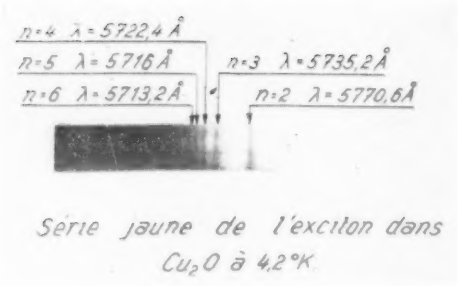


FIG. 5. Série jaune de $Cu_2O$ à 4·2°K.

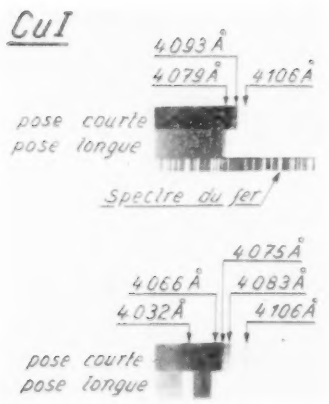


FIG. 6. Deux aspects du spectre de troisième classe (raies "sensibles") de CuI à 4·2°K).

1.1. *Spectres de première classe*

Les spectres de la grande majorité des corps étudiés appartiennent à cette classe. Ils sont caractérisés en premier lieu par une absorption très élevée. Ils comportent une première raie (comptée à partir des grandes longueurs d'onde) de très grande intensité. Le coefficient d'absorption maximum est de l'ordre de $10^5$ à $10^6$ $cm^{-1}$. Les raies suivantes, si elles sont observées, sont d'intensité rapidement décroissante. De ce fait, il est souvent difficile d'observer ces raies. L'absorption dans le spectre continu est aussi souvent beaucoup moins forte que dans la première raie. Ces spectres doivent être observés avec des lames de quelques dixièmes de micron d'épaisseur. Si on étudie des lames encore moins épaisses, la méthode photographique ne permet pratiquement plus l'observation du spectre continue ni des différentes raies de la série. Seule la première raie peut être observée ainsi que quelquefois une autre raie dans une partie éloignée du spectre ultraviolet. Nous avons appelé ces raies "ultimes". Pour les halogénures, les raies ultimes se composent souvent d'un multiplet.

Dans le cas où plusieurs rais sont observées, on peut chercher à représenter la série par une formule hydrogénoïde:

$$\nu_n = \nu_\infty - \frac{R'}{n^2}$$

où $R'$ est une constante de Rydberg réduite et $n$ le nombre quantique $n = 1, 2, 3, \ldots$ Mais l'accord n'est généralement pas très bon, peu de raies étant observables et la première étant souvent aberrante.

Les spectres de CuI, CuBr, CuCl, TiI, TiBr, TlCl ainsi que $PbI_2$ et $HgI_2$ (bien que dichroïques) appartiennent à cette classe. La Fig. 1 représente la première et deuxième raies (qui sont des doublets) et le bord d'absorption de CuI. La Fig. 2 représente le doublet de la raie ultime (première raie de la série) de CuI observée avec une lame mince. La Fig. 3 représente la première et deuxième raies ultimes de CuI. Cette deuxième raie se trouve dans l'ultraviolet. On notera que le spectre continu entre les raies n'est plus observable sur le spectrogramme.

Le spectre de réflexion présente généralement au voisinage des "raies ultimes" des anomalies caractéristiques correspondant à une bande de "rayons restants" (maximum de réflexion) et à une bande de "rayons manquants" de plus courtes longeurs d'onde (minimum de réflexion). La Fig. 4 représente les bandes des rayons manquants et restants de CuCl ainsi que des franges de spectres cannelés; la lame est lenticulaire.

1.2. *Spectres de deuxième classe*

Jusqu'à présent, seul le $Cu_2O$ permet d'observer des spectres de cette catégorie. L'absorption dans ce spectre est beaucoup plus faible que dans les spectres de première classe. L'absorption dans $Cu_2O$ est au moins 500 fois plus faible que dans CuI par exemple, corps qui présente un spectre de première classe très caractéristique. Dans $Cu_2O$, on observe plusieurs séries de raies à caractère hydrogénoïde prononcé. Dans chacune de ces séries, les raies sont d'intensité comparable. Elles peuvent être représentées par des formules hydrogénoïdes dans lesquelles la première raie de la série correspond au nombre quantique $n = 2$. La faiblesse de l'absorption permet de présumer que ces spectres appartiennent à une classe de transitions faiblement défendues. La Fig. 5 représente l'une des séries (jaune) de la cuprite.

1.3. *Spectres de troisième classe*

Suivant les observations connues actuellement, les corps qui présentent un spectre de première classe ne présentent pas de spectre de deuxième classe simultanément. Mais certains de ces corps présentent, en plus des raies du spectre de première classe, un spectre de raies que nous appellerons de *troisième classe*. Il est constitué par des raies nombreuses et fines formant des séries convergentes. Le caractère hydrogénoïde de ces séries n'a pas été établi clairement. L'intensité de l'absorption est de 10 à 30 fois plus faible que les raies du spectre de première classe. De tels spectres ont été observés pour CuI, CuBr[1] et CdS[2]. Ils sont dans ces cas légèrement décalés vers les grandes longueurs d'onde par rapport aux spectres de première classe. On peut alors observer les spectres de troisième classe avec des lames épaisses (plusieurs $\mu$ pour CuI) et les spectres de première classe avec des lames minces de la même substance ($0{,}1\mu$).

Les raies des spectres de troisième classe ont des longueurs d'onde bien définies, mais leurs intensités sont variables dans de larges limites d'une

raie à une autre et d'un échantillon à l'autre. Le facteur dont dépend cette variation n'a pas été clairement dégagé, mais il est probable qu'il dépend de la qualité du cristal, c'est-à-dire du nombre des dislocations et défauts. On a pu en particulier noter des variations importantes d'intensité de ces raies en différents points d'un même cristal. Il est certain que l'intensité de ces raies pourra servir à l'étude de la qualité du cristal, quand cette dépendance sera quantitativement établie. Pour cette raison, nous avons suggéré d'appeler ces raies "sensibles". La Fig. 6 représente deux aspects du spectre de raies "sensibles" de CuI.

Il est à noter que les spectres des halogénures alcalins forment une classe qui se rapproche des spectres de première classe, mais qui présente des particularités tout au moins au point de vue théorique.

Les mesures ont été effectuées dans notre laboratoire avec des substances spectroscopiquement pures. Il est certain que les spectres étudiés ne sont pas dus à des impuretés, mais nous n'avons pas pu contrôler jusqu'à quel point la proportion stoechiométrique était en défaut dans les échantillons préparés. Dans certains cas, des lames fondues et sublimées ont été comparées sans que l'on ait observé de différence. Pour $PbI_2$, les longueurs d'onde des raies de lames monocristallines sont un peu différentes de celles de lames sublimées.

Des spectres de luminescence, manifestement apparentés avec les spectres d'absorption, ont été observés pour la grande majorité des corps étudiés. Ils sont composés de raies fines appelées $\alpha$, trés voisines des raies d'absorption et des bandes larges appelées $\beta$ fortement déplacées vers les grandes longueurs d'onde par rapport aux raies d'absorption. Souvent, ces bandes présentent des structures vibrationnelles.

## 2. COMPARAISON AVEC LA THÉORIE

La théorie de l'exciton a fait des progrès notables récemment. Dresselhaus,[4] Haken,[5] et surtout Elliott[6] ont calculé des probabilités de transition d'un état excité du cristal à un état excitonique. On prévoit deux classes de transitions:

2.1. *Transitions de première classe*

Ces spectres correspondent à des transitions avec le vecteur $\mathbf{k} = 0$ et $\Delta\mathbf{k} = 0$, à des états excitoniques $S$, toute autre transition étant interdite. Ces transitions (permises) donnent lieu à des séries de raies qui devraient être hydrogénoïdes (sauf la première raie, voir Haken). La première raie doit correspondre à $n = 1$. Les valeurs des intensités d'oscillateurs $f$ des différentes raies sont données par la formule:

$$f = \frac{V_p}{\pi a^3_{\text{lexc}}} \frac{f_B}{n^3}$$

où

$$f_B = g|Q|^2 \text{ et } g = \frac{\hbar}{\pi m \nu_{\text{on}}} \quad Q = \int U^*_{\text{oc}} \operatorname{grad} U_{\text{ov}}\, d\tau$$

ou $\nu_{\text{on}}$ est la fréquence de la raie correspondante, $U_{\text{oc}}$ et $U_{\text{ov}}$ respectivement les fonctions d'onde de Bloch du niveau le plus bas ($\mathbf{k} = 0$) de la bande de conduction et du niveau le plus haut de la bande de valence. $V_p$ est le volume de la cellule élémentaire divisé par le nombre d'ions intéressés dans la transition par cellule. $a_{\text{lexc}}$ est le rayon de la première orbite de Bohr de l'exciton et $n$ le nombre quantique excitonique. La deuxième raie devrait être huit fois plus faible que la première et les autres raies encore beaucoup plus faibles. Nous avons évalué récemment[7] le facteur de $f$ d'une façon approchée pour la première raie de CuI et obtenu une valeur de l'ordre de $4{,}5 \times 10^{-3}$.

2.2. *Transitions de deuxième classe*

Dans certains cas, les transitions de première espèce sont interdites. Alors, pour de faibles valeurs de $\mathbf{k}$, une deuxième classe de transitions peut être permise. Elle correspond à des passages à des états excitoniques $P$, toute autre transition étant interdite. Dans ces transitions, la série hydrogénoïde doit commencer avec la raie correspondant à $n = 2$. Les valeurs de $f$ pour les différentes raies sont grossièrement de l'ordre de:

$$f \simeq \frac{C}{\epsilon_s{}^5} \frac{n^2-1}{n^5}$$

où $C$ est un facteur numérique de l'ordre de quelques unité, $\epsilon_s$ la constante diélectrique statique. Pour la première raie ($n = 2$), cette valeur est grossièrement $10^{-3}$ fois plus petite que dans les spectres de première classe. Les intensités des

raies décroissent moins rapidement que dans le premier cas.

### 3. TENTATIVES D'INTERPRÉTATION DES SPECTRES EXPÉRIMENTAUX

On voit que la première classe de spectres observés expérimentalement est très bien décrite par la théorie. En particulier, la valeur de $f$ obtenue expérimentalement[7] est de $6 \times 10^{-3}$ pour CuI à la température de $N_2$ liquide. Un accord aussi bon est accidentel. Il semble donc possible de conclure que les spectres expérimentaux de première classe sont des spectres excitoniques de première classe. Les spectres de tous les corps étudiés, sauf ceux de $Cu_2O$ et peut-être de AgI et BaO correspondent probablement à cette classe.

Il est remarquable ensuite de noter que les spectres de $Cu_2O$ sont également bien décrits par la théorie des transitions de deuxième classe. Les spectres de la cuprite seraient donc des spectres excitoniques de deuxième classe (faiblement interdits).

Les spectres de troisième classe observés avec certaines substances ne sont pas encore prévus par la théorie. Mais il est probable que le développement de la théorie permettra de prévoir une troisième classe de transitions.

Nous croyons donc pouvoir conclure que la bonne concordance entre la théorie des spectres d'exciton et les spectres observés de première et deuxième classes apporte un argument peut-être décisif en faveur de l'interprétation excitonique des spectres observés.

### LITERATUR


1. Pour la bibliographie des travaux expérimentaux effectués par E. F. Gross et ses collaborateurs et au laboratoire de l'auteur, voir une mise au point de l'auteur, *J. Chim. Phys.*, à paraître. Voir également *Phil. Mag.* souspresse.
2. Gross E. F. *et coll. Zh. tekh. fiz. SSSR* **25,** 2061 (1955); *Ibid.* **27,** 1149 (1957); *Ibid.* **27,** 2175 (1957); voir aussi Broude V., Eremenko V. *et* Pashba E., *Dokl. Akad. Nauk. SSSR* **114,** 520 (1957).
3. Martienssen W., *J. Phys. Chem. Solids*, **2,** 257 (1957); Taft E. A. et Philipp H. R., *J. Phys. Chem. Solids* **3,** 1 (1957).
4. Dresselhaus, *J. Phys. Chem. Solids* **1,** 14 (1956); *Phys. Rev.* **106,** 16 (1957).
5. Haken H., *Rapport sur l'état actuel des recherches sur l'exciton, Halbleiterprobleme IV*, édité par W. Schottky. Vieweg Brunswick (1958).
6. Elliot J., *R.R.E. Memorandum*, N. 1342 (1957); *Phys. Rev.* **108,** 1384 (1957).
7. Nikitine S., El Komoss S. G., Reiss R. et Ringeissen J., à paraître au *J. Chim. Phys.*


## DISCUSSION

*Compiled by* B. Lax

### G.1 H. Haken

B. Goodman (Univ. Missouri): The depression of the level of the lowest exciton state may also be due to exchange effects. In the effective mass approximation the relative contribution of exchange is given by an expression proportional to the optical absorption strength. If the $n = 1$ transition were allowed in $Cu_2O$, the exchange term alone could account for the depression in that level as observed by Gross and Nikitine.

H. Haken: The orbits of the exciton in the lower state are of the order of 20 Å which are larger than the critical radius responsible for electron-electron interaction. This lowering of the lowest state is due to the interaction of the lattice vibrations.

J. Krumhansl (National Carbon Company): For what material was this orbit calculated?

H. Haken: For cuprous oxide.

J. Krumhansl: Goodman's comment is more appropriate for alkali halides where the orbits are very small and the electron exchange is equivalent to saying that there is an appreciable difference between the energies of the $4s$ level in the $3p^5$ shell potential and the $3p^6$ potential, and this will give a deviation from the hydrogen-like structure.

H. Haken: I agree.

### G.2 E. F. Gross

A. M. Portis (Univ. of California): Professor Gross has stated that he has obtained evidence for a role of excitons in the photoconductivity. In further support of his statement, I would like to present some results that have been obtained recently by J. H. Apfel at the University of California. Fig. 1 shows a plot of the approximate change in the conductivity of cuprous oxide in the region of the absorption edge. The vertical lines labeled 2, 3, 4 and 5, give the positions of the hydrogen-like series which Professor Gross has described. We will see that the $K = 2$ line and the $K = 3$ line are resolved in the photoconductivity and the further lines are said to be resolved into the series limit. These results were obtained at the temperature of liquid nitrogen.

R. J. Elliott (Clarendon Laboratory, Oxford): I thought you said the Landau levels, that is, the equally spaced lines in the "continuum", were somehow different from the magneto-absorption of Lax and

Burstein. I think this probably is not so. The Coulomb interaction will not bind the electron in the hole above the series limit and you can still get peaks of this kind theoretically from simple holes and electrons which are unbound. The theory of this effect predicts different kinds of results for the case when the transitions between the bands are allowed, say between the $s$-band and the $p$-band, than those for forbidden transitions as between the $s$-band and a $d$-band. Now the fact that the $N = 1$ line of your series is practically absent would agree with the second kind, namely that these are forbidden transitions. The simple theory of the continuous absorption of forbidden transitions predicts peaks of this kind when

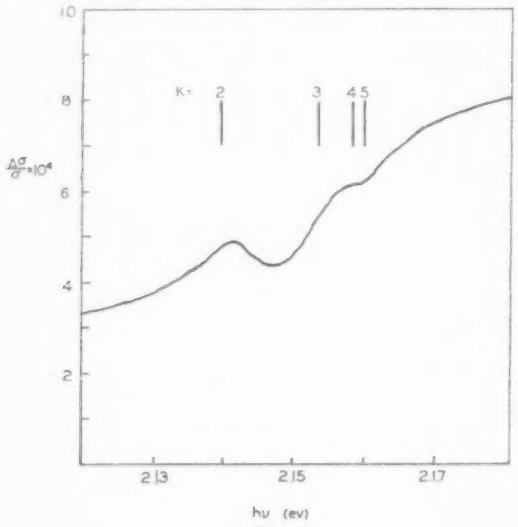

Fig. 1

the electric vector is polarized perpendicular to the magnetic field. The simple theory says that they should not be there if the $E$-vector is polarized parallel to the field. More extensive calculations show that these peaks might return. The spectra would be different for the two different kinds of polarization. Have you studied the spectrum for the two different polarizations?

E. F. Gross: Yes, we have studied this question. The Landau levels are the diffuse lines above the series limit. I am not certain about the relative intensities of these lines. They will have to be measured more exactly. Apparently the intensity of the Landau lines above the series limit appear in almost equal intensity for the two polarizations.

R. J. Elliott: Do the lines shift at all or change in intensity when you change the polarization?

E. F. Gross: These maxima are very diffuse. It appears that the picture is not quite the same for the two polarizations. This needs further examination.

R. J. Elliott: If $m_e = m_h$ then you say that they would not shift?

E. F. Gross: Yes, then the maxima are not quite equidistant. Above the series limit the lines are separated by 7 $cm^{-1}$. In the series limit the maxima can be seen to have fine structure, and in this part of the spectrum we cannot discern the fine structure.

S. H. Koenig (I.B.M.): In a magnetic field, the analogy between positronium and excitons breaks down because the sign of the gyromagnetic ratio of a positron and electron is opposite, whereas that of an electron and hole are the same. Thus, for example, positronium in both a singlet and triplet state has no linear Zeeman effect, whereas a triplet $s$-state exciton would have a magnetic moment and a linear Zeeman splitting. In particular, the fine structure of excited states will be completely different for positronium and excitons.

G.3. I. Broser and R. Broser-Warminsky

P. Aigrain (Sorbonne, Paris): Is the radiation from the crystal strongly absorbed by the crystal, or not?

I. Broser: No. The scattering is a result of a great deal of total reflection within the crystal. The crystal has a very high index of refraction and the light is not highly absorbed.

P. Aigrain: If it is not re-absorbed, how can you excite it?

I. Broser: I didn't say it isn't reabsorbed. It must be absorbed with monochromatic light. This crystal cannot be irradiated in the same manner as with blue light which gives fluorescence.

P. Aigrain: Is this a single photon which has been emitted, then fluoresces and then is reabsorbed by chance, just at the right point?

I. Broser: No. You have fluorescent emission, which travels through the crystal and is reabsorbed giving rise to photoconductivity.

P. Aigrain: That should be a very low efficiency process because only those which are reabsorbed at the right spot would be effective.

I. Broser: It has exactly the required efficiency. We have measured this.

E. E. Loebner (R.C.A.): The likely phenomenon is that of an imprisonment of radiation in which the photon is absorbed and re-emitted several times before reaching the site. This could explain some of the dependencies on temperature. What happens in this transit in which a photon gets absorbed and re-emitted several times before it reaches the spot where you measure the photoconductivity?

I. Broser: Why do you want this effect?

P. Aigrain: This multiple reflection would be very strongly dependent on the surface condition of your crystal.

I. Broser: It is, if you shape the crystal.

R. A. Halsted (General Electric Research Laboratory): In a publication to appear momentarily[1] data is presented indicating that holes can be ionized from Cu, Ag, or Au acceptor levels in ZnS by radiation at wavelengths extending from near the fundamental absorption edge to a long wavelength limit determined by the identity of the acceptor impurity. In crystals containing uncompensated acceptors such absorption sites would exist throughout the volume. Do your measurements

VOL 8 195

permit the possibility that the radiative energy transfer mechanism provided by absorption of luminescence light at such sites could contribute to your results?

I. BROSER: I would think not if you only have energy transfer for holes. I think we have electrons making the photoconductivity. We measured this with Hall effect and then I think it could be an energy transfer effect but I don't think this applies in this case.

## REFERENCES

1. HALSTED R. E., APPLE E. F., and PRENER J. S., *Phys. Rev. Letters*, **1**, 134 (1958).

G.4 M. BALKANSKI

I. BROSER (Fritz Haber Institute, Berlin): Is this proposed energy transfer possible even if the energy of the photon is lying in the fundamental absorption band?

M. BALKANSKI: Yes, if the excited electron lies low in the conduction band, it can still interact with the hole giving an excition.

I. BROSER: Could there be, by the repetition of your two-step process, a change of the energy of the primary photon and if so, how big would this change be?

M. BALKANSKI: If it is a simple excited state, (I think that it has been shown that this can be extended to a triply excited state) then you have a difference of the wavelength. Now if you do not have interaction, that is, if the simply excited state propagates, then you shouldn't expect an important shift in frequency.

E. E. LOEBNER (R.C.A.): Did you attempt to compare the results of the calculations on your model with those of a model that dispenses with the exciton propagation step in energy transport and assumes only a multiple photon absorption and emission process along fluorescent centers? Such a comparison might be helpful to suggest an experiment that distinguishes between these possibilities.

M. BALKANSKI: The only difference should be in the frequency shift. If we work with an impurity center it is more likely to maintain exactly the same frequency as it absorbs. Only experiments and further work could distinguish them.

G.5 G. DIEMER

H. S. SOMMERS, JR. (R.C.A.): Crystal studies had very little photoconductive response for wavelengths shorter than the band edge. This indicates a very high surface recombination velocity. Would not this be just the case where exciton diffusion would not be important because of destruction of the excitons at the surface sites which capture the free minority carriers?

D. POLDER: There may be some surface recombination. Nobody has said that the actual value of the lifetime of the excitons which is found in this way doesn't partly contain the effect of the surface.

T. S. MOSS (Royal Aircraft Establishment, Farnborough): Wouldn't it be interesting to cut the crystal in half?

M. BALKANSKI: Such an experiment has been done. Another experiment immerses the crystal in a medium with the same refractive index and there is no effect on the photoconductivity. One could also apply strain on the crystal to distort the band.

*J. Phys. Chem. Solids* Pergamon Press 1959. Vol. 8. pp. 196–204. Printed in Great Britain

SESSION H:

GENERAL*

# H.1 THE EFFECT OF PRESSURE ON THE PROPERTIES OF GERMANIUM AND SILICON†

WILLIAM PAUL

Harvard University, Cambridge, Massachusetts

**Abstract**—Measurements of the pressure dependence, in germanium and silicon, of the intrinsic resistivity, the fundamental absorption edge, the carrier mobilities, the magnetoresistance coefficients, and the dielectric constant are reviewed, and an explanation based on the shift of the band edges presented. Experimental evidence for similar behavior of corresponding band extrema in germanium, silicon and the intermetallics is given. The cases of the (111) and (100) minima in germanium and silicon and the Ge–Si alloys are discussed in detail. The results of measurements of the change of ionization energy of shallow and deep lying impurity levels in germanium and silicon are also reviewed.

## 1. INTRODUCTION

WHEN the research on silicon and germanium which will be reported in this review paper was started, the properties of the electrons and holes of minimum energy, such as their reduced momentum and effective mass, were unknown. Accordingly, the pressure measurements were interpreted by deductive or inductive reasoning, depending on the knowledge of semiconductor band structure current at the time of a particular experiment. However, the presentation in this brief communication will be simplified if we describe first our present understanding of the behavior under pressure of important electronic states in the semiconductor conduction band, and then demonstrate the overall agreement of several deduced properties with experimental results.

## 2. CONDUCTION BAND STATES OF GERMANIUM

Several sources of evidence indicate that there are three important sets of minima for the conduction band structure of germanium, shown in familiar form in Fig. 1.

(1) The lowest set of minima in the conduction band energy versus momentum surface at atmospheric pressure lies at the boundary of the Brillouin zone in the (111) directions. At high pressures, the energy of these states "increases" relative to the energy of the valence band maximum at a rate of $5 \times 10^{-12}$ eV dyn$^{-1}$cm$^2$.[1] The tensor effective mass for states in these minima is slightly and anisotropically changed by the decrease in lattice constant.[2]

(2) Optical data show that there is a minimum at the center of the Brillouin zone approximately 0·15 eV above the (111) minima at 300°K.[3] The minimum moves away from the valence band with pressure at a rate approximately two and a half times greater than that for the (111) minima (for references and comments, see below). There is probably a large increase in the effective mass of electrons in this minimum with pressure, of the order of 15 per cent in 10,000 kg/cm$^2$.

(3) The interpretation of measurements of electrical resistivity in impure *n*-type germanium samples to 30,000 kg/cm$^2$ requires a third set of minima approximately 0·15 to 0·20 eV above the (111) set at atmospheric pressure.[4] These minima probably lie in the (100) direction in the Brillouin zone, although the present pressure experiments do not prove this. Under pressure, these minima remain essentially static relative to the valence

* *Chairman*: G. BUSCH; *Co-Chairman*: J. H. CRAWFORD, JR.

† This work was supported by the U.S. Office of Naval Research under Contract No. 1866(10).

band; the effective mass changes with pressure are probably very small.

### 3. CONDUCTION BAND STATES OF SILICON AND SILICON–GERMANIUM ALLOYS

In silicon the lowest set of conduction band minima lie in the (100) direction: we shall stress a similarity in properties between this set and that required in (3) above.[5] These minima *approach* the valence band at a rate of $1{\cdot}5\times10^{-12}$ eV dyn$^{-1}$cm$^2$.[6] The (111) and (000) minima have not yet been identified as contributing to any measurable property of pure silicon. In silicon–germanium alloys rich in germanium, the (111) minima are the lowest, the (100) set next lowest, and the (000) minimum highest in energy. As the silicon content is increased the energy gap increases, but the (100) minima move so as to be closest to the valence band after 15 per cent silicon in germanium content is reached.[5] The effect of pressure on the position of the minima in the alloys is substantially the same as in the pure substances.[7]

### 4. VALENCE BAND STATES

Experiments on the conductivity,[8,9] drift mobility,[9] Hall mobility[8] and magnetoresistive coefficients[8] of holes in germanium all indicate small, anisotropic effects due to high pressure. These effects, which have not been fully analysed, will not be required in this discussion.

### 5. IMPURITY STATES IN GERMANIUM AND SILICON

Electrical and optical data have been used extensively to determine the energy levels of impurities in germanium and silicon. If the change in electrical conductivity of suitable samples is measured at carefully chosen low temperatures, the pressure coefficient of the impurity ionization energy can be found, and shown to be strongly dependent on the type of impurity, the particular impurity energy level, and the characteristics of the host lattice. The effect of pressure on the so-called hydrogenic impurity levels is roughly deducible from the pressure coefficients of the effective mass[4,9] and dielectric constant, and is small; for

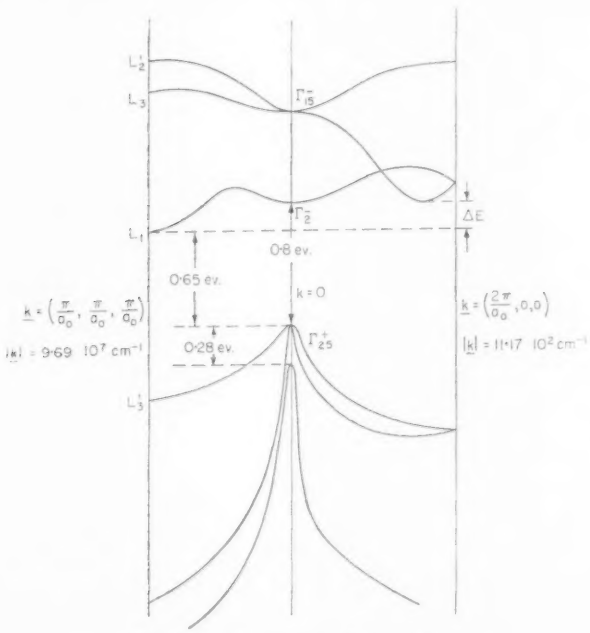


FIG. 1. Band structure of germanium.

example, for donors in silicon,[10] $d\epsilon/dP \approx$ $\approx -1\times10^{-14}$ eV dyn$^{-1}$cm$^2$. On the other hand, the pressure coefficients for the deeper lying impurity levels can be very large; for example, the pressure coefficient of an acceptor level due to gold in germanium, 0·20 eV from the (111) conduction band edge, is $d\epsilon/dP = 2.9\times10^{-12}$ eV dyn$^{-1}$cm$^2$.[10] We shall renew this discussion below; the present comment is given since the effect of the pressure coefficient of the ever-present impurity levels has to be considered in evaluating all the data.

### 6. ELECTRICAL CONDUCTIVITY OF GERMANIUM

The shift of the different sets of minima in germanium with pressure is shown in Fig. 2.

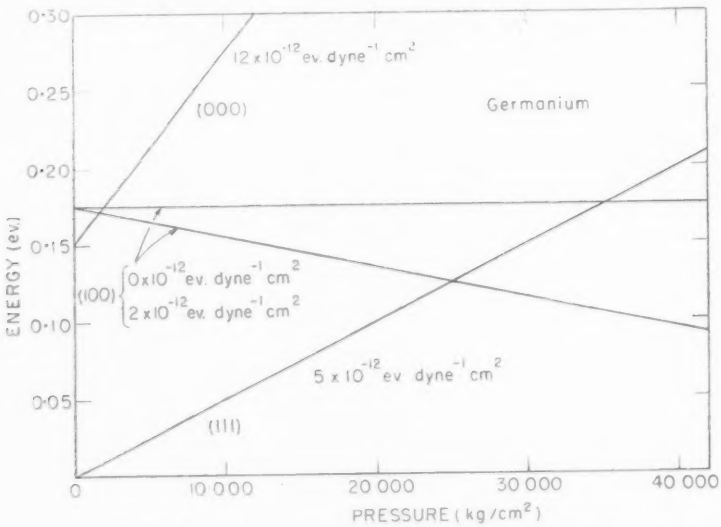


FIG. 2. The effect of pressure on the (111), (100) and (000) conduction band minima in germanium.

Let us suppose the pressure is kept below 10,000 kg/cm$^2$, that the sample is non-intrinsic $n$-type, and that the temperature is high enough so that the impurity levels are all ionized. Any change in electrical conductivity with pressure must then be caused by a change in electronic mobility, which must in turn be related to changes in the effective mass, elastic coefficients, deformation potential, or dielectric constant. Sound qualitative arguments indicate that the net effect of changes in these will be a mobility pressure coefficient of a few per cent in 10,000 kg/cm$^2$, which is what is found. The separation of the different components of the change requires further experiments, several of which have been done. For example, BAILYN[11] has measured the pressure coefficients of some of the elastic coefficients, and CARDONA, PAUL and BROOKS[12] the pressure coefficient of the dielectric constant. Hall effect and magneto-resistance measurements can be used to separate out the changes in the different effective mass components. This has been done in a preliminary way;[2] the interpretation was, however, hampered by the presence of interband scattering (see below) which will be factored out when a current series of galvanomagnetic measurements to higher pressures has been completed. The change of a certain combination of elastic coefficients is also required; apart from the fact that the choice of the proper combination of elastic constants presents some difficulty, Bailyn's data are somewhat inadequate, so that a second determination of the change in elastic coefficients with pressure is desirable. In consequence, the final correlation of the pressure coefficients is incomplete, but it is reasonably clear that no gross errors are being made.

If the impurity content and temperature are

such that the sample becomes "intrinsic", the change in electrical conductivity with pressure is largely determined by the change in the energy gap. Corrections for mobility and density-of-states mass can be applied from measurements on impure samples. The pressure coefficient of the (111) minima relative to the valence band is thus determined, up to 10,000 kg/cm$^2$. There is no way to separate out, from this experiment alone, the perturbation of the conduction and valence band edges by the pressure, which is required for a deformation potential theory of the lattice scattering mobilities. Moreover, if correlation with the measured gap change is attempted by combining in some way deformation potentials derived from the measured mobilities, the scattering of carriers by modes of vibration other than longitudinal acoustical ones must also be estimated.

Next let us suppose that the pressure is raised above 10,000 kg/cm$^2$, so that more and more electrons populate the (100) minima. The average mobility of a non-intrinsic sample will decrease, partly because of the reduced mobility in the (100) minima (this is not immediately evident, but can be demonstrated) and partly because the density of final states of almost the same energy to which any electron can be scattered is increased. This combination of interband scattering and of lower mobility in the (100) minima should cause the average mobility (1) to decrease rapidly as the pressure forces the (111) and (100) minima to approach each other, (2) to reach a minimum when the (111) and (100) minima have roughly the same energy, and (3) to increase when the (100) minima become the lower set. The rapid change in mobility observed is shown in Fig. 3, taken from measurements by Smith of the drift mobility,[9] which completely eliminate any reservations we may have concerning possible carrier density effects. The minimum in mobility has been observed on several occasions at about 50,000 kg/cm$^2$ in partially non-hydrostatic pressure measurements[13] by Bridgman to 100,000 kg/cm$^2$.

If the germanium is in its intrinsic range, the average energy gap is defined by both (111) and (100) sets of minima: the rate of increase of the average gap will therefore decrease at the higher pressures, and eventually the change in the gap will be wholly determined by the behavior of the (100) minima. The identification of the second set of minima as a (100) set can be made from magnetoresistance measurements at pressures greater than 10,000 kg/cm$^2$, and this is at present being done. There is, however, already a fair amount of subsidiary evidence, much of it from the work at RCA and elsewhere on the silicon–germanium alloys, supporting this identification of the minima.

The existence of a minimum in the conductivity constitutes almost undeniable evidence for interband scattering of the type sketched above. It is straightforward to develop a phenomenological theory of the conductivity in the two sets of minima as a function of pressure, both in the intrinsic and non-intrinsic ranges, and to deduce from it[4] and measurements on various samples at different temperatures that (1) the pressure coefficient of the energy difference between the (100) minima and the valence band is between zero and $-2\times10^{-12}$ eV dyn$^{-1}$cm$^2$, (2) the atmospheric pressure separation of the (100) and (111) sets of minima is between 0·15 and 0·20 eV, the matrix elements for inter- and intra-band scattering are about equal.

### 7. ELECTRICAL CONDUCTIVITY OF SILICON AND SILICON–GERMANIUM ALLOYS

Our discussion of the effect of pressure on the mobility of carriers in a single set of minima in germanium applies also to silicon, where the effects are of the same order of magnitude.[6,9] More striking is the effect on the intrinsic conductivity: this *increases* with increasing pressure,[6] allowing us to deduce that the (100) minima in silicon approach the valence band at a rate of $1{\cdot}5\times10^{-12}$ eV dyn$^{-1}$cm$^2$. No subsidiary effects at very high pressures due to other conduction band minima have yet been observed.

As silicon is alloyed with germanium the (100) minima in the alloy approach closer to the (111) set, which is also the effect of pressure. The effects of interband scattering appear at lower pressures in those alloys where the (111) minima are still contributing to the conduction. For example, a 10 per cent silicon alloy measured by Bridgman and Paul[14] showed a minimum in electrical conductivity near 15,000 kg/cm$^2$. The minimum in conductivity should appear at any pressure down to zero as the silicon content is

increased, up to the point where the (111) and (100) minima are approximately equal in energy.

### 8. OPTICAL ABSORPTION IN GERMANIUM

Disregarding the fine structure caused by exciton formation and phonon interaction for the moment, two distinct and abrupt edges exist in the curve relating absorption coefficient and photon energy, the one caused by the appearance of indirect (forbidden) transitions from the valence band into the (111) minima, the other by direct (allowed) transitions into the (000) minimum. Observation of the shift of the lower energy edge with pressure should give the pressure coefficient of the (111) minima, previously found from conductivity measurements. In fact, all measurements of the edge shift except our own[15] give a coefficient 60 per cent higher than that derived from conductivity data. We believe that this is caused by the neglect of changes in the shape of the absorption edge with pressure, since we have been able to find agreement between the electrical and optical coefficients by including these. There do remain, however, some disquieting features in this interpretation, stemming from the difficulties involved in the identification of the intermediate states for the indirect transition, which seems to be tacitly ignored in the literature on this subject up to this time.

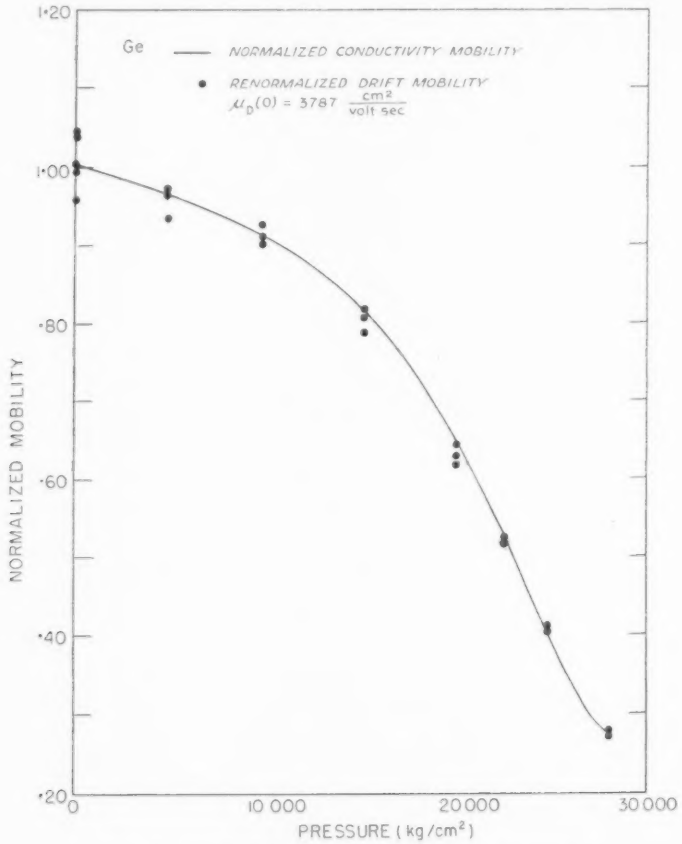


FIG. 3. Variation of the drift mobility of electrons in germanium with pressure.

Optical experiments are the only reliable means

at present of obtaining information about the (000) minima. Early measurements by FAN *et al.*,[16] and by NEURINGER,[16] on the optical absorption of thin films under pressure, seemed to show that the separation of the (000) minima from the valence band increased at a rate of about $1{\cdot}2\times10^{-11}$ eV $dyn^{-1}cm^2$. More recent experiments on the optical absorption into the (000) minimum as a function of magnetic field have established that the early pressure measurements were carried out at photon energies less than the minimum energy gap at the center of the Brillouin zone. However, more recent experiments carried out by us up to 7000 $kg/cm^2$[17] at photon energies much greater than this minimum gap energy give a pressure coefficient identical with that of the original measurements. The agreement between these determinations is not entirely understood, but it may indicate the presence of absorption at energies less than the (000) energy gap through the interaction of optical phonons of very small wave number.

If the absorption edge due to indirect transitions is measured to very high pressures, it should be possible to observe if and when the (100) minima become the set of lowest energy in the conduction band. This has been seen in very striking experiments by DRICKAMER,[18] who has measured the shift in the indirect transition absorption edge, under essentially hydrostatic conditions, to 100,000 $kg/cm^2$. DRICKAMER finds that the optical energy gap increases at a rate of $5\times10^{-12}$ eV $dyn^{-1}$ $cm^2$ below 40,000 $kg/cm^2$, and decreases at about $2\times10^{-12}$ eV $dyn^{-1}cm^2$ above this pressure. Furthermore, he can deduce from his experiments a separation of the (111) and (100) minima at atmospheric pressure of 0·2 eV, in agreement with our deductions from electrical data at much lower pressures.

## 9. OPTICAL ABSORPTION IN SILICON AND IN SILICON–GERMANIUM ALLOYS

From the above discussion we expect to find that the optical energy gap given by indirect (forbidden) transitions into the (100) minima decreases slowly with pressure. This is confirmed, although the effects are very small at low pressures. Our optical absorption edge coefficient of $-2\times10^{-12}$ eV $dyn^{-1}cm^2$[6] has been confirmed exactly in recent measurements by DRICKAMER[18] to 140,000 $kg/cm^2$.

Optical absorption into the (000) minimum has not been observed in silicon at the time of writing.

In the silicon–germanium alloys we again expect a gradual changeover from the behavior of the (111) minima to that of the (100) minima as the silicon content is increased. This has been found, as is demonstrated in Fig. 4. However, there remain several unexplained elements in the absorption spectra of the alloys, such as absorption edge shape changes and apparent non-linearity of the pressure coefficient with pressure.[7]

## 10. DIELECTRIC CONSTANT OF GERMANIUM AND SILICON

Data on the dielectric constant changes with pressure are presented in the following paper by CARDONA, PAUL and BROOKS. The pressure coefficient of the dielectric constants is related to the average change in energy separation of states of the same momentum value, and so is not simply related to the changes in the band edge states. One notable feature of these measurements is the existence of a large explicit effect of temperature on the dielectric constant. The pressure measurements generally have contributed much to the separation of implicit (volume) and explicit effects on the band gap, the effective masses and the dielectric constant.

## 11. IONIZATION ENERGIES OF IMPURITIES[10,19]

The small change in the ionization energy of the hydrogenic impurities in silicon found experimentally verifies predictions made on the basis of the pressure coefficients of effective mass and dielectric constant. No measurements have yet been made on germanium but no strikingly different behavior is anticipated.

Table 1 shows the pressure coefficients for gold in germanium and gold and indium in silicon.[10,19] The smallness of the coefficient for indium (only slightly greater than for the hydrogenic impurities) is rather surprising. The pressure coefficient of the impurity level—conduction band energy separation is usually much greater than that for the energy separation of a level from the valence band. This is most strikingly illustrated for the 0·54 eV acceptor level in silicon. Incidentally, it

is possible to measure the change with pressure of the separation of this single level from both the conduction and the valence bands, and to verify the pressure coefficient for the total silicon gap from the sum of these two coefficients. Experimental difficulties have so far prevented our measuring the pressure coefficients of the two shallow levels given by gold in germanium; these are particularly interesting since we speculate that similar properties may be found for the same type of level in both silicon and germanium.

The interpretation of our measurements on the deep lying impurity levels will become easier when electron spin resonance studies at General Electric develop a better understanding of the atmospheric pressure properties; conversely the pressure measurements may help a little in the overall interpretation.

*Table* 1

| Crystal | Type | De-ionizing level | Ionization energy (eV) | Pressure coefficient of ionization energy (eV $dyn^{-1}$ $cm^2$) |
|---|---|---|---|---|
| Silicon C–D–2 | P | Acceptor* | 0·62 | $-0{\cdot}3\times10^{-12}$ |
| Silicon C–309 | N | Acceptor* | 0·54 | $-1{\cdot}2\times10^{-12}$ |
| Silicon C–308 | P | Donor | 0·35 | $<5\times10^{-14}$ |
| Silicon–In–1 | P | Acceptor | 0·16 | $+2\times10^{-13}$ |
| Silicon–Al–1 | P | Acceptor | 0·06 | $+1{\cdot}4\times10^{-13}$ |
| Germanium–DP–85 | N | Acceptor | 0·20 | $+2{\cdot}9\times10^{-13}$ |
| Germanium–DP–63 | P | Acceptor | 0·15 | $+6\times10^{-13}$ |
| Germanium | N | Acceptor | 0·04 | Unmeasured |
| Germanium | P | Donor | 0·05 | Unmeasured |

* These are the same level.

## 12. GENERAL DISCUSSION

We wish to mention several general conclusions that can be drawn from the pressure measurements.

(1) If the pressure coefficients of the different energy gaps are used in order to calculate the volume dependent part of the temperature coefficient of the gaps, an explicit temperature dependence due to electron-phonon interaction is found. For the (111) germanium minimum the explicit part is some four times greater than the implicit one, and has the same sign.[20] For the (100) silicon minimum the explicit contribution to the temperature coefficient is similarly far greater than the implicit one; also, they have opposite signs. Only in the case of the (000) minimum does the implicit volume dependence contribute a major portion of the temperature coefficient. Assuming a pressure coefficient for this minimum of $1{\cdot}25\times$ $\times10^{-11}$ eV $dyn^{-1}cm^2$, and the known thermal expansion and compressibility coefficients of germanium, we obtain for the implicit part of the temperature coefficient $-1{\cdot}8\times10^{-4}$ eV $(°K)^{-1}$. The observed total coefficient is almost exactly twice this figure.

(2) The average effective masses in the (111) and (100) minima change very little with pressure. The implicit (volume) contribution to the temperature coefficient of these effective masses is probably less than 3 per cent in 300°K,[2,9,19] so that the large temperature coefficient claimed by some workers can probably only be explained by some electron–phonon interaction effect. The effective mass of electrons in the (000) minimum, and of light mass holes, can, however, change by 8 per cent in 300°K due to volume effects only.

(3) There is a distinct similarity in the behavior under pressure of the (100) minima in silicon, germanium, and in the silicon–germanium alloys. Similar comparison can be made between the pressure coefficients of the (000) conduction band minima found in germanium, indium antimonide, and probably in gallium arsenide, gallium

VOL 8 195

antimonide and gray tin. This seems to imply that other (atmospheric pressure) properties of these minima may be similar, independent of whichever group IV or group III–V compound is being considered. Also, there seems to be a correlation between the effects of altering the lattice constant through pressure and through alloying, so that the alloying may be regarded as providing a built-in positive or negative pressure.

VOL. 8 1959

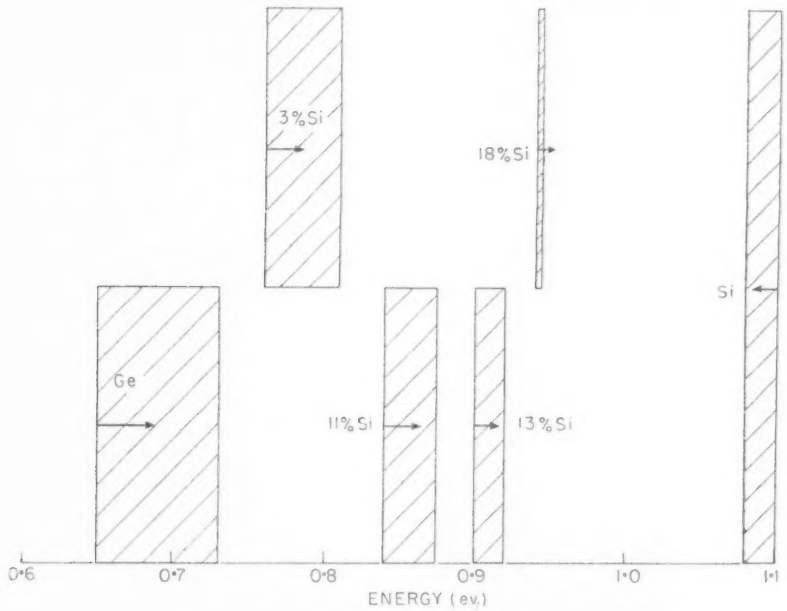


FIG. 4. Schematic representation of the shift of the indirect transition absorption edge in several silicon–germanium alloys, in 10,000 kg/cm².

*Acknowledgments*—Many individuals and research organizations have contributed to the research work described in this short review. I would like to thank especially however our friends at the General Electric, RCA, Sylvania, Bell and Lincoln Laboratories and at several other institutions for so kindly providing us with samples. As will be evident from the references, a very large part of the work was carried out by my colleagues Drs. G. B. BENEDEK, M. CARDONA, M. G. HOLLAND, M. I. NATHAN, A. C. SMITH and D. M. WARSCHAUER.

Professor HARVEY BROOKS directed the program with his usual enthusiasm and efficiency; I am much indebted to him for this example and for much personal encouragement.

## REFERENCES

1. PAUL W. and BROOKS H., *Phys. Rev.* **94,** 1128 (1954).
2. BENEDEK G. B., PAUL W. and BROOKS H., *Phys. Rev.* **100,** 1129 (1955); NATHAN M. I., PAUL W. and BROOKS H., *Bull. Amer. Phys. Soc.* **3,** 14 (1958).
3. ZWERDLING S. and LAX B., *Phys. Rev.* **106,** 51 (1957).
4. See (1). Also BROOKS H. and PAUL W., *Bull. Amer. Phys. Soc.* **1,** 48 (1956); NATHAN M. I., PAUL W. and BROOKS H., to be published.
5. HERMAN F., *Phys. Rev.* **95,** 847 (1954).
6. PAUL W. and PEARSON G. L., *Phys. Rev.* **98,** 1755 (1955); PAUL W. and WARSCHAUER D. M., *J. Phys. Chem. Solids* **5,** 102 (1958); NATHAN M. I. and PAUL W., *Bull. Amer. Phys. Soc.* **2,** 134 (1957).
7. PAUL W. and WARSCHAUER D. M., *J. Phys. Chem. Solids* **6,** 6 (1958).
8. BENEDEK G. B., PAUL W. and BROOKS H., unpublished.
9. SMITH A. C., Harvard University Thesis (1958).
10. HOLLAND M. G., Harvard University Thesis (1958).
11. BAILYN M., unpublished.

12. CARDONA M., PAUL W. and BROOKS H., *J. Phys. Chem. Solids* **8**, 204 (1958).
13. BRIDGMAN P. W., *Proc. Amer. Acad. Sci.* **81**, 221 (1952).
14. Unpublished.
15. PAUL W. and WARSCHAUER D. M., *J. Phys. Chem. Solids* **5**, 89 (1958).
16. FAN H. Y., SHEPHERD M. L. and SPITZER W. *Photoconductivity Conference*. Wiley, New York (1956); NEURINGER L., *Bull. Amer. Phys. Soc.* **2**, 134 (1957).
17. CARDONA M., PAUL W. and BROOKS H., unpublished.
18. DRICKAMER H. G., private communication.
19. NATHAN M. I., Harvard University Thesis (1958).
20. BROOKS H., *Advances in Electronics and Electron Physics*, **7**, p. 121. Academic Press, New York (1955).

*J. Phys. Chem. Solids* Pergamon Press 1959. Vol. 8. pp. 204–206. Printed in Great Britain

VOL
8
195

H.2

# DIELECTRIC CONSTANT OF GERMANIUM AND SILICON AS A FUNCTION OF VOLUME*

MANUEL CARDONA, WILLIAM PAUL AND HARVEY BROOKS

Division of Engineering and Applied Physics, Harvard University
Cambridge, Massachusetts, U.S.A.

## 1. INTRODUCTION

THE variation of the r.f. (10 mc/s) dielectric constant of germanium and silicon with pressure and temperature has already been reported by the authors.[1] The pressure coefficients were small, and the volume dependent part of the temperature coefficients much smaller than an explicit temperature dependence attributed to electron–phonon interactions. This paper reports complementary measurements of the changes in refractive indices of the two elements at infra-red wavelengths beyond the fundamental absorption edge. Since the effect of free carriers on both the r.f. measurements and the infra-red measurements is judged to be negligible for our experimental conditions, and the effect of the long wavelength lattice absorption[2] is very small,[1] the refractive index changes are expected to be simply one-half of those in the dielectric constant. The refractive index measurements provide an unambiguous independent check on those of the dielectric constant and extend the temperature range which was limited formerly by the conditions of measurement.

## 2. EXPERIMENT

The refractive index changes with temperature were deduced from two types of experiment, one involving the shift of the interference maxima and minima in the transmission of thin single crystal films, and the other the change in the angle of minimum deviation of single crystal prisms. The changes with pressure were found from the interference method only.

The optically polished, plane parallel films,† 3–10$\mu$ thick, were mounted in a conventional cryostat with $CaF_2$ windows in front of the entrance window of a Perkin Elmer 12C single beam, single pass spectrometer, also fitted with $CaF_2$ windows and prism. A radiation thermocouple detected the radiation. Suitable diaphragms collimated the beam so that near parallel rays were used in the measurement. The temperature of the film was measured with a thermocouple attached to its holder. The film thickness can be deduced from the measurement but is not needed; a correction for the thickness change with temperature has to be applied, however, using the known thermal expansion coefficient of the semiconductor.

* This work was supported by the U.S. Office of Naval Research under Contract Nonr 1866(10).

† We are grateful to Dr. W. C. Dash and General Electric Laboratory for providing these films.

The pressure measurements on the films followed our usual practices;[3] $CS_2$ was used as pressure transmitting fluid, and care taken to recognize the influence of its change in index with pressure in interpreting the shifts in interference patterns.

The 5° prisms were mounted in a single window cryostat and the cryostat placed on top of a goniometer. The Perkin–Elmer spectrometer provided monochromatic radiation. The prism was mounted against a plane mirror and the Abbe autocollimation method applied to measure the deviation angle to $\pm 1'$.

### 3. RESULTS

Figs. 1 and 2 show the variation of refractive index with wavelength for Ge and Si, deduced

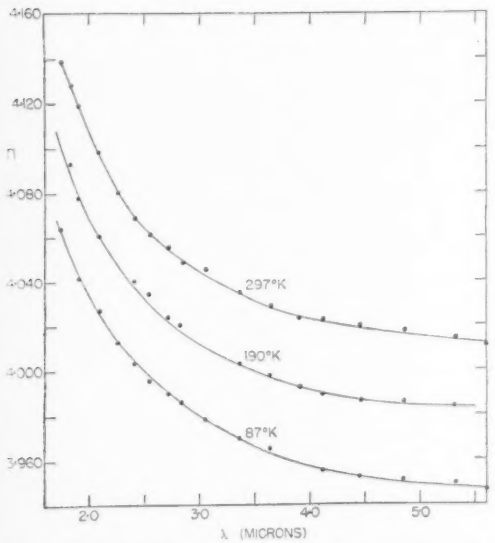


FIG. 1. Variation of refractive index of germanium with wavelength at several temperatures.

from measurements on prisms at several temperatures. Fig. 3 shows the variation of the long wavelength refractive index with temperature, from film and prism measurements; many of the points were taken with fixed long wavelength ($3\mu$) radiation incident on a prism whose temperature slowly rose after being reduced to that of boiling nitrogen.

The long wavelength temperature coefficient

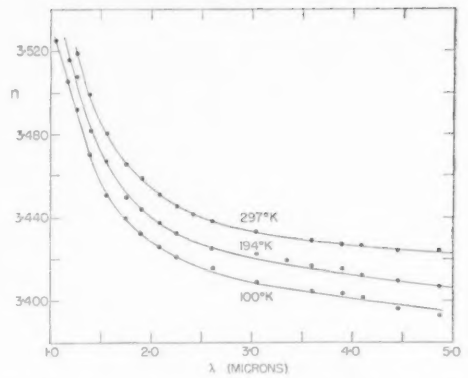


FIG. 2. Variation of refractive index of silicon with wavelength at several temperatures.

$1/n(dn/dT)$ is $(6{\cdot}9\pm0{\cdot}4)\times10^{-5}(°C)^{-1}$ for germanium and $(3{\cdot}9\pm0{\cdot}4)\times10^{-5}(°C)^{-1}$ for silicon (between 77°K and 400°K). These coefficients agree well with those for the dielectric constant determined at low temperatures; an explanation for the discrepancy that appears at high temperatures has been advanced by the authors.[1] This explanation involves inhomogeneities in samples of the elements doped with gold or manganese; because this seems quite possible, and because of the simplicity of interpretation of measurements of refractive index, we believe the variation of Fig. 3 to be the correct one.

The curve for silicon in Fig. 3 shows a perceptible flattening at low temperatures, as expected. The absence of this feature in germanium is probably due to the lower Debye $\theta$ for this element.

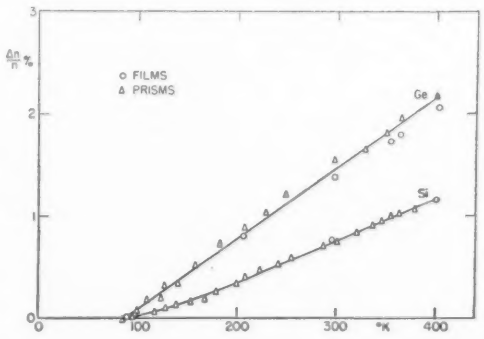


FIG. 3. Variation of long wavelength refractive indices of germanium and silicon with temperature.

The pressure coefficient of the refractive index of Ge at 297°K is

$$1/n(dn/dP) = -7\pm2\times10^{-7}\text{kg}^{-1}\text{cm}^2.$$

The coefficient for Si is $-3\pm2\times10^{-7}$ kg$^{-1}$ cm$^2$.

These changes are in close agreement with those deduced from the r.f. dielectric constant measurements (1)— $-6\pm1{\cdot}5\times10^{-7}$ kg$^{-1}$ cm$^2$ for Ge, $-2\pm0{\cdot}5\times10^{-7}$ kg$^{-1}$ cm$^2$ for Si—and are of the order of magnitude expected from shifts in band edges with pressure determined in other experiments.[1]

The pressure measurements confirm that the temperature dependence of the refractive index and dielectric constant is very much larger than that deduced from volume effects only.

The dielectric constant depends, at least in part, on the values of allowed electronic energies for all electron wave vectors, which are usually unknown. It should not therefore be possible to deduce variations in the dielectric constant from data on the electronic energies of band edges. Both the pressure and temperature data confirm this.

ARCHER[4] has determined the refractive index at room temperature from his data on the absorption coefficient versus frequency and the Kramers–Kronig relations. The lack of similarly complete data at another temperature prevents a deduction of the temperature coefficient of the refractive index in this manner. However, DASH and NEWMAN[5] have determined the variation of the absorption coefficient with temperature at frequencies close to the absorption edge. These data are sufficient to allow us to calculate with fair accuracy the difference between the change in the long wavelength refractive index and that close to the edge. This difference is small, close to our experimental error; however, examination of Figs. 1 and 2 shows that this difference is indeed present, and agrees with the calculated one.

### REFERENCES

1. CARDONA M., PAUL W. and BROOKS H., *Conference on Solid State Physics*, Brussels, June (1958). To be published by Academic Press.
2. COLLINS R. J. and FAN H. Y., *Phys. Rev.* **93,** 674 (1954).
3. PAUL W. and WARSCHAUER D. M., *J. Phys. Chem. Solids* **5,** 89 (1958).
4. ARCHER R. J., *Phys. Rev.* **110,** 354 (1958).
5. DASH W. C. and NEWMAN R., *Phys. Rev.* **99,** 1151 (1955).

VOL
8
195

*J. Phys. Chem. Solids* Pergamon Press 1959. Vol. 8. pp. 206–211. Printed in Great Britain

H.3

# THE MAGNETIC SUSCEPTIBILITY OF SEMICONDUCTORS

R. BOWERS

Westinghouse Research Laboratories, Pittsburgh, Pennsylvania

**Abstract**—Some recent work on the magnetic susceptibility of charge carriers in semiconductors is reviewed briefly. This review covers work done during the last two years and is a sequel to Busch's review at the 1956 Garmisch Conference. The principal topics covered are related to the author's work on *n*-Ge and *n*-InSb; experiments on *n*-Si are also discussed.

## 1. INTRODUCTION

THE purpose of magnetic susceptibility measurements on carriers in semiconductors is twofold. Firstly, such measurements may be used to obtain information concerning the band structure of semiconductors and, secondly, such measurements may be used to examine the validity of the theories of susceptibility.

The usefulness of susceptibility measurements as a means of studying the electronic structure of semiconductors was first established by BUSCH and MOOSER[1,2] with their work on grey tin.

These authors and also STEVENS *et al.*[3] have given a detailed account of the analysis of susceptibility measurements.

The total susceptibility of a semiconductor is the sum of the lattice susceptibility $\chi_L$ and the susceptibility of the charge carriers $\chi_C$. The lattice susceptibility may be determined from measurements on a high-purity crystal. The effect of substitutional donor or acceptor impurities on $\chi_L$ is negligible for the impurity densities used in most semiconductor experiments. Hence, the carrier contribution in a doped crystal may be obtained by substracting from its total susceptibility, the susceptibility of a pure crystal.*

The carrier contribution to the susceptibility consists of two parts, a paramagnetic contribution $\chi_s$ resulting from the spin of the carrier and a diamagnetic contribution $\chi_0$ resulting from the carrier's orbital motion. In the case of non-localized states, the former is usually interpreted with the Pauli theory and the latter by using the Landau–Peierls formula.[2,3] It should be kept in mind that there are conditions under which the latter formula is not expected to be valid[4] (see discussion of InSb, below) in which case one must attempt a more basic analysis of the susceptibility. For carriers localized at donor or acceptor sites, the spin and orbital susceptibilities are given by the Langevin relations.[2,3] In those semiconductors where the appropriate effective masses are small, the orbital susceptibility $\chi_0$ is much larger than $\chi_s$; hence, the carrier susceptibility, which is so easily extracted from the data, is almost completely orbital in character.

The electronic diamagnetism $\chi_0$ is of special interest for theoretical purposes. It is instructive to contrast the ease with which we can study conduction-electron diamagnetism in certain semiconductors with the difficulty of making a similar study in simple metals. In a metal, one cannot determine the lattice susceptibility in the direct manner described above. Furthermore, in most metals, the spin susceptibility and the orbital susceptibility of the carriers are of approximately the same magnitude making it difficult to separate the orbital contribution with precision. In addition, the electron gas in a simple metal is always degenerate, so that susceptibility measurements at various temperatures yield essentially the same information. In many semiconductors, on the other hand, the Fermi temperature is readily attainable, and the susceptibility can be studied in both degenerate and classical conditions. Another advantageous feature of semiconductors is that the number of carriers can be varied over several orders of magnitude.

* For a criticism of this method of obtaining carrier susceptibilities see DORFMANN (*Izv. Akad. Nauk* **21**, 796 (1957)). His criticism concerns the anomalous temperature dependence of the lattice susceptibility exhibited by some semiconductors (refs. 3, 5, 6, 8, 10) and possible effects of impurities on this dependence. In this paper, DORFMANN considers some resonance techniques for measuring carrier susceptibilities in semiconductors.

## 2. THE SUSCEPTIBILITY OF UNBOUND ELECTRONS

### 2.1. *Germanium*[1,3,5–9]

Until recently, most of the published measurements of the extrinsic carrier contribution to the susceptibility of Ge had been made in the temperature range 300°K to 77°K, and the principal features observed were due to nonlocalized carriers obeying classical statistics. These studies have now been extended to liquid-helium temperatures.[5,6,8] Furthermore, a larger range of electron densities has been studied.[8]

There are several reasons why it was desirable to extend the measurements into the low-temperature region. Firstly, for free carriers, it is desirable to have $kT$ very small compared to the Fermi level so that the limit of occupation in the band is well defined. Secondly, the degenerate carrier susceptibility observed at low temperatures is proportional to the cube root of the carrier density, whereas in the non-degenerate case it is proportional to the first power of the carrier density; hence, the results of measurements in the degenerate range are less sensitive to uncertainties in the knowledge of the carrier density. Thirdly, as will be discussed later, low temperatures are necessary for studies of the susceptibility of localized carriers.

Our measurements[8] of the conduction electron susceptibility in Ge cover a carrier density range from $1\times10^{17}$ to $3\times10^{19}$ cm$^{-3}$. The ionization energy of donors falls to zero at approximately $1\times10^{17}$ cm$^{-3}$ so that the carriers remain in the conduction band to the lowest temperatures. The carrier susceptibility observed in the liquid-helium

range was found to be independent of temperature. This was expected because the electron gas is degenerate at these temperatures for all the specimens.

In Fig. 1, we show the observed degenerate conduction electron susceptibility plotted against the cube root of the carrier density ($n$) as determined from Hall measurements. We also show a plot of the theoretical conduction electron susceptibility based on the Landau–Peierls and Pauli formulae, using the effective masses given by cyclotron resonance. The two straight lines cor-

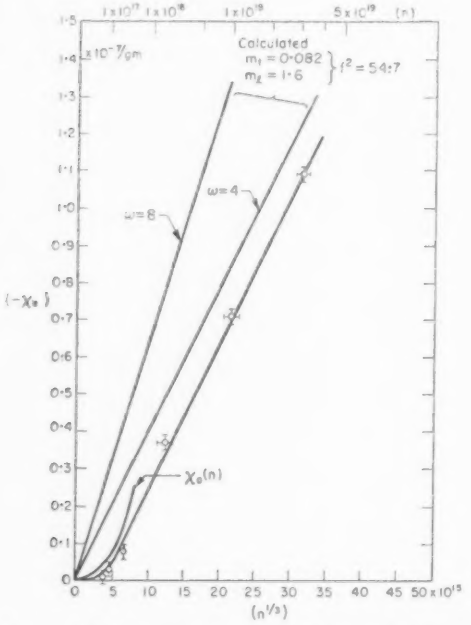


FIG. 1. The magnetic susceptibility of degenerate conduction electrons in Ge plotted against the cube root of the carrier density.

respond to the two possible numbers (4 and 8) of conduction band energy minima. The curve $\chi_A(n)$ in Fig. 1, gives a rough estimate of the *diamagnetism* which would have been expected had the electrons remained in atomic states instead of moving in the conduction band.

The observed carrier susceptibility is seen to parallel the 4 ellipsoid line except at small carrier densities. The departure from an $n^{\frac{1}{3}}$ dependence at low concentrations is understandable, for in this range the electron donor wave functions do not overlap very much, and we expect an "atomic-like" susceptibility $\chi_A(n)$ proportional to the number of carriers. While the observed susceptibility runs parallel to the theoretical 4 ellipsoid line at the higher concentrations, they do not merge in the measured range. The disparity between the two is small but seems to be real; we are not certain of its cause.

Apart from this small disparity, the observed susceptibility substantially exhibits the form expected from the cyclotron resonance masses and 4 ellipsoids. Any reasonable analysis of the observed susceptibility of the more highly doped specimens leads to effective masses which differ only slightly from the cyclotron resonance values. The Fermi levels at absolute zero of the 3 most highly doped specimens have been computed to be ·01, ·04 and ·08 eV above the bottom of the conduction band. Hence, we conclude that: (1) the parabolic part of the conduction band extends to at least an energy of 0·8 eV and (2) our results support a 4 ellipsoid model of the conduction band of Ge, substantiating earlier tentative evidence.[9]

The susceptibility of conduction electrons was also measured in the temperature range from 300°K to 77°K. In this range the data exhibits the transition from degenerate to classical statistics.

With regard to the deviation of the observed carrier susceptibility from that expected theoretically, our conclusions differ from those of STEVENS *et al.*[3] This difference is due to a difference in interpretation of our respective data and not in the experimental measurements. They had concluded that between 300°K and 77°K, for carrier densities in excess of about $10^{18}$, the susceptibility data required effective masses which increase drastically with increasing carrier density. We believe that this drastic dependence of effective mass on carrier density is spurious, and results from an interpretation of the Hall coefficient by STEVENS *et al.* which is no longer thought to be correct.[8]

HEDGECOCK[6] has investigated the low temperature conduction electron susceptibility at carrier densities near $10^{17}$ cm$^{-3}$. He has attempted to interpret some of his results in terms of effective masses in the impurity band. The absence of a theory of the impurity band is a serious impediment to such an interpretation. It is difficult to compare his low temperature results with our

own because our measurements were made in a somewhat different temperature range. However, there appears to be no major discrepancy in our data at 4·2°K, although he obtains a temperature dependence just above 4·2°K which appears to be inconsistent with our liquid helium data.

GEIST[7] has made magnetic susceptibility measurements on $n$-Ge ($8\times10^{16}$ cm$^{-3}$) at 297°K and 138°K. His analysis of the data, based on provisional estimates of the carrier density, leads to effective masses which are appreciably temperature dependent. In our work, no appreciable temperature dependence of effective mass was apparent.

### 2.2. *Silicon*

SONDER and STEVENS[10] have recently published an extensive study of the magnetic susceptibility of $n$-Si, in the temperature range from 300°K to 3°K and covering a range of donor densities from $3\times10^{16}$ to $3\times10^{19}$ cm$^{-3}$. At the higher temperatures, the diamagnetic contribution of unbound conduction electrons was derived from the data. The observed susceptibility was smaller than theoretical estimates based on effective masses determined in cyclotron resonance experiments. If one derives effective masses from the data of Sonder and Stevens, the values obtained are appreciably higher (~25 per cent) than those calculated from the cyclotron resonance results.

GEIST[7] presents magnetic data on a single $n$-Si ($6\times10^{18}$) specimen at 297°K and 138°K. His provisional analysis of this data leads to an effective mass which is quite close to the cyclotron resonance value.

### 2.3. *InSb*

Among the earliest attempts to estimate the effective mass of conduction electrons in InSb were the magnetic susceptibility measurements of STEVENS and CRAWFORD.[11] There is special interest in the susceptibility of conduction electrons in InSb in view of the fact that the conduction band in InSb is known to depart from a simple parabolic form.

In order to investigate the influence of the band shape on the carrier susceptibility, we have measured the extrinsic degenerate conduction electron susceptibility in InSb[12] covering a range of carrier densities from $1\times10^{16}$ to $6\times10^{18}$ cm$^{-3}$. The Fermi level at absolute zero for the highest carrier density is about ·33 eV, so that we can claim in these experiments to be probing the form of the conduction band to a level of ·33 eV above the band minimum.

In Fig. 2 we show the observed degenerate

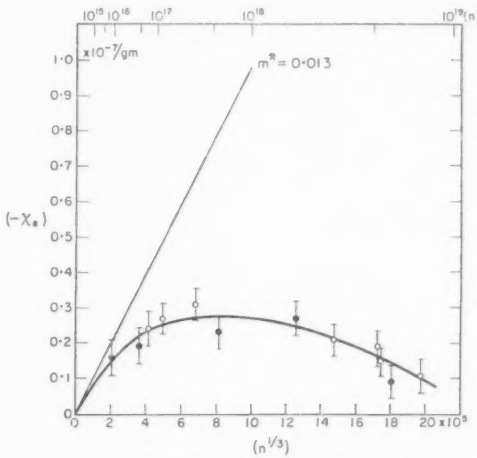


FIG. 2. The magnetic susceptibility of degenerate conduction electrons in InSb plotted against the cube root of the carrier density.

electron susceptibility plotted against $n^{\frac{1}{3}}$. The straight line represents the Landau–Peierls value with $m^* = ·013$, the mass at the band minimum as determined by cyclotron resonance. The dependence of the observed susceptibility on $n^{\frac{1}{3}}$ is in striking contrast to the behavior of electrons in Ge (Fig. 1); in InSb the deviation of the conduction band from parabolic form is strongly manifested in the behavior of the magnetic susceptibility.

A theoretical analysis of the susceptibility has been made by YAFET[12] using the result of Kanes' band structure calculations.[13] The departure of the conduction band from parabolic form precludes any direct application of the Landau–Peierls formula. The results of Yafet's calculations are as follows: (1) If only that part of the Hamiltonian connecting the conduction and valence bands is considered, the calculated susceptibility differs appreciably from that observed. (2) The effect of higher bands is appreciable at the higher concentrations, and if these bands are taken into account, the calculated susceptibility is in reasonable agreement with to that observed. In view of this

fact, the observed susceptibility is consistent with Kanes' model.

2.4. *InAs*

Measurements by GEIST[14] show that the deenpdence of the conduction electron susceptibility on the density of carriers in InAs is similar to that found in InSb.

## 3. THE SUSCEPTIBILITY OF CARRIERS IN BOUND STATES

In order to study the susceptibility of bound states, it is necessary to work at temperatures which are low enough to freeze the carriers out of the conduction band. One must also work at concentrations which are low enough for the carriers to remain localized. In germanium this means working with less than $10^{17}$ cm$^{-3}$, while with Si, the limit is $10^{18}$ cm$^{-3}$.

We have attempted to study electrons and holes in localized states by measurements on *n*- and *p*-Ge with carrier concentrations near $6 \times 10^{16}$ cm$^{-3}$.[8] At this concentration we expect the carriers to be "frozen-out" below 4°K; they cannot, however, be completely localized since impurity band conduction is observed.

We determined the paramagnetism of bound states by means of the temperature dependence of the susceptibility below 4°K. For $N$ non-interacting simple spins, one would expect a contribution to the susceptibility of $\chi_s = N\mu^2/kT$; where $\mu$ is the Bohr magneton. For both the *n*- and *p*-Ge, the observed susceptibility exhibited a temperature dependence which was *less* than that expected from $6\times10^{16}$ independent spins. For *n*-Ge, this probably results from antiparallel spin coupling due to exchange through the overlap of neighboring donor wave functions. This explanation is supported by comparable measurements made on *n*-Si ($6\times10^{16}$). The donor wave functions in Si have radii which are 1/3 of those in Ge, and theoretical estimates indicate that exchange effects should be negligible in this Si specimen. We did indeed find in this case, a temperature dependence in reasonable agreement with the free spin value.

Our experiments on Ge suggest that the magnetic interaction between neighboring impurities is quite strong at the density $6\times10^{16}$ cm$^{-3}$, but they give no information concerning the magnetic moment of independent impurities. Measurements at much lower carrier densities were required and this was beyond the capability of our experimental techniques. Our measurements on *n*-Si showed that conditions in this material were more favorable for bound state studies.

It is obviously of interest to examine the overlap of donor wave functions by measuring the spin susceptibility as a function of the concentration of donors, starting at low enough concentrations for free spins and then reaching concentrations where the spins are coupled. Such an investigation has very recently been carried out by SONDER and STEVENS,[10] for electrons in Si. Their work covered a range of donor densities from $4\times10^{16}$ to $5\times10^{18}$ cm$^{-3}$. In the temperature range 20°K to 4°K, they found that specimens with densities of approximately $4\times10^{16}$ and $2\times10^{17}$ exhibited a simple $1/T$ dependence whose magnitude was equal to $N\mu^2/kT$ where $N$ was the number of donors. For donor densities higher than these, deviations from a simple $1/T$ dependence were observed, due to the interactions between the more closely spaced donors. Except for the most highly doped specimen, $N = 5\times10^{18}$ cm$^{-3}$, the limiting slope at high temperatures of the $1/T$ plot for all specimens was equal to $N\mu^2/k$.

## 4. OTHER TOPICS

The reader is referred to references 5, 6 and 8 for recent work on anomalies in the host crystal susceptibility of germanium.

A statistical analysis of the susceptibility of impurity states has been published by GEIST;[15] this analysis is only appropriate for very dilute impurities.

A theoretical study of the susceptibility of semiconductors of the tellurium type has been published by FIRSOV.[16]

A theory of the susceptibility of excitons in semiconductors has been given by KORENBLIT.[17]

KLINGER[18] has calculated the susceptibility in an impurity band in strong magnetic fields for an ordered distribution of impurities. He finds that an oscillatory behavior of the susceptibility results from this model.

The susceptibility of $Mg_2Sn$ has been measured by KORENBLIT and KOLESNIKOV.[19] Selenides and tellurides of the heavier elements have been studied by MATYAS.[20]

## 5. SUMMARY

We shall summarize what has been learned from the susceptibility measurements of various workers since the last International Semiconductor Conference.

(1) *Ge*[5–8]—While small disparities still exist between theory and experiment, the results of recent susceptibility measurements provide strong evidence that the conduction band of Ge is parabolic to at least ·08 eV and has 4 minima in $k$-space. Attempts to study *non-interacting* localized states have been unsuccessful. Data concerning the susceptibility of electrons in the impurity band region near $10^{17}$ cm$^{-3}$ are now available.

(2) *Si*[10]—The observed conduction electron susceptibility in silicon is not as large as theoretical values which are based on the effective masses obtained from cyclotron resonance experiments. Successful studies have been made of the spin susceptibility of localized donor electrons, and magnetic data has been obtained on the growth of the interaction between neighboring donors as their density is increased.

(3) *III–V Compounds*[12,14]—Measurements of the extrinsic electron susceptibility in InSb have been made. The deviation of the conduction band from parabolic form is strongly apparent in the results. The observed susceptibility has been interpreted with reasonable success using Kane's band structure calculations. Similar experimental results have also been obtained in InAs.

## REFERENCES


1. Busch G., *Semiconductors and Phosphors*, p. 158. Vieweg, Braunschweig (1958).
2. Busch G. and Mooser E., *Helv. Phys. Acta* **26**, 611 (1953).
3. Stevens D. K., Cleland, J. W., Crawford J. H. and Schweinler H. C., *Phys. Rev.* **100**, 1084 (1955).
4. Kjeldaas T. and Kohn W., *Phys. Rev.* **105**, 806 (1957).
5. Van Itterbeck A. and Duchateau W., *Physica* **22**, 649 (1956).
6. Hedgecock F. T., *Canad. J. Phys.* **34**, 43 (1956); *J. Electronics* **2**, 513 (1956).
7. Geist D., *Naturwiss.* **45**, 33 (1958).
8. Bowers R., *Phys. Rev.* **108**, 683 (1957).
9. Crawford J. H., Schweinler H. C. and Stevens D. K., *Phys. Rev.* **99**, 1330 (1955).
10. Sonder E., and Stevens D. K., *Phys. Rev.* **110**, 1027 (1958).
11. Stevens D. K. and Crawford J. H., *Phys. Rev.* **99**, 487 (1955).
12. Bowers R., *Bull. Amer. Phys. Soc.* **3**, 120 (1958); Bowers R. and Yafet Y. (to be published).
13. Kane E. O., *J. Phys. Chem. Solids* **1**, 249 (1957).
14. Geist D. *Z. Naturf.* **13a**, 699 (1958); and private communication.
15. Geist D., *Z. Naturf.* **12a**, 873 (1957).
16. Firsov Iu. A., *Zh. tekh. fiz. SSSR* **27**, 2212 (1957); *Sov. Phys., Tech. Phys.* **2**, 2053 (1957).
17. Korenblit L. L., *Zh. tekh. fiz. SSSR* **27**, 484 (1957); *Sov. Phys., Tech. Phys.* **2**, 434 (1958).
18. Klinger M. I., *Zh. eksp. teor. fiz. SSSR* **33**, 379 (1957); *Sov. Phys., J. Exp. Theor. Phys.* **6**, 292 (1958).
19. Korenblit L. L. and Kolesnikov A. P., *Zh. tekh. fiz. SSSR* **26**, 941 (1956); *Sov. Phys. Tech. Phys.* **1**, 924 (1956).
20. Matyas M., *Czech. J. Phys.* **8**, 301, 1309 (1958).


*J. Phys. Chem. Solids* Pergamon Press 1959. Vol. 8. pp. 211–216. Printed in Great Britain

# H.4 STATE DENSITY IN THE VALENCE BAND OF SILICON

**HOMER D. HAGSTRUM**

Bell Telephone Laboratories, Murray Hill, New Jersey

**Abstract**—The distribution in kinetic energy of electrons ejected by the Auger neutralization of 10 eV $He^+$ ions at a clean silicon surface is related through an integral transform to the state density function in the valence band. Estimates of the width of the degenerate $p$-band and of the total valence band are obtained from the fitting of a theoretical distribution to the experimental one.

## 1. INTRODUCTION

THERE is at present considerable interest in the electronic band structures of solids including those of the elemental semiconductors silicon and germanium. The present paper presents work in which information concerning some of the principal features of the state density function in the valence band of silicon is obtained. The only previous experimental work yielding such information for silicon has been that of SKINNER[1] using soft X-ray spectroscopy. Theoretical work on the band structure of silicon has provided, among many other results, estimates of the widths of the individual valence bands.[2–4] In this paper it will be possible to present the method and results in abbreviated form only. Much of the necessary discussion must await subsequent publication.

## 2. THE PHENOMENON STUDIED

The present work is one of a series of studies of the interaction of slowly moving ions with solid surfaces. When a $He^+$ ion of 10 eV kinetic energy is neutralized at an atomically clean silicon surface, secondary electrons of considerable kinetic energy (up to 12 eV) are produced. The process responsible for these electrons is the two-electron Auger-type process illustrated in Fig. 1. When the ion is close enough to the surface two valence band electrons, at any energies such as $\epsilon'$ and $\epsilon''$ in the figure, interact. One electron drops into the vacant ground state of the atom and the other rises on the energy diagram to a state at $\epsilon_k$ above the vacuum level, $\epsilon_0$. Those excited electrons which are properly directed will leave the solid where they can be detected and their kinetic energies measured.

The large well depth of the atomic ground state restricts the atomic wave function to the vicinity of the atom. It results that the matrix element of the Auger process has value principally in the region of the atom and that the relative participation of a valence band electron is determined primarily by the magnitude of the tail of its wave function outside the solid in the vicinity of the atom. Thus the process involves surface electrons only, a fact which makes the conclusions drawn in this paper possible because energy straggling of the secondary electrons on leaving the solid may be neglected.

The method of obtaining information concerning the state density in the valence band is to fit the experimentally determined kinetic energy distribution of the secondary electrons with a theoretical curve. The theoretical kinetic energy distribution function depends critically on the parameters chosen to characterize the state density in the valence band.

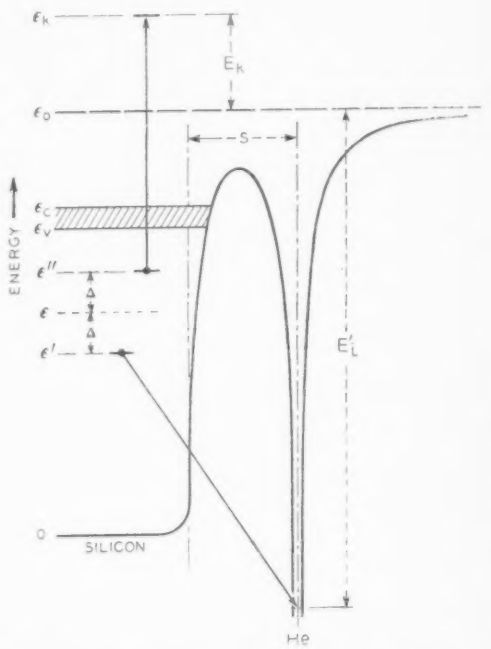


FIG. 1. Energy level diagram indicating the electronic transitions of an Auger-type which occur when a $He^+$ ion is neutralized at a Si surface.

## 3. EXPERIMENT

A focused beam of 10 eV $He^+$ ions is allowed to strike a face of a single crystal Si target. The electrons ejected in the neutralization process are collected on a surrounding electrode. Both total yield and electron energy distribution can be measured. The experimental apparatus and technique employed are those already described for studies of the refractory metals.[5] The silicon surface was cleaned by heating to 1550°K and the adsorption cycle for background gases or for known gases admitted to the instrument could be followed. The evidences that the surface was clean are to be presented elsewhere.[6] All the data given here were

obtained within minutes after cooling the silicon from a high temperature flash. Adsorption of a monolayer of oxygen, for example, completely alters the results.

We concentrate in this paper on the experimentally determined kinetic energy distribution, $N_0(E_k)$, of electrons ejected from the (111) face of silicon. The data are shown in Fig. 2. The plotted points are experimental; the curve is a theoretical one to be discussed presently. The experimental function is seen to have structure for which the state density in the valence band is responsible.

## 4. THEORY

The theory of the Auger neutralization process for $He^+$ ions incident on silicon is in principle the same as that already published for tungsten.[7] From an assumed form for the state density function, $N_v(\epsilon)$, in the valence band one calculates the density, $N_i(\epsilon_k)$, of excited electrons produced in the conduction band by the Auger process (Fig. 3). The theoretical distribution in energy, $N_0(E_k)$, of electrons which leave the solid is obtained from $N_i(\epsilon_k)$ by multiplying by the probability of escape, $P_e(\epsilon_k)$. We shall proceed as though the energy bands extended level to the surface as shown in Fig. 1 and that the population of surface states is small enough to be neglected. These matters will be discussed below.

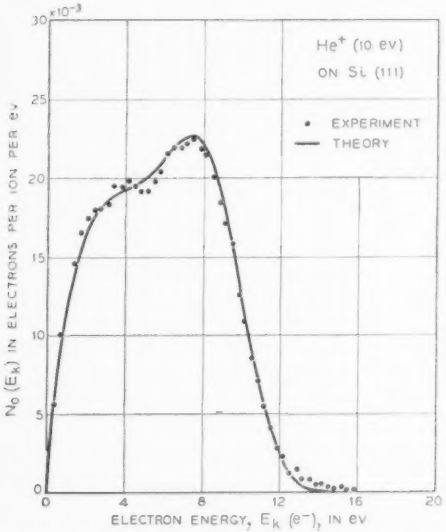


FIG. 2. Kinetic energy distribution of the electrons ejected from a clean (111) surface of Si by 10 eV $He^+$ ions. The points are experimental. The curve is theoretical for the following parameters: $\epsilon_v = 16{\cdot}0$ eV; $\epsilon_0 = 20{\cdot}7$ eV; $\epsilon_c = 17{\cdot}1$ eV; $E_i' = 22{\cdot}6$ eV; $p = 0{\cdot}68$; $r = 0{\cdot}35$; $\sigma = 0{\cdot}3$; $f = 3{\cdot}92$.

The general form of the state density function in the valence band of silicon is known.[2] (Curve 1 of Fig. 3.) Two of the four valence electrons lie in juxtaposed bands, V3 and V4, whose combined width, $\epsilon_v$, may be of the order of 10 to 15 eV or more. The remaining two electrons lie in degenerate bands, V1 and V2, (spin–orbit interaction neglected) whose high energy limits coincide with that of V3 and whose width, $(1-p)\epsilon_v$, is considerably less, perhaps 25 per cent of the over-all width, $\epsilon_v$, of the total valence band. A reasonable assumption to make is that the density function is made up of sections of parabolas starting at each band edge as shown in curve 1 of Fig. 3, each section being normalized to an area beneath the curve of one electron. Values of the total width, $\epsilon_v$, and the position of the lower limit of the V1, V2 bands at $p\epsilon_v$ are determined in this work.

The density of excited electrons in the conduction band arising from the Auger neutralization process is proportional to an integral transform of $N_v(\epsilon)$. This arises from the fact that a given element of energy space at $\epsilon_k$ is populated by all processes having the same $\epsilon$, midpoint between energies $\epsilon'$ and $\epsilon''$ of participating electrons in the valence band (Fig. 1). Thus $N_i(\epsilon_k)$ is proportional to the integral $\int N_v(\epsilon+\Delta)N_v(\epsilon-\Delta)d\Delta$ taken over appropriate limits, after a change of variable from $\epsilon$ to $\epsilon_k$ has been effected. As has been shown elsewhere[7] this function must be broadened to account for the effects of variation of the effective ionization energy of He near the silicon surface and of the Heisenberg uncertainty principle. This procedure yields curve 5 of Fig. 3 which has been normalized to an area of 1 electron per incident ion corresponding to the Auger neutralization of each ion incident upon the surface.

One proceeds from curve 5 for $N_i(\epsilon_k)$ to obtain the externally observed kinetic energy distribution function, $N_0(E_k)$, by multiplying by the probability of escape of electrons from the solid, curve 7 of Fig. 3. As shown earlier[7] this depends upon the angular opening of the cone about the surface normal in which the internal velocity vectors

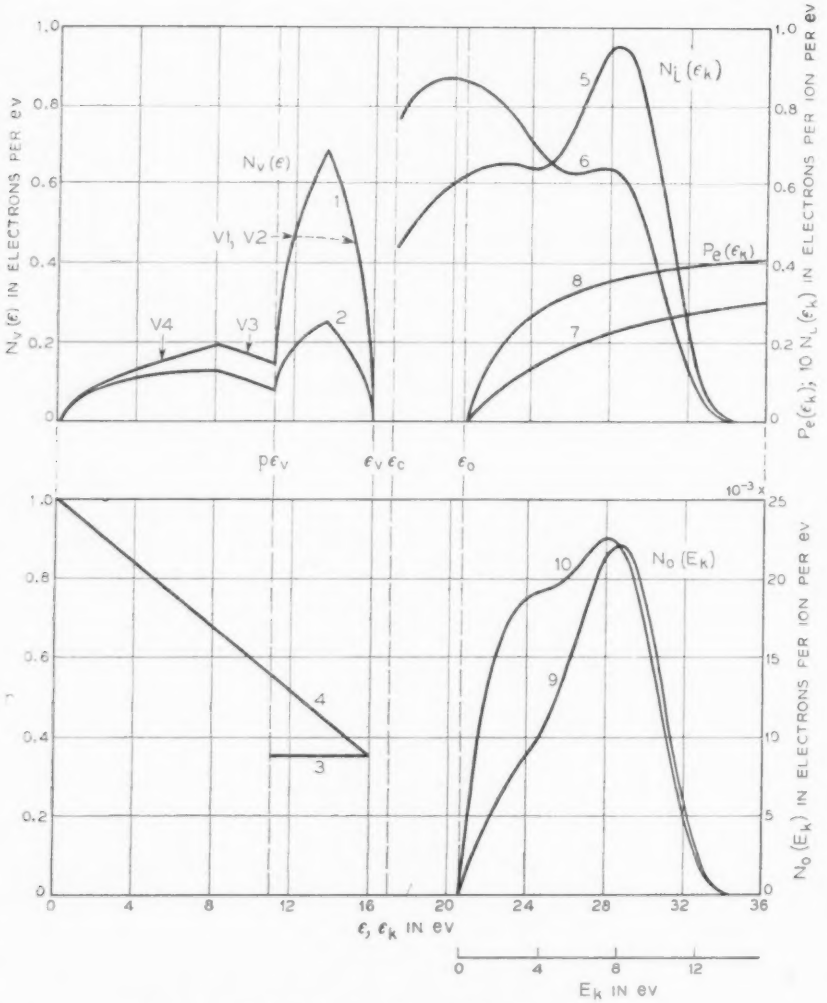


FIG. 3. Graph of the state density function, $N_v(\epsilon)$, in the valence band; the density, $N_L(\epsilon_k)$ of excited electrons in the conduction band; the probability of escape, $P_e(\epsilon_k)$, and the kinetic energy distribution, $N_0(E_k)$, of externally observed electrons. Curves are shown for no correction relative to the *s*- and *p*-character of the valence electrons (1, 5 and 9) and with such a correction (2, 6 and 10). The parameter used to correct the $N_v(\epsilon)$ function is plotted in the lower left-hand part of the graph.

must lie for escape and upon the ratio, $f$, of the matrix elements for escaping and internally reflected electrons. The ratio $f$ is a parameter which generally is adjusted to give the experimental value of the total electron yield $\gamma_1 = \int_0^\infty N_0(E_k)dE_k$. Here, however, the parameter $f$ was chosen so that curve 9 had the same total height rather than area as curve 10 for ready comparison of their forms. It is seen that the form of curve 9 is considerably at variance with the experimental data of Fig. 2. The reason for this discrepancy lies in the fact that all electrons in the valence band have thus far been treated alike as regards the extent of their participation in the Auger process.

It has been indicated above that the relative participation of any given valence band electron depends upon the magnitude of its wave function outside the solid at the position of the incoming atomic ion when the neutralization occurs. One factor affecting the size of this tail of the wave function is the depth, $\eta$, in the band below the vacuum level since the wave function falls off as $\exp(-2m\eta s/\hbar^2)^{\frac{1}{2}}$ for sufficiently large distances, $s$, outside the surface. A second factor, which seems to be controlling here, is the difference in protrusion of the $s$- and $p$-type wave functions associated with the valence electrons. We know that the electrons in the V1 and V2 bands are both $p$-type and that the character changes from $s$- to $p$-type as one proceeds through the other valence bands from the bottom of V4 to the top of V3. Because of the lobed character of the $p$ functions and their positions relative to the surface normal, it is evident that $p$ wave functions are of considerably smaller magnitude near the ion than the spherically symmetric $s$ functions.

In any event it is found possible to fit the theory to the experiment only if one "demotes" the $p$ electrons as far as their participation in the Auger process is concerned. This is accomplished in the theory by multiplying the $N_v(\epsilon)$ functions for the V1, V2 bands by a constant factor $r$ less than unity and by multiplying the $N_v(\epsilon)$ for the V3 and V4 bands by a variable factor $1-(1-r)\epsilon/\epsilon_v$. These factors are plotted in Fig. 3 below the $N_v(\epsilon)$ function as curves 3 and 4, respectively. This procedure yields curve 2 as an effective state density function. The Auger transform of curve 2, when shifted by the change of variable from $\epsilon$ to $\epsilon_k$, yields curve 6 for $N_1(\epsilon_k)$, which when multiplied by the appropriate $P_e(\epsilon_k)$, curve 8, gives curve 10 for $N_0(E_k)$. It is curve 10 which is compared with the experimental data in Fig. 2 and found to be in quite good agreement.

## 5. DISCUSSION

If one applies the theoretical model without any limitation on the parameters involved, one finds that there is a series of solutions. These solutions lie along a space curve in the three dimensional space of the parameters $p$, $E'_1$ and $\sigma$. These parameters specify the width of the degenerate V1, V2 bands, $(1-p)\epsilon_v$, the effective ionization potential, and the broadening, respectively. One limit may be predicted with certainty. It is that for little broadening, $\sigma \sim 0$. This corresponds physically to such high transition probability that the Auger neutralization process proceeds when the wave functions of atomic and solid electrons have just begun to overlap and before $E'_1$ has been reduced by much more than the image force attraction. This limiting solution for $He^+$ yields $E'_1 = 22{\cdot}6$ eV and $p = 0{\cdot}68$. The width 5·1 eV for the V1, V2 bands ($\epsilon_v = 16$ eV) thus obtained is the maximum value possible for this parameter. If the neutralization process is of lower probability and thus occurs closer to the silicon surface, $E'_1$ is reduced, $\sigma$ and $p$ increased, and thus the width of the degenerate $p$ band reduced below the 5·1 eV maximum. The details of this matter must await more detailed publication. However, it is probable that for the slow ions used the process does proceed before much wave function overlap has occurred as was found to be the case in tungsten.[7] Thus one expects the width of the V1, V2 bands to be near the 5·1 eV maximum predicted by the present results. Fig. 3 is drawn for this limiting case. Phillips[8] has estimated on theoretical grounds that the width of these bands is 3·3 eV.

The best fit of theory to experiment for $N_0(E_k)$ can be achieved only if the total width of the valence band is near 16 eV, the figure used in the present work. The fit is not as sensitive to this parameter as it is to the degenerate $p$ band width. A reasonable fit is also accomplished at 14 eV. However, for $\epsilon_v = 12$ eV or less a satisfactory fit becomes impossible. Thus the present work stands in considerable disagreement with WOODRUFF'S theoretical result[4] of 8·42 eV for the energy

separation of the $\Gamma_{25'}$ and $\Gamma_1$ states. An earlier calculation of JENKINS[3] using a different theoretical method gave 13 eV as the total width of the valence bands. Skinner's so-called reduced width for the $L_3$ X-ray emission band in silicon is $16{\cdot}7 \pm 1$ eV.[1] The free electron model gives 12·7 eV.[1]

It is possible that the experimental energy distribution (Fig. 2) is somewhat different from the true distribution by virtue of distortion caused by the retarding potential method used. Any such effect would tend to fill in the minimum observed between the two peaks which it appears difficult for the theory to reproduce. It would also make the two band widths quoted above a little high. It appears that the effect is not large. Another effect which should not be overlooked is the broadening of the $N_i(\epsilon_k)$ distribution by the finite lifetime in the final state of the Auger process. This effect is the same as that discussed by SKINNER[1] and LANDSBERG[9] and arises from the secondary Auger processes by which low lying holes left in the valence band by the ion neutralization move upward through the band. It is most marked at the low energy edge of the band which is not observed in this work but it might have a small effect on the value of $\epsilon_v$ needed to fit the upper parts of the $N_i(\epsilon_k)$ distribution.

The above theory was carried through as though the energy bands remained level to the surface and for negligible population of surface states. We know that the bands may bend near the surface giving rise to states which are localized there and that there may be states in the energy gap of appreciable density. However, only filled surface states are of significance in this work. It is now evident that for one reason or another the surface of atomically clean Si used in this work is $p$-type and that the bands bend up by a few tenths of an electron volt at the surface.[10] This will modify the valence band density function over only a few tenths of an electron volt near its ends. The present results are compatible with a population of filled surface states in the energy gap of silicon not much greater than the $10^{13}/cm^2$, or about 0·25 per cent of the density of filled states in the valence band proper, estimated by HANDLER[11] as a lower limit on the clean Ge surface.

VOL. 8 195

## REFERENCES


1. SKINNER H. W. B., *Phil. Trans. Roy. Soc.*, **A239,** 95 (No. 801) (1940).
2. HERMAN F., *Proc. Inst. Radio Engrs.* **43,** 1703 (1955).
3. JENKINS D. P., *Proc. Phys. Soc.* **A69,** 548 (1956).
4. WOODRUFF T. O., *Phys. Rev.* **103,** 1159 (1956).
5. HAGSTRUM H. D., *Phys. Rev.* **96,** 325 (1954); *Ibid.* **104,** 317 (1956), W; *Phys. Rev.* **104,** 672 (1956), Mo; *Rev. Sci. Instrum.* **24,** 1122 (1953).
6. ALLEN F. G., EISINGER J., HAGSTRUM H. D. and LAW J. T., to be published.
7. HAGSTRUM H. D., *Phys. Rev.* **96,** 336 (1954).
8. PHILLIPS J. C., private communication.
9. LANDSBERG P. T., *Proc. Phys. Soc.* **A62,** 806 (1949).
10. ALLEN F. G., *J Phys. Chem. Solids* **8,** 119 (1959).
11. HANDLER P., *Semiconductor Surface Physics*, p. 23. University of Pennsylvania Press (1956).


*J. Phys. Chem. Solids* Pergamon Press 1959. Vol. 8. pp. 216–218. Printed in Great Britain

# H.5 CHEMICAL SHIFT OF DONOR STATES IN GERMANIUM

**GABRIEL WEINREICH**

Bell Telephone Laboratories, Incorporated,
Murray Hill, New Jersey

GREAT progress has been made in the past few years on the theory of semiconductor impurity states.[1] Very convincing calculations of ionization energy have been made in the effective-mass approximation, and for the case of the phosphorus donor in silicon some work has also been done on corrections to this approximation, which are sometimes referred to as "central-cell corrections".

It is the purpose of this paper to point out that

an appreciable change of ionization energy occurs owing to a factor which is still within the realm of effective-mass theory, but which has not heretofore been taken into account. This factor is the local strain of the lattice produced by the impurity atom. We shall discuss this for the group V donors in germanium; the effect in this case is especially pronounced owing both to the large value of the deformation potential constant $\Xi_u$ and to the strong mass anisotropy of the conduction band.

While it would be rather difficult to calculate such an effect with great precision, a very simple model can be constructed which ought to give a fair estimate of the energy shift. In this model we consider the germanium lattice to be elastically homogeneous and isotropic, and we represent the donor by a spherical cavity to whose surface a (positive or negative) displacement is applied. The amount of this displacement can be estimated from known values of the donor's tetrahedral radius as compared to that of germanium.

This simple problem in elasticity has the following solution for the strain tensor:

$$u_{ij} = Ar^{-3}(\delta_{ij} - 3x_i x_j/r^2) \tag{1}$$

where the $x_i$'s are any three Cartesian co-ordinates, $r^2 = \Sigma x_i^2$, and $A$ is an arbitrary constant. Note that (1) represents a pure shear; this is a result of our assumption of elastic isotropy.

The deformation potential due to the strain (1) can be calculated in the usual way. For a particular valley, it is given in the notation of HERRING[2] by

$$V = (\Xi_d \delta_{ij} + \Xi_u \mathbf{k}_i \mathbf{k}_j) u_{ij}, \tag{2}$$

where $\mathbf{k}$ is a unit vector pointing from the center of the Brillouin zone to the position of the valley. Substitution of (1) into (2) yields

$$V = \Xi_u A r^{-3}(1 - 3\cos^2\theta), \tag{3}$$

where $\theta$ is the angle between the radius vector and the valley axis.

We next have to compute the expectation value of (3) for an electron bound in the ground state of the donor. In effective-mass approximation this state is, of course, quadruply degenerate, and "valley" is a good quantum number. We can therefore figure the energy shift in a particular valley. Because the strain has cubic symmetry, the effect will be the same for all valleys and will not lift the quadruple degeneracy. In fact, of course, the ground state is split into a singlet and a triplet,[1] but the present calculation applies equally to both of these states.

The expectation value of (3) would obviously vanish in a spherically symmetric state. It is known, however, that because the energy ellipsoids are highly prolate, the wave function is compressed into the equatorial plane.[1] Let us for the moment assume that the wave function vanishes entirely outside of the equatorial plane; while this will certainly overestimate the magnitude of the effect, it will nevertheless provide us with a convenient order of magnitude. If we simplify the problem further by assuming that the square of the wave function is constant for $r < \frac{1}{2}a_0$ and zero for $r > \frac{1}{2}a_0$, where $a_0$ is the transverse Bohr radius, we obtain

$$\langle V \rangle \sim 8\Xi_u A/r_0 a_0^2. \tag{4}$$

Here $r_0$ is a lower cutoff on the integral which should correspond roughly to the radius of the donor.

It remains to estimate the size of the constant $A$. Let $\Delta$ be the fractional oversize of the donor; then

$$A = \tfrac{1}{2}\Delta r_0^3 \tag{5}$$

which in turn yields

$$\langle V \rangle \sim 4\Xi_u \Delta (r_0/a_0)^2. \tag{6}$$

Finally, we may substitute into (6) the values $\Xi_u = +17$ eV,[3] $a_0 = 64$Å,[1] $r_0 \sim 1{\cdot}5$ Å. The result turns out to be

$$\langle V \rangle \sim 0{\cdot}040\Delta \text{ eV}. \tag{7}$$

This result must not, of course, be taken too literally. The assumption of a perfectly flat wave function certainly leads to an overestimate, in addition to which the whole model we have used is quite crude. On the other hand, the difference in tetrahedral radii between antimony and phosphorus is about 25 per cent, so that on the basis of (7) we would predict a chemical shift of 0·010 eV, with antimony being the higher-lying level. The actual measured[4] energy difference has the same sign, but is only 0·0023 eV. In view of the expected overestimate, the result is thus quite plausible.

The same type of qualitative agreement is found

in comparing antimony and arsenic, but a contradiction occurs in the arsenic–phosphorus pair. For these two elements the donor ionization energies, as well as the tetrahedral radii, are rather close together; but the relative order is inverted. While the tetrahedral radii vary monotonically as one descends column V of the periodic table, the donor ionization energies do not. On the other hand, we could hardly expect that an effect which is non-monotonic in the periodic table, and therefore obviously depends on the detailed electronic structure of the atom, should be well described by a model as simple as the one we have used.

However, even if we accepted the local strain as the explanation of the variation of binding energy among various donors, we would still be left with an absolute energy shift which presumably represents a true failure of effective-mass theory. Thus the arsenic donor (whose size is almost exactly that of a germanium atom) has a binding energy which exceeds the effective-mass value by more than 0·003 eV.[1,4] Although this shift has not been calculated, its existence is not surprising; for a splitting of the order of millivolts between the ground state singlet and ground state triplet is indicated by measurements of both Hall effect[4] and acoustoelectric effect.[5] It is worth noting in this connection that since the germanium valleys are at the edge of the Brillouin zone, the triplet state wave functions reach their first maximum on the boundary of the central cell. Thus in this case the central-cell correction to the triplet energy could well be comparable to that of the singlet.

VOL. 8 195

## REFERENCES

1. KOHN W., *Solid State Physics* **5**, 257 (1957).
2. HERRING C., *Bell Syst. Tech. J.* **34**, 237 (1955).
3. HERRING C. and VOGT E., *Phys. Rev.* **101**, 944 (1956).
4. GEBALLE T. and MORIN F. J., *Phys. Rev.* **95**, 1085 (1954).
5. WEINREICH G., *Bull. Amer. Phys. Soc.* **3**, 102 (1958); WEINREICH G., SANDERS T., and WHITE H., submitted to *Phys. Rev.*

## DISCUSSION

*Compiled by* J. H. CRAWFORD

### H.1. WILLIAM PAUL

H. H. WOODBURY: With regard to the variation of ionization energies of impurity states with pressure and/or temperature, it is interesting to note that recent experiments on copper-doped germanium confirm the results reported here. It is possible to determine $dE_i/dT$ in copper-doped specimens by altering the degree of compensation. Our studies on this point indicate that the copper levels are "tied" to the valence band, i.e., $d(E_i - E_v)/dT = 0$.

G. BUSCH: Does the point at 30,000 atm where the $\langle 111 \rangle$ and the $\langle 100 \rangle$ minima coincide occur at the same lattice constant as observed in 15 per cent Si–Ge alloys in which the same correspondence of band minima occurs?

H. BROOKS: No, the lattice constant is different for the two situations. One must conclude that the processes leading to coincidence of the two conduction band minima are different for the effects of pressure and of alloying.

### H.4 HOMER D. HAGSTRUM

P. T. LANDSBERG: One sometimes has difficulties in these problems due to non-orthogonality of the four-wave functions involved in the construction of the matrix element. Has the speaker looked into or come across such a difficulty?

H. D. HAGSTRUM: We made no first principal estimates of the value of the matrix element involved in the two-electron transition.

W. KOHN: As regards the calculated width of the valence band, it should be pointed out that the one-electron approximation is perhaps not as effective here as in other applications. This may be the reason that the theoretical estimates of the valence band width are somewhat smaller than that indicated by this study.

J. C. PHILLIPS: The one-electron approximation gives the reasonable value of 13 eV for the valence band width.

### H.5 GABRIEL WEINREICH

H. BROOKS: Fletcher and I made an attempt to apply a central cell correction to the effective-mass approximation of impurity levels in both Ge and Si. It seemed possible to explain the deviation in silicon by this correction, but not in germanium. In silicon the central cell correction may be important but in germanium the effect of shear strain as considered here may be the important effect.

P. AIGRAIN: Recent experiments by Pavodi, Benoit and Gosnet show that free holes can recombine radiatively without phonon emission on Sb bound electrons. This can only occur through the singlet state which is slightly contaminated with Bloch functions from the $k = (0, 0, 0)$ conduction band minimum. The binding energy (9·5 meV) is in good agreement with the thermal value (9·7 meV). This strongly indicates that the singlet state of the Sb donor is either very close to (within 0·5) meV or is actually lower than the triplet state.

*J. Phys. Chem. Solids* Pergamon Press 1959. Vol. 8. pp. 219–223. Printed in Great Britain

SESSION I:
TRANSPORT*

# ELECTRON IMPACT IONIZATION IN SEMICONDUCTORS

**JAN TAUC**
Institute of Technical Physics, Czechoslovak Academy of Sciences,
Prague, Czechoslovakia.

**Abstract**—Experimental facts are presented showing that the quantum yield of the inner photoelectric effect increases if the photon energy exceeds a certain value. This is interpreted as due to the intrinsic electron impact ionization. A theory of this effect is discussed. The relation of the high energy quantum yield to the low energy parameters is shown. Some other effects related to the intrinsic impact ionization are mentioned.

## 1. INTRODUCTION

If the kinetic energy of an electron or a hole attains a certain value, an interaction with the valence band electrons can take place leading to the generation of a new electron–hole pair. In semiconductors this intrinsic impact ionization was first observed in the breakdown of silicon[1–5] and germanium[6–8] $p$–$n$ junctions. Considering the breakdown as a solid state analog of the Townsend $\beta$-avalanche breakdown in gases, it was possible to deduce some fundamental information on the impact ionization process.

## 2. EXPERIMENTAL STUDIES OF THE QUANTUM YIELD

We have dealt with this effect from another standpoint, studying the dependence of the quantum yield of the inner photoelectric effect on the energy of the absorbed photon. The quantum yield $\eta$ is the number of the electron–hole pairs created by the absorption of one photon. It was known from measurements with low energy photons that the quantum yield near the infrared limit is one. Measurements with high energy photons in the region of X-rays showed that $\eta$ is proportional to the energy of the photon[9] or, in other words, in this region the energy $\epsilon$ needed for the creation of one electron–hole pair is constant (in Ge, $\epsilon = 2{\cdot}5$ eV). It was obviously of interest to study the transition between the two regions. The measurement was performed by Koc[10] (Fig. 1). As in the work of reference 9, he used the photovoltaic effect in a germanium $p$–$n$ junction. It is apparent that the quantum yield $\eta$ increases with the photon energy $E_v$ if it exceeds the value $E'_v = 2{\cdot}2$ eV. The tangent at the point $E_v = E'_v$ passes through the origin. It is remarkable that its slope is nearly the same as the slope of the corresponding straight line $\eta = \eta\ (E_v)$ in the X-ray region. A more detailed examination of the curve reveals a certain structure the nature of which can be shown more clearly in InSb (see below).

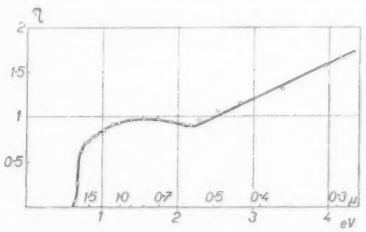


FIG. 1. Quantum yield $\eta$ in Ge as a function of the energy of the photon $E_v$.

The measurement of $\eta$ in Ge was recently repeated by Vavilov and Britsin[11] by a similar method. They have found qualitatively the same curve but the critical energy $E'_v$ was found to be 2·9 eV. The difference is probably due to different methods of measuring the reflectivity. Vavilov and Britsin measured the reflectivity using a hollow sphere coated with MgO thus taking

* *Chairman*: P. Aigrain; *Co-Chairman*: R. W. Keyes.

into account diffused light which was neglected by Koc.

Recently, VAVILOV and BRITSIN have measured the quantum yield in silicon by a similar method; the energy $E'_\nu$ was found to be about 3·25 eV.[12]

The uncertainty in the reflectivity is much smaller with InSb where it is practically constant near the energy $E'_\nu$. With this material it is difficult to use $p$–$n$ junctions, but it is easy to measure the photomagnetoelectric and the photoconductive effects. The former effect increases with increasing absorption coefficient, the latter decreases. If the two effects have the same dependence on $E_\nu$ it is considered probable that the change of the absorption coefficient with $E_\nu$ has negligible influence on the result. This was the case in our measurements,[13] a typical result of which is in Fig. 2.

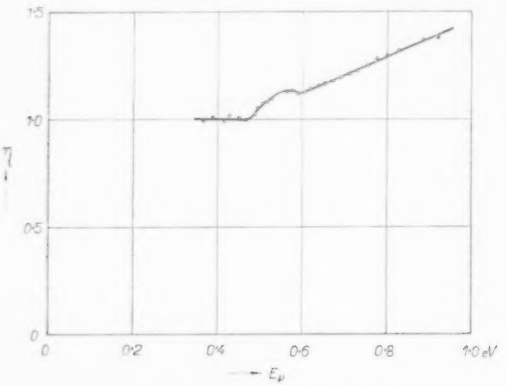


FIG. 2. Quantum yield $\eta$ in InSb.

The increasing of $\eta$ with $E_\nu$ starts at $E'_\nu = 0{\cdot}47$ eV at room temperature. The initial tangent at this point passes again through the origin but the rise in the curve soon diminishes and even stops. At the energy $E''_\nu = 0{\cdot}6$ eV $\eta$ starts to increase again with a lower slope than at the point $E'_\nu$. Although the exact shape of the curve was not well reproducible with different samples and surface treatments, nevertheless the points $E'_\nu$, $E''_\nu$ were always noticeable. They move towards higher values with decreasing temperature; the order of magnitude of this change is $10^{-4}$ eV/grad.

### 3. IRRADIATION WITH ELECTRONS

The quantum yield in germanium was also determined in the high energy region with irradiation by fast electrons[14–16] and α-particles.[17,18] These measurements gave values of $\epsilon$ somewhat higher (3 eV or more) than the above-mentioned value of 2·5 eV determined with X-rays. We have tried to measure $\eta$ in germanium with low energy electrons. Koc[19] used the electron-voltaic effect in germanium $p$–$n$ junctions (grown or alloyed). The measurements showed the existence of a certain threshhold energy $E_{\min}$, below which no signal was observed. For the energy of the electrons $E < E_{\min}$ $\eta$ is a linear function of $E$. The threshhold energy $E_{\min}$ is several hundred volts and changes with the condition of the surface.

We suppose that $E_{\min}$ corresponds to the energy necessary for the electrons to penetrate through the oxide layer on the surface. The estimate of the thickness of the layer based on this assumption agrees with that obtained by other methods (tens of Angströms).

EHRENBERG *et al.*[20] have found an energy threshhold of several thousands of eV in selenium barrier layer cells. LI TSCHI-TSZIAN has bombarded CdS and CdSe polycrystalline layers with very slow electrons and measured the changes of the conductivity.[21] He has found a very low threshhold of the incident energy (tenths of an electronvolt) and abrupt jumps in the signal at the multiples of the energy gap (2·5 eV in CdS, 1·8 eV in CdSe).

### 3. INTERPRETATION OF THE LOW ENERGY CURVE

The observed dependence of $\eta$ on $E_\nu$ can be explained by the following mechanism. By the absorption of a photon, an electron in the conduction band and a hole in the valence band are created which have in the first moment excess kinetic energies. If these energies are lower than the ionization energies necessary for the creation of a new electron–hole pair, they are transferred to the lattice and lost. If the kinetic energy of an electron or a hole exceeds the ionization energy new pairs are created by impact ionization and the quantum yield is larger than one. The number of the created electron–hole pairs increases with the kinetic energies of the electron $E_n$ or the hole $E_p$.

A theory based on this idea was worked out by ANTONČÍK.[22] He considers ionizing action only by electrons in the conduction band. The minimum energy $E_{n,\text{ion}}$ which an electron must have to be

able to ionize the valence band electrons is determined by the conservation laws for energy and crystal momentum in the process

1 fast electron → 1 hole+2 electrons.

$E_{n,\mathrm{ion}}$ depends on the band structure. With a somewhat schematized model of the band structure Antoncík obtained for Ge $E_{n,\mathrm{ion}} = 0{\cdot}82$ eV $= 1{\cdot}24\,E_G$, for Si $1{\cdot}23$ eV $= 1{\cdot}14\,E_G$.[22]

Antončík then calculates the number of electron–hole pairs created by impact ionization in the neighborhood of $E_{n,\mathrm{ion}}$, assuming that a fast electron can ionize only once. If the band structure is not spherically symmetrical (as is the case for Ge, Si, InSb) the conservation laws are fulfilled for $E_n = E_{n,\mathrm{ion}}$ only in a finite number of directions in the Brillouin zone. In Ge these are the (111) directions connecting the centre of the zone with the minima of the conduction band. Antončík then shows that if $E_n > E_{n,\mathrm{ion}}$ the conservation conditions hold in a certain solid angle around the starting (111) direction which increases with $E_n$. Supposing that all electrons in this solid angle give new pairs by ionization, one obtains for the number of the pairs created by impact ionization (corresponding to one absorbed photon):

$$\eta_{\mathrm{ion}} = \frac{s}{2\sigma}\cdot\frac{1+\alpha}{D}\,\frac{1}{E_{n,\mathrm{ion}}}(E_n - E_{n,\mathrm{ion}}). \qquad (1)$$

This formula holds for schematized "many valley" conduction bands such as these of Ge and Si, $s$ is the number of minima in the conduction band, $\sigma$ the number of ellipsoids ($\sigma = \frac{1}{2}s$ for Ge, $\sigma = s$ for Si). $\alpha$ and $D$ are parameters depending on the band structure ($\alpha = 0{\cdot}221$, $D = 1{\cdot}242$ for Si, $\alpha = 0{\cdot}303$, $D = 1{\cdot}525$ for Ge[22]).

The ionization actually starts at some energy $E'_n > E_{n,\mathrm{ion}}$ owing to the interaction of the electron with the lattice. As the cross-section for the impact ionization very steeply increases with the electron energy $E_n$ (once it exceeds $E_{n,\mathrm{ion}}$) while the cross-section for the interaction with the lattice slowly varies with $E_n$, the energy $E'_n$ should not differ much from $E_{n,\mathrm{ion}}$ (some tenths of an eV[22]).

In principle, similar considerations should hold for the impact ionization by holes.

If we are going to apply these considerations for the determination of $\eta$ the question arises; how are the energies of electrons and holes distributed just after the absorption of a photon? This is a difficult problem not solved yet. Antončík[22] makes a very rough assumption that in Ge the electron takes all the excess energy. Using equation (1) one obtains for the quantum yield for $E_\nu$ slightly larger than $E'_\nu$:

$$\eta = 1+\eta_{\mathrm{ion}} = 1+\Delta(E_\nu - E'_\nu), \qquad (2)$$

where $\Delta = s(1+\alpha)/2\sigma D E_{n,\mathrm{ion}} = 1\ (\mathrm{eV})^{-1}$. This is in reasonable agreement with experiment. The energy $E'_n = E'_\nu - E_G = 1{\cdot}5$ eV is considerably higher than $E_{n,\mathrm{ion}} = 0{\cdot}82$ eV and agrees with the value determined from the breakdown of the $p$–$n$ junctions by Miller.[6] Using the same argument for Si we get with the data from Vavilov and Britsin[12] $E'_n = 3{\cdot}25 - 1{\cdot}1 = 2{\cdot}15$ eV which is in better agreement with the result obtained by Chynoweth and McKay[5] (2·25 eV) than with that by Miller[4] (1·5 eV).

The assumption that the electron has all the excess energy is certainly not well fulfilled in Ge and Si and we should expect that the actual values of $E'_n$ are somewhat lower. But it may be a very good assumption for InSb where the effective mass of an electron is far smaller than that of a hole. The observed curve $\eta = \eta\ (E_\nu)$ in Fig. 2 could be explained by a band structure schematically suggested in Fig. 3. For small energy

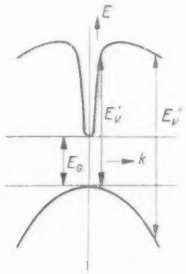


Fig. 3. Suggested band structure of InSb to explain qualitatively the curve given in Fig. 2.

differences $E_\nu - E_G$ practically all the energy $E_\nu - E_G$ is taken by the electron. With increasing $E_\nu - E_G$ the holes obtain a larger and larger part of this energy. This energy is lost as long as the holes do not attain the ionization energy. Therefore in this region the initial rise of $\eta$ with $E_\nu$ slows down and eventually stops. As soon as the holes are able to ionize $\eta$ starts to increase again (at the point $E''_\nu$).

An essential point in the theory of Antončík is

the anisotropy of the band structure. For a spherically symmetrical band structure $\eta$ should change abruptly at $E'_v$ (as was observed in reference 21).

## 5. HIGH ENERGY REGION

By further increasing the photon energy we get into a region where at present there is neither experimental nor theoretical information available. The situation is simple again at high energies $E_v \gg E_G$ where $\eta$ is proportional to the energy of the photon or the particle. We may assume that in any case high energy electrons are first created which lose their energy by impact ionization. The process is undoubtedly complex and complicated by emissions and reabsorptions of photons. However if we take the energy losses by secondary X-ray emission into account we find that the net energy $\epsilon$ needed for the creation of an electron–hole pair is little dependent on the energy of the photon.[9] It follows that electrons with high energies ($E_n \gg E'_n$) transfer little energy to the lattice. This is also to be expected on simple theoretical considerations.

By successive ionization processes the energies of the electrons and holes finally sink under $E'_n$, $E'_p$. If we suppose that no losses to the lattice occur for $E_n > E'_n$, $E_p > E'_p$ we have

$$\epsilon = E_G + \langle E_n \rangle + \langle E_p \rangle \qquad (3)$$

where $\langle E_n \rangle$, $\langle E_p \rangle$ are the mean values in the intervals $0,E'_n$ and $0,E'_p$. Supposing, as is occasionally done,[4,5] that the energy is uniformly distributed in these intervals we have $\epsilon = E_G + \frac{1}{2}E'_n + \frac{1}{2}E'_p$.

The value determined by equation (3) must be considered as the lowest limit of $\epsilon$. We know from the measurement of $\eta$ that not all electrons and holes with energies somewhat greater than $E'_n$, $E'_p$ can ionize. A part of the energy in this region is necessarily lost to the lattice. Using here the experimentally determined parameters we can calculate $\epsilon$ assuming we know the distribution of the energies of electrons and holes. This is a rather difficult problem not yet satisfactorily solved. The relation between the high and low energy effects are being experimentally and theoretically studied in our laboratory.

## 6. OTHER EFFECTS RELATED TO IMPACT IONIZATION

Most of the information on the ionization process during the breakdown of $p$–$n$ junctions was obtained by an analysis of the electrical data. However, it is to be expected that interesting facts, especially on the energy distribution of electrons and holes, may be deduced from the study of electroluminescence[23,24] and external electron emission.[25,26] Important deductions were obtained by the study of the yield of the external photoelectric emission that appreciably diminishes if the energy of the excited electrons attain the ionization energy.[27]

Recently Landsberg has been able to predict the rise of the quantum yield with $E_v$ in InSb from a comparison of the radiative lifetimes determined by direct measurement of the radiation or by calculation from the optical constants.[28]

*Acknowledgments*—Thanks are due to Dr. E. Antončík for his helpful discussions during the preparation of this paper.

## REFERENCES

1. McKay K. G. and McAfee K. B., *Phys. Rev.* **91,** 1079 (1953).
2. McKay K. G., *Phys. Rev.* **94,** 877 (1954).
3. Wolff P. A., *Phys. Rev.* **95,** 1415 (1954).
4. Miller S. L., *Phys. Rev.* **105,** 1246 (1957).
5. Chynoweth A. G. and McKay K. G., *Phys. Rev.* **108,** 29 (1957).
6. Miller S. L., *Phys. Rev.* **99,** 1234 (1955).
7. Vul B. M., *Zh. tekh. fiz. SSSR* **26,** 2403 (1956).
8. Shotov A. P., *Zh. eksp. teor. fiz.* **26,** 1634 (1956); *Zh. tekh. fiz. SSSR* **28,** 437 (1958).
9. Drahokoupil J., Malkovská M. and Tauc J., *Czech. J. Phys.* **7,** 57 (1957).
10. Koc S., *Czech. J. Phys.* **7,** 91 (1957).
11. Vavilov V. S. and Britsin K. I., *Zh. eksp. teor. fiz. SSSR* **34,** 521 (1958).
12. Vavilov V. S. and Britsin K. I., *Zh. eksp. teor. fiz.* **34,** 1354 (1958).
13. Tauc J. and Abraham A., *Czech. J. Phys.* to be published.
14. Rappaport P., *Phys. Rev.* **93,** 246 (1954).
15. Pfann W. G., van Roosbroeck W., *J. Appl. Phys.* **25,** 1422 (1954).
16. Vavilov V. S., Smirnov L. S. and Packevitsh V. M., *Dokl. Akad. Nauk. SSSR* **112,** 1020 (1957).
17. McKay K. G., *Phys. Rev.* **84,** 829 (1951).
18. McKay K. G., McAffee K. B., *Phys. Rev.* **91,** 1079 (1953).
19. Koc S., to be published.

20. EHRENBERG W., LANG CHI-SHI and WEST R., *Proc. Phys. Soc.* A**64**, 424 (1951).
21. TSCHI-TSZIAN LI, Dissertation, University, Leningrad (1958).
22. ANTONČÍK E., *Czech. J. Phys.* **7**, 674 (1957).
23. NEWMAN R., *Phys. Rev.* **100**, 700 (1955).
24. CHYNOWETH A. G. and MCKAY K. G., *Phys. Rev.* **102**, 369 (1956).
25. BURTON J. A., *Phys. Rev.* **108**, 1342 (1957).
26. TAUC J., *Nature, Lond.* **181**, 38 (1958).
27. TAFT E. A., PHILIPP H. R. and APKER L., *Phys. Rev.* **110**, 876 (1958).
28. LANDSBERG P. T., *Proc. Phys. Soc.* B**70**, 1175 (1957).

*J. Phys. Chem. Solids* Pergamon Press 1959. Vol. 8. pp. 223–226. Printed in Great Britain

VOL. 8 1959

# ON PHOTO-IONIZATION BY FAST ELECTRONS IN GERMANIUM AND SILICON

VICTOR S. VAVILOV

P. N. Levedev Physical Institute, Moscow, USSR

**Abstract**—Experimental results are presented on quantum yield at photon energies high as compared with energy gap, and on ionization by fast electrons for germanium and silicon.

THE investigation of electron–hole pairs generated by absorption of photons or by fast particles in pure crystals may give new data on the interaction of electrons with the crystal lattice and complete the results obtained in experiments with impact ionization in high fields. The values of photo-ionization quantum yield and the average ionization energies are also important from the practical point of view.

In our work in the Semiconductor Lab. of the P. N. Lebedev Physical Institute[1,2] and in Moscow University,[3,4] for the investigation of ionization processes we used germanium and silicon crystals with $p$–$n$ junctions. The carrier generation took place in the region outside the space charge of the junction. $p$–$n$ junctions were made in germanium by indium alloying, and in silicon by the diffusion of phosphorus. The arrangement of the experiment for the determination of photo-ionization quantum yield can be seen in Fig. 1.

The general expression for the carrier collection efficiency, $\alpha$, given by Pfann and ROOSBROECK,[5] for the strongly absorbed light becomes simply:

$$\alpha = \frac{2}{[1+(sL/D)]e^{d/L}+[1-(sL/D)e^{-d/L}} \qquad (1)$$

If $R_1 \ll R_0$, which is easily satisfied at low generation level,

$$\alpha = \frac{I}{qN_{h\nu}(1-R)Q} \qquad (2)$$

where $Q$ is the quantum yield and $q$ the charge of electron.

It is known that for photon energies near the photoionization threshold, lying for pure germanium near 0·7 eV, the quantum yield is equal to 1,[6] which is explained by the usual concept of electron–hole pair generation by the absorption of a photon. If the photon energy is large enough as compared to the threshold energy, additional conduction electrons may be generated as a result of impact ionization by initial photo-electrons or holes. S. I. VAVILOV[7] pointed out in 1947, that the photo-luminescence quantum yield may be greater than unity for excitation by photons with energies higher than twice the luminescence quantum energy. This phenomenon was observed

experimentally by BUTAEVA and FABRIKANT[8] for the short-wave excitation of luminophors and by KOC, investigating the inner photoelectric effect in germanium.[9] We have determined the photoionization quantum yield in *n*-germanium in the region of wavelengths between 1·5 and 0·254 $\mu$. In our experiments we used single crystals with a resistivity of 10–20 ohm-cm and diffusion lengths near 1·5 mm. The spectrum was separated by means of a monochromator with a LiF or quartz prism. The energy of the incident radiation was

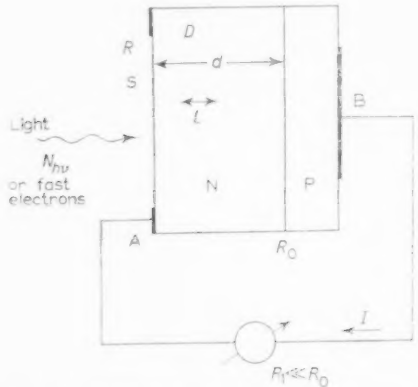


FIG. 1. The method of the experiment. The meaning of the symbols is as follows:
N, *n*-type region; P, *p*-type region; A, B, ohmic contacts; *L*, carrier diffusion; *D*, ambipolar diffusion coefficient; $R_0$, junction resistance with zero bias; $R_1$, resistance of meter; *s*, surface recombination velocity; *R*, reflectivity; *I*, photocurrent.

determined with the help of a compensated thermopile, calibrated with a Hefner candle. In the ultraviolet region, for 366, 313, 289 and 254 m$\mu$ mercury lines, a luminescent compound (lumogene), having a constant luminescence yield, and a photomultiplier was used. The calibration was made by direct comparison with a thermopile at 365 m$\mu$. The quantum yield $Q$ was calculated from expression (2). The reflectivity, $R$, as has already been pointed out,[10] depends on the surface treatment of the semiconductor. For the determination of $R$, an integrating sphere, permitting the comparison of reflectivities of the specimen studied and of a thick MgO layer, was used.

In Fig. 2 are presented the curves of $R$ as a function of photon energy and the calculated values of $Q$ in germanium for $h\nu$ between 0·83 and 4·9 eV. The dependence of quantum yield on photon energy clearly indicates a substantial increase of $Q$ beginning at energies much higher than the minimum electron–hole pair formation energy. One had to expect this, following the theoretical calculations of CHUENKOV,[11] according to whom the probability of impact ionization by carriers with energies only slightly higher than $E_g$, i.e. forbidden gap width, is extremely low. According to CHUENKOV's calculation, the impact ionization probability in germanium is near to $\frac{1}{2}$ for a

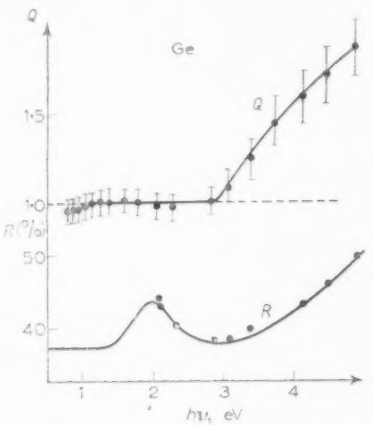


FIG. 2. Quantum yield in germanium.

carrier energy of 2 eV. It is necessary to point out that according to our data for high $h\nu$, the rate of the quantum yield increase becomes slower, i.e. the mean energy $\epsilon$ of the pair formation, increases.

It could be expected that the process described above takes place in other semiconductors, particularly in silicon.* We had at our disposal silicon photocells with *p–n* junctions obtained by thermal diffusion of phosphorus.[12] It was found that cells with a very thin *n*-type layer have a quite good sensitivity for ultraviolet radiation. For the measurement of photocurrent, $I$, and the determination of $R$ and $N_{h\nu}$ the same technique as for

* Dr. J. TAUC (Prague, In–Te of Techn. Physics) kindly informed us, that the increase of $Q$ with photon energy in InSb has been observed in his laboratory.

germanium was used. However, the interpretation of the results in this case, as compared with quantum yield determination for germanium, was made less straightforward by the following circumstances: the value of collection efficiency depends on the mobility and the diffusion length. In the case of the impurity introduced by diffusion, the mobility changes strongly with depth and is small within the strongly doped region. The diffusion length also changes with depth. As a result of it, the direct calculation of $\alpha$ is not possible and one has to use the natural assumption that in the region of photon energies $E_g < h\nu < 2E_g$, where $E_g = 1{\cdot}1$ eV is the energy gap for silicon, the quantum yield is equal to 1. Experimental dependence of $R$ and the product of quantum yield $Q$ and collection efficiency $\alpha$ on $h\nu$ is given in Fig. 3. It can be seen that, beginning approxi-

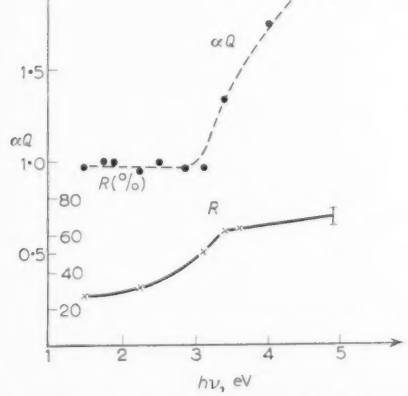


FIG. 3. The product $Q\alpha$ as a function of $h\nu$ in silicon.

mately from $h\nu = 3{\cdot}25$ eV,* the product $\alpha Q$ increases strongly. Taking into account that an increase of $\alpha$ with $h\nu$ seems to be impossible, we conclude that the observed dependence shows an increase of $Q$ due to the impact ionization by photoelectrons and holes.

It is interesting to compare the photon energy, corresponding to this increase (3·2–3·3 eV) with the threshold impact ionization energy in silicon recently determined by MCKAY and CHYNOWETH,[13] studying carriers multiplication in high electric fields. According to this data, $E_{i\min} = 2.25$ eV; our results (3·25–1·1 = 2·15 eV) correspond to it closely.

Some estimates of the average energy of ionization $\epsilon$ by fast electrons in germanium and silicon are given in several works connected with energy conversion by beta-particles.[5,14] MCKAY and MACAFEE determined the value of $\epsilon$ for ionization by alpha-particles.[15] In our experiments we studied the ionization by electrons with energies between 5 and 30 keV. Working with germanium, we used $n$-type crystals with $p$–$n$ junctions made by indium alloying. The electrons lost their energy completely in the $n$-type region. Let the ratio of the nonequilibrium carrier flow, $N_2$, through the junction to the flow, $N_1$, of fast electrons be equal to $\beta_1$; in this case

$$\beta_1 = \frac{N_2}{N_1} = \frac{I_2}{I_1} \tag{3}$$

where $I_2$ is the short-circuit current (see Fig. 1) and $I_1 = qN_1$ is the current of fast electrons.

As a result of recombination, $N_2$ is always smaller than the number $N_0$ of the pairs generated in a unit of time, but these quantities are proportional at low generation levels:

$$N_2 = \alpha_1 N_0 \tag{4}$$

The "multiplication coefficient" $\beta$ can be expressed as

$$\beta = \frac{N_0}{N_1} = \frac{\beta_1}{\alpha_1} = \frac{I_2}{\alpha_1 I_1} \tag{5}$$

and the average ionization energy $\epsilon$ as

$$\epsilon = \frac{W}{\beta} = \frac{\alpha_1 I_1 W}{I_2}\text{eV}, \tag{6}$$

where $W$ is the energy of fast electrons. The value of $\alpha_1$ changes strongly with the surface conditions; during the evacuation and at the time of electron bombardment of $n$-germanium the surface recombination velocity $s$ increases by several orders of magnitude. The control of the value of $\alpha_1$ in our experiments was achieved by simultaneous irradiation of the sample by electrons and monochromatic light ($\lambda = 1{\cdot}05\mu$) of known intensity, absorbed mainly in a layer 2–3$\mu$ thick. The values

* Measurements at $T = 293°$K.

of $\epsilon$ for germanium were practically independent of $W$ between 5 and 25 keV and did not change with different surface treatment. The average value of $\epsilon$ was equal to $3{\cdot}7 \pm 0{\cdot}4$ eV, i.e., somewhat higher than the value given by McKAY ($2{\cdot}9 \pm 0{\cdot}15$ eV). At much higher electron energies (400 keV) we obtained $\epsilon \simeq 4{\cdot}5 \pm 1{\cdot}5$ eV; the greater error is due to difficulties of estimation of the spatial distribution of the generation and with the backscattering of electrons.

For the determination of $\epsilon$ in silicon, we used single crystal wafers with $p$–$n$ junctions at $20\mu$ from the surface. Electrons were absorbed in the phosphorus-doped $n$-type region. It was found that in the case of silicon the value of $\alpha_1$ does not change during the evacuation and electron bombardment as a result of the existence of a stable thin $SiO_2$ layer.*

The collection efficiency $\alpha_1$ in the samples investigated depended strongly upon the distribution of generation in the sample. For the estimation of the ionization loss spatial distribution, we used calculations of YURKOV[16] based on Spencer's method. The average value of $\epsilon$ was determined for each $W$ by using the experimental "multiplication coefficient" $\beta_1$ and $\alpha$ for the wavelength for which the (absorption coefficient)$^{-1}$ is equal to the mean depth of electron beam penetration; $\epsilon$ was calculated from expression (6). The value obtained was equal to $4{\cdot}2 \pm 0{\cdot}6$ eV for $W$ between 10 and 30 keV. The dependence of $\beta_1$ on $W$ indicates the existence of a "dead layer" near the surface, the nature of which is not yet clear.

## DISCUSSION

The results obtained are thought to give additional data on the impact ionization by photoelectrons and holes; the quantitative agreement with McKAY's results for silicon[13] and with CHUENKOV's calculations of the impact ionization probability in germanium are of interest.

The dependence of the photoionization quantum yield on photon energy agrees qualitatively with the results of KOC[9] and theoretical conclusions of TAUC and ANTONČÍK.[17] However, we think that a sharp breaking point of the curve at the beginning of the impact ionization in ANTONČÍK's theory is a result of the simplifying assumptions.

We think that interesting data can be obtained from the investigation of the temperature dependence of $Q$ in the region of impact ionization. Our values of the mean energy of ionization by fast electrons[3,7] are somewhat higher than the results of DRAHOKOUPIL, MALKOVSKA and TAUC,[18] who studied the pair generation at the X-rays absorption in germanium (2·5 eV). We think that Q must grow very slowly with the energy of fast electrons, rather than remain constant.

The results presented here were obtained by the author in collaboration with K. I. BRITZIN (Moscow University), L. S. SMIRNOV and V. N. PATSKEVICH (P. N. Lebedev Phys. In-te).

*Acknowledgments*—It is a great pleasure to express my gratitude to B. M. WUL, N. N. ALENTZEV, V. A. CHUENKOV and A. P. SHOTOW for their interest and valuable discussions.

## REFERENCES

1. VAVILOV V. S., SMIRNOV L. S. and PATSKEVITCH V. M., *Dokl. Akad. Nauk. SSSR* **112,** 1020 (1957).
2. PATSKEVITCH V. M., VAVILOV V. S., and SMIRNOV L. S., *Zh. eksp. teor. fiz.* **33,** 804 (1957).
3. VAVILOV V. S. and BRITZIN K. J., *Zh. eksp. teor. fiz.* **34,** 521 (1958).
4. VAVILOV V. S. and BRITZIN K. J., *Zh. eksp. teor. fiz.* **35,** 5 (1958).
5. PFANN W. and VAN ROOSBROECK W., *J. Appl. Phys.* **25,** 1422 (1954).
6. GONCHER F. S., *Phys. Rev.* **78,** 816 (1950).
7. VAVILOV S. J., *The Duration of Luminescence*, 1947, Vol. 2, p. 293. A.S. USSR (1952).
8. BUTAEVA F. A., FABRIKANT V. A., *Izv. Akad. Nauk. SSSR, fiz. ser.* **21,** 541 (1957); **18,** 2 (1949).
9. KOC S. *Czech. J. Phys.* **6,** 668 (1956).
10. VAVILOV V. S., GIPPIUS A. A., GORSHKOV, M. M., *Zh. tekh. fiz.* **28,** 254 (1958).
11. CHUENKOV V. A., *Izv. Akad. Nauk. SSSR, fiz. ser.* **20,** 1550 (1956).
12. VAVILOV V. S., GALKIN G. N., MALOVETSKAYA V. M., *J. Atomic Energy*, No. 6 (1958).
13. MCKAY K., *Phys. Rev.* **108,** 29 (1957).
14. LINDER E., *Geneva Conf. on Peaceful Use of Atomic Energy*, UN edition (1955).
15. MCKAY K., MCAFEE K., *Phys. Rev.* **91,** 1079 (1953).
16. JURKOV B. YA, *Zh. tekh. fiz.* **28,** 1159 (1958).
17. ANTONČÍK E., *Czech. J. Phys.* **7,** 675 (1957).
18. DRAHOKOUPIL J., MALKOVSKA M., TAUC J., *Czech. J. Phys.* **7,** 57 (1957).

* Ion bombardment results in the deterioration of this layer, increase of surface recombination velocity and decrease of $\alpha_1$.

*J. Phys. Chem. Solids* Pergamon Press 1959. Vol. 8. pp. 227–234. Printed in Great Britain

I.2

# HOT AND WARM ELECTRONS – A REVIEW

S. H. KOENIG

IBM Watson Laboratory at Columbia University, New York 25, New York

**Abstract**—There are two categories of problems relating to the study of hot and warm carriers; i.e., the situation in which the mean carrier kinetic energy deviates measurably from its equilibrium thermal value. The first of these relates to the manner in which a steady state distribution is maintained. The pertinent work to date, both experimental and theoretical, is reviewed.

The second set of problems involves the phenomena which result from a non-equilibrium distribution, but that do not play a significant role in determining it. The velocity dependence of recombination cross sections, impact ionization of neutral impurities and enhanced thermionic emission are among these. The present experimental situation is discussed and related to what relevant theory exists for the various cases.

VOL. 8 1959

## 1. INTRODUCTION

ONE cannot adequately review all the aspects of the hot electron* (or hole) problem in a talk of this length. I have, therefore (to some extent arbitarily), chosen to restrict the discussion to hot and warm carrier phenomena in bulk material where the electric field dependent momentum distribution function for the carriers is independent of position. The current density and conductivity will then be functions only of the applied field, which will be uniform throughout the sample. Discussion of across the gap avalanching either in junctions or in the bulk is thus precluded.

For metals (large Fermi energies) or semiconductors at ordinary temperatures and not too high fields, Ohm's Law holds quite well. However, for semiconductors[1] and semimetals[2] in the temperature range from 50°–300°K at electric fields $\sim 100$ V/cm, and for semiconductors at helium temperatures at fields[1] $\sim 1$ V/cm, significant deviations from Ohm's Law are observed. In these cases, for the electron distribution to dissipate the energy it gains from the applied electric field, the average carrier energy must increase from its thermal equilibrium value. Hence the terms warm and hot electrons, according as one is considering small or large increases in the mean energy. A feeling for the magnitudes involved for the case of interactions with acoustic phonons may be had in the following manner. Consider a carrier with initial momentum $p$ and energy $\epsilon$ which undergoes a collision with a phonon and either gains or loses momentum $2p$. Then $\Delta\epsilon$, the energy change is given by

$$\Delta\epsilon = 2pc = (4p^2/2m)(mc^2/p) = 4\epsilon\, mc/p \quad (1)$$

where $c$ is the sound velocity. The number of phonons of energy $2pc$ is

$$n \sim [\exp(2pc/kT)-1]^{-1} \simeq (kT/2pc). \quad (2)$$

The fraction of energy losing collisions is

$$[(n+1)-n]/(2n+1) \sim \tfrac{1}{2}n \simeq pc/kT. \quad (3)$$

The energy loss per collision is then

$$(pc/kT)(mc/p)(4\epsilon) = (4mc^2/kT)\epsilon \sim T^{-1}\epsilon \text{ for Ge.} \quad (4)$$

A more exact calculation alters the numerical factor 4 in equation (4) by a small amount.[3] One sees then that for acoustic scattering the rate of energy relaxation is considerably less than the rate of momentum relaxation. If the power gained by the carriers from the field is equated to that lost by scattering, then to this approximation:

$$e\mu E^2 \cong (4mc^2/kT)(\epsilon/\tau);\ (\epsilon/kT) \cong \mu_0 E/2c \quad (5)$$

where $\tau$ is the mean free time between collisions and $\mu_0$ is the low field mobility and $(\mu/\mu_0)^2 = kT/\epsilon$.

Table 1 gives values of $(\epsilon/kT)$ for several reasonable experimental situations. It is often convenient to express $\epsilon$ in units of $kT$, and thus speak of

* The term electron will be used throughout in a generic sense to mean either sign of carrier except when discussing a specific conductivity type material.

electron "temperature." Only under special circumstances, however, when the distribution is essentially isotropic and definable by a single scalar parameter can the actual concept of temperature be generalized to describe the hot electron situation.

For the case of mixed scattering, the problem is more involved, and will subsequently be discussed in more detail. It should be noted, though, that the collisions most effective for momentum change (those that determine mobility) need not be those most effective for energy transfer. (Consider for example, a ping-pong ball rebounding from either a billiard ball or another ping-pong ball.)

*Table* 1. *Approximate electron "temperature" to be expected on the basis of Equations* 1–5 *for several experimental conditions.*

| Material | $T$(°K) | $E$(V/cm) | $\epsilon/kT$ |
|---|---|---|---|
| $n$-Ge | 300 | 100 | $\sim 1$ |
| $n$-Ge | 10 | 10 | $\sim 15$ |
| $n$-InSb | 4 | 1 | $\sim 20$ |

The effort to date on warm and hot electrons may be divided into two main classes: (1) Studies of the manner by which a hot distribution is achieved and maintained, i.e., what the energy loss mechanisms are and what form the distribution function takes. Experimental investigations generally involve measuring the dependence of drift or Hall mobility[4] on the power input to the distribution. (2) Investigation of phenomena that are observable as a result of a hot distribution, but that play little or no direct role in determining the energy distribution; e.g., the velocity dependence of lattice and impurity scattering,[5] of recombination processes,[6] impact ionization of neutral impurities,[1,6] and electron emission from bulk materials.[7]

## 2. ACOUSTIC SCATTERING

### 2.1. *Theoretical situation*

An analytic expression for the distribution function for arbitrary electric field may be obtained for the case of longitudinal acoustic scattering, spherical energy surfaces and Boltzmann statistics, assuming the mean energy loss per collision is small and that equipartition holds for the phonons. These assumptions limit the range of validity of the result to $mc^2/kT \ll T_E/T \ll kT/mc^2$, where $T_E$ is the electron "temperature", $c$ the sound velocity, $T$ the lattice temperature, $k$ Boltzmann's constant and $m$ an effective mass. The solution was first discussed by PISARENKO[8]* in 1938 and independently derived by YAMASHITA and WATANABE[9] in 1954. Fig. 1 shows the shape of the distribution for several values of electric field, calculated for parameters appropriate to Ge at 10°K. If one ignores what complications the multivalleyed conduction band of Ge may contribute, high purity $n$-type Ge in the temperature region of 8°–15°K probably affords the best experimental approximation to the theoretical model. In the limit of large electric fields, corresponding to mean electron energies $\lesssim 8$ times their thermal value, but not so large as to invalidate the equipartition assumption, the Pisarenko distribution approaches that obtained by DRUYVESTEYN[10] for hard sphere scattering in gases. In this limit the drift mobility varies as $E^{-\frac{1}{2}}$, as has been shown by SHOCKLEY.[3] More recently, SODHA and EASTMAN[11] have shown that the Hall to drift mobility ratio approaches a constant in the same limit, under the implicit assumption that the magnetic field doesn't effect the distribution.

For still larger electric fields, one would on a priori grounds expect a variation between $E^{-\frac{1}{2}}$ and $E^{-1}$. The power loss must be more rapid than for the $E^{-\frac{1}{2}}$ range since the collision frequency has increased and all collisions now involve spontaneous phonon emission only and are, therefore, all lossy. On the other hand, a variation faster than $E^{-1}$ would correspond to drift velocity decreasing with increasing $E$ and, therefore a negative differential resistance. The only relevant theoretical, work is the estimate of PARANJAPE,[12]† who, assuming a "hot" Maxwell distribution, found a mobility variation proportional to $E^{-0.8}$.

* It was noticed after this paper was written that this distribution was discussed by F. B. PIDDUCK, *Proc. Lond. Math. Soc.* **59**, 89 (1915).

See E. GUTHand J. MAYERHÖFER, *Phys. Rev.* **57**, 914 (1940), footnote (11) for a more complete history.

† See also R. STRATTON *Proc. Roy. Soc.* A **242**, 355 (1957).

It should be emphasized, though, that an experimentally observed power law variation of mobility $\mu$ with $E$ in agreement with that discussed above is not by itself sufficient to indicate that acoustic scattering is the dominant energy loss mechanism. For example, YAMASHITA and WATANABE[9] have shown that for certain cases at high fields the $\mu \alpha E^{-\frac{1}{2}}$ law will hold for an arbitrary amount of mixed acoustic and optical phonon scattering.

conductivity measurement combined with a measurement of Hall coefficient in the ohmic range. The proper Hall to drift mobility ratio to apply in this case is not certain. In addition, the 4°K data were taken on a $\langle 110 \rangle$ oriented sample. For hot electrons and this orientation, the Hall "constant" has two principal values, as yet unmeasured, and the data presented are the sum of their projections appropriate to the particular Hall

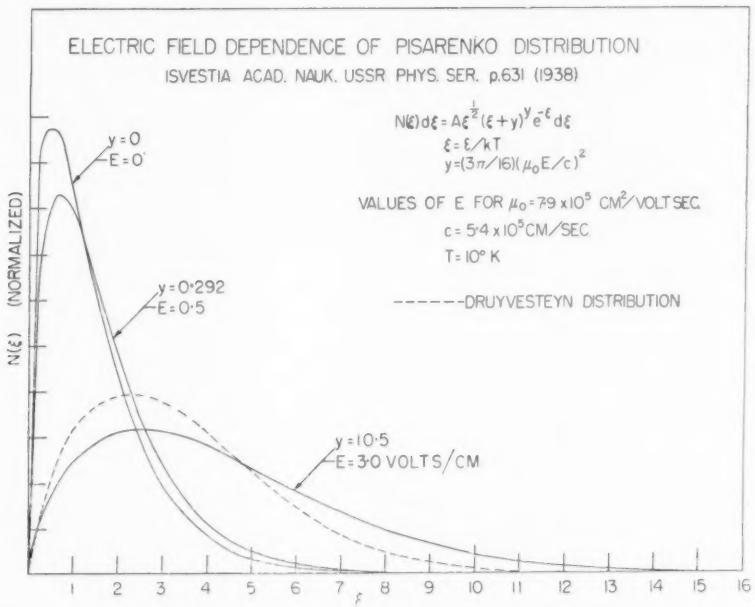
ELECTRIC FIELD DEPENDENCE OF PISARENKO DISTRIBUTION
ISVESTIA ACAD. NAUK. USSR PHYS. SER. p.631 (1938)
$N(\xi)d\xi = A\xi^{\frac{1}{2}}(\xi+y)^y e^{-\xi} d\xi$
$\xi = \mathcal{E}/kT$
$y = (3\pi/16)(\mu_0 E/c)^2$
VALUES OF E FOR $\mu_0 = 79 \times 10^5$ CM²/VOLT SEC.
$c = 5{\cdot}4 \times 10^5$ CM/SEC.
T = 10° K
------DRUYVESTEYN DISTRIBUTION
y = 0
E = 0
y = 0·292
E = 0·5
y = 10·5
E = 30 VOLTS/CM
N(ξ) (NORMALIZED)
1 2 3 4 5 6 7 8 9 10 11 12 13 14 15 16
ξ

FIG. 1. The variation with electric field of the electron energy distribution appropriate to acoustic scattering and spherical bands.

2.2. *Experimental situation*

Hot electron effects have been observed in *n*- and *p*-type Ge,[1,13] Si,[1,13] InSb,[4,14] in InP,[15] InAs,[16] and Bi.[4] The early measurements on *n*-type Ge at 20°K by RYDER[17] and recent work by KOENIG[18] and by BOK[7] are, I think, the only cases in which one may be reasonably certain that acoustic scattering controls both the momentum and energy balance. (This is discussed more fully below.) Fig. 2 shows this data in the dimensionless units appropriate to the theory. On a simple picture the two $E^{-\frac{1}{2}}$ regions would be expected to superpose. There are, however, several complications. The Koenig data is Hall mobility, whereas the Ryder data is drift mobility obtained by a direction used. The deviations from $E^{-\frac{1}{2}}$ behavior of the mobility due to failure of equipartition are expected to occur at a value of $E/E_0$ proportional to lattice temperature. This is seen to be approximately the case for the data of Fig. 2. Similar shaped curves have been obtained for *p*-type Ge at 77°K by Bray,[4] but it is hard to see why acoustic scattering should play a dominant role for this case.

## 3. WARM ELECTRONS AND OPTICAL MODES

Recent theoretical and experimental work by MORGAN[4] on slightly warm electrons in *n*-type Ge in the temperature range 77°–300°K has

demonstrated the importance of optical modes. The results may be summarized as follows: at 300°K, acoustic scattering contributes 80 per cent of the mobility but ~ 2 per cent to the energy loss. At 100°K, acoustic scattering contributes 95 per cent of the mobility, but still only ~ 12 per cent of the energy loss. The remainder of the loss is caused by optical phonons and to a lesser extent by intervalley scattering. It is only at ~ 60°K that acoustic and optical scattering make equal contribution to the energy loss. These figures were obtained by Morgan using the distribution that resulted from solving the Boltzmann equation, ignoring electron–electron scattering, rather than assuming a Maxwellian distribution, which gives a loss at 100°K greater by a factor of 4. The efficiency of electron–electron scattering in tending to restore a Maxwellian distribution centered about a drift velocity has been pointed out by FRÖHLICH and PARANJAPE.[19] Recent work by SEEGER[3,20] shows a variation with electron density in the ease with which electrons may be heated, other parameters remaining fixed, suggesting, in accordance with the preceeding ideas, the importance of electron–electron scattering.

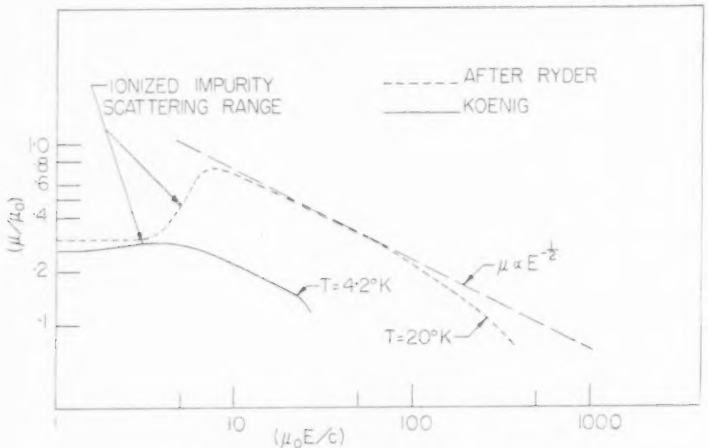


FIG. 2. The electric field dependence of mobility in reduced units. Ideally the two $E^{-\frac{1}{2}}$ regions would superpose (see text). The deviation from the $E^{-\frac{1}{2}}$ law at high fields is most probably due to failure of the assumption of equipartition for the phonons involved in the scattering. The temperature dependence is roughly correct.

## 4. ELECTRON TEMPERATURE

Attempts have been made to obtain a more direct measurement of the electron "temperature" for a hot distribution. GIBSON[21] has pointed out that the piezoresistance of *n*-type germanium should be a function of electron temperature, and has been measuring the variation of piezoresistance with electric field with some success. BOK[7] has measured the "thermoelectric power" between hot and cold electrons for extrinsic *n*-type Ge by using a T-shaped sample and by making contact to the cold electrons in the arm of the T, and to the hot electrons in the cross bar. This type of measurement has been extended by KOENIG and BROWN[22] to *n*-type Ge at 4°K in the breakdown region (Fig. 3). Though the magnitude and sign of the effect is of the order that one might expect from initial naive considerations, because in this case there is a field dependent carrier density gradient as well as energy gradient, the interpretation will not be straight forward. The observed voltage will be the sum of two terms, the difference in barrier voltage developed at the two contacts and a diffusion potential in the bulk, to some extent analogous to the Peltier and Thomson

contributions to the thermoelectric voltage under normal conditions. These two contributions may well be of opposite sign, and highly field dependent, which may account for the sudden drop observed at high fields (Fig. 3).

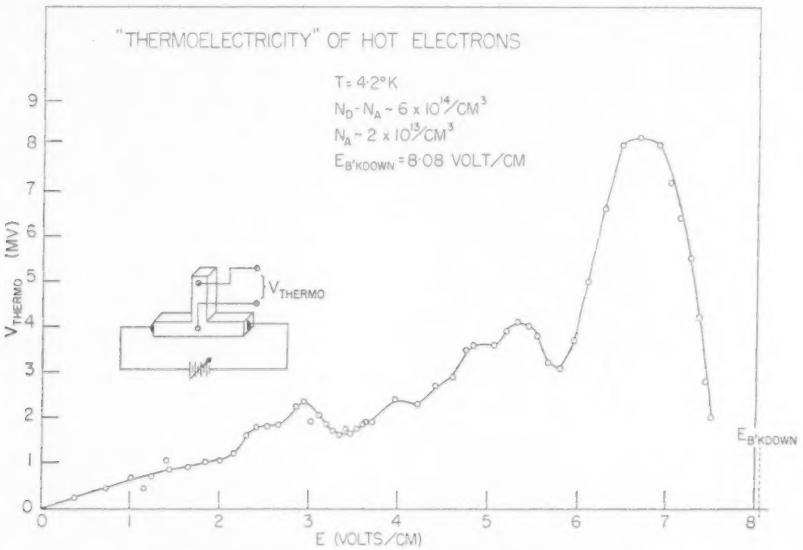


FIG. 3. The variation of the "thermoelectric" voltage developed between hot and cold electrons for the configuration shown. For $E = 8$V/cm, the electron "temperature" is $\sim 100$°K.

## 5. LOW TEMPERATURE BREAKDOWN

The most intensive investigations of phenomena resulting from the existence of hot electrons have been those relating to low temperature breakdown.[1,6] At $\sim 4$°K, the conductivity of Ge is highly non-linear, and is characterized by a reversible breakdown region in which the current increases by orders of magnitude for small changes in applied voltage (Fig. 4). It is possible to understand the shape of the current voltage characteristics by considering the balance of the rate processes that produce and annihilate carriers as these rates vary with the electron distribution function. The rate processes that need be considered are thermal ionization $A_T$, impact ionization of neutral donors by energetic electrons $A_I$, and the corresponding inverse processes, single electron recombination $B_T$, and Auger recombination $B_I$. The rate equation becomes, for carrier density $n$ small compared to both the donor and acceptor densities $N_D$ and $N_A$:

$$A_T(T)(N_D-N_A)+nA_I(f)(N_D-N_A)- -nB_T(T,f)N_A-n^2B_I(T,f)N_A = dn/dt. \quad (6)$$

The dependence of the coefficients on the lattice temperature $T$ and distribution function $f$ is indicated. For small $n$, the term in $n^2$ may be ignored, and one obtains

$$n = A_T(N_D-N_A)/[B_T-A_I(N_D-N_A)/N_A]N_A. \quad (7)$$

Breakdown occurs at an electric field such that the denominator of equation (7) approaches zero. Equation (7) predicts that the breakdown field should *increase* as $(N_D-N_A)/N_A$ (or for fixed compensation, the donor concentration) is *decreased* contrary to some ideas on the subject.[23] To demonstrate such a dependence requires samples of purity sufficiently high for the mobility to be mainly lattice determined. The data of Table 2 clearly demonstrate the effect.

The applicability of equation (6) to transient and steady state conditions, under the assumption that the distribution function "follows" changes in

*Table 2. Data showing that the low temperature breakdown field for n-type Ge may be increased by an increase in purity, in accordance with predictions of equation 7*

| Sample | $(N_D - N_A)$ | $N_A$ | $E_{b'kdown}$ |
|---|---|---|---|
| *n*WLB 28–6 | $1{\cdot}5 \times 10^{13}$ cm$^{-3}$ | $5 \times 10^{12}$ cm$^{-3}$ | 4·8V/cm |
| *n*WLP 33A | $1 \times 10^{12}$ cm$^{-3}$ | $4 \times 10^{12}$ cm$^{-3}$ | 14V/cm |

applied fields in $\gtrsim 10^{-9}$ sec, has previously been quantitatively justified and will not be discussed here.[6] By creating a non steady-state value of $n$, and observing the decay of conductivity in a sample with the electric field sufficiently low for $f$ to have essentially its thermal equilibrium value, it has been possible to measure $B_T$ for thermal electrons as a function of $T$. The significance of this quantity has been discussed by Melvin Lax earlier in this conference in his talk on "giant traps." Suffice it to say that the cross-section for capture is orders of magnitude larger than one might expect if direct capture of the carrier to the ground state were the dominant process. The data and the derived cross-section are compared with theory in Fig. 5.

Recently, it has been possible at Watson Laboratories[24] to measure directly the magnitude $B_I$, the Auger recombination term, for a range of lattice temperature of 4–10°K, but only for an electron temperature $\sim 100$°K. The result for $B_I$ is $\sim 10^{-17}$/cm$^6$ sec, which means at $n \sim 10^{10}$/cm$^3$ the Auger recombination rate and single electron capture rates are roughly equal. Calculations by SCLAR and BURSTEIN[23] of $B_I$ yield the same order of magnitude as that measured here, but the agreement is probably due to the fortuitous cancellation of several large factors in the theoretical approximations, inasmuch as the giant trap type of cascade process must be operative in Auger recombination.

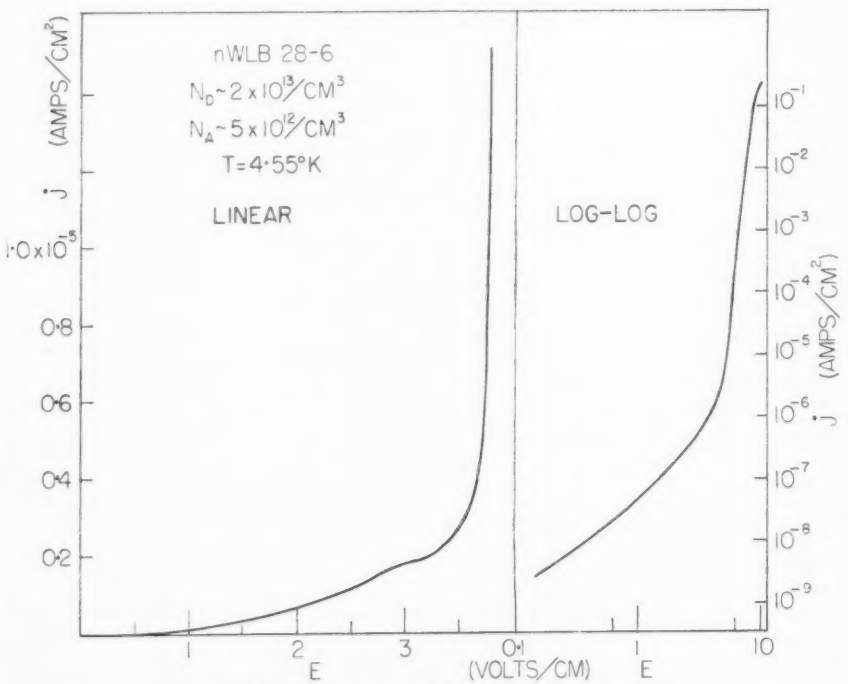


FIG. 4. Variation of current density with electric field for a high purity *n*-Ge sample at low temperature. The curves, however, typify a wide range of *n*- and *p*-type Ge.

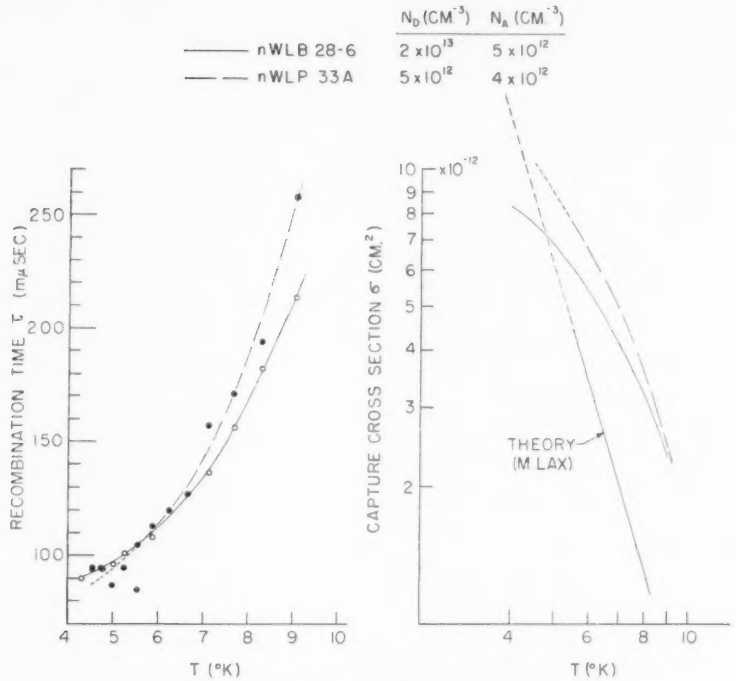


FIG. 5. The temperature dependence of the recombination time for an electron and an ionized donor for thermal electrons, and the cross section calculated from the smoothed data. The tendency to saturate at the lower temperatures is associated with an overlap of the orbits on adjacent recombination centers ($\sim 1\mu$ apart!). For the purer sample, the effect is less.

### 6. THERMIONIC EMISSION

If the electron affinity of a material is fairly low, thermionic emission may be increased by heating the electron distribution. This mechanism has been suggested by GINSBURG and SHABANSKII[7] to explain the observed anomalously high electron emission of tungsten at high current densities.[7] More recently, BOK[7] has observed such emission from bulk Si with the surface treated to lower its electron affinity.

### 7. ANISOTROPY

In the region where Ohm's Law applies, the symmetry of the conductivity tensor for a given material must be at least that of the point group of the lattice regardless of the complexities of the band structure. This ceases to be the case for hot electrons, so that from measurements of the anisotropy of conduction in the hot electron range one may obtain information regarding the band structure. SASAKI, SHIBUYA and co-workers[25] have extensively studied the anisotropy in *n*-type Ge from 77°–300°K, and will discuss their recent work at the present conference. Pertinent calculations have also been made by GOLD,[26] and observations on the variation of electric breakdown with crystalline orientation have been reported.[27] Needless to say, the results are consistent with the known multivalley structure of the conduction band of Ge. Such anisotropy measurements may be one of the simplest ways to get an idea of the symmetry of the band structure of a new semiconductor.

### 8. CYCLOTRON RESONANCE

A recent interesting application of hot electrons was made by ZEIGER[28] and collaborators, who have observed the variation in d.c. conductivity due to the absorption, at the cyclotron resonance,

of r.f. power. The sensitivity surpasses that of the conventional methods of detecting cyclotron resonance, but the complexity of the initial published results suggests that experiments of this type will yield information on both cyclotron resonance and hot electrons.

*Acknowledgments*—I should like to acknowledge the many interesting, and useful, conversations with P. J. PRICE, and in particular his critical perusal of what was to have been the final manuscript. The help of Messrs. BROWN, FRIEDMAN, HALL and SCHILLINGER in obtaining data has at times been invaluable.

## REFERENCES

1. See GUNN J. B., *Progress in Semiconductors*, Vol. 2, p. 246. John Wiley, New York (1957); KOENIG S. H., and GUNTHER-MOHR G. R., *J. Phys. Chem. Solids* **2**, 268 (1957); SCLAR N. and BURSTEIN E., *J. Phys. Chem. Solids* **2**, 1 (1957); for references to earlier work. More recent work will be referred to below.
2. BOROVIK E. S., *Dokl. Akad. Nauk. SSSR* **91**, 771 (1953); KOENIG S. H., HALL J. and FRIEDMAN A. (unpublished).
3. SHOCKLEY W., *Bell Syst. Tech. J.* **30**, 990 (1951).
4. MORGAN T., *Report. Sig. Corp. Contr.* DA-36-039-SC-52670, May (1957), Univ. of Ill; *Bull. Amer. Phys. Soc.* Ser. II, **2**, 265 (1957); *Ibid.*, **3**, 13 (1958); BRAY R., *Proc. Phys. Soc.* B, **70**, 899 (1957); GLICKSMAN M. and STEELE M. C., *Phys. Rev.* **111**, 1204 (1958); STEELE M. C., *Bull. Amer. Phys. Soc.* Ser. II, **3**, 112 (1958); SEEGER K., *Bull. Amer. Phys. Soc.* Ser. II, **3**, 112 (1958). Also reference (1).
5. CONWELL E. M., *Phys. Rev.* **90**, 769 (1953).
6. KOENIG S. H., *Phys. Rev.* **110**, 986 (1958); *Phys. Rev.* **110**, 988 (1958).
7. BOK J., *International Congress on Solid State Physics*, Brussels, June (1958) to be published; GINZBURG V. L. and SHABANSKII V. P., *Dokl. Akad. Nauk. SSSR* **100**, 3, 445 (1955); LEVEDEV S. V. and KHAIKIN S. E., *Zh. eksp. teor. fiz.* **12, 26,** 723 (1954).
8. PISARENKO N. L., *Isv. Akad. Nauk. SSSR, fiz. ser.* p. 631 (1938).
9. YAMASHITA J. and WATANABE M., *Prog. Theor. Phys. Osaka* **12,** 443 (1954).
10. DRUYVESTEYN M. J., *Physica* **10,** 61 (1930). See also CHAPMAN S. and COWLING T., *The Mathematical Theory of Non-Uniform Gases*, p. 351. Cambridge University Press (1939).
11. SODHA M. S. and EASTMAN P. C., *Phys. Rev.* **110,** 1314 (1958).
12. PARANJAPE, B. V., *Proc. Phys. Soc.* B, **70,** 628 (1957).
13. FINKE G. and LAUTZ G., *Z. Naturf.* **12,** 223 (1957); BRAY R. and MENDELSON K., *Bull. Amer. Phys. Soc.*, Ser. II, **2,** 153 (1957), BRAUNSTEIN R. *et al. Signal Corp. Contr.* DA36-039-SC-5548, 11th and 12th quarterly report (1953–1954).
14. BOK J. and AIGRAIN P., private communication.
15. STEELE M. C., *Bull. Amer. Phys. Soc.* Ser. II, **3,** 112 (1958).
16. PRIOR A. C., *J. Electronics and Control* **4,** 165 (1958).
17. RYDER E. J., *Phys. Rev.* **90,** 766 (1953).
18. KOENIG S. H., unpublished results.
19. FRÖHLICH H. F. and PARANJAPE B. V., *Proc. Phys. Soc.* B**69,** 21 (1956).
20. SEEGER K., private communication.
21. GIBSON A. F., private communication.
22. KOENIG S. H. and BROWN R., unpublished results.
23. SCLAR N. and BURSTEIN E., reference 1.
24. KOENIG S. H., to be published.
25. SASAKI W., SHIBUYA M. and MIZUGUCHI K., *J. Phys. Soc. Japan* **13,** 456 (1958); SASAKI W. and SHIBUYA M., *J. Phys. Soc. Japan* **11,** 1202 (1956); SHIBUYA M., *Phys. Rev.* **99,** 1189 (1955).
26. GOLD L., *Phys. Rev.* **104,** 1580 (1956).
27. KOENIG S. H. and GUNTHER-MOHR G. R., SCLAR N. and BURSTEIN E., reference 1.
28. ZEIGER H. J., RAUCH C. J. and BEHRNDT M. E., *Phys. Rev. Letters* **1,** 59 (1958).

*J. Phys. Chem. Solids* Pergamon Press 1959. Vol. 8. pp. 234–239. Printed in Great Britain

# I.3 LATTICE MOBILITY OF HOT CARRIERS

E. CONWELL

Research Laboratories, Sylvania Electric Products Inc.,
Bayside, New York

A THEORY of the variation of lattice mobility with electric field intensity was developed some years ago by SHOCKLEY.[1] The agreement of this theory with experimental data for germanium was not satisfactory in that it predicted deviations from Ohm's law at fields about one-third as high as actually required. Also, it predicted that beyond the Ohm's law region drift velocity should be

proportional to the square root of electric field intensity; this is not found over any substantial region.

A prerequisite for understanding lattice mobility at high fields is knowledge of the processes that determine it at low fields. The usual theory, based on acoustical mode scattering and one-phonon processes, predicts a lattice mobility varying with temperature as $T^{-1.5}$. What is found experimentally in the temperature range from about 100°K to 300°K is $T^{-2.33}$ for holes, $T^{-1.66}$ for electrons.[2] There have been a few suggestions to account for this. In the case of holes, the most promising at the moment seems to be optical mode scattering.

According to the usual treatment based on the simple model of the band structure and one-phonon processes, the square of the matrix element for scattering by acoustical or optical lattice modes of vibration is given by:[3,4]

$$|M|^2 = E_1^2 \frac{\hbar\omega}{2Vc_l}\left(n+\tfrac{1}{2}+\frac{\delta n}{2}\right) \qquad (1)$$

where $E_1$ is an interaction or coupling constant, which can be interpreted as a shift of the band edge per unit deformation suitably defined for each of the two cases, $\hbar\omega$ is the energy of the phonon which the carrier emits or absorbs in the scattering process, $V$ is the volume of the crystal, $c_l$ is an average elastic constant, $n$ is the number of phonons in the lattice mode with which the carrier interacts and $\delta n$ the change in this number due to the interaction with the carrier. The number $n$ is given by the Planck formula:

$$n = \frac{1}{\exp(\hbar\omega/kT)-1}. \qquad (2)$$

For acoustical modes and low electric fields in the range 100–300°K $\hbar\omega$ is much less than $kT$ and $n$ can be approximated by $kT/\hbar\omega$. This corresponds to equipartition of energy among the lattice oscillators. Equipartition is not valid for the optical modes in germanium in this temperature range. This is the reason why scattering by optical modes leads to a steeper temperature dependence of the matrix element, and in turn the relaxation time and the mobility.

It was shown by EHRENREICH and OVERHAUSER[5] that the experimental data for $p$-germanium could be explained with an $\hbar\omega$ for the optical modes corresponding to a characteristic temperature of 300°K. The proportion of optical to acoustical mode scattering required seemed reasonable, but unfortunately this could not be checked by calculation. Since then the characteristic temperature has been measured in neutron scattering experiments and found to be around 400° or 430°K.[6,7] Although the calculations of EHRENREICH and OVERHAUSER have not been repeated for this characteristic temperature it is felt certain that this temperature will lead to as good an agreement with experiment as did 300°.* This has also been demonstrated, as will be discussed later, using a simpler model than that of EHRENREICH and OVERHAUSER.

In the case of electrons the deviation from $T^{-1.5}$ could be due to intra-valley scattering by optical modes, inter-valley scattering by optical or acoustical modes, or some combination of these.[8] The first process is, of course, the one we have been considering for holes, and the phonons involved have a characteristic temperature around 400°K. For the inter-valley process, if the band edge is at the edge of the Brillouin zone, as is almost certain, symmetry considerations lead to the conclusion that the two lowest branches of the lattice vibration spectrum will make very little contribution.[9] Thus the phonons involved in inter-valley scattering will have energies corresponding to temperatures in the range 320°K[7] to about 400°K, being not too different from the optical phonons. Also, the form of the matrix element and therefore of $\tau$ and $\mu$ is the same for the two scattering processes.[8] Thus the present calculations would be much the same for either of the two processes, and for what follows we have chosen to consider only the intra-valley optical mode process.

In line with the preceding discussion relaxation times were obtained for acoustical and optical mode scattering from the matrix element (1) by the usual perturbation theory procedure. This involves an integration over all possible final

* EHRENREICH and OVERHAUSER did their calculations also for a characteristic temperature of 500°K and concluded that for this temperature the optical modes would not contribute enough scattering to achieve a fit with the experimental data. However, this conclusion is based on the requirement that the $T^{-2.3}$ slope be maintained down to 50°K, whereas experimentally there is no evidence for its being maintained below 100°K.

states of the system. For holes this was simplified by assuming that on scattering both light and heavy holes go into the heavy-hole band because of its much higher density of states. With this assumption both holes have the same relaxation time. For the acoustical modes, in order to obtain an expression valid at high electric field where the energy of the phonons with which the carriers interact is not much less than $kT$, the Planck distribution was used for $n$. With the simplification of neglecting the small difference in size between emitted and absorbed phonons, this leads to a relaxation time:

$$\frac{1}{\tau_{ac}} = \frac{\sqrt{(2\epsilon/m)}}{4l_{ac}} \left(\frac{2kT}{cP}\right)^4 \int_{u=0}^{cP/kT} u^4 \coth u \, du \quad (3)$$

when

$$l_{ac} = \frac{\pi\hbar^4 c_l}{m^2 E_{1ac}^2 kT} \quad (4)$$

and $P$ and $\epsilon$ are carrier crystal momentum and energy respectively. Where equipartition is valid $u$ is small and this reduces to the familiar $1/\tau_{ac} = \sqrt{(2\epsilon/m)}/l_{ac}$, or $v/l_{ac}$. For the optical modes the relaxation time obtained from (1) and (2) is:

$$\frac{1}{\tau_{op}} = \frac{(E_{1op}/E_{1ac})^2}{2l_{ac}} \frac{\theta/T}{\exp(\theta/T)-1} \sqrt{\left(\frac{2}{m}\right)} \times \times \{\sqrt{(\epsilon+k\theta)} + \exp(\theta/T)\sqrt{(\epsilon-k\theta)}\}. \quad (5)$$

where $\theta$ is the characteristic temperature. The first term in the curly bracket corresponds to phonon absorption, the second to phonon emission. The second term is present only if $\epsilon > k\theta$, i.e., if energy is conserved.

Mobility is then obtained by averaging $\tau$, the reciprocal of the sum of (3) and (5), over the carrier distribution according to:[10]

$$\mu = \frac{q}{3m} \left\langle \frac{1}{P^2} \frac{d}{dP}(P^3\tau) \right\rangle. \quad (6)$$

Since it is felt that the correct carrier distribution is not known because the effect of electron–electron collisions has not been taken into account, a Maxwell-Boltzmann distribution was used. Combination of the $\tau$'s of (3) and (5) leads to a rather complicated integral for $\mu$ as a function of electron temperature $T_e$ and this was evaluated by machine. To determine the quantity $(E_{1op}^2/E_{1ac}^2)$ $\mu$ was evaluated for $T_e = T$ and various values of the ratio, and the resulting $\mu$ vs. $T$ compared with experiment. It was found that the experimentally observed temperature dependence could be well duplicated with $\theta = 400$ and $(E_{1op}/E_{1ac})^2 = 4$ for $p$-germanium, 0·4 for $n$-germanium.

To determine how $T_e$ varies with electric field intensity it is convenient, as in past calculations, to use the requirement that in the steady state average power gain from the electric field equals average power loss, i.e.:

$$q\mu E^2 + \left\langle \frac{d\epsilon}{dt} \right\rangle = 0.$$

The expressions for the average rates of loss for a Maxwell–Boltzmann distribution are:

$$\left\langle \frac{d\epsilon}{dt} \right\rangle_{ac} = \frac{-8}{\sqrt{(\pi)}} \frac{\sqrt{(2kT/m)}}{l_{ac}} mc^2 \left(\frac{T}{T_e}\right)^{-\frac{1}{2}} \left(1 - \frac{T}{T_e}\right) \quad (7)$$

$$\left\langle \frac{d\epsilon}{dt} \right\rangle_{op} = \frac{-2}{\sqrt{(\pi)}} \frac{\sqrt{(2kT/m)}}{l_{ac}} k\theta \frac{(E_{1op}/E_{1ac})^2 \theta/T}{2[\exp(\theta/T)-1]} \times \quad (8)^*$$

$$\times \left(\frac{T}{T_e}\right)^{-\frac{1}{2}} \frac{\theta}{2T_e} K_1\left(\frac{\theta}{2T_e}\right) \left[\exp\left(\frac{\theta}{T} - \frac{\theta}{T_e}\right) - 1\right]$$

where $K_1$ is a Bessel function of the second kind with imaginary argument. It is noteworthy that (7), although derived assuming equipartition of energy, is still quite accurate at fields for which equipartition has ceased to hold. It is instructive to compare the two rates of energy loss, and this is shown in Fig. 1 for $\theta = 400$°K and a lattice temperature of 78°K. The situation is quite similar for a lattice temperature of 300°K. It is apparent that the optical modes dominate the energy loss up to quite high electron temperatures, when the acoustical modes again become important. Thus the energy loss situation is the reverse of what has very frequently been considered to be the case.[1]

The results of the calculation of mobility vs. electric field intensity for $n$-germanium at 300°K are shown in Fig. 2. Apart from $\theta$ and $(E_{1op}/E_{1ac})^2$,

* This has also been derived by T. MORGAN, IBM Laboratories.

the only parameters required for the calculation are the low field mobility, $\mu_0$, taken as 3800 cm$^2$/V sec, and the effective mass in $\langle d\epsilon/dt \rangle$. This was taken as the geometric mean of the principal masses, 0·22 $m_0$, since the mass enters mainly through the density of final states in the scattering process. The relatively good agreement of theory and experiment for the warm electron range is evidence that the deviation from $T^{-1.5}$ of lattice mobility vs. temperature is indeed due, at least predominantly, to optical or perhaps inter-valley scattering rather than variation of effective mass with crystal momentum or temperature. Beyond the warm electron range, say beyond about 3000 V/cm, agreement of theory and experiment becomes progressively less good. Indeed, agreement beyond this range is undoubtedly to some extent fortuitous because of the many effects which have been neglected. For example, when the electrons are heated sufficiently they can be scattered into other conduction band minima. This provides an additional source of energy loss, and also makes it necessary to take into account the different properties—i.e., masses and coupling constants—of electrons inhabiting the other minima. Dispersion effects for the phonons, which have been neglected, may also become significant. In addition, for hot electrons interaction with phonons from the lowest acoustic branches will no longer be small.

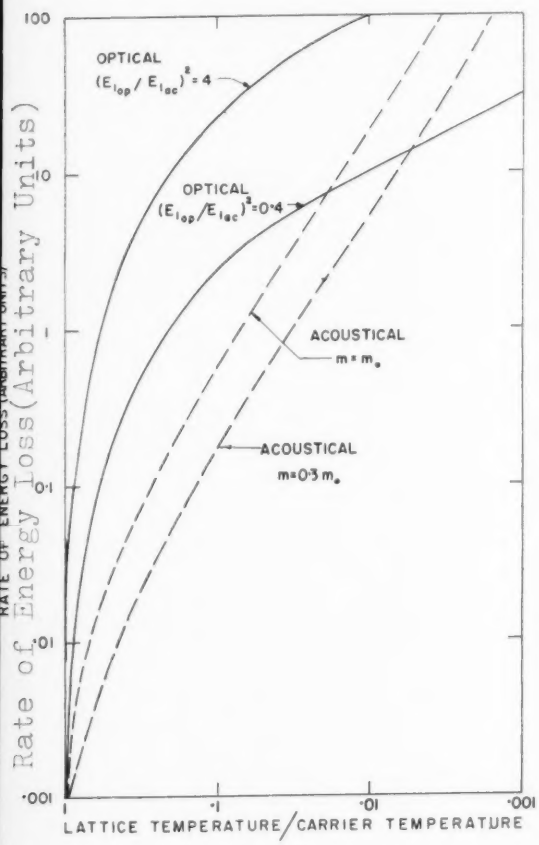


FIG. 1. Comparison of rates of loss to optical and acoustical modes at 78° K. The solid lines represent rate of loss to optical modes, the top one for $(E_{1op}/E_{1ac})^2 = 4$, the bottom one for 0·4. The dashed lines represent rate of loss to acoustical modes, the top one for an effective mass of $m_0$, the bottom one for an effective mass of 0·3 $m_0$.

The corresponding results for *p*-germanium are shown in Fig. 3. These are not nearly as good as those for *n*-germanium, the theory predicting much less heating at a given field than is actually observed except at extremely high fields. In obtaining the theoretical curve the average power loss was taken as that of the heavy holes, i.e. the mass was taken as 0·3 $m_0$. For optical modes this is quite correct, the loss rates of the two holes being equal because the $\tau$'s are. For acoustical modes this is not quite so because the size of phonons involved in a transition is somewhat different for the two. Light holes are so few in proportion, however, that the error from this source is small. A more serious source of error is the assumption that the two kinds of holes are at the same temperature. With this assumption, the calculations essentially describe the behavior of a single hole with $\mu_0 = 1800$, the average mobility. The light holes, having $\mu_0$ many times this, would start to heat up at much lower fields than this average hole and, through the media of collisions with the heavy holes and interband transitions, also produce more heating of the heavy holes than expected at a given field. This effect is thus in the right direction to reduce the discrepancy between theory and experiment. Whether it is the entire reason for the discrepancy cannot be decided without further calculation. There is some small evidence, however, that it may be. Calculations by Kane show that the curvature of the light-hole band starts changing at a few $kT$, becoming about

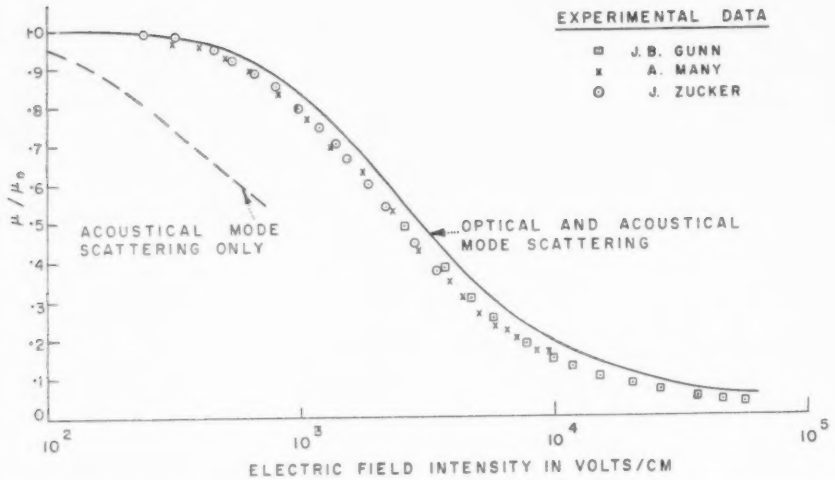


FIG. 2. Ratio of mobility to low-field mobility as a function of electric field intensity for *n*-germanium at 300°K. The solid line represents the theoretical curve obtained including both optical and acoustical mode scattering, the dashed line that obtained considering acoustical mode scattering only. The data of GUNN, J. B., *J. Electronics* **2**, 87 (1956) and ZUCKER J., Sylvania Electric Products Inc., were obtained with d.c. pulses, those of MANY A., Sylvania Electric Products Inc., with microwave pulses.

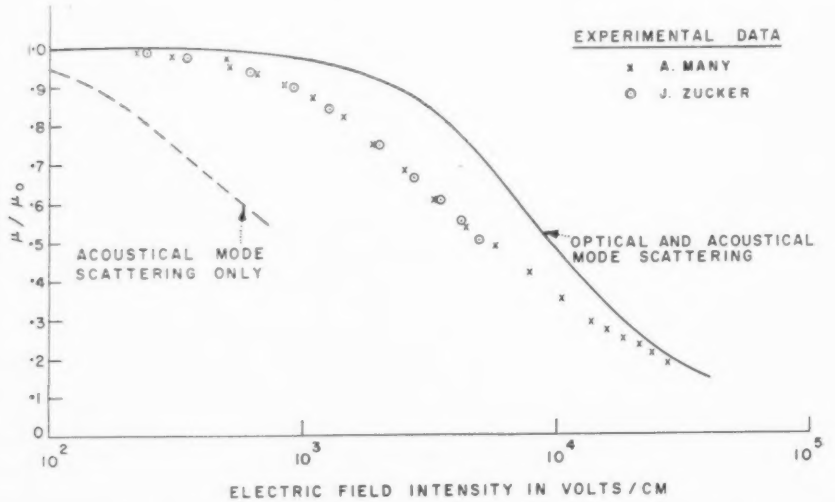


FIG. 3. Ratio of mobility to low-field mobility as a function of electric field intensity for *p*-germanium at 300°K. The solid line represents the theoretical curve obtained including both optical and acoustical mode scattering, the dashed line that obtained considering acoustical mode scattering only. The data of ZUCKER J., Sylvania Electric Products Inc., were obtained with d.c. pulses, those of MANY A., Sylvania Electric Products Inc., with microwave pulses.

the same as that of the heavy hole band around $10kT$.[11] Thus as the holes are heated the assumption of equal temperature should improve, and beyond energies of about $10kT$ should be quite good. It has been noted that the theoretical and experimental curves do come together at the highest fields. The calculated hole temperature corresponding to 40,000 V/cm is in fact ten times the lattice temperature. Thus it may be that the basic model, with optical modes accounting for the deviation from the $T^{-1\cdot5}$ dependence of lattice mobility, is correct and the poor agreement between theory and experiment seen in Fig. 3 is due to the assumption of equal temperature of the two holes.

*Acknowledgment*—The author is greatly indebted to Mr. A. Brown for the evaluation of the mobility integrals.

**REFERENCES**

1. Shockley W., *Bell Syst. Tech. J.* **30,** 990 (1951).
2. Morin F. J., *Phys. Rev.* **93,** 62 (1954).
3. Shockley W., *Electrons and Holes in Semiconductors.* D. Van Nostrand Co., New York (1950).
4. Seitz F., *Phys. Rev.* **73,** 549 (1948).
5. Ehrenreich H. and Overhauser A. W., *Phys. Rev.* **104,** 649 (1956).
6. Pelah I., Eisenhauer C. M., Hughes D. J., and Palevsky H., *Phys. Rev.* **108,** 1091 (1957).
7. Brockhouse B. N. and Iyengar P. K., *Phys. Rev.*, to be published.
8. Herring C., *Bell Syst. Tech. J.* **34,** 237 (1955).
9. Herring C. and Vogt E., *Phys. Rev.* **101,** 944 (1956).
10. Conwell E., *Phys. Rev.* **88,** 1379 (1952).
11. Kane E. O., *J. Phys. Chem. Solids* **1,** 82 (1956).

OL.
8
959

*J. Phys. Chem. Solids* Pergamon Press 1959. Vol. 8. pp. 239–241. Printed in Great Britain

I.4

# EFFECT OF ELECTRON AND IMPURITY DENSITY ON THE FIELD-DEPENDENCE OF MOBILITY IN GERMANIUM*

**J. B. GUNN**

Department of Physics, University of British Columbia, Vancouver, Canada

Previous measurements have shown that the rate of energy transfer between electrons and the lattice required to account for the electric field-dependence of mobility observed in Ge at low temperatures is greater than can be ascribed to the interaction of acoustical phonons with electrons of thermal energy.[1] A more efficient dissipation of energy would result from the emission of optical or energetic acoustical phonons, but at low temperatures such processes are unlikely because insufficient electrons have the necessary energy. The purpose of this work is to examine the possibility, suggested by Stratton,[2] that electron–electron (e–e) collisions enhance the probabilities of these processes; the collisions permit the transfer of energy from low-energy electrons, which gain it rapidly from the field, to those of high energy.

The value of electron density $n$ at which e–e scattering becomes important in this respect is calculated to be about $2\times10^{14}$ cm$^{-3}$. If this is indeed so, one would expect a dependence on $n$ of the energy dissipation rate, and hence of the magnitude of the effect of an electric field $E$ on the mobility $\mu$. In order to check this hypothesis, and simultaneously to observe the effect of impurity scattering, measurements have been made of

* Work performed under Grant No. 3801–08 from the Defense Research Board, Canada.

the variation of $\mu$ with $E$ for the region $6{\cdot}6\times10^{13} \leqslant n \leqslant 2{\cdot}9\times10^{16}$, $1 \leqslant E \leqslant 5\times10^{3}$ V cm$^{-1}$.

The measurements were made by observing the resistance $R$ of a thin filament of Ge as a function of applied voltage. A number of precautions are necessary, in order that the variation of $\mu$ with $E$ may be deduced from the results. The lattice temperature must be held constant within 0·01°K if changes in electron "temperature" of this order are to be detected. This was achieved by applying the field in infrequent pulses of 1–10$\mu$sec duration, and by directing over the specimen a vigorous flow of liquid nitrogen held at constant temperature by a feedback system. A nitrogen vapor pressure thermometer gave a check and an absolute calibration of the system. $R$ was obtained by measuring the current and voltage separately, or by a bridge method using a differential transformer. The former method, useful for large $E$, used an oscilloscope only as a null detector to indicate the equality of a pulse voltage and an accurately known direct voltage. The latter method allowed changes of 1 part in $10^4$ to be detected when $E$ was small. Spurious effects due to the end contacts were eliminated by making these as $l$–$h$ junctions by alloying a layer of Au–Sb to each end so as to retain approximately one-dimensional geometry. A plot of $\beta$ (defined below) against inverse specimen length showed no trend, indicating that contact effects could be neglected.

Intentionally added Sb was believed to be the only impurity present in the Ge, and on this assumption it is calculated that the proportion of un-ionized impurity atoms was negligible. $n$ could then be assumed constant and equal to the impurity density $N_I$, whence $\mu/\mu_0 = R_0/R$ (subscript 0 = zero field). The value of $n$, and hence of $\mu_0$, was estimated from the room-temperature resistivity and the mobility values given by PRINCE.[3] The corrections for intrinsic carriers or impurity scattering amounted to 9 and 25 per cent in the most and least pure specimens respectively.

For small $E$, the results can be represented by the equation $\mu/\mu_0 = 1+\beta E^2$, where $\beta$ is an empirically determined parameter dependent on $N_I$. The variation of $\beta$ with $N_I$ is shown in Fig. 1. For small values of $N_I$, lattice scattering is dominant, the relaxation time $\tau$ decreases with increasing electron energy, and $\beta$ is negative. For large $N_I$, impurity scattering is dominant, $\tau$ increases with energy, and $\beta$ is positive. For the intermediate value $N_I = 1{\cdot}8\times10^{15}$ cm$^{-3}$ the two effects cancel, and $\beta = 0$. The comparison of experimental and theoretical values of $\beta$ requires a knowledge of the parameter $a(N_I) \equiv 6\mu_{L0}/\mu_{I0}$ where $\mu_{L0}$, $\mu_{I0}$ are the zero-field mobilities calculated for lattice and impurity scattering, respectively. The measured curve of $\mu_0(N_I)$ agrees within 10 per cent with that calculated from the Conwell–Weisskopf expression for $\mu_{I0}$, with $m^*/m_0$ taken as 0·1, but the values of $a$ depend significantly on whether they are calculated ($a_1$) from the measured values of $\mu_0/\mu_{L0}$, or ($a_2$) from the calculated $\mu_{I0}(N_I)$ and the measured $\mu_{L0}$.

For large $E$, the quadratic expression is inadequate to represent $\mu(E)$. A test of the theory of

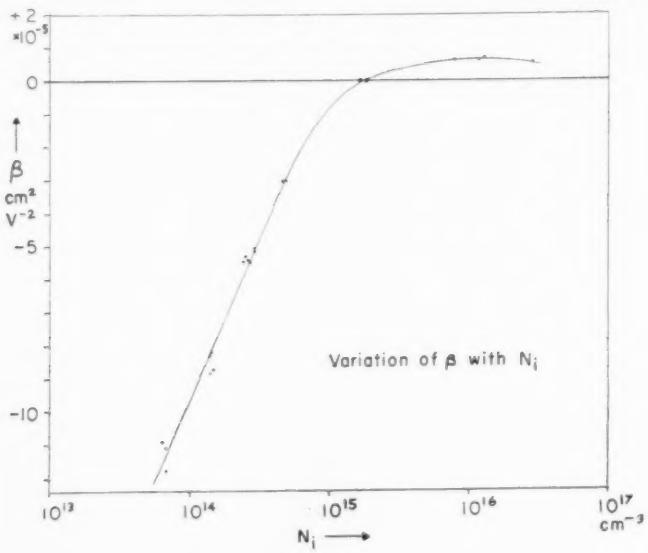


FIG. 1.

acoustical phonon emission, given by SHOCKLEY,[4] is made by plotting $\mu^{-2}$ against $\mu^2E^2$, which should give a straight line of slope $(3\pi/32)\mu_0^{-2}c^{-2}$ when impurity scattering is negligible ($c = 5{\cdot}4\times10^5$ cm sec$^{-1}$ = sound velocity). The experimental points give a sigmoid curve which lies well below the theoretical line. For large values of $N_I$, the increase in $\mu$ continues over a wide range of $E$, but $\mu$ eventually passes through a maximum and and then decreases. The curves for large and small $N_I$ do not appear to coincide even at the highest fields used. Typical results for the drift velocity $v_d(E)$ have shown in Fig. 2. Each curve represents about 50 experimental points, whose scatter is generally less than the line thickness. A rotation of axes by 45° in this figure will give log $\mu$ against log $\mu E^2$. The line corresponding to $\mu_0$ is drawn dotted in each case. Other values of $N_I$ give curves lying in a smooth sequence between those shown.

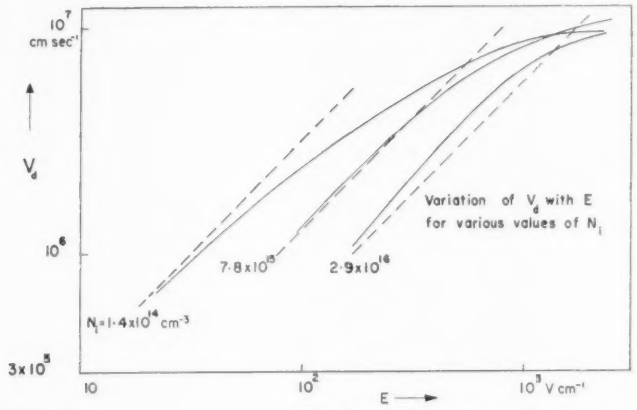


FIG. 2.

The variation of $\beta$ with $N_I$ can be compared with the theories of SODHA[5] and ADAWI.[6] The former uses a Maxwellian, and the latter a more exact, electron distribution. Both consider only scattering by acoustical phonons and impurities. The quantity $\theta \equiv \beta$ (calculated)/$\beta$ (observed), which can be interpreted as (total rate of energy loss)/(loss to acoustical phonons alone), can then be evaluated for various values of $N_I$. The results for small $N_I$ depend markedly on which theory is used, and on whether $a_1$ or $a_2$ is used in calculation. The extremes are represented by using $a_2$ and reference (5), or $a_1$ and (6). The first gives an increase of $\theta$ from 53 to 520 between $n = N_I = 6{\cdot}6\times10^{13}$ and $2{\cdot}9\times10^{16}$ cm$^{-3}$, which suggests that e–e scattering is important in the energy transfer. The second gives a variation from 170 to 390 over the same range, which is inconclusive. Thus the question remains open.

The value of $\mu_0/\mu_{L0}$ when $\beta = 0$ can be compared with theory. The calculated value depends only slightly on the distribution chosen, and not at all on the rate of energy loss. The theoretical and experimental values are 0·635 and 0·655 respectively.

The presence of a saturation region in the $v_d(E)$ curves for small $N_I$, and its apparent absence in those for large $N_I$, will be noticed. The significance of this is not understood.

## REFERENCES

1. GUNN J. B., *Progress in Semiconductors*, **2,** 213 (1957).
2. STRATTON R., *Proc. Roy. Soc.* A, **242,** 355 (1957).
3. PRINCE M. B., *Phys. Rev.* **92,** 681 (1953).
4. SHOCKLEY W., *Bell Syst. Tech. J.*, **30,** 990 (1951).
5. SODHA M. S., *Phys. Rev.* **107,** 1266 (1957).
6. ADAWI I., Private communication, to be published.

*J. Phys. Chem. Solids* Pergamon Press 1959. Vol. 8. pp. 242–244. Printed in Great Britain

I.5

# HIGH ELECTRIC FIELD EFFECTS IN *n*-INDIUM ANTIMONIDE

**M. C. STEELE and M. GLICKSMAN**

RCA Laboratories, Princeton, N.J.

In a recent report[1] the authors described experimental evidence for the creation of electron–hole pairs in *n*-InSb by means of hot electrons. These observations included current–voltage and Hall effect data taken in a 7000 oersteds magnetic field. The previous experiments have been extended to study the magnetic field dependence of the phenomena. Studies of the effect of longitudinal magnetic fields have also been undertaken, indicating a markedly different behavior from that with the magnetic field transverse.

The pulse technique for obtaining these data has already been described.[1] All the measurements were made at 77°K. The single crystal *n*-InSb specimen was the one discussed in the earlier report.[1]

Fig. 1 shows the current density–electric field characteristics for no magnetic field and for a *transverse* magnetic field, $H$, of 3500 oersteds. The Hall coefficient, $R_H$, is also shown as a function of the electric field, $E$, in the presence of the 3500 oersteds. For $E \gtrsim 150$–$200$ V/cm $R_H$ is seen to decrease rapidly for small further increases in $E$. This decrease is interpreted as evidence for the creation of electron–hole pairs by impact ionization across the forbidden gap. Other mechanisms that might have explained these results have been considered[1] and abandoned on the basis of additional critical experiments and the known properties of *n*-InSb. In particular, the possibility of minority carrier injection can be ruled out because the transit time ($\simeq 10^{-6}$ sec) was $10^2$ times longer than the lifetime ($\simeq 10^{-8}$ sec) of such carriers.[2] For $H = 0$, the current density increases as $E^{4.0}$ in the region above 240 V/cm. Although this is a rapid increase in current it might have been expected to be even steeper.[3] It is believed that the shape of the current density–electric field curve is determined principally by the electron–hole recombination processes. In particular, surface recombination may be very important. Several other second order effects can also contribute to producing the observed dependence. Both the increase[4] in the effective mass of the electron and the increase[5] in $E_g$, the band gap, as the conduction band is filled, can dictate the need for an increased electric field to get higher current densities.

Several attempts have been made to detect the band-gap recombination radiation which should be present once the threshold for creation is exceeded. A sensitive bridge circuit was used to detect possible photoconductive changes in either a gold-doped germanium or an InSb detector placed very close to the crystal. To date, these attempts have not yielded any observable signals that could be attributed to the recombination radiation. These negative results are ascribed to the strong self-absorption in the crystal and to the optical inefficiency of the detecting system.

Fig. 2 shows the results when a *longitudinal* magnetic field is applied to the crystal. In the sub-threshold region the magnetoresistance is now much less[6] than for the corresponding transverse case, as is expected for the electrons with their isotropic effective mass. There are two other marked differences between the longitudinal and transverse magnetic field data. In Fig. 2 the curve for $H = 3500$ oersteds exhibits a vertical rise in current density when $E = 268$ V/cm. This vertical rise is also observed for values of $H = 1050$ oersteds and 7000 oersteds, the onset electric field being a monotonically increasing function of the magnetic field. For $H = 350$ oersteds the curve (a portion of which is shown dotted) undergoes a peculiar loop in the interval 150–260 V/cm.

This loop is indicative of a resistance which *decreases* with increasing magnetic field from zero to 350 oersteds. A more detailed study was made of this effect by observing the resistance as a function of $H$ for a series of constant current densities. The results are given in Fig. 3. In each of the curves shown there the resistance passes through a minimum as $H$ is increased. For much lower current densities (below the threshold of ionization) the resistance is a monotonically increasing function of $H$. From the curves in Fig. 3 it is found that the value of $H$ corresponding to the resistance minimum is very nearly a linear function of the current density.

These interesting effects in longitudinal magnetic fields are not yet understood. It is believed that the focusing action of such a field may be the fundamental reason for the observed behavior, but a detailed model is not yet evident. Negative longitudinal magnetoresistances have been observed in such materials as antimony[7] and bismuth.[8] However, the present results are of a different nature in that they are dependent upon the generation of electron–hole pairs. It also appears likely that the surface conditions and possibly the internal dislocation structure of the crystal may be significant in explaining the behavior. Future experiments, with varying surface conditions, are planned.

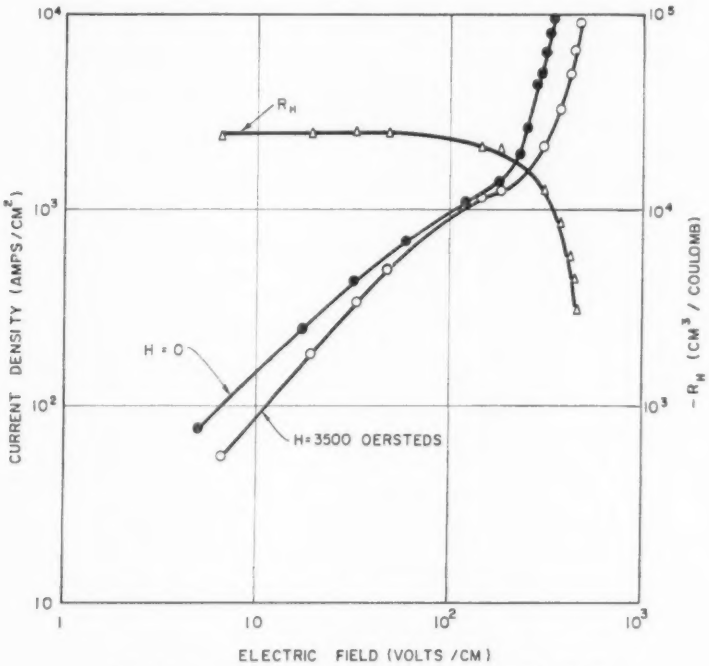


FIG. 1. Current density–electric field characteristics at 77°K for $H = 0$ and a *transverse* $H = 3500$ oersteds. Hall coefficient data are also shown.

The product of the Hall coefficient and the current density gives the average drift velocity, $v_d$, of the electrons. Such measurements have now been made at three values of magnetic field. The maximum values observed are given in Table 1. For $H = 3500$ and 7000 oersteds the values of $v_d$ exhibited saturation for electric fields greater than 300 and 150 V/cm respectively. For $H = 1050$ oersteds $v_d$ was still increasing at $E = 350$ V/cm. Of course these velocity values are average ones only. This average drift velocity of $5{\cdot}4 \times 10^7$

cm/sec can be compared to $\frac{1}{2}$ the value of $v_m$, the velocity* of a carrier having an energy sufficient to cause ionization. Using WOLFF'S[9] criterion of $1{\cdot}5\ E_g$ (or 0·3 eV), this $v_m/2$ is $9{\cdot}4\times10^7$ cm/sec.

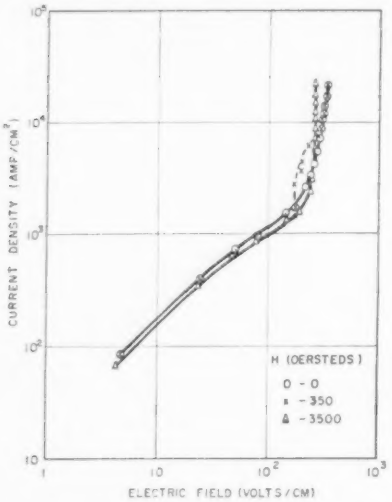


FIG. 2. Current density–electric field characteristics at 77°K for $H = 0$ and longitudinal magnetic fields of 350 and 3500 oersteds.

As is also believed to be the case in the avalanche effects in germanium and silicon, impact ionization is due to the electrons in the high energy tail of the distribution. In this model of the ionization process, a saturation in drift energy is expected due to the presence of the efficient inelastic electron–hole production process which serves as an energy

*Table* 1. *Average drift velocity of electrons in* n-*InSb at* 77°K

| $H$ (oersteds) | $v_d$ (cm sec$^{-1}$) |
|---|---|
| 1050 | $5{\cdot}4\times10^7$ |
| 3500 | $2{\cdot}8\times10^7$ |
| 7000 | $2{\cdot}4\times10^7$ |

* An effective mass of ·03 $m_0$ is assumed for this concentration of electrons. The correct value will depend on the form of the distribution function under these non-equilibrium conditions.

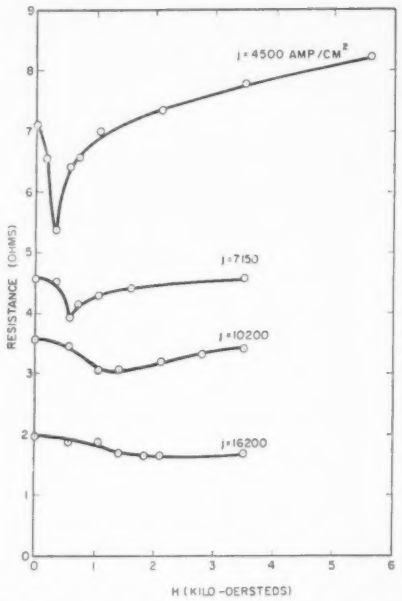


FIG. 3. Resistance at 77°K as a function of longitudinal magnetic field, with current density as a parameter.

sink. The reduction of the saturation velocity may be due to the effect of the magnetic field on the electron distribution function.

A more detailed comparison of the experimental results with available theoretical calculations of the properties of electrons in InSb (equilibrium[4,10] and non-equilibrium[11]) is planned. Additional experiments with more heavily-doped $n$-type and $p$-type InSb are in progress.

## REFERENCES

1. GLICKSMAN M. and STEELE M. C., *Phys. Rev.* **110,** 1204 (1958).
2. KURNICK S. W., STRAUSS A. J. and ZITTER R. N., *Phys. Rev.* **94,** 1791 (1954).
3. MCKAY K. G. and MCAFEE K. B., *Phys. Rev.* **91,** 1079 (1953).
4. KANE E. O., *J. Phys. Chem. Solids,* **1,** 249 (1957).
5. BURSTEIN E., *Phys. Rev.* **93,** 632 (1954).
6. FREDERIKSE H. P. R. and HOSLER W. R., *Phys. Rev.* **108,** 1136 (1957).
7. STEELE M. C., *Phys. Rev.* **97,** 1720 (1955).
8. BABISKIN J., *Phys. Rev.* **107,** 981 (1957).
9. WOLFF P. A., *Phys. Rev.* **95,** 1415 (1954).
10. EHRENREICH H., *J. Phys. Chem. Solids* **2,** 131 (1957).
11. STRATTON R., *Proc. Roy. Soc.* A **242,** 355 (1957).

VOL.
8
1959

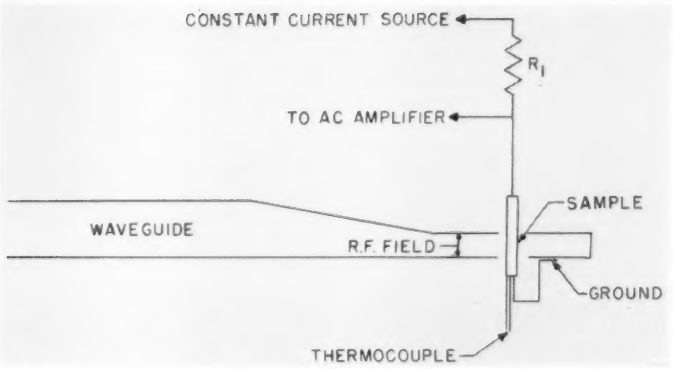


FIG. 1. Crystal mount for applying d.c. and microwave fields to a germanium sample.

facing page 245]

VOL
8
195

*J. Phys. Chem. Solids* Pergamon Press 1959. Vol. 8. pp. 245–249. Printed in Great Britain

I.6

# THE MOBILITY OF ELECTRONS HEATED BY MICROWAVE FIELDS IN *n*-TYPE GERMANIUM*

**T. N. MORGAN**
IBM Watson Laboratory, New York, N.Y.

VOL. 8 1959

MEASUREMENTS of weak field conductivity changes in semiconductors, "warm electron effects", present several experimental problems. Among these are: (1) the difficulty of introducing the disturbing electric field into the crystal without producing contact effects and (2) the inaccuracies in the measurement of the small resistivity changes produced.

In an attempt to circumvent these problems we have superimposed a constant d.c. field and a modulated microwave field along the axis of the sample. By this means the disturbing microwave field is introduced into the crystal without the use of contacts, and its presence produces a modulation of the d.c. resistance which can be measured independently of any other microwave effects.

The microwave circuit delivers a measured amount of power to the sample from which the average field strength in the material can be calculated. The modulation of the d.c. signal can be amplified and detected coherently allowing measurements to be made with microwave field strengths of less than 1 V/cm. A sample holder designed for use at 35 kMc/s is shown in Fig. 1. The unit can be enclosed and cooled from room to liquid nitrogen temperatures.

In addition to providing a convenient method for making weak field measurements, this technique places an additional parameter, the frequency, at the disposal of the experimenter. By varying this parameter he is able to study the heating effects of fields which range from nearly d.c., $\omega\tau \ll 1$, to very high frequencies where $\omega\tau \gg 1$. Here $\tau$ is the relaxation time for momentum.

It is the purpose of this paper to discuss the theory through which these experiments might be understood and to compare it with available experimental results with *n*-type germanium, where possible.

The method applied previously to the d.c. case[1] is extended to the case of two superimposed electric fields. The total field is: $E = E_0 + \mathrm{Re}(E_1 e^{i\omega t})$, parallel to the $z$-axis.

The simpler d.c. case will be treated first, as it defines the quantities appearing later. Both acoustical and optical phonon scattering processes are included and the Boltzmann equation is reduced for solution on a high-speed digital computer. Spherical energy surfaces are assumed except where it is possible to use appropriate averages of the effective mass components.

The Boltzmann equation may be written:

$$\frac{df(v)}{dt} = \frac{-eE_0}{m_z}\frac{\partial f(v)}{\partial v_z} + \frac{\partial f(v)}{\partial t}\Big)_{\text{coll}} \qquad (1)$$

and the function, $f(v)$, expanded in Legendre polynomials in the usual way:

$$f(v) = \sum_{l=0}^{\infty} v^l P_l(\cos\theta) f_l(x);\ x = \frac{mv^2}{2kT}. \qquad (2)$$

For a d.c. field the left side of equation (1) vanishes and $\partial f(v)/\partial v_z$ can be evaluated from equation (2) using terms up to $f_2(x)$. The relaxation time for scattering out of an energy range near $x$ is given in terms of the scattering parameters for acoustical and optical phonons:

$$\begin{aligned} 1/\tau(x) &= W_0\{\sqrt{(x)} + \\ &\quad + B[\sqrt{(x+x_0)} + u(x-x_0)e^{x_0}\sqrt{(x-x_0)}]\} \\ &= W_0\sqrt{(x)}/h(x). \end{aligned} \qquad (3)$$

Here

$$W_0 = \frac{1}{l_{\text{ac}}}\sqrt{\left(\frac{2kT}{m_d}\right)}$$

determines the acoustical scattering; $x_0 = T_0/T$, $T_0$ is the characteristic temperature for the optical phonons, $B = bx_0/2(e^{x_0}-1)$ is the relative scattering strength for

* This project has been supported by the United States Department of Defense.

the optical modes, as $b$ is the ratio of the matrix elements of optical to acoustical phonon scattering; and

$$u(x) = \begin{matrix} 0 & x \leqslant 0 \\ 1 & x > 0 \end{matrix}$$

From a more complete expression for the transition rates out of and into a region of energy space, the collision term can be derived:

$$\frac{\partial f(v)}{\partial t}_{\text{coll}} \equiv \frac{-f(v)+f_0(x)}{\tau(x)} - \frac{W_0 x_1}{6} v P_1(\cos\theta)\left[x f_1''(x)+(x+3)f_1'(x)+\left(\frac{2x}{3}-\frac{3}{2}+\frac{7}{4x}\right)f_1(x)\right]+$$
$$+W_0 x_1 \sqrt{(x)}\left[\frac{x}{2}f_0''(x)+\left(1+\frac{x}{2}\right)f_0'(x)+f_0(x)\right]+$$
$$+W_0 B\{\sqrt{(x+x_0)}[e^{x_0}f_0(x+x_0)-f_0(x)]-u(x-x_0)\sqrt{(x-x_0)}[e^{x_0}f_0(x)-f_0(x-x_0)]\}. \quad (4)$$

Here $x_1 = 4m_d c^2/kT$ specifies the strength of the inelastic part of the acoustical phonon scattering.

Of the four expressions on the right side of equation (4), the first is the normal elastic relaxation term, the last two are the inelastic part for isotropic scattering, and the second contains the angular dependence of the inelastic part.

These equations when combined can be separated into one equation for each value of $l$, and the functions. $f_l(x)$, can be replaced by the dimensionless functions $\phi_{l0}(x)$.

$$f_l(x) = A\beta^l \phi_{l0}(x),$$
$$\phi_{00} = e^{-x}[1+\gamma E_0^2 g_0(x)];$$
$$\int_0^\infty \sqrt{(x)} g_0(x) e^{-x}\,dx = 0; \quad (5)$$

where

$$A = e^{-\frac{\epsilon_c - \epsilon_F}{kT}}; \beta = \frac{eE_0}{W_0 kT};$$
$$\gamma = \frac{2e^2}{3m_\sigma kTW_0{}^2}.$$

The separated equations are:

Equation (7) contains the usual conductivity term plus the field-dependent part, $\delta\phi_{10}(x)$, derived from $\phi_{20}(x)$ and $g_0(x)$. The desired mobility change is

$$\frac{\Delta\mu}{\mu_0} = \int_0^\infty x^{\frac{3}{2}}\delta\phi_{10}(x)dx \Big/ \int_0^\infty x^{\frac{3}{2}}\phi_{10}(x)dx$$

Equation (6) gives the "heating" of the isotropic part of the distribution function. Its physical interpretation is as follows: the field redistributes electrons in energy space as described by the source function, $S'(x)$, while the inelastic phonon processes, represented by $\Gamma g_0(x)$ return the function toward equilibrium, $g_0(x) = 0$. The function $g_0(x)$ is a kind of thermodynamic potential for the flow of particles in energy space. The difference terms arise from the emission and absorption of optical phonons, while the differential terms arise from the acoustical phonon processes.

Solutions have been found to equation (6) with the aid of the University of Illinois digital computer for several values of $x_0$, as reported previously.[1] The parameters were chosen to fit the mobility data for $n$-type germanium; $W_0 = 4{\cdot}14\times \times 10^{12} x_0{}^{-\frac{1}{2}}$ sec$^{-1}$ and $b = 0{\cdot}35$. These give a straight line region in the mobility of slope $1{\cdot}66\pm1$ per cent from 90°K to 340°K. The characteristic optical phonon temperature, $T_0$, was chosen as 436°K as found by BROCKHOUSE snd IYENGAR[2] from neutron scattering. The coefficient of inelasticity for acoustical scattering, $x_1 = 4m_d c^2/kT$, calculated from the longitudinal

$$\Gamma g_0(x) = [x^{\frac{3}{2}}\phi_{10}(x)]' \cong [x^2 h(x)e^{-x}] = S'(x) \quad (6)$$

where

$$\Gamma g = B\sqrt{(x)}\{\sqrt{(x+x_0)}e^{-x}[g(x+x_0)-g(x)]-u(x-x_0)\sqrt{(x-x_0)}e^{-(x-x_0)}[g(x)-g(x-x_0)]+(x_1/2)(x^2e^{-x}g'(x)]'$$

$$\frac{\phi_{10}(x)}{h(x)}+\frac{x_1}{6}\left[x\phi''_{10}(x)+(x+3)\phi'_{10}(x)+\left(\frac{2x}{3}-\frac{3}{2}+\frac{7}{4x}\right)\phi_{10}(x)\right] = x^{-\frac{1}{2}}e^{-x}+\frac{\delta\phi_{10}(x)}{h(x)} \quad (7)$$

$$\delta\phi_{10}(x) = -\gamma E^2 h(x)[x^{-\frac{1}{2}}(g_0(x)e^{-x})'+\tfrac{2}{3}x^{-2}(\phi_{2C}(x)x^{\frac{3}{2}})'] \quad (8)$$

and

$$\phi_{20}(x) = -\tfrac{2}{3}h(x)x^{-\frac{1}{2}}\phi'_{10}(x), \quad (9)$$

VOL 8 195

sound velocity, the density-of-states effective mass, and the value of $T_0$, is $x_1 = x_0/300$. From these $\gamma = 1{\cdot}52 \times 10^{-8} x_0^4$. The results of this calculation are shown in Fig. 2 for the case $x_0 = 2$ corresponding to a temperature of about 220°K. The quantity plotted, $\sqrt{(x)}e^{-x}g_0(x)$, is proportional to the number of electrons of energy $x$, above or below the equilibrium number. The Maxwellian type function corresponding to the same energy transfer is shown for comparison. The striking difference between the two curves is a result of the large energy carried by each optical phonon. These optical phonons account for over 98 per cent of the energy transfer for the Maxwellian function and over 96 per cent for the non-Maxwellian at this temperature. Consequently the most efficient energy loss should occur through electrons having energies slightly above $x_0$, the threshold for the emission of optical phonons. The increased transition probability above this threshold reduces the number of electrons in this region, producing the minimum seen above $x = 2$ and reducing the efficiency of the energy loss. As the total energy lost to the lattice must equal that supplied by the field, the amplitude of $g_0(x)$ increases as its efficiency in transferring energy decreases.

The Maxwellian approximation assumes the existence of another scattering mechanism acting to remove such irregularities and to maintain the Maxwellian shape. Such a mechanism is provided by interelectronic collisions.

The dissimilarity between the two functions explains why a small amount of electron–electron scattering can produce a significant change in the field dependence of the mobility, as discussed by GUNN in his paper, earlier in this session and by SEEGER.[3] The field dependence of the mobility predicted by the non-Maxwellian function is greater by a factor of 4 than that derived with the Maxwellian.

Cases intermediate between these two extremes can be calculated approximately if a relaxation term is added to the Boltzmann equation to describe the relaxation of the isotropic part of the distribution function toward the Maxwellian:

$$\left.\frac{df_0(x)}{dt}\right)_{e-e} = -\frac{f_0(x)-f_{0M}(x)}{\tau_e};$$

$$f_{0M}(x) = A\left(\frac{T}{T^*}\right)^{\frac{3}{2}} e^{-(T/T^*)x}.$$

The effective electron temperature, $T^*$ is chosen to represent the same total energy as the solution, $f_0(x)$:

$$\int x^{\frac{3}{2}} f_0(x)dx = \int x^{\frac{3}{2}} f_{0M}(x)\,dx$$

For small electron concentrations an estimate of the change produced by a constant value of $\tau_e$ is given by the quantity $1/W_0\tau_e$. For the temperature discussed above a 10 per cent effect should be produced by a value of $\tau_e \cong 10^{-11}$. The same value of $\tau_e$ applied to momentum relaxation would reduce the low field mobility by less than 1 per cent. These effects should be enhanced at low temperatures where both $W_0$ and $\tau_e$ are smaller ($\alpha T^{\frac{3}{2}}$).

When superimposed d.c. and a.c. fields are applied to the sample, two new effects appear. The $E^2$ heating now arises through 3 terms—one d.c. part, $E_0^2$, one a.c. part of frequency $\omega$, $E_0E_1 \sin \omega t$ and one a.c. part in $\sin^2 \omega\tau$, $\frac{1}{2}E_1^2$ $(1-\sin 2\omega t)$. The first and the constant part of the third describe a d.c. modulation of the resistance. The second describes a.c. modulation of the resistance, which is coherent with the a.c. field and can therefore cause a change in the d.c. current. The other time dependent terms produce no average current flow.

The equations for this case resemble equation (6), (7), (8) and (9) except that there are three sets—one for each term of $E^2$.

Let the functions associated with $E_0^2$ be $g_0(x)$, $\phi_{10}(x)$, and $\phi_{20}(x)$ as before, those with $E_0E_1e^{i\omega t}$ be $g_1(x)$, $\phi_{11}(x)$ and $\phi_{21}(x)$ and those with $\frac{1}{2}E_1^2$ be $g_2(x)$ and $\phi_{22}(x)$. The functions $g_1(x)$, $\phi_{11}(x)$, and $\phi_2(x)$ may be complex, as their phases will, in general differ from that of the a.c. field.

For the d.c. functions equations (6), (7), (8) and (9) are the same except that $\delta\phi_{10}(x)$ now includes the added terms in $g_1(x)$, $g_2(x)$, $\phi_{21}(x)$ and $\phi_{22}(x)$.

$$\delta\phi_{10}(x) = -\gamma h(x)\{x^{-\frac{1}{2}}[E_0^2(g_0(x)e^{-x})' + \tfrac{1}{2}E_1^2(\mathrm{Re}\,g_1(x)e^{-x} + g_2(x)e^{-x})'] + \\ + \tfrac{6}{5}x^{-2}[E_0^2(\phi_{20}(x)x^{5/2})' + \tfrac{1}{2}E_1^2(\mathrm{Re}\,\phi_{21}(x)x^{5/2} + \phi_{22}(x)x^{5/2})']\} \quad (8a)$$

with $\omega\tau = q(x) = \dfrac{\omega}{W_0}\dfrac{h(x)}{\sqrt{(x)}}$ the a.c. contributions are:

$$\Gamma g_2(x) = \mathrm{Re}(x^{\frac{1}{2}}\phi_{11}(x))' \cong [s(x)/\{1+q^2(x)\}]' \tag{10}$$

$$\phi_{22}(x) = -\tfrac{2}{3}x^{-\frac{1}{2}}h(x)\mathrm{Re}\phi'_{11}(x) \tag{11}$$

$$\mathrm{Re}\Gamma g_1(x) + \frac{\omega}{W_0}\sqrt{(x)}e^{-x}\mathrm{Im}\,g_1(x) = \{x^{\frac{1}{2}}[\phi_{10}(x)+\mathrm{Re}\phi_{11}(x)]\}'$$

$$= \left[s(x)\left(1+\frac{1}{1+q^2(x)}\right)\right]' \tag{12}$$

$$\mathrm{Im}\Gamma g_1(x) + \frac{\omega}{W_0}\sqrt{(x)}e^{-x}\mathrm{Re}g_1(x) \cong \left[s(x)\frac{q(x)}{1+q^2(x)}\right]'$$

$$\frac{\phi_{11}(x)}{h(x)} + \frac{x_1}{6}\left[x\phi''_{11}(x)+(x+3)\phi'_{11}(x)+\left(\frac{2x}{3}-\frac{3}{2}+\frac{7}{4x}\right)\phi_{11}(x)\right] = x^{-\frac{1}{2}}e^{-x}/\{1+iq(x)\} \tag{13}$$

and

$$\mathrm{Re}\phi_{21}(x) = -\tfrac{2}{3}x^{-\frac{1}{2}}h(x)[\phi_{10}'(x)+\mathrm{Re}\phi_{11}'(x)+q(x)\mathrm{Im}\phi'_{11}(x)]/[1+q^2(x)] \tag{14}$$

The terms of interest in the interpretation of the experiment described above are those in $\delta\phi_{10}(x)$ containing $E_1^2$. In the low frequency limit, $q \to 0$, all of the equations reduce to their d.c. counterparts except that:

$$\phi_{21}(x) = 2\phi_{20}(x);\ g_1(x) = 2g_0(x)$$

and the $E_1^2$ components of $\delta\phi_{10}(x)$ are three times the $E_0^2$ components. Thus the a.c. method provides a signal gain of a factor of three over similar d.c. measurements.

As the frequency is increased, $q(x)$ becomes appreciable for low energy electrons and reduces the effectiveness of the a.c. field. These high frequencies, like the electron–electron and ion scattering, produce more pronounced effects at low temperatures. The solution of these equations for high frequencies has been begun at the IBM Computing Center in Poughkeepsie although no results are available. However, the frequencies at which these effects should become apparent can be estimated from the magnitudes of $q(1)$ at different temperatures.

At the temperature considered above, 220°K, $q(1) = 6\times10^{-13}\omega$ and $q^2(1) = 0{\cdot}01$ at a frequency of 26 kMc/s in the microwave $k$-band. At this same frequency, however, $q^2(\frac{1}{10})$, where the minimum appears in Fig. 2, is approximately

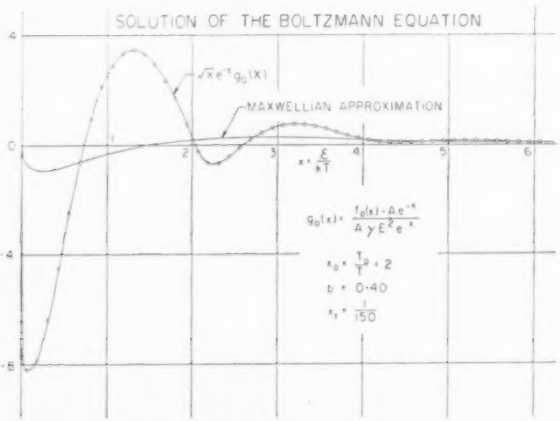


FIG. 2. Redistribution of electrons in energy space. The ordinate is proportional to the change produced by an electric field on the electron concentration in germanium at 220°K.

0·08. At 110°K nearly the same $q(x)$ values would occur at 9 kMc/s.

A plot of data taken with a 20 Ω-cm $n$-germanium sample, $n = 6{\cdot}7\times10^{13}$, at 35 kMc/s, ($\omega = 2{\cdot}2\times10^{11}$) is compared in Fig. 3 with the calculated d.c. theory for the two limiting distribution functions. The experimental values are seen to approach at high temperatures the curve calculated from the Boltzmann equation but to deviate towards the Maxwellian solution at low temperatures. This is as expected, although the low temperature deviation can be attributed to either interelectronic and ionic collisions or high frequency effects. Frequency effects are surely present at $x_0 = 4$ as $q^2(1) \simeq \frac{1}{4}$ at this temperature. Additional experiments are now being run at 8 kMc/s ($\omega = 5\times10^{10}$) for comparison with the higher frequency results. The excellent agreement at high temperatures is undoubtedly fortuitous as only partial corrections have been made for the anisotropy of the valleys, and the orientation of the sample is not known. The mass $m_\sigma$ which occurs in $\gamma$ (following equation (5)) should be replaced by $(m_s/m_\sigma)^2$ where $1/m_s^2$, the average value of $1/m_z^2$ in the four valleys, depends on the sample orientation. The ratio $(m_\sigma/m_s)^2$ can range from 1·0 to about 1·2.

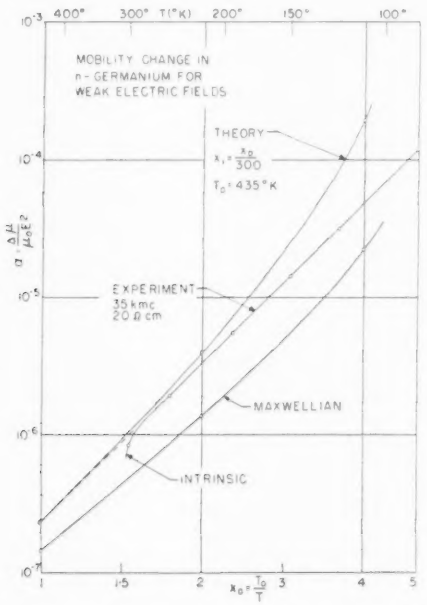


FIG. 3. Electric field dependence of the electron mobility in germanium: theory and experiment.

*Acknowledgments*—Of the many people who have contributed to this work I wish particularly to thank Dr. J. BARDEEN, Dr. P. J. PRICE, and the University of Illinois Computing Center for their generous help given from the initiation of this project.

## REFERENCES

1. MORGAN T. N., *Bull. Amer. Phys. Soc.*, Ser. II, **2**, 265 (1957); *Ibid.* Ser. II, **3**, 13 (1958).
2. BROCKHOUSE B. N. and IYENGAR P. K., *Bull. Amer. Phys. Soc.* Ser. II, **3**, 192 (1958).
3. SEEGER KARLHEINZ, *Bull. Amer. Phys. Soc.* Ser. II, **3**, 112 (1958).

*J. Phys. Chem. Solids* Pergamon Press 1959. Vol. 8. pp. 250–256. Printed in Great Britain

# I.7 ANISOTROPY OF HOT ELECTRONS IN GERMANIUM

W. SASAKI, M. SHIBUYA, K. MIZUGUCHI AND G. M. HATOYAMA

Electrotechnical Laboratory, Physics Section, Nagatacho, Tokyo, Japan

**Abstract**—An electromotive force perpendicular to the current flowing in *n*- and *p*-type germanium samples is observed. The angle of deviation of the electric field vector from the current vector is a function of field strength, temperature, and current orientation, and exceeds 20° in some cases. This anisotropy of electric conduction can be attributed to the anisotropy of the energy surfaces of the conduction and valence bands of germanium.

VOL
8
195

## 1. INTRODUCTION

ELECTRIC conduction in cubic crystals, such as silicon and germanium, is expected to become anisotropic under high electric fields where Ohm's law fails.[1] When the conduction becomes anisotropic the direction of the electric field vector is not always parallel to that of the current vector. Such deviations can be observed as a component of electric field perpendicular to the current direction.[2,3]

We have measured this effect in *n*- and *p*-type germanium specimens as a function of electric field, temperature, and the direction of current relative to the crystal axis. In this paper, these experimental results are described, and the mechanisms involved are considered.

## 2. EXPERIMENTAL

Germanium samples with room temperature resistivity of 5 to 20 Ω-cm were chosen from *n*- and *p*-type single crystals prepared by zone levelling. Slices were cut about 3 mm thick in the (110) plane of the crystal lattice, and filaments with large area current electrodes and transverse potential electrodes, as shown in Fig. 1, were prepared by a magnetostrictive cutter. Filaments lying along various directions between ⟨110⟩ and ⟨001⟩ were prepared. The angle $\theta$ defining the filament direction is chosen as shown in Fig. 1.

Filaments were etched with CP 4.

Measurements were made with pulsed current in order to avoid a temperature rise in the filaments at high electric fields. The voltage pulses were measured by measuring the pulse height on the cathode ray tube of a synchroscope. In many cases pulses of 0·3 to 0·5 μsec duration and repetition rate of 50 pulses per second were used.

Measurements were carried out at temperatures of 290°K, 200°K, and 90°K.

Fig. 2 shows the field dependence of the current density and the transverse voltage of an *n*-type germanium filament, whose direction deviates by 30° from ⟨001⟩ axis, at 90°K. Three regions are seen in the current density curve as has been pointed out by RYDER and SHOCKLEY.[4–6] In the first region Ohm's law is valid, in the second Ohm's law fails and the current is nearly proportional to the square root of electric field, and in the third the current is almost constant.

A spurious transverse voltage proportional to the longitudinal electric field, caused by assymmetry in the transverse probes, appears in the first region. Another component of transverse voltage, which differs from that in the first region in regard to its dependence on longitudinal field, appears in the second region. This component grows rapidly and attains its maximum value before the third region begins.

In order to obtain the transverse field due to the anisotropy of hot electrons, the spurious component due to the probe asymmetry, which is easily estimated from the low field data, must be subtracted from the observed voltage. Thus the tangent of the angle $\epsilon$ between current and electric field vectors due to anisotropy of hot electrons is calculated and is shown in Figs. 3 and 4.

In these figures, tan $\epsilon$ is plotted against longitudinal electric field for an *n*-type filament with $\theta = 30°$ (Fig. 3) and for a *p*-type one with $\theta = 15°$ (Fig. 4) for the various temperatures indicated.

The arrows in these figures show the value of tan $\epsilon$ at the critical field, which is defined as the intersection of two straight lines representing the first and second regions in the current vs. field plot mentioned above. It is seen that the lower the temperature the lower is the field where the angle becomes observable, the lower the field $E_d$ where the angle attains the maximum value, and the larger the maximum angle. It seems that the curves corresponding to different temperatures

## 3. DISCUSSION

### 3.1. *n-type*

The anisotropy of hot electrons in cubic semiconductors with spheroidal energy surfaces was calculated by one of the authors (M.S.).[1] His theory, which explains the hot electron anisotropy is illustrated in a simplified model in Fig. 6(a) where only two spheroids A and B are considered. An electric field $E$ is applied in the direction nearer to the rotation axis of spheroid

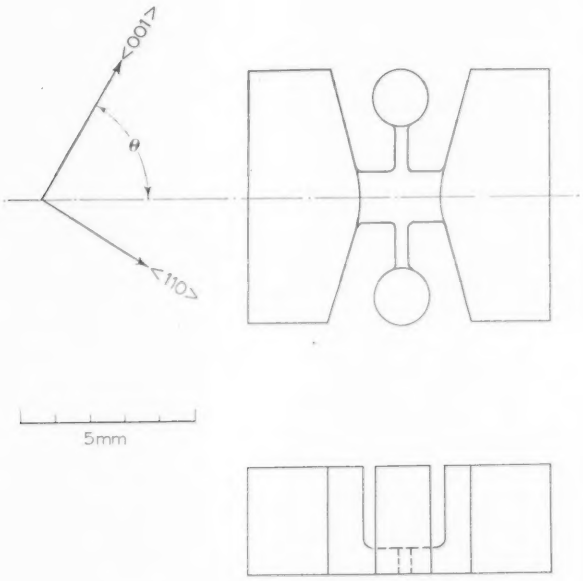


FIG. 1. Shape of the specimens.

tend asymptotically to a single curve which depends only on the type of conduction and $\theta$ of the specimen.

The direction of the deviation of the electric field vector from the current vector is such that the electric field lies nearer to $\langle 111 \rangle$ axis than the current vector in $n$-type and the reverse is in $p$-type specimens. Fig. 5 shows the angle $\epsilon$ as a function of $\theta$ measured at the field strength of $E_d$, or 750 V/cm for $n$-type and 2000 V/cm for $p$-type specimens, and at the temperature of 90°K. The sign of $\epsilon$ was taken positive for $n$-type specimens with $\theta$ smaller than 50°.

A. The electric current produced by electrons with prolate spheroidal energy surfaces lies further from the axis of rotation, and current components as shown in Fig. 6(a) are produced. These components sum up to an electric current vector parallel to the electric field vector as long as Ohm's law holds. The magnitude of the effective mass of an electron with prolate energy surface is a function of the direction of the electric field relative to the axis of rotation of the spheroid, and is larger the smaller the angle between electric field and the rotation axis. When the electric field becomes larger, the temperature of the electrons in valley B,

with smaller effective mass, becomes higher than that of those in valley A, and this difference of electron temperatures makes the current shared by group A larger than that by group B at higher

is shown in Fig. 5 by a broken line. The result is in good qualitative agreement with experiment, but the theory gives values of $\epsilon$ that are too small. Also the theory can not predict the

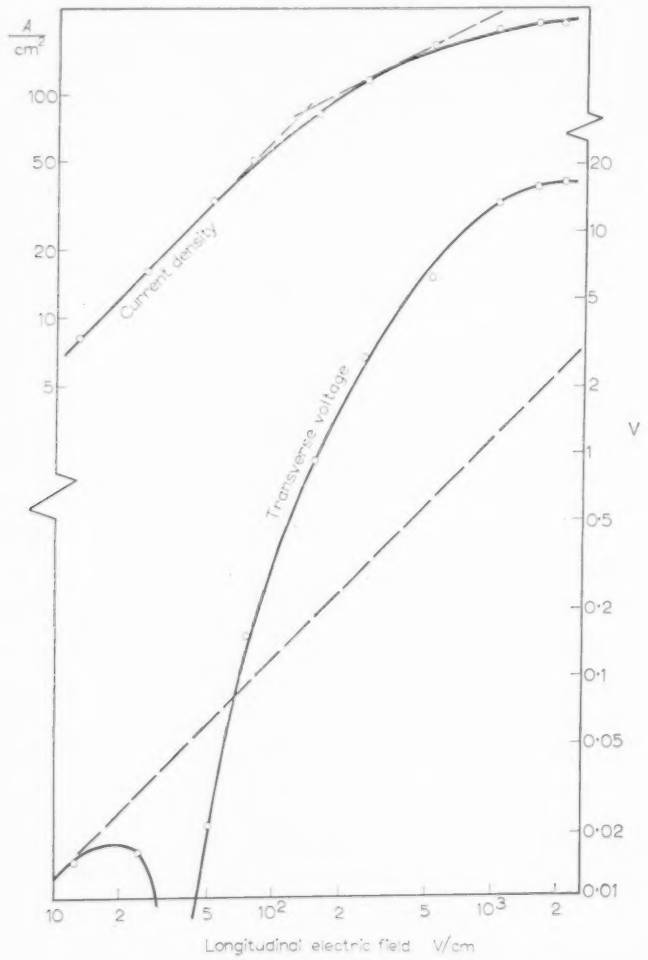


FIG. 2. Dependence of current density and transverse voltage on longitudinal electric field in an $n$-type specimen with $\theta = 30°$, measured at 90°K.

electric field. These situations are shown in Fig. 6(b). For $n$-type germanium of course, the four spheroids with their axes lying along $\langle 111 \rangle$ directions should be taken into account.[7] The result of Shibuya's calculation for $n$-germanium field and temperature dependence of $\epsilon$ observed experimentally.

In Shibuya's calculation it is assumed that the number of electrons in a valley does not change from that at thermal equilibrium in spite of the

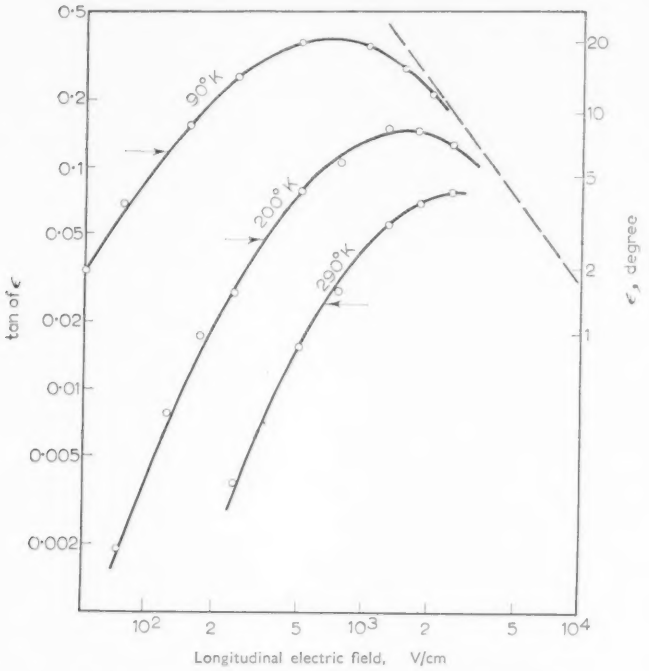


FIG. 3. Tan $\epsilon$ vs. electric field for an $n$-type specimen. Arrows show the value of tan $\epsilon$ at the critical field.

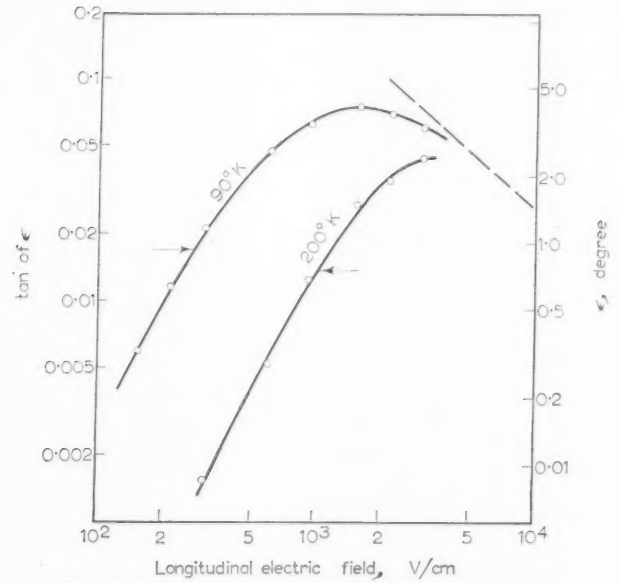


FIG. 4. Tan $\epsilon$ vs. electric field for a $p$-type specimen. Arrows show the value of tan $\epsilon$ at the critical field.

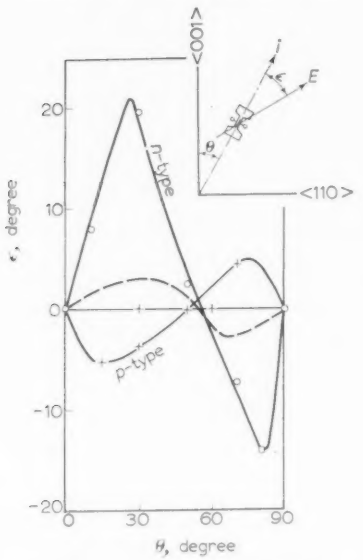


FIG. 5. $\epsilon$ vs. $\theta$ measured at 90°K. Full lines show the experimental data and the broken line shows SHIBUYA's calculation for $n$-type germanium.

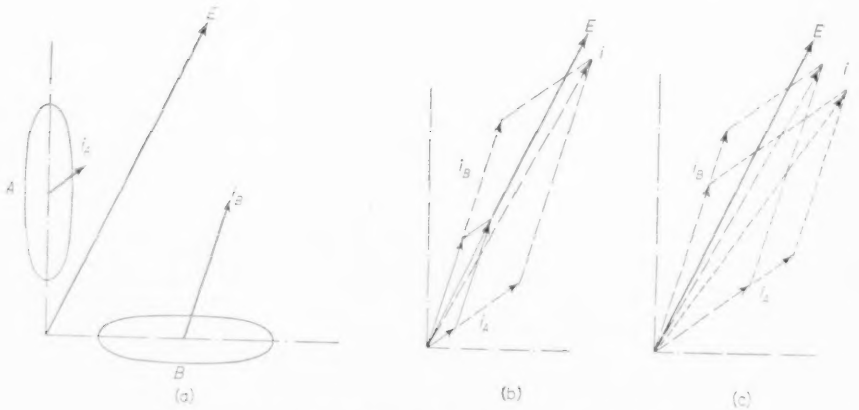


FIG. 6. (a) Simplified spheroidal model. $i_A$ and $i_B$ show the current components shared by valleys A and B. (b) Current directions in low field (full lines) and high field (broken lines). (c) Current directions in high fields without (broken lines) and with (dotted lines) intervalley transitions.

difference between the temperatures of the electrons in different energy valleys. There must be a natural tendency, however, for the electrons in a valley at higher temperature to be scattered to a valley at lower temperature, and consequently for the electron density in high temperature valleys to become smaller than that in the low temperature valleys. This tendency will make the current carried by electrons in high temperature valleys less and that in low temperature valleys more than the case calculated by Shibuya, and the angle of deviation will become larger. This situation is also shown in Fig. 6(c). If we refer to Fig. 5, the major part of $\epsilon$ is due to the latter mechanism, i.e., a difference in electron density among valleys.

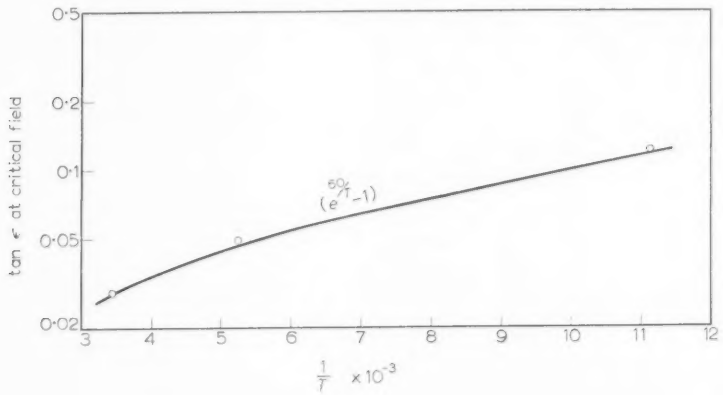


FIG. 7. Tan $\epsilon$ in logarithmic scale vs. inverse absolute temperature.

This difference of electron density should be inversely proportional to the number of intervalley phonons by which electrons in low temperature valleys are scattered back to high temperature valleys. Thus the angle of deviation depends on the lattice temperature. In Fig. 7, $\epsilon$ at the critical field is plotted as a function of the temperature of the crystal. The curve in the figure is proportional to $\exp(60/T)-1$. This shows that the energy of the intervalley phonons is approximately 60°K.

The existence of a maximum in the $\epsilon$ vs. electric field curve suggests that the electron density difference between valleys becomes smaller for fields greater than $E_q$. A possible reason for this is intervalley transitions, which become more frequent when the temperature of the electrons in all valleys becomes very high. Another reason may be the possible existence of fairly low energy saddle points in $k$ space between the valleys.

### 3.2. *p-type*

The valence band of germanium consists of a set of warped spheres:[7] the holes making the major contribution to the conductivity are in one of them, whose shape is approximated by a cube. The $\theta$-dependence of $\epsilon$ shown in Fig. 5 may be realized with such an energy surface as follows: An electric field lying nearer to the $\langle 001 \rangle$ axis as shown in Fig. 8 accelerates holes on cube sides AD and BC only by its $\langle 001 \rangle$ component and those on AB and CD only by its $\langle 110 \rangle$ component. The two current components $i_{AB+CD}$ and $i_{AD+BC}$ sum up to a total current which is parallel to the electric field when Ohm's law holds. However, for electric fields sufficiently high to make holes on sides AD and BC hot enough to decrease their mobility and not so high as to decrease the mobility of the holes on the other sides, the total current deviates towards a direction nearer the $\langle 111 \rangle$ axis than the electric field. This mechanism explains the $\epsilon$ vs. $\theta$ curve qualitatively. In order to explain the difference in temperature of the holes on different parts of the same energy surface it is necessary to assume a very peculiar energy surface in $q$ space of the phonons which allow more frequent transitions between opposite sides

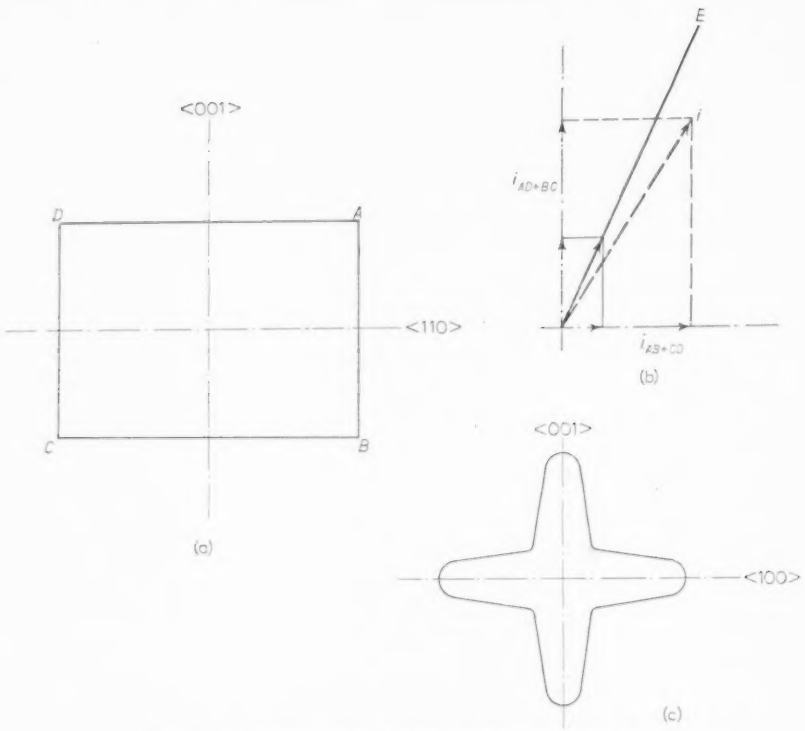


FIG. 8. (a) Approximated warped sphere energy surface for *p*-type germanium.
(b) Current directions in low electric fields (full lines) and high fields (broken lines).
(c) Projection of an energy surface for phonons in *q* space on (010) plane.

compared to those between adjacent sides. One such energy surface is proposed in Fig. 8(c).

*Acknowledgments*—The authors are grateful to M. KIKUCHI for the preparation of good crystals and to Z. ISHII for X-ray determination of the crystal axes.

## REFERENCES

1. SHIBUYA M., *Phys. Rev.* **99,** 1189 (1955).
2. SASAKI W. and SHIBUYA M., *J. Phys. Soc. Japan* **11,** 1202 (1956).
3. SASAKI W., SHIBUYA M. and MIZUGUCHI K., *J. Phys. Soc. Japan* **13,** 456 (1958).
4. RYDER E. J. and SHOCKLEY W., *Phys. Rev.* **81,** 139 (1951).
5. SHOCKLEY W., *Bell Syst. Tech. J.* **30,** 990 (1951).
6. RYDER E. J., *Phys. Rev.* **90,** 766 (1953).
7. LAX BENJAMIN, *Rev. Mod. Phys.* **30,** 122 (1958).

*J. Phys. Chem. Solids* Pergamon Press 1959. Vol. 8. pp. 257–259. Printed in Great Britain

I.8

# THE EFFECT OF UNIAXIAL TENSILE STRESS ON IMPURITY CONDUCTION IN GERMANIUM*

H. FRITZSCHE

Institute for the Study of Metals, University of Chicago

## 1. INTRODUCTION

A STUDY of the effect of stress on impurity conduction in semiconductors,† containing small concentrations of impurities, may yield interesting information concerning the factors which determine the probability of charge carriers for jumping from occupied to neighboring unoccupied impurity states. Since neighboring impurity sites are energetically not completely equivalent,[1,2] the jump frequency is not simply the resonant exchange frequency as obtained from the exchange integral for the two localized orbitals, but is expected to be affected by the interaction of the charge carriers with the lattice.

In unstrained *n*-type germanium the impurity ground states are degenerate because of the 4 equivalent conduction band minima.[3] The corresponding wavefunctions have cubic symmetry leading to an isotropic resistivity. Upon the application of uniaxial stress the degeneracy will in general be removed[3,4] and the form of the wavefunctions will change to adjust to the new symmetry conditions. One consequently expects the resistivity $\rho_\chi$ of the strained crystal to become anisotropic and quite different from $\rho_0$, the resistivity at zero strain.

This paper reports measurements of the piezoresistance of *n*-type germanium, which contained $1{\cdot}4\times10^{16}$ antimony atoms/cm$^3$ and 2–6 per cent compensation, in the temperature range of impurity conduction (1·3 to 5°K) and at higher temperatures. Tensile stress $\chi$ extending from $1\times10^7$ to $3\times10^8$ dynes/cm$^2$ was applied in the [110] direction. Three directions for the current I were considered, I in direction [110] (case A), [001] (case B), and [$\bar{1}$10] (case C).

## 2. EXPERIMENTAL

The specimens were oriented to within 0·5°, cut to rectangular bars of about 0·01 cm$^2$ cross-section and 2·5 cm length, the surface was etched, and leads were attached by soldering. The contacts were found to be ohmic at all temperatures. The presence of the contacts influences the results by a few per cent due to their different thermal expansion coefficient. In case A the contacts were repeatedly resoldered and dummy contacts were added in their vicinity. In the cases B and C the lengths of the two large area contacts were doubled. Re-alignment of the specimens in their holders gave rise to changes in $\rho_\chi/\rho_0$ of several per cent without, however, affecting the essential features of the measurements.

In Fig. 1 the ratio $\rho_\chi/\rho_0$ is plotted against stress for the cases A, B, and C for various temperatures in the impurity conduction range. The dependence of $\rho_\chi/\rho_0$ on $\chi$ is far from being linear. In case A small stresses cause $\rho$ to decrease at $T > 2{\cdot}2$°K. At higher $\chi$, $\rho_\chi/\rho_0$ increases rapidly until it approaches a saturation value near $\chi = 2{\cdot}5\times10^8$ dyn/cm$^2$. In the transverse cases B and C $\rho_\chi/\rho_0$ increases less rapidly at large stresses but without showing a saturation.

Fig. 2 shows in its upper half the temperature dependence of $\rho_0$ and in its lower half that of $\rho_\chi/\rho_0$ measured at $\chi = 3\times10^8$ dyn/cm$^2$ for the three current directions. At higher temperatures $\rho_\chi/\rho_0$ agrees very well with the results obtained at the Bell Laboratories.[5] In the range of impurity conduction, i.e. below $T = 5$°K, the temperature dependence of $\rho_\chi/\rho_0$ has the form $\rho_\chi/\rho_0 \sim \exp(\epsilon/kT)$. The value of $\epsilon$, which is to within a few per cent the same for all three current directions is a function of $\chi$. It increases from zero with

* This work was supported in part by the National Science Foundation through the grant NSF-G-3489 and by the U.S. Atomic Energy Commission through the Contract AT(11-1)-357.

† For further references to papers on impurity conduction see reference 2.

increasing $\chi$, approaches a value of $\epsilon = 1{\cdot}6\times10^{-4}$ eV near $\chi = 2\times10^{8}$ dyn/cm, and then remains constant up to the highest $\chi$ applied. The resistivity of the stressed specimen is anisotropic. The values of $\rho_\chi$ measured at $\chi = 3\times10^{8}$ dyn/cm$^2$ in the three current directions are related as $\rho_\chi$(A): $\rho_\chi$(B): $\rho_\chi$(C) = 1:1·4:2.

discussed by PRICE,[4] and the changes of the ground state wave-functions should have a strong effect on impurity conduction. A stress of $3\times10^{8}$ dyn/cm$^2$ in the [110] direction causes one pair of ground state levels to move down by about $10^{-3}$ eV, the other pair to move up by approximately the same amount. This splitting is large compared

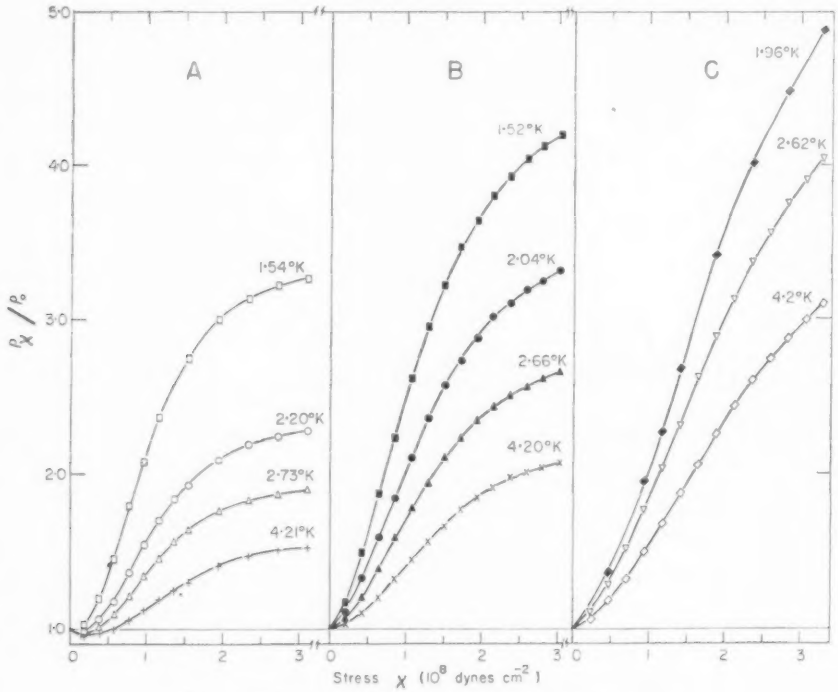


FIG. 1. The ratio $\rho_\chi/\rho_0$ as a function of uniaxial tensile stress in the [110] direction for three directions of the current $I$. Case A: $I$ [110], case B: $I$ [001], case C: $I$ [$\bar{1}$10].

### 3. DISCUSSION

It is difficult to determine accurately the influence of the contacts and the influence of possible inhomogeneities in the stress distribution and in the distribution of the impurities. The results have, therefore, to be considered preliminary. Because of the large size of the resistivity changes, one can however exclude the stress induced changes of the average impurity separation and of the dielectric constant as possible explanations for the observed effects.

The splitting of the impurity ground states, first to $kT$ below 4°K so that one can assume that only electrons occupying the lowest two ground state levels participate in impurity conduction.

These two lowest states are degenerate in the effective mass approximation. They split up, however, if corrections due to the potential in the immediate vicinity of the impurity atoms are taken into account.[3,4] This "chemical shift" is of the order of $1{\cdot}5\times10^{-4}$ eV for antimony in germanium. The corresponding two wavefunctions are, at large stresses, the symmetric and antisymmetric linear combinations of the solutions

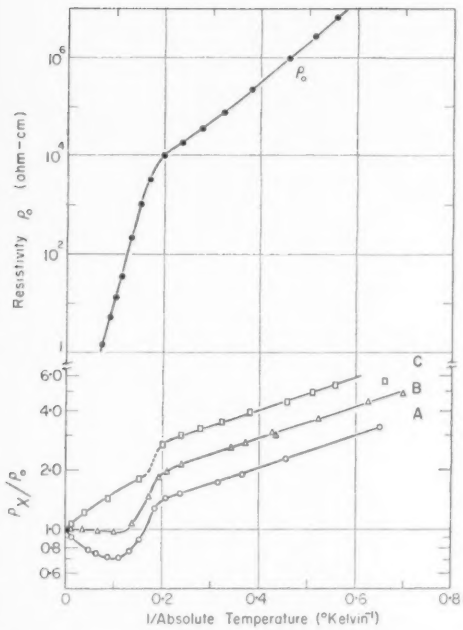


FIG. 2. *Upper part*: zero strain resistivity $\rho_0$ as a function of $1/T$. From the slope of the curve below 3°K one obtains $\epsilon_3 = 1{\cdot}5 \times 10^{-3}$ eV (for a definition of $\epsilon_3$ see reference 2).
*Lower part*: The ratio $\rho_\chi/\rho_0$ measured at $\chi = 3 \times 10^8$ dyn/cm$^2$ as a function of $1/T$ for the longitudinal case A and the two transverse cases B and C. The slope of the curves below 5°K yields $\epsilon = 1{\cdot}6 \times 10^{-4}$ eV (see text).

of the effective mass equation for the two depressed valleys, which lie in the $[1\bar{1}0]$ and the $[1\bar{1}\bar{1}]$ direction respectively. These wavefunctions extend farther in the [110] direction than in the [001] direction and fall off most rapidly in the $[\bar{1}10]$ direction. This fact may possibly give rise to the observed anisotropy of $\rho_\chi$ in the range of impurity conduction.

It has so far been impossible to explain the exponential temperature dependence of $\rho_\chi/\rho_0$. Since the impurity ground state levels are broadened by approximately $3 \times 10^{-4}$ eV due to zero point vibrations of the lattice[6] and due to exchange interaction with neighboring impurities, $\epsilon$ cannot be interpreted as a splitting of electronic energy levels. The fact that $\epsilon$ is observed in a temperature range in which $kT \geq \epsilon$ indicates that $\epsilon$ is more likely a stress induced change of the ten times larger low temperature slope $\epsilon_3$[2] of the zero strain resistivity curve.

## REFERENCES

1. JAMES H. M., *Quarterly Report*, Oct.–Dec. 1956, Purdue University.
2. FRITZSCHE H., *J. Phys. Chem. Solids*, **6**, 69 (1958).
3. KOHN W., *Solid State Physics* **5**, 257 (1957).
4. PRICE P. J., *Phys. Rev.* **104**, 1223 (1956).
5. SMITH C. S., *Phys. Rev.* **94**, 42 (1954); MORIN F. J., GEBALLE T. H. and HERRING C., *Phys. Rev.* **105**, 525 (1957).
6. LAX M. and BURSTEIN E., *Phys. Rev.* **100**, 592 (1955).

*J. Phys. Chem. Solids* Pergamon Press 1959. Vol. 8. pp. 259–263. Printed in Great Britain

I.9

# LOW TEMPERATURE IMPURITY CONDUCTION IN SILICON

T. A. LONGO, R. K. RAY AND K. LARK-HOROVITZ

Department of Physics, Purdue University, Lafayette, Indiana

## 1. INTRODUCTION

IMPURITY conduction has been observed in silicon samples containing B, Al, As or Sb. The measurements were made using standard techniques for measuring Hall coefficient and resistivity at low temperature. In the family of Hall curves for any one impurity the Hall maximum, which indicates the onset of impurity conduction, moves to higher temperature and lower values as the impurity concentration of the samples is increased.[1] In

the region of impurity conduction, the resistivity curves have slopes corresponding to activation energies about an order of magnitude less than that for impurity ionization energies. The curves for samples with $10^{18}$ cm$^{-3} < N_{maj} < 5\times10^{18}$ cm$^{-3}$ are of rather complex nature and exhibit more than one resistivity slope and often more than one Hall maximum.

## 2. DISCUSSION OF THE SEPARATE RANGES OF IMPURITY CONDUCTION

The breakdown of the phenomenon into separate ranges can best be illustrated by the plot of resistivity at 14.2°K against $N_{maj}$ for many B doped samples in Fig. 1. This curve is similar to one

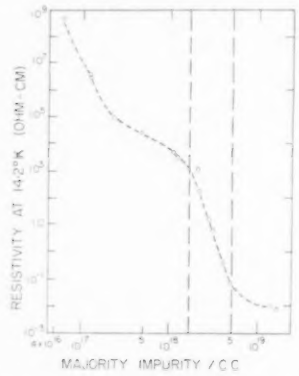


FIG. 1. The resistivity of B doped silicon at 14·2°K vs. the majority impurity concentration.

used by FRITZSCHE[2] and discussed at length by JAMES[3] for germanium.

For $N_{maj} < 10^{18}$ cm$^{-3}$ the conduction process is believed to be one of charge permutation between randomly distributed impurities. This can only occur if at least a small amount of compensation exists for the purpose of providing empty majority sites. Additional compensation should enhance the effect in this range. According to MOTT[4] when $N_{maj} \gg N_{min}$ the activation energy for this type of impurity conduction should be of the order $\epsilon = 2e^2k^{-1}N_{maj}^{\frac{1}{3}}$. The activation energies, taken from the low temperature slopes of sample resistivities in the low impurity concentration range, increase with increasing impurity concentration approximately in the manner indicated by MOTT.

For samples with $N_{maj} > 5\times10^{18}$ cm$^{-3}$ the Hall mobilities are higher than for samples in the low concentration range. This conduction is believed to take place in a band within the forbidden gap which is made up of randomly distributed impurity states which are close enough together such that the wave functions overlap. The conduction in such a band would then be similar to metallic conduction in a half filled band. For such a case compensation should decrease the number of carriers participating, without improving the mobility of these carriers and thereby decrease the effect.

The sharp drop in resistivity between the high and low concentration range has been termed the transition range by JAMES, who reasons that in going from the isolated impurity case to the overlapping wave function condition there may be a transition range in which conduction may take place along preferred paths of impurities.

## 3. INTRODUCTION OF IMPURITY COMPENSATION

Irradiation with 10 MeV deuterons was used to introduce controlled amounts of compensation in B and Sb doped samples. Previous knowledge[5] of the location of the irradiation introduced defect states made it possible to tailor the experiments in such a way that the defect states did not influence the observation of the chemical impurity conduction, other than the effect desired due to compensation. The Hall coefficient curves of Fig. 2 show the chemical impurity conduction for three B doped samples from the low, intermediate and

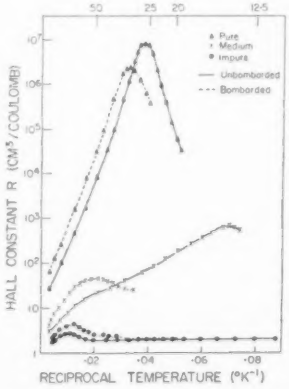


FIG. 2. The effect of compensation by deuteron irradiation on the Hall coefficient of B doped silicon samples in the impurity conduction temperature range.

high impurity ranges before and after introducing about 15–25 per cent compensation by irradiation.

For the purest sample, the manner in which the process is enhanced by compensation is strikingly evidenced by the shift of the Hall maximum to higher temperature and lower value. The corresponding resistivity curves showed a decrease in the activation energy characterizing the process from $5{\cdot}34\times10^{-3}$ eV to $3{\cdot}4\times10^{-3}$ eV. This amount of decrease agreed rather well with that predicted by the approximate relation, after KOENIG and GUNTHER-MOHR,[6] for the activation energy in samples containing appreciable compensation $\epsilon \cong 0{\cdot}62e^2k^{-1}(N_{\mathrm{maj}}^{\frac{1}{3}}-N_{\mathrm{min}}^{\frac{1}{3}})$.

The results from the most impure sample indicate that the impurity conduction has decreased considerably at intermediate temperatures but is relatively unaffected at temperatures below about 25°K. The corresponding resistivity curve however shifted upward over the whole temperature range. The Hall coefficient results for the same sample are shown again in Fig. 3 before and after

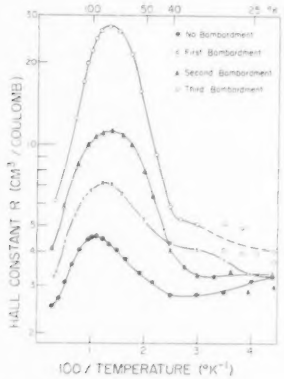


FIG. 3. Hall coefficient of near degenerate B doped silicon in the impurity conduction range after successive deuteron irradiations.

three successive irradiations. It is not clear why the curve after the second irradiation crossed over that for the first irradiation in the vicinity of 40°K. However all four curves come approximately together below about 25°K (not shown in Fig. 3). The Fermi level remains between the acceptor state introduced by deuteron irradiation and the valence band for every stage of irradiation. Therefore it is possible that the hole filled defect acceptor states have formed a second band which manifests itself below about 25°K and the sum of the contributions from the partially filled chemical band and the filled defect band is approximately equal to the contribution from the filled chemical impurity band before compensation.

Still another interesting result in Fig. 3 is the increase in the B impurity ionization energy from 0·0095 eV to 0·017 eV after successive irradiations. This is due, in part at least, to the removal of screening of the impurity states by free carriers.

Referring back to Fig. 2, the intermediate sample has been selected from the transition range. After the first maximum the Hall coefficient curves rise again; a second maximum sometimes follows. The resistivity curves for such samples can be characterized by three slopes in the manner indicated by FRITZSCHE.[2]

$$\frac{1}{\rho} = c_1\exp(-\epsilon_1/kT)+c_2\exp(-\epsilon_2/kT)+ +c_3\exp(-\epsilon_3/kT)$$

where $\epsilon_1$ is the usual impurity ionization energy, $\epsilon_3$ is the activation energy for impurity conduction found in the low concentration samples and $\epsilon_2$ is a new intermediate activation energy that is found for samples in the transition range. The compensation introduced for this intermediate sample has decreased the impurity conduction in the overlap region but enhanced it considerably at lower temperatures. This suggests that perhaps intermediate range samples show conduction by an excited state band in the higher temperature regions[7,8] followed by freezeout to the ground state and then conduction through the carrier jumping process for the ground states in the lowest temperature regions.

## REFERENCES

1. RAY R. K., LONGO T. A. and LARK-HOROVITZ K., *Bull. Amer. Phys. Soc.* II, **3**, 101 (1958).
2. FRITZSCHE H., *U.S. Signal Corps Quart. Rep.* Purdue University, Oct.–Dec. (1956).
3. JAMES H. M., *U.S. Signal Corps Quart. Rep.* Purdue University, Oct.–Dec. (1956).
4. MOTT N. F., *Canad. J. Phys.* **34**, 1356 (1956).
5. LONGO T. A. and LARK-HOROVITZ K., *Bull. Amer. Phys. Soc.* II, **2**, 157 (1957).
6. KOENIG S. H. and GUNTHER-MOHR G. R., *J. Phys. Chem. Solids*, **2**, 268 (1957).
7. SWARTZ G. A., *Bull. Amer. Phys. Soc.* II, **2**, 134 (1957).
8. KOENIG S. H. and GUNTHER-MOHR G. R., see ref. 6, p. 278.

## DISCUSSION

*Compiled by* R. W. KEYES

### I.1 J. TAUC

M. GLICKSMAN: Is the negative curvature shown for high $k$ values in the InSb conduction band necessary to explain the data?

J. TAUC: No.

P. T. LANDSBERG: The conservation laws determine the energy at which band–band impact ionization commences. The same laws control band–band Auger recombination of electrons and holes. When this mechanism dominates, a $\ln \tau$ vs. $1/T$ curve should enable one to estimate the minimum energy change of an electron for which Auger recombination is possible. Since this energy can also be deduced from an analysis of the impact ionization process, it is to be hoped that a satisfactory comparison between results in these two fields will be found when sufficient experimental data are available.

### I.2 S. H. KOENIG

MELVIN LAX (Bell Tel. Labs.): Do you have data for the dependence of the capture cross-section of electrons on their energy?

S. H. KOENIG: Yes, we find a lifetime $\tau$ that varies as the field (and hence the electron energy) to the 1·75 power. This would imply a cross-section that decreased faster than 1/(electron energy)$^2$ and accounts in part for the $1/T^3$ behavior of the cross-section for thermal electrons.

### I.3 E. CONWELL

T. MORGAN: Another explanation of the discrepancy between the curves for $p$-type Ge (and to a lesser extent for $n$-type) is found in the distribution function assumed. The actual function will be depleted in those regions of energy space which are most important in transferring energy, and thus the energy transfer efficiency will be decreased.

P. AIGRAIN: In very impure samples the energy loss through collisions with impurities may dominate.

E. CONWELL: The mechanism by which this can happen is not clear.

### I.4 J. B. GUNN

T. MORGAN: Firstly, it appears from your results that electron–electron scattering does contribute to the energy dissipation rate. The correct distribution function near zero energy lies between those used by SODHA and ADAWI. The optical phonon scattering is strong enough, even at 80°K, to remove the $\log \epsilon$ singularity near the origin and to reduce the effect of impurity scattering on the value of $\beta$ predicted by ADAWI's results. The field dependence of the distribution function at the origin goes as $\sqrt{\epsilon}$, when optical phonon scattering is included. This is still steeper than the Maxwellian function, which varies as $\epsilon$. It would be desirable to extend these experiments to materials of much higher purity or to higher temperatures. Secondly, the disappearance of the high field plateau with increasing impurity concentration can be understood as an effect of electron–electron scattering. According to Shockley's model electrons are scattered to low energies as soon as they cross the threshold energy for the emission of optical phonons, and there is a range of field strengths for which the distribution function is cut off rather sharply at the threshold energy. This phenomenon will appear rather suddenly at a certain critical field and will persist until the field is strong enough to keep many electrons above this threshold. However, electron–electron scattering would also enable electrons to cross the threshold and to emit optical phonons, even for low field strengths. Thus the effectiveness of the energy loss mechanisms would increase gradually.

### I.5 M. C. STEELE and M. GLICKSMAN

P. J. PRICE: The longitudinal magnetoresistance for hot electrons in $n$-InSb is of special interest because any such effect (apart from what would be due to the deviation of the energy function from spherical symmetry), if measured for a homogeneous current distribution in the sample, has to be due to quantization of Larmor orbits.

M. C. STEELE: The quantum condition is satisfied in the experiments in question and this may provide the explanation.

### I.6 T. MORGAN

G. C. DOUSMANIS: Microwave measurements on Ge and Si have been made by an inverse procedure, similar to that of Gibson: The carriers are heated by means of pulsed d.c. fields and the changes in mobility are detected by the changes in the microwave absorption of the samples. The microwave interaction under equilibrium conditions has also been studied in the temperature range of 300° to 4°K. The results on the ranges of frequency and temperatures, where $\omega\tau$ becomes comparable to or larger than unity, are in close agreement with the ones reported by Dr. MORGAN.

### I.7 W. SASAKI *et al.*

C. HERRING: The apparent activation energy for intervalley scattering (60°K) seems surprising, since scattering between band edge points by the lowest acoustic branch is forbidden, and the experiments of Weinreich give a phonon energy of 300° for this process. The explanation may be in the breakdown of the selection rule for states with the $k$ of the hot electrons.

### I.8 H. FRITZSCHE

W. KOHN: With some other impurities the splitting of the singlet and triplet is larger, and one might hope that the experimental detection of the difference would be easier.

R. W. KEYES: The data suggests that in a strained crystal the impurity band conductivity is the product of a temperature independent, anisotropic factor and an isotropic activated term. Symmetry considerations might suggest that the former term depends on the shear part of the stress and the latter term on the dilation.

H. FRITZSCHE: Measurements of the dependence of resistivity on hydrostatic pressure show that dilation has only a very small effect on the resistivity and that this effect is temperature independent between 2°K and 4°K. Thus they do not agree with such an interpretation.

C. HERRING: What limits can one set on relative contributions to the activation energy from Mott's "freeing" energy and from an activation energy for jumping?

H. FRITZSCHE: The activation energy of impurity conduction observed in the low concentration range is about $5 \times 10^{-4}$ eV larger than Mott's freeing energy. In strongly compensated specimens one finds an activation energy also of the order of $5 \times 10^{-4}$ eV which cannot be accounted for by Mott's model. This may indicate the presence of a different process which requires thermal activation.

Ig, T. A. LONGO *et. al.*

H. FRITSZCHE: At 15 per cent compensation every majority impurity is a nearest neighbor of a minority impurity. Hence, one cannot apply in this case MOTT's model, which distinguishes a number of majority centers as trap states. The agreement found between the activation energy of the bombarded sample and MOTT's model must be accidental. We found that in Ge the activation energy of impurity conduction remains almost constant in the range of 20–80 per cent compensation.

S. H. KOENIG points out that MOTT's model is of a qualitative and approximate nature. One should not try to compare on a quantitative basis measured activation energies in impurity conduction with the values calculated from this model.

*J. Phys. Chem. Solids* Pergamon Press 1959. Vol. 8. pp. 264–269. Printed in Great Britain

SESSION J:
OPTICAL PROPERTIES*

J.1

# THEORY OF INFRARED ABSORPTION BY CONDUCTION ELECTRONS IN GERMANIUM

**H. J. G. MEYER**

Philips Research Laboratories, N. V. Philips' Gloeilampenfabrieken
Eindhoven–Netherlands

VOL
8
195

**Abstract**—It is shown that a theory of infrared absorption by conduction electrons which takes into account the structure of the conduction band and acoustical as well as optical intravalley scattering can be developed without any serious approximation. In combination with an estimate of the possible influence of impurity scattering the theoretical results can be used for the determination of one of the acoustical and of the optical deformation potential constants. From available experimental data the approximate numerical value of the latter is determined. The general limits of validity of the theory are discussed.

## 1. INTRODUCTION

EVEN if the band structure of a certain semiconductor is known the analysis and interpretation of experiments on transport phenomena to obtain data on the various scattering mechanisms may be very difficult and often somewhat uncertain. This is due to the necessity of solving a Boltzman transport equation which often can only be done approximately. However, there is another physical process from which data on the scattering mechanisms of mobile charge carriers can be obtained *without* necessitating the solution of a Boltzmann equation, viz. the absorption of light due to these carriers.

It is the purpose of this paper to indicate briefly how for the case of conduction electrons in germanium the theory of this process, at least for intravalley lattice-scattering, can be developed in great detail and with great accuracy and to show how certain experiments (which for a great part still remain to be done) can yield valuable information about the deformation potential constants for acoustical as well as for optical modes. Still other experiments are mentioned which might be of help in exploring the band structure or which may shed light on the impurity band problem.

* *Chairman:* L. SOSNOWSKI; *Co-Chairman:* E. BURSTEIN.

## 2. GENERAL EXPRESSION FOR THE ABSORPTION CONSTANT DUE TO INTRAVALLEY LATTICE-SCATTERING

As is well known, due to the requirement of simultaneous conservation of energy and crystal-momentum, no light can be absorbed by an electronic transition of an electron within one band, unless simultaneously phonons are emitted or absorbed.† Thus, the absorption of light by a conduction electron has to be treated by a second-order perturbation calculation in which the interaction of the electron with the lattice vibrations and with the radiation field is dealt with simultaneously. Then, the probability per unit time that the total system, consisting of the radiation field, the lattice vibrations and the conduction electron, makes a transition of an initial state $i$ to a final state $f$ is given by

$$W_{(f/i)} = (2\pi/\hbar)\times$$
$$\times\left[\sum_u \left|\langle f|H|u\rangle\langle u|H|i\rangle\right| \Big/ (E_i - E_u)\right]^2 \delta(E_f - E_i). \tag{2.1}$$

Here the sum over $u$ goes over all intermediate

† The influence of the other possibility that momentum is taken up by an impurity in the lattice will briefly be discussed in section 5.

(virtual) states compatible with the special requirements of the system and $H$ is the total interaction operator causing the transition. In our case it consists of the sum of the operators representing the interaction of the conduction electron with the radiation field, the acoustical and the optical modes respectively. It can be shown[1] that, as far as absorption of an infrared photon is concerned, these three interactions may be considered to vary only little over a distance of the order of a lattice parameter. In that case the effective-mass approximation may be applied and the matrix elements occurring in (2.1) are easily calculated.[1] Using these, the absorption coefficient at frequency $\nu$, $\mu(\nu)$, due to intravalley scattering of conduction electrons is found to be given by:[1]

$$\mu(\nu) = n\frac{1}{3\cdot 8^2\cdot\pi^4}(\det\boldsymbol{\alpha})^{\frac{1}{2}}\frac{\hbar e^2 v}{m^2 Mc\epsilon^{\frac{1}{2}}}\times$$

$$\times\left(\frac{\hbar^2}{2\pi mkT}\right)^{\frac{3}{2}}\frac{1}{\nu^3}\int d\mathbf{k}'\int d\mathbf{k}\,\exp[-E_{\mathbf{k}}/kT]\cdot$$

$$\cdot\sum_{s=1}^{4}(Q_s^2/\omega)(n_s\delta[E_{\mathbf{k}}-(E_{\mathbf{k}}+h\nu+\hbar\omega_s)]+$$

$$+(n_s+1)\delta[E_{\mathbf{k}}-(E_{\mathbf{k}}+h\nu-\hbar\omega_s)]. \qquad (2.2)$$

Here $n$ is the density of the conduction electrons, $\boldsymbol{\alpha}$ is the reciprocal effective mass tensor with the components (in diagonal form) $\alpha_1$, $\alpha_1$, $\alpha_2 \equiv m/m_1$, $m/m_1$, $m/m_2$, where $m_1$ and $m_2$ are the transverse and longitudinal effective mass respectively; $v$ is the volume of a unit cell of the crystal, $\epsilon$ its dielectric constant, $M$ the mass of a germanium atom and $\mathbf{k}\mathbf{k}'$ and $E_{\mathbf{k}}$, $E_{\mathbf{k}'}$ are the initial and final wave vectors and energies of the electron. The index $s$ indicates the various sorts of modes contributing to the absorption constant, and $s = 1 \ldots 4$ corresponds to acoustical-longitudinal and transverse, and optical-longitudinal and -transverse respectively; $\omega_s$ is the frequency of the mode $s$ at wave vector $\mathrm{q} = \mathbf{k}'-\mathbf{k}$ and $n_s$ is the thermal average of the number of phonons in the corresponding mode. The coefficients $Q_s$ are given by:

$$Q_1 = |\mathbf{k}'-\mathbf{k}|(\Xi_d+\Xi_u\cos^2\vartheta),$$

$$Q_2 = -|\mathbf{k}'-\mathbf{k}|\Xi_u\cos\vartheta\sin\vartheta,$$

$$Q_3 = D\cos\vartheta, \quad Q_4 = -D\sin\vartheta,$$

where $\Xi_d$ and $\Xi_u$ are the acoustical deformation potential constants[2] and $D$ is the "optical deformation-potential" constant;[3] $\vartheta$ is the angle between $\mathbf{k}'-\mathbf{k}$ and the $z$-axis.

### 3. THE ABSORPTION CONSTANT DUE TO ACOUSTICAL MODES

The acoustical modes of vibration are characterized by the dispersion relation for the vibrational frequency $\omega$, which for longitudinal and transverse modes of long wavelengths reads at $\mathrm{q} = \mathbf{k}'-\mathbf{k}$:

$$\omega_{1,t}(\mathbf{k}'-\mathbf{k}) = u_{1,t}\left(\frac{\mathbf{k}'-\mathbf{k}}{|\mathbf{k}'-\mathbf{k}|}\right)|\mathbf{k}'-\mathbf{k}|. \qquad (3.1)$$

Here $u_1$ and $u_t$ are the velocities of sound for the longitudinal and the transverse acoustic waves. Using this dispersion law, a detailed analysis shows[1] that, in performing the integration for the first two terms ($s = 1$, $s = 2$) contributing to $\mu$ (formula (2.2)) and corresponding to the contribution due to the acoustical modes, $\hbar\omega$ may to a very good approximation be neglected in the arguments of the corresponding $\delta$-functions. At the same time $n_s$ and $n_s+1$ may with great accuracy be approximated by $n_s \approx n_s+1 \approx kT/\hbar\omega_s$. The actual evaluation of the integrals is straightforward though somewhat lengthy. It has been described in more detail in [1]. The result of this integration then yields us the absorption constant at frequency $\nu$ due to microscopic absorption of a photon by a conduction electron which is scattered by an acoustic lattice wave. It should be noted however that an incident light beam not only causes transitions corresponding to *absorption* of a photon but also transitions corresponding to induced *emission* of a photon.* As is well known the probability for this second process to occur is a factor $\exp(-h\nu/kT)$ smaller than the probability for the first process and the net macroscopic absorption constant, which is the quantity which one determines from experiments, is proportional to the difference of the two mentioned probabilities. We then find for the net absorption constant due to acoustical intravalley scattering:

$$\mu_{\text{net}}^{\text{ac}} = n\frac{\sqrt{2}}{3\cdot\pi^{\frac{1}{2}}}\frac{e^2k^{\frac{1}{2}}m^{\frac{1}{2}}}{\hbar^5 c}\frac{1}{\alpha_2^{\frac{1}{2}}\epsilon^{\frac{1}{2}}c_1}\frac{T^{\frac{7}{2}}}{\nu^3}\times$$

$$\times(1-e^{-2z})e^z z^2 K_2(z)(\Xi^2)_{\text{av}}. \qquad (3.2)$$

* As was pointed out by Dr. R. ROSENBERG (privately through Dr. HERRING) this was already remarked by H. SCHMIDT.[4]

Its behaviour as a function of frequency and temperature depends mainly on the dimensionless parameter $z$ defined by:

$$z = h\nu/2kT \tag{3.3}$$

$K_2$ is the modified Bessel function of index 2 and $c_l$ is some combination of the elastic constants.[1] $(\Xi^2)_{av}$ is a quadratic form in $\Xi_u$ and $\Xi_d$ given by:

$$(\Xi^2)_{av} = 1{\cdot}07\Xi_u^2 + 1{\cdot}66\Xi_u\Xi_d + 1{\cdot}34\Xi_d^2. \tag{3.4}$$

The coefficients appearing in (3.4) depend on the elastic constants and, though very weakly, on the ratio $m_2/m_1 \equiv \alpha_1/\alpha_2$.

If we take $\Xi_u$ and $\Xi_d$ to be 17 eV and $-3{\cdot}4$ eV[2] respectively we get from (3.2) as an approximate numerical result:*

$$\mu_{net}^{ac} = n1{\cdot}51 \times 10^{-27} \times$$
$$\times \lambda^{*3} T^{\frac{1}{2}}(1-e^{-2z})e^z z^2 K_2(z)[\mathrm{cm}^{-1}], \tag{3.5}$$

where $\lambda^*$ is the wave length in vacuum of the absorbed light expressed in $\mu$'s ($10^{-4}$ cm). It should be noted that within the general limits of the theory (cf. section 7) this expression holds for all wave lengths and all temperatures and that it was derived without any serious approximation.

As the modified Bessel function $K_2(z)$ is tabulated our final results (3.2) or (3.5) for the absorption coefficient due to the interaction of conduction electrons with the acoustical modes can easily be evaluated for any $z$. For small or large values of $z$ simple approximations can easily be given.[1]

## 4. THE ABSORPTION CONSTANT DUE TO THE OPTICAL MODES

The optical modes are characterized by the fact that their frequency $\omega_0$ shows only a small dispersion; it is of the same order of magnitude as the maximum frequency of the acoustical modes. In the following the dispersion is completely neglected (as is usual in treating optical modes) so that $\omega_0$ is regarded as a constant. Hence, though now the vibrational energy is no longer small as compared to $kT$, the calculation of the integrals occurring in (2.2) can be performed without any additional approximation. The final result for the total net absorption constant (taking stimulated emission into account) due to the interaction of the conduction electrons with the optical modes is:

$$\mu_{net}^{opt} = n\frac{\sqrt{2}\cdot 0.684}{6\cdot\pi^{\frac{1}{2}}}\frac{e^2 k^{\frac{1}{2}} m^{\frac{1}{2}}\vartheta}{\hbar^4 c M\omega_0\alpha_2^{\frac{1}{2}}\epsilon^{\frac{1}{2}}}D^2\frac{T^{\frac{1}{2}}}{\nu^3}\times$$
$$\times\frac{e^{z_+}(1-e^{-2z})}{e^{\hbar\omega_0/kT}-1}[z_+^2 K_2(z_+)+z_-^2 K_2(z_-)]. \tag{4.1}$$

Here, instead of $z$, two parameters, $z_+$ and $z_-$ occur which are given by:

$$z_\pm = (h\nu \pm \hbar\omega_0)/2kT. \tag{4.2}$$

$D$ is the coupling constant defined in (2.3).

It is obvious that under a number of limiting conditions simpler approximate expressions can be derived from (4.1) for the discussion of which we refer to [1].

It should be mentioned, that the influence of possible intervalley scattering will, at least qualitatively, be very similar to that of intravalley scattering by optical modes. Therefore in the following an unknown amount of intervalley scattering is understood to be included in what is loosely called contribution of the optical modes.

## 5. THE INFLUENCE OF IMPURITY SCATTERING ON THE ABSORPTION CONSTANT

As the main purpose of this work is to obtain information on the scattering of conduction electrons by lattice waves we shall content ourselves here with an expression for the influence of impurity scattering on the absorption constant which does not take into account the real structure of the conduction band in germanium. Such an expression can be considered to be of sufficient accuracy to allow us to indicate those regions of temperature, photon wavelength and impurity content for which the influence of impurity scattering may be neglected as compared to that due to acoustical lattice scattering.

The problem of absorption of radiation by impurity scattering may be treated as the inverse process of Bremsstrahlung by scattering in a Coulomb field. By using an approximation due to Ehlert, quoted by BETHE and SALPETER,[5] for the dipole matrix element between Coulomb wavefunctions the following expression for the net

* In the same communication Dr. HERRING pointed out that $-5{\cdot}8$ eV is probably a better value for $\Xi_d$. This would lower the value of (3.5) by about 20 per cent.

VOL 8 195

absorption constant, including again the influence of stimulated emission, may be derived:

$$\mu_{\text{net}}^{\text{imp}} = nN_i \frac{2}{3\pi} \frac{Z^2e^6}{\hbar^2 cE^{\frac{1}{2}}m^*} \left(\frac{\hbar^2}{2\pi m^* kT}\right)^{\frac{3}{2}} \times$$

$$\times 4\pi \int_0^\infty dkk' \exp\left[-\frac{\hbar^2}{2m^*kT}k^2\right] \ln\left(\frac{k'+k}{k'-k}\right). \quad (5.1)$$

Here $Z$ is the number of charges on the ionized impurity centers which are present in a concentration $N_i$ and $m^*$ is an effective mass which is some average over the more significant transverse and longitudinal masses occurring in the conduction band. In practice $m^*$ is of the order 0·1 m.[6] Finally $k$ and $k'$ are the absolute values of the electron wave-vector before and after the absorption process. It should be noted that due to the use of a somewhat more accurate approximation the integrand occurring in our formula (5.1) differs by a factor $k'/k$ from the corresponding expression used by FAN *et al.*[6] Unfortunately the integral (5.1) cannot be expressed in a closed form for all $z = h\nu/2kT$. Approximations for small and large $z$ yield:

$$\mu_{\text{net}}^{imp} \approx n\frac{4\sqrt{2}}{3\pi^{\frac{1}{2}}} \frac{N_i Z^2 e^6}{\epsilon^{\frac{1}{2}} m^{*\frac{1}{2}} ch k^{\frac{1}{2}}} \frac{1}{T^{\frac{1}{2}}\nu^3}(1-e^{-2z}) \times$$

$$\times \begin{cases} \frac{1}{2}\{\ln(2/z) - \Gamma + 1{\cdot}38z\} & (z \ll 1) \\ 1 & (z \gg 1) \end{cases} \quad (5.2)$$

where $\Gamma$ is Euler's constant ($\Gamma = 0{\cdot}577$). Whereas for $z \ll 1$ this result becomes (except for the factor $(1-e^{-2z})$) equal to that of reference (6), for $z \gg 1$ it is larger by a factor $(8z/\pi)^{\frac{1}{2}}$. This is in accordance with the fact remarked by FAN *et al.*, that at low temperatures his formula for absorption by impurity scattering yielded too small results.

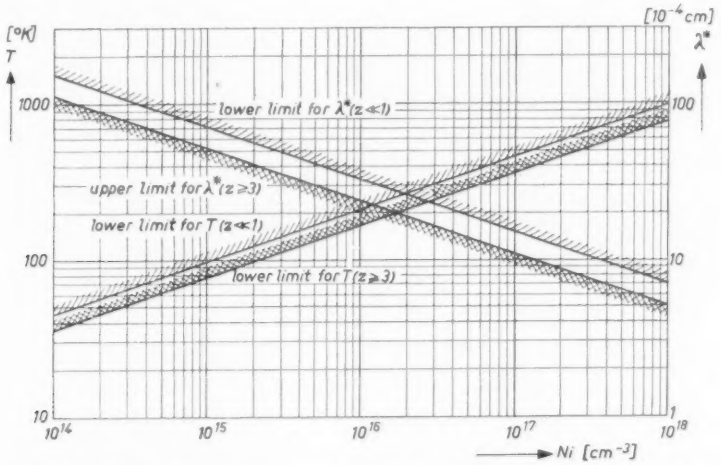


FIG. 1. Regions of temperature, wavelength and impurity content for which the influence of impurity scattering on the absorption constant is negligible. At a certain impurity content $N_i$, indicated along the horizontal axis, the temperature, plotted along the left vertical axis is determined from the condition that $\mu^{\text{imp}}/\mu^{\text{ac}}$ be smaller than 1/10 for both $z \ll 1$ and $z \gg 1$. The lines "lower limit for $T$" indicate the minimal temperature which at a certain impurity content is permissible according to this criterion. At that minimal temperature an extremal permissible wavelength exists, determined by the condition $z = 1$ and $z = 3$ respectively. The wavelength is plotted along the right vertical axis and the line "lower (upper) limit for $\lambda^*$" indicates the extremal wavelength belonging to the minimal temperature at a certain impurity content.

By comparing (5.2) with (3.5) (using $m^* = 0{\cdot}1m$) Fig. 1 can be obtained where we have indicated those regions of temperature, wavelength and impurity concentration for which the absorption

constant due to impurity scattering is smaller than one tenth of that due to acoustical scattering. It is seen immediately that large regions are available in which the influence of impurity scattering can be neglected.

## 6. COMPARISON WITH AVAILABLE EXPERIMENTAL DATA[6]

As the above does *not* provide a theory for impurity scattering which could be used for obtaining absolute quantitative results whereas this could indeed be expected from our formulae for lattice scattering, only those experimental data are suitable for a comparison between theory and experiment which may be expected not to contain any appreciable contribution due to impurities. The most direct experimental evidence of the absorption constant $\mu^{\text{latt}}$ of conduction electrons in germanium due to lattice scattering alone is due to FAN *et al.*[6] who measured the absorption constant $\mu$ at 78°K and $\lambda = 10\,\mu$ of a number of samples of various impurity content $N_i$. From a plot of $\mu$ versus $N_i$, $\mu^{\text{latt}}$ (at 78° and $\lambda = 10\,\mu$) is found to be:

$$(1/n)\mu_{\text{exp}}{}^{\text{latt}} = 1{\cdot}7\times10^{-17}\text{cm}^2 \qquad [T = 78°\text{K}, \lambda = 10\mu]. \quad (6.1)$$

From our theoretical formula (3.5) for *acoustical* lattice scattering we find at the same wavelength and temperature ($z = 9.23$)

$$(1/n)\mu_{\text{net}}{}^{\text{ac}} = 0{\cdot}34\times10^{-17}\text{cm}^2 \qquad [T = 78°\text{K}, \lambda = 10\mu]. \quad (6.2)$$

As no serious approximation was made in deriving (3.5) and as $\Xi_u$ is known with reasonable accuracy whereas $\Xi_d$, the numerical value of which is rather uncertain, is in any case relatively small, the theoretical value given above should be accurate to about 25 per cent. Thus if we would take the experimental value of FAN *et al.* at its face value, which, due to the difficulties in determining the impurity content and the number of free carriers, may be somewhat optimistic, we come to the conclusion that an appreciable amount of optical scattering (which may contain some intervalley scattering) must be present. In fact by putting

$$\mu_{\text{theor}}{}^{\text{latt}} \equiv \mu_{\text{net}}{}^{\text{ac}} + \mu_{\text{net}}{}^{\text{opt}} = \mu_{\text{exp}}{}^{\text{latt}} \quad (6.3)$$

we find that

$$(1/n)\mu_{\text{net}}{}^{\text{opt}} = 1{\cdot}36\times10^{-17}\text{cm}^2 \qquad [T = 78°\text{K}, \lambda = 10\mu], \quad (6.4)$$

from which the optical deformation-potential constant follows as $D = 3{\cdot}24\times10^{-3}$ erg cm. As is easily verified, with this value of $D$ formula (6.3) would yield at 450°K and $\lambda = 10\mu$ a value for $1/n)\ \mu_{\text{theor}}{}^{\text{latt}}$ equal to $12{\cdot}5\times10^{-17}$ cm$^2$. This, however, disagrees with experiments by FAN *et al.*[6] at that high temperature by a factor of about 1·75. A discrepancy of about the same factor is also present at $\lambda = 5\mu$ and the same temperature ($z = 3{\cdot}2$). As is immediately apparent from our Fig. 1, at this temperature the influence of impurity scattering should be less than 10 per cent of acoustical scattering for samples with $N_i \lesssim 3{\cdot}10^{17}$ cm$^{-3}$ (which is approximately the impurity content of sample 8 of SPITZER and FAN) and at any wavelength such that $z \geqslant 3$ ($\lambda \lesssim 8\mu$). We now tentatively assume that in the experimental value of the absorption constant at $\lambda = 10\mu$ and $T = 450$°K the contribution of impurity scattering is indeed 10 per cent of that due to acoustical scattering, which probably is an upper limit, and that the temperature dependence of $\mu^{\text{imp}}$ is rightly given by (5.2). With $m^* = 0{\cdot}1$, this amounts to assuming a concentration of $1{\cdot}7\times10^{17}$ impurities to be present per cm$^3$. Furthermore we choose the contribution of the optical modes such that the total theoretical absorption constant at that temperature and wavelength is about equal to the corresponding experimental value, by which choice we have fixed $D$ to be given by:

$$D \approx 1{\cdot}85\times10^{-3}\text{erg cm}. \quad (6.5)$$

We then get Table 1 indicating the various contributions and a comparison between theory and experiment at $\lambda = 10\mu$ and three temperatures.

The results of this table show that also from the data at high temperatures one has to conclude that an appreciable amount of optical scattering must be present in order to explain the experimental data on the absorption constant at $\lambda = 10\mu$. The contribution of the optical modes is very roughly equal to that of the acoustical ones at the three indicated temperatures. Furthermore it seems likely that at 78°K the amount of impurity scattering in the experiments of SPITZER and FAN

has been larger than one would conclude from their paper.

Finally the plausibility of our numerical result (6.5) for $D$ may be checked by comparing it with the numerical value of $(\Xi^2)_{\text{av}}$. It is then found that

$$D^2 = (\Xi^2)_{\text{av}} \cdot \mathbf{q}_{\text{eff}}^2 \qquad (6.6)$$

where the numerical value of the wave vector $\mathbf{q}_{\text{eff}}$ is found to be $\mathbf{q}_{\text{eff}} \approx 0{\cdot}77 \times 10^8$ cm$^{-1}$. This means that the coupling strength of the optical modes to the conduction electrons is about equal to that of the acoustical modes of shortest possible wavelength, which seems to be a reasonable result indeed.

In the above an attempt was made to determine the value of $D$ from the few experimental data available, an attempt which was handicapped by the uncertainty about the numerical value of $\Xi_d$. From the obtained estimate for $D$ it follows that the contribution of the optical modes will only be negligible at temperatures as low as about 50°K and at wavelengths of about $80\mu$ and longer. Such experiments on samples with low impurity content could not only lead to a more reliable determination of $D$ but might at the same time yield more accurate values for $\Xi_d$ than hitherto available. Once more information about these constants has been gained in this way, experiments at large values of $h\nu$ might help in exploring those regions of the conduction band which cannot be reached by the electrons in an experiment on transport phenomena.

*Table* 1. *Theoretical and experimental absorption constants at* $\lambda = 10\mu$

| I<br>$T$<br>(°K) | II<br>$(1/n)\mu^{\text{ac}}{}_{\text{theor}}$<br>($10^{-17}$ cm$^2$) | III<br>$(1/n)\mu^{\text{opt}}{}_{\text{theor}}$<br>($10^{-17}$ cm$^2$) | IV<br>$(1/n)\mu^{\text{imp}}{}_{\text{theor}}$<br>($10^{-17}$ cm$^2$) | V<br>$(1/n)\mu^{\text{tot}}{}_{\text{theor}}$<br>($10^{-17}$ cm$^2$) | VI<br>$(1/n)\mu^{\text{tot}}{}_{\text{exp}}$<br>($10^{-17}$ cm$^2$) |
|---|---|---|---|---|---|
| 450 | 3·9 | 2·8 | 0·4 | 7·1 | 7·0 |
| 293 | 2·0 | 1·5 | 0·5 | 4·0 | 4·2 |
| 78 | 0·34 | 0·44 | 0·9 | 1·7 | 1·7 |

## 7. GENERAL DISCUSSION AND CONCLUSIONS

As was shown above, the theory of the absorption of electromagnetic radiation by conduction electrons due to intravalley lattice scattering can be given at all relevant wavelengths and temperatures. Obviously, relevant temperatures are those at which the number of conduction electrons is sufficiently large and that of free holes sufficiently small. However, valuable information about impurity band formation could probably be obtained from absorption experiments at $\lambda \gtrsim 200\mu$ down to liquid helium temperatures. The region of relevant wavelengths is on the short wavelength side limited by the necessity of avoiding fundamental absorption, the limit on the long wavelength side is set by the fact that the above treatment is based on perturbation theory. In our case it appears to be valid only for

$$\lambda \ll 5 \times 10^2 T^{-1.66} \text{ cm}.^{(1)}$$

*Acknowledgments*—The author would like to thank his colleagues C. HAAS and F. H. STIELTJES for helpful and stimulating discussions. He is especially indebted to D. POLDER for valuable criticism. Finally his thanks are due to Dr. C. HERRING of Bell Telephone Labs. for a stimulating correspondence on the comparison between theory and experiment.

### REFERENCES

1. MEYER H. J. G. *Phys. Rev.* (in press).
2. HERRING C. and VOGT E. *Phys. Rev.* **101,** 944 (1956).
3. HARRISON W. A. *Phys. Rev.* **104,** 1281 (1956).
4. SCHMIDT H. *Z. Phys.* **139,** 433 (1954).
5. BETHE H. A. and SALPETER E. E. *Encyclopedia of Physics,* Vol. 35. Berlin (1957).
6. FAN H. Y., SPITZER W. and COLLINS R. J. *Phys. Rev.* **101,** 566 (1956).
7. DONOVAN B. and MARCH N. H. *Proc. Phys. Soc.* B.**70,** 833 (1957).

*J. Phys. Chem. Solids* Pergamon Press 1959. Vol. 8. pp. 270–272. Printed in Great Britain

# ABSORPTION SPECTRA OF GROUP V DONORS IN GERMANIUM*

J.2

**H. Y. FAN and P. FISHER**

Purdue University, Lafayette, Indiana

**Abstract**—Some recent investigations of infrared absorption associated with lattice imperfections in germanium and silicon are reported. The ionization and excitation bands of group III and group V impurities in germanium were observed at liquid helium temperature and long wavelengths, up to 300 microns. Ionization energies are deduced which are close to the values given by electrical measurements. A number of excitation bands were observed in each case. The spectra of the impurities are compared with each other and with the theoretical calculations of KOHN. The experimental results can be interpreted on the basis of the theory to a certain extent but give extra excitation bands which cannot be explained by the theoretical calculation. The effects of different factors, such as the concentration of impurities, have been studied.

Irradiation by high energy neutrons and electrons produces in silicon infrared absorption bands associated with the introduced lattice defects. Several bands have been observed. The possibility of observing a particular absorption band depends on the Fermi level in the irradiated sample which determines the state of ionization of the defects. The absorption was studied after annealing the sample at different temperatures. It was found that the various absorption bands are associated with different types of defect centers. One of the bands, at 20·5 microns, increased or decreased with temperature annealing, depending on the Fermi level. The observation is understandable on the assumption that the anneal of the type of absorption center depends upon the state of ionization of the defects.

THE absorption spectra of Group III and Group V impurity atoms in silicon have been observed by many authors. Similar investigations have now been made for these impurities in germanium.(1) We shall discuss here only the donor impurities. Due to the small ionization energies of these impurities it is necessary to use radiation of wavelengths $\lesssim 100\,\mu$. The measurements were made near 4·2°K and by using a far infrared grating spectrometer. The monochromator was calibrated from the atmospheric water vapour absorption spectra reported by PLYLER and ACQUISTA.(2)

Fig. 1 shows the absorption spectrum due to arsenic impurity in germanium. Various samples from different ingots and with different impurity concentrations have been examined and it is found that the lines B and E are always present with about the same relative strengths. For samples which have room temperature resistivities $\gtrsim 1{\cdot}5\Omega$-cm the lines A and C have been observed. For more impure samples the line B is broader and lines A and C are not observed. This is attributed to increasing overlap of orbitals of neighbouring

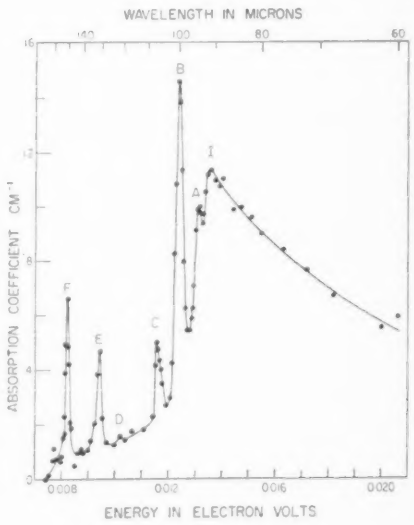


FIG. 1.

* Work supported by an Office of Naval Research Contract.

VOL.
8
1959

*Table* 1. *Energy level spacings for Group V impurities in germanium in units of* $10^{-3}$ *eV; experimental error is* 0·1 *unit.*

| Theoretical | | Experimental | | | | |
|---|---|---|---|---|---|---|
| | | | As | Bi | Sb | P |
| $2p, \pm1$–$3p, \pm1$ | 0·75 | B–A | 0·7 | | | 0·7 |
| $2p, \pm1$–$3p, 0$ | 0·75 | B–C | 0·8 | | | 0·8 |
| | | B–D | 2·2 | 1·8 | 1·5 | 1·8 |
| | | | | | 1·8 | 2·1 |
| $2p, \pm1$–$2p, 0$ | 2·9 | B–E | 2·9 | 2·8 | 2·6 | 2·8 |
| | | | | | 3·0 | 3·0 |
| | | B–F | 4·2 | | | |
| Ionization energy | | Optical | 14·0 | 12·5 | 9·8 | 12·8 |
| | | Thermal | 12·7 | 12 | 9·6 | 12·0 |

[facing page 270

VOL.
8
195

impurity atoms. The strength of the F-line has been observed to vary randomly with impurity concentration and from ingot to ingot, and for this reason is not attributed to As. Line D is always very weak and has not been investigated thoroughly. The lines A, B, C, and E may be attributed to electronic transitions from the ground state to the excited states of arsenic. The slowly varying absorption which reaches a maximum at I is associated with the photoionization.

For each of the other impurities, P, Bi, and Sb, a characteristic strong line (B) close to an ionization limit is observed. This line is at 99·8, 111, 113, and 151·5 $\mu$ for As, P, Bi, and Sb respectively. There is a corresponding E-line for Bi, but in the case of P and Sb a doublet appears instead of one line. Lines corresponding to A and C have also been observed for P. For both P and Sb the D-line is a weak doubtlet whereas for Bi, D appears as a broad peak.

Table 1 lists the energy spacings between the B-line and each of the other lines for a given impurity. The E doublet for Sb has been measured only once so far and must be considered tentative. As would be expected from the large dielectric constant of germanium and the small electronic effective mass, the energy spacings of the excited states are very nearly independent of the parent impurity element. Table 1 includes KOHN'S[3] calculated energy spacings. Good agreement is obtained between theory and most of the experimental spacings by assigning the A, B, C and E lines to the transitions, $1s \rightarrow 3p, \pm 1$, $1s \rightarrow 2p, \pm 1$, $1s \rightarrow 3p, 0$ and $1s \rightarrow 2p, 0$ respectively. This assignment is borne out by the observation of the Zeeman effect for As and P described below.

Table 1 also shows values for the "optical" ionization energies. These values were obtained by adding to the energy of each B-line the energy calculated by Kohn for the separation of the $2p, \pm 1$ level from the conduction band.

Fig. 2 shows the effect of a transverse magnetic field on the transmission spectrum of arsenic. The field is applied along (100) so as to be symmetrical with respect to the energy ellipsoids along $\langle 111 \rangle$. It is seen that the strong B-line of Fig. 1 had split into two lines, $B_1$ and $B_2$. The oscillatory pattern at higher energies is associated with the Landau grouping of the energy levels in the conduction band. On the low energy side of $B_1$ and $B_2$, the absorption has decreased slightly upon the application of the field due to the shift of the photoionization background to higher energy. Similar results have been obtained for P.

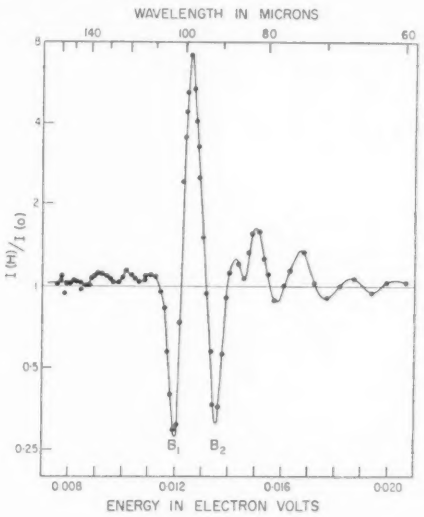


FIG. 2.

The splitting of the B-line confirms the assignment of a $p, \pm 1$ level to the excited state concerned. The separation between $B_1$ and $B_2$ has been examined as a function of the magnetic field. It was found to increase linearly with $H$ in the range of field used, 6200 to $1{\cdot}6 \times 10^4$ oersteds for P and $10^4$ to $1{\cdot}6 \times 10^4$ oersteds for As, giving $8{\cdot}7 \times 10^{-8}$ eV/oersted for P and $9{\cdot}0 \times 10^{-3}$ eV/oersted for As.

On the basis of the effective mass approximation with a wave function of the form $f(x^2+y^2, z^2), e^{im\phi}$ it can be shown [4] that the linear paramagnetic splitting of a $p, \pm 1$ level is given by $(e\hbar/m_t c)H_z$, where $m_t$ is the transverse effective mass of the conduction electrons and $H_z$ is the component of H along the axis of the ellipsoid of constant energy. According to this expression, the observed splitting of the B line of P corresponds to $m_t = (0{\cdot}077 \pm 0{\cdot}005)m$. The result is to be compared with the value of 0·082 $m$ obtained from cyclotron resonance experiments. It should be pointed out that even the smallest field used, $H = 6200$ oersteds, may be somewhat too high to justify the

use of weak field approximation for the Zeeman splitting. Experiments are being made at lower fields; the resolution (about $0{\cdot}5\mu$) may be a limiting factor for the accuracy of the result.

The separation in the Landau grouping of energy levels has been shown to be $(2\pi e\hbar H)/(c\partial S/\partial E)$[5], where $S$ is the area of intersection of a plane perpendicular to $H$ with the surface of constant energy $E$. For ellipsoidal surfaces of constant energy, $(\partial S/\partial E)/2\pi$ can be readily reduced to the well known expression of cyclotron effective mass, $m_c$, which depends on the direction of $H$. For $H\|[100]$, we expect $m_c = 0{\cdot}135\, m_0$. From the oscillations in the ionization absorption a value of $(0{\cdot}12\pm 0{\cdot}01)m_0$ is obtained.

## REFERENCES


1. Fisher P. and Fan H. Y. *Bull. Amer. Phys. Soc.* **3,** 128 (1958).
2. Plyler E. K. and Acquista N. *J. Res. Nat. Bur. Stand.* **56,** 149 (1956) R.P. 2660.
3. Kohn W. *Solid State Physics* Vol. 5, p. 257. Academic Press, New York (1957).
4. Lax B., Puff R. D. and Kleiner W. H. *Bull. Amer. Phys. Soc.* **3,** 31 (1958).
5. Lifshitz I. M. and Kosevich A. M.. *Zh. eksp. teor. fiz.* SSSR, **29,** 730 (1955).


VOL
8
195

*J. Phys. Chem. Solids* Pergamon Press 1959. Vol. 8. pp. 272–274. Printed in Great Britain

# J.2a INFRARED ABSORPTION IN NEUTRON IRRADIATED SILICON*

**H. Y. FAN and A. K. RAMDAS**

Purdue University, Lafayette, Indiana

Absorption bands associated with lattice defects produced by irradiation have been reported before.[1–3] An absorption band at $1{\cdot}8\,\mu$ was observed in samples irradiated with neutrons, deuterons and electrons. A study of neutron irradiated samples revealed bands with peaks at $3{\cdot}3\,\mu$, $3{\cdot}9\,\mu$, $6{\cdot}0\,\mu$, and $20{\cdot}5\,\mu$, and recently another one at $5{\cdot}5\,\mu$. Table 1 gives the relevant information about the bands. As the absorption bands anneal out at temperatures above 100°C, the uncontrolled heating of samples in the reactor pile often produces fluctuations in the results of irradiation and hence in the values given in column 2 of Table 1.

In order to observe an absorption band the sample must receive sufficient irradiation as well as have a suitable Fermi level as indicated in column 3, Table 1. Thus the $3{\cdot}3\,\mu$ and the $5{\cdot}5\,\mu$ bands are seen only in $n$-type samples, and the $3{\cdot}9\,\mu$ and $6{\cdot}0\,\mu$ bands are seen only with $p$-type samples. In samples sufficiently bombarded to have the Fermi level near the middle of the energy gap, only the $1{\cdot}8\,\mu$ and $20{\cdot}5\,\mu$ bands can be seen. The various bands can be seen in Figs. 1 and 2.

Absorption bands associated with the excitation of defect centers may depend on Fermi level which determines the number of electrons bound to them. Thus column 3 in the Table indicates the energy levels associated with the defects produced by irradiation. A dependence on the Fermi level has been found for all bands except the $20{\cdot}5\,\mu$ band which also corresponds to a much smaller energy than the others. It is close to the $16{\cdot}5\,\mu$ lattice vibrational band of unbombarded silicon and may be interpreted as an absorption associated with lattice vibration in the presence of defects.[2] The energy levels determined by various investigators using electrical measurements in irradiated silicon are given in Table 1. (Column 6 indicates the type of observation.) Observations[6] of

* Work supported by a Signal Corps contract.

*Table* 1. *Absorption bands and energy levels in irradiated silicon*

| Wavelength of Peak absorption ($\mu$) | peak absorption / neutron flux ($cm^{-1}/cm^{-2}$) $\times 10^{18}$ | Fermi level (eV) | Energy level (eV) | Irradiation | Type of measurement |
|---|---|---|---|---|---|
| 1·8 | ~30 | $E_c-0{\cdot}21$ | $E_c-0{\cdot}025$ | deuteron[7] | carrier removal |
| 3·9 | 7 | $E_v+0{\cdot}25$ | $E_v+0{\cdot}055$ | deuteron[7] | carrier removal |
| 6·0 | 14·0 | $E_v+0{\cdot}13$ | $E_c-0{\cdot}17$ | electron[4] | $R$ vs. $T$ |
| 3·3 | 8 | $E_c-0{\cdot}21$ | $E_c-0{\cdot}16$ | electron[5] | life time, $R$ vs. $T$ |
| 5·5 | 4 | $E_c-0{\cdot}14$ | $E_c-0{\cdot}23$ | deuteron[6] | mobility |
| 20·5 | 0·4 | — | $E_v+0{\cdot}27$ | electron, neutron[5] | life time, $R$ vs. $T$ |
| | | | $E_v+0{\cdot}3$ | electron[4] | $R$ vs. $T$ |
| | | | $E_v+0{\cdot}25$ | deuteron[6] | mobility |

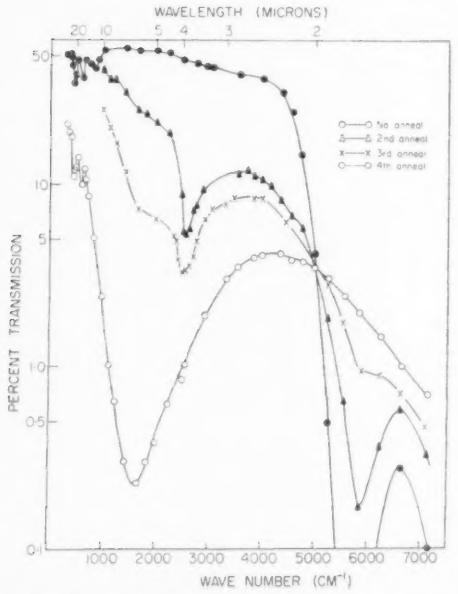


FIG. 1. Transmission of neutron irradiated $p$-type Si. Sample thickness = 0·0515 cm. Sample resistivity at room temperature was 0·007Ω-cm before irradiation and $1{\cdot}2\times10^3$ Ω-cm after irradiation.

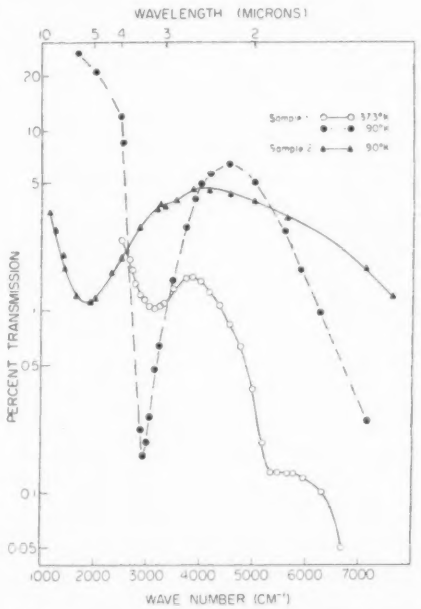


FIG. 2. Transmission of neutron irradiated $n$-type Si. Sample 1: Thickness = 0·062 cm; Fermi level $\zeta = E_c-0{\cdot}22$ eV at room temperature. Sample 2: Thickness = 0·058 cm; Fermi level $\zeta = E_c-0{\cdot}14$ eV at room temperature.

variation of Hall coefficient, $R$, with temperature have given a number of levels in the range $E_v+0{\cdot}17$ eV to $E_v+0{\cdot}3$ eV in addition to those given in column 4. The levels $E_v+0{\cdot}27$ eV, $E_v+0{\cdot}25$ eV and $E_v+0{\cdot}3$ eV reported by different authors are reasonably close to the $E_v+0{\cdot}25$ eV level determined from the 3·9 $\mu$ band. The level $E_c-0{\cdot}23$ eV is close to the $E_c-0{\cdot}21$ eV level obtained from the 3·3 $\mu$ band, whereas the levels $E_c-0{\cdot}17$ eV and $E_c-0{\cdot}16$ eV may be associated with the 5·5 $\mu$ band. Carrier removal rates showed that the levels at $E_c-0{\cdot}025$ eV and $E_v+0{\cdot}055$ eV are introduced by irradiations at much faster rates than the other levels. Absorption bands associated with these levels have not yet been observed because samples of low resistivities have to be used.

Considering the data for the 3·3 $\mu$ and 5·5 $\mu$

bands, we note that in each case the photon energy is higher than the corresponding energy given in column 3 of the table. The latter should be the thermal ionization energy i.e. the energy necessary to lift the electron from the defect and remove the absorption band. Briefly, the optical excitation energy is higher than the thermal ionization energy. This may occur if there is lattice relaxation around the defect when the defect is ionized; the lattice relaxation lowers the thermal ionization energy whereas the Franck-Condon principle applies to optical excitations. An alternative explanation is that a potential barrier exists around the defect. The same remarks could be made about the 3·9 $\mu$ and the 6·0 $\mu$ bands.

By observing the change of an absorption band as a result of heat treating the sample, the annealing of the defect responsible for the absorption may be studied. For this purpose it is necessary to avoid or to take into account the effect of the shift of the Fermi level which is produced by the heat treatment. By heat treating suitable samples at temperatures from 100°C to 200°C, it has been found that the defects giving the 1·8 $\mu$ band anneal out by a monomolecular process with an activation energy of 0·8 eV. It is likely that these defects are close interstitial-vacancy pairs. The 20·5 $\mu$ band shows an interesting behavior. In samples in which the Fermi level remained high above the valence band, the absorption vanished after a few hours heating at ~200°C. However, in *p*-type samples where the resistivity became low with annealing the absorption band grew stronger as the heat treatment was carried up to 250°C. A possible explanation is that the absorption is caused by aggregates of defect centers, the formation and dispersion of which depend on the state of ionization of the centers.

There is evidence indicating that the 1·8 $\mu$ and the 3·3 $\mu$ bands are associated with the same defects. Absorption was measured for an *n*-type sample at various temperatures; curves for this sample at two temperatures are shown in Fig. 2. It is seen that the 1·8 $\mu$ band is pronounced only in the 373°K curve. On the other hand the 3·3 $\mu$ band is stronger at the lower temperature. A study of the variations of the two bands shows the increase of one is about proportional to decrease of the other. It appears therefore that the same center gives either of the absorption bands depending upon whether one more or less electron is bound to the center. In addition to this case, there is the possibility that the 3·9 $\mu$ and the 6.0 $\mu$ bands are due to the same defects.

VOL
8
195

## REFERENCES

1. Becker M., Fan H. Y. and Lark-Horovitz K. *Phys. Rev.* **85,** 730 (1952); Fan H. Y. *Rep. Progr. Phys.* **19,** 107 (1956).
2. Spitzer W. G. and Fan H. Y. *Phys. Rev.*, **109,** 1011 (1958).
3. Fan H. Y. and Ramdas A. K. *Bull. Amer. Phys. Soc.* Ser. II, **3,** 129 (1958).
4. Hill D. E. and Lark-Horovitz K. *Bull. Amer. Phys. Soc.* Ser. II, **3,** 142 (1958).
5. Wertheim G. K. *Phys. Rev.* **105,** 1730 (1957); *Phys. Rev.* **110,** 1272 (1952); *Bull. Amer. Phys. Soc.* Ser. II, **3,** 142 (1958).
6. Longo T. A. *Bull Amer. Phys. Soc.* Ser. II, **2,** 355 (1957); Ph.D. Thesis (1957).
7. Longo T. A. and Lark-Horovitz K. *Bull. Amer. Phys. Soc.* Ser. II, **2,** 156 (1957).

*J. Phys. Chem. Solids* Pergamon Press 1959. Vol. 8. pp. 275–277. Printed in Great Britain

# J.3 INFRARED ABSORPTION OF FREE CARRIERS PRODUCED IN SEMICONDUCTORS BY PHOTOEFFECT

F. R. KESSLER

II. Physikalisches Institut der Universität Köln, Germany

VOL. 8 1959

In the following paper will be found the results of the infrared absorption of free carriers produced in semiconductors by the inner photoelectric effect in the range of the fundamental lattice absorption. The number of electrons and holes is equal because of the electrical neutrality of the crystal. The carrier absorption is modulated by the use of chopped light and detected by a tuned amplifier. Absorption measurements on *injected* carriers have been carried out in the case of germanium but with contradictory results.[1–3] The following investigation with photoelectrically-produced excess carriers tries to clear up these results for germanium and gives the absorption cross-section for electron–hole pairs in silicon.* Because the investigation method is independent of the macroscopic structure of the sample and is independent of an electrical contact or barrier layer it is hoped to extend the measurements to other polycrystalline semiconductors or photoconductors.

The following questions are connected with the production of carriers by photons:

(1) If the energy of the photon is greater than the energy gap, the carriers may have a large kinetic energy. The question of the decay of this energy is connected with the dependence of the effective mass on the kinetic energy. On the other hand, it is possible that the relative population of overlapping bands is changed.

(2) If one has a sufficiently high trap density one might have an optical regeneration of the carriers out of these traps and find the corresponding absorption band. In this case the trap level is given by the wavelength of the absorption maximum.

For germanium, the product of the absorption cross section and the number of electron–hole pairs is plotted against the wavelength in Fig. 1. One sees the well-known band spectrum that is due to the direct transitions of the free holes between the three valence bands. Relative to the holes the absorption by the electrons can be neglected. The spectrum coincides with that of $p$-type crystals in thermal equilibrium.[4] In the present work only the first $p$-band seems to have a preceding stage. In $p$-type samples this part is masked by the absorption edge. The measurements of NEWMAN[1] and BRIGGS and FLETCHER[2] with injected carriers are verified. In the present investigation, most of the carriers are produced by photons of 1·3 eV. Although the carriers then have an average kinetic energy of 0·3 eV, the relative population of the three valence bands is the same as in the thermal equilibrium. This is a result we expected because of the great lifetime of 150 $\mu$ sec and the collision time of $10^{-13}$ sec. Concerning the quantitative interpretation we are able to follow the calculations of KAHN[5] and KANE.[6]

The spectrum at 90°K is just the spectrum of $p$-type samples in regard to its quality, but the absorption is generally four times smaller. This is to be attributed to a decrease of the carrier density because the recombination rate is greater. In our case, the number of carriers is proportional to the generation rate and so the Shockley–Read mechanism for the recombination is valid.

The temperature dependence of the product $(q\bar{N})$ at constant wavelength and constant generation rate (Fig. 1) gives the temperature dependence of the lifetime, if one divides by the absorption cross section. It is done here according to the calculations of KAHN. In our case, the excess carrier density is about one hundred times greater

* These results have also been reported at the *International Conference on Solid State Physics in Electronics and Telecommunications*, Brussels, June, 1958.

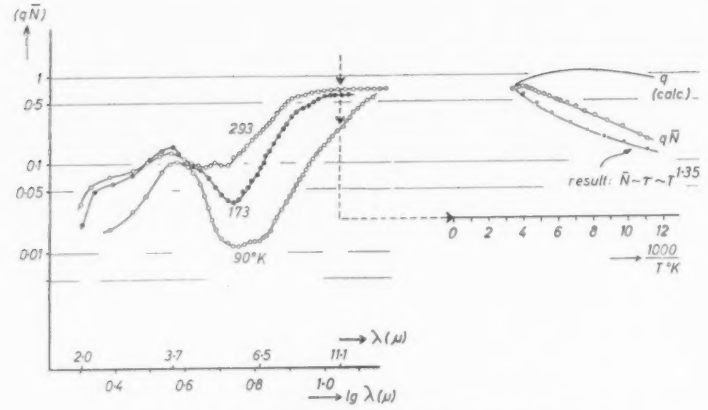


FIG. 1. Absorption of electron–hole pairs in germanium at constant photoelectric generation rate.

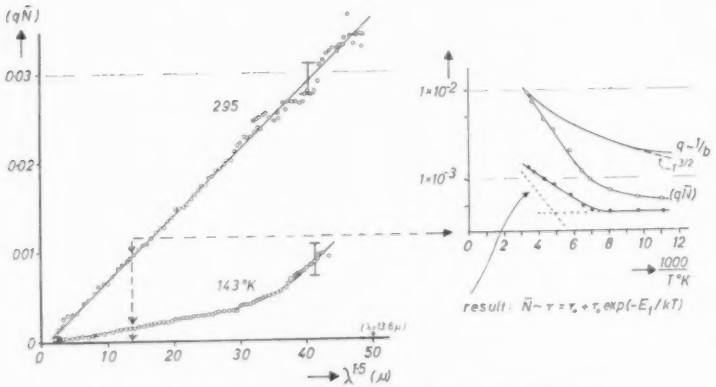


FIG. 2. Absorption of electron–hole pairs in silicon at constant photoelectric generation rate. $q$ = absorption cross-section ($cm^2$); $\bar{N}$ = Number of electron–hole pairs ($cm^{-2}$); $\lambda$ = wavelength; $b$ = mobility; $\tau$ = lifetime

than the equilibrium density and many orders of magnitude greater than the trap density. Therefore, as has been pointed out by HALL[7] the lifetime has reached its limiting value. Experimentally, we find for the lifetime $\tau \sim \Gamma^{1.35}$. Such a great temperature dependence can be understood only if the recombination is a three-body process in which a free carrier recombines with an ionized center and simultaneously excites a second free carrier to a higher energy state. For this process BURSTEIN, PICUS and SCLAR[8] find theoretically $\tau \sim \Gamma^2$.

Electron–hole pairs in silicon show very exactly the wavelength dependence with the power 1·5 according to the theory of Drude–Fröhlich (Fig. 2). Here the absorption cross-section of holes is greater than the cross-section of electrons as in germanium, because the absorption band of electrons at 2·3 $\mu$ is not visible as has been pointed out by SPITZER and FAN.[9] On the other side we expect an absorption band at 25 $\mu$ according to the transition of holes between the valence bands. In the range to 15 $\mu$ we find no sign of an increase of absorption.

The absorption at low temperature is perhaps sixteen times smaller and so we approach the limit at which we are able to detect the absorption of the excess carriers. Nevertheless, we find a characteristic deviation from the $\lambda^{1.5}$ law of Drude–Fröhlich. The absorption seems to increase to an absorption band which is above 15 $\mu$. We might assume that this is due to the influence of the $p$-band of the holes.

Another point is also considered. As in germanium, we are able to derive from the temperature dependence of the product $(q\bar{N})$ the temperature dependence of the number of carriers. The temperature dependence of the absorption cross-section lies in the mobility only. The mobility in a sample of about 100Ω-cm follows mainly the $T^{-3/2}$ law of the lattice scattering. For the lifetime one finds a temperature dependence of the form $\tau = \tau_0 + \tau_0 \exp(-E_t/kT)$ which is in accordance with the Shockley–Read recombination theory for small excess carrier densities. For the activation energy we find 0·05 eV which corresponds to the boron level. The absorption band at lower temperatures is possibly due to the regeneration of electrons out of these traps. 0·05 eV corresponds to a wavelength of 25 $\mu$ which lies at a position where we expect the $p$-band.

In conclusion we would like to add another remark. In experiments on recombination radiation one must pay attention to the fact that excess carriers give rise to an emission of long wave radiation corresponding to a real temperature radiation. According to Kirchhoff's law the absorption of the excess carriers increases the emissivity. At *constant* temperature one finds a modulated temperature radiation if the excess carrier density is modulated. This radiation was found and can not be neglected.[10]

### REFERENCES


1. Newman R. *Phys. Rev.* **91,** 1311 (1953); *Ibid.* **96,** 1188 (1954).
2. Briggs H. B. and Fletcher R. C. *Phys. Rev.* **91,** 1342 (1953).
3. Gigson A. F. *Proc. Phys. Soc.* **B66,** 588 (1953)
4. Kaiser W., Collins R. J. and Fan H. Y. *Phys. Rev.* **91,** 1380 (1953).
5. Kahn A. H. *Phys. Rev.* **97,** 1647 (1955).
6. Kane E. O. *J. Phys. Chem. Solids* **1,** 82 (1956).
7. Hall R. N. *Phys. Rev.* **87,** 387 (1952).
8. Burstein E., Picus G. and Sclar N. *Photoconductivity Conference,* New York (1956).
9. Spitzer W. and Fan H. Y. *Phys. Rev.* **108,** 268 (1957).
10. Kessler F. R. *Z. Naturf.* **13a,** 295 (1958).


*J. Phys. Chem. Solids* Pergamon Press 1959. Vol. 8. pp. 277–280. Printed in Great Britain

# J.4 EFFECTS ASSOCIATED WITH A LINEAR ENERGY TERM IN THE VALENCE BAND OF INTERMETALLIC SEMICONDUCTORS

FRANK STERN

U.S. Naval Ordnance Laboratory, White Oak, Silver Spring, Maryland

## 1. INTRODUCTION

Energy bands in III-V intermetallic semiconductors, which have a zincblende structure, differ somewhat from those in diamond-structure crystals. For the latter,[1] the bands are doubly degenerate and have zero slope for wave vector $\mathbf{k} = 0$. Neither of these restrictions need hold in the case of a zincblende structure.[2,3] It is, therefore, of some interest to investigate the differences in behavior of these two classes of semiconductors

that result from the differences in their band structure.

A convenient measure of the effect of the linear term is $E_{max}$, the height of the valence band* energy maximum relative to the energy at $\mathbf{k} = 0$. Theoretical estimates of this quantity for indium antimonide[3,4] give a value of the order of $10^{-4}$ eV. Analysis of the observed intrinsic optical absorption of InSb has not given conclusive information about $E_{max}$.[5]

## 2. OPTICAL ABSORPTION

A powerful tool for studying the linear term in the valence band is the temperature dependence of the optical absorption, in $p$-type material, associated with transitions between the light- and heavy-hole bands. Conditions for such a study appear to be most favorable in indium arsenide. Results of optical absorption experiments on a $p$-type sample of InAs have been reported by MATOSSI and STERN.[6] They compared the observed optical absorption with curves calculated according to KANE's theory.[4] Good agreement between theory and experiment could be obtained only if a linear term was included in the energy. The value of $E_{max}$ was estimated to be $0{\cdot}003 \pm 0{\cdot}003$ eV.

## 3. ELECTRICAL PROPERTIES

At low temperatures the presence of a linear term in the valence band will influence not only the optical absorption, but also the electrical properties of a $p$-type semiconductor. A sufficiently pure sample would have a much smaller ratio of light holes to heavy holes at low temperature than at room temperature; in germanium, the ratio is relatively insensitive to temperature. A study of the magnetic field dependence of the Hall constant at various temperatures can give information regarding the ratio of light holes to heavy holes.

The linear term causes substantial warping of the valence band near $\mathbf{k} = 0$, producing regions in which one or two principal effective mass components have the "wrong" sign. SHOCKLEY[7] called holes in such a region of the band "anomalous holes".†

We have carried out a numerical calculation of the density-of-states mass, of the conductivity mass, and of $\mu_H/\mu$, the ratio of Hall mobility to conductivity mobility, as functions of the position of the Fermi level for a completely degenerate heavy hole band. These calculations are based on the band structure approximations given by KANE,[4] which can be written in a dimensionless form in which $E_{max}$ enters only as a scale factor. We used two different sets of parameters to characterize the warping of the heavy hole band, because the experimental data presently available are not sensitive to the values of these parameters.

Results of the calculations are shown in Fig. 1. The most prominent feature is the strong reduction in $\mu_H/\mu$ near the energy at $\mathbf{k} = 0$. Our results are somewhat uncertain in this region, because the band structure approximation we used is not accurate there. The qualitative features of Fig. 1 are likely to be preserved in a more accurate treatment, in which DRESSELHAUS' quartic equation[3] could be used to find the valence band energies near $\mathbf{k} = 0$. The parameters of Fig. 1a, which give more warping near the valence band maximum than those of Fig. 1b, lead to negative values of $\mu_H/\mu$ for some positions of the Fermi level.

An electrical measurement to compare directly with the calculations presented in Fig. 1 is difficult to make, because an uncompensated sample at a low enough temperature to be degenerate would have most of its holes bound to acceptors, with very few carriers in the valence band. Anomalous effects have been reported[8] for InAs doped with zinc, but at a temperature higher than expected if $E_{max}$ is of the order of $3 \times 10^{-3}$ eV. DIXON[9] has prepared well-behaved samples in the same carrier concentration range as the anomalous samples.

A $p$-type sample of InAs studied by Dr. DIXON has a Hall constant of $+26$ cm$^3$/coulomb at room temperature, but a value only one-tenth as big at $4{\cdot}2$°K, with an intermediate maximum of $+50$ cm$^3$/coulomb. The large reduction in the Hall

* The splitting of the conduction band of InSb and InAs is probably of third order in the wave vector,[4] and will be neglected here.

† The Hall current involves the product of mobilities (hence reciprocal effective masses) in two mutually perpendicular directions. Thus if the principal effective mass components are not all of the same sign, anomalous contributions to the Hall constant arise.

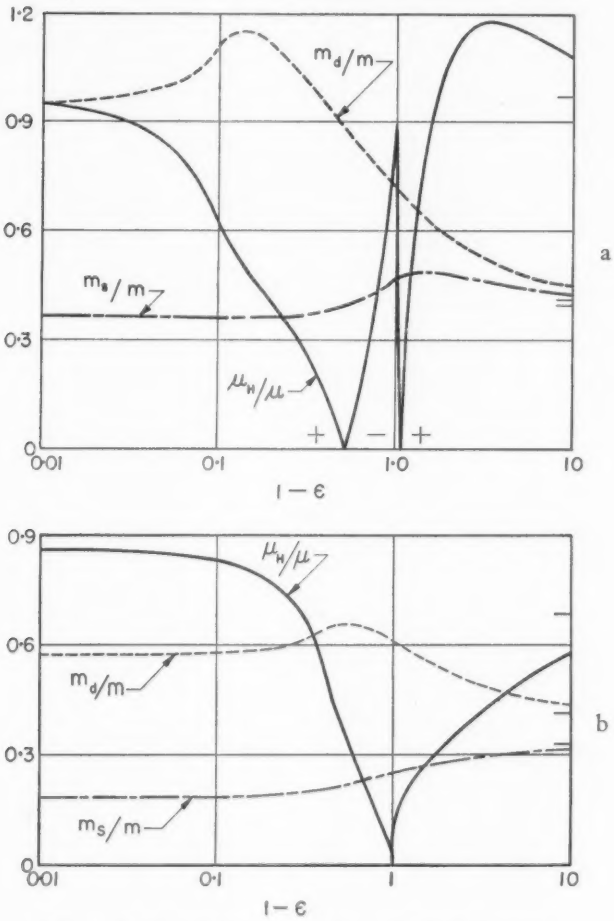


FIG. 1. Density-of-states mass $m_d$, conductivity mass $m_s$, (both relative to the free electron mass $m$) and ratio of Hall mobility to conductivity mobility $\mu_H/\mu$, for the heavy hole band of a degenerate intermetallic semiconductor are shown as functions of a dimensionless energy parameter $(1-\epsilon) = (E_v - E_F)/E_{max}$, where $E_{max}$ is the energy of the valence band maximum relative to the energy at $\mathbf{k} = 0$, and $E_v$ and $E_F$ are the energies of the top of the valence band, and of the Fermi level, respectively. The masses are defined by $m_d = \frac{1}{2}(3\pi^2\hbar^3 p)^{\frac{2}{3}}(E_v - E_F)^{-1}$ and $m_s = e\tau\mu^{-1}$, where $p$ is the hole concentration and $\tau$ is the mean scattering time at the Fermi level. The two groups of curves correspond to different valence band parameters; for Fig. 1a, $B = -5{\cdot}6(\hbar^2/2m)$, $C = -3{\cdot}0(\hbar^2/2m)$; for Fig. 1b, $B = -2{\cdot}0(\hbar^2/2m)$, $C = -5{\cdot}0(\hbar^2/2m)$; in both cases $A = D = F = 0$ (the notation is from reference 4). These two sets of parameters give approximately the same density-of-states mass far from the top of the valence band, but correspond to bands of different shape. Note that $\mu_H/\mu$ is negative near $\epsilon = 0$ in FIG. 1a.

constant of this sample at low temperatures may be associated with the effects we have described.

## 4. SUMMARY

The existence of the linear term in the valence band of indium arsenide has already been established from analysis of the optical absorption at low temperatures.[6] Additional calculations are reported in this paper which show that the linear term will substantially affect the electrical properties of $p$-type intermetallic semiconductors. Experimental tests of these predictions are complicated by the fact that most holes will be bound to acceptors at the low temperatures for which the effect of the linear term is most pronounced.

*Acknowledgment*—I am grateful to Dr. JACK R. DIXON for making his unpublished measurements available, and for valuable discussions.

## REFERENCES

1. ELLIOTT R. J. *Phys. Rev.* **96,** 280 (1954).
2. PARMENTER R. H. *Phys. Rev.* **100,** 573 (1955).
3. DRESSELHAUS G. *Phys. Rev.* **100,** 580 (1955).
4. KANE E. O. *J. Phys. Chem. Solids* **1,** 249 (1957).
5. POTTER R. F. *Phys. Rev.* **103,** 861 (1956); FAN H. Y. and GOBELI G. W. *Bull. Amer. Phys. Soc.* Ser. II **1,** 111 (1956); BLOUNT E., CALLAWAY J., COHEN M., DUMKE W. and PHILLIPS J. *Phys. Rev.* **101,** 563 (1956).
6. MATOSSI F. and STERN F. *Phys. Rev.* **111,** 472 (1958).
7. SHOCKLEY W. *Electrons and Holes in Semiconductors*, p. 338. Van Nostrand, New York (1955).
8. FOLBERTH O. G. and WEISS H. *Z. Naturf.* **11a,** 510 (1956).
9. DIXON J. R. *Bull. Amer. Phys. Soc.* Ser II **3,** 120 (1958).

VOL 8 195

*J. Phys. Chem. Solids* Pergamon Press 1959. Vol. 8. pp. 280–282. Printed in Great Britain

# J.5 INTERVALENCE BAND TRANSITIONS IN GALLIUM ARSENIDE*

**R. BRAUNSTEIN**

Radio Corporation of America, RCA Laboratories, Princeton, New Jersey

THE infrared absorption due to free holes in $p$-type gallium arsenide exhibits three absorption bands on the low-energy side of the intrinsic absorption edge.[1] $n$-Type gallium arsenide does not show this characteristic structure, but instead exhibits a monotonically increasing absorption with wave length. The same structure is found in all $p$-type samples and consequently the evidence is that these bands are not due to the presence of unknown impurities or lattice defects. The spectra can be explained in terms of hole transitions between various branches of the valence band of gallium arsenide. Similar intervalence band transitions have been identified in germanium[2] and indium arsenide.[3] From a consideration of the atomic spin-orbit splitting of gallium, arsenic, and germanium obtained from atomic spectra and the values obtained in the solid of gallium arsenide and germanium, it is expected that intervalence band transitions should be observable in a number of other semiconducting compounds and alloys.

The absorption spectra of gallium arsenide as a function of temperature are shown in Fig. 1. This sample was specifically doped with zinc. Aside from slight differences in the positions of these bands, the structure is very similar to that seen in $p$-type germanium.[2] At 295°K, there is a band at 0·42 eV, a partially resolved band at 0·31 eV, and the onset of a band at 0·25 eV. As the temperature is decreased, the bands sharpen and become slightly displaced from the room temperature positions. Cobalt-doped samples show identical

* Supported in part by the U.S. Air Force.

structures and a similar temperature dependence. Fig. 2 shows the absorption spectra of $p$-type gallium arsenide at 295°K for a range of carrier concentrations. The absorption cross section, i.e. absorption coefficient/free carrier density, at a given energy is approximately constant. Some samples that were measured had anomalously high absorption cross sections, although their free carrier densities were less than those shown in Fig. 2. These samples were found to have a high density of compensating impurities.

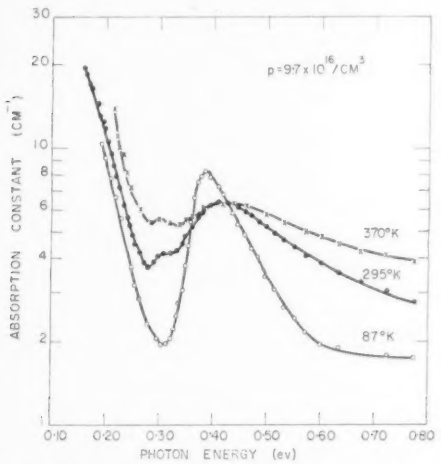


FIG. 1. The absorption spectra of $p$-type gallium arsenide as a function of temperature.

If one assumes, for simplicity, a valence band structure for gallium arsenide similar to that of germanium[4,5] the features of the spectra in Fig. 1 can be explained in terms of vertical transitions between different branches of the valence band of gallium arsenide. The band at 0·42 eV is attributed to transitions between band 3, the band split off by spin–orbit interaction, and band 1, the heavy-hole band; the peak at 0·31 eV is attributed to transitions between band 3 and band 2, the light-hole band. The onset of the absorption band at 0·25 eV is then attributed to transitions between the light- and heavy-hole bands. The designations of the bands are the same as used for germanium. The value of the spin–orbit splitting obtained from the above analysis is $\simeq 0{\cdot}33$ eV; the ratios of the effective masses for the holes are: $m_1^*/m_3^* = 3{\cdot}38$ and $m_3^*/m_2^* = 1{\cdot}70$. This evidence for the existence of light- and heavy-holes will necessitate their consideration in transport theories for gallium arsenide. Since the gallium arsenide lattice lacks a center of inversion, it is expected that the degeneracy of the heavy-hole bands will be split.[6,7] Consequently, the energy maxima of the valence band would lie above the energy at the center of the zone. To obtain evidence for the linear term requires a quantitative study of the shape of the peak due to transitions between the light- and heavy-hole bands. Such work is in progress at this laboratory.

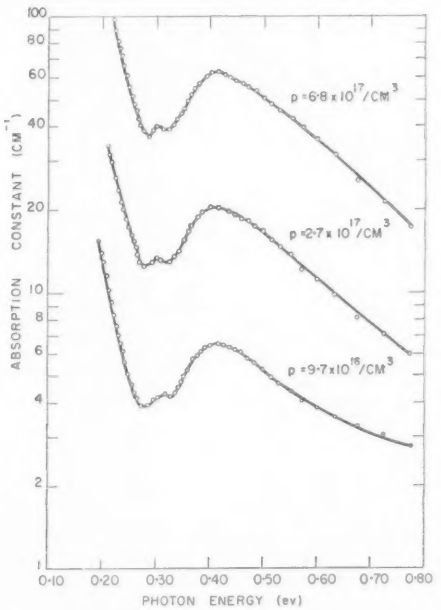


FIG. 2. The absorption spectra of $p$-type gallium arsenide at 295°K for a range of carrier concentrations.

The value of 0·33 eV obtained for the spin–orbit splitting in gallium arsenide allows an estimate to be made of the time a valence electron spends, at $\mathbf{k}=0$, on a gallium and arsenic atom. The spin–orbit splitting of atomic $p$-functions of Ga, As, and Ge as estimated from atomic spectra are 0·10, 0·30, and 0·20 eV respectively.* The splitting for germanium in the solid is 0·29 eV.[4,5] If we assume the same normalization factor for gallium arsenide as seems appropriate for germanium in estimating the spin–orbit splitting in the solid

* These estimates were kindly supplied by E. O. KANE.

from the free atom value, namely 29/20, it is found that an electron at the top of the valence band spends 65 per cent of its time on arsenic and 35 per cent of its time on gallium.

The only reported structures due to intervalence band transitions are for germanium,[2] indium arsenide,[3] and gallium arsenide. In indium arsenide only one transition was observed; the transitions from the split-off valence band to the light- and heavy-hole bands occur at energies which overlap the intrinsic edge and consequently were not resolved. If the assumption is made that in indium arsenide a valence electron at $k = 0$ spends 65 per cent of its time on arsenic and 35 per cent of its time on indium, and that the same normalization factor of 29/20 as was used for germanium and gallium arsenide applies, one would expect a spin–orbit splitting of 0·43 eV. This value is in surprisingly good agreement with the observed value of 0·43 eV.* If the same simple criterion for estimating the spin–orbit splitting in other III-V compounds is applied, one would expect to observe all three intervalence band transitions in InP, GaP, AlP, AlAs, AlSb. The essential factor for their observation is that the spin–orbit splitting be less than the band gap and that free carrier absorption does not broaden or obscure the structures.

* Reference 3 give this value as 0·46 eV from initial measurements; the value of 0·43 eV was kindly supplied by F. STERN (private communication).

In pure silicon, the intervalence band transitions have not been observed, since the structure is probably obscured by free carrier absorption. In the germanium–silicon alloy system, one might hope to observe a shift of the bands from the positions in pure germanium due to the addition of silicon and hence obtain a value for the silicon spin–orbit splitting by extrapolation. In the germanium–silicon alloys an electron at the top of the valence band should have an equal probability of residing at a silicon or germanium site, weighted by the relative proportions of silicon and germanium. Indeed, in this system three well resolved bands have been observed at this laboratory. Similar considerations to the above lead one to expect that intervalence band transitions should be observable in other alloy systems.

*Acknowledgment*—I wish to thank D. A. KRAMER for his assistance in this work.

## REFERENCES

1. BRAUNSTEIN R. and MAGID L. *Phys. Rev.* **111,** 480 (1958).
2. BRIGGS H. B. and FLETCHER R. C. *Phys. Rev.* **87,** 1130 (1952); *Ibid.* **91,** 1342 (1953).
3. STERN F. and TALLEY R. M. *Phys. Rev.* **108,** 158 (1957).
4. KAHN A. H. *Phys. Rev.* **97,** 1647 (1955).
5. KANE E. O. *J. Phys. Chem. Solids* **1,** 83 (1956).
6. PARMENTER R. H. *Phys. Rev.* **100,** 573 (1955).
7. DRESSELHAUS G. *Phys. Rev.* **100,** 580 (1955).

*J. Phys. Chem. Solids* Pergamon Press 1959. Vol. 8. pp. 282–285. Printed in Great Britain

# J.6 INFRARED LATTICE VIBRATION STUDIES OF POLAR CHARACTER IN COMPOUND SEMICONDUCTORS

G. PICUS, E. BURSTEIN, B. W. HENVIS and M. HASS

U.S. Naval Research Laboratory, Washington, D.C.

THE presence of some polar bonding in III-V compound semiconductors has been found to have important effects on electronic energy level structure and transport properties in these materials. It is therefore of importance to have some means of characterizing the magnitude of the polar contribution to the crystal bond. One measure of this in simple diatomic lattices is the effective charge

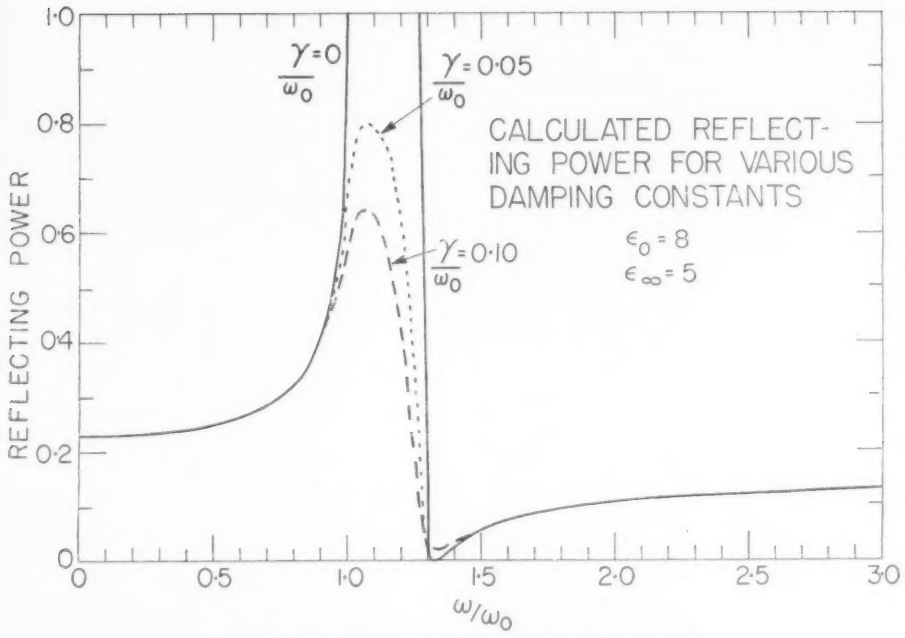


FIG. 1. Theoretical reflectivity curves for a simple polar material for different dissipative forces.

residing on the atoms. This effective charge can be deduced from a study of the optical properties of a polar material in the anomalous dispersion region associated with the interaction of electromagnetic radiation with the optical lattice vibration modes. For materials with any polar character there will be, in this frequency region, a strong rest-strahlen reflection peak from which the frequencies of the transverse and longitudinal optical vibration modes of the crystal can be determined. From this information together with data on the optical and static dielectric constants, the effective ionic charge can be calculated. In this paper we report the results of measurements of the far infrared spectra of five of the III-V compound semiconductors, the transverse and longitudinal optical lattice vibration frequencies determined from the measurements, and the effective charges calculated therefrom.

The dispersion theory applicable to this problem has been developed by BORN, SZIGETI,[1] and HUANG and is comprehensively treated by BORN and HUANG.[2] The features of importance to us will be briefly reviewed here. If dissipative forces are neglected, the dependence of the dielectric constant of an ionic lattice on frequency is given by:

$$\epsilon(\omega) = \epsilon_\infty + \frac{\epsilon_0 - \epsilon_\infty}{1-(\omega/\omega_0)^2} \qquad (1)$$

where $\epsilon_\infty$ is the optical (high frequency) dielectric constant, $\epsilon_0$ is the static (low frequency) dielectric constant, and $\omega_0$ is the circular infrared dispersion frequency, i.e., the lattice vibration frequency for long wavelength transverse waves. The reflectivity for this material is given by

$$R = \left|\frac{n-1}{n+1}\right|^2 \qquad n = \sqrt{\epsilon}$$

where $n$ is the index of refraction.

In the region $0 < \omega < \omega_0$ $R$ increases from its low-frequency value, $\{(\sqrt{\epsilon_0}-1)/(\sqrt{\epsilon_0}+1)\}^2$, up to 1. From $\omega_0$ up to a frequency $\omega_1 = \sqrt{(\epsilon_0/\epsilon_\infty)}\omega_0$, $\epsilon(\omega)$ is negative, $n$ is therefore imaginary, and $R = 1$. Above $\omega_1$, $R$ decreases rapidly to zero at a frequency $\omega_m = \omega_0\{1+(\epsilon_0-\epsilon_\infty)/(\epsilon_\infty-1)\}^{\frac{1}{2}}$, and beyond $\omega_m$, $R$ increases slowly until it attains its high-frequency limit of $\{(\sqrt{\epsilon_\infty}-1)/(\sqrt{\epsilon_\infty}+1)\}^2$. The $\gamma/\omega_0 = 0$ curve in Fig. 1 is characteristic of

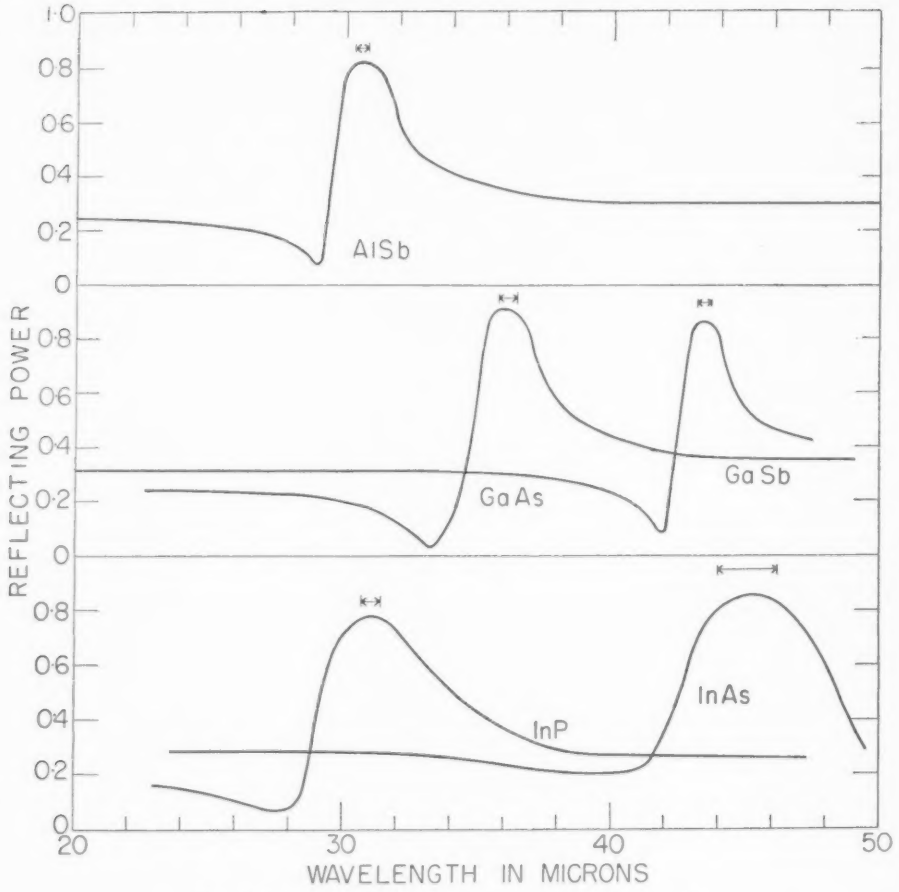


FIG. 2. Rest-strahl reflection spectra of III-V compound semiconductors.

such a reflection peak. The other two curves show the effect of the introduction of dissipative forces into the lattice equations of motion. The peak reflectivity does not rise to one and the minimum does not fall all the way to zero. In addition, the position of the minimum moves to higher frequencies. However, it is still possible to estimate $\omega_0$ and $\omega_1$ from the curves. $\omega_1$ has the significance that it is the frequency of the long-wavelength longitudinal lattice vibration mode.

The effective charge is given in terms of the dielectric constants and vibration frequencies by BORN and HUANG[2]

$$se = \omega_0\left(\frac{\epsilon_0-\epsilon_\infty}{4\pi}\right)^{\frac{1}{2}}\left(\frac{3}{\epsilon_\infty+2}\right)(\bar{M}v_a)^{\frac{1}{2}}$$

where $\bar{M}$ is the reduced mass of the positive and negative ion pair and $v_a$ is the volume of a primitive unit cell. The quantity $s$ is the ratio of the effective charge to the free electron charge $e$.

The values of $\epsilon_\infty$ were obtained from the optical data of OSWALD and SCHADE[3] at short wavelength. $\omega_0$ and $\omega_1$ were estimated from our reflection measurements, the results of which are presented in Fig. 2. $\epsilon_0$ was calculated from the relation

$\epsilon_0/\epsilon_\infty = \omega_1^2/\omega_0^2$, and finally $s$ was calculated using equation (2).

The results are presented in Table 1. In the case of InSb we used the data of YOSHINAGA and OETJEN[4] to determine $\omega_0$ and $\omega_1$. Our result agrees well with the value of 0·34 reported by FAN and SPITZER[5] from their measurements.

*Table* 1. *Transverse and longitudinal lattice vibration frequencies and effective charge*

| Compound | $\omega_0$ ($sec^{-1}$) | $\omega_1$ ($sec^{-1}$) | $s$ |
|---|---|---|---|
| AlSb | $5{\cdot}92\times10^{13}$ | $6{\cdot}32\times10^{13}$ | ·48 |
| GaAs | $5{\cdot}04$ | $5{\cdot}35$ | ·43 |
| GaSb | $4{\cdot}25$ | $4{\cdot}40$ | ·30 |
| InP | $5{\cdot}74$ | $6{\cdot}38$ | ·60 |
| InAs | $3{\cdot}95$ | $4{\cdot}38$ | ·56 |
| InSb | $3{\cdot}28$ | $3{\cdot}46$ | ·34 |

The units for the circular frequencies are $sec^{-1}$. $s$ is a dimensionless quantity.

There are several factors which must be borne in mind in interpreting these data, since a small change in $\omega_0$ or $\omega_1$ produces a much larger change in $s$. First, wavelength calibration is accurate only to about 2 per cent beyond 30 $\mu$. Second, no attempt has been made to correct for the effect of the rather large finite slit width used. Third, the presence of free carriers can affect the reflection spectra (particularly in InAs and InSb) although the data of YOSHINAGA and OETJEN[4] indicate that this effect is most pronounced at the minimum and has little effect at the peak. There is also uncertainty in the estimates of $\omega_0$ and $\omega_1$ from the reflection data.

It is of interest to compare the optically measured vibration frequencies of GaAs with those measured for Ge by BROCKHOUSE and IYENGAR[6] using inelastic neutron scattering techniques. $\bar{M}$ and $v_a$ are the same for these two materials BROCKHOUSE finds $5{\cdot}7\times10^{13}\,sec^{-1}$ for $\omega_0$ in Ge as compared to $5{\cdot}0\times10^{13}\,sec^{-1}$ in GaAs.

*Acknowledgments*—We wish to acknowledge the contribution of S. I. SLAWSON of the U.S. Naval Research Laboratory who prepared the reflection samples for us. The materials used in these experiments were obtained through the kindness of F. BECKER of the National Bureau of Standards (AlSb and GaSb), D. A. JENNEY and R. BRAUNSTEIN of RCA Laboratories (GaAs and InP) and S. TALLEY of the Naval Ordnance Laboratory (InAs).

## REFERENCES

1. SZIGETI B. *Proc. Roy. Soc.* A**204,** 52 (1950).
2. BORN M. and HUANG K. *Dynamical Theory of Crystal Lattices.* Oxford Press (1954).
3. OSWALD F. and SCHADE R. *Z. Naturf.* **9a,** 611 (1954).
4. YOSHINAGA H. and OETJEN R. A. *Phys. Rev.*, **101,** 526 (1956).
5. FAN H. Y. and SPITZER W. G. *Phys. Rev.* **99,** 1893 (1955).
6. BROCKHOUSE B. N. and IYENGAR P. K. *Bull. Amer. Phys. Soc.* **3,** 192 (1958).

## DISCUSSION

*Compiled by* E. BURSTEIN

### J.1. H. J. G. MEYER

H. Y. FAN: The calculation uses the same approach employed in my previous calculations, but takes into account the multi-ellipsoidal band structure explicitly. We note that the $T$ and $\lambda$ dependences of the acoustic phonon effect, in the range $h\nu > kT$, given by the two calculations are the same: $\lambda^{\frac{1}{2}}T$. Numerically, a difference of 30 per cent is obtained depending on the values of deformation potentials used in Meyer's calculation and the values of effective mass and mobility used in our calculation. As to the use of our experimental data, higher temperature data should be used for deducing the lattice effect. At low temperature, impurity scattering is important and lattice effects are obtained less reliably by extrapolation. I wish also to point out that in the paper by FAN, COLLINS and SPITZER, the calculated $\mathcal{L}(\nu)$ curve for 78°K inadvertantly omitted a factor of 78/293.

H. G. Meyer: The principle of the method used in the calculations is indeed the same as that of Professor FAN's calculation. In fact the aim of our calculation was only to incorporate the modern knowledge about band structure and scattering mechanisms in the theory of light absorption so that experiments in this field can be used for obtaining data on the scattering mechanism and possibly on the band structure. It should be mentioned, however, that there are qualitative differences between our results and those following from Professor FAN's calculation, namely in the case of acoustical lattice scattering for $h\nu < 2kT$ and in the case of impurity scattering for $h\nu \gg 2kT$. In both cases, the present calculations seem fit to the data somewhat better.

*J. Phys. Chem. Solids* Pergamon Press 1959. Vol. 8. pp. 286–289. Printed in Great Britain

## SESSION K:
## IONIC CRYSTALS*

# K.1 ELECTRONIC STRUCTURE OF AN EXCITON IN ALKALI HALIDES†

**T. MUTO, S. OYAMA and H. OKUNO**

The Institute for Solid State Physics, University of Tokyo, Tokyo

VOL. 8 195

### 1. INTRODUCTION

THE common characteristic features of the previous theoretical methods of treating an exciton in ionic crystals may be described in the following way. At first, the appropriate one-electron orbital is constructed in which an electron is moving in the specified electrostatic field in a Hartree sense, and then Slater's determinantal functions are set up corresponding to each electron configuration. The configuration interaction is worked in a suitable way, taking account of the effective electron configurations. In previous theories of the exciton, however, the exciton characteristics do not make their appearances in the zero-th order description (one-electron approximation) but only in the higher order approximation through the configuration interaction (correlation effect).

The self-consistent procedure for constructing the Hartree field on a crystal electron can scarcely be carried out owing to mathematical difficulties, but instead the periodic field assumption is usually adopted on physical grounds. Thus, it seems worthwhile to investigate carefully the one-electron potential in the ionic crystal that is best for the exciton problem. Now, crude considerations regarding the excess positive charge left after the removal of an electron seem to show that the average electrostatic field on an electron in a metallic crystal will presumably be sufficiently periodic in space owing to screening by the remaining electrons. For the ionic crystal, however, the residual positive charge may be reasonably supposed to be more or less localized around an ion or a group of ions within the crystal since the electrons of an ionic crystal may be regarded as relatively strongly bound to the individual ions in the crystal. The Hartree field in an ionic crystal, therefore, will probably be considered to become non-periodic in the vicinity of the mentioned ion or a group of ions.

Our new approach to the exciton structure is to adopt the one-electron orbitals in the mentioned perturbed periodic field as a starting point for the conventional method in the many electron treatment of ionic crystals. In fact, the suitably chosen, perturbed periodic field for potassium chloride has been shown[3] to give rise to a number of localized states just below the conduction continuum, which have actually some of the exciton characteristics and are seen to correspond to Dexter's excitation model. The comparison of the results with experiment seems to be rather good,[3] compared with the earlier model of von Hippel. In order to extend the validity of our method of procedure for the zero-th order description of an exciton in alkali halides, similar calculations were carried out for all alkali chlorides and furthermore, for an exciton localized around a negative ion vacancy in alkali chlorides, which corresponds to one of the Greek letter bands observed by PRINGSHEIM and others in alkali iodides and bromides.

As a next higher approximation, we shall deal with a moving exciton by taking into account the configuration interaction based on the one-electron orbitals mentioned above. The results

* *Chairman:* S. AMELINCKX; *Co-Chairman:* P. H. MILLER, Jr.

† A full account of the present article will be published in *Prog. Theor. Phys., Japan* (1958).

seem to correspond roughly to some refinement of the pioneer work by FRENKEL[1] and will be valid for the small size exciton. Finally, a brief discussion of the effect of the spin-orbit coupling on the exciton structure will be added and a possible interpretation for the doublet splitting of the exciton peak in KCl and NaCl at low temperatures will be proposed.

## 2. THE ZERO-ORDER DESCRIPTION OF AN EXCITON IN ALKALI HALIDES

The previous method of procedure[3] has been extended to all alkali chlorides in which the main task is to solve numerically the Slater–Wannier's effective mass equation of an electron in the field of a positive hole in a Cl $3p$ state, allowing for the polarization of the surrounding ions. The results are shown in Table 1, in which $\kappa$ denotes the effective dielectric constant, $m^*$ the effective mass

*Table* 1.

| | $\kappa$ | $m^*/m$ | $-E'_{cal}$(eV) | $-E'_{obs}$(eV) |
|---|---|---|---|---|
| LiCl | 2·75 | 0·6 | 0·89 | 0·86 |
| NaCl | 2·25 | 1·0 | 1·81 | 1·83 |
| KCl | 2·13 | 0·85 | 1·83 | 1·80 |
| RbCl | 2·19 | 0·7 | 1·53 | 1·50 |
| CsCl | 2·60 | 0·9 | 1·33 | 1·39 |

of the conduction band and $-E'$ the energy of an exciton ground state measured from the conduction band edge.

For an exciton in the immediate vicinity of a negative ion vacancy, we have to solve numerically the Slater–Wannier equation for the field constructed by allowing for both contributions from a positive hole in a Cl $3p$ state as well as the effect of a missing nearest neighbour chlorine ion and the polarization of the surrounding medium. According to the variational method, the trial function is assumed to be given by a superposition of a $p$-type function on to an $s$-type one, taking account of the fact that the attractive field extends towards a negative ion vacancy. The numerical results are shown in Table 2, in which B.I. expresses the result obtained by BASSANI and INCHAUSPE[4] through a cycle method similar to that adopted in the semi-classical treatment of VON HIPPEL. $\Delta E'$ in Table 2 expresses the energy difference between a normal exciton peak and a localized exciton around a missing anion. The comparison seems to be rather fair, although Greek bands in alkali chlorides have not yet been observed experimentally. According to DEXTER,[5] the oscillator strength and the charge distribution of the present model have been shown to be a satisfactory zero-order description.

*Table 2.*

| | $\Delta E'_{cal}$(eV) | B.I. (eV) | $\Delta E'_{obs}$(eV) |
|---|---|---|---|
| LiCl | 0·30 | — | — |
| NaCl | 0·58 | 0·50 | — |
| KCl | 0·54 | 0·53 | — |
| RbCl | 0·56 | — | — |
| CsCl | 0·23 | — | — |
| KBr | — | 0·49 | 0·59 |
| KI | — | 0·44 | 0·59 |

Summing up the results obtained so far, the one-electron orbitals in a suitably chosen perturbed periodic potential may be considered to afford a good zero-th order description of an exciton in alkali halides, compared with the previous model.

## 3. A MOVING EXCITON

In the following computation of a moving exciton the above mentioned, localized exciton state below the conduction band is adopted as a one-electron orbital of the excited state. The ground states of the valence electrons are supposed to be described approximately by the one-electron orbitals of the simple band theory since the majority of valence electrons is expected to lie in the region of a valence continuum which behaves quite similarly to the valence band and a few of them are brought into the localized states below a valence continuum, as revealed in the $K_\beta$ emission line in KCl.[6] Furthermore, the inner shell electrons within each ion are amalgamated into the atomic core whose interaction with the valence electrons is represented by a suitable periodic potential $V_p(\boldsymbol{r})$. As for the available electron configurations, we shall confine ourselves to the configuration with one electron excited to a ground state of the localized exciton below the conduction band from any one level of a valence band and the other configurations are approximately disregarded mainly for the sake of mathematical simplicity.

According to the different spin orientations of an excited electron and a positive hole, we have singlet and triplet states, whose determinantal functions are

$$^1\Psi^{(nl;el)} = 1/\sqrt{2}\{\Phi^{(nl\uparrow;el\downarrow)} + \Phi^{(nl\downarrow;el\uparrow)}\} \quad (1)$$

$$^3\Psi_0^{(nl;el)} = 1/\sqrt{2}\{\Phi^{(nl\uparrow;el\downarrow)} - \Phi^{(nl\downarrow;el\uparrow)}\}, \quad (2)$$

and

$$^3\Psi_{+1}^{(nl;el)} = \Phi^{(nl\uparrow;el\uparrow)}, \quad (3)$$

$$^3\Psi_{-1}^{(nl;el)} = \Phi^{(nl\downarrow;el\downarrow)} \quad (4)$$

where the suffix on $\Phi$ denotes the states and locations of an excited electron and a positive hole, including spins.

In accordance with the general procedure of configuration interaction, we obtain, for an exciton wave function,

$$^i\Psi = \sum_n {}^iA_n \sum_l e^{i\boldsymbol{K}\cdot\boldsymbol{R}_l} {}^i\Psi^{(nl;el)} (i = 1, 3) \quad (5)$$

and the corresponding secular equation leads to a $3\times3$ determinant corresponding to three branches of a valence band. Closer examination of the energy matrix reveals that, for $\boldsymbol{K} = 0$, i.e. an exciton peak, the off-diagonal elements become quite small compared with the diagonal ones, which take the following form:

$$^iE^{(n,n)} = Eg + E^{\text{exc}} - (E_{\text{atom}}(3p) + V_M) \pm$$

$$\pm E_{\text{exch}} - \sum_{l'} S_{ll'} \cdot \epsilon_n(\boldsymbol{R}_{l'} - \boldsymbol{R}_l) + \Delta E \quad (6)$$

where $E_g$, $E^{\text{exc}}$, $E_{\text{atom}}(3p)$ and $V_M$ express the ground state energy of the crystal as a whole, a localized exciton energy, an atomic energy of a $3p$ electron in $Cl^-$ and the Madelung potential at a $Cl^-$, respectively. The fourth term represents the exchange energy of an exciton-electron with a hole at the same location, $S_{ll'}$ the overlap-integral of localized exciton wave functions with different locations and $\epsilon_n(\boldsymbol{Rj})$ the Fourier transform of the Bloch energy of a valence band. $\pm$ stands for a singlet or triplet state and $\Delta E$ represents the minor contribution from the various quantities of small magnitude.

Thus, the peak frequency is given by

$$h\nu(\boldsymbol{K} = 0) = {}^iE^{(n,n)} - E_g. \quad (7$$

Substituting into (6) and (7) the appropriate estimates of the various quantities involved, using the previous results[3] and the numerical data of HOWLAND,[7] we get $h\nu(\boldsymbol{K} = 0) = 8{\cdot}3$ eV $\sim 9{\cdot}0$eV for a singlet exciton peak at $T = 0{\cdot}$K, which is to be compared with the observed value of 7·8 eV at room temperatures. The agreement seems rather good in view of the observed shift to shorter wavelength of a peak frequency with decreasing temperatures and the many crude estimates of the various quantities involved in (6), together with the disregard of a contribution from $\Delta E$.

For $\boldsymbol{K} \neq 0$, we have at most three components of an exciton multiplet. However, taking account of the spin–orbit coupling of $N$ electrons leads to a $12\times12$ secular determinant whose matrix elements can easily be computed. Then, we have at most twelve components of an exciton multiplet and the singlet wave functions are mixed up with the triplet ones, making possible the transition to the mostly triplet exciton states. Unfortunately, the numerical solution of the above secular determinantal equation has not been obtained as yet. In this connection, it should be remarked that not all the exciton multiplet components are always observed experimentally on account of the limited resolution of the optical instrument and the temperature-broadening.

Finally, we should like to add some discussion on the recent experiment by HARTMAN, NELSON and SIEGFRIED.[8] In their reflection experiment, they have actually observed the apparent doublet splitting of an exciton peak of KCl and NaCl below 150°K. The observed splitting at 6°K becomes 0·14 eV for KCl. Their result may probably be interpreted as follows. In view of the relatively small spin–orbit coupling in alkali chlorides, a singlet exciton peak will be practically unchanged and the splitting of a triplet exciton peak will perhaps be too small to be resolved experimentally in the presence of temperature broadening. The only sizable effect of the spin-orbit coupling is to mix the singlet wave function with the triplet one, which results in the weak transition to the mostly triplet state. If the above consideration were really valid, the short wave length peak of high intensity would correspond to a mostly singlet exciton and the long wave length peak of low intensity to a mostly triplet one. For the energy separation between a singlet exciton and a triplet one, Equation (6) gives

$2 \times E_{exch}$, whence $E_{exch}$ becomes 0·07 eV, making use of the observed data mentioned above. The result seems to be reasonable.

### REFERENCES


1. FRENKEL J. *Dokl. Akad. Nauk SSSR, fiz. ser.* **8,** 185 (1936); *Ibid.* **9,** 158 (1936).
2. SLATER J. C. and SHOCKLEY W. *Phys. Rev.* **80,** 705 (1936).
3. MUTO T. and OKUNO H. *J. Phys. Soc. Japan* **11,** 633 (1956).
4. BASSANI F. and INCHAUSPE N. *Phys. Rev.* **105,** 819 (1957).
5. DEXTER D. L. *Phys. Rev.* **108,** 707 (1957).
6. PARRATT L. G. and JOSSEM S. L. *Phys. Rev.* **97,** 916 (1955).
7. HOWLAND L. P. *Phys. Rev.* **109,** 1927 (1958).
8. HARTMAN P. L., NELSON J. R. and SIEGFRIED J. G. *Phys. Rev.* **105,** 123 (1956).


*J. Phys. Chem. Solids* Pergamon Press 1959. Vol. 8. pp. 289–290. Printed in Great Britain

VOL. 8 959

# K.2 EXCITON-LATTICE INTERACTION AND A THEORY OF THE LINE SHAPE OF EXCITON ABSORPTION BANDS


**Y. TOYOZAWA**

Research Institute for Fundamental Physics, Kyoto University, Kyoto, Japan


A NUMBER of theoretical investigations have been made on the electronic structures[1] of the exciton in insulators, and the results of calculations of energy levels and oscillator strengths have been compared with the peak positions and the strengths of exciton absorption bands. Also the problem of exciton–lattice interaction[1] has been attacked by several authors; however, the theoretical conclusions can be compared with experiment only in an indirect way, because most of the experimental data available at present are optical. The purpose of the present paper is to develop a theory for the line shapes of exciton absorption bands.[2]

The exciton–lattice interaction Hamiltonian $H_I$ is derived with the use of Wannier's exciton wave function. It consists of the contributions from the electron in the conduction band and the hole in the valence band, each multiplied with an effectiveness factor which depends on the phonon wave-number as well as on the internal states (bound or ionized) of the exciton before and after scattering. Due to the electrical neutrality of an exciton, the optical mode of vibration is not important in the *intra*band scattering, especially in the scattering of thermal excitons to which long wave phonons alone can contribute. On the other hand, the contribution of the optical mode may be as large as that of the acoustical mode in the case of the *inter*band scattering in which the internal state of the exciton changes.

For the investigation of the line shapes of exciton absorption bands, it is convenient to introduce a generating function—the Fourier transform ($\omega \to t$) of the absorption coefficient—which, in the present case, can be written as

$$A(t) = \sum_{\lambda} \sum_{\lambda'} F_{\lambda\lambda'} Tr_L \times$$

$$\times \{e^{-(\beta - it/\hbar)H_L} \langle \lambda 0 | e^{-iHt/\hbar} | \lambda' 0 \rangle\} / Tr_L(e^{-\beta H_L}).$$

Here $H$ consists of the exciton energy $H_e$, the lattice vibrational energy $H_L$ and the interaction $H_I$, $|\lambda K\rangle$ represents the eigen-state of $H_e$ with internal quantum number $\lambda$ and the translational momentum $K$, and $(F\mu)^{\frac{1}{2}}$ is proportional to the transition dipole moment between the ground and the $\lambda$-th excited state of the crystal.

The exponential in the formula can be expanded in power series of $H_I$, but in the following two

limiting cases, the series for each diagonal term ($\lambda = \lambda'$) reduces to closed forms, leading to typical line shapes of each absorption peak ($\lambda$).

(1) When the exciton–lattice interaction and the exciton effective mass $m^*$ are not large and the temperature $T$ is not too high, the absorption band has a *Lorentzian* shape (motional narrowing), provided that $\boldsymbol{K} = 0$ is neither at the top nor at the bottom of the exciton energy band. The half-value width is given by $\hbar/\tau$, $\tau$ being the life-time of the $\boldsymbol{K} = 0$ exciton due to the phonon scattering, whereas the shift is given by the self-energy of the exciton.

(2) When the interaction of $m^*$ is very large, or when $T$ is very high, the absorption band is of a *Gaussian* shape. In this case the localized exciton model is sufficiently good, and the situation is similar to the case of a trapped electron.

The ultra-violet exciton absorption bands observed in alkali halides and silver chloride seem to belong to case (1). The line shapes are Lorentzian in the main,[3–5] and the widths are proportional to $T$ (except at low temperatures where zero-point vibration is not negligible), as is expected from the theory. Absolute values of width are also in qualitative agreement with theoretical estimates. In the case of the (direct) exciton absorption band of Ge,[6] the dissociation process, rather than the intraband scattering, of the exciton by a phonon seems to be responsible for the greatest part of the width $\hbar/\tau$.

When the crystal becomes very imperfect, it has the same effect as an increase in temperature; the line shape is expected to approach a Gaussian type. FISCHER's data[3] on KI support this conclusion. On the other hand, the X-ray exciton should belong to case (2) at any temperature, due to its large effective mass. Experimental data on the $K$ X-ray absorption of KCl crystal [7] favor this view, though the observed width seems too large to be explained by exciton–lattice interaction alone.

Taking into account the interaction between different exciton energy bands (terms with $\lambda \neq \lambda'$ in the above formula) through phonons, which has been neglected in the above discussion, one can explain the repulsion (as $T$ rises) of adjacent absorption bands observed in CsI,[8] as well as the asymmetric shape of each. The detailed features of FISCHER's data are also qualitatively explained in the same way.

The exciton–lattice Hamiltonian is then utilized in estimating the cross sections for various elementary processes related to the exciton. Unless the bottom of the exciton energy band is at $\boldsymbol{K} = 0$, the exciton, after it is created by light, will lose its kinetic energy until it is thermalized. In a perfect crystal, the thermal exciton is annihilated by emitting a photon, through an indirect process at low temperatures and through a direct process at high temperatures, because the latter requires an activation energy. However, if, in addition, the bottom of the ionization continuum is lower than the energy of $\boldsymbol{K} = 0$ exciton by 0·1 eV or more, the exciton will, after a number of collisions with phonons, certainly dissociate into a free electron and hole before it is thermalized. In this case we should expect photoconductivity even if the exciton absorption peak is distinct. Further, when the contribution of this dissociation process to the band width $\hbar/\tau$ is larger than the binding energy of the exciton, the absorption peak may hardly be distinguished from the continuum.

Among those processes which possibly take place when a free electron and a hole encounter each other, the predominant one is reunion into an exciton with emission or absorption of a phonon. This annihilation process becomes unimportant, if the bottom of the conduction band and the top of the valence band do not coincide in **k**-space.

## REFERENCES


1. HAKEN H., Der heutige Stand der Exzitonenforschung in Halbleitern, *Halbleiterprobleme IV*. V. Vieweg, Braunschweig.
2. TOYOZAWA Y. *Prog. Theor. Phys., Japan* **20,** 53 (1958).
3. FISCHER F. *Z. Phys.* **139,** 328 (1954).
4. MARTIENSSEN W. *J. Phys. Chem. Solids* **2,** 256 (1957).
5. TUTIHASI S. *Phys. Rev.* **105,** 882 (1957).
6. ZWERDLING S., ROTH L. M. and LAX B. *Phys. Rev.* **109,** 2207 (1958).
7. KIYONO S. *Sci. Rep. Töhoku Univ.* **36,** 1 (1952). PARRAT, L. G. and JOSSEM E. L. *Phys. Rev.* **97,** 916 (1955).
8. PHILIPP H. R. and TAFT E. A. *J. Phys. Chem. Solids* **1,** 159 (1956).

*J. Phys. Chem. Solids* Pergamon Press 1959. Vol. 8. pp. 291–294. Printed in Great Britain

K.3

# INTERACTION OF EXCITONS WITH LATTICE VIBRATIONS*

B. GOODMAN and O. S. OEN†

University of Missouri, Columbia, U.S.A.

THIS work consists of two distinct parts, each concerning the theory of an experimental observation pertaining to exciton–phonon interactions.

The first part is a calculation of the thermal dissociation rate $w$, of excitons in polar materials. Not long ago PHILIPP[1] reported some photoelectric studies on barium oxide which indicate that the exciton-enhanced yield is governed by the rate of destruction of the excitons, presumably by dissociation. The process is temperature activated; $w \propto \exp(-Q/kT)$, with $Q \simeq 0{\cdot}15$ eV, about three times the polar mode quantum energy. At 300°K, $w$ is estimated to be greater than $10^{11}\,\mathrm{sec}^{-1}$.

The theory of multiphonon transitions as given by HUANG and RHYS, and PEKAR considers initial and final states in the Born–Oppenheimer approximation and the transition between them as due to the "non-adiabatic" residue in that formalism. There does not seem to be any alternative theory at the present time. However, it may be that one of the two states involved is better represented in some other manner. The HUANG–RHYS prescription is still applicable with the non-adiabatic operator defined with respect to the adiabatic state.

The final states were taken to be products of electron and hole polaron states of the type found by GURARI[2] and for intermediate temperatures by FULTON[3]

$$\Psi_f = \Omega^{-1} e^{i\mathbf{K}\cdot\mathbf{R}} e^{i\mathbf{k}\cdot\mathbf{r}} D^{-1} \prod_{\mathbf{w}} \prod (1+(n_{\mathbf{w}}+1)^{-\frac{1}{2}} f_e e^{-i\mathbf{w}\cdot\mathbf{r}_e} a_{\mathbf{w}}^{+} + n_{\mathbf{w}}^{-\frac{1}{2}} g_e e^{i\mathbf{w}\cdot\mathbf{r}_e} a_{\mathbf{w}})$$

$$\times (1+(n_{\mathbf{w}}+1)^{-\frac{1}{2}} f_h e^{-i\mathbf{w}\cdot\mathbf{r}_h} a_{\mathbf{w}}^{+} + n_{\mathbf{w}}^{-\frac{1}{2}} g_h e^{i\mathbf{w}\cdot\mathbf{r}_h} a_{\mathbf{w}}) |n_{\mathbf{w}}>,$$

$$D = \prod_{\mathbf{w}} \prod (1+|f_e|^2+f_h|^2+|g_e|^2+|g_h|^2)^{\frac{1}{2}},$$

$$\mathbf{r}_e = \mathbf{R}-\mu_h\mathbf{r}, \qquad \mathbf{r}_h = \mathbf{R}+\mu_e\mathbf{r}, \qquad \mu_{e,h} = m_{e,h}/(m_e+m_h).$$

The center of mass coordinate, $\mathbf{R}$, of the electron and hole may be eliminated by the unitary transformation, $\psi' = U\psi$, where

$$U = \exp\left\{-i\left(K_T - \sum_{\mathbf{w}} \mathbf{w} a_{\mathbf{w}}^{+} a_{\mathbf{w}}\right)\cdot R\right\},$$

and $\hbar\mathbf{K}_T$ is the *total* momentum, $\hbar(\mathbf{K}+\Sigma_{\mathbf{w}}\mathbf{w}n_{\mathbf{w}})$. Under this transformation the center of mass kinetic energy, $\mathbf{P}^2/2(m_e+m_h)$, is replaced by

$$\hbar^2\left(K_T - \sum_{\mathbf{w}} \mathbf{w} a_{\mathbf{w}}^{+} a_{\mathbf{w}}\right)^2 \Big/ 2(m_e+m_h).$$

The quartic terms in $a$ and $a^+$ give the mathematical difficulties in polaron theory. They are already included in the form of $f$ and $g$.

For the initial exciton state the basic approximation is made that $\Sigma_{\mathbf{w}}\mathbf{w}a_{\mathbf{w}}^{+}a_{\mathbf{w}}$ is a $c$-number, i.e., the recoil of the exciton when it emits and absorbs phonons is neglected. The adiabatic method is then applied to the light particle coordinate, $\mathbf{r}(=\mathbf{r}_h-\mathbf{r}_e)$, and the heavy particle coordinates, $q_{\mathbf{w}}$, the normal mode coordinates. The electronic part of the initial state is taken to be a hydrogenic type that can polarize in the phonon field,

$$\phi(\mathbf{r}, q_{\mathbf{w}}) \propto e^{-\lambda r}\left(1+\sum_{\mathbf{w}} c_{\mathbf{w}} q_{\mathbf{w}} \mathbf{w}\cdot\mathbf{r}\right).$$

The parameters, $\lambda$ and $c_{\mathbf{w}}$, are found by the variational method. Only polar modes are considered, which is

* Supported in part by the Office of Naval Research.

† Now at Oak Ridge National Laboratory, U.S.A.

expected to be a reasonable approximation for dissociation if not for scattering.

As in the work of HUANG and RHYS, the transition probability contains the Bessel functions, $I_p(z)$, where $p$ is the net number of phonons absorbed. The argument, $z$, is now more complicated, containing $q_{0w}$, the mode displacements in the initial state, $f$, $g$, the corresponding polaron terms, *and* $\mathbf{r}$, the relative coordinate which must be integrated over.

The complicated expression reduces, under the assumption that the polaron radii are small compared with $\lambda^{-1}$ and with other approximations that restrict it to $m_e \sim m_h$, to the following form,

$$w = C\sum_{p>p_0} \int_0^{K\max} K^2 dK\{(2\pi\langle K_x^2\rangle)^{-\frac{1}{2}} e^{-K^2/2\langle K_x^2\rangle}\}[\hbar\omega(p-p_0)-\hbar^2K^2/2M]R_p,$$

where

$$\hbar^2K_{\max}^2/2M = \hbar\omega(p-p_0), \qquad M = m_e+m_h,$$

and

$$C = 2^{19}5^23^{-8}\hbar\omega^2e^4\lambda^{-5}\left(\frac{\hbar^2}{m}+\frac{e^2}{\epsilon_\infty\lambda}\right)^{-2}\left(\frac{1}{\epsilon_\infty}-\frac{1}{\epsilon}\right)^2(4\bar{n}^2+4\bar{n}+1),$$

where $m$ is the reduced mass, and $\bar{n}$ is the thermal average of $n_w$.

Fig. 1 shows $w$ vs. temperature for some different cases, where $p_0$ is the minimum number of phonons required for dissociation. The dashed lines correspond to the dielectric constants of barium oxide and the curve, $p_0 = 2$, is in fair agreement with the results of PHILIPP.[1]

The second part is an application of the model of the lowest excited states of alkali halide crystals, which has been used by VON HIPPEL and others and recently made more precise by OVERHAUSER. The present results are more suggestive than conclusive and more work will have to be done to gain some sense of its reliability.

Attention will be confined to the alkali iodides and to the low energy optical absorption bands which can be reasonably identified as a spin-orbit doublet. The fine structure to be expected in this doublet due to the crystalline symmetry has been estimated approximately using the prescription of OVERHAUSER. The basic excited configuration

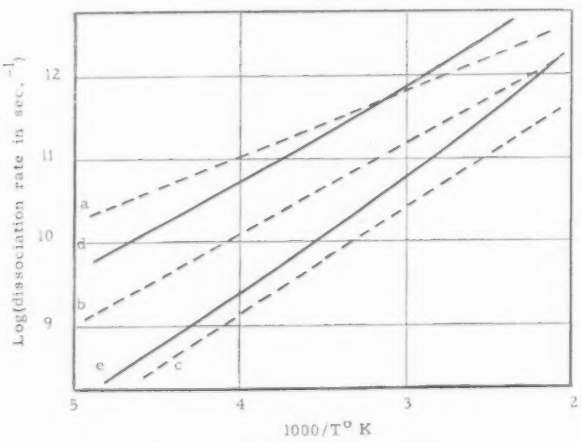


FIG. 1. Dissociation rate vs. temperature for different parameters. The dashed lines correspond to the dielectric constants of BaO.

has the electron and hole in non-orthogonal states on neighboring ions. This must be symmetrized with respect to crystal rotations and translations.

In finding these symmetry functions and energy eigenfunctions it is convenient to be able to treat the electron and hole on an equivalent basis and to carry the Pauli exclusion principle with a less cumbersome notation than $N$ by $N$ determinants. The creation and annihilation operator notation of second quantization is well adapted for this purpose. It is clear that everything done in this way can be done in conventional notation but, it seems to us, with considerably more difficulty.

Let $u_i(x)$ be a complete but not necessarily orthonormal set of one-electron states, $(u_i, u_j) = \Delta_{ij}$. The quantized field, $\Psi(x)$, may be expanded, $\Psi(x) = a_i u_i(x)$ (summation convention). Now consider the set of states, $v_i(x)$, "reciprocal" to $u_i(x)$, $(u_i, v_j) = \delta_{ij}$. In the expansion, $\Psi(x) = c_i v_i(x)$, the operator $c_i^+$ *creates an electron in the state* $u_i(x)$, and has the same transformation properties as $u_i(x)$.

The various anticommutators are:

$$\{a_i^+, a_j\} = d_{ji},\ d = \Delta^{-1},\ \{c_i^+, c_j\} = \Delta_{ij},$$
$$\{c_i^+, a_j\} = \delta_{ij};$$

all others are zero.

The complete Hamiltonian is

$$H = a_i^+ a_j(u_i, H_1 u_j) + \tfrac{1}{2} a_i^+ a_j^+ a_k a_l (u_i u_j, H_{12} u_l u_k),$$

where $H_1$ is the one-particle part, $T_1 + V_{\text{Core}} + H_{\text{Spin Orbit}}$ and $H_{12} = e^2/r_{12}$.

The separation of $\Psi(x)$ into electron and hole parts is made more symmetrical by first writing $\Psi \equiv \Psi^e$, and $\Psi^h = C\Psi^e$, where $C$ is the Wigner time reversal operation, $i\sigma_y$(h.c.); $C^2 = -1$. Then $\Psi^e = \Phi^e - C\Omega^h$, so that $\Psi^h = \Omega^h + C\Phi^e$, where $\Phi^e$ and $\Omega^h$ are the parts belonging to normally filled electron states, $u_\beta$, and normally empty electron states, $u_\gamma$, respectively,

$$\Phi^e = a_\beta u_\beta, \qquad \Omega^h = C(a_\gamma u_\gamma) = h_{-\gamma} w_{-\gamma},$$

where $-\gamma$ denotes reversed momenta due to C.

The operators $c_i$, reciprocal to $a_i$ become in this notation,

$$a_\beta \to \epsilon_\beta = c_\beta, \text{ and } h_{-\gamma} \to \eta_{-\gamma} \propto c_\gamma^+,$$

along with the anticommutators,

$$\{\epsilon_{\beta'}^+, \epsilon_{\beta'}\} = (u_\beta, u_{\beta'}),\ \{\eta_{-\gamma}^+, \eta_{-\gamma'}\} = (w_{-\gamma}, w_{-\gamma'}),$$
$$\{\epsilon_\beta, \eta_{-\gamma}\} = (w_{-\gamma}, Cu_\beta),\ \{\epsilon_\beta^+, a_{\beta'}\} = \delta_{\beta,\beta'},$$
$$\{\eta_{-\gamma}^+, h_{-\gamma'}\} = \delta_{\gamma,\gamma'};$$

all others are zero.

The basic one-electron states in the exciton model are:

Electron states: $s_{\alpha L}(\pm)$, $L$ is halogen site, $\alpha$ is n.n. site; Symmetrized orbitals $U_{iL} = \Sigma_\alpha d_{\alpha i} s_{\alpha L}$.

Hole states: $X_{iL}(\pm)$, $X_i = p_x, p_y, p_z$ on halogen.

The excited states are:

$$\chi_v = N^{-\frac{1}{2}} \sum_L b^{(v)}{}_{i_\alpha, j_\beta} U_{iL}(\alpha) X_{jL}(\beta) \Pi,$$

where $U$, $X$ are the electron and hole creation operators, and $\Pi$ is the closed shell configuration,

$$\prod_L X_L(\pm) Y_L(\pm) Z_L(\pm) |\text{Core}\rangle$$

With the assumption of n.n. overlap only, i.e., that $(s_{\alpha L}, X_{iL}) = \pm\gamma$, 0 and all others are zero, the normalization matrix, $\rho_{\mu\nu} = (\chi_\mu, \chi_\nu)$, and the Hamiltonian matrix can be evaluated using the anticommutators only. The resulting coulomb and kinetic energy matrix for the optically allowed states ($\Gamma_4'$) is, after division on the left by $\rho$ and removal of the constant part:

| | | | | NaCl | CsCl |
|---|---|---|---|---|---|
| $e_1$ | $\sqrt{2}(gE_c + e_4)$ | 0 | 0 | 0 | 0 |
| $\sqrt{2}(gE_c + e_4)$ | $e_2 + b$ | 0 | 0 | 0 | 0 |
| 0 | 0 | 0 | $\sqrt{2}gE_a$ | 0 | 0 |
| 0 | 0 | $\sqrt{2}gE_c f$ | $b$ | 0 | 0 |
| 0 | 0 | 0 | 0 | c | 0 |
| 0 | 0 | 0 | 0 | 0 | c |

$e_1$, $e_2$, $e_4$ are inequivalent exchange terms.

For the NaCl structure $e_1 \cong e_4 \cong \frac{1}{2} e_2$ and $f = 1$.

For the CsCl structure $e_1 > e_4 > e_2$ and $f < 1$.

The rest are "direct" coulomb terms due to non-spherical symmetry.

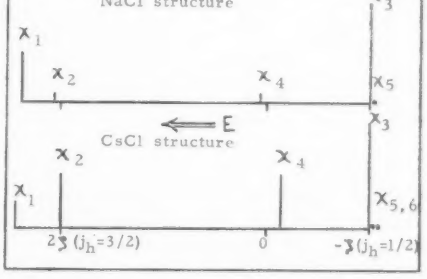


Fig. 2. Estimated positions and intensities of absorption lines in lowest spin–orbit "doublet".

When the exchange part is evaluated in the strong spin–orbit coupling case, the levels and relative intensities are as shown in Fig. 2. The "extra"

line observed in CsI seems to be merely a matter of intensities rather than extra degeneracy as suggested by OVERHAUSER.

It is suggested that the special temperature dependence of line $\Omega_3$ in CsI is due to the repulsion by states lying below $\Omega_3$ which are mixed with it by the lattice vibrations. In second order perturbation theory the energy displacement is proportional to the mean square vibrational amplitude. The mean position of all the $j_h = 3/2$ levels (allowed and unallowed) is between $\Omega_3$ and $\Omega_4$ in accord with the rapid temperature displacement of $\Omega_4$ to low energy.

## REFERENCES

1. PHILIPP H. R. *Phys. Rev.* **107**, 687 (1957).
2. GURARI M. *Phil. Mag.* **44**, 329 (1953).
3. FULTON T. *Phys. Rev.* **103**, 1712 (1956).

*J. Phys. Chem. Solids* Pergamon Press 1959. Vol. 8. pp. 294–296. Printed in Great Britain

VOL
8
195

# K.4 THE OPTICAL ABSORPTION EDGE IN IONIC CRYSTALS

W. MARTIENSSEN

Erstes Physikalisches Institut der Universität Göttingen, Germany

THE absorption near the edge in nonmetallic crystals is caused by two different processes: band-to-band transitions and creation of excitons. The band-to-band transitions are connected with photoconductivity and produce a continuous spectrum with a rather sharp edge, which is determined by the energy gap of the crystal. The exciton absorption on the other hand shows no photoconductivity. In ionic crystals with low dielectric constants this exciton absorption is widely determined by properties of the isolated ions. In semiconducting materials with high dielectric constants, like germanium, the exciton absorption has been detected only in recent years, because it requires spectrometers with very high resolution, in order to separate the faint lines from the strong band-to-band absorption. Just the contrary has come out in ionic crystals: here the strong exciton absorption nearly completely covers the edge of the band-to-band transitions, so that for a long time it has been impossible to determine the energy gap of these crystals directly. In this paper some recent experiments about the shape of the absorption edge of ionic crystals and its temperature dependence will be discussed. For clearness only two substances with typical behaviour will be treated: KI and TlCl.

The exciton bands of alkali halide crystals are extensively investigated. The first bands from the low energy side of the spectrum are well understood as electronic transitions from the halogen ions to direct neighbouring alkali ions. This concept is established by the fact that light absorption in the tail of this absorption band is not connected with photoconductivity. In the last years PHILIPP and TAFT[1] measured the external photoelectric emission of alkali halide layers and found a pronounced threshold for the emission which in most cases lies about 1–2 eV beyond the first exciton band. From a detailed comparison of the spectral dependence of photoelectric yield with the optical spectra they conclude that in the spectra of alkali iodides the edge for band-to-band transitions is marked by a distinct step between the first two exciton bands. This edge lies several tenths of an electron volt beyond the first band in the alkali iodides, so that this band is well separated from the continuous absorption.

Fig. 1 shows measurements of U. HAUPT[2] about the temperature dependence of the first exciton band in KI. The absorption constant is drawn in a logarithmic scale versus the photon energy. Similarly as has been previously shown[3]

for KBr, the tail at the low energy side of the exciton absorption band in KI perfectly obeys the exponential law

$$K = K_0 \exp\left(-\sigma \frac{h\nu_0 - h\nu}{kT}\right),$$

which has first been found by URBACH[4] and which

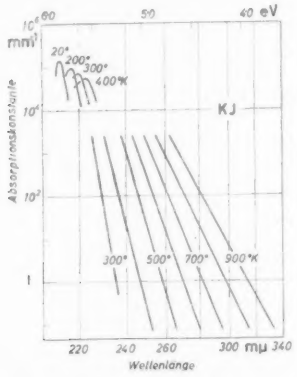


FIG. 1. The absorption edge of KI between 300°K and 900°K. Near the maximum the exciton band can be measured only beneath 500°K because of coagulation of thin layers at higher temperatures.

is called Urbach's rule. The three quantities $K_0$, $\nu_0$, and $\sigma$ are material constants. The absorption constant drops exponentially with the frequency over many decades. The steepness of the different straight lines proves to be proportional to $1/kT$, which is demonstrated in Fig. 2, where

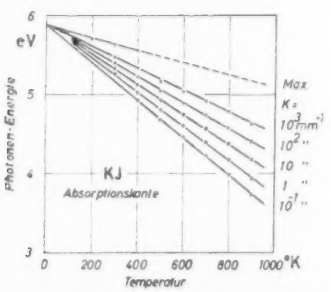


FIG. 2. The shift of the absorption edge of KI with temperature for different values of the absorption constant K.

the position of the absorption edge is plotted versus the temperature. For different values of the absorption constant one gets straight lines, which intersect at absolute zero.

At low temperatures there are deviations from this simple law because of lattice imperfections and zero point energy. But by extrapolation one can conclude, that at absolute zero the band degenerates into an absorption line at frequency $\nu_0$ with the height $K_0$. This is what one would expect for the exciton absorption in a static lattice. But the band shape at higher temperatures seems to be in contradiction to all shapes of absorption bands so far discussed. The striking point of these new measurements on KI is the fact that the constant $\sigma$ which determines the thermal broadening of the exciton band proves to be exactly the same for KBr and KI, that is $\sigma = 0{\cdot}79$.

The complete isolation of the first exciton absorption from band-to-band transitions has been found only in crystals with predominantly ionic bond. Generally the exciton bands are superimposed on the continuous absorption, as for instance has been shown for the silver halide crystals.[5] Here the spectrum of TlCl may be discussed which has been investigated by H. ZINNGREBE.[6] Fig. 3 gives the exciton bands in

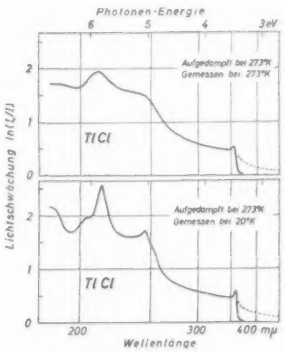


FIG. 3. The optical absorption of a 40 mμ layer of TlCl at 20°K and 273°K.

TlCl measured at a thin evaporated layer. In contrast to other substances these bands are marked by an inverse temperature shift, that means they are shifted to shorter waves when heating the crystal. This is a special property of the $Tl^+$-ion absorption, which can be understood in a configurational co-ordinate model, as developed by WILLIAMS[7] for KCl: Tl phosphors.

The investigation of the absorption edge of TlCl yields a strange behaviour (Fig. 4). Between 200 and 600°K the absorption edge shifts to longer waves with rising temperature, but below 150°K it shifts towards the opposite direction. This can be interpreted by a superposition of two different absorption processes with opposite temperature dependence. At about 200°K the edge of band-to-band transitions coincides with the tail of the exciton band. The former is shifted to longer waves with rising temperatures and then alone determines the absorption edge of the crystal, also indicating evidence for direct and indirect transtions. But at low temperatures this absorption disappears beyond the tail of the exciton band and only the latter can be observed. As for KI, the shape of this band follows an exponential law over many decades, and the steepness is very similar to the one in KI at low temperatures. So in this case the study of the temperature dependence of the absorption edge allows directly the distinction of the two superimposed absorption processes.

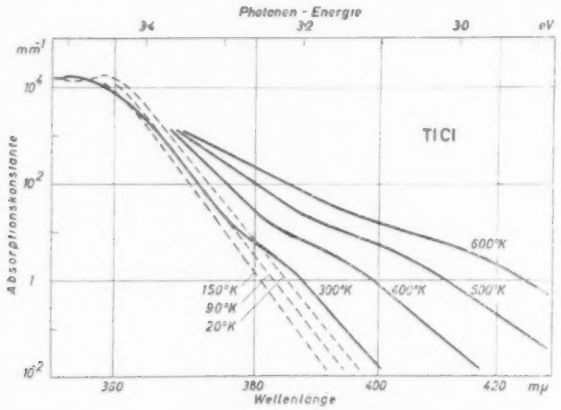


FIG. 4. The absorption edge of TlCl between 20°K and 600°K. The low temperature curves are dashed for better distinction.

## REFERENCES

1. PHILIPP H. R. and TAFT E. A. *J Phys. Chem. Solids* **1,** 159 (1956); TAFT E. A. and PHILIPP H. R. *J. Phys. Chem. Solids* **3,** 1 (1957).
2. HAUPT U., Diplomarbeit, Göttingen (1958).
3. MARTIENSSEN W. *J. Phys. Chem. Solids* **2,** 257 (1957).
4. URBACH F. *Phys. Rev.* **93,** 1324 (1953); MOSER F. and URBACH F. *Phys. Rev.* **102,** 1519 (1956).
5. TUTIHASI S. *Phys. Rev.* 105, 882 (1957). OKAMOTO Y. *Nachr. Akad. Wiss. Göttingen* **14,** 275 (1956).
6. ZINNGREBE H., Dissertation, Göttingen (1958).
7. WILLIAMS F. E. *J. Chem. Phys.* **19,** 457 (1951).

*J. Phys. Chem. Solids* Pergamon Press 1959. Vol. 8. pp. 297–300. Printed in Great Britain

K.5

# PHOTOCONDUCTIVITY IN CRYSTALS OF SILVER BROMIDE

E. A. BRAUN* and J. W. MITCHELL

H. H. Wills Physical Laboratory, University of Bristol

VOL. 8 1959

## 1. INTRODUCTION

QUANTITATIVE measurements of the electronic photoconductivity of single crystals of silver chloride and silver bromide were first made by HECHT[1] and by LEHFELDT.[2] They determined the range of the photoelectrons at a temperature of −170°C but were unable to detect any drift of positive holes in the electric field. The photocurrents steadily decreased to values which could not be measured with their apparatus when the illumination was prolonged. This was attributed to polarization as a result of the establishment of space charges.

The crystals which were used for these measurements had been exposed to light during preparation and this led to the separation of some photolytic silver. Before the measurements were made, they were heated in air for a period to "restore them to their original state." Crystals of silver halides grown from the melt in air by the Kyropoulos method probably contain silver oxide either in the form of a very dilute solution or as segregated particles. If the coloration during exposure were due to the formation of colloidal silver, this would be converted to silver oxide when the crystals were annealed in air so that the original state might, in this case, be re-established.

More recently, crystals which had been annealed in air in similar circumstances have been used as crystal counters by VAN HEERDEN,[3] ALLEMAND and ROSSEL[4] and BROWN.[5] Although the sensitivity is high, so that the shapes of the electron pulses may be resolved with a high speed oscillograph, pulses which could be attributed to the displacement of positive holes have never been detected.

HAYNES and SHOCKLEY[6] (see also HAYNES[7]) have also used air-annealed crystals for experiments in which they followed the displacement of the photoelectrons at room temperature by observations on the separation of photolytic silver.

The object of the present investigation was therefore to study the photoconductive properties of large single crystals of silver bromide free from silver oxide and other possible sensitizing impurities, which have an extremely small photolytic sensitivity. The photochemical observations suggest that holes and electrons, when liberated in such crystals, recombine without the production of photochemical changes (CLARK and MITCHELL[8]).

## 2. EXPERIMENTAL PROCEDURE

The silver bromide used for this work was prepared by methods described in detail by CLARK and MITCHELL.[8] The material was kept molten for several hours in a high vacuum so as to pump away volatile impurities, including cuprous compounds, and to break down silver oxide into free silver and oxygen, which was pumped away. The silver was converted into silver bromide by admitting pure bromine to the molten silver bromide; the excess bromine was subsequently removed by condensation in a liquid air trap. This procedure appears to eliminate traces of silver oxide.

The crystals were grown in vacuum by the Bridgman method and cut into slabs 10mm × 7mm × 3mm, which were ground and polished. The slabs were annealed first in bromine and then in vacuum.

Every care was taken to produce crystals of high purity and perfection. Particular attention was paid to the elimination of silver oxide and cuprous compounds.

The crystals were provided with graphite

* On leave of absence from the Department of Physics, the Hebrew University, Jerusalem, Israel.

electrodes such that the crystal was illuminated with the light beam either (1) at right angles to the electric field or (2) parallel to the field. Light of 436mm wavelength at a rate of quantum incidence of $10^{10}$ quanta $sec^{-1}$ was used.

The specimens were mounted in a vacuum cryostat and cooled to various temperatures between −183°C and −78°C.

Instead of using the recent pulse techniques for measuring the photoconductive response (ALLEMAND and ROSSEL[4] and BROWN[5]), we used a current measuring circuit in which two electrometer triodes formed two arms of a Wheatstone bridge. The reason for this was twofold. First, the pulse technique is less sensitive than the current measurement and therefore useful only for crystals with fairly large electron ranges; we both expected and obtained rather small electron ranges in our crystals. Secondly, the d.c. measurement technique enabled us to study the behavior of the photocurrents over large periods, and this in turn gave information on the internal polarization which builds up in the crystals. One of the striking results of these measurements was the fact that the photocurrent did not decrease to zero even during periods of exposure to many hours.

### 3. EXPERIMENTAL RESULTS

Results of measurements at temperatures between −183°C and −150°C will be described first. The general pattern of the photoconductive response of the crystals was as follows: When a field of about 1000 V $cm^{-1}$ was applied, the current rose abruptly on illumination from zero to a maximum value $I_m$ and then slowly fell according to a law of the form

$$I = I_s + 1/b[\{b(I_m - I_s)\}^{-\frac{1}{2}} + t]^2$$

to an equilibrium value $I_s$; $t$ is the time and $b$ a constant. Equilibrium was reached within a few minutes. The value of the equilibrium current was about a tenth or more of the maximum current and was stable as long as the illumination and applied field were left unchanged.

When the light was switched off, the current fell rapidly to zero. No dark current was ever observed at low temperatures. When the field was removed and the crystal illuminated again, a transient photocurrent in a direction opposite to that of the original photocurrent was observed. This "back-current" was due to the internal polarization caused by holes and electrons trapped during the flow of the forward photocurrent.

The peak value of the forward photocurrent corresponds to the primary photocurrent measured by HECHT, LEHFELDT and others. We have applied HECHT's formula to calculate the mean range of carriers in unit field from the extrapolated peak value of the photocurrent. The initial mean range for electrons was of the order of $10^{-6}$ $cm^2$ $V^{-1}$ and for holes it was $10^{-7}$ $cm^2$ $V^{-1}$. The fact that the photocurrent, although decreasing after the initial peak due to internal polarization, reaches an equilibrium value different from zero, provides further proof of some finite, if small, range for the holes.

The internal polarization could be detected even after very short exposures and reached its equilibrium value at the same time as the photocurrent. This equilibrium value clearly could not eliminate completely the applied field in the illuminated region. The "back-current" was always proportional to the steady state photocurrent. At low temperatures, the internal polarization which decayed very slowly over periods of hours during dark storage scarcely decayed at all if the electric field was maintained. At higher temperatures, the internal polarization was less persistent, but no single trap depth could be ascertained from thermal decay of the polarization.

The voltage dependence of the equilibrium photocurrent followed a law of the type $I = AE^b$ where $I$ is the current, $E$ the field and $b$ a constant. The value of $b$ was unity or slightly higher for the case of parallel illumination and about 1·5 for the perpendicular case.

At temperatures above −150°C, the photoconductive response remained very much the same as at low temperatures as long as the ionic current did not exceed the electronic current by orders of magnitude. Above −100°C the surface photoconductivity was markedly increased compared with the bulk photoconduction. This is consistent with previous observations by EVANS, HEDGES and MITCHELL[9] on the displacement of the latent image in single crystals of silver bromide by electric fields. The photochemical sensitivity

of these crystals was remarkably low and the printing out of photolytic silver during even prolonged periods of intense illumination was almost impossible to achieve.

## 4. CONCLUSIONS

It has now been shown that crystals of silver chloride and silver bromide, of the highest attainable purity and perfection, have two characteristic properties. Their sensitivity for the separation of photolytic silver is extremely small and the range of the conduction electrons which are liberated under illumination is $3 \times 10^{-6}$ cm$^2$ V$^{-1}$. It would be surprising if there were no correlation between these properties.

The absence of any photochemical change shows that conduction electrons and positive holes, if they are actually liberated by the absorption of energy in the crystals must recombine. The bulk of the energy of the absorbed photons is therefore converted into lattice vibrational energy.

Crystals of silver halides may be sensitized for both photochemical change and photoconductive response by heating them in oxygen in contact with a piece of silver foil. Silver oxide is then formed which diffuses into the crystals to form a very dilute solid solution and possibly also segregated particles. Such sensitized crystals darken, due to the separation of discrete particles of silver, during exposure and the range of the conduction electrons is found to be of the order of $10^{-4}$ cm$^2$ V$^{-1}$. The drift of the positive holes which may be liberated with the conduction electrons cannot be detected and their range in these sensitized crystals must be extremely small. It therefore becomes clear that there must be a fundamental difference between the properties of the positively charged centres produced by the trapping of the positive holes in the pure and in the sensitized crystals which results in a reduction in the amount of recombination between trapped positive holes and electrons and in an increase in the lifetime of the conduction electrons. Before we discuss this in greater detail, we shall refer to an alternative interpretation of the sensitizing influence of silver oxide which has been suggested by SUPTITZ[10] and by BROWN.[11]

Following the general lines of argument of the Gurney–Mott theory of photolysis, SUPTITZ and BROWN focus their attention upon the capture of the conduction electrons by traps of an unspecified nature as the process which determines the range. They do not consider recombination between conduction electrons and trapped positive holes. With this approach, it is necessary to postulate that the electron traps are inactivated or removed, possibly by segregation, when the crystals are annealed in oxygen.

In our view, heating the crystals under conditions which allow silver oxide to diffuse into them produces a very dilute solid solution of silver oxide in the silver halide, together with segregated silver oxide, if the treatment is prolonged. The function of the dissolved silver oxide is to provide traps for positive holes which are not recombination centres. In the crystal, the excess negative charge of a doubly charged oxide ion is compensated by an interstitial silver ion and the drift of these ions in electric fields is responsible for the enhanced conductivity of crystals containing silver oxide compared with pure crystals. During illumination, the positive holes are trapped by the oxide ions to give singly negatively charged ions. The positive charge of the interstitial silver ion is then compensated by the negative charge of the conduction electron for which both the interstitial silver ion and the singly charged oxide ion have small capture cross sections. The lifetime of the conduction electron at room temperature is determined by the time required for its combination with an interstitial silver ion on the external surface or on an internal surface of the crystals. That other trapping processes are unimportant is established by the equality between the Hall and the drift mobilities for electrons in silver chloride found by HAYNES and SHOCKLEY.[6] This accounts directly for the correlation between the increased photosensitivity and the increased photoconductive response of crystals containing silver oxide at room temperature.

## REFERENCES

1. HECHT K. *Z. Phys.* **77,** 235 (1932).
2. LEHFELDT W. *Nachr. Ges. Wiss. Göttingen* **1,** 171 (1935).
3. HEERDEN P. J. VAN, *Physica*, **16,** 505 (1950).
4. ALLEMAND CH. and ROSSEL J. *Helv. Phys. Acta* **27,** 212, 519 (1954).

5. BROWN F. C. *Phys. Rev.* **97**, 335 (1955).
6. HAYNES J. R. and SHOCKLEY W. *Report on Conference on Strength of Solids* p. 151. Physical Society, London (1948); *Phys. Rev.* **82**, 935 (1957).
7. HAYNES J. R. *Rev. Sci. Instrüm.* **19**, 51 (1948).
8. CLARK P. V. McD. and MITCHELL J. W. *J. Phot. Sci.* **4**, 1 (1956).
9. EVANS T., HEDGES J. M. and MITCHELL J. W. *J. Phot. Sci.* **3**, 75 (1955).
10. SUPTITZ P. *Naturwissenschaften* (1957).
11. BROWN F. C. *J. Phys. Chem.* **4**, 206 (1958).

*J. Phys. Chem. Solids* Pergamon Press 1959. Vol. 8. pp. 300–304. Printed in Great Britain

VOL
8
195

# K.6 ELECTRONIC PROCESSES IN THE SILVER HALIDES AT LOW TEMPERATURE*

F. C. BROWN and K. KOBAYASHI

University of Illinois

THE mobility of electrons at room temperature in ionic crystals is considerably smaller than in atomic semiconductors because of the strong interaction between conduction electrons and optical mode vibrations. Below the Debye temperature $\Theta$ associated with the longitudinal optical mode, mobility increases rapidly with decreasing temperature according to $\mu = A \exp[(\Theta/T)-1]$.[1] If impurity scattering is not too important acoustical mode scattering with a $T^{-\frac{1}{2}}$ dependence will predominate at very low temperatures.[2]

Electron drift mobility has been measured over a wide range of temperatures by transit time techniques in the case of AgCl and AgBr.[3–6] The results are not in agreement with the above expectations. Drift mobility is found to be small at low temperatures and to have a maximum in the vicinity of 50 to 90°K depending upon sample preparation. Scattering by imperfections such as ionized impurities could cause such an effect, but an unreasonably high density of impurities ($10^{17}$ to $10^{18}$ cm$^{-3}$) is required. It seems more reasonable to ascribe the drift mobility results to multiple trapping effects.

Recently the situation has been clarified by observations of the Hall effect for photo-carriers using a modification of the Redfield technique.[7] Details will be given elsewhere,[8] but some essential results are shown in Fig. 1 for a simple crystal of AgCl. Both Hall mobility† and drift mobility for electrons are plotted as a function of temperature. Note that the Hall mobility, which is independent of trapping effects, rises to very high values at low temperature. The sign of the observed Hall effect was negative since holes make a small or negligible contribution to photoconductivity in all samples studied so far. This result is in agreement with transient photoconductivity experiments.[9] The drift of holes in an applied field has not been observed and, if present at all, must be several orders of magnitude less than the drift of electrons.

The Hall mobility data shown in Fig. 1 can be approximated by a $T^{-\frac{1}{2}}$ dependence below about 50°K indicating the importance of acoustical scattering. There is also evidence for scattering by other imperfections at the lowest temperatures. The crystals are relatively pure but may contain ionized impurities of the order of $10^{15}$ cm$^{-3}$. Optical mode scattering becomes apparent at the

* Supported in part by the U.S. Air Force Office of Scientific Research.

† Obtained from the Hall angle in the range of linear dependence on magnetic field.

higher temperatures and is in reasonable agreement with a Debye temperature of $\Theta = 280°K$ as computed from Restrahl data for AgCl. Comparison of the experimental data with polaron theory[10] gives a ratio of polaron mass to free electron mass $m^*/m_0 = 0{\cdot}4$ and an interaction constant $\alpha = 2{\cdot}2$.

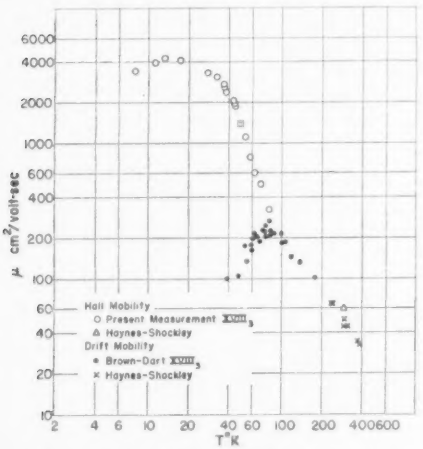


FIG. 1. The mobility of electrons in silver chloride as a function of temperature. The crosses and the triangle were obtained from the migration of the "print out effect" in electric fields.[6] The solid circles were derived from the measurement of transient photoconductivity.[3] The open circles show the recent results[8] on the photoelectric Hall effect. Roman numerals refer to the particular crystal used.

The general features of electron trapping in AgCl have been revealed by experiments such as those carried out by VAN HEYNINGEN[9] and also by BRAUN and MITCHELL.[11] Although electron mobility rises to high values at low temperature the range of electrons has been observed to decrease below 35°K and to become still smaller below 15°K. Furthermore, isolated electrical glow peaks have been observed near these same temperatures. This leads one to adopt the point of view that discrete trapping levels exist. In several samples the very shallow traps associated with a glow peak at 15°K appear to be present in the greatest concentration. These levels, about 0·03 eV from the bottom of the conduction band (computed from the position of the glow peak and a choice of frequency factor $s = 10^{10}\,\text{sec}^{-1}$) appear to be largely responsible for the decrease in drift mobility in the range of temperature from 50 to 80°K.

Drift mobility for these insulating crystals is computed from the observed transit time for a sheet of electrons moving in an applied electric field. Under the conditions of measurement diffusion is small and can be neglected. The relation between drift mobility $\mu_D$ and microscopic mobility $\mu_m$ can be readily derived in the case of a single set of trapping levels. Assume that the conduction electrons are in quasi equilibrium, that is they are distributed classically between states near the bottom of the conduction band and a set of shallow traps of depth $E$ and uniform concentration $N_t$. The density of empty traps is high and the number of electrons in the moving sheet of charge is small. During the transit time the electrons spend a fraction of their time in the conduction band and a fraction of the time in the shallow traps. The effect of deep electron traps can be minimized and will be neglected. Let $\tau$ equal the mean scattering time for electrons in the conduction band, $\tau_t$ equal the mean trapping time for electrons in the conduction band and $\tau_g$ the average time an electron remains in a shallow trap. For $c$ lattice collisions an electron in an applied field $E$ will have displaced a distance $s = eEc\tau^2/m$ on the average. This will require a total time $T = c\tau + c\tau\tau_g/\tau_t$ because of the $c\tau/\tau_t$ trapping events. Using $\mu m = e\tau/m$ one arrives at

$$\mu_D = \frac{s}{TE} = \mu_m\left(\frac{1}{1+\tau_g/\tau_t}\right). \qquad (1)$$

If $\tau_g/\tau_t$ is considered constant with electron energy the mobilities in the above expression may be replaced by the average values which are observed.

The ratio $\tau_g/\tau_t$ can be derived under the stated conditions by assuming that the rate of trapping is equal to the rate of release from traps. Neglecting possible trap degeneracy the result is

$$\mu_D = \mu_m\left(\frac{1}{1+(N_t/N_c)\exp(E/kT)}\right). \qquad (2)$$

Here $N_t$ and $E$ are parameters characteristic of the traps as previously defined and $N_c$ is the effective density of states near the bottom of the conduction band. For simple band structure

$$N_c = 4{\cdot}82\times10^{15}\left(\frac{m}{m_0}\right)^{\frac{3}{2}} T^{\frac{3}{2}}. \qquad (3)$$

The effective mass $m$ in equation (3) should be identical with the polaron effective mass determined by other means. Relations similar to the above are frequently used especially in the approximate form[12]

$$\mu_D \simeq \mu_m \frac{N_c}{N_t} \exp\frac{-E}{kT}, \qquad \tau_g \gg \tau_t.$$

Over the temperature range of interest for the drift data of Fig. 1 $\mu_m$ is determined primarily by

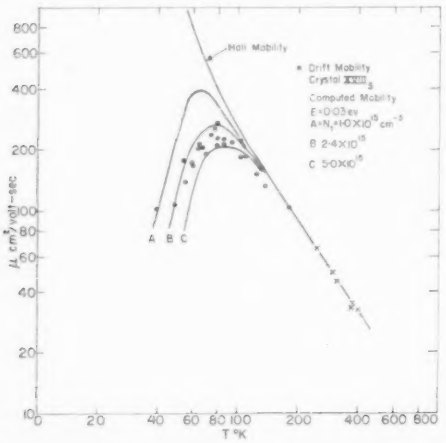


FIG. 2. The uppermost curve is taken from the Hall data of Fig. 1 whereas the dots represent the data on drift mobility. Curves A, B and C were computed for different values of trap concentration, $N_t$, as discussed in the text. They illustrate the effect of multiple trapping.

optical mode scattering. In this case electron mean free path is proportional to velocity so that $\tau$ is a constant and $\mu_m = \mu_H$. The curves labelled A, B and C in Fig. 2, corresponding to different values of $N_t$, were computed from equations (2) and (3) by replacing $\mu_m$ with the observed Hall mobility. A choice of $E = 0{\cdot}03$ eV was made in order to fit the shape of the curve. A value of 0·05 eV, for example, with correspondingly lower $N_t$, produces a much steeper drift mobility at low temperatures and does not fit the data at intermediate temperatures. The curves are strongly dependent upon trap concentration and the fit is best for $N_t = 2{\cdot}4\times10^{15}$ cm$^{-3}$, which is of the order of impurities observed spectrographically in crystals such as these.

Observations have been made on a crystal having a smaller number of shallow traps. The drift mobility rises to a maximum well above that shown in Fig. 1 and it also extends to lower temperatures. For the crystal discussed above the values of $E$ and $N_t$ are quite reasonable in view of the photoconductivity and glow curve results. Although the situation is undoubtedly oversimplified by the assumption of a single trapping level, the analysis illustrates the essential features of multiple trapping in the silver halides.

VOL 8 195

## REFERENCES

1. FROHLICH H. *Advanc. Phys., Phil. Mag. Suppl.* **5,** 412 (1956).
2. KONTOROVA T. A. *Zh. tekh. fiz., AIP Translation,* **2,** 237 (1957).
3. BROWN F. C. and DART F. E. *Phys. Rev.* **108,** 281 (1957).
4. ALLEMAND C. and ROSSEL J. *Helv. Phys. Acta* **28,** 212 (1954).
5. YAMANAKA C. and SUITA T., *J. Phys. Soc. Japan* **10,** 238 (1955).
6. HAYNES J. R. and SHOCKLEY W. *Phys. Rev.* **82,** 935 (1951).
7. REDFIELD A. G. *Phys. Rev.* **94,** 526 (1954).
8. KOBAYASHI K. and BROWN F. C. tc be published.
9. VAN HEYNINGEN R. and BROWN F. C. *Phys. Rev.* **111,** 462 (1958).
10. LOW F. and PINES D. *Phys. Rev.* **98,** 414 (1955).
11. BRAUN E. A. and MITCHELL J. W. Private communication.
12. ROSE A. *R.C.A. Rev.* **12,** 363 (1951).

## DISCUSSION

*Compiled by* D. DUTTON.

K.1. T. MUTO *et al.*

J. A. KRUMHANSL (National Carbon Co.): Is the term $E$(exchange) the same as the one found by HELLER and MARCUS?

T. MUTO: Yes.

(There was further discussion among MUTO, HEINE, and ELLIOTT about the factors responsible for the differences between localized and hydrogen-like excitons,

including the influence of the dielectric constant and the effective mass.)

K.2. Y. Toyozawa

H. Haken (Erlangen) and Toyozawa discussed difficulties which would arise in the intermediate-coupling theory of exciton–lattice interaction. R. J. Elliott (Oxford), Y. Toyozawa, and J. A. Krumhansl discussed mechanisms of absorption-line broadening and possible asymmetry. S. Nikitine (Strasbourg) commented that he has observed continuous absorption on both sides of the exciton lines in CuI, and remarked that both the line shape and the shape of the dispersion curve agree with Drude's formula.

K.3. B. Goodman and O. S. Oen

H. Haken and B. Goodman discussed the problem of the non-orthogonality of the wave functions used.

K.4. W. Martienssen

J. J. Markham (Zenith Radio): Have you found that the absorption edge in KI is structure sensitive?

W. Martienssen: Yes. In KI the edge is a simple exponential only down to about 300°K. At lower temperatures, in ordinary material, there is a tail of lower slope; when the material is zone-refined, this tail goes away. It is rather important to have pure material, and it always seems more difficult to purify KI than KBr.

D. Dutton (Rochester): I might mention that we have measured the edge shape in CdS, which shows photoconductivity in the edge even at very low temperatures, but which has an edge shape very much like KBr; it obeys Urbach's rule from about 20 $cm^{-1}$ to $10^4$ $cm^{-1}$.

S. Nikitine: In TlI, and also in TlBr, we find after the first exciton peak a step in the absorption spectrum, which we presume to be the continuum. A second point I should like to mention is that the temperature shift of the excitonic spectrum in CuO and $HgI_2$ is parabolic, i.e. the shift reverses sign at some temperature.

R. J. Elliott: I would like to point out that the behavior of thallous chloride is very similar to that of germanium, namely an exciton band due to a direct transition and perhaps a continuum edge beyond it, while at lower energies and at absorption coefficient values of the order of 100 $cm^{-1}$ one sees indirect transitions, involving phonons, between the valence band and the conduction band with extrema at different points in **k**-space. This absorption rises sharply with temperature at the lower energies because of the number of phonons involved. I would suggest that the tail which you see in TlCl is really a quite different thing and is due to such indirect transitions, and that TlCl has a band structure like Ge with minima at different places in **k**-space.

W. Martienssen: Would you say the tail is due to indirect exciton transitions or indirect band-to-band transitions?

R. J. Elliott: It looks from the shape of the absorption as if the binding energy of the excitons in these substances is quite low. The shape of the edge is almost exactly that of germanium as measured by Lax and by MacFarlane and in my opinion is due to a series of other exciton lines, further up the hydrogen series, which are not resolved, running into a continuum.

F. Brown (Illinois): The situation in the silver and thallium halides may be slightly different from that in germanium since in the former materials it is likely that the conduction band is simple, rather than the valence band, so that indirect transitions would produce a hole at $k \neq 0$ and an electron near $k = 0$.

R. J. Elliott: How can you tell?

F. Brown: Some of the conduction and photoelectric experiments indicate that the properties of the electron in the conduction band are simple and isotropic—there are just the beginning indications of this—and one expects this in these wider band gap materials. I would like to ask if this would make any difference in the theory for indirect transitions?

R. J. Elliott: There should be no difference in the theory, I think: one would expect an $E^{\frac{1}{2}}$ dependence in the edge, changing into an $E^2$ dependence in the usual way.

Further discussion among F. Brown, R. J. Elliott, and W. Martienssen brought up the comments that an $E^2$ edge fits the AgCl spectrum fairly well, while in the alkali and thallous halides the edge shape is exponential. J. A. Krumhansl pointed out a basic difference, involving the role of the $2S$ electrons, between the silver and thallium halides, and suggested that a closer analog to TlCl would be PbS, which might also be expected to show the anomalous temperature shift.

K.5. E. A. Braun and J. W. Mitchell

G. Luckey (Eastman Kodak Company): What is the nature of the etch used, in your second picture?

J. W. Mitchell: The second series of etches have all been developed by adding antifoggants of the mercaptobenzimidazole type to a 3N solution of sodium thiosulfate. The crystal has to be dipped in the etch and then plunged into water in the shortest possible time, since if etching is continued longer than a fraction of a second the dislocations just disappear completely. We found we could obtain more controllable etching times by using a tenth-normal solution of sodium thiosulfate, with a final concentration of mercaptobenzimidazole of about 1 in 20,000, a very clear demonstration of the behavior which Sears observed in LiF.

M. Silver (O.O.R.): After the initial decay of photoconductivity, if the light is turned off and then reapplied, does the current just reach the saturation value?

J. W. Mitchell: The current reaches the saturation value, but at a slow rate.

M. Silver: What about the persistence of the space charge?

J. W. Mitchell: We have studied the persistence of the space charge very carefully because we have to measure the trap depth of the electrons by following its decay. So long as the field is applied the space charge remains in the crystal almost indefinitely; if the field is not applied, there is a slow decay of the space charge over a period of four or five days.

There was some further discussion between M. SILVER and J. W. MITCHELL regarding the temperature dependence of the space charge decay.

H. F. IVEY (Westinghouse): You indicated that you had expected electroluminescence in these crystals but didn't see it. Could you say why you expected electroluminescence?

J. W. MITCHELL: Because of what one might call the previous experiments along these lines. Since the war most of the effective work on conduction in the silver halides has been done by pulse techniques. We have in effect gone back to the old techniques of the Göttingen school, as used by HECHT and LEHFELDT; in their experimental work, HECHT observed a beautiful electroluminescence. We have also observed electroluminescence in crystals containing silver oxide; the luminescence is rather poor, of course, but well known.

K.6. F. C. BROWN and K. KOBAYESHI

H. HAKEN: If one considers the order of magnitude of the trapping energy it is apparent that it is of the same magnitude as one would expect for the self-energy of a polaron. Therefore one might think that the trapping centers are due to a polarization field surrounding the electron. If such a trapping effect is important it seems to be a question not only of the strength of the electron-lattice coupling but also of the validity of the continuum approximation, a question which has not yet been completely treated in the literature, so far as we know.

(There was further discussion between F. C. BROWN and H. HAKEN regarding the possible influence of polaron self-trapping on the high temperature drift mobility.)

G. HEILAND: Is there any influence of previous treatment? If there were self-trapping effects one would not expect much structure dependence.

F. C. BROWN: The trap density is very structure dependent. The exact position of the glow peak, and the apparent concentration as deduced from the drift data, vary widely from crystal to crystal. We have not as yet found any systematic behavior.

J. W. MITCHELL: Would it have been possible to perform the transit time experiments on the clean AgBr crystals mentioned in connection with high Hall mobility?

F. C. BROWN: Just barely. The range was shorter by a factor of 10 to 100 than in the crystals we talked about here, so it would be rather difficult.

*J. Phys. Chem. Solids* Pergamon Press 1959. Vol. 8. pp. 305–311. Printed in Great Britain

SESSION L:
MAGNETO-OPTICAL EFFECTS*

# L.1 ZEEMAN TYPE MAGNETO-OPTIC STUDIES OF ENERGY BAND STRUCTURE

**E. BURSTEIN,† G. S. PICUS, R. F. WALLIS and F. BLATT‡**

U.S. Naval Research Laboratory, Washington, D.C.

VOL. 8 1959

**Abstract**—The energy levels associated with an energy band in a magnetic field are characterized by the following quantum numbers: $\hbar k_H$, the crystal momentum along the magnetic field direction; $l$, the Landau magnetic quantum number; and $M_J$ the component of the total angular momentum along the magnetic field which is characteristic of the atomic states in the tight binding limit. In the case of degenerate valence bands, the effect of a magnetic field is complicated by degeneracy effects and the levels in a magnetic field are characterized by two or more pairs of ($l$, $M_J$) values. The selection rules, polarization effects, and the character of the absorption spectra of interband transitions in a magnetic field are discussed and illustrated by experimental data for Ge.

The purpose of the present paper is to discuss the physics underlying the Zeeman type interband magneto-optic (IMO) effects in semiconductors. The effect of a magnetic field on the electronic energy levels of a semiconductor will be presented and the various optical transitions that can take place between these levels will be discussed. Finally, data on the room temperature IMO effect in Ge will be reported and compared with the theoretical calculations.

## 1. ENERGY LEVELS IN A MAGNETIC FIELD

In a magnetic field the energy levels of a "simple" conduction band, such as one arising from $s$-type atomic levels, can be written to first order as

$$\epsilon_c(k_H, l, M_J) = \epsilon_c + \frac{\hbar^2 k_H^2}{2m_c^*} + (l+\tfrac{1}{2})\hbar\omega_{0c} + g\beta H M_J \tag{1}$$

where $\epsilon_c$ is the energy at the band edge; $\hbar k_H$ is the component of crystal momentum of the electrons along the magnetic field; $l$ is the Landau magnetic quantum number; $\omega_{0c} = eH/m_c^* c$ is the circular cyclotron resonance frequency; $g$ is the effective $g$-factor of the electrons; $M_J$ is the component of angular momentum along the magnetic field having values of $+1/2$ and $-1/2$ corresponding to the two possible orientations of the electron spin; and $\beta = e\hbar/2mc$ is the Bohr magneton. The energy levels are magnetically quantized in the plane perpendicular to the applied magnetic field, but remain quasi-continuous along the magnetic field direction, forming a double series of "one dimensional sub-bands" characterized by the quantum numbers $l$ and $M_J$. The wave functions of the levels can be written to first order in effective mass theory as

$$\Psi(\mathbf{r}) = F_l(\mathbf{r})\phi_{M_J}{}^{(J)}(\mathbf{r}) \tag{2}$$

where $\phi_{M_J}{}^{(J)}(\mathbf{r})$ are the Bloch functions at $k = 0$ having symmetry properties characterized by the angular momentum quantum numbers $J$ and $M_J$ of the atomic states to which they reduce in the tight binding limit, and $F_l(\mathbf{r})$ are the wave functions for a free electron in a constant magnetic field which are characterized by the magnetic quantum number $l$. The density of states in a particular sub-band is given by

$$N_{l,M_J}(\epsilon) = \frac{eH}{c\hbar}\left(\frac{2m^*}{h^2}\right)^{\frac{1}{2}}(\epsilon - \epsilon_{l,M_J})^{-\frac{1}{2}} = \frac{eH}{ch}N^{(1)}(\epsilon) \tag{3}$$

where $\epsilon_l$, $M_J$ is the energy at the sub-band edge;

* *Chairman:* D. Polder; *Co-Chairman:* H. V. Fan.

† Address after September 15, 1958: Department of Physics, University of Pennsylvania, Philadelphia, Pa.

‡ Permanent address: Physics Department, Michigan State University, East Lansing, Michigan.

$(eH/ch)$ is the degeneracy of the levels; and $N^{(1)}$ is the density of states of a non-degenerate one-dimensional energy band. The density of states at the edge of each sub-band is infinite, a consequence of their one-dimensional character; this is in contrast to the zero density of states at the edge of "three-dimensional" energy bands in the absence of a magnetic field.

The effect of magnetic field on degenerate valence bands is much more complicated. LUTTINGER and KOHN[1] have developed an effective mass formalism for calculating the energy levels and wave functions in degenerate energy bands with spin–orbit coupling for crystals with a center of symmetry. They show that the wave function of a given magnetic state in the valence band is given to a first approximation, by a linear combination of products $F_l(\mathbf{r})\phi_{M_J}{}^{(J)}(\mathbf{r})$. For Ge the valence band Bloch functions can be written as $\phi_{3/2}{}^{(3/2)}, \phi_{1/2}{}^{(3/2)}, \phi_{-1/2}{}^{(3/2)}$ and $\phi_{-3/2}{}^{(3/2)}$ for the $V_1$ and $V_2$ bands and $\phi_{1/2}{}^{(1/2)}$ and $\phi_{-1/2}{}^{(1/2)}$ for the split off $V_3$ band. The mixing of the $\phi_{M_J}{}^{(3/2)}$ and $\phi_{M_J}{}^{(1/2)}$ Bloch functions is quite small in Ge for magnetic fields ordinarily available in the laboratory. Furthermore, under conditions which are reasonably well satisfied in Ge* for the magnetic field directed along the 100 axis the wave functions for the magnetic states of the $V_1$ and $V_2$ bands at $k_H = 0$ can be written as linear combinations of two terms of the form

$$\begin{aligned}
\Psi_1{}^+ &= a_1{}^+F_{l-2}\phi_{\frac{3}{2}}{}^{(\frac{3}{2})} + a_2{}^+F_l\phi_{-\frac{1}{2}}{}^{(\frac{3}{2})}, \quad l \geqslant 0 \\
\Psi_1{}^- &= a_1{}^-F_{l-2}\phi_{\frac{3}{2}}{}^{(\frac{3}{2})} + a_2{}^-F_l\phi_{-\frac{1}{2}}{}^{(\frac{3}{2})}, \quad l \geqslant 2 \\
\Psi_2{}^+ &= b_1{}^+F_{l-2}\phi_{\frac{1}{2}}{}^{(\frac{3}{2})} + b_2{}^+F_l\phi_{-\frac{3}{2}}{}^{(\frac{3}{2})}, \quad l \geqslant 0 \\
\Psi_2{}^- &= b_1{}^-F_{l-2}\phi_{\frac{1}{2}}{}^{(\frac{3}{2})} + b_2{}^-F_l\phi_{-\frac{3}{2}}{}^{(\frac{3}{2})}, \quad l \geqslant 2
\end{aligned} \tag{4}$$

The corresponding energy eigenvalues consist of four ladders of non-uniformly spaced levels $\epsilon_1{}^+(n)$, $\epsilon_2{}^+(n)$, $\epsilon_1{}^-(n)$ and $\epsilon_2{}^-(n)$ where $n = 0, 1, 2 \ldots$ for the plus ladders and $n = 2, 3, 4 \ldots$ for the minus ladders. Each magnetic state is characterized by two $(l, M_J)$ pairs of quantum numbers, except for the two uppermost levels of each of the $\epsilon_1{}^+(n)$ and $\epsilon_2{}^+(n)$ ladders which are characterized by only a single $l$ and a single $M_J$ (Fig. 1). The

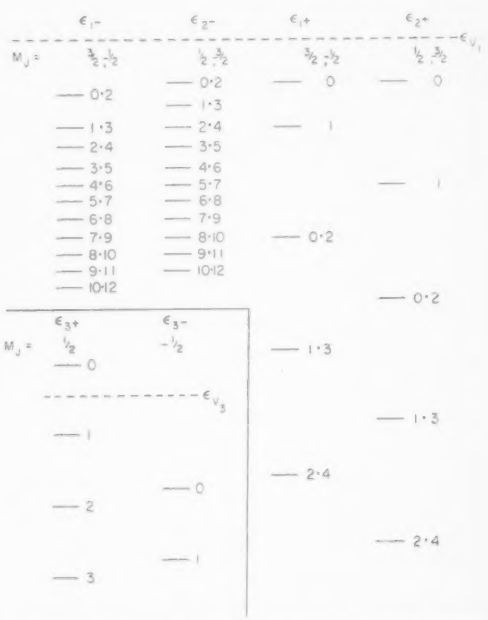


FIG. 1. Energy levels of the $V_1$, $V_2$ and $V_3$ bands in Ge in the presence of a magnetic field. Numbers next to each level are the $l$-values that characterize that level.

value of $n$ corresponds to the larger of the two $l$ values characterizing a given state. On the limit of large $n$ the $\epsilon_1{}^+(n)$ and $\epsilon_2{}^+(n)$ levels approach a uniform spacing characteristic of the effective mass for light holes, while the $\epsilon_1{}^-(n)$ and $\epsilon_2{}^-(n)$ levels approach a uniform spacing characteristic of the effective mass for heavy holes. When $k_H$ is not restricted to zero, the energies of the $V_1$ and $V_2$ magnetic states become complicated functions of $k_H$ and each magnetic state forms a "one-dimensional sub-band" which is parabolic only for small values of $k_H$.

The magnetic levels of the $V_3$ band are characterized by only a single $l$ and a single $M_J$, have a uniform spacing and form simple parabolic sub-bands of the type described by equation (1). An estimate of KOHN[2] leads to a value of $g = +54$ for the $V_3$ band. As a result of this large $g$-factor the separation between the $M_J = +1/2$ and the

* The exact conditions are that $k_H = 0$ and that the effective mass parameters $\gamma_2$ and $\gamma_3$ defined by LUTTINGER[2] are equal. The latter condition is equivalent to neglecting warping of the $V_1$ and $V_2$ bands. The magnetic levels under these assumptions are independent of the relative orientation of crystallographic axes and magnetic field.

$M_J = -1/2$ sub-bands for the same $l$ value is about two times greater than the separation between adjacent sub-bands with the same $M_J$ but having $l$ values differing by one.

The calculation of the energy levels and wave functions for magnetic levels in the valence bands of crystals lacking a center of symmetry such as InSb differs in certain important details. As a consequence of the absence of a center of symmetry, the $V_1$ and $V_2$ bands are not doubly degenerate except at $k = 0$. The expressions for the energy levels contain terms linear in $k$ for certain directions in $k$ space and the maxima of the bands do not occur at $k = 0$ as in Ge, nor do they coincide. The linear terms in $k$ make the calculations of the magnetic levels of the valence band in InSb much more complicated than for Ge and at present such a calculation is not available.

## 2. OPTICAL TRANSITIONS BETWEEN ENERGY BANDS IN A MAGNETIC FIELD

### 2.1. *Density of states effects*

The absorption spectrum, neglecting broadening, for vertical transitions from a single valence sub-band to a single conduction sub-band is given by

$$a_{ll'}(\omega) = \frac{2\alpha h^2 |I_{ll'}|^2}{\eta m^2 \hbar\omega}\left(\frac{eH}{ch}\right)\left(\frac{2\bar{m}^*}{h^2}\right)^{\frac{1}{2}}(\hbar\omega - \epsilon_{ll'})^{-\frac{1}{2}}$$

$$= \frac{2\alpha h^2}{\eta m^2}\frac{\bar{N}_{ll'}|I_{ll'}|^2}{\hbar\omega} \qquad (5)$$

where we have omitted the subscripts designating the $M_J$ quantum numbers. $\alpha$ is the fine structure constant and $\eta$ is the refractive index. $I_{ll'}$ is the momentum matrix element for vertical optical transitions, $\bar{m}^*$ and $\bar{N}_{ll'}$ are the reduced effective mass and reduced density of states respectively for the two sub-bands, and $\epsilon_{ll'}$ is the corresponding energy gap given by

$$\epsilon_{ll'} = \epsilon_{nn'} + (l+\tfrac{1}{2})\hbar\omega_{0n} + \\ + (l'+\tfrac{1}{2})\hbar\omega_{0n'} - g_n\beta HM_J + g_{n'}\beta HM_{J'} \qquad (6)$$

in which $\epsilon_{nn'}$ is the energy gap between the two energy bands $n$ and $n'$ at zero magnetic field.

For allowed first order transitions, the matrix element, which we denote by $I_{ll'}^{(1)}$, is effectively independent of $k$, so that $a_{ll'}(\omega)$ will be infinite at the absorption edge (i.e., at $\hbar\omega = \epsilon_{ll'}$) and decrease as $(\hbar\omega - \epsilon_{ll'})^{-1/2}$ near the edge. The infinity in the absorption constant at the absorption edge is typical of allowed transitions between one-dimensional energy bands and arises from the infinities in the densities of states at the band edges of one-dimensional energy bands just as the zero absorption constant at the absorption edge for zero magnetic field arises from the zero in the density of states at the band edges of three-dimensional bands. In actual semiconductors, energy level broadening will remove the infinities at the absorption edge. A complete IMO spectrum for a given state of polarization and direction of propagation of the radiation relative to the magnetic field will consist of the superposition of the spectra of appropriate pairs of sub-bands, specified by the selection rules $\Delta l = 0$ and $\Delta M_J = 0, \pm 1$ for first order transitions, and will exhibit absorption peaks at photon energies given by equation (6). One can see from equations (5) and (6) that the positions of the IMO peaks and their dependence on magnetic field can yield information about the energy gap $\epsilon_{nn'}$, the effective masses $m^*_n$ and $m^*_{n'}$ and the effective $g$-factors $g_n$ and $g_{n'}$. The presence of sharp peaks at the absorption edges makes it possible to obtain very accurate values of $\epsilon_{nn'}$ by extrapolation of the first absorption peak position to zero magnetic field.

The second order matrix elements, $I_{ll'}$,(2) which apply to vertical transitions involving intermediate states will include terms which are proportional to $k_H$ as well as terms which are independent of $k_H$. The terms which are independent of $k_H$ will yield peaked absorption spectra of the form given by equation (5). On the other hand the terms which are proportional to $k_H$ will yield absorption spectra in which the absorption constants vary as $(\hbar\omega - \epsilon_{ll'})^{+1/2}$ and do not therefore exhibit absorption peaks. The second order spectra will thus consist of a superposition of two types of spectra and may be expected to be much more complicated than the first order spectra.

When the extremum of one of the energy bands is not at $k = 0$, the absorption edge will involve non-vertical optical transitions with the simultaneous emission or absorption of phonons. In the presence of a magnetic field, the absorption or emission of phonons introduces an additional factor of the form $(\hbar\omega - \epsilon_{ll'})^{1/2}$ into the expression

for the absorption constant.† The absorption constant for indirect transitions between magnetic sub-bands will be of the form

$$a_{ll}(\omega, l'', p) \sim |I_{ll''}|^2 |M_{l''l'p}|^2 \frac{(\hbar\omega - \epsilon_{ll'p})^0}{\hbar\omega} \quad (6)$$

where $I_{ll''}$ is the matrix element for vertical optical transitions between sub-band $l$ and an intermediate sub-band $l''$, $M_{l''l'p}$ is the electron–lattice interaction matrix element involving transitions between the intermediate sub-band $l''$ and sub-band $l'$ via a given phonon $p$, and $\epsilon_{ll'p} = \epsilon_{ll'} \pm \epsilon_p$ where $\epsilon_p$ is the phonon energy. When the matrix elements are constant, the absorption constant will be finite at the absorption edges. On the other hand, when a given term in the matrix elements is proportional to $k$, the corresponding term in the absorption constant will be of the form

$$a_{ll}(\omega, l'', p) \sim \frac{(\hbar\omega - \epsilon_{ll'p})}{\hbar\omega} \quad (7)$$

so that the absorption constant will be zero at the absorption edge and increase as $(\hbar\omega - \epsilon_{ll'p})$ near the edge. The IMO spectrum for indirect transitions may be expected to be a superposition of spectra for each type of intermediate state and each type of phonon transition involved.

### 2.2. *Selection rules and polarization effects*

The matrix elements which characterize the optical transitions between bands $n$ and $n'$ in the presence of an applied magnetic field are of the form

$$I_\beta = \int \Psi_n^*(\mathbf{r}) P_\beta \Psi_{n'}(\mathbf{r}) d\mathbf{r} \quad (8)$$

where we have omitted the subscripts $n$ and $n'$ on $I_\beta$; $P_\beta$ is the $\beta$ component of the kinetic momentum operator $\mathbf{P} = \mathbf{p} + (e/c)\mathbf{A}$. If we consider only first order terms in the wave functions, the matrix elements would have the form

$$I_\beta^{(1)} = \int F_n^*(\mathbf{r}) \left( p_\beta + \frac{e}{c} A_\beta \right) F_{n'}(\mathbf{r}) d\mathbf{r} \times$$

$$\times \int \phi_n^*(\mathbf{r}) \phi_{n'}(\mathbf{r}) d\mathbf{r} + \int F_n^*(\mathbf{r}) F_{n'}(\mathbf{r}) d\mathbf{r} \times$$

$$\times \int \phi_n^*(\mathbf{r}) p_\beta \phi_{n'}(\mathbf{r}) d\mathbf{r} \quad (9)$$

Because of the orthogonality of the Bloch functions of different energy bands, the first term is non-zero only for transitions between states in the same energy band. The second term is non-zero for allowed direct transitions between states in different energy bands. The first term is thus responsible for cyclotron resonance transitions while the second term is responsible for IMO transitions.

From the first integral of the IMO term and the orthogonality of the $F_n(\mathbf{r})$ wave functions, it follows that the selection rules for first order IMO transitions are $\Delta k_H = 0$ and $\Delta l = 0$. The second integral of the IMO term yields the selection rule that $\Delta M_J = 0, \pm 1$.

Associated with the selection rule $\Delta M_J = 0, \pm 1$ are characteristic polarization effects. For light propagating along the external magnetic field (Poynting vector parallel to the external magnetic field and therefore $E \perp H$) $\Delta M_J = +1$ transitions occur for left circularly polarized radiation (they correspond to the $\sigma_L$ transition in atomic Zeeman spectra) and the $\Delta M_J = -1$ transitions do not occur for this configuration of the Poynting vector and the external magnetic field.

For light propagating perpendicular to the external magnetic field (Poynting vector perpendicular to this magnetic field, the $\Delta M_J = 0$ transitions occur for plane polarized radiation with $E \parallel H$ (these correspond to the $\pi$ transitons in atomic Zeeman spectra). Both the $\Delta M_J = +1$ and $\Delta M_J = -1$ transitions occur for plane polarized radiation with $E \perp H$.

When we include second order terms in the wave function, the optical matrix elements for IMO transitions are given by‡[3]

$$I_\beta = I_\beta^{(1)} + I_\beta^{(2)}$$

$$I_\beta^{(1)} = p_{nn'\beta} \int F_n^*(\mathbf{r}) F_{n'}(\mathbf{r}) d\mathbf{r} \quad (10)$$

$$I_\beta^{(2)} = -\frac{1}{\hbar m} \left[ \sum_{n'' \neq n'} \frac{p_{nn''\beta} p_{n''n'\alpha}}{\omega_{n''n'}} + \sum_{n'' \neq n} \frac{p_{nn''\alpha} p_{n''n'\beta}}{\omega_{n''n}} \right]$$

† In the absence of a magnetic field the factor would be of the form $(\hbar\omega - \epsilon_{nn'p})^{\frac{1}{2}}$.

‡ The second order matrix element also contains an additional term which like $I_\beta^{(1)}$ is proportional to $p_{nn'}$. However this additional term is negligible compared to $I_\beta^{(1)}$ for semiconductors studied thus far.

$$\int F_n^*(\mathbf{r})\left[p_\alpha+\frac{e}{c}A_\alpha\right]F_{n'}(\mathbf{r})d\mathbf{r}$$

where

$$p_{nn'}{}^{\beta}=\frac{(2\pi)^3}{\Omega}\int\phi_n^*(\mathbf{r})p_\beta\phi_{n'}(\mathbf{r})d\mathbf{r}$$

($\Omega$ is the volume of a unit cell.) The $I_\beta^{(2)}$ term is the counterpart of the second order matrix element in the absence of a magnetic field with the integral involving the modulating functions taking the place of the factor $k_\alpha$. For crystals with a center of symmetry $I_\beta^{(2)}$ makes a contribution only if the corresponding first order transition is not allowed. It is applicable, for example, to IMO transitions among the $V_1$, $V_2$ and $V_3$ bands in Ge. For crystals lacking a center of symmetry, non-zero contributions may raise from both $I_\beta^{(1)}$ and $I_\beta^{(2)}$.

The integral involving the modulating functions in $I_\beta^{(2)}$ has the same form as that appearing in the first order term for CR transitions, and yields the selection rule $\Delta l=\pm1$, 0 and $\Delta k_H=0$. The contributions involving $\Delta l=0$ are proportional to $k_H$ and independent of $l$ and $H$, whereas those involving $\Delta l=\pm1$ are independent of $k_H$ and are proportional to $(Hl^+)^{1/2}$ where $l^+$ is the larger of the two $l$ values involved. The factor which involves the products of momentum matrix elements yields the selection rule $\Delta M_J=0$, $\pm1$, $\pm2$.†

The values for $\Delta l$ and $\Delta M_J$ are further restricted by a selection rule on their sum given by $(\Delta l+\Delta M_J)=0$, $\pm1$ which is consistent with the conservation of total angular momentum of electron and photon.‡

### 2.3. *Direct optical transitions between the valence bands and the $\Gamma_2$ conduction band in Ge*

Direct IMO transitions from the $V_1$, $V_2$ and $V_3$ bands to the $\Gamma_2$ conduction band in Ge are allowed to first order since the corresponding transitions are allowed in the absence of a magnetic field.

† The possibility of $\Delta M_J=\pm2$ arises because the intermediate state $n''$ can have $M_J$ values differing by $\pm1$ from both the initial and final states.

‡ The polarization effects associated with the selection rule $(\Delta l+\Delta M_J)=0$, $\pm1$ in second order spectra are the same as those for the selection rule $\Delta M_J=0$, $\pm1$ for first order IMO spectra.

The $\Gamma_2$ band is spherically symmetric and has a two-fold spin degeneracy. The energy levels are given to first order by equation (1) and are characterized by a single $l$ and a single $M_J$. ROTH[4] has shown that the $g$-factor for electrons in the $\Gamma_2$ band is given approximately by

$$g=2\left[1-\left(\frac{m-m^*}{m^*}\right)\left(\frac{\Delta}{3\epsilon_G+2\Delta}\right)\right] \qquad (11)$$

where $\epsilon_G$ is the band gap between the $V_1$ band and the $\Gamma_2$ band, and $\Delta$ is the energy separation between the $V_3$ band and the $V_1$ and $V_2$ bands at $k=0$. The $g$-factor turns out to be negative ($g\simeq-3$) so that the order of the two spin states in a magnetic field is reversed from the usual order.

Transitions between the $V_3$ band and the $\Gamma_2$ band may be expected to yield spectra which are similar to those that occur for simple energy bands. The transitions between the $V_1$ and $V_2$ bands and the $\Gamma_2$ band, on the other hand, yield a greater number of absorption peaks, since the wave functions of the $V_1$ and $V_2$ magnetic states consist of the sum of two or more terms, each term involving a different $l$, $M_J$ pair of quantum numbers.

For illustration, the experimental room temperature $\sigma_R$ and $\pi$ absorption spectra for Ge with $H$ directed along (100) are illustrated in Figs. (2) and (3) together with the corresponding theoretical positions of the absorption peaks.[3]

The experimental curves were obtained from transmission measurements on a 3-$\mu$ thick sample of Ge, made from material kindly supplied by C. Goldberg, Westinghouse Research Laboratories. IR polaroid films were used to produce plane polarized radiation for the $\pi$ spectrum, and one such film together with a Fresnel rhomb made of NaCl was used to produce circularly polarized radiation for the $\sigma_R$ spectrum. The theoretical positions of the absorption peaks were calculated using values of the valence band energy levels kindly supplied to us by R. Goodman, together with $\Gamma_2$ band energy levels calculated by assuming an effective mass of 0·038 $m$. This particular value of the $\Gamma_2$ band effective mass gave the best match between theoretical and experimental data in the $\sigma_R$ spectrum. Although the assumption of uniform spacing of the magnetic sub-bands in the $\Gamma_2$ band is not strictly valid because of non-parabolic effects, it is probably sufficiently accurate for the present data.

The individual absorption peaks are not resolved. Nevertheless it is evident that there is

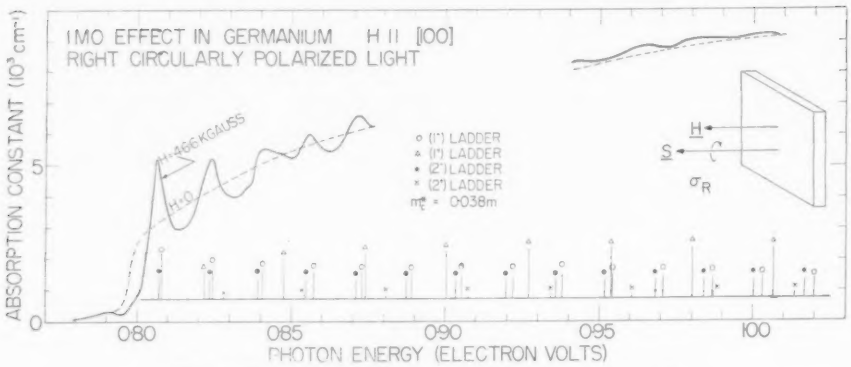


FIG. 2. Experimental absorption spectrum and theoretical absorption peaks for right circularly polarized light in Ge in a magnetic field at room temperature.

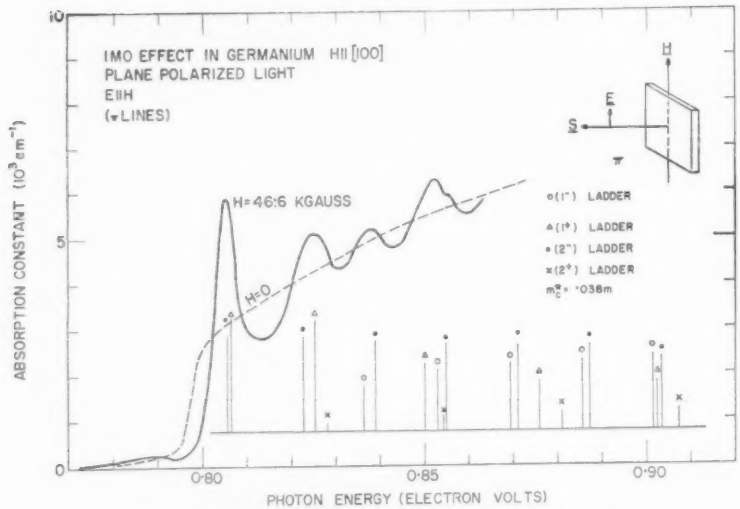


FIG. 3. Experimental absorption spectrum and theoretical absorption peaks for plane polarized light with $E \parallel H$ in Ge in a magnetic field at room temperature. Beyond 0·94 eV the $H = 0$ curve and the high field curves are coincident.

reasonable agreement between the experimental and theoretical positions of the peaks. It is possible to resolve additional structure by going to lower temperature as has recently been demonstrated by the Lincoln Laboratory Group.[5] The latter estimate a value of 0·035 $m$ for the effective mass of the carriers in the $\Gamma_2$ band from the low temperature data. Efforts to observe structure associated with transitions from the $V_3$ to the $\Gamma_2$ band have not yet been successful. Low temperature, thinner specimens and higher magnetic fields may eventually enable one to observe such structure.

The IMO spectra of InSb[6,7] have also been investigated, although not as extensively as those for Ge. Roth's suggestion that the separation between the first two absorption peaks corresponds to the separation between the conduction band

spin states for $l = 0$ appears to be a reasonable one. In the absence of an adequate theory for the magnetic levels in the valence band, further speculation about the details of the IMO spectra in InSb is unwarranted at this time.

2.4. *Optical transitions among the $V_1$, $V_2$ and $V_3$ valence bands in Ge*

The $\epsilon_1^+(n)$ and $\epsilon_1^-(n)$ ladders have similar wave functions as do the $\epsilon_2^+(n)$ and $\epsilon_2^-(n)$ ladders. First order CR type transitions, those which yield terms in the matrix elements with the same Bloch functions in the initial and final states, can accordingly take place between $\epsilon_1^+(n)$ and $\epsilon_1^-(n)$ sub-bands and between $\epsilon_2^+(n)$ and $\epsilon_2^-(n)$ sub-bands, as well as between sub-bands in the same ladder. These absorption transitions between the + and − ladders involve $\Delta l = -1$ as well as $\Delta l = +1$, and therefore involve both right and left circularly polarized radiation. Furthermore, as a result of the differences in curvature of the + and − sub-bands, they lead to absorption peaks with extended tails, as in the case of IMO transitions, rather than to symmetrically broadened lines obtained for the usual CR transitions.

IMO type transitions among the valence bands, those which yield terms in the matrix elements with different Bloch functions in the initial and final states, can take place only to second order. The interband transitions from $V_1$ and $V_2$ to $V_3$ levels are of particular interest for Ge since they yield spectra which occur in an easily accessible region of wavelength. However, efforts to observe structure in the $V_1$ and $V_2$ to $V_3$ IMO spectra in $p$-type Ge have thus far been unsuccessful. The experiments which were carried out at low temperatures with fields up to 25,000 gauss are now being extended to higher magnetic fields.

*Acknowledgments*—We wish to express our appreciation to E. N. Adams, R. R. Goodman, E. O. Kane, W. Kohn and J. M. Luttinger for valuable discussions.

## REFERENCES

1. Luttinger J. M. and Kohn W. *Phys. Rev.* **97,** 869 (1955).
2. Luttinger J. M. *Phys. Rev.* **102,** 1030 (1956).
3. Burstein E., Picus G. S., Wallis R. F. and Blatt F. *Phys. Rev.* (to be published).
4. Roth L. *Lincoln Laboratory Solid State Res. Quart. Prog. Rep.* p. 47. 1 Nov. 1957.
5. Zwerdling S., Roth L. M. and Lax B. *Phys. Rev.* **109,** 2207 (1958).
6. Burstein E. and Picus G. S. *Phys. Rev.* **105,** 1123 (1957).
7. Zwerdling S., Lax B. and Roth L. M. *Phys. Rev.* **108,** 1402 (1957).

*J. Phys. Chem. Solids* Pergamon Press 1959. Vol. 8. pp. 311–318. Printed in Great Britain

L.2

# QUANTUM MAGNETO-ABSORPTION PHENOMENA IN SEMICONDUCTORS*

**B. LAX, L. M. ROTH and S. ZWERDLING†**

Lincoln Laboratory, Lexington, Mass.

**Abstract**—The existence of quantized magnetic or Landau levels in a semiconductor in a magnetic field can give rise to a variety of magneto-absorption phenomena. The oscillatory magneto-absorption of the direct transition has been observed in germanium, indium arsenide and indium antimonide.

* The research reported in this document was supported jointly by the Army, Navy and Air Force under contract with the Massachusetts Institute of Technology.

† Staff Members, Lincoln Laboratory, Massachusetts Institute of Technology.

The fine structure of the low temperature data in germanium has been correlated with the theory, taking into account the complex band structure. The indirect magneto-absorption spectrum in germanium has also been observed and in accordance with theory, it appears as a sequence of steps which is modified by a finite line width. A third type of magneto-absorption associated with transitions between the degenerate and split-off bands as in germanium and gallium arsenide is shown to have both oscillatory and non-oscillatory components. The Zeeman effect of impurities and excitons which is closely related to the above phenomena can give information about the band structure of semiconductors. For ellipsoidal energy surfaces, the linear effect evaluates the transverse mass and the anisotropy of the quadratic Zeeman effect for electrons is exactly analogous to the results of cyclotron resonance. Finally, quantum effects can occur in the Faraday rotation and free carrier absorption in a magnetic field.

A NUMBER of phenomena in semiconductors arise due to the creation of quantized levels in the conduction and valence bands in the presence of a magnetic field. These phenomena can be readily observed by the absorption of optical radiation in semiconducting materials. The best known among these is (1) the cycloton resonance which is associated with transitions between magnetic levels in the same band. Other phenomena which have been observed are (2) the oscillatory magneto-absorption of the direct transitions in semiconductors and (3) the magneto-absorption of the indirect transition in germanium. These are transitions between magnetic levels of the valence and conduction bands. A related type of magneto-absorption effect due to (4) the transition of electrons between the valence bands has been analyzed theoretically and is yet to be seen experimentally. Still another class of quantum phenomena are (5) the Zeeman effect, which involves transitions between impurity levels, or, as in the exciton, between the valence band and bound exciton levels. The last class of phenomena are those associated with (6) the quantum effects of the Faraday rotation and the free carrier absorption in a magnetic field which would show up best at low temperatures.

## DIRECT TRANSITION MAGNETO-ABSORPTION

The energy momentum relation for two simple parabolic bands in a semiconductor is given by $\epsilon_1 = \epsilon_{10} - \hbar^2k^2/2m_1$ and $\epsilon_2 = \epsilon_{20} + \hbar^2k^2/2m_2$, where $\epsilon_{10}$ and $\epsilon_{20}$ are the energies at the edges of the valence and conduction bands and $m_1$ and $m_2$ are the effective masses of the hole and electron, respectively. In a magnetic field, for each of these two simple parabolic bands we can write an effective-mass Schroedinger equation. The solution of this type of equation has been obtained by Landau and gives rise to discrete magnetic levels in both the conduction and valence bands of the form $\epsilon_n = \pm(n+\frac{1}{2})\hbar\omega_c \pm \hbar^2k_z^2/2m^*$, where $\omega_c = eH/m^*c$ is the cyclotron frequency for the carrier in a magnetic field $H$, and the energy levels are referred to the bottom of the conduction and top of the valence bands. In order to calculate the optical absorption in a semiconductor, the transition probability of an electron from band 1 to band 2 has to be evaluated. This involves the product of Bloch functions at the band edges which are evaluated over a unit cell and the Landau functions which are evaluated over the crystal. From the former we obtained the condition that the first-order transition is possible when the two bands are of different symmetry and from the latter we obtained the selection rules $\Delta n = 0$ and $\Delta \mathbf{k} = 0$. Such a calculation has been carried out for $\alpha_H$, the absorption coefficient in a magnetic field:

$$\alpha_H = \tfrac{1}{2}K\hbar(\omega_{c1}+\omega_{c2}) \times \times \sum_n \left[h\nu - \epsilon_g + (n+\tfrac{1}{2})\hbar(\omega_{c1}+\omega_{c2})\right]^{(-\frac{1}{2})}$$

where $h\nu$ is the energy of the photon, $\epsilon_g = \epsilon_{20} - \epsilon_{10}$ is the energy gap, $K$ a constant involving the density of states and the momentum matrix element.

The above expression for $\alpha_H$ can be modified to include a relaxation time for a Lorentzian line which then gives an absorption coefficient which shows an oscillatory character above the absorption edge with absorption peaks corresponding to transitions between discrete magnetic levels with the selection rule $\Delta n = 0$. This type of phenomenon was observed independently by the group at Lincoln Laboratory[1] in germanium and by the NRL group in indium antimonide.[2] The experimental observation obtained in germanium[3] is shown in Fig. 1 where at energies above the absorption edge we obtain distinct oscillations

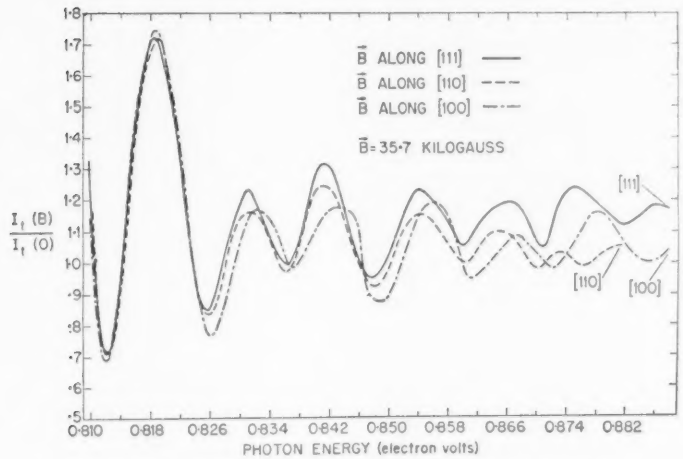


FIG. 1. Anisotropy of the oscillatory magneto-absorption effect in germanium for a d.c. magnetic field intensity of 35·7 kG. The data was taken at room temperature with a prism spectrometer.

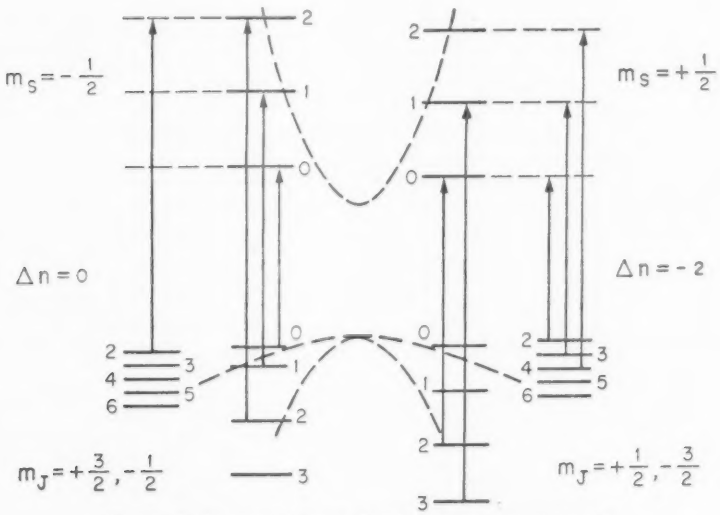


FIG. 2. Schematic diagram showing the magnetic levels for the valence and $k = 0$ conduction bands in germanium. The transitions shown are those allowed for $\mathbf{E} \parallel \mathbf{H}$.

which are most appropriately presented as a ratio of the transmitted signal with a magnetic field to that with zero magnetic field. The anisotropy expected from the known properties of the valence band in germanium is shown. The energy band scheme in germanium is rather complex as indicated by the diagram of Fig. 2 in which we have drawn a somewhat simplified diagram of the valence band and part of the conduction band at $k = 0$. The latter is somewhat higher than the usual minimum in germanium which is located at the edge of the Brillouin zone along

the (111) direction. The magnetic levels for the degenerate valence bands are obtained from the solution of a $4\times4$ matrix equation including the magnetic field. This has been worked out by Luttinger and Kohn and we have used the values of the parameters obtained from cyclotron resonance at microwave frequencies to plot an energy diagram as shown in Fig. 2, which shows four sets of magnetic levels; two associated with the small holes and two with the heavy holes. The analogous problem for the conduction band is relatively simple since the levels are separated into two levels due to the spin. Since the magnetic levels of the valence band are a composite of Landau states with quantum numbers $n$ and $n-2$, the selection rules for the levels shown are $\Delta n = 0$ and $\Delta n = -2$. Additional selection rules take into account the total angular momentum, which for **E**/**H** requires that $\Delta m_J = 0$; and for **E**/**H** $\Delta m_J = +1$ or $-1$ for circular polarization, and $\Delta m = \pm 1$ for a linearly polarized electric field.

The results of the theoretical spectrum indicate that the lines of Fig. 1 are composites of several lines. In order to observe the fine structure we built a liquid helium dewar to be used with a high resolution grating spectrometer and fields up to 38·9 kG. The results obtained with this spectrometer are shown in Fig. 3 for the light polarized with electric vector parallel to the d.c. magnetic field. The theory and experiment agree quite satisfactorily. The two prominent unaccounted for lines are exciton lines which are discussed by ZWERDLING, ROTH and LAX.[4]

We have observed oscillatory spectra for indium antimonide, indium arsenide and gallium antimonide. Fig. 4 shows the results of data obtained in indium antimonide. In accordance with theory, the motion of the energy level as a function of the magnetic field is linear in $H$. The extrapolation of all the lines to zero field gives an accurate measurement of the energy gap which is $\epsilon_g = 0{\cdot}180 \pm 0{\cdot}001$ eV at room temperature.

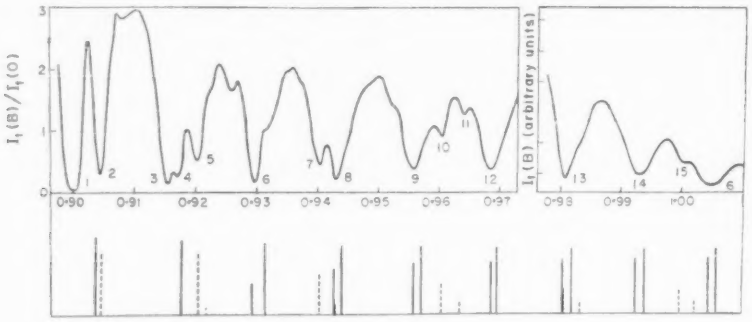


FIG. 3. Comparison of the theoretical spectrum for germanium with the experimental data taken at low temperature with the high-resolution grating spectrometer and a field of 38·9 kG (**E**||**H**).

Taking the known data from cyclotron resonance for the effective mass of the electron and assuming that the mass of the hole is large, the dotted line was drawn to represent a hypothetical transition to the first Landau level. Since it appears to bisect the first two lines in Fig. 4, we concluded that the $\Delta n = 0$ transition was split due to a spin–orbit coupling effect. The effective $g$-factor corresponding to the energy splitting from the experiment is 50. ROTH has worked out a theory[5] which takes into account the effect of the valence bands and the split-off bands as in germanium. This results in an expression for the $g$-value given by

$$g = 2\left[1+\left(1-\frac{m}{m^*}\right)\frac{\Delta}{3\epsilon_g+2\Delta}\right].$$

From values $m^* = 0{\cdot}013 m_0$, $\epsilon_g = 0{\cdot}18$ eV and

$\Delta = 0{\cdot}9$ eV, the theoretical value of $g = -54$.

The most recent data obtained with the high resolution spectrometer at low temperature is that shown in Fig. 5 for GaSb.[6] The fine structure was not resolved due to the high impurity concentration. However, the analysis of the data yielded a direct energy gap $\epsilon_g = (0{\cdot}813 \pm 0{\cdot}001)$eV at $1{\cdot}5$°K and a value of effective mass for the electron of $m^* = (0{\cdot}047 \pm 0{\cdot}001)m_0$.

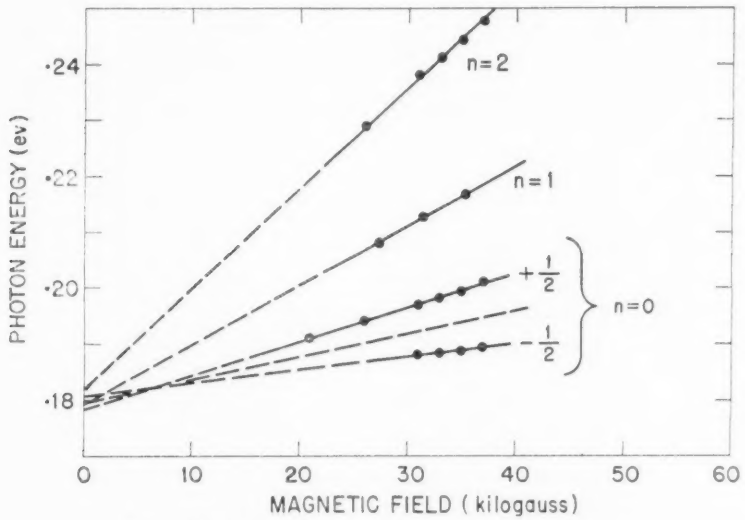


FIG. 4. Plot of the positions of the transmission minima in terms of photon energy vs. magnetic field intensity. The experimental points were taken from the oscillatory magneto-absorption data for InSb at room temperature. The extrapolation of the data to zero field gives a direct energy gap of $0{\cdot}180 \pm 0{\cdot}001$ eV. The first level ($n = 0$) is split by spin–orbit interaction.

### INDIRECT TRANSITION

Theoretical work on the indirect transition magneto-absorption in germanium predicted[5] a "staircase" type of spectrum. Experimentally this was observed[7] as shown in Fig. 6. The first line which appears also at zero field is the exciton line[8] whereas the other lines only appear at low temperatures and high magnetic fields. The latter are Landau transitions between the valence bands and the conduction band minimum at the (111) edge of the Brillouin zone. These transitions involve the emission of a longitudinal acoustical phonon whose value has been determined.[8] Using the plot of the spectrum as a function of magnetic field (see Fig 2 of ZWERDLING, ROTH and LAX, this issue) we obtain the indirect energy gap of $0{\cdot}744 \pm 0{\cdot}001$ eV at $1{\cdot}5$°K.

### "FORBIDDEN" DIRECT TRANSITION

The theory for the magneto-absorption of the transitions between the split-off valence bands at $\mathbf{k} = 0$ applicable to germanium and GaAs has also been developed. The absorption coefficient for simple bands is given by

$$\alpha_H = \frac{3}{2}(\omega_{c1}+\omega_{c2})K\sum_{nn'}\left\{\frac{1}{3}(h\nu-\epsilon_{nn'})^{\frac{1}{2}}+\right.$$

$$\left.+\frac{1}{6}(\omega_{c1}+\omega_{c2})\frac{n\delta_{n,n-1}+n'\delta_{n,n+1}}{(h\nu-\epsilon_{nn'})^{\frac{1}{2}}}\right\}$$

$$\epsilon_{nn'} = \epsilon_g+(n+\tfrac{1}{2})\omega_{c1}+(n'+\tfrac{1}{2})\omega_{c2},$$

where $K$ is a constant and $\omega_{c1}$, $\omega_{c2}$ are of the opposite sign.

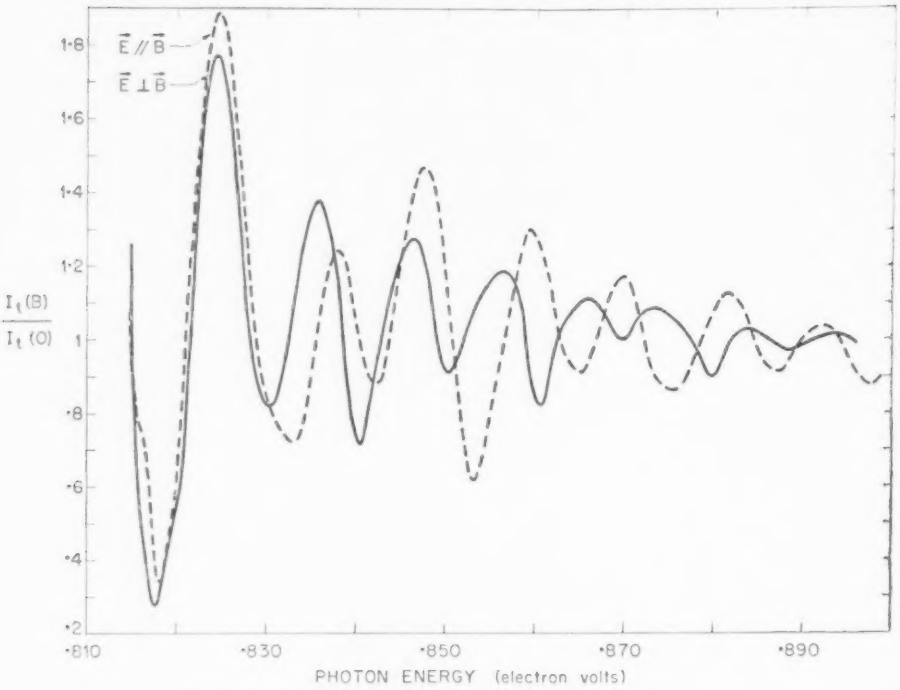


FIG. 5. Oscillatory magneto-absorption in GaSb at 1·5°K and magnetic field of 38·9 kG along the (111) direction. The fine structure which was not resolved, is indicated by the shoulders in the first minimum and by the broadening and shift of the second minimum for the electric vector parallel to the d.c. magnetic field, **B**.

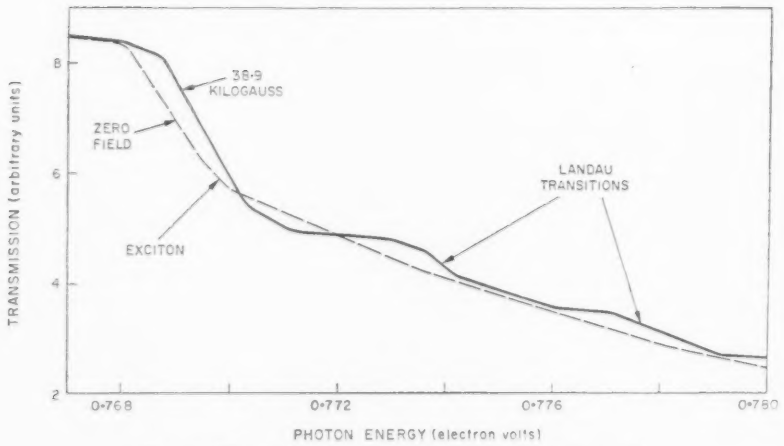


FIG. 6. The series of absorption edges of "staircase" spectrum at 1·5°K characteristic of magneto-absorption for indirect transitions. The Landau transitions are observable only at high magnetic fields; the exciton absorption persists at zero field.

The selection rules for the first term is $\Delta n = 0$ and corresponds to a series of absorption edges, whereas for the second term, $\Delta n = \pm 1$, we obtain absorption peaks. This spectrum should be observable at low temperature and high resolution using $p$-type samples.

### THE ZEEMAN EFFECT

We have carried out some preliminary studies of the Zeeman effect of impurities and excitons. Using perturbation theory, we have calculated the anisotropy spectrum of the $2p\pm$ states for electrons in silicon and germanium using an effective mass Schroedinger equation for ellipsoidal energy surfaces. The important result is that $\Delta\epsilon_\pm = \hbar\omega_t \cos\Psi$, where $\omega_t = eH/m_t{}^*c$ and $m_t{}^*$ is the transverse effective mass and $\Psi$ is the angle of $H$ with the principal ellipsoidal axis. Using this result we have plotted a Zeeman spectrum as shown in Fig. 7a. A similar spectrum has been plotted by HAERING[9] of the University of Birmingham.

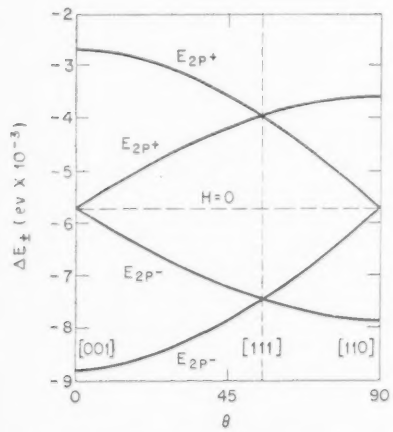


FIG. 7a. Anisotropy of the linear Zeeman effect in silicon for the $2p_\pm$ states.

The quadratic Zeeman effect is of particular importance since it has been observed to occur for the direct and indirect exciton. For ellipsoidal surfaces the theory for the quadratic Zeeman effect has been worked out for the ground state using the appropriate effective mass Hamiltonian and the variational solution at zero magnetic field. The result for the energy shift as a function of angle $\Psi$ is

$$\Delta\epsilon = \frac{K^2\hbar^4\omega_c{}^2}{16m_te^4}[(3+\epsilon)+(1-\epsilon)\cos 2\Psi]$$

where

$$\epsilon = m_t/m_l,\ \omega_c = eH/m^*c \text{ and } 1/m^* = \tfrac{1}{3}m_t+\tfrac{1}{3}m_l.$$

If these results are applied to germanium, the anistropy of the Zeeman effect, where all four

$$\Delta E = \frac{K^2\hbar^4\omega_c^2}{16m_te^4}\left[(3+\epsilon)+(1-\epsilon)\cos 2\theta\right]$$

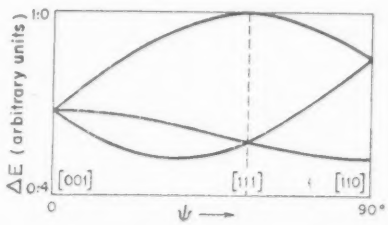


FIG 7b. Anisotropy of the quadratic Zeeman effect for the ground state in $n$-type germanium and also $n$-type silicon.

ellipsoidal surfaces along the cube diagonal are taken into account, is shown in Fig. 7b. The importance of this result is that the quadratic term in the magnetic field is responsible for the anisotropy, not only of the ground state, but of higher states. In the high field limit the higher states are bound Landau states wherein the Coulomb term is a small perturbation. The anisotropy which is obtained from the cyclotron resonance data results in a diagram almost identical with that of Fig. 7b. The conclusion is that, in principle the transitions from impurity states to higher magnetic states will give information about the band structure.

We have recently made some preliminary observations of the photo-excitation spectrum of electronic transitions from the ground state of bismuth in silicon in magnetic fields in the (111) direction up to 39·9 kG. The $3p_0$ level was found to shift to higher energy quadratically with the field, and both the $2p_\pm$ and $3p_\pm$ levels split linearly

with field and also appeared to shift to higher energy for the highest fields used. The splitting of the $2p_{\pm}$ level amounted to $\sim 10^{-3}$ eV and the shift of the $3p_0$ level was $\sim 5 \times 10^{-4}$ eV at maximum field. The data were obtained using a 6 mm thick sample at $\sim 1{\cdot}3$°K having $9 \times 10^{14}$ impurities/cm$^3$. These results are in reasonable agreement with theory.

Quantum effects of the Faraday rotation and the free carrier absorption in a magnetic field at low temperature can give rise to phenomena analogous to the de Haas–van Alphen effect. Under certain conditions, for a simple band, the oscillatory character is absent but may occur for more complicated energy surfaces and energy-dependent scattering time. These will occur in degenerate semiconductors as found for InSb and InAs by FREDERIKSE[10] and also SLADEK.[11]

*Acknowledgments*—We wish to thank W. H. KLEINER and R. PUFF for their work on the Zeeman effect, and K. J. BUTTON for his work on magneto-absorption.

## REFERENCES

1. ZWERDLING S. and LAX B. *Phys. Rev.* **106,** 51 (1957).
2. BURSTEIN E. and PICUS G. S. *Phys. Rev.* **105,** 1123 (1957).
3. ZWERDLING S., LAX B. and ROTH L. M. *Phys. Rev.* **108,** 1402 (1957).
4. ZWERDLING S., ROTH L. M. and LAX B. *J. Phys. Chem. Solids* **8,** 397, 525, 66 (1959).
5. ROTH L. M., LAX B. and ZWERDLING S. *Phys. Rev.* (to be published).
6. ZWERDLING S., LAX B., BUTTON K. J. and ROTH, L. M. submitted to *J. Phys. Chem. Solids.*
7. ZWERDLING S., LAX B., ROTH L. M. and BUTTON K. J. *Phys. Rev.* (to be published).
8. MACFARLANE G. G., MCLEAN T. P., QUARRINGTON J. E. and ROBERTS V. *Phys. Rev.* **108,** 1377 (1957).
9. HAERING R. R. (private communication).
10. FREDERIKSE H. P. R. and HOSLER W. R. *Phys. Rev.* **108,** 1136 and 1146 (1957).
11. SLADEK R. J. *J. Phys. Chem. Solids* (this issue).

VOL 8 195

*J. Phys. Chem. Solids* Pergamon Press 1959. Vol. 8. pp. 318–320. Printed in Great Britain

# L.3 THEORY OF THE ZEEMAN EFFECT IN THE PHOTO-IONIZATION OF IMPURITIES

**R. F. WALLIS and H. J. BOWLDEN***

U.S. Naval Research Laboratory, Washington 25, D.C.

THE quantization of the energies of free electrons or holes into sub-bands or "Landau levels" when a magnetic field is applied to a semiconductor[1] and the infinite densities of states at the edges of the sub-bands lead to the expectation that the photo-ionization absorption spectrum of impurities in semiconductors should exhibit a series of peaks in an external magnetic field $H$. These peaks correspond to optical transitions from bound impurity levels to the various magnetic sub-bands of the continuum. We shall designate this phenomenon as the impurity photoionization magneto-optic (IPMO) effect.

A theory of the IPMO effect has been developed[2] for impurity levels associated with simple energy bands. Two cases may be distinguished depending upon whether the impurity ionization energy in zero magnetic field, $E_I$, is greater than or less than $1/2\hbar\omega_c$ where $\omega_c = eH/m^*c$ and $m^*$ is the effective mass. These cases will be referred to as the low and high field cases, respectively.

A plot of a theoretical IPMO spectrum for the low field case with simple energy bands is shown in Fig. 1 together with the spectrum for zero field. In the calculations it was assumed that the

* Permanent address: National Carbon Research Laboratories, National Carbon Company, Division of Union Carbide Corporation, Parma, Ohio.

continuum states are unaffected by the impurity potential while the ground state of the impurity is unaffected by the magnetic field. Collision broadening was included for $H > 0$ but not for $H = 0$. One sees that the magnetic field introduces peaks with separations $\hbar\omega_c$ into the spectrum. From an observed value of the separation one can determine the effective mass $m^*$. Another feature of the IPMO spectrum is that the absorption rises more sharply at the threshold than for zero field. Rather accurate values of $E_I$ should result from extrapolation of the position of the first peak to zero field. It should be mentioned that well-defined peaks occur for simple bands only if the electric vector $\mathscr{E}$ of the radiation is perpendicular to the external magnetic field $H$. If $\mathscr{E}$ is parallel to $H$, the peaks are washed out.

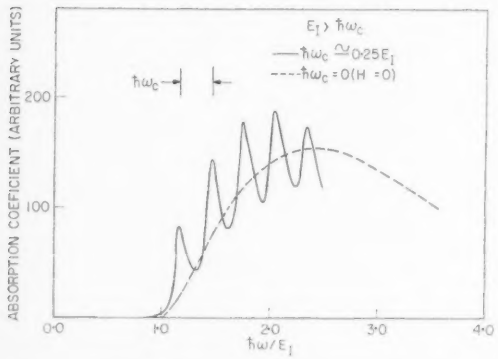


FIG. 1. Typical photoionization absorption spectrum for the low field case with a simple energy band.

If the effect of a Coulomb-like impurity potential on the continuum states is included in the theory, it appears from comparison with the zero field case that the peaks near threshold should be enhanced relative to those at higher photon energies. The spacing of the peaks near threshold may also be modified.

The IPMO spectrum for the high field case with simple energy bands differs from the low field case mainly in having the first two peaks dominant with the remaining peaks washed out.

It is clear that the IPMO effect can be observed experimentally only if the sample is at sufficiently low temperature to freeze out the charge carriers at the impurities. For materials such as germanium with Group III or Group V impurities, temperatures below that of liquid hydrogen are required. In common with cyclotron resonance and the interband magneto-optic effect there are requirements on $\tau$, the effective collision relaxation time, in order to see well-defined absorption peaks. Since the IPMO experiments must be done at low temperatures, one is necessarily in a rather favorable position for satisfying requirements on $\tau$. A further condition to be fulfilled for a successful IPMO experiment is that the impurities be sufficiently dilute so that impurity banding is not excessive. In InSb, for example, it appears that impurity concentrations not greater than about $10^{14}$ cm$^{-3}$ are required.[3]

Donor impurities in InSb provide an example which is reasonably well described by the discussion given for simple energy bands. Only the high field case, however, is easily accessible to experiment since donor impurities are largely ionized even at liquid helium temperatures in small fields.

Complications arise when one considers some of the other common cases. For example, donor impurities in silicon and germanium are associated with conduction bands which are ellipsoidal rather than parabolic and which have their minima at a number of equivalent positions in $k$-space away from $k = 0$. The ellipsoidal character of these conduction bands may cause the IPMO spectrum to be a sensitive function of the relative orientation of magnetic field and the crystallographic axes. The major axes of the various ellipsoids in a given material will not, in general, make the same angle with the magnetic field. Consequently, more peaks may appear in the spectrum than would be predicted by the theory for simple bands. This is similar to the situation in cyclotron resonance.

The degeneracy of the $V_1$ and $V_2$ valence bands at $k = 0$ in silicon and germanium is another type of complication. The ground state of acceptor impurities associated with the $V_1$ and $V_2$ bands has been shown by KOHN and SCHECHTER[4] to be four-fold degenerate. In an external magnetic field the degeneracy of the ground state is removed as has been shown by KOHN.[5] It appears from KOHN'S calculations that in germanium the energy separations of these four levels are on the order of $10^{-4}$ eV at a field of 60,000 G. All four

levels should therefore be appreciably populated at liquid helium temperatures with fields smaller than 60,000 G.

LUTTINGER[6] has shown that the continuum states associated with the $V_1$ and $V_2$ bands in a magnetic field can be grouped into four sets or

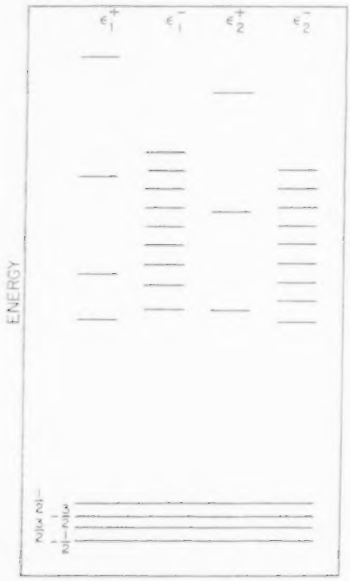


FIG. 2. Energy level diagram for free and bound holes in germanium in a magnetic field. Only the four lowest bound levels are shown.

"ladders" of one-dimensional sub-bands. A diagram of the continuum sub-band edges and the four lowest bound states is given in Fig. 2 for germanium. Two of the ladders, the $\epsilon^+$ ladders, are associated with light holes and the other two, the $\epsilon^-$ ladders, with heavy holes.

A general discussion of the IPMO effect for acceptor states is rather difficult, but some progress can be made if the effective mass parameters[6] $\gamma_2$ and $\gamma_3$ are equal. The latter condition is fairly well satisfied in germanium. If one uses the ground state wave functions given by KOHN and SCHECHTER and the continuum state wave functions given by LUTTINGER, one finds for $\gamma_2 = \gamma_3$ that absorption peaks occur with $\epsilon \perp H$ corresponding to transitions from bound states $F_{3/2}$ and $F_{-1/2}$ to the sub-bands of the $\epsilon_1^+$ and $\epsilon_1^-$ ladders. Similarly, transitions from the $F_{1/2}$ and $F_{-3/2}$ bound states to the $\epsilon_2^+$ and $\epsilon_2^-$ ladders lead to absorption peaks for $\epsilon \perp H$. The complete spectrum to be expected is therefore a rather complicated superposition of absorption peaks.

In contrast to the situation for simple bands the $\epsilon \| H$ configuration may also lead to absorption peaks. The latter correspond to transitions from the $F_{3/2}$ and $F_{-1/2}$ bound states to the $\epsilon_2^+$ and $\epsilon_2^-$ ladders and from the $F_{1/2}$ and $F_{-3/2}$ bound states to the $\epsilon_1^+$ and $\epsilon_1^-$ ladders. Detailed calculations of the IPMO effect for acceptor states in germanium are being carried out and will be reported at a later date.

In conclusion we wish to thank ELIAS BURSTEIN for many helpful discussions.

## REFERENCES

1. See, for example, BURSTEIN E., PICUS G. S., WALLIS R. F. and BLATT F. J., *J. Phys. Chem. Solids*, **8,** 305 (1959).
2. WALLIS R. F. and BOWLDEN H. J. *J. Phys. Chem. Solids*, **7,** 78 (1958).
3. KEYES R. W. and SLADEK R. J. *J. Phys. Chem. Solids* **1,** 143 (1956).
4. KOHN W. and SCHECTER D. *Phys. Rev.* **99,** 1903 (1955).
5. KOHN W., preprint entitled "Theory of Magnetic Susceptibility of Impurity States in Germanium."
6. LUTTINGER J. M. *Phys. Rev.* **102,** 1030 (1956).

*J. Phys. Chem. Solids* Pergamon Press 1959. Vol. 8. pp. 321–323. Printed in Great Britain

VOL. 8 1959

# L.4 FAR INFRARED MAGNETO-OPTIC EFFECTS FROM IMPURITIES IN GERMANIUM

W. S. BOYLE

Bell Telephone Laboratories, Inc., Murray Hill, New Jersey

We have studied the effect of a magnetic field on the excited impurity states and the photoionization spectrum of single crystals of germanium. The experimental information has been obtained from far infrared transmission measurements performed at liquid helium temperatures. Our attention has been confined to donor impurities and to the simplest crystallographic orientation with the direction of propagation of the radiation and the magnetic field both applied along a (100) direction in the crystal. This leaves corresponding Landau levels in the four valleys degenerate and provides the simplest case of the Zeeman splitting of the bound states about an impurity.

In Fig. 1 is shown the absorption spectrum of a sample with $3\times10^{15}$ As atoms per cm$^3$. The positions of the absorption lines and their assignment together with their calculated position[1] are given in Table 1. Since the calculated value of the ground state is not expected to be as precise as the excited states, we have arbitrarily put the $2p\ m=0$ calculated and experimental values into coincidence. This also gives a more reliable theoretical value for the ionization energy of the donor. We note that the transitions from the ground state to the $2p$ states both have a half-width of approximately 3 cm$^{-1}$. This is considerably narrower than the corresponding transitions that have been observed in Si[2] and tends to confirm the theory that most of the broadening at low temperatures occurs in the $1S$ state through the electron interaction with the zero point vibrations of the lattice.[3]

*Table* 1. *Donor spectrum in* As *doped* Ge

| Transition | Experimental (cm$^{-1}$) | Calculated (cm$^{-1}$) |
|---|---|---|
| $1S\rightarrow 2p\ m=0$ | 76·0±·5 | 76·0 |
| $1S\rightarrow 3p\ m=0$ | 93·6 | 93·2 |
| $1S\rightarrow 2p\ m=\pm1$ | 99·8 | 99·3 |
| $1S\rightarrow$ Cont. | (108·0?) | 112·2 |

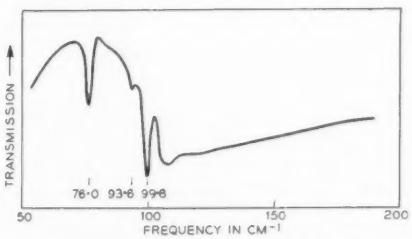


FIG. 1. The absorption spectrum of Ge from 50 to 200 cm$^{-1}$ with $3\times10^{15}$ As/cm$^3$.

When a magnetic field is applied, the $1S\rightarrow 2p\ m=0$ line remains unchanged up to the largest fields available (23 kG). The $1S\rightarrow 2p\ m=\pm1$ line on the other hand at low fields splits into a symmetrical doublet. This is illustrated in Fig. 2 where we show the splitting of this line when the ground state is a phosphorous impurity atom and the $1S\rightarrow 2p\ m=\pm1$ line occurs at 91·5cm$^{-1}$.[4] The expected value of the splitting of this line has been discussed in terms of first order perturbation theory.[5] This corresponds to taking the component of the field along the symmetry axis of a constant energy surface at any of the four equivalent minima in the Brillouin zone and using a Bohr magneton appropriate to the cyclotron mass normal to this symmetry axis. The splitting calculated in this way using a mass of 0·08 $m$ agrees well with the experimental observations.

We shall now discuss the effect of the magnetic field on the photoionization spectrum. In the presence of a magnetic field, the states in the continuum of the conduction band break up into Landau sub-bands. The energy of these bands

above the bottom of the conduction band at zero fields is given by

$$E(nk_z) = (n+\tfrac{1}{2})\hbar\omega_c + \frac{\hbar^2 k_z^2}{2m^*}$$

where $\omega_c = eH/m^*c$, and $n$ is a quantum number

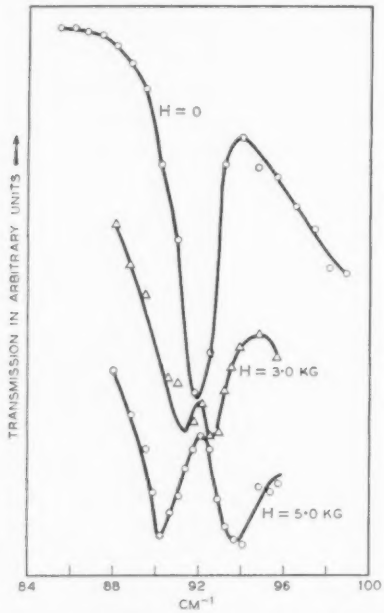


FIG. 2. Zeeman splitting of the $2p\,m = \pm 1$ level about a phosphorus impurity.

which labels the Laundau levels. This energy level structure leads to oscillations in the absorption coefficient.[6]

The oscillations in the absorption coefficient can be observed most easily by fixing the frequency of the incident radiation at a value which leads to a transition from the ground state of the impurity to a point some distance up from the bottom of the conduction band and then increasing the magnetic field slowly. Fig. 3 shows such a periodic (in $1/H$) variation of the transmission of a sample with $3\times10^{15}$ As atoms/cm$^3$ taken at a wavelength of $73\mu$. Such a series of measurements taken at different wavelengths gives a simple method of determining the correct $n$ label to apply to a given absorption maximum.

In Fig. 4 we show the ratio of the transmission with $H = 21{\cdot}8$ kG to $H = 0$, for the same sample as in Fig. 3, as a function of frequency.

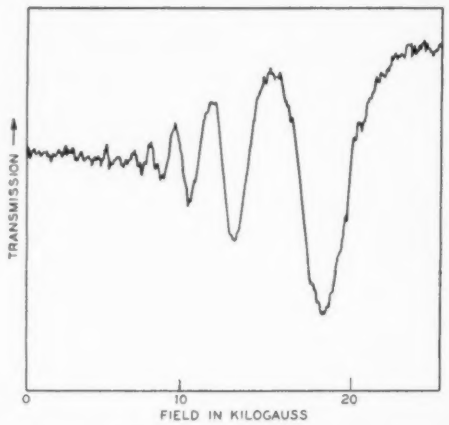


FIG. 3. Oscillations in the transmission coefficient with a steadily increasing magnetic field. The sample is the same as in Fig. 1. $\lambda = 73\ \mu$.

Having determined the proper $n$ label from experiments as in Fig. 3, this type of experiment lends itself to a more direct comparison with theory.

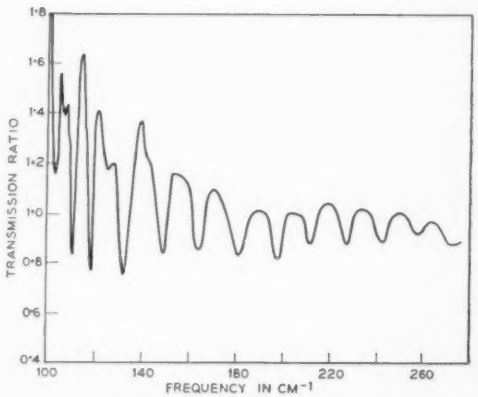


FIG. 4. The ratio of the transmission coefficients with $H = 21{\cdot}8$ kG and $H = 0$ shown as a function of frequency.

The frequencies of the successive minima have been plotted in Fig. 5 as the abscissa, the ordinate of the figure gives the quantum integer $n$. We

show the results for two different magnetic fields. Both series of points fall on smooth curves which according to simple theory[6] should intersect at the band edge with $n = -1/2$.

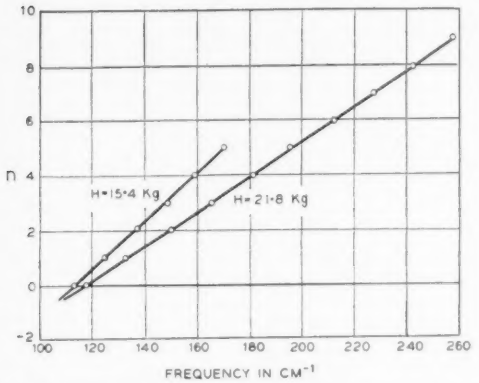


FIG. 5. The location in frequency of the successive maxima in the absorption coefficient at two different fields.

It is interesting to note that the amplitude of the oscillations does not fall off smoothly with $n$ as predicted by theory. There is a reduction in amplitude in the region of 180 $cm^{-1}$ and at frequencies higher than 240 $cm^{-1}$ the amplitude falls rapidly to zero. We attribute this to a decrease in relaxation time of the carrier when it becomes energetically possible to impact, ionize or excite to the $2p$ levels the electrons on other impurity centers.

The oscillations near the band edge have not yielded to any simple interpretation. At the highest fields the Zeeman splitting of the $2p$ $m = \pm 1$ level merge into the Landau levels of the continuum. In addition the lowest Landau levels in the continuum show some incompletely resolved fine structure. If we ascribe the point of maximum absorption in the first few levels to the bottom of each free Landau sub-band, then the extrapolated curves for $H = 21{\cdot}8$ kG and $15{\cdot}4$ kG intersect near the point $n = -1/2$. In this way we obtain an ionization energy of 108 $cm^{-1}$ for As impurities. This is to be compared with the corrected theoretical ionization energy of 112·2 $cm^{-1}$ as given in Table 1 and an experimental value of 103·5 $cm^{-1}$ obtained from thermal measurements.[7]

We note finally that the high field results, which extend up to $n = 9$, show a slight curvature over this whole range. The sense of the curvature is such that the effective mass has increased by about 3 per cent at ·015 eV above the bottom of the conduction band. At the bottom of the band we determine $m^* = {\cdot}13_2\ m_0$ for this particular crystallographic orientation.

## REFERENCES

1. KOHN W. *Solid State Physics*, Vol. 5, p. 286. Academic Press, New York (1957).
2. BURSTEIN E., BELL E. E., DAVISSON J. W. and LAX M. *J. Phys. Chem.* **57**, 849 (1953).
   HROSTOWSKI H. J. private communication.
3. LAX M. and BURSTEIN E. *Phys. Rev.* **100**, 592 (1955).
4. FISHER P. and FAN H. Y. *Bull. Amer. Phys. Soc.* **3**, No. 2, 128 (1958).
5. HAERING R. R. in press.
6. WALLIS R. F. in press.
7. GEBALLE T. H. and MORIN F. J. *Phys. Rev.* **95**, 1805 (1954).

*J. Phys. Chem. Solids* Pergamon Press 1959. Vol. 8. pp. 323–326. Printed in Great Britain

L.5

# THE INFRARED FARADAY EFFECT DUE TO FREE CARRIERS IN INDIUM ANTIMONIDE

**T. S. MOSS, S. D. SMITH and K. W. TAYLOR**
Royal Aircraft Establishment, Farnborough

## 1. INTRODUCTION

THE rotation of the plane of polarization of a beam of radiation under the influence of a magnetic field along the direction of propagation is known as the Faraday effect.

This rotation has been observed by RAU and

CASPARI[1] in germanium at microwave frequencies where it gives some information about mobilities. At infrared frequencies the experiment provides a valuable method of studying the effective mass (as shown by MITCHELL[2]) and the shape of the $E-k$ curve.

## 2. THEORY

The Faraday rotation per unit length of specimen at frequency $\omega$ is:

$$\theta = \tfrac{1}{2}\omega(n^+ - n^-)/c \qquad (1)$$

A quasi-classical treatment gives the two refractive indices from

$$(n-ik)^2 = \epsilon + \frac{Ne^2 m\omega\epsilon_0}{-\omega \pm \omega_c \pm i/\tau} \qquad (2)$$

where $N$ is the carrier density and $\omega_c = eB/m$ is the cyclotron resonance frequency. (This treatment is valid when the average energy of the electron $\gg \hbar\omega_c$ and the wavelength $\lambda \gg \sqrt{(h\tau/2\pi m)}$ so that a wave packet approach is justified).

Thus the rotation is proportional to the difference in refractive index for the two circularly polarized waves given in equation (2), so that in effect the Faraday rotation measures the differential dispersion caused by cyclotron resonance absorption.

Making the assumptions,

(1) Absorption is small, i.e. $k^2 \ll n^2$

(2) Relatively short wavelengths used, i.e. $\omega^2 \gg (1/\tau^2)$

(3) Small magnetic fields, i.e. $\omega_c{}^2 \ll \omega^2$

we obtain,

$$n\theta = BNe^3/2c\epsilon_0 m^2\omega^2 \qquad (3)$$

or alternatively

$$\theta = (\omega_c\lambda/2c)dn/d\lambda = (eB\lambda/2mc)dn/d\lambda. \qquad (4)$$

Equation (4) shows that at a given wavelength the rotation is determined only by the dispersion and the cyclotron resonance frequency, so that the experiment can be regarded as a method of determining $\omega_c$ without the necessity of satisfying the rather stringent requirements for resonance. From equation (3) the product of $n\theta$ should increase as $\lambda^2$ and be inversely proportional to the (effective mass)$^2$. This latter dependence implies that the experiment is a potentially accurate way to determine effective mass. A further valuable feature shown by equations (3) and (4) is that the rotation is independent of $\tau$ and thus of the scattering mechanism as noted previously.[2] This is also true of pure (free carrier) dispersion.[3] A more detailed theoretical treatment by STEPHEN and LIDIARD[4] starting from the Boltzmann transport equation shows that for the case of a degenerate semiconductor with spherical energy surfaces an expression identical with equation (3) is obtained provided that

$$\frac{1}{m} = \frac{1}{\hbar^2}\left(\frac{dE}{kdk}\right)_F$$

where subscript F means the value at the Fermi surface.

Thus for a non-parabolic band—as in InSb—the Faraday effect measures a reciprocal mass which represents the slope $dE/dk$ rather than the curvature $d^2E/dk^2$ of the $E-k$ curve. This same concept has also been found by SPITZER and FAN[3] to apply to free carrier dispersion measurements on degenerate semiconductors. It is easy to see algebraically that for a parabolic band

$$\frac{1}{\hbar^2}\left(\frac{dE}{kdk}\right) = \frac{1}{\hbar^2}\frac{d^2E}{dk^2}$$

so the two concepts are then identical.

STEPHEN and LIDIARD[4] have also shown the value of $N$ to be used in equation (3) is given from the Hall constant

$$R = 1/Ne$$

for degenerate systems, even for non-parabolic bands, provided the energy surfaces are spherical.

For non-degenerate statistics and a parabolic band the Faraday rotation gives

$$1/m = \frac{1}{\hbar^2}\frac{d^2E}{dk^2}$$

i.e. for a parabolic band the mass measured is independent of the statistics. If the band is non-parabolic the expression is not simple but can be evaluated if the band shape is known.

## 3. EXPERIMENTAL RESULTS AND DISCUSSION

Details of the experiment have already been published.[5] The rotation has been found to be

linear with magnetic field up to at least 4000 G and the dependence of $n\theta$ on $\lambda^2$ is well satisfied over the wavelength range 10–20$\mu$ (Fig. 1).

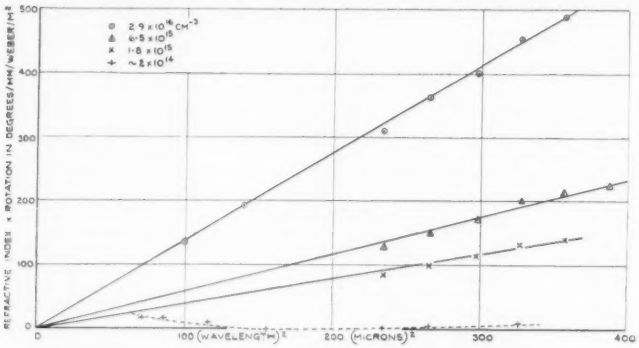


FARADAY ROTATION IN N-TYPE INDIUM ANTIMONIDE.

FIG. 1.

Measurements of effective mass were made on specimens with electron concentrations from $6{\cdot}4\times10^{17}$ cm$^{-3}$ to $1{\cdot}8\times10^{15}$ cm$^{-3}$. The most impure material was highly degenerate at room temperature. For purer materials degeneracy was ensured by cooling to 77°K. Measurements on a very pure sample ($2\times10^{14}$ cm$^{-3}$ at 77°K) showed only small rotations due to free carriers and also that rotation due to bound carriers (i.e. arising from dispersion associated with band to band absorption) was so small beyond 10$\mu$ that it was negligible compared with the free carrier effect in all other specimens.

Results are summarized in Table 1.

*Table* 1.

| $N$(cm$^{-3}$) | $m/m_0$ | Fermi energy (eV) | $\frac{1}{2}(dk^2/dE)$ (from Kane[11]) |
|---|---|---|---|
| $6{\cdot}4\times10^{17}$ | ·0288 | ·135 | ·0265 |
| $2{\cdot}9\times10^{16}$ | ·0178 | ·027 | ·0158 |
| $7{\cdot}3\times10^{15}$ | ·0137 | ·010 | ·0141 |
| $2{\cdot}6\times10^{15}$ | ·0131 | ·005 | ·0136 |
| 0 | — | 0 | ·0130 |

The effective mass was evaluated over a range of carrier concentration of 300: 1 and more impure specimens could easily be measured. The masses obtained give the slope of the $E-k$ curve at various energies up to $\sim$ 0·15 eV from the bottom of the conduction band.

The highest mass value in Table 1 agrees well with SPITZER and FAN[3] for a similar material. The Faraday determination should be more accurate because of the square root dependence on $n$, $N$ and $\theta$. For pure specimens the dispersion method[3] cannot be used because of Restrahlen dispersion. This does not contribute to the Faraday rotation as the mass in equation (4) is now that of an atom. This value is also consistent with the higher values obtained by KEYES *et al.*[6] from high field infrared cyclotron resonance.

Values for the mass nearer the bottom of the band have been found by BURSTEIN *et al.*[7] (0·015 $m_0$ from I.R. cyclotron resonance at 300°K with fields $\sim$ 60 kG), by BOYLE and BRAILSFORD[8] (0·0146 from I.R. resonance at 4°K and 20 kG), by DRESSELHAUS *et al.*[9] (0.013$\pm$0·001 from microwave resonance at 2°K with small fields) and ZWERDLING *et al.*[10] (0·014 from magneto-absorption with fields $\sim$ 30 kG at 300°K).

Compared with all these determinations except the microwave resonance, the Faraday effect is measured at a much lower magnetic field.

If over the region of the $E-k$ curve covered in these measurements the band is parabolic all the determinations should give the same result. Our measurements show that the band is non-parabolic down to the lowest concentrations measured and under these conditions further analysis is required to understand what is measured in the

resonance and magneto-absorption experiments in relation to the Faraday method.

The Faraday effect has been used in this work to obtain values of effective mass over a larger part of the $E-k$ curve than has been achieved in any other single experiment.

*Acknowledgments*—Acknowledgment is due to R. R. E., Malvern for assisting in the supply of InSb crystals, to Dr. A. B. LIDIARD and Dr. M. J. STEPHEN for helpful discussion and to Miss D. WEBBER and Mr. I. D. BIRCH for experimental assistance.

## REFERENCES

1. RAU R. and CASPARI M. E. *Phys. Rev.* **100,** 632 (1955).
2. MITCHELL E. W. J. *Proc. Phys. Soc.* B.**68,** 973 (1955). See also MOSS T. S. *Optical Properties of Semiconductors.* Butterworths, London (1958).
3. SPITZER W. G. and FAN H. Y. *Phys. Rev.* **106,** 882 (1957).
4. STEPHEN M. J. and LIDIARD A. B. *J. Phys. Chem. Solids,* in press.
5. SMITH S. D. and MOSS T. S. *Solid State Conference,* Brussels. Wiley, New York (1958).
6. KEYES R. J., ZWERDLING S., FONER S., KOLM H. H. and LAX B. *Phys. Rev.* **104,** 1804 (1956).
7. BURSTEIN E., PICUS G. S. and GEBBIE H. A. *Phys. Rev.* **103,** 825 (1956).
8. BOYLE W. S. and BRAILSFORD A. D. *Phys. Rev.* **107,** 903 (1957).
9. DRESSELHAUS G., KIP A. F., KITTEL C. and WAGONER G. *Phys. Rev.* **98,** 556 (1955).
10. ZWERDLING S., LAX B. and ROTH L. M. *Phys. Rev.* **108,** 1402 (1957).
11. KANE E. O. *J. Phys. Chem. Solids* **1,** 249 (1957).

VOL
8
195

*J. Phys. Chem. Solids* Pergamon Press 1959. Vol. 8. pp. 326–329. Printed in Great Britain

# L.6 MICROWAVE FARADAY ROTATION: MEASUREMENT OF THE CONDUCTIVITY TENSOR*

**A. M. PORTIS**

Department of Physics, University of California, Berkeley 4, California

## 1. INTRODUCTION

WE discuss here the application of microwave Faraday rotation to the measurement of magneto-conductivity. The bimodal cavity which we employ for these measurements has been described.[1] It is similar in principle to a cavity used by NISHINA and SPRY[2] for the study of high mobility semiconductors. Both cavities are bimodal. The incident microwaves excite the first mode, which in turn excites currents in the sample. These currents excite the second mode, which is itself coupled to the detector. The use of a resonant cavity in this way with high impedance samples results in a sensitivity three or four orders higher than can be attained with the usual guided wave approach.[3]

The present cavity was designed with the measurement of photocarrier mobilities in mind where both the carrier concentrations and the mobilities are expected to be small. In order to obtain good sensitivity it must be possible to achieve a high degree of isolation between the cavity modes in the absence of sample excitation. For this purpose a cylindrical cavity with coupling irises in the ends so as not to reduce the cylindrical symmetry was used. It was found that in order to balance out the coupling between modes produced by inaccuracies in machining and by dielectric and dark-carrier effects in the samples it was necessary to use four metallic probes and two resistive probes. The metallic probes are adjusted to make the resonance frequency of the cavity the same for the two normal modes. This does not however completely eliminate the transfer of

* This research was supported in part by the Office of Naval Research, the Signal Corps, the Air Force Office of Scientific Research, and the National Security Agency.

power to the detector. It is found that unless an adjustment of the resistive probes is made, the mode that is excited by the incident power may couple directly to the detector. The resistive probes adjust the losses in the normal modes so that the two modes are now completely equivalent electrically. In order that the variation in power coupled to the detector be a function of the sample conductivity to first order, it is necessary to couple a small amount of unbalance power through the cavity. This may be done either with the resistive probes or the metallic probes. By observing the change in transmitted power under both kinds of unbalance, one may obtain the real and imaginary parts of the off-diagonal elements and the real part of the diagonal elements of the conductivity tensor.

## 2. MEASUREMENT OF CONDUCTIVITY

We take the normal cavity modes to be directed along the $x$ and $y$ axes. A static magnetic field $H_0$ is established along $z$. In the experiment described here we are interested just in the currents flowing transverse to the magnetic field. We write

$$\boldsymbol{j}_{xy} = \bar{\bar{\sigma}} \cdot \boldsymbol{E}_{xy}$$

where $\bar{\bar{\sigma}}$ is the conductivity tensor and

$$\bar{\bar{\sigma}} = \begin{pmatrix} \sigma_{xx} & \sigma_{xy} \\ \sigma_{yx} & \sigma_{yy} \end{pmatrix}$$

As will be seen below, the results of the microwave measurements may be related directly to the elements of the conductivity tensor.

A discussion of the effects of conducting samples on microwave cavities has been given by BERK and LAX.[4] PORTIS and TEANEY[1] have developed an equivalent circuit of lumped elements from which the effects of samples may be discussed in terms of circuit analysis. From the point of view of the equivalent circuit we introduce an impedance tensor $\bar{\bar{z}} = \bar{\bar{r}} + j\bar{\bar{x}}$ which characterizes the sample. If we couple power through the cavity by means of the metallic probes we say that the cavity is unbalanced reactively. Under these conditions the variation in coupled power associated with the sample is

$$\frac{\delta P_2}{P_2} = \frac{\cot\theta}{[(1+\beta_1)(1+\beta_2)]^{\frac{1}{2}}}\left(\frac{x_{xx}-x_{yy}}{R}+\frac{x_{xy}-x_{yx}}{R}\right) - \left(\frac{1}{1+\beta_1}+\frac{1}{1+\beta_2}\right)\frac{r_{xx}+r_{yy}}{R}\cos^2\theta - \left(\frac{1}{1+\beta_1}-\frac{1}{1+\beta_2}\right)\frac{r_{xy}+r_{yx}}{R}\cos^2\theta - \frac{1}{[(1+\beta_1)(1+\beta_2)]^{\frac{1}{2}}}\frac{x_{xx}-x_{yy}}{R}\sin 2\theta.$$

The ratio of the power coupled through the cavity to the maximum possible coupling is expressed by $\sin^2 2\theta$; $R$ is the equivalent resistance associated with the cavity losses, $\beta_1$ and $\beta_2$ are coupling coefficients. When the cavity is unbalanced by means of the resistive probes we obtain for small coupling

$$\frac{\delta P_2}{P_2} \cong \frac{2\operatorname{cosec} 2\theta}{[(1+\beta_1)(1+\beta_2)]^{\frac{1}{2}}}\left(\frac{r_{xx}-r_{yy}}{R}+\frac{r_{xy}-yx}{R}\right) - \left(\frac{1}{1+\beta_1}+\frac{1}{1+\beta_2}\right)\frac{r_{xx}+r_{yy}}{R} - \left(\frac{1}{1+\beta_1}-\frac{1}{1+\beta_2}\right)\frac{r_{xy}+r_{yx}}{R}.$$

It now remains to obtain the connection between the impedance tensor for the sample and its conductivity tensor. In the equivalent circuit analysis the energy in the electric field is associated with a charged capacitor. If a sample with a dielectric tensor stores a fraction $f$ of the electric field energy we write for the tensor admittance of the equivalent capacity

$$\bar{\bar{Y}} = j\omega C(\bar{\bar{I}} + 4\pi f\bar{\bar{\chi}})$$

To first order the impedance tensor

$$\bar{\bar{Z}} = \frac{1}{j\omega C}[\bar{\bar{I}} - 4\pi f\bar{\bar{\chi}}].$$

Since the dielectric susceptibility is related to the conductivity by the relation

$$\bar{\bar{\chi}} = \bar{\bar{\sigma}}/j\omega$$

we have finally for the sample impedance tensor

$$\frac{\bar{\bar{Z}}}{R} = Q_0\frac{4\pi f\bar{\bar{\sigma}}}{\omega}$$

where $Q_0$ is the cavity quality factor and is equal to $1/\omega RC$. In the treatment presented here we have assumed that the sample filling factor $f$ is the same for both modes. If this is not the case a tensor filling factor must be introduced.

### 3. SENSITIVITY

The sensitivity of the present equipment to changes in sample conductivity is limited by the noise generated in the microwave detector, which is a crystal diode. The noise power developed by a crystal may be written[5]

$$P_n = \left(kT + \frac{CI^2}{\nu}\right)\Delta\nu$$

where $I$ is the short circuit crystal current, $\nu$ is the frequency at which the noise power is being measured, and $\Delta\nu$ is the band width. The power in the signal may similarly be written as

$$P_s = \frac{2}{\pi^2}(\delta I)^2 R.$$

Assuming that the second term in the expression for crystal noise is dominant the signal to noise ratio is given by

$$\frac{P_s}{P_n} = \frac{2}{\pi^2}\frac{R}{C}\left(\frac{\delta P_2}{P_2}\right)^2 \frac{\nu}{\Delta\nu}$$

For a 1*N*23*C* crystal detector $R$ is approximately 5000 Ω. We measure $C$ to be about $1{\cdot}5\times10^{-4}$ Ω. For a 1 c/s bandwidth at 15 c/s we find that for a signal to noise ratio of one we can expect to detect fractional changes in transmitted power of one part in $10^4$. The stability of the balance of the bimodal cavity is such that we can work with coupled powers as much as 60dB below the maximum coupled power or with values of $\sin 2\theta$ as small as $10^{-3}$. Then the lower limits for detectability of diagonal and off-diagonal elements of the impedance tensor are

$$\frac{r_{xx}}{R} \sim 10^{-4} \qquad \frac{r_{xy}}{R} \sim 2\times10^{-8}.$$

These limits assume of course that it is possible to distinguish $r_{xx}$ from the ordinary cavity losses and that it is possible to distinguish $r_{xy}$ from the rotation produced by carriers in the walls or by ferromagnetic impurities which may be present. These sensitivities are rather low when compared with what can be done with direct measurements on a sample. This is because of the high noise and low conversion efficiency of microwave crystal detectors. There may be other factors however which dictate the use of microwave measurements as discussed below. The precision with which mobilities may be obtained is limited by the measurement of the microwave parameters and the validity of the equivalent circuit which we use. We expect that our mobility values are reliable to between 10 and 20 per cent. It should be emphasized that the filling factor which is less well known fortunately does not enter into the mobility determination.

### 4. MOBILITY OF PHOTOCARRIERS IN CADMIUM SULFIDE

As an example of the use of the bimodal cavity we report on a measurement of the mobility of photocarriers in cadmium sulfide. A sample approximately ·02 cm thick and ·015 cm² in area was made available to us by Dr. JOHN E. JACOBS of the General Electric Company. The sample was placed in the region of maximum electric field in a cylindrical bimodal cavity resonant at 8·92 kMc/s with an unloaded $Q$ of 3400. On illumination of the sample with white light the $Q$ of the cavity was reduced by 0·69 per cent. From this reduction in $Q$ we compute an increase in sample conductivity of $1{\cdot}09\times10^{-4}$ (Ω-cm)$^{-1}$ in the light. From the change in coupled power on the application of a magnetic field of 8000 G we compute that the $xy$ component of the photoconductivity is $1{\cdot}80\times10^{-6}$ (Ω-cm)$^{-1}$. The Hall angle is simply the ratio of these two components or ·0165 rad. This angle corresponds to a mobility of 210 cm²/V sec in good agreement with published values for CdS.[6]

### 5. FREQUENCY EFFECTS

We finally wish to mention briefly a number of effects which must be considered on comparing low frequency and microwave measurements. We do not discuss at all here phenomena such as cyclotron resonance which arise when the carrier collision relaxation time is comparable to the period of the microwaves. Instead we wish to consider surface charge effects arising from the fact that we are dealing with finite samples and volume effects arising from non-uniformity of the sample. The effect of non-ohmic contacts on the measurement of Hall mobilities has been discussed by MACDONALD and ROBINSON.[7] These writers find that in some cases these effects can

be eliminated by producing an alternating Hall voltage. They observe however that there may be cases where the relaxation time of the barriers is shorter than the charge relaxation time of the sample itself. Under these circumstances it is not possible to obtain the Hall voltage. One advantage of the microwave measurements is that they do not depend on the development of an electrostatic field. Actually at microwave frequencies it is not possible to set up a Hall field in a period of one cycle except in very low impedance materials. Therefore one expects that the currents will flow at the Hall angle with respect to the driving field. Then it is the transverse microwave current which excites the second mode. It should of course be possible to measure the inductive effects of Hall currents at radio frequencies although it may not be possible to achieve the kind of stable balance that is possible in a microwave cavity.

A second problem which must be considered in comparing low frequency with microwave measurements is the effect of shunt capacity in a finite sample. This is particularly important in the study of high impedance films where a significant accumulation of surface charge takes place.[8] In the comparable microwave experiment with high impedance samples the field configuration is determined by the cavity design rather than by the sample. We therefore expect no decrease in effective resistance below the d.c. value because of this effect. Of course the presence of film inhomogeneities will still result in an increase in film conductance at high frequencies.

*Acknowledgments*—I would like to thank Dr. N. T. MELAMED for his generous assistance during the early development of the present technique. Mr. DALE TEANEY very kindly assisted with the mobility measurements on CdS.

## REFERENCES

1. PORTIS A. M. and TEANEY D. *J. Appl. Phys.* (in press).
2. NICHINA Y. and SPRY W. J. *J. Appl. Phys.* **29,** 230 (1958).
3. RAU R. R. and CASPARI M. E. *Phys. Rev.* **100,** 632 (1955); HAMBLETON G. E. and GARTNER W. W. *Bul. Amer. Phys. Soc.* Ser. II **3,** 259 (1958).
4. BERK A. D. and LAX B. *Conv. Record, Inst. Radio Engrs., National Convention,* Part **10,** 70 (1953). See also SPENCER E. G., LECRAW R. C. and AULT L. A. *J. Appl. Phys.* **28,** 130 (1958).
5. TOWNES C. H. and SCHAWLOW A. L. *Microwave Spectroscopy,* see especially Section 14–18. McGraw-Hill Book Company, New York (1955).
6. KROGER F. A., VINK H. J. and VOLGER J. *Physica* **20,** 1095 (1954); and *Philips Res. Rep.* **10,** 39 (1955).
7. ROSS MACDONALD J. and ROBINSON JOHN E. *Phys. Rev.* **95,** 44 (1954).
8. BROUDY R. and LEVINSTEIN H. *Phys. Rev.* **94,** 285 (1954); LAX M. and SACHS R. *Phys. Rev.* **107,** 650 (1957).

*J Phys. Chem. Solids* Pergamon Press 1959. Vol. 8. pp. 329–332. Printed in Great Britain

L.7

# MICROWAVE HALL EFFECT IN GERMANIUM AND SILICON AT 20 kmc/s

**G. E. HAMBLETON and W. W. GÄRTNER**

U.S. Army Signal Research and Development Laboratory, Fort Monmouth, New Jersey

THE response of an assembly of carriers to a rapidly varying electric field becomes limited at high frequencies by the inertia of the carriers. This effect manifests itself, e.g. in a frequency dependence of the Hall mobility. If one considers the solid as containing only non-interacting carriers with a constant relaxation time $\tau$, and an isotropic effective mass, $m^*$, one obtains the following expression for the Hall mobility.

$$u_H = \frac{q}{m^*(\omega_c + i\omega)} \qquad (1)$$

where $q$ is the electronic charge, $\omega_c = 1/\tau$ is the collision frequency and $\omega$ is the frequency of the sinusoidally varying applied electric field. A solution of the Boltzmann equation for varying electric field and constant magnetic field and for any of the customary band structure schemes predicts essentially the same dependence.

Some theoretical and experimental work on high-frequency transport phenomena has been published previously[1-10] and it is the purpose of this paper to report some experiments on the microwave Hall mobility of germanium and silicon.

At lower frequencies a coaxial system has been used which consists of a rectangular metal box containing the sample. The electrical contacts are made to the four sides of coaxial leads. Hall effect can thus be measured with ease up to several hundred Mc/s and no deviations from d.c. values have been observed.

The microwave measurements have been carried out in a waveguide system. The block diagram of Fig. 1 indicates the experimental

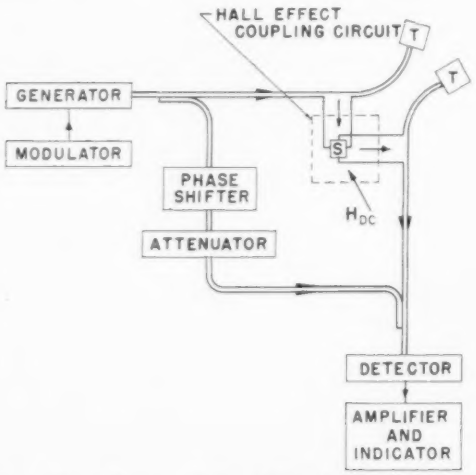


FIG. 1. Block diagram of experimental arrangement for Hall effect measurement at microwave frequencies.

arrangement. A Hewlett Packard $K$-band generator with a maximum calibrated output of more than ten milliwatts is modulated by a Hewlett Packard Audio Signal Generator, and the resultant microwave signal is applied to the input guide of the microwave circuit which contains the Hall effect crystal specimen. The bridge arrangement shown is used to reduce the undesired leakage signal, which appears in the output waveguide of the circuit, to a low value. This allows for detection of smaller Hall effect signals than would otherwise be possible, and it avoids the difficulty of separating the vector sum of Hall power and leakage power.

The d.c. magnetic field is obtained from a Varian V-4012-3B twelve inch electromagnet with an air gap of three inches. It provides fields up to 10,000 G.

The circuit which contains the crystal specimen is shown in Fig. 2. It consists of two sections of

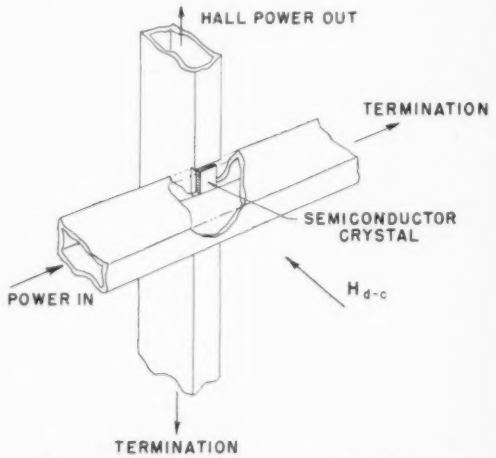


FIG. 2. Microwave circuit for Hall effect study.

waveguides whose axes are perpendicular and whose common wall section has been replaced by the Hall effect crystal specimen. The d.c. magnetic field applied perpendicular to the face of the crystal generates a microwave Hall voltage which couples to the output waveguide.

The Hall mobility is simply related to the microwave powers in the applied and observed fields at the face of the crystal.

$$u_H = \frac{1}{H}\left(\frac{P_y}{P_x}\right)^{\frac{1}{2}}. \tag{2}$$

The measurement of applied and resultant Hall signal powers, in a known magnetic field, thus yields an indication of Hall mobility at microwave

frequencies. Matching of input and output waveguides to the Hall sample and attenuation in the waveguide system must be measured and taken into account in the evaluation of the results.

The experimental results are shown in Fig. 3. Plotted are the microwave Hall mobility at 20 kmc/s and at d.c. for germanium and silicon, *N*-type and *P*-type samples. The samples on

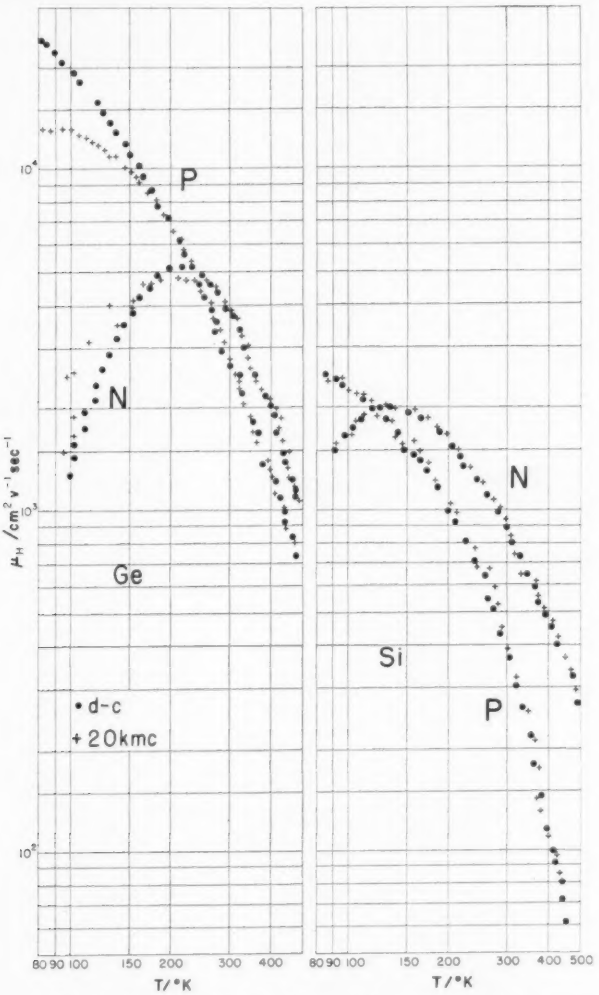


FIG. 3. Hall mobility at d.c. and 20 kmc/s in *N*- and *P*-type germanium and silicon as a function of temperature. Magnetic field strength: 5000 G.

The low temperatures were obtained in a liquid nitrogen metal dewar which permits one to evacuate the portion of the waveguide arrangement which is cooled below room temperature. The high temperatures were produced by heater windings around the sample holder.

which the d.c. Hall mobility has been measured were cut from the same crystal immediately adjacent to the microwave sample. The measurements were made for magnetic fields between 0 and 10,000 G, in steps of 1000 G. The decrease in Hall mobility with magnetic field is noticeable

but relatively small and has not been reported, in particular, since no attempt has yet been made to orient the crystals for magnetoresistance measurements. The curves shown correspond to a magnetic field strength of 5000 G.

The curves for silicon indicate that within the error of the measurement there is no deviation from the d.c. Hall mobilities at these frequencies and temperatures. In germanium, however, and in particular in *P*-type samples the Hall mobility at microwave frequencies and low temperatures appears to be lower than the d.c. values, which could be explained by a collision frequency comparable to the microwave frequency used. The deviations in the *N*-type samples with pronounced impurity scattering are not as readily explained and will require additional investigation.

The conclusion of this work is clear: The measurements must be extended to lower temperatures and higher frequencies in oriented samples. The system described lends itself to these extensions and the results of such experiments shall be the subject of a forthcoming publication.

*Acknowledgments*—The authors would like to thank Prof. N. MARCUVITZ for a discussion on the microwave problems involved, and Miss C. LOSCOE and H. METTE of the U.S. Army Signal Research and Development Laboratory, Fort Monmouth, for carrying out the d.c. Hall mobility measurements.

The germanium and silicon crystals used have kindly been supplied through the co-operation of F. P. LYONS and H. R. STROBEL of Western Electric, and W. MAHER of Philco Corporation. T. SAAD of Sage Laboratories, Inc., has supervised the construction of the improved sample holder used.

## REFERENCES

1. COOKE S. P. *Phys. Rev.* **74,** 701(L) (1948).
2. BARLOW H. E. M. *Proc. Inst. Elect. Engrs.* **102B,** 179 (1954).
3. DONOVAN B. *Proc. Phys. Soc.* **A67,** 305 (1954).
4. DONOVAN B. *Proc. Phys. Soc.* **A68,** 1026 (1955).
5. RAU R. and CASPARI M. *Phys. Rev.* **100,** 632 (1955).
6. BARLOW H. E. M. and STEPHENSON L. M. *Proc. Inst. Elect. Engrs.* **103B,** 110 (1956).
7. DONOVAN B. and MARCH N. *Proc. Phys. Soc.* **B69,** 528 (1956).
8. FUKUROYI T. and DATE M. *Sci. Rept. Res. Inst., Tohoku Univ.* Ser. A, **9,** 190 (1957).
9. NISHINA Y. and SPRY W. J. *J. Appl. Phys.* **29,** 230 (1958).
10. HAMBLETON G. E. and GÄRTNER W. W. *Bull. Amer. Phys. Soc. Ser.* **3,** 259 (1958).

*J. Phys. Chem. Solids* Pergamon Press 1959. Vol. 8. pp. 332–337. Printed in Great Britain

# L.8 EFFET ELECTROMAGNETOPHOTONIQUE DANS LE GERMANIUM

**MAURICE BERNARD**

Departement Physique, Centre National d'Etudes des Telecommunications, Issy-les-Moulineaux (France)

**Abstract**—In an intrinsic Germanium sample the thickness of which is substantially less than the ambipolar diffusion length, it is shown that simultaneous electric and magnetic field must induce infrared emission through recombination transitions; this electromagnetophotonic effect (EMP) which is the reciprocal of the photomagnetoelectric effect (PME), has been observed. Volume recombination (direct rediative process) near the face of the sample where carriers are accumulated by the Laplace force seems responsible for the observed emission. The efficiency of radiative processes in surface recombinations, for wavelengths less than 3·3 $\mu$ is not appreciable but is in any case inferior to $10^{-6}$.

SOIT un échantillon semiconducteur de forme parallélépipédique placé dans un champ magnétique uniforme parallèle á $Oz$ (Fig. 1); si on

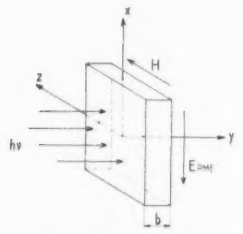


FIG. 1. L'effet photomagnetoelectrique.

l'éclaire suivant $Oy$ par un rayonnement fortement absorbé il apparaît un champ électrique parallèle á $Ox$; ce phénomène est bien connu sous le nom d'effet photomagnétoélectrique.

Réciproquement, supposons que l'échantillon, toujours placé dans un champ magnétique uniforme, soit soumis á un champ électrique d'origine extérieure parallèle á $Ox$; on peut montrer que dans certaines conditions il en résulte une émission de rayonnement.[1]

Il a été démontré en effet que, dans une plaquette semiconductrice intrinsèque d'épaisseur inférieure á la longueur de diffusion ambipolaire, la concentration des paires électron-trou s'écarte considérablement de la concentration d'équilibre[2] sous l'influence d'un champ électrique et d'un champ magnétique croisés. Soit $E_x$ le champ électrique d'origine extérieure parallèle á $Ox$ et $H$ le champ magnétique parallèle á $Oz$; on montre[3] qu'en régime permanent la concentration des paires électron-trou $n$ $(y)$, $n_i$ étant la concentration à l'équilibre, s'écrit:

$$n(y) = n_i(\lambda e^{-y/y_0}+\mu) \qquad (1)$$

$$\text{Avec } y_0 = \frac{2kT}{qE_xH(\mu_n+\mu_p)}$$

où $\nu$ et $\mu$ sont deux constantes; la face $F_1(y = b/2)$, appauvrie en porteurs, engendre des paires électron-trou qui vont se recombiner sur la face $F_2(y = -b/2)$ où il existe, au contraire, un excès de paires électron-trou (Fig. 2a); si la recombinaison en volume est négligeable, ce qui est réalisé si l'épaisseur $b$ de la plaquette est inférieure à la longueur de diffusion des paires électron-trou, le flux de particules de la face $F_1$ à la face $F_2$ est conservatif; le taux de génération de la face $F_1$ est égal au taux de recombinaison de la face $F_2$; si $A$ est la valeur commune de ces taux, on a, en admettant une recombinaison superficielle linéaire:

$$A = \mu\mu_n\mu_pE_xHn_i = s_1(n_i-n_1) = s_2(n_2-n_i) \quad (2)$$

$$\text{où} \quad n_1 = n(+b/2) \qquad n_2 = n(-b/2).$$

Ces relations permettent de calculer $A$, $\lambda$ et $\mu$ en fonction des champs $E_x$, $H$, de l'épaisseur $b$ de la plaquette et des vitesses de recombinaison superficielles $s_1$ et $s_2$; on trouve:

$$\lambda = \frac{\alpha_1+\alpha_2}{(t-1/t)+\alpha_1t+\alpha_2/t}$$

$$\mu = \frac{t-1/t}{(t-1/t)+\alpha_1t+\alpha_2/t}$$

$$A = \mu_n\mu_pE_xHn_i\frac{t-1/t}{(t-1/t)+\alpha_1t+\alpha_2/t}$$

où l'on a posé:

$$t = e^{b/2y_0} \qquad \alpha_1 = \frac{\mu_n\mu_pE_xH}{s_1} \qquad \alpha_2 = \frac{\mu_n\mu_pE_xH}{s_2}$$

Si certaines des recombinaisons qui ont lieu sur la face $F_2$ ou à son voisinage sont radiatives on doit s'attendre à l'émission de rayonnement; nous avons cherché à mettre ce phénomène en évidence.

## DISPOSITIF EXPÉRIMENTAL

Des plaquettes de dimensions $15\times5\times1$ mm ont été taillées dans des cristaux de Germanium trés purs; la teneur en impuretés résiduelles $N_d-N_a$, déterminée par la conductivité à basse température est de 2 à $5\times10^{12}$ at/cm$^3$; la recombinaison en volume est faible, la durée de vie étant supérieure à $10^{-3}$ sec; les mesures sont faites en plaçant les plaquettes dans l'entrefer d'un aimant donnant un champ magnétique uniforme de 4800 Oe. Le rayonnement est mesuré par une cellule PbS[4] refroidie à la neige carbonique.

### VÉRIFICATION DE LA RÉPARTITION DES PORTEURS

Une plaquette a subi le traitement suivant: la face $F_1$ a été doucie de façon à présenter une grande vitesse de recombinaison superficielle $s_1$; la face $F_2$ a été polie et attaquée chimiquement de façon à présenter une faible vitesse de recombinaison $s_2$. La formule (1) montre que pour un champ électrique $E_x$ positif assez grand (quelques V/cm) la répartition des paires électron-trou à l'allure représentée sur la courbe (a) de la Fig. 2; pour un champ électrique $E_x$ négatif la répartition des paires électron-trou est représentée sur la courbe (b) de la Fig. 2. La conductance de l'échantillon, proportionelle au nombre de porteure, est donc très grande dans un sens et très faible dans l'autre (3). La Fig. 3 représente (courbe a) la

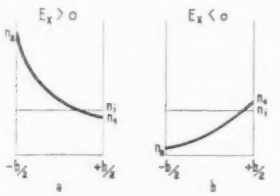


FIG. 2. Répartition des paires électrons-trous le long de $Oy$.

caractéristique $V$–$I$ relevée expérimentalement; la courbe théorique (courbe b) qui interpôle au mieux cette caractéristique expérimentale est celle qui corespond aux valeurs suivantes de la recombinaison superficielle:

$$s_1 = 10000 \text{ cm/sec}$$
$$s_2 = 200 \text{ cm/sec}$$

Ces valeurs sont en bon accord avec ce que l'on trouve dans le Germanium pour des surfaces ainsi préparées; on en déduit que la répartition de porteurs prévue par la formula (1) est bien vérifiée expérimentalement.

En adoptant les valeurs de $s_1$ et $s_2$ déterminées ci-dessus on calcule que, par exemple, pour $E_x = 10$ V/cm, le nombre de paires électron-trou engendrées par seconde par la face $F_1$ et recombinées par la face $F_2$ est d'environ $5 \times 10^{16}$; le calcul du nombre de paires recombinées en volume, à partir de la valeur connue de la durée de vie de volume, donne environ $2 \times 10^{15}$ paires par seconde, soit 4 pour cent de la recombinaison superficielle, ce qui montre que négliger la recombinaison de volume, était justifié et que la répartition des paires électron-trou dépend essentiellement des vitesses de recombinaison de surface des faces $F_1$ et $F_2$.

### MESURE DU RAYONNEMENT

La formule (2) montre que le nombre de recombinaisons superficielles sera d'autant plus grand, à $E_xH$ donné, que $\mu$ sera grand; en général $t \gg 1$ et l'on a $\mu \simeq 1/(1+\alpha)$; $\mu$ sera maximum ($\mu = 1$) si $\alpha_1$ est minimum, c'est-à-dire si $s_1$ est grand, la valeur de $\alpha_2$ (c'est-à-dire de $s_2$) n'ayant alors aucune influence sur $A$; ceci montre que si la vitesse de recombinaison de la face $F_1$ est assez grande c'est elle seule qui commande le flux de paires électron-trou. L'échantillon est alimenté par une tension électrique à 125 c/sec, redressée, une alternance; l'expérience montre que pour une tension électrique et un champ magnetique suffisamment grands, on obtient un signal à 125 c/sec; le signal décroît et s'annule avec $H$ (à $E_x$ fixe) et décroît et s'annule avec $E_x$ (à $H$ fixe); la Fig. 4 (Courbe 1) représente le signal obtenu en fonction du champ électrique ($H = 4800$ Oe).

### INTERPRÉTATION

Il faut distinguer entre la recombinaison de volume et la recombinaison de surface. La recombinaison de volume dans le Germanium est soit directe, soit indirecte; la recombinaison directe par un processus de la bande de conduction à la bande de valence est radiative et provoque l'émission de photons de longueur d'onde comprise entre 1·7 et 1·9 $\mu$[5]; la durée de vie corréspondante est environ 0·3 sec à température ordinaire; la durée de vie des échantillons examinés étant d'environ $1 \times 10^{-3}$ sec est due à un processus de recombinaison 200 fois plus efficace que la précédent; cette recombinaison doit être attribuée à des centres d'impuretés[6] et n'est pas radiative à température ordinaire.[7]

La recombinaison de surface est très mal connue; on peut penser que la recombinaison directe radiative est quasi inexistante; c'est en effet le processus inverse de l'absorption des photons par la matière que est essentiellement un phénomène de volume; le seul processus envisagé est un pro-

cessus indirect en l'on ignore si de telles transitions sont radiatives.[8]

Le signal obtenu étant trop faible pour permettre de déterminer le spectre du rayonnement, nous avons examiné l'influence de différents filtres sur l'amplitude du signal; la Fig. 4 montre les

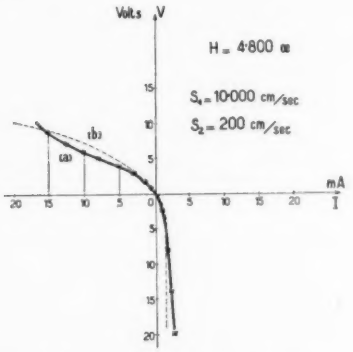


FIG. 3. Caracteristique courant-tension.

résultats obtenus; en tenant compt de la reflectivité on soit que le filtre en verre n'absorbe pratiquement pas le signal, la longueur d'onde du rayonnement détecté est donc inférieure à 2·5 $\mu$; on voit de même que le rayonnement n'étant pas absorbé par le filtre en Silicium et faiblement absorbé par les filtres en Germanium la longueur d'onde est supérieure à 1·7 $\mu$.

On a alors étalonné la cellule détectrice PbS à l'aide du rayonnement de corps noir et l'on a porté sur la même figure (Fig. 5) la courbe (a) du nombre de photons recueillis, calculé á partir de l'étalonnage de la celluel, et la courbe (b) du nombre de photons provemant de la recombinaison de volume directe (radiative) en tenant compte de la réflexion à l'interface Germanium-air et de l'ouverture optique du système. Si l'on considère les erreurs importantes, naturelles dans ce genre de calculs, l'accord est très satisfaisant.

On peut tirer de ces expériences deux conclusions. D'une part une mince plaquette de Germanium très intrinsèque ($N_a - N_d \ll n_i$) et de grande durée de vie ($\tau \geqslant 10^{-3}$ sec) placée dans un champ électrique et dans un champ magnétique croisés doit émettre un rayonnement infrarouge;

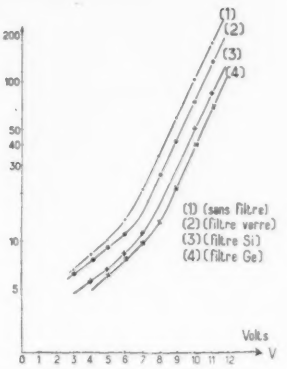


FIG. 4. Emission Infrarouge en fonction de la tension appliquée

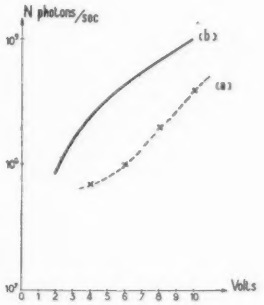


FIG. 5. Flux de photons recus (courbe thermique et courbe experimentale).

un tel rayonnement a éte observé. Cet effet électromagnétophotonique (EMP) apparaît comme l'effet réciproque de l'effet photomagnetoélectrique (PME).

D'autre part, le rayonnement détecté est dû, en grande partie si non en totalité á la recombinaison de volume, directe, ai voisinage de la face $F_2$ ou sont concentrés les porteurs par les champs électrique et magnétique; les recombinaisons de surface, si elles sont radiatives, le sont avec un très faible rendement (de l'ordre de $10^{-6}$) ou bien correspondent à des photons de longueur d'onde supérieure à 3·3 $\mu$ (limite de réponse spectrale de la cellule PbS).

**BIBLIOGRAPHIE**

1. KIKOIN et NOSKOV *Phys. Z. Sowjet* **5,** 586 (1934); *Ibid.* **6,** 478 (1934).
2. BERNARD M. et LOUDETTE J. *C.R. Acad. Sci., Paris.* **246,** 1177 (1958).
3. WELKER H. *Z. Naturf.* **6a,** 184 (1951); WEISSHAAR E. et WELKER H. *Z. Naturf.* **8a,** 681 (1953); MADELUNG O., TEWORDT I. et WELKER H. *Z. Naturf.* **10a,** 476 (1955); WEISSHAAR E. *Z. Naturf.* **10a,** 448 (1955); PIKUS G. E. *Zh. tekh. fiz. SSSR* **26,** 22 (1956).
4. Cette cellule de grande sensibilité et de faible bruit a été tres aimablement fournie par le Professeur LALLEMAND, Observatoire de Paris.
5. HAYNES J. R. et BRIGGS H. B. *Phys. Rev.* **86,** 647 (1952); NEWMAN R. *Phys. Rev.* **91,** 1313 (1953); VAN ROOSBROECK W. et SHOCKLEY W. *Phys. Rev.* **94.** 1558 (1954).
6. HALL R. N. *Phys. Rev.* **87,** 387 (1952); SHOCKLEY W. et READ W. T. *Phys. Rev.* **87,** 835 (1952).
7. AIGRAIN P. *Physica* **20,** 1010 (1954); BENOIT C. A LA GUILLAUME *C. R. Acad. Sci., Paris.* **243,** 704 (1956).
8. BRATTAIN W. H. et BARDEEN J. *Bell. Syst. Tech. J.* **82,** 1 (1953).

## DISCUSSION

*Compiled by* H. Y. FAN

### L.1. E. BURSTEIN *et al.*

D. R. FRANKL raised the question about the transition of density of states from the $H = 0$ condition to the large field condition described by Landau levels.

E. BURSTEIN replied that energy level broadening, which is important for small fields, was not considered.

### L.2. B. LAX, *et al.*

W. KOHN asked about the value of the transverse effective mass of electrons in silicon, as estimated from the effect of magnetic field on the excitation lines of donor impurities.

B. LAX replied that the observed effect was about 10 per cent smaller than that expected from the effective mass given by cyclotron resonance experiments.

E. BURSTEIN asked about the interpretation of exciton absorption in $Cu_2O$ on the basis of the energy band structure.

R. J. ELLIOTT commented that the observations on $Cu_2O$ fit the theory; two series of lines have been observed which should correspond to transitions between *s* and *d* bands, the latter being split by spin–orbit interaction.

H. BROOKS: Could the experimentally determined energy gap for indirect transitions be affected by strain produced in the sample by the mounting process.

B. LAX: In the measurement of indirect transitions, the sample was mounted without backing and was therefore not strained; in the measurement of direct transitions the sample was mounted on glass with cement, and there might be some effect of strain.

### L.3. R. F. WALLIS and H. J. BOWLDEN

R. F. WALLIS in reply to a question by W. KOHN: We have realized that the acceptor bound state energies in a magnetic field are quite sensitive to the values of the effective mass theory parameters. We have not investigated the sensitivity of these energies to the form of the variational wave functions.

B. LAX: Have you considered the effect of large spin orbit effect and the effect or higher order or $k^4$ terms on the Zeeman effect?

R. F. WALLIS: We have assumed that the conduction band in InSb is parabolic. Under these conditions, the states of spin $+1/2$ and those of spin $-1/2$ are shifted in energy by a constant amount and do not mix with each other. The two spin states give identical spectra. It is felt that the inclusion of non-parabolic terms in the energy band structure would produce relatively small effects under the conditions assumed in the calculation.

L. ROTH: In regard to the splitting of InSb cyclotron resonance absorption observed by BOYLE and BRAILFORD, the effect of the large *g* value and the change of mass could account for the positions of the lines; however in their experiment the spin splitting was much larger than $kT$, so that all of the electrons would be in the same spin state.

### L.4. W. S. BOYLE

W. KOHN: According to theory, there should be a shoulder to the excitation lines. Is there such indication in the excitation absorption of impurities in germanium?

W. S. BOYLE: No such indication has been observed.

S. H. KOENIG: Judging from the carrier lifetime and donor density quoted, the possibility of impact ionization being important in determining the shape of the absorption curves would require a larger cross-section for impact ionization than is measured in breakdown experiments.

R. J. ELLIOTT: It seems unlikely that discrete levels will exist with the same energy as continuum states, in an exact solution of the problem. They clearly do exist if it is possible to separate the equation into $z$ and $(x^2+y^2)$, but on adding the mixed terms matrix elements will exist between the states and mix them. If these elements are small it may still give rise to an absorption peak at this point in analogy to the Auger effect in complex atoms, where the description in terms of localized

and ionized states are only strictly valid in a perturbation theory limit.

R. F. WALLIS: Split-off from the bottom of each Landau level are a number of discrete states characterized by a set of quantum numbers including $m$, the component of angular momentum parallel to the magnetic field. In large magnetic fields the discrete levels associated with higher Landau levels may have energies equal to energies of continuum states of the lowest Landau level. Some of the higher discrete states are perturbed by the continuum states of equal energy. Others, however, have different $m$ values (positive) from the permitted $m$ values (zero or negative integers) for the lowest Landau level. The latter discrete state are accordingly not disturbed.

W. H. KLEINER: R. PUFF and I have been examining the problem of hydrogen atom in a magnetic field. The azimuthal quantum number $m$ and parity are good quantum numbers for any field strength $H$. The bound energy eigenstates are conserved as $H$ increases from 0 to $\infty$. They are non-degenerate for $H > 0$, aside from accidental degeneracy. Bound states with energy above the lowest Landau level are degenerate with continuum states. It is not clear whether an eigenstate which is bound for small $H$ necessarily acquires an admixture of continuum character when it crosses a Landau level. There is no mixing if the eigenstate has $m$ and parity different from all continuum states of lower energy. For large enough $H$, the bound eigenstates are separated into groups, one group being associated with each Landau level. There are an infinite number of bound eigenstates in a group. The binding energy (energy from the associated Landau level) of each of these except one is bounded as a function of $H$. The binding energy of the remaining eigenstate increases with $H$ asymptotically as $(\ln H)^2$.

G. H. WANNIER: The levels pulled out of the Landau band by the Coulomb field are also the ones with large matrix elements because of local proximity. This may produce an apparent shift of Landau peaks to lower frequency.

### L.5. T. S. Moss *et al.*

S. ZWERDLING: Radiation reflected from a dielectric at Brewster's angle is completely polarized, and its intensity increases with increasing refractive index. Germanium with its high refractive index is an excellent material for wavelengths longer than those corresponding to intrinsic absorption. I designed a polarizer using reflection from germanium and mirror surfaces in such a way that the beam would not be deviated. The polarizer built by Mr. BROWN of our laboratory has been used successfully over the range of NaCl and KBr prisms in conjunction with Faraday rotation experiments on semiconductors.

B. LAX: In determining the effective mass from Faraday rotation, the carrier density has to be determined from the Hall effect. The accuracy is then determined by the Hall measurement.

T. S. MOSS: For the degenerate samples used the carrier density is simply related to the Hall coefficient by $n = 1/Re$.

B. LAX: Hohanberg at our laboratory has worked out the quantum theory of the Faraday rotation and showed that the classical result is correct for the degenerate case with the effective number of electrons equal to the total number of electrons in the Fermi sea.

### L.6. A. M. PORTIS

B. LAX: The normal modes in your degenerate TE111 cavity are two circularly rotating modes which are optically the tensor medium. How do you bring them into coincidence?

A. M. PORTIS replied that this causes no problem since $\Delta\nu$ is very small.

B. LAX: If the dispersive effect is small then you must be measuring ellipticity due to the differential loss for the two rotating modes.

A. M. PORTIS replied that the effect of absorption is negligible in the observed result which is mainly produced by the difference in refractive index.

*J. Phys. Chem. Solids* Pergamon Press 1959. Vol. 8. pp. 338–339. Printed in Great Britain

SESSION M:
THERMAL CONDUCTION AND THERMOMAGNETIC EFFECTS*

# M.1 EXPERIMENTAL STUDIES ON THE THERMAL CONDUCTIVITY IN SEMICONDUCTORS

**Y. KANAI and R. NII**
Electrical Communication Laboratory, Tokyo, Japan.

A FEW years ago BUSCH and SCHNEIDER[1] found an anomalous behaviour of thermal conductivity in InSb. FRÖHLICH and KITTEL[2] suggested that this anomaly might be explained by the heat conduction due to the ambipolar diffusion of electrons and holes in intrinsic semiconductors. PRICE's calculation,[3] however, showed that the contribution from the ambipolar thermo-diffusion in InSb was too small to explain the experimental data. Recently STUCKES[4] measured the thermal conductivity of InSb and found that there was no anomaly in his sample. Meanwhile JOFFÉ[5] and DEVYATKOVA[6] also found a similar anomalous behaviour of the thermal conductivity in PbTe. JOFFÉ proposed heat conduction due to the diffusion of excitons as an explanation of their experimental data. In order to clarify the mechanism of anomalous heat conduction we thought it worthwhile to carry out measurements of the temperature dependence of the thermal conductivity in semiconductors.

We will report here the thermal conductivity of $Bi_2Te_3$, PbTe and InSb determined from (the improved) Ångström's method. The apparatus for our measurement is shown schematically in Fig. 1. The sample was soldered to the bar of copper which carries the heater I. The thermocouples $T_1$ and $T_2$ of copper–constantan were soldered to each end of the sample. When the on–off current of about 4 sec is passed through the heater I a damped sine shaped temperature wave is travelling through the sample and is reflected at the upper end but decays practically to zero amplitude before reaching $T_1$. Under these conditions the thermal emfs at $T_1$ and $T_2$ are given by:

$$V_1 = A\cos\omega t + C_1$$

$$V_2 = B\cos(\omega t - \beta) + C_2$$

The following relations hold between $A$, $B$ and $\beta$

$$\kappa = \frac{\omega l^2}{2ln^2 2A/B} = \frac{\omega l^2}{2\beta^2} = \frac{K}{c\cdot\rho}$$

where $K$ is the thermal conductivity, $c$ the specific heat, $\rho$ the density, $\kappa$ the temperature (thermometric) conductivity, and $l$ the length of the specimen. Hence the measurement of the amplitude ratio $A/B$ and phase difference $\beta$ give independently the temperature conductivity $\kappa$.

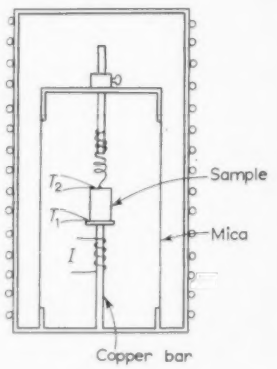


FIG. 1.

Figs. 2–4 the symbol ● shows the values calculated from the experimental data of $A/B$ and the symbol X shows those calculated from $\beta$. It is seen that the agreement between these two values is very good.

We show first in Fig. 2 a typical example of the temperature dependence of $1/\kappa$ of a $Bi_2Te_3$ sing

* *Chairman*: A. JOFFÉ: *Co-Chairman*: H. P. R. FREDERIKSE.

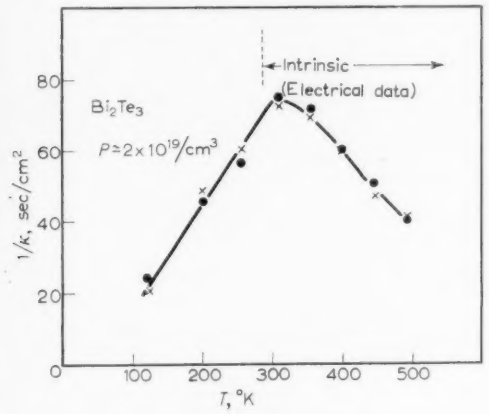


FIG. 2.

crystal. As shown, the curve bends over near the temperature where the Hall coefficient of the sample begins to decrease. This behaviour corresponds to the results given by GOLDSMID[7] and by SATTERTHWAITE and URE,[8] and can be well explained by PRICE's theory.[3]

Next we show in Fig. 3 a typical example of the temperature dependence of $1/K$ of a PbTe single crystal. The thermal conductivity was calculated from the measured value of $\kappa$ and the values of $c$ and $\rho$. For $c$ we used the values given by PARKINSON and QUARRINGTON[9] below room temperature, and we assumed 12cal/mol above room temperature. The dotted curve in Fig. 3 is the result given by JOFFÉ.[5] In spite of the similarity of the electrical properties of JOFFÉ's sample and ours, there is a rather large difference in the high temperature behaviour of the thermal conductivity. The $1/K$ curve of our sample deviates from a straight line at higher temperature where the sample becomes intrinsic and does not show the abnormal bend of thermal conductivity due to excitons.

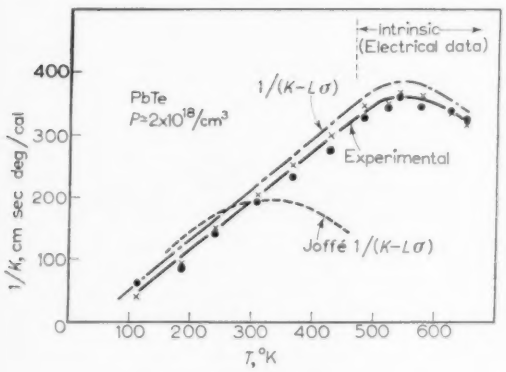


FIG. 3.

Finally we show in Fig. 4 a typical example of the temperature dependence of $1/K$ of InSb single crystal. In determining $K$, we assumed 12 cal/mol for the value of the specific heat. For comparison, we also show the results of BUSCH and SCHNEIDER and STUCKES.[1] It is seen that our results are in good agreement with STUCKES' data.

Corrections due to radiation losses were estimated to be negligible in our experiments.

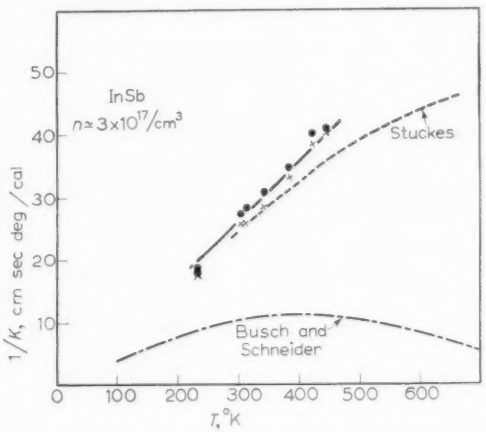


FIG. 4.

## REFERENCES

1. BUSCH G. and SCHNEIDER M., *Physica* **20,** 1084 (1954).
2. FRÖHLICH H. and KITTEL C., *Physica* **20,** 1086 (1954).
3. PRICE P. J., *Phil. Mag.*, **46,** 1252 (1955).
4. STUCKES A. D., *Phys. Rev.* **107,** 427 (1957).
5. JOFFÉ A. F., *Canad. J. Phys.* **34,** 1342 (1956).
6. DEVYATKOVA E. D., *Sowjet. fiz. tekh. fiz.* **2,** 414 (1957).
7. GOLDSMID H. J., *Proc. Phys. Soc.* B**69,** 203 (1956).
8. SATTERTHWAITE C. B. and URE, Jr. R. W., *Phys. Rev.* **108,** 1164 (1957).
9. PARKINSON D. H. and QUARRINGTON J. E., *Proc. Phys. Soc.* A**67,** 569 (1954).

*J. Phys. Chem. Solids* Pergamon Press 1959. Vol. 8. pp. 340–343. Printed in Great Britain

# M.2 THERMAL CONDUCTIVITY OF GERMANIUM IN THE TEMPERATURE RANGE 300°—1080°K.

**B. ABELES**

RCA Laboratories, Princeton, N.J.

PREVIOUS determinations of the thermal conductivity $\kappa$ in germanium at high temperatures were made by PANKOVE,[1] JOFFÉ,[2] and KETTEL.[3] The latter two authors have reported an anomalous behaviour of $\kappa$ at high temperatures and attributed it to bipolar electronic conduction.[4–6]

In the present work measurements of $\kappa$ on single crystals of germanium were extended to 1080°K. A conventional measuring method was used in which the sample was placed between a heater and sink. Simultaneous measurements of the thermoelectric power and electrical conductivity were made. A drawing of the apparatus is shown in Fig. 1. The germanium samples were nickel brazed to molybdenum discs and the molybdenum discs, in turn, were tin soldered to the copper sink and heater. Temperatures were measured by chromel–alumel thermocouples welded to the molybdenum discs. The measurements were made in a vacuum furnace.

Measurements of $\kappa$ on four *n*-type germanium samples of different extrinsic carrier concentrations were made. The cross-sectional areas of the samples were about 0·4 cm$^2$ and the lengths 0·3 cm for all samples except sample No. 3 which had a length of 0·8 cm. At the highest temperatures measured, the radiation losses for the short samples were about 5 per cent and for the long sample about 30 per cent of the power supplied by the heater. The radiation correction was estimated from the measured value of the radiation losses from the heater and assuming a value of 0·55 for the total emissivity of germanium.[7]

In Fig. 2 are plotted the measured values of $\kappa$ after the above corrections were made. The room temperature resistivities of the samples are indicated in the figure. The results of JOFFÉ and KETTEL are shown for comparison. Good agreement is obtained with other published room temperature values of the thermal conductivity,[8,9] and with Kettel's data up to 600°K. The agreement with Joffé's data is satisfactory only at the high temperatures. Up to about 800°K, $\kappa \sim (1/T)$ within the experimental uncertainty. Above this temperature $\kappa$ deviates from the $1/T$ law for samples No. 1, 2, and 3 and goes through a minimum. For the degenerate sample, No. 4, the minimum is shifted to a higher temperature. The measurements of the electrical conductivity $\sigma$ on

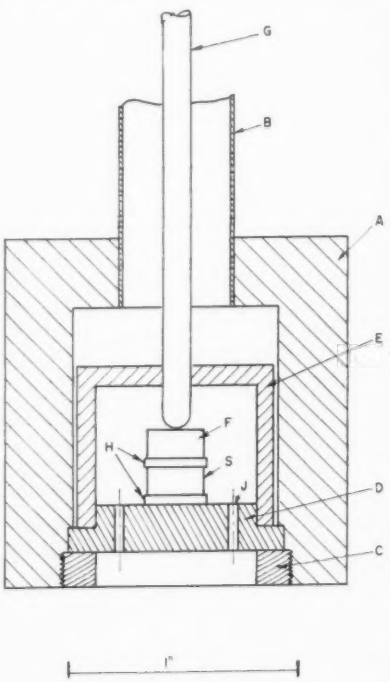


FIG. 1. Apparatus for thermal conductivity measurements: A, Stainless steel holder; B, Inconel tube; C, Clamping screw; D, Copper sink; E, Copper radiation shield; F, Heater; H, Molybdenum discs; S, Sample; J, Holes for electrical leads; G, Spring loaded alundum tube.

samples No. 1, 2 and 3 are shown in Fig. 3. The agreement with other published data is satisfactory.[10]

To interpret the data we make the assumption that $\kappa = \kappa_{ph} + \kappa_{el}$ where $\kappa_{ph}$ is the lattice component and $\kappa_{el}$ is the total electronic component of $\kappa$ respectively. Assuming $\kappa_{ph} \sim (1/T)$, $\kappa_{el}$ is given by the deviation of $\kappa$ from the straight line in Fig. 2. This deviation is plotted in Fig. 4. The values of the radiation losses and $\kappa_{ph}$. Agreement with theory appears to be qualitative; however, the experimental values tend to rise more steeply than theory predicts.

The theory predicts that $\kappa_{el}$ should be small in the extrinsic range. The behaviour of $\kappa$ and the thermoelectric power $Q$ for the degenerate sample verifies this prediction qualitatively. For this sample $\kappa_{el}$ is negligible up to 900°K above which

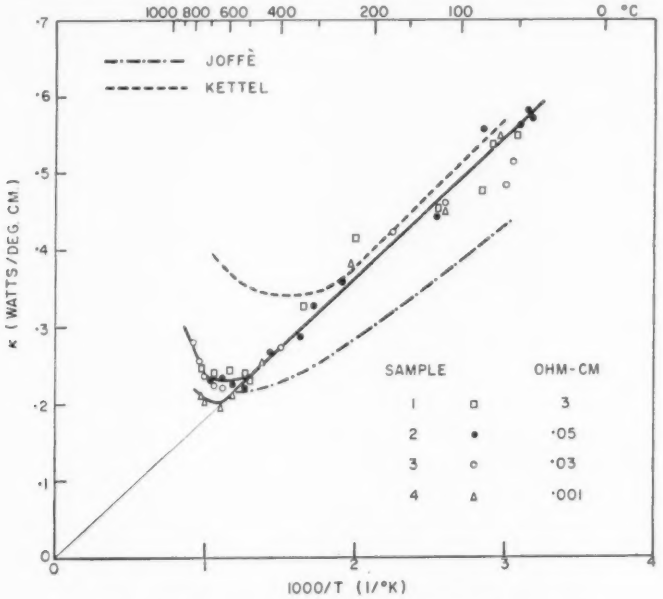


FIG. 2. Measured thermal conductivity of *n*-type germanium as a function of temperature. The room temperature resistivities of the samples are indicated in the figure. The dashed curves are the work of JOFFÉ and KETTEL, respectively.

theoretical expression for $\kappa_{el}$ in the intrinsic range is given by:[5]

$$\kappa_{el} = 2(k/e)^2\sigma T\left[1+\tfrac{1}{2}\frac{1}{b+2+(1/b)}\left(\frac{E_g}{kT}+4\right)^2\right] \quad (1)$$

The dashed curve in Fig. 4 was calculated from equation (1). We assumed for the ratio of electron to hole mobility[11] $b = 2{\cdot}5$, for the band gap[12] $E_g = 0{\cdot}67 - 0{\cdot}0004\ (T-300)$, and for $\sigma$ the measured values given in Fig. 3. In estimating the possible experimental errors of the points in Fig. 4, account was taken of the uncertainty in the temperature it rises sharply. The simultaneous sharp drop observed in $Q$ indicates that the sample has become intrinsic at this temperature.

Within the accuracy of the experiment and the parameters used in the calculation, no definite conclusions can be drawn at this time about the quantitative validity of the theory. The above work is being continued and will be extended to higher temperatures.

*Acknowledgments*—The author wishes to thank G. D. CODY for valuable discussions, R. W. EASTON for assistance in the measurements, R. J. BREINIG and J. J.

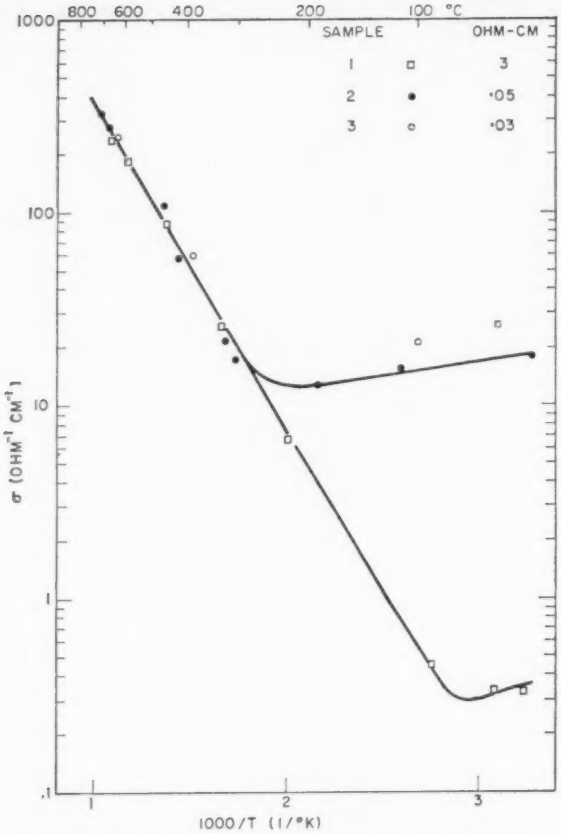


FIG. 3. The measured electrical conductivity of *n*-type germanium as a function of temperature.

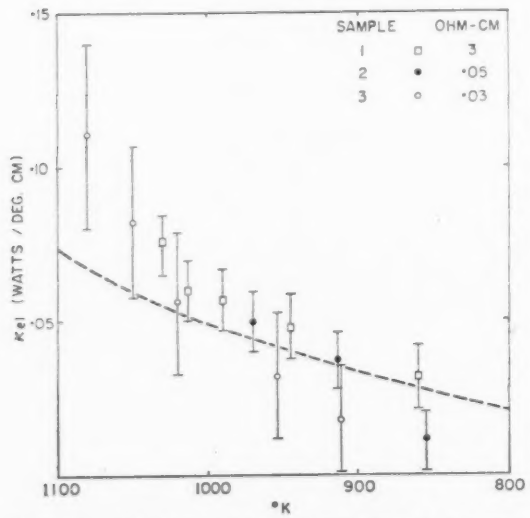


FIG. 4. Total electronic thermal conductivity in *n*-type germanium as a function of temperature. The dashed line has been computed from equation (1).

GANNON for preparation of the high temperature contacts to the germanium crystals and R. J. MOEHS for construction of the equipment.

## REFERENCES

1. PANKOVE J., *Semiconductor Symp. Electr. Div. Electrochem. Soc.* May 3, 1956, San Francisco.
2. JOFFÉ A. F., *Canad. J. Phys.* **34,** 1342 (1956).
3. KETTEL F., Munster meeting of the *German Phys. Soc.*, April 1957.
4. DAVYDOV and SCHMUSHKEVICH, *Usp. Fiz. Nauk* **24,** 21 (1940).
5. PRICE P. J., *Phys. Rev.* **95,** 596 (1954); *Phil. Mag.* **46,** 1192 (1955).
6. FRÖHLICH H. and KITTEL C., *Physica.* **20,** 1086 (1954).
7. ALLEN F. G., *J. Appl. Phys.* **28,** 1510 (1957) reports the value 0·55 for the spectral emissivity of germanium at $0{\cdot}65\eta$. The spectral emissivity of silicon is very nearly independent of wave length (*American Institute of Physics Handbook*, p.6–72. McGraw–Hill, New York 1957) and it is reasonable to assume that this is also true for germanium.
8. GRIECO A. and MONTGOMERY H. C., *Phys. Rev.* **86,** 570 (1952).
9. MCCARTHY K. A. and BALLARD S. S., *Phys. Rev.* **99,** 1104 (1955).
10. MORIN F. J. and MAITA J. P., *Phys. Rev.* **94,** 1525 (1954).
11. $\kappa_{el}$ computed from equation 1 is not sensitive to the numerical value of $b$; $b = 2{\cdot}5$ was estimated from the temperature dependence of the thermoelectric power.
12. MACFARLANE G. T., MCLEAN T .P., QUARRINGTON J.E. and ROBERTS V., *Phys. Rev.* **108,** 1377 (1957). Since $\log \sigma_{intr} \sim 1/T$ in the whole temperature range it is a reasonable assumption that $E_g$ has a linear temperature dependence throughout the entire temperature range.

OL.
8
959

*J. Phys. Chem. Solids* Pergamon Press 1959. Vol. 8. pp. 343–345. Printed in Great Britain

# M.3 THERMAL CONDUCTIVITY IN SEMICONDUCTORS

**J. A. KRUMHANSL**

National Carbon Research Laboratories, National Carbon Company, Cleveland, Ohio

THE subject of thermal conductivity in solids is a complex and interesting one for several fundamental reasons. First, it is a transport problem, which automatically involves many parameters; heat content, excitation transfer mechanisms, and structure sensitive factors all affect this property in an essential way. In the second place, particularly at high temperatures, it is quite possible to have several different heat transporting mechanisms operating simultaneously. For example, heat can be transported in a solid at high temperatures by lattice vibrations, electronic excitation, and radiation heat transport—all operating simultaneously.

To discuss in detail the many types of thermal conduction mechanisms possible requires treatment of a wide variety of subjects, such as: lattice vibrations in solids, anharmonicity, defect scattering of phonons, phonon–electron interaction, electron transport, ambipolar diffusion in semiconductors, excitons, dielectric properties and electromagnetic wave propagation. On the other hand a relatively simple model often suffices to estimate thermal conductivity and exhibit the essential features fairly well.

The thermal conductivity $\kappa$ in a variety of cases can be expressed as

$$\kappa = vLC_v$$

where $C_v$ measures the local heat content in the system transporting the heat, $v$ is a characteristic speed of transport (velocity of sound, electron diffusion velocity etc.), and $L$ is a characteristic length for damping out temperature differences. There are obvious oversimplifications in the above expression with regard to geometric factors; but over and above this there is a basic limitation to the "linear" region where $L$ and $C_v$ are independent of $Q$, i.e., of $dT/dx$. This seems to be true in all

practical cases although it would appear to be quite possible in principle that $L$ might well be taken as $L(T, dT/dx)$ which would introduce a non-linear flux dependence of the conductivity.

Considering the various modes of thermal conduction, there is a sharp division between cases wherein thermal excitation requires little energy, and those where considerable energy is involved. The former are important at low temperatures, the latter must be considered at high temperatures. Representative cases are:

Low excitation energy:

(1) classical gas (in porous solids); electrons in semiconductors
(2) electron gas (in metals)
(3) elastic phonons (in all solids)
(4) electromagnetic photons (continuous spectra)
(5) spin wave quanta

High excitation energy:

(1) molecular dissociation
(2) excitons in solids
(3) electron–hole pairs in semiconductors
(4) plasma oscillations in metals.

In passing, it should be noted that some of these heat transporting systems also transport electrical charge, and thereby are coupled with thermoelectric effects.

The above subdivision may also be looked at as one based on the total energy spectrum of the system under consideration. In the former case there is a continuum of energy states immediately above the ground state; in the latter case there is an energy gap between the ground state and the first excited state. Of course the accurate formulation of the theory in any of the above cases will require consideration of a distribution of states so that $v$, $L$, and $C_v$ must be considered as average quantities. This is particularly true for the case of low temperature lattice vibration heat conductivity where scattering of phonons by various imperfections in a solid shows quite characteristically different temperature (frequency) dependences.

There has been considerable discussion of the low temperature thermal conductivity, with reviews by BERMAN,[1] KLEMENS,[2] and OLSEN and ROSENBERG.[3]

While the study of low temperature thermal processes in solids has received considerable attention from a basic point of view, this has not been true for high temperature thermal conductivity until recently. Physicists, restricting considerations largely to electronic and lattice conduction, probably saw little of interest in the rather limited variety of behavior possible at high temperature. Moreover, reproducible measurement of thermal conductivity at high temperatures, particularly on small samples, is a difficult experimental problem. On the other hand there has been some interest in this topic on the part of ceramists (KINGERY[4]) and glass technologists (CZERNY and GENZEL[5]). Recent interest among physicists has been engendered by data reported on semiconductors (JOFFÉ[6]). What is often observed in both ceramics and semiconductors is an "anomalous" rise in the thermal conductivity at high temperatures (at a few hundred degrees Centigrade and up, depending on the material). With these comments we pass on to the subject of high temperature conductivity.

Radiation transport really begins to gain importance at high temperature, being possible but unimportant at lower temperature. A somewhat simplified expression obtained by using appropriate expressions (CZERNY and GENZEL[5]) for $C_v$, $v$, and $L$ is

$$\kappa = \frac{16}{3}\frac{bT^3}{\alpha}n^2 \text{ cal cm}^{-2} \text{ sec}^{-1} \text{ deg}^{-1}$$

where $b = 1{\cdot}37 \times 10^{-12}$ cal cm$^{-2}$ sec$^{-1}$ deg$^{-4}$

$\alpha$ = optical absorption constant in cm$^{-1}$ for wavelength corresponding to peak of black body radiation at $T$

$n$ = index of refraction.

In glasses and refractories this contribution usually does not become important until temperatures of several hundred degrees Centigrade are reached. In semiconductors, on the other hand, the index of refraction is quite high, and radiation conduction can be important at much lower temperatures. As a specific example, consider the thermal conductivity of PbTe (JOFFÉ[6]). Typical minimum values are $\kappa \simeq 5 \times 10^{-3}$ cal cm$^{-2}$ sec$^{-1}$ deg$^{-1}$ at 0°C. The peak of the black body radiation is at $\lambda \simeq 10\ \mu$ for this temperature. The index of refraction (LEVINSTEIN[7]) is about 5. Assuming an absorption constant $\alpha$ of about 10 per cm, one calculates a radiation conductivity $\kappa = 5 \times 10^{-4}$. In good single

crystals $\alpha$ might be lower than this for sufficiently low free carrier concentration.*

We conclude with a brief discussion of another major class of heat transporting mechanisms—systems in which there is an excitation energy $E$ between the ground state and first excited states of the system. Such would be the case for energy transport by electron–hole pairs in semiconductors, excitons, or dissociated gas molecules. One general feature of all these processes can be nicely brought out by a simple model. Assume that all current carrying states, $g$ in number, are at energy level $E$ above the ground state and calculate the specific heat for this two level system. This is

$$C_v = \frac{d}{dT}[gEe^{-E/KT}/(1+ge^{-E/KT})]$$

and for $E/KT \gg 1$, which usually holds,

$$C_v = K\left(\frac{E}{KT}\right)^2 g^2 e^{-E/KT}$$

$$\kappa = KLv\left(\frac{E}{KT}\right)^2 g^2 e^{-E/KT}$$

which shows that in those energy carrying states excited there is an amplification of $(E/KT)^2$ over $K$, the Boltzmann specific heat per degree of freedom. Depending on the specific case $E$ may be the band gap, exciton, dissociation, or ionization energy; the characteristic lengths and velocities are chosen in appropriate manner. Detailed studies of heat conduction by such excitation processes are few and scattered (PRICE[8]) (JOFFÉ[6]), and quantitative experimental checks of these models are nonexistent. However, enough data have been taken on a few materials to indicate order of magnitude agreement with theory. Actually, better information on exciton and energy band structure is also needed.

*Note added at Conference*: A clean separation of radiation thermal conduction and its relation to carrier concentration was shown by JOFFÉ for various samples of tellurium.

* In the case of PbTe measurements referred to had carrier concentrations such that $\alpha$ is probably greater than $10^3$ per cm, so JOFFÉ's data can not be explained by radiation conduction in this case. Similarly in many semiconductor materials the electrical conductivity will be high enough so that free carrier absorption will reduce radiation transfer to negligible values.

## REFERENCES


1. BERMAN R., *Advanc. Phys.* **2,** 103 (1953).
2. KLEMENS P. G., *Handbuch der Physik* **14**, p. 349. Springer, Berlin (1956).
3. OLSEN J. L. and ROSENBERG H. M., *Advanc. Phys.* **2,** 103 (1953).
4. KINGERY W. D. and CHARVAT F. R., *J. Amer. Ceram. Soc.* **40,** 306 (1957).
5. CZERNY M. and GENZEL L., *Glastech. Ber.* **25,** 387 (1952).
6. JOFFÉ A. F., *Canad. J. Phys.* **34,** 1342 (1956).
7. LEVINSTEIN H., *Photoconductivity Conference*, p. 601. John Wiley, New York (1956).
8. PRICE P. J., *Phil. Mag.* **46,** 1252 (1955).


*J. Phys. Chem. Solids* Pergamon Press 1959. Vol. 8. pp. 345–347. Printed in Great Britain

M.4

# THERMAL RESISTANCE DUE TO ISOTOPES AND OTHER POINT DEFECTS

**P. G. KLEMENS**

Division of Physics, C.S.I.R.O., Sydney

THE lattice thermal conductivity of solids[1,2] can be expressed in the form

$$\kappa = \frac{1}{3}\int S(\omega)vl(\omega)d\omega \qquad (1)$$

where $S(\omega)d\omega$ is the contribution to the specific heat per unit volume from lattice waves of frequency $(\omega, d\omega)$, $v$ is the velocity of the waves and $l(\omega)$ the phonon mean free path. The inverse mean free path $1/l$ is composed of contributions from

various scattering processes. At low temperatures, $\kappa \propto T^{3-n}$ if $l(\omega) \propto \omega^{-n}$. This allows the nature of imperfections to be deduced from the temperature variation of the thermal resistance. To a sufficient degree of approximation

$$1/\kappa = W = W_B + W_U + W_I \qquad (2)$$

where at low temperatures the resistivity due to boundaries $W_B \propto T^{-3}$, the resistivity due to Umklapp-processes $W_U \propto T^{-3}e^{-\theta/\alpha T}$, $\alpha \sim 1$, and the resistivity due to structural imperfections $W_I \propto T^m$, where $m \leqslant +1$. At high temperatures, however, $W_U \propto T$.

If the structural imperfections are point defects, $l(\omega) \propto \omega^{-4}$ and the thermal resistance is proportional to the temperature. It is possible to calculate the phonon scattering cross-section from second-order perturbation theory,[3] and from (1) one obtains, after allowing for the mutual interaction among phonons[4]

$$W_P/T = \frac{3(2\pi)^2}{0{\cdot}90}\frac{a^3}{hv^2}nS^2 \qquad (3)$$

where $a^3$ is the volume per unit cell and $n$ the point defect concentration (atom fraction). The parameter $S^2$ depends upon the nature of the defect. If the defect scatters because a defect site has a mass differing by $\Delta M$ from that ($M$) of a normal lattice site,

$$S^2 = \frac{1}{12}\left(\frac{\Delta M}{M}\right)^2. \qquad (4)$$

However, if $n$ approaches unity, the factor $nS^2$ in (3) must be replaced by

$$\epsilon/12 \equiv \frac{1}{12}\sum_a n_a(M_a - M)^2/M^2 \qquad (5)$$

where $M$ is the average mass and $n_a$ and $M_a$ are the concentration and mass of sites of type $a$.

A defect scatters not only in virtue of its mass difference but also because of misfit (changes in the strength of the nearest linkages, as well as distortions of the lattice). Scattering due to misfit is more difficult to calculate, partly because the form of the perturbation Hamiltonian is more complex, partly because the relevant parameters can be inferred only with difficulty.[3] Thus the theory leading to (3) is best tested quantitatively by impurities which scatter mainly because of their mass difference.

While impurities and vacancies produce a thermal resistivity proportional to temperature,[5] the natural isotopic constitution of some solids can also be responsible for an appreciable point defect resistance, as pointed out by SLACK.[6] In such crystals $W$ would not show the exponential temperature variation characteristic of $W_U$ at low temperatures, but rather would decrease with temperature not faster than linearly. While the exponential variation had been observed in some crystals, it had not been observed in others, notably silicon, germanium, potassium chloride and diamond, and SLACK pointed out that in these latter the isotopic mass variation (5) was large: only in solids with $\epsilon < \sim 10^{-4}$ is $W_P$ small enough to allow $W_U$ to be observed in the exponential region. However, the observed resistances exceeded the isotopic resistances calculated from (3) and (5) in all these materials by factors ranging from 2 upwards, so that either the theory leading to (3) must be quantitatively in error or these materials contain other point defects contributing to $W_P$.

The magnitude of the point defect resistance has been shown to be in fair agreement with the theory in the following cases:

KEMP *et al.*[7] deduced the lattice component of thermal conductivity $\kappa_g$ of two copper–gold alloys from their thermal and electrical conductivities. At liquid oxygen temperatures $\kappa_g$ is limited by point defect scattering. The heavy gold atoms scatter phonons mainly in virtue of their mass excess; the misfit of a gold atom in the copper lattice is relatively small. It was shown[8] that the observed resistance was *less* than the resistance from (3) and (5) by factors of order 2, the discrepancy increasing with $\epsilon$. Since in these cases $\epsilon$ was 0·2 and 0·33 respectively, perturbation theory may be expected to break down. On correcting for this empirically by putting

$$W_P = a\epsilon - b\epsilon^2, \qquad (6)$$

it was found that the linear term agreed with the theoretical value from (3) and (5).

TOXEN[9] measured $W_P$ for four germanium–silicon alloys (0·5 per cent, 3 per cent, 6 per cent and 7 per cent Si). He found good agreement with theory for the 0·5 per cent alloy, but for the other alloys the observed values of $W_P$ were again too small by factors ranging from 1·6 to 2 and increasing with $\epsilon$. Since his values of $\epsilon$ are smaller by a factor $\sim 10$, it is not possible to describe the variation of $W_P$ with $\epsilon$ by (6) with the same value of $b$. Whether higher order perturbations are more important in germanium than in copper alloys, or

whether the silicon atoms are not distributed completely at random, remains to be investigated.

In any case the results on these two alloys make it unlikely that (3) and (5) should seriously underestimate the isotope resistance.

A direct test of the theory is provided by the measurements of GEBALLE and HULL[10] on two germanium crystals, one of natural isotopic constitution ($\epsilon = 5{\cdot}7 \times \times 10^{-4}$) and one isotopically enriched to be practically mono-isotopic. In the relevant temperature region (above 15°K) the conductivity of the enriched specimen was higher by a factor $\sim 3$, but was still limited by an apparent point defect resistance. The decrease of resistivity may be identified with the isotope resistance; it has the right temperature dependence and is only a factor 1·2 higher than the value calculated from (3) and (5). In view of the approximations in the theory, this must be considered good agreement.[2] The apparent residual point defect resistance of the enriched specimen corresponds to $nS^2 \simeq (3 \times 10^{-4})/12$, and its removal would be noticeable even in a specimen of natural isotopic constitution. The hypothetical point defect has no effect on the electrical properties. The possibility of dissolved gases was explored by GEBALLE and HULL;[10] however, they found no appreciable increase in the thermal conductivity after regrowing *in vacuo*.

At Sydney, carbon as substitutional impurity was thought to be perhaps an important source of resistance: since germanium is frequently in contact with graphite, a carbon concentration of $10^{-4}$ did not seem impossible. Dr. L. W. DAVIES, of the C.S.I.R.O. Division of Radiophysics, prepared a specimen by twice regrowing a crystal in a silica crucible in vacuo, each time discarding the ends. However, the thermal conductivity[11] showed no improvement, so that either carbon was not present initially in the required concentration or it was not removed by that procedure. The second possibility does not seem very likely. Precision hydrostatic density measurements[12] showed that the silica-grown crystal was slightly denser; however, the relative density change was only $\sim 4 \times 10^{-5}$ so that not enough carbon could have been removed to change the thermal conductivity significantly.

GEBALLE and HULL[10] suggested that this apparent residual point defect resistance is not due to point defects, but due to Umklapp-processes. Owing to a low phase velocity of the phonons in special directions, Umklapp-processes are not frozen out in the exponential manner until temperatures lower than $\sim 15$°K are reached, and $W_U$ varies little faster than linearly with $T$ above that temperature. The general lack of success of attempts to eliminate this resistance lend strong support to their suggestion. Whether a similar explanation holds in the case of other crystals where the observed point defect resistance exceeds the calculated isotope resistance, and whether the theory leading to (3) holds in all crystals, are questions requiring further investigation.

## REFERENCES


1. KLEMENS P. G., *Encyclopaedia of Physics* Vol. 14, p. 198. Springer, Berlin (1956).
2. KLEMENS P. G., *Solid State Physics*, Vol. 7. Academic Press, New York (1958).
3. KLEMENS P. G., *Proc. Phys. Soc.* A**68,** 1113 (1955).
4. KLEMENS P. G., *Proc. Roy. Soc.* A**208,** 108 (1951).
5. SLACK G. A., *Phys. Rev.* **105,** 832 (1957).
6. SLACK G. A., *Phys. Rev.* **105,** 829 (1957).
7. KEMP W. R. G., KLEMENS P. G. and TAINSH R. J., *Aust. J. Phys.* **10,** 454 (1957).
8. KLEMENS P. G., *Proc. Phys. Soc.* A**70,** 833 (1957).
9. TOXEN A. M., *Phys. Rev.* **110,** 585 (1958).
10. GEBALLE T. H. and HULL G. W., *Phys. Rev.* **110,** 773 (1958).
11. BIRCH J. A., KEMP W. R. G. and TAINSH R. J., private communication.
12. BELL G. A., private communication.


*J. Phys. Chem. Solids* Pergamon Press 1959. Vol. 8, pp. 347–353. Printed in Great Britain

M.5

# PHONON-DRAG THERMOMAGNETIC EFFECTS IN N-GERMANIUM

**T. H. GEBALLE, C. HERRING and J. E. KUNZLER**

Bell Telephone Laboratories, Incorporated Murray Hill, New Jersey

**Abstract**—An investigation of the thermomagnetic properties of extrinsic germanium shows that the phonon-drag contribution far outweighs that due to electron diffusion at all temperatures except when near intrinsic. All the results are understandable theoretically in terms of a model which assigns

to each ellipsoidal energy shell in crystal-momentum space an anisotropic phonon-drag Peltier tensor. The temperature and energy dependence of the two components of this tensor give valuable information on the law of phonon–phonon scattering. The transverse high-field magnetoresistance, and at high temperatures the thermomagnetic effects, are found to be sensitive to small amounts of surface conduction.

## 1. INTRODUCTION

THE interesting "phonon-drag" effects observed recently in the low temperature values of the thermoelectric power $Q$ of single-crystal semiconductors have led us to undertake a program designed to sort out and evaluate the important interactions which are involved. These effects and their theoretical interpretation were reviewed at the 1956 conference.[1] The phonon-drag contribution, $Q_p$, to the thermoelectric effect is caused by a build-up of charge carriers in the cold end of the sample—in addition to that caused by their tendency to diffuse from hot to cold which we shall denote by $Q_e$—due to preferential scattering of the charge carriers from hot to cold by the asymmetric distribution of phonons which exists of necessity in the thermal gradient. The measured effect, $Q$, is the sum $Q_e+Q_p$. From elementary considerations $Q_p$ can be shown to be proportional to the strength of the electron–phonon coupling and to the relaxation time for randomization of the motions of the long-wavelength phonons with which the carriers interact. Its study provides an opportunity to learn things about electron–phonon interactions which are not revealed by the study of purely electrical transport, and to study phonon–phonon interactions in a region of the vibrational spectrum different from that which dominates the thermal conductivity.

Previous studies of $Q_p$ itself, and of the effect of changing the sample dimensions on $Q_p$ and on the thermal conductivity[1] (at temperatures high enough so that only low-energy phonons suffered appreciable boundary scattering) have furnished substantial proof for the correctness of the ideas involved. The present investigation of the thermomagnetic properties has furnished new data from which some important microscopic parameters are deduced. The full details of this work are being published elsewhere.[2]

## 2. EXPERIMENT

Measurements have been made of the voltage changes which occur when a magnetic field is applied to a sample of $n$-germanium in a temperature gradient $\nabla T$. These include the Nernst voltage, given by a field $E_y = -BH_z dT/dx$ which is perpendicular to $\nabla T$, and increases in $Q$ measured parallel to $\nabla T$ upon application of $\mathbf{H}$ parallel or perpendicular to $\nabla T$. We shall refer to the latter as the longitudinal or transverse $\Delta Q$ effects respectively. In the above expression $B$ is the Nernst coefficient; $x$, $y$ and $z$ were restricted to symmetry directions of the crystal as well as being at right angles. Measurements of the corresponding galvanomagnetic effects, namely the Hall effect and the longitudinal and transverse magnetoresistances, were also made in order to be able to obtain relevant information all on the same sample.

It has proved convenient to use the sample itself (Fig. 1) as a thermometer both for measuring the absolute temperature (making use of separately determined resistance-temperature characteristics) and for measuring the temperature gradient (making use of known thermoelectric properties in zero magnetic field). The limiting values at low and high magnetic fields have been found by measuring the effects at fixed values of $H$ between 0 and 18,000 G and making parabolic extrapolations to $H = 0$ and $H = \infty$. Typical raw data are shown in Fig. 2.

## 3. THEORY

The theory is formulated[2] in terms of the Peltier tensor $\mathbf{\Pi}$ of the electrons, where $\mathbf{\Pi} \cdot \mathbf{j}$ is the energy flux relative to the Fermi energy accompanying the current. The generalized Kelvin relation connects $\mathbf{\Pi}$ to the thermoelectric power tensor $\mathbf{Q}$:

$$Q_{\alpha\beta}(\mathbf{H}) = \Pi_{\beta\alpha}(-\mathbf{H})/T \qquad (1)$$

The "electron-group" model[3] is used as a basis for the calculations. In this model the possible states of motion of the charge carriers are divided into a number of groups $g$. For a multi-valley semiconductor like $n$-germanium, a natural choice is to let a group $g$ consist of the states in an ellipsoidal shell, of energy range $\epsilon$ to $\epsilon+d\epsilon$, in a particular valley. It is assumed (1) that the distribution function over $g$ is determined by the contribution

$\mathbf{j}_g$ which the states of this group make to the current density, and (2) that the partial currents $\mathbf{j}_g$ are determined by the applied fields in a manner independent of the other groups. Detailed theoretical examination[2] of these conditions indicates that they are favorably met in high-purity *n*-type germanium. Further, the model has been confirmed by experiment to the extent that it leads to valley, which for *n*-germanium is axial symmetry about a [111]-type direction. Thus $\mathbf{\Pi}_g$ is describable in terms of its two principal components $\Pi_{\parallel}(\epsilon)$ along this direction (the high-mass direction) and $\Pi_{\perp}(\epsilon)$, normal to it. Each of these components, in turn, is a sum of an electron-diffusion term (subscript e) and a phonon-drag term (subscript p). Here $\Pi_{e\parallel} = \Pi_{e\perp}$ and is a linear function of $\epsilon$, while

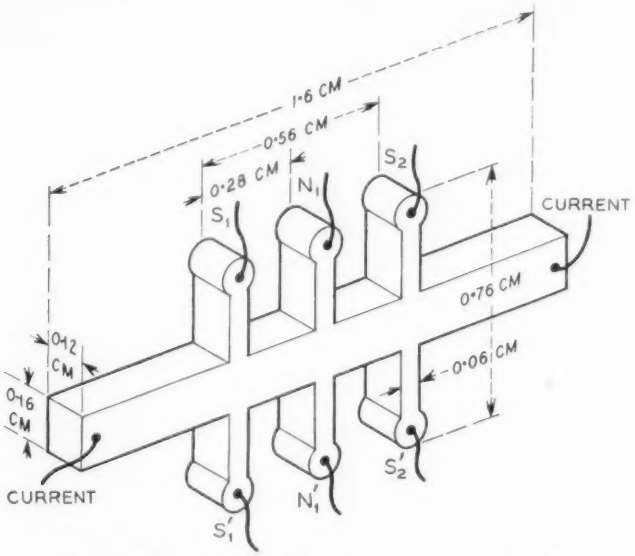


FIG. 1. Schematic drawing of the six-armed samples used. The transverse voltages were normally read across $N_1N_1'$ and the longitudinal voltages across $S_1S_2$. $S_1'$ and $S_2'$ were used with $S_1$ and $S_2$ respectively for checking homogeneity of the sample.

phenomenological relationships which are satisfied quite closely. This is illustrated, for example, by the data shown in Fig. 2, as will be discussed below. Each such group $g$ has its characteristic Peltier tensor $\mathbf{\Pi}_g$, which must be independent of $\mathbf{H}$ if the model is applicable, and the total Peltier tensor of he medium can be compounded out of those of the different groups. Explicitly,

$$\mathbf{\Pi}(\mathbf{H}) = \sum \mathbf{\Pi}_g \cdot \boldsymbol{\sigma}_g(\mathbf{H}) \cdot \boldsymbol{\rho}(\mathbf{H}) \qquad (2)$$

where $\boldsymbol{\sigma}_g$ is the conductivity tensor of group $g$ and $\boldsymbol{\rho} = (\Sigma_g \boldsymbol{\sigma}_g)^{-1}$ is the total resistivity tensor. For any one of the ellipsoidal shells just mentioned the Peltier tensor $\mathbf{\Pi}_g$ must have the symmetry of the

$\Pi_{p\parallel}(\epsilon) > \Pi_{p\perp}(\epsilon)$, as we shall see. As an example of the anisotropy of $\mathbf{\Pi}_p$ consider the longitudinal data shown in Fig. 2. In the electron-group approximation each energy-shell group is characterized by a relaxation-time tensor with components $\tau_{\parallel}$ and $\tau_{\perp}$. The magnetoresistance depends only on the ratio $w = m_{\perp}\tau_{\parallel}/m_{\parallel}\tau_{\perp}$. A single choice, $w = 0{\cdot}061$, fits $\rho_{\infty}/\rho_0$ for all three curves to within a few per cent, as should be the case if the electron group model holds. If all the phonon modes had the same relaxation time and velocity, then $p = \Pi_{p\parallel}/\Pi_{p\perp}$, which is the ratio of crystal momentum loss to the lattice for unit current flow in the high-mass to that in the low-mass direction, would be just equal to $w^{-1}$. If this were true the $\Delta Q_p/Q_p$ curves would coincide with the magneto-

resistance curves. Actually, after subtracting out the electron diffusion terms and converting the $\Delta Q/Q$ data of Fig. 2 to $\Delta Q_p/Q_p$ it is found that the corresponding magnetoresistance curves are similar, but somewhat higher. This simply means that the momentum transferred to the lattice by the low-mass electrons is dissipated less rapidly than that transferred by the high-mass electrons.

were independent of energy. Thus $Q_p$ is determined relatively more by the contributions of the higher energy groups at high fields. The anisotropy factor arises because in zero field the current contribution $\mathbf{j}_g$ for each valley tends to prefer the low-mass directions with a correspondingly low $\Pi_p$, whereas at high fields an increase in the contribution of the high-mass direction must result as a

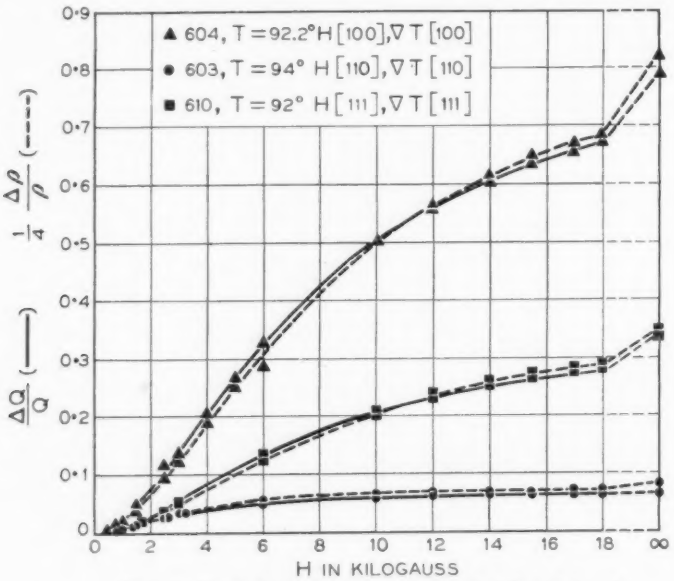


FIG. 2. Typical curves of longitudinal $\Delta Q$ and longitudinal magnetoresistance for three orientations. The values indicated for infinite magnetic field are obtained by a parabolic extrapolation of the high field data against $H^{-2}$.

In reference 2 analytic expressions are obtained for eleven different properties involving $\Delta Q$ and $B$ in crystallographically nonrelated directions in the limits of zero and infinite magnetic field. The analytic expressions depend upon the product of a factor $f(w, p)$, which we shall call the anisotropy factor, and a factor dependent on the energy variation of $\mathbf{\Pi}_{pg}$ and $\mathbf{m}^* \cdot \boldsymbol{\tau}^{-1}$ which we shall call the energy factor. The energy factor arises in the transverse infinite-magnetic-field cases because the current comes more from high-energy electrons at high fields than at low fields. This is because in zero field the relaxation time $\tau$ increases with decreasing energy, whereas at infinite field the distribution of current over the energy groups approaches that which would obtain at $H = 0$ if $\tau$ consequence of the Lorentz force on the electrons. Therefore relatively more crystal momentum is fed into the phonon system and $Q_p$ increases.

The longitudinal increase in $Q$ depends only on the anisotropy factor because the distribution of the $\mathbf{j}_g$'s in energy is the same for $H = 0$ and $\infty$. Fig. 3 shows the dependence of $Q_p(\infty)/Q_p(0)$ on $p$ using the empirical value 0·06 for $w$ (solid curves), and a value $w = 0{\cdot}08$ (dotted curves), the latter being to illustrate the dependence on $w$. The anisotropy factors from which these curves are calculated are also given. It is found that the empirical values of $Q_p(\infty)/Q_p(0)$ obtained from data such as Fig. 2 correspond to a value $p \sim 9{\cdot}5$ for all three directions.

Once $p$, the anisotropy of the Peltier tensor, has

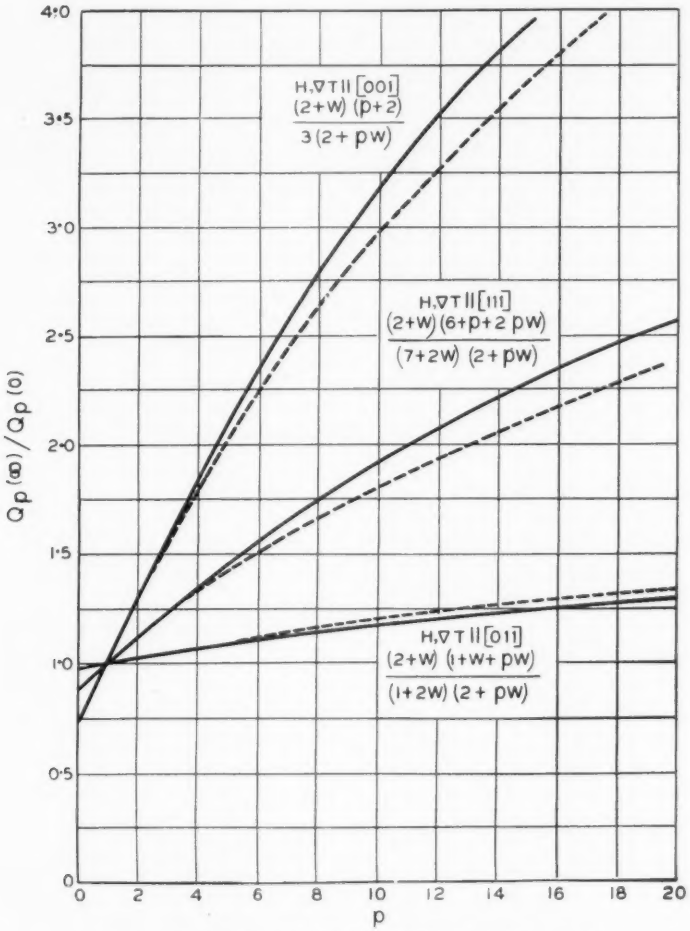


FIG. 3. Dependence of $Q_p(\infty)/Q_p(0)$ on $p$ for **H** parallel to $\nabla T$ for three orientations in $n$-germanium. The analytic functions are given. The full curves apply for $w = m_\perp \tau_\parallel / m_\parallel \tau_\perp = 0{\cdot}06$, the dashed values for $w = 0{\cdot}08$.

been determined, the transverse high-field cases can be analyzed and the energy factors determined. The same parameters enter into the low-field longitudinal and transverse $\Delta Q$ effects and the Nernst effect. The low-energy electrons contribute more heavily in the low-field cases. In the second part of reference 2, the detailed analysis of all these data is carried out; here, we have just attempted to illustrate the method.

## 4. CONCLUSIONS

Some of the important deductions which result from the detailed analysis are:

(1) The phonon-drag Peltier coefficient $\mathbf{\Pi}_p$ decreases slowly with increasing electron energy. In fact, $\Pi_{p\perp}$ is proportional to about $\epsilon^{-0{\cdot}08}$ and $\Pi_{p\parallel}$ to about $\epsilon^{-0{\cdot}3}$ at liquid nitrogen temperatures. The significance of these energy dependences is in what they tell about phonon–phonon scattering. The contribution to the heat flux from an energy-shell group $g$ of energy $\epsilon$ is, for the parallel direction,

$$\Pi_{p\parallel} j_{g\parallel} \propto [\tau_\parallel(\epsilon)]^{-1} m^*_\parallel j_{g\parallel} \tau_{ph}(\bar{q}, \parallel), \qquad (3)$$

and a similar equation holds for the perpendicular

direction; here $\tau_{ph}(\bar{q}, \|)$ or $\tau_{ph}(\bar{q}\perp)$ is the relaxation time of an "average" phonon-drag phonon. This equation follows from the proportionality of heat flux to crystal momentum for low-frequency phonons, hence to the product of the average relaxation time with the rate of loss of crystal momentum by the electrons to these phonons. If we take $\tau_{ph}(\bar{q}) \propto \bar{q}^n$, with $\bar{q} \propto \epsilon^{\frac{1}{2}}$ and $\tau(\epsilon) \propto \epsilon^{-\frac{1}{2}}$, (3) gives

$$\Pi_{pg} \propto \epsilon^{(1+n)/2}. \tag{4}$$

Comparing (4) with the empirically-determined energy variations quoted above, we can conclude that the average phonon interacting with an electron in the low-mass direction has $\tau_{ph}(\bar{q}, \perp)$ proportional to $\omega^{-1\cdot15}$, where $\omega$ is the frequency, and in the high-mass direction has $\tau_{ph}(q, \|)$ proportional to $\omega^{-1\cdot6}$. It has been shown[1] that if three-phonon collisions are the dominant source of relaxation then in the limit as $q$ or $\omega$ approaches zero

$\tau_{ph} \propto \omega^{-2}$ for longitudinal modes

$\tau_{ph} \propto \omega^{-1}$ for transverse modes.

Thus the data suggest that $\tau_{ph}(\|)$ is determined in a large part by longitudinal phonons and $\tau_{ph}(\perp)$ principally by transverse ones. Deformation-potential theory predicts that transverse modes should affect $\Pi_{p\perp}$ more than $\Pi_{p\|}$. However for them to dominate $\Pi_{p\perp}$ they must have relaxation times larger than longitudinal modes of comparable frequency; this had not been expected.

(2) The anistropy $p$ of the phonon-drag Peltier tensor is $\Pi_{p\|}/\Pi_{p\perp} \sim 9{\cdot}5$. This rather large anisotropy is less than the anisotropy $1/w = m_\| \tau_\perp / m_\perp \tau_\|$ which measures the anisotropy of the rate at which a given current feeds crystal momentum into the phonon system. Therefore the phonons interacting with the electrons in high-mass directions must dissipate their momentum faster, i.e., have lower relaxation times than those interacting in low-mass direction. This is in part due to the inverse relationship between $\tau_{ph}$ and $q$ since the large-mass electrons interact with modes of larger $q$ than the low-mass electrons, as well as depending on the magnitude of the $\tau_{ph}$'s of the longitudinal and transverse branches. Also, anisotropy of the $\tau_{ph}$'s within any one branch must be considered.

(3) Over the range 60° to about 200°K for which the analyses have been made, only very moderate temperature variations in the ratio of $\Pi_{p\|}$ to $\Pi_{p\perp}$ and in their energy dependence have been found. Phonon scattering must be chiefly due to three-phonon processes over most of this range; for if four-phonon processes were at all appreciable in the lower part of the range they would dominate at higher temperatures, and almost certainly cause an abrupt change in the observed temperature variations.

### 5. SURFACE DAMAGE

A number of side issues were investigated in order to obtain empirical values of various possible complicating effects which must be known before the raw experimental data can be compared with theory. These include, among other things, the magnitude of the effect of orbital quantization of the conduction band states by the magnetic field, the effect of the sample side arms (Fig. 1) in distorting the linear flow of current, the effect of impurity scattering, and the effect of concentration fluctuations in the crystal. In trying to estimate the first of these effects we found a value of transverse magnetoresistance for **H** in a [100] direction much higher than that predicted by the electron-group model and many times the expected effect of orbital quantization deduced from other evidence. If the large Hall field present were short-circuited by a surface conduction of only a few-thousandths of the bulk conduction of the sample such an effect could occur. This was confirmed by etching about a mil off the originally sandblasted surface and finding a marked reduction in $\Delta\rho/\rho$, and then repeating the sandblasting-etching cycle. It seems clear that reliable high-field transverse magnetoresistance measurements can be made only when there is no path for shorting out the large Hall fields.

The low-field Nernst effect has been found to be extremely sensitive to surface conduction just below the intrinsic range, and the high-field effect at all temperatures. It is believed that a more detailed study of this sensitivity might well yield valuable information about surface conduction. For example, the sign of $B$ should be negative above 175°K when the electron-diffusion contribution to the Nernst effect exceeds that of phonon drag. It has been reported by other workers to be positive; however, it has been found by us to be negative as expected when surface conduction is believed to be negligible, but positive and of

VOL
8
195

variable magnitude for some high-purity samples when sandblasted. It is estimated that a surface conduction of only a few per cent of the bulk conduction can be responsible.

### REFERENCES

1. HERRING C., *Halbleiter und Phosphore* (edited by M. SCHÖN and H. WELKER), p. 184. Vieweg, Braunschweig (1958).
2. HERRING C., GEBALLE T. H. and KUNZLER J. E. *Phys. Rev.*, **111**, 36 (1958); *Bell Syst. Tech. J.* to be published.
3. HERRING C. and VOGT E., *Phys. Rev.* **101**, 944 (1956).

*J. Phys. Chem. Solids* Pergamon Press 1959. Vol. 8. pp. 353–358. Printed in Great Britain

VOL. 8 1959

M.6

# THEORY OF THERMOELECTRIC AND THERMOMAGNETIC EFFECTS IN NONPOLAR ISOTROPIC SEMICONDUCTORS

J. APPEL

OSRAM, Studiengesellschaft, Augsburg, Germany

## 1. INTRODUCTION TO THE PHYSICAL AND MATHEMATICAL PROBLEM

IN the theory of electrical and thermal transport phenomena of nonpolar isotropic solids one is concerned with two major components, the electrons and the longitudinal acoustical phonons. The possible scattering processes are: electron–electron, electron–phonon and phonon–phonon. If the corresponding collision operators are known, the steady state distribution functions $f$ of the electrons and $N$ of the phonons must be determined simultaneously as solutions of the two Boltzmann equations:

$$\left(\frac{\partial f}{\partial t}\right)_{\text{coll}}^{\text{el–ph}} + \left(\frac{\partial f}{\partial t}\right)_{\text{coll}}^{\text{el–el}} = -\left(\frac{\partial f}{\partial t}\right)_{\text{field}} \quad \text{(1a)}$$

$$\left(\frac{\partial N}{\partial t}\right)_{\text{coll}}^{\text{ph–el}} + \left(\frac{\partial N}{\partial t}\right)_{\text{coll}}^{\text{ph–ph}} = -\left(\frac{\partial N}{\partial t}\right)_{\text{temp}} \quad \text{(1b)}$$

In the conventional theory of BLOCH *et al.* both equations are treated independently of each other. Therefore, when calculating $f$ it is assumed that the phonons are in equilibrium; that is, that $N = N_0$, where $N_0$ is the Bose function.

In the same way, when solving (1b) for $N$, which determines the lattice heat conductivity, one assumes $f = f_0$, where $f_0$ is the Fermi function.

The need to check the theory of transport phenomena, taking into account the deviation of both the electrons and the phonons from equilibrium, was necessitated by experiments. FREDERIKSE,[1] and later GEBALLE and HULL[2] observed a strong increase of thermoelectric power in Ge single crystals at low temperatures. The effect is caused by the anisotropy of the phonon distribution and the corresponding anisotropy of the transition probabilities for electron scattering. The electrons are scattered preferentially in the direction of $-\text{grad } T$.

HERRING[3] first calculated the additional thermoelectric power considering the energy flux and the crystal momentum of the phonon system. Later, SONDHEIMER[4] showed explicitly that equations (1a, b) have to be solved in a consistent fashion, taking into account exactly the deviation of both distribution functions. Otherwise the Kelvin relations for the thermoelectric effects may be violated.

With simple but consistent assumptions, i.e. spherical energy surfaces and isotropic relaxation times for both electrons and phonons, we have solved the Boltzmann equations analytically for nondegenerate semiconductors in some important limiting cases, and iteratively with numerical methods in general cases. Electron–electron

scattering may be neglected. Scattering of electrons by ionized impurity atoms and scattering of phonons at grain boundaries are described by the appropriate mean free paths.

The mathemetical procedure of solving the two coupled integral equations for the steady state distribution functions $f$ and $N$, which are linear in first approximation, have already been described.[5] In principle, the solution depends on expanding the perturbation $\Phi(\mathbf{k}) = f - f_0$ and $\psi(\mathbf{q}) = N - N_0$ in a power series of a coupling parameter $\lambda$. The parameter $\lambda$ is given by

$$\lambda = 4,48 \cdot 10^{12} \left(\frac{m^*}{m}\right)^{\frac{3}{2}} \frac{T^{\frac{5}{2}} \mu_g}{u_0 l_g n}$$

where $l_g$ represents the mean free path and $u_0$ the sound velocity of low-frequency phonons, which interact essentially with the nondegenerate electron gas (HERRING[3]). $\mu_g$ is the lattice scattering mobility of the electrons. The coupling parameter $\lambda$ determines the relative influence of phonon–electron scattering on the deviation of phonons from equilibrium. In the limit $\lambda = \infty$, the deviation $\psi(\mathbf{q})$ is determined only by the lattice term, which is proportional to $(\hbar u_0 l_g / T)$ grad $T$. The smaller the parameter $\lambda$, the greater is the reduction of the lattice term owing to electron–phonon interaction. When $\lambda \gtrsim 1$, which is the case in nondegenerate semiconductors, we obtain:

$$\Phi|\mathbf{k}| = \phi_0 + \sum_1^\infty \phi_j \left(\frac{1}{\lambda}\right)^j \tag{2a}$$

$$\Psi|\mathbf{q}| = \psi_0 + \sum_1^\infty \psi_j \left(\frac{1}{\lambda}\right)^j \tag{2b}$$

The coefficients $\phi_0$, $\psi_0$ represent the drift terms. The coefficients $\phi_j$, $\psi_j (j \geqq 1)$ are not independent of each other, they have to be calculated in a consistent fashion as functions of the wave vectors $\mathbf{k}$, $\mathbf{q}$ and the external fields $\boldsymbol{E}$, $\mathbf{H}$, $-$grad $T$. A necessary consequence of the preliminary statement (2a, b) is, that the transport quantities are divided into two parts, an electronic and a lattice part. They are coupled by $\lambda$.

There are two important cases in which we can obtain the exact values for $\Phi$ and $\psi$. In the absence of an electric current, these are given by:

(1) $\lim \lambda = \infty$, $|\boldsymbol{H}|$ arbitrary value

(2) $\lim |\boldsymbol{H}| = \infty$, $\lambda$ arbitrary value

Under these conditions the Boltzmann equations are decoupled. Thus, the thermoelectric power $Q$ for (1) and lattice scattering of the electrons only is given by:

$$Q = -\frac{1}{eT}(2kT - \zeta) - \frac{u_0 l_1}{T \mu_g}$$

This result is in accordance with the Kelvin relation $Q = \pi / T$.

## 2. SOME RESULTS FOR THE THERMOELECTRIC AND THE THERMOMAGNETIC EFFECTS

The absolute thermoelectric power (t.p.), $Q$ and the Ettingshausen Nernst coefficient, $B$ (E.N.c.) are defined by:

$$\frac{\left(E_1 + \frac{1}{e}\frac{\partial H}{\partial x_1}\right)}{(\partial T / \partial x_1)} = Q; \quad -\frac{\left(E_2 + \frac{1}{e}\frac{\partial H}{\partial x_1}\right)}{(H/C)/(\partial T / \partial x_1)} = B$$

$F_j$ is the strength of an electric field in $x_j$-direction, $H$ is the strength of a magnetic field in $x_3$-direction, $-|e|$ = electron charge.

When a magnetic field is present we have to distinguish between the adiabatic effects (index a, no heat transfer in $x_2$-direction) and the isothermal effects (index i, $\partial T / \partial x_2 = 0$). We find a general relation connecting these:

$$Q_a = Q_i + B_i \frac{H}{c} \frac{\partial T}{\partial x_2} \Big/ \frac{\partial T}{\partial x_1}; \quad B_a = B_i - Q_i \frac{c}{H} \frac{\partial T}{\partial x_2} \Big/ \frac{\partial T}{\partial x_1}$$

The detailed investigation of heat conductivity yields $\partial T / \partial x_2 \ll \partial T / \partial x_1$ if:

(1) The electronic part $\kappa_e$ of the heat conductivity is small compared with the lattice part $\kappa_g$ *and* if $\kappa_g$ is not markedly reduced by phonon–electron scattering processes.

(2) The effects are measured in strong magnetic fields.

In zero field case $H = 0$ the lattice component of t.p. $Q_g(\lambda)$ is shown in Fig. 1. The parameter $\beta^2$ measures the relative influence of ion-scattering on the mobility $\mu$ of the electrons. $\mu_g$ and $\mu_i$ are the

electron mobilities corresponding to lattice and impurity scattering. When $\lambda$ decreases the lattice component of the t.p. $Q_g$ becomes smaller owing to the increasing reduction of the deviation $\psi_0$ of the phonons as consequence of phonon–electron scattering. This result is in accordance with experiments of GEBALLE and HULL,[2] e.g. on $p$-silicon with different impurity concentrations. Some of and limited $\lambda$-values are shown in Figs. 2 and 3. If impurity scattering takes part, one should observe changes of sign. This result holds likewise, if the screening effect is taken into account. Since screening reduces the $\beta^2$-values, the changes of sign shift to stronger magnetic fields. The E.N.c. part $B_1$ in an isotropic or two carrier model can only change its sign if $\beta^2 \neq 0$. In order to compare

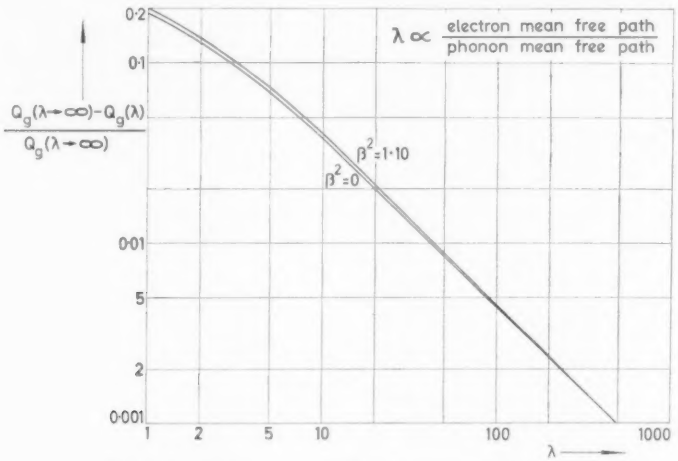


FIG. 1. Lattice component $Q_g$ of thermoelectric power as a function of $\lambda$.

the results for the heat conductivity $\kappa$ in zero field limit are:

$$\kappa_e(N = N_0) < \kappa_e(N \neq N_0);\ \kappa_g(f = f_0) > \kappa_g(f \neq f_0);$$

$$\delta\kappa_g = \kappa_g(f = f_0) - \kappa_g(f \neq f_0)$$

$$= \frac{2}{9\pi}\frac{ne}{T\mu_g}(u_0 l_g)^2 \text{ if } \lambda \gg 1$$

For $H \neq 0$ and $\lim \lambda = \infty$, the effects may be calculated analytically in weak and strong magnetic fields. In weak fields the coefficients of the relative change of the two parts of t.p. and E.N.c. are proportional to $H^2$. Their sign depends on the scattering mechanisms. In strong magnetic fields the effects tend to saturation values. For example with $\beta^2 = 0$ (lattice scattering only) these values become:

$$\lim_{H\to\infty}\frac{Q}{\infty} = -\frac{1}{eT}\left(\frac{5}{2}\frac{k}{e}\zeta\right) - \frac{32}{9\pi}\frac{u_0 l_g}{T\mu_g};\ \lim_{\lambda\to\infty} B = 0$$

Some of the results for intermediate field strengths our results with the experimental data, we show in Fig. 4 the field dependence of t.p. for a $p$-Ge single crystal at 80°K as measured by ERDMANN and SCHULTZ of our laboratories. The dotted curves represent the calculated changes of both parts of t.p. for a one carrier model. If one takes into account the degeneracy of the upper valence band level and uses an isotropic two carrier model, one gets satisfactory agreement between theory and experiment in weak and intermediate magnetic fields just as in the case of galvanomagnetic effects.[6]

Fig. 5 shows the anisotropy of t.p. in $n$-Ge as measured by the above authors at 80°K ($\beta^2 = 0$). To discuss these results we must extend our investigation to anisotropic semiconductors. In the limit $\lambda = \infty$, the case of interest here, the Boltzmann equations are decoupled, and therefore may be solved without difficulty, using the method of Abeles and Meiboom. In agreement with Erdmann we found that in weak and strong magnetic fields the thermomagnetic effects are isotropic in spite of

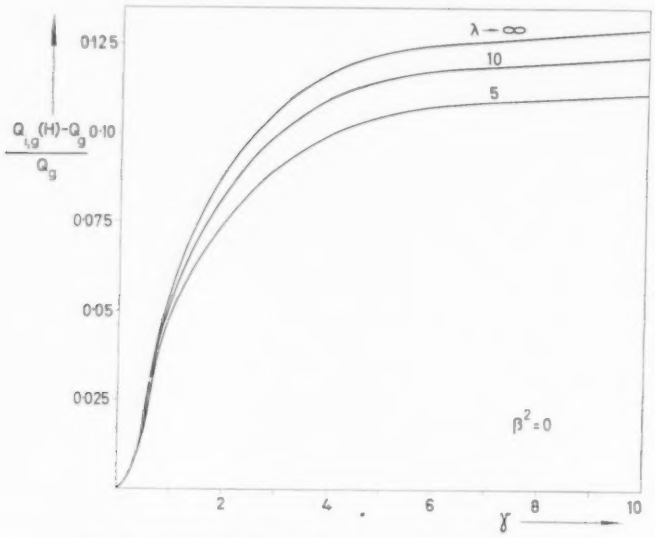


FIG. 2. Change of phonon drag term with magnetic field strength $\gamma = (3\sqrt{\pi}/4)\,10^{-8}\mu_g H$, relative change of component $Q_{i,g}$ of thermoelectric power as a function of $H$.

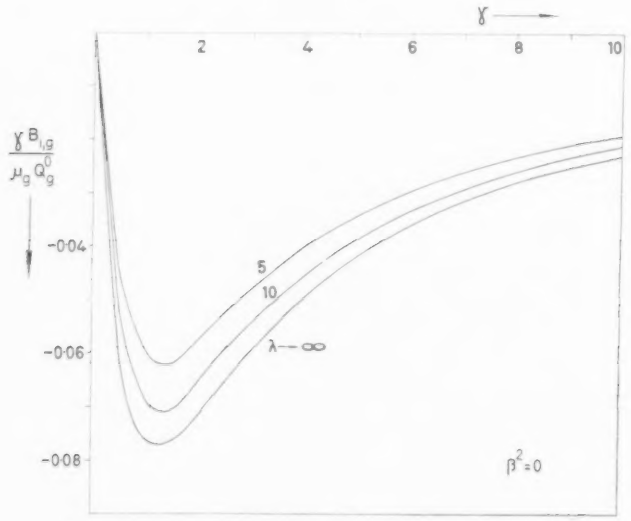


FIG. 3. Phonon drag part of Ettingshausen–Nernst–Koeffizient $B_{i,g}$ as a function of magnetic field strength $\gamma=(3\sqrt{\pi}/4)\,10^{-8}\mu_g H$; $\beta^2=0$, change of E.N.c., part $B_{i,g}$ with $H$.

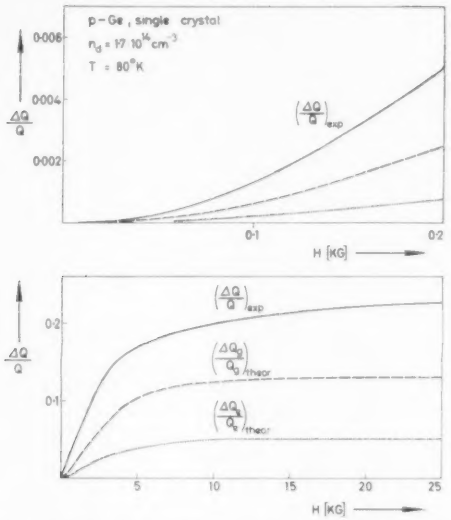


FIG. 4. Measured (80°K) and calculated ($\beta^2 = 0$, one carrier model) relative change of t.p. $Q_i$ for a $p$-Ge single crystal.

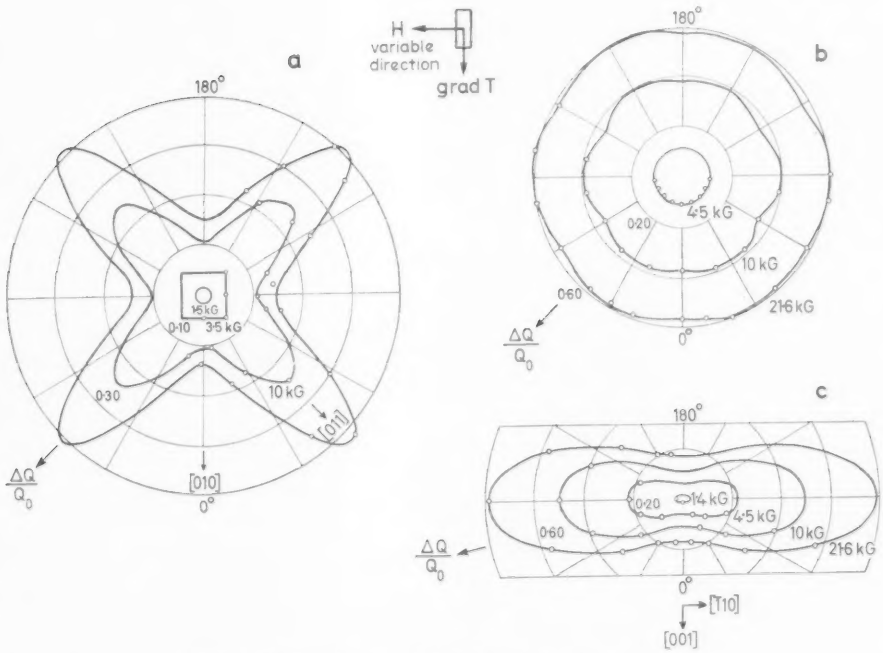


FIG. 5. Anisotropy of relative change of thermoelectric power, $T = 80°K$. grad $T$: $a$[100], $b$[111], $c$[110]. After J. ERDMANN and H. SCHULTZ.

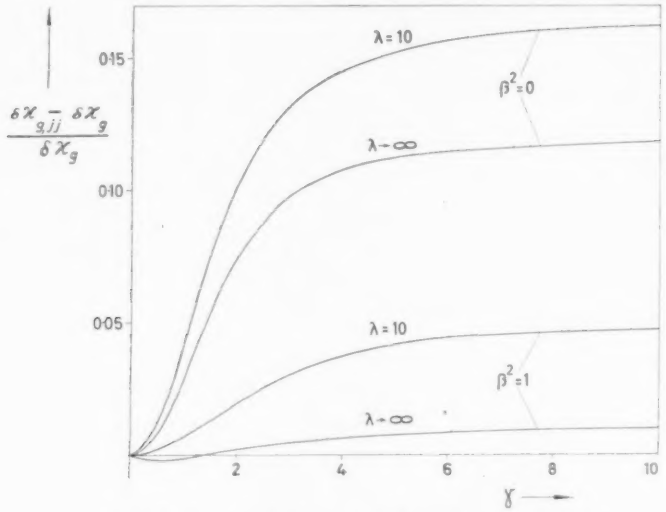


FIG. 6. $\delta\kappa_g$ = reduction of isolator heat-conductivity owing to scattering of phonons by electrons, relative change of $\delta\kappa_g$ with $H$.

the energy band anisotropy. We suggest that this discrepancy between theory and experiment is caused by the assumption of isotropic relaxation times $\tau_{el} = \tau_{el}(E)$ and $\tau_{ph} = \text{const.}$ (independent of $\mathbf{q}$). To clear up the situation it would be useful to investigate the longitudinal t.p. of $n$-Ge. The longitudinal t.p. should have a maximum at intermediate field strengths and should go to zero in strong fields.

*Acknowledgment*—I wish to thank Prof. KRAUTZ for his interest.

REFERENCES

1. FREDERIKSE H. P. R., *Phys. Rev*, **91,** 491 (1933).
2. GEBALLE T. H. and HULL G. W. *Phys. Rev.* **98,** 940; (1955); *Ibid.* **94,** 1134 (1954).
3. HERRING C., *Phys. Rev.* **96,** 1163 (1954).
4. SONDHEIMER E. H., *Proc. Roy. Soc.* **234,** 391 (1956).
5. APPEL J., *Z. Naturf.* **12**a (1957) 410; *Ibid.* **13**a, 386 (1958).
6. WILLARDSON R. K., HARMAN T. C. and BEER A. C. *Phys. Rev.* **96,** 1512 (1954).

*J. Phys. Chem. Solids* Pergamon Press 1959. Vol. 8. pp. 358–362. Printed in Great Britain

M.7

# SUR LES EFFETS DE TRANSPORT DANS L'ANTIMONIURE D'INDIUM*

**M. RODOT**

Laboratoire du Magnétisme et de Physique du Corps Solide du C.N.R.S., Bellevue, (S. & O.) France

LE mécanisme de dispersion des électrons dans l'antimoniure d'indium est actuellement encore controversé. Les premiers travaux sur ce composé utilisaient implicitement ou explicitement l'hypothèse "classique" de la dispersion par les phonons acoustiques, combinée avec la dispersion par les impuretés ionisées; en 1957 EHRENREICH[1] au

* Not presented at Conference.

contraire, par l'étude de la mobilité, conclut à la prédominance de la dispersion par les phonons optiques, dite dispersion "polaire".

Les mesures de résonance de cyclotron ont fourni très directement une valeur précise de la masse efficace des électrons $m_n = 0{\cdot}013m_0$. Cette valeur est difficilement compatible avec les mesures d'effet thermoélectrique dans l'hypothèse de la dispersion "classique".

Nous avons tenté d'apporter des éclaircissements à cette question par l'étude des effets thermomagnétiques. La théorie de ces effets est élaborée avec les hypothèses suivantes: (1) les effets sont supposés "isothermes", c'est-à-dire que, le gradient de température $\Delta T$ étant dirigé suivant $0x$ et le champ magnétique $H$ suivant $0z$, il n'apparaît pas de gradient de température suivant $0y$; (2) la bande de conduction est conforme au modèle de KANE, la masse efficace étant $m_n = 0{\cdot}013m_0$ au bas de la bande; (3) il existe un seul mécanisme de dispersion, caractérisé par un temps de relaxation $\tau$ lié à l'énergie $\epsilon$ de l'électron par $\tau \propto \epsilon^r$. Cette dernière hypothèse n'est pas valable dans le cas de la dispersion "polaire".

Considèrons d'abord les effets dûs aux seuls *électrons* libres. Le pouvoir thermoélectrique $Q$ et le coefficient de Nernst $B$ sont définis par:

$$Q = \frac{E_x - d\zeta/qdx}{dT/dx}; \; BH = \frac{E_y}{dT/dx} \qquad (1)$$

($q$ = charge de l'électron, $E$ = champ électrique, $\zeta$ = énergie de Fermi).

Résolvant l'équation de Boltzmann en tenant compte de nos conditions aux limites, nous obtenons:

$$\frac{q}{k}Q = \frac{1}{kT}\frac{(K_2/K_1)+(L_1/K_1)^2(L_2/L_1)}{1+(L_1/K_1)^2} - \eta \; ; \qquad (2)$$

$$\frac{q}{k}BH = \frac{1}{kT}(L_1/K_1)\frac{(K_2/K_1)-(L_2/L_1)}{1+(L_1/K_1)^2}$$

où $k$ = constante de Boltzmann, $\eta = \zeta/kT$ et:

$$\begin{cases} K_1 = \displaystyle\int_0^\infty \frac{\tau(dn/d\epsilon)d\epsilon}{1+(\alpha\tau H)^2}; & K_2 = \displaystyle\int_0^\infty \frac{\tau\epsilon(dn/d\epsilon)d\epsilon}{1+(\alpha\tau H)^2} \\ L_1 = \displaystyle\int_0^\infty \frac{\tau\alpha\tau H(dn/d\epsilon)d\epsilon}{1+(\alpha\tau H)^2}; & L_2 = \displaystyle\int_0^\infty \frac{\tau\epsilon\,.\,\alpha\tau H(dn/d\epsilon)d\epsilon}{1+(\alpha\tau H)^2} \end{cases} \qquad (3)$$

($\alpha = q/m_n c$; $dn$ = nombre d'électrons libres d'énergie cinétique comprise entre $\epsilon$ et $\epsilon+d\epsilon$). Les résultats s'experiment commodément en fonction du paramètre de champ $y = \mu_H H/c$ ($\mu_H$ = mobilité de Hall, $c$ = vitesse de la lumière).

*Cas des champs magnétiques faibles* ($y \ll 1$)

On n'introduit qu'une faible erreur en calculant les intégrales (3) comme si la bande de conduction était parabolique, *à condition que le niveau de Fermi $\zeta$ soit calculé en tenant compte de la structure exacte, non parabolique, de la bande.* Si nous posons:

$$\mathcal{F}_i = (i+1)\int_0^\infty \frac{x^i dx}{1+\exp(x-\eta)} \quad (x = \epsilon/kT) \qquad (4)$$

l'effet magnétothermoélectrique (ou MTE) $\Delta Q = Q(H) - Q(0)$ et le coefficient de Nernst $B$, aux champs magnétiques faibles, s'écrivent

$$\begin{cases} \Delta Q(0) = (k/|q|)y^2(A_1+A_2) \\ B(0) = (k/|q|)(y/H)A_1 \end{cases} \qquad (5)$$

avec:

$$\begin{cases} A_1 = \dfrac{\mathcal{F}_{\frac{3}{2}+r}}{\mathcal{F}_{\frac{1}{2}+r}} - \dfrac{\mathcal{F}_{\frac{3}{2}+2r}}{\mathcal{F}_{\frac{1}{2}+2r}} \\ A_2 = \dfrac{\mathcal{F}_{\frac{3}{2}+3r}\mathcal{F}_{\frac{1}{2}+r} - \mathcal{F}_{\frac{3}{2}+r}\mathcal{F}_{\frac{1}{2}+3r}}{(\mathcal{F}_{\frac{1}{2}+2r})^2} \qquad (r \neq -\tfrac{1}{2}) \end{cases} \qquad (6)$$

Les formules (5) se simplifient si la distribution d'électrons est très dégénérée (cas "métallique") ou, au contraire, obéit à la statistique de Boltzmann (cas "classique"):

$$\Delta Q_m(0) = (k/|q|)(\pi^2 ry^2/3\eta); \; B_m(0) = (-k/|q|H)(\pi^2 ry/3\eta) \text{(cas "métallique")} \qquad (7)$$

$$\Delta Q_c(0) = (k/|q|)ry^2(\theta-1); \; B_c(0) = (-k/|q|H)ry \text{ (cas "classique")} \qquad (8)$$

($\theta-1$) désigne un nombre, combinaison de fonctions eulériennes, qui est positif et faible, et qui croît avec $r$.

L'effet Nernst et l'effet MTE théoriques pour des champs magnétiques infiniment faibles, donnés par les formules (5), sont représentés sur la Fig. 1. Il est possible aussi de les déterminer expérimentalement. Des mesures ont été faites[2] sur des échantillons de type $n$, pour lesquels $\eta$ était compris entre $-1$ et $+5$, à des températures comprises entre 77°K et 350°K; l'appareillage était tel que la condition (1) ci-dessus était exactement remplie; les relations $\Delta Q \propto y^2$ et $BH \propto y$ étaient bien vérifiées. Dans tous les cas, on a trouvé que les points représentatifs des mesures étaient compris entre les courbes $r = 0$ et $r = +1/2$. Ceci semble incompatible avec l'hypothèse que le mécanisme de dispersion est une combinaison de la dispersion par les phonons acoustiques et par les impuretés ionisées, dans la mesure où l'on n'a jamais trouvé de points voisins des courbes $r = -1/2$ (même à haute température), ni voisins des courbes $r = +3/2$ (même à basse température). Cependant aucune conclusion sûre ne peut encore être tirée. En effet:

(1) la théorie des effets thermomagnétiques dans le cas d'une dispersion mixte, bien qu'élaborée partiellement par BEER *et al.*[3] (avec des conditions aux limites différentes des nôtres), ne peut encore conduire à des prévisions quantitatives dans le cas de l'antimoniure d'indium où l'emploi de la statistique de Fermi–Dirac est le plus souvent nécessaire;

(2) la théorie des effets thermomagnétiques dans le cas de la dispersion polaire n'est pas non plus élaborée. On sait que, dans ce cas, il n'y a pas de temps de relaxation; il est donc nécessaire de traiter le problème par la méthode déjà employée par EHRENREICH[1] en l'absence de champ magnétique. Qualitativement, les effets thermomagnétiques résultent alors d'un compromis entre l'action des électrons très énergiques ($\epsilon \gg h\nu_1$, $h\nu_1$ étant l'énergie des vibrations optiques de nombre d'onde nul) pour lesquels $r = +1/2$, l'action des électrons dont l'énergie $\epsilon$ est juste supérieure à $h\nu_1$, pour lesquels $r$ est grand et négatif,[4] et celle des électrons dont $\epsilon < h\nu_1$, pour lesquels il n'existe pas de temps de relaxation.

*Cas des champs magnétiques quelconques*

Revenons à la théorie des effets thermomagnétiques dans le cas où existe un temps de relaxation $\tau \propto \epsilon^r$. On peut encore donner une formule exacte pour les champs infiniment grands:

$$\begin{cases} \dfrac{q}{k}Q(\infty) = \dfrac{\mathfrak{F}_3(\eta)}{\mathfrak{F}_1(\eta)} - \eta \\ B(\infty) = 0 \end{cases} \tag{9}$$

L'intérêt de ce résultat est qu'il ne dépend pas du mode de dispersion (cette situation est la même que pour la constante de Hall); mais les formules (9) ne deviennent valables que dans des champs magnétiques en général supérieurs à 10 kG.

Aux champs magnétiques compris entre 1000 et 7 000 G, c'est seulement dans le cas de l'approximation "métallique" qu'on peut écrire une formule simple:

$$\begin{cases} \Delta Q(H) = \dfrac{y^2}{1+y^2}\Delta Q(\infty) \\ B(H) = \dfrac{1}{1+y^2}B(0) \qquad \text{(cas "métallique")} \\ \Delta Q(\infty) = -E(0)c/\mu_H = \dfrac{k}{|q|}\dfrac{r\pi^2}{3\eta} \end{cases} \tag{10}$$

L'expérience vérifie assez bien les formules (10).

*Cas des échantillons à conductivité mixte (effet ambipolaire)*

Sur un échantillon de type $p$, on observe[2] des effets thermomagnétiques beaucoup plus importants, qui passent par un maximum à la température où les contributions des électrons et des trous, $\sigma_1$ et $\sigma_2$, à la conductivité totale $\sigma$, sont égales. Si le champ magnétique est assez faible pour que les effets des trous seuls soient négligés et que les effets des électrons seuls soient donnés par

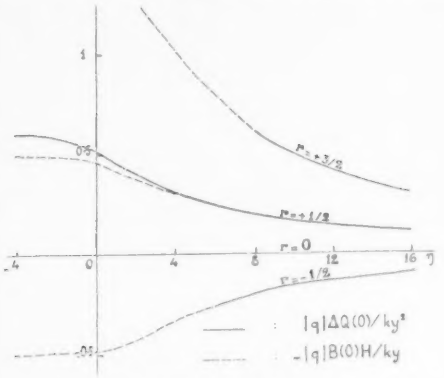


FIG. 1. Effets MTE: $(|q|\Delta Q(0)/ky^2)$ et Nernst $(-|q|B(0)H/ky)$ en fonction de l'énergie de Fermi réduite $\eta$, pour différents mécanismes de dispersion.

les formules (8), et si l'on suppose que $v_1 = \sigma_1/(\sigma_1+\sigma_2)$ n'est pas voisin de 1 ni de 0, le calcul peut être mené jusqu'au bout. Il montre que *les effets ambipolaires dépendent peu des mécanismes de dispersion des électrons et des trous.* En particulier, contrairement aux effets des seuls électrons libres, ils ne sont pas nuls si $r = 0$, mais ils sont alors proportionnels à $v_1(1-v_1)(5-\delta)$, où $\delta = E_g/kT$ est l'énergie d'activation réduite. Il est impossible de tirer de l'étude des effets *ambipolaires* une conclusion sur les mécanismes de dispersion.

En conclusion de cette étude, nous soulignons la nécessité d'élaborer la théorie exacte des effets thermomagnétiques dans le cas de la dispersion "polaire", pour pouvoir affirmer si ce mécanisme de dispersion est, ou non, prédominant.

### BIBLIOGRAPHIE

1. EHRENREICH H., *J. Phys. Chem. Solids* **2,** 131 (1957).
2. RODOT M., *Compte Rendu du Congrès de Bruxelles* (1958).
3. BEER A. C., ARMSTRONG J. A. et GREENBERG I. N. *Phys. Rev.* **107,** 1506 (1957).
4. CALLEN H. B., *Phys. Rev.* **76,** 1394 (1949).

## DISCUSSION

*Compiled by* H. P. R. FREDERIKSE

### M.1 Y. KANAI and R. NII

G. C. DANIELSON pointed out that the radiation—although sometimes rather small—cannot be neglected.(1)

A. JOFFÉ remarked that he considered the best method for determining the heat conductivity that in which this quantity is deduced from Peltier effect measurements.

R. BOWERS, J. A. KRUMHANSL and H. P. R. FREDERIKSE stated that measurements of the thermal conductivity of InSb in their respective laboratories agree essentially with the results of A. STUCKES.(2)

R. P. CHASMAR: Recent experiments on the heat-conductivity of InAs and InP are in reasonable agreement with PRICE's theory.

A. JOFFÉ reported that measurements in his laboratory have shown a 15 per cent difference in thermal conductivity between *n*- and *p*-type Ge.

C. HERRING answered that such a difference had not been observed by GEBALLE.

### M.2 B. ABELES

C. HERRING pointed out that it is not right (1) to consider $K_{ph} = a/T$ with constant $a$, because of isotope scattering, (2) to use a constant mobility ratio $b$; the variation of $b$ can be deduced from high temperature thermoelectric power measurements.

P. AIGRAIN remarked that it was not clear what value of $E_g$ (energy gap) should be used in the expression for bipolar diffusion.

P. J. PRICE: The effect of the temperature dependence of the energy levels on the formula for bipolar diffusion can be discussed by means of the Onsager relations. It appears that the energy gap factor is $(E_g+\delta_n kT+\delta_p kT)^2$ in general, where $E_g$ is the (thermal) gap *at the particular temperature* and $\delta_n$ and $\delta_p$ are as previously defined.(3) The difference between $E_g(T)$ and $E_g(T=0)$ given by KETTEL's procedure, and the difference between $(\delta_n+\delta_p)$ and the "classical" value of 4, should not be neglected at temperatures where the bipolar effect is appreciable.

### M.4 P. G. KLEMENS

J. CALLAWAY: The statement that point defects contribute a thermal resistivity ($W_P$) proportional to temperature is not well founded theoretically. If only point defects scattered phonons, the thermal conductivity would diverge at the lower limit because of the $\omega^{-4}$ dependence of the relaxation time. The contribution of point defect scattering to the thermal resistance will depend sensitively on the presence of additional scattering mechanisms which limit the contribution of the low energy modes.

P. G. KLEMENS: The theory leading to equation (3) does take account of anharmonicity interactions ($N_1$ processes) in an approximate way. These processes make the effective mean free path of low frequency phonons ($< kT/h$) independent of frequency, but do not seriously affect higher frequency modes (see reference 4).

The thermal resistance is certainly not additively compounded of $W_{bound}$ and $W_P$, since the scattering processes have widely different frequency variations (see reference 4). SLACK has published the results of exact computations for the case of combined boundary and point defect scattering (see reference 5); these results are at least in rough agreement with the curves of GEBALLE and HULL (reference 10). I understand that HERRING, too, has treated this case and found good agreement with experiment (reference 10).

I do not claim, however, that my theory is valid for all cases, even though it seems to be a satisfactory approximation in many cases of practical interest. A full and exact treatment of the combined effects of all processes producing thermal resistance seems very difficult and has not yet been achieved.

M.5 T. H. GEBALLE *et al.*

P. G. KLEMENS: Do these results on the frequency dependence of the longitudinal and transverse phonon mean free path imply that one does not have to worry about low frequency divergence in thermal conduction?

T. H. GEBALLE: We don't know if we will be able to sort out the relative contributions of the longitudinal and transverse phonons at low temperatures; moreover, we have not investigated the asymptotic limit of the phonon spectrum.

M.6 J. APPEL

C. HERRING questioned the significance of a comparison of theoretical and experimental results pertaining to the thermomagnetic effects in *p*-type Ge at low temperature; these effects depend very sensitively on the frequency dependence of the phonon mean free path, which is not exactly known.

Another remark by HERRING concerned the symmetrical treatment of the two Boltzmann equations (for electrons and phonons) in the case of a temperature gradient. Although this point has been stressed considerably in the literature (SONDHEIMER, APPEL, etc.), he does not believe that the error made by neglecting the influence of phonon–electron scattering in the phonon equation is serious for rather pure semiconductors.

## REFERENCES

1. SIDLES P. H. and DANIELSON G. C., *J. Appl. Phys.* **25,** 58 (1954).
2. STUCKES A., *Phys. Rev.* **107,** 427 (1957).
3. PRICE P. J., *Phys. Rev.* **104,** 1223 (1956).

VOL
8
195

*J. Phys. Chem. Solids* Pergamon Press 1959. Vol. 8. pp. 363–366. Printed in Great Britain

SESSION N:
THEORY III*

# N.1 COHESIVE ENERGIES AND BAND STRUCTURES OF COVALENCE AND IONIC CRYSTALS

A. MORITA
Physical Institute, Tôhoku University, Sendai, Japan

VOL. 8 1959

RECENTLY we proposed a new method to investigate the influences of homopolar binding on the cohesive energies of ionic crystals and the influences of ionic binding on the cohesive energies of covalent crystals.[1,2] This method is called the method of "Semilocalized Crystalline Orbital" or briefly "SLCO".

Semilocalized crystalline orbitals consist of a set of linear combinations of atomic orbitals and each of them has a semilocalized character. Only a part of them are occupied in the ground state of a crystal and the rest may be used to describe certain excited states. The detailed forms of SLCO are determined so as to minimize the expectation value of the energy of the ground state, the wave function of which is expressed by the single Slater determinant consisting of the part of SLCO corresponding to the ground state.

The method of SLCO is a natural generalization of the Heitler–London method and is applicable to insulators and intrinsic semiconductors having an energy gap. This method also offers a useful method to compute the conduction and valence bands of these crystals.

Here I shall avoid the detailed explanation of the method of SLCO and present only the results of its applications to the computation of the cohesive energy of the LiH crystal and the band structure of Si and Ge crystals.

*Cohesive energy of the LiH crystal*

The first quantum mechanical treatment of the cohesive energy of the LiH crystal was carried out by HYLLERAAS[3] and then a more detailed computation was carried out by LUNDQVIST.[4] Their calculations were performed on the basis of the so-called "ionic approximation", in which only ionic states were taken into account. Their results are shown in Table 1 in comparison with the experimental data. The theoretical value of the cohesive energy obtained by LUNDQVIST is smaller than the observed one by about 18 kcal/mol.

We have computed[1] the cohesive energy of the LiH crystal by taking into account homopolar binding by the use of the SLCO method and have obtained 25 kcal/mol as the correction due to the homopolar binding effect. In our calculation, we have taken into account only the 2*s* orbital of the Li atom as the atomic orbital responsible for the homopolar binding and also have used the so-called Mulliken approximation to reduce many-centered Coulomb integrals to two-centered integrals. In view of the approximations used in our calculation, I think that our result is very satisfactory.

*Energy band structure of silicon and germanium crystals*

So far various methods of computing the energy band structure of crystals have been proposed.[5] The SLCO method also presents another useful method to compute the energy band structure, which is very similar to the so-called tight binding methods. Our method has some advantages compared with the other methods for the following reasons, although it is only applicable to insulators and intrinsic semiconductors having an energy gap. First, the method of SLCO is intimately related to the theory of cohesive energy. Namely, the effective one-electron Hamiltonian and its matrix elements are given automatically through the computation of cohesive energy. Therefore, there is no ambiguity formally in the construction of the

* *Chairman:* T. MUTO; *Co-Chairman:* F. HERMAN.

*Table* 1a. *The cohesive energy and lattice constant of the LiH crystal* (LUNDQVIST[4])

| | A | B | C | D | observed |
|---|---|---|---|---|---|
| cohesive energy (kcal/mol) | 199·3 | 196·4 | 203·9 | −199·1 | −217±7 |
| lattice constant ($10^{-8}$ cm) | 4·50 | 4·34 | 4·16 | 4·10 | 4·085 |

A. Overlap between neighbours of the first order
B. Overlap between neighbours of the 1st and 2nd order
C. Overlap between neighbours of the 1st, 2nd and 4th order } $S^2$-approximation
D. Overlap between neighbours up to the 6th order—complete expression.

*Table* 1b

| | | |
|---|---|---|
| $\Delta E_{COH}$ | = $E_{COH}$ (observed)—$E_{COH}$ (LUNDQVIST; D) | = 17·9±7 kcal/mol. |
| $\Delta E_{COH}$ | (calculated by using the SLCO method) | = 25 kcal/mol. |

effective one-electron Hamiltonian and we need not be troubled with self-consistent calculations. Second, the difficulty concerning non-orthogonalities of atomic orbitals are avoided. Third, in our method, the conduction and valence bands are determined independently by two separate secular equations. In diamond-type crystals such as Si and Ge, therefore, we have two 4–4 secular equations.

Since we have not yet carried out the computation of the cohesive energies of Si and Ge, we cannot calculate the band structure of these crystals directly by the use of SLCO. But we can determine the matrix elements of SLCO secular equations by making use of the information derived from cyclotron resonance and optical absorption experiments on these crystals, obtaining the band structure of these crystals semi-empirically. This method is very similar to SLATER and KOSTER's LCAO interpolation scheme,[6] but there are some differences. Our method takes into account the over-lapping effect of atomic orbitals correctly. Furthermore, in our method, conduction and valence bands are determined independently by two separate secular equations. This fact simplifies the interpolation procedure very much.

Fig. 1 is the band structure of Si. The quantities that we adopted to determine this band structure are listed in Table 2. In the table, $\Delta E$ is the energy

*Table* 2

(a) *The conduction band*

| | $m_l/m$ | $m_t/m$ | $\Delta E$ | Energy gap | $Kc/K(100)$ |
|---|---|---|---|---|---|
| Our values | 0·97 | 0·19 | 0·54 eV | 1·21 eV | ~3/5 |
| Experimental | 0·97±0·02 | 0·19±0·01 | 0·6 eV | 1·21 eV | ~3/4 |

(b) *The valence band*

| | A | B | C | L | M | N |
|---|---|---|---|---|---|---|
| Our values ($\hbar^2/2m$) | −4·1 | −1·6 | 3·3 | −7·3 | −2·5 | −7·45 |
| Experimental ($\hbar^2/2m$) | −4·1±0·2 | ±1·6±0·2 | 3·3±0·5 | — | — | — |

difference between the [000] position in $k$-space and the minima in the direction [100]. We have had to take this value smaller than 0·04 Rydberg units (= 0·54 eV) in order to keep the minima in the direction [111], that is to say, $E_{L1}$ higher than the minima in the direction [100]. On the other hand, we have experimental indications that this value is larger than 0·6 eV.[8]

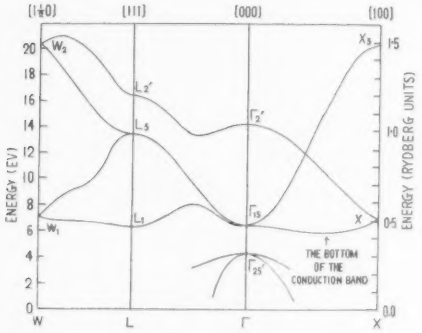


FIG. 1. The energy band structure of silicon. The spin–orbit splitting has been omitted.

To determine the complete diagrams of the valence bands, we have to know the total width of the valence bands. However we have not got available data having the same accuracy as the cyclotron resonance data. So we have shown only the neighbourhood of the top of the valence bands.

According to DRESSELHAUS, KIP and KITTEL,[7] the structure of the valence band edge without spin–orbit splitting is given by the secular equation

$$\begin{vmatrix} Lk_x^2+M(k_y^2+k_z^2)-E(k) & Nk_xk_y & Nk_xk_z \\ Nk_xk_y & Lk_y^2+M(k_z^2+k_x^2)-E(k) & Nk_yk_z \\ Nk_xk_z & Nk_yk_z & Lk_z^2+M(k_x^2+k_y^2)-E(k) \end{vmatrix} = 0$$

On the other hand, the upper two valence bands containing the spin–orbit splitting are given by

$$E(k) = Ak^2 \pm \pm[B^2k^4+C^2(k_x^2k_y^2+k_y^2k_z^2+k_z^2k_x^2)]^{\frac{1}{2}},$$

where

$$A = \tfrac{1}{3}(L+2M),\ B = \tfrac{1}{3}(L-M),$$
$$C^2 = \tfrac{1}{3}[N^2-(L-M)^2].$$

We can prove the identity $L \equiv N$ by making use of the SLCO method. This relation is satisfied by the cyclotron resonance data of Si and Ge when and only when we assume $B < 0$.

Fig. 2 is the energy band structure of Ge. Unfortunately, we could not determine the conduction band structure of Ge consistently with the cyclotron resonance data in the range of reasonably

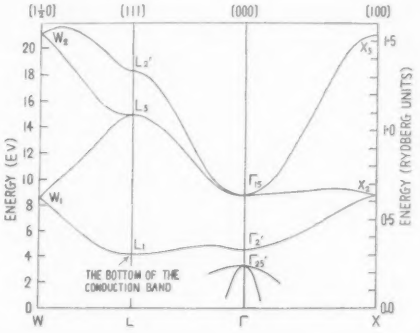


FIG. 2. The energy band structure of germanium. The spin–orbit splitting has been omitted.

*Table* 3.

(a) *The conduction band*

| | $m_l/m$ | $m_t/m$ | $E_{\Gamma'_2}-E_{L1}$ | Energy gap |
|---|---|---|---|---|
| Our values | 1·10 | 0·136 | 0·4 eV | 0·785 eV |
| Experimental | 1·58±0·04 | 0·082±0·001 | 0·18 eV | 0·785 eV |

*Table 3—cont.*

(b) *The valence band*

| | A | B | C | L | M | N |
|---|---|---|---|---|---|---|
| Our values ($\hbar^2/2m$) | −13·0 | −8·9 | 10·3 | −31 | −4 | −32·3 |
| Experimental ($\hbar^2/2m$) | −13·0±0·2 | ±8·9±0·1 | 10·3±0·2 | — | — | — |

acceptable structures. The quantities that we used to determine this band structure are listed in Table 3 in comparison with the experimental values[7] derived by cyclotron resonance. As is shown in the Table, we have had to take the value of the longitudinal effective mass $m_l$ a little smaller and the value of the transverse effective mass $m_t$ considerably larger than the cyclotron resonance data, respectively.

We can refine our theory by taking into account more distant resonance integrals. But in view of the fact that our available data are confined to effective mass data derived from cyclotron resonance experiments and a few data concerning energy gaps derived by optical absorption experiments, such an attempt may be impractical.

**REFERENCES**

1. MORITA A. and TAKAHASHI K., *Progr. Theor. Phys.* **19,** 257 (1958).
2. MORITA A., *Progr. Theor. Phys.* **19,** 534 (1958).
3. HYLLERAAS E. A., *Z. Phys.* **63,** 771 (1930).
4. LUNDQVIST S. O., *Arkl. fys.* **8,** 177 (1954).
5. See, for example, HERMAN F., *Rev. Mod. Phys.* **30,** 102 (1958).
6. SLATER J. C. and KOSTER G. F., *Phys. Rev.* **94,** 1498 (1954).
7. DRESSELHAUS G., KIP A. F. and KITTEL C., *Phys. Rev.* **98,** 368 (1955).
8. FAN H. Y., SHEPHERD M. L. and SPITZER W. *Photoconductivity Conference* Atlantic City, pp. 184–203 (1954).

*J. Phys. Chem. Solids* Pergamon Press 1958. Vol. 8. pp. 366–369. Printed in Great Britain

# N.2 ON THE CONNECTION BETWEEN BONDS AND BANDS IN METALS AND SEMICONDUCTORS

**Ph. CHOQUARD, A. JANNER and E. ASCHER**

Batelle Memorial Institute, Geneva, Switzerland

THESE last years, various investigators in semiconductor and metal physics have expressed the need for a chemical approach to solid state problems. This means an approach using the localized electron picture and the valence bond scheme. They take as an example PAULING's "resonating valence bond theory of metals". The interest of this theory seems to justify a further investigation into its nature and its connection with the band theory. We shall illustrate how one might attempt this by using a theorem of LÖWDIN and formulating the resonances in terms of configuration interaction.

A chemical approach to solid state problems implies, as must any correct description of cohesive, magnetic or electric properties of solids, an appropriate treatment of electron–electron correlation due mainly to Coulomb interaction. This

fact has led SLATER to develop the method of configuration interaction by which he was able to show the equivalence of valence bond and molecular orbital treatment of the hydrogen molecule, where three configurations were necessary. Later LÖWDIN demonstrated that this equivalence could be extended to the $N$ electron problem, showing that a sufficient condition was realized if one started from two complete sets of orbitals $\varphi_K$ and $\psi_e$ related by an infinite unitary matrix:

$$\varphi_K = \sum_{=1}^{\infty} U_{Ke} \cdot \psi_e$$

For our purpose however, we will discuss and use a practical version of this theorem in choosing appropriate bases of one-electron wave functions.

For the sake of simplicity let us consider from now on a simple case of the $N$ electron problem, namely the linear chain consisting of $N$ atoms with one electron per atom. This model is not only of academic interest but also of practical interest since such properties as electrical properties may be handled one-dimensionally. The representation suited for molecular orbital treatment is naturally the Bloch representation whereas the one most suited for a valence bond treatment will be the Wannier representation. The Bloch functions $b_q(K, x)$ and Wannier functions $a_q(x-R)$ are connected by the known relation:

$$b_q(\mathbf{K},\mathbf{x}) = N^{-\frac{1}{2}} \sum_R [\exp(i\mathbf{KR})] a_q(\mathbf{x}-\mathbf{R})$$

By this selection, the infinite unitary matrix gets a simple physical meaning in being reduced to a direct sum of unitary matrices enumerated along the diagonal by the quantum number $q$. The matrix elements are:

$$N^{-\frac{1}{2}}[\exp(i\mathbf{KR})]\delta_{qq'}$$

From the structure of the unitary matrices we notice that a necessary condition for equivalence is contained in the simple requirement of at least one orbital per electron. Generally the same number, say $M$ of orbitals is required in both representations in order to treat both schemes to the same order of approximation, that means taking into account a specific number of bands. The minimum of one band corresponds to $M_{\min} = N$.

Let us enumerate the number of ways we may distribute the $N$ electrons over $M$ orbitals taking into consideration the exclusion principle but forgetting for a moment the spin variables. First we have the number of ways of distributing $N/2$ doubly filled orbitals, then $N/2-1$ doubly filled orbitals multiplied by the number of distributions of two electrons over the rest of $M-(N/2-1)$ orbitals and so on, until the number of distributions of $N$ singly occupied orbitals. So we have:

$$\mathcal{N} = \binom{M}{N/2} + \binom{M}{N/2-1} \times \times \binom{M-(N/2-1)}{2} + .. + \binom{M}{N}$$

Whatever the spin configuration one imposes on the electrons, any determinantal wave function of the $N$ electrons expressed in one scheme becomes, via the unitary transformation, a linear combination of determinantal wave functions in the other scheme—the number of which is never larger than $\mathcal{N}$. So a configuration in one scheme is a superposition of configurations in the other scheme with definite coefficients given by the unitary transformation.

Next we consider the spin degeneracy. We must specify further the state of the chain and say for instance that it is diamagnetic, characterized therefore by $S_z = S^2 = 0$. Then the total number of singlets will be given by

$$C = \binom{M}{N/2}\rho_0 + .. + \binom{M}{N/2-K} \times \times \binom{M-(N/2-K)}{2K} \cdot \rho_{2K} + \cdots \binom{M}{N} \cdot \rho_{NA}$$

where

$$\rho_{2K} = \frac{1}{K+1}\binom{2K}{K}$$

is Rumer's number.

These singlet states, antisymmetric in spin and symmetric in space variables are linear combinations of configurations with $S_z = 0$; in order to be eigenvectors of $S^2 = 0$, they are produced for example by the projection operator method of LÖWDIN or by the bond configuration method of EYRING. EYRING's bond configurations involve

each $2^{N/2}$ of the $\binom{N}{N/2}$ spin configurations having $S_z = 0$ and are conventionally known under SLATER–PAULING's form. LÖWDIN's singlets are orthogonal whereas EYRING's are not, but the latter have a simple interpretation in terms of bond diagrams. The relation between both descriptions has recently been given by LÖWDIN but only for small values of $N$. For our purpose we keep the bond configuration description since even in the Bloch scheme they may be constructed by the simple device of placing on Rumer's circle the $N$ values of the wave vector $\mathbf{K}$ instead of the $N$ positions of the atoms. Equivalence is achieved if one writes the solution $\psi$ of the $N$ electron problem as linear combinations of all $C$ singlets in both schemes.

We shall now illustrate how PAULING's resonances may be formulated.

*Synchronized resonance*

According to PAULING, this resonance implies a change of at least two bonds. It requires the same number of orbitals as electrons: in particular this will be our chain made of hydrogen-like atoms with $M = N$. In principle all the singlet states enumerated above contribute to the resonance but as an illustration of the prototype of this resonance which in fact has not been treated by PAULING, we shall consider only the bond configurations $A_1$, $A_2$ given by the diagrams

$$\binom{1}{2}\binom{3}{4}\ldots\binom{N-1}{N} \text{ and } \binom{N}{1}\binom{2}{3}\ldots\binom{N-2}{N-1}$$

and the $N$ bond configurations $B\nu$ given by the diagrams

$$\binom{1}{2}\ldots\binom{\nu}{\nu+3}\binom{\nu+1}{\nu+2}\ldots\binom{N-1}{N}$$

These bond configurations are not stationary but if we impose the cyclic condition to the chain, we may, as in the Bloch scheme, form bases for irreducible representations of the cyclic group by the transformations

$$\mathscr{A}_N = A_1 + A_2 \qquad \mathscr{A}_{N/2} = A_1 - A_2$$

$$\mathscr{B}_\mu = \sum_{\nu=1}^{N}\left[\exp\left(\frac{2\pi i\mu\nu}{N}\right)\right]B_\nu \qquad \mu = 1,2\ldots N$$

$\mathscr{A}_{N/2}$ interacts with $\mathscr{B}_{N/2}$, $\mathscr{A}_N$ with $\mathscr{B}_N$ since they belong to the same representation $\Gamma_{N/2}$, $\Gamma_N$. In this example the ground state is given by the following ansatz

$$\psi_N = c_A(A_1 + A_2) + c_B(B_1 + B_2 + \ldots B_N)$$

from which we get two solutions. The same is true for $\psi_{N/2}$ whereas the others $\psi_\mu = \mathscr{B}_\mu$ are unaffected. Since the $\psi$ belong to different representations, they are stationary states. Having found the $N+2$ values $E_\lambda$ of the energy spectrum, we may easily deduce the behaviour in time of the original bond configurations $A$ and $B$, imposing a definite configuration at an initial time $t = 0$, and formulate in this way the resonance theory of synchronized type. This procedure may be generalized to include all the sets of $N$ Rumer's bond configurations and in principle also the ionic configurations, but for those it might be advisable to take into account their participation by introducing new orbitals which are linear, but not orthogonal combinations of the basic Wannier functions and calculating the mixing parameters by minimization of the energy.

*Pivoting resonance*

This resonance occurs for example when there are reasons to attribute two orbitals on at least one or a certain number $n$ of foreign atoms, such as lithium atoms, placed on the chain so that no two such atoms are nearest neighbours. If some superlattice is obtained by this arrangement, we may apply the same procedure as described before with $M_{\min} = N + n$. Here $n$ is the number of PAULING's metallic orbitals.

*Uninhibited resonance*

This is obtained in the case of a chain of lithium-like atoms in which one has two orbitals per atom, that means $M = 2N$. In treating this resonance, PAULING has however reduced the $N$ electron problem to a one-electron approximation. He assumes that the resonance energy depends on hybridization as binding energy depends on hybridization in a diatomic molecule.

One may recall the connection between resonance-type and conductivity character: uninhibited resonance is responsible for the metallic character of solids, whereas pivoting and synchronized resonances are characteristic of semiconductors, as MOOSER and PEARSON have shown.

In conclusion we may say that PAULING's scheme

is equivalent to the molecular orbital scheme. If the calculations are pursued far enough both theories will give the same result since solid state properties are invariant with respect to unitary transformation applied to one of their description. However, further work must be carried out on simple models in order to obtain these results.

**REFERENCES**

1. PAULING L., *Proc. Roy. Soc.* A**196,** 343 (1949).
2. SLATER J. C., *Handbuch der Physik*, XIX, Chap 7. Springer, Berlin (1956). See also this text for references.
3. LÖWDIN P. O., *Advanc. Phys.* **5,** 3 (1956).
4. EYRING H., WALTER J. and KIMBALL G. E., *Quantum Chemistry*. Wiley, New York (1944).

*J. Phys. Chem. Solids* Pergamon Press 1959. Vol. 8. pp. 369–371. Printed in Great Britain

VOL. 8 1959

# N.3 ENERGY BANDS OF SILICON AND GERMANIUM*

J. C. PHILLIPS

Department of Physics, University of California, Berkeley 4, California

IN recent years there has been a great increase in both theoretical and experimental knowledge of the electronic energy bands of Si and Ge. The following information can be deduced from various experiments (energy values are measured relative to the top of the valence band):

(1) The direct energy gap at the center of the Zone, as determined optically by DASH and NEWMAN[1] (0·18 and 0·06 Ryd., for Si and Ge, respectively);

(2) The indirect energy gaps to the conduction-band minima along the (100) and (111) directions in Si and Ge, respectively;

(3) The obverse values, as determined from extrapolating optical measurements[2,3] on Ge–Si alloys; together with the results of (2) this yields[4] $E(X_1^{(2)}) = 0{\cdot}09$ and 0·08 Ryd., and $E(L_1^{(2)}) = 0{\cdot}22$ and 0·045 Ryd., respectively, for Si and Ge; and

(4) The location of the minimum in the (100) direction in the lowest conduction band in Si at $k_0 = (0{\cdot}86 \pm 0{\cdot}06)2\pi a^{-1}$, as determined from the hyperfine structure of donor spin resonance.[5]

In addition the curvatures (effective masses) of the top of the valence and bottom of the conduction bands are known from cyclotron resonance experiments.[6,7] These curvatures can be used to estimate certain term values, as will be discussed presently.

On the theoretical side the calculations of HERMAN[8] for Ge and WOODRUFF[9] and BASSANI[10] for Si have shown that an orthogonalized plane wave calculation can yield results that are in good qualitative agreement with experiment. Indeed, HERMAN[11] has recently emphasized that the qualitative features of the energy bands of semiconductors can be understood in terms of a nearly free electron picture.

Since the plane wave formalism gives a good qualitative account of the variation of energy with wave-vector, the author constructed an interpolation scheme based on the plane-wave formalism which replaced the orthogonalization terms by a repulsive pseudopotential.[12] The basic assumption here is that the core has relatively little effect on the variation of energy with wave vector for bands near the energy gap. This assumption can be justified by noting that the orthogonalization terms related to the core are chiefly represented by high Fourier components, and the latter are not important in determining effective masses, although they may affect the overall convergence of the levels. If the energy gaps at a few points of the Zone are fitted correctly by a suitable choice of the parameters the latter difficulty is eliminated. In this way 3-parameter pseudopotentials were constructed for Ge and Si that agreed very well with

* The calculations presented in this paper were carried out at Bell Telephone Laboratories, Murray Hill, New Jersey.

all the experimental facts discussed above and also with the theoretical calculations of HERMAN, WOODRUFF, and BASSANI. The parameters are taken to be the first three Fourier coefficients of the pseudopotential. Calculations were carried out at Γ, X, and L, and along Δ. Using the same pseudopotentials, calculations have been carried out along Σ (at $(\frac{1}{2}, \frac{1}{2}, 0)$ and $(\frac{3}{4}, \frac{3}{4}, 0)$) and at W. Since the pseudopotential values differed from the experimental term values by a few hundredths of a Rydberg, the pseudopotential bands can be made to agree with experiment completely by making minor changes in the bands. In this way the energy bands of Si and Ge have been sketched with some accuracy in the (100) and (111) directions.[12] Figs. 1 and 2 show similar sketches for the (110) direction, and Table 1 lists the calculated values at W. The results of the calculations for Ge are similar to the ones already obtained by HERMAN,[8] but of course agree more nearly with experiment.

masses at the center of the Zone can be explained[14] if $\epsilon \sim 0{\cdot}3$. This result is plausible since it is known that the Slater approximation overestimates exchange effects.

With this value of $\epsilon$ one is now tempted to deduce other features of the band structure. For example, the small transverse masses in the conduction band minima in Si and Ge are a consequence of repulsion of the conduction bands by the top valence bands. Thus one might hope to determine the direct energy gaps at X and L for Si and Ge, respectively. Unfortunately the value of $\epsilon$ that should be used here is not necessarily the same as that deduced for the center of the Zone.

The Slater approximation tries to take into account density variations by assuming that the exchange hole at any point has the same form as that of a free electron gas having the local density. A more general treatment was given by HERRING and HILL,[15] but their results could be expected to be

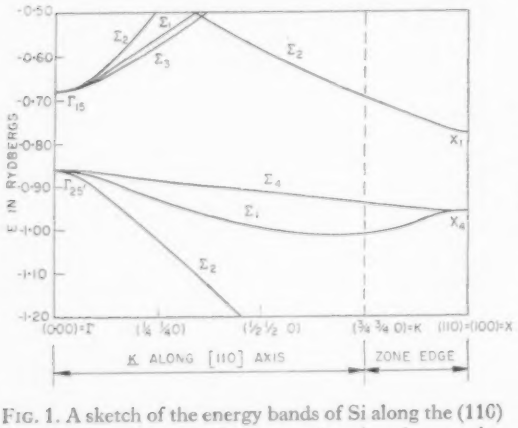


FIG. 1. A sketch of the energy bands of Si along the (110) direction based on calculations made using the pseudopotential interpolation scheme described in the text.

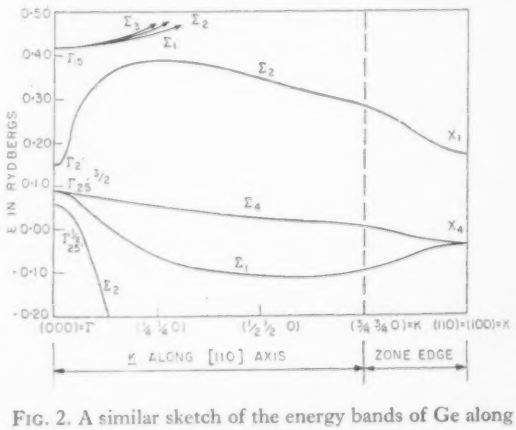


FIG. 2. A similar sketch of the energy bands of Ge along the (110) direction.

Recent work by KANE[13] and the author[14] has shown that the hole effective masses in Si and Ge, as measured by cyclotron resonance, can be calculated using the plane-wave formalism, providing the matrix elements of $\mathbf{p}$ in the usual $\mathbf{k} \cdot \mathbf{p}$ formalism are multiplied by a factor $(1+\epsilon)$. Here $\epsilon$ is a measure of the non-local nature of the crystal potential. If this is ascribed entirely to exchange with other valence electrons and the Slater approximation is made for the exchange hole, one finds[13] $\epsilon \sim 0{\cdot}6$. On the other hand, the experimental

accurate only for monatomic metals where the Fermi surface does not come too close to the Zone edge. The levels at X and L in Si and Ge are of course at the Zone boundary, so that a free-electron approximation might not be appropriate. Thus it is difficult to give a general treatment of exchange effects on the band structure; it does appear, however, that $\epsilon \sim 0{\cdot}3$ is also approximately consistent with the band picture we have sketched and the transverse cyclotron masses in the conduction band.

We conclude by remarking that the lowest conduction band at W is higher than the conduction band minimum by 3·5 eV in Si and 5·5 eV in Ge, according to the present calculations. Group-theoretical arguments[16,17] suggest that W might be a minimum in the conduction band for zinc-blende-type crystals, but our results suggest that this would be unlikely. Thus the optical gap in GaAs is only about 0·4 eV larger than that in Ge, and this quantity provides a rough estimate of the shift in bands caused by going from the diamond to the zinc-blende potential.[18] For AlP the increase from Si is 2 eV, which makes it possible but still unlikely that the conduction-band minimum would occur at W. From the over-all similarity between the bands of Si, Ge, and grey Sn it seems more likely that the conduction-band minima in zinc-blende-type crystals would occur either at Γ (for crystals containing either In or Sb) or X or L.

*Table* 1

| | Si | Ge |
|---|---|---|
| $W_1^{(1)}$ | −1·34 | −0·49 |
| $W_2^{(1)}$ | −1·15 | −0·09 |
| $W_1^{(2)}$ | −0·33 | 0·55 |
| $W_2^{(2)}$ | −0·45 | 0·57 |

Term values obtained from the pseudopotential interpolation scheme described in the text. The energies are measured in Rydbergs, and the zeros of energy are the same as those used in Figs. 1 and 2.

*Acknowledgments*—These calculations were carried out at Bell Telephone Laboratories, Murray Hill, New Jersey, with the assistance of Mrs. W. MAMMEL.

## REFERENCES

1. DASH W. C. and NEWMAN R., *Phys. Rev.* **99,** 1151 (1955).
2. JOHNSON E. R. and CHRISTIAN S. M., *Phys. Rev.* **95,** 560 (1954).
3. BRAUNSTEIN R., MOORE A. R. and HERMAN F., *Phys. Rev.* **109,** 695 (1958).
4. The notation used for the irreducible representations and symmetry points of the Zone is that of HERRING C., *J. Franklin Inst.* **233,** 525 (1942).
5. FEHER G., private communication.
6. DRESSELHAUS G., KIP A. F. and KITTEL C., *Phys. Rev.* **98,** 368 (1955).
7. DEXTER D. L., ZEIGER H. J. and LAX B., *Phys. Rev.* **104,** 637 (1956).
8. HERMAN F., *Physica* **20,** 801 (1954).
9. WOODRUFF T. O., *Phys. Rev.* **103,** 1159 (1956).
10. BASSANI F., *Phys. Rev.* **108,** 263 (1957).
11. HERMAN F., *Rev. Mod. Phys.* **30,** 102 (1958).
12. PHILLIPS J. C., submitted to *Phys. Rev.*
13. KANE E. O., *J. Phys. Chem. Solids* **6,** 236 (1958).
14. PHILLIPS J. C., *J. Phys. Chem. Solids* **7,** 52 (1958).
15. HERRING C. and HILL A. G., *Phys. Rev.* **58,** 132 (1940).
16. DRESSELHAUS G., *Phys. Rev.* **100,** 580 (1955).
17. PARMENTER R. H., *Phys. Rev.* **100,** 573 (1955).
18. Energy gaps for zinc-blende-type crystals are listed by HERMAN F., *J. Elect.* **1,** 103 (1955).

*J. Phys. Chem. Solids* Pergamon Press 1959. Vol. 8. pp. 371–374. Printed in Great Britain

N.4

# BAND STRUCTURE CALCULATIONS OF SEMICONDUCTORS BY THE KOHN-ROSTOKER-KORRINGA METHOD: APPLICATION TO GERMANIUM

B. SEGALL

General Electric Research Laboratory, Schenectady, New York

THE concept of band structure has played an important role in the development of solid state physics and will probably continue to do so. However, there are some unsettled questions about the band theory and some difficult problems that must be surmounted in the carrying out of an accurate *a priori* calculation. Concerning the basic theory, there is the formidable question of the validity of the band picture inasmuch as correlations are neglected or, at best, treated in an approximate

manner. Even assuming the validity of the one-electron picture there remain the problems of determining the crystalline potential and of developing methods for solving the wave equation with a periodic potential. In order to obtain quantitatively accurate information about the potential, it is necessary to have some knowledge of the solution—i.e. to have achieved some degree of self-consistency. As for the method, it must yield accurate results without requiring excessive labor.

We feel that the method which has been derived independently and by different approaches by KORRINGA[1] and by KOHN and ROSTOKER[2,3] for "simple" crystals and which has been extended to "complex" crystals[4] (i.e. those having several atoms per unit cell), promises to help solve the problems involved in band calculations. The method requires that the crystalline potential can be reasonably approximated by a potential which is spherically symmetric inside nonoverlapping spheres about the lattice sites and effectively constant elsewhere. If the solutions for the zeroth-order potential lead to a potential which can be approximated by one of the required form and the difference treated by perturbation theory, the method offers the possibility for attaining self-consistency.

We will very briefly outline the method in terms of the approach taken by KOHN and ROSTOKER. It was shown by them that the variational principle

$$\delta\Lambda = 0$$

$$\Lambda = \int \psi^*(\mathbf{r})V(\mathbf{r})[\psi(\mathbf{r}) - \int G(\mathbf{r}, \mathbf{r}')V(\mathbf{r}')\psi(\mathbf{r}')d\mathbf{r}']d\mathbf{r} \tag{1}$$

is equivalent to the integral equation

$$\psi(\mathbf{r}) = \int G(\mathbf{r}, \mathbf{r}')V(\mathbf{r}')\psi(\mathbf{r}')\mathbf{r}d' \tag{2}$$

for the Schrödinger wave function. In the above, $G(\mathbf{r}, \mathbf{r}')$ is the Green's function for the problem and hence obeys the Bloch condition $G(\mathbf{r}+\mathbf{r}_n; \mathbf{r}') = e^{i\mathbf{k}\cdot\mathbf{r}_n}G(\mathbf{r}, \mathbf{r}')$ with $\mathbf{r}_n$ being one of the lattice translation vectors. From the experience with variational principles of this type in other fields of physics, one would expect very good convergence to result from (1).

The trial function in the $j$-th "atomic sphere" in the unit cell is expanded as[4]

$$\psi(\mathbf{r}) = \sum_{l,m}^{l_{\max}} C_{lm}{}^{(j)}\mathscr{R}_l{}^{(j)}(|\mathbf{r}-\mathbf{a}_j|)Y_{lm}(\mathbf{r}-\mathbf{a}_j) \tag{3}$$

where $Y_{lm}(\mathbf{x})$ is a spherical harmonic (or lattice harmonic for a point of symmetry) and $\mathscr{R}_l{}^{(j)}(\mathbf{r})$ satisfies the radial Schrödinger equation with the appropriate potential for the $j$-th sphere. For a potential of the type described above, the variational principle (1) with equation (2) leads to the following set of homogeneous equations for the expansion coefficients[4]

$$\sum_{l'm'j'} \Lambda_{lm;l'm'}^{(jj')} \quad C_{l'm'}^{(j')} = 0 \tag{4}$$

$$\Lambda_{lm;l'm'}^{(jj')} = (j_l\mathscr{R}_l{}^{(j)} - j_l{}'\mathscr{R}_l{}^{(j)})|_{r=R_j} \times$$
$$\times \{A_{lm;l'm'}^{(jj')}(E, \mathbf{k})(j_{l'}\mathscr{R}_{l'}{}^{(j')} - j_{l'}{}'\mathscr{R}_{l'}{}^{(j')})|_{r=R_{j'}} + \sqrt{(E)}\delta_{ll'}\delta_{mm'}\delta_{jj'}[n_l\mathscr{R}_l{}^{(j)} - n_l{}'\mathscr{R}_l{}^{(j)}]|_{r=R_j}\} \tag{5}$$

In order for the system of equation (4) to have a nontrivial solution, the determinant of the matrix $\Lambda$ must vanish. This yields the relationship between $E$ and $\mathbf{k}$.

The coefficients $A_{lm;l'm'}^{(jj')}$ which derive from the expansion of the Green's function, are related to a smaller set of coefficients, $D_{LM}^{(jj')}$, by

$$A_{lm;l'm'}^{(jj')} = 4\pi i^{l-l'}\sum_{LM} i^{-L}C_{lm;l'm'}^{LM}\, D(E, k)_{LM}^{(jj')} \tag{6}$$

with the $C_{lm;l'm'}^{LM}$ being certain tabulated[5] constants. The $D_{LM}^{(jj')}$ which will be called the "structure coefficients" are given by[4]

VOL 8 195

$$D_{LM}^{jj'} = -\frac{4\pi}{\tau}\frac{i^L}{j_{L(R\sqrt{E})}} \sum_{K_n} \frac{\exp\{i(\mathbf{K}_n+\mathbf{k})\cdot(\mathbf{a}_j-\mathbf{a}_{j'})\} j_L(|\mathbf{K}_n+\mathbf{k}|R) Y_{LM}^*(\mathbf{K}_n+\mathbf{k})}{(\mathbf{K}_n+\mathbf{k})^2-E} + \\ + \sqrt{\frac{E}{4\pi}}\delta_{jj'}\delta_{LO}\cot(R\sqrt{E}) \tag{7}$$

where $\tau$ is the cell volume, $\mathbf{K}_n$ a reciprocal lattice vector and $j_L(x)$ a spherical Bessel function of order $L$.

The structure coefficients have been evaluated by Dr. F. S. HAM and the author for $\mathbf{k}$ vectors lying on the (100), (111) and (110) axes for a wide range of $E$ values for the body-centered cubic, the face-centered cubic, the zinc-blende and rock-salt structures.

As our first application of this method we chose to study the electronic structure of crystals having the diamond structure, in particular Ge.† We have set up a program for the IBM 704 digital computer to solve for the eigenvalues and eigenfunctions.

As a check on the machine program and to gain some idea of the efficiency of the method, we studied some problems for which the eigenvalues are known or are readily calculable. The first was for a potential consisting of spherical wells which are sufficiently deep and well separated so that the tight-binding approximation could be used for comparison. In Tables 1 and 2 are listed the results for the lowest two bands obtained by the tight-binding approximation and by the present method for the (100) and (111) axes respectively. It can be seen that the agreement is generally better than $\frac{1}{2}$ per cent, which is about the accuracy that can be expected for the use of the extreme tight-binding calculation in this case. It should be noted that the convergence for these bands was excellent. This bears out the expectation about the power of the variational principle (1).‡

Another case in which we can compare our results with known band structure is the empty-lattice. Here, as $V = 0$, $\mathscr{R}_l = j_l$, and all the matrix elements $\Lambda_{lm;l'm'}^{(jj')}$ vanish. A further analysis of (4), (5), and (7) shows that for this case the eigenvalue must lie at one of the poles of the structure coefficients and hence that $E = (\mathbf{K}_n+\mathbf{k})^2$. For a further check on our program, however, we calculated the eigenvalues for several shallow wells and extrapolated to $V = 0$. Our results, which are given in Table 3 for two points on the (100) axis, are in satisfactory agreement with the free electron values considering the extrapolation used.

For the Ge calculations we used a modified

*Table* 1

The table lists the two lowest eigenvalues for $\mathbf{k}$ on the (100) axis for deep and well-separated spherical wells with radius, $R$, one-third the interatomic distance and $V_0R^2 = 7$. The $\epsilon_{\text{t.b.}}$ are the values computed by the tight-binding approximation and the $\epsilon_{K-R-K}$ by $K$–$R$–$K$ method. The units are such that the cube edge is $2\pi$.

| | $1_1$ | | $1'_2$ | |
|---|---|---|---|---|
| $k_x$ | $\epsilon_{\text{t.b.}}$ | $\epsilon_{K-R-K}$ | $\epsilon_{\text{t.b.}}$ | $\epsilon_{K-R-K}$ |
| 0 | −3·049 | −3·041 | −2·459 | −2·447 |
| $\frac{1}{4}$ | −3·025 | −3·019 | −2·484 | −2·471 |
| | −2·961 | −2·956 | −2·548 | −2·539 |
| | −2·867 | −2·863 | −2·643 | −2·638 |
| 1 | −2·755 | −2·745 | −2·755 | −2·745 |

*Table* 2

The values given in the table are the two lowest levels for the (111) axis for the same potential as described in Table 1.

| | $1_1 \to \Gamma_1$ | | $1_1 \to \Gamma'_2$ | |
|---|---|---|---|---|
| $k_x$ | $\epsilon_{\text{t.b.}}$ | $\epsilon_{K-R-K}$ | $\epsilon_{\text{t.b.}}$ | $\epsilon_{K-R-K}$ |
| $\frac{1}{8}$ | −3·031 | −3·024 | −2·479 | −2·465 |
| $\frac{1}{4}$ | −2·986 | −2·977 | −2·523 | −2·511 |
| $\frac{3}{8}$ | −2·930 | −2·920 | −2·579 | −2·572 |
| $\frac{1}{2}$ | −2·901 | −2·893 | −2·608 | −2·607 |

† Dr. F. S. HAM is presently using the Kohn–Rostoker–Korringa method in his investigations of the alkali metals.

‡ Dr. HAM also finds good convergence in his calculations on the alkali metals.

Hartree–Fock procedure to obtain the radial functions. Here the boundary condition for the atomic case, that $\psi \to 0$ as $r \to \infty$, is replaced by the condition that the Hartree–Fock functions be normalized in an "equivalent" sphere. In the first step we obtained the self-consistent radial functions for the

*Table* 3.

The tabulated values are those obtained by extrapolating the eigenvalues for shallow spherical wells to $V = 0$ for $\mathbf{k}$ on the (100) axis.

| $k_x$ | $k^2$ | $\epsilon_{ext.}$ |
|---|---|---|
| $\frac{1}{2}$ | 0·250 | 0·253 |
| | 0·5625 | 0·556 |

so-called valence state,[6] ($^5S$—$(4s)(4p)^3$), using a modification of Dr. W. W. PIPER's IBM 650 program[7]* for atomic wavefunctions. The Hartree–Fock eigenvalue parameters for the $4s$ and $4p$ functions were chosen so that the self-consistent solutions had zero slope at the radius of the touching sphere. The radial functions, $\mathscr{R}_l(r)$, for the crystal wavefunction were then obtained by solving the radial equation with a potential (including exchange) due to a "core" consisting of the inner closed shells,[8] one $4s$ electron and two $4p$ electrons spherically averaged. The spin state for this configuration was taken to be a quintet so that the "last" electron experiences maximum exchange to compensate for the neglect of correlations.

The level structure at $\mathbf{k} = 0$ was calculated using only $s$ and $p$ functions. In Table 4, we have listed the eigenvalues for the valence band levels $\Gamma_1$ and $\Gamma_{25}$ and for the two lowest conduction band levels, $\Gamma'_2$ and $\Gamma_{15}$. It can be seen that the results

*Table* 4.

The eigenvalues for Ge at $\mathbf{k} = 0$ are given in Rydberg units with the zero energy coinciding with the constant part of the potential. The value of the potential in the constant region is taken from the modified Hartree-Fock calculations to be −2·033 Ryd.

| | $\epsilon$ |
|---|---|
| $\Gamma_1$ | −0·367 |
| $\Gamma'_{25}$ | 0·892 |
| $\Gamma'_2$ | 0·927 |
| $\Gamma_{15}$ | 1·250 |

for this application of the method for Ge are quite reasonable. From our experience, we expect that the inclusion of higher $l$-values will not alter the results appreciably.

Besides studying the effect of including more terms in the wavefunction, we hope soon to calculate $E(\mathbf{k})$ along the three principal axes. Finally, we hope to study the result of modifying the potential, particularly the exchange part.

*Acknowledgments*—The author wishes to thank Drs. F. S. HAM, E. O. KANE, and W. W. PIPER for many helpful discussions and Miss E. L. KREIGER and Mrs. M. T. GRAY for their invaluable assistance with the numerical analysis.

## REFERENCES

1. KORRINGA J., *Physica* **13,** 392 (1947).
2. KOHN W. and ROSTOKER N., *Phys. Rev.* **94,** 1111 (1954).
3. MORSE P. M., *Proc. Nat. Acad. Sci. U.S.* **42,** 276 (1956).
4. SEGALL B., *Phys. Rev.* **105,** 108 (1957).
5. CONDON E. U. and SHORTLEY G. H., *The Theory of Atomic Spectra*, p. 175ff. Cambridge University Press (1951).
   HAM F. S., unpublished.
6. HERMAN F., *Phys. Rev.* **93,** 1214 (1953).
7. PIPER W. W., *I.E.E. Trans. Comm. and Elect.* p. 152, May 1956.
8. PIPER W. W., to be published in *Phys. Rev.*

* The author wishes to thank Dr. PIPER for making his program available to him and for several discussions concerning its use.

*J. Phys. Chem. Solids* Pergamon Press 1959. Vol. 8. pp. 375–377. Printed in Great Britain

# N.5 ENERGY BAND STRUCTURE OF SODIUM ATOMS IN THE DIAMOND LATTICE*

FRANCO BASSANI

Istituto di Fisica Teorica, University of Pavia, Pavia, Italy

VOL. 8 1959

## 1. INTRODUCTION

THE energy-band structure of diamond and silicon has been theoretically investigated by various authors.[1] The most recent calculations have been made using the method of Orthogonalized Plane Waves and have explained the existence of an energy gap between the valence states and the unoccupied conduction states. The O.P.W. method has been also used successfully to evaluate a large number of energy bands in typical metals such as potassium and lithium.[2]

The symmetry of the lattice, the lattice constant, and the crystal potential are the physical factors on which the relative positions of the energy bands depend. It seemed to be of interest to investigate which is the most important factor in determining the energy-band structure. For this purpose a calculation of the energy-band structure of a pseudolattice made of sodium atoms in the diamond structure has been performed, using the method of Orthogonalized Plane Waves. The lattice parameter of the pseudolattice has been chosen to be $a = 12{\cdot}688a_0$, which gives the same electron density as in metallic sodium.

The results obtained for the pseudolattice of sodium atoms are to be compared with the results for silicon, since the two atoms have the same core states, the only difference being in the density of electrons and in the lattice potential.

## 2. CRYSTAL POTENTIAL AND O.P.W. PARAMETERS

A one-electron crystal potential is obtained in the approximation described by WOODRUFF.[3]

The self-consistent equations of atomic sodium have been solved by HARTREE and HARTREE.[4] From their numerical values for the wave functions and for the effective nuclear charge an atomic potential has been constructed, using the Slater free-electron exchange approximation.[5] The atomic potential thus obtained is then approximated by an analytical expression, and the Fourier coefficients with reciprocal vector $\mathbf{h}$ different from zero are evaluated.

By making a direct numerical integration for the case of $\mathbf{h} = 2\pi a^{-1}(1, 1, 1)$ it has been found that the analytical approximation to the atomic potential introduces an error of the order of 1 per cent only.

The Fourier coefficient of the lattice potential $V(0, 0, 0)$ has been evaluated by numerical integration from the data of HARTREE and HARTREE within the approximation described by WOODRUFF[1] and by CASELLA.[6] All the values of the Fourier coefficients which have been used in the calculation of the crystal potential are listed in Table 1.

The orthogonality coefficients can be expressed by the formula

$$A_{nl}(|\mathbf{K}+\mathbf{h}|) = (\Omega_0)^{-\frac{1}{2}} \int_{\infty} u_{nl}^* \exp[i(\mathbf{K}+\mathbf{h}) \cdot \mathbf{r}]dv,$$

where $u_{nl}$ is the wave-function of the atomic-core state and $\Omega_0$ is the volume per atom. Because of the advantage of having analytical expressions easy to integrate, the orthogonalized Slater atomic orbitals[7] have been used as the core wave-functions of sodium. This introduces a slight inconsistency which is believed to be not very important for the purpose of the present work.

The values given by HARTREE and HARTREE:[4] $E_{1s} = -81{\cdot}46$, $E_{2s} = -6{\cdot}15$, $E_{2p} = -3{\cdot}603$, in Rydberg units, have been used as the energy parameters of the core states.

## 3. NUMERICAL RESULTS AND CONCLUSIONS

The values of the energies have been calculated

* This work was started at the University of Illinois, under a contract of the Office of Naval Research.

at four symmetry points of the reduced zone: $K = 0$, $K = 2\pi a^{-1}(1, 0, 0)$, $K = 2\pi a^{-1}(\frac{1}{2}, \frac{1}{2}, \frac{1}{2})$, $K = 2\pi a^{-1}(\frac{1}{2}, 0, 0)$. Plane waves which originate from the sets of reciprocal-lattice vectors $\mathbf{h} = 0$, $\mathbf{h} = \langle 1, 1, 1\rangle$, $\mathbf{h} = \langle 2, 0, 0\rangle$, $\mathbf{h} = \langle 2, 2, 0\rangle$ have been used. The resulting secular equations are at most of the fifth order, and have been solved in some cases with the aid of the digital computer of the Engineering School of Milano.

*Table* 1. *Fourier coefficients of the crystal potential (in Rydbergs)*

| | |
|---|---|
| $V(000) = -1{\cdot}1278$ | $V(331) = -0{\cdot}1278$ |
| $V(111) = -0{\cdot}3549$ | $V(422) = -0{\cdot}1094$ |
| $V(220) = -0{\cdot}2124$ | $V(511) = V(333) = -0{\cdot}1008$ |
| $V(311) = -0{\cdot}1783$ | $V(440) = -0{\cdot}0892$ |
| $V(400) = -0{\cdot}1425$ | |

The Fourier coefficients of the potential are defined as $V(|\mathbf{h}|) = (N\Omega_0)^{-1}\int_\infty V \exp(i\mathbf{h}\cdot\mathbf{r})dv$, where $N$ is the number of atoms, $\Omega_0$ the volume per atom and $V$ the total crystal potential.

The values of the energies at different stages of approximation are given in Tables 2 and 3 for the points $K = 0$ and $K = 2\pi a^{-1}(1, 0, 0)$. In Fig. 1

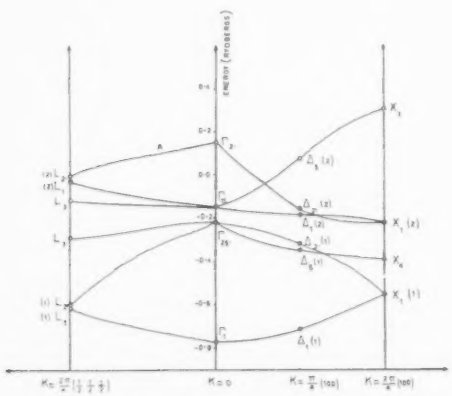

FIG. 1. Energy-band profile for a diamond-type lattice made of sodium atoms.

the probable profiles of the energy bands are drawn in the directions [1, 0, 0] and [1, 1, 1] taking into account the final results for the two other points of symmetry $K = 2\pi a^{-1}(\frac{1}{2}, 0, 0)$ and $K = 2\pi a^{-1}(\frac{1}{2}, \frac{1}{2}, \frac{1}{2})$.

It can be seen at once that the energy bands of Fig. 1 display a strict similarity with the bands of silicon.[1] A comparison of Tables 2 and 3 with Table 4 of WOODRUFF's paper and with Table 2 of BASSANI's paper[1] shows that the order of appearance of the energies corresponding to the various irreducible representations is the same in the case of the lattice made of sodium atoms as in the case of the lattice made of silicon atoms. The separation between the energies is smaller in the case of sodium, mainly because of the higher value of the lattice constant. The energy at $X_1(2)$ lies lower than at $\Gamma_{15}$ and this indicates a tendency for

*Table* 2. *Energies at the point* $K = 0$ *(in Rydbergs)*

| | $\Gamma_1$ | $\Gamma_{25}'$ | $\Gamma_{15}$ | $\Gamma_2'$ |
|---|---|---|---|---|
| $E_1$ | $-0{\cdot}753$ | $-0{\cdot}116$ | $-0{\cdot}116$ | $0{\cdot}168$ |
| $E_2$ | $-0{\cdot}763$ | $-0{\cdot}207$ | $-0{\cdot}147$ | $0{\cdot}147$ |
| $E_3$ | $-0{\cdot}767$ | $-0{\cdot}218$ | | |

The subscripts attached to $E$ indicate the order of the secular determinant used in obtaining the energies.

*Table* 3. *Energies at the point* $K = 2\pi a^{-1}(1, 0, 0)$ *(in Rydbergs)*

| | $X_1(1)$ | $X_4$ | $X_1(2)$ | $H_3$ |
|---|---|---|---|---|
| $E_1$ | $-0{\cdot}521$ | $-0{\cdot}358$ | | $0{\cdot}352$ |
| $E_2$ | $-0{\cdot}529$ | $-0{\cdot}399$ | $-0{\cdot}209$ | $0{\cdot}305$ |
| $E_3$ | $-0{\cdot}536$ | $-0{\cdot}400$ | $-0{\cdot}209$ | |
| $E_4$ | $-0{\cdot}546$ | | $-0{\cdot}220$ | |
| $E_5$ | $-0{\cdot}554$ | | $-0{\cdot}226$ | |

The subscripts attached to $E$ indicate the order of the secular determinant used in obtaining the energies.

the conduction bands to have a minimum near the edge of a zone in the direction [1, 0, 0]; it lies also lower than at $\Gamma_{25}'$ but the difference between the two energies is too small to be significant. It seems possible to conclude that the sequence of the energy bands is mainly determined by the lattice symmetry and their separation by the electron density.

*Acknowledgments*—The writer wishes to thank Professor F. SEITZ who suggested this problem. He is also indebted to Professor F. FUMI for his encouragement and to Dr. G. BORTONE for his generous help in the last stage of the calculations.

**REFERENCES**

1. HERMAN F., *Phys. Rev.* **88,** 1210 (1952); *Ibid.* **93,** 1214 (1954).
   JENKINS D. P., *Proc. Roy. Soc.* A**69,** 548 (1956).
   WOODRUFF T. O., *Phys. Rev.* **103,** 1159 (1956).
   BASSANI F., *Phys. Rev.* **108,** 263 (1957).
2. CALLAWAY J., *Phys. Rev.* **103,** 1219 (1956).
   GLASSER M. L. and CALLAWAY J., *Phys. Rev.* **109,** 1541 (1958).
3. WOODRUFF T. O., "The Orthogonalized Plane-Wave Method", *Solid State Physics,* Vol. 4. Academic Press, New York (1957).
4. HARTREE D. R. and HARTREE W., *Proc. Roy. Soc.* A**193,** 299 (1948).
5. SLATER J. C., *Phys. Rev.* **81,** 385 (1951).
6. CASELLA R., *Phys. Rev.* **109,** 54 (1958).
7. SLATER J. C., *Phys. Rev.* **36,** 57 (1930).
   SLATER J. C., *Phys. Rev.* **42,** 33 (1932).


VOL. 8 1959

*J. Phys. Chem. Solids* Pergamon Press 1959. Vol. 8. pp. 377–379. Printed in Great Britain

# N.6 THE MASS-ACTION LAWS FOR FREE CARRIERS AND AMPHOTERIC IMPURITIES IN SEMICONDUCTORS


**F. W. G. ROSE**

Research Laboratory, British Thomson Houston Co. Ltd., Rugby


## 1. INTRODUCTION

IT is usually assumed that impurities or other centres in semiconductors can only act either as donors, i.e. give away one electron and become positively charged, or as acceptors, i.e. attach one electron and become negatively charged, and it is often not considered that "amphoteric" impurities may exist which possess both properties. The existence of such amphoteric impurities is probable from experimental investigations (compare DUNLAP's review[1]) and a theoretical treatment of their effect on the carrier concentration and recombination will be given here (*cf.* SHOCKLEY and LAST[2]).

## 2. CALCULATION OF THE CARRIER CONCENTRATION

In the following calculations it will be assumed that the amphoteric impurity exists in two neutral modifications, $D^x$ and $A^x$, which are in equilibrium. The modification $D^x$ can give away one electron and become a positively charged donor $D^+$, the modification $A^x$ can accept one electron and become a negatively charged acceptor $A^-$. The ratio of the concentration of $D^x$ to the concentration of $A^x$ may be given in equilibrium by

$$\frac{n_{D^x}}{n_{A^x}} = a \tag{1}$$

where $n$ is the concentration of the particle written as subscript and where $a$ is a constant at constant temperature.

### 2.1. *p-Type semiconductors*

The reactions between free holes $h$ and the $A^x$, $D^x$, $A^-$, $D^+$ are the following:

$$A^x \rightleftharpoons A^- + h \tag{2}$$

$$D^+ \rightleftharpoons D^x + h \tag{3}$$

From equations (1), (2) and (3) the mass-action laws

$$\frac{p n_{A^-}}{n_{A^x}} = K_A \tag{4}$$

$$\frac{p n_{D^x}}{n_{D^+}} = \frac{p a n_{A^x}}{n_{D^+}} = K_D \tag{5}$$

can be derived, where $n$ is as above, $p$ the hole concentration and where $K_A$ and $K_D$ are the temperature dependent mass-action constants. These are

given in non-degenerate semiconductors by

$$K_A = \frac{f_1}{g_1} N_v \exp\left[\frac{-(\epsilon_A - \epsilon_v)}{kT}\right] \quad (6)$$

$$K_D = \frac{g_2}{f_2} N_v \exp\left[\frac{-(\epsilon_D - \epsilon_v)}{kT}\right] \quad (7)$$

where $N_v$, $\epsilon_A$, $\epsilon_D$, $\epsilon_v$, $k$, $T$ are the effective density of energy levels in the valence band, the energy level of the amphoteric impurity's acceptor modification, the energy level of the donor modification, the highest energy level in the valence band, and where $f_1$, $g_1$, $f_2$, $g_2$ are the numbers of possible values for the resultant electron spin in $A^-$, $A^x$, $D^+$, $D^x$ respectively. It has been shown (ROSE[3]) that in a degenerate semiconductor $N_v$ must be replaced by $(N_v - p)$ and that the value of $N_v$ and $(N_v - p)$ at various values of $p$ can be calculated from tables or evaluated from graphs. Introducing the total concentration

$$N = n_{D^x} + n_{A^x} + n_{D^+} + n_{A^-} \quad (8)$$

of amphoteric impurities, one has from equations (4) to (8)

$$n_{A^-} = \frac{N}{1 + \frac{(a+1)p}{K_A} + \frac{ap^2}{K_A K_D}} \quad (9)$$

$$n_{D^+} = \frac{N(ap^2/K_A K_D)}{1 + \frac{(a+1)p}{K_A} + \frac{ap^2}{K_A K_D}} \quad (10)$$

For the case that genuine donors $\bar{D}$ and acceptors $\bar{A}$ are also present in the semiconductor it follows from neutrality that

$$\begin{aligned} p &= n_{\bar{A}^-} - n_{\bar{D}^+} + n_{A^-} - n_{D^+} \\ &= n_{\bar{A}^-} - n_{\bar{D}^+} + \frac{N[1-(ap^2/K_A K_D)]}{1 + \frac{(a+1)p}{K_A} + \frac{ap^2}{K_A K_D}} \end{aligned} \quad (11)$$

in an "extrinsic" semiconductor, i.e. where the concentration of free electrons is neglected.

Analogous equations can be derived in $n$-type semiconductors, i.e.

$$n_{D^+} = \frac{N}{1 + \frac{(b+1)n}{k_D} + \frac{bn^2}{k_D k_A}} \quad (12)$$

$$n_{A^-} = \frac{N(bn^2/k_D k_A)}{1 + \frac{(b+1)n}{k_D} + \frac{bn^2}{k_D k_A}} \quad (13)$$

$$n = n_{\bar{D}^+} - n_{\bar{A}^-} + \frac{N[1-(bn^2/k_D k_A)]}{1 + \frac{(b+1)n}{k_D} + \frac{bn^2}{k_D k_A}} \quad (14)$$

$$b = \frac{1}{a} = \frac{n_{A^x}}{n_{D^x}} \quad (15)$$

$$k_D = \frac{f_2}{g_2} N_c \exp\left[\frac{-(\epsilon_c - \epsilon_D)}{kT}\right] \quad (16)$$

$$k_A = \frac{g_1}{f_1} N_c \exp\left[\frac{-(\epsilon_c - \epsilon_A)}{kT}\right] \quad (17)$$

$$K_A k_A = K_D k_D = N_c N_v \exp\left[\frac{-(\epsilon_c - \epsilon_v)}{kT}\right] \equiv n_i^2 \quad (18)$$

where $n$ is the concentration of free electrons, $\epsilon_c$ the lowest level in the conduction band, and $N_c$ the effective density of energy levels in the conduction band.

### 3. THE STEADY STATE RECOMBINATION OF FREE CARRIERS VIA AMPHOTERIC IMPURITIES

In a steady state the concentration of the charged donor modification and the concentration of the neutral donor modification do not change. This implies that

$$\alpha_{pD} p n_{D^x} + b_{2D} n_{D^x} = \alpha_{nD} n n_{D^+} + b_{1D} n_{D^+} \quad (19)$$

where in analogy to the paper by ROSE and SANDIFORD[4] $\alpha_{pD}$ and $\alpha_{nD}$ are the recombination constant for the recombination of free holes with neutral donor type centres and the recombination constant for the recombination of free electrons with positively charged donor type centres respectively and where

$$b_{2D} = \alpha_{nD} k_D; \; b_{1D} = \alpha_{pD} K_D$$

The surplus of the rate of recombination of free holes with amphoteric donor centres over the

generation rate of free holes from these centres is from ROSE and SANDIFORD[4] and from equations (19), (18) and (12).

$$\Delta(R_p-G_p)_D = \alpha_{pD}pn_{D^x}-b_{1D}n_{D^+}$$

$$= \frac{\alpha_{pD}\alpha_{nD}N(pn-n_i^2)}{\left[1+\frac{(b+1)n}{k_D}+\frac{bn^2}{k_Dk_A}\right](\alpha_{pD}p+\alpha_{nD}k_D)} \quad (20)$$

In a similar way the recombination of free carriers via the acceptor modification of the amphoteric impurities may be calculated and one finds for the recombination via both modifications

$$\Delta(R_p-G_p) = \Delta(R_n-G_n) = \frac{N(pn-n_i^2)}{\left[1+\frac{(b+1)n}{k_D}+\frac{bn^2}{k_Dk_A}\right]}\left[\frac{\alpha_{pD}\alpha_{nD}}{\alpha_{pD}p+\alpha_{nD}k_D}+\frac{\alpha_{pA}\alpha_{nA}bn^2}{k_Dk_A(\alpha_{nA}n+\alpha_{pA}K_A)}\right] \quad (21)$$

If only small deviations $\Delta n$ and $\Delta p$ from the equilibrium concentrations $p_0$ of holes and $n_0$ of electrons and sufficiently small concentrations of amphoteric impurities are considered it is easy to derive the steady state lifetime $\tau = \Delta p/\Delta(R_p-G_p) = \Delta n/\Delta(R_n-G_n)$ of free carriers in a semiconductor containing amphoteric impurities. For this case $\Delta p \simeq \Delta n$ and $pn-n_i^2 \simeq p_0\Delta n+n_0\Delta p$.

## 4. CONCLUSIONS

Equations for the concentration of the positively charged, negatively charged and neutral amphoteric impurities have been calculated. From these it can be shown that the same amphoteric impurity may act as a donor in $p$-type material and as an acceptor in $n$-type material if the donor level is near to the conduction band and the acceptor level nearer to the valence band. However, in both $p$ and $n$-type material an amphoteric impurity will act as a donor if both its levels are near to the conduction band, and as an acceptor when both levels are near to the valence band. With other positions of the levels it may act as an acceptor in $n$-type material and be ineffective in $p$-type material, or with certain positions of the levels it may act as a donor in $p$-type material and be ineffective in $n$-type material.

The steady state recombination of free carriers via the amphoteric impurities can be calculated and it can be shown that the amphoteric impurities do not simply act as if they were independent donor centres and acceptor centres.

One interesting aspect of various impurities should be mentioned in connection with amphoteric action, i.e. that some of them may act as donors as well as acceptors not because they are amphoteric in themselves but because they are built into the lattice in different ways. This type of amphoteric action needs a different theoretical treatment and, therefore, is not included in the results given here.

*Acknowledgments*—The author would like to thank Mr. N. H. SAUNDERS for helpful discussions and his other colleagues in the Research Laboratory for their encouragement and assistance.

### REFERENCES

1. DUNLAP Jr., W. C., *Progress in Semiconductors* II edited by A. F. GIBSON, R. E. BURGESS and P. AIGRAIN. Heywood, London (1957).
2. SHOCKLEY, W., and LAST, J. T., *Phys. Rev.* **107**, 392 (1957).
3. ROSE F. W. G., *Proc. Phys. Soc.* **71**, 699 (1958).
4. ROSE F. W. G. and SANDIFORD D. J., *Proc. Phys. Soc.* B**68**, 894 (1955).

## DISCUSSION

*Compiled by*: F. HERMAN

### N.1 A. MORITA

J. BIRMAN (Sylvania): What is the relation between your method and that of SCHMID?[1]

A. MORITA: SCHMID works with two-electron wave functions, while I work with one-electron wave functions.

J. BIRMAN: Are you able to carry the ionic character along as a parameter in your calculations?

A. MORITA: Not yet, but I'm trying to do something along these lines.

### N.2 P. L. CHOQUARD *et al.*

E. MOOSER (ETH, Zurich): It seems to me that your attempt to relate bonds and bands in solids is essentially a *quantitative* formulation of the "semiconducting bond"

model which PEARSON and I proposed some time ago (see, for example, E. MOOSER and W. B. PEARSON[2]). I would, therefore, like to ask you whether, on the basis of your treatment, you come to conclusions similar to ours as regards the transition from semiconducting to metallic behavior which is found on transforming amorphous antimony into the crystalline (hexagonal) phase?

P. CHOQUARD: In both amorphous and hexagonal antimony the same double layers of atoms occur, each atom having three nearest neighbors. The difference between the two phases is due to the fact that in crystalline antimony these double layers are ordered with respect to one another, thereby allowing a strong interaction between neighboring sheets to occur. In amorphous antimony on the other hand, the sheets are disordered, the interaction between them being only of the van der Waals type. In this phase the three $p$ electrons therefore form three saturated covalent bonds and semiconducting properties would be expected. The strong interaction between the layers in the hexagonal phase indicates the existence of some covalent bonding between the sheets. This bonding can be explained by assuming uninhibited resonances involving $d$ orbitals. Because of these resonances metallic properties result.

### N.3 J. C. PHILLIPS

F. HERMAN (RCA Laboratories): PHILLIPS' work is perhaps best understood as a bold and interesting attempt to relate the band structures of silicon and germanium to the corresponding empty-lattice band-structure. This is accomplished by introducing a suitably chosen pseudopotential. In order to grasp the physical significance of this pseudopotential, and the nature of the underlying approximations, it is instructive to examine the matrix elements of the crystal Hamiltonian in the OPW representation (see, for example, C. HERRING[3]). For our purposes, it is convenient to write the energy matrix elements connecting the extended wave vectors $\mathbf{K}'$ and $\mathbf{K}$ as follows:

$$\langle \mathbf{K}'|H|\mathbf{K}\rangle = K^2\delta(\mathbf{K}',\mathbf{K}) + V(\mathbf{K}-\mathbf{K}') - \sum_l Q_l(\mathbf{K}',\mathbf{K})R_l(\mathbf{K}',\mathbf{K}),$$

where the Fourier coefficients of the (ordinary) crystal potential, $V(\mathbf{r})$, are denoted by $V(\mathbf{K}-\mathbf{K}')$, and the orthogonality coefficients and the geometrical phase factors associated with all the core states of type $l$ by $Q_l(\mathbf{K}',\mathbf{K})$ and $R_l(\mathbf{K}',\mathbf{K})$, respectively. (For simplicity, we shall ignore the non-orthogonality matrix elements $\langle \mathbf{K}'|1|\mathbf{K}\rangle$ which also occur in the OPW method.)

Since the crystal potential terms are attractive, and the orthogonality terms repulsive, there is a partial cancellation of these sets of terms. The more complete the cancellation, the more nearly does the actual band structure resemble the empty-lattice band-structure, which is given simply by the kinetic energy terms $K^2\delta(\mathbf{K}',\mathbf{K})$.

PHILLIPS' primary goal is to exploit this "partial cancellation" feature to the utmost. With this in mind, he arbitrarily drops all orthogonality terms associated with $p$ and $d$ core states ($l = 1$ and 2). The $s$ orthogonality terms are retained, but all the $Q_0(\mathbf{K}',\mathbf{K})$ are approximated by a constant, $Q_0$. Since, $R_0(\mathbf{K}',\mathbf{K}) = R_0(\mathbf{K}-\mathbf{K}')$, it is now possible to introduce a pseudopotential $P(\mathbf{r})$ with Fourier coefficients $P(\mathbf{K}-\mathbf{K}') = V(\mathbf{K}-\mathbf{K}') - Q_0R_0(\mathbf{K}-\mathbf{K}')$. Because corresponding $V(\mathbf{K}-\mathbf{K}')$ and $Q_0R_0(\mathbf{K}-\mathbf{K}')$ tend to partially cancel each other, $|P(\mathbf{K}-\mathbf{K}')| <$ or $\ll |V(\mathbf{K}-\mathbf{K}')|$. Thus, the pseudopotential $P(\mathbf{r})$ is much weaker than the ordinary crystal potential $V(\mathbf{r})$.

As a first approximation for the pseudopotential, PHILLIPS assumes that $P(\mathbf{K}-\mathbf{K}') = P$, a constant, for all $\mathbf{K}-\mathbf{K}'$. This corresponds to a delta function placed at each lattice site. In the next approximation, a few of the leading $P(\mathbf{K}-\mathbf{K}')$, such as $P(000)$, $P(111)$, and $P(220)$, are permitted to depart from the constant value $P$. These deviations from $P$, and $P$ itself, constitute the disposable parameters of PHILLIPS' interpolation scheme.

In order to avoid the possibility of convergence difficulties, and in order to simplify the numerical work, the secular equations are truncated at a suitable point, i.e., it is required that $\langle \mathbf{K}'|H|\mathbf{K}\rangle = 0$ for $\mathbf{K}'$ or $\mathbf{K} > \mathbf{K}^{\max}$, where the choice of $\mathbf{K}^{\max}$ depends upon the symmetry classification of the state under consideration (see J. C. PHILLIPS,[4] for a more adequate discussion of this aspect). In the discussion to follow, we will ignore the non-local character introduced into the pseudopotential by this truncation procedure.

In order to obtain fits to the experimental band structure, PHILLIPS finds it necessary to choose $P(111) < 0$, i.e., attractive, and $P > 0$, i.e., repulsive. Roughly speaking, the pseudopotential thereby defined consists of a repulsive delta function at each lattice site (this serves to keep the valence and conduction band electrons out of the lower-lying core states), and a shallow attractive well centered at the midpoint of each interatomic bond. The latter feature may be interpreted as a manifestation of the covalent bonding implicit in diamond-type crystals: the attractive wells encourage the valence charge density to pile up along the chemical bonds.

It is important to observe that in order to introduce a forbidden band in the perturbed empty-lattice band-structure of diamond-type crystals, it is necessary to place a *repulsive* delta function (or a more spread out but peaked function) at each lattice site. I obtained this result about three years ago (in unpublished work) while attempting to evaluate the physical significance of one-dimensional Kronig-Penney models of diamond-type and zinc-blende-type crystals [cf. B. SERAPHIN[5] and I. ADAWI;[6] for another viewpoint on this question, see A. I. GUBANOV[7]]. In the one-dimensional case, it is necessary to place an *attractive* well at each lattice site in order to separate the bands which are conventionally chosen as the valence and conduction bands. In order to separate the valence and conduction bands in the actual three-dimensional case, it is necessary to introduce a weak repulsive potential at each lattice site (this corresponds to PHILLIPS' result), or an attractive potential sufficiently strong to have bound (core) states (this is the actual situation). If a weak attractive potential (without bound states) is placed as each lattice site, as in the one-dimensional studies cited above, no forbidden band is

formed. Thus, one must exercise considerable caution in attaching a physical significance to the results of such one-dimensional studies.

In conclusion, I wish to point out that while PHILLIPS' scheme is certainly a step in the right direction, a great deal of work remains to be done before its conclusions can be considered physically significant. Without a careful examination of the consequences of the various approximations described above, particularly the neglect of $p$ and $d$ orthogonality terms, and the abruptness of the truncation procedure, it is difficult to distinguish results which are artifacts of the method, and results which are not.

J. TIEMANN (General Electric Research Laboratory): On physical grounds, the assumption of a repulsive potential more spread out than a delta function is preferable to the assumption of a delta function repulsive potential. This may be advantageous in providing an additional parameter (the spread), and also in alleviating the truncation problem, since $P(\mathbf{K}-\mathbf{K}')$ = constant is replaced by a decreasing function of $|\mathbf{K}-\mathbf{K}'|$.

J. CALLAWAY (University of Miami): One is a bit concerned about the ultimate convergence of PHILLIPS' procedure as more and more plane waves are included in the expansion. By putting $P|\mathbf{K}-\mathbf{K}'|$ = constant for large $|\mathbf{K}-\mathbf{K}'|$, the off-diagonal matrix elements of the Hamiltonian do not decrease with distance from the diagonal.

J. C. PHILLIPS: In my scheme, convergence difficulties are avoided by suitably truncating the secular equations. Truncation is much more effective in hastening the convergence than in making $P|\mathbf{K}-\mathbf{K}'|$ a decreasing function of $|\mathbf{K}-\mathbf{K}'|$.

B. S. GOURARY (Johns Hopkins University): How do you determine the maximum number of plane waves that you *may* use with your effective potential?

J. C. PHILLIPS: By trial and error.

B. S. GOURARY: As I recall from the work of HELLMAN and HELLMAN and KASSATOTSCHKIN on effective potentials for atoms, *too much freedom* in the variational trial wave function can lead to incorrect results, unless the effective potential is further refined.

J. C. PHILLIPS: Since I am not actually dealing with variational trial wave functions, this consideration is presumably not relevant.

E. O. KANE (General Electric Research Laboratory): How can you expect to get energy values accurate to 0·05 Ryd, when the matrix elements of $\epsilon(\mathbf{k}\cdot\mathbf{p})$ between the valence and conduction bands near the edge of the zone are of order 0·3 Ryd for $\epsilon = 0{\cdot}3$?

J. C. PHILLIPS: Non-zero values of $\epsilon$ will not be important when the main contribution to the variation of $E$ with $\mathbf{k}$ is given by the kinetic energy terms. Off-diagonal matrix elements of $\mathbf{k}\cdot\mathbf{p}$ between the lowest conduction and highest valence bands exist only for $\mathbf{k}$ transverse to the [100] and [111] directions. Thus if the direct energy gap $\Delta E$ is determined to fit experiment at the center of the zone, it is possible to get correct values for $\Delta E$ along the [100] and [111] directions. To calculate the density of states in the conduction band, however, it would be necessary to include exchange effects explicitly for regions of the zone away from the [100] and [111] directions.

### N.4 B. SEGALL

J. BIRMAN (Sylvania): What is the relative importance of errors arising from truncation and errors arising from the assumption of a spherically symmetric potential inside each "atomic sphere" and a constant potential elsewhere?

B. SEGALL: From what I have already done, the truncation errors appear to be of negligible importance. I am not yet able to assess the importance of errors arising from the assumed form of the crystal potential.

J. CALLAWAY (University of Miami): Even if nonspherical effects are neglected, the Kohn–Rostoker potential cannot be self-consistent. According to electrostatics, the fact that the potential is flat between the inscribed sphere and the cell boundary means that there are no electrons in this region. Also, the method necessitates a discontinuity in the potential or its derivative inside the cell.

W. KOHN (Carnegie Institute of Technology): The difficulties just mentioned are compensated by the many favorable aspects of the method, such as the rapid convergence, and the immediate applicability to all crystals of a given structure, once the scattering matrix for this structure is determined.

### N.5 F. BASSANI

J. CALLAWAY (University of Miami): Qualitative considerations of crystal symmetry may quite properly be used to determine the order of levels at symmetry points, provided the levels are basically of the same type (as $\Gamma_{15}$ and $\Gamma_{25'}$ are $p$ levels in the diamond lattice). It is not possible to deduce the relation between levels of different types in this way (as $\Gamma_{2'}$ and $\Gamma_{15}$, for instance). This depends more strongly on the crystal potential, and is, in fact, different in germanium and silicon.

F. BASSANI: Under favorable conditions, it is also possible to predict the order of related levels by examining the corresponding plane wave expansions. For example, consider the lowest non-core $\Gamma_{25'}$ and $\Gamma_{15}$ states in the diamond lattice. The leading plane wave terms in the expansion for $\Gamma_{25'}$ are [111], [200], [220]... The leading terms for $\Gamma_{15}$ are [111], [220]... The occurrence of the [200] terms in the former, and not in the latter, suggests that a variational trial wave function for $\Gamma_{25'}$ will have a lower energy than that for $\Gamma_{15}$. This expectation is borne out in practice.

## REFERENCES


1. SCHMID L. A., *Phys. Rev.* **92,** 1373 (1953); *Amer. J. Phys.* **22,** 255 (1954).
2. MOOSER E. and PEARSON W. B., *Canad. J. Phys.* **34,** 1369 (1956).
3. HERRING C., *Phys. Rev.* **57,** 1169 (1940).
4. PHILLIPS J. C., *Phys. Rev.*, **112,** 685 (1958).
5. SERAPHIN B., *Z. Naturf.* **9a,** 450 (1954).
6. ADAWI I., *Phys. Rev.* **105,** 789 (1957).
7. GUBANOV A. I., *Sov. Phys., J. Tech. Phys.* **1,** 2107 (1957).

*J. Phys. Chem. Solids* Pergamon Press 1959. Vol. 8. pp. 382–388. Printed in Great Britain

SESSION O:

EXCITONS AND PHOTONS*

# O.1 THEORY OF FINE STRUCTURE ON THE ABSORPTION EDGE IN SEMICONDUCTORS

**R. J. ELLIOTT and R. LOUDON**

Clarendon Laboratory, Oxford, England

**Abstract**—General equations are derived for the details of the direct absorption edge in a semiconductor when the effects of excitons and of an applied external magnetic field are included. The effects produced by magnetic fields and excitons separately are readily derived as special cases and these are briefly reviewed with reference to work already published. The problem including both simultaneously could not be solved in general but expressions for the continuous absorption are obtained in an approximation valid in large magnetic fields. Simple spherical bands are assumed throughout and spin effects neglected.

VOL
8
195

## 1. INTRODUCTION

THE important properties of semiconductors are largely determined by those one-electron energy states which lie immediately above and below the forbidden energy gap. A great deal of information about the nature of these states can be obtained from the study of the optical absorption in a crystal—in particular that associated with transitions in which an electron is transferred from the valence band to the conduction band, leaving behind a hole. This creation of a hole–electron pair requires a minimum energy roughly equal to the band gap and the absorption rises steeply as the photon energy is increased from this value. This absorption edge shows in high resolution a complicated shape which may form a series of lines. These are due to the formation of excitons, which are essentially bound hole–electron pairs, and they have been extensively studied in ionic semiconductors (notably $Cu_2O$) by GROSS,[1] NIKITINE[2] and others (the references give review papers). More recently lines of this kind have been observed in Ge by MACFARLANE *et al.*[3] and LAX *et al.*[4] In the presence of a magnetic field the continuous absorption beyond the exciton lines changes shape and may form a series of peaks. This magneto-optic effect has been observed by BURSTEIN,[5] LAX[6] and co-workers and proves a powerful method of determining effective masses in the bands. The magnetic field also affects the excitons and when the magnetic energy is much less than the exciton binding energy, linear and quadratic Zeeman effects have been observed in the lines of $Cu_2O$ by GROSS.[1] In larger fields more complex effects have been seen by LAX, ROTH and ZWERDLING.[4]

In this paper the theoretical form of this absorption will be discussed. An attempt is made to set up a general form of the theory within the framework of the effective mass approximation which includes exciton and magnetic field effects simultaneously. Simple spherical bands are assumed and spin effects neglected. This problem is only solved in an approximation valid for large magnetic fields to give the shape of the continuous absorption under various conditions of allowed and forbidden transitions between the band edges. The fine structure arising from excitons[7] alone and the theory of magneto-optic effect[8] without excitons have already been treated theoretically. These results are reviewed however as they are readily obtained as special cases of the general expression.

This theory is confined to direct optical absorption and does not discuss the indirect transitions involving phonons investigated by MACFARLANE *et al.*[9] where exciton effects were also observed.[8]

*Chairman*: R. A. SMITH; *Co-Chairman*: M. LAX.

## 2. WAVE FUNCTIONS

The single particle wave functions are Bloch functions of form

$$u_{\mathbf{k},j}(\mathbf{r})\exp(i\mathbf{k}\cdot\mathbf{r}) \tag{1}$$

where $\mathbf{k}$ specifies the wave vector and $j$ the band. The ground state of the system is a determinantal function for $N$ electrons which just fill the states available in the valence bands. The excited state consists of a similar function with one electron in a conduction band state $\mathbf{k}_e, c$ and an electron missing in $-\mathbf{k}_h, v$. This latter may be regarded as a hole with $\mathbf{k}_h, v$ so that the state may be regarded as two particles with a product function:

$$u_{\mathbf{k}_e,c}(\mathbf{r}_e)u_{\mathbf{k}_h,v}(\mathbf{r}_h)\exp i(\mathbf{k}_e\cdot\mathbf{r}_e+\mathbf{k}_h\cdot\mathbf{r}_h) \tag{2}$$

The effective mass approximation for one particle systems has been given its most complete exposition by KOHN and LUTTINGER[10] and applied to the two particle problem of excitons by DRESSELHAUS.[11] The wave function of the two particle system including the Coulomb attraction of the particles and the magnetic field may be written as a linear combination.

$$\Psi_{n,\mathbf{K}}(\mathbf{r}_e,\mathbf{r}_h)= \sum_{\mathbf{k}_e,\mathbf{k}_h} B(\mathbf{k}_e,\mathbf{k}_h)e^{i(\mathbf{k}_e\cdot\mathbf{r}_e+\mathbf{k}_h\cdot\mathbf{r}_h)}\phi_{\mathbf{k}_e,c}(\mathbf{r}_e)\phi_{\mathbf{k}_h,v}(\mathbf{r}_h) \tag{3}$$

where the functions $\phi_{\mathbf{k}}$ are expanded as a linear combination of the complete set of functions formed by the Bloch functions of a specific $\mathbf{k}$ in all the bands. For convenience we assume that the conduction and valence band edges are at $\mathbf{k}=0$ and only spin degenerate. Then

$$\phi_{\mathbf{k},c}=u_{0,c}+\sum_{a\neq c}\frac{\mathbf{p}^{\alpha}_{ac}}{mE_{ac}}\left[\hbar k_\alpha+\frac{e}{c}A_\alpha\right]u_{0a}$$

$$\phi_{\mathbf{k},v}=u_{0v}+\sum_{a\neq v}\frac{\mathbf{p}^{\alpha}_{av}}{mE_{av}}\left[\hbar k_\alpha-\frac{e}{c}A_\alpha\right]u_{0a} \tag{4}$$

where there is a summation over the three cartesian directions $\alpha$.

$E_{ac}$ is the energy difference between the $\mathbf{k}=0$ states in bands $a$ and $c$ and $\mathbf{p}_{ac}$ is the momentum matrix element

$$\frac{(2\pi)^3}{\Omega}\int_{\text{unit cell}} u_{0c}^{*}(-i\hbar\nabla)u_{0a}d\mathbf{r} \tag{5}$$

and $A$ is the vector potential, $\Omega$ is the volume of a unit cell.

The functions $\phi$ represent the modulation introduced by the atom cores on the total wave function. The overall motion of the two particles is given by the function

$$\Phi_{n\mathbf{K}}(\mathbf{r}_e,\mathbf{r}_h)=\sum_{\mathbf{k}_e,\mathbf{k}_h}B_{n,\mathbf{K}}(\mathbf{k}_e,\mathbf{k}_h)e^{i(\mathbf{k}_e\cdot\mathbf{r}_e+\mathbf{k}_h\cdot\mathbf{r}_h)} \tag{6}$$

In the effective mass approximation this function is found to be a solution of a Schrodinger-type equation with the effective masses $m_e$, $m_h$ of the bands included and the perturbing potentials of the magnetic field and a Coulomb potential in a medium of dielectric constant $\epsilon$

$$\left[\frac{1}{2m_e}\left(\mathbf{p}_e+\frac{e}{c}\mathbf{A}_e\right)^2+\frac{1}{2m_h}\left(\mathbf{p}_h-\frac{e}{c}\mathbf{A}_h\right)^2-\frac{e^2}{\epsilon|\mathbf{r}_e-\mathbf{r}_h|}\right]\Phi=E\Phi \tag{7}$$

$E$ gives the energy of the state relative to the band gap energy.

The states which are of interest in optical transition are only those in which $\mathbf{K}=0$. This is because of a selection rule of conservation of momentum or wave vector and because photons in the optical range have essentially no momentum on the electronic scale. In this case equation (7) may be considerably simplified as shown by LAMB[12] by changing the variables to the centre of mass co-ordinate

$$\mathbf{p}=m_e\mathbf{r}_e+m_h\mathbf{r}_h/m_e+m_h \tag{8}$$

and relative position $\mathbf{r}=\mathbf{r}_e-\mathbf{r}_h$

and making the substitution

$$\Phi(\mathbf{r}_e,\mathbf{r}_h)=U(\mathbf{r})\exp\left[-\frac{ie}{2\hbar c}\mathbf{H}\times\mathbf{p}\cdot\mathbf{r}\right] \tag{9}$$

Then

$$\left[-\frac{\hbar^2}{2\mu}\nabla^2+\frac{ie\hbar(m_e-m_h)}{2c\ m_em_h}\mathbf{H}\cdot\mathbf{r}\times\nabla+\frac{e^2}{8\mu c^2}(\mathbf{H}\times\mathbf{r})^2-\frac{e^2}{\epsilon r}\right]U(\mathbf{r})=EU(\mathbf{r}) \tag{10}$$

$\mu$ is the reduced mass $m_e m_h/m_e+m_h$. Solutions of this equation under various conditions will be considered below.

### 3. ABSORPTION COEFFICIENT

The transition probability that the crystal be excited from its ground state into an excited state with a wave function such as (3) is proportional to the square of the matrix element of $\sigma = e^{i\mathbf{q}\cdot\mathbf{r}}.\xi j$ where $\mathbf{q}$, $\xi$ are the photon wave and polarization vectors and $j$ is the current operator to be taken between electron states. Since $\mathbf{q}$ is essentially zero, transitions are only possible to states with zero total momentum; i.e. $\mathbf{K} = \mathbf{k}_e+\mathbf{k}_h = 0$. If the relative motion of the electron–hole pair is localized and $U(\mathbf{r})\to 0$ as $\mathbf{r}\to\infty$ it is found that the absorption takes the form of discreet lines with $f$ values

$$f_n = \frac{2m}{he^2\nu}|\langle 0|\sigma|0, n\rangle|^2 \tag{11}$$

where $\nu$ is the photon frequency. If the relative motion is not localized there is continuous absorption with coefficient

$$\kappa = \frac{2\pi}{\nu c}|\langle 0|\sigma|0, n\rangle|^2 s_n(E) \tag{12}$$

where $s_n(E)$ is the density of excited states per unit volume per unit energy range.

The matrix elements of $j$ between the ground state and (3) are conveniently written in terms of the momentum matrix element (5). After some manipulation one finds

$$\langle 0|\xi\cdot\mathbf{p}|0, n\rangle = \left\{\xi\cdot\mathbf{p}_{cv}+\frac{iehH}{2mcE_{cv}}[\xi\times\mathbf{p}_{cv}]_z\right\}U_n(0)+\mathbf{M}_{cv}\cdot\Pi U_n(0) \tag{13}$$

where

$$\mathbf{M}_{cv} = \frac{1}{m}\sum_a\left[\frac{\mathbf{p}_{ac}}{E_{ca}}(\xi\cdot\mathbf{p}_{va})-\frac{\mathbf{p}_{av}}{E_{av}}(\xi\cdot\mathbf{p}_{ca})\right] \tag{14}$$

$$= \frac{1}{\hbar}[\nabla_k(\xi\cdot\mathbf{p}_{cv}^{(\mathbf{k})})]_{\mathbf{k}=0} \tag{15}$$

and

$$\Pi = \mathbf{p}+\frac{e}{c}\mathbf{A} \tag{16}$$

an operator written as a function of $r$. The direction $z$ is that of $\mathbf{H}$.

There are clearly two quite distinct cases which arise according as $\mathbf{p}_{cv}\neq 0$ or is 0. In the former case the first bracket of (13) gives the dominant effect and the second term of that bracket is negligible. This case is referred to as that of allowed transitions since transitions can take place between the states at the edges of the conduction and valence bands.

If $\mathbf{p}_{cv} = 0$ these transitions are forbidden and in this case the results are given by the final term in (13) alone.

Band to band transitions neglecting both coulomb and magnetic field effects are particularly simple. The overall wave functions are plane waves and the relative motion is simply $e^{i\mathbf{k}\cdot\mathbf{r}}$ and the density of states is $2\pi(2\mu/\hbar)^{\frac{3}{2}}E^{\frac{1}{2}}$. Here $\pi U(0)=\hbar k$ and $\pi U'(0)=(2\mu E/N\Omega)^{\frac{1}{2}}$. The expressions for $\kappa$ are then

$$\frac{e^2}{2\pi\nu cm^2}\left(\frac{2\mu}{\hbar^2}\right)^{\frac{3}{2}}|\mathbf{p}_{cv}|^2E^{\frac{1}{2}} \tag{17}$$

$$\frac{e^2\hbar^2}{6\pi\nu cm^2}\left(\frac{2\mu}{\hbar^2}\right)^{\frac{5}{2}}|\mathbf{M}_{cv}|^2E^{\frac{3}{2}} \tag{18}$$

for the allowed and forbidden cases respectively.

### 4. MAGNETO ABSORPTION

The theory of the shape of the absorption edge in the presence of a magnetic field has been given in detail in reference 8. The results of that paper relevant to simple spherical bands can however be readily obtained by neglecting the Coulomb term in (10). The most useful form of these solutions is that given by DINGLE[11] in cylindrical polar co-ordinates. The component of angular momentum $l$ about the $z$ axis is fixed and the motion along the $z$ axis is free. The solutions are

$$U(\mathbf{r}) = \left[\frac{eH\,n!}{hcL_z[(n+|l|)!]^3}\right]^{\frac{1}{2}}e^{ik_z z}e^{-il\phi}\eta^{\frac{1}{2}|l|}e^{-\frac{1}{2}\eta}L^{|l|}_{n+|l|}(\eta) \tag{19}$$

$$E=\frac{\hbar^2k_z^2}{2\mu}+\frac{e\hbar H}{2\mu c}(2n+|l|+1)+\frac{e\hbar H(m_e-m_h)l}{2cm_em_h} \quad (20)$$

Here $\eta$ is $eH(x^2+y^2)/2\hbar c$, $L^{|l|}{}_{n+|l|}$ an associated Laguerre polynomial and $L_z$ is the length of the specimen in the $z$ direction. $U(0)$ is only non zero for states with $l=0$ when $L_n{}^0(0)=n!$ Thus allowed transitions take place only to $l=0$ states and the absorption consists of a series of edges beginning at energy $E_{gap}+(e\hbar H/2\mu c)(2n+1)$. The density of states associated with motion in one dimension is now $\frac{1}{2}L_z(2\mu/E)^{\frac{1}{2}}/h$ so that the absorption in each sub-band has a peaked form.

$$\kappa=\frac{1}{2}\sum_{n=0}^{\infty}\frac{e^2}{2\pi\nu cm^2}\left(\frac{2\mu}{\hbar^2}\right)^{\frac{3}{2}}|\mathbf{p}_{cv}|^2\frac{e\hbar H}{2\mu c}\left[E-\frac{e\hbar H}{2\mu c}(2n+1)\right]^{-\frac{1}{2}} \quad (21)$$

For forbidden transitions the absorption coefficient is obtained from the second term in (13).

$$\Pi_zU(0)=\hbar k_zU(0) \quad (22)$$

and again only $l=0$ states give an effect. Thus for radiation polarized along the direction of **H** the absorption has the form of a series of steps instead of peaks given by

$$\kappa=\frac{1}{2}\sum_{n=0}^{\infty}\frac{e^2\hbar^2}{2\pi\nu cm^2}\left(\frac{2\mu}{\hbar^2}\right)^{\frac{5}{2}}|\mathbf{M}_{cv}|^2\frac{e\hbar H}{2\mu c}\left[E-\frac{e\hbar H}{2\mu c}(2n+1)\right]^{\frac{1}{2}} \quad (23)$$

For radiation polarized perpendicular to **H** the transitions take place to states of $l=\pm1$ since $U_{n,l}\neq0$ only if $l=1$ and

$$\begin{aligned}\Pi^+U_{n,-1}&=i\sqrt{\left(\frac{2e\hbar H}{c}\right)}\sqrt{(n+1)}U_{n+1,0}\\ \Pi^-U_{n,1}&=i\sqrt{\left(\frac{2e\hbar H}{c}\right)}\sqrt{(n+1)}U_{n,0}\end{aligned} \quad (24)$$

where

$$\Pi^{\pm}=\pi^x\pm i\pi^y$$

This absorption is again peaked but at different energies to that of (21) because of the form of (20). In fact

$$\kappa=\frac{e^2\hbar^2}{8\pi\nu cm^2}\left(\frac{2\mu}{\hbar^2}\right)^{\frac{3}{2}}|\mathbf{M}_{cv}|^2\left(\frac{e\hbar H}{2\mu c}\right)^2\sum_{n=0}^{\infty}(n+1)\left\{\left[E-\frac{e\hbar H}{2c}\left(\frac{2n+1}{\mu}+\frac{2}{m_e}\right)\right]^{-\frac{1}{2}}+\left[E-\frac{e\hbar H}{2c}\left(\frac{2n+1}{\mu}+\frac{2}{m_h}\right)\right]^{-\frac{1}{2}}\right\} \quad (25)$$

The experimental observations[4–6] appear so far to have been confined to the allowed kind of transition.

## 5. EXCITONS

The theory of the absorption edge taking account of the Coulomb attraction between hole–electron pairs is given in reference 7 in essentially the form of this theory and will not be reproduced here. The solutions of (10) with $H=0$ are hydrogen like states, bound when $E<0$ and with unbound Coulomb wave functions if $E>0$. The predicted hydrogenic like series runs together as the photon energy increases to $E_{gap}$ and merges with the continuous absorption without discontinuity. The form of this continuous absorption is given in reference 7 as ($\alpha=(e^2/2\hbar\epsilon)\sqrt{(2\mu/E)}$)

$$\kappa=\kappa_A\frac{\pi\alpha e^{\pi\alpha}}{\sinh\pi\alpha} \quad (26)$$

$$\kappa=\kappa_F\frac{\pi\alpha(1+\alpha^2)e^{\pi\alpha}}{\sinh\pi\alpha} \quad (27)$$

where $\kappa_A$ and $\kappa_F$ are the plane wave forms of $\kappa$ for allowed and forbidden transitions respectively given by (17) and (18) which neglected the effect of the Coulomb attraction. It therefore seems that a correct evaluation of the magneto-optic effects discussed in Section 4 should include the effect of the Coulomb attraction, which produces such a marked effect close to the band edge.

### 6. EXCITONS IN A MAGNETIC FIELD

The general problem therefore requires the solution of equation (10), particularly for those states where the component of angular momentum $l$ is 0 or $\pm 1$. For the bound hydrogenic states in very small fields the second term in (10) is a dominant perturbation and gives a linear Zeeman splitting. The term in $H^2$ gives a quadratic Zeeman splitting which becomes dominant as $H$ increases. When the magnetic energy is of the order of the Coulomb energies such a procedure breaks down. The higher energy hydrogenic states are close together and are affected at smaller fields than the lower states. In atoms this has been investigated by SCHIFF and SNYDER.[13] The energy of the lowest bound state of an equation similar to (10) has also been considered by a variational technique by ADAMS, YAFET and KEYES.[14]

We shall be concerned here with an attempt to determine the wave functions of the unbound pairs which will still form a series of sub-bands beginning at energies given by (20) relative to the gap. Because of the localized nature of the Coulomb perturbation it does not alter the energy of unbound states as the magnetic field does. It is assumed along the lines of reference 14 that in large magnetic fields the wave functions in the direction perpendicular to $z$ are determined entirely by the magnetic field and have the $\eta$ dependence of (19), $f(\eta)$ say. The motion in the $z$-direction then takes place in an effective potential

$$V_0(z) = -\int \frac{e^2}{\epsilon r}|f(\eta)|^2 dxdy \tag{28}$$

For the lowest band $n = 0$, $l = 0$ this has the form

$$-2e^2\beta^{\frac{1}{2}}\epsilon^{\beta z^2}Erfc(\beta^{\frac{1}{2}}|z|)\epsilon^{-1} \tag{29}$$

where $\beta = eH/2\hbar c$. Solutions of the $z$ dependence of the wave function are of course impossible in closed form with (29). It is however possible to proceed by approximating (29) by

$$-e^2/\epsilon(a+|z|) \tag{30}$$

where $a = (\pi\beta)^{-\frac{1}{2}}$. This has the same value at $z = 0$ and the same asymptotic form as (29) and has a discontinuity in slope at the origin.

The solutions of the equation

$$-\frac{\hbar^2}{2\mu}\frac{d^2\psi}{dz^2} - \frac{e^2\psi}{\epsilon(a+|z|)} = E_z\psi \tag{31}$$

can be written, when $E_z = \hbar^2\mathbf{k}^2/2\mu$, $\alpha = \mu e^2/\hbar^2\epsilon\mathbf{k}$

$$e^{i\mathbf{k}z}g(2i\mathbf{k}[a+|z|]) \tag{32}$$

where $g(x)$ is a linear combination of solutions of

$$\frac{d^2g}{dx^2} - \frac{dg}{dx} + \frac{i\alpha}{x}g = 0 \tag{33}$$

One of these is a confluent hypergeometric function

$$x\,{}_1F_1(i\alpha+1, z, x) \tag{34}$$

and the other is defined by ERDÉLYI[15] as

$$x\Psi(i\alpha+1, 2, x) \tag{35}$$

$\Psi$ is irregular at the origin where it has the form

$$\frac{1}{\Gamma(i\alpha)}\,{}_1F_1(i\alpha+1, 2, x)\log x + \\ + \frac{1}{\Gamma(i\alpha+1)}\left[\frac{1}{x} + (1-i\alpha) + 0(x)\right] \tag{36}$$

A convenient alternative function is defined as

$${}_1G_1(1+i\alpha, 2, x) = i\,{}_1F_1(1+i\alpha, 2, x) + \\ + \frac{2ie^{-\pi\alpha}}{|\Gamma(1-i\alpha)|}\Psi(1+i\alpha, 2, x) \tag{37}$$

when the solutions $e^{-ikz}kz\,{}_1F_1(i\alpha+1, 2, 2ikz)$ and $e^{-ikz}kz\,{}_1G_1(i\alpha+1, 2, 2ikz)$ have asymptotic forms like the imaginary and real parts respectively of

$$\exp i(kz+\alpha\log 2kz - \arg\Gamma(1+i\alpha)) \tag{38}$$

In these terms there are two orthogonal solutions of (31) which are respectively even and odd for reflection in the origin.

$$\Psi_g = e^{\frac{1}{2}\pi\alpha}\left(\frac{\alpha(1+\alpha^2)}{\sinh\pi\alpha}\right)^{\frac{1}{2}}e^{-i\mathbf{k}(a+z)}\mathbf{k}(a+z)\,\frac{[{}_1F_1(a+z)\,{}_1G_1{}^{\mathrm{I}}(a) - {}_1G_1(a+z)\,{}_1F_1{}^{\mathrm{I}}(a)]}{({}_1G_1{}^{\mathrm{I}}(a)^2 + {}_1F_1{}^{\mathrm{I}}(a)^2)^{\frac{1}{2}}} \tag{39}$$

$$\Psi^{u} = e^{\frac{1}{2}i\pi\alpha}\left(\frac{\alpha(1+\alpha^2)}{\sinh\pi\alpha}\right)^{\frac{1}{2}} e^{-i\mathbf{k}(a+z)}\mathbf{k}(a+z)\frac{[{}_1F_1(a+z)\,{}_1G_1(a)-{}_1G_1(a+z)\,{}_1F_1(a)]}{({}_1G_1(a)^2+{}_1F_1(a)^2)^{\frac{1}{2}}} \tag{40}$$

where

$${}_1F_1{}^{\mathrm{I}}(a) = (1-i\mathbf{k}a)\,{}_1F_1(a)+a\,{}_1F_1{}'(a)$$

and a similar definition holds for ${}_1G_1{}^{\mathrm{I}}$.

For allowed transitions we need the value of the function at the origin substituted in (13) and (12). Only the even function (39) gives an effect which, very close to the edge when $\alpha \gg 0$ (i.e. at energies where $E_z$ is less than the Coulomb energy) is

$$\kappa = \left(\frac{e\hbar H}{mc}\right)\frac{\alpha^4 a^2\mathbf{k}^2\epsilon}{\pi v mc\hbar^2}\,\frac{{}_1F_1(a)^4}{{}_1F_1{}^{\mathrm{I}}(a)^2} \times \frac{|p_{cv}|^2}{(\log 2\mathbf{k}a)^2(1-e^{-2\pi\alpha})} \tag{41}$$

For forbidden transitions with light polarized along $H$ the second term in (13) is non zero for $\partial\psi/\partial_z$ of the odd function (40). Here

$$\kappa = \left(\frac{e\hbar H}{mc}\right)\frac{\alpha^4\mathbf{k}^2\epsilon|M_{cv}|^2\,{}_1F_1(a)^2}{\pi v mc(\log 2\mathbf{k}a)^2(1-e^{-2\pi\alpha})} \tag{42}$$

The results for other sub-bands with $n\neq 0$ beginning at $E = e\hbar H(2n+1)/2\mu c$ may be obtained in a similar way. The radius of the orbit around the magnetic field is different and hence so is the effective potential (28) and (29). They may however be approximated by (30) with larger values of $a$. As a result the absorption in these bands will, under the above conditions, have forms (41) and (42) with different values of $a$. The approximate expression (41) and (42) will hold over a smaller range of $\mathbf{k}$.

For forbidden transitions with light polarized perpendicular to $H$ one again needs $\Psi(0)$ for even functions like (39) together with the properties of $f(\eta)$ given by (24). However the effective potential for $l = \pm 1$ states is different from (28) and can reasonably be approximated by replacing $a$ by $2a$. The shape of each absorption contribution is then of the same form as (41) and there are two series of peaks as in the magneto-absorption case (25).

Thus the Coulomb attraction is seen to sharpen considerably the peaks of the magneto-absorption from a form $E^{-\frac{1}{2}}$ to $E^{-1}(\log E)^{-2}$ in the allowed and perpendicular forbidden cases. For the parallel polarization in the forbidden case it induces in this approximation peaks of this same form, whereas in the absence of Coulomb terms there was a series of $E^{\frac{1}{2}}$ steps. This result is probably less reliable than the others since it depends on the slope of $\Psi$ at the origin obtained from an approximate potential. The general formulae of this section tend to the results of the magneto-absorption calculation[8] at large values of $\mathbf{k}$.

Unfortunately the experimental data at present available is not sufficiently accurate to allow a check on the detailed form of the absorption, but confirms the existence of sharp peaks in the allowed case. It is clear from this work that the effect of the coulomb attraction is of prime importance in considering the shape of the continuous absorption. It is planned to extend this work; in particular towards a more detailed study of the bound exciton states and the absorption from impurities in a magnetic field which has so far been treated only with the Coulomb effects neglected.[16]

## REFERENCES


*1. Gross E. F., *Nuovo Cim. Suppl.* **3,** 672 (1956).
*2. Nikitine S., *Phil. Mag.* in press (1958).
*3. Macfarlane G., McLean T. P., Quarrington J. and Roberts V., *Proc. Phys. Soc.* **71,** 863 (1958).
*4. Lax B., Roth L. and Zwerdling S., *Phys. Rev.* **109,** 2207 (1958).
5. Burstein E. and Picus G. S., *Phys. Rev.* **105,** 1123 (1957).
6. Lax B., Roth L. and Zwerdling S., *Phys. Rev.* **106,** 51 (1957); **108,** 1402 (1957).
7. Elliott R. J., *Phys. Rev.* **108,** 1383 (1957).
8. Elliott R. J., McLean T. P. and MacFarlane G. G., *Proc. Phys. Soc.* **72,** 553 (1958).
9. MacFarlane G., McLean T. P., Quarrington J. and Roberts V., *Phys. Rev.* **108,** 1377 (1957).


*Footnote*

Correction: All formulae for absorption coefficients $\kappa$ should contain a factor $n'/\epsilon$ where $n'$ is the refractive index.

10. KOHN W. and LUTTINGER J., *Phys. Rev.* **97**, 869 (1955).
11. DINGLE R., *Proc. Roy. Soc.* **A211**, 500 (1952).
12. LAMB W., *Phys. Rev.* **85**, 259 (1952).
13. SCHIFF L. and SNYDER H., *Phys. Rev.* **55**, 59 (1939).
14. ADAMS E., YAFET Y. and KEYES W., *J. Chem. Phys. Solids* **1**, 137 (1956).
15. ERDÉLYI A., MAGNUS W., OBERHETTINGER F. and TRICOMI F. G., *Higher Transcendental Functions* (1953).
*16. BOWDEN H. and WALLIS R. *J. Chem. Phys. Solids* **7**, 78 (1958).

*See also papers by these authors in Proceedings of this Conference.

*J. Phys. Chem. Solids* Pergamon Press 1959. Vol. 8. pp. 388–392. Printed in Great Britain

# O.2 EXCITON AND PHONON EFFECTS IN THE ABSORPTION SPECTRA OF GERMANIUM AND SILICON

G. G. MACFARLANE, T. P. MCLEAN, J. E. QUARRINGTON and V. ROBERTS

Royal Radar Establishment, Malvern, England

**Abstract**—Evidence for exciton creation in Ge and Si by indirect and direct transitions has been obtained from high resolution absorption spectra. At low levels of absorption fine structure is observed, which is characteristic of indirect transitions involving the emission and absorption of phonons. For Ge four different phonons with energies of 90°K, 320°K, 350°K and 420°K and for Si four phonons with energies 212°K, 670°K, 1050°K and 1420°K contribute to the absorption. They correspond with the TA, LA, LO, and TO vibrational modes respectively. Each component is interpreted as being due to the formation of excitons and free electron–hole pairs. The exciton binding energy is found to be about 0·0027 eV for Ge and about 0·010 eV for Si. Absorption to the first excited state of the exciton is also observed. This state is estimated to be about 0·0010 eV above the ground state for Ge and 0·0055 eV for Si. The structure of the exciton absorption is smoothed out as the temperature is raised. The effect is explained as due to a temperature dependent relaxation time for the excitons. Direct exciton transitions have been observed as a line structure at high levels of absorption in Ge. By taking into account the coulomb interaction of the electron and hole in the theory of the direct band-to-band absorption, the energy dependence of the absorption above the exciton line can be explained and a value of about 0·0012 eV obtained for the exciton binding energy.

## 1. INTRODUCTION

In recent publications[1,2] we have shown that the low-level absorption edge spectra of Ge and Si can be interpreted in terms of indirect transitions involving phonons. In general each branch of the vibrational spectrum makes two contributions, one in absorption, the other in emission. In Si and Ge four phonon energies have been found corresponding to wave vectors in the ⟨100⟩ and ⟨111⟩ directions respectively. At temperature $T$ and frequency $\nu$ the absorption constant can be described by the formula

$$K(h\nu) = \sum_{i=1}^{4} \frac{a_i(T)}{\exp(\theta_i/T)-1}[\alpha_i(h\nu-E_{ia}, T)+\rho_i \exp(\theta_i/T)\alpha_i(h\nu-E_{ie}, T)], \quad (1)$$

where $E_{ie}-E_{ia} = 2k\theta_i$.

The factor $\rho$ depends on the difference in energy of the intermediate and final states.[3] Its theoretical maximum value is about 2·2 for Ge and little

more than unity for Si. A knowledge of $\rho$ is useful in deciding which of the intermediate states is predominant. The shape of the components, $\alpha_i(h\nu)$, is found to vary slowly with the temperature and we have explained this as relaxation broadening. In this paper we summarize the main results for Si, and give new data and revised values for Ge.

## 2. SILICON

In Fig. 1 we show the observed absorption spectrum of Si at various temperatures. Components due to four phonons are recognizable,

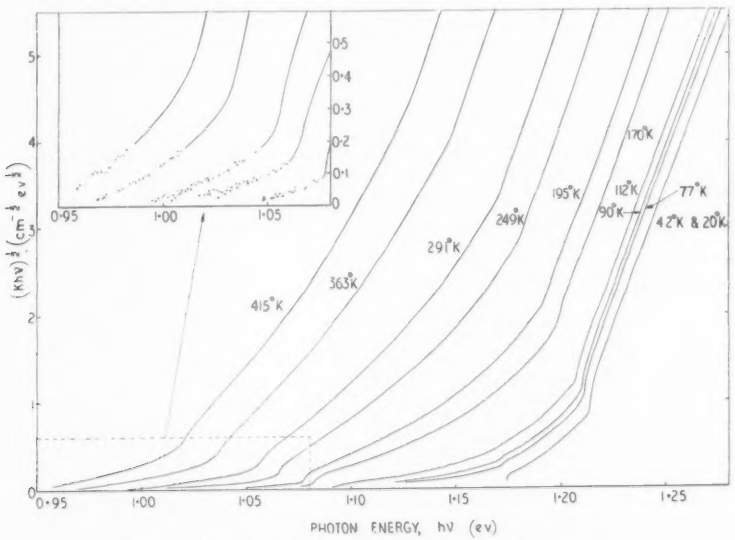


FIG. 1. Low-level absorption spectrum of high purity Si at various temperatures.

two in emission and absorption at low temperatures with energies of 212°K and 670°K and two in absorption only at very low levels and higher temperatures with energies of 1050°K and 1420°K. These energies, in ascending magnitude, are thought to refer to the TA, LA, LO and TO branches of the vibrational spectrum at a wavevector about 0·81 of the distance from the centre to the edge of the Brillouin zone in the $\langle 100 \rangle$ direction. The occurrence of four phonons confirms the view that the conduction band energy minima are not at the zone edge but at the above six equivalent points. The factor $\rho$ is found to be practically unity.

The basic shapes of the 212°K and 670°K components, $\alpha_1$ and $\alpha_2$, reveal exciton effects. In each two parts with the form $(\Delta E)^{\frac{1}{2}}$, characteristic of exciton absorption, with thresholds separated in energy by 0·0055 eV are clearly evident. Subtracting them out we find that the residue rises as $(\Delta E)^{\frac{3}{2}}$ from an energy zero about 0·010 eV, above the first exciton threshold. ELLIOTT[4] has shown that when coulomb interaction of the electron and hole is included, the band-to-band absorption in an indirect transition should become $(\Delta E)^2$ only when $\Delta E$ is well over $\pi^2$ times the exciton binding energy. Near the threshold one can show from Elliott's formula that the energy dependence is $(\Delta E)^{\frac{3}{2}}$. We appear to observe only the $(\Delta E)^{\frac{3}{2}}$ behaviour. With this theory in mind we estimate the exciton binding energy to be about 0·010 eV, and the first excited state of the exciton to be about 0·0055 eV, above its ground state. An unexplained feature of the data is the difference in relative magnitudes of the exciton and band-to-band parts of $\alpha_1$ and $\alpha_2$. As we shall show below this difference is even more marked in Ge.

The relaxation time $\tau$ of the exciton was obtained by comparing the shape of $\alpha_2(T)$ with a set of curves obtained by convolving the basic

shape with a Gaussian distribution function of half-width $\sigma = h/\tau$. It is constant at $3{\cdot}4\times10^{-12}$ sec for $T < 100°$K, approximately the binding energy of the exciton, but above 100°K it falls roughly as $T^{-\frac{1}{2}}$. To produce a broadening the relaxation processes must be inelastic so that $\tau$ is essentially the lifetime of the exciton in its energy band.

absorption branch of the 320°K component and has a phonon energy of about 350°K. We identify these four $\theta$s, in ascending magnitude, as the energies of the TA, LA, LO and TO phonons at the boundaries of the Brillouin zone in the $\langle 111 \rangle$ directions. They are in good agreement with the values obtained from neutron scattering studies by BROCKHOUSE and IYENGAR.[5]

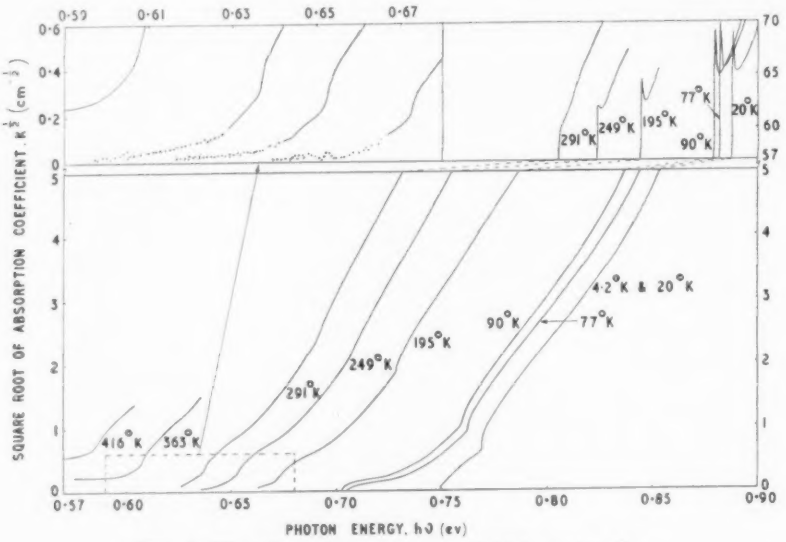


FIG. 2. The absorption spectrum of high purity Ge at various temperatures showing the characteristic exciton features in both the indirect and direct transition regions.

We have also looked for components that could be attributed to the lower valence band, which is split off by spin–orbit coupling, but so far we have not identified any.

### 3. GERMANIUM

The spectrum for Ge is more complicated but in some respects more interesting. The absorption data is shown in Fig. 2. Here again formula (1) for indirect transitions describes the features of the low-level absorption. At low temperature two phonons with energies 90°K and 320°K are clearly seen. At higher temperatures new components appear at very low levels, one of which is easily identified and has phonon energy of about 420°K; the other is resolved only after detailed analysis of the data. It appears as an additional tail on the

The basic shapes of the 90°K and 320°K components, $\alpha_1$ and $\alpha_2$, are markedly different; so also are the values of $\rho_1$ and $\rho_2$. $\alpha_1$ is very accurately of the form $(\Delta E)^{\frac{1}{2}}$ and $\rho_1 = 1{\cdot}01 \pm {\cdot}005$, but $\alpha_2$ shows evidence of three distinct contributions, and $\rho_2 \sim 2$. The basic shape of $\alpha_2$, from which the observed shapes at all temperatures can be deduced by a Gaussian form of relaxation broadening, can be well represented by a formula of the form

$$\alpha_2 = a(\Delta E)^{\frac{1}{2}} + b(\Delta E - 0{\cdot}0010)^{\frac{1}{2}} + c(\Delta E - 0{\cdot}0027)^{\frac{1}{2}}, \quad (2)$$

in which the first two terms have the form expected for excitons and the third term characterizes band-to-band transitions. The excited state of the exciton is therefore $0{\cdot}0010 \pm {\cdot}0001$ eV in energy

*Table* 1.

The values of the threshold energies $E_{1a}$, $E_{2a}$, $E_{3a}$, $E_{4a}$, $E_{1e}$ and $E_{2e}$ found from the analysis of the absorption curves and the corresponding values of the energy gaps $\bar{E}_1$ and $\bar{E}_2$ at various temperatures T for Ge.* Also shewn are the four phonon temperatures $\theta_1$, $\theta_2$, $\theta_3$ and $\theta_4$ and the exciton lifetime $\tau = \frac{h}{\sigma}$.

| $T$(°K) | $E_{4a}$ (eV) | $E_{3a}$ (eV) | $E_{2a}$ (eV) | $E_{1a}$ (eV) | $E_{1e}$ (eV) | $E_{2e}$ (eV) | $\theta_1$(°K) = $\frac{1}{2k}(E_{1e}-E_{1a})$ | $\theta_2$(°K) = $\frac{1}{2k}(E_{2e}-E_{2a})$ | $\theta_3$(°K) = $\frac{1}{k}(\bar{E}-E_{3a})$ | $\theta_4$(°K) = $\frac{1}{k}(\bar{E}-E_{4a})$ | $\bar{E}_1$ (eV) = $\frac{1}{2}(\bar{E}_{1e}+E_{1a})$ | $\bar{E}_2$ (eV) = $\frac{1}{2}(E_{2e}+E_{2a})$ | $\tau$(sec) $\times 10^{11}$ |
|---|---|---|---|---|---|---|---|---|---|---|---|---|---|
| 4·2 | | | | | 0·7485 | 0·7686 | | | | | 0·7407[a] | 0·7410[b] | 1·53 |
| 20 | | | | | 0·7480 | 0·7679 | | | | | 0·7402[a] | 0·7403[b] | 1·53 |
| 77 | | | 0·7063 | 0·7264 | 0·7419 | 0·7614 | 90 | 320 | | | 0·7342 | 0·7339 | 1·38 |
| 90 | | | 0·7035 | 0·7238 | 0·7393 | 0·7587 | 90 | 320 | | | 0·7315 | 0·7311 | 1·38 |
| 195 | 0·6633 | 0·6694 | 0·6718 | 0·6919 | 0·7073 | 0·7269 | 89 | 320 | 349 | 420 | 0·6996 | 0·6994 | 1·03 |
| 249 | 0·6435 | 0·6492 | 0·6523 | 0·6718 | 0·6868 | 0·7072 | 87 | 319 | 356 | 422 | 0·6793 | 0·6797 | 0·52 |
| 291 | 0·6273 | 0·6332 | 0·6367 | 0·6570 | 0·6724 | 0·6913 | 88 | 317 | 357 | 426 | 0·6647 | 0·6640 | 0·42 |
| 363 | 0·5980 | 0·604 | 0·6073 | | | | | | 359 | 426 | | 0·6349[c] | 0·26 |
| 416 | | | 0·5877 | | | | | | | | | 0·6153[c] | 0·21 |

* All these energy values have been corrected by the factor 0·99955 as explained in reference (2).

a. Calculated from $\bar{E}_1 = E_{1e} - k\theta_1$ with $\theta_1 = 90°\text{K}$.

b. Calculated from $\bar{E}_3 = E_{2e} - k\theta_2$ with $\theta_2 = 320°\text{K}$.

c. Calculated from $\bar{E}_2 = E_{2a} + k\theta_2$ with $\theta_2 = 320°\text{K}$.

above the ground state and the exciton binding energy is $0{\cdot}0027 \pm 0{\cdot}0004$ eV.

The fact that $\rho_2 \sim 2$ indicates that the principal intermediate state is the one in the conduction band with wave-vector (0, 0, 0). Thus $\rho^{\frac{1}{2}} = (\delta E + k\theta)/(\delta E - k\theta)$, where $\delta E$ is the difference in energy of the intermediate and final states* of the electron or hole. For the above intermediate state $\delta E \simeq 0{\cdot}146$ eV which gives $\rho_2 = 2{\cdot}16$. For any other possible intermediate state $\delta E > 0{\cdot}5$ eV and $\rho_2 < 1{\cdot}2$.

The properties of the 90°K component, $\alpha_1$, are quite different. There is no evidence for any contribution beginning as $(\Delta E)^{\frac{1}{2}}$, instead the whole shape is accurately given by the simple form $(\Delta E)^{\frac{3}{2}}$. The question now arises whether excitons contribute at all to $\alpha_1$. If they do not the energy gap, $\frac{1}{2}(E_{1a}+E_{1e})$ should be larger than the energy gap $\frac{1}{2}(E_{2a}+E_{2e})$ by the binding energy 0·0027 eV of the exciton. In the table we give the results of a detailed analysis of all the absorption data from which it appears that these two energy gaps do not differ by more than $\pm 0{\cdot}0007$ eV. We conclude therefore that exciton absorption is present in $\alpha_1$ as well as $\alpha_2$. A three-halves power law may arise in an indirect transition for which the optical part of the transition probability is not primarily constant but increases linearly with the wave-number.

Again we find $\rho_1 = 1{\cdot}01 \pm 0{\cdot}005$. This indicates that the principal intermediate state is not the one with an electron in the conduction band with wave-vector (0, 0 ,0), because then one should find $\rho_1 = 1{\cdot}23$.

The relaxation time of the exciton is found to decrease with rise in temperature in the same way as for Si but the constant low temperature value is larger at $1{\cdot}5 \times 10^{-11}$ sec, as given in Table 1.

We have also looked for and found evidence for direct transitions which produce excitons.[6] These transitions show up clearly in the absorption curve around levels of 4000 $cm^{-1}$ as well-defined lines broadened into sharp peaks. They are shown in the insert of Fig. 2. We have analysed these data using the recent theory of ELLIOTT,[4] which takes account of coulomb interaction between the electron and hole, and find that the form of the continuous absorption spectrum above the exciton line can be very well accounted for. Out of this analysis we get the band-to-band energy gap from which the exciton binding energy is found to be about 0·0011 eV.

*Acknowledgments*—This paper is published by permission of the Controller, Her Britannic Majesty's Stationery Office.

*The necessity to include the $k\theta$ term in $\rho$ for germanium was pointed out to the authors by HARVEY BROOKS (private communication).

## REFERENCES

1. MACFARLANE G. G., MCLEAN T. P., QUARRINGTON J. E. and ROBERTS V., *Phys. Rev.* **108,** 1377 (1957).
2. MACFARLANE G. G., MCLEAN T. P., QUARRINGTON J. E. and ROBERTS V., *Phys. Rev.* (in press).
3. ELLIOTT R. J., MCLEAN T. P., MACFARLANE G. G., *Proc. Phys. Soc.* (in press).
4. ELLIOTT R. J., *Phys. Rev.* **108,** 1384 (1957).
5. BROCKHOUSE G. N. and IYENGAR P. K., *Bull. Amer. Phys. Soc.* **3,** 192 (1958).
6. MACFARLANE G. G., MCLEAN T. P., QUARRINGTON J. E. and ROBERTS V., *Proc. Phys. Soc.* **71,** 863 (1958).

*J. Phys. Chem. Solids* Pergamon Press 1959. Vol. 8. pp. 392–396. Printed in Great Britain

# O.3 ANALYSIS OF INTRINSIC RECOMBINATION RADIATION FROM SILICON AND GERMANIUM

**J. R. HAYNES, M. LAX and W. F. FLOOD**

Bell Telephone Laboratories, Incorporated, Murray Hill, New Jersey

EXCESS minority carriers were produced in silicon and germanium in two ways: (1) by passing a current in the forward direction through grown *p–n* junctions and (2) by shining a high intensity

light beam having wavelengths greater than $0{\cdot}6\mu$ on single crystals. In either case the excess carriers recombine within a diffusion length and in thermal equilibrium with the crystal lattice giving intrinsic recombination radiation. This radiation was analyzed with a spectrometer equipped with a grating, detected by a lead sulfide cell and automatically recorded on a chart.

The production of intrinsic recombination radiation in silicon and germanium involves a change in crystal momentum since for both materials the valence band maximum is at the center of the Brillouin zone while the conduction band minima are at a crystal momentum of $k_0$, which is at the zone edge in germanium and near it in silicon. Recombination of electrons at the conduction band minima with holes at the valence band maximum therefore involves a change in crystal momentum of from $k_0$ to $k = 0$ and this crystal momentum must be conserved. This can be accomplished by the electron either emitting or absorbing a phonon having a crystal momentum wave vector of $k_0$. The phonon spectrum of both silicon and germanium has four branches in the direction of the conduction band minima and hence there are four phonons of different energies all having the required crystal momentum of $k_0$. Since energy as well as crystal momentum must be conserved in the transition we may expect the intrinsic radiation from these materials to consist of eight lines: four with energies less than the energy gap due to the emission of four phonons of four different energies, and four lines with energies higher than the energy gap produced by absorption of these four different phonons.

A reproduction of a recorder trace of recombination radiation from silicon at 101° Kelvin is shown in Fig. 1. The horizontal axis is the photon energy in electron volts. The vertical response is nearly proportional to the number of photons per unit energy interval. The signal-to-noise ratio is typical of the more than 60 radiation characteristics taken over a temperature range of from 40 to 350° Kelvin. The radiation shown in the slide is independent of sample thickness and surface treatment. It is also insensitive to donor and acceptor concentration. From these facts we conclude that the radiation is due to intrinsic volume recombination and that the photon energy distribution is unaltered by absorption in its escape from the silicon specimen. The radiation is seen to consist mainly of a single line broadened by the sum of the thermal kinetic energies of the recombining electrons and holes. However, fine structure can be seen on either side of the main line, produced by additional radiation.

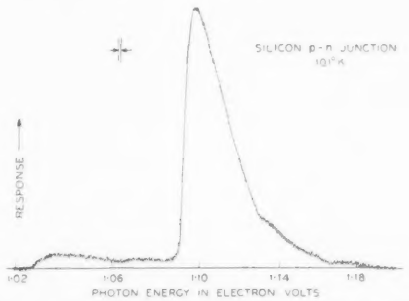


FIG. 1. Reproduction of a recorder trace of recombination radiation from silicon showing typical signal-to-noise ratio and effective slit width.

The line shape is of interest since it gives a clue to the behavior of the interaction cross-section of electrons and holes. The result obtained by replotting a recorder trace in terms of the relative number of photons per unit energy interval as a function of the thermal energy involved is shown in Fig. 2 as a solid line. Obtaining this solid line involved correcting for overall spectrometer and detector response and locating a point $h\nu_0$ by extrapolating the low energy side of the line to zero number of photons. The point $h\nu_0$ is then the photon energy produced when the recombining hole and the electron each have zero thermal kinetic energy. In this case $h\nu_0$ equals the energy gap minus the phonon energy associated with the transition, since, as we shall show, this line is produced by emission of the acoustic longitudinal phonon. Energies higher than $h\nu_0$ are the result of the sum of the thermal kinetic energies of the electrons and holes making radiative transitions. We have shown this energy in units of $\Delta h\nu/kT$ at the bottom of the slide and in electron volts at the top.

The dashed curves give the line shapes predicted by theory with the following assumptions: the recombination rate $R = N_e N_h \sigma v$, where $N_e$ and $N_h$ are the concentrations of electrons and holes, $v$ is the relative velocity of an electron and hole,

and the capture cross-section $\sigma$ is assumed proportional to $v^n$. If $n = 0$ so that the cross-section is independent of the relative velocity of the carriers we obtain a curve which is obviously not a good fit to the data. However, if $n = -2$ so that the cross-section varies inversely as the square of the relative velocity a good fit to the data is obtained especially at low energy. This shows that there is a highly weighted probability of recombination for those electrons and holes which approach each other with low relative velocities.

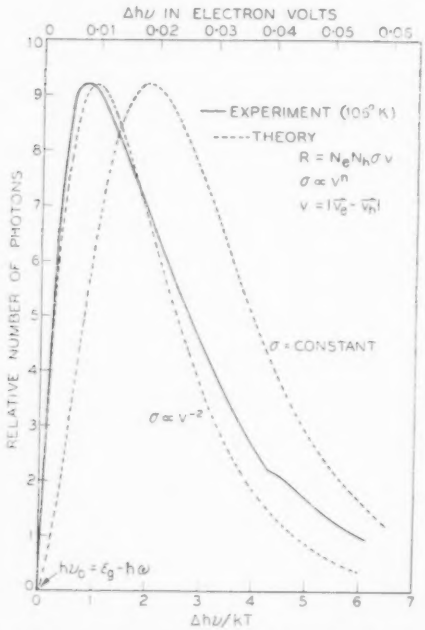
Δhν IN ELECTRON VOLTS
0 0·01 0·02 0·03 0·04 0·05 0·06
—EXPERIMENT (105° K)
-----THEORY
R = N_e N_h σ v
σ ∝ v^n
v = |v_e − v_h|
σ = CONSTANT
σ ∝ v^-2
hν_0 = ε_g − hω
RELATIVE NUMBER OF PHOTONS
Δhν/kT
0 1 2 3 4 5 6 7

FIG. 2. The solid line shown is the result of replotting a recorder trace in terms of the relative number of photons per unit energy interval as a function of the kinetic energy involved in the transition. The dotted curves are the predictions of theory with the assumptions shown.

If the electrons and holes form excitons before recombining, as indicated by the preceeding[1] and following papers,[2] the kinetic energy shown is that of the recombining excitons. If the probability of recombination of an exciton were independent of its kinetic energy a Boltzmann distribution would result. The solid line is not a Boltzmann energy distribution which has a maximum at $kT/2$. However, an equally good fit to the data could doubtless be made for excitons by assuming a velocity dependence of recombination probability.

In either event our construction of the point $h\nu_0$ by extrapolating the low energy side of the line is very nearly correct.

The effect of temperature change on the radiation is shown in Fig. 3. Here we have traced

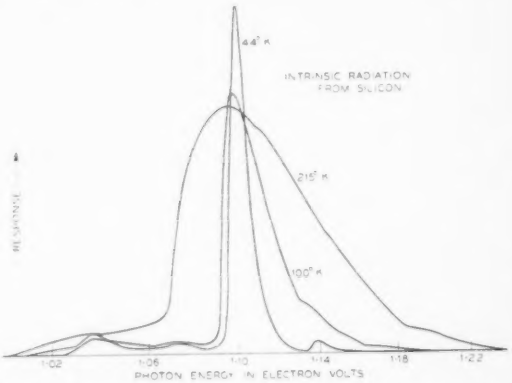


FIG. 3. Recombination radiation from silicon obtained at three different temperatures.

the response as a function of photon energy in electron volts for three different temperatures. At 44° Kelvin we clearly have four lines. These lines are all due to phonon emission since at this low temperature there are not enough of any of the required phonons to permit appreciable absorption. The $h\nu_0$ points for the four phonons are easily identified. The $h\nu_0$ point for transitions involving the acoustic transverse phonon is at 1·135 eV, for the acoustic longitudinal phonon 1·096 eV, for the optical longitudinal phonon 1·068 eV and for the optical transverse phonon 1·032 eV. Thus determination of the difference in energies of the four phonons can be made at low temperature.

At 100° the lines are broadened by increased thermal energy but the $h\nu_0$ points can still be identified by the breaks in the curve produced by the onset of additional radiation and at this temperature we are able to observe radiation produced by the absorption of the acoustic transverse phonon. The absolute energy of this phonon, which has an $h\nu_0$ point of 1·129 eV for emission and an $h\nu_0$ point of 1·161 eV for absorption if

half of the energy difference of these $h\nu_0$ points and the energy gap at this temperature lies midway between the two points.

At a still higher temperature of 215° Kelvin the energy gap is visibly decreased lying again midway between the absorption and emission $h\nu_0$ points of the acoustic transverse phonon. At this temperature, however, we obtain appreciable radiation due to absorption of the acoustic longitudinal phonon with an $h\nu_0$ point at 1·182 eV. The absolute energy of this phonon is half of the difference of its $h\nu_0$ points and the energy gap is also midway between these two points. In this way we obtain both the phonon spectrum at $k_0$ and the energy gap.

Intrinsic recombination radiation from germanium obtained at three different temperatures is shown in Fig. 4. It is seen to be quite similar

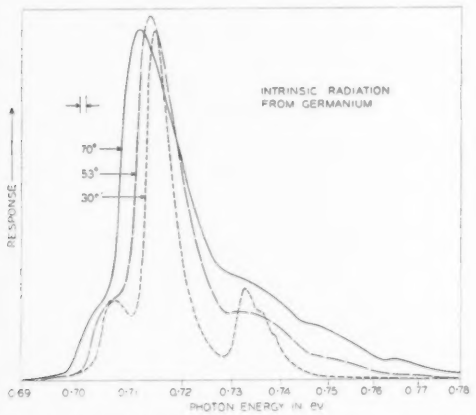


FIG. 4. Recombination radiation from germanium obtained at three different absolute temperatures. The effective slit width used is indicated.

to that obtained from silicon. At 30°K we have three prominent lines. These lines are all due to phonon emission. The $h\nu_0$ point for transitions involving the acoustic transverse phonon is at 0·730 eV, for the acoustic longitudinal phonon is 0·712 eV, and for the optical transverse phonon 0·703 eV. Weak lines may be seen near the energy gap with $h\nu_0$ points at 0·735 and 0·738 eV. At the higher temperature of 53°K we see transitions involving both emission and absorption of the acoustic transverse phonon. The $h\nu_0$ point for emission of the acoustic transverse phonon is at 0·728 eV and that for absorption is at 0·746 eV. At 70°K absorption of the acoustic longitudinal phonon becomes visible with an $h\nu_0$ point at 0·726 eV. We do not see transitions involving the optical longitudinal phonon probably because these lie between the strong acoustic longitudinal and the optical transverse phonon transitions.

The change in energy of the $h\nu_0$ points with temperature in germanium is shown in Fig. 5.

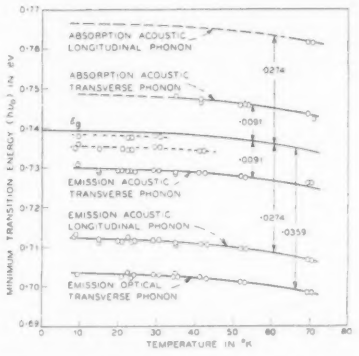


FIG. 5. The energies of the $h\nu_0$ points of recombination radiation from germanium as a function of temperature. The phonons involved in the transitions and their energies are shown. If recombination occurs through exciton states the energy gap is larger than $\epsilon_g$ by an amount equal to the exciton binding energy.

At higher temperatures than those shown only the $h\nu_0$ points of transitions involving emission and absorption of the acoustic longitudinal phonon remain distinct. If the strong lines are due to recombination of electrons and holes the energy gap, $\epsilon_g$, lies midway between the $h\nu_0$ points of emission and absorption of the acoustic transverse phonon and also midway between the $h\nu_0$ points of emission and absorption of the acoustic longitudinal phonon as shown. The unidentified lines near the gap can be ascribed to the recombination of excitons in the ground and first excited state without phonon co-operation. This can occur by exciton scattering from neutral impurity atoms. If, however, the prominent transitions are due to the recombination of excitons the lines near the gap cannot be due to exciton transitions since the energy gap then lies above $\epsilon_g$ by an amount equal to the exciton binding energy and we must find some other explanation.

The phonon energies for silicon and germanium determined from recombination radiation measurements are shown in Table 1. These results are in good agreement with both those of MACFARLANE *et al.*[1] obtained from optical absorption measurements and with the values for germanium obtained by BROCKHOUSE[3] from neutron diffraction.

*Table 1. Phonon energies at wave vector* $\mathbf{k}_0$ (eV)

| Element | Acoustic transverse | Acoustic longitudinal | Optical transverse | Optical longitudinal |
|---|---|---|---|---|
| Silicon | ·016 | ·055 | ·083 | 0·119 |
| Germanium | ·0091 | ·0274 | ? | ·0359 |

The energy gaps derived from the analysis of recombination radiation of electrons and holes in germanium and silicon are shown in Fig. 6 as a function of temperature. If the electrons form excitons before recombining, as now appears probable, then the energy gaps are higher than those indicated by the exciton binding energies. Our principal reason for caution in this regard stems from the line shapes. If the radiation were partly due to electron–hole recombination and partly due to exciton annihilation we would expect to see a break in the line at an energy above the $h\nu_0$ points equal to the exciton binding energy. No such breaks are observed at any temperature from which we conclude that the radiation is either all due to the recombination of electrons and holes or it is all due to exciton recombination. Calculation based on the ratio of the number of excitons to electron–hole pairs and the average distance of electrons and holes in the two states indicates that electron–hole recombination should dominate, at least at the higher temperatures. For some unknown reason, apparently, the exciton recombination is the more favorable.

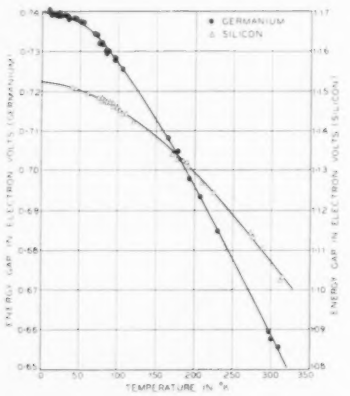


FIG. 6. The energy gaps of silicon and germanium as a function of temperature. If holes and electrons form excitons before recombining the energy gaps are greater than those shown by an amount equal to the exciton binding energy.

In any event we would expect the energies shown in Fig. 6 to agree with those found by MACFARLANE *et al.*[1] from optical absorption measurements. In the case of germanium the agreement is quite satisfactory, their results lying only about ·001 eV higher than ours over the entire range of measurements. In the case of silicon, however, their results are consistently about ·005 eV higher than ours. Although this difference is small, it is well outside of experimental error and it is not presently understood.

*Acknowledgments*—It gives us pleasure to thank many persons at Bell Telephone Laboratories for assistance during the course of this work, particularly H. R. MOORE for design of electronic circuits and J. A. BURTON for helpful discussions and advice.

*Note*—A note added in proof appears on p. 422.

## REFERENCES

1. MACFARLANE G. G., MCLEAN T. P., QUARRINGTON J. E. and ROBERTS V., *J. Phys. Chem. Solids* **8**, 388 (1959).
2. ZWERDLING S., ROTH L. M. and LAX B., *J. Phys. Chem. Solids* **8**, 397 (1959).
3. BROCKHOUSE B. N., *J. Phys. Chem. Solids* **8**, 400 (1959).

*J. Phys. Chem. Solids* Pergamon Press 1959. Vol. 8. pp. 397–400. Printed in Great Britain

# 0.4 THE DIRECT AND INDIRECT TRANSITION EXCITONS IN GERMANIUM*

**S. ZWERDLING, L. ROTH and B. LAX†**

Lincoln Laboratory, M.I.T., Lexington, Massachusetts

VOL. 8 1959

A STUDY of the direct and indirect transition excitons in germanium was undertaken subsequent to their discovery in the course of experiments to observe the fine structure of the quantum magneto-absorption spectrum of these transitions at low temperatures. In order to resolve the predicted fine structure, it was necessary to build a high resolution magneto-spectrophotometric system. The apparatus consisted of a double pass grating monochromator employing the first order of a 15,000 line/in. blazed echellette grating in the wavelength region between 1·0–1·8 $\mu$, a special liquid helium optical cryostat, and an electromagnet capable of providing a field of 38,900 G. An operating chromatic resolving power up to 20,000 (spectral slit width $5\times10^{-5}$ eV) was achieved in these experiments. For studying the direct transition, pure samples $\sim 4\mu$ thick were prepared and used cemented to a glass substrate. For the indirect transition, the samples were 6 mm. thick with polished parallel faces. Operating times of 12–16 hr. were possible with one filling of 2·5 l. of liquid helium.

Two intense absorptions were observed in the magneto-spectrum of the direct transition in germanium at 4·2°K[1] which could not be accounted for theoretically as being due to Landau transitions (those between magnetically quantized levels of the valence and conduction bands, respectively). Such transmission minima were expected at this temperature to be due to the formation of excitons of the direct transition, a possibility considered theoretically by DRESSELHAUS[2] and by ELLIOTT.[3] In order to substantiate this hypothesis, a study was made of the motion of these minima in energy as a function of magnetic field down to zero intensity for various relative orientations of the magnetic field vector, the electric vector of the linearly polarized radiation, and the principal crystallographic axes, at temperatures of 1·5°K, 4·2°K and 77°K. The curves in Fig. 1 show some of this data, including both exciton and Landau transition absorptions. For the various temperatures, the values of the direct transition energy gap found were (1) at 1·5°K and 4·2°K, 0·898$\pm$·001 eV, (2) at 77°K, 0·889$\pm$·001 eV, and (3) at 293°K, 0·805$\pm$·001 eV. The exciton lines showed a non-linear dependence on magnetic field in accordance with the theoretically anticipated quadratic Zeeman effect. Since the extrapolation of Landau transition lines establishes the forbidden energy gap,[4] the binding energy of the ground state of this exciton is $\sim$0·0025 eV at both lower temperatures and $\sim$0·0020 eV at 77°K. These values compare favorably with a theoretical estimate of 0·0017 eV obtained for an assumed hydrogen-like exciton structure, from $\epsilon_N^{\text{exc}} = 13{\cdot}60\ \mu^*/K^2N^2m_0$ with $\mu^* = 0{\cdot}031\ m_0$ for the reduced effective mass and $K = 16$ for the dielectric constant. The high field binding energy at 38·9 kG, as defined by YAFET, KEYES and ADAMS,[5] was 0·0043 eV at 4·2°K and 0·0035 eV at 77°K, compared with a theoretical estimate of 0·0045 eV using their curves. An anomalous absorption at zero field at an energy above the gap was observed in these spectra using two different samples at all temperatures, the origin of which is as yet unexplained.

The line widths found are the natural widths for the samples used, since they are an order of magnitude larger than the spectral resolving power of the apparatus. The minimum line width of the absorption corresponding to the exciton ground state yields a lower limit of the

*The research in this document was supported jointly by the Army, Navy and Air Force under contract with the Massachusetts Institute of Technology.

†Staff Members.

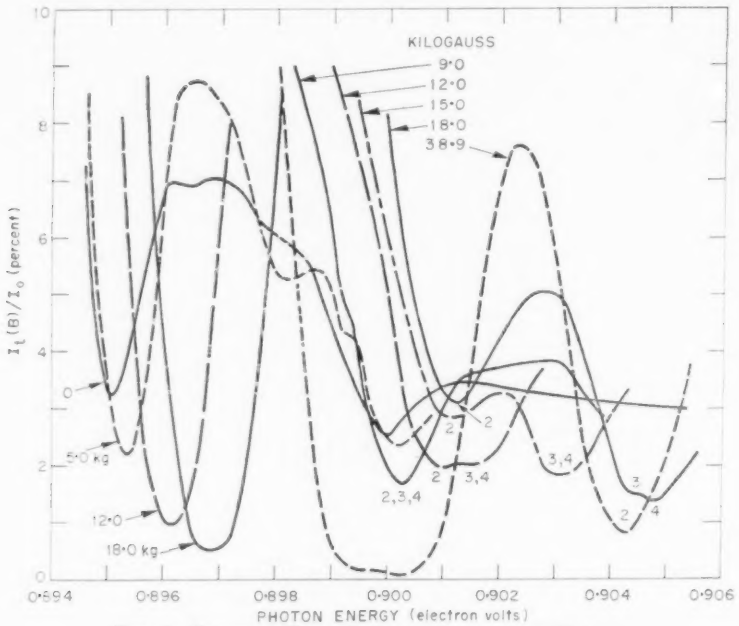


FIG. 1. Zeeman effect of the exciton and oscillatory magneto-absorption of the direct transition in germanium. Detailed traces for $\boldsymbol{E}\|\boldsymbol{B}$ at 1·5°K. Lowest exciton absorption broadens threefold and begins to split at 38·9 kG.

exciton lifetime of $8\times10^{-12}$ sec, and the maximum line width, a lifetime of $4\times10^{-12}$ sec.

Since the instrumentation developed proved to be so powerful, another attempt was made to study the magneto-absorption spectrum of the indirect transition in germanium which an earlier experiment had failed to disclose at room temperature using lower resolution. Theory now indicated, however, that the magneto-spectrum should not be oscillatory, but should consist of a series of *steps*, or absorption edges, with increasing energy above the forbidden gap. These new experiments were conducted at 4·2°K and 1·5°K and clearly showed this predicted magneto-spectrum. In addition, an absorption was observed corresponding to the formation of the indirect transition exciton involving the emission of a longitudinal acoustic phonon which was first reported by MACFARLANE, MCLEAN, QUARRINGTON and ROBERTS.[6] The Zeeman effect and fine structure of this exciton absorption is shown in Fig. 2, where the shift to higher energy with increasing field is clearly evident. In order to evaluate the data quantitatively, a plot was made of the positions of the centers of the series of steps including that of the exciton versus magnetic

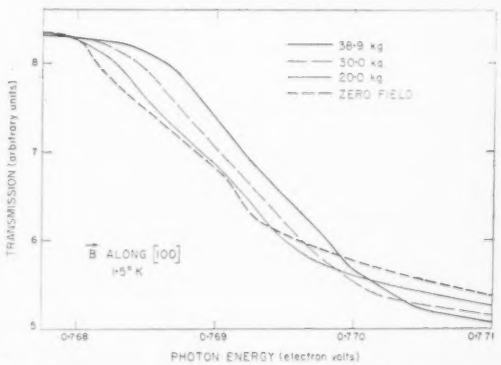


FIG. 2. Zeeman effect and fine structure of the indirect transition exciton in germanium. Transmission trace at 1·5°K shows absorption edge at zero field and non-linear shift with magnetic field intensity.

field, as shown typically in Fig. 3. Two very important results can be obtained from this plot. Firstly, the value of the indirect transition energy gap can be found very accurately as the difference

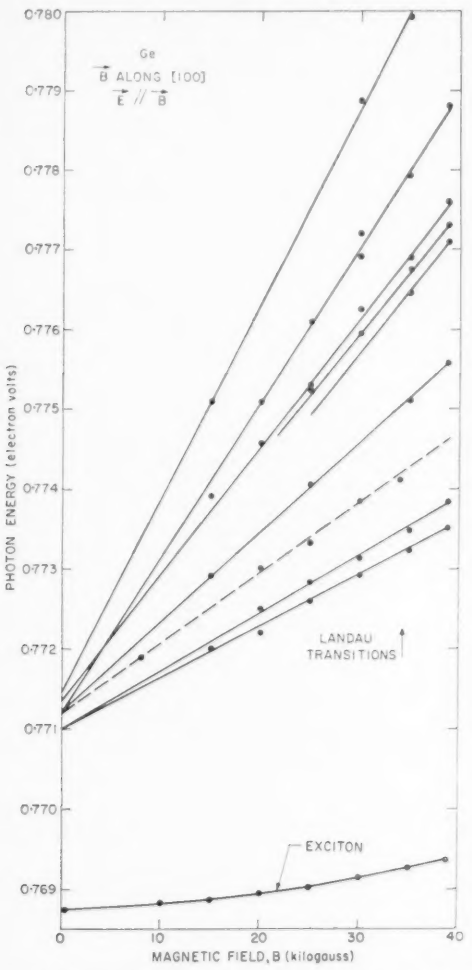


FIG. 3. Convergence plot of Landau transitions and the quadratic Zeeman effect of the indirect transition exciton in germanium. Data for 1·5°K with $\boldsymbol{B}$ along [100] and $\boldsymbol{E}\|\boldsymbol{B}$.

between the mean extrapolated energy of the Landau transition lines at zero field (0·7713± 0·0004 eV) and the energy of the emitted phonon of Debye temperature 312°±6°K (0·0276±·0005 eV) as found by MMQR.[6] Thus, the indirect energy gap is $E_e = 0{\cdot}744 \pm {\cdot}001$ eV at 1·5°K. Secondly, from the energy separation between this extrapolated value and the apparent center of the exciton absorption at zero field, the binding energy of the indirect transition exciton ground state is 0·0025±·0005 eV. This value is smaller by about a factor of 2 than that predicted theoretically by DRESSELHAUS[2] and ELLIOTT[3] and experimentally by MMQR.[6](*)

The fine structure of the indirect exciton is evident from the two resolved inflections in its absorption edge at zero field as shown in Fig. 2. This structure arises from a splitting of the ground state resulting from the complex nature of the degenerate valence band and the ellipsoidal conduction band. It may be analyzed further by evaluating the slope of the transmission trace as a function of photon energy. The resulting curve shows two peaks corresponding to the principal absorptions. Preliminary calculations involving the actual band structures gave two values for the binding energy of 0·0025 eV and 0·0033 eV in rather close agreement with the experimental peak values of 0·0021 eV and 0·0032 eV, respectively. The order of magnitude of the energy shift of the center of the exciton absorption at maximum field, which amounted to 0·0006 eV, has also been accounted for by the quadratic Zeeman effect of the exciton.

The low temperature magneto-absorption experimentation reported is yielding very accurate data concerning energy bands and excitons in semiconductors. Similar measurements have been made at 1·5°K of the indirect transition in a 6 mm thick sample of silicon where the exciton absorption edge was clearly observed at zero field to be centered at 1·2053±·0006 eV, but the magneto-absorption was too small at 38·9 kG for quantitative evaluation, due to the larger effective masses relative to that in germanium. Further measurements involving the binary intermetallic semiconductors should furnish much information concerning their energy band structures.

*We have learned since our report of these results earlier this year at a meeting of the Physical Society, Malvern, England, that a re-evaluation by MMQR of their experimental results (6) now gives a value of the indirect exciton binding energy in very close agreement with ours. For the indirect energy gap at these temperatures both our value and theirs are also in complete agreement within experimental error.

**REFERENCES**

1. ZWERDLING S., ROTH L. and LAX B., *Phys. Rev.* **109,** 2207 (1958); *Bull. Amer. Phys. Soc.* **3,** 128 (1958); *Bull. Amer. Phys. Soc.* **3,** 16 (1958).
2. DRESSELHAUS G., *J. Phys. Chem. Solids* **1,** 14 (1956).
3. ELLIOTT R. J., *Phys. Rev.* **108,** 1384 (1957).
4. ZWERDLING S., LAX B. and ROTH L., *Phys. Rev.* **108,** 1402 (1957).
5. YAFET Y., KEYES R. W., and ADAMS E. N., *J. Phys. Chem. Solids* **1,** 137 (1956).
6. MACFARLANE G. G., MCLEAN T. P., QUARRINGTON J. E. and ROBERTS V., *Phys. Rev.* **108,** 1377 (1957).

*J. Phys. Chem. Solids* Pergamon Press 1959. Vol. 8. pp. 400–405. Printed in Great Britain

# O.5 LATTICE VIBRATIONS OF SEMICONDUCTORS BY NEUTRON SPECTROMETRY

B. N. BROCKHOUSE

Physics Division, Atomic Energy of Canada Limited, Chalk River, Ontario, Canada

VOL. 8 195

**Abstract**—By study of the energy distribution of neutrons scattered by a single crystal it is possible to determine the frequency-wave number relation ($\nu(\mathbf{q})$ relation) of the normal modes of the crystal. In this paper the ideas involved are reviewed, and discussed with particular application to the diamond-type lattices of silicon and germanium. The published $\nu(\mathbf{q})$ relation for germanium determined by BROCKHOUSE and IYENGAR, and its relation to elastic constant, specific heat, and infrared measurements in the literature, is discussed. By comparing similar measurements in the literature for silicon with those for germanium, in the light of the new knowledge of the lattice frequencies for germanium, it is concluded that the lattice frequencies for silicon are higher than those for germanium at the same position in the zone, by a roughly constant factor of 1·75. The Raman frequency for silicon is deduced to be 515 cm$^{-1}$.

## 1. INTRODUCTION AND THEORY

In the Born–Von Kármán theory of crystal dynamics[1–4] a crystal is considered to be a dynamical system whose normal modes are lattice waves which behave as uncoupled harmonic oscillators. The frequencies of the normal modes are related to their wave vectors $\mathbf{q}$ (of magnitude $2\pi$/wavelength) by the dispersion relation

$$\nu = \nu_j(\mathbf{q}) \tag{1}$$

where the index $j$ signifies the branch, and takes values from 1 to $3n$ where $n$ is the number of atoms in the primitive unit cell. This frequency-wave vector relation completely describes the crystal dynamics insofar as the motions are harmonic, and from it can be deduced the frequency distribution $g(\nu)$ which describes the thermodynamic properties of a harmonic crystal.

In common with electromagnetic waves of all frequencies, neutrons can be scattered by a crystal in processes which involve the emission and/or absorption of zero, one, or more phonons. The scattering is governed by interference conditions and by conservation of energy. For a large crystal, the one-phonon process, in which the quantum number of one normal mode changes by one and the quantum numbers of the other modes remain the same, is governed by the equations[5,6]

$$\mathbf{Q} \equiv \mathbf{k}_0 - \mathbf{k}' = 2\pi\tau - \mathbf{q} \tag{2a}$$

$$|E_0 - E'| = h\nu \tag{2b}$$

where $\mathbf{k}_0$ and $\mathbf{k}'$ are, respectively, the wave vectors of the incident and outgoing neutron, $E_0$ and $E'$ are its incident and outgoing energies*, $\nu$ and $\mathbf{q}$ are the frequency and wave vector of the particular phonon with which the neutron interacted, belonging to the dispersion relation (1), and $\tau$ is a vector of the reciprocal lattice. For a cubic crystal $\tau = a^{-1}(h, k, 1)$ where $a$ is the

*The neutron energy $E = (\hbar^2/2M_n)|\mathbf{k}|^2$ where $M_n$ is the neutron mass.

lattice constant and $h$, $k$, 1 is a set of Miller indices. The wave vector is normally limited to the zone of reciprocal space about $\tau$, the equal zones filling all reciprocal space.

One phonon (coherent) scattering occurs if, and only if, equations (2) are satisfied by pairs of values of $\nu$ and $\mathbf{q}$ which also satisfy equation (1). If neutrons of known initial energy are incident on a single crystal of known orientation, and the energies of the neutrons after scattering through a given angle are measured, then $\mathbf{k}_0$, $\mathbf{k}'$, $E_0$ and $E'$ are all experimentally determined. The vector $\tau$ has a limited number of possible values, and hence, for each $\tau$ and $j$, equations (1) and (2) constitute five equations in four unknowns ($\nu$ and the three components of $\mathbf{q}$). These equations can be satisfied only rarely and hence neutrons appear in isolated groups in the angular and energy distributions. Each group defines a pair of values of $\nu$ and $\mathbf{q}$ which belong to the dispersion relation equation (1), and by repeated observation of different groups under different experimental conditions the dispersion relation can be built up.

This possibility was recognized many years ago, independently by PLACZEK and VAN HOVE, by J. M. CASSELS, by the author, and perhaps by others. In particular PLACZEK and VAN HOVE[7] showed that there are always at least $3n$ solutions to equations (1) and (2) when all $\tau$'s and $j$'s are included. It is only in the last few years that experimental techniques advanced to the stage at which the measurements were feasible.

In principle determination of the $\nu(\mathbf{q})$ relation could be carried out in the same way using electromagnetic radiation. The reason that neutrons are so much more effective than electromagnetic radiation for this purpose is that the relations between energy and wavelength are so different for the two radiations. If a phonon of wave vector $\mathbf{q}$ is to be observed, then $\mathbf{k}_0$ and $\mathbf{k}'$ must differ by at least this amount, and hence either $\mathbf{k}_0$ or $\mathbf{k}'$ or both must be of the order of $\mathbf{q}$ or larger. Thus the wavelength must be small, of the order of a lattice spacing if large $\mathbf{q}$'s are to be observed. Electromagnetic radiations of wavelength, say, 2Å have quantum energies of about 6000 eV while neutrons of the same wavelength have energies of about 0·02 eV. Thus phonon energies, generally of the order $10^{-3}$ eV to $10^{-1}$ eV, are much more readily observable with neutrons than with electromagnetic radiation.*

The study of neutron energy distributions, which we call neutron spectrometry, is therefore a powerful tool for studying lattice vibrations. It is equally useful for studying the dynamics of other systems, and since the first energy distributions were measured by the author[8] and by JACROT[9] in 1954, a considerable variety of systems have been studied.[10–12] In particular the frequency-wave number relation for germanium has been well determined through the work of BROCKHOUSE and IYENGAR[13] and of PELAH, EISENHAUER, HUGHES, and PALEVSKY.[14]

In addition to determining the frequency and wave vector of the vibrations it is desirable to characterize the branch of the spectrum to which the particular vibration belongs. This is particularly necessary if the results are to be fitted to the Born theory in order to determine the interatomic force constants. For a monatomic crystal this can be done from the intensities as pointed out by BROCKHOUSE and STEWART.[10] The intensities of the neutron groups are proportional among other things to a factor $|\mathbf{Q} \cdot \xi_j(\mathbf{q})|^2$ where $\xi_j(\mathbf{q})$ is the unit polarization vector of the normal mode. For a given $\mathbf{q}$ the three polarization vectors are orthogonal. In general $\xi_j(\mathbf{q})$ is a function of the interatomic forces, but sometimes its direction is known from symmetry. In particular for symmetric directions the polarization vectors are often either parallel to $\mathbf{q}$ (longitudinal waves), or perpendicular to $\mathbf{q}$ (transverse waves). For $\mathbf{q}$ in such directions assignment of the observed phonon to the proper branch is simple: if $\mathbf{q}$ is nearly parallel to $\mathbf{Q}$ the phonon is longitudinal, if $\mathbf{q}$ is nearly perpendicular to $\mathbf{Q}$ the phonon is transverse. For a multiatomic crystal[6] the intensity is proportional to a quantity which is the analog of the structure factor for elastic scattering, and which represents the distrubance to the neutron wave caused by motions of the atoms in the direction of the scattering vector $\mathbf{Q}$, viz:[13]

$$g_j^2(\tau, \mathbf{q}) = \left| \sum_k \frac{b_k(\boldsymbol{\xi}_{jk}(\mathbf{q}) \cdot \mathbf{Q})}{(M_k \nu_j)^{\frac{1}{2}}} \exp(i\mathbf{Q} \cdot \mathbf{R}_k) \right|^2$$

where $b_k$, $M_k$ and $\mathbf{R}_k$ are the scattering amplitude, mass and position of the $k$th atom in the unit cell. [Rigorously a Debye–Waller factor exp $(-W_k)$ should also be included.] The complex polarization vectors $\xi_{jk}$ obey ortho-normality relations and in general depend on the interatomic forces. Again however in certain symmetric directions the directions of $\xi_{jk}$ may be known by symmetry, as in the particular case of the [111]

*Measurements of the $\nu(\mathbf{q})$ relation using X-rays employ a different principle, and are based on comparison with theory of measurements of the intensity of diffusely scattered neutrons as a function of $\mathbf{q}$.

and [100] directions in the diamond lattice for which the direction of the polarization vectors is, for both atoms in the unit cell, either longitudinal or transverse. Hence the transverse or longitudinal character can be assigned in the same way as for monatomic lattices. The optical or acoustic character of the vibrations can be assigned by comparing the intensity of a group observed at a certain point in the reciprocal lattice with intensities calculated at that point for simple models using Born lattice theory. Further details are given elsewhere.[13]

## 2. LATTICE VIBRATIONS OF GERMANIUM

The frequency-wave number dispersion relations in the [100] and [111] directions of germanium have been determined by BROCKHOUSE and IYENGAR[13] and are shown in Fig. 1. For these

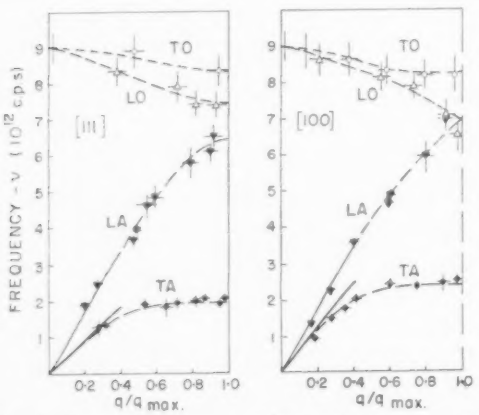


FIG. 1. Frequency-wave number relations for the [100] and [111] directions in germanium (after BROCKHOUSE and IYENGAR).

symmetric directions there are four branches to the frequency spectrum; doubly-degenerate transverse optical (TO) and transverse acoustic (TA) branches, and non-degenerate longitudinal optical (LO) and longitudinal acoustic (LA) branches. Each measured phonon was assigned to the appropriate branch by the intensity and position in the reciprocal lattice of the neutron group. The dashed lines represent the best estimate of the dispersion curves taking into account what is known of the errors. The heavy lines represent the $\nu(\mathbf{q})$ relation for the acoustic branches at long wavelengths, as calculated from the elastic constants.* The agreement for small $\mathbf{q}$ is seen to be satisfactory. The general level of the optical modes is in agreement with neutron measurements made independently by PELAH *et al.*[14] The results for a few special phonons are in agreement with deductions from infrared measurements by MACFARLANE, MCLEAN, QUARRINGTON and ROBERTS,[16] and by HAYNES *et al.*[17] and from acoustoelectric effect measurements by WEINREICH *et al.*[18] as shown in Table 1. Because the special phonons depend for their assignments on

*Table* 1. *Frequencies of phonons in germanium at* $\mathbf{q} = 0$ *and at the zone boundary in the symmetric directions, with probable errors.*

| Designation | Frequencies ($10^{12}$ c/s) reference 13 | Frequencies ($10^{12}$ c/s) other work | Reference |
|---|---|---|---|
| TO [100] | 8·25±0·3 | | |
| L [100] | 6·9 ±0·4 | 6·6 | 18 |
| TA [100] | 2·45±0·15 | | |
| TO [111] | 8·4 ±0·3 | 8·6 | 17 |
| LO [111] | 7·4 ±0·3 | | |
| LA [111] | 6·45±0·3 | 6·65 | 16 |
| | | 6·65 | 17 |
| TA [111] | 1·95±0·10 | 1·88 | 16 |
| | | 2·06 | 17 |
| O [$\mathbf{q} = 0$] | 9·0 ±0·3 | 8·9 | 14 |

the accepted placement of the maximum of the valence band at $\mathbf{q} = 0$ and of the minimum of the conduction band at $\mathbf{q} = 2\pi/a(\frac{1}{2}, \frac{1}{2}, \frac{1}{2})$, the agreement is further evidence for this placement of the bands.

BROCKHOUSE and IYENGAR showed that a frequency distribution consistent with Fig. 1 would probably account for the unusual ($\Theta_D$, $T$) curve for germanium obtained from specific heat measurements. In fact, using the data of Fig. 1 with only very minor modification, PHILLIPS[19] has been able to construct a

*From the equation $\nu = (c_j/\rho)^{\frac{1}{2}}|\mathbf{q}|/2\pi$ where $\rho$ is the density and $c_j = c_{11}$, $c_{44}$, $(c_{11}+2c_{12}+4c_{44})/3$, $(c_{11}-c_{12}+c_{44})/3$ for, respectively, the LA[100], TA[100], LA[111] and TA[111] modes. The elastic constants measured at room temperature by MCSKIMMIN[15] were used.

frequency distribution that gives, for all practical purposes, complete agreement with the very accurate specific heat data of MORRISON, FLUBACHER and LEADBETTER.[20] Brockhouse and Iyengar also showed that the far infrared spectrum[21,22] of germanium (Fig. 2) is very probably composed entirely of combination bands, and made plausible assignments based on Fig. 1. The intensities of the combination bands are consistent with the second order electric moment theory of LAX and BURSTEIN.[23] The matrix elements turn out to be large enough so that they may be important in other aspects of the physics of germanium, but not so implausibly large that they cast doubt on the applicability of the theory.

MACFARLANE *et al.*[16] and BROCKHOUSE and IYENGAR[13] showed that the dispersion curves of Fig. 1 cannot be fitted by the Born–Von Kármán model with general forces out to second neighbors, given by HELEN SMITH.[3] Individually HERMAN,[24] LAX[25] and POPE[26] have very recently studied other, more complicated, models which may give agreement with the observed dispersion law. In any case it is clear that either there is a hitherto unsuspected system of long range forces in germanium, or else the Born–Von Kármán theory is in need of revision.

### 3. LATTICE VIBRATIONS IN SILICON

It had been hoped to have neutron experiments on silicon completed in time for the Conference. For reasons quite beyond the author's control this proved impossible. Nevertheless it has been possible to draw interesting conclusions about the lattice vibrations in silicon by studying other physical properties of silicon in the light of the neutron results for germanium. The results of this study are summarized in Table 2.

First, the ratios of the Debye characteristic temperatures $\Theta_D$ obtained from specific heat measurements,[20] (a) near 0°K ($\Theta_0$), (b) at the minimum of the ($\Theta_D$, $T$) curve ($\Theta_{min}$), and (c) at comparatively high temperatures ($\Theta_\infty$), are approximately constant for the two elements. The quantity $\Theta_\infty$ represents an average of all the modes, $\Theta_{min}$ is dominated by the TA modes, and $\Theta_0$ is a measure of the very low acoustic frequencies in the spectrum. The value of $\Theta_0$ as calculated from the elastic constants[4] is also shown.

By comparing the far infrared spectra[22] of silicon and germanium (Fig. 2) one identifies immediately the strongest peaks in the two substances at 345 $cm^{-1}$ for germanium and 610 $cm^{-1}$ for silicon. For germanium this peak has been assigned by BROCKHOUSE and IYENGAR to a two phonon (TA+O) process and for silicon the same assignment is made. The ratio 610/345 = 1·77 is in agreement with the specific heat and elastic constant ratios. In germanium the two-phonon cut-off, identified in Fig. 2 by the letter A, occurs at twice the Raman frequency of 300 $cm^{-1}$, that is at 600 $cm^{-1}$. In silicon there is a band around 1130 $cm^{-1}$ (B) which has been shown by KAISER *et al.*[27] to be due to oxygen impurity. The cut-off of the intrinsic spectrum occurs at about 1030 $cm^{-1}$, and indicates that the Raman frequency in silicon is 515 $cm^{-1}$. The two-phonon cut-off frequencies for the far infrared spectra of silicon and germanium are thus in the ratio 1·72, in substantial agreement with the other ratios of Table 2. Similar arguments for other data can be produced. Thus fairly direct evidence has been presented that the very low frequencies, the Raman frequency, the general level of all frequencies, and the general level of the TA and TO branches for the two elements, are all in approximately the ratio 1·75. Differences in the elastic constant ratios, in the shapes of the bowls of the ($\Theta_D$, $T$) curves, and especially in

*Table 2. Parameters form measurements of specific heat, elastic constants, and far infrared spectra of silicon and germanium.*

| | $\Theta_\infty$ | $\Theta_{min}$ | Measured $\Theta_0$ | Calculated $\Theta_0$ | Strongest I.R. peak (TA, O) | Two phonon I.R. cut-off |
|---|---|---|---|---|---|---|
| Silicon | 674° | 463° | 645° | 648° | 610 $cm^{-1}$ | 1030 $cm^{-1}$ |
| Germanium | 395° | 254° | 374° | 374° | 345 $cm^{-1}$ | 600 $cm^{-1}$ |
| Ratio Si/Ge | 1·71 | 1·82 | 1·72 | 1·73 | 1·77 | 1·72 |

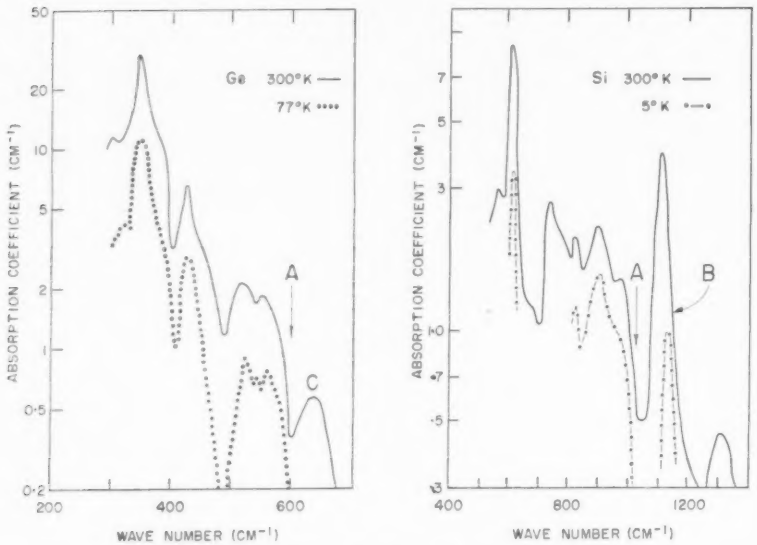


FIG. 2. Far infrared absorption of germanium and silicon (after COLLINS and FAN). The assigned positions of the two-phonon cut-offs are indicated by "A". The band marked "B" arises from oxygen impurity in the silicon lattice.

the details of the far infrared spectra of the two elements, indicate that the frequency spectra do have quite measurable differences. However to a useful degree of approximation we can conclude that the frequency spectrum of silicon resembles the spectrum of germanium, except that the frequencies at similar positions in the zone are greater for silicon by a factor of about 1·75. Similar qualitative arguments have been made by other workers.[21]

From measurements of the infrared absorption edge by MACFARLANE *et al.*[16] and of the spectrum of the intrinsic recombination radiation by HAYNES, LAX and FLOOD,[28] the values of some frequencies corresponding to $\mathbf{q}$ at the position of the minimum of the conduction band have been obtained. These frequencies are listed in Table 3. The low frequencies for the two experiments probably represent the same phonon, which would be the TA mode. The exact position of the conduction band minimum along the [100] direction[29] is not known but it is likely closer to the zone boundary than to $\mathbf{q} = 0$. The frequencies of the TA mode for silicon and germanium are then in roughly the ratio of 1·75 suggested here. The higher frequencies have been assigned by HAYNES *et al.*[28] to LA, LO and TO modes respectively. We believe the mode obtained at $\sim$0·056 eV ($\sim$460 cm$^{-1}$) in the two experiments is more probably an optical frequency

*Table 3. Energies in cm$^{-1}$ of phonons in silicon at the position of the minimum of the conduction band*

| | | | | |
|---|---|---|---|---|
| HAYNES *et al.*[28] | 129 | 445 | 670 | 960 |
| MACFARLANE *et al.*[16] | 147 | 465 | 730 | 985 |
| Previous assignments[28,16] | TA | LA | LO | TO |
| Assignments, this work | TA | O | (TA+O) | (O+O) |

and that the two higher frequencies are two-phonon combinations, probably (TA+O) and (O+O), in which case the values given are consistent with the hypothesis advanced above.

When a more exact idea of the silicon frequency dispersion laws are obtained it may be possible to locate precisely the minimum of the conduction band by comparing frequencies measured by methods such as those used by MACFARLANE *et al.* and by HAYNES *et al.*, with those measured with neutrons. Because of the steep slope of the longitudinal acoustic branch, this branch offers the best hope; the transverse branches are particularly unsuitable for this purpose (see Fig. 1). Theoretical work to identify the phonons observed in the optical experiments, and experimental work to locate the longitudinal acoustic mode, would thus be amply justified.

VOL. 8 1959

## REFERENCES


1. BORN M. and VON KÁRMÁN T., *Z. Phys.* **13,** 297 (1912).
2. BORN M. and HUANG K., *Dynamical Theory of Crystal Lattices.* Oxford (1954).
3. SMITH H. M. J., *Trans. Roy. Soc., Lond.* **241,** 105 (1948).
4. DELAUNAY J., *Solid State Physics,* Vol. 2 (edited by SEITZ F. and TURNBULL J.) Academic Press Inc., New York (1956).
5. WEINSTOCK R., *Phys. Rev.* **65,** 1 (1944).
6. WALLER I. and FROMAN P. O., *Ark. Fys.* **4,** 183 (1952).
7. PLACZEK G. and VAN HOVE L., *Phys. Rev.* **93,** 1207 (1954).
8. BROCKHOUSE B. N., *Phys. Rev.* **98,** 1171 (1955).
9. JACROT B., *C.R. Acad. Sci. Paris* **240,** 745 (1955).
10. BROCKHOUSE B. N. and STEWART A. T., *Phys. Rev.* **100,** 756 (1955). *Rev. Mod. Phys.* **30,** 236 (1958).
11. EISENHAUER C. M., PELAH I. M., HUGHES D. J. and PALEVSKY H., *Phys. Rev.* **109,** 1046 (1958).
12. BROCKHOUSE B. N., *Phys. Rev.* **99,** 601 (1955); *Ibid.*, **106,** 859 (1957); *Acta Cryst.* **10,** 827 (1957); *Nuovo Cim., Suppl.* in press; YARNELL J. L., ARNOLD G. F., BENDT P. J. and KERR F. C., *Phys. Rev. Letters* **1,** 9 (1958).
13. BROCKHOUSE B. N. and IYENGAR P. K., *Phys. Rev.* **108,** 894 (1957); *Bull. Amer. Phys. Soc.* **3,** 192 (1958); *Phys. Rev.* in press.
14. PELAH I., EISENHAUER C. M., HUGHES D. J. and PALEVSKY H., *Phys. Rev.* **108,** 1091 (1957); *Bull. Amer. Phys. Soc.* **3,** 60 (1958).
15. MCSKIMMIN H. J., *J. Appl. Phys.* **24,** 988 (1953).
16. MACFARLANE G. G., MCLEAN T. P., QUARRINGTON J. E. and ROBERTS V., *Phys. Rev.* **108,** 1377 (1957). Conference paper. *Phys. Rev.* to be published.
17. HAYNES J. R., LAX M. and FLOOD W. F., private communication.
18. WEINREICH G., private communication.
19. PHILLIPS J. C., *Phys. Rev.*, to be published.
20. MORRISON J. A., FLUBACHER P., LEADBETTER A. J., private communication.
21. SIMERAL W. G., *The Infrared Absorption Spectra of Diamond, Silicon and Germanium.* Thesis, University of Michigan (1953).
22. COLLINS R. J. and FAN H. Y., *Phys. Rev.* **93,** 674 (1954).
23. LAX M. and BURSTEIN E., *Phys. Rev.* **97,** 39 (1955).
24. HERMAN F., *J. Phys. Chem. Solids* **8,** 405 (1959).
25. LAX M., *Phys. Rev. Letters* **1,** 133 (1959).
26. POPE N. K., private communication.
27. KAISER W., KECK P. H. and LANGE C. F., *Phys. Rev.* **101,** 1264 (1956).
28. HAYNES J. R., LAX M. and FLOOD W., *Bull. Amer. Phys. Soc.* **3,** 30 (1958).
29. HERMAN F., *Rev. Mod. Phys.* **30,** 102 (1958).


*J. Phys. Chem. Solids* Pergamon Press 1959. Vol. 8. pp. 405–418. Printed in Great Britain

# O.6 LATTICE VIBRATIONAL SPECTRUM OF GERMANIUM*

**FRANK HERMAN**

Radio Corporation of America, RCA Laboratories Division, Princeton, N.J.

**Abstract**—The Born–von Kármán theory of crystal dynamics has been applied to the diamond structure, and the most general force system involving interactions between each atom and its

*A preliminary account of this work was presented at the Symposium on Spectroscopy of Solids, Malvern, England, May 29, 1958.

first through sixth order neighbors has been derived. The macroscopic elastic constants and the frequencies of selected lattice vibrational modes have been expressed in terms of the 21 independent parameters entering into this force system.

It will be shown that the experimental elastic constants and lattice frequencies along the [100] and [111] axes cannot be fitted to force models based only on general 1° and 2° neighbor interactions. The addition of general 3° and 4° neighbor interactions does not improve the situation, but the further addition of 5° (and higher order) neighbor interactions does. It is possible to obtain physically plausible force models which fit all the data considered within experimental error by the use of only general 1° through 5° interactions. The nature and the limitations of the derived force models will be discussed.

## 1. INTRODUCTION

RECENT work by four experimental groups has added greatly to our knowledge of the lattice vibrational spectrum of germanium. The infrared absorption studies of MACFARLANE, MCLEAN, QUARRINGTON and ROBERTS,[1] the infrared emission studies of HAYNES, LAX and FLOOD,[2] and the inelastic neutron scattering experiments of PELAH, EISENHAUER, HUGHES and PALEVSKY,[3,4] and of BROCKHOUSE and IYENGAR,[5] have provided us with a comprehensive picture of the dispersion curves along the [100] and [111] axes of the reduced zone, and a tentative picture of those along the [110] axis.[4]

On the basis of available experimental information, it is possible to account for the detailed form of the infra-red lattice absorption spectrum,[5] and for the observed temperature dependence of the specific heat.[5–7] These explanations, and the consistency of the values of particular lattice mode frequencies obtained by different experimental techniques, evidence the essential correctness of the observed lattice vibrational spectrum.

It has already been noted by several authors[8] that the experimental elastic constants[9] and lattice mode frequencies[1–5] cannot be fitted to force models based on the Born–von Kármán theory of crystal dynamics[10–13] and involving general forces between each atom and its 1°, 2°, 3° and even 4° neighbors. Moreover, the discrepancy between experiment and theory is not materially improved by adding general 3° and 4° neighbor forces to general 1° and 2° neighbor forces.

In order to satisfy our curiosity regarding the effect of adding forces between still more distant neighbors, we extended the previous work to include general forces between 1° through 6° neighbors. In section 2 we will present a concise summary of the application of the Born–von Kármán theory to the diamond structure. For a detailed discussion of the methods employed, which we omit in the interest of brevity, see the classic paper by HELEN SMITH.[11] In section 3 we discuss the problem of fitting theory to experiment. Numerical results are presented, and the nature of the derived force models is considered. In the final section, the limitations of the present work are discussed.

## 2. APPLICATION OF BORN–VON KÁRMÁN THEORY TO DIAMOND STRUCTURE

According to the Born–von Kármán theory of crystal dynamics,[10,11] the nuclear motion is determined by an effective potential function $\Phi$ which depends only upon the nuclear coordinates (assuming that the electronic system remains in its adiabatic ground state). It is convenient to expand $\Phi$ in powers of the cartesian components of the displacements of the nuclei from their equilibrium positions. For a study of harmonic nuclear motion, it is sufficient to consider only the second order terms in this expansion:

$$\Phi_2 = \tfrac{1}{2} \sum_s \sum_{s'} \sum_i \sum_j \Phi_{ij}(s, s') u_i(s) u_j(s'), \qquad (1)$$

where

$$\Phi_{ij}(s, s') = \left[ \frac{\partial^2 \Phi}{\partial x_i(s) \partial x_j(s')} \right]_0. \qquad (2)$$

The cartesian components of the equilibrium position of lattice site $s$ are denoted by $x_i(s)$, $i = x, y, z$. The displacements from this equilibrium position are denoted by $u_i(s)$. In (1), the sums on $s$ and $s'$ range over all lattice sites, and those on $i$ and $j$ over $x$, $y$ and $z$. We will refer to the matrix elements—$\Phi_{ij}(s, s')$ as interatomic force constants.

For a given crystal structure, it is possible to reduce the number of independent interatomic force constants by noting that:
(a) the order of differentiation in (2) is irrelevant; (b) the potential function $\Phi$ is invariant to all symmetry operations belonging to the space group of the crystal; and (c) the potential function $\Phi$ is invariant to rigid translations and rotations of the crystal.

In the case of the diamond structure, which has two atoms per unit cell, it is convenient to introduce two cartesian coordinate systems, one centered at the lattice site [0, 0, 0], and the other at $(a/4)[1, 1, 1]$, where $a$ is the lattice constant. Lattice sites will be identified in the former coordinate system by the symbol $s$, and in the latter by $s^*$. The lattice sites corresponding to the 1° through 6° neighbors of the central atom in each coordinate system are listed in Table 1.

In diamond-type crystals, the lattice sites can be classified into nine categories. Expressed in units of $(a/4)$, and in terms of $Q$, $R$ and $S$, three different, non-zero integers, these are: (i) $[0, 0, Q^e]$; (ii) $[Q^e, Q^e, 0]$; (iii) $[Q^e, Q^e, Q^e]$; (iv) $[Q^e, Q^e, R^e]$; (v) $[Q^e, R^e, 0]$; (vi) $[Q^e, R^e, S^e]$; (vii) $[Q^0, Q^0, Q^0]$; (viii) $[Q^0, Q^0, R^0]$; and (ix) $[Q^0, R^0, S^0]$, where the superscripts e and o denote even and odd integers. The general form of the force constant matrices is the same for all sets of neighbors belonging to the same category. By suitably ordering the lattice sites associated with each set of neighbors, it is possible to bring out the characteristic similarities and differences among the various categories. This has been done in Fig. 1 and Table 2, where the most general forms of the

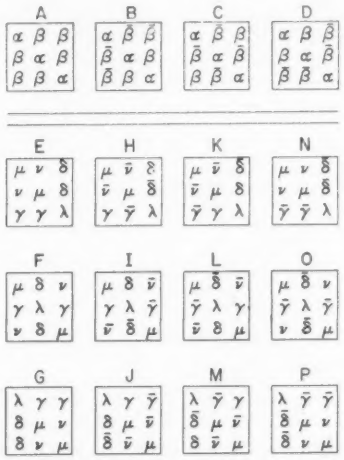


FIG. 1. The interatomic force constant matrices $-\Phi(s, s')$ and $-\Phi(s^*, s^{*\prime})$. Overhead bars denote minus signs.

*Table* 1. *Rectangular coordinates of lattice sites s and s* in units of* $(a/4)$. *The* 1° *neighbors of s or* $s^* = 0$ *are given by* $1 \leq s$ *or* $s^* \leq 4$. *The* 2° *neighbors of s or* $s^* = 0$ *are given by* $5 \leq s$ *or* $s^* \leq 16$, *with* $Q = 2$ *and* $R = 0$. *Similarly, the* 3° *neighbors are given by* $17 \leq s$ *or* $s^* \leq 28$, *with* $Q = -1$ *and* $R = -3$; *the* 4° *neighbors by* $29 \leq s$ *or* $s^* \leq 34$; *the* 5° *neighbors by* $35 \leq s$ *or* $s^* \leq 46$, *with* $Q = 3$ *and* $R = 1$; *the* 6° *neighbors by* $47 \leq s$ *or* $s^* \leq 58$, *with* $Q = 2$ *and* $R = 4$, *and by* $59 \leq s$ *or* $s^* \leq 70$, *with* $Q = -2$ *and* $R = -4$.

| $s$ $s^*$ | $x(s)$ $-x(s^*)$ | $y(s)$ $-y(s^*)$ | $z(s)$ $-z(s^*)$ | $s$ $s^*$ | $s$ $s^*$ | $s$ $s^*$ | $s$ $s^*$ | $s$ $s^*$ | $x(s)$ $-x(s^*)$ | $y(s)$ $-y(s^*)$ | $z(s)$ $-z(s^*)$ |
|---|---|---|---|---|---|---|---|---|---|---|---|
| 0 | 0 | 0 | 0 | 5 | 17 | 35 | 47 | 59 | $Q$ | $Q$ | $R$ |
| 1 | 1 | 1 | 1 | 6 | 18 | 36 | 48 | 60 | $Q$ | $R$ | $Q$ |
| 2 | 1 | −1 | −1 | 7 | 19 | 37 | 49 | 61 | $R$ | $Q$ | $Q$ |
| 3 | −1 | 1 | −1 | 8 | 20 | 38 | 50 | 62 | $-Q$ | $Q$ | $-R$ |
| 4 | −1 | −1 | 1 | 9 | 21 | 39 | 51 | 63 | $-Q$ | $-R$ | $Q$ |
| | | | | 10 | 22 | 40 | 52 | 64 | $-R$ | $-Q$ | $Q$ |
| 29 | 0 | 0 | 4 | 11 | 23 | 41 | 53 | 65 | $Q$ | $-Q$ | $-R$ |
| 30 | 0 | 4 | 0 | 12 | 24 | 42 | 54 | 66 | $Q$ | $-R$ | $-Q$ |
| 31 | 4 | 0 | 0 | 13 | 25 | 43 | 55 | 67 | $-R$ | $Q$ | $-Q$ |
| 32 | 0 | 0 | −4 | 14 | 26 | 44 | 56 | 68 | $-Q$ | $-Q$ | $R$ |
| 33 | 0 | −4 | 0 | 15 | 27 | 45 | 57 | 69 | $-Q$ | $R$ | $-Q$ |
| 34 | −4 | 0 | 0 | 16 | 28 | 46 | 58 | 70 | $R$ | $-Q$ | $-Q$ |

*Table 2. Identification of $-\Phi(s, s')$ and key to Fig. 1. The symbols A through P refer to matrices displayed in Fig. 1, and the symbols $\tilde{A}$ through $\tilde{P}$ to the transposes of these matrices. The entry 5–10 under the heading E—J indicates that the matrix E corresponds to $s' = 5$, the matrix F to $s' = 6$, the matrix G to $s' = 7$ ... and the matrix J to $s' = 10$.*

| Neighbors | $s$ or $s^*$ | $s'$ or $s^{*\prime}$ | | | | | | Remarks |
|---|---|---|---|---|---|---|---|---|
| | | $A-D$ | $\tilde{A}-\tilde{D}$ | $E-J$ | $K-P$ | $\tilde{E}-\tilde{J}$ | $\tilde{K}-\tilde{P}$ | |
| 1° | 0 | 1—4 | | | | | | |
| 1° | 0* | | 1*—4* | | | | | |
| 2° | 0 | | | 5–10 | 11–16 | | | Set $\gamma = -\delta$ |
| 2° | 0* | | | | | 5*–10* | 11*–16* | |
| 3° | 0 | | | 17–22 | 23–28 | | | Set $\gamma = \delta$ and add primes |
| 3° | 0* | | | | | 17*–22* | 23*–28* | |
| 4° | 0 | | | 29–34 | | | | Set $\nu = \gamma = \delta = 0$ and add double primes |
| 4° | 0* | | | | | 29*–34* | | |
| 5° | 0 | | | 35–40 | 41–46 | | | Set $\gamma = \delta$ and add triple primes |
| 5° | 0* | | | | | 35*–40* | 41*–46* | |
| 6° | 0 | | | 47–52 | 53–58 | 59–64 | 65–70 | Merely add quadruple primes |
| 6° | 0* | | | 59*–64* | 65*–70* | 47*–52* | 53*–58* | |

force constant matrices for 1° through 6° neighbors are displayed. [These belong to categories (i), (ii), (iv), (vii) and (viii).] For future reference, note that for 2° and 6° neighbors, there are both symmetric [$\nu$, $\nu''''$, $(\frac{1}{2})(\delta''''+\nu'''')$] and antisymmetric [$\delta$, $(\frac{1}{2})(\delta''''-\nu'''')$] off-diagonal matrix elements. SMITH[11] incorrectly set the 2° antisymmetric element $\delta$ equal to zero.[14–16]

To get some physical insight into the nature of the various parameters, it is helpful to consider a few special force models. In Fig. 2 we compare the matrices for the most general force system involving 1° through 6° neighbors with those for pure central forces, pure angular forces, and pure torsional forces. These three models have been chosen for consideration because they are commonly used in molecular vibration problems,[17] and moreover, because central, angular, and torsional forces are examples of two-, three-, and four-body forces, respectively.

In the case of central forces, it may be seen from Fig. 2 that there is only one parameter $P_i$ for each set of neighbors. There is one parameter for angular forces ($Q$) and one for torsional forces ($T$). By definition,[17] angular forces tend to resist deformation of the angle formed by each pair of concurrent bonds, and torsional forces tend to resist deformation of the dihedral angle between each pair of planes determined by the atoms A-B-C and B-C-D, respectively, where

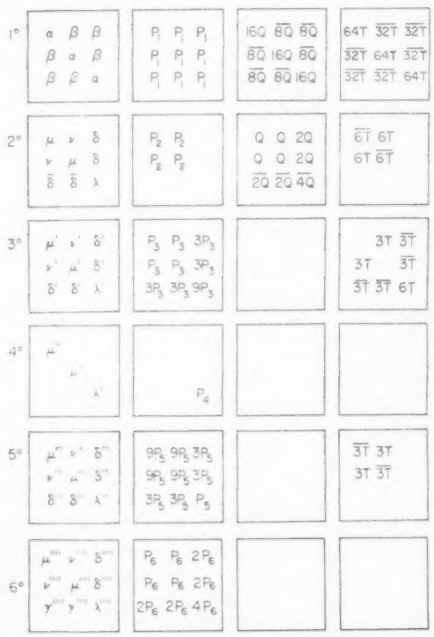

FIG. 2. Interatomic force constant matrices for general forces (column 1), central forces (column 2), angular forces (column 3), and torsional forces (column 4). Overhead bars denote minus signs.

atoms A-B-C-D are bonded in sequence. The matrices shown in Fig. 2 were obtained by calculating the individual matrices for all bond and

dihedral angles defined in part by the central atom, and then summing. Since the three and four atom chains which define bond and dihedral angles can link the central atom with its 1° and 2° neighbors, and with its 1°, 2°, 3°, and 5° neighbors, respectively, there are terms in $Q$ and $T$ for each of these sets of neighbors.

Central and angular force models have often been introduced in previous work[18] in order to reduce the total number of independent parameters. We have displayed the matrices for these force models, and for the torsional force model as well, not with this in mind, but rather to indicate how these forces are apportioned among the various general parameters. Thus we see, for example, that central forces contribute equally, and angular and torsional forces unequally, to the 1° parameters $\alpha$ and $\beta$. (If these were the only forces present, we would have: $\alpha = P_1+16Q+64T$; $\beta = P_1-8Q-32T$.) Note that angular forces contribute to the anti-symmetric 2° parameter $\delta$, but that central and torsional forces do not.

It is possible to relate the macroscopic elastic constants to the interatomic force constants by the method of long waves.[10] In the case of diamond-type crystals, it can be shown that the three elastic constants ($c_{11}$, $c_{12}$ and $c_{44}$) can be expressed in terms of five characteristic linear combinations of interatomic force constants, as is indicated in Fig. 3. The quantities $A_i$ appearing in this figure are closely related to the non-vanishing elements of the fourth rank tensors in terms of which the elastic constants are defined.[19]

Note that the diagonal matrix elements [e.g., $\alpha$, $\mu$, $\lambda$] appear only in $A_1$, $A_3$ and $A_5$, while the symmetric off-diagonal elements [e.g., $\beta$, $\nu$, $\delta_+'''' = (\frac{1}{2})(\delta''''+\gamma'''')$] appear only in $A_2$ and $A_3$. For reasons already given by WALLER and LUNDQVIST,[20] the anti-symmetric off-diagonal elements [e.g., $\delta$, $\delta_-'''' = (\frac{1}{2})(\delta''''-\gamma'''')$] do not appear at all in the expressions for the elastic constants.

Also note the rapid increase in the numerical coefficients with increasing order of neighbor. This behavior is to be expected, since the fourth rank tensors which define the elastic constants are quadratic functions of the $x_i(s)$. It follows that the interatomic force constants must fall off quite rapidly with interatomic separation if the expressions in Fig. 3 are to converge, as they must on physical grounds.

$ac_{11} = A_1 \qquad ac_{12} = A_2 - A_3 \qquad ac_{44} = A_3 - \frac{A_4^2}{A_5}$

| NEIGHBORS | | 1° | 2° | 3° | 4° | 5° | 6° |
|---|---|---|---|---|---|---|---|
| PARAMETERS | | $\alpha, \beta$ | $\mu, \nu, \lambda, \delta$ | $\mu', \nu', \lambda', \delta'$ | $\mu'', \lambda''$ | $\mu'', \nu'', \lambda'', \delta''$ | $\mu'''', \nu'''', \lambda'''', \delta'''' \gamma''''$ |
| $A_1$ | = | $\alpha$ | $+8\mu$ | $+2\mu'+9\lambda'$ | $+8\lambda''$ | $+18\mu''+\lambda''$ | $+16\mu''''+32\lambda''''$ |
| $A_2$ | = | $2\beta$ | $+8\nu$ | $+2\nu'+12\delta'$ | | $+18\nu''+12\delta''$ | $+16\nu''''+32\delta'''' +32\gamma''''$ |
| $A_3$ | = | $\alpha$ | $+4\mu+4\lambda$ | $+10\mu'+\lambda'$ | $+8\mu''$ | $+10\mu''+9\lambda''$ | $+40\mu''''+8\lambda''''$ |
| $A_4$ | = | $\beta$ | | $-3\nu'-2\delta'$ | | $+\nu''+6\delta''$ | |
| $A_5$ | = | $\alpha$ | | $+2\mu'+\lambda'$ | | $+2\mu''+\lambda''$ | |

FIG. 3. Method of long waves.

In order to determine the normal modes of vibration, it is necessary to solve a set of sixth order secular equations of the form

$$||\mathbf{G}(\mathbf{q})-\mathbf{I}M\omega^2|| = 0, \tag{3}$$

where $(2\pi/a)(\mathbf{q})$ is the reduced wave vector, $\mathbf{I}$ is the $6\times6$ unit matrix, $M$ the nuclear mass, and $\omega$ the angular frequency. The matrix elements of $\mathbf{G}(\mathbf{q})$ are given in Appendix I for the general point in the reduced zone. For $\mathbf{q}$ lying along a symmetry axis, or at a symmetry point, it is possible to factor the above sixth order secular equation into a number of lower-order ones, and in the most favorable cases, to obtain solutions in closed form. Such results are presented in Appendix II.

### 3. FITTING THEORY TO EXPERIMENT

Historically, the first indication that a force model based on general forces between 1° and 2° neighbors was inadequate for germanium came with the report of MACFARLANE *et al.*[1] that the equivalent temperatures of the LA and TA modes at $\mathbf{q} = (\frac{1}{2}, \frac{1}{2}, \frac{1}{2})$ were 320°K and 90°K, respectively. Expressed in wave numbers, these become 222 and 62·5 $cm^{-1}$. Since the lattice mode frequencies of this $\mathbf{q}$ are independent of $\delta$, there are only five independent parameters in such a force model, namely, $\alpha$, $\beta$, $\mu$, $\nu$ and $\lambda$. If it be required that these parameters fit the three elastic constants, through the relations given in Fig. 3, there are only two degrees of freedom left. It is convenient to choose these as $\alpha$ and $\beta/\alpha$.

In Fig. 4 we have plotted the wave numbers for the six normal modes at $\mathbf{q} = (\frac{1}{2}, \frac{1}{2}, \frac{1}{2})$ (TO and TA are each doubly degenerate) for selected values of $\alpha$ and $\beta/\alpha$, for general 1° and 2° neighbor force models which fit the three elastic constants. While it is not difficult to obtain a fit to LA = 222 $cm^{-1}$, it is impossible to fit TA = 62·5 $cm^{-1}$ for reasonable choices of $\alpha$, or what amounts to the same thing, for reasonable choices of the Raman frequency. At the time Fig. 4 was drawn, the actual value of this frequency was unknown. The best current values (for the Raman wave number) are: Brookhaven[4]: 294±10 $cm^{-1}$; Chalk River:[5] 300±10 $cm^{-1}$. Incidentally, it should be noted that there are actually two fits to LA = 222 $cm^{-1}$ for RA = 300 $cm^{-1}$. We shall return to this point later.

As has already been emphasized by previous authors,[1,5] the principal difficulty of the above force model is its failure to accommodate to the experimental values for the TA mode frequencies at $\mathbf{q} = (\frac{1}{2}, \frac{1}{2}, \frac{1}{2})$ and at $\mathbf{q} = (1, 0, 0)$, once it has been fitted to the experimental values of the elastic constants and of the Raman frequency. More specifically, the model predicts transverse

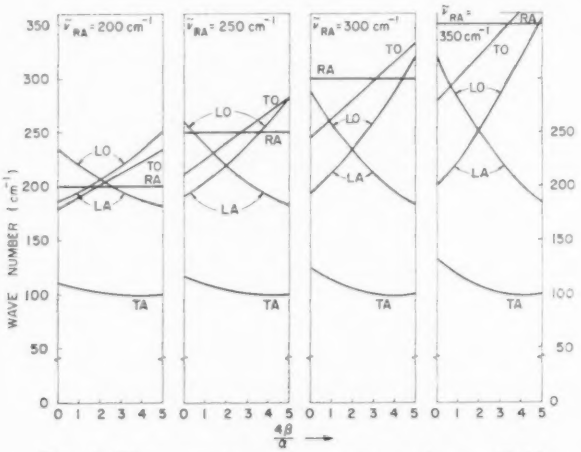


FIG. 4. Wave numbers for normal modes at [111] face points.

acoustic mode frequencies in the outer part of the reduced zone that are considerably higher than the experimental values.

Even if we work with a force model involving the 12 independent parameters corresponding to general forces between 1° through 4° neighbors, it is not possible to obtain a fit, within experimental error, to the three elastic constants, the Raman frequency, and the LO or LA and TA frequencies at $\mathbf{q} = (\frac{1}{2}, \frac{1}{2}, \frac{1}{2})$. It is rather curious that the nature of the fit is actually not improved as the original force model (general 1° and 2° neighbor forces) is rendered more flexible by the addition of general 3° and 4° neighbor forces. That this is the case may be seen from the following relations:

$$ac_{11} = A_1;\ ac_{12} = A_2 - A_3;\ ac_{44} = A_3 - A_4^2/A_5; \quad (4)$$

$$(\tfrac{1}{8})M\omega^2_{\mathrm{RA}} = A_5; \quad (5)$$

It is clear from equations (6) through (9) that the required improvement in flexibility can only come about through the addition of 5° and still higher order neighbor parameters.

In order to determine the nature of the force models required to fit the experimental data, and in particular to determine the minimum number of additional neighbors beyond 4° neighbors that have to be taken into account, we undertook three numerical investigations. In all three cases, we used the nineteen experimental data given in Table 3 as the basis of our work. These are: the three elastic constants, the Raman frequency, and the 15 normal mode frequencies at the mid- and end-points of the [100] and [111] axes (see also Fig. 5).

*Table 3. Experimental data for lattice frequencies (based on* BROCKHOUSE *and* IYENGAR, *reference 5).*

| Mode | Frequency $\nu \times 10^{12}$ sec$^{-1}$ | No. | Mode | Frequency $\nu \times 10^{12}$ sec$^{-1}$ | No. |
|---|---|---|---|---|---|
| RA (0 0 0] | 9·0 ±0·3 | (1) | TO [¼ ¼ ¼] | 8·8 ±0·3 | (9) |
| TO [½ 0 0] | 8·45±0·3 | (2) | TA [¼ ¼ ¼] | 1·85±0·15 | (10) |
| TA [½ 0 0] | 2·2 ±0·15 | (3) | LO [¼ ¼ ¼] | 8·05±0·3 | (11) |
| LO [½ 0 0] | 8·2 ±0·3 | (4) | LA [¼ ¼ ¼] | 4·15±0·2 | (12) |
| LA [½ 0 0] | 4·2 ±0·2 | (5) | TO [½ ½ ½] | 8·4 ±0·3 | (13) |
| TO [1 0 0] | 8·25±0·3 | (6) | TA [½ ½ ½] | 1·95±0·10 | (14) |
| TA [1 0 0] | 2·45±0·15 | (7) | LO [½ ½ ½] | 7·4 ±0·3 | (15) |
| L [1 0 0] | 6·9 ±0·4 | (8) | LA [½ ½ ½] | 6·45±0·3 | (16) |

$$(\tfrac{2}{3})(M\omega^2_{\mathrm{LX}} + 2M\omega^2_{\mathrm{TA}}) = A_1 + 2A_3 + A_5 - \Delta; \quad (6)$$

$$(\tfrac{2}{3})(M\omega^2_{\mathrm{LX}} - M\omega^2_{\mathrm{TA}}) = A_2 + 2A_4 - \Delta'; \quad (7)$$

where

$$\Delta = 16[2\mu''' + \lambda''' + 6\mu'''' + 3\lambda''''] + \text{higher order parameters}; \quad (8)$$

$$\Delta' = 16[\nu''' + 2\delta''' + 2\nu'''' + 2\delta'''' + 2\gamma''''] + \text{higher order parameters}; \quad (9)$$

and where LX is to be identified with either the experimental LO or LA mode, but in either case, $M\omega^2_{\mathrm{LX}}$ is given by the same linear combination of parameters. We have deliberately expressed $M\omega^2_{\mathrm{LX}}$ and $M\omega^2_{\mathrm{TA}}$ in the form of two identities in order to be able to investigate the effect of ignoring 5° and higher order neighbor interactions.

If we confine ourselves to general 1° through 4° neighbor interactions, $\Delta$ and $\Delta'$ are zero, and we find that the six experimental quantities under consideration actually depend upon the five characteristic linear combinations of parameters already encountered in Fig. 3. Since this dependence remains the same whether the highest order neighbors considered are 2°, 3° or 4°, we see that the addition of 3° and 4° neighbor parameters does not actually increase the flexibility of the model, at least so far as fitting the above six experimental quantities is concerned.

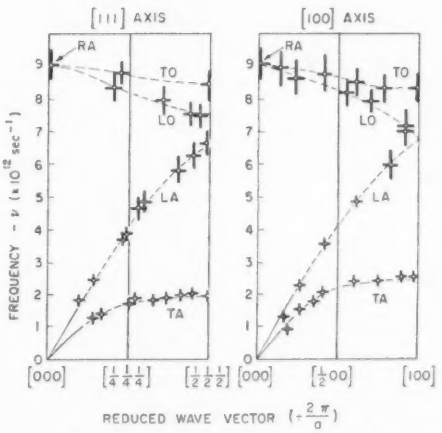


FIG. 5. Inelastic neutron scattering data, after BROCKHOUSE and IYENGAR, reference 5.

In the first two sets of calculations, we confined ourselves to 1° through 5° neighbor interactions. Since the 2° parameter $\delta$ does not enter into the expressions for any of the 19 experimental quantities mentioned above, this force model contains 15, rather than 16 pertinent parameters. However, it is easily shown that in these 19 expressions, the 15 parameters occur in 13 distinct linear combinations. Thus, it is not possible to obtain a unique fit to the data, but rather a fit with two degrees of freedom. Actually, the term "unique fit" is misleading, since at best there would be four solutions, owing to the quadratic forms in the expressions for $ac_{44}$ and for the longitudinal modes at $\mathbf{q} = (\frac{1}{2}, \frac{1}{2}, \frac{1}{2})$. For future reference, we observe that these four solutions can be distinguished from one another by the their respective experimental uncertainties. This solution, which of course is not an optimum one, is as follows (all parameters are in units of $10^4$ dyn cm$^{-1}$):

$$\alpha = 4{\cdot}9536$$

$$\beta - 2\nu' = 2{\cdot}5835 \qquad \mu = 0{\cdot}2366$$

$$\beta + 2\nu''' = 3{\cdot}2032 \qquad \nu = 0{\cdot}4638$$

$$\beta + \nu''' - 2\delta''' = 3{\cdot}0217 \qquad -\lambda = 0{\cdot}3194$$

$$-2\mu' - \lambda' = 0{\cdot}5900 \qquad \mu'' = 0{\cdot}1088$$

$$\nu' - 2\delta' = 0{\cdot}8069 \qquad -\lambda'' = 0{\cdot}1197$$

$$\lambda' + 2\mu''' = 0{\cdot}1999 \qquad 2\mu''' + \lambda''' = 0{\cdot}3962$$

In order to demonstrate the existence of solutions for which the parameters become

*Table 4. Derived values for inter-atomic force constants (in units of $10^4$ dyn cm$^{-1}$).*

| Force Constant | I | II | III | IV | V | VI |
|---|---|---|---|---|---|---|
| $\alpha$ | 4·9536 | 3·7119 | 3·7095 | 4·0161 | 3·7092 | 4·0161 |
| $\beta$ | 3·0822 | 2·6564 | 3·4032 | 2·5758 | − 4·0000 | − 4·3385 |
| $\mu$ | 0·2366 | 0·2643 | 0·3312 | 0·2694 | 1·9079 | 1·7432 |
| $\lambda$ | −0·3194 | −0·4213 | − 0·5924 | − 0·5282 | − 3·7458 | − 3·4758 |
| $\nu$ | 0·4638 | 0·3593 | 0·0792 | 0·1243 | 0·0791 | 0·1243 |
| $\mu'$ | −0·2629 | 0·3740 | 0·3954 | 0·2396 | 3·8471 | 3·8243 |
| $\lambda'$ | −0·0643 | −0·8471 | − 0·7707 | − 0·9756 | − 7·6741 | − 8·1449 |
| $\nu'$ | 0·2494 | −0·6579 | − 0·1441 | − 0·2686 | − 3·8457 | − 3·7257 |
| $\delta'$ | −0·2788 | −0·4573 | − 0·1975 | − 0·5186 | − 2·0483 | − 2·2471 |
| $\mu''$ | 0·1088 | 0·1077 | 0·2466 | 0·1915 | 3·4001 | 3·1390 |
| $\lambda''$ | −0·1197 | −0·1747 | − 0·5118 | − 0·3469 | − 6·8186 | − 6·2420 |
| $\mu'''$ | 0·1321 | 0·5415 | 0·5262 | 0·6096 | 3·9779 | 4·1942 |
| $\lambda'''$ | 0·1321 | | 0·0041 | 0·0267 | − 6·8990 | − 7·1426 |
| $\nu'''$ | 0·0605 | 0·7389 | 0·5056 | 0·7108 | 4·2074 | 4·1680 |
| $\delta'''$ | 0·0605 | | 0·2453 | 0·1949 | − 1·6054 | − 1·5336 |
| $\mu''''$ | | | − 0·0471 | − 0·0124 | − 0·8354 | − 0·7493 |
| $\lambda''''$ | | | 0·0768 | 0·0438 | 1·6534 | 1·5176 |
| $\nu''''$ | | | − 0·1751 | − 0·1474 | − 0·1752 | − 0·1474 |
| $\delta_+''''$ | | | 0·0175 | 0·0843 | 0·0175 | 0·0843 |
| $A_3$ | | | 11·8488 | 12·1234 | 11·8519 | 12·1233 |
| $A_4$ | | | 6·2075 | 6·2991 | 6·2087 | 6·2991 |
| $A_5$ | | | 4·7861 | 4·7656 | 4·7860 | 4·7656 |

following conditions: (i) $\beta > 0$, LX = LO; (ii) $\beta > 0$, LX = LA; (iii) $\beta < 0$, LX = LO; (iv) $\beta < 0$, LX = LA.

Proceeding by trial and error, and using condition (ii), we were able to find a family of solutions which fitted all 19 experimental data well within progressively smaller with increasing order of neighbor, we can select special cases of the above family of solutions. For example, by setting $\mu''' = \lambda'''$, and $\nu''' = \delta'''$, we eliminate the two degrees of freedom, and obtain the solution denoted in Table 4 by I. Note that in this solution,

the 1° parameters are an order of magnitude larger than the 2° parameters, and beyond 2° neighbors, the parameters fall off gradually with increasing order of neighbor. On physical grounds, this is a very attractive result.

The existence of this solution, and of others like it, proves that the experimental elastic constants and lattice spectrum of germanium (at least along the [100] and [111] axes) can in fact be fitted by force models based on general 1° through 5° neighbor interactions. While we have not made a thorough study of the lattice spectrum predicted in the remainder of the reduced zone by the above force model, the indications are that it is a physically reasonable one. Moreover, with the vast amount of freedom afforded by a 16 parameter model—we are now adding the 2° parameter $\delta$—we feel that no difficulty should be encountered in fitting this model to data elsewhere in the zone, when such data becomes available.

In the next set of calculations (also using 1° through 5° neighbors), we proceeded by the method of least squares, weighting each of the 19 data by the inverse square of its probable error. For reasons of computational expediency, we ignored the experimental uncertainty in the reduced wave vector in the inelastic neutron scattering measurements, and admitted only uncertainties in angular frequency. Instead of working directly with the raw data, as given by BROCKHOUSE and IYENGAR[5] we considered lattice modes at specific points in the reduced zone, using the overall data to obtain the best possible estimates of $\nu$ and $\Delta\nu$ for each such mode. The values actually used are given in Table 4. Some of these are taken from the paper by BROCKHOUSE and IYENGAR.

Since many of the expressions for the normal mode frequencies are non-linear, and since the expression for $c_{44}$ is non-linear, we found it necessary to linearize the problem, and solve it by successive iteration.[21] Since there are only 13 independent parameters, it was necessary to delete 2 of the 15. For the purposes of illustration, we show in Table 4 under the heading II the least-squares solution [based on condition (i): $\beta > 0$, LX = LO] for the case $\lambda''' = \delta''' = 0$. Note that the parameters do not show the progressive fall-off with increasing order of neighbor exhibited by the trial-and-error, non-optimum solution I. We did not consider it worthwhile to attempt to juggle the parameters so that this progressive fall-off would result, though we believe this could be readily accomplished. (In this process, we would, of course, stay within experimental error, so far as the fit is concerned.) In any event, solution II demonstrates that a straight-forward least-squares fit does not give as physically attractive a model as does a judiciously executed trial-and-error fit.

In the final set of calculations, we introduced the four pertinent 6° parameters [$\mu''''$, $\lambda''''$, $\nu''''$, and $\delta''''_{+} = (\frac{1}{2})(\delta'''' + \gamma'''')$], and set out to fit the 19 experimental data with the 19 pertinent 1° through 6° parameters. Fortunately, these 19 parameters are linearly independent, so that one can obtain specific solutions, rather than families of solutions. The system of 19 equations in 19 unknowns was actually solved with the program originally devised for solving the linearized least-squares problem by successive iteration. [The numerical work was done on an IBM 650 Computor.] The numerical results, which are good to two and sometimes three decimal digits, are shown in Table 4 as III, IV, V, and VI. These correspond to conditions (i), (ii), (iii) and (iv), respectively.

Solutions V and VI may be dismissed immediately as unphysical, since the force parameters of distant neighbors have the same order of magnitude as those for close neighbors. While solutions III and IV are physically reasonable, they exhibit a much slower fall-off with increasing order of neighbor than solution I. As we have already said in connection with solution II, the parameters can be modified to give a more rapid fall-off, at the same time staying within the experimental uncertainty of all the data.

It is instructive to compare solutions II and III for evidence of convergence, since both of these refer to the same condition, namely, (i). While there is a distinct similarity between the two solutions, the evidence for convergence is meagre. Of course, the above comparison would be more significant if solution II referred to a least-squares solution for general 1° through 5° neighbor interactions, rather than one for general 1° through 4° and special 5° neighbor interactions. In view of this circumstance, and in view of the small amount of data used, relative to the number of parameters used, it is not out of the question

that the convergence of the solution is actually more rapid than a comparison of solutions II and III would suggest.

*Note added in proof:* COLE and KINEKE have recently calculated the frequency distribution function and the dispersion relations along the [100], [110], and [111] axes on the basis of solutions III to VI of our Table 4 [COLE H., private communication; and COLE H. and KINEKE E., *Phys. Rev. Letters* **1**, 360 (1958)]. Solutions III and IV gave essentially the same frequency distribution but different dispersion relations along the [110] axis. In contrast to solutions III and IV, which gave physically reasonable dispersion relations everywhere in the reduced zone, the unphysical solutions V and VI gave imaginary frequencies along the [110] axis and in other directions. The author wishes to thank Dr. COLE for bringing this work to his attention prior to publication, and for valuable correspondence.

## 4. DISCUSSION

In the previous section, it was shown that the experimental elastic constants and lattice frequencies along the [100] and [111] axes cannot be fitted to force models based on general 1° and 2° neighbor interactions. It was also shown that the addition of general 3° and 4° interactions does not improve the situation, but that the further addition of 5° (and higher order) interactions does. In fact, it is possible to obtain physically plausible force models which fit all the data considered within experimental error by the use of only general 1° through 5° interactions.

However, the number of parameters used is so large, relative to the number of experimental data employed, and the experimental uncertainty of the various lattice frequencies is sufficiently great, that except for the 1° and possibly the 2° parameters, the derived values of the force constants are not statistically significant [see Appendix III for details]. This rules out any attempt to establish the physical nature of the derived force model by decomposition into component force models each of which has a clear-cut physical significance.

Moreover, there is no guarantee that force models based on short- and medium-range interactions are sufficient for a proper representation of the actual force system, even though such force models fit a representative set of data within experimental error. In order to demonstrate the sufficiency of such force models, it would be necessary to examine their convergence properties more thoroughly than we have been able to.

Thus, while we do not actually need to introduce long-range interactions in order to fit the data, it does not follow that such interactions can be safely ignored.

It is with these thoughts in mind that we now turn to a brief consideration of recent work by MELVIN LAX, which came to our attention only after the present work was in its final stages.[22] LAX[23] has made the important suggestion that the asymptotic behavior of the inter-atomic forces in diamond-type crystals is determined by quadrupole–quadrupole interactions, and that such interactions have a long-range character. An important consequence of this long-range character is that the expressions for the elastic constants [cf. Fig. 3] converge very slowly.

The physical picture is as follows: When a given nucleus is displaced from its equilibrium position, there is a deformation of the local charge density, which may be resolved into multipole moments. For reasons of crystal symmetry, only $2^{2n}$-pole moments ($n = 1, 2, 3 \ldots$) are induced by the motion of the nucleus. If all the multipoles are assumed to be concentrated at lattice sites, the interaction between any pair of atoms (separated by the distance R) can be expressed as the sum of a quadrupole–quadrupole interaction (which falls off as $1/R^5$), a quadrupole–hexadecapole interaction (which falls off as $1/R^7$), a hexadecapole–hexadecapole interaction (which falls off as $1/R^9$), etc.

LAX proposes to fit the experimental data to a force model involving one parameter to represent the quadrupole–quadrupole interaction (only one parameter is necessary), and as many low order neighbor parameters as proves necessary. It is hoped that the latter will take the higher multipole–multipole interactions into account, and will compensate for the error made by assuming that the induced multipoles are concentrated at lattice sites.

We would like to suggest that when this program is completed, the solution for the force system is not likely to be radically different from the ones obtained in the present work, apart from the addition of a (possibly small) quadrupole–quadrupole term. In order to justify this view, let us consider the induced quadrupoles more closely.

When a nucleus is displaced from its equilibrium position, a real (as opposed to an ideal or point)

dipole is induced along each of the four lines joining the nucleus to its nearest neighbors.[22–26] The characteristic length of each of these real dipoles is of the order of half an inter-atomic spacing. The sum of the four dipoles radiating from the central nucleus is a real quadrupole, with characteristic lengths of the order of an inter-atomic spacing.

It is well known[27] that the interaction between two real multipoles may be many times that between two analogous ideal multipoles if the separation between them is less than about twice the characteristic lengths. In the present application, this means that the interaction between real quadrupoles would give contributions to 1° through 3° (and possibly 4° and 5°) neighbor force constants much larger than those predicted by the $1/R^5$ law, which applies only to ideal quadrupoles at short distances.

Thus, it would not be unreasonable to expect a force model which contains: (i) very large 1° neighbor force constants (arising primarily from the higher order multipole–multipole interactions); (ii) smaller but still appreciable 2°, 3° and possibly 4° and 5° neighbor force constants (arising primarily from the effects of interactions between real quadrupoles); and (iii) still smaller higher order neighbor force constants well described by the ideal quadrupole–quadrupole interaction law.

*Acknowledgments*—The author wishes to thank Mr. SHERWOOD SKILLMAN for programming the numerical computations on an IBM 650 Magnetic Drum Calculator, and for other able assistance in many phases of this work. The author is grateful to Dr. MAURICE GLICKSMAN, Dr. MELVIN LAX, Dr. DWIGHT O. NORTH, and Dr. JAMES C. PHILLIPS for many interesting discussions, and to the many individuals who sent him preprints of their work prior to publication. Finally, the author wishes to express his deep appreciation to Dr. B. N. BROCKHOUSE, Mr. C. M. EISENHAUER, Dr. J. R. HAYNES, Dr. D. J. HUGHES, Dr. G. G. MACFARLANE, Dr. H. PALEVSKY and Dr. I. PELAH for the privilege of seeing their data at an early stage, and for much valuable correspondence.

## REFERENCES

1. MACFARLANE G. G., MCLEAN T. P., QUARRINGTON J. E. and ROBERTS V., *Phys. Rev.* **108,** 1377 (1957).
2. HAYNES J. R., private communication; see also HAYNES J. R., LAX M. and FLOOD W. F., *J. Phys. Chem. Solids* **8,** 392 (1959).
3. PELAH I., EISENHAUER C. M., HUGHES D. J. and PALEVSKY H., *Phys. Rev.* **108,** 1091 (1957).
4. HUGHES D. J. and PALEVSKY H., private communication; for a subsequent account of this work, see: GHOSE A., PALEVKY H., HUGHES D. J., PELAH I. and EISENHAUER C. M., *Phys. Rev.*, to be published.
5. BROCKHOUSE B. N. and IYENGAR P. K., *Phys. Rev.* **108,** 894 (1957); *Ibid.* **111,** 747 (1958); BROCKHOUSE B. N., *J. Phys. Chem. Solids* **8,** 400 (1959).
6. PHILLIPS J. C., *Phys. Rev.*, to be published.
7. MARCUS P. M. and KENNEDY A. J., *Phys. Rev.*, to be published.
8. See, for example, references 1 and 5, also MACFARLANE G. G., private communication, and PHILLIPS J. C., private communication.
9. MCSKIMIN H. J., *J. Applied Phys.* **24,** 988 (1953). In the present paper, we shall use MCSKIMIN's data at 25°C, which in units of $10^{12}$ dyn cm$^{-2}$ is: $c_{11} = 1{\cdot}2897$, $c_{12} = 0{\cdot}48346$, and $c_{44} = 0{\cdot}67130$. The estimated experimental uncertainty in these values is 1 per cent. For the lattice constant of germanium, we shall use the value $a = 5{\cdot}65754 \times 10^{-8}$ cm (at 25°C); the nuclear mass can be determined from the density, which is 5·32674 g cm$^{-3}$ (at 25°C); source: SMAKULA A. and KALNAJS J., *Phys. Rev.* **99,** 1737 (1955), and SMAKULA A. and SILS V., *Phys. Rev.* **99,** 1744 (1955).
10. BORN M. and HUANG K., *Dynamical Theory of Crystal Lattices*. Oxford (1954).
11. SMITH H. M. J., *Phil. Trans. Roy. Soc. Lond.* **241,** 105 (1948).
12. HSIEH Y.-C., *J. Chem. Phys.* **22,** 306 (1954).
13. EASTWOOD D. E., Ph.D. Thesis, Illinois Institute of Technology, Chicago, Illinois (June 1957), unpublished.
14. BRAUNSTEIN R., MOORE A. R. and HERMAN F., *Phys. Rev.* **109,** 695 (1958), see Appendix.
15. SAINT-JAMES D., *J. Phys. Chem. Solids* **5,** 337 (1958).
16. To the author's knowledge, the first specific reference to a fourth 2° parameter appears in: RAMANATHAN K. G., *Proc. Indian Acad. Sci.* A**26,** 481 (1947); see also KRISHNAMURTI D., *Ibid*, A**33,** 325 (1951).
17. WILSON Jr. E. B., DECIUS J. C. and CROSS P. C., *Molecular Vibrations*, Chap. 4. McGraw-Hill, New York (1955). Note, on page 61, equation (22), there should be a plus, rather than a minus sign in front of the second term.
18. CHELAM E. V., *Proc. Indian Acad. Sci.* A**18,** 334 (1943); HARRISON W. A., Ph.D. Thesis, University of Illinois (1956), unpublished; see also references 10–15.
19. See reference 10, sections 26 and 27.
20. WALLER I., *Ark. Fys.* in press; see also LUNDQVIST S. O., *Ibid.* **9,** 435 (1955); *Ibid.* **12,** 263 (1957), also reference 15.
21. WHITTAKER E. T. and ROBINSON G., *The Calculus of Observations*, 4th edn., section 109. London, (1946).

22. LAX M., private communication.
23. LAX M., *Phys. Rev. Letters* **1**, 133 (1958).
24. SHOCKLEY W., *Electrons and Holes in Semiconductors* page 531, problem 1. D. Van Nostrand, New York (1950).
25. NORTH D. O., private communication. The author wishes to thank Dr. NORTH for bringing reference 24 to his attention, and for pointing out the desirability of expanding the inter-atomic forces in terms of a complete, mutually orthogonal set of interactions, such as the multipole–multipole interactions.
26. LAX M., *Phys. Rev. Letters* **1**, 131 (1958).
27. HIRSCHFELDER J. O., CURTISS C. F. and BIRD R. B., *Molecular Theory of Gases and Liquids*, chapters 12 and 13; see, for example, Fig. 12. 1–6, p. 850. Wiley, New York (1954).

## APPENDIX I

*The matrix elements of* $\mathbf{G}(\mathbf{q})$ [*cf. equation* (3)].

These will be denoted below by $\mathbf{G}_{ab}(\mathbf{q})$, where $a$ or $b = 1, 2, 3$ for $s = 0$, and $a$ or $b = 4, 5, 6$ for $s = 1$. The rows and columns of $\mathbf{G}(\mathbf{q})$ are ordered in the same fashion as in Smith's paper [cf. reference 11, equation (3.13)].

$$\begin{aligned}
\mathbf{G}_{11}(\mathbf{q}) = \mathbf{G}_{44}(\mathbf{q}) &= 4\alpha+4\lambda(1-\cos\pi q_y\cos\pi q_z)+4\mu(2-\cos\pi q_z\cos\pi q_x-\cos\pi q_x\cos\pi q_y)\\
&\quad+8\mu'+4\lambda'+2\lambda''(1-\cos 2\pi q_x)+2\mu''(2-\cos 2\pi q_y-\cos 2\pi q_z)\\
&\quad+8\mu'''+4\lambda'''+8\lambda''''(1-\cos 2\pi q_x\cos\pi q_y\cos\pi q_z)\\
&\quad+8\mu''''(2-\cos 2\pi q_y\cos\pi q_z\cos\pi q_x-\cos 2\pi q_z\cos\pi q_x\cos\pi q_y).
\end{aligned}$$

$\mathbf{G}_{22}(\mathbf{q}) = \mathbf{G}_{55}(\mathbf{q})$ and $\mathbf{G}_{33}(\mathbf{q}) = \mathbf{G}_{66}(\mathbf{q})$ can be obtained from the above by cyclic permutation.

$$\begin{aligned}
G_{12}(\mathbf{q}) = \mathbf{G}^*_{21}(\mathbf{q}) &= G_{54}(\mathbf{q}) = G^*_{45}(\mathbf{q}) = 4\upsilon\sin\pi q_x\sin\pi q_y-i4\delta\sin\pi q_z(\cos\pi q_x-\cos\pi q_y)\\
&\quad+8\upsilon''''\sin\pi q_x\sin\pi q_y\cos 2\pi q_z+8\delta_+''''\cos\pi q_z(\sin\pi q_x\sin 2\pi q_y-\sin\pi q_y\sin 2\pi q_x)\\
&\quad-i8\delta_-''''\sin\pi q_z(\cos\pi q_x\cos 2\pi q_y-\cos\pi q_y\cos 2\pi q_x).
\end{aligned}$$

$\mathbf{G}_{23}(\mathbf{q}) = G^*_{32}(\mathbf{q}) = G_{65}(\mathbf{q}) = G^*_{56}(\mathbf{q})$ and $G_{31}(\mathbf{q}) = \mathbf{G}^*_{13}(\mathbf{q}) = G_{46}(\mathbf{q}) = G^*_{64}(\mathbf{q})$ by cyclic permutation: $G_{12}(\mathbf{q})\to G_{23}(\mathbf{q})\to G_{31}(\mathbf{q})$.

$$\begin{aligned}
G_{14}(\mathbf{q}) = \mathbf{G}^*_{41}(\mathbf{q}) &= -\alpha[1+\exp-\pi i(q_x+q_y)+\exp-\pi i(q_y+q_z)+\exp-\pi i(q_z+q_x)]\\
&\quad-\lambda'[\{1+\exp-\pi i(q_y+q_z)\}\exp-2\pi iq_x+(\exp-\pi iq_y+\exp-\pi iq_z)\exp\pi iq_x]\\
&\quad-\mu'[\{1+\exp-\pi i(q_z+q_x)\}\exp-2\pi iq_y+(\exp-\pi iq_z+\exp-\pi iq_x)\exp\pi iq_y]\\
&\quad-\mu'[\{1+\exp-\pi i(q_x+q_y)\}\exp-2\pi iq_z+(\exp-\pi iq_x+\exp-\pi iq_y)\exp\pi iq_z]\\
&\quad-\lambda'''[\{\exp-\pi i(2q_y-q_z)+\exp-\pi i(2q_z-q_y)\}\exp-\pi iq_x+\exp\pi i(q_y+q_z)+\exp-2\pi i(q_y+q_z)]\\
&\quad-\mu'''[\{\exp-\pi i(2q_z-q_x)+\exp-\pi i(2q_x-q_z)\}\exp-\pi iq_y+\exp\pi i(q_z+q_x)+\exp-2\pi i(q_z+q_x)]\\
&\quad-\mu'''[\{\exp-\pi i(2q_x-q_y)+\exp-\pi i(2q_y-q_x)\}\exp-\pi iq_z+\exp\pi i(q_x+q_y)+\exp-2\pi i(q_x+q_y)]
\end{aligned}$$

$\mathbf{G}_{25}(\mathbf{q}) \equiv \mathbf{G}^*_{52}(\mathbf{q})$ and $\mathbf{G}_{36}(\mathbf{q}) = \mathbf{G}^*_{63}(\mathbf{q})$ by cyclic permutation: $\mathbf{G}_{14}(\mathbf{q}) \to \mathbf{G}_{25}(\mathbf{q}) \to \mathbf{G}_{36}(\mathbf{q})$

$$\begin{aligned}
G_{15}(\mathbf{q}) = \mathbf{G}^*_{51}(\mathbf{q}) &= G_{24}(\mathbf{q}) = G^*_{42}(\mathbf{q}) = -\beta[1+\exp-\pi i(q_x+q_y)-\exp-\pi i(q_y+q_z)-\exp-\pi i(q_z+q_x)]\\
&\quad-\delta'[\{-1+\exp-\pi i(q_y+q_z)\}\exp-2\pi iq_x+(-\exp-\pi iq_y+\exp-\pi iq_z)\exp\pi iq_x]\\
&\quad-\delta'[\{-1+\exp-\pi i(q_z+q_x)\}\exp-2\pi iq_y+(+\exp-\pi iq_z-\exp-\pi iq_x)\exp\pi iq_y]\\
&\quad-\upsilon'[\{+1+\exp-\pi i(q_x+q_y)\}\exp-2\pi iq_z+(-\exp-\pi iq_x-\exp-\pi iq_y)\exp\pi iq_z]\\
&\quad-\delta'''[\exp\pi i(q_y+q_z)-\exp-2\pi i(q_y+q_z)+\{+\exp-\pi i(2q_y-q_z)-\exp-\pi i(2q_z-q_y)\}\exp-\pi iq_x]\\
&\quad-\delta'''[\exp\pi i(q_z+q_x)-\exp-2\pi i(q_z+q_x)+\{-\exp-\pi i(2q_z-q_x)+\exp-\pi i(2q_x-q_z)\}\exp-\pi iq_y]\\
&\quad-\upsilon'''[\exp\pi i(q_x+q_y)+\exp-2\pi i(q_x+q_y)+\{-\exp-\pi i(2q_x-q_y)-\exp-\pi i(2q_y-q_x)\}\exp-\pi iq_z].
\end{aligned}$$

$G_{26}(\mathbf{q}) = \mathbf{G}^*_{62}(\mathbf{q}) = G_{35}(\mathbf{q}) = G^*_{53}(\mathbf{q})$ and $G_{34}(\mathbf{q}) = G^*_{43}(\mathbf{q}) = G_{16}(\mathbf{q}) = G^*_{61}(\mathbf{q})$ by cyclic permutation: $G_{15}(\mathbf{q})\to G_{26}(\mathbf{q})\to G_{34}(\mathbf{q})$.

Note that the anti-symmetric parameters [$\delta$ and $\delta_-'''' = (\tfrac{1}{2})(\delta''''-\gamma'''')$] do not contribute to $\mathbf{G}(\mathbf{q})$ along the [100] and [111] axes. Along the [110] axis, their influence on $\mathbf{G}(\mathbf{q})$ is greatest at $\mathbf{q} = (\tfrac{1}{2}\ \tfrac{1}{2}\ 0)$, which is midway between the zone center and a [100]-type face point. Along the [1$q$0] axis, their influence on $\mathbf{G}(\mathbf{q})$ is greatest at $\mathbf{q} = (1\ \tfrac{1}{2}\ 0)$, i.e., at the zone corner, which is midway between two [100]-type face points.

## APPENDIX II

*Special solutions of the secular equation* $\|\mathbf{G}(\mathbf{q})-\mathbf{I}M\omega^2\| = 0$.

(i) [000] Raman frequency: $M\omega^2_{\mathrm{RA}} = 8A_5 = 8(\alpha+2\mu'+\lambda'+2\mu'''+\lambda''')$.

(ii) [100] axis: $q_x = q$; $q_y = q_z = 0$; $0 \leqslant q \leqslant 1$.

$$\left.\begin{matrix}M\omega^2_{\mathrm{LO}}\\ M\omega^2_{\mathrm{LA}}\end{matrix}\right\} = (\tfrac{1}{2})M\omega^2_{\mathrm{RA}}+8(\mu+2\mu'''')(1-\cos\pi q)+2(\lambda''+4\lambda'''')(1-\cos 2\pi q)$$
$$\pm 4[(\alpha+2\mu'+\lambda''')\cos(\pi q/2)+(\lambda'+2\mu''')\cos(3\pi q/2)]$$

$$\left.\begin{matrix} M\omega^2_{\mathrm{TO}} \\ M\omega^2_{\mathrm{TA}} \end{matrix}\right\} = (\tfrac{1}{2})M\omega^2_{\mathrm{RA}}+4(\mu+\lambda+2\mu''''+2\lambda'''')(1-\cos\pi q)+2(\mu''+4\mu'''')(1-\cos 2\pi q)$$
$$\pm 4[\{(\alpha+\mu'+\lambda'+\mu''')\cos(\pi q/2)+(\mu'+\mu'''+\lambda''')\cos(3\pi q/2)\}^2$$
$$+\{(\beta-2\delta'+\nu''')\sin(\pi q/2)+(-\nu'+2\delta''')\sin(3\pi q/2)\}^2]^{\frac{1}{2}}$$

(iii) [111] axis: $q_x = q_y = q_z = q$; $0 \leqslant q \leqslant \frac{1}{2}$.

$$\left.\begin{matrix} M\omega^2_{\mathrm{LO}} \\ M\omega^2_{\mathrm{LA}} \end{matrix}\right\} = F+2J\pm[(A_1+2B_1)^2+(A_2+2B_2)^2]^{\frac{1}{2}}$$

$$\left.\begin{matrix} M\omega^2_{\mathrm{TO}} \\ M\omega^2_{\mathrm{TA}} \end{matrix}\right\} = F-J\pm[(A_1-B_1)^2+(A_2-B_2)^2]^{\frac{1}{2}}$$

where:
$F = (\frac{1}{2})M\omega^2_{\mathrm{RA}}+4(2\mu+\lambda)(1-\cos^2\pi q)+2(2\mu''+\lambda'')(1-\cos 2\pi q)$
$+8(2\mu'''+\lambda''')(1-\cos^2\pi q\cos 2\pi q)$;
$J = 4\nu\sin^2\pi q+8\nu''''\sin^2\pi q\cos 2\pi q$;
$A_1 = (\alpha+4\mu'+2\lambda')+(3\alpha+2\mu'+\lambda'+6\mu'''+3\lambda''')\cos 2\pi q+(2\mu'+\lambda'+2\mu'''+\lambda''')\cos 4\pi q$;
$A_2 = -(3\alpha+2\mu'+\lambda'+2\mu'''+\lambda''')\sin 2\pi q-(2\mu'+\lambda'+2\mu'''+\lambda''')\sin 4\pi q$;
$B_1 = (\beta-2\nu')+(-\beta+\nu'-2\delta'-\nu'''+2\delta''')\cos 2\pi q+(\nu'+2\delta'+\nu'''-2\delta''')\cos 4\pi q$;
$B_2 = -(-\beta+\nu'-2\delta'-3\nu'''-2\delta''')\sin 2\pi q-(\nu'+2\delta'+\nu'''-2\delta''')\sin 4\pi q$.
At $q = \frac{1}{2}$ (the [111] face point), $A_2$ and $B_2$ are zero, so that
$\left.\begin{matrix} M\omega^2_{\mathrm{TO}} \\ M\omega^2_{\mathrm{TA}} \end{matrix}\right\} = F-J\pm|A_1-B_1|$, and $\left.\begin{matrix} M\omega^2_{\mathrm{LO}} \\ M\omega^2_{\mathrm{LA}} \end{matrix}\right\} = F+2J\pm|A_1+2B_1|$.
Assuming that $\alpha > 0$ and $\beta > 0$, there is no ambiguity in the case of the transverse modes, since:
$M\omega^2_{\mathrm{TO}} = F-J-A_1+B_1 = 6\alpha+2\beta+\ldots$; $M\omega^2_{\mathrm{TA}} = F-J+A_1-B_1 = 2\alpha-2\beta+\ldots$
In the case of the longitudinal modes, we write: (if LW = LO, LX = LA, and vice versa)
$M\omega^2_{\mathrm{LW}} = F+2J-A_1-2B_1 = 6\alpha-4\beta+\ldots$; $M\omega^2_{\mathrm{LX}} = F+2J+A_1+2B_1 = 2\alpha+4\beta+\ldots$

(iv) [1$q$0] axis: $q_x = 1$, $q_y = q$; $0 \leqslant q \leqslant \frac{1}{2}$; $q_z = 0$. There are three doubly-degenerate branches along this axis. The secular equation has the form:
$[G_{11}-\omega^2)(G_{22}-\omega^2)(G_{33}-\omega^2)-(G_{11}-\omega^2)|G_{26}|^2-(G_{22}-\omega^2)|G_{31}|^2-(G_{33}-\omega^2)|G_{15}|^2$
$+G_{15}G^*_{26}G_{31}+G^*_{15}G_{26}G^*_{31}]^2 = 0$,
where:
$G_{11} = 4[\alpha+\mu(3+\cos\pi q)+\lambda(1-\cos\pi q)+2\mu'+\lambda'+(\frac{1}{2})\mu''(1-\cos 2\pi q)+2\mu'''+\lambda'''$
$+2\lambda''''(1-\cos\pi q)+2\mu''''(2+\cos\pi q+\cos 2\pi q)]$;
$G_{22} = 4[\alpha+2\mu+2\lambda+2\mu'+\lambda'+(\frac{1}{2})\lambda''(1-\cos 2\pi q)+2\mu'''+\lambda'''+4\mu''''+2\lambda''''(1+\cos 2\pi q)]$;
$G_{33} = 4[\alpha+\mu(3-\cos\pi q)+\lambda(1+\cos\pi q)+2\mu'+\lambda'+(\frac{1}{2})\mu''(1-\cos 2\pi q)+2\mu'''+\lambda'''$
$+2\lambda''''(1+\cos\pi q)+2\mu''''(2-\cos\pi q+\cos 2\pi q)]$;
$G_{12} = G_{23} = G_{14} = G_{25} = G_{36} = G_{34} = 0$;
$G_{31} = -8i[\delta\sin\pi q+2\delta_-''''\sin\pi q]$;
$G_{15} = -2[(\beta+\nu'-\delta'-\delta''')(1-\exp-\pi iq)+(\delta'+\delta'''-\nu''')(\exp\pi iq-\exp-2\pi iq)]$;
$G_{26} = -2[(\beta+\nu'-\delta'-\delta''')(1+\exp-\pi iq)-(\delta'+\delta'''-\nu''')(\exp\pi iq+\exp-2\pi iq)]$.

(v) [110] axis: $q_x = q_y = q$, $q_z = 0$; $0 \leqslant q \leqslant 1$. The $6\times6$ secular equation factors into a $2\times2$ and a $4\times4$ secular equation. The solution of the former is as follows:
$M\omega^2 = F-J\pm[(A_+-B_+)^2+(A_--B_-)^2]^{\frac{1}{2}}$. The $4\times4$ secular equation is as follows:

$$\begin{vmatrix} F+J+A_++B_+-M\omega^2 & A_-+B_- & (2)^{\frac{1}{2}}C_+ & (2)^{\frac{1}{2}}(C_--K) \\ A_-+B_- & F+J-A_+-B_+-M\omega^2 & (2)^{\frac{1}{2}}(C_-+K) & -(2)^{\frac{1}{2}}C_+ \\ (2)^{\frac{1}{2}}C_+ & (2)^{\frac{1}{2}}(C_-+K) & H+A'_+-M\omega^2 & A'_- \\ (2)^{\frac{1}{2}}(C_--K) & -(2)^{\frac{1}{2}}C_+ & A'_- & H-A'_+-M\omega^2 \end{vmatrix} = 0$$

where:
$A_+ = (\frac{1}{2})(A+A^*)$; $iA_- = (\frac{1}{2})(A-A^*)$; and similarly for $A'$, $B$, and $C$;
$F = (\frac{1}{2})M\omega^2_{\mathrm{RA}}+4\mu(2-\cos\pi q-\cos^2\pi q)+4\lambda(1-\cos\pi q)+2\mu''(1-\cos 2\pi q)$
$+2\lambda''(1-\cos 2\pi q)+8\mu''''(2-\cos^2\pi q-\cos\pi q\cos 2\pi q)+8\lambda''''(1-\cos\pi q\cos 2\pi q)$;
$H = (\frac{1}{2})M\omega^2_{\mathrm{RA}}+8\mu(1-\cos\pi q)+4\lambda(1-\cos^2\pi q)+4\mu''(1-\cos 2\pi q)$
$+16\mu''''(1-\cos\pi q\cos 2\pi q)+8\lambda''''(1-\cos^2\pi q)$;
$J = 4\nu\sin^2\pi q+8\nu''''\sin^2\pi q$;
$K = 4\delta\sin\pi q(1-\cos\pi q)-8\delta_-''''\sin\pi q(\cos\pi q-\cos 2\pi q)$;

EE

$$
\begin{aligned}
A &= -\alpha(1+\exp -2\pi iq+2\exp -\pi iq)-\mu'(\exp \pi iq+2+2\exp -\pi iq+2\exp -2\pi iq+\exp -3\pi iq)\\
&\quad -\lambda'(\exp \pi iq+1+\exp -2\pi iq+\exp -3\pi iq)-\lambda'''(\exp \pi iq+1+\exp -2\pi iq+\exp -3\pi iq)\\
&\quad -\mu'''(\exp 2\pi iq+\exp \pi iq+1+2\exp -\pi iq+\exp -2\pi iq+\exp -3\pi iq+\exp -4\pi iq);\\
A' &= -\alpha(1+\exp -2\pi iq+2\exp -\pi iq)-2\mu'(\exp 2\pi iq+1+\exp -2\pi iq+\exp -3\pi iq)\\
&\quad -\lambda'(1+2\exp -\pi iq+\exp -2\pi iq)-2\mu'''(\exp \pi iq+1+\exp -2\pi iq+\exp -3\pi iq)\\
&\quad -\lambda'''(\exp 2\pi iq+2\exp -\pi iq+\exp -4\pi iq);\\
B &= -\beta(1+\exp -2\pi iq-2\exp -\pi iq)-\upsilon'(1-2\exp -\pi iq+\exp -2\pi iq)+2\delta'(\exp \pi iq-1-\exp -2\pi iq\\
&\quad +\exp -3\pi iq)-2\upsilon'''(\exp -\pi iq)(\cos 3\pi q-1)-4\delta'''(\exp -\pi iq)(\cos 2\pi q-\cos \pi q);\\
C &= -\beta(1-\exp -2\pi iq)+\upsilon'(\exp \pi iq+1-\exp -2\pi iq-\exp -3\pi iq)+\delta'(\exp \pi iq-\exp -3\pi iq)\\
&\quad -2i\upsilon'''(\exp -\pi iq)(\sin 2\pi q-\sin \pi q)-2i\delta'''(\exp -\pi iq)(\sin \pi q+\sin 2\pi q+\sin 3\pi q).
\end{aligned}
$$

## APPENDIX III

*Probable errors of derived force constants*

Using the eight identities listed below, and the experimental data given in Table 3, it is possible to determine the values and the probable errors of eight linear combinations of inter-atomic force constants. Identifying the various lattice modes by the numbers given in Table 3 [e.g., $\omega_1$ = RA (0 0 0)], we have:

$$(\tfrac{1}{16})M\omega^2_1+(\tfrac{1}{24})[2(M\omega^2_{13}-M\omega^2_{14})\mp(M\omega^2_{15}-M\omega^2_{16})] = \alpha+2\mu'''+\lambda''' \quad \text{(III.1)}$$

$$(\tfrac{1}{16})M\omega^2_1-(\tfrac{1}{24})[2(M\omega^2_{13}-M\omega^2_{14})\mp(M\omega^2_{15}-M\omega^2_{16})] = 2\mu'+\lambda' \quad \text{(III.2)}$$

$$(\tfrac{1}{16})[M\omega^2_6-M\omega^2_7]+(\tfrac{1}{24})[(M\omega^2_{13}-M\omega^2_{14})\pm(M\omega^2_{15}-M\omega^2_{16})] = \beta+\upsilon'''-2\delta''' \quad \text{(III.3)}$$

$$(\tfrac{1}{16})[M\omega^2_6-M\omega^2_7]-(\tfrac{1}{24})[M\omega^2_{13}-M\omega^2_{14})\pm(M\omega^2_{15}-M\omega^2_{16})] = \upsilon'-2\delta' \quad \text{(III.4)}$$

In the above identities, the upper sign corresponds to LX = LO, and the lower to LX = LA.

$$(\tfrac{1}{32})[2M\omega^2_8-M\omega^2_1] = \mu+2\mu'''' \quad \text{(III.5)}$$

$$(\tfrac{1}{32})[2M\omega^2_6+2M\omega^2_7-2M\omega^2_8-M\omega^2_1] = \lambda+2\lambda'''' \quad \text{(III.6)}$$

$$(\tfrac{1}{24})[M\omega^2_{15}+M\omega^2_{16}-M\omega^2_{13}-M\omega^2_{14}] = \upsilon-2\upsilon'''' \quad \text{(III.7)}$$

$$(\tfrac{1}{24})[M\omega^2_{15}+M\omega^2_{16}+2M\omega^2_{13}+2M\omega^2_{14}]$$
$$-(\tfrac{1}{32})[M\omega^2_1+2M\omega^2_6+2M\omega^2_7+2M\omega^2_8] = 2\mu''+\lambda''-4\mu''''-2\lambda'''' \quad \text{(III.8)}$$

$$\alpha+2\mu'''+\lambda''' = \begin{Bmatrix}+4\cdot797\\ +5\cdot319\end{Bmatrix} \pm 0\cdot282$$

$$\beta+\upsilon'''-2\delta''' = \begin{Bmatrix}+3\cdot431\\ +2\cdot909\end{Bmatrix} \pm 0\cdot214$$

$$\mu+2\mu'''' = +0\cdot212 \pm 0\cdot183$$

$$\upsilon-2\upsilon'''' = +0\cdot436 \pm 0\cdot154$$

$$\lambda+2\lambda'''' = -0\cdot418 \pm 0\cdot236$$

$$2\mu'+\lambda' = \begin{Bmatrix}+0\cdot023\\ -0\cdot499\end{Bmatrix} \pm 0\cdot282$$

$$\upsilon'-2\delta' = \begin{Bmatrix}+0\cdot261\\ +0\cdot783\end{Bmatrix} \pm 0\cdot214$$

$$2\mu''+\lambda''-4\mu''''-2\lambda'''' = +0\cdot036 \pm 0\cdot331$$

where all quantities have been expressed in units of $10^4$ dyn cm$^{-1}$, and where the upper and lower numbers correspond to LX = LO and LX = LA, respectively. (Note that the choice LX = LO favors smaller 3° neighbor parameters.) The various solutions given in Table 4 are consistent with these results.

If it is assumed that the 1° parameters are much larger than the 5° ones, and that the 2° parameters are much larger than the 6° ones, then the first five results give approximate values for the 1° and 2° parameters, and the associated probable errors. While the 1° parameters are determined with moderate precision by these simple considerations, the 2° parameters are determined with marginal precision, and the 3° through 6° parameters are not determined at all. In any event, the above results give a general picture of the expected nature of the force model.

*J. Phys. Chem. Solids* Pergamon Press 1959. Vol. 8. pp. 419–422. Printed in Great Britain

# 0.7 THE VIBRATION SPECTRA OF DISORDERED LATTICES

C. DOMB, A. A. MARADUDIN, E. W. MONTROLL and G. H. WEISS

University of Maryland, College Park, Maryland

VOL. 8 1959

ONE of the fundamental problems in the investigation of the properties of disordered crystals is the determination of the vibrational frequency spectrum. A formal solution has been given by DYSON[1] for the one-dimensional chain, but it has not proved amenable to detailed calculation in cases of physical interest. The one-dimensional problem has also been discussed by other authors,[2] but with the same negative results from the standpoint of constructing an actual frequency spectrum. For two- and three-dimensional models even less information is available.

However, the moments of the spectrum of the disordered lattice can be calculated using the moment-trace method,[3] and these calculations can be substantially simplified using the theory of random walks on lattices. In one dimension a combinatorial expression can be derived for the $2n$th moment.

We have considered in detail the problem of a disordered chain consisting of a random mixture of atoms of two masses. In the limit when one of the two masses becomes infinite an exact spectrum can be calculated. Although it has peculiar analytic properties (it consists of delta-functions at a set of points in one-to-one correspondence with the rational numbers in the interval (0, 1)), it provides considerable insight into the behavior of the spectrum as one of the masses becomes large. Also, the asymptotic behavior of the moments of a chain with finite unequal masses follows closely that of a chain with the masses of one of the isotopic constituents infinite.

We have been able to draw the following conclusions rigorously. (1) The maximum frequency of a disordered chain is the maximum frequency of an ordered chain of light atoms. (2) The singularity at the upper end of the spectrum disappears when the chain becomes disordered, the corresponding spectrum tending to zero. (3) At low frequencies to a good approximation the spectrum corresponds to an ordered chain of mean mass.

By evaluating the even moments of the spectrum up to 20 on the IBM 704 computer at the U.S. National Bureau of Standards we have calculated approximations to the spectrum for varying concentrations and mass ratios of the two constituents.

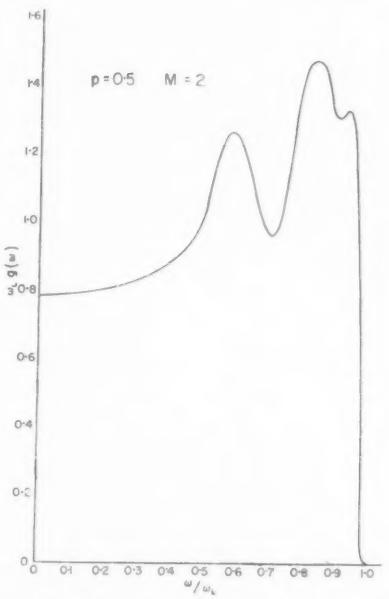


FIG. 1. Approximate spectrum for $M_1/M_2 = 2$ and $p = 0{\cdot}5$.

We have obtained our results by the use of Legendre polynomial expansions, by a new method which uses polynomial approximations to the delta function, and by a perturbation method which is accurate at the low frequency end of the spectrum.[4]

We found it necessary to do our calculations in double precision (i.e., keeping twenty decimal places), since in the Legendre polynomial calculations many of the terms arise as small differences of large numbers, thus necessitating increased accuracy.

Fig. 1 shows the spectrum which corresponds to a chain with $M_1 = 2M_2$ and $p$, the fraction of light masses, equal to $\frac{1}{2}$; major peaks in the spectrum appear consistently in the last three approximations and we feel confident that they are not spurious. Also there are strong indications (by comparison with the corresponding approximations in the ordered case) that they do not represent infinite peaks.

Fig. 2 has been derived for $M_1 = 3M_2$ and

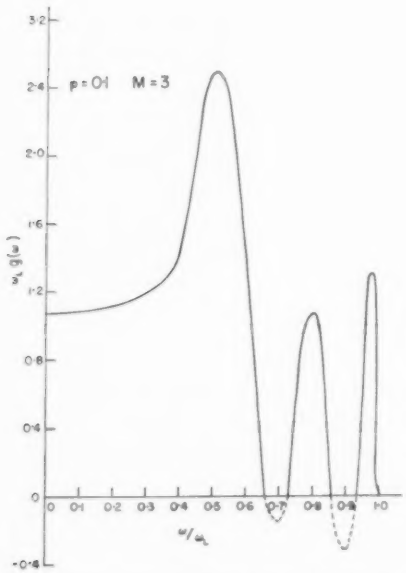


FIG. 2. Approximate spectrum for $M_1/M_2 = 3$ and $p = 0{\cdot}1$.

$p = 0{\cdot}1$. This represents a spectrum of a homogeneous lattice with a small impurity concentration. There are clear indications of two impurity bands emerging from the main spectrum.

In Fig. 3 we have plotted the zero point energy per particle for the ordered (ABAB....) lattice, for the random lattice, and for the separated phases (AAA...BBB...) as a function of the mass ratio for $p = \frac{1}{2}$. We see that in all cases the ordered lattice has the highest zero point energy, while

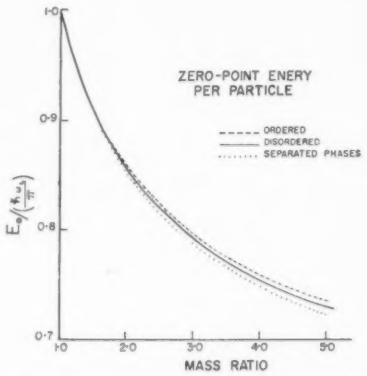


FIG. 3. Zero-point energy for different chain configurations.

the separated phases have the lowest. These results are in agreement with the results of previous investigations.[5]

Finally Fig. 4 has been drawn to illustrate

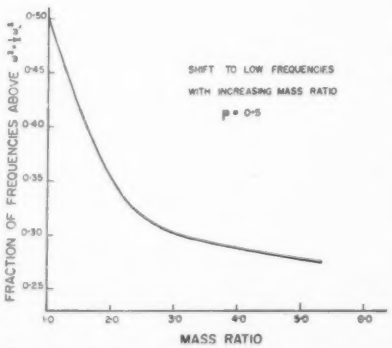


FIG. 4. Fraction of frequencies above $\omega_L^2/2$.

Rayleigh's theorem[6] that the increase of any mass of a vibrating system decreases the normal mode frequencies. We have plotted the fraction of normal modes of a disordered chain whose frequencies satisfy $\omega^2 \geq \frac{1}{2}\omega^2_L$ (where $\omega_L$ is the

maximum frequency of a homogeneous chain of light masses) as a function of the mass ratio $M_1/M_2$. This fraction equals $\frac{1}{2}$ for the homogeneous chain, but decreases rapidly for $M_1/M_2 > 1$ until it approaches the value for $M_1/M_2 = \infty$.

Further deails and results will be presented in a forthcoming paper. The methods can also be applied to higher dimensional models and corresponding work is in progress.

*Acknowledgment*—We would like to thank Mr. ANDREAS SCHOPF of the National Bureau of Standards for his expert programming assistance.

VOL. 8 1959

## REFERENCES

1. DYSON F. J., *Phys. Rev.* **92,** 1331 (1953).
2. LIFSCHITZ I. M. and STEPANOVA G. I., *Zh. eksp. teor. fiz.* **3,** 656 (1956). SCHMIDT H., *Phys. Rev.* **105,** 425 (1957). KERNER E. H., *Proc. Phys. Soc.* A**69,** 234 (1956). HORI J. and ASAHI T., *Progr. Theor. Phys.* **17,** 523 (1957). HORI J., *Progr. Theor. Phys.* **18,** 367 (1957).
3. MONTROLL E., *J. Chem. Phys.* **10,** 218 (1942).
4. WEISS G. H. and MARADUDIN A. A., *J. Chem. Phys. Solids,* to be published.
5. PRIGOGINE I., BINGEN R. and JEENER J., *Physica* **20,** 383, 516 (1954).
6. LORD RAYLEIGH, *The Theory of Sound.* Reprint by Dover Publications (1945).

# DISCUSSION

*Compiled by* M. LAX

### O.1 R. J. ELLIOTT and R. LONDON

E. BURSTEIN (University of Pennsylvania): Have you considered the effect on the absorption selection rules of the $m_j$ character of the levels. The selection rules $\Delta l = 0$, $\Delta l = \pm 1$ would then no longer be adequate, and additional peaks might occur?

R. J. ELLIOTT (Clarendon Laboratory): I have not taken into account spin-orbit coupling, although this would certainly be possible.

### O.2 G. G. MACFARLANE *et al.*

G. H. WANNIER (Bell Telephone Laboratories): Why is the indirect exciton absorption spread out, and not a line?

G. G. MACFARLANE (Radio Research Establishment): Because the transition is to a continuum. Phonons permit the excitons to have all propagation constants.

W. P. DUMKE (International Business Machines): Have you seen indirect transitions induced by impurities rather than phonons?

G. G. MACFARLANE: No.

M. LAX (Bell Telephone Laboratories): (added later) One of Haynes' weak lines might have this interpretation.

H. J. G. MEYER (Philips Research Laboratories): Have you examined the intensity of exciton absorption lines to see if such an extrapolation of deformation potential theory to phonons of large propagation constant is anywhere near correct?
(MACFARLANE defers to ELLIOTT).

R. J. ELLIOTT (Clarendon Laboratory): No, but it could certainly be done.

A. MOORE (R.C.A.): Have you examined the lifetime of the direct transition exciton?

G. G. MACFARLANE (Radio Research Establishment): No.

B. LAX (Lincoln Laboratory, MIT): You originally quoted an exciton binding energy of ·005 eV. Now you quote one in the vicinity of ·0025 eV. What accounts for the change?

G. G. MACFARLANE (Radio Research Establishment): The first was just a crude estimate that neglected fine structure at 4° and at 90°. It was based on a mixing of $(\Delta E)^{\frac{1}{2}}$ and $(\Delta E)^2$. We know, now, from Elliott, that in the presence of Coulomb forces $(\Delta E)^2$ should be replaced by $(\Delta E)^{\frac{3}{2}}$.

### O.3 J. R. HAYNES *et al.*

P. AIGRAIN (Ecole Normale Superieure): We have evidence from extrinsic radiation that supports your (Haynes') picture of phonon assisted recombination. Extrinsic radiation to an impurity center can occur with and without a phonon. The difference supplies a phonon energy that agrees with the strong one of HAYNES.

J. R. HAYNES (Bell Telephone Laboratories): Fine.

### O.4 S. ZWERDLING *et al.*

G. C. DOUSMANIS (RCA Laboratories): How did you compute your reduced mass in the presence of light and heavy holes, and an anisotropic electron mass?

S. ZWERDLING (Lincoln Laboratory, MIT): The reduced mass is always heavily weighted by the light masses involved—the light mass hole, and the light mass directions of the heavy hole.

### O.5 B. N. BROCKHOUSE

H. BROOKS (Harvard): If you interpret the two larger HAYNES phonons in silicon as two-phonon processes, where are the other two phonons that should show up in the HAYNES experiment?

B. N. BROCKHOUSE (Atomic Energy of Canada Limited): I am not an expert on group theory, but it is possible that some lines are forbidden by symmetry selection rules.

### O.6 F. HERMAN

M. LAX (Bell Telephone Laboratories): I want to thank FRANK HERMAN for so ably presenting my idea

that the long range focus (proven by HERMAN to be necessary to explain the Brockhouse spectrum) could be supplied by quadrupole–quadrupole interactions. The $Q$–$Q$ force constants decrease as $1/R^5$, and might seem to be short range, but the number of atoms increases as $R^2$, so that a sum over shells up to $R$ goes as

$$\int_1^R (1/R^3)dR \propto 1-1/R^2.$$

Thus one per cent accuracy requires the use of shells out to $R = 10$ times the first shell distance, perhaps forty shells.

One may visualize my quadrupoles as dipole moments induced on an atom and its neighbors by displacing an atom. The total moment so induced is zero, and we have an extended quadrupole consisting of dipoles at the corners and center of a tetrahedron.

My present preliminary calculations neglects this extended nature, which makes an error only at small distances, that can be allowed for by modifying the other near neighbor force constants.

I have made a preliminary calculation by hand of the three elastic constants, and the Raman frequency, and of the four frequencies at the [1, 1, 1] zone boundary. Three parameters (two first neighbor, and the one quadrupole) were adjusted to fit the Raman frequency, $c_{11}$ and $c_{12}$, and the remaining five values were computed and compared with the experiment. The worst error, in one case, was 20 per cent. The others were 10 per cent or better. The ratio $\omega_{LA}/\omega_{TA}$ was found to be 2·9 as compared with an experimental value of 3·4. This is a big improvement over calculations involving only a small number of neighbors, for which it is hard to get a ratio larger than 2. Of course, our results depend on a long series of hard computations, and until they are checked by machine calculation, regard them as highly tentative.

H. BROOKS (Harvard): The dispersion in the TA mode as reflected in the initial departure from the phase velocity is a sensitive function of the range of the forces. Can you conclude anything from this about the suitability of $1/R^5$ forces?

M. LAX (Bell Telephone Laboratories): I have not done so, but it could be done by the Fourier transform argument of FOREMAN and LOMER.

A more critical test, in my opinion, of the $Q$–$Q$ interaction will be whether the angular dependence of the fourth order cubic harmonics in $Q$–$Q$ will reproduce the marked angular dependence shown by the TA mode.

(*See page* 396)

*Note added in proof*—Recent neutron scattering measurements (personal communications from B. N. BROCKHOUSE and also D. J. HUGHES) show that some of our assignments of phonon energies involved in recombination radiation from silicon are incorrect. We made the simplest assignment for the four-phonon energies observed (see Table 1). It now appears that, as predicted by BROCKHOUSE,[3] our two highest phonon energies are probably due to multiple phonon processes and also that the phonon energy labeled acoustic longitudinal may be one of the optical phonons. The germanium assignments remain correct.

*J. Phys. Chem. Solids* Pergamon Press 1959. Vol. 8. pp. 423–428. Printed in Great Britain

SESSION P:
SEMICONDUCTING COMPOUNDS*

# P.1 RECENT ADVANCES IN THE OPTICAL AND ELECTRONIC PROPERTIES OF PbS, PbSe, PbTe AND THEIR ALLOYS

W. W. SCANLON
United States Naval Ordnance Laboratory, White Oak, Maryland

**Abstract**—The optical and electrical properties of PbS, PbSe, and PbTe are reviewed as they contribute to the understanding of the electronic band structure in these compounds. The optical absorption data generally favors a model in which the maximum of the valence band and the minimum of the conduction band occur at about the same value of the wave vector, **k**. Magnetoresistance data for these crystals are similar for *n*- and *p*-type crystals and the longitudinal magnetoresistance is generally larger (in some cases four or five times larger) than the transverse magnetoresistance at 77° and 4·2°K. The magnetoresistance data suggest that both band edges have the same structure and that constant energy surfaces are ellipsoids of revolution about the ⟨111⟩ direction with centers away from $k = 0$. A ratio of longitudinal to transverse effective mass of from 4–6 is thought to be most appropriate for PbTe.

## 1. INTRODUCTION

THE structures of the conduction and valence bands are of considerable importance in understanding many of the properties of a semiconductor. In germanium and silicon where the method of cyclotron resonance absorption has been used, the band structures are known in considerable detail. In the lead salts, on the other hand, cyclotron resonance experiments have not proven successful as yet. The failure appears to be due to the high carrier concentration as well as the relatively large effective masses in these substances which lead to the condition $\hbar\omega > kT$ only for temperatures less than about 1°K for moderate magnetic fields. Hence it is necessary to deduce the nature of the bands from other kinds of experiments. In this paper we shall describe some of the most recent advances in this subject on the lead salt semiconductors. The experimental results will be based upon two kinds of studies: optical absorption and magnetoresistance.

## 2. OPTICAL ABSORPTION IN THE PURE COMPOUNDS

The fundamental optical absorption near the long wavelength edge of a material can be interpreted as due to electron transitions between the conduction and valence bands. These optically induced transitions are subject to certain selection rules and under some conditions transitions from the top level of the valence band to the bottom level of the conduction band may be forbidden.

An electron may make a direct transition from the conduction band to the valence band provided that the wave number vectors for the initial and final states are the same. This selection rule corresponds to the conservation of momentum. Under this condition it has been shown by several authors[1] that absorption coefficients are generally large, of the order $10^4$ cm$^{-1}$, and that the absorption coefficient is proportional to $(h\nu - h\nu_t)^{\frac{1}{2}}$ where $\nu$ is the photon frequency and $\nu_t$ is the threshold frequency. From the dependence of the optical absorption on photon energy one may evaluate the minimum vertical separation between the valence and conduction band edges.

Violations of this selection rule may occur in cases where the crystal lattice becomes involved in the excitation process. Conservation of momentum expressions may under these conditions include the momentum of lattice phonons. Transitions of this type are called indirect. The analysis of the absorption process by indirect transitions is not so well understood, but current theories suggest that the absorption is relatively low and is a quadratic or

* *Chairman:* H. WELKER; *Co-Chairman:* P. H. KECK.

cubic function of the photon energy. From the variation of absorption with photon energy it is possible to estimate the minimum energy for indirect optical transitions between the band edges.

One might expect the three compounds, PbS, PbSe and PbTe to be related in band structure. However, the fact that PbSe is out of step in the series by having the smallest energy gap suggests the possibility of crossing of energy bands as one goes from one compound to another. A situation like this is known to occur for germanium and silicon. Some insight into this behavior might be gained by studying the optical absorption in alloys of the lead compounds. These materials are isomorphic so that it is a relatively easy matter to grow crystals of solid solutions of the compounds in all proportions.

Absorption edges in the lead salts have been studied in the past by a number of observers.[2] However, because of the wide range of absorption coefficients, $\alpha$, covered by an edge, from 1 to $10^6$ $cm^{-1}$, two different experimental methods were used to encompass the whole edge. One method, used for the low absorption range was based upon transmission measurements and the other, for the high absorption range, was based upon reflection measurements. Unfortunately, the data did not fit together in the overlap region of wavelengths.

Recent advances in techniques have made possible the measurement of the absorption coefficient throughout the absorption edge by transmission measurements.[3] Because of the ease with which crystals of the lead salts split along {100} planes it is difficult to prepare thin specimens of large enough area for optical transmission measurements as was done with germanium and silicon. However, by means of a microscope technique it was possible to make transmission studies on crystal areas as small as $600 \times 50\,\mu$. The resolution in these measurements was satisfactory, ranging from $0{\cdot}4\,\mu$ at a wave length of about $4\,\mu$ to $0{\cdot}06\,\mu$ at $2{\cdot}5\,\mu$. Crystal thickness used ranged from 1 mm down to a few microns. On the thinner ones interference patterns were used to evaluate the thickness while the thickest ones could be measured by conventional methods.

The absorption edges for the pure compounds PbS, PbSe and PbTe are shown in Fig. 1.[4] The three curves are of a similar nature and indicate the onset of direct transitions at about 3000 $cm^{-1}$. This absorption data was analyzed in terms of the different dependences upon photon energy of direct and indirect transitions. A plot of $\alpha^2$ vs. $E$ gave the curves shown in Fig. 2 which are linear above values of $\alpha$ of about 3000 $cm^{-1}$. This was interpreted as evidence of direct transitions and from the zero intercept on the energy axis the threshold energy was obtained. It is clear from these results that there is no evidence of the much larger values once predicted[5] for direct transitions in these compounds.

If the absorption coefficient is plotted as $\alpha^{\frac{1}{2}}$ against $E$ as shown in Fig. 3, an approximately linear portion of the curve seems to exist below values of $\alpha$ of about 3000 $cm^{-1}$ which might be interpreted as evidence of indirect transitions. The threshold energy was obtained from the intercept on the energy axis.

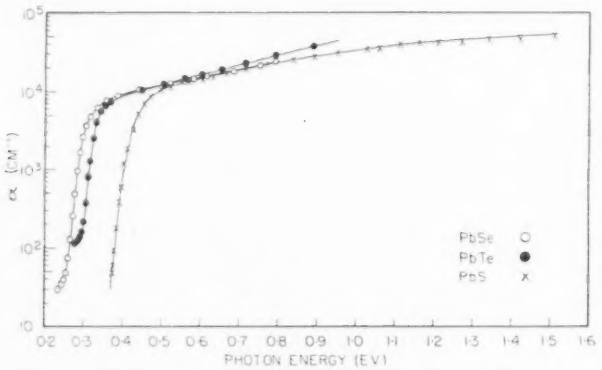


FIG. 1. The optical absorption coefficient for PbS, PbSe and PbTe as a function of photon energy.

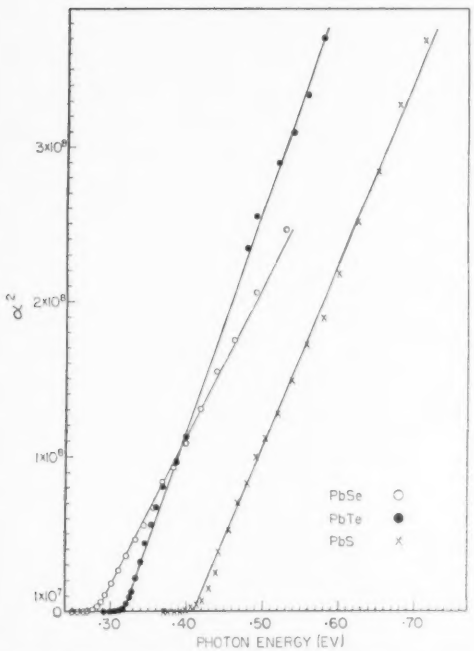


FIG. 2. The absorption coefficient squared as a function of photon energy for direct transitions in PbS, PbSe and PbTe.

The threshold energy results are summarized in Table 1. It will be noted that the energies for direct and indirect transitions are very close together in the lead salts, unlike Ge and Si.

*Table* 1. *Energy gaps obtained from absorption edge*

| Material | Energy gap at 300°K (eV) | |
|---|---|---|
| | Direct | Indirect |
| PbS | 0·41 | 0·37 |
| PbSe | 0·29 | 0·26 |
| PbTe | 0·32 | 0·29 |

Published values for the Debye temperature for these compounds range from 150 to 200°K.[8] Thus transitions involving lattice phonons could account for the observed small differences between direct and indirect transitions, and it would not be necessary to assume a minimum in the conduction band away from the maximum in the valence band.

### 3. OPTICAL ABSORPTION IN THE ALLOYS

Due to the isomorphism of the three compounds, PbS, PbSe and PbTe, the common cation and nearness of anion sizes, one may expect alloys of the compounds to exist in all proportions. This has been established experimentally at a number of laboratories. We have made single crystals of a number of alloys of PbS + PbSe and PbSe + PbTe by applying the techniques used in growing single crystals of the pure compounds.[4] These alloys ranged in composition from a few per cent to 50 at. per cent. The cleavage properties and general appearance of the alloy crystals are similar to those of the pure compounds.

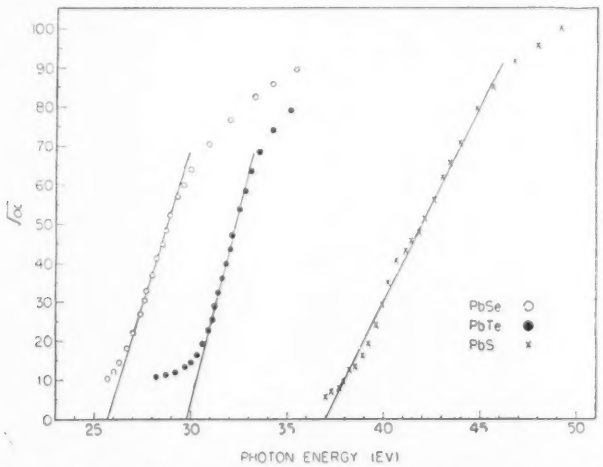


FIG. 3. The square root of the absorption coefficient as a function of photon energy for indirect transitions in PbS, PbSe and PbTe.

The optical absorption edge was measured for each of the alloys in the same way as for the pure compounds. The shapes of the curves for the alloys were the same as for the compounds except that there was a shift in the position of the absorption edge. The values for the direct and indirect transition energies for each alloy were obtained and the results are summarized in Fig. 4. Here we see that

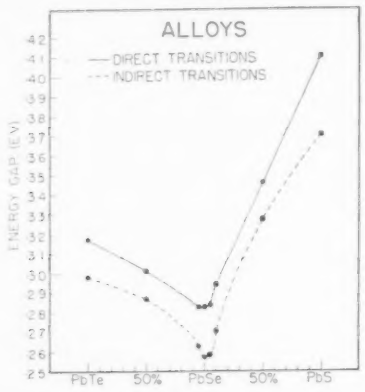


FIG. 4. Direct and indirect threshold energies for alloys of PbTe + PbSe and PbSe + PbS.

the energy gaps change approximately linearly with alloy composition with the minimum transition energies occurring in PbSe. There appears to be no remarkable difference between the absorption edges in the alloys and in the compounds. On the basis of these studies there is no evidence of crossing of energy bands in the lead salts for the composition range investigated.

Additional information on the band structure may be obtained from studies of the magnetoresistance. The magnitude of the magnetoresistance depends on the directions of the sample current and magnetic field relative to each other and to the direction of the symmetry axes of the sample.

Small field theory predicts that

$$\frac{\Delta\rho}{\rho_0} = M_{\text{abc}}^{\text{def}} \frac{\mu_H{}^2 H^2}{C^2}$$

where $\Delta\rho/\rho_0$ is the fractional change in the zero field resistivity, $M$ is the magnetoresistance coefficient, abc and def specify the current and magnetic field directions respectively, $\mu_H$ is the Hall mobility of the current carriers and $H$ is the magnetic field. In e.m.u., gaussian and practical units, the constant $C$ has the values 1, $3 \times 10^{10}$ cm/sec and $10^8$ cm$^2$ G/V-sec respectively. Small fields imply that $\mu_H H/C \ll 1$.

For the case of spherical energy surfaces with origin at $k = 0$ and in the lattice scattering range $M_{\text{abc}}^{\text{def}} = 0{\cdot}27 \sin^2\theta$ for non-degenerate samples, where $\theta$ is the angle between the current and magnetic field. For the case of complete degeneracy and if $\tau = \tau(E)$, $M_{\text{abc}}^{\text{def}} = 0$.

For the case of a cubically symmetric model in which the constant energy surfaces are ellipsoids of revolution along the $\langle 100 \rangle$ direction in $k$ space, the coefficient $M_{100}$ is zero for all values of the shape parameter $K$. The parameter $K$ is the ratio of longitudinal to transverse effective mass which characterizes the ellipsoid. On the other hand if the ellipsoids are oriented along the $\langle 110 \rangle$ or $\langle 111 \rangle$ directions they may be distinguished by the value of the ratio $M_{100}/M_{100}^{001}$. This ratio is plotted in Fig. 5 as

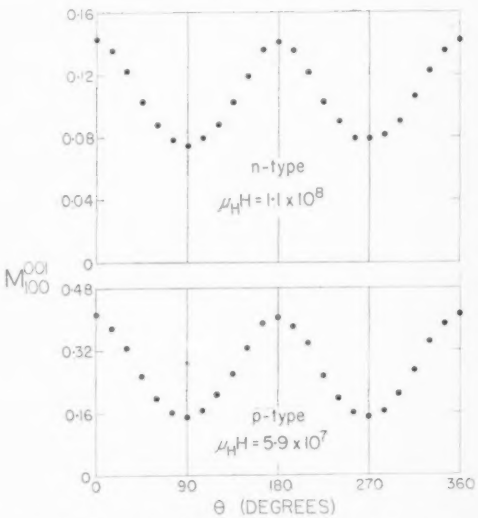


FIG. 5. Ratio of $M_{100}/M_{100}^{001}$ as a function of the effective mass ratio, $K$.

a function of $K$ for the $\langle 110 \rangle$ and $\langle 111 \rangle$ cubic models for both classical statistics and degenerate statistics.[7] Note that the highest ratio for the $\langle 110 \rangle$ model is 2 while for the $\langle 111 \rangle$ model it is 4.

In a recent paper ALLGAIER[8] reported magnetoresistance data obtained on the lead salts at 77·4° and 4·2°K. The samples generally contained about $10^{18}$ carriers per cm$^3$; consequently, classical statistics were a rather poor approximation at

77·4°K, and all the samples were highly degenerate at the lower temperature. The measurements were made only on cleaved crystals which restricted the direction of current flow to a [100] axis.

ALLGAIER found that the longitudinal coefficient $M_{100}$ was generally as large or larger than the transverse coefficient $M_{100}^{001}$ for both *n*- and *p*-type material in all three lead salts. Fig. 6 exhibits

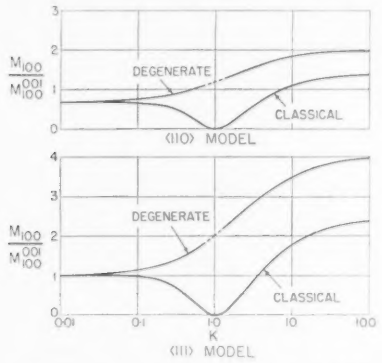


FIG. 6. Magnetoresistance coefficient as a function of angle between current and magnetic field for *n*- and *p*-type PbTe at 77·4°K.

typical data obtained on PbTe samples at 77·4°K, and illustrates the similarity between the results for *n*- and *p*-type material. These results suggested that the conduction and valence bands in the lead salts may be similar, a situation which is in sharp contrast to that suggested by magnetoresistance data in germanium[9] and silicon.[10]

The relatively large longitudinal magnetoresistance which ALLGAIER found for all samples immediately eliminates the simple band model and also the ⟨100⟩ cubic model as being appropriate for these compounds.

ALLGAIER's experimental data for PbS were not precise nor extensive enough to choose between the ⟨110⟩ and the ⟨111⟩ models. The ratios of $M_{100}/M_{100}^{001}$ for PbSe were mostly between 1 and 2 so that either model with prolate ellipsoids ($K > 1$) could be satisfied by the data. Four of the five PbTe samples he studied had ratios between 2 and 5, and thus the ⟨111⟩ model seems more appropriate for PbTe. This agreed with the conclusions of SHOGENJI and UCHIYAMA.[11]

ALLGAIER[8] pointed out that small field theory was not applicable to most of his results, especially those at 4·2°K, where the high sample mobilities led to values of $\mu_H H/C$ between 1 and 20. He used calculations of GOLD and ROTH,[12] valid for any value of $\mu_H H$, and the saturation coefficients (i.e. as $H \to \infty$) calculated by SHIBUYA[13] and by GOLD and ROTH[14] to show that outside the small field region, the ratio $M^{100}/M_{100}^{001}$ should increase for the ⟨111⟩ model and decrease for the ⟨110⟩ model. Thus his high experimental values of this ratio strengthen the choice of the ⟨111⟩ model for PbTe; for this material, he concluded that a value of $K$ between about 4 and 6 was appropriate.

## 4. CONCLUSIONS

On the basis of experimental studies of the optical absorption edge and magnetoresistance in the lead compound semiconductors, we now have information on some of the characteristics of the energy band edges. The optical studies show a great similarity between the three compounds and their alloys as far as the shape of the band edge is concerned. The small difference between the direct and the indirect transition energies suggests that the maximum of the valence band and the minimum of the conduction band occur at about the same value of the wave vector, **k**. The magnetoresistance data suggest that the band edges in both the conduction band and valence band are similar and that they lie along ⟨111⟩ directions with the centers not near $k = 0$. This is consistent with the optical data.

Released by the Commander, U.S. Naval Ordnance Laboratory, Silver Spring, Maryland.

GORDON W. HIRTLE, JR.
*Technical Information Officer*

*Acknowledgment*—The author gratefully acknowledges the help given him by Dr. R. S. ALLGAIER in the preparation of this manuscript and R. RIEDL for his help in making the optical measurements.

## REFERENCES

1. BARDEEN J., BLATT F. and HALL L. *Photoconductivity Conference*, edited by Breckenridge, Russell and Hahn, p. 146. John Wiley, New York (1956).
   DEXTER D. *Ibid.* p. 155.
   FAN H. Y., SHEPPARD and SPITZER. *Ibid.* p. 184; FAN H. Y. *Rep. Progr. Phys.* **19,** 107 (1956).
2. PAUL, JONES and JONES. *Proc. Phys. Soc.* B**64,** 528 (1951).
   GIBSON A. F. *Proc. Phys. Soc.* B**65,** 378 (1952).
   AVERY D. G. *Proc. Phys. Soc.* B**67,** 2 (1954).
3. SCANLON W. W. *Phys. Rev.* **109,** 47 (1958).
4. SCANLON W. W. and RIEDL H. R. unpublished.
5. BELL, HUM, PINCHERLE, SCIAMA and WOODWARD. *Proc. Roy. Soc.* A**217,** 71 (1953).

6. PARKINSON D. H. and QUARRINGTON, J. E. *Proc. Phys. Soc.* B67, 644 (1954).
7. The approximation of completely degenerate statistics becomes inadequate for the specimens considered in the dotted portion of the curve. See reference 8.
8. ALLGAIER R. S. *Phys. Rev.* to be published.
9. PEARSON G. L. and SUHL H. *Phys. Rev.* **83,** 768 (1951).
10. PEARSON G. L. and HERRING C. *Physica* **20,** 975 (1954).
11. SHOGENJI K. and UCHIYAMA S. *J. Phys. Soc. Japan* **12,** 1164 (1957).
12. GOLD L. and ROTH L. M. *Phys. Rev.* **107,** 358 (1957).
13. SHIBUYA M. *Phys. Rev.* **95,** 1385 (1954).
14. GOLD L. and ROTH L. M. *Phys. Rev.* **103,** 61 (1956).

*J. Phys. Chem. Solids* Pergamon Press 1959. Vol. 8. p. 428. Printed in Great Britain

## P.2 THE ELECTRICAL PROPERTIES AND CRYSTAL STRUCTURE OF $IV_b$–$VI_b$ INTERMETALLIC-COMPOUNDS*

**TOSHIHIRO OKADA**
Kyusyu University, Hukuoka, Japan

SYSTEMATIC researches on the electrical resistivity and Hall constant and their relation to the crystal structure were made on the selenide and telluride of tin and germanium, especially on SnTe, GeTe and SnSe, in our laboratory. Specimens were prepared by means of artificial syntheses. SnSe and GeSe were proved to have the structure of the type SnS (B-29), and to be semiconductive in electrical conduction; whereas SnTe, whose lattice is rock-salt type, is semimetallic and has positive temperature coefficients for the resistivity as well as the Hall constant. From the analysis of the observed temperature dependencies of the resistivity and the Hall constant of SnTe, it may be concluded that in this crystal the conduction band possibly overlaps with the filled band as in the case of bismuth. GeTe is semimetallic in the resistivity, while the Hall constant is semiconductive in contrast with SnTe. These properties might also be explained by the above assumption of overlapping bands. The binary systems PbTe–SnTe and SnSe–SnTe were also investigated. The former system was continuous in electrical properties and in structure for change in its composition, while the latter system seemed to be discontinuous.

* Not presented at conference.

*J. Phys. Chem. Sclids* Pergamon Press 1959. Vol. 8. pp. 428–430. Printed in Great Britain

## P.3 GALVANOMAGNETIC EFFECTS IN BISMUTH TELLURIDE

**J. R. DRABBLE**
Research Laboratories of The General Electric Company Limited, Wembley, England

BISMUTH telluride belongs to the crystal class $R\bar{3}m$ in which the principal symmetry elements are a three-fold axis of rotation, a centre of inversion and three equivalent reflection planes containing the rotation axis. It possesses a well defined cleavage normal to the rotation axis. Defining the relevant

galvanomagnetic coefficients by the tensor relation between the electric field $E$, the current density $J$, and the magnetic induction $B$

$$E_i = \rho_{ij}J_j - \rho_{ijk}J_jB_k + \rho_{ijkl}J_jB_kB_l$$

then symmetry requirements limit the number of independent components to two for the resistivity tensor, two for the Hall tensor and to eight for the magnetoresistance tensor. These will be referred to a coordinate system on which $Ox_3$ is parallel to the rotation axis and the $(x_1\, x_3)$ plane is parallel to one of the reflection planes.

In principle, all twelve components can be measured using the three experimental arrangements shown in Fig. 1. In each arrangement the electric field can be measured in each of three mutually perpendicular directions and the magnetic field can be rotated about an axis normal to the current flow. Expressions for the electric field components as a function of the angle $\phi$ between the magnetic field and the current can be derived phenomenologically and used to check the experimental techniques. In performing the experiments at liquid nitrogen temperature, very good consistency in this respect was obtained for the Hall effects and for the longitudinal and transverse magnetoresistance effects involving measurement of the electric field parallel to the current. The remaining magnetoresistance measurements contained discrepancies, probably due to the small signals involved and mis-orientation effects. For $n$-type material, the third arrangement was not used owing to the lack of uniform specimens of a suitable length. In all, six coefficients out of a total of twelve were obtained accurately for $n$-type material in these experiments. A seventh coefficient ($\rho_{33}$) has been measured independently. For $p$-type material, the third arrangement was used and a total of nine coefficients was obtained. The value of the Hall coefficient $\rho_{312}$ can be obtained from both the first and third arrangements and good agreement was found between the two values.

The results for both $n$- and $p$-type material have been found to be consistent with a "many-valley" form of the corresponding band, in which the surfaces of constant energy are ellipsoids centred on the reflection planes. The number of valleys will be three if they are centred on the edge of the Brillouin zone and six otherwise. In the analysis, it was assumed that the relaxation time was a function of energy only. This assumption can be justified to a considerable extent on the basis of the observed thermoelectric power which is isotropic in $p$-type and nearly so in $n$-type material. The more extensive measurements on $p$-type material made it possible to extend the analysis to include measurements of the thermoelectric power and thus to obtain the absolute value of the effective mass tensor for a single valley, subject to the uncertainty of whether three or six valleys were involved. For $n$-type material, only the ratios of the principal effective masses have been derived. The results are summarized in Table 1. The angle $\theta$ is the angle through which the valley axes have to be rotated about the normal to the reflection plane to coincide with the crystal axes.

On the basis of the above analysis, galvanomagnetic coefficients contain anisotropy factors which are functions of the valley parameters. For the Hall coefficient associated with the magnetic field parallel to the rotation axis, these factors are about one third and one half for $n$- and $p$-type material respectively.

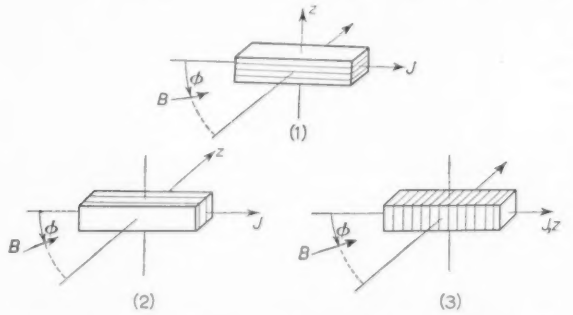


FIG. 1. Experimental arrangements. The rotation axis is indicated by Z.

*Table 1. Data on effective masses for bismuth telluride. $m_1$, $m_2$ and $m_3$ are the principal effective masses within a valley, and $m^*$ is the density of states effective mass*

| | *n*-type | *p*-type |
|---|---|---|
| $m_2$ | unknown | $0{\cdot}0505m_0$ |
| $m_1/m_2$ | 1·21 | 4·13 |
| $m_3/m_2$ | 0·093 | 7·64 |
| $\cos^2\theta$ | 0·055 | 0·305 |
| $m^*$ | unknown | $0{\cdot}51\ m_0$ |

The relations between the conductivity mobility and the Hall mobility are correspondingly affected. It has been found that the conductivity mobility for current flow in the cleavage planes at room temperature is about 1200 cm²/V-sec for electrons and about 500 for holes for specimens studied in this work.

A further point of interest in the work on *p*-type material was that the ratio of the resistivities for current flow perpendicular and parallel to the cleavage planes and the ratio of the two Hall coefficients were both practically independent of temperature over the range liquid nitrogen to room temperature, indicating that any changes in the form of the valence band are negligibly small over this range.

VOL
8
195

*J. Phys. Chem. Solids* Pergamon Press 1959. Vol. 8. pp. 430–433. Printed in Great Britain

P.4

# TRANSPORT PROPERTIES OF THE PSEUDO-BINARY ALLOY SYSTEM $Bi_2Te_{3-y}Se_y$

**N. FUSCHILLO, J. N. BIERLY and F. J. DONAHOE**
Franklin Institute, Philadelphia, Pa.

## 1. INTRODUCTION

THE alloy system $Bi_2Te_{3-y}Se_y$ has been the subject of a number of investigations[1–8] in recent years because of the possible application of these alloys in thermoelectric devices. This binary system, however, presents some interesting intermetallic and semiconductor situations which are of fundamental interest in the study of compound semiconductors. In this paper is presented a systematic study of the temperature variation of the electrical conductivity, $\sigma$, and the Seebeck coefficient, $S$, and the room temperature thermal conductivity, $K$, as selenium is substituted for tellurium in the molecular formula $Bi_2Te_{3-y}Se_y$ until $Bi_2Te_3$ is transformed into $Bi_2Se_3$. Our X-ray and metallographic examinations have uncovered no evidence of any phase transformations in this system and all available evidence points to the existence of a continuous solid solution range between $Bi_2Te_3$ and $Bi_2Se_3$. In particular the careful determinations of MCHUGH and TILLER[3] show that the distribution coefficient of bismuth is unity, so that $Bi_2Te_{3-y}Se_y$ is truly a pseudo-binary alloy system.

## 2. EXPERIMENTAL

The test specimens were prepared by encapsulating the semiconductor grade purity materials in evacuated Vycor tubes which were heated to above the melting point and shaken vigorously. The melt was frozen as rapidly as possible by plunging the Vycor tube containing the liquid alloy into water. The resulting ingots consisted of columnar crystals extending to the axis of the alloy rod. Since the *c*-axis of the hexagonal structure is perpendicular to the direction of most rapid growth the *c*-axis will be randomly orientated with respect to the longitudinal axis of the specimen. All of the transport properties were measured along the long axis of the specimen and therefore represent a value averaged over all possible orientations of the *c*-axis. The Seebeck coefficient and electrical conductivity respectively were measured by the standard d.c. and a.c.

(60 c/s) methods, in a vacuum cryostat operating between 77 and approximately 600°K.* The total thermal conductivities were measured by the method described by JOFFÉ.[7]

### 3. RESULTS AND DISCUSSIONS

Fig. 1 shows the temperature dependence of the specific electrical conductivity of ten specimens of different compositions. Seven of these specimens of composition $y = 0$ ($Bi_2Te_3$), $y = 1{\cdot}5$, $1{\cdot}8$, $2{\cdot}1$, $2{\cdot}4$, $2{\cdot}7$, and $3{\cdot}0$ ($Bi_2Se_3$) are clearly highly degenerate semiconductors over the whole temperature range studied. The natural temperature coefficient of resistivity is positive, and with the exception of $Bi_2Te_3$, is constant throughout the temperature range investigated. Moreover, both the temperature coefficient of resistivity and the magnitude of the conductivity decrease regularly with increasing tellurium starting from $Bi_2Se_3$ up to $y = 1{\cdot}5$. Specimens of these compositions are thus behaving like semimetals rather than semiconductors.

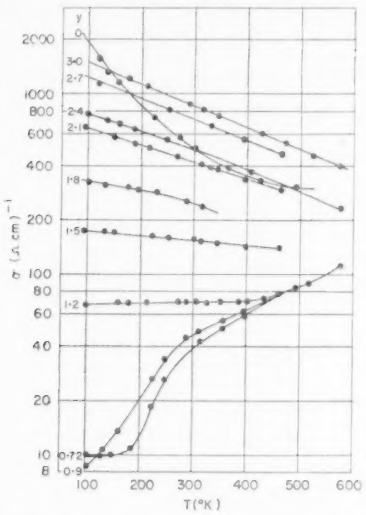


FIG. 1. Electrical conductivity of $Bi_2Te_{3-y}Se_y$ vs. temperature.

This behavior may be contrasted with the semiconductor behavior represented by the compositions $y = 0{\cdot}72$ (except below 200°K), $y = 0{\cdot}9$, $y = 1{\cdot}2$ (above 450°K). The energy gap deduced from the temperature dependence of electrical conductivity is of the order of 0·13 eV. This is smaller by a factor of the order of two from the optical band gap.[5] This factor is not difficult to explain if the maximum energy in the valence band and the minimum energy in the conduction band occur in different regions of $k$-space. It should be noted that the compositions having the largest optical band gap in this series of alloys are those which exhibit near intrinsic behavior around 300°K.

In Fig. 2 is shown the temperature variation of the Seebeck coefficient for the same series of alloys. The general features of these curves are in agreement with the conclusions drawn from the

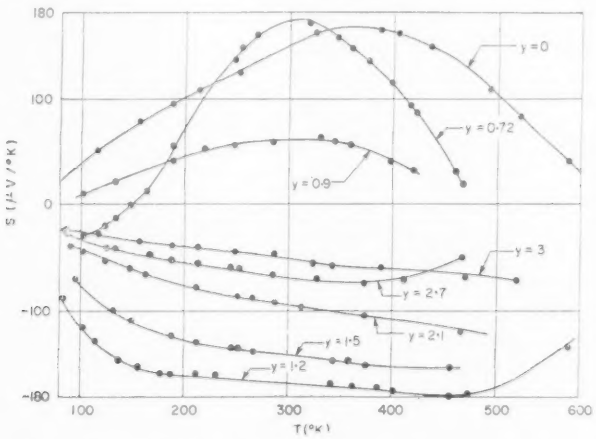


FIG. 2. Seebeck coefficient of $Bi_2Te_{3-y}Se_y$ vs. temperature.

* Seebeck coefficients are measured relative to copper. Of course this constitutes a negligible departure from the measurement of an absolute value except near regions where the Seebeck coefficient of the alloy is in the process of reversing sign and has a low value.

conductivity data of Fig. 1. For example, the Seebeck coefficient of $Bi_2Se_3$ ($y = 3$) increases in absolute magnitude with temperature in an almost linear fashion throughout the whole temperature range. The $Bi_2Te_3$ specimen ($y = 0$) has a Seebeck coefficient which, at low temperature, indicates strong degeneracy, but which in the neighborhood of 400°K is starting to bend back towards the $S$-equal-to-zero axis at about the same temperature at which the electrical conductivity appears to be approaching a minimum. On the other hand the variation of $S$ with temperature is greatest in the specimens ($y = 0{\cdot}72$, $0{\cdot}9$) which were judged to be near intrinsic at 300°K.

It is instructive to consider various isotherms of these results. Thus in Figs. 3 and 4 are shown the

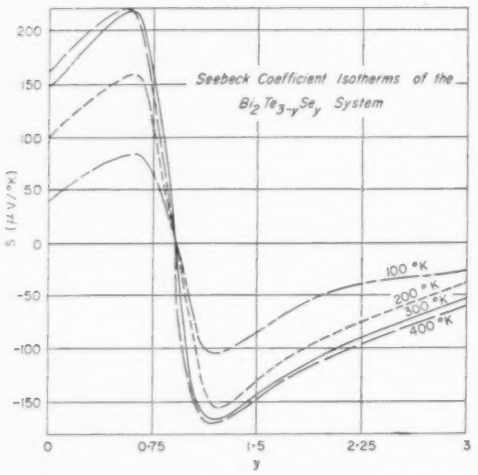


FIG. 3. Seebeck coefficient isotherms of the $Bi_2Te_{3-y}Se_y$ system.

isothermal variations of $S$ and $\sigma$ respectively at 100, 200, 300 and 400°K. These results indicate a rather unusual behavior at values of $y$ in the neighborhood of 0·9. There is a pronounced minimum in the electrical conductivity and the Seebeck coefficient reverses sign on passing through zero near this composition, although the former effect occurs at a slightly smaller value of $y$ than does the reversal in the Seebeck coefficient. In addition the room temperature Hall mobility is minimal at compositions in the neighborhood of $Bi_2Te_2Se$ ($y = 1$) and varies as $T^{-1}$, which is intermediate between the $T^{-3}$ dependence found for $Bi_2Te_3$ ($p$-type) and the $T^{-\frac{1}{2}}$

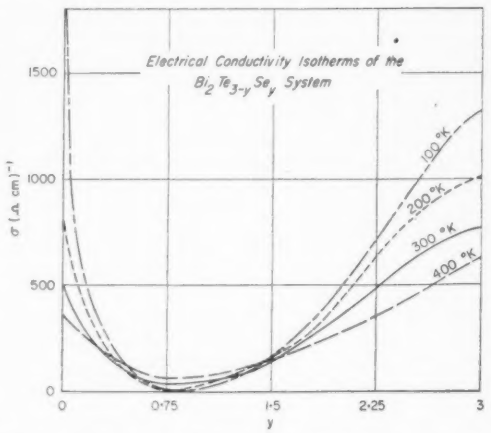


FIG. 4. Electrical conductivity isotherms of the $Bi_2Te_{3-y}Se_y$ system.

dependence found for $Bi_2Se_3$ ($n$-type).* The latter variation is characteristic of ionic lattice type scattering[8] above the Debye temperature. The $T^{-3}$ variation for $Bi_2Te_3$ has not been adequately explained.

An isothermal (300°K) representation of $S$ vs. $\log_{10}\sigma$ is shown in Fig. 5. The form of this curve

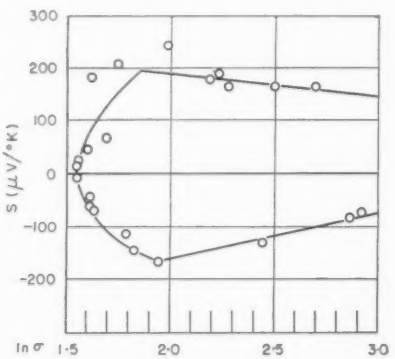


FIG. 5. Dependence of the Seebeck coefficient on electrical conductivity at $T = 300$°K.

has the shape predicted by PRICE.[9] The specimen points in the intrinsic region where the graph crosses the axis ($S = 0$) were from a series of alloys of $y$ very close to 0·9. While this figure may be considered interesting it is not worthwhile to apply the

* The Hall mobility of the other compositions is still under investigation.

analysis suggested by PRICE to the present series of alloys. To do so would involve the assumption that the effective masses and mobilities are unchanged in the $Bi_2Te_{3-y}Se_y$ system as $y$ ranges from 0 to 3.

A final isotherm is shown in Fig. 6, where the

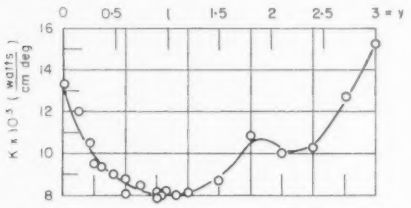


FIG. 6. The total thermal conductivity of the $Bi_2Te_{3-y}Se_y$ system at $T = 300°K$.

total thermal conductivity is plotted against $y$ for values at 300°K. The expected pronounced minimum is found in both the total and lattice (not plotted) thermal conductivity. This, however, occurs in the neighborhood of $y = 0{\cdot}9$. The secondary minimum behavior at $y = 2$ to 2·5 is as yet unexplained but is in agreement with the results of ROSI, ABELES and JENSEN.[6]

The anomalous behavior of the transport properties in the neighborhood $y = 0{\cdot}9$ is also accompanied by an optical band gap anomaly observed by AUSTIN and SHEARD.[5] The graph of band gap versus percentage of $Bi_2Se_3$ added to $Bi_2Te_3$ exhibits a linear variation from $y = 0$ to $y = 0{\cdot}9$. At $y = 0{\cdot}9$ a cusp-like maximum appears and the band gap decreases sharply at first and then more gradually to the value for $Bi_2Se_3$.

The full explanation of these phenomena has not yet been determined and awaits the detailed consideration of recent X-ray and Hall mobility data. However, some preliminary observations indicate that their explanation may lie largely in the structure and bonding scheme for alloys of this series.

Structurally this series of alloys belongs to the crystal class $\bar{3}m$ and is isomorphous with the naturally occurring mineral tetradymite ($Bi_2Te_2S$).[10] The atomic arrangement is a layered structure in which the layers repeat the unit

$$B_1\text{–}A\text{–}B_2\text{–}A\text{–}B_1 \cdot B_1\text{–}A\text{–}B_2\text{–}A\text{–}B_1,$$

where B represents a Group VI element and A a Group V element. DRABBLE and GOODMAN have proposed a bonding scheme which explains the band gap anomaly in the $Bi_2Te_{3-y}Se_y$ system.

This bonding scheme indicates that $B_2$ sites are energetically more favorable than are $B_1$ sites. Thus a Group VI element which is more electronegative than tellurium should preferentially occupy $B_2$ sites. At the nominal composition $Bi_2Te_2Se$ all the $B_2$ sites should be occupied by selenium and the remaining $B_1$ sites by tellurium. (Entropy considerations may well shift the best ordered composition to $y = 0{\cdot}9$.) The naturally occurring mineral tetradymite ($Bi_2Te_2S$) has this structure [10] with sulfur occupying $B_2$ sites. Although these structures are ordered, no superstructure lines should appear since the $B_2$ sites are crystallographically nonequivalent to the $B_1$ sites.

This model accounts for the variation in band gap but gives no clue to the reason why the alloy should be intrinsic at this composition when prepared from stoichiometric materials. It would be convenient if one could point to some feature in the liquidus–solidus curve of the pseudo-binary system which could be used to explain the reason for this behavior. Unfortunately the experimentally determined liquidus–solidus curve shows no anomaly at this composition.[3] For the present, it seems rather fortuitous that the critical point in the Seebeck coefficient of this pseudo-binary system should coincide with the energy gap maximum.

*Acknowledgments*—The authors are indebted to Mr. L. C. BENNETT for his assistance, to Messrs. J. R. WIESE and R. PYLE for alloy preparation and to the sponsors of the thermoelectric effects research program for their financial support.

## REFERENCES

1. SIANI S. S. and GORDYAKOVA G. N. *Zh. tekh. fiz.* **26,** 2398 (1956).
2. AIRAPETYANTS S. V., EFIMOVA B. A., STAVITSKAYA T. S., STILBANS L. S. and SYSOEVA L. M. *Zh. tekh. fiz.* **27,** 2167 (1957).
3. MCHUGH J. P. and TILLER W. A. *Westinghouse Scientific Paper No.* 431FD271-P1 (1958).
4. DRABBLE J. R. and GOODMAN C. H. L. *J. Phys. Chem. Solids.* **5,** 142 (1958).
5. AUSTIN I. G. and SHEARD, A. *J. Electronics* **3,** 236 (1957).
6. ROSI F. D., ABELES B. and JENSEN R. V. Private communication.
7. JOFFÉ, A. F. *Canad. J. Phys.* **34,** 1342 (1956).
8. KOLOMOETS N. V., STAVITSKAYA T. S. and STILBANS L. S. *Zh. tekh. fiz.* **27,** 73 (1957).
9. PRICE P. J. *Phys. Rev.* **104,** 1223 (1956).
10. HARKER D. *Z. Krïstallogr.* **89,** 175 (1934).

*J. Phys. Chem. Solids* Pergamon Press 1959. Vol. 8. pp. 434–437. Printed in Great Britain

P.5

# SEMICONDUCTORS OF THE TYPE $A^{III}B^{VI}$

P. FIELDING,* G. FISCHER and E. MOOSER†

## 1. INTRODUCTION

THE search for new semiconducting materials has led us to investigate the electrical and optical properties of compounds of the type $A^{III}B^{VI}$. These compounds are of some interest because of their odd number of valency electrons. Insofar as they contain nine valency electrons per anion, i.e. one more than the number usually found in semiconductors, they form the counterpart to the $A^{II}B^{V}$ compounds which contain only seven valency electrons per anion. The structure of the $A^{II}B^{V}$ phases (ZnSb, CdSb) indicates the formation in these materials of *anion pairs* and it was pointed out by MOOSER and PEARSON[1] that this pair formation compensates for the *electron deficiency* so that a complete filling of the valence band results.

In the $A^{III}B^{VI}$ compounds essentially two types of structures, and hence two mechanisms, for compensating the *electron excess* are observed:

(1) GaS, GaSe, GaTe, InS and InSe all crystallize in layer structures which are built up of fourfold layers of the type —BAAB—BAAB—. Within each of these multiple layers the atoms are covalently bonded such that each A atom (cation) is surrounded tetrahedrally by three B atoms (anions) and one A atom. The *cation pairs* which thus occur in these structures compensate for the *electron excess* and a typical semiconductor band structure results.

The bonding between neighbouring multiple layers is of the van der Waals type and the arrangement of the layers with respect to one another varies from compound to compound.

(2) InTe, TlS, and TlSe on the other hand crystallize in the B37 type of structure in which chains of composition $AB_2$ are formed. In these chains each A atom is surrounded tetrahedrally by four B atoms. The remaining A atoms are located between the chains. The chemical formulae of these compounds are, therefore, better written in the form $A^+(AB_2)^-$ from which it is readily recognized that half of the A atoms are univalent, the rest being trivalent. The occurrence in the heaviest In-compound and in the Tl-compounds of a structure containing half the cations in a univalent state is consistent with the tendency of the heavier Group IIIB elements to form stable univalent ions.

## 2. EXPERIMENTAL PROCEDURE

Samples of GaSe, GaTe, InSe, InTe, and TlSe were prepared by fusion of the components in evacuated and sealed quartz tubes. The sulfides have not so far been prepared. Research grade Tadanac brand indium, 99·999 per cent gallium from the United Mineral and Chemical Corp. and high purity thallium, selenium and tellurium as supplied by A. D. Mackay Inc. were used in preparing the samples. Except in the case of TlSe the ingots obtained by fusion of the components were subsequently zone melted in an evacuated and sealed quartz tube which normally was maintained at temperatures some 100 to 200°C below the melting point of the compound. Graphite coated quartz boats were used for zone melting to prevent the ingots from adhering to the boats. While large single crystals of InTe could be grown in this manner the zone melted samples of GaSe, GaTe and InSe were all polycrystalline. Nevertheless the size of the crystallites ($\sim 10\ mm^2$) was big enough to allow optical measurements to be carried out on single crystals. In preparing the samples for electrical measurements, care was taken to cut them from regions of the ingots in which the layers of the crystal lattice were nearly parallel to one another. In all electrical measurements the current was flowing parallel to the layers. For the Hall measurements the magnetic field was applied perpendicular to the layers.

For measurements at or below room temperature contacts were painted on the samples with silver paste. For higher temperatures indium dots were soldered to the specimen. The current and potential leads were pressed against these dots by springs.

Resistivity and Hall voltage were measured to an accuracy of about $\pm 10$ per cent with an a.c. bridge described by DAUPHINEE and MOOSER,[2] the error being mainly due to uncertainties in the geometry and inhomogeneities arising from the polycrystalline nature of the samples. The Hall measurements were all carried out in a magnetic field of 8000 oersteds.

* Division of Pure Chemistry, National Research Council, Ottawa, Canada.

† Division of Pure Physics, National Research Council, Ottawa, Canada.



VOL
8
195

The optical absorption curves reproduced in Fig. 1 were obtained by means of a Beckman spectrometer. These results were confirmed by measurements on a Cary spectrometer and a Hilger medium spectrograph. The samples were cleft from single crystals and their thicknesses measured with a dial gauge. The dial gauge measurements introduce an error of approximately $\pm 10$ per cent in the absolute values of the data in Fig. 1.

The photo response was measured with a Wheatstone bridge arrangement, the samples being placed in an evacuated cryostat. An Osram HBO–160 xenon arc lamp formed the light source and the beam was passed through a Beckman spectrometer. The incident energy was measured with a Kipp thermopile and the response corrected for equal energy.

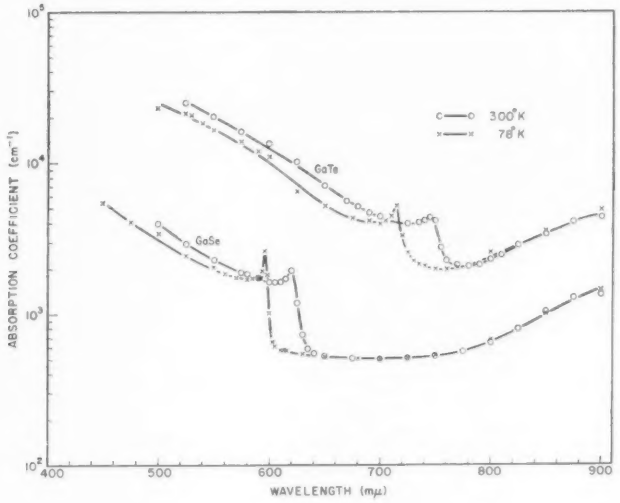


FIG. 1. Absorption coefficients of GaSe and GaTe.

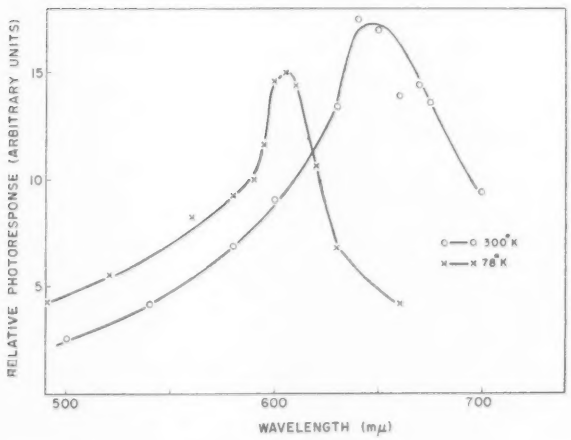


FIG. 2. Photo response of GaSe.

## 3. THE RESULTS

### 3.1 GaSe

Resistivity and Hall coefficients of GaSe were measured between 300°K and 500°K. An extrinsic activation energy of 0·2 eV was found in this region. The intrinsic region was not reached. At 500°K a resistivity of $\rho = 14{\cdot}5\ \Omega$ cm and a Hall coefficient of $A_H = +285$ cm$^3$ coulomb$^{-1}$ were measured, corresponding to a hole mobility $A_H/\rho = \mu = 20$ cm$^2$/V-sec.

The absorption coefficient of a GaSe sample (thickness 12 $\mu$) is plotted in Fig. 1 as a function of wavelength. Taking the peak occurring in the absorption edge as a measure for the activation energy $\Delta E$, we find $\Delta E$ (300°K) = 2·01 eV and $\Delta E$ (78°K) = 2·09 eV. These values compare well with that ($\Delta E = 2{\cdot}04$) found by RYVKIN and KHANSEVAROV[3] from photo response measurements. The shift $d\Delta E/dT$ of the peak with temperature is found to be $-3{\cdot}6 \times 10^{-4}$ eV/°K.

In Fig. 2 the photo response of GaSe is plotted against wavelength for room temperature and for 78°K. As compared to the Russian work[3] the peak in our photo response curve is shifted towards longer wavelengths.

### 3.2 GaTe

Resistivity and Hall coefficient of an *n*-type sample of GaTe are plotted in Fig. 3. An intrinsic activation energy of $\Delta E = 1{\cdot}8$ eV is found from these measurements. The electron mobility as calculated from $\mu = A_H/\rho$ is reproduced in Fig. 4.

The absorption coefficient of a GaTe sample (thickness 5 $\mu$) is plotted in Fig. 1. As in GaSe a marked peak occurs near the absorption edge. Its position indicates an activation energy $\Delta E$ (300°K) = 1·66 eV and $\Delta E$ (78°K) = 1·74 eV, which again is in good agreement with that given by RYVKIN and KHANSEVAROV[3] ($\Delta E = 1{\cdot}65$ eV), as well as with the value found from electrical measurements. The same value $d\Delta E/dt = -3{\cdot}6 \times 10^{-4}$ eV/°K as in GaSe is found.

The photo response of GaTe was too weak to be measured accurately with our equipment.

### 3.3. InSe

Only optical absorption measurements were carried out on this compound. It is remarkable that even though the structure of InSe is very similar to those of GaSe and GaTe no peak was observed in absorption. However, the absorption edge which was found in the present work is considerably better defined than that given by DAMON and REDINGTON[4] and indicates that at 300°K the value of the activation energy is $\Delta E$ (300°K) = 1·8 eV.

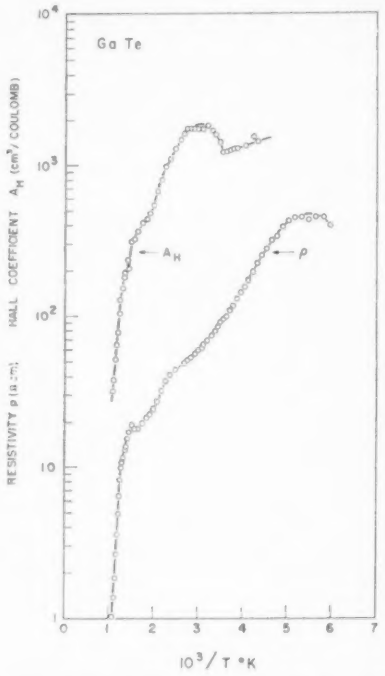


FIG. 3. Electrical resistivity and Hall cofficient of GaTe.

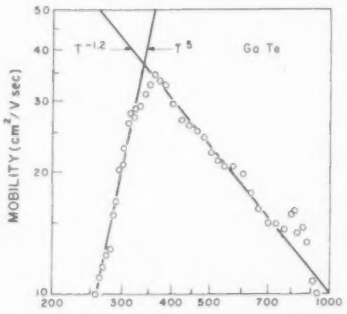


FIG. 4. Electron mobility in GaTe.

### 3.4. TlSe

The resistivities of two samples of TlSe are plotted as functions of the temperature in Fig. 5. The intrinsic activation energy derived from this plot is 0·57 eV.

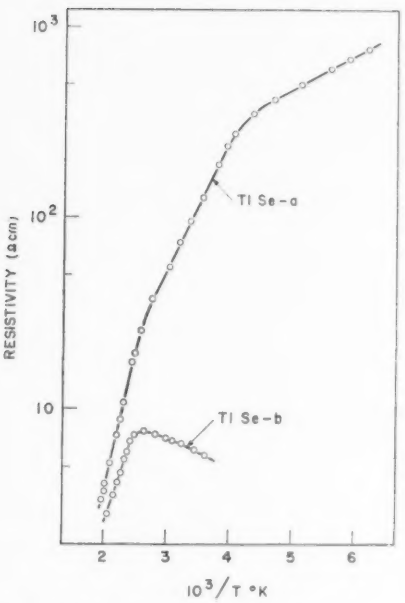


FIG. 5. Electrical resistivity of TlSe.

### 3.5. InTe

In spite of the fact that InTe has the same crysta structure as TlSe and even though zone purified single crystals were grown, we did not succeed in finding any semiconducting characteristics in InTe. The room temperature values of resistivity and Hall coefficient are respectively $\rho = 1\,4 \times 10^{-3}\ \Omega$ cm and $A_H = 0{\cdot}15$ cm³/coulomb. Preliminary low temperature measurements of the thermal conductivity $k$ of InTe show a flat maximum $k_{max} = 50$ mW/cm °K at 10°K. At the same temperature a thermal e.m.f. of 16 $\mu$V/°K was observed.

#### REFERENCES

1. MOOSER E. and PEARSON W. B. *J. Electronics* **1**, 629 (1956).
2. DAUPHINEE T. M. and MOOSER E. *Rev. Sci. Instr.* **26**, 660 (1955).
3. RYVKIN S. M. and KHANSEVAROV R. Iu. *Sov. Phys., Tech. Phys.* **1**, 2688 (1956).
4. DAMON R. W. and REDINGTON R. W. *Phys. Rev.* **96**, 1498 (1954).

*J. Phys. Chem. Solids* Pergamon Press 1959. Vol. 8. pp. 437–439. Printed in Great Britain

# INTERMETALLIC SEMICONDUCTORS CONTAINING ALKALI METALS

**W. E. SPICER and A. H. SOMMER**
RCA Laboratories, Princeton, N.J.

## 1. INTRODUCTION

THE materials to be discussed here have, for the most part, been prepared by reacting Sb or Au films, deposited by evaporation on a glass or quartz substrate, with alkali metal vapors to form a film of the compound about 500 Å thick. However, for X-ray analysis the alkali vapors were reacted with Au or Sb powders.

## 2. ALKALI ANTIMONIDES

The alkali metals combine with antimony to form semiconducting compounds of the form $M_3Sb$ where M represents one or more alkali metals. By measuring photoemission, photoconduction and optical absorption as a function of the energy of the incident radiation, values for the band gap, $E_G$, and for the electron affinity, $F_A$, have been obtained for a number of these materials. The band gap was determined from the threshold of photoconduction and optical absorption; and the electron affinity from the threshold of photoemission.

Since the threshold of photoemission is not sharply defined, an expression for the photoemission from the valence band was derived on the basis of the following assumptions:

(1) The absorption to states above the vacuum level is proportional to $[h\nu - (E_A + E_G)]^{3/2}$ ($h\nu$ = photon energy).

(2) The absorption to states below the vacuum level is constant in the spectral range where $h\nu > E_A + E_G$.

(3) The escape probability of an excited electron decreases exponentially with distance from the surface.

The solid curve in Fig. 1 indicates the type of fit

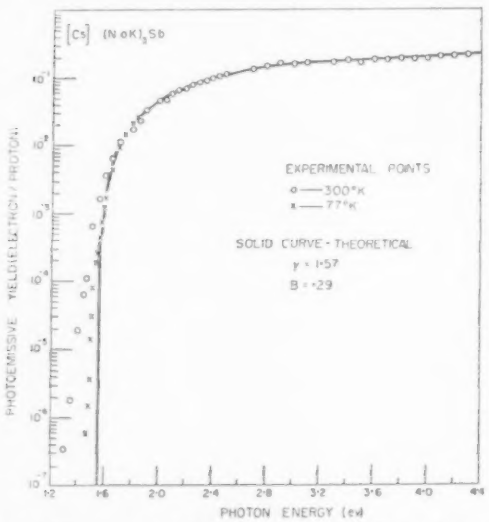


FIG. 1. Photoemission from [Cs](NaK)$_3$Sb. The points are experimental and the solid line is the theoretical curve. The theoretical curve indicates a value of 1·55 eV for the sum of the band gap plus electron affinity energies.

which is obtained between theory and experiment. The divergence of the experimental data from the theoretical curve at low photon energies is interpreted as photoexcitation from thermally ionized acceptors. This is confirmed by the reduced emission on cooling (see Fig. 1). The photoemissive yield curves from $Cs_3Sb$, $Rb_3Sb$, and the "multi-alkali" antimonides, $(NaK)_3Sb$, $[Cs](NaK)_3Sb$, and $[Rb](NaK)_3Sb$,[1] can be fitted by this model, but those from $Na_3Sb$ and $K_3Sb$ cannot be. Therefore the electron affinity values of these two materials can only be stated within a relatively wide energy range. The effect of excess Na or K and the temperature dependence of the spectral response curve indicate the presence of *n*-type impurities due to an excess of alkali metal.

The polarity of conductivity was also determined by measuring the change of resistivity if additional alkali metal or Sb is introduced into the material[2] and by correlating this with published results.[3] The resistivity measurements indicated that $Cs_3Sb$ and the multi-alkali antimonides are *p*-type due to Sb excess; whereas, $Na_3Sb$ and $K_3Sb$ were found to be *n*-type due to excess alkali metal. These results are in agreement with the conclusions drawn from photoemission measurements.

In Table 1, the values of band gap and electron affinity obtained for the materials investigated are summarized. The band gap of the materials with identical crystal structures, namely, $Na_3Sb$, $K_3Sb$, and $Rb_3Sb$, is little affected by the alkali constituent. This finding has an analogy in the alkali-halides

*Table* 1

| Material | $E_G$ (eV) | $E_A$ (eV) | Conductivity type |
|---|---|---|---|
| $Na_3Sb$ | 1·1 | 2·0–2·4 | *n* |
| $K_3Sb$ | 1·1 | 1·1–1·8 | *n* |
| $Rb_3Sb$ | 1·0 | 1·2 | ? |
| $Cs_3Sb$ | 1·6 | 0·45 | *p* |
| $(NaK)_3Sb$ | 1·0 | 1·0 | *p* |
| $[Rb](NaK)_3Sb$ | 1·0 | 0·70 | not measured |
| $[Cs](NaK)_3Sb$ | 1·0 | 0·55 | *p* |

where the band gap also does not vary appreciably with the alkali constituent. On the other hand, the electron affinities of the antimonides increase with decreasing atomic number of the alkali constituent.

### 3. GOLD–CESIUM COMPOUND

It has been found that the intermetallic compound AuCs[4, 5] has semiconducting properties. This is remarkable since it is a semiconducting compound formed from two elements which are both in the first column of the Periodic Table. X-ray analysis[6] indicates a CsCl type structure. Superlattice lines were observed, showing that the lattice was ordered, in agreement with the formula AuCs.[4]

Between 0·5 eV and 2·0 eV, the optical absorption is much smaller than that of the gold film from which the layer was formed. The fundamental absorption (Fig. 2) starts at about 2·0 eV and is dominated by what are apparently strong exciton peaks at 2·6, 3·05, and 3·35 eV. The peak absorption

coefficients here are in the $10^5$/cm to $10^6$/cm range. As was to be expected for exciton absorption, the structure became much sharper on cooling from 300°K to 77°K. The lack of absorption in the range 0·5 eV to 2·0 eV and the fundamental absorption with exciton lines above 2·0 eV can be taken as strong evidence that the material is a semiconductor.

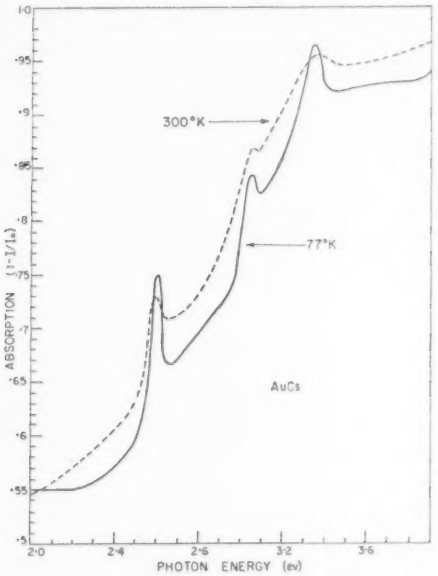


FIG. 2. Absorption of AuCs. Note the exciton type peaks at 2·6, 3·05, and 3·35 eV. These become much sharper at 77°K.

The X-ray work indicates an Au–Cs separation of 3·69 Å which is almost 10 per cent less than the sum of the metallic radii, 4·04 Å. This, together with the nature of the exciton absorption, is suggestive of an ionic character with Au forming the negative partner in the compound.

This work is being extended to RbAu and KAu. Preliminary results indicate that RbAu is also a semiconductor, but with much less pronounced exciton peaks. By contrast, KAu seems to be either metallic or a semiconductor with a very small band gap.

*Note added in proof.*—For a fuller description of the work reported in Section 2 see: SPICER, W. E. *Phys. Rev.* **112,** 114 (1958).

L. APKER has pointed out to us that P. G. BORZYAK [*Trud. Inst. fiz. Akad Nauk Ukr. SSR* **2,** 3 (1952)] has reported an $E_A$ of 0·4 and an $E_G$ of 1·6eV for $Cs_3Sb$.

## REFERENCES

1. The symbols [Cs](NaK)$_3$Sb and [RB](Nak)$_3$Sb refer to (Nak)$_3$Sb with an added surface layer of Cs or Rb. For a description of these materials see SOMMER A. H. *Rev. Sci. Instr.* **26,** 729 (1955); *Inst. Radio Engs. Trans.* NS**3,** 8 (1956).
2. SOMMER A. H. *J. Appl. Phys.* in press.
3. SAKATA T. *J. Phys. Soc. Japan* **8,** 125, 272 (1953); *Ibid* **9,** 1030 (1954).
   BORZYAK P. G. *Zh. tekh. fiz.* **20,** 925 (1950).
4. SOMMER A. H. *Nature, Lond.* **152,** 215 (1943).
5. BORZYAK P. G. *Trud. Inst. fiz., Akad. Nauk. Ukr. SSR* **2,** 1924 (1952).
6. WHITE J., to be published.

*J. Phys. Chem. Solids* Pergamon Press 1959. Vol. 8. pp. 439–443. Printed in Great Britain

# P.7 CONDUCTING STATES IN ORGANIC MOLECULAR CRYSTALS

**DAVID FOX**

Institute of Optics, University of Rochester, Rochester, N.Y., and IBM Research Laboratory, Poughkeepsie, N.Y.

IN a number of crystals of aromatic molecules, the temperature dependence of the conductivity indicates the existence of an activation energy.[1] These substances were therefore classified as semiconductors. It seems unlikely, however, that the usual one-electron approximation will be good in these crystals.

LYONS[2] proposed a model for anthracene and naphthalene in which he considered the following states, among others: (a) An electron is removed from a molecule, leaving a positive ion, and is placed in a conducting state, with a wave function which is large in the relatively empty spaces between the molecules. (b) The freed electron is

trapped by another molecule, so that there is an ion pair in the crystal of otherwise neutral molecules. LYONS estimated the excitation energies of these states. For (a), he obtained values which were several eV higher than the measured gaps. On this basis, the latter would appear not to be intrinsic.

Several modifications of the above model seem to be necessary. As GARRETT[1] pointed out, in a perfect crystal, states in which an ion is located at a definite lattice site are not good quantum states; instead, the lowest approximation must consist of appropriate linear combinations of the degenerate set of states in which the ionic charge is on different molecules. These states, ($b'$), would then be conducting states, with lower excitation energies than (a), since the molecules have positive electron affinities. (Conduction in such states may be pictured classically as involving the hopping of electrons and/or holes from one molecule to the next.) The remaining corrections are in the numerical calculations. In determining the energy of polarization of the neutral molecules by the ions, LYONS summed over a few neighbors. It may be shown that the convergence in such a procedure is not good; a crude estimate indicates that there is an approximately equal contribution from the remainder of the crystal. Further, the interaction between the induced dipoles (which contributes significantly in the case of polarization by a uniform field) was not included. The polarization energies are being calculated at present, with the above corrections and the anisotropy of the molecular polarizability taken into account. According to preliminary estimates, the new value, taken together with the introduction of the additional conducting states below (a), will bring the band gap into reasonable agreement with the observed activation energy for conductivity. Since experiments with doped crystals[3] give evidence that the measured gap in anthracene is intrinsic, it seems worthwhile to develop the model further.

In a crystal containing one extra electron, the wave functions of the states ($b'$) are $\phi_{\mathbf{k}} = \sum_{\mathbf{R}} e^{i\mathbf{k}\cdot\mathbf{R}}\psi_{\mathbf{R}}$, where $\psi_{\mathbf{R}}$ is a product wave function in which there are $N-1$ neutral molecules, and one negative ion at $\mathbf{R}$; the molecules and the ion are all in their respective ground states. Each $\phi_{\mathbf{k}}$ is a many-electron state, in which the correlation between the extra electron and the remaining electrons of the ion on which it is located at any moment are taken into account; in the absence of such correlation, $\phi_{\mathbf{k}}$ reduces to the product of the ground-state function of a neutral crystal by a one-electron Bloch function. Matrix elements of the operators of interest, taken between $\psi_{\mathbf{R}'}$ and $\psi_{\mathbf{R}''}$, where $\mathbf{R}'$ and $\mathbf{R}''$ are nearest neighbors, are said to be of the order of a small parameter $S$; this definition of $S$, though not precise, is adequate for our purposes.

In a similar way, one may build states of a neutral crystal with a mobile carrier of each sign. These states, $\phi_{\mathbf{k}\mathbf{k}'}$, may then be improved, to zeroth order in $S$, through a perturbation expansion or, in principle, by exact diagonalization of certain submatrices of the Hamiltonian; the latter process leaves off-diagonal terms of higher order in $S$. The energy obtained in this way is just the classical energy of a widely separated ion pair in a crystal of polarizable molecules, so that to zeroth order in $S$, one may calculate the energy from experimental molecular and ionic parameters, with no knowledge of the wave functions. Such a calculation implicitly takes into account most of the correlation between each carrier and the particles of the molecules it polarizes, as well as the more limited correlation described above.

The band width will be of order $S$. With the present knowledge of molecular wave functions, $S$ cannot be determined with any reasonable accuracy, but from the crystal and molecular structure, it is reasonable to expect that in such solids as naphthalene and anthracene, $S$ will be small enough for the model to be applicable. In the absence of a good estimate, the approach adopted is to carry out the zero-order calculations, and to make certain qualitative predictions in the next order.

A higher conduction band, related to (a), above, may presumably be adequately treated in the one-electron approximation, with correlation effects taken as perturbations.

On the basis of the above model, one may draw a number of conclusions, which are listed below, together with available supporting experimental evidence.

(1) LYONS' essentially classical calculation of the band gap, modified as described above, is justified. The quantity actually computed is the distance between centers of the "valence" and first "conduction" bands; it differs from the gap by quantities of order $S$.

VOL
8
195

(2) The valence and first conduction bands are narrow (of order $S$) compared with the bandgap. The mobilities of carriers in these bands should therefore be low. (On the assumption that the measured band gaps are intrinsic, MANY, HARNICK and GERLICH[4] estimated the mobilities to within one or two orders of magnitude, and found that in nearly all the aromatic compounds which were measured, the mobilities were in the range $10^{-2}$ to $10^{-12}$ cm$^2$/V-sec. An estimate based on measurements of impurity conductivity in doped anthracene roughly agrees with their result, with no assumption as to the size of the intrinsic gap. The assumption of an exponentially temperature-dependent mobility[1] leads to an even smaller estimate of this quantity.)

(3) A second gap may appear between the first ("hopping" electron) and the second ("free" electron) conduction bands.

(4) The usual prediction, based on the one-electron model, that exciton states will appear below the bottom of the conduction band, applies here to excitons of radius equal to, or larger than, the nearest-neighbor distance. Excitation energies of the tightly-bound excitons (which are essentially mobile molecular excitations) have little relationship to the band gap;[1] the former does not contain the large polarization terms discussed above, and so may be larger than the latter.

(5) Transitions between ionized and non-ionized states will be very weak. For large $S$, band-to-band transition probabilities will be roughly of order $S$ compared with those in conventional semiconductors, and will decrease much more rapidly than $S$ as this parameter is made smaller. (Although considerable experimental work has been done on the naphthalene and anthracene spectra, no band-to-band transitions have been reported, even where thick samples were used.)

(6) The crystal structures of naphthalene and anthracene are such that the mobilities of holes and of the "hopping" electrons in the direction perpendicular to the ab-plane should be many orders of magnitude lower than those in this plane, which are themselves small. The mobilities of the "free" electrons should be considerably larger, and more nearly comparable in the various directions. (The conductivity is much larger in the ab-plane than in the perpendicular direction.[5] Further, measured temperature dependences of the conductivities give different activation energies in the parallel and perpendicular directions. The measurements were carried out by different observers and were interpreted to indicate a difference in sample purity.[5,6]) However, in view of the evidence indicating that the lower gap is intrinsic, an alternate explanation should be considered: the holes or first-band electrons may determine the ab-plane conductivity, but may have such low mobilities in the perpendicular direction that the "free" electrons may dominate, in spite of their lower population. An experiment on a single sample is now being carried out by INOKUCHI.[7] (There is evidence that a similar situation exists in $ZnAs_2$ crystals, where not only the conductivity but also the Hall coefficients show a directional dependence of the activation energy.[8])

## REFERENCES


1. GARRETT C. G. B. Organic semiconductors, chap. 12 in *Semiconductors*, edited by N. B. Hannay, to be published. This chapter, an excellent review and critique of work on organic crystals, contains a lengthy bibliography.
2. LYONS L. E. *J. Chem. Soc.* 5001 (1957).
3. NORTHROP D. C. and SIMPSON O. *Proc. Phys. Soc.* **B67,** 892 (1954).
4. MANY A., HARNIK E., and GERLICH D. *J. Chem. Phys.* **23,** 1733 (1955).
5. METTE H. and PICK H. *Z. Phys.* **134,** 566 (1953).
6. INOKUCHI H. *Bull. Chem. Soc. Japan* **29,** 131 (1956).
7. INOKUCHI H. private communication.
8. TURNER W. and FISCHLER A. private communication.

## DISCUSSION

*Compiled by* P. H. KECK

### P.1. W. W. SCANLON

H. BROOKS (Harvard University) raised the question whether Hall mobility measurements had been made on alloys.

W. W. SCANLON replied they had not been measured in the alloys yet but in the pure compounds. PbTe has the largest mobility, PbSe intermediate and PbS the lowest mobility, which does not indicate band crossing.

H. BROOKS pointed out further that possibly two minima in the band structure of these compounds could explain their properties.

H. EHRENREICH (General Electric Research Laboratory) raised the question whether a break in the optical absorption edge could be expected if the band minimum would change from (111) to (110).

W. W. SCANLON: Yes.

C. HERRING (Bell Telephone Laboratories) asked whether one could measure all three low field magnetoresistance constants and get a more sensitive check of the (111) hypothesis.

W. W. SCANLON replied that these measurements have not yet been made but will be carried out in the near future.

C. HERRING further pointed out that a comparison of low and high field values of magnetoresistance anisotropy is risky because the energy dependence of $\tau$ affects the latter.

H. BROOKS asked how an indirect transition could be visualized.

W. W. SCANLON: It could be a transition either to a minimum in the conduction band near the same $K$-value as the maximum in the valence band or else a lattice phonon interaction. A study of the variation of the absorption coefficient with temperature will clarify this.

M. GREEN (U.S. Army Signal Laboratories) asked whether the absorption edge had been measured for the binary alloys of PbS and PbTe.

W. W. SCANLON replied that this has not yet been done. Such an alloy composition may behave like synthetic PbSe.

### P.3. J. R. DRABBLE

B. ABELES (R.C.A.) raised the question, what is the criterion for the thermoelectric power to be isotropic in an otherwise anisotropic material.

C. HERRING (Bell Telephone Laboratories) commented that anisotropy of thermoelectric power reflects differences in the energy dependence of relaxation times in different directions, but not in their absolute values.

R. WOLFE (Bell Telephone Laboratories) pointed out that it can be shown that both of the Hall coefficient anisotropy factors are less than, or equal to unity for this six-valley model with any ellipsoid shape. Therefore, a better estimate for the carrier density is obtained if the larger of the two Hall coefficients is used.

### P.4. N. FUSCHILLO *et al.*

T. C. HARMAN (Battelle Memorial Institute) pointed out that quenching of $Bi_2Te_3$ from a stoichiometric melt may lead to differences in the composition within the ingot. At Battelle it was found that quenching in oil from a temperature of 200°C above the melting point resulted in high resistivity material. Additions of excess Bi yielded low resistivity $p$-type while excess Te yielded low resistivity $n$-type crystals. Slow recrystallization by the Bridgman technique confirmed the phase diagram published by SATTERTHWAITE and URE.[1]

J. ROTHSTEIN (Edgerton, Germeshausen, and Grier, Inc.) raised the question whether specific heat anomalies had been sought in this system. The author answered that no evidence of anomalies were observed.

R. W. FRITTS (Minnesota Mining and Manufacturing Company) asked what gain in the thermoelectric figure of merit is obtained by alloying $Bi_2Se_3$ and $Bi_2Te_3$ and how does this figure vary with temperature.

F. J. DONAHOE replied that the thermal conductivity decreases by a factor of two but the figure of merit ($S^2/K\rho$) is not improved by the same factor. For some compositions the figure of merit is independent of temperature between 200 and 350°K.

### P.5. P. FIELDING *et al.*

E. E. LOEBNER (R.C.A.) pointed out that a band gap of approximately 2·6 eV was measured for GaS at the R.C.A. Laboratory. He further commented that both GaS and GaSe are highly anisotropic and one might expect a dependence of the absorption on the optical arrangement.

E. MOOSER confirmed LOEBNER's value for the band gap in GaS: preliminary absorption measurements carried out at the laboratories of the National Research Council of Canada on GaS give $\Delta E \approx 2{\cdot}7$ eV.

E. MOOSER also pointed out that the crystal structure of GaS and GaSe as well as examination under a polarizing microscope indicate that these crystals are uniaxial, the optical axis being normal to the cleavage plane. Since all the absorption measurements reported here have been carried out with the light beam perpendicular to the cleavage plane no effect of polarization upon the position of the absorption edge would be observed in these experiments.

G. A. WOLFF (U.S. Army Signal Laboratory) pointed out that crystals of $A^{III}B^{VI}$ compounds can be prepared in good purity from their metallic solutions. GaS, for instance, crystallizes from an appropriate solution in liquid Ga in the form of yellow flakes. In reply to a question from the floor MOOSER stated that the absorption measurements reproduced in Fig. 1 are not corrected for reflection losses.

### P.6. W. E. SPICER and A. H. SOMMER

The discussion after this paper centered around the

question of Au having a negative valence and the reasonableness of AuCs being a semiconductor.

R. C. SANGSTER (Texas Instruments) pointed out that mercury has a strong tendency to have either none or two *s*-electrons in its valence shell, so that an $Au^-$ ion may be plausible. He further pointed out that nominally monovalent mercury actually appears in dimeric forms, such as $Hg_2^{++}$, with a pair of *s*-electrons being shared between the two mercury atoms.

P.7. D. Fox

S. L. MATLOW (Hoffman Electronics) raised the question whether the band gap for anthracene equals the energy difference between the highest filled and lowest unfilled $\pi$ orbitals.

D. FOX answered yes, but pointed out that this is presumably a coincidence. There is no theoretical reason for the excitation energy of a bound triplet state to have anything to do with the excitation energy for conduction. For a more thorough discussion of this point see reference 1 of the paper.

G. A. WOLFF (U.S. Army Signal Laboratories) made the following comments. In this presentation conducting states in ideal molecular crystals have been investigated. There are many examples of crystalline materials which are imperfect in the sense that some of the intramolecular bonds are broken and intermolecular bonds are formed instead which give rise to optical absorption and semiconduction.

## REFERENCE

1. SATTERTHWAITE C. B., and URE R. W. *Phys. Rev.* **108,** 1164 (1957).

OL.
8
959

*J. Phys. Chem. Solids* Pergamon Press 1959. Vol. 8. pp. 444–449. Printed in Great Britain

SESSION Q:
LARGE BAND GAP SEMICONDUCTORS*

Q.1

# A REVIEW OF RECENT WORK ON DIAMOND

E. W. J. MITCHELL

Physics Research Labs., The University, Reading, England

**Abstract**—The following properties are discussed: the intrinsic absorption apectra (5·4 eV and 3 to 6 $\mu$) and the various extrinsic absorption features; the electrical and optical properties of semiconducting diamonds; the luminescence of diamonds and the study of the symmetry of the centres from the polarization of the emission; and the optical spectra associated with radiation induced defects and their effect on the electrical properties of semiconducting diamonds.

VOL
8
195

## 1. INTRODUCTION

THE discovery of semiconducting diamond has meant that it is possible to obtain more information about defects in diamond and about its band structure than was previously possible. In addition the availability of high energy electrons has enabled the various effects of interstitial carbon atoms and vacancies to be investigated. This review is primarily of the work at Reading.

## 2. ABSORPTION SPECTRA

The purest diamond so far investigated is probably one of the specimens (D 100) studied by CLARK.[1] There is a transparent region limited in the ultraviolet (5·4 eV) by the temperature dependent indirect band to band transitions, and in the infrared by vibrational absorption between 3 and 6 $\mu$. STEPHEN[2] has extended the two phonon, charge deformation theory of LAX and BURSTEIN[3] and obtained sufficiently good agreement with the spectrum of the 3 to 6 $\mu$ absorption to indicate that the theory is basically correct. It seems, therefore, that the ultraviolet and infrared absorption in this specimen corresponds to the intrinsic absorption characteristic of the diamond lattice.

Diamonds which are more commonly encountered have a variety of extrinsic features. These are summarized as follows:

(1) Absorption lines superposed on the vibrational absorption and a region of continuous absorption extending into the visible. These diamonds are blue. The lines occur[4] at 0·307, 0·346, 0·363, 0·372, 0·514, 0·537, and 0·675 eV. The strength of the lines and the strength of the continuum vary from specimen to specimen but the relative strengths remain constant.[4] Diamonds showing these absorption features are semiconductors having room temperature resistivity ca. $10^2$ $\Omega$ cm. The strength of the lines and of the continuum decreases with increasing temperature.

(2) Diamonds in which the effects described in (1) are absent but which have a specimen dependent tail to the absorption edge. These are usually referred to as Type IIa diamonds. It was found by CLARK *et al.*[5] that the strength of this absorption could be increased by heat treatment after electron, gamma or pile irradiation, and that the spectral form was the same in the two cases.

(3) Various absorption bands which occur in the diamonds commonly referred to as Type I. In the infrared there is additional absorption at 8 $\mu$—that is, at the Raman frequency. This absorption is specimen dependent. The absorption systems shown in Fig. 2 of reference (12) and Fig. 8 of reference (15) are also specimen dependent. These two centres show absorption on the high-energy side of main lines at 2·99 eV (4150 Å) and 2·47 eV (5032 Å) respectively, and emission on the low-energy side.[6] The absorption and emission spectra comprise relatively sharp lines superposed on broad (ca. 1 eV) bands. Type I diamonds also exhibit strong specimen dependent absorption

* *Chairman:* E. F. GROSS; *Co-Chairman:* W. C. DUNLAP, Jr.

beginning near 4 eV. There is evidence of a plateau in this absorption and measurements on cleavage flakes[7] indicate that the absorption curve is tending towards the intrinsic curve at higher energies.

### 3. SEMICONDUCTING DIAMONDS

Semiconducting diamonds were first reported by CUSTERS.[8] Measurements of the Hall constant and conductivity between 200 and 800°K have been made on the 6 semiconducting diamonds for which the optical spectra were referred to above.[4] It was found that in this temperature range the Hall constant ($R$) could be represented by:

$$\frac{A/Re(A/Re+N_D)}{N_A-N_D-A/Re}=\left(\frac{2\pi m^*kT}{h^2}\right)^{3/2}e^{-\epsilon/kT} \quad (1)$$

where if $A=3\pi/8$, the concentration of acceptor levels $N_A$ varied for different crystals between $5\times10^{15}$ and $10^{17}$ cm$^{-3}$, the concentration of donors $N_D$ between $2\times10^{15}$ and $10^{16}$ cm$^{-3}$, and values of the effective mass $m^*$ varied between 0·25 and 0·6 $m_e$. At room temperature the hole concentration—$p=A/Re$—was between $10^{13}$ and $10^{14}$ cm$^{-3}$.

The method of analysis used by WEDEPOHL[9] was as follows: $\epsilon$ was determined from the temperature variation of the Hall constant in the region where $p<N_A$ or $N_D$; then equation (1) was written in the form

$$p/f(T)=N_A\left(\frac{m^*}{m_e}\right)^{3/2}\left(\frac{1}{p+N_D}\right)-\left(\frac{m^*}{m_e}\right)^{3/2} \quad (2)$$

in which, using the previously determined value of $\epsilon$, $f(T)$ is a known function of temperature. In the high temperature region $pf(T)$ should vary linearly with $1/(p+N_D)$. $N_D$ was chosen by trial and error to give a linear relation, from the interpret of which $m^*$ could be found and used to determine $N_A$ from the slope. The estimated errors involved in this procedure were given as 10 per cent on $N_A$ and 40 per cent on $N_D$ and $m^*$.

In the 6 semiconducting diamonds investigated the strength of the infrared lines listed above correlated with the values of $(N_A-N_D-p)$—that is, with the concentration of unoccupied acceptor levels. WEDEPOHL[9] pointed out that the energy intervals between the first 3 excited levels, as determined from the energies of the first 4 lines,† were in the ratio 100 : 44 : 23. Applying a hydrogenic model to the excited states it would be expected that the energy intervals would be in the ratios 100 : 35 : 16. WEDEPOHL also pointed out that by continuing to apply this model to the excited states photoionization would be expected to begin at 0·38 eV. It is not possible in this way to account for the lines at 0·514, 0·537, and 0·675 eV and it is necessary to establish from photoconductivity experiments at what energy photoionization begins. Semiconducting diamonds show photoconductivity under white light illumination but a high resolution infrared experiment has not yet been carried out.

Magnetoresistance coefficients have been measured[10] at room temperature on a specimen whose face normals were arbitrary directions, the direction cosines being given in the reference. In the range of magnetic fields investigated—up to 4000 oersted—the fractional change in resistance was proportional to $H^2$. The current $I$ was along the length axis of the crystal while $H$ was varied from the length axis through the thickness axis in one experiment, and through the width axis in the second experiment. In both experiments the maximum effect was obtained with $H$ perpendicular to $I$ and the minimum with $H$ parallel to $I$. There was a small crystalline anisotropy. The observed magnetoresistance variation is consistent with nearly spherical energy surfaces in one or more bands whose edges are at $k=0$.

At room temperature semiconducting diamonds are transparent beyond 6 $\mu$. At higher temperatures, however, there is absorption present which increases with increasing wavelength. This absorption is not found in non-semiconducting diamonds. The effect is associated with the presence of free carriers and the absorption per carrier increases with increasing temperature. Near 10 $\mu$ the absorption increases with wavelength according to a power between 1·5 and 2, but at longer wavelengths tends to increase linearly. Since the crystals have to be heated to obtain sufficient carriers to see the effect most of the measurements are being made under conditions for which $h\nu\sim kT$. Values of

† A weak line at 0·295 eV having a linear correlation coefficient of only 68 per cent with $(N_A-N_D-p)$ was omitted from this series.

$kT$ up to 0·05 eV have been used. Details of these measurements and the analysis of the results will be published separately.

## 4. THE LUMINESCENCE OF DIAMONDS

Most diamonds luminesce. The frequently occurring centres emit in the green (5032 Å centre) and in the blue (4150 Å centre), respectively. DYER and MATTHEWS[6] found these centres in all the diamonds which they examined except the semiconducting diamonds. However, the strength of the emission was much less in Type IIa specimens than in Type I, such that the absorption spectra could not be detected in Type IIa crystals.

The emission spectra for the two centres are shown in Figs. 3 and 4 of reference (6). These spectra were recorded at 80°K, the structure being only poorly resolved at room temperature. Two interesting characteristics of the centres are:

(1) The main line shows negligible Frank–Condon shift.

(2) Both centres have spectra comprising relatively sharp lines superposed on broad bands. This structure is temperature dependent and therefore probably vibrational structure.

Some information concerning the atomic nature of the centres is available for the 5032 Å centre since it can be produced in Type I diamonds by particle irradiation followed by heat treatment, as will be described below. CLARK *et al.*[5] suggested that the centre was in some way associated with a vacancy or interstitial carbon atom which migrated during the heat treatment to become finally anchored to an impurity atom.

Further information about the nature of this centre has been obtained by ELLIOTT *et al.*[11] from studies of the degree of polarization of the emission when the centres are excited with plane polarized light. The measurements were made on 5032 Å centres induced by pile irradiation followed by heat treatment in a specially cut crystal having (100) faces. The variation of the degree of polarization of the emitted light as a function of $E$ of the exciting light relative to one of the crystal axes was determined. From the analysis of the results for both the "straight through" experiment and for perpendicular viewing it was shown that centres having ⟨100⟩ or ⟨111⟩ axes were not involved. The predicted curves for a transition involving a wave function directed along the axes of centres having ⟨110⟩ axes ($\pi$ oscillators) exhibited the main features of the experimental results for both kinds of experiment. From the evidence of the way the centres are formed and the conclusion that they have ⟨110⟩ axes, ELLIOTT *et al.*[11] suggested that a 5032 Å centre consisted of an interstitial carbon atom anchored to an interstitial impurity. The other simple combinations of vacancy or interstitial carbon with impurity have principal axes along ⟨111⟩ directions.

The emission from the 4150 Å centre is also partially polarized when the exciting light is plane polarized. These experiments have been carried out mainly on one crystal having arbitrary faces. The results for the various combinations of directions are close to the predicted curve for ⟨111⟩ $\sigma$ centres—that is transitions involving two wave-functions both perpendicular to the axis of the centre. However, CLARK and MAYCRAFT have found that there are systematic differences between the predicted and experimental results and improved agreement is obtained if it is assumed that there are 4 ⟨111⟩ $\sigma$ oscillators equivalent to 6 ⟨110⟩ $\pi$ oscillators involved in the emission. Several other possibilities have been tried—absorption in $\pi$ centres followed by emission in $\sigma$ centers, and the reverse process, ⟨100⟩, ⟨311⟩ centres—all unsuccessfully.

It is not clear yet what kind of centres could give the symmetry indicated by these results. We can summarize the experimental evidence relevant to the atomic nature of the 4150 Å centre as follows:

(1) It is not produced in any diamond by irradiation, or by irradiation followed by heat treatment. This indicates that the centre is not a vacancy, an interstitial carbon, a vacancy pair (see below), or any product of damage anchored to impurities. In the latter case one has to make the proviso that such a model would be possible if in all the Type I and IIa diamonds investigated at Reading, the anchoring impurities were saturated with defects.

(2) The centre is not isotropic. It is therefore not likely to be an isolated impurity atom.

## 5. DEFECTS INTRODUCED BY IRRADIATION

CLARK *et al.*[12] found that two separated regions of absorption were induced in Type IIa diamond by electron irradiation—one with a main line at 1·673 (7410 Å) and structure on the high-energy

side, and the second rising into the ultraviolet. The structure of the 7410 Å system has been investigated under various conditions and the results of the above and more recent work may be summarized as follows:

(1) The major line becomes extremely sharp at 80°K.

(2) The detailed form of the spectrum at 80° K depends on the nature and temperature of the irradiation, in spite of the fact that the specimen is warmed to room temperature between irradiating and measuring. As shown in Fig. 1 the lines are not well resolved when the band is induced by

It is suggested that sharp lines are obtained when defects are well separated. This situation may be brought about by the thermal annealing of close pairs of defects during irradiation—as in the case of electron irradiation. When the effective flux of ionizing radiation is much lower—as with gamma and pile irradiation—close pairs may only recombine during subsequent heat treatments.

The 7410 Å system was also induced by irradiation in Type I diamonds but the radiation induced ultraviolet absorption, if it occurred, would be obscured by the natural ultraviolet absorption in these specimens.

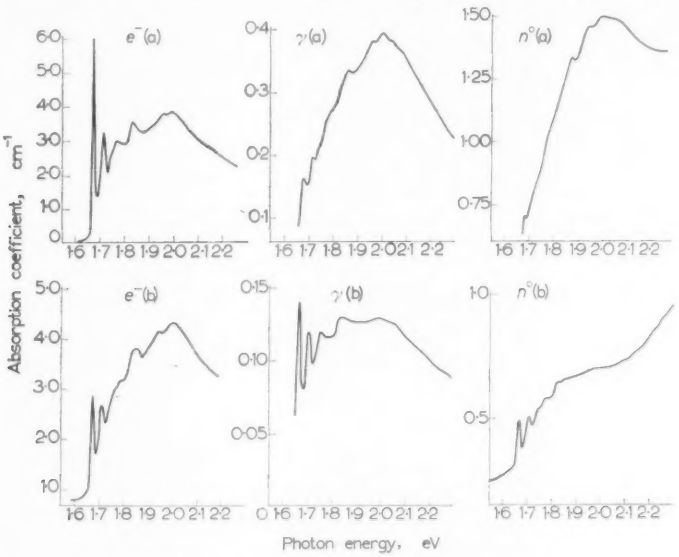


FIG. 1. The absorption coefficient as a function of photon energy for the 7410 Å band under various conditions:

$e^-$ (a) produced by electron irradiation at room temperature;
(b) produced by electron irradiation at 195°K.;
$\gamma$ (a) produced by gamma irradiation;
(b) after heating at 723°K;
$n°$ (a) produced by pile irradiation at about 313°K.;
(b) after heating at 723°K.

gamma irradiation, although they sharpen—but decrease in strength—after heating to 723°K. The same effect is observed with pile irradiated crystals. The lines are sharpest after electron irradiation near room temperature, and are less sharp when the ambient temperature during the irradiation was 195°K.

CLARK *et al.*[5] found that the effects of heat treatment after irradiation were different for the two types of crystals:

*Type IIa.* Heating at 870°K causes a large reduction in the radiation induced lines and new lines appear in the region 2·543—2·618 eV (4876–4736 Å). At 870°K the rate curves for

the two effects were found to be complementary and bimolecular. It was suggested that the new lines were associated with a vacancy pair or interstitial pair. The lines disappear during heat treatment at high temperatures leaving only the continuous absorption referred to in Section 2.

*Type I.* Heating at temperatures above 770°K leads to the formation of the 5032 Å absorption system which was discussed in Section 4. This centre is also found naturally in Type I diamonds in varying concentrations. Unlike the absorption induced by heating irradiated IIa diamonds the 5032 Å system is permanent.

Further information about the defects introduced by electron irradiation has been obtained from measurements on a semiconducting diamond.[9, 13] The crystal was irradiated at an ambient temperature of 80°K and afterwards warmed to room temperature and measured. Fig. 2 shows the carrier concentration as a function of $1/T$ for this diamond before irradiation and after each of two electron irradiations of $2 \times 10^{16}$ ($e^-$ cm$^{-2}$). It will be seen that the carrier concentration has been reduced although the temperature dependence in the low-temperature region ($1/T$ greater than 0·003) has not changed appreciably.

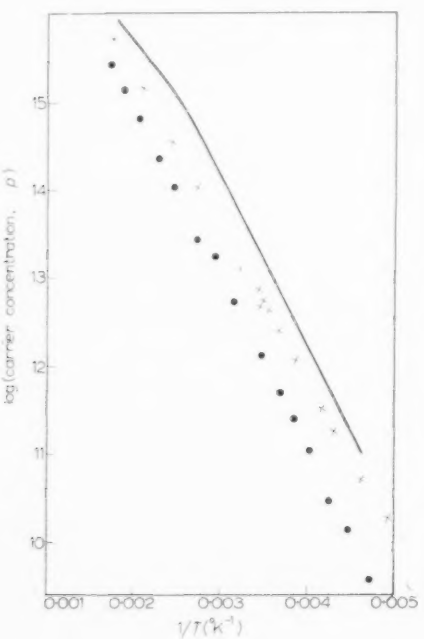


FIG. 2. Logarithm of the carrier concentration of D 108 as a function of $1/T$ (°K$^{-1}$).
———— before irradiation (Wedepohl);
xxxxxxxxxx after the first 2 MeV. electron irradiation (Wedepohl);
..... after the second electron irradiation (Kemmey).

It is to be expected that the centres induced by electron irradiation will provide both donor and acceptor levels. The precise positions of these levels in diamond are not known but the absence of an appreciable change of temperature coefficient of the carrier concentration in the low-temperature region indicates that the induced levels are remote from the "impurity" acceptor level. Furthermore, assuming that the vacancy provides the acceptor level,[14] and that the assignment of the induced optical absorption between 1·67 and 3·0 eV is correct,[15, 16] then the acceptor level cannot be a shallow level lying close to the valence band. The main factor influencing the carrier concentration would then be the concentration of induced donor levels.

Subsequent illumination of the crystal with light from a high pressure mercury lamp produced no permanent change in the conductivity indicating that the electron distribution after irradiation corresponded closely to the equilibrium distribution. The proposed interpretation of the results is that the carrier concentration has decreased because of the introduction of additional donor levels. Their concentration may be calculated from the low temperature form ($p < N_A$ or $N_D$) of equation 1 and for $1/T$ of 0·0034 we find the concentration of induced donors ($N_R$) equal to $7{\cdot}4 \times 10^{15}$ for the first irradiation and $8{\cdot}2 \times 10^{15}$ for the second. These numbers represent the concentration of induced donor centres only if each centre donates one electron. If two or more electrons are donated then the concentration of centres is less than the above values. In either case the numbers are less than the calculated concentration of displaced atoms of $2{\cdot}0 \times 10^{16}$ cm$^{-3}$. It seems, therefore, that some annealing of defects had occurred during the irradiation.

WEDEPOHL[9] also found that the strengths of the infrared lines in the semiconducting diamond decreased with electron irradiation. Assuming that the lines are associated with transitions to vacant "impurity" acceptor levels as indicated in Section 3

then the ratios of the line strengths before and after irradiation should be $(N_A - N_D)/(N_A - N_D - N_R)$. From these results WEDEPOHL found $N_R = 11 \times 10^{15}$ cm$^{-3}$. This value is higher than that deduced from the electrical measurements after irradiation but the difference is probably not significant owing to the difficulties of determining the strengths of the infrared lines accurately. Further details of the effect of irradiation on the properties of semiconducting diamond will be published later.

*Acknowledgments*—The work described in this review has been carried out in Professor DITCHBURN's laboratory at Reading and the contributions of different members of the group are indicated in the references. We are grateful to Dr. J. F. H. CUSTERS, Director of Research, Diamond Research Laboratory, Johannesburg for his interest and for providing the variety of polished diamonds used in the work.

## REFERENCES

1. CLARK C. D. *J. Phys. Chem. Solids* **8**, 481 (1959).
2. STEPHEN M. J. *Proc. Phys. Soc.* **71**, 485 (1958).
3. LAX M. and BURSTEIN E *Phys. Rev.* **97**, 39 (1955).
4. WEDEPOHL P. T. *Proc. Phys. Soc.* B **70**, 177 (1957).
5. CLARK C. D., DITCHBURN R. W., and DYER H. B. *Proc. Roy. Soc.* A **237**, 75 (1956).
6. DYER H. B. and MATTHEWS I. G. *Proc. Roy. Soc.* A **243**, 320 (1957).
7. CUSTERS J. F. H. and RAAL F. A. *Nature, Lond.* **179**, 268 (1957).
8. CUSTERS J. F. H. *Nature, Lond.* **176**, 173 (1955); *Physica* **18**, 489 (1952).
9. WEDEPOHL P. T. Ph.D. Thesis, Univ. of Reading (1958).
10. MITCHELL E. W. J. and WEDEPOHL P. T. *Proc. Phys. Soc.* B **70**, 527 (1957).
11. ELLIOTT R. J., MATTHEWS I. G., and MITCHELL E. W. J. *Phil. Mag.* **3**, 360 (1958).
12. CLARK C. D., DITCHBURN R. W., and DYER H. B. *Proc. Roy. Soc.* A **234**, 363 (1956).
13. KEMMEY P. to be published.
14. JAMES H. M. and LARK-HOROVITZ K. *Z. Phys. Chem.* **198**, 107 (1951).
15. CLARK C. D. Ph.D. Thesis, Univ. of Reading (1955).
16. MITCHELL E. W. J. *Brit. J. Appl. Phys.* **8**, 179 (1957).

*J. Phys. Chem. Solids* Pergamon Press 1959. Vol. 8. pp. 449–457. Printed in Great Britain

# INFRARED PHOSPHOR-SEMICONDUCTORS

G. F. J. GARLICK
University of Hull, England

**Abstract**—The development of sensitive photoconducting detectors for infrared radiation has made possible the study of luminescence emission from a new variety of solids including those of considerable interest as semiconductors. A review of progress over the past few years is given with special reference to the emission of zinc and cadmium sulphide phosphors, lead sulphide, lead telluride and mercury sulphide. The infrared emission found in zinc sulphide is ascribed to electron transitions from the valence band to the ground states of visible emission centers. In mercury sulphide the characteristics of the excitation and emission spectra suggest a different mechanism. This also applies to lead sulphide and lead telluride.

New results on cadmium telluride made *p*- or *n*-type under controlled conditions show a number of emission bands extending to 2·6 $\mu$. Excitation and photovoltage excitation curves coincide with emission bands, there being no Franck–Condon shift. The results are given a tentative theoretical explanation.

## 1. INTRODUCTION

THE extension of luminescence studies to the infrared region of the spectrum was begun in the author's laboratory in 1952–3. It was hoped that results of such investigation would not only improve knowledge of luminescence processes in solids, but would also provide a new approach to semiconductor research by measurements of optical transitions associated with such phenomena as photoconduction and the photovoltaic effect.

The present paper attempts to provide a critical and up-to-date review of progress in the production and measurement of infrared emitting phosphors and of the resulting advances in knowledge of luminescence and related phenomena. Some of the work has already been published[1–4] but the more complete account below includes much work which has not been previously reported.

Luminescence effects in solids may be confined to luminescence centres or may involve energy transfer and storage outside such centres. Examples of both are found in infrared emitting phosphors, e.g. molecular systems like iodine or transition element activators like $Co^{2+}$ ions show luminescence of a confined form, while such infrared emitters as zinc and cadmium sulphides, mercury and lead sulphides, cadmium telluride and cuprous oxide show emission which is closely related to charge carrier motion in the solid, i.e. with photo- and semiconduction. These different types are dealt with in separate sections below.

In attempting to look for infrared emitting phosphors new techniques of radiation detection have had to be adopted. Advantage was taken of the availability of lead sulphide and lead telluride photoconducting cells. The use of these together with "chopped" radiation—narrow band tuned amplifier techniques have enables us to explore the region up to 5 $\mu$ with sensitivities not too far below those attainable with photomultipliers in shorter wavelength studies.

## 2. PHOSPHORS OF NON-PHOTOCONDUCTING TYPES

### 2.1. *The solid halogens*

Quite early in our investigations DUMBLETON[2] discovered near infrared emission from the solid halogens and inter-halogen compounds (fluorine excepted due to its very low solidification temperature). Their excitation and emission spectra are given in Figs. 1(a) and 1(b). More recently FRANKS[4] remeasured the spectra for iodine and also investigated the absorption and diffuse reflection spectra and temperature dependence of emission. From these, and using the method of KLICK and SCHULMAN[5] he was able to construct the energy configurational diagram of Fig. 2 and to compare his curves (shown by solid lines) with those proposed much earlier for molecular iodine vapour by MULLIKEN.[6] It is interesting to note

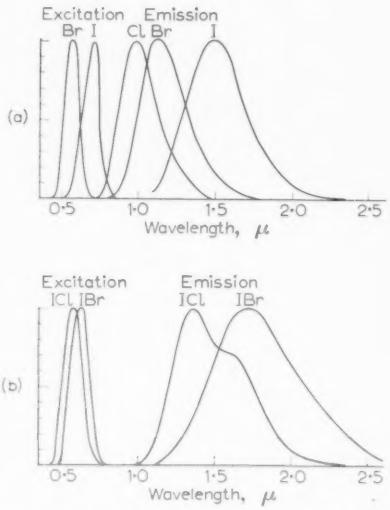


FIG. 1(a) Excitation and emission spectra of solid halogens. 1(b) Excitation and emission spectra of solid halogen compounds (after DUMBLETON [2a]).

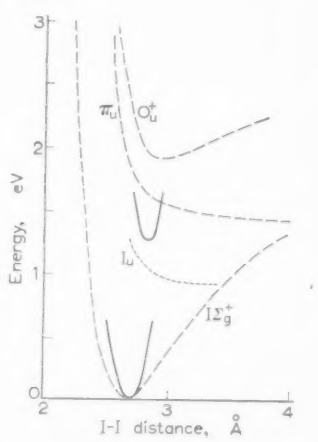


FIG. 2. Energy configurational co-ordinate diagram for solid iodine (full curves) compared with previous results for vapour state (broken lines) (after FRANKS[4]).
———solid iodine – – – – vapour (after MULLIKEN[6]).

that the infrared excitation and emission correspond to transitions between ground and second excited states of the molecule. However, an absorption but no emission was found at 1·12 $\mu$ corresponding to transitions to the first excited state. The absence of emission is expected from the curve for the $1u$ state in Fig. 2. We were unable to find any relation

between luminescence and the photoconduction characteristics for iodine reported by Moss[7] except perhaps indication from absorption curves that the two processes are competing ones for the absorbed quanta.

2.2. *Transition element activators*—ZnS : $Co^{2+}$

In zinc sulphide addition of a few parts per million of cobalt produces relatively deep electron traps[8] but in larger concentration this activator "kills" the normal visible emission completely. However, an infrared emission characteristic of transitions in the 3*d* shell of the $Co^{2+}$ ions is observed and this reaches an optimum efficiency for a concentration of about one part $Co^{2+}$ per thousand ZnS. Mutual perturbation of activator ions causes a drop in efficiency above these concentrations. It is of interest to note that the above concentration limit corresponds roughly to the appearance of dipole–dipole broadening effect in the paramagnetic resonance spectra of such transition ions, dispersed in solids. Fig. 3 shows the excitation, diffuse reflection and emission spectra of ZnS–$Co^{2+}$ phosphors and indicates the close correlation between absorption and excitation. We are hoping to have single crystal specimens available in the near future which will enable us to make much more quantitative investigations of the details of the emission centres and their interaction with the surrounding lattice. One interesting problem to be solved is that we have not observed the infrared emission for cobalt ions dispersed in any other matrix although similar diffuse reflection spectra have been observed (e.g. $Co^{2+}$ dispersed in a borax bead or in a zinc silicate lattice). A further interesting problem is to determine why the corresponding emission about 1 $\mu$ for iron-activated zinc sulphide is relatively feeble compared with those for manganese (yellow–orange emission) and cobalt (3 $\mu$ region). We have so far failed to detect any emission from ZnS–$Ni^{2+}$ phosphors in the region up to 5 $\mu$ and at temperatures down to 77°K.

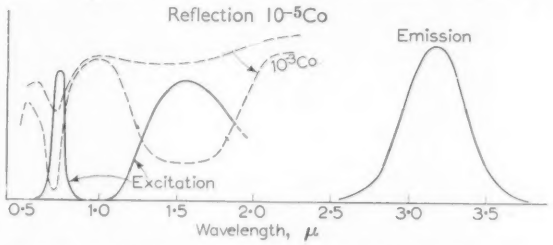


FIG. 3. Excitation, diffuse reflection and emission spectra for cobalt activated zinc sulphide (after DUMBLETON[2b]).

## 3. PHOTO- AND SEMI-CONDUCTING PHOSPHORS

3.1. *Cuprous oxide*

As shown some years ago by Russian workers[9] cuprous oxide specimens can be excited to give an emission at 1 $\mu$. Since cuprous oxide is important as a semiconductor, considerable attention was devoted to it in the author's laboratory. The results were previously reviewed in 1956[10] and an energy band scheme, correlating the photoconduction photovoltaic and luminescence characteristics shown in Fig. 4, proposed. This is given in Fig. 5 together with a modified scheme proposed more recently by BLOEM[11] following his more extensive measurements and discovery of another emission region at 0·7–0·8 $\mu$ predicted by the author.[10] The emission bands of cuprous oxide have a

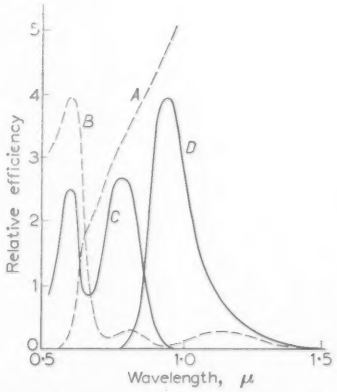


FIG. 4. Electrical and optical properties of cuprous oxide. A. Optical transmission, B. Photoconduction response spectrum, C. Luminescence excitation spectrum, D. Emission spectrum.

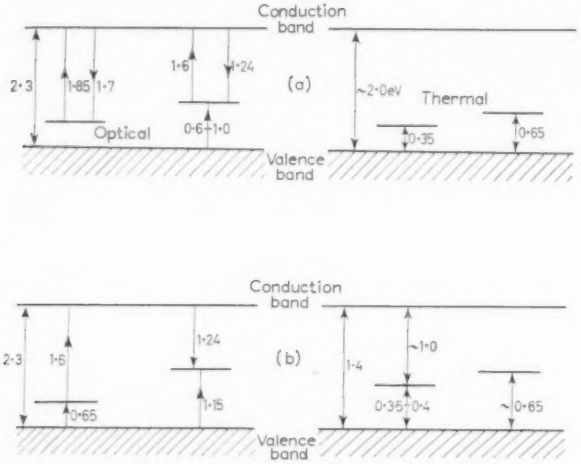


FIG. 5. Energy band schemes for cuprous oxide: (a) modified scheme due to BLOEM,[11] (b) proposed by GARLICK.[10]

doublet nature and the forbidden gap levels of Fig. 5 are thought to arise from lattice defects, a copper vacancy giving rise to the 1 $\mu$ emission. More copper-rich specimens contain oxygen vacancies which provide levels, one of which is assumed to be associated with the shorter wavelength emission.[11]

In cuprous oxide we have a relatively tractable material for such investigations. More detailed studies are still required, e.g. the relation between types of carrier and the several luminescence processes and comparison of carrier life time measurements in photoconduction with luminescence decay times over a wide temperature range.

### 3.2. *Lead sulphide*

Lead sulphide is well known as a member of the photoconductor group lead sulphide–selenide–telluride. Infrared emission from lead sulphide was first reported by Russian workers.[12] We subsequently measured the spectral distribution of the emission[1] and more recently R. A. Fatehally, of the author's laboratory, measured the excitation spectrum for the emission. The excitation and emission spectra for a typical specimen are given in Fig. 6, together with the photoconduction response spectra. It will be seen that one emission band appears where photoconduction response is falling off with increasing wavelength and that this band moves to longer wavelengths with a fall in temperature as does the photoconduction response curve. So far doping of specimens with impurity has failed to produce different emission bands. The band observed is most intense in specimens prepared to give maximum photoconduction efficiency, i.e. in specimens which are *p*-type produced by oxidation of *n*-type material under closely specified conditions.[13] We assume from detailed consideration of results that the emission arises from electron transitions between levels very close to the bottom of the conduction band and the top of the valence band, charge carriers being trapped before these transitions occur. This would appear to be supported by BLOEM's work on defect levels in lead sulphide.[14]

It would be interesting now, as in the case of cuprous oxide above, to make measurements of carrier and luminescence decay times at various temperatures in order to correlate photoconduction and emission processes.

### 3.3. *Mercury sulphide*

Mercury sulphide in the form of red cinnabar has been known for a long time as a photoconductor. In recent years HAMILTON[15] of the author's laboratory succeeded in making single crystals of the material of higher purity than natural crystals. The emission of mercury sulphide is shown in Fig. 7 together with examples of mixed cadmium–mercury sulphide.[1]

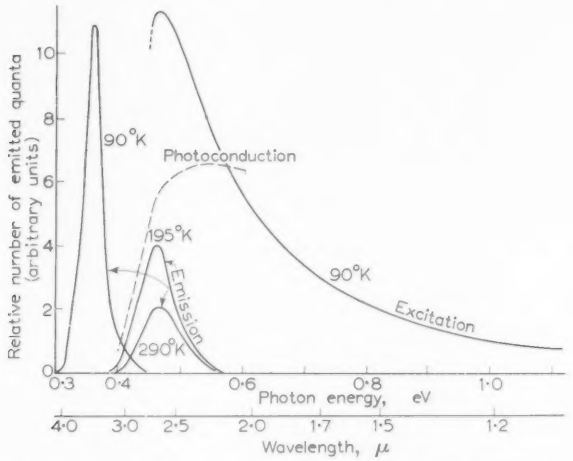


FIG. 6. Excitation, emission and photoconduction response spectra for a typical lead sulphide specimen.

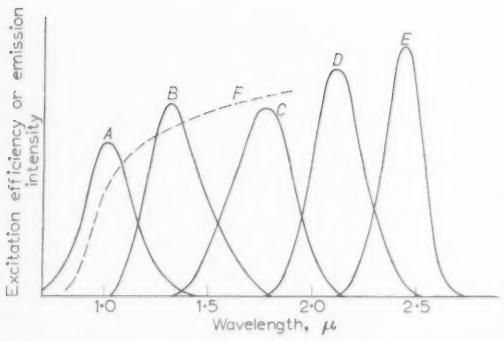


FIG. 7. Emission spectra of cadmium–mercury sulphide phosphors and excitation spectrum for mercury sulphide. A. CdS; B. CdS(70%)–HgS(30%); C. CdS(25%)–HgS(75%); D. HgS at 290°K; E. HgS at 90°K; F. Excitation spectrum for D.

For pure mercury sulphide it will be seen that the emission band is single and, as in the case of lead sulphide, moves to longer wavelengths with decreasing temperature. The excitation spectrum is similar to that of lead sulphide but the position of the emission is well outside the absorption edge and well beyond the usual limit of photoconduction response. Although for the mixed cadmium–mercury sulphides a complete range of solubility is shown and although the emission band shifts uniformly with mercury content, the excitation spectra show a more complex behaviour. BROWNE[3] suggests that, in contrast to the usual emission for zinc and cadmium sulphides, the emission for mercury sulphide is due to transitions in anion rather than cation vacancies, it being difficult to retain mercury in the lattice during preparation. We hope to re-explore the matter by reheating single crystals made by Hamilton's techniques in mercury vapour under controlled vapour pressure and temperature conditions. Again more effort to try and correlate photoconduction and luminescence characteristics is indicated.

### 3.4. *Zinc and cadmium sulphides*

Following the initial discovery of infrared emission in zinc sulphide[1] BROWNE[3] has made a much more extensive investigation of the emission in the zinc–cadmium sulphide system. Typical emission and excitation spectra are shown in Figs. 8 and 9 respectively. A series of important conclusions have been reached from his results which provide the bases of a much more comprehensive theory of zinc sulphide phosphors:

(1) The emission bands do not shift much in position from zinc to cadmium sulphide in contrast to the shift of the usual emission bands from the visible into the near infrared region. This suggests that they are associated with perturbed levels of the valence band (characteristic of anions).

(2) The excitation bands for infrared emission coincide with the quenching spectra for the visible emission and photoconduction. This supports the conclusion in (1) above.

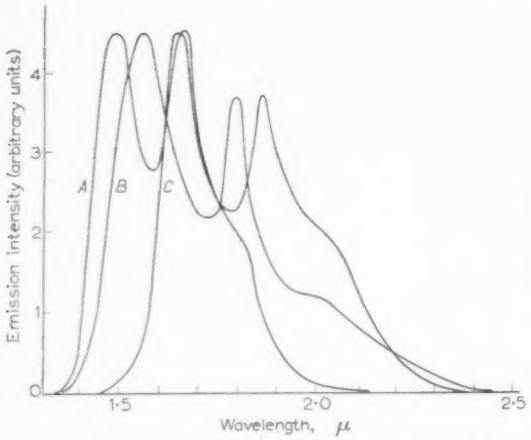


FIG. 8. Infrared emission spectra of zinc and cadmium sulphide phosphors. (a) ZnS (b) ZnS (50%)–CdS (50%) (c) CdS (after BROWNE[3]).

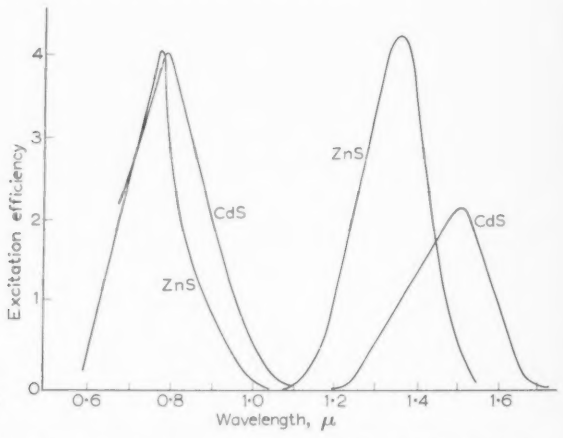


FIG. 9. Excitation spectra for infrared emission for zinc and cadmium sulphide phosphors (after BROWNE[3]).

(3) The relation of infrared emission excitation conditions to phosphor preparation conditions suggests that the important luminescence centres in these phosphors are due to cation vacancies.

(4) It is possible to explain both visible and infrared emission in terms of transitions to and from the cation vacancy levels as given by BROWNE's energy band scheme, shown in Fig. 10(a).

From further consideration of BROWNE's results in relation to more recent measurements on cadmium telluride in this laboratory by R. A. Fatehally and data on this group as photoconductors obtained by BUBE,[16] we prefer the model shown in Fig. 10(c) which is a modified form of that due to BUBE shown in Fig. 10(b). The levels lying close to the valence band are brought into evidence in the study of the anomalous dependence of the decay time of the infrared emission on temperature (see later for cadmium telluride). The latter is constant up to a certain temperature beyond which it increases rapidly due to the depopulation of the levels by thermal activation of positive holes into the valence band. At present the above models are not completely satisfactory and we are planning further experiments on the luminescence and electrical properties of single crystal specimens.

### 3.5. *Cadmium telluride*

The zinc, cadmium and mercury sulphides are characterized by a hexagonal lattice structure (zinc sulphide can also of course exist in the zinc-blende form) but the basic lattice unit is tetrahedral. Cadmium telluride exists in the zinc-

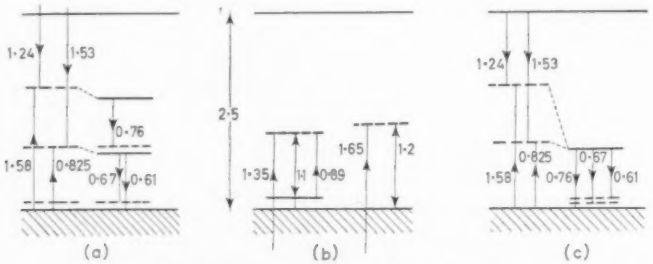


FIG. 10. Energy band models for luminescence in zinc and cadmium sulphide phosphors: (a) due to BROWNE,[3] (b) due to BUBE,[16] (c) modified model (all energy values in eV).

blende form but with the same basic lattice unit as for the above phosphors. However, its luminescence shows different features from the other phosphors and provides interesting new information on a II–VI compound which is already of considerable interest as a photo- and semi-conductor. It has been extensively studied from the point of view of emission by R. A. Fatehally of the author's laboratory and independently, with marked differences in results, by DE NOBEL.[17]

Cadmium telluride is synthesized with relative ease from its constituent elements, but to make specimens of controlled constitution and departure from stoichiometry ($p$- or $n$-type) is more difficult. We found it most suitable to adopt the preparation techniques developed by KRÖGER and DE NOBEL[18] and by VAN DOORN and DE NOBEL[19] using a controlled vapour pressure of cadmium over the previously prepared specimen, and with a selected temperature to obtain $p$- or $n$-types. We also deliberately "doped" some specimens by small additions of, e.g., chlorine (as HCl vapour) or copper. Fig. 11 gives R. A. Fatehally's results for specimens (notably In and Ag as in the experiments of KRÖGER and DE NOBEL) we were able by electrical measurements to determine the specimen type and approximate carrier concentrations (as given in Fig. 11).

No Franck–Condon shift between excitation and emission bands is found for cadmium telluride and coincidence with excitation bands for photoconduction and photovoltaic effects is also found. This would appear to indicate that cadmium telluride has a predominantly homopolar binding. Measurements of refractive index by apparent depth measurements using an infrared microscope have been made by J. Hough of the author's laboratory. Results indicate little difference between the optical and static dielectric constants and confirm the assumption of homopolar binding. This is a somewhat different conclusion from those reached separately by DE NOBEL[17] and by GOODMAN.[20]

Addition of copper chloride produces a new emission peak at 1·35 $\mu$. This suggests that copper behaves as an acceptor impurity providing a

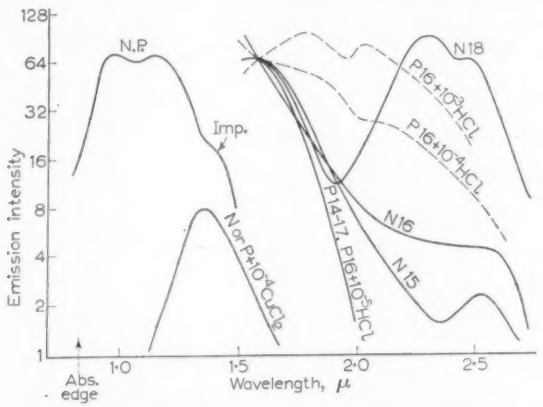


FIG. 11. Typical emission spectra of cadmium telluride specimens. $n = n$ type; $p = p$ type; Numbers 14–18 signify approximate $\log_{10}$ carrier concentration.

the emission spectra of various specimens. Five different bands are found in undoped specimens, their occurrence depending on specimen type as shown. It seems clear that the longer wavelength bands occur when energy states in defect centres have their normal electron population increased by increasingly "$n$-type" preparation conditions. By using various electrode materials on the level (or levels) near to the valence band, the necessary electron being supplied by the chlorine inclusion. The latter by itself produces more $n$-type behaviour in otherwise $p$-type specimen (see curves of Fig. 11) with some shift of the longer wavelength band peaks being evident. This could be explained by the perturbation due to chlorine substitution in the lattice. DE NOBEL has shown that the rate of

cooling of specimens after preparation has a marked effect on properties. He uses a rapid rate, ostensibly to avoid aggregation of lattice vacancies, but it would seem to encourage the formation of large strain regions in the specimens. He only observes the two shorter wavelength emission bands of Fig. 11. We employed much slower cooling for our specimens. However, further work on the effect of cooling rate is important and also on doping with elements such as gold and indium as carried out by DE NOBEL.

Decay time measurements by R. A. Fatehally have revealed an anomalous variation with temperature as shown by BROWNE[3] for zinc and cadmium sulphides. A quantitative theory for this behaviour has now been developed and will be published later. It enables the complex decay characteristics to be correlated with the efficiency–temperature relations for each band and also prompts further measurements on carrier life times in the single crystal specimens now available to us.

With respect to the energy band diagram for cadmium telluride the correlation between emission bands and specimen type (*n* or *p*) suggests that increase in electron population fills the vacancy levels already existing. It might be assumed with some safety that the two shorter wavelength emission bands are characteristic of transitions involving cation vacancies. Longer wavelength bands might be due to higher-lying levels in those vacancies or to levels of the anion vacancies (cation and anion being used to distinguish cadmium and tellurium respectively although the ionic charge on each in the lattice may be very small under predominantly homopolar conditions). Detailed results from R. A. Fatehally's work suggest the energy diagram of Fig. 12(b). In Fig. 12(a) we give a tentative energy band scheme proposed by DE NOBEL.[17] There are similar features in the two diagrams although DE NOBEL requires fewer levels in the forbidden zone than we do to explain his results. His cation vacancy levels when combined would provide one of the centres of our model and would explain three of the observed emission bands of Fig. 11 (1·3, 0·78 and 0·54 eV) and the occurrence of only one of them in *p* type specimens (1·3 eV) since a low Fermi level position would obtain. A new band in the emission for copper activation, would also be expected by inspection of DE NOBEL's results. If, as is found in our results (see Fig. 11) copper impurity causes a suppression of the usual emission bands of cadmium telluride then we may assume that it is likely to be sited in the cadmium vacancies. To explain the 1·06 and 0·48 eV emission bands is more difficult although from Fermi level considerations we would expect the 1·06 eV band to occur in most specimens and the 0·48 eV band only in *n*-type specimens. Reference to DE NOBEL's results rules out the possibility of these levels being due to interstitial cadmium (this would in any case be absent in *p*-type specimens). The occurrence of these levels may be due to vacancy aggregates in our specimens which were cooled slowly after preparation compared with the rapid quenching of DE NOBEL's specimens. We hope to have more single crystal studies completed soon. Until then, the model shown must be regarded as tentative.

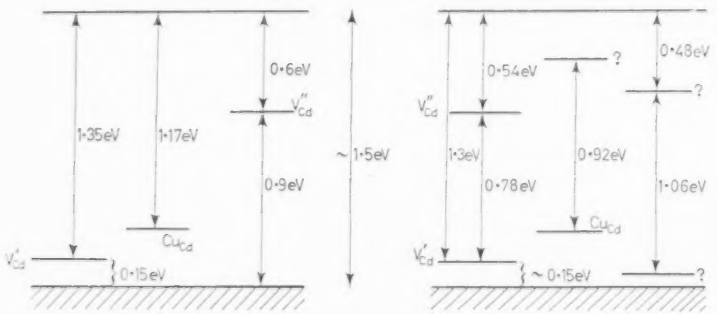


FIG. 12. Energy band schemes for cadmium telluride: (a) due to DE NOBEL,[17] (b) scheme deduced from our own results.

It will also be valuable to divert some effort to a further study of cadmium selenide since this is intermediate between the zinc–cadmium sulphides and cadmium telluride. In early studies of cadmium selenide we found emission at 1·35 eV and 1·03 eV the total band gap being 1·74 eV. However, we found no smaller energy emission bands further into the infrared at that time. BUBE's results for quenching of photocurrents in cadmium sulphide show quenching bands at 1·2, 1·05 and 0·79 eV which are difficult to correlate with the emission bands with which there is marked overlap. Clearly, new observations on emission and conduction in single crystals are desirable to examine these differences. We have also measurements proceeding on cadmium–mercury telluride mixed crystals.

## 4. CONCLUSION

Luminescence research has now reached the stage where specimens are available in which emission properties can be correlated with other characteristics such as photoconduction. Such specimens are already of considerable importance as semiconductors. Infrared emission studies could be extended to various solids not dealt with above. For example, we have had no opportunity so far to apply our techniques to doped germanium and silicon crystals having forbidden zone levels likely to involve transitions in the energy region covered by our detectors. It would also be interesting to look for infrared electroluminescence as distinct from the injection and recombination emission already measured in this region for germanium, etc. With the likely development of efficient detectors such as indium antimonide and doped germanium in the near future it should be possible, with the help of very low temperatures, to extend the field of luminescence studies to much longer wavelengths.

## REFERENCES


1. GARLICK G. F. J. and DUMBLETON M. J. *Proc. Phys. Soc.* B **67,** 442 (1954).
2. (a) DUMBLETON M. J. *Proc. Phys. Soc.* B **68,** 53 (1955); (b) *Brit. J. Appl. Phys. Suppl.* **4,** S.88 (1955).
3. BROWNE P. F. *J. Electronics* **2,** 1, 95 (1956).
4. FRANKS J. *Proc. Phys. Soc.* B **70,** 892 (1957).
5. KLICK C. C. and SCHULMAN J. H. *J. Opt. Soc. Amer.* **42,** 910 (1952).
6. MULLIKEN R. S. *Rev. Mod. Phys.* **4** (1932).
7. MOSS T. S. *Photoconductivity in the Elements.* Butterworths, London (1952).
8. HOOGENSTRAATEN W. *J. Electrochem. Soc.* **100,** 356 (1953).
9. LASHKAREV V. E. and KOSSONOGOVA K. M. *Dokl. Akad. Nauk. SSSR* **54,** 125, (1946).
10. GARLICK G. F. J. Photoconductivity *Handbuch der Physik* **19,** 316. Springer, Berlin (1956).
11. BLOEM J. *Philips Res. Rep.* **13,** 167 (1958).
12. GALKIN L. N. and KOROLEV N. V. *Dokl. Akad. Nauk. SSSR* **92,** 529 (1953).
13. SMITH R. A. *Advanc. Phys.* **2,** 321 (1953) (Review).
14. BLOEM J. *Philips Res. Rep.* **11,** 273 (1956).
15. HAMILTON D. R. *Brit. J. Appl. Phys.* **9,** 103 (1958).
16. BUBE R. H. *Proc. Inst. Radio Engrs.* **43,** 1836 (1955).
17. DE NOBEL D. Dissertation, Leiden (May 1958).
18. KRÖGER F. A. and DE NOBEL D. *J. Electronics* **1,** 2, 190 (1955).
19. VAN DOORN C. Z. and DE NOBEL D. *Physica* **22,** 338 (1956).
20. GOODMAN C. H. L. *J. Electronics* **1,** 2, 115 (1955).


*J. Phys. Chem. Solids* Pergamon Press 1959. Vol. 8. pp. 457–461. Printed in Great Britain

Q.3

# TEMPERATURE DEPENDENCE OF THE OPTICAL BAND GAP IN ZnS

**W. W. PIPER, P. D. JOHNSON and D. T. F. MARPLE**
General Electric Research Laboratory, Schenectady, New York

## 1. INTRODUCTION

THE temperature dependence of the band gap of ZnS[1] is in part due to the effects of lattice dilatation, as determined by measurements on single crystals under hydrostatic pressure.[2] It has been found that above room temperature the expression derived by FAN[3] for the shift due to electron–phonon coupling in polar crystals can account for

the remaining shift in absorption edge only if large effective electron or hole masses are assumed.[2] We have now extended the measurements to 4°K in order to further study the temperature dependence of the band gap at low temperatures.

## 2. EXPERIMENTAL

Transmission measurements were made with a recording spectrophotometer and a previously described cryostat[4] with sample holder modified to improve heat shielding and provided with a copper–constantan thermocouple for approximate indication of temperature. Measurements with dry ice–acetone, liquid $N_2$, liquid $H_2$ and liquid He were not detectably affected by increasing radiation intensity incident on the sample up to several times the intensity used in the measurements reported here. The temperatures were taken to be published temperatures of the coolants. The optical system used previously[2] was converted to a ratio measuring system similar in principle to that developed by HORNIG *et al.*[5] Adjacent to the 1 mm hole in the sample holder covered by the crystal was another similar hole for measurement of the unattenuated beam. The spectral band width was 3 to 5 Å at the absorption edge. For more accurate determination of the wavelengths and widths of absorption bands and for a search for absorption lines a 2 m Bausch and Lomb grating spectrograph with 4 Å/mm dispersion was used. The spectral band width used with this instrument was less than 0·05 Å. Spectra were obtained with both polarized and unpolarized ultraviolet light.

Measurements were made on synthetic single crystals of hexagonal ZnS ranging in thickness from 0·08 to 40 $\mu$ thick as determined from interference fringes. These crystals were grown from the vapor phase in this laboratory. They were platelets with good optical surfaces and a surface area greater than 1 mm². The $c$-axis was parallel to the plane of the surface.

The spectral variation of the absorption coefficient was deduced from the transmission data with the aid of an expression derived by BARNES and CZERNY for a flat plate.[6] If $\alpha\lambda \ll 4\pi$ and interference effects are averaged, their expression reduces to:

$$T_{av} = \frac{(1-R)^2 \exp(-\alpha d)}{1-R^2 \exp(-2\alpha d)} \qquad (1)$$

where $\alpha$ is the absorption coefficient and $d$ the thickness of the plate. $R$ is the reflectivity at one interface and was calculated by Fresnel's equation using the index of refraction determined as a function of wavelength and temperature from the spacing of interference fringes. For the crystals which were thinner than 5 $\mu$, the band width of the recording spectrophotometer was only a small fraction of an interference fringe and a strong interference pattern resulted. In these cases the expression, which is exact for ideal interference with zero band width,

$$T_{av} = (T_{max} \times T_{min})^{\frac{1}{2}}, \qquad (2)$$

was used to obtain a $T_{av}$. A correction factor, constant for a given crystal, always less than 5 per cent and thought to be due to scattering by the crystal, was used to correct $T_{av}$ computed from observed transmission to agree with the theoretical value at a wavelength where no absorption would be expected.

## 3. RESULTS AND DISCUSSION

In Fig. 1 the absorption coefficient is plotted as a function of photon energy for $T = 300$°K with the electric vector of the incident light both perpendicular and parallel to the $c$-axis. These curves were computed from data on several crystals. Of particular interest is the fact that the absorption curve shifts with temperature but retains the same shape up to an absorption coefficient of 5000 cm$^{-1}$, in conflict with Urbach's rule. This is also evident in Fig. 2 where the temperature shift is seen to be the same at coefficients of 300 cm$^{-1}$ and 5000 cm$^{-1}$. DUTTON[7] has reported that Urbach's rule applies to CdS up to an absorption coefficient of $10^4$ cm$^{-1}$. It will be noticed also that the temperature shift is independent of the polarization of the incident radiation.

At low temperatures it is quite evident from Fig. 1 that there is structure in the region of strong absorption. Narrow bands are observed at 3107, 3155, 3179 and 3202 Å, at 4°K.† The strongest band, at 3179 Å, is found to shift with temperature the same amount as the rest of the absorption

† The two bands at shorter wavelengths are approximately 15 Å wide at half their peak absorption whereas the other two bands are only about 4 Å wide.

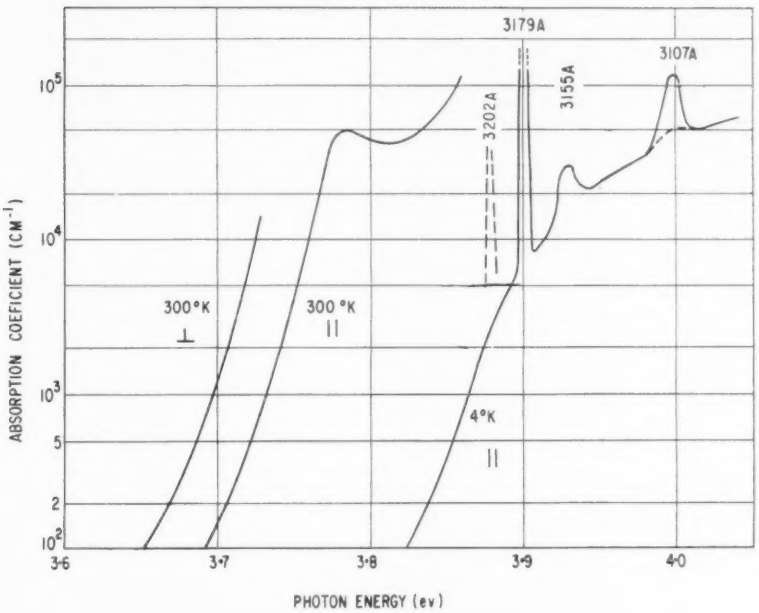


FIG. 1. Absorption coefficient as a function of photon energy and polarization direction as deduced from several crystals of hexagonal ZnS. The solid curve at liquid helium temperature is for the electric vector polarized parallel to the $c$-axis. Perpendicular to the $c$-axis absorption peaks are found at 3155 Å, 3179 Å and 3202 Å.

curve. The position of this band at liquid He, $H_2$ and $N_2$ temperatures was measured carefully with the Bausch and Lomb spectrograph.

Using the temperature dependence of volume reported by ADENSTEDT[8] for cubic ZnS and the pressure dependence of the band gap,[2] the shift of the band gap due to dilatation, $\Delta E_d$, can be computed. The shift due to the electron interaction with optical phonons, $\Delta E_{ep}$, may be computed from the FAN expression if the effective masses are known.[3] The total shift that would be expected from these two effects,

$$\Delta E = \Delta E_d(T) + \Delta E_{ep}(m^*, T),$$

has also been plotted in Fig. 2 for the two cases $(m^*/m_0) = 3{\cdot}3$ for both electrons and holes and $(m^*/m_0) = 1$. As we have previously pointed out, effective masses of $3{\cdot}3\ m_0$ will account for the magnitude of the shift at room temperature and above, although such a mass results in a coupling constant so large that the perturbation calculation of FAN is no longer valid.

Independent of the effective mass one chooses to assume, there remains a temperature dependence below 150°K which cannot be explained by either the thermal contraction of the crystal or the interaction with optical phonons. The crystals were cemented at one corner on to a flat copper plate. The grossly different geometry of the crystals examined and the agreement among the crystals would seem to eliminate the possibility of strain inducing a spurious shift.

MEIJER and POLDER[9] have pointed out that in ZnS there are piezoelectrically active acoustical modes which become relatively more important than the optical modes for electron scattering below 150°K. The shift of the band edge due to these piezoelectric modes has not been calculated, but this would appear to be the most probable explanation of the temperature dependence or the band edges in the region of low temperature.

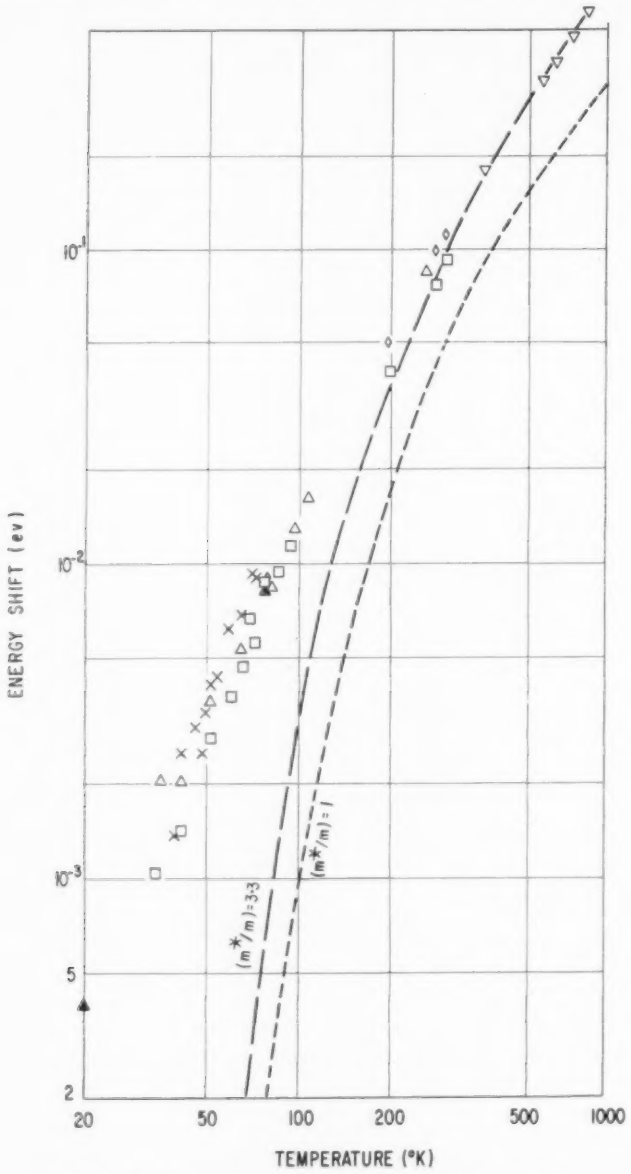


FIG. 2. The temperature dependence of the fundamental absorption edge and absorption band. The energy shift relative to 4·2°K is plotted for the 3179 Å band (x = recording spectrometer and ▲= spectrograph), for $\alpha =$ 5000 $cm^{-1}$ and $E \parallel C$ (△), for $\alpha = 300$ $cm^{-1}$ and $E \parallel C$ (□), for $\alpha = 300$ $cm^{-1}$ and $E \perp C$ (◇), and for $\alpha = 50$ $cm^{-1}$ (VAN DOORN[1]) (▽). The theoretically expected shift due to the combined effects of dilatation and electron interaction with optical phonons is plotted for $(m^*/m_0)=$ 3·3 and 1·0.

*Acknowledgments*—We are indebted to T. H. RAUTENBERG and F. C. MOSTEK for extensive help in obtaining high dispersion data on the Bausch and Lomb spectrograph. The assistance of S. J. POLICH in growing specimens of ZnS is also gratefully acknowledged.

### REFERENCES

1. VAN DOORN C. Z. *Physica* **20,** 1155 (1954).
2. PIPER W. W., MARPLE D. T. F., and JOHNSON P. D. *Phys. Rev.* **110,** 323 (1958).
3. FAN H. Y. *Phys. Rev.* **82,** 900 (1951).
4. JOHNSON P. D. and STUDER F. J. *Phys. Rev.* **82,** 976 (1951).
5. HORNIG D. F., HYDE G. E. and ADCOCK W. A. *J. Opt. Soc. Amer.* **40,** 497 (1950).
6. BARNES R. B. and CZERNY M. *Phys. Rev.* **38,** 338 (1931).
7. DUTTON D. *Phys. Rev.* **112,** 785 (1958).
8. ADENSTEDT H. *Ann. Phys., Lpz.* [5] **26,** 69 (1936).
9. MEIJER H. J. G. and POLDER D. *Physica* **19,** 225 (1953).

VOL. 8 1959

*J. Phys. Chem. Solids* Pergamon Press 1959. Vol. 8. pp. 461–464. Printed in Great Britain

# SOME CHARACTERISTICS OF LARGE BAND GAP COMPOUND SEMICONDUCTORS

**J. S. PRENER and F. E. WILLIAMS**
General Electric Research Laboratory, Schenectady, New York

## 1. COMPENSATION OF DONOR OR ACCEPTOR IMPURITIES

DONOR or acceptor impurities present in small concentrations in a solid binary compound constitute charged species, when ionized at the high temperatures used in the preparation of semiconducting solids. The ionized impurities must be charge compensated in the solid and one mechanism for doing this is by means of free charge carriers. For example, donor impurities $D^+$ in the solid MX may be compensated by conduction electrons $n$:

$$D^0 \text{ (in solid MX)} \rightarrow (D^+ + n) \text{ (in solid MX)} \quad (1)$$

In addition, however, metal or non-metal vacancies or interstitials may give rise to acceptor or donor states and thereby provide charged imperfections for the compensation of charged impurities. For example, the donor impurities $D^+$ may be compensated by metal vacancies $V_M^-$:

$$D^0 \text{ (in solid MX)} \rightarrow (D^+ + V_M^-) \text{ (in solid MX)} + M \text{ (gas phase)} \quad (2)$$

The solid MX containing donors or acceptors in equilibrium with a vapor phase containing M and X is a trivariant system; the temperature, total pressure and impurity concentration determine the composition of the solid phase. For a given material, temperature and impurity concentration, the mechanism of compensation which dominates will therefore depend on the total pressure which in turn fixes the pressure of M and X. Charge compensation of ionized donors will occur primarily by mechanism (1) if $\Delta F_1 < \Delta F_2$, whereas mechanism (2) will dominate if the reverse is true. The free energy changes for the two reactions can be computed with the result that if

$$\ln p_M < \ln\left[\tfrac{1}{4}N_0 kT\left(\frac{m_M}{m_e}\right)^{3/2}\right] + \frac{(E_g - E_A) - E_M}{kT} \quad (3)$$

mechanism (2) will dominate. The metal pressure in the gas phase is $p_M$, $N_0$ is the number of metal atoms per cm$^3$ in the solid, $m_M$ and $m_e$ are the masses of the metal atom and the electron, $(E_g - E_A)$ the band gap less the energy of the acceptor level and $E_M$ the energy required to

form a neutral metal vacancy. For acceptor impurities, compensation by non-metal vacancies will occur in accordance with an expression identical with equation (3) except that the subscripts M and A are replaced by X and D. We conclude that the pressure limits which lead to compensation by vacancies are exponential in the approximate difference between the band gap and the energy of formation of the appropriate vacancy. Association of donors and acceptors, the presence of multiple donors and acceptors, and the existence of $X_2$ in the gas phase complicate the analysis but similar conclusions can be obtained.

## 2. ASSOCIATION OF DONORS AND ACCEPTORS

Since ionized donors and acceptors constitute charged species in the solid, they interact coulombically and consequently are not randomly distributed.[1] Using the analysis developed for the association of ions in aqueous solutions,[2] but modifying the treatment to take into account the discretized nature of the solid, the fraction $\alpha_i$ of pairs of oppositely charged species separated by the distance $r_i$ in the solid is given by:[3]

$$\alpha_i = AcZ_i[\exp(-q_1q_2/Kr_ikT)][\exp(-c\sum_{j=1}^{i}Z_j)] \quad (4)$$

Here $c$ is the concentration of the charged species, $Z_i$ the number of sites available to a charged defect at a distance $r_i$ from a defect of the opposite sign, $q_1$ and $q_2$ the charges of the defects, $K$ the static dielectric constant of the solid and $A$ a normalization constant. The application of equation (4) to ZnS with $10^{18}$ cm$^{-3}$ donor and acceptor densities indicates a high degree of association at the temperature below which diffusion over interimpurity distances cannot occur. The electronic and optical properties of these materials will, therefore, depend on the characteristics of associated donor-acceptor pairs.

## 3. ENERGY LEVEL STRUCTURES OF ASSOCIATED PAIRS

The associated pairs have different energy level structures depending on the interimpurity separation $r_i$ of donor and acceptor. For nearest neighbor pairs the system has been approximated by considering the electron and hole individually bound in a finite dipole field and neglecting electron–hole interactions.[1] These dipole states have energies several orders of magnitude smaller than the coulomb states of the separated donor or acceptor. More recently, HOOGENSTRAATEN[4] has considered the energy levels of the pairs as perturbed coulomb states but neglected the effect of the overlap of the separated donor and acceptor wavefunctions. We have re-examined the problem taking into account electron–hole interactions. The analysis follows closely the Heitler–London treatment of the hydrogen molecule. The system can be described as an exciton bound in the field of a finite dipole and, therefore, involves excited crystal states. The Hamiltonian for this system in a medium of dielectric constant $K$ is

$$H = -\frac{\hbar^2}{2}\left(\frac{1}{m_-}\Delta_- + \frac{1}{m_+}\Delta_+\right) + \frac{e^2}{K}\times$$
$$\times\left(-\frac{1}{r_{A+}} - \frac{1}{r_{D-}} + \frac{1}{r_{A-}} + \frac{1}{r_{D+}} - \frac{1}{r_{+-}} - \frac{1}{r_i}\right) \quad (5)$$

where $r_{kj}$ refers to the interparticle distances of the electron $-$, hole $+$, donor D, and acceptor A. The two particle wavefunction is taken as a single product of the separated donor and acceptor wavefunctions:

$$\psi(-,+) = \psi_D(-)\psi_A(+). \quad (6)$$

The permuted function $\psi_D(+)\psi_A(-)$ is not part of the bound exciton state since this product refers to a configuration of quite different energy. From the Hamiltonian and the wavefunction, the total energy $E$ is found to be:

$$E = E_D + E_A + J \quad (7)$$

where $E_D$ and $E_A$, respectively, are the energies of the separated donor and acceptor, and $J$ can be described as the coulombic integral and is equal in magnitude but opposite in sign to the corresponding integral for the hydrogen molecule in a medium with dielectric constant $K$. No exchange integral appears in the energy of the donor–acceptor pair. For donor and acceptor states both characterized by one particle wavefunction of the form $\pi^{-\frac{1}{2}}a^{-\frac{3}{2}}e^{-r/a}$, $J$ is:

$$J = -\frac{e^2}{Ka}e^{-r_i/a}\left[\frac{a}{r_i} + \frac{5}{8} - \frac{3}{4}\frac{r_i}{a} - \frac{1}{6}\frac{r_i^2}{a^2}\right] \quad (8)$$

The parameter $a$ contains the dielectric constant $K$ and the effective masses of electron and positive hole which in the above analysis have been taken to be equal. The ionization energy $E_I$ involved in ionizing both hole and electron into their respective conduction bands is:

$$E_I = E_D + E_A + J + \frac{e^2}{Kr_i}. \quad (9)$$

The term $e^2/Kr_i$ arises because the core interaction remains following ionization.

Except for systems in which $a/r_i \geqslant 1$ where the Heitler–London method is no longer valid, $E_I$ decreases monotonically with increasing degree of association; the coulomb states being perturbed towards their respective band edges. For $a/r_i \ll 1$, $J \to 0$ and equation (9) becomes equal to the result obtained neglecting overlap of the donor and acceptor wavefunctions. The energy level structure of an associated pair depends, of course, on the state of excitation since $r_i$ and the other nuclear coordinates are different for different states of excitation.

### 4. RADIATIVE RECOMBINATION IN ASSOCIATED DONOR-ACCEPTOR SYSTEMS

As a consequence of the association of donors and acceptors into pairs in binary semiconductors with relatively low dielectric constants, it is necessary to consider radiative recombination in these pairs, as well as the direct interband transition and transitions between the bands and isolated donors or acceptors. The luminescent emission of ZnS containing Group IB or VB acceptors and Group IIIB or VIIB donors has been attributed to pairs with interimpurity spacing $r_i$ such that radiative transitions occur from excited donor states to the ground state of the acceptor.[1] The transition energy for emission is therefore dependent on the identity of the acceptor but not of the donor. The ground state of the donor for these pairs will function as an electron trap. More recently, an additional longer wavelength emission band has been investigated in ZnS containing Cu or Ag acceptors and Ga or In donors. This emission arises from donor–acceptor pairs sufficiently closely associated so that radiative transitions occur directly from the ground state of the donor to the ground state of the acceptor.[5] The transition energy for the longer wavelength emission is, therefore, dependent on the chemical identity of both donor and acceptor. The spectra and the dependence on temperature and on pair concentrations of the intensities of the short and long wavelength bands are in accord with the identification of the pairs and of the transitions responsible for radiative recombination.

### 5. METAL VACANCY-IMPURITY DONOR PAIRS

The study of ZnS containing IIIB or VIIB donor impurities has also indicated that negatively charged Zn vacancies can associate strongly with the positively charged donor to give an associated pair of defects which give rise to localized acceptor states and is responsible for the blue fluorescence observed in these materials.[6] That this luminescent center contains a zinc vacancy is indicated by the decrease in intensity of the blue fluorescence with decreasing sulfur pressure. The model also predicts a decrease in the concentration of these centers at high sulfur pressures, and this has been observed by KRÖGER *et al.* in CdS:Ga.[7] That the donor is part of the center is shown by the difference in emission spectra depending on whether a Group IIIB or VIIB donor is used. The observed shift in peak position of the emission of 80 Å is in accord both as to magnitude and direction with the prediction based on a model of the center in which the vacancy and donor are considered to be point charges, $-2$ and $+1$, imbedded in a polarizable medium whose static dielectric constant is that of ZnS.[8]

### 6. NON-METAL VACANCY DONORS IN ZnS

Recently we have investigated the infrared emission in ZnS containing copper as an acceptor impurity. In certain phosphors this emission can be excited by infrared radiation alone and has been interpreted as indicating the presence of un-ionized copper acceptors. The addition of donor impurities such as Al causes a marked decrease in the intensity of this emission. That sulfur vacancies may also act as donors is indicated by an increase in the intensity of this emission with increasing sulfur pressure.*

* This has been observed independently by AVEN and POTTER of the Lamp Development Department of G.E. and by APPLE and PRENER of this laboratory.

**REFERENCES**

1. PRENER J. S. and WILLIAMS F. E. *J. Phys. Radium* **17,** 667 (1956); *Phys. Rev.* **101,** 1427 (1956).
2. FUOSS R. M. *Trans. Faraday. Soc.* **30,** 967 (1934); REISS H. *J. Chem Phys.* **25,** 400 (1956).
3. PRENER J. S. *J. Chem. Phys.* **25,** 1294 (1956).
4. HOOGENSTRAATEN W. Thesis, Univ. of Amsterdam (1958).
5. APPLE E. F. and WILLIAMS F. E. *J. Electrochem. Soc.*, in press.
6. PRENER J. S. and WILLIAMS F. E. *J. Chem. Phys.* **25,** 361 (1956).
7. KRÖGER F. A., VINK H. J., and VAN DEN BOOMGAARD J. Z. *Phys. Chem.* **203,** 1 (1954).
8. PRENER J. S. and WEIL D. J. *J. Electrochem. Soc.*, in press.

*J. Phys. Chem. Solids* Pergamon Press 1959. Vol. 8. pp. 464–466. Printed in Great Britain

Q.5

# SPACE-CHARGE-LIMITED CURRENTS AS A TECHNIQUE FOR THE STUDY OF IMPERFECTIONS IN PURE CRYSTALS

**M. A. LAMPERT, A. ROSE and R. W. SMITH**
RCA Laboratories, Princeton, New Jersey

VOL
8
195

BY sweeping the Fermi level through the forbidden gap a great deal of information can be obtained about localized defect states in a crystal. The *minimum possible* departure from thermodynamic equilibrium is achieved if the position of the SSFL (steady-state Fermi level) is controlled through manipulation of a *single* type of carrier, namely through the voltage-controlled injection of excess carriers of one sign of charge. So long as the applied field does not substantially alter the velocity distribution of the free carriers, *all* states in the forbidden gap remain, under steady-state conditions, in normal thermal contact with the free carriers. For this reason, *all* localized states in the forbidden gap are "felt out" by the SCLC (space-charge-limited current).

The usefulness of the SCLC technique for obtaining data on imperfections is forcefully illustrated by recent measurements on single crystals of CdS. An experimental current–voltage curve* is shown in Fig. 1. As we shall see later, these measurements correspond to a situation where a set of defect states at a single, discrete energy level $E_t$ dominates the nearby energy region in the forbidden gap, and further where the defect level lies above the thermal-equilibrium Fermi level $E_{\bar{F}}$. This situation is illustrated by an energy-band diagram in Fig. 2. $E_c$ and $E_v$ are the conduction-band minimum and valence-band maximum energy levels respectively. $E_F$ is the steady-state electron† Fermi level, defined with respect to the free electron density is in the usual manner through the relation: $n = N_c \exp[(E_F - E_c)/kT]$ with $N_c$ the effective density of states in the conduction band. At thermal equilibrium $E_F$ coincides with $E_{\bar{F}}$.

In order to interpret and make use of the experimental curve of Fig. 1 we shall first examine the general structure of the $J$–$V$ (current density–voltage) characteristic to be expected theoretically from a crystal with the energy-level configuration shown in Fig. 2. This $J$–$V$ characteristic is the solid curve ABCDE, shown on a log–log plot, in Fig. 2. Its structure may be readily understood by following the motion of the Fermi level $E_F$ through the forbidden gap as a function of applied voltage.

(1) At low voltages there is negligible injection of excess charge into the crystal (no significant departure of $E_F$ from $E_{\bar{F}}$) and Ohm's law is observed (portion AB of the $J$–$V$ curve).

(2) SCL current sets in at that voltage $V_{TR}$ at which the density of *excess* free carriers equals $\bar{n}$, the thermal-equilibrium density, i.e. $n = 2\bar{n}$ and correspondingly $n_t = 2\bar{n}_t$, with $n_t$ and $\bar{n}_t$ the trapped carrier density under

* This work was reported on at the Chicago meeting of the APS, March 1958. See SMITH R. W. *Bull. Amer. Phys. Soc.* II **3,** 129 (1958).

† We are concerned throughout this article with one-carrier currents. For the sake of definiteness we assume that the carriers are electrons.

voltage and at no voltage respectively. This corresponds to a departure of $E_F$ from $E_{\bar{F}}$ by approximately $kT$. For a plane-parallel geometry and for $\bar{n}_t \gg \bar{n}$, $V_{TR} = ea^2\bar{n}_t/2\epsilon$ (m.k.s. units)[3], with $e$ the electronic charge, $\epsilon$ the static dielectric constant, and $a$ the cathode–anode spacing.

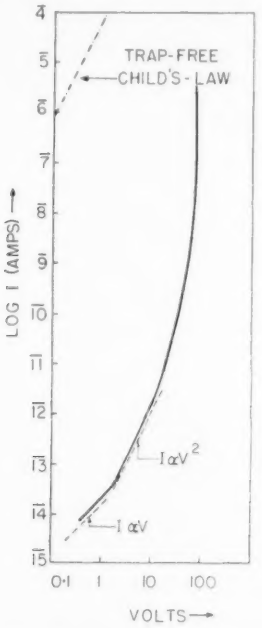


FIG. 1. Experimental current–voltage characteristic (solid line) for a single crystal of CdS. The cathode–anode spacing $a = 1{\cdot}7 \times 10^{-3}$ cm and the electrode area $\simeq 3{\cdot}5 \times 10^{-3}$ cm². The dashed lines indicate linear and square-law slopes respectively. The stippled curve is the (hypothetical) trap-free Child's law current for the same crystal.

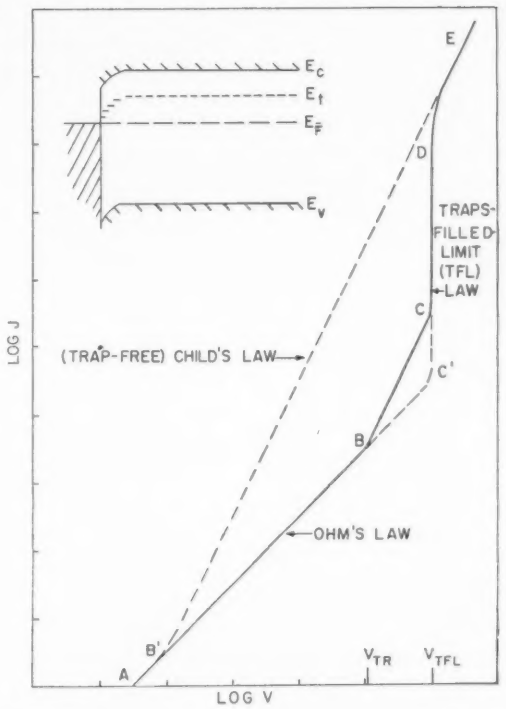


FIG. 2. Theoretical current density–voltage characteristic for a solid with plane-parallel geometry. The solid curve ABCDE refers to the case where the (dominant) traps lie at a single, discrete energy-level $E_t$ lying above the thermal-equilibrium Fermi level $E_{\bar{F}}$, illustrated by the accompanying energy-band diagram. If $E_t \lesssim E_{\bar{F}}$, then a curve such as AC′DE would be expected. If there were no traps the curve AB′E would be expected.

(3) With further increase of voltage beyond $V_{TR}$ additional excess charge is injected into the crystal and accordingly the Fermi level $E_F$ moves closer to the conduction band. So long as $E_F$ remains below $E_t$ the ratio of free to trapped carriers, $n/n_t$, is a constant independent of voltage. It follows directly from this[2] that $J \propto V^2$ in this voltage range (portion B to C of the $J$–$V$ curve).

(4) After the Fermi level $E_F$ passes through the defect level $E_t$ the current $J$ rises steeply, but reversibly, with voltage (portion CD of the $J$–$V$ curve). This sharp rise occurs[3] at the voltage $V_{TFL} = ea^2N_t/2\epsilon$, corresponding to complete filling of the defect states of density $N_t$. For $V < V_{TFL}$ excess charge is held almost exclusively in the defect states. After saturation of the defect states additional excess charge must appear in the conduction band. Thus, comparing the SCLC at voltage $2V_{TFL}$ with that at voltage $V_{TFL}$, $J(2V_{TFL})/J(V_{TFL}) \simeq (N_t/N_c)\exp[(E_c - E_t)/kT]$. At $T = 300°K$, $N_c \approx 10^{19}$ cm$^{-3}$. Taking $N_t = 10^{14}$ cm$^{-3}$ and $E_c - E_t = 0{\cdot}4$ eV, this current ratio is about 100.

(5) For $V > 2V_{TFL}$, the excess free charge dominates the excess trapped charge so that the current–voltage characteristic coincides with that for a trap-free solid, namely the Child's (square) law of Fig. 2.

What information is obtained from measurement of a $J$–$V$ characteristic such as curve ABCDE of Fig. 2? The crucial elements are the "vertical" rise CD and the square-law portion BC preceding it. The latter portion guarantees that the defect energy level lies above the thermal-equilibrium Fermi level, $E_t > E_{\bar{F}}$, and therefore that the defect states are practically all empty at the outset. Knowing this, we obtain the density of defect

states from the voltage at the "vertical" rise in current: $N_t = 2\epsilon V_{TFL}/ea^2$ (m.k.s.). A remarkable feature of this density determination is that it does not require any knowledge of basic transport quantities of the crystal, such as the effective mass $m^*$ or mobility $\mu$ of the carriers. Consequently the error in measurement should be considerably less than a factor of two—which corresponds to unusually high accuracy in the current state of the art. The minimum defect density, $N_{t,min}$, that can be measured depends on the energy location $E_t$ and the temperature. Thus, at 300°K, if $E_c - E_t = 0{\cdot}80$ eV then $N_{t,min} \approx 10^6$ cm$^{-3}$ whereas if $E_c - E_t = 0{\cdot}40$ eV then $N_{t,min} \approx 10^{13}$ cm$^{-3}$.

Further information from SCLC measurements is contingent upon knowledge of transport quantities. Thus, the $J$–$V$ characteristic in the square-law region preceding the vertical rise, segment BC of Fig. 2, can be explicitly written:[2]

$$J = \frac{2{\cdot}4\times 10^6}{gN_t}\left\{\exp\frac{(E_t - E_c)}{kT}\right\}\times$$

$$\times K\mu\left(\frac{m^*_{ds}}{m}\right)^{3/2}\frac{V^2}{a^3}\text{A/cm}^2$$

where all quantities are expressed in practical units and $T = 300$°K. Here $K$ is the relative static dielectric constant and $m^*_{ds}$ is the density-of-states effective mass. If $g$, $m^*_{ds}/m$ and $\mu$ are all known, then $E_c - E_t$ is determined from the measured current in the square-law range BC of Fig. 2. Uncertainties in these quantities are reflected in a corresponding error in $E_c - E_t$. If $E_c - E_t$ is known from other measurements then the measured square-law current, portion BC of Fig. 2, yields a determination of the product $(\mu/g)(m^*_{ds}/m)^{\frac{3}{2}}$.

If no square-law portion is observed *preceding* the vertical rise, that is, if a $J$–$V$ curve of type AC′DE of Fig. 2 is obtained, then accordingly less information is obtained from the SCLC measurement. In this case the effective defect states lie energetically at or below the Fermi level $E_{\bar{F}}$ and the vertical rise determines only the density of holes in the defect states at thermal equilibrium.

Applying the foregoing theory it is clear that the experimental current–voltage curve of Fig. 1, for a single crystal of CdS, is characteristic of a discrete defect level lying above the Fermi level $E_{\bar{F}}$. The vertical portion yields a defect density of $3 \times 10^{14}$ cm$^{-3}$. The square-law portion yields a defect energy level $E_c - E_t = 0{\cdot}8$ eV, taking $g = 2$, $\mu = 100$ cm$^2$/V-sec and $m^*_{ds}/m = 1/4$. Uncertainties in the latter quantities produce an uncertainty in $E_c - E_t$ probably not exceeding $2kT = 0{\cdot}05$ eV.

This report has been confined to discussion of *steady-state* SCL current measurements. Further information can be obtained by additional measurements of *transient* SCL currents in the same crystal on which steady-state measurements have been made. Thus the measurement of current decay can yield the capture cross-section of the defect center for free electrons. Also, recent theoretical and experimental studies (as yet unpublished) have revealed an intimate connection between SCL currents and photoconductivity. Consequently, the combination of SCLC and photoconductivity measurements provides a powerful means to disentangle kinetically occupied (recombination) centers from thermally occupied (trapping) centers. For example, photoconductive measurements on the CdS crystal responsible for the $J$–$V$ characteristic of Fig. 1 have established unambiguously that the defect centers associated with the vertical rise do not function as electron traps under photo-excitation of the crystal, but rather have a kinetically-determined occupancy and must therefore be associated with recombination centers.

Further details on the theory of SCLC in solids are contained in references 1–3. Earlier experimental work is reported in reference 4.

## REFERENCES

1. Mott N. F. and Gurney R. W. *Electronic Processes in Ionic Crystals*. Oxford University Press, New York (1940).
2. Rose A. *Phys. Rev.* **97,** 1538 (1955).
3. Lampert M. A. *Phys. Rev.* **103,** 1648 (1956).
4. Smith R. W. and Rose A. *Phys. Rev.* **97,** 1531 (1955).

*J. Phys. Chem. Solids* Pergamon Press 1959. Vol. 8. pp. 467–472. Printed in Great Britain

# ELECTRONIC PROPERTIES OF ZnO

A. R. HUTSON

Bell Telephone Laboratories, Incorporated, Murray Hill, New Jersey

**Abstract**—Hall effect measurements on doped, *n*-type single-crystals of ZnO have yielded: a density-of-states mass of $0{\cdot}5m$, a shallow donor ionization energy of 0·05 eV, and the temperature dependence of mobility. An effective mass of $0{\cdot}27m$, is derived from the donor binding energy. It is used in the computation of the optical-mode scattering, which together with some acoustical-mode scattering, fits the mobility data. Thermoelectric power measurements show the presence of a large phonon-drag ($Q_p$) contribution. The $Q_p$ saturation effect yields an effective inertial mass of $0{\cdot}07m$, and it is shown that it is approximately isotropic. Magnetoresistance measurements show that there must be at least 12 valleys in the ZnO conduction band and that the valleys are not greatly anisotropic. The small inertial mass is compatible with the density-of-states mass and the 12 valleys of small anisotropy; however, the donor binding energy and the optical-mode scattering both seem to require an effective mass larger by a factor of 4. A tentative model is suggested which might resolve this difficulty.

## 1. INTRODUCTION

Zinc oxide is well known as an electronic semiconductor with a large energy gap (3·2 eV). Its conductivity is extrinsic and *n*-type for all of the measurements to be discussed here. The donors which can be added in controlled fashion by diffusion at high temperatures followed by a rapid quench are: hydrogen,[1] interstitial zinc,[2] indium,[3] and interstitial lithium.[4] There are other donors which always seem to be present, though at very low concentrations in some crystals, which may be chemical impurities or perhaps oxygen vacancies.

Zinc oxide has the wurtzite crystal structure of crystal class 6 mm. There are two ZnO molecules per unit cell. The samples upon which most of the measurements have been performed were thin needles of hexagonal cross-section about 0·02 cm in diameter and about 1 cm in length with the needle axis corresponding to the 6-fold *c*-axis.

The experimental results which are to be discussed here have been obtained from measurements of the electrical conductivity, Hall effect, thermoelectric power, and magnetoresistance. They all relate in various ways to the structure of the conduction band in the neighborhood of the energy minima, and the interaction of conduction electrons with acoustical and optical phonons. These results will be intercompared with the aim of understanding the conduction band of ZnO on the basis of a many-valley[5] model.

We shall assume that the electric polarizability of the ZnO lattice is specified by three experimentally determined quantities: the low-frequency dielectric constant, $\varkappa = 8{\cdot}5$;[6] the high-frequency dielectric constant, $\varkappa_\infty = n^2 = 4$;[7] and the rest-strahlen frequency $\nu_t = 440\ \text{cm}^{-1}$.[8] (The polarizability appears to be very nearly isotropic.) We shall also make the usual assumption that the relaxation time giving the time rate of change of the electronic distribution function is a function of electron energy only.

## 2. DONOR IONIZATION ENERGY AND DENSITY-OF-STATES MASS

In a previous publication,[6] measurements were reported of the Hall effect and conductivity of single crystals of ZnO which had been selected for purity and then doped with hydrogen and zinc donors, allowing an analysis of the statistics of donor ionization in terms of a single donor level at an energy $E_D$ below the conduction band. The expression for the carrier concentration is then

$$\frac{n^2}{(N_D - n)N_C} = \left[\frac{m^{(N)}}{m}\right]^{3/2} D^{-1} \exp\left(\frac{-E_D}{kT}\right) \quad (1)$$

where $N_D$ is the donor concentration, $D$ is the donor degeneracy, $N_C = 2(2\pi mkT/h^2)^{\frac{3}{2}}$, and $m^{(N)}$ is the density-of-states mass for the conduction band. The logarithm of the left-hand side of equation (1) was plotted vs. $1/T$ for a number of

samples containing different concentrations of hydrogen, interstitial zinc, or interstitial lithium donors. From the common intercept of these plots, $m^{(N)}$ was estimated to have the value $0{\cdot}5m$ under the assumption that $D = 2$, corresponding to the simple spin degeneracy. The carrier concentrations were obtained from the Hall measurements assuming that $\mu_H/\mu = 3\pi/8$. For donor concentrations less than $5 \times 10^{16}$ cm$^{-3}$ $E_D$ was found to be 0·05 eV for both zinc and hydrogen donors. This result suggested that an effective mass could be estimated from a hydrogen-atom model of the donor states where

$$E_D = \frac{13{\cdot}6(m^{(H)}/m)}{\kappa^2}\text{eV} \qquad (2)$$

with the result that $m^{(H)} = 0{\cdot}27m$.

### 3. HALL MOBILITY, OPTICAL-MODE SCATTERING, AND CONDUCTIVITY ISOTROPY

The temperature dependence of the Hall mobility for a typical crystal of carrier concentration less than $5 \times 10^{16}$ cm$^{-3}$ is shown in Fig. 1.

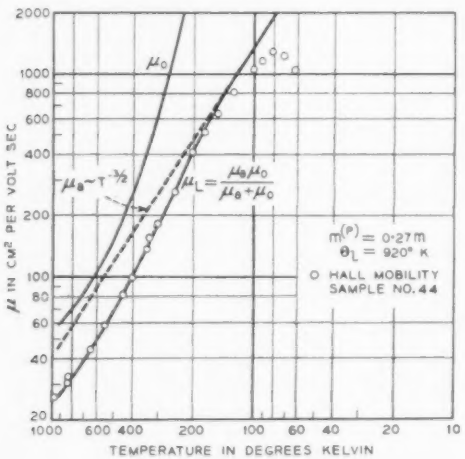


FIG. 1. Hall mobility of a typical crystal of ZnO and its analysis in terms of optical-mode and acoustical-mode scattering. $m^{(P)}$ is the polaron mass and $\Theta_l$ is the Debye temperature for the longitudinal optical modes of long wavelength.

There is some variability in $\mu_H$ from crystal to crystal at low temperatures, however, above 150°K the scattering seems to be characteristic of the ZnO lattice. The theoretical fit to the data of Fig. 1 was made assuming a mixture of acoustical-mode and optical-mode scattering. The optical-mode scattering mobility, $\mu_0$, was computed from the polarizability properties of ZnO and a polaron mass $m^{(P)} = m^{(H)} = 0{\cdot}27m$ with the perturbation theory.[9]* The intermediate coupling theory[10] gives essentially the same $\mu_0$ for the coupling constant, $\alpha = 0{\cdot}85$, calculated for ZnO. In Fig. 1, the fit to the data was obtained by adjusting the magnitude of only the acoustical-mode scattering, $\mu_a \sim T^{-\frac{3}{2}}$, and combining the reciprocals of $\mu_a$ and $\mu_0$. From the quality of the fit in Fig. 1, it appears that the magnitude of the optical-mode-scattering is just about right, indicating that the effective mass used in its computation cannot be too far wrong since $\mu_0 \sim (m^{(P)})^{-\frac{3}{2}}$.

In general in a uniaxial crystal, such as ZnO, the electrical conductivity tensor will have two components, giving the conductivity parallel and perpendicular to the axis. A large anisotropy of this type would be very troublesome in the interpretation of Hall and conductivity measurements with current restricted to the axial direction due to the needle-like sample geometry. Our inability to prepare large-area, low-resistance, ohmic contacts prevented a direct measurement of the conductivity ratio on the small, single-crystal samples available. However, some single crystals† with diameters approaching 1 mm and conductivities of about 0·02 $\Omega^{-1}$ cm$^{-1}$ were ground and polished into thin, nearly square, rectangular slabs with the $c$-axis in the plane of the slab. These slabs were then positioned in a 9 kMc/s microwave cavity so that the cavity's maximum electric field was in the plane of the slab and either parallel or perpendicular to the $c$-axis. Measurements of the cavity losses for the two crystal orientations demonstrated that the conductivity of ZnO is isotropic to within the experimental uncertainties of the order of 10 per cent. Thus the only mass anisotropy

* In reference 6, a similar calculation of $\mu_0$ was made with a Debye temperature $\Theta_l$ for the longitudinal optical modes which was too small because of an incorrect estimate of the reststrahlen frequency which must be used in the Lyddane–Sachs–Teller relation in order to obtain $\Theta_l$.

† These crystals were obtained from Mr. Robert Ammon of the American Zinc, Lead, and Smelting Co., St. Louis, Mo.

factor which will come into $\mu_H/\mu$ will be that associated with the anisotropy of the individual valleys, and this factor should be close to unity for valleys which are not too anisotropic.[5]

**4. THERMOELECTRIC POWER—PHONON-DRAG**

Measurements of thermoelectric power, $Q$, were originally undertaken in conjunction with Hall effect measurements in order to ascertain the density-of-states mass, $m^{(N)}$, in ZnO. It has now been established[11] that in many semiconductors $Q$ is the sum of two contributions; the electronic part, $Q_e$, which gives the electric field necessary to oppose the diffusion of electrons in a temperature gradient, and the phonon-drag part, $Q_p$, which measures the electric field necessary to halt the drift of electrons from hot regions to cold regions brought about by interaction with the phonon system which possesses net crystal momentum in a temperature gradient. It is $Q_e$ which is related to $m^{(N)}$ through the familiar formula

$$Q_e = -86{\cdot}2\left[\ln\frac{4{\cdot}7\times10^{15}}{n}+\frac{3}{2}\ln\frac{m^{(N)}}{m}+\right.$$
$$\left.+\frac{|\Delta E|}{kT}+\frac{3}{2}\ln T\right], \qquad (3)$$

where $Q_e$ is in $\mu$V/deg, $n$ is in cm$^{-3}$, and $\Delta E$ is of the order of $2kT$. The theory of $Q_p$ has been given by HERRING[12] who shows that it may be expressed as

$$Q_p = -\bar{c}^2 f\bar{\tau}/\mu T \qquad (4)$$

where $\bar{c}$ is an average velocity of sound, $\bar{\tau}$ is an average relaxation time for the very long-wavelength acoustical phonons with which the electrons interact, $\mu$ is the electron mobility, and $f$ is the fraction of electron drift momentum which is given to the acoustical phonons. The large values of $Q_p$ and its rapid increase as temperature is lowered are due to large values of $\bar{\tau}$ and the fact that it is proportional to a negative power of the temperature.

The situation for ZnO is illustrated in Fig. 2 where the product $QT$ as measured on a crystal of relatively low carrier concentration is compared with $Q_eT$ computed from Hall effect carrier concentration data according to equation (3) for $m^{(N)}$ equal to $m$ and $0{\cdot}5m$. The phonon-drag effect makes the major contribution to $Q$ at all temperatures, hence $m^{(M)}$ cannot be determined from a comparison of thermoelectric and Hall data. However, the phonon-drag effect itself can provide

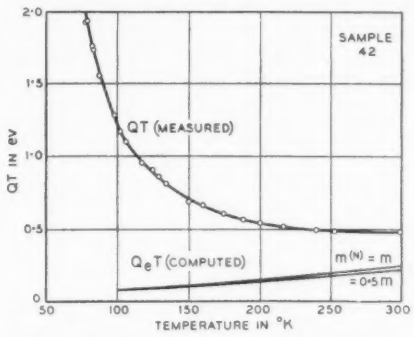


FIG. 2. Thermoelectric data for a sample of ZnO compared with the theory for the electronic part of $Q$, showing the large contribution of the phonon-drag effect.

information which bears upon the effective mass problem in ZnO.

Fig. 3 shows $Q_p$ plotted as a function of tem-

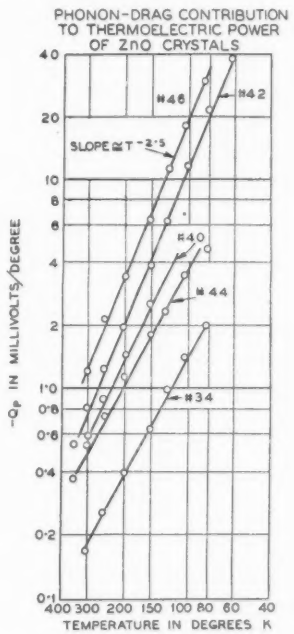


FIG. 3. $Q_p$ as a function of temperature for ZnO crystals with the following room-temperature carrier concentrations: # 46, $1{\cdot}2\times10^{15}$; # 42, $1{\cdot}8\times10^{16}$; # 40, $6{\cdot}7\times10^{16}$; # 44, $8{\cdot}2\times10^{16}$; and # 34, $3{\cdot}3\times10^{17}$ cm$^{-3}$.

perature for five crystals of different carrier concentration. $Q_p$ was obtained from the measured values of $Q$ by subtracting $Q_e$, computed from Hall data and equation (3), setting $m^{(N)} = 0{\cdot}5m$ and $\Delta E/kT = 2$. The temperature dependence of $Q_p$ for the samples with lowest carrier concentration is about $T^{-2{\cdot}5}$ which is less steep than the $T^{-3{\cdot}5}$ dependence predicted by the simple theory. This may be because the temperatures over which $Q_p$ has been measured are not sufficiently small compared to the Debye temperature for acoustical modes.

The largest observed magnitude of $Q_p$ (at the lowest temperature) can be used to set an upper bound on the acoustical-mode scattering mobility, $\mu_a$. This comes about because at sufficiently low temperatures, the $\bar{\tau}$ of equation (4) would result in phonon mean free paths longer than sample dimensions. There is, therefore, a boundary-scattering limit on the magnitude of $Q_p$ which may be obtained by substituting $\bar{\tau}_b = L/\bar{c}$ for $\bar{\tau}$ in equation (4), where $L$ may be taken as approximately the sample diameter, thus

$$Q_{pb} = -\bar{c}fL/\mu T \text{ and } |Q_p| < |Q_{pb}|. \quad (5)$$

If we assume that $\mu/f$ is the mobility, $\mu_a$, which one would have if acoustical mode scattering were operative alone, then it follows from equation (5) that

$$\mu_a < \frac{\bar{c}L}{|Q_p|T}. \quad (6)$$

Our datum point which sets the lowest upper bound on $\mu_a$ is $Q_p = 0{\cdot}04$ V/deg at 60°K on sample 42 ($L = 0{\cdot}022$ cm). The velocity of sound for ZnO can be estimated from its Young's Modulus of $10^{12}$ dyn/cm$^2$ [13] and its density of 5·6 g/cm$^3$ to be $\bar{c} = 4 \times 10^5$ cm/sec. Substituting in equation (6), we obtain an upper bound for $\mu_a$ at 60°K of about 4000 cm$^2$ V-sec. On the basis of the fit to the experimental Hall mobility in Fig. 1, the predicted value of $\mu_a$ at 60°K is 3000 cm$^2$/V-sec, which is in agreement with this upper bound.

The decrease in $Q_p$ with increasing carrier concentration which is evident in Fig. 3 is due to the saturation effect discussed by HERRING.[12] It should occur when the phonon relaxation time $\bar{\tau}$ of equation (4) becomes appreciably shortened due to phonon–electron collisions. With a number of simplifying assumptions, HERRING has calculated curves of $Q_p/Q_p^{(0)}$ as a function of the ratio of carrier concentration to a quantity $n_1$. $Q_p^{(0)}$ is the value $Q_p$ would have in the limit of vanishing carrier concentration. If a comparison between experiment and theory can be made at a temperature where the electron mobility is dominated by longitudinal-acoustical-mode scattering, the expression for $n_1$ may be written as

$$n_1 = \frac{1}{4\pi}\frac{(k/e)}{Q_p^{(0)}} \cdot \frac{1}{\lambda^3}, \quad (7)$$

where $\lambda$ is the reduced electron wavelength in the direction of the thermal gradient, $(\hbar^2/2m^{(I)}kT)^{\frac{1}{2}}$. The saturation effect can thus give us a measure of the inertial effective mass.

From the mobility analysis of Section 3, $\mu_a$ appears to be dominant at 150°K. Therefore, in Fig. 4 we have plotted the ratios of $Q_p$ for a number of samples to the $Q_p$ measured on sample 46 as a

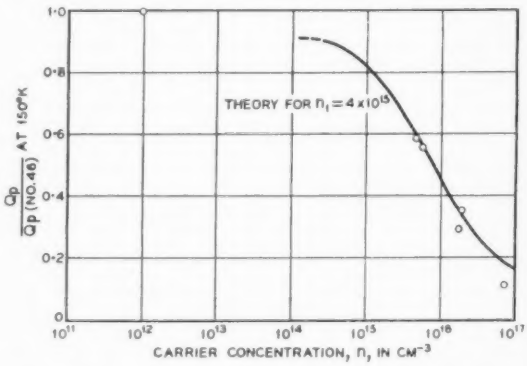


FIG. 4. Fit of $Q_p$ data at 150°K to Herring's theory of the saturation effect resulting in a determination of the parameter $n_1$.

function of log carrier concentration at 150°K. (Since sample 46 had an extremely low carrier concentration, we assume that it does not show the saturation effect.) HERRING's curve of $Q_p/Q_p^{(0)}$ has been fitted to the data in Fig. 4 yielding a value of $n_1 = 4 \times 10^{15}$ cm$^{-3}$ at 150°K, and consequently an inertial mass $m^{(I)} = 0{\cdot}07m$. This value of inertial mass seems extraordinarily low when compared with the effective mass which gives best agreement with the binding energy of shallow donor states and the magnitude of the optical-mode scattering which fits the temperature

dependence of the mobility. However, recent measurements by R. J. COLLINS[8] of the free-carrier contribution to the infrared reflectance of ZnO are in agreement with this low value of inertial mass and show, furthermore, that it is nearly isotropic.

### 5. MAGNETORESISTANCE

The magnetoresistance of a number of synthetic single crystal needles of ZnO has been measured at room temperature and 77°K. The current was along the *c*-axis because of sample geometry. Fig. 5 shows the variation of $\Delta\rho/\rho\theta^2$ as a function of the angle between the magnetic field and the *c*-axis

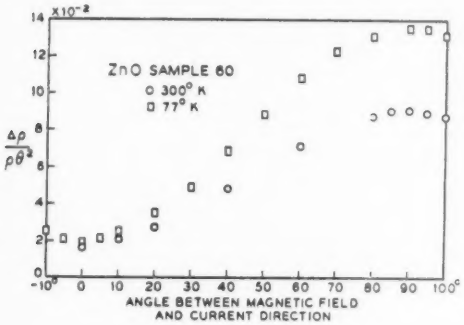


FIG. 5. Magnetoresistance as measured on a hydrogen-doped, single-crystal needle of ZnO with the current along the needle (*c*) axis. The magnetic field was 1·56 Webers/m².

at both temperatures. ($\theta$ is the Hall angle, $\mu_H B$, for current along the *c*-axis.) These data were taken with a magnetic field strength of 1·56 Webers/m². In both the transverse and longitudinal directions the magnetoresistance had the proper $B^2$ dependence from the lowest fields at which it could be measured up to 1·56 Webers/m². From Fig. 5 it can be seen that the magnetoresistance scales approximately as $\mu_H^2$ from 77°K to room temperature.

For the present discussion, the most important result of these measurements is the fact that *the longitudinal magnetoresistance does not vanish* for current along the *c*-axis. In order to be certain of this result the crystals were mounted in a holder which could be positioned with two angular degrees of freedom about the direction of the magnetic field, and special care was exercised in the doping of the crystals in order to insure homogeneity of carrier concentration.

In terms of a simple-many-valley model for the conduction band of ZnO, the non-zero longitudinal magnetoresistance along the *c*-axis implies that the *c*-axis cannot be a principal axis of all of the valleys. (It can be shown that the longitudinal magnetoresistance for a single valley is identically zero along its principal axes.[12]) The first Brillouin zone for crystals of the class 6 mm is a cylinder of hexagonal cross-section bounded by planes perpendicular to the hexagonal (*c*) axis. It possesses two sets of three reflection planes containing the *c*-axis and a center of inversion. A consideration of the possible valley positions in this zone shows that a minimum of 12 valleys is required by the condition that the *c*-axis is not a principal axis of all of the valleys.

An approximate idea of the mass anisotropy for the individual valleys may be obtained from the transverse and longitudinal magnetoresistance parameters using a method developed by KEYES[14] He defines an anisotropy parameter $\Lambda$:

$$\Lambda = \frac{\alpha_1(\alpha_2-\alpha_3)^2+\alpha_2(\alpha_3-\alpha_1)^2+\alpha_3(\alpha_1-\alpha_2)^2}{2\alpha_1\alpha_2\alpha_3}, \quad (8)$$

where $\alpha_1$, $\alpha_2$ and $\alpha_3$ are the reciprocals of the three principal masses of each valley. He then shows that upon averaging over all valley orientations, $\Lambda$ is related to the magnetoresistivity coefficients by

$$\frac{(\Delta\rho/\rho\theta^2)_{\text{long}}}{1+(\Delta\rho/\rho\theta^2)_{\text{trans}}} = \frac{2\Lambda}{4\Lambda+15} \quad (9)$$

Upon substituting the values of the coefficients from Fig. 5 at 77°K we find that $\Lambda = 0{\cdot}14$, indicating a rather small degree of anisotropy. (If the valleys were to turn out to be ellipsoids of revolution, this value of $\Lambda$ would indicate that the mass ratio was either 1·4 or 0·7.) A more thorough investigation of the magnetoresistivity must take account of the actual orientations of the valleys, however, the isotropy of conductivity would indicate that the analysis above is close to the truth.

### 6. DISCUSSION

The evidence presented above strongly favors a many-valley model for the conduction band of ZnO, although there appear to be some internal

inconsistencies. The value of $m^{(N)}$ of $0{\cdot}5m$ derived from the temperature dependence of carrier concentration yields a value of $0{\cdot}095m$ for $(m_1m_2m_3)^{\frac{1}{3}}$ for a 12-valley model. This agrees well with both the inertial mass of $0{\cdot}07m$ as determined from phonon-drag saturation and the degree of valley anisotropy indicated by the magnetoresistance data. The difficulty lies with the large quantity of optical-mode scattering (low value of $\mu_0$) required to fit the temperature dependence of the Hall mobility above 150°K, and the binding energy of 0·05 eV for the shallow donor states. These latter two results seem to be best fitted by an average effective mass of about $0{\cdot}25m$.

While one might suppose that the explanation of the donor binding energy might turn out to be simply a large central cell correction or the failure of the assumption that the low frequency dielectric constant is appropriate to the hydrogen-atom donor state model, it is difficult to see how either of these explanations would sufficiently increase the binding energy. Furthermore, they offer no explanation for the large amount of optical-mode scattering.

A more inclusive tentative explanation (evolved in discussion with D. A. KLEINMAN and J. HOPFIELD) is based upon the assumption that the 12 low-mass valleys are rather shallow depressions in a region of **k** space characterized by a considerably larger mass. The bound donor states are then assumed to be made up of a superposition of unperturbed states from *both* the neighborhood of the low-mass minima and some of the surrounding high-mass region with a correspondingly large binding energy. The probability for scattering of a low-mass electron by an optical phonon of energy corresponding to about 900°K will also be appreciably larger if the valleys are sufficiently shallow so that the electron must be scattered to one of the more numerous high-mass states just outside the valley in order to conserve energy.

*Acknowledgments*—The author would like to acknowledge a number of very helpful discussions with C. HERRING, D. A. KLEINMAN, J. HOPFIELD, and R. J. COLLINS. The experimental work was aided by G. FOULDS, E. KANKOWSKI, and R. B. ZETTERSTROM.

## REFERENCES

1. THOMAS D. G. and LANDER J. J. *J. Chem. Phys.* **25,** 1136 (1956).
2. THOMAS D. G. *J. Phys. Chem. Solids* **3,** 229 (1957).
3. THOMAS D. G. in press.
4. LANDER J. J. private communication.
5. HERRING C. *Bell Syst. Tech. J.* **34,** 237 (1955).
6. HUTSON A. R. *Phys. Rev.* **108,** 222 (1957).
7. MOLLWO E. *Z. Angew. Phys.* **6,** 257 (1954).
8. COLLINS R. J. to be published.
9. FROHLICH H. and MOTT N. F. *Proc. Roy. Soc.* A.**171,** 496 (1939).
   HOWARTH D. and SONDHEIMER E. *Proc. Roy. Soc.* A**219,** 53 (1953).
10. LOW F. E. and PINES D. *Phys. Rev.* **98,** 414 (1955).
11. FREDERIKSE H. P. R. *Phys. Rev.* **91,** 491 (1953); *Ibid.* **92,** 248 (1953); GEBALLE T. H. *Phys. Rev.* **92,** 857 (1953).
    GEBALLE T. H. and HULL G. W. *Phys. Rev.* **94,** 1134 (1954).
12. HERRING C. *Phys. Rev.* **96,** 1163 (1954).
13. PEARSON G. L. private communication.
14. KEYES R. W. *Phys. Rev.* **109,** 43 (1958).

VOL
8
195

*J. Phys. Chem. Solids* Pergamon Press 1959. Vol. 8. pp. 473–481. Printed in Great Britain

# Q.7 OPTICAL INVESTIGATION OF SEMICONDUCTORS AT THE UNIVERSITY OF ROCHESTER*

D. L. DEXTER

Institute of Optics and Department of Physics and Astronomy
University of Rochester, Rochester, New York, U.S.A.

**Abstract**—A survey is given of recent investigations at this institution of optical properties of non-metals. The fundamental absorption of the alkali, silver, and thallous halides and of cadmium sulfide; intrinsic photoconductivity in the alkali halides; electron multiplication in lead sulfide and selenide; and the theory of excitons in the tight binding approximation are among the topics discussed.

VOL. 8 1959

THIS paper is presented on behalf of the solid state physics group of the Institute of Optics and the Physics Department, namely, Drs. M. P. GIVENS, D. B. DUTTON, D. FOX, K. J. TEEGARDEN, S. TUTIHASI, the writer, and co-workers. It contains a representative selection of material pertinent to this conference, on optical and electrical investigations of non-metallic crystals; its aim is more to introduce the host institution than to serve as an ordinary scientific outlet.

In view of the title of this session, and of this university's initiation of the Annual High Energy Conferences, it seems particularly appropriate to begin with a discussion of one of the "highest-energy" semiconductors imaginable. R. S. KNOX in his thesis has carried out a treatment of the ground and "exciton" states of solid argon, in which the "band-gap" is perhaps 12 eV, or about 2000 times the melting temperature multiplied by Boltzmann's constant. The computation is based on one of the two basic models of solids, the "tight binding" approximation, which should be valid in this system if in any. It evidently represents the first quantitative attempt to treat excited states of solids by this scheme.

It is well known that the Heitler–London model, when used to describe excited states of solids, leads to states which cannot be described by the basic Bloch scheme, and which are generally expected to lie below the lowest conduction band in large-band-gap semiconductors. FRENKEL[1, 2] and PEIERLS[3] originally proposed that these states, called by FRENKEL "exciton" states, were linear combinations of states of localized atomic excitation. SLATER and SHOCKLEY[4] and WANNIER[5] proposed another description of exciton states in which the optically excited electron is able to leave the site of excitation but remains bound to the hole it leaves behind, and showed how this set of states could be related to Bloch states. The original model is particularly suited to a numerical computation because knowledge of ground and excited state atomic functions is sufficient to construct a complete set of trial crystal functions. Because of the success of the Heitler–London model in computing first-order ground state (binding) energies, it is of interest to test it in a computation of excited state energies.

Since its inception, the Frenkel–Peierls model has received considerable qualitative attention, including work on the fine structure of exciton bands due to non-simple unit cell symmetries (Davydov splitting), the problem of energy transfer in ionic crystals by excitons,[6] the quantum mechanical basis of the Lorentz local field,[7] and the position and strength of absorption due to transitions to exciton states.[8] In each case a single-valence electron model was employed for simplicity and lattice vibrations were not explicitly taken into account.

KNOX[9] has made what appears to be the first numerical computation based directly on the

* The work described herein has been supported in part by the U.S. Air Force Office of Scientific Research of the Air Research and Development Command.

Frenkel–Peierls model. Using Hartree–Fock functions for ground[10] and excited state[11] atomic argon, he has computed the excitation energies, band structures, and integrated absorption coefficients associated with exciton states built from the argon ($3p^5 4s$) configuration. The basic crystal model chosen in his work was the same as the one used in references 6–8, but extended to include complications due to spin–orbit coupling, overlapping of wave functions in the solid, and the fact that each atom contains many electrons. These extensions modify the formalism from a simple exercise in quantum mechanics to a complex theoretical structure; the numerical evaluation is equally formidable, even with modern computing machines. These difficulties are mentioned in order to emphasize that even when the tight-binding approximation is applicable a realistic treatment is still far from simple. As a result of these numerical computations, he predicts two absorption bands at $\sim 9$ eV with a separation of $\lesssim 0{\cdot}17$ eV, the line of lower energy being about twice as intense as the other. The effective masses which may be ascribed to excitons in the argon $3p^5 4s$ bands are found to be positive near $k = 0$, and range from 4·5 to 6·5 electron masses, the exact value depending on the direction of propagation and the particular exciton band involved. The fact that the band of lower energy is more intense is due to its containing a larger admixture of the singlet state. The presence of the Heller–Marcus dipole–dipole interaction lowers a singlet exciton state and may even cause an inversion of the usual relative singlet–triplet position. This happens to be the case in solid argon.

Excited atomic argon functions are greatly extended spatially, and this fact is of considerable quantitative importance in the computation. Lattice sums extending through the shell of third neighbors were usually sufficient; however, because of the inadequacy of the Hartree–Fock method, there was poor accuracy in the numerical evaluation of some of the large contributions to excitation energies, and KNOX considers the value of 9 eV reliable only to within $\pm 1$ eV. Furthermore, he was not able to prove conclusively that the Lowdin orthonormalization process used either converged or diverged. All overlap contributions through the second power of Lowdin's overlap parameter $S$ were included. It is interesting to note that the Heller–Marcus dipole–dipole interaction, even when corrected through terms of order $S^2$, is of much less importance than exchange-like terms in determining exciton effective masses. Moreover, the part of these exchange-like terms which depends on explicit overlap integrals was found to be entirely responsible for the positive sign of the exciton effective mass in argon. Had the explicit overlap terms been neglected, as they have been in earlier formalisms, the entire band structure would have been inverted. KNOX feels that the same conditions will prevail in the other rare gases* and in the alkali halides if described on an excitation model.

An evaluation of the usefulness of the Heitler–London method in describing excited states on the basis of this computation must await experimental data on the optical properties of solid argon and in any event is qualified by the question of the convergence of the orthonormalization method. Knowledge of the widths of the absorption bands will determine whether the predicted doublet can be observed. This must be decided by experiment or by an accurate analysis of the effect of phonons in the computation. A rigorous formalism for line breadth consistent with the Heitler–London method and following the work of PEIERLS[3] does not seem to have been given, although TOYOZAWA[12] has recently reopened the problem using the Wannier model.

Towards the other extreme from solid argon we may consider the lead salts of sulfur and selenium. DUTTON and co-workers have investigated electron multiplication in these materials, a process in which an electron, originally excited from the valence band by a photon, may excite secondary electrons which contribute to the photo-current if its kinetic energy is high enough. In Fig. 1 is plotted the observed relative photocurrent per incident photon in PbS as a function of the incident photon energy $E$. For energies above the band gap (about 0·4 eV) the photocurrent rises to become approximately constant from about 1·3 to 2·0 eV, above which the photocurrent rises linearly with photon energy.[13] In PbSe, on the other hand (see Fig. 1), the process is considerably more

* For example, excited neon $3s$ functions computed with exchange (unpublished data of A. GOLD and R. S. KNOX) are as greatly extended as the $4s$ function in argon.

complicated. Here the photocurrent per incident photon reaches a peak at 3·7 eV, about 14 times the band gap, and falls off with increasing photon energy. It is not clear what would cause such an effect, and an interpretation has not been given.

in the absorption spectrum raise the possibility that exciton transitions may be responsible for part or all of the absorption in the edge. This possibility is further suggested by recent indications at several laboratories of the diffusion of

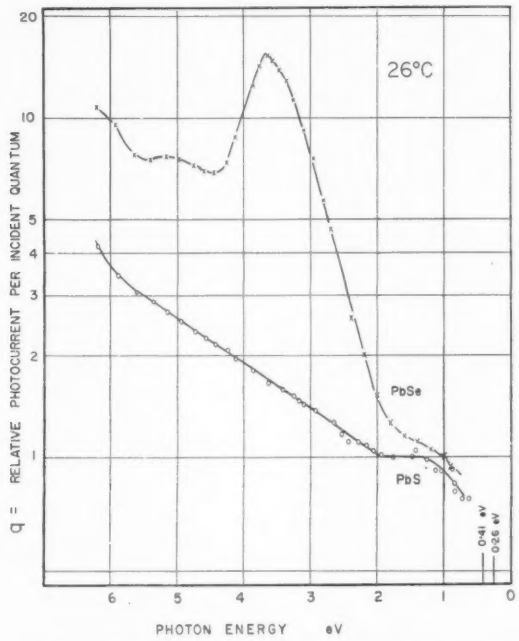


FIG. 1. Relative photocurrent per incident quantum, $q$. is plotted on a logarithmic scale against photon energy. The scales for PbS and PbSe are not the same. The quantity $q$ is interpreted as proportional to the number of charge carriers produced per absorbed photon; the absolute value of this number, in both cases, is approximately that given by the ordinate scale.

The most obvious explanation, that the film is not absorbing the incident higher energy light, has been ruled out. Work is continuing on this system.

CdS represents an intermediate crystal, with a band gap of about 2·5 eV. Since in CdS there is apparently a close correspondence between the thresholds of intrinsic photoconductivity and optical absorption, the mechanism of absorption in the edge has long been considered to be band-to-band transitions, and the position of the absorption edge has usually been taken as the optical energy band gap. However, recent observations by E. F. GROSS and others[14] of exciton-like fine structure

excitons created by optical means. In the hope of clarifying the absorption mechanism, and correlating the absorption edge itself with the absorption lines and bands observed by GROSS, DUTTON has undertaken a series of detailed measurements of the shape of the absorption edge, covering a wide range of the absorption coefficient, at temperatures between 90° and 360°K, for analysis in the light of recently developed analytical models[15] for band-to-band transitions, and also for comparison with other materials.

These observations consist of direct point-by-point photoelectric transmittance and reflectance

measurements on single crystals of CdS, grown by various modifications of the Frerichs vapor-phase technique. In view of the small size of the samples, a microscopic technique is employed. The crystals may be of the order of 200 $\mu$ or larger in linear dimensions and range in thickness from about 1 $\mu$ to 200 $\mu$.

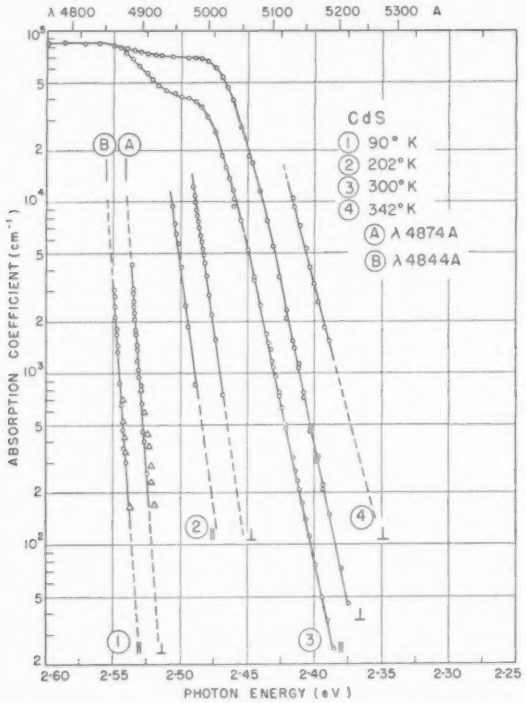


FIG. 2. Absorption coefficient of crystalline CdS. The linear portions of the solid curves are plots of the form $\ln \alpha = \beta h\nu/kT + \text{const.}$, where $\beta = 2{\cdot}17$. The vertical lines A and B are the positions of absorption peaks inferred from the reflection spectrum at 90°K. $\parallel$ and $\perp$ indicate absorption for polarized light with **E** vector parallel or perpendicular, respectively, to the crystalline $c$-axis. Absorption coefficient $= 1/t \log_e (I)^{-1}$ where $I$ is the optical transmittance corrected for reflection, and $t$ = sample thickness.

Fig. 2 shows the complete absorption data to date, as obtained on a number of crystals, mainly RCA type I (obtained from Dr. R. H. Bube of RCA Laboratories), crystals grown by D. C. Reynolds at Wright Air Development Center, and crystals grown by P. Mauer at the Eastman Kodak Company. Over several decades the absorption coefficient can quite accurately be represented as an exponential function of photon energy, following the rule first noted by F. URBACH.[16] The frequency dependence of the absorption coefficient, the steepening of the edge with decreasing temperature, and the shift toward shorter wavelengths are all compactly described by an expression of the form

$$\alpha(\nu) = \alpha_0 \exp -(B/kT)[E_{00} - CT - h\nu], \quad (1)$$

where $\beta$ is a dimensional constant of order unity in several materials, $C$ is a thermal coefficient of "edge expansion", and $E_{00}$ and $\alpha_0$ are characteristic energies and absorption coefficients at absolute zero. As pointed out by GOBRECHT and BARTSCHAT,[17] CdS is dichroic, the absorption

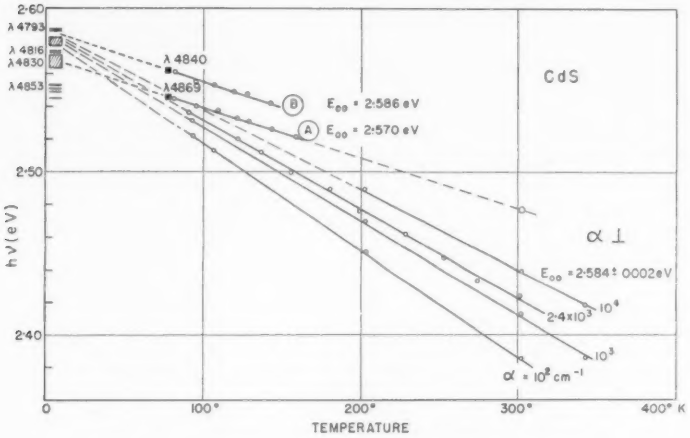


FIG. 3. Temperature shift of the absorption spectrum of CdS. The photon energy $h\nu$ at which the $\perp$ absorption coefficient $\alpha_\perp$ has a given value is plotted on a linear scale against absolute temperature. Curves A and B denote the positions of absorption peaks as inferred from the reflection spectrum. The points 4840 and 4869 Å are the positions of absorption lines reported by GROSS. The line absorption spectrum at 4°K, after GROSS, is shown by the rectangular boxes on the left. The point at 300°K on curve A is taken from the room-temperature absorption spectrum.

near the edge being appreciably strongest for light polarized with **E** vector perpendicular to the crystalline $c$-axis. Except for temperatures below about 160°K the expression (1) serves equally well to describe the edge shape in both polarizations, with different values of the parameter $E_{00}$ but the same values of $\alpha_0$, $\beta$ and $C$. Below 160°K, $C$ decreases slightly for light polarized parallel to the $c$-axis, so that the energy separation of the two edges is somewhat less at 90°K than at room temperature.

The temperature shift of the edge is shown in Fig. 3, which is a linear plot of the photon energy at which the absorption coefficient has a given value, against the absolute temperature. Equation (1) may be written

$$h\nu|_{\alpha=\text{const.}} = E_{00} - \left[\frac{k}{\beta}\ln(\alpha_0/\alpha) + C\right]T, \qquad (2)$$

i.e., plots of this kind should be straight lines, as is the case.

Some clue as to the relationship of the absorption edge and the absorption fine structure is provided by observations of this structure in the reflectance spectrum at 90°K, shown in Fig. 4. For light

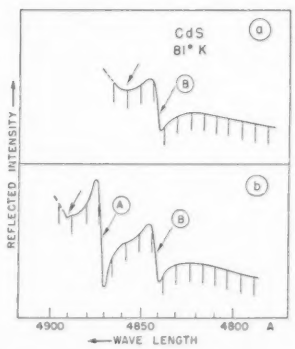


FIG. 4. Reflection spectrum of CdS. Reproductions of original data records giving reflected light intensity as a function of wavelength, (a) for $\parallel$ light, (b) for $\perp$ light. The upturn at the left of each curve, marked by heavy arrows, is due to additional reflection from the second surface, since the crystal becomes transparent at these points. The vertical pips are wavelength markers. Note the similarity of anomaly B in the two polarizations

polarized with the **E** vector parallel to the *c*-axis, there is a sharp anomaly in the reflectance spectrum at 4840 Å; for light polarization perpendicular to the *c*-axis, this structure is again present in about equal strength and a somewhat stronger anomaly appears at 4874 Å. These correspond to absorption lines observed photographically at 77°K by GROSS and IAKOBSON.[14] The temperature shift of these lines, as deduced from the reflectance somewhat stronger line appears at 4874 Å, shifting the absorption edge toward longer wavelengths by a corresponding amount.

This behavior does not all resemble that expected for band-to-band transitions (see reference 15), in which the absorption coefficient varies as some power of the difference of the photon energy and the band gap, and is in fact strikingly similar to that observed in KBr, near the first

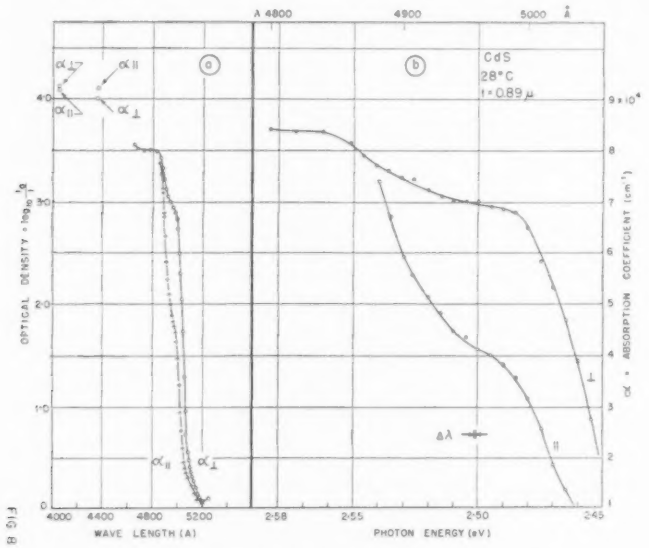


FIG. 5. Absorption spectrum of CdS at room temperature. (a) Based on measured transmittance of a single specimen 0·89$\mu$ thick. The apparent structure at 5100 Å is an interference effect. (b) Detail of 5(a).

spectrum, is shown in Fig. 3, which also includes the positions of lines and bands at 4°K as reported by the above authors.[14] Some trace of this structure, which is observable in the reflectance spectrum only at temperatures below 160°K, is still present in the room-temperature absorption spectrum (Fig. 5), with a proportionate temperature shift in position.

In summary, the absorption edge may be described as an exponential "tail", extending over many decades, of an absorption band or line which becomes very sharp and narrow at low temperatures; for one polarization ($E \| c$) there is one such line, at 4840 Å at 90°K; for the other polarization ($E \perp c$) an additional and apparently exciton band, by MARTIENSSEN.[18] One is inclined to describe the absorption process as a discrete exciton-like one, true band-to-band transitions presumably occurring at slightly higher energies. Efficient photoconductivity is, however, observed in the "exciton" region, and the most recent photoconductivity data obtained by the Soviet workers[19] reflect the absorption structure, the 4840 and 4870 lines appearing either as maxima or as minima in the photoconductivity spectrum, depending on the conditions of the sample surface. (The important influence of the surface condition is likewise indicated by DUTTON's observation that in optically-polished samples the anomalies in reflection are not present even at 90°K.) DUTTON

has observed these lines as maxima in the excitation spectrum of the green low-temperature "edge" luminescence.[20]

This green emission may give further information about the band structure of CdS. It is commonly observed in most samples below about liquid nitrogen temperature, and consists of a series of equally spaced sharp lines. DUTTON has found this luminescence to be strongly polarized at 90°K, independent of the polarization of the exciting light, with an intensity perpendicular to the *c*-axis 6·3 times as great as that parallel to it. Since the electron trap associated with this emission is shallow (only a few hundredths of an eV), the electron's orbit is large, and this anisotropy cannot be reasonably attributed to any microscopic structure of the trap. (A possible exception might be a trap associated with a grain boundary, dislocation, or other large-scale imperfection.) Thus this anisotropy probably results from an anisotropy in the energy band structure near the bottom of the conduction band (whose states comprise the trapped electron's wave packet) or the top of the valence band, or both. (From discussions of preliminay measurements of cyclotron resonance in CdS with R. N. DEXTER, the former alternative seems more likely.) If as the absorption spectra indicate, there are two proximate bands of states of different polarization, one might expect the degree of polarization of the emission to vary with temperature, since the latter would determine the admixture of states from the different bands; the indications are that this is the case, the polarization increasing as the temperature decreases.

Considerable attention has been devoted at this laboratory to the measurement of intrinsic absorption spectra of solids in the ultraviolet. TEEGARDEN and R. E. HOPKINS have modified B and L quartz prism monochromators, along lines suggested by the work of Apker, with the use of Corning fused silica, to operate down to about 1700 Å. (Now in operation also is a grating monochromator whose range is 1000–2500 Å and Givens has for some time been working in the range 100–1000 Å.) With the prism instruments TEEGARDEN has been able to obtain new structure in the absorption spectra of films of several alkali halides, an example of which for RbI is shown in Fig. 6. On the basis of external photoelectric yield measurements, Apker has proposed that the low plateau in absorption at 6.1 eV corresponds to the onset of band-to-band transitions. The low-energy peak in absorption appears to be a simple unique one, sharpening in a regular way with decreasing temperature.

TUTIHASI has performed similar absorption measurements on the silver halides, whose absorption spectra had previously been believed to be relatively temperature-insensitive, and to consist of relatively broad bands, even at low temperatures. Fig. 7 indicates the sharpening of the

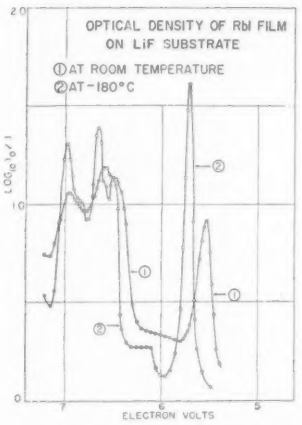


FIG. 6. The optical absorption spectrum of a thin film of RbI at − 180°C and at room temperature.

spectrum at low temperatures in AgCl films, when prepared with a suitable anneal, and the shift, similar to that in the alkali halides, to higher energies with decreasing temperatures.

From the silver halides, TUTIHASI was led to the thallous halides, whose spectra he also found to be considerably sharpened at low temperatures, as compared with older data, upon annealing the films. In these materials, as shown in Fig. 8 for TlCl, the first fundamental peak shifts towards *lower* energies with decreasing temperature, but, since the exponential edge not only shifts but also sharpens, the two curves cross at about $3 \times 10^3$ $cm^{-1}$ and the apparent edge in macroscopic crystals would seem to shift toward higher energy. The question of whether or not this phenomenon is peculiar to the CsCl crystal structure remains open. The writer is unfamiliar with a theoretical basis for this observation.

The question of the optical band gap in the alkali halides has been a matter of considerable

theoretical and experimental interest for many years. As noted by other workers, the direct measurement of photoconductivity in these materials is made difficult by the Apker–Taft phenomenon, namely, the indirect external release of photoelectrons from traps in the crystal, which give rise to most of the observed photocurrent. TEEGARDEN, in attempting to avoid this common difficulty, hit upon the scheme of coating the crystal of, say, KI, with an evaporated layer of KCl, which, though transparent to light of energy expected to produce intrinsic photoconductivity in KI, would nevertheless produce a barrier to the escape of photoelectrons released from traps in the KI crystal, thus reducing the spurious, external photocurrent. Preliminary measurements by this technique agree with a tentative assignment of the energy of the band gap as noted above for RbI.

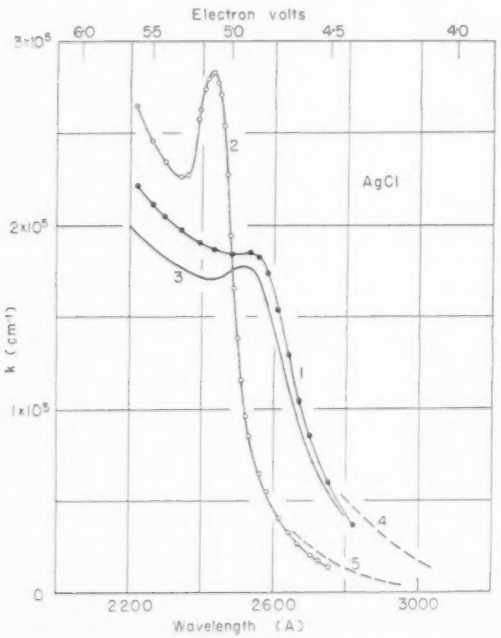


FIG. 7. The absorption spectrum of AgCl at room temperature and liquid nitrogen temperature. Curve 1 is the absorption curve at 26°C, and curve 2 is at − 184°C. The measurements were taken on a thin (210 mμ) evaporated film. Curve 3 shows the absorption curve measured by MILLIMAN at room temperature on fused films. Curves 4 and 5 are data measured by KAISER on an evaporated film of 510 mμ thickness at 27°C and at − 183°C respectively.

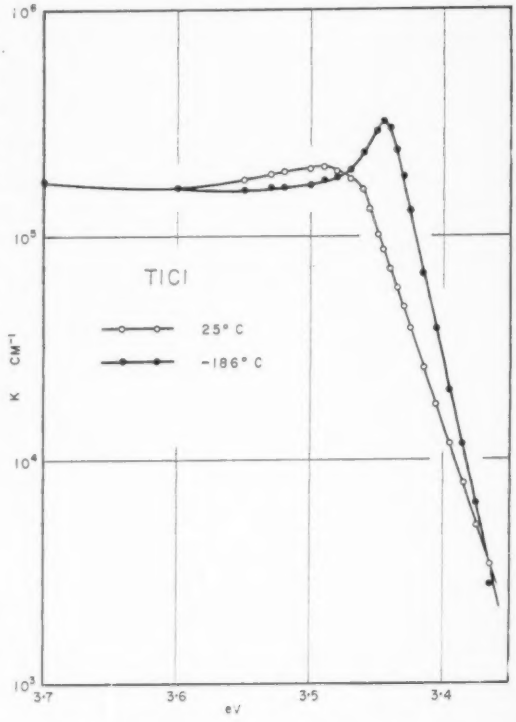


FIG. 8. The absorption of TlCl near the edge.

In an investigation of "intrinsic" luminescence in KI crystals at low temperatures, TEEGARDEN studied an emission band at about 3·3 eV excited with high quantum efficiency by light absorbed in the fundamental absorption region. The origin of this luminescence was uncertain, but it did not appear to be associated with any known activators for KI. Furthermore, various lines of investigation indicated that it did not arise from a direct recombination of excitons created by the incident light. Consequently it has seemed of interest to investigate the relationship, if any, between this emission and processes of charge transfer. Several measurements along this line have been carried out by TEEGARDEN and co-workers, with the aim not only of investigating the phenomena of luminescence in "pure" alkali halides, but also with a view toward obtaining information about the energy level structure of these interesting materials. For the interpretation of these experiments it is necessary to draw upon the vast lore

of photochemical reactions in the alkali halides, which we may not enter into here. The principal conclusion is that the 3·3 eV emission results from the recombination of a free electron with a trapped hole. By an extension of the present techniques, which involve the simultaneous irradiation of the crystal with steady *u–v* light and chopped light absorbed in the *F*-band, it seems likely that the onset of band-to-band transitions may be detected. Work is continuing with this end in view.

### REFERENCES


1. FRENKEL J. *Phys. Rev.* **37,** 17, 1276 (1931).
2. FRENKEL J. *Phys. Z. Sowjet.* **9,** 158 (1936).
3. PEIERLS R. E. *Ann. Phys. Lzg.* **13,** 905 (1932).
4. SLATER J. C. and SHOCKLEY W. *Phys. Rev.* **50,** 705 (1936).
5. WANNIER G. H. *Phys. Rev.* **52,** 191 (1937).
6. HELLER W. R. and MARCUS A. *Phys. Rev.* **84,** 809 (1951).
   DEXTER D. L. and HELLER W. R. *Phys. Rev.* **84,** 377 (1951).
7. DEXTER D. L. and HELLER W. R. *Phys. Rev.* **91,** 273 (1953).
8. DEXTER D. L. *Phys. Rev.* **101,** 48 (1956).
9. KNOX R. S. Thesis, University of Rochester (1958); *J. Phys. Chem. Solids*, submitted for publication.
10. HARTREE D. R. and HARTREE W. *Proc. Roy. Soc.* **A166,** 450 (1938).
11. KNOX R. S. *Phys. Rev.* **110,** 375 (1958).
12. TOYOZAWA Y. *Progr. Theor. Phys.* **19,** 214 (1958).
13. DUTTON D. B. *J. Opt. Soc. Amer.*, submitted for publication.
14. GROSS E. F. and IAKOBSON M. A. *Dokl. Akad. Nauk. SSSR* **102,** 485 (1955).
    GROSS E. F. *Nuovo Cim. Suppl.* **3,** 672 (1956).
    GROSS E. F. and RAZBIRIN B. S. *Zh. tekh. fiz. SSSR* **28,** 237 (1958).
15. BARDEEN J., BLATT F. J., and HALL L. H. *Photoconductivity Conference, Atlantic City* 1954, edited by Breckenridge, Russel, and Hahn, p. 146. Wiley, New York (1956).
    DEXTER D. L. *Ibid*, p. 155.
    DRESSELHAUS G. *Phys Rev.* **105,** 135 (1957); DEXTER D. L. *Proceedings of the* 1957 *Varenna Summer School*, Nuovo Cim. Suppl. **7,** 245 (1958).
16. URBACH F. *Phys. Rev.* **92,** 1324 (1953).
17. GOBRECHT H. and BARTSCHAT A. *Z. Phys.* **136,** 224 (1953).
18. MARTIENSSEN W. *J. Phys. Chem. Solids* **2,** 257 (1957).
19. GROSS E. F. and NOVIKOV B. V. *Zh. tekh. fiz*, **28,** 782 (1958).
20. DUTTON D. *J. Phys. Chem. Solids* **6,** 101 (1958).
21. KOC S. *Czech. J. Phys.* **7,** 91 (1957).


*J. Phys. Chem. Solids* Pergamon Press 1958. Vol. 8. pp. 481–485. Printed in Great Britain.

# Q.8 THE ABSORPTION EDGE SPECTRUM OF DIAMOND

C. D. CLARK

University of Reading, England

## 1. INTRODUCTION

MACFARLANE *et al.*[1] and ELLIOT[2] have been successful in giving an interpretation of the temperature dependence of the fine structure observed near the absorption edge in silicon and germanium. This paper deals with similar measurements on a relatively pure diamond.

## 2. RESULTS

The changes in the optical absorption of diamonds in the energy range 4·9 to 5·6 eV have been measured as a function of temperature between 80 and 650°K. The one type IIa and two type IIb diamonds chosen for the investigation all showed impurity absorption of different strengths in the region of the absorption edge. This impurity absorption increased steadily with increasing photon energy and, within experimental error, was temperature independent in the energy range below that considered in this paper. The absorption was substracted from the absorption spectra when investigating the variations induced by temperature change.

Several absorption spectra of the relatively pure diamond D 100 (type IIb) recorded at temperatures between 80 and 522°K, and corrected for impurity

absorption (approximately 0·3 $cm^{-1}$) are shown in Fig. 1. (The square root of the absorption coefficient is plotted against photon energy.) The 80°K spectrum shows no absorption up to 5·48 eV, and above this energy absorption increases rapidly. At 195°K additional absorption appears in the range above 5·30 eV and becomes stronger as

It is clear from Fig. 1 that the threshold photon energy for absorption in either of the branches moves to lower energies as the temperature is raised, e.g., $E_1$ changes from 5·30 eV to 5·25 eV when the temperature is raised from 195°K to 293°K. In fact for any given temperature change $E_1$ and $E_2$ both suffer the same energy change.

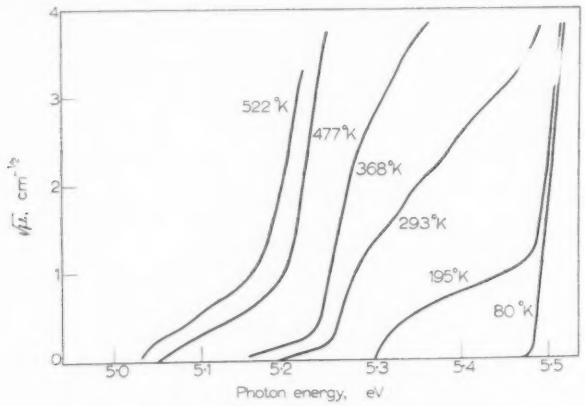


FIG. 1. Optical absorption in diamond D100 as a function of temperature.

the temperature rises. It is found that the strength of the absorption in this "branch" at a temperature $T$ can be represented by the equation

$$\mu \propto \left\{\frac{1}{e^{\theta/T}-1}\right\} f \qquad (1)$$

where $\theta=\theta_1=1050\pm60$°K ($k\theta_1=0{\cdot}09\pm0{\cdot}005$ eV). The term $f$ is independent of temperature and represents the shape of the branch in the absorption spectrum. $f$ is a function of $(h\nu-E)$ where $h\nu$ = photon energy and $E=E_1$, is the threshold photon energy of the absorption in the branch at temperature $T$.

At 293°K and higher temperatures a second temperature dependent branch occurs. Absorption in this branch extends to lower photon energies than observed for the first branch. Within experimental error the shape of the first and second branches is the same. Thus the second branch may be fitted also to equation (1), with

$$\theta=\theta_2=2800\pm120\text{°K}, (k\theta_2=0{\cdot}24\pm0.01)$$
$$\text{and } E=E_2.$$

The function $f$ is best illustrated by the 293 °K curve in Fig. 1. The experimental curve rises fairly sharply at 5·25 eV and over an energy range 0·04 eV can be fitted to the power law $\mu \propto (h\nu - 5{\cdot}25)^{1\cdot4}$ but falls below the curve given by this equation at higher energies. The experimental curve continues to rise with increasing photon energy, but two dips in the absorption curve are apparent at approximately 5·31 eV and 5·38 eV.

Fig. 2 shows an analysis of the 293°K absorption curve shown in Fig. 1. In doing this allowance has to be made for the finite band width used for scanning the spectrum. The full line curve A is the experimental result. The broken curve B is that calculated for $\mu \propto (h\nu - 5{\cdot}252)^{\frac{1}{2}}$ but corrected for the experimental band width of about 10 Å. There is not bad agreement between the two curves in the range 5·24 to 5·31 eV.

The difference between curves A and B is given by the full curve C of Fig. 2. Over the energy range 5·315 to 5·352 eV the shape of curve C is similar to the initial shape of curve A, and thus lies close to the function $\mu \propto (h\nu - 5{\cdot}327)^{\frac{1}{2}}$ when

corrected for experimental conditions (see broken curve D).

The open circles in Fig. 2 are the differences between C and D at these energies. Up to 5·48 eV they lie on the straight line given by $\mu = 209\ (h\nu - 5{\cdot}342)^2$, but there is evidence of slight curvature at lower values of $\mu^{\frac{1}{2}}$ in the lower energy region.

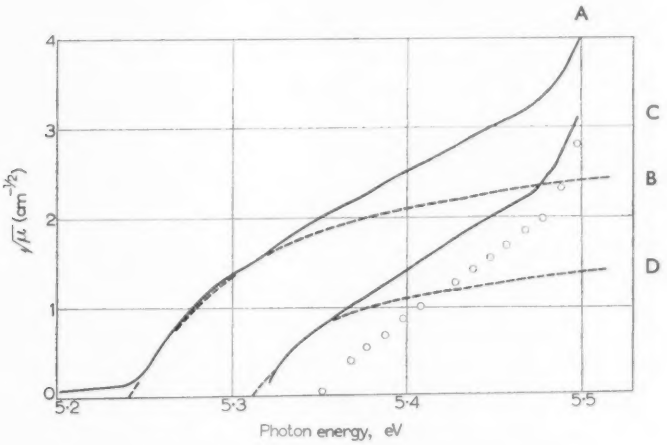


FIG. 2. Analysis of the 293°K absorption spectrum.

Thus the experimental curves between 5·0 and 5·48 eV in Fig. 1, recorded between 80 and 522°K, may be fitted to two absorption contributions written in the form

$$\mu \propto \left(\frac{1}{e^{\theta/T}-1}\right)\{(h\nu-E)^{\frac{1}{2}}+0{\cdot}4(h\nu-E-0{\cdot}075)^{\frac{1}{2}}+ +c(h\nu-E-0{\cdot}102)^2\}. \qquad (2)$$

and $\theta = 1050$ and 2900°K. $c$ is a constant.

Measurements on two other diamonds (BP2 and D80) were in quantitative agreement with the results for D100 described above in spite of having much greater impurity absorption.

### 3. DISCUSSION

The above results are attributed to indirect transitions into conducting and exciton states of the crystal. Theoretically[2] if the band extrema are at different values of $K$ indirect transitions involving the absorption or creation of phonons occur giving absorption proportional to $(h\nu - E)^{\frac{1}{2}}$ for each exciton band, and $(h\nu - E)^2$ for the continuum. Thus the first term in $(h\nu - E)$ of equation (2) represents transitions into the ground state of the exciton, the next term transitions into the first excited exciton band. There is evidence of weak absorption due to transitions into higher energy exciton bands. The last term represents transitions into the continuum.

It follows from this interpretation that $E_1$ and $E_2$ are related to the binding energy $\epsilon$ of an exciton, the forbidden energy gap $E_G$, and the energy of the phonon absorbed during the transition. Thus

$$E_1 = E_G - k\theta_1 - \epsilon \qquad (3)$$

$$E_2 = E_G - k\theta_2 - \epsilon. \qquad (4)$$

From equations (3) and (4) a value of 5·330 eV has been estimated for $(E_G - \epsilon)$ at room temperature. A value of $E_G$ may be obtained if $\epsilon$ is known. This is uncertain but is approximately 0·1 eV.

Now the maximum energy of a phonon in diamond as determined from the Raman frequency is 0·16 eV. The phonon energies $k\theta_1$ and $k\theta_2$ are 0·09 and 0·24 eV, respectively. Thus it is concluded

that $k\theta_2$ comprises the sum of the energies of at least two phonons involved in the indirect transitions. If the extrema in the conduction band lie along the 100 directions as in silicon then calculations of the phonon spectrum in diamond[3] indicate that the 0·09 eV phonon is certainly acoustical, and that if the 0·24 eV value represents two phonons one must be from the acoustical and one from the optical bands.


**REFERENCES**

1. Macfarlane G. G., McLean T. P., Quarrington J. E. and Roberts V. *Phys. Rev.* **108,** 1377 (1957).
2. Elliot R. J. *Phys. Rev.* **108,** 1384 (1957).
3. Smith H. M. J. *Trans. Roy. Soc.* A **241,** 105 (1948).


## DISCUSSION

*Compiled by* W. C. Dunlap, Jr.

### Q.1 E. W. J. Mitchell

F. E. Williams (General Electric Research Lab.): There is theoretical work which supports Dr. Mitchell's identification of the emission from diamonds with associated imperfections or impurities. Donors and acceptors are expected to be present in nearly equivalent concentrations in large band-gap semiconductors and to associate into donor–acceptor pairs. Associated pairs have been shown to have energy level structures and capability for radiative transitions consistent with emission from zinc sulfide. The emission reported by Mitchell for diamond appears consistent with recombination of electrons and holes at donor–acceptor pairs.

G. F. Garlick (University of Hull, England): Early glow curve experiments indicated the blue and green emissions were related. Can you say if perhaps the blue is a transition from one state, the green from another state, of the same center?

E. W. J. Mitchell: That is, if you do something to increase the blue emission, the green should also increase?

G. F. Garlick: Yes—perhaps the two might be related through the presence of interstitial–vacancy combinations to provide a common origin.

E. W. J. Mitchell: Perhaps this is so.

G. C. Danielson (Iowa State University): Use of diamond for crystal counters has been made for a long time. Such diamond counters also provide means for the study of trapping centers in diamond. At Iowa State we have studied the accumulation of space charge in such counters. After irradiation with light of various wavelengths we then measure the release of space charge vs. wavelength and obtain information about the trapping centers. The results will be available elsewhere.

A. C. Beer (Battelle Institute): Bate, of our laboratory, has recently measured the Hall coefficient in $p$-type II-B diamond as a function of magnetic field. He finds, after the weak field plateau, a monotonic increase beginning at about 700 G, and rising some 10 per cent to 20,000 G. The behavior is similar to that which has been observed in extrinsic $p$-type silicon and may be indicative of warping in the valence band. Although the data do not extend to sufficiently high fields to determine $R_\infty$, it seems likely that $R_H/R_\infty$, or $\mu_H/\mu$, may be less than unity at the weak-magnetic-field plateau.

### Q.3 N. W. Piper *et al.*

E. N. Adams (Westinghouse Research Laboratories): The use of the Fan calculation of the edge shift to obtain the effective mass should always give a mass that is too large, since the effect at any temperature depends on the largest phonon momenta available and measures, therefore, a mean energy denominator that is always smaller than is given in the effective mass approximation.

E. F. Gross (Leningrad): We have also studied the edge absorption of zinc sulfide and also find a fine structure, using the photographic technique I have already described. We find, in exact agreement with Piper, four lines in this structure. These studies, which are being done in collaboration with L. Suslina, are continuing.

H. F. Ivey (Westinghouse Electric Corp., Bloomfield, N. J.): To what extent did the presumably hexagonal single crystals of ZnS contain stacking faults and is it planned to study crystals of cubic structure in the future?

W. W. Piper: These crystals were shown by X-ray studies to be apparently free of stacking faults, unlike some crystals made by the same process and used for earlier work. Such stacking faults generally show up in larger crystals, whereas these were very thin, the order of 10 $\mu$. No cubic material has been observed in the product of the vapor-growth process used.

### Q.4 J. S. Prener and F. E. Williams

A. Rose (RCA Laboratories, Princeton): Is there evidence for a variation of the degree of association with temperature?

F. E. Williams: The pairs will certainly tend to become dissociated at temperatures at which appreciable solid state diffusion takes place. In fact, a random distribution where it is desired can probably be achieved by heating at very high temperatures and cooling rapidly. If cooling is slow or if annealing is used, a distribution containing associated pairs and separated donors and acceptors will be assumed for the particular conditions used.

A. Hutson (Bell Laboratories): There seem to me to be several difficulties in the calculations you describe. In the first place, care must be exercised where you are dealing with states far removed from a band edge. Here the carrier energy may be much greater than that

of the average optical phonon. Secondly, a carrier trapped in a deep state polarizes with a dielectric constant more nearly equal to the high frequency value than the d.c. value.

F. E. WILLIAMS: This is quite right. There are a number of difficulties in this theory and matters are at least as complicated as you describe. The theory presented is not intended to be the final or complete story.

Q.5 M. A. LAMPERT *et al.*

G. HEILAND (University of Erlangen): I would like to ask, what is the distribution of potential along the crystal between the electrodes? How large is the distortion of the field by the space charge?

M. A. LAMPERT: The contacts are designed and prepared so as to be essentially ohmic. While space charge does affect the potential distribution slightly, the distortion of the field is quite small.

Q.6 A. R. HUTSON

K. LEHOVEC (Sprague Manufacturing Co., North Adams, Mass.): I have shown in a paper published several years ago that by taking screening effects properly into account it is possible to determine the proper value of dielectric constant to be used in making calculations of impurity levels in ZnO. Have you made any attempt to apply this type of calculation?

A. R. HUTSON: No.

Q.7 D. L. DEXTER

A. G. CHYNOWETH (Bell Laboratories): The onset of increased quantum efficiency is interpreted as arising when electrons are raised from the top of the valence band to energies in the conduction band sufficient to produce a second free electron by collision. Is there any evidence of a second threshold in the curve of quantum efficiency vs. photon energy which could be ascribed to the complementary process, namely the raising of an electron from deep in the valence band to the bottom of the conduction band, leaving an energetic hole capable of producing another electron–hole pair? The ionization energies for these two processes may, in some cases, be appreciably different.

J. TAUC (Prague): In our work on multiplication we have noticed not one but two breaks in the current curve. It is probable that one of these breaks is due to just that mechanism suggested in the previous question.

*J. Phys. Chem. Solids* Pergamon Press 1959. Vol. 8, pp. 486–489. Printed in Great Britain

SESSION R:
RESONANCE*

R.1

# DONOR WAVEFUNCTIONS IN SILICON BY THE ENDOR TECHNIQUE

G. FEHER
Bell Telephone Laboratories Incorporated, Murray Hill, New Jersey.

**Abstract**—The Electron Nuclear DOuble Resonance (ENDOR) method was applied to the investigation of the ground state donor wavefunction in silicon. The method enables one to determine the hyperfine interaction of the donor electron with the $Si^{29}$ nuclei situated at different lattice sites with respect to the impurity. This gives one a value for the square of the electronic wavefunction at different lattice points. Both the isotropic and anisotropic h.f. interactions for arsenic, phosphorus and antimony impurities were determined. By comparing the experimental results with the theory of KOHN and LUTTINGER one obtains for the value of the conduction band minimum in silicon $k_0/k_{max}=0{\cdot}85\pm0{\cdot}03$.

VOL
8
195

## 1. INTRODUCTION

THE bound donor electron in silicon exhibits an electron spin resonance line first observed by FLETCHER *et al.*[1] They found a resonance pattern that consisted of $2I + 1$ lines, where $I$ is the nuclear spin of the donor atom. The spacing between the lines is proportional to the hyperfine interaction and provides information about $|\psi(0)|^2$, the square of the electronic wavefunction at the donor nucleus. The magnitude of this quantity was satisfactorily explained by KOHN and LUTTINGER[2] who developed a detailed theory of the donor states.

The present work deals with the determination of the square of the wavefunction not only at the central donor nucleus but also at the different silicon lattice points in the vicinity of the donor atom. Such a mapping out of the donor wavefunction is made possible by the Electron Nuclear DOuble Resonance (ENDOR) technique.[3] In this method one determines the hyperfine interaction of the electron with the different $Si^{29}$ nuclei which serve as convenient probes placed in the orbit of the donor electron.

The impurities that were investigated in greatest detail were phosphorus, arsenic, and antimony, all of which are incorporated into the silicon lattice substitutionally. The experimentally observed h.f. interactions were compared with the theory of KOHN and LUTTINGER.[2] From this comparison one obtains the position of the conduction band minimum in silicon.

## 2. THE ENDOR METHOD

Let us first consider the energy level diagram (see Fig. 1) of an electron–nuclear system which for simplicity has $I = 1/2$, $S = 1/2$ (e.g. phosphorus doped silicon). The main splitting $h\nu_e$ is due to the electron spin in the external magnetic field and gives rise to the observed paramagnetic resonance lines. The splitting $h\nu_D$ is due to the h.f. interaction with the donor nucleus and in our case can still be resolved by "ordinary" paramagnetic resonance methods. The h.f. splittings due to the $Si^{29}$ nuclei, $a_{I-Si}$, are drawn for the sake of simplicity as discrete levels although in actuality the width of each level is larger than the spacing between them. In an ordinary resonance experiment they are therefore not resolved, but are the cause of the observed line width. Such an "inhomogeneous"[4] line width which arises from the magnetic fields created by the h.f. interactions from various $Si^{29}$ configurations has the important property that part of it may be saturated without affecting the rest of it.† This forms the basis for the ENDOR technique.

Fig. 1 illustrates schematically the experimental procedure involved. The magnetic field $H_0$ (modulated for detection purposes with an audio frequency $H_M \cos \omega_M t$) is set on the center of the microwave resonance line and an additional variable radio frequency field is applied at right angles to it. The electron spin resonance signal is saturated by

* *Chairman:* O. SIMPSON; *Co-Chairman:* A. F. KIP.

† This is only approximately true. A "discrete" spin diffusion process[5] which involves a $Si^{29}$ flip and connects different parts of the line does take place.

VOL.
8
1959

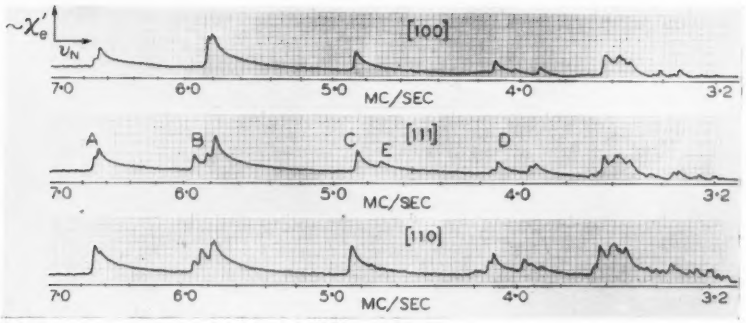


FIG. 2. Part of the ENDOR signal from arsenic doped silicon ($8 \times 10^{16}$ As/cm$^3$, $T = 1{\cdot}2°$, $\nu_e \approx 9000$ Mc/s). The lines represent the h.f. interaction of the donor electron with the $Si^{29}$ nuclei at different lattice points.

VOL
8
195

applying a strong enough microwave field. This equalizes the populations of the upper and lower electronic states, thereby reducing the observed microwave signal. The populations in the various levels are indicated in Fig. 1. Here $n$ is the total number of donors (i.e. unpaired spins) divided by the number of levels indicated. The levels that lie outside the magnetic field modulation amplitude are undisturbed, and their occupancy is given by

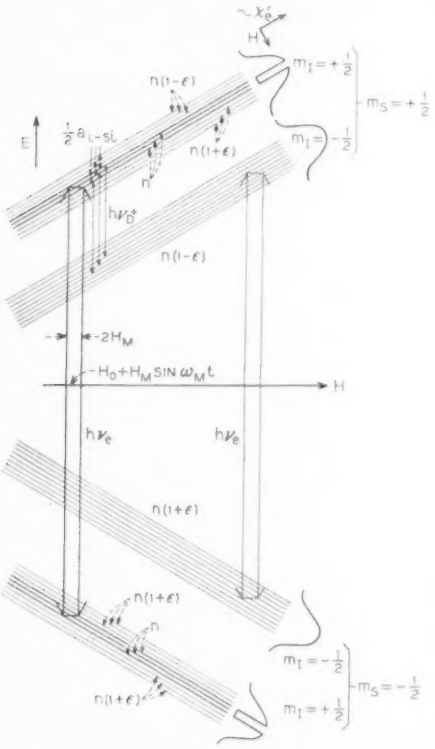


FIG. 1. Schematic representation of the energy level diagram of a donor electron in phosphorus doped silicon. We assume for simplicity that the microwave field completely saturates part of the $m_I = +1/2$ line. In the ENDOR technique, a partial desaturation (i.e. increase in the electronic signal) is observed when the "$a_{I-Si}$" or $h\nu_D$ transitions are induced.

the electronic Boltzman factor $\epsilon = \mu_0 H/kT$ as indicated. If one sweeps the radio frequency field covering the frequency range corresponding to the h.f. interactions, transitions will be induced which will change the population of the saturated electronic levels. This change in population exhibits itself as a change in the *electron* resonance signal and is recorded together with the nuclear frequency at which this change occurs.

### 3. THE EXPERIMENTAL RESULTS

We will focus our attention only on the part of the ENDOR spectrum that arises from the hyperfine interaction of the electron with the $Si^{29}$ nuclei. The main interaction is isotropic and is due to the usual scalar Fermi-Segrè h.f. interaction ($a_l$). In addition, one observes also an anisotropic h.f. interaction that arises from a dipole–dipole interaction ($b_l$). The transition frequency for flipping a $Si^{29}$ nucleus at the $l$-th lattice site is given by:

$$h\nu_l^{\pm} = \left| -\frac{\mu_{Si}}{I_{Si}} H_0 \pm \frac{a_l}{2} \mp \frac{b_l}{2}(1-3\cos^2\theta) \right| \quad (1)$$

where

$$a_l = \frac{16\pi}{3} \frac{\mu_{Si}}{I_{Si}} \mu_e |\psi(r_l)|^2$$

$$b_l = 2\mu_e \frac{\mu_{Si}}{I_{Si}} \left\langle \frac{3\cos^2\alpha - 1}{(r-r_l)^3} \right\rangle$$

$\psi(r_l)$ is the electronic wavefunction at the $l$-th silicon site, $r$ being measured from the position of the donor nucleus, $\mu_e$ is the magnetic moment of the electron, $\mu_{Si}$, $I_{Si}$, the magnetic moment and spin of the $Si^{29}$ nucleus. In the above expression we have assumed that $b_l \ll a_l$, and that the wavefunction has axial symmetry about $r_l$. $\theta$ is the angle between this axis of symmetry and the external magnetic field and $\alpha$ is the angle between $(r-r_l)$ and the axis of symmetro.

The experimental results on As doped silicon are illustrated in Fig. 2. The traces show the variation of the electronic signal as the radio frequency $\nu_N$ is varied. When this frequency corresponds to the transition of a $Si^{29}$ nucleus at a particular lattice point, an increase in the electronic signal is observed. In each of the traces, the magnetic field points along a different crystalline direction. From the center of gravity of each line (labelled A, B, C, D, E in Fig. 2) one determines the h.f. interaction constant $a_l$ (and hence, $|\psi(\mathbf{r}_l)|^2$). From the angular variation of the structure on the lines, one obtains $b_l$.

The next problem is to identify each of the ENDOR lines with a particular lattice site. This is not a trivial task, because of the nature of the wavefunction, the h.f. interactions with the $Si^{29}$'s do not

fall off monotonically with their distance from the donor nucleus. If we had only the experimental values of the isotropic part of the h.f. interaction, the correlation of the observed lines with the interaction of a silicon at a specific lattice point, $r_l$, would be nearly impossible. Fortunately, we have two additional handles which help us in the identification. One is the relative amplitudes of the ENDOR lines which have to be consistent with the number of occupied lattice points, and the other is the additional structure on each line. From the angular variation of this structure, one can find the symmetry of the particular lattice point with respect to the impurity center. We will demonstrate the last point on one particular line.

Let us consider the nearest silicon that lies along a line extending from the donor along the [100] direction. (This is the fourth nearest neighbor.) If we label the lattice sites in such a manner that four units correspond to the edge of the unit cell and the axes are chosen along the [100] directions, the silicon in question would occupy a 400 site. The three principal symmetry axes of this site lie along the [110], [1$\bar{1}$0], and [100] directions. Since this site does not have axial symmetry, equation (1) has to be modified by adding another term of the form $(b_l/2)\,(1 - 3\cos^2\phi)$. Here $\phi$ is the angle between $H_0$ and the [110] direction and $\theta$ between $H_0$ and the [100] direction.

The next step is to fit an ENDOR line with the angular variation as predicted by the above symmetry assignment. In Fig. 3 we show such a fit

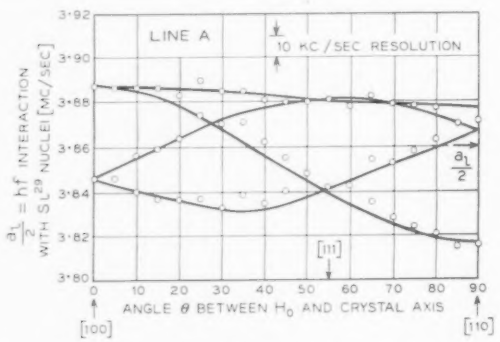


FIG. 3. H.f. interaction of the donor electron in As doped silicon with the $Si^{29}$ nuclei at the 400 site. (Line A in Fig. 2.) The magnetic field is rotated in the (110) plane of the crystal, angles are measured from the [100] direction. The full lines represent the theoretical angular variation.

with the line having the largest h.f. interaction (labelled A in Fig. 2). The dots represent the experimental points, and the full line, the theoretical fit with $b_l/2 = 23$ kc/s, $b_l'/2 = 20$ kc/s, and $a_l/2 = 3{\cdot}86$ Mc/s. In a similar fashion, the rest of the lines have been identified[5] and their amplitudes checked for consistency with the assignment.

## 4. COMPARISON OF EXPERIMENTAL RESULTS WITH THEORY

The theory with which we wish to compare our experimental results is due to KOHN and LUTTINGER.[2] They show that the wavefunction of a donor in its ground state can be represented by a linear combination of six wavefunctions corresponding to the six minima of the conduction band, which for silicon lie in the [100] direction. The wavefunctions have the form:

$$\psi(r) = \frac{1}{\sqrt{6}} \sum_{j=1}^{N} F^j(\mathbf{r}) u^j(\mathbf{r}) e^{i\mathbf{k}_0^j \cdot \mathbf{r}} \qquad (2)$$

where $N$ is the number of equivalent minima, $u^j(\mathbf{r})\, e^{i\mathbf{k}_0 \cdot \mathbf{r}}$ is the Bloch wave at the $j$th minimum, and $F^j(r)$ is a hydrogen-like envelope function obtained by solving an effective mass Schroedinger equation. From equation (2) we see that at the donor site ($r = 0$), the six wavefunctions add and $|\psi(0)|^2$ will have an appreciable amplitude. However, as $r$ is increased, the $e^{i\mathbf{k}_0^j \cdot \mathbf{r}}$ terms will cause the six wavefunctions to interfere with each other. Since the interference effects depend on the position of the conduction band minimum, a comparison of the experimental results with theory should give us a value for $k_0$.

Fig. 4 shows how the h.f. interaction of the donor electron (in As doped silicon) with the $Si^{29}$'s at different lattice points is expected to vary with the position of the conduction band minimum, $k_0/k_{\max}$. This plot was calculated from equation (2) by SCHECHTER and MOZER.[6]

Table 1 summarizes the experimental results of the isotropic h.f. interactions in arsenic doped silicon. The isotropic h.f. interactions in phosphorus and antimony doped silicon, as well as the anisotropic interactions, have also been determined.[5] The best over-all fit with theory was obtained for a value of the conduction band minimum at

$$k_0/k_{\max} = 0{\cdot}85 \pm 0{\cdot}03$$

which is in good agreement with the value obtained from infrared measurements by HAYNES *et al.*[7]* The theoretical values listed in Table 1 were based on this value of $k_0/k_{max}$ and were obtained from Fig. 4. It should be noted that none of the experimentally observed h.f. interactions differ by more than ≈ 50 per cent from the theoretical predictions. The largest deviations from theory were found for

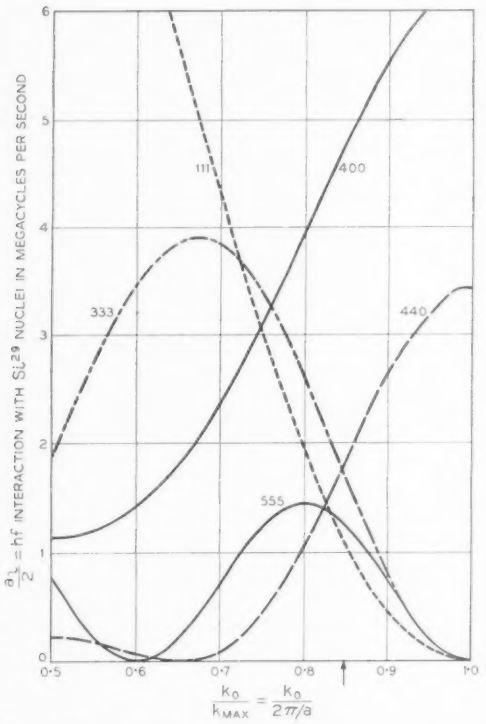


FIG. 4. The square of the electronic wavefunction $|\psi(\mathbf{r}_1)|^2$ in As doped silicon as a function of the position of the conduction band minimum $k_0/k_{max}$ for different silicon lattice sites. (After SCHECHTER and MOZER[6]). Arrow indicates the position of the conduction band minimum that gives the best fit with the experimental data.

* *Note added in proof.*—The original interpretation of the infra-red data seems at present doubtful (see HAYNES, J. R., LAX, M. and FLOOD, W. F. *J. Phys. Chem. Solids*, **8**, 392 (1959)).

*Table* 1. *Hyperfine interactions in arsenic doped silicon*

| Lattice site | Exp. h.f. interaction $(1/2\,a_{1-Si})$ (Mc/s) | Predicted h.f. interactions from KOHN and LUTTINGER'S theory assuming $k_0/k_{max} = 0{\cdot}85$ |
|---|---|---|
| 400 | 3·86 | 4·9 |
| 440 | 3·00 | 1·9 |
| 333 | 2·04 | 1·6 |
| 555 | 1·29 | 1·2 |
| 111 | 0·80 | 1·0 |

the As impurity which is the most tightly bound donor (i.e. has the largest ionization energy). This is not too surprising, since the effective mass approximation used by KOHN and LUTTINGER is expected to give the poorest results for this case. Their theory, however, fails to predict properly the magnitudes of the anisotropic interactions.

In the course of this work, electron spin resonance lines in silicon were also observed from other centers. They include Bi, Li, and Fe impurities, centers associated with the surface and centers created during the heat treatment of silicon. They were investigated in less detail than the P, As, Sb impurities and will be described elsewhere.[5]

*Acknowledgments*—I would like to thank Drs. P. W. ANDERSON and W. KOHN for many helpful discussions, and in particular for their help in the identification of the lines. I am indebted to Mr. E. A. GERE for his assistance in carrying out the experiments described.

## REFERENCES

1. FLETCHER R. C., YAGER W. A., PEARSON G. L. and MERRITT F. R., *Phys. Rev.* **95,** 844 (1954). FLETCHER R. C., YAGER W. A., PEARSON G. L., HOLDEN A. N., READ, W. T. and MERRITT F. R. *Phys. Rev.* **94,** 1392 (1954).
2. KOHN W. and LUTTINGER J. B. *Phys. Rev.* **97,** 1721 (1955); *Phys. Rev.* **98,** 915 (1955).
3. FEHER G. *Phys. Rev.* **103,** 834 (1956).
4. PORTIS A. M. *Phys. Rev.* **91,** 1071 (1953).
5. FEHER G. to be published.
6. SCHECHTER D. and MOZER B. private communication.
7. HAYNES J. R., LAX M., and FLOOD W. *Bull. Amer. Phys. Soc.* II **3,** 31 (1958).

*J. Phys. Chem. Solids* Pergamon Press 1959. Vol. 8. pp. 490–492. Printed in Great Britain

R.2

# SPIN RESONANCE OF DEEP LEVEL IMPURITIES IN GERMANIUM AND SILICON

**G. W. LUDWIG, H. H. WOODBURY and R. O. CARLSON**
General Electric Research Laboratory, Schenectady, New York.

ELECTRON spin resonance measurements have been reported for nickel[1] and manganese[2] in germanium. We have been studying several deep level impurities in germanium and silicon by resonance techniques, but only two systems, nickel in germanium and manganese in silicon, will be discussed here.

Manganese was introduced into silicon crystals either by doping the melt or by diffusion at ~1230°C followed by a relatively slow quench.[3] Manganese acts as a donor impurity in silicon with a level 0·53 eV from the conduction band.[4] If the Fermi level is at or above this level a characteristic spectrum is observed. The spectrum consists of 21 hyperfine lines when the condition $n_1^2n_2^2 + n_2^2n_3^2 + n_3^2n_1^2 = 1/5$ is satisfied, where $n_1, n_2$, and $n_3$ are the direction cosines of the magnetic field with respect to the cubic axes of the crystal. The line positions can be described by the formula

$$h\nu = g\beta H + A\sum_{k=1}^{4} m_k +$$

$$+ A^2\sum_{k=1}^{4}[I(I+1) - m_k^2]/2g\beta H_0$$

where $g = 2{\cdot}0063$, $A = 12{\cdot}8 \times 10^{-4}$ cm$^{-1}$, $I$ is the nuclear spin of manganese (5/2), and $m_k$ is the magnetic quantum number of the $k$th manganese nucleus. The spectrum is attributed to a symmetric grouping of four neutral manganese atoms, e.g. at the corners of a tetrahedron. It has a characteristic envelope, in accordance with the probability of obtaining a given $m = \sum_{k=1}^{4} m_k$ (see Fig. 1). The half width of each line is 1·4 G.

For most directions of magnetic field, each hyperfine line is split into four, evidently by crystalline field interactions. Thus it is believed that $S = 2$. However, we have not yet succeeded in tracing line positions as a function of angle, due to overlapping of the lines. The maximum crystalline field splitting is of order 40 G.

One would expect that if the clusters of four manganese atoms give rise to the 0·53 eV electrical level, they would be charged in low resistance $p$-type crystals. However, manganese associates with shallow acceptors such as boron and aluminum introduced to make crystals $p$-type. In boron-doped crystals one observes a complicated spectrum which probably is due to manganese–boron pairs. The axis of the pair appears to be a 111 direction.

If manganese is atomically dispersed in silicon at high temperatures, one might expect that clusters of four would not be formed under conditions of sufficiently rapid quenching. Preliminary data indicate that this is indeed the case. In low resistance $n$-type crystals which are quenched by blowing the silicon crystals into ethylene glycol, two overlapping six line spectra are observed which presumably are due to sites involving just one or two manganese atoms. The spectra, designated a and b, are described by $g_a = g_b = 2{\cdot}0104$, with hyperfine interaction constants $A_a = 71{\cdot}9$ and $A_b = 70{\cdot}9$ in units of $10^{-4}$ cm$^{-1}$.

The foregoing considerations lead us to conclude that the 0·53 eV electrical level of manganese-doped silicon is due to clusters of four manganese atoms. In $p$-type crystals manganese associates with the acceptor which is present.

In nickel-doped germanium, resonant absorption has been detected[1] proportional to the concentration of $Ni^-$. The spectrum, which at 20·4°K consists of six main lines having anisotropic $g$-values, is interpreted in terms of a Jahn–Teller distortion of the nickel ion (which has an effective spin of 1/2) in any cubic direction. The principal axes of the $g$-tensor are the cubic direction and two mutually

VOL.
8
1959

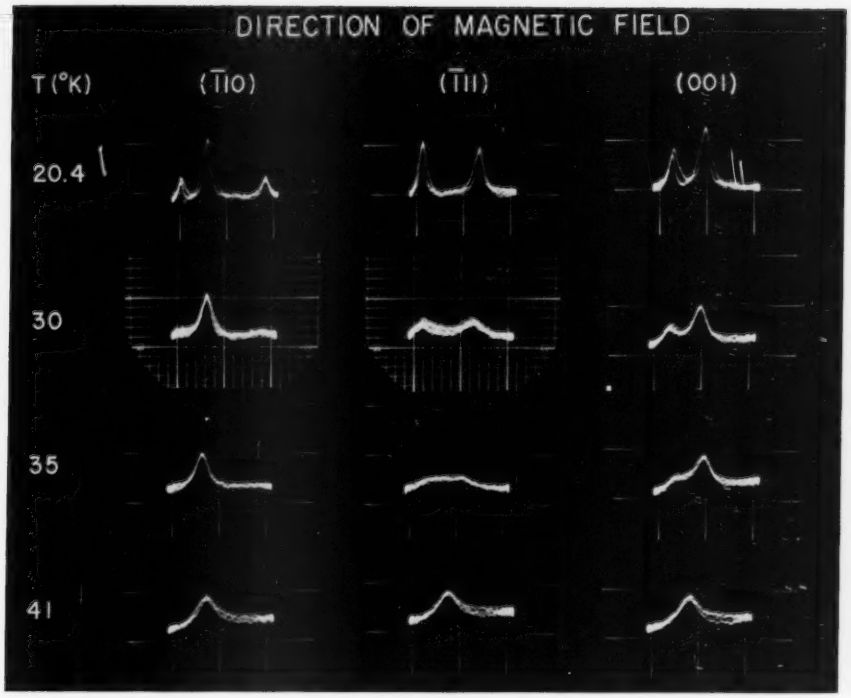


FIG. 2. Photographs of an oscilloscope display of the $Ni^{-}$ spectrum as seen in absorption, showing the broadening and merging of the lines as the temperature is raised above 20·4°K.

VOL
8
195

perpendicular (110) directions having $g$-values of 2·0294, 2·0176, and 2·1128, respectively. One observes a six-line spectrum since there are six possible orientations for the $g$-ellipsoid.

Fig. 2 shows the spectrum observed for three simple directions of magnetic field as a function of temperature. As the temperature is raised the lines broaden and then merge. Evidently the Jahn–Teller distortion is frozen in at sufficiently low temperatures, but reorients with increasing frequency as the temperature is raised. As the frequency of reorientation approaches the low temperature line width the lines broaden; as it approaches the overall splitting between lines the individual lines merge.

The width of a number of lines was measured as a function of temperature. The results were analyzed assuming that the effects of motion on line width could be represented by a temperature dependent correlation time for the persistence of a given orientation. There are two types of reorientation for the Jahn–Teller distortion, inversion and rotation. For example, a distortion in the (001) direction can reorient by inversion to the (00$\bar{1}$) direction and by rotation to the (100), ($\bar{1}$00), (010), and (0$\bar{1}$0) directions. The results seem to indicate an energy barrier of about 0·02 eV to reorientation by inversion and a slightly lower energy barrier to rotation. Nevertheless, reorientation by inversion competes with rotation in the temperature range investigated (25°–45°K) because the frequency factor ($\sim 5 \times 10^{11}$) is about a factor of five greater. The energy barrier to inversion (0·02eV) is also an estimate to the Jahn–Teller energy.

One might expect hyperfine interaction of the nickel center with $Ge^{73}$ (7·7 per cent natural abundance, nuclear spin $I = 9/2$) occupying the nearest neighbor sites. Since there are four such sites one anticipates four sets of ten hyperfine lines associated with each main line for arbitrary direction of the magnetic field relative to the crystalline axes. However, the Jahn–Teller distortion moves the nickel atom closer to two of the four nearest neighbors and further away from the other two. Only two sets of ten well resolved hyperfine lines are observed; these are attributed to a $Ge^{73}$ isotope in either of the two closer positions. The hyperfine interaction with $Ge^{73}$ in the two further nearest neighbor positions also has been detected. The splitting between adjacent hyperfine lines is apparently $\sim 4$ G, but an indication of only the outermost lines is seen since the full width is also $\sim 4$ G.

As one would expect, a principal axis for the resolved hyperfine interaction with $Ge^{73}$ is the (111) direction from the nickel to the $Ge^{73}$ atom. The hyperfine interaction is a maximum for the magnetic field along the Ni–$Ge^{73}$ axis ($T_{\parallel} = 19{\cdot}8 \times 10^{-4}\ \mathrm{cm}^{-1}$) and a minimum at right angles to the axis ($T_{\perp} = 16{\cdot}5 \times 10^{-4}\ \mathrm{cm}^{-1}$).

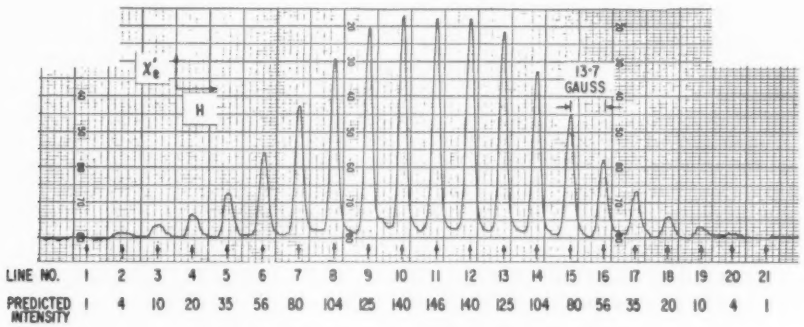


FIG. 1. Electron spin resonance spectrum of manganese-doped silicon at ~14 kMc/sec. The magnetic field direction is so chosen that the crystalline field splitting vanishes ($n_1^2 n_2^2 + n_2^2 n_3^2 + n_3^2 n_1^2 = 1/5$) and 21 hyperfine lines are observed. At the temperature chosen, ~15°K, the relaxation time is such that the real part $\chi'_e$ of the magnetic susceptibility of the sample traces out the absorption envelope.[5]

Hyperfine structure due to interaction with $Ni^{61}$ has been detected[1] in samples doped with nickel enriched to contain 83 per cent of that isotope. The principal axes of the hyperfine interaction are the same as those of the $g$-tensor, and one finds the principal values $A_1 = 10{\cdot}3$, $A_2 \leqslant 1{\cdot}6$, $A_3 = 12{\cdot}2$ (in units of $10^{-4}$ cm$^{-1}$) in the directions corresponding to $g_1 = 2{\cdot}1128$, $g_2 = 2{\cdot}0294$, and $g_3 = 2{\cdot}0176$.

## REFERENCES

1. Ludwig G. W. and Woodbury H. H. *Bull. Amer. Phys. Soc.* Ser. II, **3**, 135 (1958); Woodbury H. H. and Ludwig G. W. *Phys. Rev. Letters* **1**, 16 (1958). A more complete analysis of the nickel spectrum is in preparation.
2. Watkins G. D. *Bull. Amer. Phys. Soc.* Ser. II, **2**, 345 (1957).
3. Manganese metal was alloyed to silicon bars $\sim 3 \times 3 \times 10$ mm in dimension held in quartz tubes. The tubes were then evacuated and held at $\sim$1230°C for about 18 hr. The samples were quenched by dropping the quartz tubes into water.
4. Carlson R. O. *Phys. Rev.* **104**, 937 (1956).
5. Portis A. M. Technical Note No. 1, *Magnetic Resonance in Systems with Spectral Distributions.* Sarah Mellon Scarfe Radiation Laboratory, University of Pittsburgh (November 15, 1955).

VOL
8
195

*J. Phys. Chem. Solids* Pergamon Press 1958. Vol. 9. pp. 492–494. Printed in Great Britain

R.3

# SPIN RESONANCE OF DONORS IN CdS*

JOHN LAMBE and CHIHIRO KIKUCHI

Willow Run Laboratories, University of Michigan, Ypsilanti, Michigan.

## 1. INTRODUCTION

The subject of donor centers in cadmium sulfide has been of interest from two viewpoints. First it appears that such centers play an important role in luminescence phenomena and secondly they are, of course, important in connection with the semiconduction properties of CdS. One of the most widely studied of these donor centers is that due to the incorporation of chlorine into cadmium sulfide. It is found that this impurity gives rise to a donor level 0·03 eV below the conduction band. The center arises from the substitution of a singly negative chlorine ion for the doubly negative sulfur ion. This leaves a net positive charge in this region which can bind an additional electron. The center thus has a negatively charged core (due to $Cl^-$) with a surrounding positively charged region. The electron bound to such a center would be expected to show paramagnetic resonance. At 300°K the centers are essentially completely ionized and the crystals may have fairly high conductivity. At 4°K the free electrons are bound at the $Cl^-$ centers so that the crystals are highly insulating and spin resonance experiments can be carried out quite easily.

* This work was supported by the Air Force Office of Scientific Research.

## 2. EXPERIMENTAL METHODS AND RESULTS

In the experiments reported here an X band paramagnetic resonance spectrometer was used, operating at about 9300 Mc/s. Samples were placed along the axis of a cylindrical cavity operating in the $TE_{011}$ mode. Straight crystal detection was used with 5 kc/s magnetic field modulation and lock-in detector.

Crystals of CdS with added chlorine were measured at 4°K, and a large spin resonance signal was observed. Since CdS has hexagonal crystal structure, long needlelike crystals were used so that the $C$ axis of the crystal could be oriented with respect to the magnetic field. For such crystals a single line was observed with a $g$ value dependent upon orientation of the $C$ axis, as shown in Fig. 1.

The measured $g$ values are $g_\perp = 1{\cdot}78$, $g_{||} = 1{\cdot}79$.

The line width is approximately 8 G. No hyperfine structure was observed. The resistivity of these crystals was about 1 Ω cm at room temperature. This indicates a carrier concentration $10^{17}$ electrons/cm$^3$.

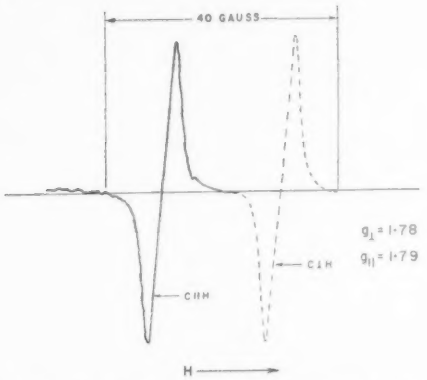


FIG. 1. Observed spin resonance spectrum of a CdS : Cl crystal at 4°K.

Measurements were also made on CdS crystals of higher resistivity to check that the signal was indeed associated with the presence of the donor center. Samples with resistivities in the range of $10^5$ to $10^6$ Ω cm were measured and no signal could be detected. This means that any signal was at least 1000 times smaller than the signal observed for the CdS : Cl sample.

### 3. DISCUSSION

The foregoing experiments indicate that the chlorine center in CdS does give rise to a paramagnetic resonance absorption. The major points of interest concern the observed $g$ value, its magnitude and the observed anisotropy. A rigorous quantitative treatment of this would be quite involved, but some semi-quantitative observations can be made which are of interest.

As a model for this center we may note some similarity to the $F$ center in the alkali halides. In the case of the $F$ center important contributions to the $g$ value arise from the fact that the electron wave function extends over neighboring potassium ions.[3, 4] The essential theoretical problem is the evaluation of the wave function at these neighboring ions. In the case of the chlorine center a similar situation should arise with extension of the wave function onto neighboring cadmium ions.

In the case of the $F$ center theoretical considerations[4] lead to the expression of the following form for the shift in $g$ value from the free electron value ($\Delta g \cong -0{\cdot}007$ for the $F$ center)

$$\Delta g \propto \frac{1}{E_F} \sum_{\alpha i} \langle F|\alpha_i\rangle \lambda_\alpha \qquad (1)$$

$E_F$ = excitation energy for $F$ center

$\langle F|\alpha_i\rangle$ measures the magnitude of the $F$ center wave function overlap with the core orbitals on surrounding ions

$\lambda_\alpha$ is the spin–orbit coupling parameter for the core orbital.

The application of the above type of expression to the CdS:Cl problem involves the evaluation of many factors in detail, however it is interesting to note the direct dependence of $\Delta g$ upon $E_F$. In the case of the $F$ centers, $E_F$ is of the order 2 eV. In the case of CdS:Cl this value would be 0·03 eV, or less. This then has a large effect on $\Delta g$. This factor alone would indicate that $\Delta g$ for CdS:Cl should be about 60 times as large as for the $F$ center. It is seen that $\Delta g \cong -0{\cdot}2$ for CdS:Cl which is in fact about 30 times as large as for the $F$ center. Needless to say the other factors in (1) will also be quite different but the above considerations illustrate the importance of excitation energy in connection with $\Delta g$.

The anisotropy in $g$ is of special interest in that the following point is involved. CdS has the typical wurzite lattice structure and is thus quite similar to ZnS. In the case of ZnS, however, a sulfur site is surrounded by a tetrahedron of zinc ions and all the zinc ions are equidistant from the sulfur site, the distance being 2·33 Å.[5] For the case of CdS, however, there is a distortion of the tetrahedron and the distances to nearest cadmium ions are not equal, being 2·51 Å and 2·53 Å.[5] On ZnS the complex of zinc ions around a sulfur site should show cubic symmetry even though the lattice is not cubic. In the case of CdS, the difference in ionic distances may be sufficient to cause the anisotropy in $g$. This point can perhaps be checked by calculation. On the other hand, if the wave function of the donor electron extends significantly beyond nearest neighbor cadmiums, this could also introduce the anisotropy in $g$.

The lack of hyperfine structure precludes the direct identification of the spin resonance with the

chlorine by this means. This lack is, however, not surprising. In this case the chlorine core is already negative and would tend to minimize the interaction of the additional electron with the chlorine nucleus. Hyperfine interaction with the cadmium may be expected but the extent of this is not known.

It was noted that with the power available in the X band spectrometer, about 25 mW, and with a cavity $Q$ of 2000, there were no apparent saturation effects. This indicates that the spin lattice relaxation time is quite short ($10^{-6}$ or less). This is consistent with the large amount of orbital motion implied by the large $\Delta g$.

*Acknowledgments*—We wish to thank the following persons for kindly providing us with various samples of CdS. Dr. R. H. BUBE of the RCA Laboratories, Dr. F. A. KROGER of the Philips Laboratories, Prof. CYZAK of the University of Detroit, Dr. Y. SIVRONEN of the General Motors Laboratories.

### REFERENCES

1. KROGER F. A., VINK and VAN DEN BOOMGAARD, *Z. Phys. Chem.* **203,** 1 (1954).
2. BUBE R. H. *Phys. Rev.* **23,** 18 (1955).
3. ADRIAN F. J. *Phys. Rev.* **107,** 488 (1957).
4. BLUMBERG W. E. and DAS T. P. *Phys. Rev.* **110,** 647 (1958).
5. WYCKOFF R. W. G. *Crystal Structures*, Vol. 1, p. 31. Interscience Publishers, New York (1948).

VOL
8
195

*J. Phys. Chem. Solids* Pergamon Press 1959. Vol. 8. pp. 494–495. Printed in Great Britain

# R.4 CYCLOTRON RESONANCE IN CADMIUM SULFIDE*

R. N. DEXTER
The University of Wisconsin, Madison, Wisconsin

## 1. EXPERIMENTAL

PRELIMINARY experiments on cyclotron resonance in CdS have been performed at liquid air and liquid helium temperatures using 1·25 cm microwaves. Free charge carriers were excited using visible and infrared light separately or in combination. In initial experiments polarized light was not used and the infrared light was that transmitted by quartz and germanium therefore in the 2–3 $\mu$ range.

CdS samples selected from those grown by D. C. Reynolds of Wright Air Development Center showed no visible edge luminescence at low temperature and were selected on that basis since they proved to have the highest mobility of free carriers. A typical sample grown by the vapor-phase reaction was about $2 \times 1 \times 0{\cdot}01$ mm and was a plane containing the $c$ axis of the hexagonal structure.

Despite strong visible light and infrared photoconductivity at 78°K, very poor photoconductivity was found at liquid helium temperatures. The sample was mounted near one end of a tapered quartz light pipe and the light from a 1000-watt tungsten projection lamp was focused into the other end. Ultraviolet and infrared sources were also used and various filters were available. Following earlier techniques of cyclotron resonance in semiconductors,[1] light was chopped at 90 c/s. Microwave magnetoconductivity changes at that frequency were recorded following a narrow band amplifier and phase sensitive detector. In samples showing high mobility, triggered light experiments demonstrated that photoconduction easily followed the 90 c/s alternation of light intensity.

## 2. RESONANCE RESULTS

Microwave magnetoconductivity of CdS at 78°K gave evidence that infrared produced carriers with a mobility of about $2 \times 10^5$ cm$^2$/V-sec and that visible light produced carriers with a mobility about one-fifth as large. Infrared quenching of the visible light photoconductivity was demonstrable in some samples as in earlier d.c. experiments.[2]

At temperatures of 1·2 to 4·2°K the following cyclotron resonance observations were made using linearly polarized microwaves.† In several samples,

* Supported by the Alfred P. Sloan Foundation, the Wisconsin Alumni Research Foundation, and the Thomas Brittingham Trust Fund.

† Insufficient carrier concentrations were produced in the circular polarization system used. This system if successful would allow determining carrier sign directly as described in DRESSELHAUS *et al.*[1]

infrared preferentially produced carriers of effective mass $\simeq 0{\cdot}07\, m_0$ where $m_0$ is the mass of the free electron. This effective mass showed a moderate anisotropy. Visible light (and infrared depending on the light intensity) produced some of these low mass carriers but more abundantly carriers on two different types of energy surfaces. One of these surfaces had an effective mass parameter of about $0{\cdot}36\, m_0$ and approximately 17 per cent anisotropy in the cyclotron mass. The other surfaces appeared to be 3 (or 6) ellipsoids having cyclotron mass parameters in the range of $0{\cdot}09\, m_0$ to $0{\cdot}22\, m_0$ and with an average or conductivity mass estimated to be about $0{\cdot}14\, m_0$. Incomplete results did not permit separation of the data to give the components of the mass tensor. A trace obtained under highest resolution appears in Fig. 1.

### 3. DISCUSSION

One tentative interpretation of these initial results is that the top of the valence band of CdS is of high curvature and is near or at $k = 0$. Holes in this band are assumed to account for the $0{\cdot}07\, m_0$ carrier excited preferentially by infrared. This identification is not entirely justified. It is based on the following results and the fact that across-the-gap excitation generally produces conduction by electrons. Less pure CdS samples having a strong visible light photoconductivity of very long lifetime due to demonstrable carrier trapping had conduction by relatively low mobility carriers. Nevertheless, infrared photoconductivity in the same sample at the same temperature followed the 90 c/s chopping rate and gave carriers of relatively high mobility as measured by the microwave magnetoconductivity effect.

The other two types of carriers which appeared to be excited by the same radiation are then assumed to correspond to minima in the conduction band in two regions near the same energy value. One minimum at $k = 0$ corresponds to the $0{\cdot}36\, m_0$ effective mass. The other minima in the conduction band correspond to 3 (or 6) ellipsoids with a mass ratio of at least 5:1 in components of the mass tensor. The location of these ellipsoids in $k$-space and energy is unknown. Electrons at $k = 0$ are produced somewhat more abundantly and are presumably at lower energy than electrons on the ellipsoids.

As discussed by DRESSELHAUS[3] optical absorption experiments in CdS[4] are consistent with band extrema at $k = 0$ although other possibilities exist. Ellipsoids at slightly higher energies might presumably be seen via indirect optical transitions.

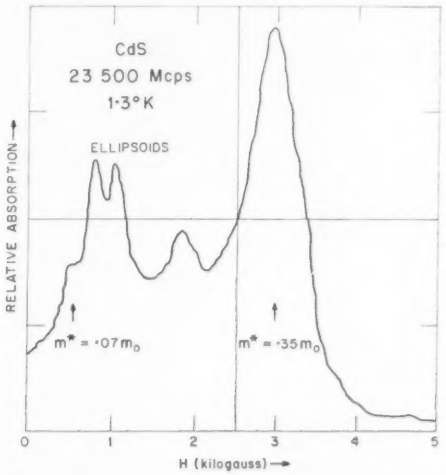


FIG. 1. Cyclotron resonance in CdS at 1·3°K and 23,500 Mc/s with preferential excitation of the $0{\cdot}36 m_0$ carrier and the carriers on ellipsoids. $H$ is nearly perpendicular to the $c$ axis. $\omega\tau \approx 10$ corresponding to $\tau \approx 6{\cdot}7 \times 10^{-11}$ sec.

We hope by further experiments to eliminate the ambiguities present in these preliminary results. Initial experiments in hexagonal ZnS showed results qualitatively similar to those in CdS but with appreciably smaller resolution.

*Acknowledgments*—The author is grateful to Prof. D. L DEXTER for suggesting the experiment, to Dr. D. C. REYNOLDS for providing the high purity CdS, to Prof. R. RETHERFORD for providing CdS samples from several sources, and to Mr. W. R. DATARS for help with some of the measurements.

### REFERENCES

1. DRESSELHAUS G., KIP A., and KITTEL C. *Phys. Rev.* **98,** 368 (1955).
   DEXTER R., ZEIGER H., and LAX B., *Phys. Rev.* **104,** 637 (1956).
2. For example see TUTIHASI S. *J. Opt. Soc. Amer.* **46,** 443 (1956).
   BUBE R. *Phys. Rev.* **99,** 1105 (1955).
3. DRESSELHAUS G. *Phys. Rev.* **105,** 135 (1957).
4. GROSS E. and JACOBSON M. *Dokl. Akad. Nauk. SSSR* **102,** 485 (1955).
   FURLONG L. and RAVILIOUS C. *Phys. Rev.* **98,** 954 (1955).

*J. Phys. Chem. Solids* Pergamon Press 1959. Vol. 8. pp. 496–498. Printed in Great Britain

R.5

# CROSS MODULATION OF D.C. RESISTANCE BY MICROWAVE CYCLOTRON RESONANCE*

H. J. ZEIGER, C. J. RAUCH, and M. E. BEHRNDT†

Lincoln Laboratory, Massachusetts Institute of Technology, Lexington, Massachusetts.

## 1. INTRODUCTION

A NUMBER of experiments on the transport properties of semiconductors at low temperatures have indicated marked deviations from Ohm's law at moderately low applied electric fields. In some of these experiments,[1] the deviations are due to a change in number density of carriers, as well as variation of mobility with carrier energy. Cyclotron resonance observations of FLETCHER[2] at low microwave powers show a considerable line narrowing, as well as the onset of low quantum state effects.

These observations indicate a heating of the carriers at high microwave powers. It might be expected that this heating would produce a change in the d.c. mobility of the carriers, so that the occurrence of cyclotron resonance could be observed by detecting changes in d.c. resistance. We have observed this effect in Ge, Si, and possibly in *p*-type InSb.

We have developed a theory of the "Cross-modulation" phenomenon, in the presence of a d.c. magnetic field, which is generalized to describe the change in current flow at a combination frequency due to the application of electric fields at a number of frequencies. The theory will be discussed in detail in a later publication. It is based on an iterative solution of the Boltzmann transport equation. The structure of the solution is analogous to that of a quantum-mechanical perturbation theory, with a current proportional to Fourier components of the field. For example

$$\mathcal{J}_3(\omega_\gamma) \sim E(\omega_\alpha)E(\omega_\beta - \omega_\alpha)E(\omega_\gamma - \omega_\beta), \quad (1)$$

with a number of resonant factors in the denominator.

For the special case of d.c. cyclotron resonance cross modulation, d.c. and r.f. electric fields are applied simultaneously, and a d.c. current $\mathcal{J}_3(0)$ is generated. (A typical contribution in this case consists of r.f. factors with $\omega_\alpha = -\omega, \omega_\beta = \omega$, and the d.c. factor with $\omega_\gamma = 0$.) The result of the general theory is that, as the magnetic field is swept through cyclotron resonance, $\mathcal{J}_3(0)$ will describe a line similar to the usual cyclotron resonance absorption line.

## 2. EXPERIMENTAL PROCEDURE

The sample (~3 mm in maximum dimension) with leads attached is supported from a quartz rod in the high electric field region of a microwave cavity immersed in a liquid-helium bath. The microwave plumbing is that of a conventional *K* band bridge. The static magnetic field is slowly swept through resonance, as in the usual technique. However, the resonance peaks are observed by detecting changes in the d.c. resistance of the sample. A convenient method of operation has been amplitude modulation of the microwave power at 260 cycles, and observation of the 260 cycle component of sample resistance by means of a phase sensitive detection system. The power modulation tends to minimize the magnetoresistance background. However, good ohmic contacts are also desirable to eliminate a rectified microwave background signal. Cross modulation seems to yield a significantly better signal-to-noise ratio than the conventional method of observing cyclotron resonance by detecting microwave power absorption.

## 3. EXPERIMENTAL RESULTS

Cross modulation was initially observed in very pure germanium having an $\omega\tau \sim 22$ at 4·2°K. Low intensity light illumination was necessary to excite carriers in the sample. A small d.c. voltage (~0·2 V) was applied across the sample and the resonance signal was observed across a small resistor in series

* The research reported in this document was supported jointly by the Army, Navy, and Air Force under contract with the Massachusetts Institute of Technology.

† Now at International Business Machines Corporation, Poughkeepsie, New York.



VOL 8 195

with the sample. Subsequently, cross modulation in germanium was observed just as easily with no externally applied voltage; apparently a kind of resonant photoelectromagnetic effect is observed.

Fig. 1 shows a recorder trace of cyclotron resonance cross modulation in germanium as a function of magnetic field with no external voltage applied. A resonance may appear as an increase or decrease in signal. Changes in light intensity and/or orientation may reverse the resonance signal of any of the carriers.

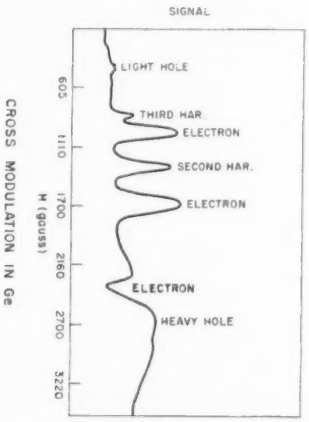


FIG. 1. Cross modulation in Ge.

A recorder trace of cyclotron cross modulation in $n$-type silicon at 1·14°K is shown in Fig. 2. The carriers are optically excited and resonance is detected with no applied d.c. voltage. The crystal has an $\omega\tau \sim 50$, which gives narrow enough lines to give an apparent splitting of the low field electron line, due to the slight tipping of the static magnetic field out of the (110) plane. The peaks of the absorption lines all exhibit small dips as does the light hole line of germanium in Fig. 1. This may be due to a decrease in the $\omega\tau$, on sweeping through resonance under high microwave power, caused by a heating of the sample.

Indications of cyclotron resonance cross modulation have been observed in $p$-type indium antimonide. However, the peculiar magnetoresistance behavior of InSb introduces complications in the observations. Frequently, lines of an apparently resonant character appear, which are due to the d.c. magnetoresistance. Magnetic field modulation of the sample in the presence and absence of the C.W. microwave electric field is used to distinguish true microwave effects from magnetoresistance phenomena. Surface effects and hysteresis effects in conjunction with bistable states have introduced further complications.

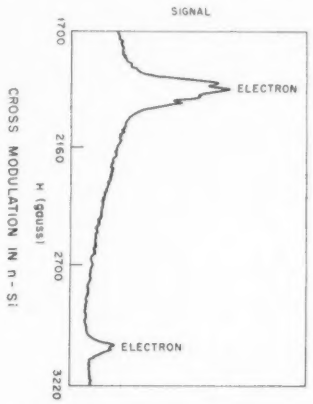


FIG. 2. Cross modulation in $n$-Si.

## 4. DISCUSSION

The theory of cross modulation shows that the effect vanishes if the carrier relaxation time is independent of the energy. Thus it appears appropriate to regard cross modulation as a carrier heating effect which produces changes in the d.c. mobility.

In addition to the usual resonances in germanium several new ones of somewhat lower intensity have been detected. Some of these may be related to the quantum transitions discussed by LUTTINGER[3] and observed by FLETCHER *et al.*[2]

For open circuit conditions, photo voltages occur and the cross modulation effect is also observed. The general theory has been extended to consider this case, by the addition of a diffusion term to the Boltzmann transport equation. It is shown that an open circuit voltage appears, which again describes lines similar to the usual cyclotron resonance absorption line.

As mentioned earlier, a resonance may appear as either an increase or a decrease in signal; furthermore, lines reverse with light intensity and orientation. A simple treatment of these phenomena has been developed for a semiconductor having a number of different spherical-energy-surface charge carriers, each characterized by an effective mass,

relaxation time function and number concentration. The theory has not been developed for ellipsoidal surfaces because of the added complications, but similar results would be expected.

Finally, it should be mentioned that the cross modulation theory also predicts the generation of a current $\mathcal{J}_3(3\omega)$, when an electric field $E(\omega)$ is applied. When a carrier with a cyclotron resonance frequency $\omega_c$ is present, $\mathcal{J}_3(3\omega)$ becomes large when $3\omega \sim \omega_c$, owing to absorption. This may be thought of as corresponding to a transition with the absorption of 3 quanta. This phenomenon may have been observed by R. N. DEXTER in Sb.[4]

*Acknowledgment*—We wish to thank our colleagues at Lincoln Laboratory for many stimulating discussions.

## REFERENCES

1. KOENIG S. H. and GUNTHER-MOHR G. R. *J. Phys. Chem. Solids* **2,** 268 (1957).
   KOENIG S. H. *Phys. Rev.* **110,** 986 (1958).
2. FLETCHER R. C., YAGER W. A., and MERRITT F. R. *Phys. Rev.* **100,** 747 (1955).
3. LUTTINGER J. M. *Phys. Rev.* **102,** 1030 (1950).
4. DEXTER R. N. private communication.

VOL
8
195

*J. Phys. Chem. Solids* Pergamon Press 1958. Vol. 8. pp. 498–504. Printed in Great Britain.

R.6

# NUCLEAR MAGNETIC RESONANCE STUDIES OF DOPED III–V COMPOUNDS

E. H. RHODERICK

Services Electronics Research Laboratory, Baldock, Herts., England.

**Abstract**—The dominant effect of impurities on the magnetic resonance of the host nuclei in III–V compounds consists of broadening brought about by the interaction of the nuclear quadrupole moments with inhomogeneous electric fields. These electric fields may be either the Coulomb fields associated with ionized impurities or the distortions of the crystalline field caused by the elastic strains around neutral imperfections. In both cases the interaction is strong enough for $\sim 10^3$ or more nuclei around each impurity atom to be affected, so that the significance of the lattice structure disappears, and information about the immediate vicinity of the imperfection is not directly obtainable. In spite of this, there are cases in which the magnitude of the broadening, in conjunction with Hall effect measurements, yields qualitative information about the type of imperfection involved. For example, nuclear resonance shows that Si atoms enter the GaAs lattice in two forms, one of which acts as a donor while the other is electrically neutral.

## 1. INTRODUCTION

ABOUT four years ago, BLOEMBERGEN[1] published a comprehensive analysis of the various ways in which nuclear magnetic resonance in a crystal may be affected by the presence of imperfections. Altogether, there are at least ten different ways in which the host nuclei may interact with various types of defect, and provided one can unravel them it is often possible to obtain useful information about the nature of the imperfection. In imperfect III–V semiconductors, the situation is simplified by the fact that there is one interaction which dominates all others, namely the coupling of the nuclear electric quadrupole moments to the inhomogeneous electric fields associated with crystal defects. This is because, apart from $P^{31}$, all the nuclei which occur in III–V compounds have large quadrupole moments, and also because, as will appear later, the properties of these compounds are such that very large field gradients may exist at the positions of the nuclei.

The main features of nuclear resonance in perfect

III–V semiconductors were first established by SHULMAN and his collaborators.[2, 3] In all of those so far studied (InSb, GaSb, InAs, GaAs), the line width in a single crystal of pure material is many times larger than would be expected from dipolar interactions, and is due to the $\mathbf{I}_1.\mathbf{I}_2$ coupling between pairs of nuclei which occurs via the electrons. This interaction is independent of the orientation of the crystal axes relative to the magnetic field; consequently, apart from possible quadrupolar effects arising from dislocations introduced during the crushing process, which will be discussed in the following section, it is immaterial whether the resonance is observed in a single crystal or in a powder.

## 2. GENERAL FEATURES OF QUADRUPOLAR INTERACTIONS IN CRYSTALS

If a nucleus having a magnetic moment and an angular momentum $I\hbar$ is placed in a magnetic field, then, in the absence of any quadrupolar effects, the $2I + 1$ Zeeman states are equidistant in energy. Since the only allowed transitions are those between adjacent states, the $2I$ possible transitions coincide in frequency and the nuclear resonance spectrum consists of a single line. If, however, the nucleus has an electric quadrupole moment and there exists in addition to the magnetic field an inhomogeneous electric field, the interaction between the quadrupole moment and the electric field gradient perturbs the Zeeman states so that they are no longer equidistant; the $2I$ allowed transitions no longer coincide, and the nuclear resonance spectrum consists of $2I$ discrete lines. When $2I$ is an odd integer, as is usually the case, the central component is unchanged in frequency by the quadrupolar interaction, and the remaining $2I$–1 lines, known as satellites, are grouped symmetrically about it. In general there exist intense electric fields within a solid and, if the crystal symmetry is such that the field gradient does not vanish at the sites of the nuclei under consideration, the nuclear magnetic resonance spectrum in a single crystal will be split into $2I$ lines, as was vividly demonstrated by POUND.[4] In perfect crystals with cubic or tetrahedral symmetry, such as those having the zincblende structure, the gradient of the electric field vanishes at the site of each nucleus, so that there are no quadrupolar effects. In the neighbourhood of a dislocation, however, the symmetry of a crystal is modified slightly by strain, so that the electric field gradient at the nucleus may no longer vanish. If this is the case, the contribution of an individual nucleus to the absorption spectrum will be split into $2I$ lines, the separation of which depends on the magnitude and symmetry properties of the field gradient tensor at the nucleus in question. Since these will vary from nucleus to nucleus according to the geometrical arrangement of the dislocations, the satellites will become smeared out into a continuous band while the central component remains unaltered, and the absorption curve becomes broader. An increase in the width of the $In^{115}$ resonance in a powdered specimen of pure InSb, compared with that in a single crystal, has been observed by RHODERICK[5] and attributed to this cause. That dislocations can be introduced into a brittle material like InSb by crushing at room temperature is rather surprising, but independent confirmation has been obtained by ALLEN[6] using etch-pit techniques. The writer has also shown[5] that the $In^{115}$ resonance in a good single crystal of high purity InSb, having the remarkably low dislocation density of $\sim 10^3$ cm$^{-2}$, is almost completely free from quadrupolar broadening. Evidently such a crystal is very near to perfection so far as its nuclear resonance characteristics are concerned.

## 3. THE EFFECT OF DOPING

In general, the introduction of foreign atoms into a crystal causes strong inhomogeneous electric fields. These electric fields may be brought about in two different ways. In the case of a charged impurity atom, such as an ionized donor or acceptor, the field is predominantly the Coulomb field of the ion. This is screened to a certain extent by the free carriers, but in a semiconductor the screening is small. In the case of neutral impurities, such as foreign group III or group V elements in III–V compounds, the field gradients at the nuclear sites are generated by the distortion of the crystalline field resulting from the strain in the lattice around the impurity atom. Since the magnitude of the electric field gradient and the direction of its symmetry axis will vary from one nucleus to another, the satellites are smeared into a continuous band in the manner already described. The theory of quadrupolar broadening by point defects has been developed by COHEN and REIF;[7] it is sufficient for the present purpose that, as the concentration increases, the average distance of a nucleus from a defect decreases and the absorption curve broadens. It is often convenient to use the maximum value of the derivative of the nuclear absorption, $(\partial\chi''/\partial\nu)_{\max}$, as a measure of the broadening, because the derivative is a sensitive function of the width of the curve and is the quantity usually recorded by nuclear resonance spectrometers.

The effect of charged impurities is illustrated by the broadening of the $In^{115}$ resonance in InSb by Te, which is a donor. Fig. 1, taken from reference (5), shows how $(\partial\chi''/\partial\nu)_{\max}$ varies with Te concentration. It follows from the discussion in the previous section that the nuclear resonance intensity should

never fall below that due to the central component alone, since this is unaffected by the quadrupolar interaction. This is the result as long as the interaction is treated only to first order; if the second order interaction is considered, one concludes that the central component is broadened also. The relative contribution of the central component is extrapolates smoothly to the value 0·15 for zero concentration, is due to second-order broadening of the central component. A surprising feature of this phenomenon is the remarkably high sensitivity of the resonance signal to a comparatively low concentration of Te atoms; the satellites are almost completely removed by a concentration of $10^{18}$ cm$^{-3}$,

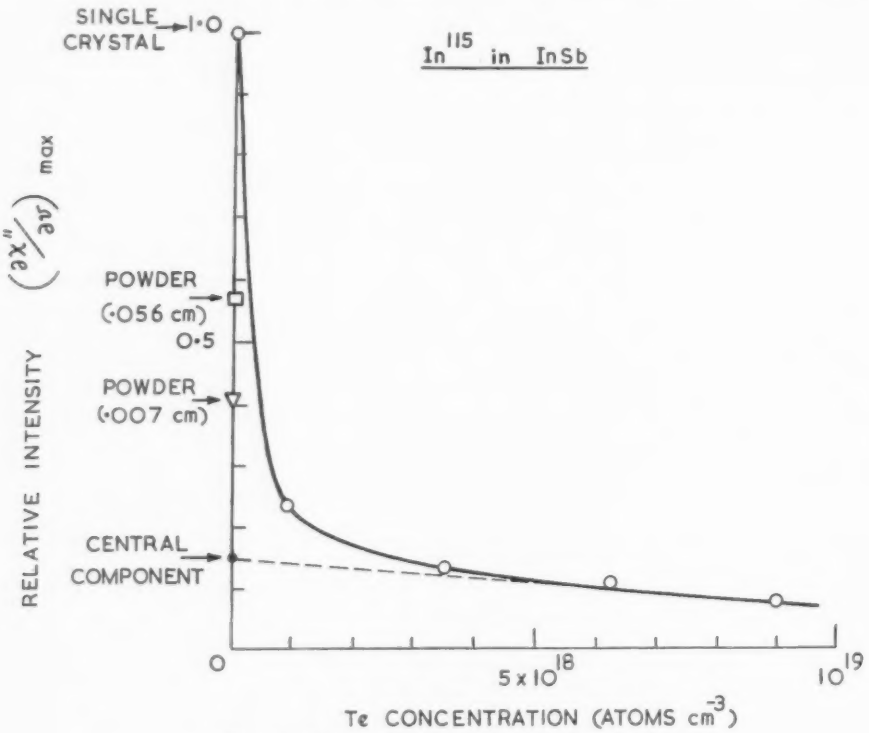


FIG. 1. Variation with Te concentration of derivative of In$^{115}$ resonance in InSb. Also shown are results for two particle sizes of the pure powdered material. (290°K).

easily calculable, since it depends only on the matrix elements connecting the various Zeeman states. For In$^{115}$, which has $I = 9/2$, the central component should contribute $25/165 = 0{\cdot}15$ of the total intensity in the perfect crystal. The fact that for large Te concentrations the amplitude of the resonance falls below this value shows that second order effects must be contributing. Fig. 1 can now be interpreted as follows. The initial sharp decrease in the intensity of the nuclear resonance signal corresponds to first-order broadening of the satellites, while the subsequent gradual fall, which for which the average distance between impurity atoms is about 100Å. To explain this high sensitivity it is necessary to multiply the field gradient $\partial^2 V/\partial r^2 = 2e/r^3$, which would obtain in free space at a distance $r$ from an ion of charge $e$, by an empirical factor $\beta$ which must be $\simeq 350$. This multiplication factor expresses the effect on the field gradient of complex polarization effects within the solid. The chief contribution to $\beta$ comes from the "antishielding factor" introduced by STERNHEIMER[8] to denote the enhancement of the field gradient at the nucleus of an atom caused by

the distortion of the surrounding electron cloud. Since the other factors involved in $\beta$ cause a three-fold reduction in the field gradient,[7] the antishielding factor must be $\sim 1000$. It has been suggested by the author[5] that this large value may be connected with the small energy gap in InSb (0·18 eV). Briefly, the argument rests on the fact that a distortion of the electron distribution around a nucleus can be achieved only by admixing with the original wavefunction new wavefunctions corresponding to excited states. The ease with which this can be done varies inversely as the difference in energy between the initial state and the excited states involved; consequently, the electron distribution around a nucleus in a semiconductor with a small energy gap should be much more easily distorted than that in, say, an insulator with a forbidden gap of several eV.

In InSb the effect of an acceptor impurity, such as Zn, is qualitatively the same as that of Te, except that, for a given impurity concentration, the increase in the line width is slightly less pronounced in *p*-type specimens because holes are more effective than electrons in screening the ionic charge, owing to their greater effective mass. The effect on the nuclear resonance in GaSb of doping with *p*- and *n*-type impurities has also been investigated by OLIVER,[9] with qualitatively similar results.

The effect of neutral impurities is typified by the behaviour of the $In^{115}$ resonance in mixed crystals of InSb and GaSb.[5] For low Ga concentrations, the variation of the derivative of the absorption with concentration is very similar to that shown in Fig. 1 except that, for a given reduction in $(\partial\chi''/\partial\nu)_{max}$, the Ga concentration must be about 30 times that of Te. In the case of neutral impurities, the field gradients result from the strain set up in the lattice by the disparity between the sizes of the foreign atoms and the host atoms which they replace. In InSb, the tensor relating the field gradient to the strain which causes it is known from some elegant experiments by SHULMAN, WYLUDA, and ANDERSON,[10] who studied the effect of elastic compression on nuclear resonance lines in single crystals. Using their results, once can show[5] that the effect of the Ga atoms in InSb is remarkably well explained by a simple model in which the strain around a Ga atom is a pure radial one whose magnitude is given by $\Delta r/r = a_2^2\,(a_2 - a_1)/r^3$, where $a_1$ and $a_2$ are the "tetrahedral covalent radii" of In and Ga atoms respectively, as given by PAULING.[11] This is the strain predicted by elasticity theory for an isotropic elastic medium if the material within a sphere of radius $a_1$ is contracted to radius $a_2$. It can also be deduced that the field gradient at a given distance from a Ga atom which replaces an In atom in InSb is about 30 times less than that produced by the Coulomb field of an ionized impurity. This result is of some importance for the interpretation of the Te experiments, since the substitution of a $Te^+$ ion for an Sb atom must also cause strain in the lattice. From a knowledge of the radii of the two atoms, we should expect this strain to be comparable in magnitude to that caused by Ga. It is therefore clear that the effect of the Te atoms on the nuclear resonance is almost entirely due to their charge.

### 4. AN EXAMPLE: THE BEHAVIOUR OF Si IN GaAs

The motive for studying the effect of impurities on the resonance of the host nuclei in III–V compounds was the hope that one might be able to learn something about the way in which the foreign atom fits into the lattice; for example, that one might be able to tell whether a given impurity is interstitial or substitutional. To obtain information of this sort it is necessary that any observed change in the nuclear resonance spectrum shall represent the behaviour of nuclei in the immediate vicinity of the impurity atom. However, even in the case of neutral impurities, the quadrupole interaction is such a long range one that about $10^3$ nuclei around the foreign atom are affected, so that the effect of the lattice structure disappears and information about the immediate vicinity of the imperfection is not directly obtainable. Nevertheless, there are cases in which nuclear resonance experiments, in conjunction with data obtained from other sources such as Hall effect or X-ray measurements, may yield useful information about the behaviour of impurities in III–V semiconductors. An example of this is the case of Si in GaAs.

In the course of an investigation of the effects of various impurities on the electrical properties of III–V compounds, EDMOND[12] in this laboratory has shown that Si behaves as a donor in GaAs, which implies that it replaces Ga. The minimum Hall constant attainable is 1·5, which means that the maximum solubility of Si atoms replacing Ga in

GaAs is about $4 \times 10^{18}$ atoms per cm$^3$. On the other hand, KOLM, KULIN, and AVERBACH,[13] on the basis of X-ray measurements of the lattice parameters of GaAs–Si alloys, assert that Si can enter the GaAs lattice in some electrically neutral form to the extent of $\frac{1}{2}$ per cent, i.e. $1{\cdot}1 \times 10^{20}$ atoms per cm$^3$, and suggest that this neutral form consists of pairs of Si atoms replacing a GaAs molecule. There is no inherent contradiction between these two statements; Si undoubtedly does make GaAs *n*-type, but there is no reason why it should not enter the lattice in some neutral manner in addition to behaving as a donor.

Let us now consider how the nuclear resonance signal will be affected in the two cases. If Si atoms can only replace Ga atoms, acting as donors, then the effect on the line width should be exactly the same as that of any other donor, such as Te, since we have already seen that the charge effect is much greater than the strain effect. On the other hand, if in addition to the $4 \times 10^{18}$ ionized Si atoms cm$^{-3}$ there are $10^{20}$ Si atoms per cm$^3$ in the form of neutral pairs, the strain effect from the pairs might well be comparable with the charge effect from the ionized atoms. If this were so, then for a given carrier concentration the line width in Si-doped GaAs would exceed that in Te-doped material.

In Fig. 2 is shown the maximum value of the derivative of the Ga$^{69}$ resonance in various specimens of Te- and Si-doped GaAs plotted against the carrier concentration obtained from Hall effect measurements. (Ga has two nuclear species, Ga$^{69}$ and Ga$^{71}$, of which Ga$^{69}$ has the larger quadrupole moment and is therefore more sensitive to quadrupolar effects.) The Te-doped specimens were taken from separate ingots, while the Si-doped specimens, apart from those labelled A and B, were taken from different parts of a single ingot. The

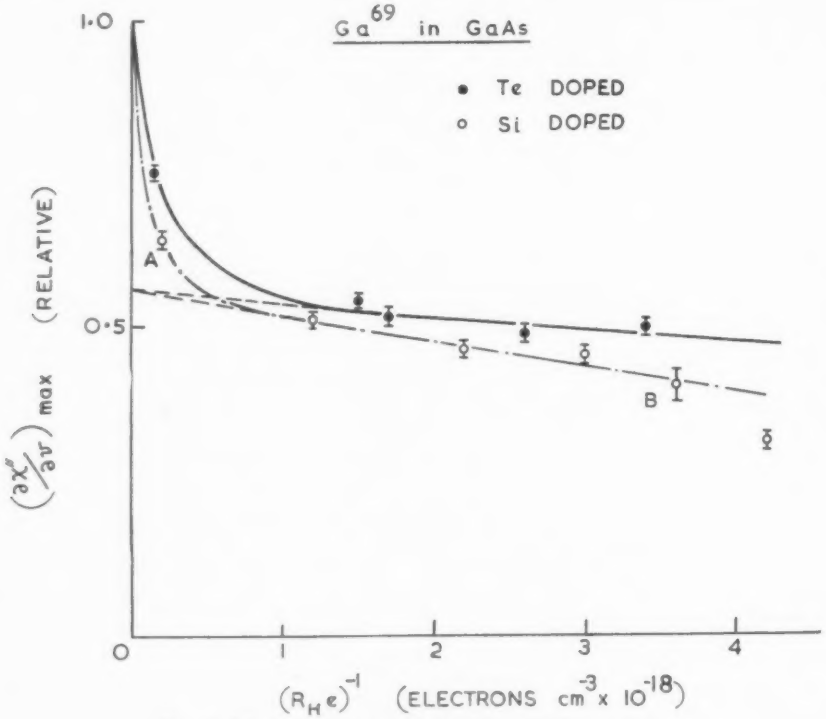


FIG. 2. Maximum value of derivative of Ga$^{69}$ resonance in Te- and Si-doped GaAs plotted against reciprocal of Hall constant. (290°K).

point B refers to one of the specimens used by KOLM, KULIN, and AVERBACH for their X-ray measurements, which is reported by them to contain $\frac{1}{2}$ per cent Si in solution. This material was *n*-type, with a Hall constant of $-1{\cdot}7$, in agreement with EDMOND's findings.

The results for the Te-doped specimens show the same general features as in the case of InSb. $Ga^{69}$ has $I = \frac{3}{2}$, for which the central component should contribute 0·4 of the total intensity, whereas the slowly falling part of the graph, which we ascribe to second order broadening of the central component, extrapolates to a value greater than 0·5. The implication of this is that the undoped specimen, which we have arbitrarily taken to represent unity on the vertical scale, was not pure enough to be completely free from quadrupolar broadening. The points representing the Si-doped specimens all lie below the corresponding Te-doped ones, the difference, although not large, lying outside the experimental error. It is evident that in the Si-doped specimens there must be some broadening mechanism additional to the effect of the ionized donors; this could well arise from strains produced by a comparatively large number of neutral impurities. The straight lines, which were fitted to the data for $(R_{\mathrm{H}}e)^{-1} > 10^{18}$ cm$^{-3}$ by the method of least-squares, intersect the vertical axis at the same point and have slopes in the approximate ratio 2 : 1. From this one can show by a simple argument that in the Si-doped specimens the charge and strain effects are roughly equal. By this we mean that if there are $N_1$ ionized donors per cm$^3$, each producing an electric field gradient $k_1 r^{-3}$ at a distance $r$, and $N_2$ and $k_2$ are the corresponding quantities for the neutral impurities, then $k_1 N_1 \simeq k_2 N_2$. If this were an exact equality it would imply that in all the Si-doped samples $N_1 \propto N_2$, which would not be true unless the segregation coefficients of the neutral and ionized forms were the same. Any difference between the segregation coefficients would have maximum effect at the most impure end of the ingot, and it is significant that the point with $(R_{\mathrm{H}}e)^{-1} = 4{\cdot}2 \times 10^{18}$ cm$^{-3}$, which represents the most impure end, lies well below the other points. The inference is that this specimen contains a much larger fraction of its Si in the neutral form than the other specimens, and we have for this reason omitted it from the least-squares determination. To prove that a large concentration of neutral impurities can affect the nuclear resonance to the required extent, we show in Fig. 3 the effect on the $Ga^{69}$ resonance of replacing some of the Ga atoms in GaAs by In. A concentration of $1{\cdot}3 \times 10^{20}$ In atoms per cm$^3$ broadens the resonance to the same extent as in the Si-doped specimen B, which according to KOLM *et al.* contains $\frac{1}{2}$ at. per cent (i.e. $1{\cdot}1 \times 10^{20}$ cm$^{-3}$) Si atoms in the form of neutral pairs. Since we have already stated that in the Si-doped specimens the charge and strain effects are roughly equal, this implies that the neutral form of Si causes approximately half as much strain as

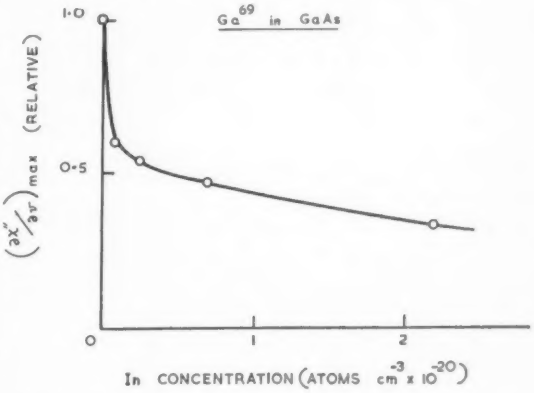


FIG. 3. Variation with In concentration of derivative of $Ga^{69}$ resonance in GaAs–InAs mixed crystal.

the same concentration of In atoms, which is reasonable. If the neutral Si consists of pairs of atoms, they may give rise to a small charge effect which would constitute an additional source of broadening, since although such a pair will have no net charge it will possess a dipole moment. The electric field of such a dipole will be much weaker than that of a point charge $e$, but may not be negligible if the pair concentration is in the region of $10^{20}$ cm$^{-3}$.

To summarize, nuclear resonance shows unambiguously that there is some broadening mechanism present in Si-doped GaAs other than the Coulomb field of the ionized donors. This additional broadening is probably due to the strain produced by some neutral form of Si, and the order of magnitude of the effect is consistent with the supposition that Si can enter the lattice in the form of pairs of atoms replacing a GaAs molecule, with a maximum solubility around $\frac{1}{2}$ per cent.

*Acknowledgments*—The author wishes to thank Dr. H. C. GATOS, of the Lincoln Laboratory, for making available one of the samples used by KOLM *et al.* and also Mr. J. T. EDMOND and Dr. J. C. WOOLLEY for providing specimens of doped GaAs. Acknowledgment is made to the Admiralty for permission to publish this paper.

## REFERENCES

1. BLOEMBERGEN N. *Report of the Bristol Conference on Defects in Crystalline Solids*, p. 1. Physical Society, London (1955).
2. SHULMAN R. G., MAYS J. M., and MCCALL D. W. *Phys. Rev.* **100,** 692 (1955).
3. SHULMAN R. G., WYLUDA B. J., and HROSTOWSKI, H. J. *Phys. Rev.* **109,** 808 (1958).
4. POUND R. V. *Phys. Rev.* **79,** 685 (1950).
5. RHODERICK E. H. *Phil. Mag.* **3,** 545 (1958).
6. ALLEN J. W. *Phil. Mag.* **2,** 1475 (1957).
7. COHEN M. H. and REIF F. *Solid State Physics*, Vol. 5, p. 321. Academic Press, New York (1957).
8. FOLEY H. M., STERNHEIMER R. M., and TYCKO D. *Phys. Rev.* **93,** 734 (1954).
9. OLIVER D. J. *Phil. Mag.*, to be published.
10. SHULMAN R. G., WYLUDA B. J., and ANDERSON P. W. *Phys. Rev.* **107,** 953 (1957).
11. PAULING L. *The Nature of the Chemical Bond*, p. 179, University Press, Oxford (1940).
12. EDMOND J. T. *Proc. Phys. Soc.*, to be published.
13. KOLM C., KULIN S. A., and AVERBACH B. A. *Phys. Rev.* **108,** 965 (1957).

VOL
8
195

*J. Phys. Chem. Solids* Pergamon Press 1959. Vol. 8. pp. 504–506. Printed in Great Britain

# R.7 NUCLEAR MAGNETIC RESONANCE IN SEMICONDUCTORS

**OLEN KRAUS**

National Bureau of Standards, Washington, D.C.

FEW measurements of nuclear spin–lattice relaxation times have been made in semiconductors. SHULMAN and WYLUDA[1] measured the spin–lattice relaxation time at room temperature as a function of carrier concentration in *n*- and *p*-type silicon. The relaxation times are the order of minutes, and relaxation takes place by means of the hyperfine interaction between carrier spins and nuclear spins for carrier concentrations greater than $10^{17}/cm^3$. Silicon has no nuclear quadrupole moment; and hence, there is no quadrupolar interaction. A theoretical expression derived by BLOEMBERGEN[2] and modified by ANDERSON[1] predicts the behavior of the spin–lattice relaxation time in semiconductors when a quadrupolar interaction is absent. According to the theory, the relaxation time is inversely proportional to the number of carriers for non-degenerate carriers in the exhaustion and intrinsic ranges.

We have observed the temperature dependence from 298°K to 180°K of the relaxation time for $Al^{27}$ nuclei in aluminum antimonide. Relaxation times were measured by means of pulsed nuclear induction at a frequency of 8·55 mc/s. A flow of nitrogen gas which passed through a coil immersed in liquid nitrogen provided a temperature bath. Crystals C–1 and C–2 were *p*-type polycrystalline specimens with a carrier concentration at room temperature of $3 \times 10^{16}/cm^3$ and $4 \times 10^{16}/cm^3$, respectively. Battelle Memorial Institute supplied these two crystals. A third specimen C–3 grown at the National Bureau of Standards was *p*-type with a carrier concentration of $2 \times 10^{17}/cm^3$ at room temperature.

Fig. 1 shows the spin–lattice relaxation time, $T_1$ as a function of $1/T^2$ where $T$ is the absolute temperature. One notices a sharp discontinuity in $T_1$ in the neighborhood of 225°K for C–3. A similar discontinuity, although not as great, appears near 250°K for C–1; and finally, one notices a shift in the curve for C–2 at a temperature of 210°K. Above and below the discontinuities the relaxation time appears to be proportional to $1/T^2$; however, one cannot be sure that a $1/T$-dependence does not fit the data as well.

Since aluminum has a nuclear spin $I = \frac{5}{2}$ and a nuclear quadrupole moment, the nuclear quadrupolar interaction should provide the dominant spin–

lattice relaxation mechanism. The relaxation times which are short compared with those for silicon where there is no quadrupolar effect indicate that the quadrupolar interaction does provide the effective coupling of the nuclear spin system to the lattice. VAN KRANENDONK[3] has presented a theory which indicates the temperature dependence of the spin–lattice relaxation time. The theory assumes that the relaxation takes place through the quadrupolar interaction with the lattice vibrations and predicts for sodium chloride in the temperature range which concerns us that $T_1 \propto 1/(T^*)^2$, where $T^*$ is the reduced temperature. In addition to the quadrupolar interaction with the lattice vibrations

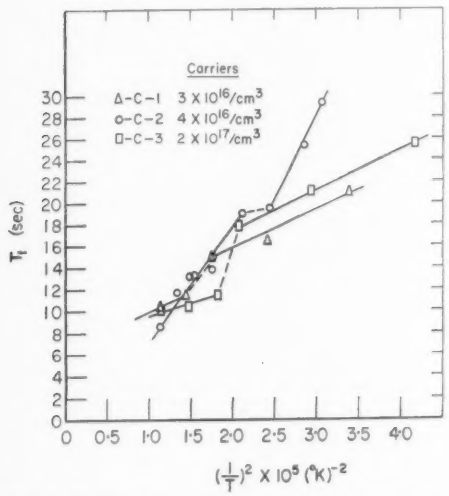


FIG. 1. Spin–lattice relaxation time for $Al^{27}$ in AlSb.

one should also consider the effect of quadrupolar interactions with moving imperfections, for example, diffusing interstitials or vacancies. Such interactions would also contribute to the spin–lattice relaxation and must be added to the effect of lattice vibrations. The relaxation time may not be proportional to $(1/T^*)^2$ in such cases.

The interaction of nuclear spins with paramagnetic impurities provides another relaxation mechanism. If this is the dominant means of relaxation, the spin–lattice relaxation time of the nuclei may be independent of the temperature or depend upon the electron spin–lattice relaxation time which in turn is temperature dependent. One model[4] of *p*-type AlSb pictures the acceptors as antimony vacancies. Such vacancies could act as paramagnetic impurities and supply strong relaxation centers. SHULMAN,[1] however, has observed that for indium-doped silicon, the neutral indium acceptors were ineffective as relaxation centers. We feel that the antimony vacancies, if they act as paramagnetic impurities, do not make an important contribution to the relaxation of the $Al^{27}$ nuclei in AlSb.

Our measurements show no obvious correlation between the purity of the specimen and the spin–lattice relaxation time. Unfortunately, no single crystals of AlSb large enough for our work were available. The local electric field gradients are very sensitive to strains in the crystal; and consequently, the quadrupolar interaction will depend strongly on the strained condition of the material. One may attribute the differences between the relaxation times of the three specimens to strains in the polycrystalline AlSb.

A discontinuity in the relaxation time could arise from a change of the quadrupolar interaction produced by a polymorphic change of the crystal; however, one does not anticipate such changes in AlSb at 220°K. The duration of the nuclear induction signal determined from the oscilloscope trace was the same for the three crystals and did not change with temperature; hence, the width of the resonance is independent of the sample and temperature. A careful investigation of the absorption line shape should be made by means of continuous techniques. Intensity measurements would indicate whether or not one observes only the central component ($m = +\frac{1}{2} \longleftrightarrow m = -\frac{1}{2}$) of the aluminum resonance.

We also observed the $Al^{27}$ induction signal at room temperature in a polycrystalline sample of AlSb doped with 0·025 molar per cent of tellurium. This specimen was *n*-type at room temperature. The duration of the induction signal was one-half its value for crystals C–1, C–2, and C–3; consequently, the tellurium broadened the resonance line. Although the signal-to-noise ratio was poor, the spin–lattice relaxation time was approximately one second.

The experiments which we have mentioned were exploratory in nature. Measurements of $T_1$ as well as line-shape studies in single crystals of AlSb will help provide an understanding of the nuclear spin–lattice relaxation in semiconductors as well as

supply information about the more general problem of relaxation in solids.

*Acknowledgments*—We thank Dr. A. C. BEER and Dr. R. K. WILLARDSON of Battelle Memorial Institute for supplying samples of AlSb.

**REFERENCES**

1. SHULMAN R. G. and WYLUDA B. J. *Phys. Rev.* **103,** 1127 (1956).
2. BLOEMBERGEN N. *Physica* **20,** 1130 (1954).
3. VAN KRANENDONK J. *Physica* **20,** 781 (1954).
4. BLUNT R. F., FREDERIKSE H. P. R., BECKER J. H., and HOSLER W. R. *Phys. Rev.* **96,** 578 (1954).

## DISCUSSION

*Compiled* by A. F. KIP

### R.2 G. W. LUDWIG *et. al.*

M. G. HOLLAND: Do the fast quenched Mn–Si samples show the 0·53 eV donor level? High pressure measurements at Harvard on the change in ionization energy of the 0·53 eV level show large hysteresis and long time drift effects, although the atmospheric resistivity remains unchanged. These effects might be explained by the presence of two levels, with different pressure coefficients, arising from the same or different Mn sites, if the effect of pressure changes one type of level to the other, and the levels have about the same ionization energy at atmospheric pressure.

G. W. LUDWIG: From our electron spin resonance measurements we cannot say whether clusters of four manganese atoms in silicon have electrical levels in addition to the 0·53 eV donor level. We have never seen the complicated spectrum present in low resistance *p*-type crystals and the spectrum depicted in Fig. 1 simultaneously; this may imply that an additional level or two is present. We have not yet made Hall and resistivity measurements on fast quenched silicon samples containing manganese, but expect that such samples when properly compensated would show one or more electrical levels distinguishable from the 0·53 eV donor level.

H. J. G. MEYER: Did you also investigate spin resonance on neutral or doubly charged Ni? Such an investigation could in principle be of great value for understanding the recombination process, as different Jahn–Teller shifts in different charge states would make understandable the possibly existing large probability for a many-phonon transition.

G. W. LUDWIG: We tried to find resonance at neutral and doubly charged Ni at various temperatures but could not find any result.

### R.4 R. N. DEXTER

F. W. QUELL: Elementary considerations based on plane wave arguments indicate that the anisotropic electron mass arises from a minimum along the line between $\Gamma$ and K r ineciprocal space. Group theory shows that the valence and conduction bands must be $\Gamma_1$, $\Gamma_4$, $\Gamma_5$ or $\Gamma_6$ bands. A study of the absorption edge and selection rules limit the possible valence band conduction band combinations to $\Gamma_1$–$\Gamma_5$, $\Gamma_4$–$\Gamma_6$, $\Gamma_5$–$\Gamma_6$. Tight binding arguments favor the $\Gamma_1$–$\Gamma_5$ combination.

### R.5 H. J. ZEIGER *et al.*

G. C. DOUSMANIS: Is there an appreciable reduction in line width when the temperature is lowered from 4°K to 1·5°K? In some cases in earlier work, no appreciable narrowing was observed. Differences in this between your new technique and the earlier one may indicate the extent of any instrumental contribution to broadening.

H. J. ZEIGER: A careful study of experimental line shapes in cross-modulation experiments has not as yet been made. Preliminary observations on a Si sample show a significant line narrowing in the cross-modulation signal going from 4°K to 1°K. However, we have as yet made no comparison with the standard microwave absorption technique.

### R.6. E. H. RHODERICK

G. W. LUDWIG: In interpreting the line broadening due to silicon in GaAs you seemed to imply that the ratio of the concentration of Si substituted for Ga to the concentration of $Si_2$ is constant as a function of total silicon content. Do you believe that such is in fact the case?

E. H. RHODERICK: If the curves showing the effects of doping with Te and Si were identical apart from a change of scale, the implication would be that the concentration of the neutral form of Si is a constant fraction of the total Si content. The data are neither accurate enough nor sufficiently complete to indicate to what extent this is true. The point corresponding to maximum Si concentration seems to show that the most impure end of the ingot contains a larger fraction of neutral Si than the other samples, which may be due to differences in segregation coefficients.

A. G. TWEET: Is the strain energy associated with the presence of the Te in the InSb capable of accounting for all of the heat of solution of this impurity?

E. H. RHODERICK: I am unaware of any data on heats of solution of impurities in InSb.

A. G. TWEET: One would expect that heat treatment of GaAs containing Si at relatively low temperature would result in a higher degree of association of the Si atoms into pairs, reducing the chemical potential of the system.

E. H. RHODERICK: I haven't investigated the effect of heat treatment.

*J. Phys. Chem. Solids* Pergamon Press 1959. Vol. 8. pp. 507–511. Printed in Great Britain

# SESSION S:
# GALVANOMAGNETIC EFFECTS*

S.1

## FINE STRUCTURE IN THE HALL COEFFICIENT

A. C. BEER
Battelle Memorial Institute, Columbus, Ohio

VOL. 8 1959

MEASUREMENTS of the Hall coefficient as a function of magnetic field in the extrinsic region of semiconductors such as *p*-type germanium, silicon, diamond, and AlSb, reveal a fine structure consisting of maxima and minima. This phenomenon occurs in nondegenerate semiconductors and is, therefore, to be distinguished from the de Haas–van Alphen oscillations. The minimum in germanium was reported by PETERSON *et al.*,[1] who measured *p*-type specimens at 77°K. Our data at several temperatures on a specimen containing $1 \times 10^{13}$ extrinsic holes/cm$^3$ are shown by the dashed lines in Fig. 1.

Simplified theoretical treatments can reasonably well account for the observed behavior when warping of the heavy-mass band is taken into account and when a mixed scattering mechanism is used. The magnetic-field dependence is introduced by the method of MCCLURE,[2, 3] which, for a magnetic field in the $Z$-direction along the [100] crystallographic axis, yields the following expressions for the conductivity coefficients:[4]

$$S_{xx} = \frac{2}{3}\frac{pe^2}{m^*kT} \alpha \left\langle \epsilon\tau \sum_{N \text{ odd}} \frac{b_N}{[1+(N\omega\tau)^2]} \right\rangle; \quad (1)$$

$$S_{xy} = \frac{2}{3}\frac{pe^2}{m^*kT} \alpha \left\langle \epsilon\omega\tau^2 \sum_{N \text{ odd}} \frac{(-1)^n b_N N}{[1+(N\omega\tau)^2]} \right\rangle, \quad (2)$$

The common symbols have their usual meanings, with $\epsilon$ being the energy of the charge carriers over which the averaging is carried out. The cyclotron frequency, $\omega$, is related to the magnetic field intensity by the relation

$$\omega = aeH/m^*c. \quad (3)$$

The parameters $\alpha$, $b_N$, and $a$ are indicative of the warped band. We determined them from cyclotron resonance information and from constraints imposed on $S_{xx}$ and $S_{xy}$ at the weak-field and strong-field limits.[4] Terms as far as $b_5$ were included.

A simple mixed-scattering mechanism was used, namely that by acoustic phonons and ionized impurities,† so that equations (1) and (2) could be expressed in terms of tabulated functions.[5] The result for a single warped band yields a Hall coefficient factor, $R_H/R_\infty$, which rises monotonically after the weak-field plateau to a maximum, and then recedes to the strong-field limit.[4] The prominence of the maximum depends on the amount of impurity scattering, and it is absent if the latter contribution is small. In the actual case, results are substantially modified by the contribution from the light-mass band. In germanium, the mobility of the fast holes is so large that the weak-field Hall coefficient ratio, $R_0/R_\infty$, is greatly augmented, with the result that $R_H$ decreases monotonically with field, until a minimum is reached.

In all calculations, the light-mass band was considered spherical. Mobility and carrier-density ratios in the two bands were taken as 8 and 0·04, respectively, for germanium (3 and 0·16 for silicon), as suggested from cyclotron resonance data.[6] The magnetic field appears through $\gamma_2$, the dimensionless parameter $(9\pi/16)$ $(\mu_2{}^L H/10^8)^2$, where $\mu_2{}^L$ is the lattice mobility representative of a *spherical* heavy-mass band.

In Fig. 1, a choice of 65,000 cm$^2$/V-sec for $\mu_2{}^L$ places the minima of the theoretical curves at a magnetic field strength in the neighborhood of the experimental data at 77°K. Such a mobility value is also consistent with expectations from magnetoresistance and $R_0\sigma_0$ data. The ordinates of the curve for $\beta_2 = 1$ were normalized to fit the data at $H = 20$ kG; the curve for $\beta_2 = 3$ was slightly depressed for the sake of clarity. The correspondence in shape between the theoretical and experimental curves seems remarkable.

Since the location and prominence of the fine structure depends on $\mu_2{}^L$ and on $\beta$, it is interesting to examine the temperature dependence of the minima, as shown in Fig. 2. For this specimen, the

* *Chairman:* H. K. HENISCH; *Co-Chairman:* P. J. PRICE.

† A parameter $\beta$, relating the ratio of lattice and impurity mobilities ($\beta \equiv 6\mu^L/\mu^I$), is a measure of the degree of impurity scattering.

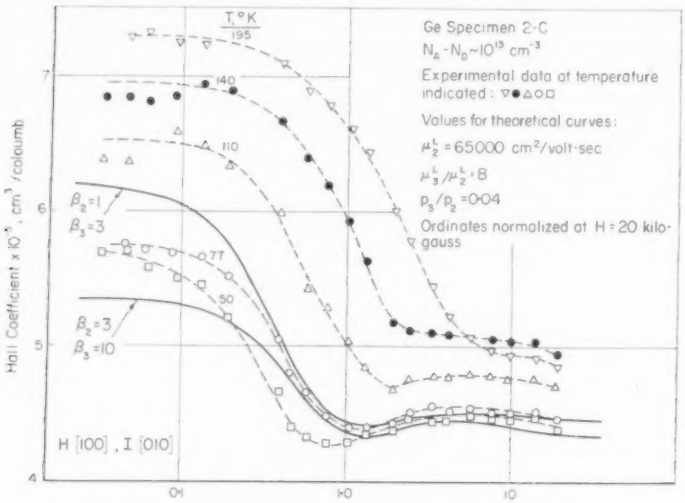


FIG. 1. Hall coefficient in $p$-type germanium. Theoretical curves (solid lines) are based on $\mu^L_2 = 65{,}000$ cm$^2$/V-sec, representative of the mobility at 77°K, and on normalization of ordinates at 20 kG (see text). Subscripts 3 and 2 refer to light- and heavy-mass bands, respectively.

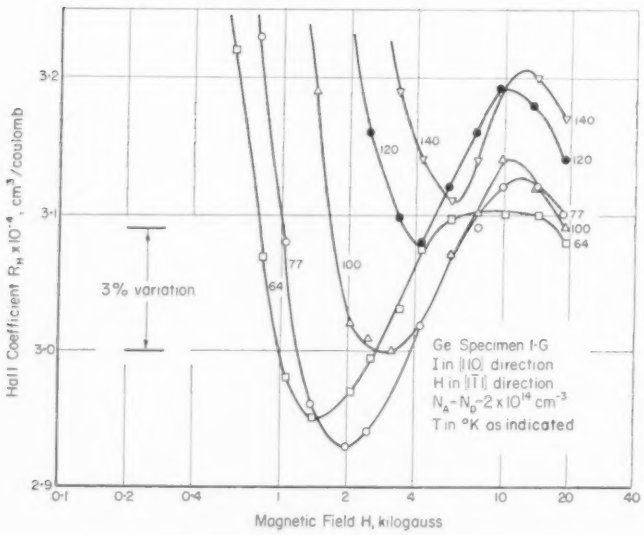


FIG. 2. Temperature dependence of the minima in germanium. This sample has a larger carrier concentration and a different orientation than sample 2–C.

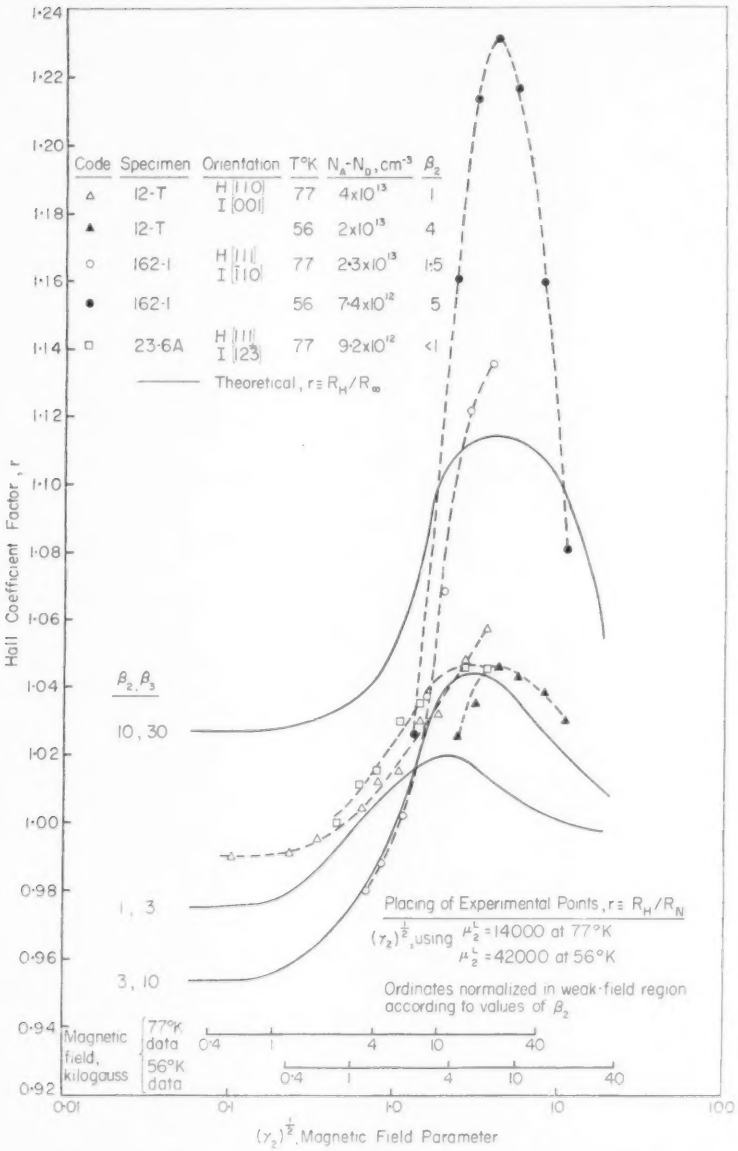
Code Specimen Orientation T°K $N_A$-$N_D$, cm$^{-3}$ $\beta_2$
△ 12-T H [110] I [001] 77 4x10$^{13}$ 1
▲ 12-T 56 2x10$^{13}$ 4
○ 162-1 H [111] I [$\bar{1}$10] 77 2·3x10$^{13}$ 1·5
● 162-1 56 7·4x10$^{12}$ 5
□ 23-6A H [111] I [123] 77 9·2x10$^{12}$ <1
Theoretical, r ≡ $R_H/R_\infty$
Hall Coefficient Factor, r
$\beta_2, \beta_3$
10, 30
1, 3
3, 10
Placing of Experimental Points, r ≡ $R_H/R_N$
$(\gamma_2)^{\frac{1}{2}}$, using $\mu_2^L$ = 14000 at 77°K
$\mu_2^L$ = 42000 at 56°K
Ordinates normalized in weak-field region according to values of $\beta_2$
Magnetic field, kilogauss
77°K data
56°K data
0·4 1 4 10 40
$(\gamma_2)^{\frac{1}{2}}$, Magnetic Field Parameter

FIG. 3. Experimental data (dashed lines) and theoretical predictions (solid lines) for $p$-type silicon.

fine structure is more pronounced—perhaps owing to the larger carrier concentration and enhanced impurity scattering, and to the lower symmetry of the orientation. Since $\mu_2{}^L$ varies inversely with temperature, the shift in the location of the minima is understandable. It is also seen that the relative prominence of the structure depends qualitatively on $\beta$ in the manner predicted by the theory. The likelihood that the degree of prominence reaches a maximum—in this case in the

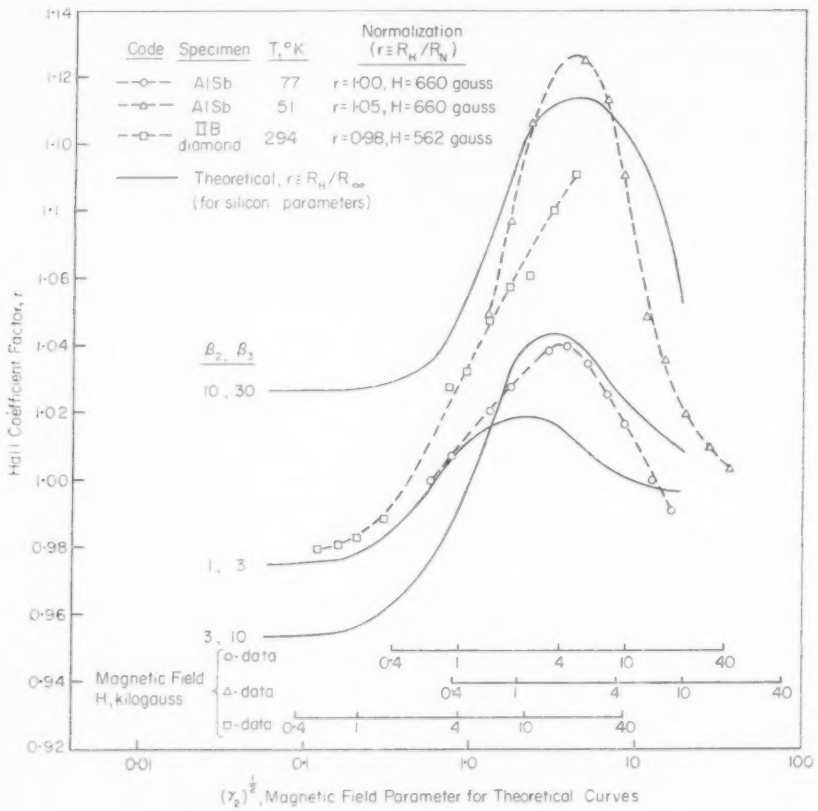


FIG. 4. Experimental data (dashed lines) for *p*-type diamond and AlSb. Superimposed are theoretical curves (solid lines) for silicon (see text).

neighborhood of 80°K—is not surprising, since it is known that the mixed-scattering mechanism yields a minimum in $R_0/R_\infty$ as a function of $\beta$.[7]

In silicon, with a lower mobility ratio between light- and heavy-mass bands, the structure resulting from the warped band is generally not obscured by contributions from the light-mass band,* and the maximum is very much in evidence in Fig. 3. Some of the observed maxima are quite large, suggesting that perhaps a somewhat greater degree of warping needs to be considered. The values of $\mu_2{}^L$ used for comparing experimental data with theory are in agreement with predictions from $R_0\sigma_0$ and magnetoresistance data.

Unpublished data of R. BATE on a II-B diamond and of F. REID and J. DUGA on AlSb are shown in Fig. 4. It is interesting that the silicon type rather than the germanium type behavior is found. The experimental data were plotted so that all maxima occurred at similar values of $\gamma_2$. This required an unrealistic value of $\mu_2{}^L$—in each case about eight times as large as expected from $R_0\sigma_0$ data and from magnetoresistance. It is possible that warping terms of higher order than $b_5$ are required. Also, our scattering treatment is perhaps less applicable to these materials. Another possibility might be warping of the light-mass band. In order to resolve

* An exception is the case of unusually pure silicon, since the germanium type of magnetic field dependence is predicted for very small values of $\beta$.[4] Just recently we have found this behavior experimentally.

some of these speculations, more detailed cyclotron resonance information is desirable.

*Acknowledgments*—The author is indebted to R. K. WILLARDSON for helpful comments, and to the Air Force Office of Scientific Research, Cambridge Research Center, and Wright Air Development Center for use of data in advance of publication. The kindness of Dr. J. F. H. CUSTERS, Diamond Research Lab., Industrial Distributors (1946) Ltd., Johannesburg, in supplying the II-B diamond is appreciated.

**REFERENCES**

1. PETERSON E., SWANSON J., and TUCKER G. *Bull. Amer. Phys. Soc.* **1,** 117 (1956).
2. MCCLURE J. W. *Phys. Rev.* **101,** 1642 (1956).
3. GOLDBERG C., ADAMS E., and DAVIS R. *Phys. Rev.* **105,** 865 (1957).
4. BEER A. C. and WILLARDSON R. K. *Phys. Rev.* **110,** 1286 (1958).
5. BEER A., ARMSTRONG J., and GREENBERG I. *Phys. Rev.* **107,** 1506 (1957).
6. DEXTER R., ZEIGER H., and LAX B. *Phys. Rev.* **104,** 637 (1956).
7. JOHNSON V. A. and WHITESELL W. J., *Phys. Rev.* **89,** 941 (1953).

VOL. 8 1959

*J. Phys. Chem. Solids* Pergamon Press 1959. Vol. 8. pp. 511–515. Printed in Great Britain

S.2

# THE MAGNETORESISTANCE OF ELECTRONS IN InP AND GaAs*

M. GLICKSMAN
RCA Laboratories, Princeton, N.J.

AVAILABLE samples of single crystal indium phosphide and gallium arsenide contain appreciable concentrations[1, 2] of impurities. It has been concluded from mobility observations that the purest indium phosphide contains[3] about $10^{16}$ cm$^{-3}$ impurities and the purest gallium arsenide[4] about $10^{17}$ cm$^{-3}$ impurities. In spite of the high concentrations it is possible to deduce information about the anisotropy of the mobility (and indirectly the effective mass) and about the form of the scattering from galvanomagnetic measurements. Reported herein are observations made on single crystal slabs of *n*-type indium phosphide and gallium arsenide which indicate that (a) in both materials the bottom of the conduction band is spherically symmetric in *k*-space, and (b) in both materials the scattering is weakly dependent on the energy.

Samples were prepared so that the magnetoresistance could be observed for the current parallel to a [110] direction or parallel to a [100] direction. In a cubic crystal the first of these provides sufficient measurements to deduce[5] the low-field magnetoresistance tensor, the second set serving as a check.

It was found during the course of these investigations that the type and size of the side contacts could materially affect[6] the results. In particular, either the use of "large" area soldered side contacts or bridge-shape samples[7] introduces a contribution to the observed change in resistance in the magnetic field caused by a shorting out of the Hall voltage in the vicinity of the contacts. This effect is strongest when the magnetic field is in the plane of the contacts, and it is observed that the transverse magnetoresistance for crystals with such contacts is larger with the magnetic field in the plane of the contacts. The magnitude of this spurious magnetoresistance will depend on the mobility, and on the form of the contact shorting. In the case of bridge samples, a contribution of about $0{\cdot}3 \times 10^6$ cm$^4$/V$^2$-sec$^2$ to $\Delta\rho/\rho_0 H^2$ was observed for *n*-type germanium, indium phosphide, and gallium arsenide, all having mobilities of about 4000 cm$^2$/V-sec. For germanium this corresponds to only 3–4 per cent of the bulk magnetoresistance; for indium phosphide and

* This work was supported in part by the U.S. Air Force.

gallium arsenide it can be as high as 100 per cent.

To minimize this spurious effect contacts were made using small diameter (0·002 in.) gold wires which were welded to the sides of the specimen. In the case of germanium samples, the spurious magnetoresistance was found to disappear (within experimental error) for this arrangement. Two approaches were used as a check on the spurious effect. One was to compare samples of the same crystal which had different contact arrangements. From these observations it was noted that in addition to an effect on the transverse magnetoresistance there is a much larger longitudinal magnetoresistance with the large area side contacts than when these are replaced by the small diameter welded wires. The other type of check was made using a sample with the current in the [100] direction and the magnetic field in the perpendicular (100) plane. In this case the bulk magnetoresistance should be independent of the direction of the magnetic field in the (100) plane. This was found to be the case only when the contacts were small diameter welded wires.

Included in the tables of values are measurements involving both forms of contacts, with those crystals with welded wires starred. These latter values are the most reliable. The spurious contributions to the unstarred group vary because of the many types of contacts used—small area pressure contacts, soldered contacts of different areas and bridge samples with well-defined areas.

Table 1 lists values for a number of *n*-type indium phosphide crystals. In all cases, $H$ [001] refers to the magnetic field in the [001] direction and perpendicular to the plane of the contacts, whereas $H$ [$\bar{1}$10] refers to the magnetic field in the [$\bar{1}$10] direction and in the plane of the contacts. It is clear from the results for the purest crystals (192) that there is a very small longitudinal magnetoresistance and a transverse magnetoresistance isotropic in the (110) plane. This is demonstrated in Figs. 1 and 2, which give the values of the magnetoresistance for one of the crystals 192 as a function of the magnetic field orientation. Fig. 3 yields a corroboratory check for another sample of the same crystal cut to give a current in the [100] direction.

*Table* 1. *Magnetoresistance of* n-*type* InP

| Crystal | Hall mobility ($cm^2$/V-sec) | Electron concentration ($cm^{-3}$) | Temperature (°K) | Magnetoresistance $\Delta\rho/\rho_0H^2$ ($10^6$ $cm^4/V^2$–$sec^2$) | | |
|---|---|---|---|---|---|---|
| | | | | $I$ [110] $H$[110] | $I$ [110] $H$[001] | $I$ [110] $H$[$\bar{1}$10] |
| 1 | 3150 | $1{\cdot}4 \times 10^{17}$ | 289 | 0·31 | 0·55 | 0·26 |
| 51 | 3150 | $1{\cdot}2 \times 10^{17}$ | 290 | 0·03 | 0·13 | 0·10 |
| 54 | 2800 | $6 \times 10^{15}$ | 290 | 0·37 | 1·15 | 1·22 |
| T43 | 4300 | $4{\cdot}3 \times 10^{16}$ | 293 | 0·20 | 0·66 | 0·25 |
| T43 | 8700 | | 77 | 0·6 | 8·2 | 6·6 |
| 192 | 4200 | $6 \times 10^{15}$ | 294 | 0·05 | 1·3 | 1·5 |
| 192 | 23400 | | 77 | 0·4 | 34·0 | 31·0 |
| 192* | 4600 | $6 \times 10^{15}$ | 292 | 0·02 | 1·11 | 1·09 |
| T5* | 2750 | $4{\cdot}6 \times 10^{17}$ | 293 | 0·02 | 0·14 | 0·10 |
| T43* | 4000 | $5 \times 10^{16}$ | 292 | 0·02 | 0·28 | 0·21 |
| T43* | 6900 | | 77 | 0·09 | 6·2 | 5·8 |

* The side contacts were 0·002 in. diameter gold wires welded to the crystal.

Although crystal 192 shows this isotropy, it is clear that more impure specimens (with larger electron concentration) show some anisotropy. In the conventional notation[5] three coefficients $b$, $c$, and $d$ may be defined by

$$\frac{\Delta\rho}{\rho_0 H^2} = b + \frac{(\boldsymbol{I}\cdot\boldsymbol{H})^2}{I^2H^2}c + \frac{\sum_i I_i^2 H_i^2}{I^2H^2}d.$$

The last three columns of Table 1 refer respectively to measurements of $b + c + \frac{1}{2}d$, $b$, and $b + \frac{1}{2}d$. The form of anisotropy shown by the observations gives a negative value for $d$, although the effect is small. From the measurements in indium phosphide, it is concluded that the mobility tensor of $e\tau/m^*$ is isotropic for crystals with electron concentrations

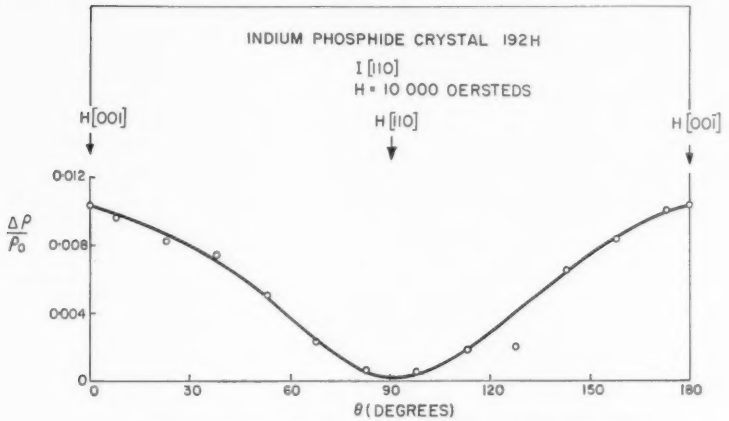


FIG. 1. The magnetoresistance of *n*-type InP crystal 192 as a function of the angle the magnetic field makes with the [001] direction in the ($\bar{1}$10) plane. The temperature was 292°K.

the order of $10^{16}$ cm$^{-3}$ or less, and shows a small anisotropy of a [100] type[8, 9] for crystals with larger electron concentrations. The first result indicates that the effective mass at the bottom of the conduction band is a scalar. The second may be due to an anisotropic scattering process entering or to a possible anisotropic second conduction band quite close to the lowest spherically symmetric one.[10] The latter suggestion seems more reasonable, and there is other evidence for the presence of such a band (with a heavier mass) from thermoelectric and optical measurements.[11] From the form of the anisotropy, this second state may be similar to the state of symmetry $\Delta$ which is the lowest conduction band in silicon.[12]

Table 2 lists a similar series of measurements for crystals of *n*-type gallium arsenide. The best measurements (on crystals 61 and M12) indicate a

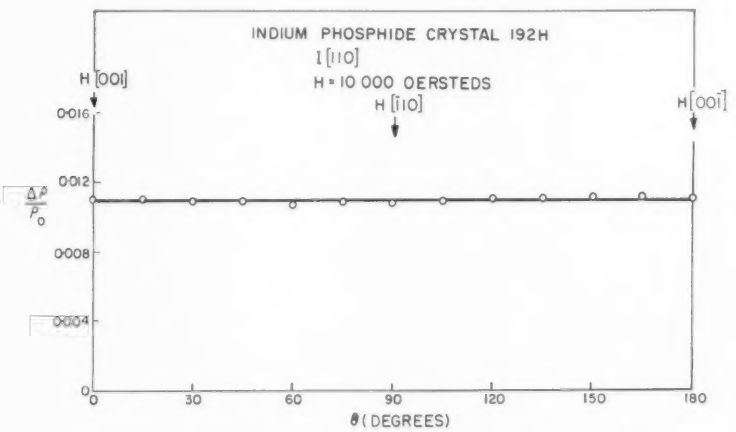


FIG. 2. The magnetoresistance of *n*-type InP crystal 192 as a function of the angle the magnetic field makes with the [001] direction in the (110) plane. The temperature was 292°K.

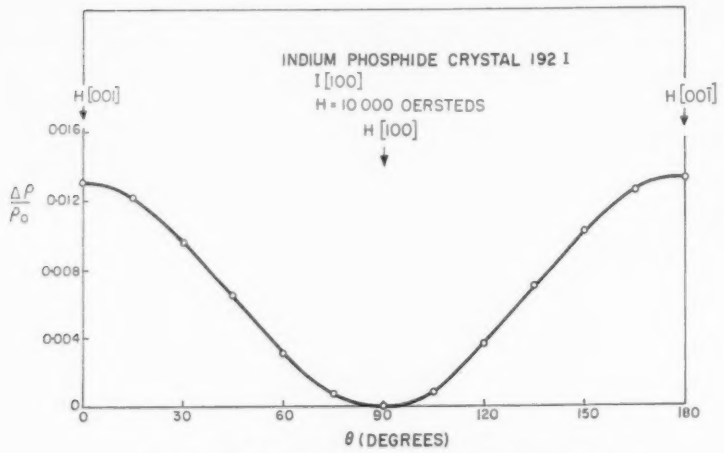


FIG. 3. The magnetoresistance of *n*-type InP crystal 192 as a function of the angle the magnetic field makes with the [001] direction in the (010) plane. The temperature was 292°K.

small longitudinal magnetoresistance in the [110] and in the [100] directions and an isotropic transverse magnetoresistance. In this case, too, it is concluded that the mobility tensor $e\tau/m^*$ is isotropic, with the effective mass $m^*$ thus a scalar. The anisotropies shown for the other crystals in Table 2 are all of the magnitude and type due to the contacts and are ascribed as spurious. The isotropic effective mass is in agreement with calculations reported by CALLAWAY.[13]

For both indium phosphide and gallium arsenide the magnetoresistance is considerably less than the 0·28 times the square of the Hall mobility expected[14] for lattice scattering with a relaxation time inversely proportional to the carrier velocity. However the scattering in these III–V compounds is likely of the type believed dominant in InSb,[15] the electrons being most strongly scattered by polar optical modes with a resulting effective relaxation time[16] weakly dependent on the energy. This would reduce the magnetoresistance, in qualitative agreement with the observations reported. It is necessary to reduce the impurity scattering effect or correct for it with confidence in order to give a more quantitative comparison of theory and experiment.

*Table 2. Magnetoresistance of* n-*type* GaAs

| Crystal | Hall mobility ($cm^2$/V-sec) | Electron concentration ($cm^{-3}$) | Temperature (°K) | Magnetoresistance $\Delta\rho/\rho_0 H^2$ ($10^6$ $cm^4/V^2$-$sec^2$) | | |
|---|---|---|---|---|---|---|
| | | | | $I$[110] $H$[110] | $I$[110] $H$[001] | $I$[110] $H$[$\bar{1}$10] |
| 59 | 4100 | $4 \times 10^{17}$ | 295 | 0·21 | 0·30 | 0·68 |
| 14 | 4400 | $7 \times 10^{16}$ | 295 | 0·15 | 0·39 | 0·57 |
| 61 | 3400 | $4 \times 10^{16}$ | 295 | 0·02 | 0·43 | 0·48 |
| M12* | 4000 | $4{\cdot}7 \times 10^{17}$ | 292 | 0·16 | 0·61 | 0·29 |
| M12† | 3800 | $4 \times 10^{17}$ | 290 | 0·02 | 0·27 | 0·27 |

* For this crystal only, the case $I$ [110] $H$ [001] corresponds to $H$ in the plane of the contacts and $I$ [110] $H$ [$\bar{1}$10] to $H$ perpendicular to the plane of the contacts.

† The side contacts were 0·002 in. diameter gold wires welded to the crystal. Measurements on a sample with current in the [100] direction gave the same results.

*Acknowledgments*—I should like to thank J. J. GANNON and R. V. VANNOZZI for their aid in making the measurements, and R. GUIRE, J. R. WOOLSTON, and Dr. K. WEISER for supplying the crystals.

### REFERENCES

1. WELKER H. and WEISS H. *Solid State Physics* Vol. 3, (edited by F. Seitz and D. Turnbull), p. 1. Academic Press, New York (1956).
2. JENNY D. *Proc. Inst. Radio Engrs.* **46,** 959 (1958).
3. GLICKSMAN M. and WEISER K. *J. Electrochem Soc.* **105,** 728 (1958).
4. WEISBERG L. R., WOOLSTON J. R., and GLICKSMAN M. *J. Appl. Phys.* **29,** 1514 (1958).
5. PEARSON G. L. and SUHL H. *Phys. Rev.* **83,** 768 (1951).
6. BROOM R. F. *Proc. Phys. Soc.* **71,** 500 (1958).
7. GLICKSMAN M. *Phys. Rev.* **100,** 1146 (1955).
8. ABELES B. and MEIBOOM S., *Phys. Rev.* **95,** 31 (1954).
9. SHIBUYA M. *Phys. Rev.* **95,** 1385 (1954).
10. GLICKSMAN M. *Bull. Amer. Phys. Soc.* **3,** 120 (1958).
11. NEWMAN R. *Phys. Rev.* **111,** 1518 (1958).
12. HERMAN F. *Phys. Rev.* **95,** 847 (1954).
13. CALLAWAY J. *J. Electronics* **2,** 330 (1957).
14. SEITZ F. *Phys. Rev.* **79,** 372 (1950).
15. EHRENREICH H. *J. Phys. Chem. Solids* **2,** 131 (1957).
16. HOWARTH D. J. and SONDHEIMER E. H. *Proc. Roy. Soc.* A **219,** 53 (1953).

VOL. 8 1959

*J. Phys. Chem. Solids* Pergamon Press 1959. Vol. 8. pp. 515–518. Printed in Great Britain

S.3

# IMPURITY BAND CONDUCTION IN STRONG MAGNETIC FIELDS

R. J. SLADEK

Westinghouse Research Laboratories, Pittsburgh 35, Pennsylvania

## 1. INTRODUCTION

THE mobility, $\mu_i$, of electrons in magnetically induced impurity bands[1] in $n$-InSb has been determined as a function of temperature and magnetic field strength by means of resistivity and Hall effect measurements at liquid-helium temperatures. Field strengths up to 28,000 G were employed. At all temperatures $\mu_i$ decreases very rapidly with increasing magnetic field strength in general accord with the decrease of the overlap between electronic wave functions centered on neighboring donors. In most cases $\mu_i$ is a weakly activated function of temperature with the activation energy increasing with field strength.

## 2. EXPERIMENT

Electrical conductivity and Hall effect data were obtained for three $n$-type InSb samples having between $1{\cdot}0 \times 10^{14}$ and $3{\cdot}3 \times 10^{14}$ excess donors per cm$^3$. The Hall data have been published recently.[1]

Representative electrical conductivity data are presented in Fig. 1. The log of the conductivity, $\sigma$ at constant magnetic field is plotted vs. the reciprocal of the absolute temperature. The magnetic field was perpendicular to the current direction as for Hall effect measurements. From Fig. 1 it can be seen that $\sigma$ decreases strongly as the temperature is decreased or the magnetic field is increased.

## 3. DISCUSSION

Previously[1] it was deduced from the Hall effect data that electrons fall from the conduction band into donor levels which have been split off from the conduction band by the strong magnetic field. Electrons in these donor levels have non-zero mobility, i.e. there is impurity band conduction. Resistivity measurements at one low temperature indicated that the impurity band mobility varied with magnetic field strength like an exchange integral in which gaussian-type donor wave functions taken from theory[2] were used. Thus it was concluded that the impurity band conduction involved electron jumps between neighboring donor ions—the jump frequency being given by the exchange integral.

Our present purpose is to determine $\mu_i$ over a range of temperatures and field strengths. Since in

the temperature range available, usually some conduction is due to electrons remaining in the conduction band (this type of conduction is negligible only at lowest temperatures), two band formulae[3] for the Hall coefficient and the conductivity were used to determine $\mu_i$ from our data. Specifically,

$$\mu_i = \frac{\sigma}{n_0 e}\left[1 - \sqrt{\left(\frac{n_c}{n_0 - n_c}\right)(R_H n_0 e - 1)}\right], \quad (1)$$

where $\sigma$ is the electrical conductivity, $e$ is the electronic charge, $n_0$ is the total concentration of electrons due to excess donors, $R_H$ is the Hall coefficient, and $n_c$ is the concentration of electrons in the conduction band. Values of $n_c$ were obtained using the results of previous analysis of Hall data.[1]

Applying equation (1) to our data we obtained values of $\mu_i$ at various temperatures and magnetic field strengths. First we shall use these values to compare the field dependence of $\mu_i$ with that given by the exchange integral. This integral is proportional to $\exp(-\text{constant}/a_\perp^2)$, where $a_\perp$ is the radius of a donor wave function in the plane perpendicular to the magnetic field, and the constant depends on the spacing between donor ions. Thus we made plots of log $\mu_i$ at constant temperature, vs. $(a_0/a_\perp)^2$ for each of our samples. ($a_0$ is the effective Bohr radius in zero magnetic field.) The value of $a_0/a_\perp$ corresponding to a given field strength was taken from a theoretical curve by YAFET, KEYES, and ADAMS.[2]

Fig. 2 presents such a plot of the field dependence

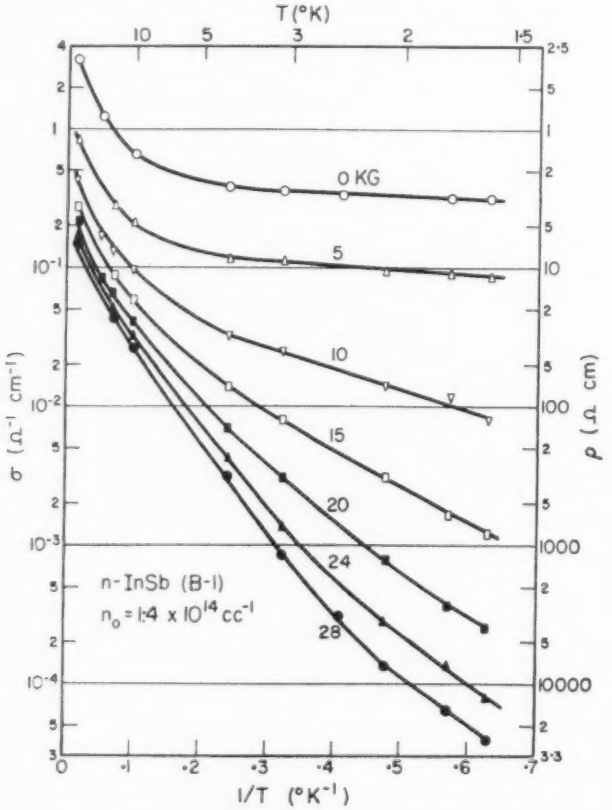


FIG. 1. The electrical conductivity of $n$-type InSb, sample B-1, vs. reciprocal absolute temperature for a number of magnetic field strengths. The magnetic field was perpendicular to the current direction in the sample.

of $\mu_i$ for sample N–3. Similar results were also obtained for the other two samples. From Fig. 2 it can be seen, that except at highest fields, log $\mu_i$ is a decreasing linear function of $(a_0/a_\perp)^2$ at all temperatures in agreement with variation of the exchange integral. This result confirms the idea that exchange jumping of electrons between neighboring donor ions is involved in impurity band conduction in strong magnetic fields.

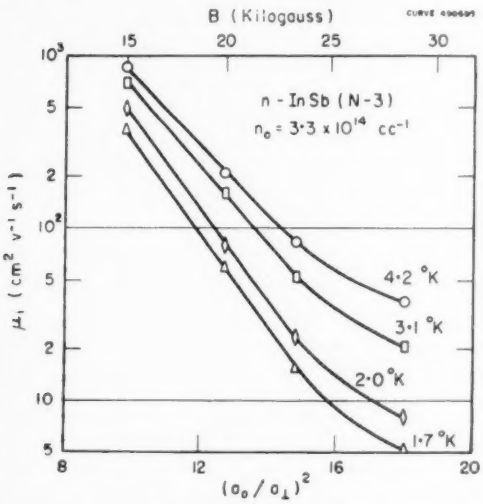


FIG. 2. Magnetic field dependence of the impurity band mobility in $n$-type InSb, sample N-3, at various temperatures. The log of $\mu_i$ is plotted vs. the square of the reciprocal of the reduced radius of the donor wave function in the plane perpendicular to the magnetic field. $a_0$ is the effective Bohr radius of a hydrogen-like donor in zero magnetic field. The dependence of $a_\perp$ on field strength is taken from reference 2.

It may be noted that the slopes of the log $\mu_i$ vs. $(a_0/a_\perp)^2$ curves decrease somewhat as the temperature increases. Since the exchange integral is independent of temperature, this effect must be due to other causes. It could be due to $\mu_i$ being an activated function of temperature with the activation energy increasing with field strength.

To examine the temperature dependence of $\mu_i$ we have plotted log $T\mu_i$ at constant field as a function of $1/T$ for each of our samples. ($T$ is the absolute temperature.) Representative results are given in Fig. 3. Note that for a given field, log $T\mu_i$ vs. $1/T$ is a straight line of negative slope. This indicates that $\mu_i$ is a singly activated function of temperature. Values of the activation energy, $\epsilon_A$, are listed in Table 1. No values for $\epsilon_A$ are given for sample O-1 at the higher fields because log $T\mu_i$ vs. $T$ was not a straight line at these fields in this sample. From Table 1 we see that $\epsilon_A$ increases with increasing field strength and with decreasing excess donor concentration. The ratio of $\epsilon_A$ to the donor ionization energy,[1] $\epsilon_I$, is approximately constant for a given sample.

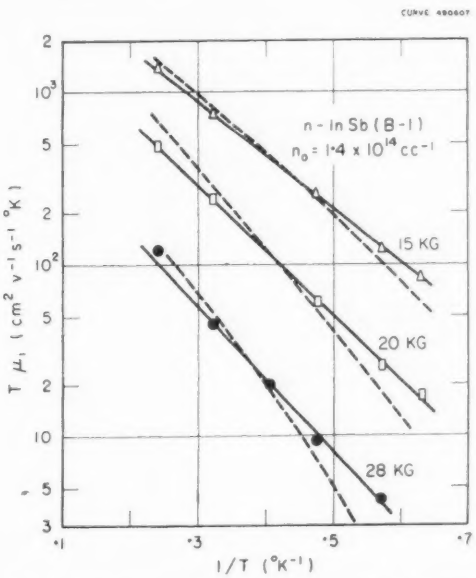


FIG. 3. The temperature dependence of the impurity band mobility in strong magnetic fields in $n$-type InSb, sample B-1. The dashed curves give the temperature dependence of the factor $1/[1 + \exp\{-(\epsilon_B - \zeta)/kT\}]$ when only excess donors provide bound levels. These curves have been drawn to intersect the lines through the data points.

To interpret the temperature dependence of $\mu_i$ we shall make use of the generalized Einstein relation,[4] $\mu = eD/[d\zeta/d \log n]$, where $D$ is the diffusion coefficient, $\zeta$ is the Fermi energy, and $n$ is the concentration of charge carriers. Thus we obtain

$$\mu_i = \frac{eD}{kT}\left[\frac{1}{1+\exp\{-(\epsilon_B-\zeta)/kT\}}\right], \qquad (2)$$

where $\epsilon_B$ is the energy at which the impurity band lies and equals $-\epsilon_I$. (The field dependence discussed previously is contained in $D$, i.e. $D = L^2\nu_{\text{jump}}$ where $L$ is the distance between donors and $\nu_{\text{jump}}$

*Table* 1. *The activation energy,* $\epsilon_A$, *for the mobility of electrons in donor levels localized by a strong magnetic field and the ratio of* $\epsilon_A$ *to the donor ionization energy,* $\epsilon_I$, *for three* n-*type* InSb *samples.*

($k$ = Boltzmann's constant)

| Magnetic field (kG) | N-3 $n_o = 3{\cdot}3 \times 10^{14}$ cm$^{-3}$ | | B-1 $n_o = 1{\cdot}4 \times 10^{14}$ cm$^{-3}$ | | O-1 $n_o = 1{\cdot}04 \times 10^{14}$ cm$^{-3}$ | |
|---|---|---|---|---|---|---|
| | $\epsilon_A/k$ | $\epsilon_A/\epsilon_I$ | $\epsilon_A/k$ | $\epsilon_A/\epsilon_I$ | $\epsilon_A/k$ | $\epsilon_A/\epsilon_I$ |
| 10 | — | — | — | — | 8·0°K | 0·49 |
| 15 | 4·5°K | 0·29 | 7·3°K | 0·38 | 9·8 | 0·51 |
| 20 | 6·2 | 0·34 | 8·7 | 0·39 | — | — |
| 24 | 7·2 | 0·33 | 9·4 | 0·39 | — | — |
| 28 | 7·8 | 0·32 | 9·8 | 0·37 | — | — |

is the jump frequency given by the exchange integral.)

According to equation (2), an explicit temperature dependence of $T\mu_4$ is contained in the bracketed factor, which represents the probability of donor levels being empty and thus providing sites into which electrons can jump. In the absence of compensation (or if only excess donors provide bound levels) this factor decreases approximately exponentially as the temperature is lowered and thus could account for the observed temperature dependence of $T\mu_4$. (See Fig. 3, for example.) However, we believe that our samples are rather highly compensated. In this case the bracketed factor would be almost independent of temperature. Thus $D$ itself would have to be a thermally activated function of temperature to account for the observed temperature dependence of $T\mu_4$. This could occur, for example, if electrons need to be raised to excited donor levels in order for them to conduct. Such a hypothesis is consistent with the fact that the ratio of the activation energy to the donor ionization energy is constant in a given sample. (See Table 1.)

*Acknowledgments*—Thanks are due to E. N. Adams and R. W. Keyes for helpful discussions.

## REFERENCES

1. Sladek R. J. *J. Phys. Chem. Solids* **5,** 157 (1958).
2. Yafet Y., Keyes R. W., and Adams E. N. *J. Phys. Chem. Solids* **1,** 137 (1956).
3. Hung C. S. *Phys. Rev.* **79,** 727 (1950).
4. Greene R. F. and Adams E. N. *Westinghouse Research Laboratories Scientific Paper* 6-94760-2-P14.

*J. Phys. Chem. Solids* Pergamon Press 1959. Vol. 8. pp. 518–523. Printed in Great Britain

S.4

# GALVANOMAGNETIC EFFECTS IN $n$-InSb AT LOW TEMPERATURES IN STRONG MAGNETIC FIELDS*

**J. C. HASLETT and W. F. LOVE**

Physics Department, University of Colorado, Boulder, Colorado

## 1. INTRODUCTION

As a result of the low effective mass in the conduction band of $n$-InSb, the magnetic quantum of energy $\hbar\omega_C$ ($\omega_C$ = cyclotron frequency) is quite large even in moderate magnetic fields. Under the condition that $\hbar\omega_C \gg E$ and $kT$, where $E$ is the electron energy, all electrons will occupy the ground oscillator state of their motion transverse to the field. This extreme case has been designated as the "quantum limit" by Argyres and Adams.[1] The purpose of these experiments was to provide

* This work was supported by the United States Atomic Energy Commission and the Council on Research and Creative Work of the University of Colorado.

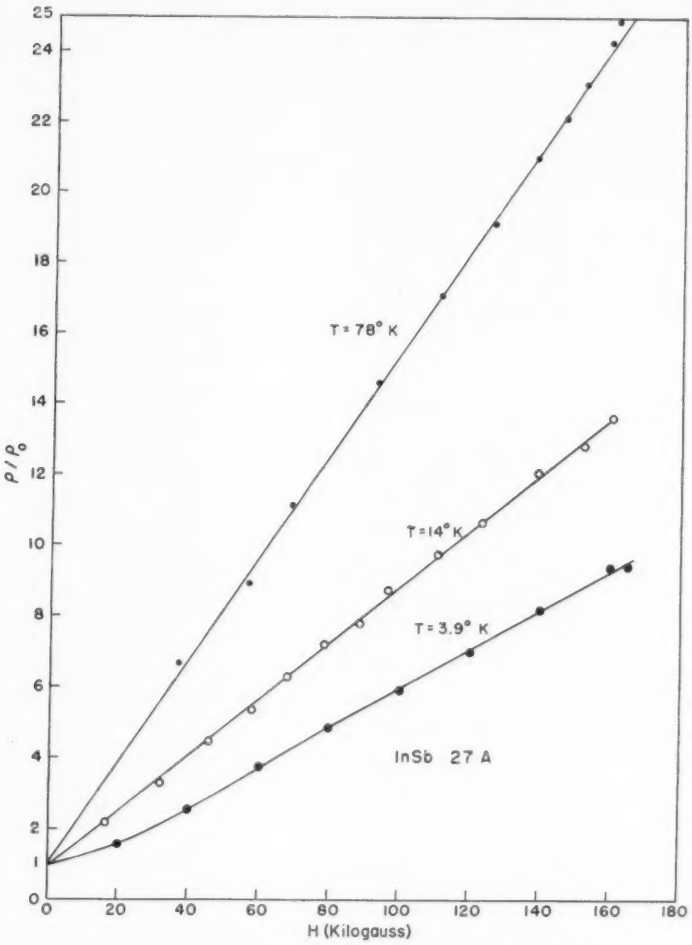


FIG. 1. Longitudinal magnetoresistance ratio of InSb 27A vs. magnetic field strength at 78°K, 14°K, and 3·9°K.

experimental data on InSb in the quantum limit.

At liquid-helium temperatures a single band picture no longer applies to *n*-InSb. In a magnetic field impurity levels split off from the conduction band to form an impurity band. This leads to "freeze out" effects in the galvanomagnetic properties.[2–4]

## 2. EXPERIMENTAL RESULTS

The technique for producing pulsed magnetic fields is described adequately in the literature.[5–7] In these experiments the original data are taken with a Tektronix 535 oscilloscope and Polaroid Land Camera. The horizontal sweep is driven by a signal proportional to the magnetic field and the vertical sweep by the sample voltage.

Data from three separate ingots of *n*-InSb having different purities have been taken. The ingots have been labeled 27, 28, and 29 with excess donor concentrations of $1{\cdot}2 \times 10^{16}$, $1{\cdot}4 \times 10^{15}$, and $2{\cdot}8 \times 10^{14}\,\mathrm{cm}^{-3}$, respectively. The authors are indebted to Dr. E. N. ADAMS for providing the indium antimonide used in these experiments. The samples had dimensions of the order of 1 mm ×

1 mm × 5 mm. Separate current and potential or Hall leads were soldered to the samples with indium solder.

Fig. 1 shows data on the longitudinal magnetoresistance ratio as a function of magnetic field strength of InSb 27A taken with the sample immersed in baths of liquid nitrogen, hydrogen, and helium. The measuring current density was 8·7 A/cm². No dependence of the magnetoresistance ratio on current was observed at 78°K. The variation is linear with field strength at the highest fields. ARGYRES and ADAMS[1] predict such

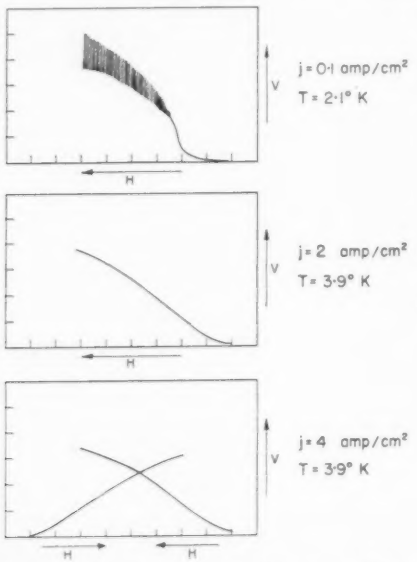


FIG. 2. Schematic drawings of typical longitudinal magnetoresistance data on InSb 28D at 4°K.

a linear variation for a non-degenerate semiconductor in the lattice scattering range. The results at 78°K do not agree quantitatively with their theory, possibly because lattice scattering is not predominant in InSb at this temperature. An unusual feature of these results is the decrease in the magnetoresistance ratio with decreasing temperature.

The results at liquid-helium temperatures are complicated by a strong dependence on measuring current density, magnetic field strength, temperature, and the nature of the soldered leads. At high current densities (~10 A/cm²) a linear variation of the longitudinal magnetoresistance ratio with magnetic field strength is generally observed. At the lowest current densities (~0·003 A/cm²) the magnetoresistance ratio varies exponentially with magnetic field strength. At intermediate current densities (~0·1 A/cm²) a combination of both types of behavior accompanied by a peculiar form of noise at the highest field strengths is found. The transition between the two types of behavior is rather abrupt.

Fig. 2 shows three schematic drawings of the original data on InSb 28D. The upper picture was taken at an intermediate current density and shows the exponential low field behavior and abrupt transition to a linear behavior accompanied by noise. The smeared out region at higher field strengths represents high frequency oscillations which have a noise-like character. A detailed examination of the oscillations showed that they had an irregular sawtooth character and a frequency of around 200 kc/s. The middle picture shows the behavior at higher current densities where the oscillations have disappeared. The lower picture shows the results for two successive pulses with the magnetic field in opposite directions.

Some typical data on InSb 28D, taken after the specimen had been etched and the leads resoldered, are shown in the schematic of Fig. 3. Results similar

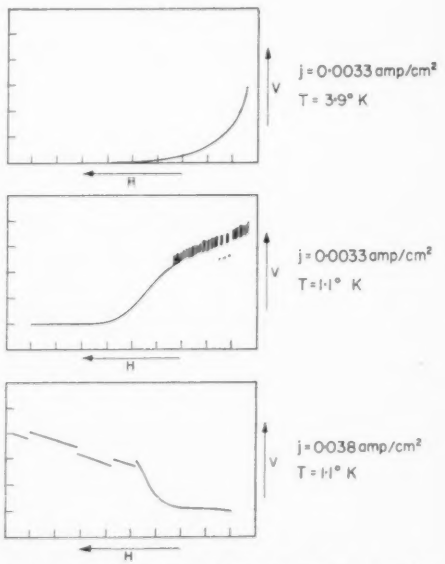


FIG. 3. Schematic drawings showing typical longitudinal magnetoresistance data on InSb 28D after sample had been etched and leads resoldered.

to those in Fig. 2 are obtained except that the character of the noise has changed considerably. The upper picture shows the exponential behavior at all field strengths for a sufficiently low measuring current density. The middle picture was taken at the same current density but at a lower temperature to illustrate the temperature dependence of these effects. The noise now appears "clipped". In the third picture the noise has almost disappeared except for a few steps in the curve.

The initial exponential behavior of sample voltage is interpreted as a "freeze-out" effect. The abrupt changes in sample voltage with magnetic field strength are interpreted as electrical breakdown due to impact ionization of bound electrons. The noise is similar in character to that found by McKay[8] associated with breakdown in silicon *p–n* junctions.

Fig. 4 supports the notion of electric breakdown occurring at high measuring current densities. The current density is plotted vs. electric field strength for InSb 29A at different values of the applied

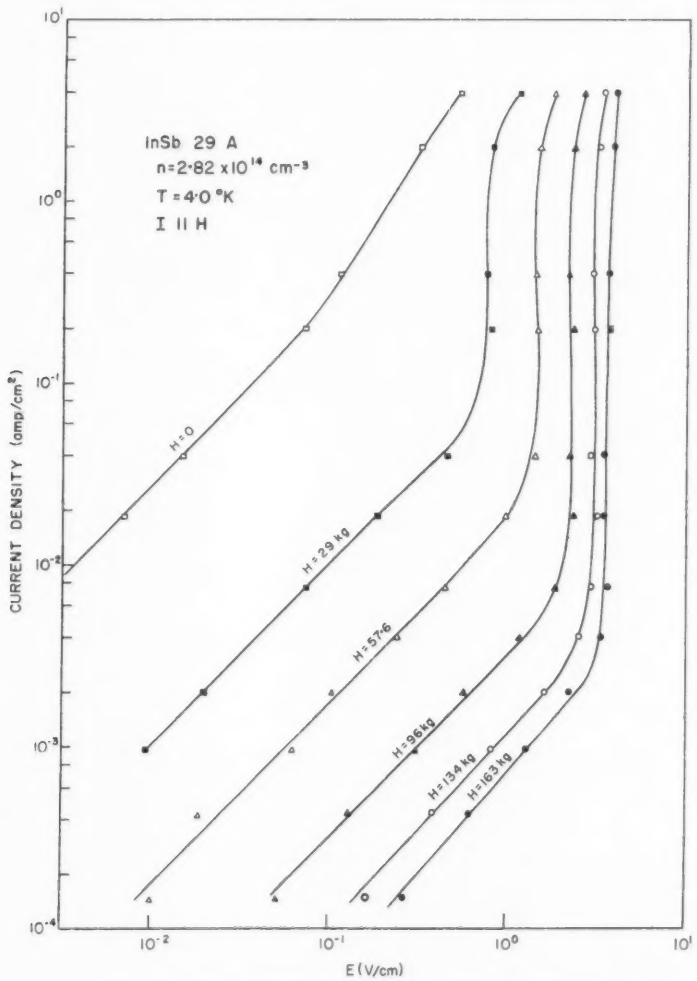


FIG. 4. Plot of current density vs. electric field strength at various values of magnetic field strength for InSb 29A.

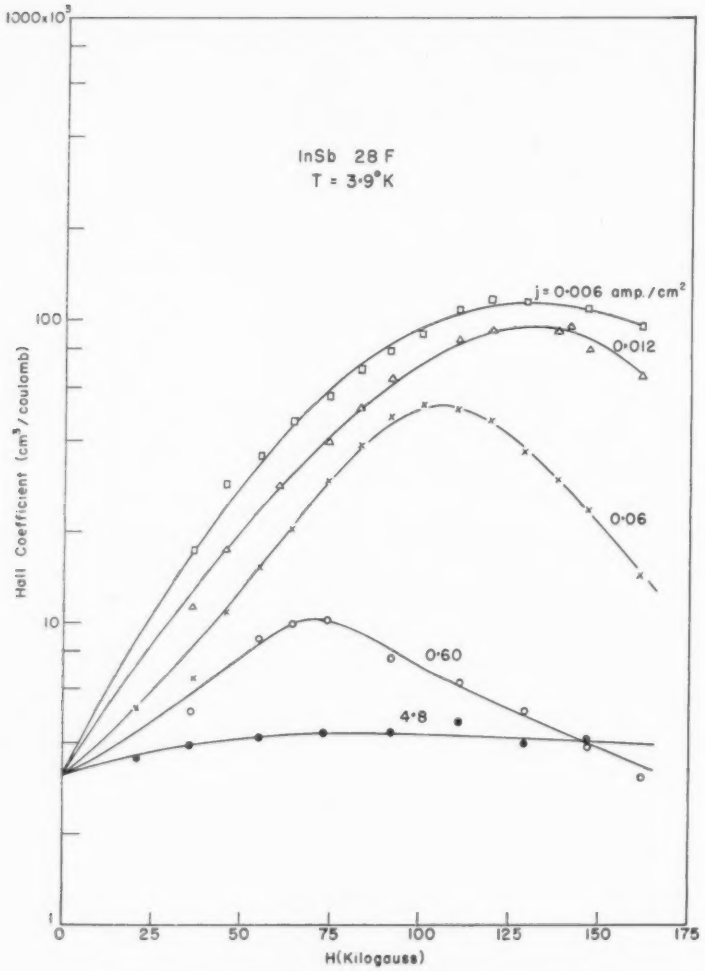


FIG. 5. Hall coefficient in InSb 28D vs. magnetic field strength for various measuring current densities.

magnetic field. These curves were obtained by an analysis of a series of pictures taken at different current densities. Note that the sample was non-ohmic even at zero magnetic field. This is probably a "hot electron" effect. The breakdown is clearly indicated by the vertical portions of the curves. It was found that the breakdown electric field increases with increasing concentration of excess donors.

Measurements of the Hall coefficient have been made to check the idea of breakdown, and the results are shown in Fig. 5. The constant Hall coefficient at high current densities indicates that complete ionization of donor impurities is maintained at all field strengths. The initial rise observed at low current densities is the "freeze-out" effect and the dropping off of the Hall coefficient at high magnetic fields is assumed to be charge multiplication by impact ionization which accompanies the breakdown.

**REFERENCES**

1. ARGYRES P. N. and ADAMS E. N. *Phys. Rev.* **104,** 900 (1956).
2. KEYES R. W. and SLADEK R. J. *J. Phys. Chem. Solids* **1,** 143 (1956).
3. SLADEK R. J. *Westinghouse Laboratories Scientific Paper* 8-1038-p28 (1957). To be published in *J. Phys Chem. Solids.*
4. FREDERIKSE H. P. R. and HOSLER W. R. *Phys. Rev.* **108,** 1136 (1957).
5. FURTH H. P. and WANIEK R. W. *Rev. Sci. Instrum.* **27,** 195 (1956).
6. FURTH H. P., LEVINE M. A., and WANIEK R. W. *Rev. Sci. Instrum.* **28,** 949 (1957).
7. FONER S. and KOLM H. H. *Rev. Sci. Instrum.* **27,** 547 (1956).
8. MCKAY K. G. *Phys. Rev.* **94,** 877 (1953).


*J. Phys. Chem. Solids* Pergamon Press 1959. Vol. 8. pp. 523–525. Printed in Great Britain

VOL. 8 1959

S.5

# ELECTRONIC PROPERTIES OF GRAY TIN SINGLE CRYSTALS*

**A. W. EWALD and O. N. TUFTE**

Department of Physics, Northwestern University, Evanston, Ill.

THE growth of gray tin single crystals from mercury solution has recently been reported.[1] Because these crystals are grown from a liquid phase they should be relatively free of the physical imperfections present in all previous specimens of gray tin prepared by the solid–solid phase transformation. Growth at a reduced temperature (−20 to −30°C) and at a low rate (~1 cm per month) should also favor a high degree of crystalline perfection. Despite their growth from an amalgam the best crystals appear to be as pure as the tin from which they are grown. These crystals of highest purity are grown at temperatures between −25 and −30°C and contain approximately $10^{17}$ *n*-type impurities per $cm^3$. Growth above −20°C produces *p*-type crystals due to mercury alloying.

The single crystal data presented here were obtained on two specimens typical of a number of *n*-type samples investigated. The samples were cut to dimensions of approximately $0{\cdot}2 \times 0{\cdot}4 \times 5{\cdot}0$ mm using an "Airbraisive" sandblast unit. Sample A was used primarily for a comparison of the electronic properties of a single crystal with those of a filament obtained by the phase transformation. The filament was prepared from Vulcan tin of the same purity (99·999 per cent) as that used in growing the crystals. Also the same electrode arrangement was used for the single-crystal specimen as for the filament and consisted of current and potential leads attached to the sample ends with Hall probes at the mid-point. Sample B was used to study the field dependence of the magnetoresistance at nitrogen and helium temperatures. For this purpose separate potential probes consisting of 0·003 in. diameter wire were attached to one edge of the sample.

A comparison of the conductivities of the single crystal and transformed filament is shown in Fig. 1. The good agreement in intrinsic slopes indicates equal purity since in gray tin of this order of purity the temperature dependence of the intrinsic conductivity is sensitive to impurity content.† The higher extrinsic conductivity of the single crystal may therefore be attributed to the higher mobility characteristic of the more perfect crystal structure. The magnetoresistance coefficients plotted in Fig. 2 also reflect the higher mobility in the single crystal

* This work was supported by the Office of Naval Research.

† This effect which was first observed in transformed filaments (EWALD A. W. and KOHNKE E. E. *Phys. Rev.* **97,** 607 (1955)) has also been found in mercury-alloyed single crystals.

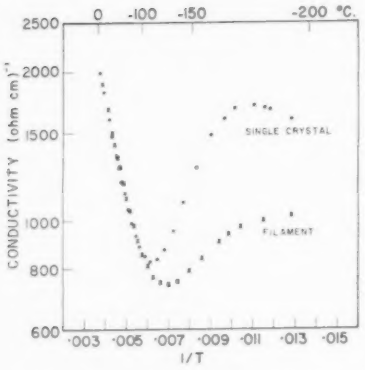


FIG. 1. Comparison of the conductivity of a single crystal with that of a filament obtained by the phase transformation.

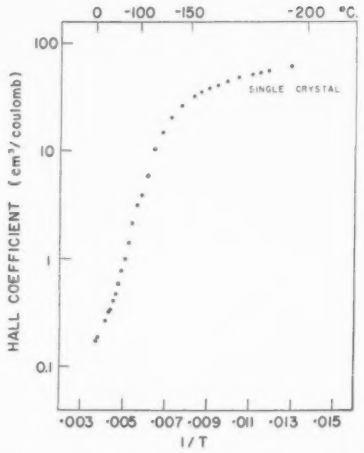


FIG. 3. Hall coefficient of a single-crystal specimen.

especially near nitrogen temperature where the coefficient for the crystal is six times greater than that of the filament. The Hall coefficient of the crystal is shown in Fig. 3. In this case the curve is very similar to those previously found for transformed gray tin.[2] The value at nitrogen temperature corresponds to an electron concentration of $1{\cdot}2 \times 10^{17}$ per cm³. A summary of the single crystal characteristics including helium temperature data is presented in Table 1. The high electron mobility at both 78 and 4·2°K may be noted.

The field dependence of the transverse magnetoresistance of sample B is shown in Fig. 4. The curve obtained at 78°K shows a quadratic range at low fields and an approximately linear behavior at the highest fields as has previously been reported for transformed gray tin.[3] Also the low field region extends nearly to 1000 gauss in satisfactory agreement with a Hall mobility of $1{\cdot}44 \times 10^5$ cm²/V-sec.

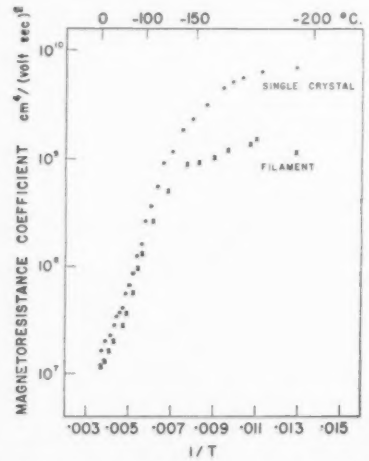


FIG. 2. Comparison of the magnetoresistance coefficient of a single-crystal specimen with that of a transformed filament.

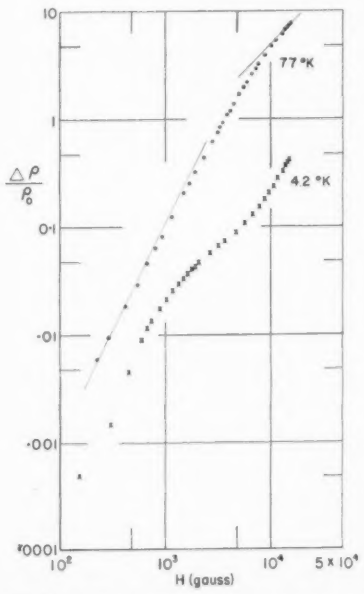


FIG. 4. Field dependence of the transverse magnetoresistance of a single crystal. The straight lines are drawn with slopes of 1 and 2 for reference.

*Table* 1. *Characteristics of gray tin single crystals*

| | $T = 273°K$ | $T = 78°K$ | | | $T = 4{\cdot}2°K$ | | |
|---|---|---|---|---|---|---|---|
| Crystal | $\sigma$ ($ohm^{-1}cm^{-1}$) | $\sigma$ ($ohm^{-1}cm^{-1}$) | $R$ ($cm^3/C$) | $(R\sigma)$ ($cm^2/V\text{-}sec$) | $\sigma$ ($ohm^{-1}cm^{-1}$) | $R$ ($cm^3/C$) | $(R\sigma)$ ($cm^2/V\text{-}sec$) |
| A | 2080 | 1600 | 61 | $0{\cdot}97 \times 10^5$ | 1100 | 99 | $1{\cdot}08 \times 10^5$ |
| B | 2640 | 2000 | 72 | $1{\cdot}44 \times 10^5$ | 1170 | 83 | $0{\cdot}97 \times 10^5$ |

The behavior at 4·2°K is more complicated an dis no unlike that of *n*-type InSb and InAs at 78°K.[4]

VOL. 8 1959


**REFERENCES**

1. Tufte O. N. and Ewald A. W. *Bull. Amer. Phys. Soc.* Ser. II, **3,** 128 (1958).
   Ewald A. W. and Tufte O. N. *J. Appl. Phys.* **29,** 1007 (1958).
2. Kohnke E. E. and Ewald A. W. *Phys. Rev.* **102,** 1481 (1956).
3. Busch G., Wieland J., and Zoller H. *Helv. Phys. Acta* **24,** 49 (1951).
   Becker J. H. Thesis, Cornell University (1957).
4. Frederikse H. P. R. and Hosler W. R. *Phys. Rev.* **108,** 1136 (1957); *Phys. Rev.* **110,** 880 (1958).


*J. Phys. Chem. Solids* Pergamon Press 1959. Vol. 8. pp. 525–530. Printed in Great Britain

# S.6 MEASUREMENT OF THE GALVANOMAGNETIC EFFECTS IN PURE TELLURIUM


**H. ROTH**

General Atomic Division of General Dynamics Corporation, San Diego, California and
Physics Department, University of Pennsylvania, Philadelphia, Pennsylvania


## 1. INTRODUCTION

Tellurium is an elemental semiconductor with a forbidden band of 0·34 eV. Its electrical properties have been studied by a number of investigators,[1–4] who always find it to be *p*-type in the extrinsic range. The band structure of tellurium has been investigated theoretically by H. B. Callen[5] and more recently by Asendorf,[6] Reitz,[7] and Firsov.[8]

The galvanomagnetic effects in a single crystal can be expressed as

$$E_i = \rho_{ij} I_j + \epsilon_{ijk} I_j R_{k,m} H_m + \rho_{ij,mn} I_j H_m H_n + \ldots$$

in the case of a weak magnetic field where these effects can be described in powers of the field. Using the point-group symmetry of the crystal, one can determine phenomenologically the independent tensor components which exist.

Tellurium crystallizes in an anisotropic structure consisting of a hexagonal array of chains containing a 3-fold screw-axis. It possesses the symmetry of the crystal class $D_3$ in the Hermann–Maughn notation and can be shown[9] to have two independent components of the resistivity tensor $\rho_{ij}$, two Hall coefficients $R_{k,m}$ and eight independent magnetoresistance coefficients, $\rho_{ij,mn}$.* By using properly oriented samples these coefficients can be experimentally determined and an ellipsoid-model of the energy surfaces can be constructed to explain the galvanomagnetic effects observed.

* The resistivity and Hall tensors are diagonal with

$$\rho_{11} = \rho_{22} = \rho_1,\ \rho_{33} = \rho_3,$$
$$R_{1,1} = R_{2,2} = R_1 \text{ and}$$
$$R_{3,3} = R_3.$$

## 2. EXPERIMENTAL

By taking Laue back reflection X-ray photographs, a crystal of tellurium, grown by the Czochralski technique at the Honeywell Research Center,[10] was found to be a single crystal with the $c$-axis along the direction of growth. The crystal was cut ultrasonically into 1·5 cm lengths, cleaved parallel to the $c$-axis into 2-mm slabs, and oriented samples of approximately square cross-section were cut (see Fig. 1) using a fine stream of sand under high pressure. The samples were polished with fine emery cloth and etched for 10 sec in CP–4 in order to remove any conducting layer present on the surface.* (The etching process removed about 50 $\mu$ of material from each face.) Current leads were attached by melting a heated 5-mil platinum wire into the ends of the sample.

Potential and Hall probes were attached by spot welding 1-mil platinum wires to the sample. Sample dimensions and probe distances were measured with a microscope.

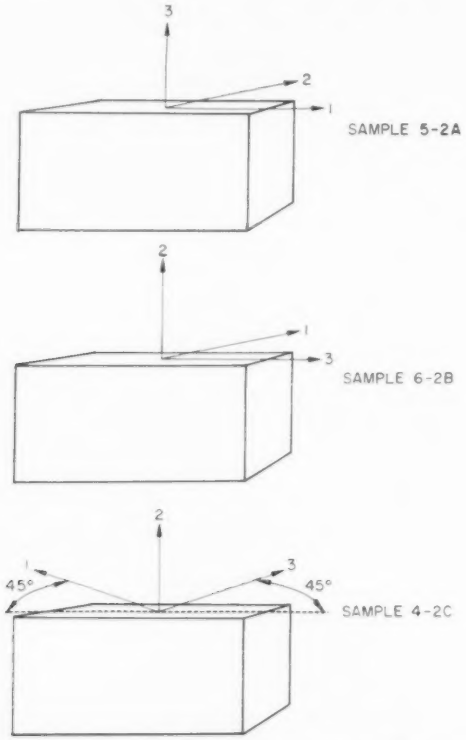


FIG. 1. Orientation of axes in three types of tellurium samples used. The 3-axis is the $c$-axis, 1 is a binary axis and 2 is perpendicular to the 1–3 plane which is taken as the cleavage plane.

The samples were mounted in a liquid helium cryostat against a copper block coated with G.E. 7031 varnish. The cryostat could be rotated a full 360° in the field of an electromagnet capable of producing up to 13,000 G. The electrical measurements were made with a Leeds and Northup K–3 potentiometer.

## 3. RESULTS

Fig. 2 shows the resistivities as a function of $1/T$ for current flow parallel ($\rho_3$) and perpendicular ($\rho_1$)

* This conducting layer was found by R. S. Caldwell at Purdue and is reported in an unpublished Purdue Report, January, 1958, "Optical Properties of Te and Se."

to the $c$-axis. It will be noticed that the anisotropy exists throughout the entire temperature range, the resistivity ratio* $\rho_1/\rho_3$ being 1·7 at 303°K and 3·3 at 78°K.

Fig. 3 gives the temperature dependence of the Hall coefficients. The ratio of the Hall coefficients $R_3/R_1$ is unity at 303°K in agreement with BOTTOM;[1] however this ratio is 2·7 at 78°K. The Hall reversal of $R_3$ occurs at the same temperature as that of $R_1$.

Fig. 4 shows the magnetoresistance $\Delta\rho/\rho$ vs. angle as the samples are rotated in a plane in a magnetic field of 5000 G. The longitudinal magnetoresistance is seen to be zero at 303°K but of the same order of magnitude as the transverse magnetoresistance at 78°K.

Fig. 5 shows a typical behavior of the magnetoresistance $\rho_{33,33}$ and $\rho_{33,11}$ vs. temperature. The temperature dependence of $\rho_{11,11}$ (not shown) is similar to that of $\rho_{33,33}$, while that of $\rho_{11,22}$ and $\rho_{11,33}$ (not shown) is similar to that of $\rho_{33,11}$.

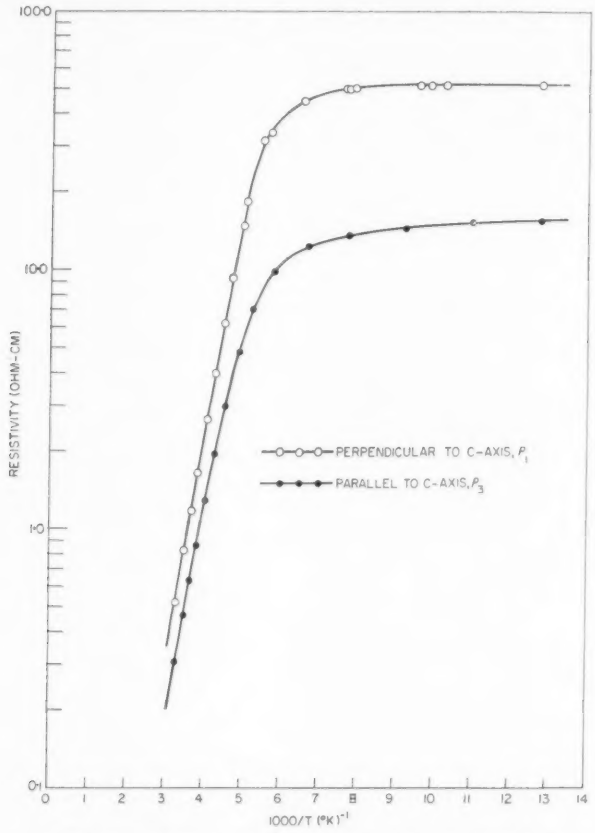


FIG. 2. Temperature dependence of the resistivity in tellurium for samples cut parallel and perpendicular to the $c$-axis.

The experimentally determined values of the galvanomagnetic coefficients at 78°K and 303°K are summarized in Table 1. It should be noted that the resistivity and Hall coefficients in the extrinsic range are almost an order of magnitude higher than previously published data, indicating a higher degree of sample purity than has been available up to this time.

The absence of any longitudinal magneto-

* BOTTOM[1] finds the ratio $\rho_1/\rho_3$ to be 1·9 in the intrinsic range.

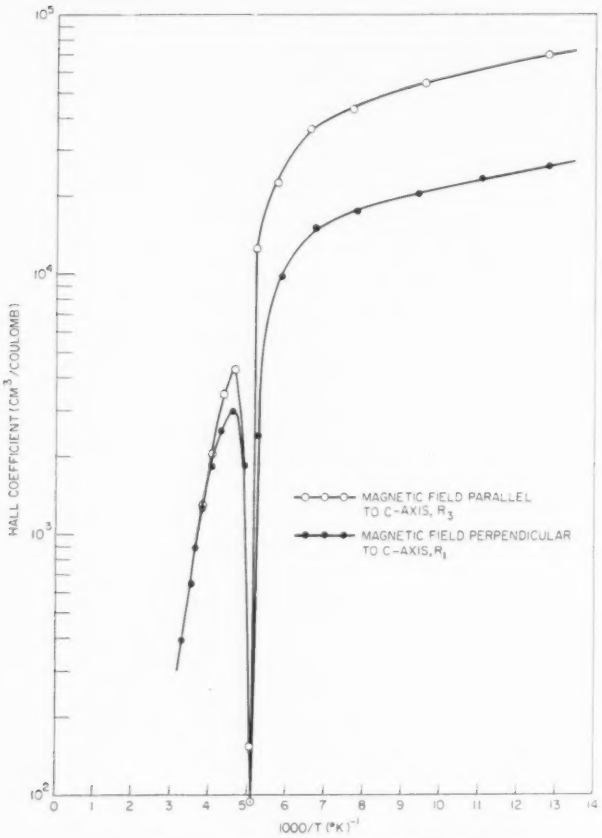
HALL COEFFICIENT (CM³/COULOMB)
10⁵
10⁴
10³
10²
0 1 2 3 4 5 6 7 8 9 10 11 12 13 14
1000/T (°K)⁻¹
MAGNETIC FIELD PARALLEL TO C-AXIS, R₃
MAGNETIC FIELD PERPENDICULAR TO C-AXIS, R₁

FIG. 3. Temperature dependence of Hall coefficients in tellurium.

*Table* 1. *Experimental values of the galvanomagnetic coefficients as measured at* 5000 *G*

| Coefficient | 303°K | 78°K |
|---|---|---|
| $\rho_1$ | 0·525 Ω-cm | 52 Ω-cm |
| $\rho_3$ | 0·307 Ω-cm | 16 Ω-cm |
| $R_1$ | $-3{\cdot}7 \times 10^2$ cm³/C | $7{\cdot}0 \times 10^4$ cm³/C |
| $R_3$ | $-3{\cdot}8 \times 10^2$ cm³/C | $2{\cdot}6 \times 10^4$ cm³/C |
| $\rho_{11,11}/\rho_1$ | ~ 0 | $7{\cdot}2 \times 10^{-10}$ G$^{-2}$ |
| $\rho_{11,33}/\rho_1$ | $2{\cdot}0 \times 10^{-10}$ G$^{-2}$ | $8{\cdot}7 \times 10^{-10}$ G$^{-2}$ |
| $\rho_{11,22}/\rho_1$ | $3{\cdot}1 \times 10^{-10}$ G$^{-2}$ | $12 \times 10^{-10}$ G$^{-2}$ |
| $\rho_{33,33}/\rho_3$ | ~ 0 | $2{\cdot}2 \times 10^{-10}$ G$^{-2}$ |
| $\rho_{33,11}/\rho_3$ | $3{\cdot}1 \times 10^{-10}$ G$^{-2}$ | $7{\cdot}2 \times 10^{-10}$ G$^{-2}$ |
| $2\rho_{13,13}/(\rho_1 + \rho_3)$ | $1{\cdot}1 \times 10^{-10}$ G$^{-2}$ | — |
| $\rho_{11,23}/\rho_1$ | ~ 0 | ~ 0 |
| $\rho_{23,11}/\rho_3$ | ~ 0 | ~ 0 |

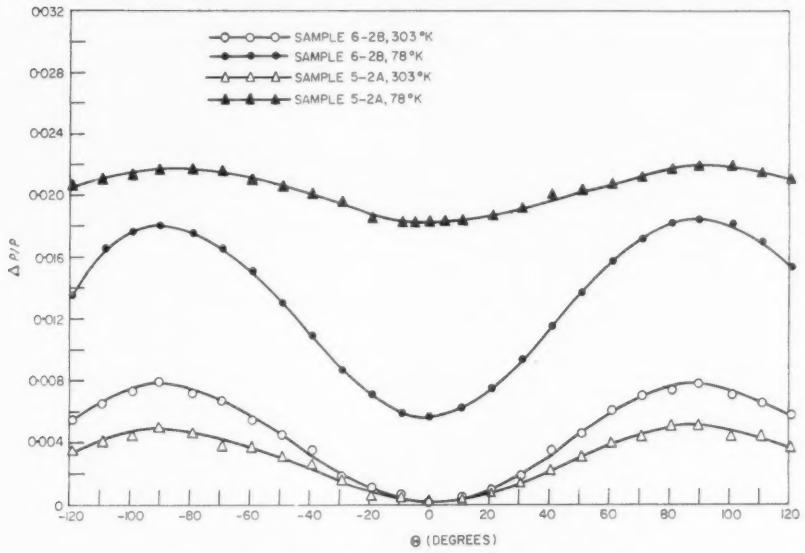


FIG. 4. Variations of $\Delta \rho/\rho$ in tellurium as the sample is rotated in a magnetic field of 5000 G. $\theta$ is the angle between the current and the magnetic field.

resistance and the equality of the Hall coefficients at 303°K indicate that a simple band model, consisting of one ellipsoid of revolution oriented along the *c*-axis, would be sufficient to describe the conduction band in tellurium. For the valence band, however, a more complicated band model must be employed because of the existence at 78°K of longitudinal magnetoresistance and the anisotropic Hall effect.[11] Either a three ellipsoid model, with the ellipsoids centered on the two-fold axis but no ellipsoid axis parallel to the *c*-axis of the crystal, or a general six-ellipsoid model might be appropriate.

*Acknowledgments*—I am indebted to Dr. P. H. MILLER, Jr. for suggesting this problem and for his constant

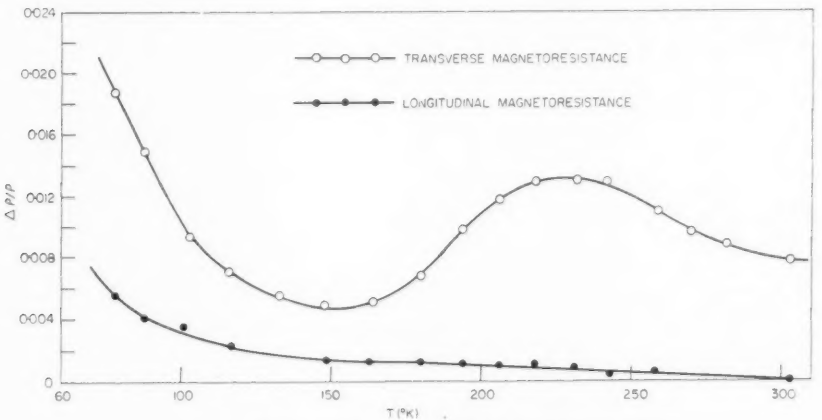


FIG. 5. Temperature dependence of magnetoresistance in tellurium. The current direction is parallel to the *c*-axis. The magnetic field is 5000 G.

MM

encouragement during the investigation, and to Dr. W. B. TEUTSCH for many helpful discussions and suggestions.

## REFERENCES

1. BOTTOM V. *Science* **115,** 570 (1952).
2. FUKUROI T., TANUMA S., and MUTO Y. *Sci. Rep. Res. Inst. Tôhoku Univ.* **A6,** 18 (1954).
3. NUSSBAUM A. *Phys. Rev.* **94,** 337 (1954).
4. SHALYT S. S. and OBRAZTSOV YU. N. *Zh. tekh. fiz.* **27,** 189 (1957).
5. CALLEN H. B. *J. Chem. Phys.* **22,** 518 (1954).
6. ASENDORF R. H. *Bull. Amer. Phys. Soc.* Ser. II, **2,** 147 (1957).
7. REITZ J. R. *Phys. Rev.* **105,** 1233 (1957).
8. FIRSOV IU. A. *Soviet Phys., J. Exp. Theor Phys.* **5,** 1101 (1957).
9. OKADA T. *Mem. Fac. Sci., Kyusyu Univ.* **1B,** 157 (1955).
10. DAVIES T. J. *Bull. Amer. Phys. Soc.* Ser. II, **2,** 301 (1957).
    The author is indebted to T. J. DAVIES and G. D. LONG of the Honeywell Research Center who supplied the crystals for the measurements reported here.
11. See, for example, DRABBLE J. R. and WOLFE R. *Proc. Phys. Soc.* B **69,** 1101 (1956).

## DISCUSSION

*Compiled by* P. J. PRICE

### S.2 M. GLICKSMAN

H. EHRENREICH: For GaAs, both the rise in the Hall constant from 500°K to intrinsic and Spitzer's data on free carrier absorption indicate that the next higher conduction band edge is as close as 0·2 to 0·4 eV above the main [0, 0, 0] one. This closeness, having effects in the extrinsic range, may be general for the III–V compounds.

R. K. WILLARDSON: Our data on transverse magnetoresistance of *n*-GaAs (with $4 \times 10^{15}$ electrons per cm$^3$ at 300°K) between 77° and 300°K is well accounted for by a simple model with spherical symmetry and combined lattice ($T^{-3/2}$) and ionic ($T^{+3/2}$) mobilities.

C. HERRING: The theory for ionic scattering is not simple.

H. EHRENREICH: Polar optical-mode, rather than acoustic-mode, scattering would dominate in GaAs.

### S.3 R. J. SLADEK

M. C. STEELE: How was the activation energy determined?

R. J. SLADEK: From the temperature dependence of the Hall constant, assuming the temperature dependence of the ratio of mobilities (conduction band and impurity) could be neglected in this calculation. For details see SLADEK *J. Phys. Chem. Solids* **5,** 157 (1958).

### S.4 J. C. HASLETT and W. F. LOVE

E. N. ADAMS explained (in reply to a question) that he could account for the observed dependence of mobility on electric field by a modification of Shockley's calculation with momentum relaxation dominated by ionic scattering. Optical-mode scattering was not significant in the energy relaxation because the electron "temperatures" concerned did not exceed 8°.

I. ESTERMANN asked about geometry effects, and

E. N. ADAMS commented that deflection of current towards the side electrodes might be a serious source of error.

C. HERRING remarked that surface conduction might also lead to errors.

W. F. LOVE responded with information about homogeneity of the samples.

### S.5 A. W. EWALD and O. N. TUFTE

L. J. VAN DER PAUW: (in reply to a question) explained his theorem for the transresistances of a thin flat crystal (effectively two-dimensional and isotropic in the plane, and with any shape of the perimeter): If $R_{AB,CD}$ gives the potential between small electrodes C, D for current between small electrodes A, B, and the conductivity times the thickness is $s$, then

$$\exp(-\pi\, s\, R_{AB,CD}) + \exp(-\pi\, s\, R_{BC,AD}) = 1$$

however the electrodes are placed on the circumference. Exploitation of this theorem might allow simpler preparation of samples for resistance measurements on these small crystals. See *Phillips Research Reports,* **13,** 1 (1958).

J. H. BECKER: My measurements (thesis, Cornell 1957) indicated no negative magnetoresistance. Silver paint contacts (with higher resistance than the sample) eliminated shorting. The small ratios of longitudinal-to-transverse magnetoresistance found suggest that the energy surfaces are spherical in the conduction band and only slightly warped in the valence band. The electron lattice-scattering mobility was found considerably higher than the values reported by EWALD and TUFTE, at 78°.

### S.6 H. ROTH

J. APPEL suggested that the increase of the longitudinal magnetoresistance with decreasing temperature reflected anisotropy of lattice-mode scattering, with the phonon density factor becoming a Boltzmann exponential.

C. HERRING commented that the anisotropy of the mass tensor could not be overlooked.

D. LONG explained that at 300°K, where Roth's samples were intrinsic, the electron contribution dominated the conduction, but at 77° the hole contribution dominated. Thus there was essentially a transition from *n*- to *p*-type as the temperature decreased, and the increase in anisotropy indicated by the magnetoresistance is probably largely due to this.

*J. Phys. Chem. Solids* Pergamon Press 1959. Vol. 8. pp. 531–536. Printed in Great Britain

SESSION T:
SUMMARY SESSION

T.1

# STATIONARY STATES OF SEMICONDUCTORS

HARVEY BROOKS
Harvard University

VOL. 8 1959

## 1. INTRODUCTION

THE remarks in this summary are organized under six headings: the validity of the band theory, band calculations, the bond picture, information on the band structure of actual materials, impurity levels, and lattice vibrations.

## 2. VALIDITY OF THE BAND THEORY

It is convenient to classify the approximations of band theory under the three general headings suggested by Professor SLATER (B.1). These are, with some modification:

(1) The use of a one-electron potential.

(2) The neglect of the multiplet structure on individual atoms.

(3) Treatment of electron lattice interaction as a small perturbation.

Various types of semiconductors may be discussed in terms of the degree to which these various approximations are violated. For example, Ge, Si, the III–V compounds, the Pb salts of the PbS family, $Bi_2Te_3$ and analogous compounds, the II–VI compounds, graphite—these form a class of high mobility semiconductors in which only approximation (1) is violated. However, in this case the work of KOHN (B.6) suggests that the band description is still formally valid, although the actual parameters which describe the bands may not be calculable from a one-electron potential. The importance of KOHN's result lies in the fact that for all these high mobility semiconductors the significant electronic properties arise from electrons occupying a very small fraction of the Brillouin Zone. In consequence the low lying excitations of the solid are of long wavelength and behave as quasi particles. KOHN's analysis also shows that the band description is formally valid in the presence of slowly varying electric fields, whether external or internal, arising from impurity centers. Furthermore, the dielectric constant enters in the expected way into the ionization energy of impurities provided the orbits are sufficiently large (B.6, B.7). The theory has not yet been extended to the motion in a magnetic field. Hence the argument is not yet complete, since ultimately it would be desirable to show that the band parameters derived from cyclotron resonance are the same ones needed in the description of impurity centers and of motion in an electric field. Empirically this is so, and the verification by BOYLE (L.4) of the theory of the Zeeman effect for impurity levels by WALLIS and BOWLDEN (L.3) gives further confidence that the vital theoretical connection can in fact be made.

When multiplet effects within individual atoms cannot be neglected we see the type of electronic behavior illustrated by the transition metal oxides and other compounds discussed by ZENER (B.2). Since these materials contain *d* electrons in incomplete shells they would be expected to be conductors according to the simple band picture. However, because of the stabilization of parallel spins within the atom in accordance with Hund's rule, the energy cost of transferring an electron to a neighboring atom is greatly increased and the materials are nonconducting.

Apparently, assumptions (2) and (3) often break down simultaneously as ZENER points out, since in the transition metal oxides the excited atomic configurations which transport current become self-trapped through distortion of the lattice, with the consequence that there is an activation energy associated with the carrier mobility. It is not surprising that the breakdown of both assumptions (2) and (3) is often associated with *d* electrons, since

their spatial degeneracy favors a low kinetic energy penalty for self-trapping and in addition the lattice can relax by Jahn–Teller distortion as well as by the more usual polarization effects.

It appears, however, that the lattice self-trapping mechanism alone can often give rise to an activated mobility as was nicely brought out by Professor JOFFÉ (A.3) in the case of $In_2Se_3$. JOFFÉ has emphasized that many semiconductors with mobilities less than 100 $cm^2V^{-1}$ $sec^{-1}$ have a nominal free path which is less than the wavelength of thermal electrons, and for these the ordinary band description is inappropriate owing to strong electron–lattice coupling, i.e. to the breakdown of assumption (3).

In cases where the simple band picture is inappropriate, there does not yet exist a calculus comparable with band theory which is capable of describing the electronic structure in a quantitative way.

It is to be observed also that the temperature dependence of the band gap in high mobility semiconductors is a manifestation of a small violation of assumption (3). Although this is understood qualitatively,[1] we are still far from a quantitative understanding of such effects as illustrated by the paper by PIPER *et al.* (Q.3).

Returning now to the high mobility semiconductors, KANE (B.5) and PHILLIPS (N.3) have both indicated that exchange and correlation effects on semiconductor band structure can be represented by including a non-local potential in the Schrödinger equation for each electron. Both PHILLIPS and KANE have attempted to estimate the contribution of exchange to the effective mass near the conduction and valence band edges. Their estimates still differ considerably. KANE concludes that the many-electron aspects of the problem do not make an important contribution to the band parameters. This controversy probably cannot be resolved without a detailed comparison of an accurate *a priori* and calculation with experiment.

### 3. BAND CALCULATIONS

During the past two years emphasis has shifted from *a priori* band calculations to a semi-empirical approach in which experimental information, especially cyclotron resonance data, is used to fix some of the parameters in the theory. One such approach, the so-called $\mathbf{k} \cdot \mathbf{p}$ approximation, has been reviewed by KANE (B.5). It has been very successful in fitting the cyclotron resonance data on Ge, Si, and InSb, and essentially this method has been used in the very successful determination of the complex band structure of graphite by MCCLURE and SOULE (B.3).

The alternative approach suggested by PHILLIPS (N.3) has the potential advantage of permitting us to predict the band structure far away from the Fermi level from a knowledge of the band edge positions and effective masses of the valence and conduction bands. PHILLIPS' method consists in doing an OPW calculation for a crude potential having a small number of disposable parameters, and adjusting these parameters to fit experimental data. Such methods will be useful in interpreting results such as those of HAGSTROM (H.4) on the energy structure deep in the valence band.

As pointed out in the preceding section a crucial test of band theory will ultimately depend on our being able to make an *a priori* calculation of band structure for which both the calculational errors and the limits of error of the self consistent one-electron potential can be accurately estimated. This stage has not yet been reached even for Ge and Si. The two computational methods which seem now to be most favored are the orthogonalized plane wave method (OPW) and the augmented plane wave (APW) method or its close relative, the variational method of KOHN and ROSTOKER.[2] The OPW method has the disadvantage of rather slow convergence, and hence poor estimation of purely calculational errors, but can be conveniently carried out with a non-spherical potential, which may be rather important in valence semiconductors. The APW method can only be carried out with a spherically symmetric potential having a rather artificial cut-off at the surface of the sphere inscribed in the atomic polyhedron. Thus, to make computations with a realistic potential, accurate wave functions as well as eigenvalues are needed for a perturbation calculation, and the greater speed of convergence may be offset by the necessity for computing wave functions. It is too early to say how the two methods of approach are going to work out on the diamond structure semiconductors. However, according to SEGALL (N.4) the necessary preliminaries to a Kohn–Rostoker calculation for both diamond and zinc-blende structures have now been completed, and another calculation for Ge by

VOL. 8 1959

HERMAN should be available soon. Both of these calculations, when complete, should have the kind of accuracy needed for an honest test of band theory. They will be one-electron calculations only in the sense that exchange and correlation effects among valence electrons will be neglected, but exchange with the core will be included.

### 4. THE BOND PICTURE

The chemical viewpoint has continued to prove its usefulness as a guide to the discovery of new semiconducting materials. There remains a problem in relating the qualitative considerations of the bond picture to the more quantitative details of the band picture. The dilemma is illustrated by Professor WELKER'S (A.4) interesting explanation of the high electron mobility in compound semiconductors in terms of the polarization of the valence electrons. As pointed out by HERMAN in the discussion, it seems clear that the differences between the various compounds are a function of the type of energy minimum in the conduction band. In compounds like InSb and GaAs the (000) minimum, with a characteristic low effective mass, is lowest in the conduction band and is responsible for the high mobility. However, it is not clear how the relative positions of the energy minima can be derived from WELKER'S picture.

The exploration for new semiconductors continues to yield interesting results.

Compounds of the type $A_3Sb$, where A is an alkali metal, have been studied systematically by SPICER and co-workers (P.6). Some of these compounds have long been of interest as strong photoelectric emitters, but the study of their band structure is only just beginning. They are noteworthy for their small electron affinity and for the fact that the band gap is relatively insensitive to the alkali metal.

Particularly interesting is the compound AuCs, a compound between nearly ideal metals, which is nevertheless a large band gap semiconductor (P.6).

The so-called III–VI compounds form another interesting group reported on at this meeting (P.5). These compounds are remarkable in that the chemical formula corresponds to an odd number of valence electrons, nine outside closed shells, and despite this they are semiconductors. It is a measure of the usefulness of the bond viewpoint that the semiconducting properties of these compounds were successfully predicted.

### 5. ACTUAL BAND STRUCTURES

With respect to our knowledge of their band structure semiconductors naturally divide themselves into two classes. In the first class are those materials for which good cyclotron resonance and magneto-optical data are available. For these we have a very detailed knowledge of the energy surfaces within 0·1 eV or so of the Fermi level. In the second class are those materials for which our knowledge of band structure depends mainly on the interpretation of transport properties supplemented by optical measurements of the band gap or of transitions between sub-bands of a degenerate valence band.

In what follows I have attempted to summarize the main contributions to our knowledge of semiconductor band structure which have emerged from the conference.

A. *Class* 1 *semiconductors*

(1) *Ge and Si*—The energy and curvature of the (000) minimum in the conduction band of Ge has been established with extremely high precision by the magneto-optical absorption technique (L.1, L.2).

The very complete theoretical understanding and experimental verification of the magnetic field effects on the three types of interband optical transitions is strong evidence for the effective mass type theory.

The recent optical work of the Malvern group (O.2) and of HAYNES (O.3) has established the energy of the (111) minimum in Ge, that is the energy gap, with great accuracy.

Work on electrical transport properties of Ge under pressure (H.1) has fixed the position of the (100) minimum in Ge at $0{\cdot}16 \pm 0{\cdot}01$ eV above the conduction band edge. The curvatures are much more approximately fixed as close to those of Si.

Exploration of the donor wave functions in Si by the ENDOR technique (R.1) has established the position of the (100) conduction band minimum at a point 85 per cent of the way out to the zone boundary.

Magnetic susceptibility measurements on conduction electrons in Ge (H.3) have established that there are four rather than eight minima and that

the conduction band is parabolic to at least 0·08 eV above its edge. For Si there are still unresolved discrepancies with the six-ellipsoid model.

The technique of ejection of electrons from the valence band through interaction with positive ions approaching the surface (H.4) has provided a new tool for exploring deep into the valence band. With certain plausible theoretical assumptions a density of states curve for Si has been obtained which shows a high density $p$ band of 5·1 eV width at the top of the valence band, and a total valence band width of 16 eV. Both results are larger than theory predicts. It is hard to understand why the valence band width should be so much larger than the free electron value of 13 eV.

Electron impact ionization (I.1) holds great promise for exploring rather deep into the conduction band, but even the simple energetics of the process has not been worked out theoretically to the point where it can be used for interpreting complex band structures.

(2) *Graphite*—Despite its great complexity the band structure of graphite is now known as well as that for Ge and Si, the most complete and detailed work being that described by SOULE and MCCLURE (B.3). Briefly the picture presented is that of a valence and conduction band overlapping about 0·03 eV with the carriers in highly anisotropic and warped energy surfaces corresponding to low effective mass. Such thorough exploration is possible because, though graphite is a semi-metal in the strict sense, the volume of the significant part of the Brillouin Zone is small as in a semiconductor.

(3) *III–V intermetallics*—The only materials that fall strictly in class 1 are InSb and InAs, although data are becoming available for GaAs (L.2).

The use of the magnetic susceptibility technique (H.3) has made it possible to explore as much as 0·33 eV into the conduction band, verifying the large deviation from parabolic form deduced from the $\mathbf{k} \cdot \mathbf{p}$ theory of KANE (B.5).

B. *Class 2 semiconductors*

1. *III–V intermetallics*—BRAUNSTEIN (J.5) has studied the optical transitions within the valence band of GaAs and has thence been able to deduce the magnitude of the spin-orbit splitting and the ratios of the three hole effective masses. It is interesting that the valence band is quite like that of Ge, as is probably true for all the III–V compounds. The effective mass ratios are about as would be expected from the relative size of the band gap in Ge and GaAs. It is interesting to note that the magnitude of the spin orbit splitting in GaAs is consistent with a picture in which the valence electron spends 65 per cent of its time on the As.

An interesting question is whether the top of the valence band lies strictly at $\mathbf{k} = 0$ in the intermetallics or whether it is split in accordance with the group theoretical considerations of DRESSELHAUS and others.[3] From optical data on the inter-valence-band transitions STERN (J.4) believes there is evidence that the maxima in InAs are displaced from $\mathbf{k} = 0$, being about $3 \times 10^{-3}$ eV above the energy at $\mathbf{k} = 0$, and there is evidence for similar splitting in the case of GaAs (J.5). The present evidence is inconclusive, however, but might be resolved by a study of galvanomagnetic properties at very low temperature.

In contrast to the similarity of the valence bands, there is considerable variation in the conduction bands. Three types of minima (000), (111), and (100), are present and which lies lowest is a systematic function of atomic number, lattice constant, and degree of ionicity. For example, low atomic number favors the (100) minimum as does smaller lattice constant (H.1). Ionic character seems to favor the (000) minimum, as this lies lowest in GaAs which is isoelectronic with Ge. Apparently high atomic number also favors the (000) minimum, but it is to be noted that in grey tin the mobility is not consistent with the effective mass one would expect from a (000) conduction band (S.5). The systematics of the relative positions of the types of minima as a function of pressure and composition in the intermetallics appears to be a fruitful field for further study.

(2) *PbS, PbSe, and PbTe*—These materials present two rather puzzling features. In the first place, the band gap appears to be smallest for PbSe, a fact which is further substantiated by SCANLON's studies (P.1) on alloys with PbS and PbTe, though the evidence is not conclusive. This is difficult to understand unless there is a change in the character of the conduction or valance band extrema as a function of composition. The incomplete evidence from magnetoresistance suggests (111) ellipsoids in both valence and conduction bands in all three

VOL 8 195

compounds. A further puzzle is that the minima in the conduction band appear to lie vertically above the maxima in the valence band, a coincidence which is unlikely unless both sets of ellipsoids lie on the zone boundaries.

(3) *$Bi_2Te_3$*—The interesting work reported by DRABBLE (P.3) illustrates the difficulty of interpreting galvanomagnetic data in terms of band structure when the symmetry is lower than cubic. Nevertheless, by a sufficient number of measurements it has been possible to determine that both the conduction and valence bands are of the multi-ellipsoid type, and the effective mass ratios have been found.

(4) *ZnO*—A multi-ellipsoid model also appears probable for this material (Q.6).

(5) *CdS and ZnS*—Incomplete theoretical (B.4) and experimental (R.4) evidence suggest that the conduction band minimum is at $\mathbf{k} = 0$ with, hence, an isotropic effective mass. It is interesting that this material is available in high enough perfection to permit observation of cyclotron resonance.

(6) *Impurity levels*—Impurity levels with sufficiently large orbits to be describable by the effective mass approximation and an effective dielectric constant (B.6, B.7) are fairly well understood, although there are still puzzling discrepancies for acceptors in Si. In practice this means that only the excited states of group III acceptors and group V donors in Ge and group V donors in Si are fully understood. In this connection the work of the Purdue group in the far infrared on both donors and acceptors in Ge (J.2a, J.2b) provides us with a detailed verification of the classical theory of KOHN.[4]

An important further extension, new at this conference, is the theoretical work of WALLIS (L.3) and the experimental verification by BOYLE (L.4) on the Zeeman effect of the hydrogenic impurity levels.

There exists scarcely any theory for the deep lying impurities, despite a wealth of experimental data (C.2). It is interesting to note that there is no experimental evidence for excited states of these impurities. The only unifying viewpoint which emerges from the experiments is provided by the valence bond picture: the number of donor or acceptor levels corresponds to the number of electrons that have to be added or subtracted from the atomic configuration to just provide a complete set of tetrahedral bonds. Recently the evidence for this picture has been further extended by the discovery of donor levels due to S in Si (C.7).

Despite the success of the bond picture, it is important to identify the structural nature of the imperfection giving rise to the deep levels. These are not always simple substitutional atoms, and the spin resonance technique (R.2) is just beginning to provide a powerful new tool for investigating the detailed structure. These studies have already shown that Mn in Si appears often in clusters of four, and that Ni in Ge distorts the Ge lattice anisotropically, apparently tending to lower the symmetry of its environment through the Jahn–Teller effect.

The importance of association of impurities and imperfections is further emphasized by the interesting theoretical work of PRENER and WILLIAMS (Q.4), who show that association effects are of special importance in large band gap semiconductors such as ZnS.

(7) *Lattice vibrations*—Three different lines of evidence on the lattice vibration spectrum of semiconductors were discussed at the conference. These are: the observation of optical effects due to polar modes (J.6), the study of the fine structure of indirect transitions between the valence and conduction bands (O.3, O.2), and experiments on the inelastic scattering spectra of neutrons (O.5). The first complete lattice spectrum of a semiconductor was reported (O·5), and it is interesting to note that the results are quite consistent with the optical data for Ge, although there is a puzzle as to why the phonon transitions that are theoretically forbidden should actually appear. The most interesting feature of the lattice spectrum is the extremely high dispersion in the transverse acoustic mode, much greater than observed in common metals such as Al or Cu. High dispersion always suggests long range forces, and the fact that it is chiefly in the transverse mode suggests non-central forces. These considerations have led M. LAX (O.6 discussion) to postulate quadrupole forces between atoms falling off as $r^{-4}$ and superposed on the short range valence bond forces. Such forces are physically plausible in high dielectric constant semiconductors. Furthermore, since Si has stronger bonds but considerably smaller polarizability, one might expect that the lattice

spectrum for Si would have less dispersion. However, the optical data on Si suggest phonon energies for Si which are hard to reconcile with any plausible extrapolation from the lattice spectrum of Ge, and the unravelling of this problem must await neutron data on Si.

**REFERENCES**

1. FAN H. Y. *Phys. Rev.* **82,** 900 (1951).
2. KOHN W. and ROSTOKER N. *Phys. Rev.* **94, 1111** (1954).
3. DRESSELHAUS G. *Phys. Rev.* **100,** 580 (1955).
4. KOHN W. *Phys. Rev.* **98,** 1856 (1955).

*J. Phys. Chem. Solids* Pergamon Press 1959. Vol. 8. pp. 536–538. Printed in Great Britain

VOL
8
195

T.2

# FUNDAMENTAL TRANSITION PROCESSES

**D. POLDER**

Philips Research Laboratories, N. V. Philips' Gloeilampenfabrieken, Eindhoven-Netherlands

EXCITONS have come to stay. This is perhaps the most important conclusion that can be drawn from the papers I shall review. There is now convincing evidence of the existence of excitons both in the elemental and in compound semiconductors. To a large extent the evidence is convincing because of the existence of a more detailed theory of excitons and the corresponding optical transitions which can be compared with the experimental observations. Though the theoretical concept of an exciton is an old one, the recent progress in the theory has only been possible because of our increased knowledge of the structure of energy bands. Theoretical calculations and experimental exploration of energy bands with cyclotron resonance were some of the main topics at the 1954 conference. In the meantime the subject has progressed rapidly. The study of optical band-to-band transitions, also in the presence of magnetic fields, has made important contributions. Spectroscopy of the solid state is now a fashionable subject for the investigation of the intrinsic properties of semiconductors and defects.

Let us review some of the papers relevant to this subject. First of all there is ELLIOTT's paper which summarizes the theory of band-to-band transitions of the direct type (either allowed or forbidden) or of the indirect type involving the emission or absorption of phonons. It includes the fine structure due to excitons in these cases and the effect of a magnetic field. A major refinement of the theory is the inclusion of the effect of the Coulomb interaction between electron and hole on the shape of the absorption vs. frequency curve in the continuum range. It is perhaps worth pointing out that many of the qualitative features of the theory of the absorption curves can be obtained with a few simple considerations on the density of final states and the structure of the matrix-elements, taking into account the usual conservation laws.

Very precise measurements of the fundamental absorption of Ge and Si by the R.R.E. group have now revealed the direct exciton transition in Ge. A detailed analysis of the indirect edge at different temperatures, with the aid of curve fitting and adding based on theory, shows that in Si and Ge four different phonons are active. A precise determination of the phonon energies has been made. The shape of the elementary parts of the absorption curve shows the presence of the indirect exciton in Si and Ge. This interpretation is verified by photoconduction experiments. The latest results about its binding energy in Ge (0·0025 eV) now seem to be in agreement with the earlier results obtained by the Lincoln group, which I shall review a little later.

HAYNES reports intrinsic recombination emission experiments on Si and Ge which are complementary to the absorption data. In a way the emission experiments are even clearer as the different phonon

processes show up as emission peaks. The phonon energies are in good agreement with those given by the R.R.E. group. At present there is still some uncertainty whether the emission takes place from excitons or not.

Application of a magnetic field provides a further tool to solid state spectroscopists. The magneto-optics of direct transitions in Ge and InSb was discussed by BURSTEIN *et al.*, in which the complications due to the complex valence band structure were included. The Lincoln group presents high resolution low temperature magneto-optical data (and their interpretation) for both the direct and the indirect transitions in Ge. Two direct exciton peaks are observed and their positions as a function of $H$ are interpreted, in addition to the usual peaks due to Landau levels. The indirect magneto-optical spectrum which shows steps rather than peaks can also be interpreted in terms of Landau-transitions and an exciton transition, the latter again being characterized by a non-linear dependence of its energy on the magnetic field. One of the many further points of interest is the anomalously high $g$-factor of the electron because of spin-orbit coupling evident in the direct Landau-transitions.

I believe we may say that the exciting development in the elemental semiconductors has now come to a stage where the field is open for a more quantitative analysis of the absorption strength of the transitions together with a further study of the line broadening on which both the R.R.E. group and the Lincoln group have already given some experimental data.

It is natural that the increased knowledge will greatly help the interpretation of line spectra in compounds such as reported by GROSS in $Cu_2O$ and CdS and by NIKITINE in several salts. Hydrogen-like series are often found here. To mention one example, a particular series in $Cu_2O$ has the $n = 1$ member missing which, according to ELLIOTT, could be interpreted as an exciton series of the forbidden direct-transition type. The large diamagnetic effect in magnetic fields clearly indicates the large size orbits, the absence of an appreciable linear Zeeman effect points to the approximate equality of the electron and hole effective mass.

The success of the theory in the cases mentioned above largely depends on the smallness of the interaction between charge carriers and lattice vibrations. In the polar lattices of alkali halides the situation is surely more difficult to handle. There is little doubt that eventually observations on the optical edge such as reported by MARTIENSSEN will be better understood and that semi-empirical rules like Urbach's rule will be replaced by a clearer physical picture. However, at present, the theory here is not yet in a very good state. Several theoretical papers in this field at the conference do not easily lend themselves for reviewing. I wish to mention HAKEN's paper that contains a fundamental discussion of the role of the different dielectric constants ($\epsilon_0$, $\epsilon_\infty$ or 1) in the attraction that binds a hole and an electron together.

A paper by PIPER on the temperature dependence of the energy gap in ZnS, which seems to be existent down to quite low temperatures, indicates a strong interaction with low energy phonons. This gives me the opportunity to remark that also in Ge and Si where the band gap as a function of $T$ is now accurately known, relatively little attention has been paid to a quantitative interpretation of this phenomenon. Furthermore, the application of statistical mechanics to a system of temperature-dependent energy levels must have consequences for energy-transport processes, which are not yet fully explored.

In the field of the spectroscopy of semiconductors there are three more papers I would like to review.

First, a paper by the U.S.N.R.L. group on optical vibration spectra in polar crystals summarizes results obtained on effective charges by this classical method. Secondly, a paper on the Faraday rotation by conduction electrons (MOSS) contains a potentially useful method to determine the effective mass of charge carriers from dispersion and rotation data, especially useful, perhaps, for substances where other methods are not so easily available. Thirdly, MEYER'S paper on infrared absorption by carriers in Ge discusses the role of impurity, optical-phonon, and acoustical-phonon scattering using the latest data on deformation potential constants. Free carrier absorption measured as a function of temperature and wavelength should give further information on these scattering processes.

A few words should be said about the theory of trapping and recombination. It appears that in those cases where the Shockley–Read theory applies, capture cross-sections of centres which are not

definitely repulsive are little dependent on temperature. Large and strongly temperature-dependent trapping in low-lying donor levels is observed in some of KOENIG's low temperature experiments which essentially measure the transient effect of the disappearance of carriers into these traps. MELVIN LAX has made a theory for this in which he points out that electrons have effectively already been trapped as soon as they are about $kT$ in energy down the ladder eventually leading to the lowest state of the trap. It may be pointed out that this theory does not necessarily apply to recombination centres as the bottle-neck of the recombination process may be further down in the energy scale.

Progress has been reported on the theory of band-to-band Auger recombination (LANDSBERG). Because of the simultaneous conservation laws of energy and momentum the process is only effective if the sum of hole and electron kinetic energies is a considerable fraction of the band gap. This feature is also present in TAUC's paper on band-to-band impact ionization, where the electron must have considerably more than the band gap energy in order to produce ionization of this type. Essentially LANDSBERG's process is the inverse of that involved in TAUC's experimental work.

Finally I shall review only some of the work reported at this conference on nuclear and spin resonance in centres.

Nuclear resonance has been used to study quadrupole fields in cubic compounds (RHODERICK, InSb) set up either by strains due to incorporation of different-sized atoms (Ga) or by the (much more effective) electric fields from differently charged impurities (Te). The aim of this sort of investigation is obviously to get more quantitative information that can be used again in other cases to make deductions on the structure of defects.

In the G.E. laboratories a systematic investigation is being made of spin resonance in deep lying levels of transition metals in Ge and Si. In Ge it appears that in many cases no resonance was detected, while in other cases only certain ionization states did give signals. $Ni^-$ in Ge appears to be in an anisotropic surrounding. Presumably $Ni^-$ is shifted away from the substitutional position by a Jahn–Teller effect, though above 21°K reorientation and an isotropic line is observed. Manganese in Si appears to cluster in groups of four atoms. These first results already show considerable complexity and promise interesting future developments. As a tool for the investigation of deep levels spin resonance is likely to be a prominent feature on the next semiconductor conference program.

*J. Phys. Chem. Solids* Pergamon Press 1959. Vol. 8. pp. 538–541. Printed in Great Britain

# T.3 RECOMBINATION, TRAPPING, AND OPTICAL PHENOMENA

L. APKER

MY assignment is to summarize the progress reported at this meeting on recombination, trapping, and certain optical phenomena. Dr. POLDER has already discussed electronic transition processes, with emphasis on theory. I shall talk more about the statistical interplay of these transitions, with emphasis on experiments.

The first part of this subject, then, concerns recombination of electrons and holes in semiconductors. Speakers at this conference have treated three main aspects of the problem. They are the following:

(1) Auger recombination.

(2) Radiative recombination involving no crystal defects (but sometimes involving phonons).

(3) Recombination, both radiative and non-radiative, at defects such as chemical impurities or dislocations.

The previous summary has mentioned Auger phenomena and their relation to impact ionization

effects. The latter are important in the quantum efficiency measurements on photoconduction in Ge as reported in Session I and in the analogous experiments on lead salts surveyed in Q.7. Accurate experimental values for the impact ionization threshold are also of interest in understanding the external photoelectric effect and in the theory of junction avalanche breakdown as worked out by P. A. WOLFF.[1] Investigation of the related effects in this area will be of continuing interest.

We turn now to the second aspect of recombination in the list above. This concerns radiative processes in the ideal crystal. The summary by POLDER covers progress in observing and understanding the elementary transition processes that are involved. In available samples of germanium and silicon, this kind of radiative recombination is outweighed by radiationless processes at defects. It may be detected separately, however, by observation of the emitted radiation. Moreover, measurements (such as those in C.5) involving the mixed process are interpretable and are in agreement with present theory. In the lead salts, measurements of optical absorption (P.1) show that the radiative lifetime is lower than $10^{-4}$ sec in intrinsic material at room temperature.

Point three in our list above involves a much more extensive and difficult area: namely, recombination catalyzed by chemical impurities and by imperfections in the crystal structure. It stands in contrast to the two types of recombination just discussed. It is not determined by the properties of the ideal crystal alone. Different samples of the same semiconductor obviously may have different recombination centers and correspondingly different properties. It is especially interesting, therefore, that gratifying progress has been made in this diverse and complicated field. Understandably, the work is slow and painstaking. Many different recombination centers must be studied one at a time in a semiconductor such as Ge, for which other conditions are well understood and precisely controllable.

Considerable progress has been made with chemical impurities of the "deep level" type (C.2, 7). Measurements are made on the Hall effect, resistivity, and photoconductivity of carefully doped samples. This determines the energy levels and the charge states associated with specific impurities. It also gives some information about cross sections for trapping or recombination. With this approach, the trap model for photoconductivity, as developed by ROSE for CdS, has been quantitatively verified in Ge. Other techniques, such as electron spin resonance measurements, are giving interesting detailed information on the manner in which impurities are incorporated into the crystal (R.1, 2).

As reported by KALASHNIKOV (C.1) detailed studies of recombination have been carried out on germanium deliberately doped with copper. The dependence of the recombination on the carrier concentration and on temperature was analyzed. When only a single energy level was important, the Shockley–Read–Hall theory adequately described the observed effects. Copper in germanium gives rise to more than one energy level, however. The theory has been extended to cover the case in which more than one recombination level is important. Comparison with experiments indicated that cross sections were only weakly temperature and concentration dependent. From this it was deduced that phonon processes probably dissipated the recombination energy. Plasma and impact processes (as well as Auger processes at defects) may be ruled out. The upper energy level for copper was found to be 0·18 eV below the conduction band. It was established in discussions here at the conference that this number corresponds closely with the value in paper C.2, provided that the latter (previously specified at 0°K) is corrected to room temperature. We may thus conclude that this type of recombination is well understood. Interesting and even clearer results have been obtained with nickel (there was no time to do more than mention these at Session C). Interest will focus on extension of this type of work to other recombination centers.

Attention is also turning toward the theory of detailed mechanisms by which energy is dissipated at a recombination center (C.3).

We should note two ways in which the understanding of deep-level impurities differs from that of the shallow-level centers. First, a quantitative theory of deep-levels is difficult and has not yet been worked out. Second, as pointed out in the summary by Brooks, there apparently has not yet been a direct experimental observation of excited states for deep-level centers in Ge or Si. On this particular kind of problem, there has been more progress in wide-band-gap materials such as phosphors.

Experimental techniques for measuring recombination, at least in Ge and Si, have become reliable and straightforward. Difficulties and discrepancies, once so numerous, are no longer discussed at any length in the case of these two semiconductors.

Recombination sometimes exhibits, however, a behavior more complex than that described for copper and nickel above. When this happens, a common explanation is that the character of the sample itself is complex (we pass over geometrical difficulties due to surface effects or sample inhomogeneity). The reasons are diverse. Several different chemical impurities may be present simultaneously (C.6). Conceivably, unfamiliar impurities may also be involved. Or, the recombination may be due to crystal imperfections such as dislocations.

Defects in the crystal structure of Ge are not yet controlled as precisely as chemical impurities. There are many varied and complex kinds of dislocations, for example. As in the case of surfaces, they may be demonstrably clean, or they may not. In spite of this, progress is evident, for example, in the papers of Session F. There is fair agreement on the nature of the acceptor behavior of dislocations or grain boundaries in Ge. The associated space-charge sheaths have been investigated in considerable detail. The effect of dislocations on recombination is being measured. The recombination radiation from dislocations shows interesting detail. There is still much to be understood in this field.

Progress is being made on other materials. Luminescence is a valuable tool for studies of defects in diamond, in CdS, and in other wide-gap semiconductors (Session Q).

It is agreed that hole-trapping drastically reduces the recombination rate in silver halides that have been grown in air. We note in passing that in the course of work on silver salts at Bristol (K.5), the stress-induced prismatic dislocation, as conceived by SEITZ, was detected for the first time experimentally. In this same laboratory, detection of effects explainable by hole motion in silver halides delineates an area of future interest. At Illinois (K.6) Hall mobilities as large as 5000 $cm^2\ V^{-1}\ sec^{-1}$ have been measured at low temperatures for electrons in AgCl. This approach has overcome the difficulties usually presented by traps. Interesting recombination phenomena are under investigation in the alkali-halides and in CdS at Rochester (Q.7). Cyclotron resonance has been detected in CdS at Wisconsin (R.4). A sensitive, powerful new method for detecting impurity levels in the forbidden gap of crystals like CdS has grown out of the work by LAMPERT, ROSE, and SMITH on currents limited by space charge (Q.5).

As discussed in Session G, the optical absorption of CdS, as well as that of other crystals, shows line structure indicative of exciton formation. Several talks concerned the behavior of excitons after they are formed in CdS and ZnS. Well-defined luminescence with line structure has been observed in the Leningrad, Paris, and Strasbourg work. It is ascribed, at least in some cases, to exciton annihilation. The talk by GROSS mentioned photoconductivity that shows spectral structure directly connected with that of the optical absorption. Related observations are being made in Kiev.[2] This field appears to be developing in a very interesting direction.

Paper G.5 described an experimental sample in which diffusion of excitons as electrically neutral carriers of energy over millimeter distances in CdS was not ruled out. The theory of a possible process involving both exciton and photon transport is the subject of G.4. In G.3, scattered and reabsorbed luminescent radiation turned out to be of dominant importance in an extensive series of experiments on energy transport over millimeter lengths in CdS. In the presence of this phenomenon, exciton diffusion could not be detected. In summary, it appears that we have not yet reached the point where exciton diffusion over millimeter distances in CdS is being reproduced or demonstrated at will in different laboratories. There does seem to be agreement that scattered radiation can be an important effect in energy transport over such distances in CdS and ZnS. An interesting possibility for future progress in CdS, then, is direct demonstration of exciton diffusion (such as has been carried out for distances of order $10^{-5}$ cm in organic molecular crystals by O. SIMPSON).[3] For the alkali halides and BaO, photoemission studies have shown that the efficiency of energy transfer from excitons to *F*-centers is high, sometimes as much as 10 per cent. In these materials also, however, we still lack a direct and reproduced demonstration of exciton migration. Such an experiment might be like SIMPSON'S experiment, or it might be based on careful measurements as a function of *F*-center concentration at average center separations more than

$10^{-6}$ cm.[4] It appears that luminescence studies such as those being made at Rochester may be most convenient for this purpose. Before leaving this point, we should note that the lifetimes deduced from line broadening for excitons in Ge and Si give information on the fate of these particles after they are created. The expanding effort on excitons in diamond will clearly be followed with attention.

In the alkali halides, the first fundamental absorption peak has been termed an exciton peak because observable photoconductivity does not result as a primary consequence of photon absorption. This reasoning is not entirely sound, because it tacitly assumes that observable photoconductivity *does* occur at some higher photon energy, which corresponds to interband transitions. While there is some indirect evidence for this, the effect has never been directly observed, as far as I am aware. At least one search has been made in the past. In this situation, tentative observation of photoconduction in RbI here at Rochester's Institute of Optics is of great interest. The phenomenon sets in at an understandable point, namely, at the absorption edge located by MARTIENSSEN (K.4) at a photon energy about 0·5 eV higher than the first fundamental absorption peak. Both this effect and the related investigations of luminescence due to recombination in alkali halides mark an area of interesting development.

The part of semiconductor research typified by work on Ge and Si has attained an impressive maturity. These materials have a characteristic complexity, but in large part they have been understood with unprecedented precision. Progress reminiscent of early work on Ge and Si has appeared at this conference in the area covered by this summary. It has concerned solids with rather longer histories—alkali halides, silver salts, lead salts, and crystals such as CdS. Those familiar with this field will probably not be greatly surprised by other interesting parallel developments in the future.

### REFERENCES

1. WOLFF P. A. *Phys. Rev.* **95,** 1415 (1954).
2. BROUDE V. L. *et al Doklady Akad. Nauk. USSR* **119,** 911 (1958).
3. SIMPSON O. *Proc. Roy. Soc.* **238,** 402 (1956).
4. A related experiment with excitation by gamma rays has already been explored by VAN SCIVER W. and HOFSTADTER R. *Phys. Rev.* **97,** 1181 (1957).

*J. Phys. Chem. Solids* Pergamon Press 1959. Vol. 8. pp. 541–543. Printed in Great Britain

T.4

# SURFACES

**WALTER H. BRATTAIN**

Bell Telephone Laboratories Inc., Murray Hill, New Jersey

I HAD some hopes that maybe after HERRING's talk you would all decide you had had enough and then I would not have to give mine. The papers on surface properties at this conference covered four main categories.* These are as follows: the so-called "real surfaces" of germanium and silicon; the type of surface that I like to call "imaginary" but might better be called "clean"; the transport properties of electrons and holes in surface layers; and finally the chemistry of adsorption and structure of these surfaces.

The physical properties of the "real surface" of a germanium crystal are now becoming quite clear. Such a surface has some kind of an oxide layer. Between this layer and the semiconductor are certain states or traps in which electrons or holes can

* I have purposely refrained from using names. One can easily find the source by referring to the original papers on Surfaces.

be trapped, thus contributing to the surface charge. Under normal conditions these "fast traps" are in good thermal equilibrium with the interior of the crystal. These trapping levels appear to be discrete rather than having a continuous distribution in energy. There appear to be four of them: two close to the conduction and valence bands, respectively; another is just above the intrinsic level; and, the other is about 0·1 to 0·2 eV below the intrinsic level. The latter surface level or trap under normal conditions is the most accessible one for study and appears to be primarily responsible for surface recombination of holes and electrons. For this reason its properties are better known than the others. These states have a density of about $10^{11}$ per cm$^2$ of surface. The ratio of capture cross section for holes is greater than that for electrons by about 50. This indicates that these are acceptor levels, i.e. negatively charged when filled with an electron and neutrally charged when empty. While the field effect measurements vs. frequency confirm the idea that these traps are not distributed in energy but discrete, nevertheless, the analysis of this latter data does not agree too well with the previous results on the position in energy of these traps. This needs more investigation. Finally there is the area of reaction of the surface with the ambient gas at the outer surface of—or in—the "oxide layer". These are so-called slow states since it takes seconds to minutes for this part of the surface to reach equilibrium with the interior after sudden changes in potential of the surface. The evidence is that chemical changes here add to or subtract from the total charge dipole layer at the surface; thus, changing the potential at the surface and this change is more or less equivalent to the application of an electrical field at the surface—i.e. the density and energy levels of the fast traps are not to the first approximation affected by the chemical reactions at the outer surface. One should remark, however, that the nature of the fast traps can be changed by surface pretreatment, such as the type of etch, etc., used to prepare the surface for study. The density of the fast traps is most sensitive to such treatments while the energy levels and cross sections do not appear to change so much. As a result of one paper, we now know that the slow surface states react to the contact potential field set up when a metal is brought in contact with the surface in the same way as to an applied electric field, i.e. a sudden change in potential of the surface with a slow relaxation back towards the original surface potential. These slow surface states and/or the chemistry of the surface still need further studies. One would hope to really understand the oxygen water vapor cycle in surface potential in the sense that one knows chemically what is actually going on as the potential of the surface changes. These slow states appear to have larger densities than the fast states—$10^{13}$ to $10^{14}$ per cm$^2$. It was also brought out, that by working at low temperatures, the charge can be changed and this change maintained for long periods, by illuminating the surface with light of various frequencies. The use of this technique to study the dependence of the relaxation times of these effects as a function of temperature looks promising.

A number of reports were given concerning the clean surfaces of germanium and silicon. It now appears that such surfaces are usually quite *p*-type. The only exception to this was the report that cleaved germanium surfaces appear to be nearly intrinsic. This last conclusion depended on whether neighboring noncleaved surfaces were having an undue effect on the measurements. Particularly convincing was the evidence that the surface of a silicon crystal can be made what one might define as thermionically clean by heat treatments at 1550°K. Field emission, contact potential, photo emission, thermionic emission, and secondary electron emission results, all lead to this conclusion. Such a surface is highly *p*-type regardless of whether the crystal was *n*- or *p*-type in the interior. More important still was the discovery that after this treatment this *p*-type surface could only be removed by actually etching away a definite amount of the silicon. This indicates that the treatment used to produce this clean surface had introduced a special "chemical" *p*-type layer on the surface and for silicon, at least, the problem of producing a clean surface on an otherwise homogeneous crystal was still a problem for the future. This also suggests that tests should be made in all cases of clean semiconductor surfaces to see if the surface has been altered in a manner that needs more than a simple surface charge to explain it.

The transport properties of charges flowing in the surface space-charge layer show that as the depth of the potential well at the surface is increased the mobility decreases as previously predicted by

VOL
8
195

Schrieffer. The results reported, however, indicate that the reduction in mobility is in general somewhat less than would result from completely diffuse scattering at the surface.

We were told that oxygen take-up or oxidation of clean germanium and silicon surfaces follows the logarithmic rate law. These surfaces can be regenerated both by ion bombardment and by heat treatment. One is inclined to remark that this reaction is taking place on an admittedly *p*-type surface which in the case of silicon may be of a special "chemical" type as we have seen. One would like to ask what law or laws would this oxidation or adsorption follow on a highly *n*-type "clean" surface of silicon that might well be made by special doping of the surface. The electron diffraction study of the silicon surface suggests that the atomic arrangement of silicon atoms at the surface is much more complicated than for the case of germanium.

One might conclude this summary by expressing the hope that in the future ways will be found to study the essential chemistry of the semiconductor surface and to correlate these properties with the now measurable physical properties of the surface. Then maybe we will really begin to understand such surfaces whether "real" or "imaginary."

VOL. 8 1959

*J. Phys. Chem. Solids* Pergamon Press 1959. Vol. 8. pp. 543–549. Printed in Great Britain

T.5

# TRANSPORT

C. HERRING
Bell Telephone Laboratories, Murray Hill, New Jersey

## 1. OUTLINE

MOST of the current work on transport in semiconductors is centered about the idea of entities in motion, pushed by an external agency, and trying to return to equilibrium by scattering processes. These mobile entities may be either the free charge carriers themselves, or they may be uncharged entities, of which the most important for the field of transport are phonons and to a lesser extent excitons. However, as JOFFÉ (A.3) pointed out rather clearly, not all interesting semiconductor phenomena can be understood in such terms. In Table 1, which outlines the topics to be covered in the present review, the last two of the four headings are for things whose understanding requires other concepts, although these things do not occupy by any means half of the papers in this conference. One of these headings is quantum transport, the application of modern quantum-mechanical methods to gain a conception of the transport process better than that provided by the usual Boltzmann equation; the other heading has to do with the rather vague concept of hopping of charges that are bound to particular sites and just occasionally change their position.

## 2. FREE CARRIERS

Let us take up first the most familiar of the fields, that of free-carrier transport. Before discussing transport itself, it is appropriate to say a little about the fundamental scattering interactions. These are of the familiar types: acoustic scattering, polar-mode scattering, intervalley scattering, impurity scattering, and so on. There is not enough space to survey here the exact state of present knowledge on all of these, so we shall be content to draw attention to one or two things of especial interest which have come out only recently.

It has now become quite clear that polar-mode scattering is very important and in fact dominates the mobility in semiconductors which have even a slightly polar character and at the same time a very small effective mass. EHRENREICH (E.5) has shown quite convincingly that the mobility of indium

*Table* 1. *Major areas in the field of semiconductor transport*

| Free carriers only | Phonons and excitons | Quantum transport | Hopping |
|---|---|---|---|
| Scattering interactions → | | Strong interactions | Low-mobility materials |
| Near-equilibrium transport | Thermal conduction | High magnetic fields | Impurity conduction |
| Hot electrons | Exciton migration | | |
| | Phonon drag | | |

antimonide is quantitatively calculable from the polar-mode scattering model—augmented at high temperatures by electron-hole scattering—with input data obtained wholly from fields other than conduction. The reason that polar-mode scattering is especially important when the effective mass is very small is of course that the polar mode, being a polarization wave in the lattice, sets up an E field that is proportional to polarization and so sets up potential fluctuations that are inversely proportional to the wavelength; if very long wavelengths are involved, as in the case of low-mass carriers, these potential fluctuations become much larger than those due to other sources of scattering. Polar scattering also seems to be dominant in some of the other III–V compounds such as indium phosphide and gallium arsenide.

An interesting and sometimes important effect, long familiar in the case of ionized-impurity scattering, but only recently pointed out for polar-mode scattering (E.5), is the screening of the scattering interaction by the free carriers themselves. This screening of course becomes especially serious if the density of the carriers is high. For intrinsic indium antimonide it gets quite appreciable. It is even possible—especially for materials with a high static dielectric constant—for this effect to outweigh impurity scattering and make the mobility increase with doping.

Let us now pass on to the application of some of the known scattering interactions to the details of transport phenomena. The first type of transport we shall discuss is what may be called "near-equilibrium" transport. This is the familiar type of transport in which a small electric field is applied with or without magnetic fields, stresses, etc. and a small perturbation of the equilibrium carrier distribution is produced. In this field the picture seems to be one of increasing refinement in the correlation of the theory and experiment; whereas a few years ago people were happy if they understood the qualitative features of experimental results, the trend now is to try to explain things like magnetoresistance, Hall-to-drift mobility ratio, variations of Hall coefficient with magnetic field, etc., in very fine quantitative detail. This is succeeding fairly well for semiconductors like germanium and silicon and we are extending our understanding more and more to other materials.

In this program it is now becoming necessary to use more and more refined methods for the solution of the transport equation, especially when one wants to treat anisotropic energy surfaces and scattering laws, or the simultaneous action of more than one type of scattering mechanism. Here a great opportunity is provided by variational principles. Very often one can show that the solution of the equation one is trying to solve gives a minimum or at least a stationary value to some certain functional of the distribution function, subject to certain constraints. In such cases one can assume a distribution function with a few adjustable parameters, minimize the functional, and get a pretty good idea of the distribution. This approach has been applied to optical-mode and electron-hole scattering (E.5), to transport in warped bands (E.7), and to various other problems. It can be generalized to cases where a magnetic field is present.[1]

VOL 8 195

It may be instructive to make a little digression illustrating the power of the variational method as a means of obtaining a conclusion which might be hard to prove in any other way. The question has occasionally been raised as to whether peculiar types of scattering interactions or peculiar types of warped energy surfaces might be capable of giving a negative magnetoresistance. Now KOHLER'S general variational principle[2] states that the distribution function which occurs for conduction in the absence of a magnetic field is one which minimizes the dissipation for a given current. The dissipation is a certain quadratic functional of the distribution function which does not depend on the external fields explicitly. So if for a given current the distribution which occurs in the presence of a magnetic field differs from that in the absence of such a field, the former must give the higher dissipation. The conclusion from this is that it is not possible to obtain a negative magnetoresistance from any theory based on a Boltzmann equation with scattering interactions in crystal-momentum space. Negative magnetoresistance can arise only from an effect of the magnetic field on the carrier concentration, from phenomena peculiar to quantum transport theory, or as a consequence of a transport equation which treats transport not in momentum space alone but in momentum and position space together.

The next topic under the heading of free carriers is a very active one at this conference—hot electrons. Here one can divide the subject, as KOENIG (I.2) pointed out very clearly, into first, the factors which determine the distribution function of a given number of electrons under the action of a strong electric field, and second, the way in which this distribution function can interact with bound electrons or electrons in the valence band to produce ionization and avalanche phenomena, etc.

As regards the distribution function, the phenomena are determined by different factors in different temperature ranges. At high temperatures, even in non-polar semiconductors, the energy loss is determined primarily by scattering by optical modes, and in germanium, even at liquid-air temperature and somewhat below, the overwhelming proportion of the energy loss of hot electrons is to optical modes, in spite of the fact that optical modes have negligible influence on the mobility. However, one can go to low enough temperatures—down in the hydrogen and helium ranges, for germanium—so that the dominant cause of energy loss is acoustical phonons and here the mechanism of energy loss is better understood; at least there is not an unknown coupling constant coming into it. There is hope that in the near future a fairly complete correlation of theory and experiment on the distribution function and mobility of hot electrons can be achieved. In the higher-temperature range where the optical modes come in, some rather difficult calculations are involved to get the distribution function of hot electrons, and if the electrons are sufficiently numerous things like screening and electron–electron collisions may also play a role. In spite of these difficulties, hot-electron studies are now beginning to give useful information on the strength of the coupling of electrons to optical modes, and this knowledge is helpful in a number of applications.

Some interesting techniques are starting to be employed in the study of hot electrons, notably the action of magnetic fields on them (I.5, S.4). A lot of the phenomena that are being observed are not yet understood but seem to be capable of eventually providing useful information.

A very interesting effect was pointed out in a paper by SASAKI, SHIBUYA, MIZUGUCHI, and HATOYAMA (I.7) on the anisotropy of hot-electron conduction. In *n*-type germanium the valleys are anisotropic and if the direction of the electric field makes different angles with the large-mass directions of different valleys, then electrons in some valleys will get hotter than those in others. In such case the electrons in the hotter valleys, having higher energies, will tend to pass to the lower energy states of the other valleys by intervalley scattering; this gives a redistribution of population among the different valleys. The overall anisotropy of hot electrons is thus compounded out of this redistribution and the anisotropy which would be present even for fixed populations. The suggestion has been made (I.2) that perhaps a measurement of the anisotropy of hot electrons may be the easiest type of experiment to do to get information on the band structures of new semiconductors.

Breakdown processes can be studied very easily with hot electrons, especially if our understanding of the distribution function of hot electrons is fairly advanced. For in such cases the observed carrier multiplication is related in a known way to the

various energy-dependent ionization and recombination processes, and by observing this relationship at various electron "temperatures" one can sort out the details of the cross sections involved. The work reported by KOENIG (I.2) has in this way yielded a fair confirmation of the theory of giant traps (C.3) for germanium at helium temperatures.

Now I would like to comment on an area in which few new results have been presented at this conference, but in which the need for an improved theoretical understanding is becoming more and more evident. This is the area of impurity scattering. The by now classical theory of Conwell and Weisskopf has proven extremely useful in the correlation of effects that are attributable to ionized-impurity scattering, especially when the impurity scattering is rather slight. At low ion densities a theory of this type can in fact be given a rather rigorous justification, although the correct theory differs from the form usually used in the semiconductor literature through the inclusion of the effects of electron–electron collisions, effects which for some purposes are almost as important as electron–ion collisions. However, at densities where the number of carriers in a cubic Debye length is of the order of unity or less or where the Debye length is of the order of an electron wavelength, the logical basis of this type of treatment of impurity scattering breaks down and no one has done enough work to know just how much the theory needs to be modified. We have good indications that the modification may be considerable, and whereas crude versions of the theory may be all right for qualitative purposes, a much more refined theory is needed for those cases, which occur more and more often nowadays, where an accurate correlation of theory and experiment is sought. It may even be that one cannot formulate the theory of strong ionized-impurity scattering simply as a scattering in crystal-momentum space; one may have to consider coordinate and momentum space together.

Impurity scattering is, of course, an essential feature in the understanding of highly-doped semiconductors, and some of the interesting things that may occur in this field have been suggested by the report of STIL'BANS (E.2) on mobilities in degenerate lead telluride and bismuth telluride. He found the apparent impurity-scattering cross section to depend on temperature, as if there might be some sort of interaction of impurity and phonon scattering. This area is still quite a mystery.

### 3. PHONONS AND EXCITONS

Now let us consider the second column of Table 1, phonons and excitons. The first topic listed here is thermal conduction. Now although thermal conduction by phonons alone does not belong in the area of semiconductor physics, it is of considerable interest to us because any thermal conduction or thermal resistance which one cannot account for by phonons may involve free carriers, excitons, and things like that which are central to the semiconductor field. Here of course the most exciting event has been the controversy, which has raged for a number of years now, regarding the increase in the thermal conduction of a number of semiconductors at high temperatures. To account for such increases people have invoked the ambipolar transport of gap energy by electron–hole pairs,[3] exciton migration, and internal radiation (M.3).

The different experimenters working on materials like indium antimonide, lead telluride, etc., have for a long time been disagreeing with each other, but I think we have now reached a stage where the different experiments are gradually starting to come together. In all cases where reasonable agreement has been reached it seems that there are no thermal conduction effects which cannot be understood in terms of phonon transport, ambipolar transport, and possibly sometimes radiative transport within the solids; however, not all the discrepancies in the experimental data have been tracked down and the possibility of other types of transport should not be completely ruled out.

Exciton transport is only a rather remote possibility; the reason it is remote is the very large statistical factor arising from the fact that an exciton is a single particle, while an electron-hole pair is two particles. If, as is usually the case, the energy required to produce an exciton is comparable with that to produce a pair, the equilibrium concentration of pairs will be much greater than that of excitons, because of the greater number of momentum states accessible. Only if the exciton has a very much lower activation energy—say than half the band gap—could it make a comparable contribution to the conduction.

The third field in this area, which of course is of especial interest to semiconductors, is phonon drag.

Here we have passed from the period of mere discovery of new effects into a phase of very detailed correlation of experiment and theory (M.5), in which the one unknown is the form of the phonon–phonon scattering laws. The wide variety of possible thermoelectric and thermomagnetic observations which one can make on a given material allows us both to check up on the adequacy of our understanding of the purely electronic aspects of the transport process, and to pin down many details of the phonon–phonon scattering laws.

### 4. COMMENTS ON CURRENT TRENDS

Before going on to the last two headings in Table 1, I would like to make a little digression. About three-quarters of the transport papers presented at this conference have pertained to the two areas we have already discussed. In these areas the current trend is toward a more and more detailed and accurate correlation of theory and experiment, often extending into the second decimal place. One may ask, what is the value and significance of this? Is it just an exercise for the specialist? I would like to advance the thesis that this trend is of interest to everybody because it supplies a solid platform of thoroughly-understood material which we can use as a taking-off point for investigating new areas of the completely unknown. The conference has provided a few examples of how this works out, and of how areas other than transport can benefit from refinement of our understanding of transport phenomena. One such example is the use of hot electrons to study the ionization and recombination cross sections of donor centers. A good determination of the energy and temperature dependence of these cross sections depends upon an accurate understanding of the distribution function of the hot electrons. Another example is the phonon-drag area, which is now yielding information about the frequency and temperature dependence of phonon–phonon scattering in a frequency range inaccessible to almost all other types of investigation. This quantitative analysis of phonon drag would have been impossible, however, without the foundation of a detailed understanding of electronic transport processes in germanium, a foundation to which many theoretical and experimental researches have contributed. As a final example we may cite the use, to be discussed below, of the piezoresistance effect to study impurity band conduction (I.8). Because the study of piezoresistance in normal conduction has given us a thorough understanding of the effects of strain on free-carrier states, we can start to employ these effects to study the structure of donor levels and the nature of the hopping process.

If we grant that the current trend toward quantitative accuracy in the correlation of theory and experiment is a valuable step in the advance of semiconductor science, and that this trend should be strengthened, we must take to heart a corollary which, though obvious, is sometimes in danger of being overlooked. This is that for this stage a much more sophisticated attention to experimental technique is necessary than has been usual in semiconductor work in the past. In what have come to be regarded as routine types of electrical and galvanomagnetic measurements it is beginning to be realized that one must relentlessly track down such things as geometrical effects of contact area, surface conduction, and inhomogeneities. In measurements of thermal conduction, contact resistance and radiative connections require careful attention. In all areas, measurements should not be given quantitative credence until it has been established that they are accurately reproducible from specimen to specimen.

### 5. QUANTUM TRANSPORT

There are two quite common situations in which the conception of free carriers undergoing occasional scattering processes breaks down. One is if the random perturbations which we would like to call scattering interactions are so strong that they make a major, rather than just an occasional, modification in the motion of the carriers; in mathematical terms, this occurs if the perturbations damp out a current in a time $\tau$ so short that $\hbar/\tau$ exceeds the energy of the carriers. The other situation is one in which the most natural choice of what we would like to call stationary states turns out to involve states of zero mean velocity, rather than running-wave states of finite velocity. For either of these cases a really adequate description of the conduction process has to be in terms of how an electric field alters the diagonal and off-diagonal elements of the quantum-mechanical density matrix.

To illustrate this, let us consider a specific example, namely, the conductivity of a semiconductor in a very strong transverse magnetic field. In such a field the states of the carriers are quantized into Landau levels. Now these Landau

levels, although they can have a velocity along the magnetic field, cannot have any average velocity perpendicular to the magnetic field. They are just stationary circular motions. So if we wish to calculate the current in a direction at right angles to the magnetic field, we cannot use the usual type of Boltzmann equation. In fact, to get a state with a mean velocity perpendicular to the magnetic field one must take a linear combination of Landau states with quantum numbers $n$ and $n \pm 1$. Therefore a knowledge of the mean number of electrons in each Landau level does not suffice to determine the mean velocity of the electrons. One must know the probabilities for electrons to be in states describable as linear combinations of different Landau levels, in other words, the off-diagonal elements of the density matrix. When the spacing of the Landau levels is very much less than $kT$ and when the scattering interactions are weak, one expects on physical grounds that the result of a correct calculation of these off-diagonal elements should be the same as the result of the very much simpler calculation based on the usual Boltzmann equation and ignoring quantization. But when the level spacing is $\gtrsim kT$, one expects the effects of quantization to be important, and the current can only be computed from a fully quantum-mechanical theory.

A number of different approaches have been used in the recent literature to set up quantum transport theory.[4] There were just two papers in this field at this conference, one of which, by ARGYRES (E.4), was on the high-field magnetoresistance problem just mentioned. This paper made a very logical analysis of the problem of determining the density matrix in a magnetic field with different kinds of scattering. However, it should be pointed out that there are some unresolved questions in connection with quantum magnetoresistance which may or may not affect other aspects of quantum transport theory. For it seems that by equally plausible methods of setting up quantum transport theory one can derive for the case, say, of acoustic scattering and cyclotron spacing $\gg kT$, a high-field magnetoresistance going very nearly as $H$ (ARGYRES), or very nearly as $H^2$.[5] The logical error which must be present in one of these lines of reasoning has not yet been demonstrated. This question ought to be resolved in the interest of safe progress for quantum transport theory.

Another type of application of quantum transport theory has been described by LUTTINGER and KOHN (E.1). This work starts with the picture of free carriers in running-wave states, but tries to develop the quantum-mechanical density matrix to a higher order of approximation than that which corresponds to the solution of the ordinary Boltzmann equation. This is an approach which will be useful in cases where the latter approach is at least a rough approximation but where something better is needed. Such a need occurs, for example, in semiconductors of moderately low mobility, where the carriers would probably behave as fairly ordinary free particles if the scattering interactions were absent, but where in practice these interactions are so strong that it is hard to speak of a free motion of the carriers in between scatterings.

Though quantum transport theory is at present still in its infancy, it is, I believe, the route through which will be made the most fundamental of the future advances in our understanding of semiconductor transport.

### 6. HOPPING

A hopping of charges from one local site to another is the only picture that we now have to understand low-mobility semiconductors. There are a good many of these, e.g. the transition-metal oxides and the ring compounds. As JOFFÉ pointed out (A.3), the study of these semiconductors has been somewhat neglected. It is to be hoped that in the future this neglect will be made up, not by a flurry of routine measurements, but by profoundly conceived theories and by experiments so designed as to isolate and reveal the features of the theoretical picture which are of the most fundamental importance.

Not much was reported on low-mobility materials at this conference. Perhaps the most interesting thing is the remark by ZENER (B.2) to the effect that one can correlate peaks in the internal friction as a function of frequency or temperature with the hopping of electrons from one ion to another. This, then, gives an independent way of studying the hopping frequencies that enter into conduction processes.

We shall close with a discussion of the great field of impurity conduction, a field in which there was considerable activity at this conference. More and more experiments are being reported in support of the idea, which I think occurred independently to a

VOL 8 195

number of workers, but which was most forcefully expounded by MOTT,[6] that impurity conduction takes place—at least in lightly-doped material—by the hopping of electrons from an occupied donor center to a neighboring unoccupied one, or of holes between occupied and unoccupied acceptor centers. This sort of conduction is thus sensitive to the degree of compensation, and would disappear in the absence of compensation. At low compensations the conduction should have an activation energy representing an average energy to move a charge from the majority impurity nearest to a compensating impurity ion away from the field of the latter and into the fields of other compensating ions. A general confirmation of this picture has been obtained in experiments of LONGO, RAY, and LARK-HOROVITZ (I.9), using the method of bombardment with high-energy particles to produce an accurately-controllable compensation in silicon. However, it does not seem to have been established yet whether there is sometimes another source of an activation energy for this type of transport, e.g. whether the hopping sometimes takes place via low-lying excited states of the centers.

A very powerful tool for the study of this kind of impurity conduction has been demonstrated by FRITZSCHE (I.8), namely, the piezoresistance effect. A shearing strain is known to lift the degeneracy of the band-edge states; for *n*-type germanium the relative shifts of the different valleys are rather accurately known from piezoresistance measurements in the range of normal conduction. According to theory the band-edge degeneracy should entail a degeneracy or a near-degeneracy of the ground state of a hydrogenic impurity level. It turns out, therefore, that an elastic shear of attainable magnitude can produce a rather large—and essentially calculable—perturbation of the energy and wave function of an impurity center. This produces, as might be anticipated, a large change in the impurity conduction, and there is real hope that in the near future studies of this effect will lead to an establishment of the nature of the hopping process.

Another powerful tool is the use of large magnetic fields, which can modify the wave functions and energies of impurity levels in a calculable way. For *n*-type indium antimonide the effect is especially large because of the small effective mass, and it makes it possible to freeze out electrons onto donors, an effect not observed in the absence of a magnetic field. The mobility of these frozen-out electrons does indeed seem to vary with magnetic field in somewhat the same way as the theoretical overlap of the donor wave functions (S.3); however, the temperature dependence of the conduction is not yet fully understood. Another interesting effect of the magnetically-induced freeze-out is that it makes possible the study of collision ionization by hot electrons in indium antimonide (S.4).

Although at low impurity densities there is abundant evidence that impurity conduction is due to the compensation-dependent Mott mechanism, there is at least a suggestion that for a certain range of rather high impurity densities ($10^{19}$ or so per $cm^3$ for boron in silicon) the low-temperature conduction corresponds more nearly to the older concept of carriers moving more or less independently in an "impurity band" (I.9).[7] The evidence comes from specimens which with decreasing temperature show a certain amount of freeze-out, followed by a maximum in the Hall constant and a low-temperature plateau with temperature-independent conduction. On passing from light to moderate compensation the impurity conduction in these specimens decreases, instead of increasing as in the Mott region.

## REFERENCES


1. GARCIA MOLINER F. and SIMONS S. *Proc. Cam. Phil. Soc.* **53,** 848 (1957).
   SEEGER A. *Canad. J. Phys.* **34,** 1278 (1956).
2. KOHLER M. *Z. Phys.* **124,** 772 (1948).
3. DAVYDOV B. I. and SHMUSHKEVICH I. M. *Usp. fiz. Nauk.* **24,** 24 (1940).
   FRÖHLICH H. and KITTEL C. *Physica* **20,** 1086 (1954).
   PRICE P. J. *Phil. Mag.* **46,** 1252 (1955).
4. KUBO R. *J. Phys. Soc. Japan* **12,** 570 (1957).
   NAKANO H. *Progr. Theor. Phys.* **17,** 145 (1957).
   KOHN W. and LUTTINGER J. M. *Phys. Rev.* **108,** 590 (1957).
   LUTTINGER J. M. and KOHN W. *Phys. Rev.* **109,** 1892 (1958).
5. KLINGER M. I. and VORONYUK P. I. *Zh. eksp. teor. fiz.* **33,** 77 (1957). The explicit evaluations of this paper are only given for fantastically high fields, at which the mean energy of the phonons which scatter the electrons becomes $\gg kT$. However, intermediate formulas given in this paper can be applied to the calculation of the magnetoresistance in the "quantum limit" as usually defined and give a resistivity nearly proportional to $H^2$; the same conclusion has been reached in unpublished calculations of a number of other workers.
6. MOTT N. F. *Canad. J. Phys.* **34,** 1356 (1956).
7. FRITZSCHE H. *J. Phys. Chem. Solids* **6,** 69 (1958).